AL.2.2003-533
C.2

The Chemistry of Alberta Oil Sands, Bitumens and Heavy Oils

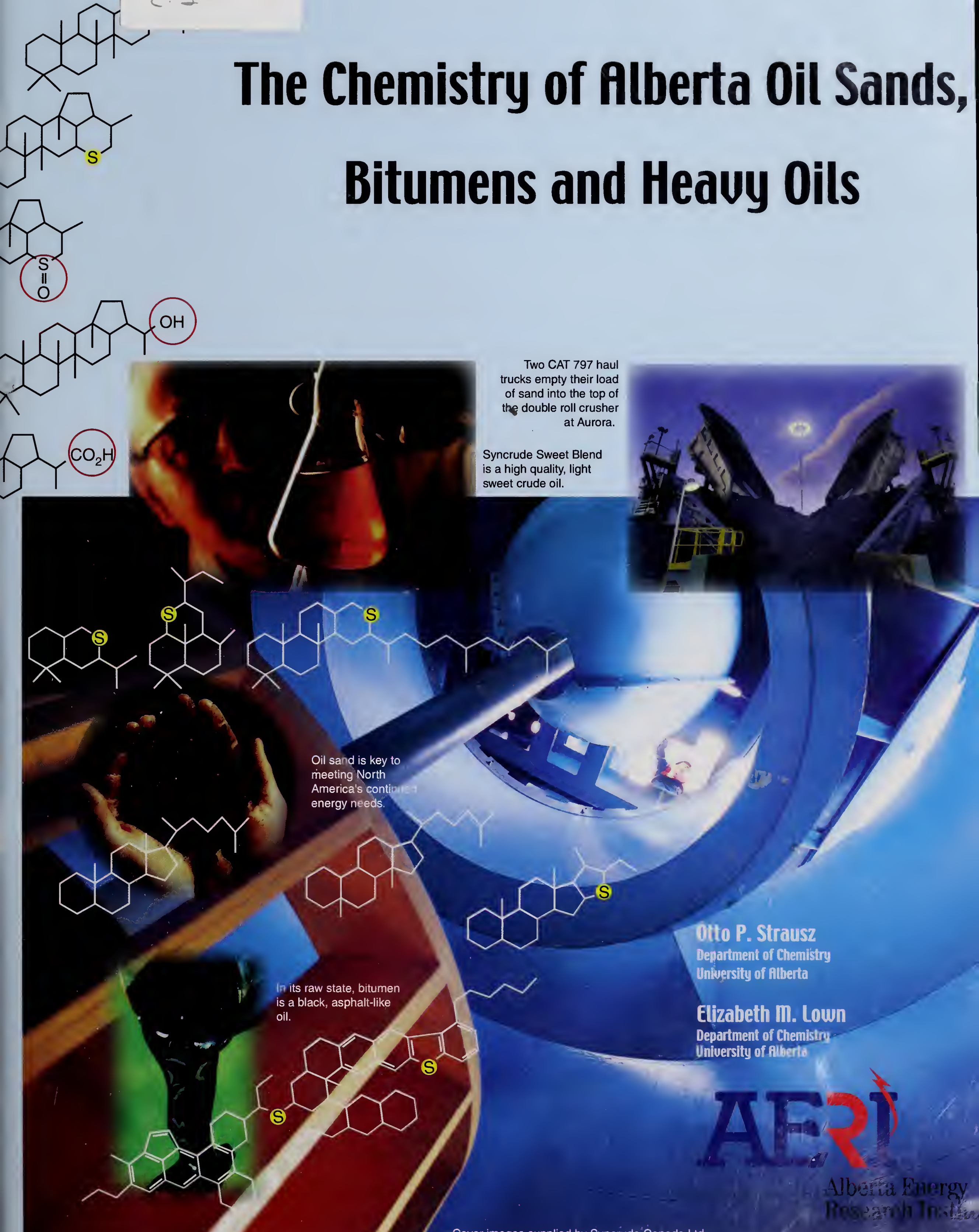

Two CAT 797 haul trucks empty their load of sand into the top of the double roll crusher at Aurora.

Syncrude Sweet Blend is a high quality, light sweet crude oil.

Oil sand is key to meeting North America's continued energy needs.

In its raw state, bitumen is a black, asphalt-like oil.

Otto P. Strausz
Department of Chemistry
University of Alberta

Elizabeth M. Lown
Department of Chemistry
University of Alberta

AERI
Alberta Energy Research Institute

Cover images supplied by Syncrude Canada Ltd.

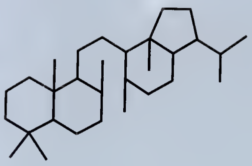

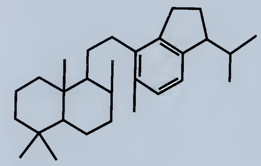

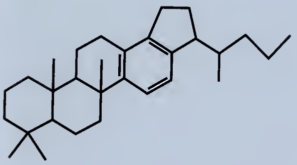

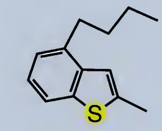

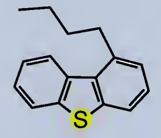

Enormous wood bison sculptures
mark the entrance to the
Syncrude site.

Digitized by the Internet Archive
in 2015

https://archive.org/details/chemistryofalber00stra

The Chemistry of Alberta Oil Sands, Bitumens and Heavy Oils

Otto P. Strausz
Department of Chemistry
University of Alberta

Elizabeth M. Lown
Department of Chemistry
University of Alberta

This book is dedicated to the explorers, engineers and scientists who have contributed to the advancement of our knowledge and understanding of the mysteries of Alberta's oil sands.

The Alberta Energy Research Institute and Her Majesty the Queen in right of Alberta make no warranty, express or implied, nor assume any legal liability or responsibility for the accuracy, completeness, or usefulness of any information, contained in this publication, nor that use thereof will not infringe on privately owned rights. The views and opinions of the author expressed herein do not necessarily reflect those of the Alberta Energy Research Institute or Her Majesty the Queen in right of Alberta. The Government of Alberta, its officers, employees, agents and consultants are exempted, excluded and absolved from all liability for damage or injury, howsoever caused, to any person in connection with or arising out of the use by that person for any purpose of this publication or its contents.

Copyright © Dr. Otto Strausz 2003

ISBN 0778530965

Published by:

Alberta Energy Research Institute
Suite 2540, Monenco Place
801 6th Avenue S.W.
Calgary, Alberta, Canada T2P 3W2
www.aeri.ab.ca

Preface

"The Chemistry of Alberta Oil Sands, Bitumens and Heavy Oils" is a somewhat expanded, specialized version of general petroleum chemistry and comprises different facets of chemical sciences and related interdisciplinary areas, such as physics, geology, earth sciences, biology and microbiology. Within chemistry, many branches and subspecialties incorporate the chemistry of petroleum. Since petroleum is a mixture of organic molecules, it comes under the general purview of organic chemistry and many of its subspecialties, including analytical chemistry, biochemistry, biomarker chemistry and organic geochemistry, as well as physical, colloid and geochemistry.

Each of the above subspecialties has become exceedingly complex over the years, accumulating enormous bodies of intricate, detailed technical and fundamental knowledge. For the specialists immersed in their own field it may not always be easy to pierce through the horizon and develop an idea of the terrain that lies beyond. This circumstance, and the also the need for a textbook for an introductory course at the undergraduate or graduate level in technical and engineering schools providing an overview of the field, prompted the writing of this book.

Research in oil sand chemistry, hand-in-hand with petroleum chemistry, has made gigantic strides in the past decades but the direction of research does not always follow straight boulevards and often spirals down labyrinths. To illustrate this point, there are still many problems in petroleum chemistry about which ideas have changed numerous times over the years and decades, and yet they are still in a state of flux. A typical example is asphaltene, the highest-molecular weight supramolecular compound class component of petroleum and especially of heavy oils and oil sand bitumens. The molecular structure, shape, size and physical and chemical properties of this material are still not fully understood and aspects of them are even now earnestly debated.

Owing to space limitations, this book does not cover all the elements of oil sand chemistry. The selection of topics was somewhat arbitrary and dictated in part by the authors' own research interests. Consequently, to our regret, many fine and important pieces of research had to be omitted. Nonetheless, we believe that the coverage presents a reasonably broad overview of the field,with attention to some of the problems such as the molecular structure, size and shape of the asphaltene molecule, the composition of the resin fractions and their interaction with asphaltenes, the composition and distribution of biological markers, and others.

This book was made possible by the active support and contributon of a multitude of people to whom the authors owe a great deal of indebtedness. First of all, we would like to pay tribute to Dr. Harry E. Gunning, former Professor and Head of the Department of Chemistry and President of the University of Alberta whose helpful support, contagious enthusiasm and inspirational encouragement meant so much to us. We also gratefully acknowledge the vital support of Dr. Clement W. Bowman, former Vice-President for Research, Esso Resources, Chairman of the Board, Alberta Oil Sands Technology and Research Authority and President of the Alberta Research Council, who recognized the necessity for fundamental knowledge to develop new technologies for the utilization of Alberta's oil sand resources. It is also a great pleasure to thank Dr. Douglas S. Montgomery for his helpful and enjoyable collaboration and generous willingness in sharing with us his insight into the science and technology of petroleum.

A special thank you to our colleague Dr. Imre Safarik for his invaluable help in literature searches, his many useful suggestions and the painstaking job of proofreading the manuscript.

We also thank each and every one of our former colleagues and coworkers for their enthusiastic dedication to research on oil sand chemistry and their contributions to its advancement.

It is a pleasure to acknowledge our indebtedness to Ms. Lorna Pregoda for her expert graphic art work and meticulous professional editing.

We also thank Mr. Conrad Gietz for proofing an early version of the manuscript.

Last but not least, we would like to thank the Alberta Oil Sand Technology and Research Authority and the Alberta Energy Reseach Institute for financial assistance in the preparation of the manuscript, the Alberta Oil Sands Technology and Research Authority and the Natural Sciences and Engineering Council of Canada for their generous support of our research efforts, and the Department of Chemistry of the University of Alberta for providing facilities for the preparation of the manuscript.

Contents

Introduction 1
  Bibliography 7

1. The Origin of Petroleum 9
  1.0 Genesis of Petroleum 12
  2.0 Migration and Accumulation of Oil 14
  3.0 Chemical Alteration of Oil During Migration 15
  4.0 Chemical Alteration of Pooled Oil 16
    4.1 Thermal processes 16
    4.2 Deasphalting 17
    4.3 Biodegradation and water washing 17
  Bibliography 19

2. Geology of the Alberta Bitumen and Heavy Oil Deposits 21
  1.0 Athabasca Oil Sands Area 23
  2.0 Carbonate Trend (Carbonate Triangle) 24
  3.0 Peace River Oil Sands Area 25
  4.0 Cold Lake Oil Sands Area 26
  5.0 Lloydminster Heavy Oil Deposit 26
  Bibliography 26

3. Composition and Structure of Alberta Oil Sands and Oil Carbonates 29
  1.0 The Composition and Structure of Oil Sands 29
    1.1 Interfacial properties 39
      1.1.1 Interfacial tension 40
      1.1.2 Electric properties 50
        a) Electric double layer and the zeta potential of the bitumen/water interface 50
        b) Electric double layer and the zeta potential of the mineral/water interface 53
    1.2 Microstructure of oil sands 55
  2.0 Physical Chemistry of the Water Flotation Process 57
    2.1 The hot water process 57
    2.2 The cold water process 61
  3.0 Interfacial Effects in the *In-situ* Water Flood Displacement of Bitumen 61
  4.0 Migrational History of the Oil Precursor to the Bitumen 62
  5.0 Summary 62
  Bibliography 63
  Appendix 3.1 67

4. Organic Chemistry: Nomenclature and Some Basic Concepts 69
  1.0 Acyclic Alkanes 69
  2.0 Cycloalkanes 73
  3.0 Aromatics 76
  4.0 Heteroatom-Containing Compounds 78
  5.0 More About Isomerism in Carbon Compounds 79
  6.0 Chemical Structures of the Bioorganic Precursor Source Materials of Petroleum 82
  7.0 Types of Functional Groups and Chemical Structures in Alberta Bitumens 86

5. **Composition and Properties of Bitumen** 89
  - 1.0 Definition, Characterization, Separation 89
  - 2.0 Elemental Composition 93
  - 3.0 Physical Properties 99
    - 3.1 Density and specific gravity 99
    - 3.2 Viscosity 102
    - 3.3 Thermal properties 107
      - 3.3.1 Liquid-solid transition 107
      - 3.3.2 Liquid-vapor transition 109
      - 3.3.3 Carbon residue 110
      - 3.3.4 Specific heat and latent heat 114
        - a) Specific heat 114
        - b) Latent heats of vaporization and fusion 115
        - c) Heat of combustion 116
  - 4.0 Optical Properties 118
    - 4.1 Refractive index 118
    - 4.2 Optical rotation 119
  - 5.0 Class Composition 120
    - 5.1 Distribution in the reservoir 126
  - 6.0 Summary 127
  - Bibliography 129
  - Appendix 5.1 Inorganic Constituents of Petroleums 132

6. **Minerals** 135
  - Bibliography 140

7. **Reservoir Water** 143
  - Bibliography 149

8. **Methylene Chloride–Insoluble Organic Matter** 151
  - 1.0 Bitumen-Related Organic Matter 151
  - 2.0 Bitumen-Unrelated Organic Matter 158
    - 2.1 Characterization of bitumen-unrelated organic matter 158
    - 2.2 Distribution of the bitumen-unrelated organic matter in the oil sand tailing fractions 164
    - 2.3 Bonding between humic and inorganic substances 168
  - 3.0 Summary 174
  - Bibliography 176

9. **Reservoir Gases** 179
  - Bibliography 188

10. **Chemical Composition of the Saturate Fraction** 189
  - 1.0 Athabasca Bitumen Saturates 190
  - 2.0 Other Alberta Bitumen Saturates 200
  - 3.0 The Nondistillable Portion of Athabasca Saturates 208
  - 4.0 Summary 210
  - Bibliography 210
  - Appendix 10.1 Field Ionization, GC–FI Mass Spectrometry 212
  - Bibliography 215
  - Appendix 10.2 Adduction Chromatography 216
  - Bibliography 218

11. Chemical Composition of the Aromatic Fraction 219
- 1.0 Monoaromatic Subfraction 220
  - 1.1 Subfraction 1c 220
  - 1.2 Subfraction 1d 220
- 2.0 Diaromatic Subfraction 223
  - 2.1 Subfraction 2a 223
  - 2.2 Subfraction 2b 225
  - 2.3 Subfraction 2c 227
  - 2.4 Subfraction 2d 228
  - 2.5 Subfraction 2e 228
- 3.0 Triaromatic Subfraction 229
  - 3.1 Subfraction 3b 229
  - 3.2 Subfraction 3c 231
  - 3.3 Subfraction 3d 233
  - 3.4 Subfraction 3e 233
  - 3.5 Subfraction 3f 235
- 4.0 General Properties of Distillable Aromatics 236
- 5.0 Composition of the Nondistillable Aromatics 240
  - 5.1 NMR studies 240
  - 5.2 Thermolysis 242
    - 5.2.1 The *n*-pentane eluent of the pyrolysis oil 242
    - 5.2.2 The 50% toluene/*n*-pentane eluent of the pyrolysis oil 244
      - a) Distillable subfraction 245
        - i) Hydrocarbons 245
        - ii) Sulfides 245
        - iii) Thiophenes 246
      - b) Nondistillable subfraction 246
    - 5.2.3 The 10% methanol/toluene eluent of the pyrolysis oil 250
  - 5.3 Ruthenium ions-catalyzed oxidation 252
- 6.0 Aromatics in Other Alberta Bitumens 253
- 7.0 Aromatic Compounds Identified 254
- 8.0 Summary 258
- Bibliography 259

12. Chemical Composition of the Polar Fraction 261
- 1.0 Mass Spectroscopic Studies on the Lower Molecular Weight Components of Athabasca Polars 265
  - 1.1 Subfractions 4 to 7 266
  - 1.2 Subfraction 8 270
  - 1.3 Subfractions 9 and 10 271
  - 1.4 Subfraction 11 271
  - 1.5 Subfraction 13 271
  - 1.6 Subfraction 14 274
  - 1.7 Subfraction 15 276
  - 1.8 Comments on the mass spectroscopic studies 276
- 2.0 Chemical Studies on Athabasca Polars 277
  - 2.1 Sulfur-containing components 277
    - 2.1.1 Saturated sulfides and sulfoxides 277
      - a) Bicyclic terpenoid sulfides and sulfoxides 282

b) Tetracyclic terpenoid sulfides and sulfoxides ... 286
c) Tricyclic terpenoid sulfides and sulfoxides ... 288
d) Hexacyclic terpenoid sulfides and sulfoxides ... 289
e) Monocyclic sulfides and sulfoxides ... 291
f) Pentacyclic terpenoid sulfides and sulfoxides ... 293
g) Terpenoid sulfides and sulfoxides complexed to asphaltene ... 293
h) Conclusion ... 293
2.1.2 Thiophenes ... 295
2.2 Oxygen-containing components ... 298
2.2.1 Carboxylic acids and esters ... 299
a) Tricyclic acids and esters ... 299
b) Pentacyclic acids and esters ... 303
c) Acyclic acids and esters ... 304
d) Miscellaneous carboxylic acids ... 305
2.2.2 Acid anhydrides and esters ... 311
2.2.3 Ketones ... 313
2.2.4 Alcohols ... 316
2.3 Nitrogen-containing components ... 319
2.3.1 Carbazoles in the acetone extract of asphaltene ... 321
2.3.2 Basic nitrogen compounds ... 326
2.3.3 Porphyrins ... 335
3.0 Composition of the Nondistillable Polars ... 346
3.1 NMR studies ... 347
3.2 Flash pyrolysis of the nondistillable polars ... 349
3.2.1 The *n*-pentane eluent of the distillate ... 349
3.2.2 The toluene eluent of the distillate ... 353
a) Distillable toluene eluent ... 353
b) Nondistillable toluene eluent ... 361
3.2.3 The polar (CH_3OH/toluene) eluent of the distillate ... 364
3.2.4 Pyrolysis oil recovered from the reactor ... 368
3.3 Summary and conclusions ... 368
4.0 Thermolysis of the Polars ... 369
Bibliography ... 371

13. Biomarkers in Bitumens ... 375
Part I. Biomarkers in the Bitumen ... 376
1.0 Hydrocarbon-type Biomarkers ... 376
1.1 Cyclic terpenoid biomarkers ... 376
1.1.1 Pentacyclic terpenoid hydrocarbons ... 380
1.1.2 Tetracyclic terpenoid hydrocarbons ... 387
a) Saturated steroids ... 387
b) Aromatic steroids ... 391
c) Secohopanes ... 393
1.1.3 Tricyclic terpenoid hydrocarbons ... 393
1.1.4 Bicyclic terpenoid hydrocarbons ... 397
1.1.5 Monocyclic terpenoid hydrocarbons ... 398
1.2 Acyclic terpenoid biomarkers ... 398
1.3 Geochemical conclusions from early studies on hydrocarbon biomarkers ... 400
2.0 Sulfur-Containing Biomarkers ... 406

    2.1 Origin of sulfides and incorporation of sulfur into the sedimentary organic matter 407
    2.2 Bicyclic terpenoid sulfides 408
    2.3 Tricyclic terpenoid sulfides 411
    2.4 Tetracyclic terpenoid sulfides 413
    2.5 Pentacyclic steroid sulfides 415
    2.6 Hexacyclic terpenoid sulfides 415
    2.7 Cyclic terpenoid sulfoxides 416
    2.8 Thiophenes 416
  3.0 Biodegradation of Petroleum 417
  4.0 Water Washing of Petroleum 426
  5.0 Oxygen-Containing Biomarkers 429
    5.1 Carboxylic acids 429
    5.2 Ketones 431
    5.3 Alcohols 432
  6.0 Nitrogen-Containing Biomarkers 433
  7.0 Secondary Migration of Petroleum 437
  Part II. Biomarkers in the Alkaline Process Water 438
  1.0 Hydrocarbon-type biomarkers 438
  2.0 Oxygen-Containing Biomarkers 445
  3.0 The Origin of Alberta Oil Sands and Their Secondary Migration 450
    3.1 Timing of hydrocarbon generation and migration 451
  Bibliography 452
  Appendix 13.1 457

14. Chemical Composition of Asphaltene 459
  1.0 Introduction 459
  2.0 Solubility Characteristics and Precipitation of Asphaltenes 464
    2.1 Solubility parameters 465
      2.1.1 General solvency and chemistry 480
      2.1.2 Solubility—precipitation 482
      2.1.3 Fractionation effects in precipitation 486
    2.2 Precipitation procedures 487
      2.2.1 Volume ratio of precipitant to feedstock 487
      2.2.2 Contact time 489
      2.2.3 Temperature 490
      2.2.4 Pressure 492
      2.2.5 Exposure to oxygen and light 493
  3.0 Elemental Composition of Asphaltenes 493
    3.1 C, H, N, O and S 493
    3.2 Trace metals 495
  4.0 Experimental Probes into the Molecular Structure of Asphaltene 498
    4.1 Thermal degradation of asphaltenes 499
      4.1.1 Thermolysis of whole asphaltenes 500
      4.1.2 Thermolysis of extracted Athabasca asphaltene 507
      a) Saturate fraction of the product 508
        i) Alkanes 508
        ii) Alkylbenzenes 508
        iii) *n*-Alkylthiophenes 509

- b) Aromatic fraction of the product 509
  - i) Sulfides 510
  - ii) Benzo[b]thiophenes 512
  - iii) Dibenzothiophenes 513
  - iv) Fluorenes 515
  - v) Aromatics I and II 517
- c) Polar fraction of the product 520
- d) Product yields 522
- e) Flash pyrolysis with toluene-d_8 as the carrier 523

4.2 Reductive degradation of asphaltenes 523
- 4.2.1 Naphthalene radical anion reduction 523
- 4.2.2 Nickel boride reduction 525
  - a) Saturates from the NiB desulfurization 528
    - i) HMA saturates 528
      - 1. Alkanes 529
      - 2. Alkylcyclohexanes 531
      - 3. Tricyclic terpanes 532
      - 4. Steranes 532
      - 5. Hopanes 532
      - 6. Gammacerane 535
    - ii) LMA saturates 535
      - 1. *n*-Alkanes 535
      - 2. Bicyclic terpanes 535
      - 3. Tricyclic terpanes 536
      - 4. Steranes 536
      - 5. Hopanes 536
      - 6. Pristane/phytane 536
    - iii) Summary and conclusions from the NiB reduction experiments 538

4.3 Hydrolytic degradation of asphaltenes 539

4.4 Oxidative degradation of asphaltenes by ruthenium ions-catalyzed oxidation (RICO) 542
- 4.4.1 Low-MW products from Athabasca asphaltene 544
  - a) Alkyl side chains attached to aromatic carbon 544
  - b) Alkyl bridges connecting two aromatic units 552
  - c) Aromatic units 553
  - d) Other types of reactions occurring in RICO 555
- 4.4.2 High-MW products 557
  - a) Elemental composition 557
  - b) Pyrolytic fragments 559
- 4.4.3 Oxidative degradation of other Alberta asphaltenes 563
- 4.4.4 Foreign asphaltenes 567

5.0 Spectroscopic Probes Into the Molecular Structure of Asphaltene 575
- 5.1 Nuclear magnetic resonance spectroscopy 575
- 5.2 Fourier transform infrared spectroscopy 584
- 5.3 Ultraviolet–visible spectroscopy 585
- 5.4 Electron paramagnetic resonance (EPR) and electron nuclear double resonance (ENDOR) spectroscopy 592

5.4.1 The vanadyl porphyrin spectrum 593
5.4.2 The organic free radicals spectrum 594
5.4.3 The nature of the free radicals 602
a) Triaryl radicals 602
b) Perinaphthyl radicals 603
c) Radical ions 604
5.5 Magnetic susceptibility 605
5.6 Conductivity and dielectric properties 606
6.0 The covalent structure of the asphaltene molecule 606
6.1 Structural elements from thermolysis 607
6.1.1 *n*-Alkanes 608
6.1.2 Alkylbenzenes 609
6.1.3 Thiophenes 609
6.1.4 Sulfides 609
6.1.5 Condensed thiophenes 609
6.1.6 Condensed aromatics 610
6.1.7 Additional compounds 610
6.1.8 Combined yield 610
6.1.9 Pattern of substitution in alkylated cyclic compounds 610
6.2 Reductive degradation 611
6.3 Oxidative degradation 614
6.3.1 Bridges between ring structures 616
6.3.2 Additional products identified in RICO experiments 617
6.4 HO^- and BBr_3 cleavage of the C–O bonds 617
6.5 The nature of the remainder of the asphaltene core 618
6.6 The size of the polyaromatic sheets 620
6.7 The covalent MW of asphaltene 621
6.7.1 MW from chromatographic and chemical studies 622
6.7.2 MW distribution 629
6.7.3 MW from mass spectrometric studies 630
6.7.4 MW from molecular rotational correlation time–fluorescence depolarization (RCT–FDP) 632
6.8 The fifth compound class of petroleum 632
7.0 The origin of asphaltene 634
8.0 Micelles: to be or not to be? 637
Bibliography 652
Appendix 14.1 663
Appendix 14.2 664
Appendix 14.3 665
Appendix 14.4 Products and their yields from the RICO of various organic compounds 666
References 667
Appendix 14.5 668
Appendix 14.6 Elemental analysis of low-molecular-weight (LMA) and high-molecular-weight (HMA) Athabasca asphaltenes and their RICO products 669
Appendix 14.7 670
Appendix 14.8 672
Appendix 14.9 673

Epilogue 675
Subject Index 679
Chemical Index 689

Introduction

The 20th century has been termed as the century of oil and it has been generally recognized that fossil fuels—coal, petroleum and natural gas, in order of historical importance—provided the material foundation for the emergence of a modern technological society. With Man's recently acquired ability to exploit fossil fuel resources, he could create conditions whereby human life could transcend the subsistence level for the first time in history.[1] As a result, world population has nearly quadrupled since the beginning of the century, Figure 1, while world oil consumption increased by a factor of 20 or more. Figure 1 was prepared in 1993 and values between 1992 and 2000 are computed projections. Figure 2 shows de facto world oil production through the year 2000 and future projection values[2] to the year 2000. The plots in Figure 2 predict that the peak year for world oil production will be between 2004 and 2008. This estimate is based on the method developed in the 1950s by M.K. Hubbert and is currently considered to be inadequate. Since then more sophisticated assessment methods have been developed.[3] Predicting the future has never been for the faint-hearted and the assessment of undiscovered petroleum resources is no exception. Details as to why this is so are found in the book by L.J. Drew[4] and in reference 3.

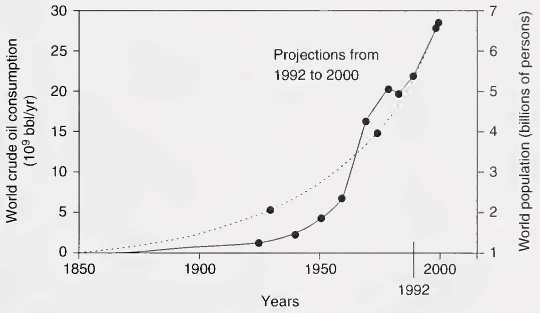

Figure 1. World oil consumption and population growth (1925–2000). Solid curve shows projected world crude oil consumption; dotted curve, projected world population. From H.L. Townes, Ref. 1. © 1993, American Association of Petroleum Geologists.

Since World War II petroleum has gradually displaced coal as the most abundantly used source of fuel, Figure 3. More recently natural gas has been gaining prominence as a principal source of energy worldwide and, in the United States, energy production in 1993 in the form of methane plus natural gas liquids exceeded that of oil or coal.

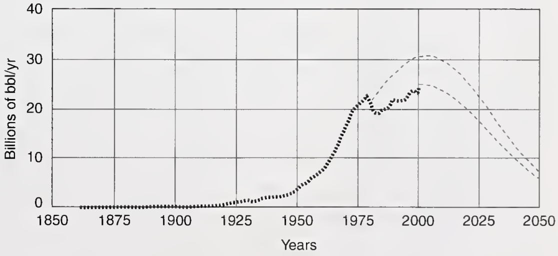

Figure 2. World oil production through the year 2000 is shown as heavy dots. The dashed lines on the right show the probable production rates if the ultimate discoverable oil is 1.8 trillion barrels (the area under the lower curve) or 2.1 trillion barrels (upper curve). From K.S. Deffeyes, Ref. 2. © 2001, Princeton University Press.

In view of the vast quantities of methane known to exist in the form of gas hydrates, coal gas and natural gas the use of natural gas is predicted to hugely increase in this century and the

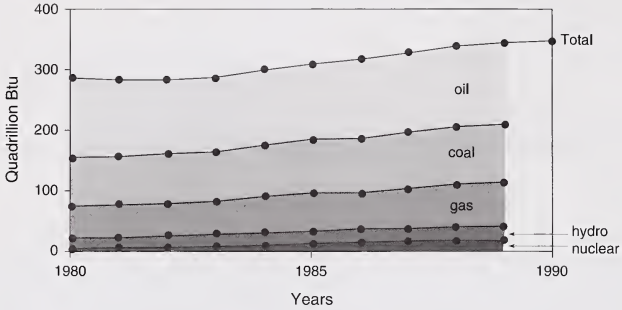

Figure 3. Cumulative worldwide energy consumption by type. From H.L. Townes, Ref. 1. © 1993, American Association of Petroleum Geologists.

21st century is being called the century of natural gas by some. Currently, petroleum provides over 90% of all transportation fuels and lubricants, and about 4% of petroleum and natural gas is used as feedstocks[5] for the manufacture of chemicals, pharmaceuticals, plastics, elastomers, paints and a host of other products we are so used to in our daily lives, Figure 4. In fact, the total value of the consumer products manufactured from crude oil, Figures 5 and 6, exceeds that of the crude itself by a factor of 10–20. Thus, petrochemicals provide a great many of the necessities of modern life and their consumption is still growing at an annual rate of about 10%. Advances in the petroleum–hydrocarbon industry are probably the most important single factor responsible for the standard of living we enjoyed in the late 20th century.[5]

Naturally, petroleum and fossil fuel resources are limited. In the United States, for example, declining domestic crude oil production fell below crude oil imports for the first time in 1994. From a historical perspective the age of petroleum and fossil fuels will be only a short "blip" in man's energy supply, "Hubbert's Peak" Figure 7, extending over a few centuries only. Proven world reserves of conventional crude oils are variously estimated to be around the 1.0, 1.8, 2.1 trillion barrel levels.[2,6] Understandably, in view of the many ill-defined, unknown, unforeseeable input parameters required, precise estimates are difficult to make and all estimates are conjectural and subject to considerable uncertainties. Indeed, it has been pointed out that because of the recent inventions of new technologies for extracting oil from beneath the deep oceans, ten of the world's largest oil companies active in research in this area have discovered new fields that will add five percent to their combined oil reserves, an increase not yet reflected in the earlier global estimates.[7] Estimates of worldwide ultimately recoverable oil resources have fluctuated between 850 and 4,000 billion barrels over the past quarter century, but the most probable value lies around the 1.8–3.0 trillion barrel mark. A more recent (1999–2000) estimate by the U.S. Geological Survey (USGS)–International Energy Agency[8] places the mean world undiscovered conventional resources at 724 billion barrels. This would place the peak in world oil production at about the year 2017. The 2000 world consumption was estimated by various authors to be 23 and 27 billion barrels per year and the discovery rate was around 6 billion barrels per year. Projected world oil demand into the next decade, Figure 8, predicts steady increases which, according to one of the many existing projections would lead to world production rates peaking around 2012 followed by a rapid drop owing to resource depletions, Figure 9. There are several other suggested dates for peak production rates but with some notable exceptions *e.g. cf.* Figure 2 they all lie in the narrow 2010–2020 range.

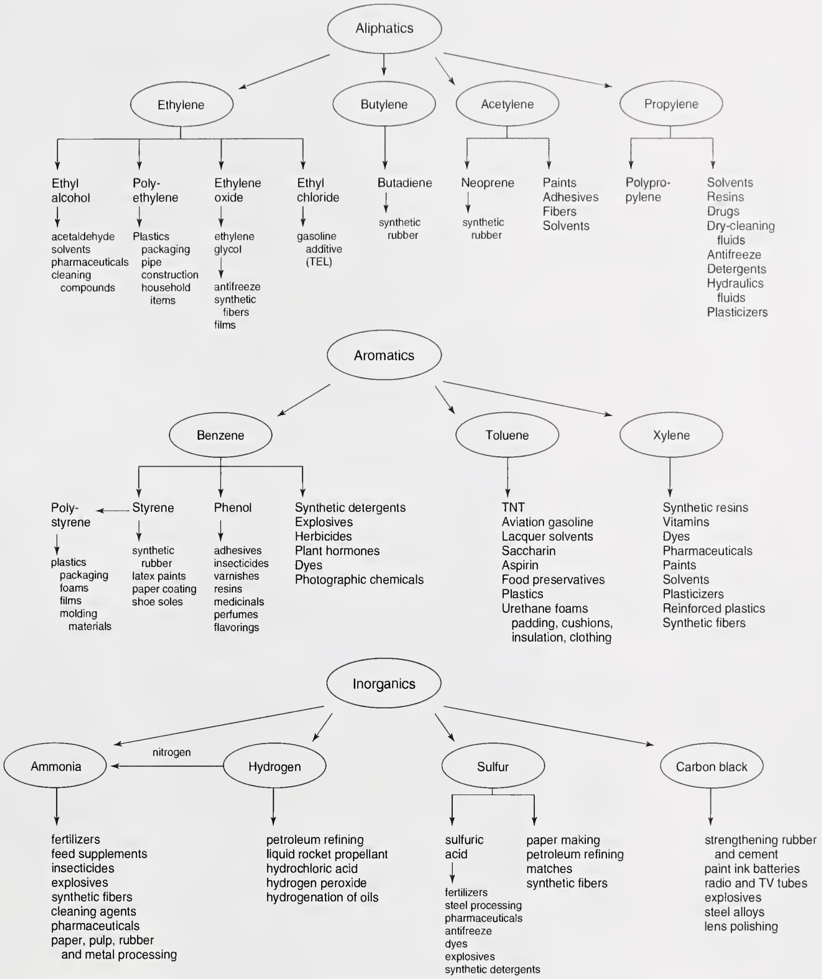
Aliphatics
Ethylene
Butylene
Acetylene
Propylene
Ethyl alcohol
acetaldehyde
solvents
pharmaceuticals
cleaning compounds
Poly-ethylene
Plastics
packaging
pipe
construction
household items
Ethylene oxide
ethylene glycol
antifreeze
synthetic fibers
films
Ethyl chloride
gasoline additive (TEL)
Butadiene
synthetic rubber
Neoprene
synthetic rubber
Paints
Adhesives
Fibers
Solvents
Polypro-pylene
Solvents
Resins
Drugs
Dry-cleaning fluids
Antifreeze
Detergents
Hydraulics fluids
Plasticizers
Aromatics
Benzene
Toluene
Xylene
Poly-styrene
plastics
packaging
foams
films
molding materials
Styrene
synthetic rubber
latex paints
paper coating
shoe soles
Phenol
adhesives
insecticides
varnishes
resins
medicinals
perfumes
flavorings
Synthetic detergents
Explosives
Herbicides
Plant hormones
Dyes
Photographic chemicals
TNT
Aviation gasoline
Lacquer solvents
Saccharin
Aspirin
Food preservatives
Plastics
Urethane foams
padding, cushions, insulation, clothing
Synthetic resins
Vitamins
Dyes
Pharmaceuticals
Paints
Solvents
Plasticizers
Reinforced plastics
Synthetic fibers
Inorganics
Ammonia
nitrogen
Hydrogen
Sulfur
Carbon black
fertilizers
feed supplements
insecticides
explosives
synthetic fibers
cleaning agents
pharmaceuticals
paper, pulp, rubber and metal processing
petroleum refining
liquid rocket propellant
hydrochloric acid
hydrogen peroxide
hydrogenation of oils
sulfuric acid
fertilizers
steel processing
pharmaceuticals
antifreeze
dyes
explosives
synthetic detergents
paper making
petroleum refining
matches
synthetic fibers
strengthening rubber and cement
paint ink batteries
radio and TV tubes
explosives
steel alloys
lens polishing

Figure 4. The petrochemical family tree. After B.D. Berger and K.E. Anderson, Ref. 5.

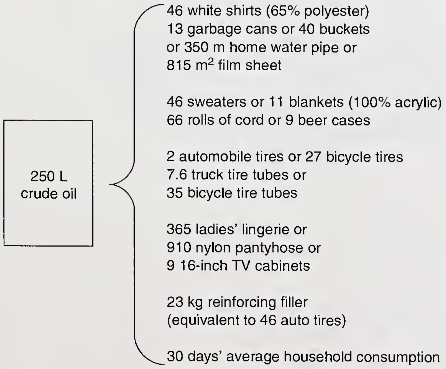
250 L crude oil
46 white shirts (65% polyester)
13 garbage cans or 40 buckets or 350 m home water pipe or 815 m² film sheet
46 sweaters or 11 blankets (100% acrylic)
66 rolls of cord or 9 beer cases
2 automobile tires or 27 bicycle tires
7.6 truck tire tubes or 35 bicycle tire tubes
365 ladies' lingerie or 910 nylon pantyhose or 9 16-inch TV cabinets
23 kg reinforcing filler (equivalent to 46 auto tires)
30 days' average household consumption

Figure 5. Products derived from 250-L crude oil. After B.D. Berger and K.E. Anderson, Ref. 5.

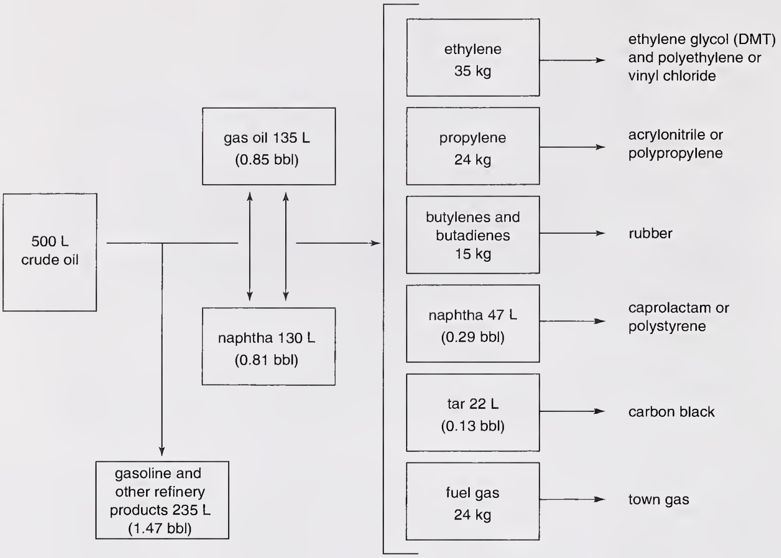
500 L
crude oil
gas oil 135 L
(0.85 bbl)
naphtha 130 L
(0.81 bbl)
gasoline and
other refinery
products 235 L
(1.47 bbl)
ethylene
35 kg
propylene
24 kg
butylenes and
butadienes
15 kg
naphtha 47 L
(0.29 bbl)
tar 22 L
(0.13 bbl)
fuel gas
24 kg
ethylene glycol (DMT)
and polyethylene or
vinyl chloride
acrylonitrile or
polypropylene
rubber
caprolactam or
polystyrene
carbon black
town gas

Figure 6. Products derived from 500-L (~3 bbl) crude oil. After B.D. Berger and K.E. Anderson, Ref. 5.

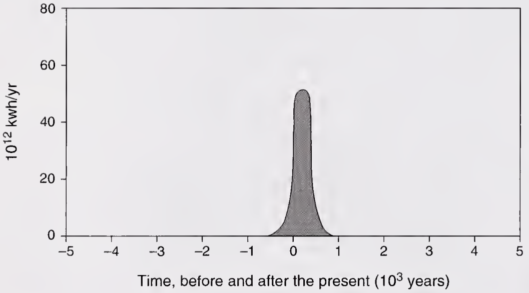

Figure 7. Epoch of exploitation of fossil fuels in historical perspective. From H.L. Townes, Ref. 1. © 1993, American Association of Petroleum Geologists.

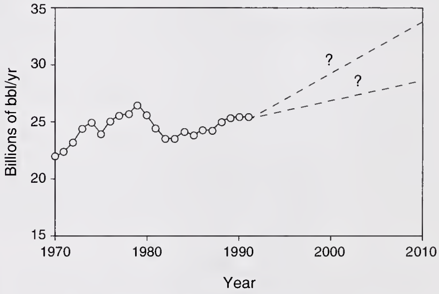

Figure 8. World oil demand (1970–1992) and range of estimates (1992–2010). From H.L. Townes, Ref.1. © 1993, American Association of Petroleum Geologists.

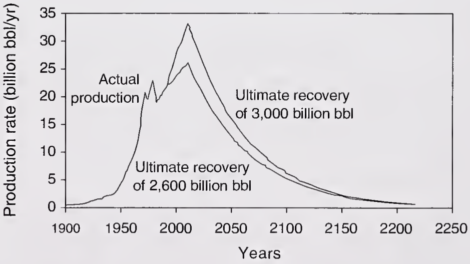

Figure 9. Possible cycles of world crude oil production. From H.L. Townes, Ref. 1. © 1993, American Association of Petroleum Geologists.

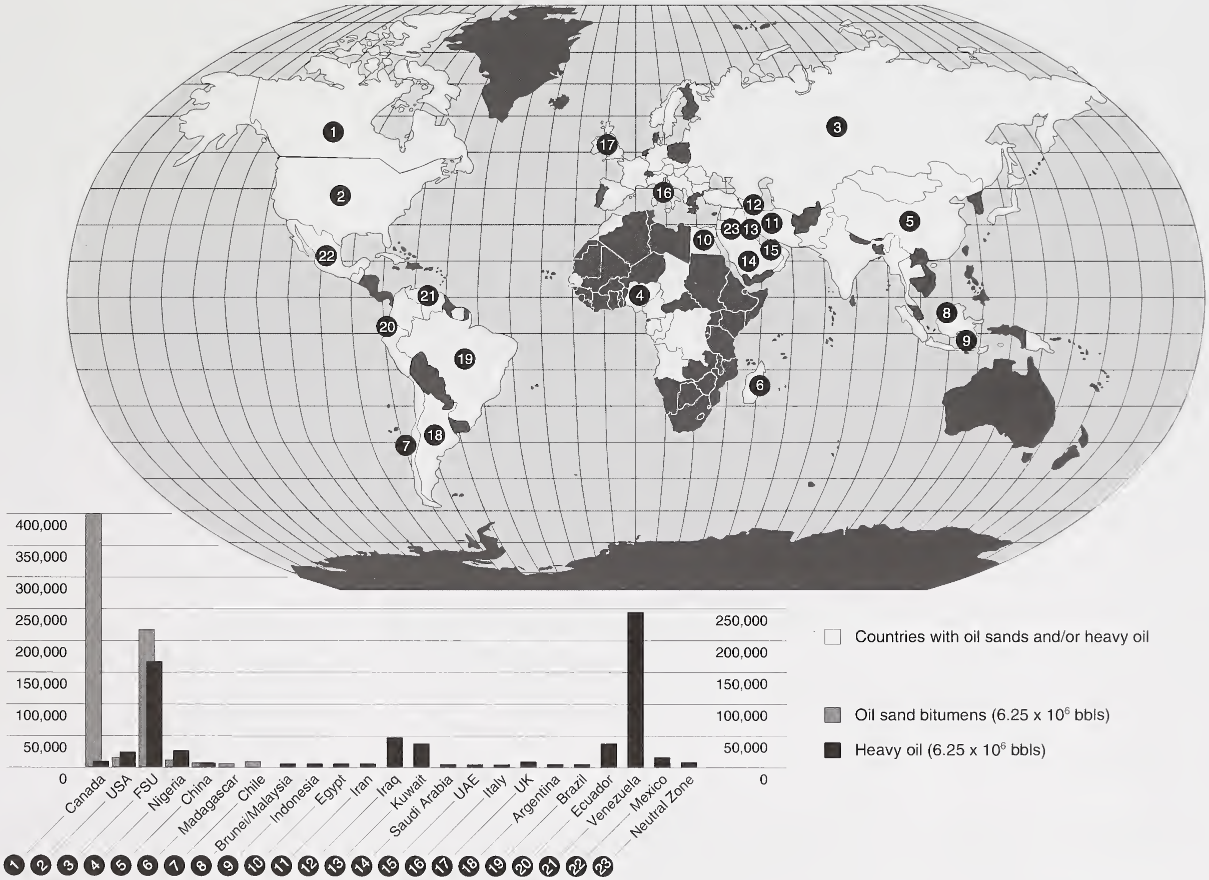
1
2
3
4
5
6
7
8
9
10
11
12
13
14
15
16
17
18
19
20
21
22
23
400,000
350,000
300,000
250,000
200,000
150,000
100,000
50,000
0
Canada
USA
FSU
Nigeria
China
Madagascar
Chile
Brunei/Malaysia
Indonesia
Egypt
Iran
Iraq
Kuwait
Saudi Arabia
UAE
Italy
UK
Argentina
Brazil
Ecuador
Venezuela
Mexico
Neutral Zone
250,000
200,000
150,000
100,000
50,000
0
Countries with oil sands and/or heavy oil
Oil sand bitumens (6.25 x 10^6 bbls)
Heavy oil (6.25 x 10^6 bbls)

Figure 10. Heavy oil and oil sands resources around the world. Source: Alberta Oil Sands Technology and Research Authority.

One of the studies representing a more optimistic view is the recently-released fifth assessment of the USGS.[9] It includes a newly-analyzed category—oil lurking in and around fields—and an expanded effort employing, for the first time, a closely-documented, uniform approach to evaluating potential deposits.[10] The study raises the estimates of world-wide existing field reserves to 612 billion barrels and of oil yet to be discovered to 732 billion barrels. It also pushes the time for peak world oil production beyond 2025.

World heavy oil and bitumen resources (about 7 trillion barrels), Figure 10, exceed the resources of conventional oils and will become the principal source of crude oils in the early decades of the 21st century. Alberta, with an estimated resource of 2.5 trillion barrels or according to a more recent estimate,[11] 1.7 trillion barrels of bitumens, occupies a prominent position in the world resources, followed by Venezuela and Russia. An additional potential source of synthetic crude oil is natural gas. With further improvements in conversion technologies, natural gas has been estimated as being capable of supplying 500 billion barrels of synthetic crude oil.[12]

Recognizing the economic potential of the bitumen and heavy oil deposits of Alberta, the Governments of Canada and Alberta, in cooperation with industry and Alberta universities, initiated long-term research and development policies and committed considerable resources to their implementation. In the last quarter century these initiatives, along with the research and development efforts of the two large oil sand plants,[13] Suncor and Syncrude, operating in the Athabasca deposit near Fort McMurray, Alberta, have resulted in tremendous forward strides in the technologies of bitumen and enhanced oil recovery, as well as bitumen upgrading. The Suncor and the larger Syncrude plant, which produce an average of about 225,000 and 250,000 barrels/day of high-quality, light, sweet synthetic crude oil (at a 2000 operating cost of around Cdn.$12/barrel), together supply over 20% of Canada's 2000 crude oil consumption. Both plants are being expanded and by 2008 and 2007 will nearly double their production capacity to over 400,000 and 460,000 barrels/day at a significantly reduced per barrel cost. The Syncrude plant produced its billionth barrel of synthetic crude oil in May, 1998. In addition, the Lloydminster heavy oil upgrader is planning to gradually increase production from 55,000 barrels/day to 80,000 barrels/day, and the recovery of bitumen by various in-situ technologies is also on the continuous rise. Beyond the expansion of existing recovery and upgrading facilities many new ones are currently under construction or in the planning stage. Undoubtedly, the time of oil sands has arrived!

In addition to the short- and long-term engineering programs aimed at improving existing processes and developing new technologies for the economic exploitation of bitumen and heavy oil deposits, high priority has been placed on basic research in order to generate fundamental data and in-depth knowledge of these resources. Much of the chemical knowledge on Alberta bitumens summarized in this monograph was generated as part of the intense research supported during the last 25 years by the Natural Science and Engineering Research Council of Canada, the Alberta Oil Sands Technology and Research Authority, and the Canada–Alberta Energy Resources Research Fund.

Most pooled bitumens (tars)—viscous, heavy petroleums with viscosities greater than 10 Pa·s and gravities less than 10°API—are found in sandstone reservoir rocks of various degrees of consolidation and, in Alberta, also in carbonate rocks. They are known to have originated from the microbiological degradation of conventional petroleum and were further altered by related water washing and oxidation processes. In terms of the major compound complements of petroleum, the paraffinic hydrocarbons, naphthenic hydrocarbons, aromatic hydrocarbons, resin and asphaltene fractions, bitumens belong to the naphthenic–aromatic class of petroleums and represent exceedingly complex mixtures of hydrocarbons and hydrocarbon-derived organic molecules with a trace contribution from inorganic constituents. The recovery and upgrading of bitumen requires different, more complex and somewhat costlier technologies and methods than those required for conventional crude oil. The challenge in bitumen chemistry then lies not only in elucidating the origin, history and current status of bitumen deposits, but also in bringing about the understanding of the properties and reactivity of bitumen with regard to the development of new, more competitive and environmentally acceptable technologies for its utilization.

Bibliography

1. H.L. Townes, "The Hydrocarbon Era, World Population Growth and Oil Use—A Continuing Geological Challenge", Am. Assoc. Petrol. Geol. Bull., 77 (1993) 723.
2. K.S. Deffeyes, *Hubbert's Peak*, Princeton University Press, Princeton, NJ, 2001.
3. R.R. Charpentier, "Locating the Summit of the Oil Peak", Science, 295 (2002) 1470.
4. L.J. Drew, *Undiscovered Petroleum and Mineral Resources: Assessment and Controversy*, Plenum Press, New York, N.Y., 1997; S. Collins, American Scientist, 86 (1998) 191 .
5. B.D. Berger and K.E. Anderson, *Modern Petroleum*, Third Edition, PennWell Publishing Co., Tulsa, OK, 1992.
6. C.J. Campbell and J.H. Laharrère, "The End of Cheap Oil", Scientific American, 278 (1998) 78.
7. R. Anderson, "Oil Production in the 21st Century", Scientific American Press,New York, N.Y., 278 (1998) 86.
8. http://energy.cr.usgs.gov/energy/worldenergy.html#top.
9. Greenwood.cr.usgs.gov/energy/worldenergy/DDS-60.
10. R.A. Kerr, "USGS Optimistic on World Oil Prospect", Science, 289 (2000) 237.
11. Alberta Energy and Utilities Board, 1999.
12. S.A. Fouda, "Liquid Fuels from Natural Gas", Scientific American, 278 (1998) 92.
13. R.L. George, "Mining for Oil", Scientific American, 278 (1998) 84.

1

The Origin of Petroleum

According to accepted theory, petroleum, along with other forms of sedimentary organic matter (coal, natural gas, kerogen), originated from the organic debris of formerly living organisms which obtained their chemical energy from solar radiation *via* the photosynthetic process. A fractional amount of the organic debris was deposited and preserved in sediments. In subsequent geological developments, part of the sedimentary organic matter was converted to petroleum-like substances.

Photosynthesis is the quintessential route to the production of organic carbon on earth. The source of the carbon is atmospheric CO_2 which, in the green parts of plants and in some bacteria, is converted to sugar by the photocatalyst chlorophyll upon the action of light:

$$6\,CO_2 + 12\,H_2O^{*} \xrightarrow[\text{chlorophyll}]{h\nu} \underset{\text{glucose}}{C_6H_{12}O_6} + 6\,\overset{*}{O}_2 + 6\,H_2O \tag{1}$$

The carbon accumulated in the vast amount of sedimentary organic matter was thus absorbed from the atmosphere *via* the photosynthetic process. A byproduct of photosynthesis is molecular oxygen which is emitted into the atmosphere; in effect, the bulk of the oxygen in the atmosphere originated from water *via* the photocatalytic reaction 1. The evolution of the present-day atmosphere and the evolution of life on earth were therefore interrelated and interdependent processes.

The theory of an inorganic origin for petroleum developed in the 19th century by Mendeleyev (1877) and others[1] has now been reduced to a historical curiosity under the weight of a mountain of irrefutable evidence in favor of a biological origin. Nevertheless, occasional attempts at its revival have been made, even as late as in the 1990s.[2] These attempts have shown, if anything, that the theory of an inorganic origin for petroleum is far removed from reality.

The organic origin of petroleum was proposed by Engler[3] (1888) a decade after Mendeleyev published his inorganic hypothesis and the debate was resolved only about a half century later by the seminal discoveries of Treibs[4] (1934). Treibs found that most petroleums exhibit optical activity and also discovered the presence of porphyrins in petroleums and coals. He recognized that the porphyrins must have been the diagenetic transformation products of chlorophyll. Both optical activity and chlorophyll are the fingerprints of life processes, providing evidence for a biological source material. Porphyrins were the heralds of many series of organic molecules—termed biological markers or biomarkers—that have since been discovered in sedimentary organic matter. Biomarkers are ancient molecules (molecular fossils) which were formed by the mild transformation of biological molecules originally synthesized by living organisms in the past, geological epochs and eras ago, and survived until the present without losing the hallmarks of their biological origin. Their chemistry provides a pillar for the foundation of the scientific theory of the origin of petroleum and is an invaluable aid to the elucidation of the chemical composition of petroleum.

The glucose product in Equation 1 is a monomeric form of sugar which, on polymerization, converts to polysaccharides, the fundamental form of photosynthesized organic matter stored in living cells. Polysaccharides represent stored chemical energy and provide the starting material for the production of organic compounds in all subsequent biosynthetic reactions.

Organisms that derive energy for the synthesis of organic carbon from light—the phototrophs—are restricted to the land and euphotic zones (zones of sunlight penetration down to a depth of 50 m in clear water) in lakes and oceans. The most important photosensitizers in aquatic environments are phototrophic microorganisms and on land, the higher plants. Their relative importance has varied over geological times. Until the Middle Devonian period (375 million years ago), when land plants made their widespread appearance, marine phytoplanktonic organisms, bacteria and blue-green algae were the dominant source of organic carbon. Even today marine phytoplanktons and bacteria account for over 40% of worldwide organic carbon production. Differences between aquatic and land phototrophs determine differences in the nature of the organic matter deposited in sediments from these environments.

Chlorophyll is the universal photosynthetic pigment which is responsible for the green color of plants; it is also found in most algae and cyanobacteria in slightly different forms. It acts in conjunction with other, auxiliary photopigments, including phycoerythrin, carotenoid compounds, quinones, iron-sulfur proteins; ferredoxin; *etc.*, in the chloroplast. Somewhat altered derivatives of chlorophyll, carotenoids and other, analogous compounds that were synthesized by photosynthetic organisms whose dead bodies became incorporated into the sediments and later gave rise to the formation of petroleum, can still be found in petroleum today. Their existence in fossil sediments proves that chlorophyll and the auxiliary photosynthetic pigments, together with the essential mechanisms of the energy pooling and photosynthetic steps, have not changed since the times of the precursor organisms. Moreover, knowledge of the chemistry of these biological markers occurring in petroleum and other sedimentary organic matter and their relationship with present-day photosynthetic organisms has given important insights into the origin of petroleum and the chemical changes which the biotic source materials have undergone.

The structures of chlorophylls and their geological transformation products, the porphyrins, will be discussed in some detail in Chapter 13.

Photosynthesis in aquatic environments is made possible by the high solubility of CO_2 in water (30 times that of oxygen) and the accumulation of dissolved carbon owing to the chemical reaction between CO_2 and water to form bicarbonate and carbonate ions which are much more soluble than CO_2 itself:

$$CO_2 + H_2O \rightleftharpoons H_2CO_3 \tag{2}$$

$$H_2CO_3 \rightleftharpoons HCO_3^- + H^+ \tag{3}$$

$$HCO_3^- \rightleftharpoons CO_3^{2-} + H^+. \tag{4}$$

Indeed, some 98.5% of the carbon in the ocean–atmosphere inventory today is found in the ocean.

Marine photosynthesis in the euphotic zone today is not limited by the availability of light or carbon dioxide. To cope with a low carbon dioxide level, phytoplanktons appear to have developed a mechanism, which may involve the enzyme carbonic anhydrase, to convert the bicarbonate ion to carbon dioxide. The limiting factor has been suggested to be the availability of micronutrients and, in particular, iron, which is required for photosynthetic electron transport and for the synthesis of chlorophylls; iron is also needed since it is a cofactor of the enzymes that reduce nitrates dissolved in seawater to a form that can be used in the synthesis of organic matter.

Oxygen gas produced in photosynthesis is discharged from the ocean into the atmosphere.

The ultimate fate of photosynthetically fixed, reduced carbon in various organisms that utilize fermentation or respiration to produce energy, and in abiogenic oxidation, is oxidation back to carbon dioxide. A tiny fraction of the organic carbon, of the order 0.01–0.1%, enters the sediment and escapes oxidation. The total amount of organic carbon and metaanthracite (which formerly represented sedimentary organic carbon) present in the earth's crust has been estimated to be about 15.6×10^{15} t, Table 1.1. About 99.99% of this is present in sediments and only about 0.01% in living organisms and the atmosphere. The process comprising the oxidation of organic carbon and the fixation of carbon dioxide as organic carbon is called the primary carbon cycle,[5] illustrated in Figure 1.1. The primary carbon cycle has an estimated turnover of about 4.6×10^{12} t of organic carbon with a half-life of a month to tens of years. The larger, secondary geocycle with an estimated quantity of carbon of 15.6×10^{15} t and with a half-life of 3.42×10^{8} years, represents organic matter accumulated over geologic times in the lithosphere. The two carbon cycles are interconnected with a small window of leakage corresponding to less than one ppm of the total organic carbon, representing the oxidation of sedimentary organic matter to carbon dioxide and the reverse process, the incorporation of organic matter into the sediment. The long-term fate of organic matter in the sediment is then mainly governed by tectonic events.[6] Phases of subsidence and increase in burial, and phases of uplift and erosion determine whether the organic matter of a sediment is preserved and transformed into petroleum, or eroded and oxidized. If, during the evolutionary history of a geosyncline, the organic matter completes the second cycle, it undergoes increasing burial accompanied by profound biological, chemical and physical alterations during the broad stages which have been termed, after Tissot and Welte,[6] diagenesis, catagenesis and finally metagenesis.

Table 1.1 Carbon reservoirs: amounts and residence times[a]

Reservoirs	Amount, t C	Residence time, years
Sedimentary carbonate C	62.4×10^{15}	3.42×10^{8}
Sedimentary organic C	15.6×10^{15}	3.42×10^{8}
Oceanic inorganic C	4.2×10^{13}	3.85×10^{2}
Necrotic C	4.0×10^{12}	20–40
Atmospheric CO_2	7.2×10^{11}	4
Living terrestrial biomass	5.6×10^{11}	16
Living marine biomass	7.0×10^{9}	0.1
Other carbon cycle parameters		**Estimated value**
Terrestrial net productivity		4.8×10^{10} t C·year^{-1}
Marine net productivity		3.5×10^{10} t C·year^{-1}
Burial of organic C in marine sediments		1.3×10^{8} t C·year^{-1}

[a] After R.E. Summons, "Biochemical Cycles, A Review of Fundamental Aspects of Organic Matter Formation, Preservation and Composition", in *Organic Geochemistry*, M.H. Engel and S.A. Macko, Eds., Plenum Press, New York, N.Y., 1993, p. 8.

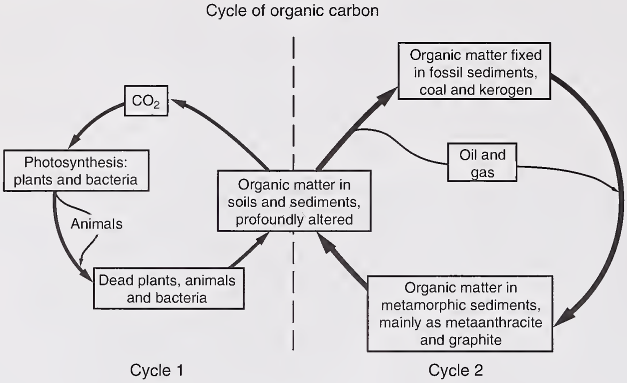
Cycle of organic carbon
CO2
Photosynthesis: plants and bacteria
Animals
Dead plants, animals and bacteria
Organic matter in soils and sediments, profoundly altered
Organic matter fixed in fossil sediments, coal and kerogen
Oil and gas
Organic matter in metamorphic sediments, mainly as metaanthracite and graphite
Cycle 1
Cycle 2

Figure 1.1 The two major cycles of organic carbon on earth. Organic carbon is mainly recycled in cycle 1. The crossover from cycle 1 to cycle 2 is a tiny leak that amounts to only 0.01–0.1% of the primary organic productivity. From D.H. Welte, Ref. 5. © 1970, Springer-Verlag.

1.0 Genesis of Petroleum

In the early stages of the chemical evolution of subaquatic sedimentary organic matter where minerals, water, dead organic matter and living microorganisms are present, thermal or pressure effects are mild and the major alterations are caused first by aerobic, and then, when the oxygen supply is exhausted, by anaerobic microorganisms. Here proteins, carbohydrates, lignins and the other biopolymers are destroyed and their constituents reassembled in new geomacromolecules, the precursors to kerogen. This process, through which the sediment normally becomes consolidated and the humic matter is converted to kerogen, is known as diagenesis, Figure 1.2. The end of diagenesis is at a vitrinite reflectance, R_o, of ~0.50. Extensive sulfur incorporation into sediments in confined environments with H_2S-saturated bottom water (produced from sulfate ions by sulfur-reducing bacteria) may result in the formation of organosulfur compounds during late diagenesis, leading to the production of a sulfur-rich petroleum like the precursor oil of the Alberta oil sand bitumens.

Among the various factors that determine the quantity and quality of organic matter preserved during diagenesis and burial of a sediment are organic productivity, oxygen contents of the water column and sediments (**oxic:** ≥ 2.0 mL $O_2 \cdot L^{-1}$ water; **anoxic:** < 0.1 mL $O_2 \cdot L^{-1}$ water; **eunoxic**: marine, anoxic with free H_2S), water circulation and sedimentation rate. The precise roles of these factors are still being argued.

With increasing depth of burial the temperature rises from ~50 to ~150°C and so does the geostatic pressure, from ~300 to ~1000–1500 bars, causing the decomposition of kerogen—first producing liquid petroleum then, in later stages, wet gas and condensate. This is the process of catagenesis. The end of catagenesis is around a vitrinite reflectance, R_o, of about 2.0, which is the beginning of the anthracite rank of coal.

At higher temperatures and pressures, petroleum formation ceases and organic matter exists as methane gas and a carbon residue. This is the stage of metagenesis, of which the more severe form is called metamorphism.

Kerogen is the immediate precursor of crude oil and is defined as the organic constituent of sedimentary rocks that are insoluble in aqueous alkaline solutions or in organic solvents.

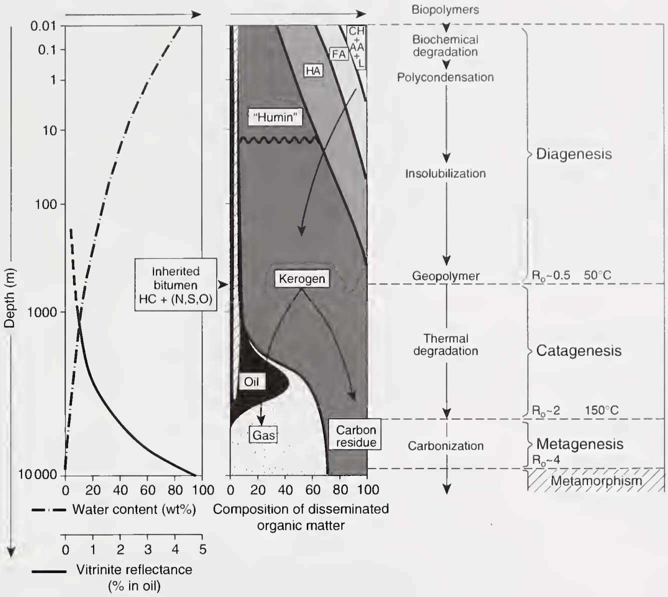
Depth (m)
0.01
0.1
1
10
100
1000
10 000
0 20 40 60 80 100
Water content (wt%)
0 1 2 3 4 5
Vitrinite reflectance (% in oil)
Inherited bitumen HC + (N,S,O)
CH + AA + L
FA
HA
"Humin"
Kerogen
Oil
Gas
Carbon residue
0 20 40 60 80 100
Composition of disseminated organic matter
Biopolymers
Biochemical degradation
Polycondensation
Insolubilization
Geopolymer
Thermal degradation
Carbonization
Diagenesis
R₀~0.5 50°C
Catagenesis
R₀~2 150°C
Metagenesis
R₀~4
Metamorphism

Figure 1.2 General scheme for the evolution of organic matter from the freshly deposited sediment to the metamorphic zone. CH = carbohydrates; AA = amino acids; FA = fulvic acids; HA = humic acids; L = lipids; HC = hydrocarbons; N, S, O = nitrogen, sulfur, and oxygen compounds. From B.P. Tissot and D.H. Welte, Ref. 6. © 1984, Springer-Verlag.

Kerogen is a yellow to dark brown solid containing a variety of organic debris called macerals and reconstituted degradation products of organic matter. Kerogen may also contain recognizable biomacromolecules (proteins, cellulose, tannins).

Of the macerals, which are recognizable remains of different types of organic matter, consisting of individual organic particles such as spores, pollens, plant tissues and algae (phytoclasts), three principal groups are distinguished:

- liptinites: Oil-prone, low-reflectance macerals containing phytoclasts such as algae, resins, spores.
- vitrinites: Gas-prone macerals, believed to originate from terrestrial plants, the reflectance (R_o) of which is used as an indicator for the thermal maturity of rock samples. They show intermediate reflectance.
- inertinites: Inert macerals showing high reflectance.

Kerogens are characterized according to their ability to produce oil on pyrolysis and the quality of the produced oil or, alternatively, according to their $(H/C)_{a(\text{atomic})}$ relative to their $(O/C)_a$ ratios (van Krevelen diagram). Customarily, four types of kerogens are distinguished:

Type I:	High $(H/C)_a$ (~1.5) and low $(O/C)_a$ (< 0.1) ratios; dominated by liptinite macerals and aliphatic structures, suggesting major contributions from lipids.
Type II:	Slightly lower $(H/C)_a$ (~1.2–1.5) than Type I, low $(O/C)_a$, dominated by liptinite macerals. Sulfur is higher than in other types and may reach 14%. They appear to generate oil at lower thermal exposures than other types and are believed to have originated from mixed phytoplankton, zooplankton and bacterial debris in marine sediments.

Type III:	The $(H/C)_a$ ratios are lower (< 1.0) than in Types I or II, and the $(O/C)_a$ ratios are high, up to 0.3. This type of kerogen is usually derived from terrestrial plants and is dominated by vitrinite macerals.
Type IV:	"Dead carbon" having $(H/C)_a$ ~0.5–0.6 and low to high $(O/C)_a$, up to ~0.3. This type of kerogen does not generate significant amounts of hydrocarbons.

It is noteworthy that kerogen is widely distributed in sedimentary rocks and that it represents the most abundant form of organic carbon on earth. Kerogen has been estimated to be 1000 times more abundant than coal plus reservoired petroleum and about 50 times more abundant than bitumen and other dispersed petroleum in nonreservoir rocks.

Kerogen is generally associated with small quantities of bitumen. This source rock bitumen is a different type of material from the pooled bitumen formed from liquid petroleum *via* microbial degradation, like the oil sand bitumens of Alberta, and the two types of bitumen should be clearly differentiated.

To conclude this section, a generalized scheme for the evolution of sedimentary organic matter leading to petroleum formation is shown in Figure 1.3.

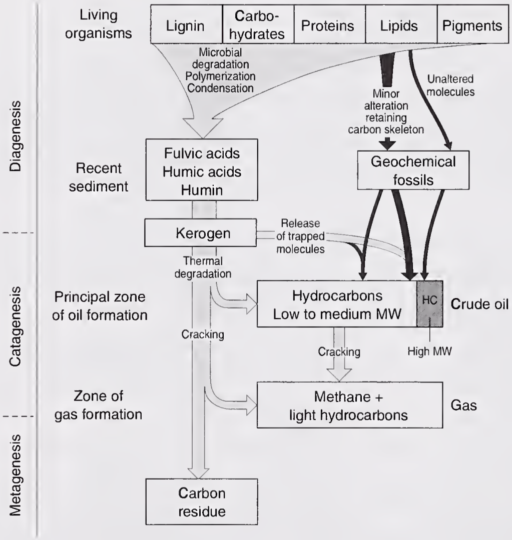
Diagenesis
Catagenesis
Metagenesis
Living organisms
Lignin
Carbo-hydrates
Proteins
Lipids
Pigments
Microbial degradation Polymerization Condensation
Minor alteration retaining carbon skeleton
Unaltered molecules
Recent sediment
Fulvic acids Humic acids Humin
Geochemical fossils
Kerogen
Release of trapped molecules
Thermal degradation
Principal zone of oil formation
Hydrocarbons Low to medium MW
HC
Crude oil
Cracking
Cracking
High MW
Zone of gas formation
Methane + light hydrocarbons
Gas
Carbon residue

Figure 1.3 Generalized scheme for the evolution of sedimentary organic matter and sources of hydrocarbons in geological situations. Geochemical fossils represent a first source of hydrocarbons in the subsurface (black solid arrows). Degradation of kerogen represents a second source of hydrocarbons (gray dotted arrows). From B.P. Tissot and D.H. Welte, Ref. 6. © 1984, Springer-Verlag.

2.0 Migration and Accumulation of Oil

Kerogen, the immediate source of crude oil, is found in abundance, but it produces significant quantities of liquid petroleum only in fine-grained sedimentary rocks. The release of liquid petroleum from the solid kerogen and its transport within and through the capillaries and narrow pores of a fine-grained source rock are defined as primary migration. The oil extruded from a source bed passes through more coarse structures and more permeable porous rock units in its secondary migration before being trapped by an impermeable barrier in the reservoir rock, forming an oil and gas accumulation. The migration of the oil takes place in the presence of the aqueous pore fluid. The movement may be due to active water flow or may take place independently of the aqueous phase, either by displacement or by diffusion as a single phase or a multiphase fluid system. Oil and gas, being lighter than saline pore waters, accumulate in structural heights, such as an anticline sealed by an impermeable caprock, known as a structural trap. Although a number of different mechanisms may be operative under specific conditions, the paramount, most effective form of primary migration which is consistent with empirical geological and geochemical data is considered to be a hydrocarbon-phase migration. Water flow is not needed as a driving force for migration.

In the secondary migration of oil and gas, buoyancy in water-saturated porous rocks is the only driving force when the aqueous pore fluids in the subsurface are stationary. If there is water flow in the subsurface, the buoyant rise of oil and gas may be modified by the water flow. The third controlling parameter is capillary pressure in the narrow rock pores causing the entrapment of the oil.

Thus, the driving forces and mechanisms of primary and secondary migrations are different and so are the effective distances covered, being meters or tens of meters in primary migration, and ten to hundreds of kilometers in secondary migration.

3.0 Chemical Alteration of Oil During Migration

Comparative studies on the chemical composition of source bitumen and the crude oil generated from the source bitumen show that the oil is lighter and it contains more hydrocarbons and fewer polar and high-molecular-weight (MW) components. This is illustrated by the class compositional data on two sets of source bitumens—crude oil samples, one for a shale/sand sequence and one for a carbonate sequence, Figure 1.4.[7] In both cases the hydrocarbon contents (saturates and aromatics) have become enhanced and the polar resins and asphaltene contents depleted in the oil, relative to the source bitumen. These results are in agreement with the well-known chromatographic properties of the materials involved and are predictable on that basis: the polar molecules have a greater affinity to the rock surface than the nonpolar molecules and the larger molecules tend to adsorb more readily than the smaller molecules. Otherwise, on the whole, hydrocarbon distributions remain similar and the homologous series as well as the individual concentration ratios are practically the same before and after migration. This is evident in the comparison of the distribution of triterpanes in the saturate fractions of two Alaskan oils and in their possible source-rock bitumens and source-rock pyrolyzates,[8] Figure 1.5.

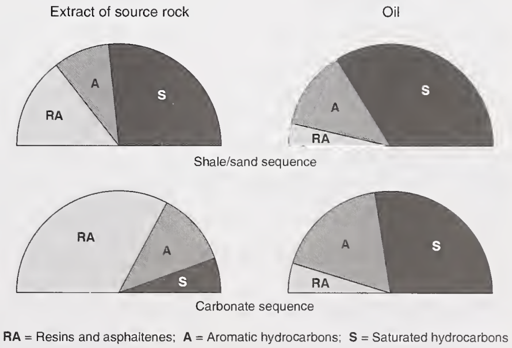

Figure 1.4 Class compositional data for source rock bitumens and crude oils, one in a shale/sand and the other in a carbonate sequence. After B.P. Tissot and R. Pelet, Ref. 7.

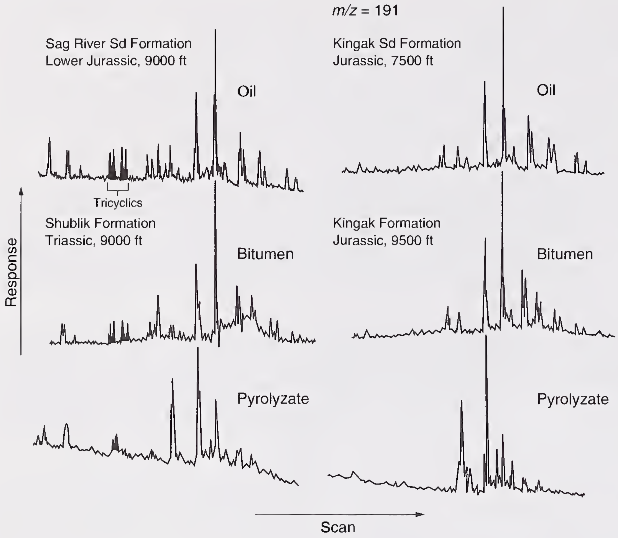

Figure 1.5 Gas chromatographic–mass spectrometric–single ion recording $m/z = 191$ cross scans of the oils and source rock bitumens from the Sag River and Kingak oils, Shublik and Kingak shales, and the pyrolyzates from these rocks. The relative amounts of tricyclic terpanes (black peaks) support a genetic relationship between the Sag River oil and the Shublik shale; similarly, their absence in the Kingak oil and shale supports a relationship between these samples. The presence and absence of tricyclic terpanes in the pyrolyzates of the Shublik and Kingak shales demonstrate the indigenous nature of the bitumen in the source rocks. After K.E. Peters and J.M. Moldowan, Ref. 8.

4.0 Chemical Alteration of Pooled Oil

There are numerous possible processes which may induce changes in the chemical composition of pooled oil and which may be physical, chemical or biological. The various types of processes are often interrelated and may proceed simultaneously, inducing changes in parallel or opposing directions. For example, water washing and biodegradation usually take place simultaneously, both causing the loss of lighter compounds and a consequent increase in the specific gravity of the oil.

The character of an oil is mainly determined by its source material. In some cases, however, the chemical alteration of the pooled oil is so drastic that it may obscure the original character of the source material. An example of this scenario is the case of Alberta oil sand bitumens. High-sulfur crude oils, like the precursor oils of these bitumens, are often associated with carbonate-type source rocks and are rich in *n*-alkanes. Alberta oil sand bitumens are, however, in practical terms, devoid of *n*-alkanes and low-MW constituents due to their extensive microbial degradation and water washing history and perhaps evaporatic losses.[9] Nonetheless, it has been shown that Alberta bitumens contain copious quantities of *n*-alkyl and *n*-alkyl derived moieties built into their constituent molecules as structural elements, revealing that indeed the precursor oils must have been rich in *n*-alkanes.

4.1 Thermal processes

The higher alkanes and aromatic hydrocarbons are thermodynamically metastable with respect to methane (lower alkanes) and carbon and some of them with respect to their constituent elements, hydrogen and carbon (graphite). Therefore, with increasing depth of burial as the temperature rises due to the geothermal gradient or, to a lesser degree, with increasing time of residence, the higher-MW constituents of oil progressively undergo disproportionation to yield gas and low-MW hydrocarbons on the one hand, and polycondensed high-MW aromatics approaching graphite (pyrobitumen) on the other. The overall result is that the pooled oil becomes lighter. This thermal maturation process in the pooled oil has been experimentally demonstrated[10] in the Western Canada Sedimentary Basin and some of the relevant results reported are reproduced in Figure 1.6. As seen from the plots, the percentage concentration of the fractions comprising molecules with less than 15 carbons linearly increases with rising temperature of the reservoir. Similar changes take place in the oxygen and sulfur compounds which result in the release of CO_2, water and H_2S. Clearly, the overall result is a crude oil which possesses improved chemical character and commercial value.

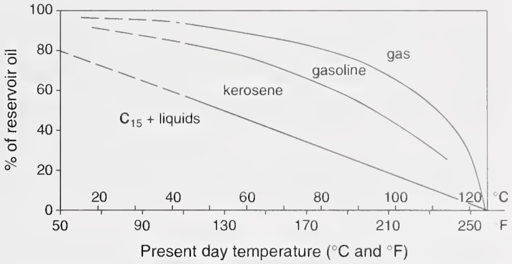

Figure 1.6 Chemical changes in crude oils of the Western Canada Sedimentary Basin with increasing reservoir temperature. From C.R. Evans *et al.*, Ref. 10. © 1971, Elsevier Science B.V.

4.2 Deasphalting

Another naturally occurring process causing the oil in the reservoir to become lighter is deasphalting. It is the consequence of the dissolution of accumulated gases in the oil, thereby causing the precipitation of asphaltene and resinous substances from the oil. Thermal maturation and deasphalting occur in parallel and produce similar results. More extensive deasphalting may occur upon injection of additional reservoir gas. Examples of massive gas injections are also found in the Western Canada Sedimentary Basin, namely in the Devonian Beaverhill Lake and Keg River oils.[10] The platform on which the reefs in the basin rest extends downdip toward the West into an organic facies of high thermal maturity. Gases flowing updip from this high-temperature zone caused the precipitation of asphaltene in reservoirs located in the migration path of the gas. The amount of asphaltene precipitated correlates with the amount of gas dissolved in the oil, while the specific gravity of the oil is a measure of the amount of asphaltene dissolved in the oil. The plot of the logarithm of the solution gas/oil ratio (GOR) *versus* specific gravity of the solution, Figure 1.7, reveals an approximate inverse linear correlation showing that the asphaltene content declines with increasing gas content.

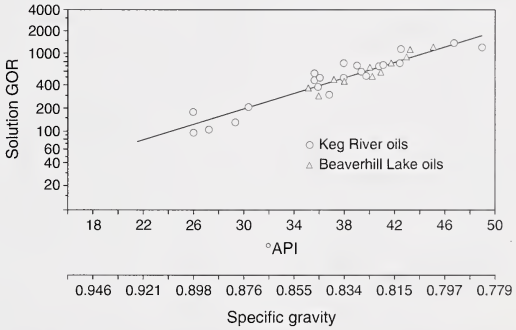

Figure 1.7 Correlation between the logarithm of the gas/oil ratio (GOR) and specific gravity for Keg River and Beaverhill Lake oils in the Western Canada Sedimentary Basin. From C.R. Evans *et al.*, Ref. 10. © 1971, Elsevier Science B.V.

4.3 Biodegradation and water washing

It is evident from the preceding sections that the chemical evolution of petroleum does not stop at the stage of accumulation of the oil in the reservoir and, in addition to nonbiological influences, the chemical composition may be impacted by biological processes. Certain aerobic bacteria are capable of metabolizing some hydrocarbon constituents of the oil and causing the biodegradation of the pooled oil. Anaerobic bacteria, such as sulfate reducers, can also oxidize hydrocarbons, but probably not as fast as aerobic bacteria, and they require aerobes to initiate the process. Under favorable conditions, laboratory degradation by aerobic bacteria can be very rapid and Prudhoe Bay and Bellshill Lake oils, for example, were found to reach the limit of their biodegradability by losing 45–50% of their weight in 168 hours of laboratory incubation with a single or mixed culture of bacteria.[11,12] The progress of biodegradation as a function of incubation time for the Prudhoe Bay oil is plotted in Figure 1.8 which shows that the saturated hydrocarbon fraction is metabolized faster than the aromatic fraction, and the polar fraction—comprising the resins and asphaltene—shows a subtle increase. Whereas the removal of certain types of saturated and aromatic hydrocarbons is well documented, the possibility of the production and injection of extraneous materials in the course of microbial degradation into the oil is not well understood and is a matter of some controversy. The end result of biodegradation of Prudhoe Bay oil is a bitumen, not unlike an Alberta oil sand bitumen, with increased heteroatom content and specific gravity.

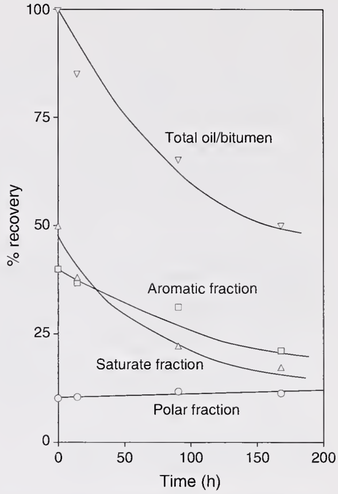

Figure 1.8 Weights of the oils recovered and their three primary component fractions from the biodegradation of Prudhoe Bay conventional oil as a function of degradation time. From I. Rubinstein *et al.,* Ref. 12. © 1977, Elsevier Science Ltd.

Severe biodegradation is generally restricted to shallow depths of burial. Biodegradation generally occurs in relatively shallow, cool reservoirs which are charged with oxygenated water.[13] Such conditions permit the growth of aerobic bacteria. In Alberta the maximum burial depth where severe biodegradation appears to have taken place is around 660 m and most oil sand bitumens are found above this level. The moderately biodegraded Lloydminster heavy oil has a depth of burial of ~670 m and the related nonbiodegraded Bellshill Lake oil deposit is at a depth of ~920 m. Evidence for biodegradation in deeper strata has also been found, for example in the Aquitaine Basin in France.[14] The depth limitation for aerobic biodegradation is related to the requirement for meteoric (low salinity and high sulfate) water that is rich in oxygen and bacteria and to the limiting (maximum) temperature of about 65°C for bacterial activity (which in some cases may be as high as ~80°C).

The effect of water washing on the oil is much less severe. At the water/oil interface, the locale for microbial degradation, the surface-derived formation water, which is undersaturated with the constituents of the oil, selectively and preferentially dissolves the more soluble constituents of the oil and carries them away as it flows through the formation, thereby changing the composition of the oil. The most water-soluble compounds are affected the most. These are, in general, the low-MW, high-polarity molecules containing heteroatoms such as carboxylic acids, sulfoxides, sulfides, thiophenes, quinolines, amines, and low-MW aromatic hydrocarbons. Among the saturated hydrocarbons, which are less soluble in water than the polar molecules, the most soluble are cyclopentane, cyclohexane and the C_1–C_6 alkanes.

The water-washing history of an oil deposit is more difficult to assess because the effect is relatively mild, and suitable reference standards for comparison are generally not available. However, it has been suggested recently that the distribution of the terpenoid di-, tri- and tetracyclic sulfides in the oil represents a highly usable indicator of the water-washing history of a deposit (see Chapter 13).

An additional chemical effect of the invasion of the oil reservoir by oxygen-rich surface-derived water is the abiogenic oxidation of the oil at the oil-water interface. All Alberta oil sands show signs of having experienced mild oxidation resulting in the production of unstable compounds which, on mild thermolysis, decompose to yield carbon monoxide, carbon dioxide, acetaldehyde, *etc.*

The various types of alterations discussed in this section are summarized diagrammatically in Figure 1.9 for a convenient overview.

Chemical alterations of crude oils analogous to water washing, involving evaporative losses of the light fraction of surface-exposed pooled oils, have also been invoked to explain the origin of Alberta oil sand bitumens.[9]

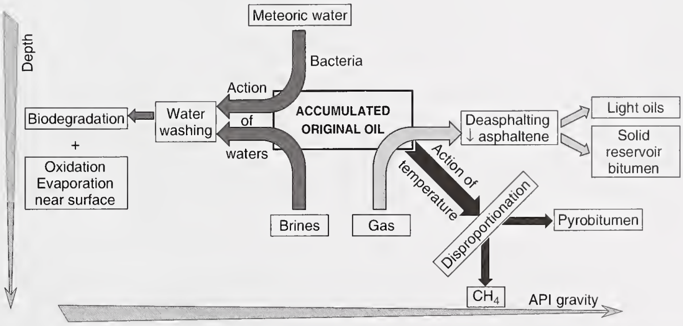
Depth
Meteoric water
Bacteria
Action
of
waters
Biodegradation
Water washing
+
Oxidation Evaporation near surface
ACCUMULATED ORIGINAL OIL
Deasphalting ↓ asphaltene
Light oils
Solid reservoir bitumen
Action of temperature
Disproportionation
Pyrobitumen
Brines
Gas
CH4
API gravity

Figure 1.9 Alteration of crude oils in reservoirs. From J. Connan, Ref. 14. © 1984, Academic Press.

Bibliography

1. D.I. Mendeleyev, Ber., (1877) 229; A. von Humboldt, "Voyage aux Régions Equinoxales du Nouveau Continent Pendant les Années 1799, 1800, 1802, 1803 et 1804", Paris (1825); M. Berthelot, "Sur L'origine des Carbures et des Combustibles Minéraux", Ann. Chim. Phys., 4e Ser., 9 (1866) 481.
2. T. Gold, "Sweden's Siljab Ring Well Evaluation", Oil & Gas J., 89 (1991) 76; T. Gold, "The Deep Hot Biosphere", Proc. Nat. Acad. Sci. U.S.A., 89 (1992) 6045; C.W. Hunt, "Obsolete Theories, New Ideas—Some Alternatives", The Resources Letters, Alberta Chamber of Resources, 5 (1994) 2.
3. C. Engler, "Zur Bildung des Erdöls", Chem Ber., 21 (1888) 1816.
4. A. Treibs, "Chlorophyll und Häminderivat in Bituminösen Gesteinen, Erdölen, Erdurechsen und Asphalten", Liebigs Ann. Chem., 510 (1934) 42.
5. D.H. Welte, "Organic Carbon and the Evolution of Photosynthesis on Earth", Naturwiss., 57 (1970) 17.
6. B.P. Tissot and D.H. Welte, *Petroleum Formation and Occurrence*, Second Edition, Springer-Verlag, New York, N.Y., 1984.
7. B.P. Tissot and R. Pelet, "Nouvelles Données sur les Mécanismes de Genèse et de Migration du Pétrole. Simulation Mathématique et Application à la Prospection", Proc. 8th World Petrol. Congr., 2 (1971) 35.
8. K.E. Peters and J.M. Moldowan, *The Biomarker Guide*, Prentice Hall, Engelwood Cliffs, N.J., 1993.
9. L.W. Vigrass, "Geology of Canadian Heavy Oil Sands", AAPG Bull., 52 (1968) 1984.
10. C.R. Evans, M.A. Rogers and N.J.L. Bailey, "Evolution and Alteration of Petroleum in Western Canada", Chem. Geol., 8 (1971) 147.

11. I. Rubinstein and O.P. Strausz, “The Biodegradation of Crude Oils: The Origin of the Alberta Oil Sands”, in *Oil Sand and Oil Shale Chemistry*, O.P. Strausz and E.M. Lown, Eds., Verlag Chemie International, New York, N.Y., 1978, p. 177.

12. I. Rubinstein, O.P. Strausz, C. Spyckerelle, R.J. Crawford and D.W.S. Westlake, “The Origin of the Oil Sands of Alberta: a Chemical and a Microbiological Study”, Geochim. Cosmochim. Acta, 41 (1977) 1341; R.J. Crawford, C. Spyckerelle and D.W.S. Westlake, “Biodegradation of Oil Reservoirs”, in *Oil Sand and Oil Shale Chemistry,* O.P. Strausz and E.M. Lown, Eds., Verlag Chemie International, New York, N.Y., 1978, p. 163.

13. S.E. Palmer, “Effect of Biodegradation and Water Washing on Crude Oil Composition”, in *Organic Geochemistry*, Eds. M.H. Engel and S.A. Macko, Plenum Press, New York, N.Y. 1993, p. 511.

14. J. Connan, “Biodegradation of Crude Oils in Reservoirs”, in *Advances in Petroleum Geochemistry*, Vol. 1, J. Brooks and D.H. Welte, Eds., Academic Press, London, 1984, p. 299.

2

Geology of the Alberta Bitumen and Heavy Oil Deposits

The Western Canada Sedimentary Basin, which includes areas of the four westernmost provinces of Canada—the Northeastern corner of British Columbia, essentially all of Alberta, southern Saskatchewan and southern Manitoba (Williston Basin)—contains rich deposits of gas, oil and bitumen, Figure 2.1. While gas deposits are found mainly in the western region of the Basin and oil deposits are distributed across the Basin, the bitumen accumulations are all located in Alberta. The size of the bitumen accumulations has been estimated by various authors to be 2.5–6 trillion barrels (the lower figure is considered to be more realistic) and far exceeds the combined amount of gas and oil in the Basin. The bitumen, which is contained in Lower Cretaceous sands and Upper Devonian to Mississippian limestones and dolomites, Figure 2.2, is grouped into three geographic areas: Athabasca (Wabasca), Peace River and Cold Lake, Figure 2.3.

Geological cross sections through the bitumen and heavy oil deposits are shown in Figures 2.4 and 5. Cross section A–B, Figure 2.4, runs approximately east–west through the Peace River, Wabasca (the southwestern tip of the Athabasca) and Athabasca deposits. The

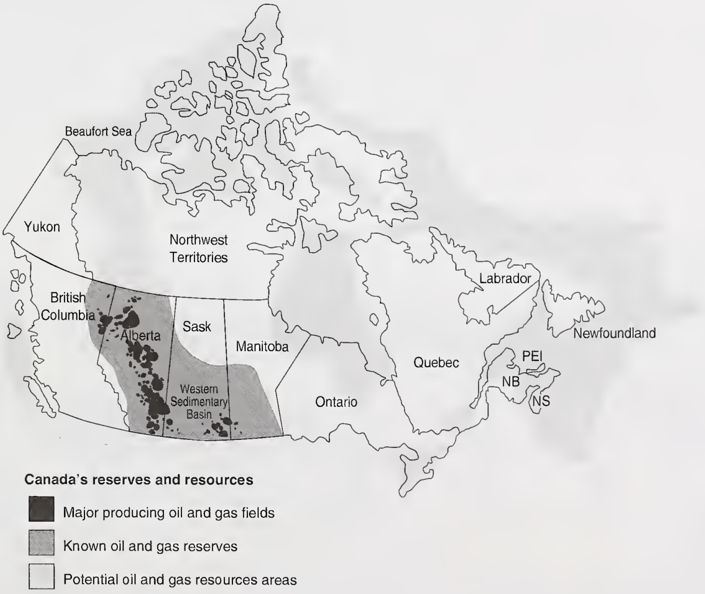
Beaufort Sea
Yukon
Northwest Territories
British Columbia
Alberta
Sask
Manitoba
Western Sedimentary Basin
Ontario
Quebec
Labrador
Newfoundland
PEI
NB
NS
Canada's reserves and resources
■ Major producing oil and gas fields
▨ Known oil and gas reserves
☐ Potential oil and gas resources areas

Figure 2.1 Canada's known oil and gas reserves (cross-hatched area) and potential oil and gas resources (stippled area). The solid black areas are major producing oil and gas fields. Source: Petroleum Resources Communications Foundation, Calgary, AB.

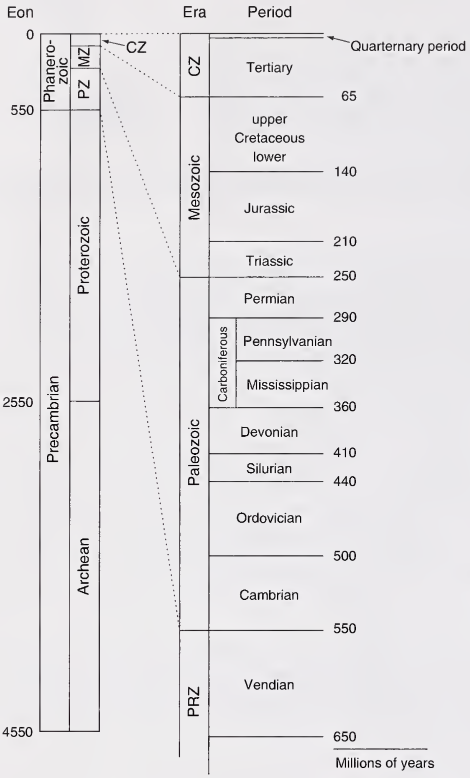
Eon
Era
Period
0
550
2550
4550
Phanero-zoic
Precambrian
MZ
PZ
Proterozoic
Archean
CZ
Quarternary period
CZ
Tertiary
65
Mesozoic
upper
Cretaceous
lower
140
Jurassic
210
Triassic
250
Paleozoic
Permian
290
Carboniferous
Pennsylvanian
320
Mississippian
360
Devonian
410
Silurian
440
Ordovician
500
Cambrian
550
PRZ
Vendian
650
Millions of years

Figure 2.2 Geological timetable.

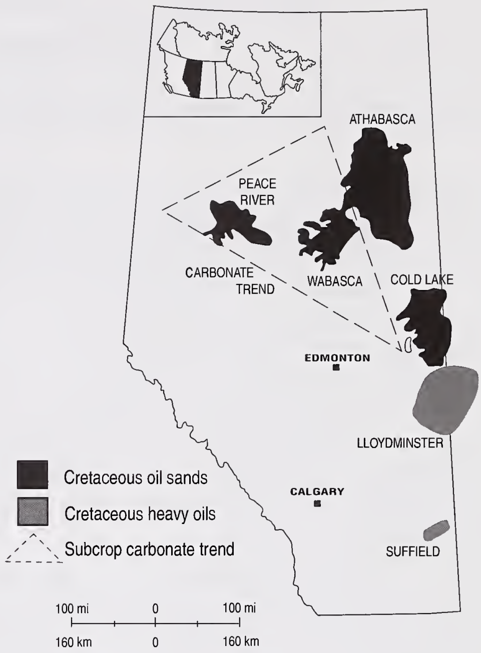
ATHABASCA
PEACE RIVER
CARBONATE TREND
WABASCA
COLD LAKE
EDMONTON
LLOYDMINSTER
CALGARY
SUFFIELD
Cretaceous oil sands
Cretaceous heavy oils
Subcrop carbonate trend
100 mi
0
100 mi
160 km
0
160 km

Figure 2.3 Bitumen and heavy oil deposits of Alberta. Source: Alberta Geological Survey, Alberta Research Council, Edmonton, AB.

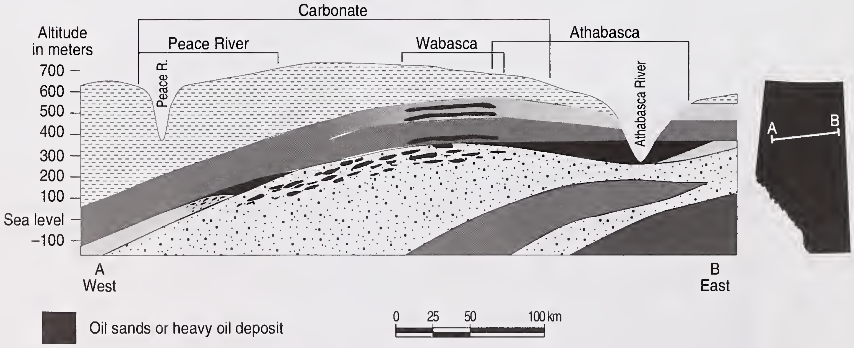
Carbonate
Peace River
Wabasca
Athabasca
Altitude in meters
700
600
500
400
300
200
100
Sea level
−100
Peace R.
Athabasca River
A
West
B
East
A
B
Oil sands or heavy oil deposit
0
25
50
100 km

Figure 2.4 East–West geological cross-section through the Alberta heavy oil and bitumen deposits. Source: Alberta Oil Sands Technology and Research Authority, Edmonton, AB. For general references on the geology of Alberta oil sands see the Bibliography and for a discussion on the origin and geochemistry, Chapter 13.

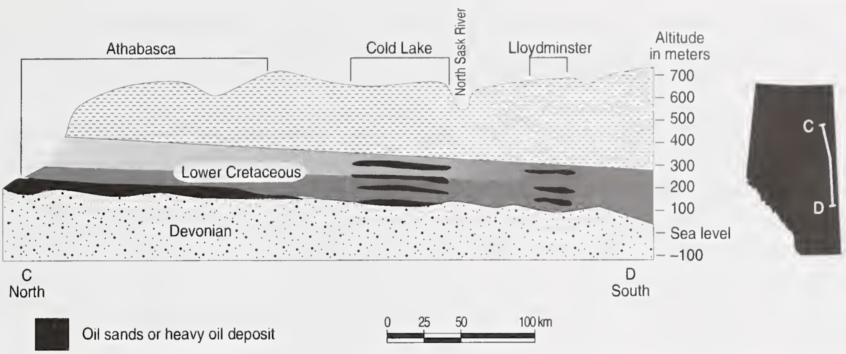
Athabasca
Cold Lake
North Sask River
Lloydminster
Altitude in meters
700
600
500
400
300
200
100
Sea level
−100
Lower Cretaceous
Devonian
C North
D South
C
D
Oil sands or heavy oil deposit
0 25 50 100 km

Figure 2.5 North–South geological cross-section through the Alberta heavy oil and bitumen deposits. Source: Alberta Oil Sands Technology and Research Authority, Edmonton, AB.

vertical scale is exaggerated to illustrate the comparative locations of the oil sand bitumen and the Devonian carbonate bitumen formation. Cross section C–D, Figure 2.5, runs approximately north and south through the Athabasca and Cold Lake bitumen deposits, the Lloydminster heavy oil pools and the underlying Devonian carbonate bitumen deposit.

1.0 Athabasca Oil Sands Area

A schematic illustration of the geological formations showing the primary oil sands and heavy oil horizons, Figure 2.6, indicates that the Athabasca oil sand deposit is contained predominantly within the Lower Cretaceous McMurray Formation which unconformably (*i.e.*, in an interrupted stratigraphic sequence) overlies the Devonian Beaverhill Lake Formation and is conformably (*i.e.*, in parallel, without interruption) overlain by the Clearwater Formation, the Wabiskaw member of which is bitumen-bearing. There are rare, thin gas zones near the top of the formation and zones that once contained gas but are now water bearing can be found. The thickness of the McMurray Formation ranges between 40 and 80 m with up to 40% porosities and 18% by

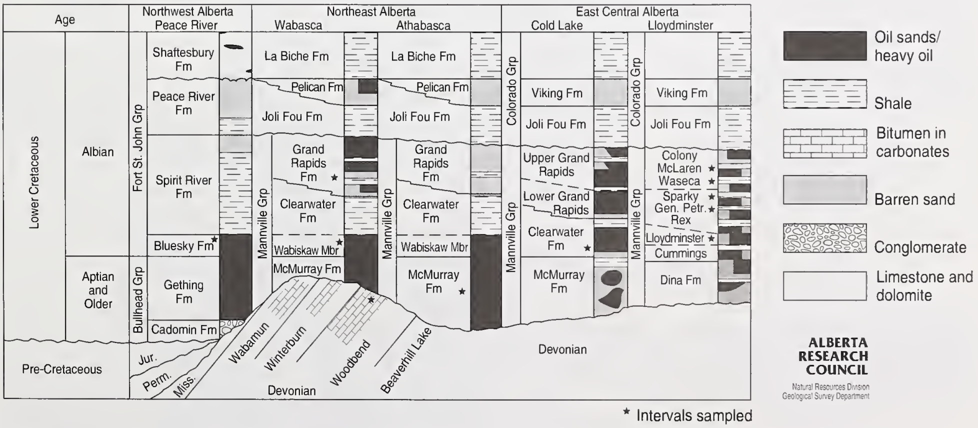
Age
Northwest Alberta
Peace River
Northeast Alberta
Wabasca
Athabasca
East Central Alberta
Cold Lake
Lloydminster
Lower Cretaceous
Albian
Aptian and Older
Pre-Cretaceous
Fort St. John Grp
Bullhead Grp
Shaftesbury Fm
Peace River Fm
Spirit River Fm
Bluesky Fm
Gething Fm
Cadomin Fm
Jur.
Perm.
Miss.
La Biche Fm
Pelican Fm
Joli Fou Fm
Grand Rapids Fm
Clearwater Fm
Wabiskaw Mbr
McMurray Fm
Mannville Grp
Wabamun
Winterburn
Woodbend
Beaverhill Lake
Devonian
Colorado Grp
Viking Fm
Upper Grand Rapids
Lower Grand Rapids
Colony
McLaren
Waseca
Sparky
Gen. Petr.
Rex
Lloydminster
Cummings
Dina Fm
Oil sands/ heavy oil
Shale
Bitumen in carbonates
Barren sand
Conglomerate
Limestone and dolomite
ALBERTA RESEARCH COUNCIL
Natural Resources Division Geological Survey Department
* Intervals sampled

Figure 2.6 Table of formations showing the primary oil sands and heavy oil horizons in Alberta. Source: Alberta Geological Survey, Alberta Research Council, Edmonton, AB.

weight bitumen saturation of the unconsolidated sand. Net pay zones—the sum of all the sands containing greater than 10% bitumen, regardless of whether the pay section is interrupted by shale beds or not—occur up to a thickness of 40 m.

The Athabasca deposit covers some 46,800 km^2 (about the size of Belgium) and contains approximately 950 billion barrels of bitumen. Where overburden thickness does not exceed 45 m and saturated beds are at least 30–60 m in thickness with a minimum of 6% bitumen saturation, recovery by surface mining technologies is considered to be economical. (With higher saturated bed thickness and bitumen saturation overburden thickness as high as 75 m may be acceptable for surface mining.) About 10% of the deposit lying in the northern region of the Athabasca area is estimated to satisfy these requirements. The Athabasca deposit is the only one where the overburden is less than the critical 45-m value in some places.

2.0 Carbonate Trend (Carbonate Triangle)

Bitumen accumulations along the eastern updip margin of the Paleozoic formations which subcrop beneath the Cretaceous deposits may be as large or larger than in the Athabasca oil sand deposits, yet they are much less studied. Only four horizons within this carbonate trend have been subjected to detailed resource estimates, the Upper Devonian Grosmont and Nisku formations (Athabasca area) and the Mississippian Shunda and Debolt formations (Peace River area).

The Grosmont Formation is a huge complex carbonate, dolomite platform underlying the McMurray Formation of the Athabasca oil sand area. The main reservoir horizons, Figure 2.7, 25–50 m in thickness, lie at depths of 250–300 m. The average porosity is as high as 20% and bitumen saturations average 70% or more of the pore space. The well-lithified reservoir has a dual porosity system with part of the bitumen contained in tunnels of various sizes interconnected with fractures, Figure 2.8, and the remaining bitumen is in intercrystalline matrix pores, the result of dolomitization of the original limestone. The bitumen of the Grosmont Formation has the lowest API gravity of all the Alberta bitumens.

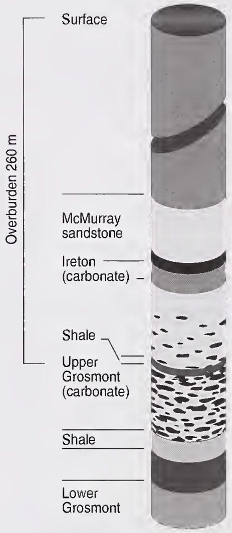

Figure 2.7. Horizons of the Grosmont Formation of the Carbonate Trend. Source: Alberta Oil Sands Technology and Research Authority, Edmonton, AB.

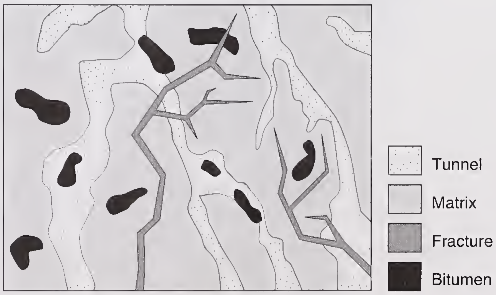

Figure 2.8. Dual porosity system of the Grosmont Formation. Source: Alberta Oil Sands Technology and Research Authority, Edmonton, AB.

The total in-place bitumen present in Paleozoic rocks was estimated in 1977 to be 1.56 trillion barrels which still can be considered a realistic ballpark figure. A summary of in-place Alberta bitumen reserves and resources is presented in Table 2.1.

Some remarks concerning the nomenclature relating to these carbonate deposits are in order here. It has been suggested that these carbonate reservoirs could be called oil "sands". However, to call the carbonate, dolomite rocks "sands" was not a practical notion and serves no purpose. Distinction in the nomenclature must be made between the sands and carbonate dolomite rock matrices because they are distinctly different chemically and morphologically. It is suggested that the deposits in the Carbonate Trend (Triangle) be called oil carbonates (by analogy with oil sands and oil shales) and their bitumens referred to as carbonate bitumens.

Table 2.1 Bitumen reserves and resources of Alberta[a]

Area	Deposit	Rock	Bitumen Reserve[b] 10⁹ bbl	Bitumen Resource 10⁹ bbl
Athabasca	McMurray/Wabiskaw	sand	906	
	Grand Rapids	sand	44	
	Grosmont/Nisku	carbonate	384	
Cold Lake	Grand Rapids	sand	126	
	Clearwater	sand	69	
	McMurray/Wabiskaw	sand	25	
Peace River	Bluesky/Gething	sand	76	
Carbonate Trend	Debolt/Shunda	carbonate	44	
	Pekisko	carbonate		250
	Banff	carbonate		
	Wabamun	carbonate		365
	Graminis	carbonate		
	Blueridge	carbonate		44
	Calmar	carbonate		
	Upper Ireton	carbonate		120
	Hondo	carbonate		
	Leduc	carbonate		76
	Ireton	carbonate		
Total			1,674	855

[a] From C.O. Outtrim and R.G. Evans, "Alberta's Oil Sand Reserves and Their Evaluation", Heavy Oil Symposium, Proceedings, 28th Annual Technical Meeting of the Petroleum Society of C.I.M., May, 1977, p.1. [b] A reserve is the total resource in a deposit less any portion thereof deemed unrecoverable by any foreseeable technology.

3.0 Peace River Oil Sands Area

Bitumen within the Peace River deposit area, covering 9,870 km^2, is trapped in an updip pinchout, Figures 2.3 and 2.4, of the Cretaceous Gething and Bluesky formations against Mississippian carbonates which form a high on the sub-Cretaceous unconformity. It is the third largest of the Alberta oil sand deposits with an in-place bitumen content of 76 billion barrels and an average porosity of 24%. It is underlain by the Debolt/Shunda formations of the Carbonate Trend deposit. An important feature of the Peace River deposit is the extensive area of thick, rich oil sands, underlain by a thin, water-sand layer which permits very effective steam injection recovery of the bitumen without fracturing the formation.

4.0 Cold Lake Oil Sands Area

With 220 billion barrels of in-place bitumen which is distributed over four main stratigraphic areas, the Cold Lake area deposit is the second largest oil sand occurrence in Alberta. The key deposits, lying 275–600 m deep, are (in ascending order) the McMurray, Clearwater and Lower and Upper Grand Rapids. The bitumen reserve in the Clearwater deposit, although not the largest in the Cold Lake area, is commercially of the greatest potential because of the great thickness of the net pay zones, up to 60 m, and good lateral continuity of the reservoir. The average rock porosity here is 30% and the bitumen in the Cold Lake area has the highest API gravity, 10–15°.

5.0 Lloydminster Heavy Oil Deposit

The Lower Cretaceous Mannville Group Lloydminster area heavy oil pools are related to the Cold Lake area bitumen deposit. They contain several billion barrels of heavy crude oil with API gravity of 12–23° and density of about 0.800 $kg \cdot m^{-3}$. This deposit extends eastward into Saskatchewan.

Bibliography

1. B.M. Benyon and S.G. Pemberton, “Resource Characterization of the Lower Cretaceous Grand Rapids Formation: Reservoir Geology and Hydrocarbon Distribution, Cold Lake Oil Sands Area, Alberta”, AOSTRA J. Res., 8 (1992) 103.
2. M.A. Carrigy, “Mesozoic Geology of the Fort McMurray Area”, in *Guide to the Athabasca Oil Sands Area*, M.A. Carrigy, Ed., Alberta Research Council Information Series, 65 (1973) 75.
3. P.D. Flach and G.D. Mossop, “Depositional Environments of the Lower Cretaceous McMurray Formation, Athabasca Oil Sands”, Am. Assoc. Petrol. Geol. Bull., 69 (1985) 1195.
4. R.S. Harrison, “The Bitumen-Bearing Paleozoic Carbonate Trend of Northern Alberta”, Am. Assoc. Petrol. Geol. Studies in Geology, 25 (1987) 319.
5. D.A.W. Keith, J.R. MacGillivray, D.M. Wightman, D.D. Bell, T. Berezniuk and H. Berhane, *Resource Characterization of the McMurray/Wabiskaw Deposit in the Athabasca Central Region of Northeastern Alberta*, Alberta Oil Sands Technology and Research Authority Technical Publication Series No.7, Edmonton, AB, 1990.
6. B.A. Rottenfusser, “Peace River Oil Sands—Regional Geology”, Alberta Oil Sands Technology and Research Authority/Alberta Research Council Internal Report, 1985.
7. D.M. Wightman, B.A. Rottenfusser, J. Kramers and R.S. Harrison, “Geology of the Alberta Oil Sand Deposit”, in *AOSTRA Technical Handbook on Oil Sands, Bitumens and Heavy Oils*, L.G. Hepler and C. Hsi, Eds., Alberta Oil Sands and Technology Technical Series No.6, Edmonton, AB, 1989, p. 1.
8. D.M. Wightman, S.G. Pemberton and C. Singh, “Depositional Modeling of the Upper Manville (Lower Cretaceous), East Central Alberta”, Soc. Econ. Paleontologists and Mineralogists, Spec. Publ., 40 (1987) 189.
9. D.M. Wightman and S.G. Pemberton, “The Lower Cretaceous (Aptian) McMurray Formation: an Overview of the Fort McMurray Area, Northeastern, Alberta”, Can. Soc. Petrol. Geol., Memoir 18 (1997) 312.

10. J. Allen and S. Creaney, "Oil Families of the Western Canada Basin", Bull., Can. Petr. Geology, 39 (1991) 107.

11. S. Creaney, J. Allen, K.S. Cole, M.G. Fowler, P.G. Brooks, K.G. Osadetz, R.W. Macqueen, L.R. Snowdon, C.L. Riediger, "Petroleum Generation and Migration in the Geological Atlas of the Western Canada Sedimentary Basin", G.D. Mossop and I. Sheben (compilers). Can. Soc. Petr. Geologists and Alberta Research Council, Alberta, (1994) p. 455.

3

Composition and Structure of Alberta Oil Sands and Oil Carbonates

Oil sands are naturally occurring bitumen-impregnated sands and similarly, oil carbonates are naturally occurring bitumen-impregnated carbonate rocks. Oil sands have been alternately referred to as "oil sands", "tar sands", or "bituminous sands". The proper technical term would be the least frequently used designation, "bituminous sands". In Canada, "oil sands"—by analogy with oil shales—has become the accepted term while in other countries the term "tar sands" is, almost without exception, in general usage. While the terms "oil sands" or "tar sands" may not be technically precise, since the bitumen these sands contain is distinctly different from a liquid oil or tar (which is a dark brown-black viscous liquid product of the destructive distillation of petroleum, coal, and other carbonaceous materials), their meaning is clear and therefore either term may be used without ambiguity.

The situation with oil carbonates is different. In view of the shorter history of resource exploration and development at the commercial scale and the less frequent worldwide occurrence and awareness of such deposits, a generally accepted term for these materials has not evolved. While the term "oil sands" has been suggested, this is not justifiable in view of the obvious compositional differences between a cemented carbonate rock and unconsolidated sands as discussed in Chapter 2. Therefore it is proposed that, to conform with the terms "oil sands" and "oil shales", these materials be named "oil carbonates" and their bitumen contents "carbonate bitumens".

Oil sands are complex multiphase systems[1] composed of bitumen, sand, fines, colloids, clay organics, salts, water, traces of gases and chemisorbed carboxylic acids, along with varying amounts of non-petroleum-derived organic matter such as humin, humic acids and fulvic acids. Fines are defined as solid materials passing through a 325-mesh (< 44 μm) sieve and they comprise some heavy minerals ($>2.96\ \mathrm{g \cdot cm^{-3}}$, about 0.8 ± 0.6% of the solids), silt, very fine quartz, and clay minerals. In some of the literature, minerals smaller than 2 μm (in equivalent spherical diameter) are termed clay and the 2–44 μm minerals are referred to as silt while, in the Wentworth Classification of Sand Particle Size, silt is defined as sand particles ranging from 5 to 62 μm in size, and clay as particles of less than 5 μm.

1.0 The Composition and Structure of Oil Sands

Most oil sands are hard rocks in which the unconsolidated clastic sand grains are cemented together by the bitumen. On removing the bitumen by dissolution (in benzene, toluene, methylene chloride, etc.) the sand collapses. On recombining the separated bitumen with all the components of the original oil sand, the oil sand rock can be reconstituted with somewhat altered properties. Among the important properties of oil sands—like those of other reservoir rocks—are micro- and macrostructures, porosity, permeability, heat conductivity, specific heat and chemical composition (bitumen, water, fines content).

The porosity (that is, the fluid-holding capacity which is determined by the grain size and grain size and shape distribution and is expressed as the percentage of the total volume occupied by channels or pores) of the reservoir rock for the case of the closely packed sands in the Athabasca oil sand deposits is fairly constant over a formation[2] and varies between 25 and 40%. Average porosities of the oil sand formations lie in the 24–35% range, Table 3.1. As a consequence, the total amount of fluid, bitumen plus water, is a relatively constant 20% by weight in the surface-mineable upper strata of the Athabasca deposit, which corresponds to about 35% porosity, that is, void space in the closely packed sand, Figure 3.1. As a consequence there is an inverse linear relationship between concentrations of water and bitumen. At the highest bitumen saturation, ~18.6%, the water content is low, about 2%. Another correlation involving fines content is also evident in that in low-grade, high-water-content oil sands, the fines content is higher. The higher the water, the higher the fines content and in oil sands with bitumen saturations of less than 6%, the fines content may exceed one-third of the mineral matter. Ores with 6–9% bitumen content are considered low grade, 9–12% average and greater than 12%, high grade. Also, the ore grade profoundly affects the efficiency of bitumen recovery in the hot water separation of the bitumen which is a principal step in the current technology for the production of synthetic crude from oil sands. Thus, the percent recovery rises steeply with increasing bitumen content in the ore and reaches a maximum efficiency of about 92% at about 12% bitumen content.

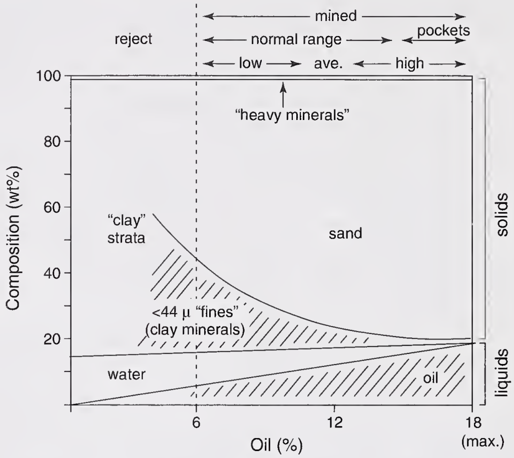

Figure 3.1 Composition of Athabasca oil sands. From J.A. Bichard, Ref. 1a.

The constituents of Alberta (primarily Athabasca) oil sands are shown diagrammatically in Figure 3.2 and listed in Table 3.2. These oil sands constituents are arranged in the oil sands rock in accordance with the history of the oil and reservoir rock, and the oil depositional history of the reservoir which gave rise to stable microstructures.

Most Alberta oil sands, unlike most American oil sands, readily break up when placed in hot water and are therefore called water wet. The easy separability of the bitumen from the sand has been attributed since the early 1900s to the presence of a water film surrounding each sand grain and separating it from the bitumen.[3] In American oil sands, for example Utah (Asphalt Ridge, P.R. Spring, Sunnyside, Tar Sand Triangle), this water film is absent and consequently the sand grains are enveloped directly by the bitumen. Such oil-wet structures are not readily broken up on contact with water. The water wetting of oil sand can be demon-

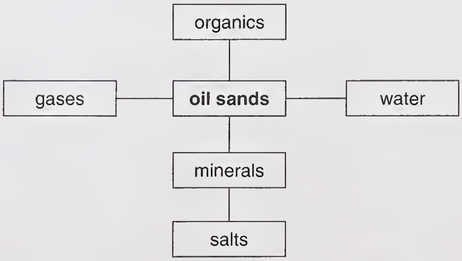

Figure 3.2 Constituents of Alberta (primarily Athabasca) oil sands.

Table 3.1 Generalized geological attributes of Alberta oil sand deposits[a]

			Depth range (m)	Average pay thickness (m)	API °	Average porosity (%)	Depositional environment	Dominant grain minerals	Dominant clay minerals	
Athabasca	Grand Rapids	Upper	200–400	9	8	30	shoreline & shallow marine	quartz chert feldspar rock fragments	kaolinite chlorite illite smectite illite	oil sands water sands
		Middle	230–430	5	8	30				
		Lower	270–470	6	8	30				
	Wabiskaw/ McMurray	Mineable	0–120	38	8–10	29	continental to marine shelf	quartz	kaolinite illite	
		In situ	80–750	19	8–10	28				
Cold Lake	Grand Rapids	Upper	275–500	6	11–15	30	continental to marine shoreline	quartz rock fragments feldspar	kaolinite illite smectite	
		Lower	325–525	12	9–12	31				
	Clearwater		375–500	12	10–11	30	marine shoreline	quartz, feldspar rock fragments altered grains	kaolinite illite smectite	
	Wabiskaw/ McMurray		425–600	5	10–12	25	marine shelf/ continental	quartz glauconite/ quartz	kaolinite illite	
Peace River	Bluesky/ Gething		460–760	14	9	24	estuarine to shallow marine	quartz, chert rock fragments	kaolinite illite	
Carbonate deposits	Debolt		500–800	32	8–10	18	open marine	limestone dolomite	not significant	
	Shundra		500–800	14	8–10	20	tidal flat to open marine	limestone dolomite		
	Grosmont		260–350	16	7	16	tidal flat to open marine	dolomite		

[a] From D.M. Wigham *et al.*, Ref. 2.

Table 3.2 Chemical composition of oil sands

Organics:

- bitumen
- humin
- humic acids
- fulvic acids
- chemisorbed aliphatic carboxylic acids
- insoluble organic – noncrystalline inorganic complexes (IONCI)

Water:

- hydration:
  - – lattice
  - – surface film
- unbonded:
  - – pendular ring
  - – retained in fines clusters
- connate water includes: unbonded water and surface hydration (as determined by Soxhlet extraction)
- total water includes: connate plus lattice water (as determined by ash analysis)

Salts:

- insoluble in water
- soluble in water
- surface adsorbed ions
- ions in water

Minerals:

• sand – α quartz 325+ mesh matter		
• silt	2–44μm	″
• clay	2 μm and less	″
• colloid	<0.5 μm	″
• IONCI		″
• heavy minerals		

Gases:

- dissolved in oil phase
- dissolved in aqueous phase
- free in structure

strated experimentally by reconstituting the separated sand, water and bitumen components of the oil sand.[1a] If the order of mixing the constituents is sand + water + bitumen, then the reconstituted oil sands can be separated readily by the hot water process. On the other hand, if the order of mixing is sand + bitumen + water, then the reconstituted oil sand does not readily break up in the hot water process. In contrast to these findings it has been shown that it is possible to get good primary recoveries for oil sands that have been completely dehydrated by exposure to the atmosphere.[1b] Since the water in the film is only a small fraction of the connate water and this water is difficult to remove, it may perhaps be possible that in these experiments most of the water films separating the sand from the bitumen remained intact. The easy water separability of the bitumen from the sand is an industrially important property of the Alberta oil sands and is the basis of the currently used hot water and cold water process for bitumen extraction.

Most of the Athabasca oil sands lie in the McMurray formation which was deposited about 110 million years ago. Three facies are recognized in this formation with the lower part having a fluvial channel origin, the middle zone deposited in an estuarian complex and the upper part originating in a variety of marine depositional environments.

The structure of the oil sand in the uppermost, surface-mineable strata has been studied to a considerable extent. The mineral composition is diverse and it has been reported to comprise >90% quartz with minor amounts of potash feldspar, chert, mica and muscovite. Clay minerals,[2] predominantly kaolinite, illite and small amounts of chlorite, smectite and montmorillonite, appear only in the fines fraction. Illustrative size distribution curves for high- and low-grade (15% and 7% bitumen) oil sands are shown in Figure 3.3. Maxima in the size distribution curves of these oil sands occur at 180 and 90 μm. In agreement with the trend illustrated in

Figure 3.1, the size distribution curve for low-grade ore is shifted to smaller particle sizes relative to the high-grade ore.

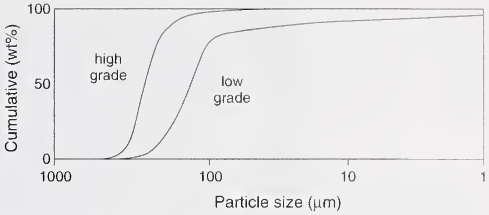

Figure 3.3 Size distribution curves for a high-grade (15% bitumen) and low-grade (7% bitumen) oil sand. From D.M. Wigham *et al.,* Ref. 2.

In addition to bitumen, varying amounts of bitumen-unrelated organic solvent-insoluble organic matter such as humic materials comprising humin, humic acids and fulvic acids with chelated ketones, bitumen-related solid-bound carboxylic acids and other, yet unidentified organic matter are also present.[4–6] The organic solvent-insoluble organic matter is present as free particles, as surface layers firmly adsorbed on inorganic particles, or as binding agents in porous aggregates of clay, sand and mineral particles. Adsorption of the organic solvent-insoluble organic matter on the originally hydrophilic, water-wettable, electrically-charged mineral surfaces endows the surfaces with hydrophobic, oil-wettable characteristics. Such surfaces could bind to bitumen but not to water, and therefore oil sands with hydrophobic minerals would not be readily separable by water extraction processes. In low-grade oil sands the bulk of the fines may be surface coated and therefore the concentration of the humic matter in the sand increases with increasing fines content. It has been found that high-grade oil sands with low fines content contain small amounts of humic materials and low-grade ores with a high fines content may carry up to 3% organic solvent-insoluble, partially inorganic-bound organic matter (based on the methylene chloride extracted sand).

Examples of close-up views using electron microscopes and energy dispersive X-ray diffraction[6] are shown in Figures 3.4 and 3.5.

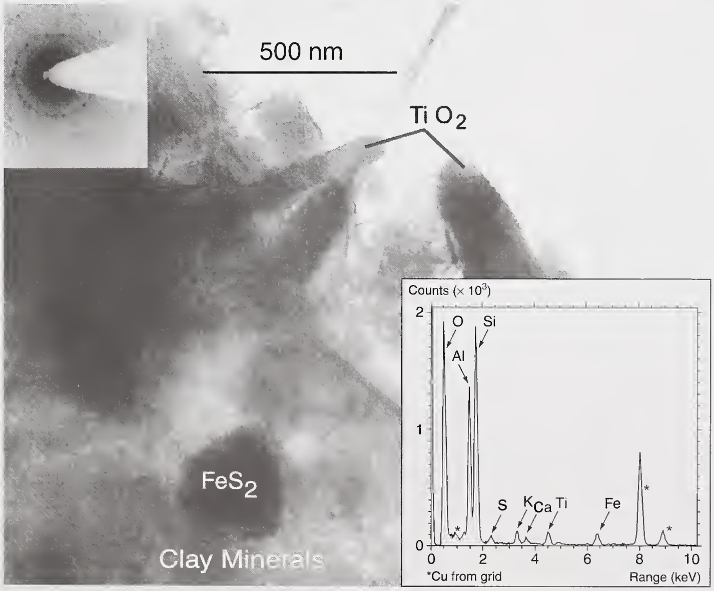

Figure 3.4 Close-up view of organic-rich solids using transmission electron microscopy (TEM) and energy dispersive X-ray diffraction (EDX) scans. After L.S. Kotlyar *et al.*, Ref. 6.

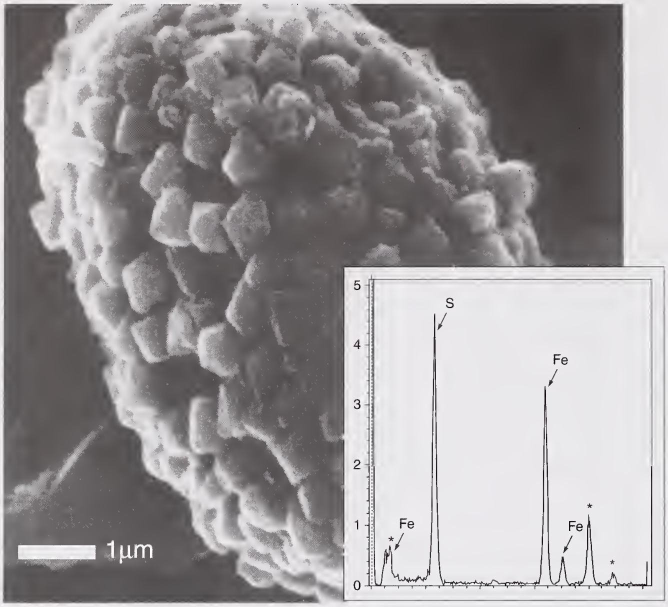

Figure 3.5 Scanning electron micrograph of a large particle identified as pyrite by EDX. After L.S. Kotlyar *et al.*, Ref. 6.

Several models have been proposed for the structure of Alberta oil sands. The essential and central feature of all of them is the presence of a thin film of connate water (*cf.* Chapter 7) surrounding each sand grain, thereby separating the bitumen from the sand. The model in current use[7] is shown in Figure 3.6. This model is thought to be in agreement with the predictions of the interfacial properties of the components of the oil sands and their irreducible water saturation (1.3–2.5%) from computed drainage-capillary pressure curves for simplified high-grade oil sand models. The connate water is present in three forms: *i)* as pendular rings surrounding the particle-to-particle contact points and covering approximately 30% of the sand surface; *ii)* as an approximately 10-nm thick film covering about 70% of the sand surfaces; and *iii)* as water retained in fines clusters. The amount of water retained in the thin film is small, less than 5% of the water and in high-grade oil sands over 95% of the water is present in the pendular rings. The stability of this film is derived from the "disjoining pressure", the resultant pressure of the repulsive forces from the electrical double layer and the London-van der Waals attractive forces.[7] Depending on the salinity of the connate water, the attractive forces dominate for film thicknesses between about 1.5 nm and 17 nm, on the average about 10 nm; in other words, the aqueous film is predicted to be stable in this thickness range. On this basis, the origin of the aqueous film around the sand grains is attributed to the displacement of the original aqueous wetting phase from the porous medium by the non-

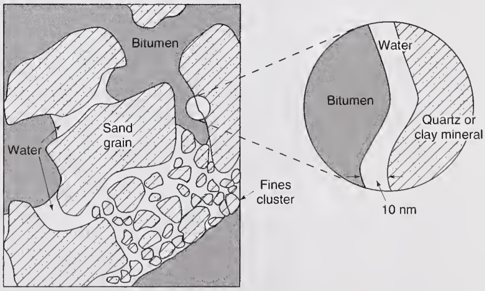

Figure 3.6 Schematic diagram showing a hypothetical microstructure for Athabasca oil sands. From K. Takamura, Ref. 7. © 1982, Canadian Society for Chemical Engineering.

wetting oil phase leaving behind the stable, thin film covering the surface, thereby separating the bitumen from the sand. (This simple picture of the process of bitumen deposition, however, is not fully satisfactory and does not take into consideration the complexity of the process; this problem will be revisited later in this chapter and in Chapter 13.) The water retained in fines clusters in high-grade oil sands is of little significance.

In the case of low-grade oil sands containing large amounts of fines, the above structure is modified by the presence of water in fines clusters and the inorganic-humic matter complexes. The latter material was suggested to be present in two forms:[5] as colloidally stable complexes in the connate water (in which case the surfaces of most of the crystalline minerals are not contaminated with insoluble organic matter and are separated from the bitumen by a water envelope as in the model discussed above); or, alternatively, as an insoluble hydrophobic phase coating the surfaces of some of the oil sand solids, thus facilitating adhesion to bitumen, Figure 3.7. The former condition has been associated with high-grade, estuarian sands and the latter with low-grade, marine deposits.

The different forms of the noncrystalline inorganic-humic matter complexes in estuarian and marine deposits have been suggested to be due to the flocculation of the colloidally dispersed amorphous aluminum silicate-organic complexes formed from dissolved aluminum and silicon ions and humic materials in water.[5] Elevated concentrations of the humic materials could inhibit the crystallization of the amorphous aluminum-silicon aggregates into clay minerals and, in the absence of a high concentration of flocculating cations (estuarine oil sands), these amorphous organic-inorganic clusters may form stable colloidal solutions. However, increased ionic concentrations of Mg, Ca and K (marine oil sands) could cause the flocculation and precipitation of these organic-rich particles on the electrically-charged surfaces of crystalline materials which would ultimately result in the formation of a hydrophobic solid phase.

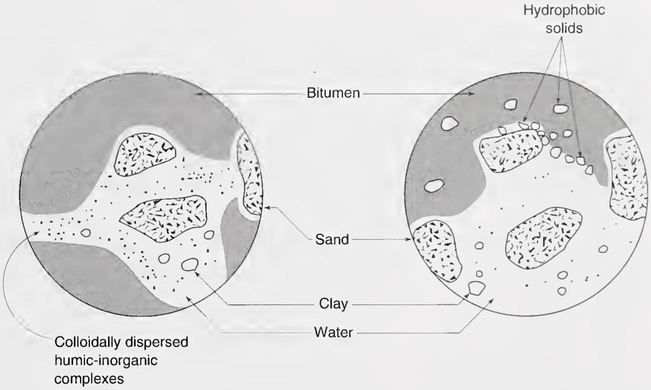

Figure 3.7 Schematic microstructures of high-grade and low-grade oil sands. From L.S. Kotlyar *et al.*, Ref. 5.

It should be pointed out that the experiment mentioned above, involving the reconstitution of the oil sand from its separated sand, bitumen and water components, suggests that in the absence of water the hydrophilic sand is capable of bonding directly to the bitumen to produce an oil-wet oil sand that is not readily separable by the hot water process. This phenomenon can be interpreted in terms of the amphiphilic components of the bitumen (*e.g.*, carboxylic acid, sulfoxide, alcohol, etc., molecules perhaps with the mediation of water bridges) acting as surfactants covering the hydrophilic surface with their polar ends bound to the surface and their nonpolar ends providing an oil-wettable cover for the adsorption of hydrocarbon molecules.

Contrary to the generally held view—as outlined above—of the structure of Alberta oil sands in which the connate water is primarily associated with the mineral matter, an electron microscopic investigation of some Alberta oil sands led to a different conclusion.[8] In that study electron micrographs of freeze-fractured Athabasca oil sands from the Suncor mine clearly showed regions of the bitumen phase that contained densely packed regular spherical globules in the 0.02–0.5 µm size range, which were assumed to be water droplets. This assumption, however, has not been substantiated and the globules could have contained gases rather than connate water. Small quantities of gases are always present in oil sands (Chapter 9) and the existence of occasional gas pockets has also been reported. Gas and vapor bubbles may be easily confused with liquid droplets or internal structures in the bitumen. In any event the micrographs show a unique picture of the bitumen phase in the oil sand structure but they have not yet been duplicated.

The composition along with the geologic, mineralogic, chemical and physical properties of oil sands vary even within a single reservoir and may change abruptly within distances of less than one meter. Data on vertical compositional variations are sparse and what is available will be discussed in Chapter 5.

The distribution of bitumen saturation in Athabasca oil sands is shown in Figure 3.8 from which it appears that over 80% of the deposit has a bitumen saturation above the economically favorable ~8% limit, although the representativeness of the data is uncertain.[9]

The chemical compositions of bitumens from the various Alberta deposits are quite similar, showing only slight, but definite and characteristic, differences. For example, the saturated hydrocarbon content of the bitumen increases and the viscosity decreases, in the order Carbonate Trend, Athabasca, Peace River and Cold Lake deposits.

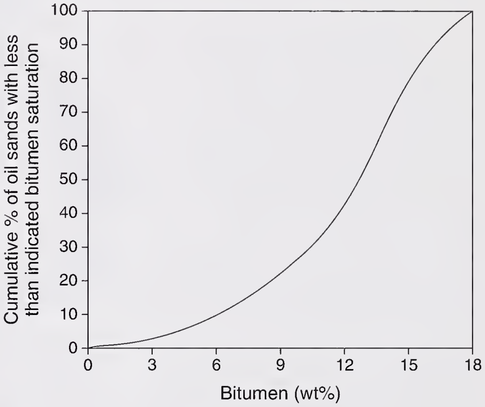

Figure 3.8 Bitumen saturation for the Athabasca deposit. From F.W. Camp, Ref. 9.

Oil sands from a worldwide distribution show considerable variability, not only in chemical composition but in grain size distribution, porosity, degree of consolidation, fluid saturation and other properties. For example, all Alberta bitumens contain a high level of sulfur, in the range 4.1–6.2%, with an average value close to 4.6%. American oil sand bitumens have considerably less sulfur, typically in the 1–2% range, and Sunnyside and Asphalt Ridge bitumens contain only 0.4–0.6% sulfur.

Free sulfur, that is, sulfur in elemental form, has been reported to be present in oil sand samples from the Athabasca deposit and from Nigeria,[10] Indonesia, Malagasy and Peru.[11] Elemental sulfur in oil sands can originate from the oxidation of pyrites and probably other sulfide minerals by atmospheric oxygen to produce sulfate ion and elemental sulfur:

$$FeS_2 + 2\,O_2 \longrightarrow Fe^{2+} + S^{o} + SO_4^{2-} \qquad (1)$$

Other oxidation mechanisms proposed[12] include the bacterially assisted reaction which produces sulfate ion and sulfuric acid, but not elemental sulfur:

$$4\,FeS_2 + 15\,O_2 + 2\,H_2O \xrightarrow[\substack{(\textit{thiobacillus}\\ \textit{ferrooxidans}\\ \text{and others})}]{\text{bacteria}} 2\,Fe_2(SO_4)_3 + 2\,H_2SO_4 \qquad (2)$$

and the reaction

$$2\,FeS_2 + 7\,O_2 + 2\,H_2O \longrightarrow 2\,FeSO_4 + 2\,H_2SO_4 \qquad (3)$$

Other sulfides found by various researchers in Athabasca oil sands such as marcasite (FeS_2, an isomorph of pyrite but reportedly oxidizes much more quickly than pyrite) and chalcopyrite ($CuFeS_2$) would also yield sulfuric acid and metal sulfates on oxidation.

In addition to reaction 1, the elemental sulfur isolated from oil sand samples could have been formed from the reduction of the sulfate ion by sulfate-reducing bacteria as well:

$$SO_4^{2-} \xrightarrow[(\textit{desulfovibrio})]{\text{bacteria}} S^{2-}/S^0 \qquad (4)$$

In the case of the Peruvian sample it was established with reasonable confidence that the elemental sulfur was representative of the in-place oil sand and was not the result of prolonged air exposure. In one oil sand sample from Indonesia elemental sulfur comprised 2.5% of the weight of the oil sand.

The oxidation by atmospheric oxygen also affects the organic matter in the oil sand and results in the formation of oxygenated compounds such as alcohols,[13] carbonyls,[14] carboxylic acids[15] and sulfoxides.[16] These oxidation reactions may be catalyzed by some components of the heavy minerals in the sand and may in part be the consequence of past or present microbial activity. On prolonged exposure to air, however, even refined petroleum products like lubricating oils are known to experience slow oxidation which leads to quality deterioration and decreased performance.

As can be predicted, the mineral composition of an oil sand has a considerable impact on its quality with respect to processability. Since most of the minerals have low solubilities, the solution chemistry of minerals does not directly affect the hot water process. Nonetheless, the role of the small amount of minerals which can undergo ion exchange reactions liberating Ca^{2+} and Mg^{2+} ions and establish equilibrium with exchangeable ions can be important. This is illustrated by the correlation between loss of recovery with oil sand fines in the aging process, Figure 3.9, and the decrease in recovery as a function of the concentration of soluble divalent ions due to aging in secondary tailings, Figure 3.10.[17]

Another property of the oil sand that is determined by the mineral composition is the *pH*. Most oil sands displaying good separability have neutral or weakly basic (7–9) *pH* values. This is attributable to the presence of an excess of alkaline earth carbonates, although many other minerals in the oil sand tend to give basic *pH* in aqueous suspensions, Table 3.3. These aqueous mineral suspensions also exhibit some buffer capacity and tend to resist changes in the

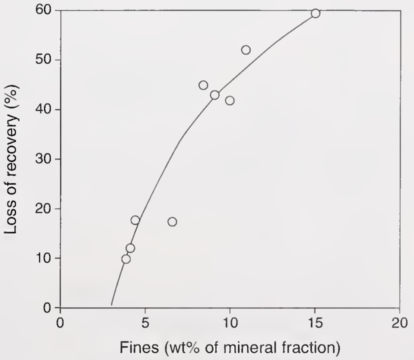

Figure 3.9 Effect of oil sand fines (<44 μm) on bitumen recovery. From E.C. Sanford, Ref. 17. © 1983, Canadian Society for Chemical Engineering.

Table 3.3 *pH* values for some minerals in aqueous suspensions (0.6 wt%)[a]

Mineral	Formula	*pH*	Mineral	Formula	*pH*
Oxides:			**Carbonates:**		
quartz	SiO_2	9.2	calcite	$CaCO_3$	9.8
sand	SiO_2	7.0	dolomite	$CaMg(CO_3)_2$	9.5
rutile	TiO_2	9.5	magnesite	$MgCO_3$	8.9
ilmenite	$FeO{\cdot}TiO_2$	7.8	siderite	$FeCO_3$	6.1
Silicates:			**Clay minerals:**		
garnet	$Mg, Al(SiO_4)_3$	10.0	kaolin	$Al_2O_3{\cdot}2SiO_2$	5.3
wollastonite	$CaSiO_3$	10.0	illite	variable	2.9
zircon	$ZrSiO_3$	9.4			
staurolite	$Fe_2Al_9O_7(SiO_4)_4OH$	9.3			
kyanite	Al_2SiO_5	8.3			
Sulfates:			**Sulfides:**		
ferrous sulfate	$FeSO_4$	4.4	pyrites	FeS_2	5.8
ferric sulfate	$Fe_2(SO_4)_3$	2.4			

[a]From Ref. 1.

pH on addition of acids or bases. As has been discussed above, the one *pH*-altering process that has been shown to affect plant operation in the hot water separation phase is the oxidation of pyrites, reactions 1–3, producing iron sulfates and sulfuric acid. These oxidation processes were found to be strongly temperature dependent, Figure 3.11; for example, Athabasca oil sand stored at 20°C for one month aged, in terms of sulfate production, to the same extent as a sample stored at –18°C for three years. A high sulfate concentration in the connate water is an indication that the sample has been exposed to air.

The hydrogen ions produced in reaction 2 react with the carbonate minerals and both the hydrogen and iron ions may also react with the clay minerals by ion exchange, resulting in an increase in the concentration of calcium and magnesium ions in the connate water. The presence of any of these

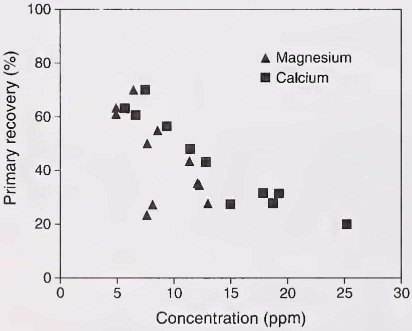

Figure 3.10 Relation between bitumen recoveries and soluble divalent ions due to aging in the secondary tailings. From E.C. Sanford, Ref. 17. © 1983, Canadian Society for Chemical Engineering.

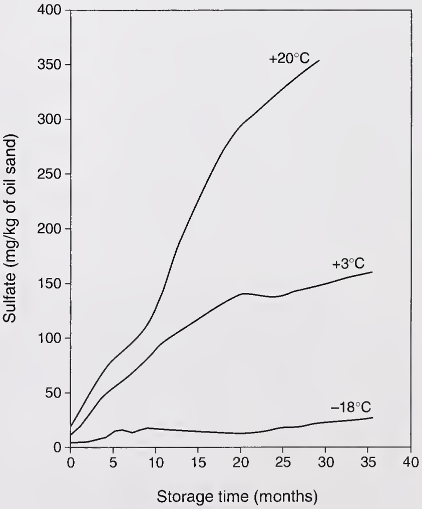

Figure 3.11 Rate of sulfate production as a function of time at different storage temperatures. After D. Wallace *et al.*, Ref. 11.

cations (H^+, Fe^{2+}, Fe^{3+}, Ca^{2+}, Mg^{2+}) in the water would increase the binding between bitumen and sand and therefore exert an adverse effect on the processability of the oil sand. Thus, the monitoring of the sulfate or, more appropriately, the metal (sodium, potassium, calcium, magnesium) and hydrogen cation concentrations in the connate water provides an indicator for the oxidative history of the oil sand sample and a basis for the prediction of its hot water processability.

The role of *pH* in the hot water process is related to the naturally present surfactants in the oil sands. These surfactants are mainly acidic compounds, carboxylic and reportedly sulfonic acids,[15,18] which can be activated by salt formation with a strong base like sodium hydroxide to form the carboxylate (and sulfonate) anions which are the actual surfactants:

$$\begin{array}{lcl} \mathrm{RCOOH} & \rightleftharpoons & \mathrm{RCOO^- + H^+} \\ \mathrm{NaOH} & \rightleftharpoons & \mathrm{Na^+ + OH^-} \\ \mathrm{H^+ + OH^-} & \rightleftharpoons & \mathrm{H_2O} \\ \hline \mathrm{RCOOH + NaOH} & \rightleftharpoons & \mathrm{RCOO^- + Na^+ + H_2O} \end{array} \quad \begin{array}{r} (5) \\ (6) \\ (7) \\ (8) \end{array}$$

The introduction of these ions then alters the stability of the oil sand structure by modifying the interfacial tensions and the electric charges at the interfaces thereby affecting the separability of the bitumen from the sand. It has been shown that there exists an optimum (critical) concentration for the natural surfactants present in the oil sand below or above which the recovery of bitumen would decrease. This optimum concentration is obtained by adding a judicial amount of NaOH to the oil sand slurry. Divalent carbonates (siderite $FeCO_3$, $MgCO_3$, $CaCO_3$) divalent clays and divalent sulfates present in the sand can consume NaOH via reactions of the type

$$\mathrm{MCO_3 + NaOH + H_2O \longrightarrow M(OH)_2\downarrow + NaHCO_3}, \tag{9}$$

where M can be Ca^{2+}, Mg^{2+} or Fe^{2+}. The M^{2+} ions produced then can react further with the carboxylate surfactant

$$\mathrm{M^{2+} + 2\ R{-}CO_2^- \longrightarrow (R{-}CO_2)_2M\downarrow} \tag{10}$$

causing their removal from the solution and the interface. Calcium carbonate and magnesium carbonate are both apparently soluble enough and reactive enough to cause the additional undesirable effect of reducing the concentration of carboxylate ion surfactants, with the need for more NaOH consumption for the regeneration of the surfactant *via*

$$\mathrm{(R{-}CO_2)_2\,M + 2\ NaOH \longrightarrow M(OH)_2 + 2\ RCO_2^- + 2Na^+}. \tag{11}$$

Some solid calcium and magnesium carboxylates are also naturally associated with the mineral phase of the oil sand from which the carboxylate ion surfactant can also be liberated by reaction (11).

1.1 Interfacial properties

Oil sands, being complex multiphase systems, exhibit properties and behavior which can be profoundly influenced by interfacial phenomena. Some of these interfacial phenomena can arise from the presence of electric charges in the bulk of the water and at the interfaces, while others are manifestations of internal cohesion forces. The structure of oil sand and its behavior during the hot water separation of the bitumen is governed by the interfacial relationships between the components—bitumen, aqueous phase, minerals, gases. For an understanding of oil sand structure and behavior during separation it is necessary to consider the energetics of the interfaces between the components, the effect of charges present, and the influence of such variables as *pH*, temperature and the presence of ions.

1.1.1 Interfacial tension

Surface or interfacial tension is the contractile force that exists in the boundary between two or more phases at equilibrium and is a direct manifestation of the action of intermolecular forces. Molecules at the surface of a liquid or a solid are subjected to unbalanced molecular forces and therefore possess additional energy, compared to the molecules in the interior. In liquids, the surface energy acts as an internal force which tends to reduce the surface area to a minimum. (In solids, owing to the lack of mobility at the surface, this additional energy is not directly observable and has to be measured by indirect means.) The excess surface energy is measured in units of force per unit length or energy per unit area:

$$\mathrm{J \cdot m^{-2} = N \cdot m^{-1}} \tag{12}$$

or on the more convenient scale,

$$\mathrm{mJ \cdot m^{-2} = mN \cdot m^{-1}\ (= erg \cdot cm^{-2} = dyn \cdot cm^{-1}\ in\ cgs\ units).} \tag{13}$$

The contractile force at the interfaces between a liquid and a gas (usually air), a liquid and a solid, or a solid and a gas is referred to as surface tension. The contractile force between two immiscible liquids is known as interfacial tension.

The determination of interfacial and surface tension is based on either of two principles (or a combination of them): measurement of the force required to create new interfacial areas and measurement of the shape of a droplet exposed to the influence of a known force.

One manifestation of surface tension is the capillary effect, the rise or lowering of the liquid level and the shape of a liquid surface in a capillary column. If the liquid level rises, the liquid wets the capillary surface and the contact angle which the liquid makes with the tube walls is <90°, resulting in a concave meniscus. Nonwetting liquids give contact angles >90° with a convex meniscus and their level in the capillary tube is depressed. The capillary pressure, P_c, is related to the surface tension, γ, by the equations

$$P_c = \frac{2\gamma \cos\theta}{r};\ P_c = \gamma\left(\frac{1}{r_1} + \frac{1}{r_2}\right);\ \text{and}\ P_c = \frac{2\gamma}{r} \tag{14}$$

where θ is the angle of contact and r is the radius of the capillary, Figure 3.12. Measurement of the contact angle, usually on a small surface of the solid, is a common method of determining wettability. For aqueous solutions contact angles of less than 90° indicate preferential water-wet conditions and contact angles greater than 90° indicate preferential oil-wet conditions. The sand in Alberta oil sands is usually water wet except after solvent extraction when its natural state could have been altered but can be restored by acid or heat treatment. Some relevant surface and interfacial tension values are listed in Tables 3.4[19,20] and 3.5[21] and are plotted in Figure 3.13 as a function of temperature. The surface tension of bitumen is dependent on the mode of extraction from the oil sand, which is not unexpected since the amount of surfactants in the bitumen may well vary with the extraction mode and the nature of the solvent. A low-boiling solvent (CS_2 or CH_2Cl_2) is easier to remove from the extracted bitumen without incurring the loss of the volatile components of the bitumen than a higher-boiling solvent. Per definition,

Table 3.4 Surface tensions (mN·m^{-1}) of pure liquids, Athabasca bitumen, Alberta and Utah bitumens, and some solids

Liquids	γ (20 °C)	Liquids	γ (20 °C)
pentane	16.0	thiophene	31.4
octane	21.8	tetralin	35.2
cyclohexane	25.0	thiolane	35.8
toluene	28.5	thiane	36.1
benzene	28.8	pyridine	38.0
ethylbenzene	29.0	naphthalene	40.6
decalin	29.9	phenol	40.9
o-xylene	30.3	quinoline	45.0

Water[19a]		Athabasca bitumen[19a]			
			γ		
t (°C)	γ	t (°C)	Centrifuged*	Hot water extracted*	Solvent extracted+
0	75.6	40	32.0		
20	72.8	50	31.2		
40	69.6	60	30.4	29.6 (64°C)	23.6 (64°C)
60	66.2	70	29.7	28.3 (75°C)	22.6 (75°C)
80	62.6	80	28.9	25.6 (104°C)	19.0 (104°C)
100	58.9	90	28.2	25.0 (112°C)	18.1 (112°C)

Alberta and Utah bitumens[19b]	*A*, 60°C, mN·m^{-1}	*B*, mN·m^{-1}·t^{-1}
Whiterocks	20.6±0.2	–0.077±0.002 (40–77°C)
Sunnyside	21.3±0.2	–0.063±0.001 (68–83°C)
PR Spring	31.2±0.2	–0.097±0.001 (49–83°C)
Asphalt Ridge	28.9±0.2	–0.078±0.001 (50–79°C)
Circle Cliffs	29.3±0.2	–0.093±0.002
Athabasca	27.2–29.6 (64°C)	–(0.19–0.095) (40–112°C)
Peace River	22.0–29.2	–(0.048–0.072) (40–90°C)
Pelican Lake	24.0–30.9	–(0.044–0.078) (40–90°C)
Fort McMurray	22.2–30.6	–(0.050–0.082) (40–90°C)

Solid	γ^{20}	Solid	γ^{20}
organoclays	22–26	fresh coal surfaces	35–60
polyethylene	31	kaolinite	170–203
graphite	33	bentonite	166–229
polypropylene	34	montmorrilonite	179–221
polystyrenes	30–40	marble	198–205
polyesters and polysilanes	40–45	silica	129–259
humic matter in oil sands	42.7–48.6	magnesium oxide	1090
		calcium oxide	1310

*g = 35 – 0.076 t (°C) mN·m^{-1}; +g = 29 – 0.074 t (°C) mN·m^{-1}. Some crudes show deviation from linear temperature dependence and above a certain temperature the trend may even reverse resulting in rising interfacial tensions with rising temperature, Ref. 21.

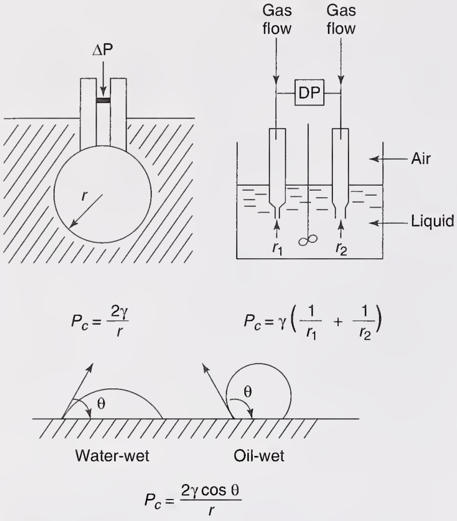
ΔP
r
$P_c = \frac{2\gamma}{r}$
Gas flow
Gas flow
DP
Air
Liquid
r_1
r_2
$P_c = \gamma\left(\frac{1}{r_1} + \frac{1}{r_2}\right)$
θ
θ
Water-wet
Oil-wet
$P_c = \frac{2\gamma \cos\theta}{r}$

Figure 3.12 Schematic illustration of the relation between capillary pressure, P_c, and surface tension γ.

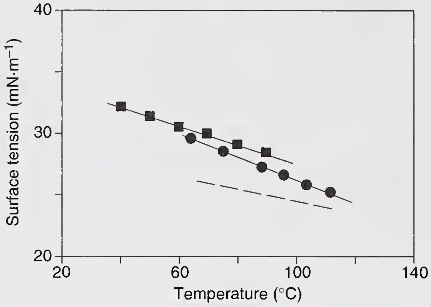

Figure 3.13 Effect of temperature on the surface tension of Athabasca bitumen samples obtained by centrifugation (■) and commercial hot water extraction (●); the dotted line corresponds to predicted values based on the principle of corresponding states. From K. Takamura and E.E. Isaacs, Ref. 21.

Table 3.5 Interfacial tensions (mN·m^{-1}) of solvent-extracted sand particles and some crude oils[a]

Solvent-extracted Athabasca sand particles[a]	γ
solid–air	36–38
solid–aqueous phase	75
solid–bitumen	88–90

Crude oil	γ	
	Distilled water	Produced water
Bonnie Glen[b]	21.1	26.4
Wainwright[b]	26.0	20.8
Epping[b]	27.1	22.0
Chauvin[b]	17.2	4.5
Lloydminster[b]	26.8	15.4
Cold Lake (bailed)[b]	15.7	–
Cold Lake (produced)[c]	15.0	7.4
Judy Creek[b]	21.9	20.5
Athabasca[d]	15.0	–

[a] From K. Takamura and E.E. Isaacs, Ref. 21. [b] Measured at 23°C; [c] Measured at 40°C; [d] Measured in D_2O at 50°C.

solvent extraction dissolves only the bitumen from the ore, whereas alkaline hot-water extraction would be expected to partially mobilize the sand-bound humic acids, fulvic acids and the various bound carboxylic acids (*cf.* Chapter 8) and to generate carboxylic acids (carboxylate ions) and alcohols by the partial hydrolysis of esters in the bitumen. Parallel to these processes, some loss of surfactant precursors from the bitumen may occur through transfer to the water phase. Data from the same laboratory[19a] indicate that the interfacial tension between water and a toluene solution of bitumen is about 10% lower for hot-water extracted *vs.* solvent-extracted bitumen, signifying the presence of higher concentrations of surfactants in the former sample. (Data from different laboratories may not be directly comparable.)

The surface tension of low-MW hydrocarbons, especially of *normal* alkanes and of low-MW petroleum fractions, increases with increasing molecular weight. Hydrocarbon-based polymers have surface tensions in the 30–40 $mN{\cdot}m^{-1}$ range whereas the values for polymers with oxygen-containing functional groups are in the 35–50 $mN{\cdot}m^{-1}$ range (Table 3.4). While the 20°C extrapolated surface tension of Athabasca bitumen, 27.5–33.5 $mN{\cdot}m^{-1}$, is not as high as would be expected on this basis, it is still in the upper range of the values for pure hydrocarbons.

The effect of increasing temperature on the surface tension of bitumen, as for all pure compounds, is to lower the surface tension. For the large majority of pure compounds the surface tension is a linear function of temperature and varies according to the general equation $\gamma = A - B\ t(°C)$, where A and B are molecular constants. The surface tension of bitumen also obeys this equation with $A = 29–35\ mN{\cdot}m^{-1}$ and $B \approx 0.075 \pm 0.001\ mN{\cdot}m^{-1}{\cdot}t^{-1}\ (°C)^{-1}$ (Table 3.4).

For bitumens and heavy oils in water, interfacial tensions (Table 3.5) are lower than surface tensions (Table 3.4). The reason for this is that, at the oil/water interface, the carboxylic acid type surfactants are activated by dissociation to a carboxylate anion and a hydrogen (sodium) cation or, by reacting with a nitrogen base present, a nitrogen base cation forming an electric double layer—much like a soap at an oil/water interface—causing a lowering of the interfacial tension.

Some approximate surface tension values for sand particles from solvent-extracted Athabasca oil sands have also been reported (Table 3.5). The values measured for the sand-air tension, 36–38 $mN{\cdot}m^{-1}$, are much lower than the values reported for silica or clay minerals, 129–259 and 166–229 $mN{\cdot}m^{-1}$, and in effect are closer to those reported for organoclays, 22–26 $mN{\cdot}m^{-1}$. This may be due to modifications of the sand particle surfaces caused by the organic solvent-insoluble organic coating.

The extent of dissociation of the natural surfactants and thereby the interfacial tension is expected to be affected by the *pH*. That this is indeed the case is seen in Figure 3.14. The steep drop in interfacial tension between *pH* ~10.0 and ~12.0 is thought to be related to the destruction of the negative charge on the oil droplets by the increased ionic strength of the aqueous solution and the formation of oil-in-water emulsion. *cf.* also Appendix 3.1. The concentration of NaOH which results in the so-called ultralow interfacial tension, $10^{-2} - 10^{-4}$ $mN{\cdot}m^{-1}$, varies with the type of crude and the salt concentration in the aqueous phase.

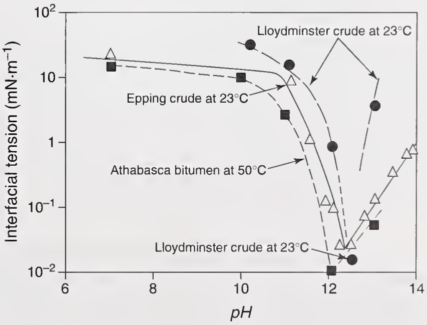

Figure 3.14 Effect of *pH* on the interfacial tensions of bitumens and heavy oils. From K. Takamura and E.E. Isaacs, Ref. 21.

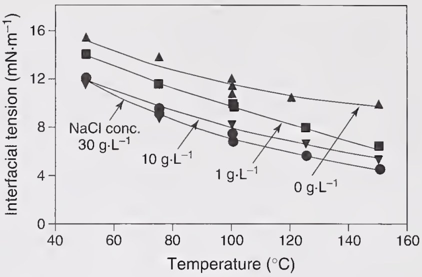

Figure 3.15 Influence of temperature and salinity on the interfacial tension of Athabasca bitumen in D_2O. From K. Takamura and E.E. Isaacs, Ref. 21.

Foreign ions from salts such as NaCl alter the interfacial tension by changing the electrical properties of the interface (*v.i.*). For example, the interfacial tension of Athabasca bitumen in heavy water (D_2O) decreases with increasing concentration of NaCl in the water, Figure 3.15. On the other hand, in the presence of NaOH the addition of NaCl has the opposite effect, it increases the interfacial tension, as will be seen below for the example of a Lloydminster heavy oil.

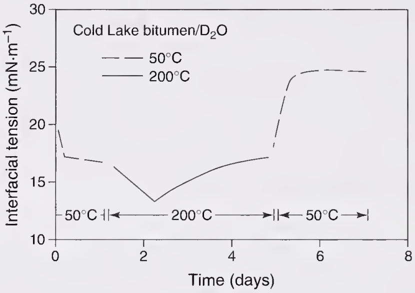

Figure 3.16 Evolution of interfacial tension for a bitumen drop in D_2O measured in sequence at 50, 200 and 50°C. From K. Takamura and E.E. Isaacs, Ref. 21.

Acid-base reactions in homogeneous aqueous solutions are very fast, practically instantaneous processes. At the bitumen/water interface, acid-base reactions are expected to be very fast as well. However, most of the acids are present not in the interface but in the bulk bitumen and are transferred to the interface by diffusion, which is a slow process. The evolution of interfacial tension for a bitumen drop in D_2O in Figure 3.16 illustrates the point. The initial drop in the interfacial tension is due to the diffusion of the acids to the interface. When the supply of acids is exhausted, a near stationary value is reached. Raising the temperature from 50 to 200°C causes a further drop in the interfacial tension as a result of the temperature effect, the mobilization of more surfactants by the increased rate of diffusion, perhaps by the hydrolysis of esters and the dissociation of asphaltene aggregates. Later, a reversal takes place due to the degradation and transfer of the interfacially-active material into the bulk aqueous phase and, after reducing the temperature to 50°C, the interfacial tension is higher than it was initially. (Owing to the extended duration of the experiment, photochemical processes taking place at the oil/water interface could have affected the observed changes (*v.i.*).) Another illustration of the temporal behavior of interfacial tension of small droplets of oil is shown in Figure 3.17a for Lloydminster heavy oil and deasphaltened heavy oil in 0.1% NaOH.[22] In these cases the rate of change in interfacial tension is much steeper than without added NaOH, Figure 3.16, and a shallow minimum is featured in both cases in the ultra-low region reached. It can also be observed that the interfacial tension increases upon addition of 0.15% NaCl or removal of the asphaltene from the oil.

The temporal behaviors of the various compound class fractions of the oil (saturates, aromatics, resins and asphaltene) have been found to exhibit somewhat similar responses. For example, resins in toluene solutions, Figure 3.17b, were observed to undergo very rapid drop in interfacial tension followed by a more gradual increase after 50 seconds. The increase is attributable to the depletion of surfactants from the interface by transferance into the bulk aqueous phase.

The kinetics of interfacial tension variation with time have also been investigated. Thus, toluene solutions of Athabasca (Syncrude) bitumen in aqueous NaOH were found to obey the equation derived on the Langmuir model for surfactant adsorption/desorption kinetics at the interface

$$\gamma = \gamma^{E} \exp\left(A \exp\left(-k_{L}{}^{t}\right)\right), \qquad (15)$$

where γ^E is the equilibrium interfacial tension, A is a constant and k_L is the Langmuir constant. Plots of interfacial tensions for various concentrations of bitumen as a function of time and bitumen concentrations are shown in Figure 3.17c and d. As seen in the concentration range of 0.1–10% bitumen, the drop in interfacial tension is larger and faster for the more concentrated solutions owing to larger amounts and more rapidly available surfactants. Also, the equilibrium interfacial tension values are lower for the more concentrated bitumen solutions, Figure 3.17d,

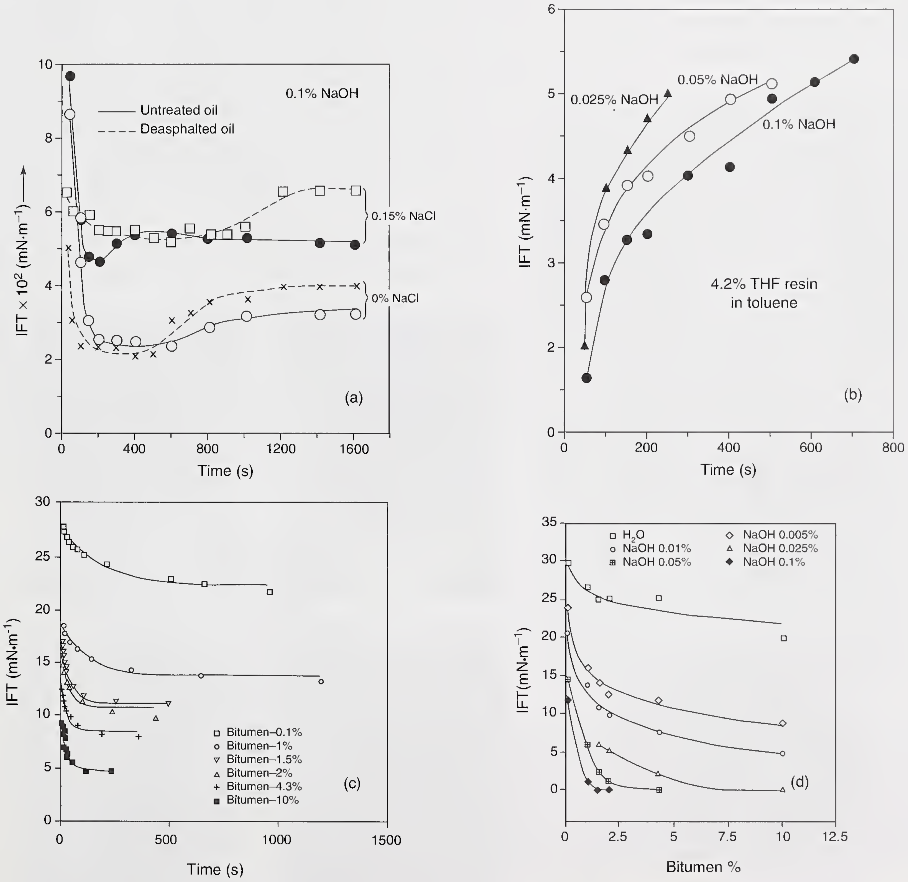

Figure 3.17 (a) Effects of interfacial age and NaCl on the interfacial tension between Lloydminster heavy oil and a 0.1% NaOH solution. From K.C. Khulbe *et al.*, Ref. 22a. (b) Effects of interfacial age on the interfacial tension between a THF resin-in-toluene mixture and various NaOH solutions. From K.C. Khulbe *et al.*, Ref. 22a. (c) Experimental data and Langmuir model fitted results for dynamic interfacial tension (IFT) of 0.01% NaOH solution and various bitumen–toluene solutions. The solid lines are Langmuir model fitted results. From Y. Xu, Ref. 22b © 1995, American Chemical Society. (d) Equilibrium interfacial tension (IFT) as a function of bitumen and NaOH concentrations. From Y. Xu, Ref. 22b. © 1995, American Chemical Society.

and in the more concentrated NaOH solutions. At higher NaOH concentrations equilibrium interfacial tension values are reached at lower bitumen concentrations. All plots appear to be describable by equation (15) except at longer elapsed times when the experimental data points in Figure 3.17c begin to deviate slightly from the kinetic model. The possible cause has been attributed to the different size and diffusion rate of the surfactants. However, loss of surfactants in the interface and the change in the chemical composition and efficiency of surfactant molecules in the interface with time should play a major role here as well.

A complicating circumstance in the measurement and interpretation of interfacial phenomena in crude oil/water systems is the formation of viscous interfacial films at the oil (bitumen)/water interface. Drops of Athabasca bitumen placed on a glass surface and immersed in water after 1–15 days standing develop a brown interfacial film and begin to wet the glass.[23] A few days after the formation of the film, the nearly spherical drops collapse onto the test surface into a flat pancake-like shape, Figure 3.18 (A and B)[23]. Film formation at the surface of drops of bitumen pendants in distilled water can only be observed upon irradiation of the drops with light, Figure 3.18. Elongation of the drops appears to be caused by a reduction of interfacial tensions which accompany film formation.[19d,23] Variations in the interfacial tension are mild in the absence of light but upon irradiation, a marked reduction in interfacial tension takes place, Figure 3.19, which is accompanied by a decrease in the *pH* of the aqueous phase. IR spectra of the aqueous phases from the irradiated and nonirradiated systems revealed the presence of carboxylic acids in the former but not in the latter. Film formation and changes in interfacial tension in the photochemical experiments are relatively slow processes compared to those observed in studies where, instead of distilled water, dilute NaOH solutions were used, *e.g.*, Figure 3.17.

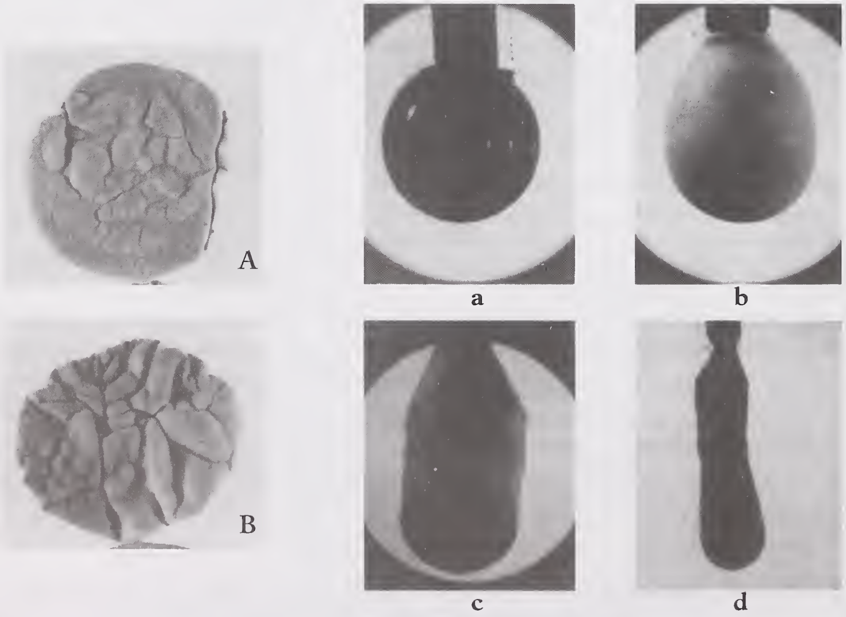

Figure 3.18 (Left): View of a collapsed drop of bitumen as seen from the top of the aqueous phase. The folding and ridge formation of the membraneous film is clearly visible after (a) 20 days, and (b) 40 days. (Right): The effect of time on the formation of interfacial film at the surface of a drop of bitumen pendant in distilled water. Photographs of the drop were taken after exposure to light for 0 (a), 4 (b), 11 (c) and 40 (d) days. From E.E. Isaacs and D.N. Morrison, Ref. 23.

Interfacial film creation has also been reported[24] in the reverse system* of micrometer size water droplets in *n*-heptane/toluene diluted bitumen. Film formation here was detected by a crumpling of the adsorbed surface layer on the water droplets upon reducing the surface area by deflating the droplets with the aid of a micropipette, Figure 3.20. Interfacial films formed at low bitumen concentrations (<1%) in the solution are rigid and tend to crumple on deflation, whereas films formed on water droplets at higher bitumen concentrations are fluid and flexible; they do not crumple, but rather disperse into small droplets upon deflation (budding), Figure 3.21.[24] Two additional properties manifested by the interfacial film at higher bitumen concentrations in the solution (up to 10%) are the slow shape recovery of the water droplets after being stretched, and the stability of the droplets with respect to coalescence—although interdroplet adhesion, which can lead to floc formation, begins to appear.

The technique of handling micrometer-size droplets in liquids has led to the development of a micromethod for the measurement of interfacial tension using a single micrometer-size droplet.[26] As illustrated in Figure 3.22, a droplet is axially stretched between two micropipettes and the change in length and the force applied as observed under a microscope are read and from these data the interfacial tension is calculated.

A better understanding of the properties of microemulsions is important for the development of improved methods for the removal of trace amounts of connate water from the bitumen. Connate water is the residue of sea water which is highly corrosive owing to the presence of high concentrations of chloride ions. Therefore, it is necessary to keep the level of water concentrations in the bitumen as low as possible.

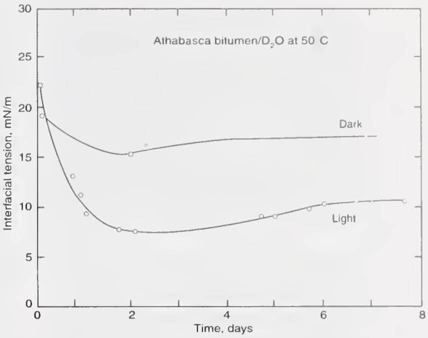

Figure 3.19 Evolution of interfacial tension for sessile drops of bitumen in D_2O at 50°C. The sample kept in the dark was exposed to light only during measurement. From E.E. Isaacs and D.N. Morrison, Ref. 23.

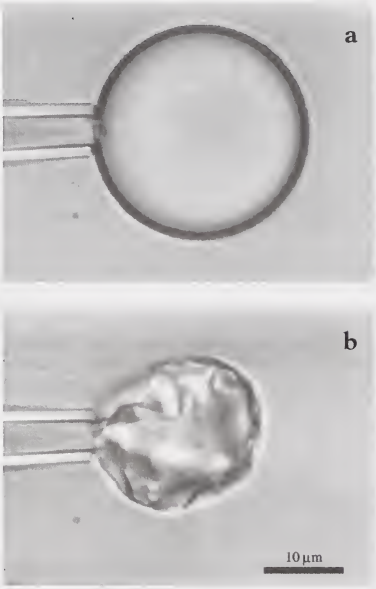

Figure 3.20 Deflating an emulsion drop using a micropipette. The surrounding oil phase contains 0.1% bitumen. The “protective” layer, which results from the adsoprtion of crude oil’s natural surfactants onto the oil–water interface, is revealed as the droplet area is reduced. From A. Yeung *et al.*, Ref. 24. © 1999, The Royal Society.

---

*The reverse system refers to reverse micelles in which surfactants in nonpolar solvents aggregate with their polar head groups pointing inward and their lipophilic end projects outward. The most important property of the reverse micelles is their ability to encapsulate a fairly large amount of water to form a “microemulsion”. The water confined in the water pool of the microemulsion differs from ordinary water in a number of ways owing to its highly organized structure constructed from “bound”, “free” and “trapped” water molecules (*cf.* also Chapter 14).

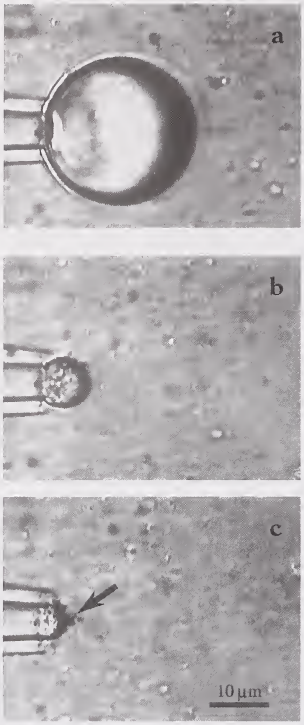

Figure 3.21 Deflating a water drop in 10% bitumen. Here, no interfacial crumpling is observed. Instead, small water droplets are seen to detach from the mother drop. The arrow in (c) points to several water droplets that have just come off the surface. From A. Yeung *et al.*, Ref. 24. © 1999, The Royal Society.

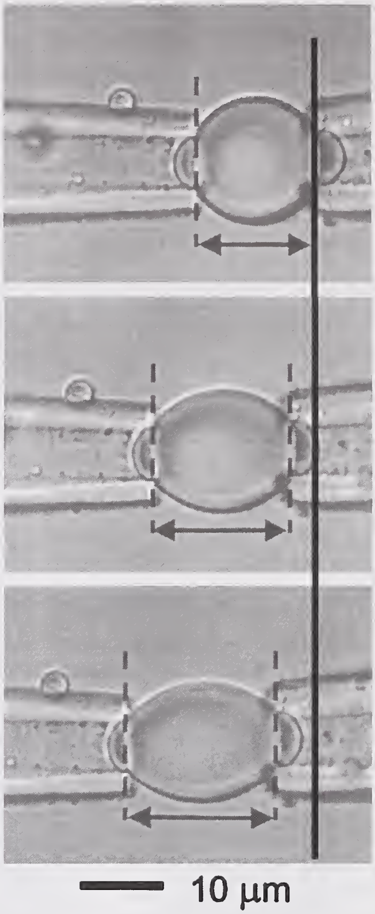

Figure 3.22 Photographs of an actual drop stretching experiment. In this case a water droplet is being elongated while submerged in chloroform. The pipette on the right is a flexible cantilever. From the deflection of the cantilever, as evidenced by its tip positions relative to the solid vertical line, the stretching force can be determined. The length of the stretched drop is also obtained from these images (shown by the arrows). From K. Moran *et al*, Ref. 26. © 1999, American Chemical Society.

The rate at which the time-dependent bitumen/water interfacial tension changes at the macroscale from an initial γ_i to a final equilibrium value γ_f, defined as the spreading rate parameter, $SRP = (\gamma_i - \gamma_f)/t$ (where t is the time required for the change) is a function of the nature and concentration of the surfactant present and has been correlated with the stability of water-in-oil emulsions.[27] SRP may be used to predict the rate of water recovery from water-in-oil emulsions upon centrifugation.

The surface tension of the aqueous phase of the water-oil sand slurry is also an important parameter in the hot water separability of the bitumen.[28] Its value is also affected by *pH*, Figure 3.23, and decreases nearly linearly with increasing *pH*.[19c]

Surface and interfacial tensions are of paramount importance to the two essential steps of the hot water separation process: the detachment of the more or less continuous bitumen layer filling the pores of the mineral matrix from the mineral grains and the flotation of the separated bitumen droplets to the surface froth. As bitumen is displaced from the sand grains, the interfacial area between bitumen and water decreases and the work needed to increase the surface of the system must obey the inequality

$$\gamma_{BS} + \gamma_{BA} > \gamma_{SA} \qquad (16)$$

(where BS = bitumen-sand, BA = bitumen-aqueous phase and SA = sand-aqueous phase) as derived on the basis of a decrease in the free energy of the system for a spontaneous process. If the reported values in Table 3.5 for the surface tensions γ_{BS} = 88 mN·m^{-1} and γ_{SA} = 75 mN·m^{-1} are correct then the inequality applies for all values of γ_{BA} and the displacement process is thermodynamically favorable under all realistic conditions.

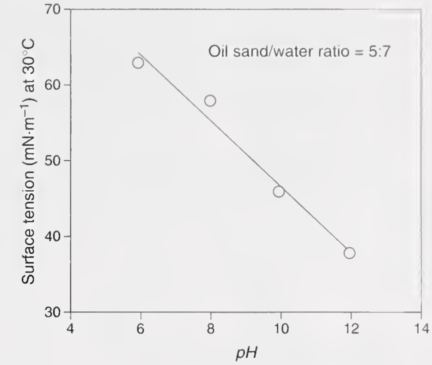

Figure 3.23 Effect of *pH* on the aqueous/vapour surface tension of an oil sand–aqueous slurry. Data from C.W. Bowman, Ref. 19c.

Even though the separation of bitumen is thermodynamically favorable at all values of γ_{BA}, the initial retraction of bitumen from sand grains, which is governed by the capillary force, is faster for high values of γ_{BA} and thus the process is more efficient. Also, under these circumstances the bitumen droplets formed are larger and they can be recovered more efficiently because of their greater upward velocity in flotation. (This velocity is proportional to the square of the droplet radius and therefore large droplets are desirable.) Also, the large size increases the likelihood of air attachment and encapsulation. Thus, a high value for γ_{BA} is beneficial in both the separation of bitumen from sand grains and the subsequent flotation of bitumen droplets.

For the flotation of bitumen, the surface tension criteria are:

$\gamma_{BA} + \gamma_{AV} > \gamma_{BV}$ for contact attachment, and

$\gamma_{BA} + \gamma_{BV} < \gamma_{AV}$ for filming,

Figure 3.24[29] (where AV = aqueous phase-vapor and BV = bitumen-vapor). From the data in Tables 3.4 and 3.5 and Figure 3.24 it can be estimated that both inequalities are satisfied under all applicable conditions and therefore both mechanisms may be operative. However, surface charges on the bitumen and air bubble* may introduce a thermodynamic or kinetic barrier and other factors such as viscosity and coagulation of fine solids may also play a role (*v.i*).

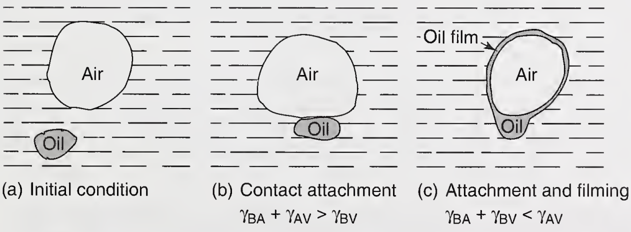

(a) Initial condition (b) Contact attachment $\gamma_{BA} + \gamma_{AV} > \gamma_{BV}$ (c) Attachment and filming $\gamma_{BA} + \gamma_{BV} < \gamma_{AV}$

Figure 3.24 Models for oil flotation. A = aqueous phase, B = bitumen, V = vapor phase. From J. Leja and C.W. Bowman, Ref. 29. © 1968, Canadian Society for Chemical Engineering.

---

* As has been shown experimentally, gas bubbles have a *pH*- and concentration-dependent negative charge in aqueous electrolyte solutions as well as in surfactant solutions. If the air bubbles are also negatively charged in the hot water system then the electrostatic repulsion between the negatively-charged air bubbles and the negatively-charged bitumen would act against attachment. The forces arising from changes in interfacial tension and interfacial areas would also have to overcome this electrostatic repulsion.[1b]

In the course of the hot water separation process, there are many other factors that influence surface and interfacial energy relationships and thus affect the separability of bitumen. The most important step determining processability has been suggested to be the alteration of the surface energy and the hydrophobic-to-hydrophilic transformation of the clay on the bitumen surface.[17]

Surface tension measurements have been suggested[30,31] for the evaluation of asphaltene aggregation in organic solvents and for the determination of critical micelle concentrations and molecular weights of asphaltene. However, the method has been found to be profoundly affected by trace amounts of moisture[32] in the solvents and to be nonapplicable for the cases of anhydrous solvents.

1.1.2 Electric properties

Interfaces in general are electrically charged and their electric properties are governed by phenomena occurring within an interfacial region that is commensurate in thickness with the connate water film surrounding the sand grains in the oil sands (~10 nm).[21,33] Within this region the chemical and physical properties change rapidly with distance and are sensitive to surface conditions and impurities. The electric charges are related to the presence of ions which can originate from the following processes:

- **dissociation of ionizable groups,** $-COOH$, $-SO_3H$, $\equiv C-OH$, *etc.* on the surface, a process which is strongly *pH* sensitive and is an important source of ions in the basic oil sand–aqueous slurry;
- **ion adsorption,** the unequal adsorption of oppositely charged ions—for example, anionic surfactants such as the carboxylate ($RCOO^-$) ion;
- **ion dissolution**, the unequal adsorption of oppositely charged ions from sparingly soluble crystals—for example, $CaCO_3$;
- **charged crystal surfaces:** when a crystal is broken, surfaces with different properties may be created—for example, clays may have opposite charges on the edges and basal surfaces; and
- **isomorphous substitution**, the exchange of an ion from the crystal surface with another one having different charge; for example, Al^{3+} may replace Si^{4+} on the surface of clays, imparting a negative charge to the surface.

Bitumens and crude oils in water acquire a negative surface charge (and ζ potential) owing to the dissociation of carboxylic acids and perhaps other anionic surfactants; this has important ramifications with regard to their surface and colloidal properties.

a) Electric double layer and the zeta potential of the bitumen/water interface

A charged surface in an electrolyte solution attracts the counter-ions and repels the co-ions. These electric interactions and the thermal motion give rise to an arrangement of the ions in the proximity of the charged surface that is referred to as an electric double layer, Figure 3.25. It consists of a thin immobile layer attached to the surface and a thicker diffuse layer extending up to tens of nanometers. From electrokinetic (electrophoretic, sedimentation potential, electro-osmotic, streaming potential) measurements, it is possible to define an electrokinetic or zeta potential (ζ) which represents a potential at the surface—the shear plane of which is located about 0.5–1 nm from the actual particle surface—that separates the immobilized fluid layer surrounding the particle from the mobile fluid. It is this potential that characterizes the electric behavior of the surface rather than the surface potential. Adsorbed ions can have marked effects on the ζ potential relative to the surface potential, and adsorbed polyvalent ions can even cause reversal of the charge in the immobilized layer, in which case the actual surface potential and the ζ potential have opposite signs.

Zeta potential is an essential static or equilibrium surface property which plays an important role in the colloid chemistry of dispersions determining the stability in the natural microstructure of oil sands and in the hot water extraction of bitumen.

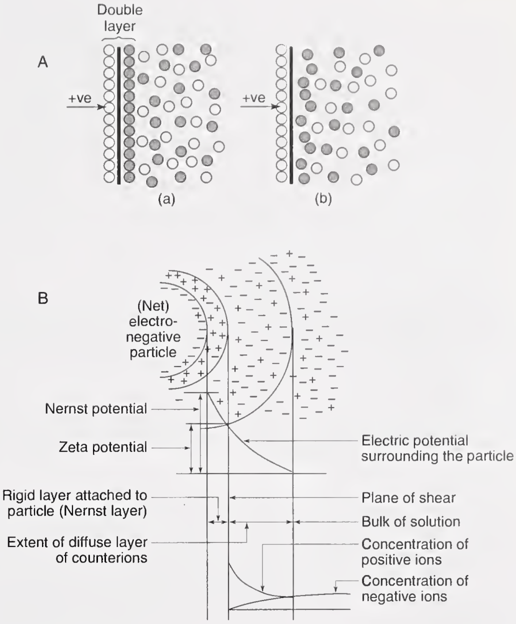
Double layer
A
+ve
+ve
(a)
(b)
B
(Net) electro-negative particle
Nernst potential
Zeta potential
Rigid layer attached to particle (Nernst layer)
Extent of diffuse layer of counterions
Electric potential surrounding the particle
Plane of shear
Bulk of solution
Concentration of positive ions
Concentration of negative ions

Figure 3.25 A. The electric double layer; a) according to the Helmholtz model. b) the diffuse double layer resulting from thermal motion. o, positive charge; ●, negative charge. From J.H. Masliyah, Ref. 33. B. Schematic illustration of the zeta potential. From J.A. Bichard, Ref. 1a.

Computed distributions of Na^+ and Cl^- ions near a negatively charged surface (surface potential Y_o = −160 mV) in a bulk liquid having a NaCl concentration of $10^{-2}M$ at pH 7 are shown as a function of distance from the surface in Figure 3.26. The Na^+ concentration near the surface is about $5M$ whereas the Cl^- concentration is only $2 \times 10^{-5}M$. The plot for Na^+ also describes the distribution of H^+ ions and although the pH of the bulk solution is 7, it is only 4.3 at the surface. In this connection it is important to note that the dissociation of ionizable entities such as carboxylic acids on the surface is determined by the pH in the vicinity of the surface and not in the bulk solution.

The value of the zeta potential for bitumen particles is a function of the nature and concentration of the salts present and the pH of the bulk aqueous phase. Examples of zeta potential variations with pH and added salts are shown in Figures 3.27–3.29. The zeta potentials for the two different Athabasca bitumens show maxima corresponding to ζ ~ −25 to −33 mV at pH ~9.7, where the carboxylic acids are dissociated to carboxylate anions. This is in approximate agreement with the computed fractional dissociation of surface carboxylic groups plotted in Figure 3.30 which predicts complete dissociation near pH 10. At lower and higher pH the double layer is effectively destroyed by high ion concentrations. The rapid decline in ζ above pH 10 coincides with the decline in the interfacial tension of the bitumen, the latter being a consequence of the former.

The effect of cations on ζ is seen in Figures 3.28 and 3.29. All cations have a suppressing effect, and their effectiveness increases with their charge, the trivalent (Fe^{3+}) ions being so effective as to cause a reversal in the sign of ζ.

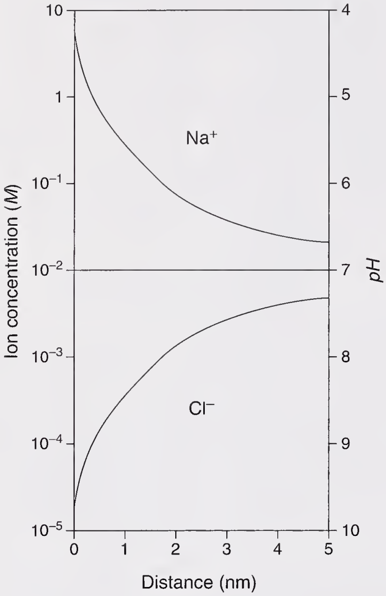

Figure 3.26 Distribution of Na^+, H^+ (*pH*), and Cl^- near the negatively charged surface. Surface potential = –160 mV in 10^{-2}*M* NaCl solution at *pH* 7. From K. Takamura and E.E. Isaacs, Ref. 21.

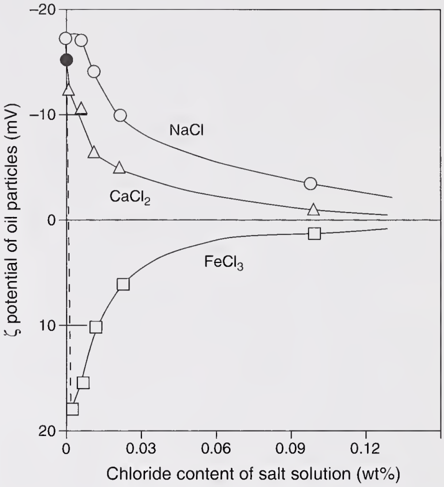

Figure 3.28 Variation of the ζ potential of oil particles with the chloride content of the salt solution. From J.A. Bichard, Ref. 1a.

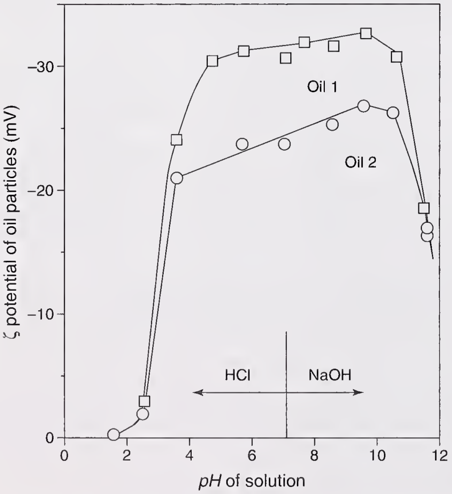

Figure 3.27 Variation of the ζ potential of oil particles from two different Athabasca bitumens with the *pH* of the solution. From J.A. Bichard, Ref. 1a.

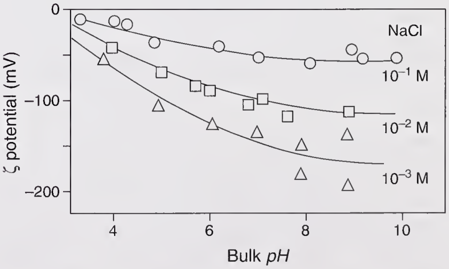

Figure 3.29 Comparison of ζ potentials calculated from measured mobilities (symbols) with those predicted (solid curves) for a bitumen emulsion using the Ionizable Surface-Group Model. From K. Takamura and E.E. Isaacs, Ref. 21.

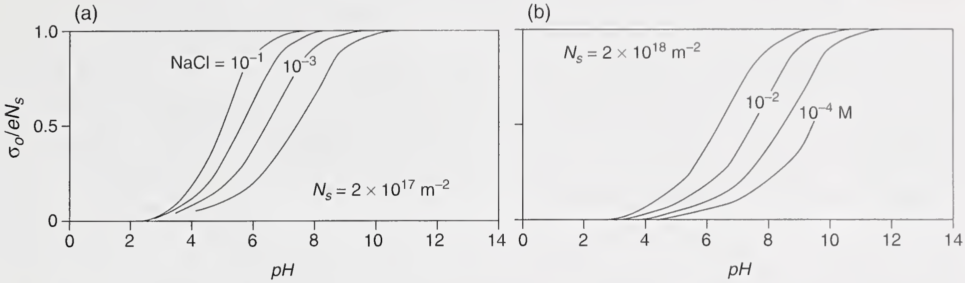

Figure 3.30 Calculated fraction of dissociated surface groups, $-\sigma_o/eN_S$, as a function of *pH* in aqueous NaCl solutions at 25°C. N_S is the total surface density of carboxylic groups and σ is that of the carboxylate ions. From K. Takamura and E.E. Isaacs, Ref. 21.

b) Electric double layer and the zeta potential of the mineral/water interface

The electric properties of the mineral/water interface can also be explained by the ionization of surface groups. The silica surface, for example, has an amphoteric character and can become positively or negatively charged by one of the following two surface ionization steps

$$\equiv\text{Si–OH}_2^+ \rightleftharpoons \equiv\text{Si–OH} + \text{H}^+ \qquad (17)$$

$$\equiv\text{Si–OH} \rightleftharpoons \equiv\text{SiO}^- + \text{H}^+ \qquad (18)$$

with equilibrium constants

$$K_{17} = \frac{[\text{SiOH}]\,[\text{H}^+]}{[\text{SiOH}_2^+]} = 0.6\ (M) \text{ and } K_{18} = \frac{[\text{SiO}^-]\,[\text{H}^+]}{[\text{SiOH}]} = 7.2\ (M)$$

Plots of theoretically and experimentally derived zeta potentials against *pH* are shown in Figure 3.31. The plots indicate that ζ becomes zero at *pH* 2.8 regardless of the electrolyte concentrations. Above the *pH* value corresponding to the point of zero charge (pzc) the surface has a net negative charge and below it, the surface has a net positive charge. The history of the surface (chemically treated, aged, *etc.*) has a major effect on the magnitude and sign of ζ.

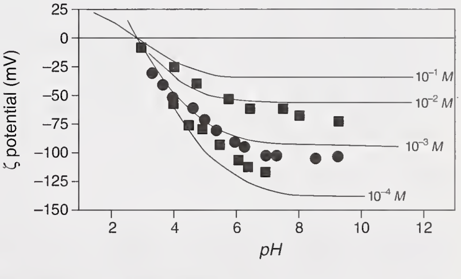

Figure 3.31 Measured (symbols) and calculated (solid curves) ζ potentials of silica in KNO_3 solution. From K. Takamura and E.E. Isaacs, Ref. 21.

Plots of ζ potentials for Athabasca sand grains and carbonate mineral particles as a function of *pH* and $CaCl_2$ concentrations are reproduced in Figures 3.32 and 3.33. Under all conditions the sand grains carry a greater negative charge than the carbonate particles.

A comparison of the computed values of ζ for bitumen, sand and fines near the operating temperature of the hot water separation process (80°C) as a function of the *pH* of the aqueous phase is shown in Figure 3.34. At low *pH* values the attractive electrostatic potential between the fines and bitumen is quite strong, but as the *pH* is increased, the zeta potential of all three kinds of particles becomes strongly negative and they repel one another, a necessary condition

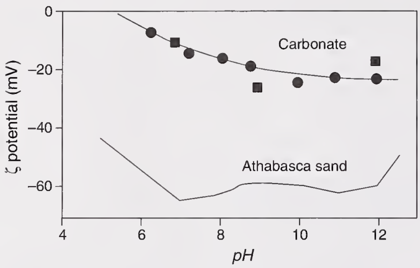

Figure 3.32 ζ potentials of ground carbonate particles (●) in $10^{-2}M$ NaCl as a function of *pH*; ■, after treating the particles in an NaOH solution of *pH* 11.5 for 3 days. Bottom curve: results for Athabasca sand grains under the same conditions. From K. Takamura and E.E. Isaacs, Ref. 21.

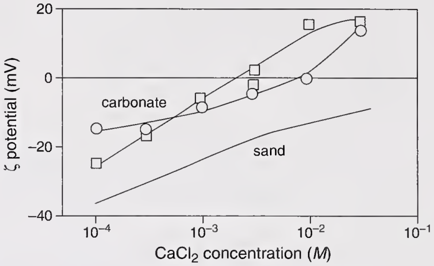

Figure 3.33 ζ potentials of carbonate particles as a function of $CaCl_2$ concentration at *pH* 7 (○) and 9 (□) in the presence of $10^{-2}M$ NaCl. The solid line (no data) is for Athabasca sand grains at *pH* 11.5. From K. Takamura and E.E. Isaacs, Ref. 21.

for good separability. The curve for bitumen may be compared to that in Figure 3.27 obtained at room temperature indicating relatively large differences owing to subtle changes in temperature and NaCl concentration.

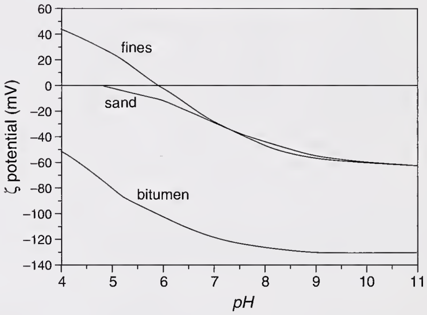

Figure 3.34 Variation of the ζ potential with *pH* at 80°C with 0.01*M* NaCl. From J.H. Masliyah, Ref. 33.

Kaolinite, the main component of clay minerals found in the oil sands, has the curious characteristic of possessing interfacial properties on the face of the crystal that are different from those on the edge:

- the edge is composed of exposed silica and alumina layers and has positive charge at low *pH* and negative charge at high *pH* with a pzc in the *pH* 5–8 range, and
- the face is negatively charged throughout the *pH* range as a consequence of a small degree of isomorphous replacement of cations (*e.g.*, exchange of Si^{4+} with Al^{3+}) within the crystal.

Figure 3.35 shows the variation in zeta potential of the edge of Na-kaolinite (as estimated from the combination of quartz + α-alumina) as a function of *pH*.[34] The pzc occurs at *pH* ~7.4; above this *pH* the edge acquires a negative zeta potential and below it, a positive zeta potential.

As a consequence of the independent electric behavior of the edges and faces in the kaolinite crystal, the kaolinite particle may undergo different kinds of coarsening processes yielding different kinds of coarser particles as indicated in Figure 3.36. At low *pH* values, below the pzc of the edge surface of kaolinite, there is an attractive electrostatic potential between the positively charged edges and the negatively charged surfaces leading to edge-to-face flocculation and a voluminous card-house structure. On the other hand, at high ionic strength, all electrical double layers are compressed and the lowest-free-energy coagulated structure is the one in which the particles are associated in a face-to-face fashion resulting in the card-pack aggregate.

We note at this point that the difference between flocculation and aggregation is not well defined and there is no universally accepted nomenclature. Flocculation is meant to imply a mode of particle association in which the specific surface area of the primary particles is

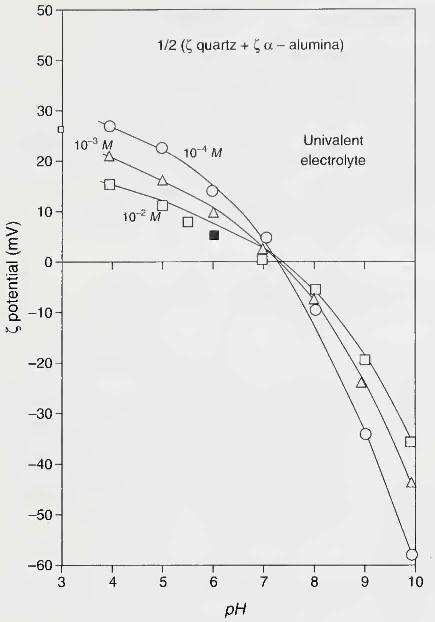

Figure 3.35 Estimated ζ potentials for the edges of Na–kaolinite particles. From D.J.A. Williams and K.P. Williams, Ref. 34. © 1978, Academic Press.

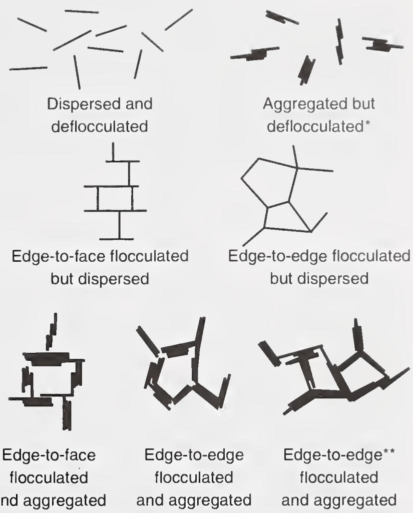
Dispersed and deflocculated
Aggregated but deflocculated*
Edge-to-face flocculated but dispersed
Edge-to-edge flocculated but dispersed
Edge-to-face flocculated and aggregated
Edge-to-edge flocculated and aggregated
Edge-to-edge** flocculated and aggregated

* Face-to-face association, or parallel or oriented aggregation
** Mixed edge-to-edge and edge-to-face

Figure 3.36 Modes of particle association in clay suspensions and the terminology used. From K. Takamura and E.E. Isaacs, Ref. 21.

nearly retained. Aggregation, on the other hand, is a colloidal process in which association leads to the formation of coarser particles with a substantially reduced specific surface area for the particle.[35]

Measurement of the sediment volume as a function of *pH* and electrolyte strength in aqueous kaolinite suspension, Figure 3.37 indicates, in accord with other measurements, that the face-to-edge flocculated structure of high sedimentation volume (and viscosity) formed at *pH* <7 changes to a face-to-face configuration at increased ionic strength, > 0.12*M* NaCl.[36]

1.2 Microstructure of oil sands

In the current model for the microstructure of Alberta high-grade oil sand,[7] most (~70%) of the sand grain surface is covered by a thin connate water film of an average thickness of 10 nm. The stability of this film is derived from the disjoining pressure assumed to be the result of repulsive electrostatic forces and London–van der Waals attractive forces.

In the physical visualization of the disjoining pressure, the force acts within the aqueous film normal to the surface with a positive direction opposing the thinning, that is, compression of the film.

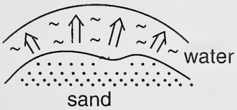

Calculated disjoining pressures as a function of the thickness of an aqueous NaCl film between sand and bitumen surfaces for 30m*M* and 100m*M* NaCl concentrations are plotted[7] in Figure 3.38. The calculated disjoining pressures, depending on the NaCl concentration, have positive values in the 1–17 nm thickness range.[37] Therefore, the aqueous films surrounding the sand grains are predicted to be stable within this NaCl concentration and thickness range, a conclusion which is thought to be in agreement with experience. This substantial disjoining pressure is credited with the retention of the connate water film, that is, the water-wet condition of the sand, in the Athabasca oil sand deposits over geologic time. The variation in the disjoining pressure–NaCl concentration relationship is due mainly to the effect of the Na^+ concentration on the magnitude of ζ. An increase in the Na^+ concentration (at $pH = 5.6$) for example, from 30m*M* to 100m*M* causes the maximum disjoining pressure to rise from 170 to 220 kPa and a contraction in the thickness of the film—that is, the separation distance of the sand and bitumen surface—from about 17 to 10 nm.

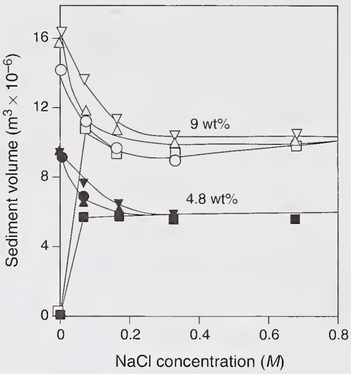

Figure 3.37 Sedimentation volume of Na kaolinite suspensions as a function of NaCl concentration at *pH* 5 (▽,▼), 7 (△,▲), 7.4 (○,●), and 8.5 (□,■). From I.E. Melton and B. Rand, Ref. 36. © 1977, Academic Press.

Figure 3.39 shows the calculated disjoining pressure as a function of connate water thickness in the presence of NaCl, NaOH and $CaCl_2$. At a given value of the disjoining pressure OH^- ions tend to increase the film thickness whereas divalent Ca^{2+} cations tend to decrease the magnitude of the disjoining pressure. At large surface separation distances (> 10 nm) the disjoining pressure drops to near zero. In the presence of $CaCl_2$ at shorter surface separations (≤10 nm), the sign of the pressure changes to negative and that of the force from repulsive to attractive, thus effectively eliminating the force that was responsible for maintaining the water-wet condition of the oil sand.

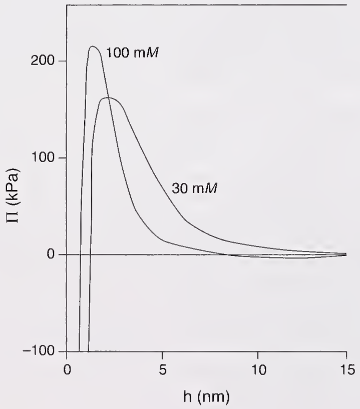

Figure 3.38 Calculated disjoining pressure, Π, of the aqueous film between sand and bitumen surfaces. From K. Takamura, Ref. 7. © 1982, Canadian Society for Chemical Engineering.

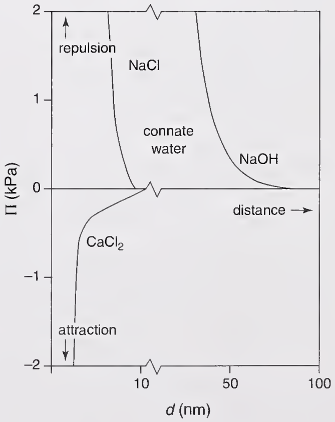

Figure 3.39 Calculated disjoining pressure, Π, of water between sand and bitumen surfaces as a function of separation distance *d*; connate water = 0.1*M* NaCl at *pH* 5.6; NaOH = *pH 11.5;* $CaCl_2$ = 10m*M*. From K. Takamura and R.S. Chow, Ref. 38. © 1983, Petroleum Society of C.I.M.

2.0 Physical Chemistry of the Water Flotation Process

The water bitumen extraction/separation process in current commercial use for the separation of bitumen exploits the water-wet property of the oil sand owing to the presence of the connate water film around each sand grain. There are, according to the temperature of the water employed, two varieties of the process; the hot-water process with T = ~ 82°C, and the cold water process with room temperature water. The former process is older and its physical and colloid chemistry has been investigated in much greater detail.

2.1 The hot water process

In the initial step of the separation process the mined ore is mixed with dilute caustic solution (0.03–0.1% NaOH) at ~82°C in a tumbler. What happens under these conditions[38] is illustrated by the scheme in Figure 3.40. Here, an oil sand particle is represented by two sand grains covered by a bitumen layer. When this aggregate is immersed in hot water the bitumen, partly under the effect of the mechanical shear applied, migrates toward the grain-to-grain contact point where it develops a toroidal shape. The interfacial area between the bitumen and the water is smaller in this configuration and therefore the aggregate is thermodynamically more stable. If the sand is water-wet (*i.e.*, the contact angle θ is less than 90°) a repulsive force develops between the two sand grains until they move apart to a somewhat larger separation. Under the influence of this repulsive force the oil sand matrix may disintegrate and, if the sand grains are covered with water ($\theta = 0°$), the bitumen retracts completely from the sand and detaches as a globule.[39] During this process the excess energy at the bitumen/water interface is dissipated through the viscous flow of the bitumen. Therefore, the criteria for a high rate of bitumen separation are:

i) high negative electric charge on the sand grains and on the bitumen,
ii) high interfacial tension between bitumen and water,
iii) lack of contact between bitumen and sand, and
iv) low viscosity of bitumen.

The amount of energy liberated in the transition from configuration (a) to configuration (b) in Figure 3.40 as a result of the decrease in the bitumen/water interfacial area is proportional to the interfacial tension, hence the requirement for a high value for γ_{BA}.

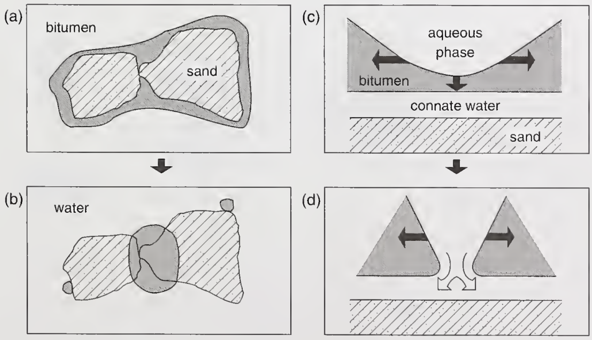

Figure 3.40 Initiation of bitumen displacement. (a) Initially the bitumen layer covers the entire surface of two sand grains. (b) In water, the toroidal shape of the bitumen at the contact point between the grains has a smaller bitumen/water interfacial area and represents the thermodynamically more stable state. (c) A connate water layer up to 10 nm thick exists between bitumen and sand surfaces. (d) Migration of the bitumen (shown by arrows in c) results in mixing of the aqueous phase with the connate water. From K. Takamura and R.S. Chow, Ref. 38. © 1983, Petroleum Society of C.I.M.

A more detailed examination of the initial stage of bitumen separation shows that as the bitumen begins to accumulate at the grain-to-grain contact area, the bitumen film undergoes local thinning, Figure 3.40c. When the bitumen film ruptures, the connate water film mixes with the process water and the stability of the aqueous film is modified according to the *pH*, the electrical charge and the concentration of the electrolytes as discussed above (Figure 3.39).

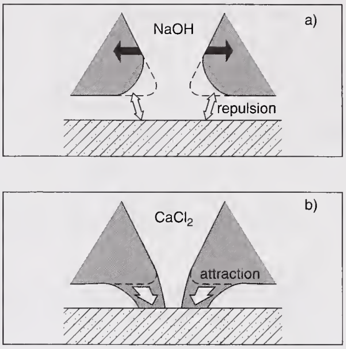

Figure 3.41 Schematic diagram showing the receding of the bitumen envelope on the sand surface (*cf.* Figure 3.38). a) The double-layer repulsion acts together with the capillary forces, thus a high receding velocity is obtained in NaOH solution. b) In $CaCl_2$ solution the van der Waals attractive force leads to contact between the bitumen and the sand and consequently, by opposing the action of the capillary forces, to low receding velocity. From K. Takamura and R.S. Chow, Ref. 38. © 1983, Petroleum Society of C.I.M.

The effects of interfacial forces on the rate of bitumen separation is schematically illustrated in Figure 3.41. In the presence of NaOH the double-layer repulsive force acts together with the capillary forces, thereby enhancing the displacement rate. In contrast, in the presence of $CaCl_2$ or high concentrations of NaCl the sand surface attracts the bitumen, resulting in contact between the sand and the bitumen.

In summary, insofar as the primary separation of the bitumen from the sand is concerned, theory predicts that a basic *pH* of about 8.5 (which increases the negative surface charges on the sand grains and on the bitumen without causing a drop in γ_{BA}), high values for the bitumen/water interfacial tension and the disjoining pressure coupled with a low value for the viscosity of the bitumen (elevated temperatures) will be beneficial. These predictions are in agreement with experimental observations.

In the second step of the separation process the oil globules must be lifted to the surface of an aqueous slurry for collection. Here, it is desirable that the bitumen globules be large (but not too large[17]) because the upward velocity is proportional to the square of the droplet radius.[39] The likelihood of air bubbles attaching to larger droplets and thus further assisting flotation is also increased. The droplet size is governed by the bitumen/water interfacial tension: high values of γ_{BA} favor large droplet size. Thus, as in the detachment of the bitumen from the sand, a high value for the bitumen/water interfacial tension is also favorable in the flotation of the free bitumen droplets to the surface of the slurry.

What may happen if the bitumen droplet size becomes too large, is illustrated on the model oil sand[40] prepared from bitumen, deionized water and (600–850 μm) sand in Figure 3.42. Here it is seen that as the sand particles, while separating from the bitumen, slide down on the surface of the droplet and thereby stretch the droplet until it breaks in the middle. The lower portion of the bitumen droplet is then held down by the sand particles and sinks to the bottom of the separator vessel, resulting in a poor recovery of the bitumen.

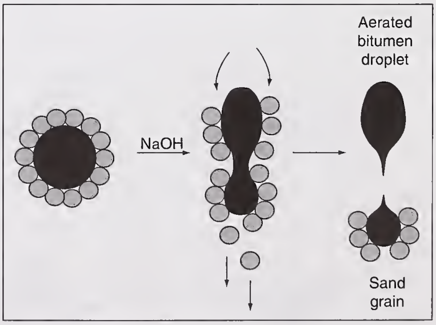

Figure 3.42 Schematic illustration of the fate of an "oversized" bitumen droplet in the hot water separation process.

Flotation efficiency may also be affected by the presence and behavior of fines. The fines in high- and medium-grade ores are suspended in the aqueous slurry, but depending on *pH*, the ions present, ζ potentials, *etc.*, they may coagulate, thereby increasing the viscosity and gel strength of the aqueous phase through which the bitumen must rise. Attachment of the bitumen to the fines solids should also be minimized because large aggregates of fines may trap bitumen and settle to the bottom of the separation vessel.

Conditions for coagulation of the fines can be predicted on the basis of computed potential energy curves calculated from double-layer interaction energies

$$V_t(h) = \int_h^0 \Pi(h)\mathrm{d}(h) \qquad (19)$$

where $\Pi(h)$ is the disjoining pressure and h is the distance between two parallel plates or surfaces. Such computed potential energy curves for fines-fines, bitumen-fines and bitumen-bitumen interactions are displayed in Figure 3.43. Without added NaOH all particle-particle interactions feature substantial barriers for the coalescence of two particles (representing the initial phase and energy barrier of coagulation) and coalescence would not be attainable with the available kinetic energies. In the presence of added sodium hydroxide, however, all the potential energy barriers are lowered and the potential energy barrier for fines-fines interaction would drop to thermally (82°C) plus hydrodynamically (in a stirred reactor) available levels, ≤ 400 *kT* (where *k* is the Boltzman constant), although this limit has been suggested to be too high. However, at 480 mg NaOH per kg oil sand the interpolated energy barrier for fines–fines interaction is only about 240 *kT*, yet experiments with a medium-grade oil sand showed 80% primary bitumen recovery, signifying the absence of fines coagulation. Therefore, 240 *kT* appears to be a sufficiently high energy barrier to prevent fines coagulation. When the same experiment was repeated, but with 300-mg NaCl added, recovery dropped to 37% and the fines-fines energy barrier was computed to be at the readily available 200 *kT* level. At a sufficiently high amount of added NaOH (~1,400 mg) the energy barrier for fines coagulation vanishes altogether, but for bitumen coalescence—a desirable process—the energy barrier is still substantial and it is not possible to reduce this energy barrier without reducing the energy barrier for fines coagulation as well. Thus, the concentrations of Na^+ and OH^- ions are two critical variables affecting the stability of fines particle suspensions. This is illustrated by the computed and directly measured (using the light scattering technique) aqueous suspension stability diagram for 5-µm kaolinite particles shown in Figure 3.44. Here the computed plot shows that above *ca* 60 m*M* Na^+ ion concentrations the suspension becomes unstable with respect to coagulation, and below *ca pH* 6 it is unstable even when the Na^+ ion

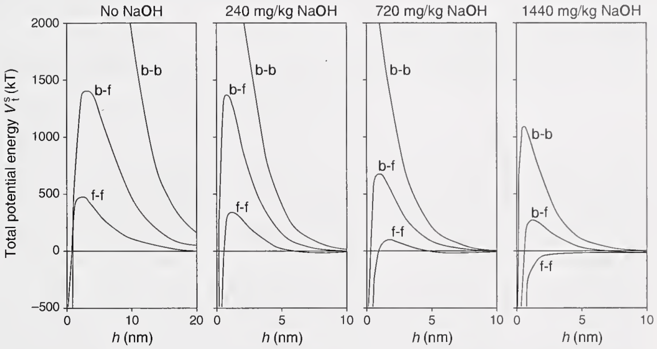

Figure 3.43 The total potential energies, V_t^s, between bitumen and bitumen (b–b), bitumen and fines (b–f) and fines and fines (f–f) particles in a medium-grade oil sand as a function of interparticle distance *h* for various levels of caustic addition. From K. Takamura and D. Wallace, Ref. 39. © 1988, Petroleum Society of C.I.M.

concentration diminishes. Direct measurements gave a stability curve different from the computed one, but when the measurements were repeated in the presence of $10^{-4}M$ sulfonate surfactant (SDS) in the suspension, the measured zone of stability increased to match the computed results. Similar stability curves for the digestion conditions of two different oil sands are shown in Figure 3.45. From the bitumen recovery plots also shown in Figure 3.45 it can be seen that the maximum recovery for the medium-grade ore passes through a maximum for NaOH addition. The recovery of the low-grade ore is low and does not exhibit a maximum because the fines are not stable at any level of NaOH addition.

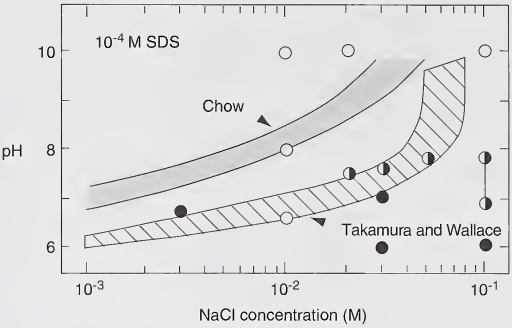

Figure 3.44 Computed stability diagram for 5-μm diameter particles of kaolinite. From K. Takamura and D. Wallace, Ref. 39, © 1988, Petroleum Society of C.I.M., and measured stabilities from R.S. Chow, Ref. 41. Symbols are for systems containing $10^{-4}M$ SDS surfactants. Open, half-shaded and full symbols refer to stable, weakly coagulated and coagulated dispersions.

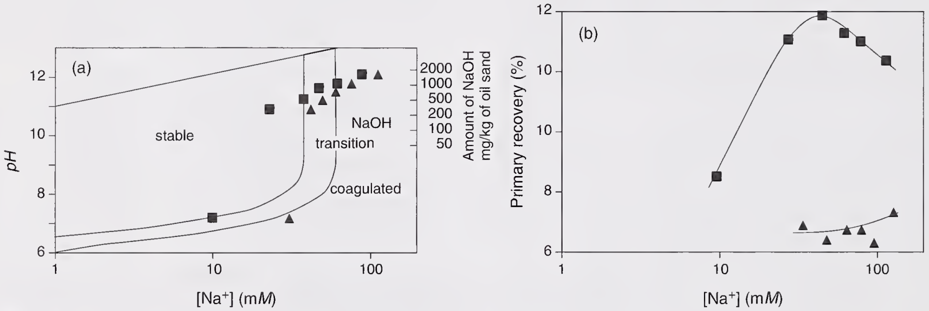

Figure 3.45 (a) Digestion conditions for medium-grade (■) and low-grade (▲) oil sands in response to various amounts of caustic addition. At zero caustic addition the sodium ion concentration depends on the salt content of the oil sand and of the digestion water. (b) The recovery curve for the medium-grade oil sand passes through a maximum caustic addition as predicted by the stability diagram. The recovery curve for the low-grade oil sand does not exhibit a maximum because the fines are not stable at any level of caustic addition. From K. Takamura and D. Wallace, Ref. 39. © 1988, Petroleum Society of C.I.M.

From the combined results of theoretical computational and experimental studies, it has been concluded that during primary separation it is necessary, not only to separate the bitumen from the sand, but also to keep the fines solids dispersed in order to minimize interference with flotation. While these conclusions in general are undoubtedly valid, it should be kept in mind that the calculations were done on pure ideal systems[37] and many of the experiments were carried out on simple model systems. Consequently, the results obtained are not necessarily directly applicable in their entirety to oil sand slurries.

As will be discussed in Chapter 8, all oil sands contain some nonpetroleum type organic matter comprising mainly humins, humic acids and fulvic acids, in addition to monocarboxylic acids chemisorbed to the benzene-insoluble portion of the oil sand. In the case of high-grade (estuarian) oil sand the organic solvent-insoluble organic content is low (~0.1% of the sand or <1% of the total organic matter) and the humic-inorganic complexes exist as colloidal dispersions in the connate water phase. In the case of low-grade (marine) oil sand with 6% bitumen content, the humic content can be as high as 2% of the sand (or ~25% of the organic content) and may contribute to the formation of a moderately hydrophobic solid coating on the sand, the hydrophobicity of which will be dependent on the insoluble organic content. Such oil sands do not lend themselves as readily to water displacement processes as high-grade oil sands.

2.2 The cold water process

This process was developed[42] in connection with the hydraulic pipeline transportation of bitumen and is a relatively new process. It can be operational above 3°C but becomes efficient above 15°C. The bitumen is liberated by mechanical shear input in the oil sand/water slurry and the bitumen particles liberated are raised to the surface by flotation *via* added chemical induced attachment to air bubbles. Thus, it is the combined effect of temperature, mechanical energy and added chemicals that makes it possible to achieve over 90% bitumen recovery in the process. This is in contrast to the hot water separation where the main driving force for flotation is the density differential between bitumen and water maximizing at 82°C.

3.0 Interfacial Effects in the *In-situ* Water Flood Displacement of Bitumen

The displacement of an oil present in the pore structure of a water-wet reservoir rock is determined by the relative magnitude of the capillary forces holding the oil in the capillary structure and the viscous forces arising from the flow of the viscous fluid (*i.e.*, water) through the rock. The water is imbibed most strongly into the smaller pores, displacing any oil present in them, until the hydrostatic and capillary pressures in the system balance. As the hydrostatic pressure of the water is increased, water invades larger capillaries and more oil is displaced from the rock. The ratio of viscous forces to capillary forces correlates well with the residual oil saturation and is termed the capillary number, N_c. In one formulation the capillary number is given as

$$N_c = \eta v/g, \tag{20}$$

where η and v are the viscosity and velocity of the displacing fluid. A generalized capillary number-residual oil correlation is shown in Figure 3.46.[43] Between $N_c \approx$ *ca* 10^{-5} and 10^{-3} the percentage residual oil in the rock decreases nearly linearly with rising N_c and reaches 0% around $N_c = 2 \times 10^{-3}$. Therefore, for efficient oil displacement N_c should have a large value. The viscous forces can be increased within practical limits; however, more significant changes in N_c can be effected by lowering the value of γ_{BA} from its value of *ca* 30 mN·m^{-1} in the absence of surfactants to the ultralow range of 10^{-3} mN·m^{-1} in the presence of an added surfactant and cosurfactant. In this way, it is possible to achieve a value of 10^{-3} for N_c for which oil recovery would be complete.

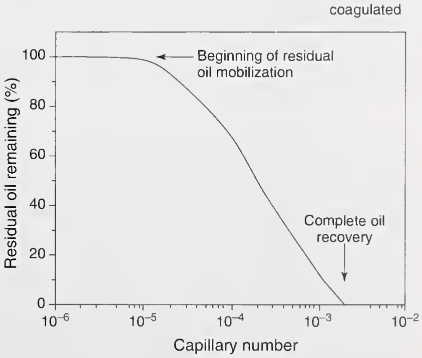

Figure 3.46 A Generalized capillary number correlation. From L.L. Schramm, Ref. 43. © 1992, American Chemical Society.

Thus, in general, very low values of γ_{BA} are required in water-flood oil recovery, unlike the case for the hot water separation of bitumen where a high value of γ_{BA} is preferred.

4.0 Migrational History of the Oil Precursor to the Bitumen

As it is well established today (*v.i.*), the bitumen is the residue of microbiological degradation of a conventional oil which migrated into the preexisting sand and carbonate formations. There are two features of the present-day oil sands that give important information regarding the timing and location of the microbiological degradation process, namely, the occasional occurrence of 100% saturation of the sand rock pores and the presence of suites of mineral-bound and bitumen-associated carboxylic acids which appear to be the metabolic products of the microbiological degradation of the precursor oil *via* the aerobic pathway of biosynthesis. This topic will be discussed again in subsequent chapters.

5.0 Summary

The principal components of Alberta oil sands, the bitumen and sand, comprise up to 18 and 95% of the ore material. Among the lesser components, water, clay, silt, heavy minerals, gases, humic matter and mineral-bound organic matter, only the heavy minerals show commercial potentials. Nevertheless, these lesser components can profoundly affect the water flotation efficiency and thus the separability of the bitumen.

A few percent of the connate water in all Alberta oil sands are present as a thin film covering the sand surfaces and separating the bitumen from the sand. This serendipitous structural feature renders the sand water wet and the bitumen separable from the sand by water flotation. The water, clay and bitumen contents in the ore are interrelated and water and clay vary in parallel and inversely to bitumen. Over 80% of the deposits has been estimated to contain bitumen above the economically inviting 8 wt% level. Only about 10% of the Athabasca deposit contains oil-bearing sand near the surface (at depths < 45–75 m) that can be recovered by surface mining. The rest of the deposits can be recovered by some form of *in situ* operation.

The properties of oil sands may exhibit significant variation owing to compositional changes, but the composition of the bitumen exhibits only modest changes with geostratigraphic location. Among the reservoirs a definite trend is apparent: on going from Carbonate Trend to Athabasca, Peace River and Cold Lake, the densities and viscosities decrease and the alkyl and aliphatic contents of the bitumens increase.

Oil sands are reactive and undergo oxidation in the presence of air; also, thermocatalytic reactions release gases and volatiles at quite low temperatures. Oxidation produces sulfuric acids from the iron sulfides present and carboxylic acids from the bitumen, along with sulfoxides and other polar molecules. The carboxylic acids are the source of the most important chemical class of natural surfactants present in the bitumen, the carboxylate anions formed upon treatment with aqueous base. The carboxylate anions fulfill another important role: they endow the bitumen surface with a negative charge necessary to maintain a repulsive force between bitumen droplets and sand grains, since the latter are negatively charged as well. Sulfuric acid releases Ca^{2+}, Mg^{2+} and other higher-valent cations from the clays and minerals which tend to bind the bitumen to the sand and thus adversely affect the separation process.

Carbonate, clay, sulfate and other minerals indirectly impact the separation of bitumen by releasing Ca^{2+}, Mg^{2+} and other higher-valent cations in a variety of ion exchange reactions. NaOH may also react with some of these minerals producing $Ca(OH)_2$ and $Mg(OH)_2$ which, in turn, could precipitate the carboxylate ions. These processes increase NaOH consumption and decrease carboxylate surfactant concentrations thereby being doubly injurious to the economy of the separation of bitumen by increasing cost and decreasing efficiency.

In the complex physical chemistry of bitumen flotation, interfacial and electric properties play a decisive role. Surface tension, interfacial tension, *pH*, surface charge, electric double layer and zeta potential are the major parameters. Since the bitumen/water interfacial area diminishes in the primary separation step, a high value for the interfacial tension and an optimum *pH* of about 8.5 to create a suitably large negative zeta potential at the bitumen surface (without diminishing the bitumen/water interfacial tension) along with a low viscosity for the bitumen are prerequisite. The disjoining pressure, responsible for maintaining the stability of the thin aqueous film separating the sand and the bitumen, can, to a first approximation, be assumed to be derived from the repulsive electrical forces and the attractive London–van der Waals forces.

In the second step of flotation a high value for the bitumen/water interfacial tension is also advantageous in lifting the oil droplets to the surface of the slurry: high interfacial tension promotes formation of large droplets with a high upward velocity and increased attachment of air bubbles, helping flotation. Flotation is also impacted by the presence and nature of fines. Here it is desirable to select conditions inducing strong repulsive potentials between fines-fines and bitumen-fines and low repulsion between bitumen-bitumen droplets.

A curious phenomenon regarding bitumen (oil)/water interfaces is the slow formation of rigid interfacial films upon irradiation with light. In the absence of irradiation but in the presence of sodium hydroxide the film forms rapidly. Its role in microemulsions is being investigated and it is exploited for the measurement of the interfacial tension of single micro droplets.

The saturation characteristics of the sand pores, in conjunction with the nature of the mineral-bound carboxylic acids, provide important information on the migrational and biodegradational history of the precursor oil which gave rise to bitumen formation.

Bibliography

1. a) *Oil Sands Composition and Behaviour Research. The Research Papers of John A. Bichard 1957-1965,* Alberta Oil Sands Technology and Research Authority Technical Publication Series No. 4, Edmonton, AB, 1987. b) L.G. Hepler and R.G. Smith, *The Alberta Oil Sands: Industrial Procedures for Extraction and Some Recent Fundamental Research*, Alberta Oil Sands Technology and Research Authority Technical Publication Series No. 14, Edmonton, AB, 1994, p. 140.

2. D.M. Wigham, B.A. Rottenfusser, J. Kramers and R. Harrison, "Geology of the Alberta Oil Sand Deposit" in *AOSTRA Technical Handbook on Oil Sands, Bitumens and Heavy Oils*, L.G. Hepler and C. Hsi, Eds., Alberta Oil Sands Technology and Research Authority Technical Publication Series No. 6, Edmonton, AB, 1989, p.1.

3. The single most important structural feature (in terms of processability) of Alberta oil sands is the presence of a thin water film enveloping each sand grain. The earliest documented recognition of this arrangement is found in a research paper authored by M.W. Ball, [Am. Assoc. Petrol. Geol. Bull., 19 (1935) 153] where T.A. Link, a Calgary geologist, commented:

    > "While experimenting with the tar sands some 15 years ago I was informed by someone at the University of Alberta, working on the same subject, that microscopic observation revealed the presence of films of water surrounding the sand grains, which films, in turn, are surrounded by the oil."

    The "someone at the University of Alberta" was probably Professor Adolph Lehmann, the first Chairman of the Chemistry Department (1909-1930) who carried out research on the Athabasca oil sands during the early years of his appointment.

4. T.M. Ignasiak, Q. Zhang, B. Kratochvil, C. Maitra, D.S. Montgomery and O.P. Strausz, "Chemical and Mineral Characterization of the Bitumen-Free Athabasca Oil Sands Related to the Bitumen Concentration in the Sand Tailings from the Syncrude Batch Extraction Test", AOSTRA J. Res., 2 (1985) 21.
5. L.S. Kotlyar, B.D. Sparks and H. Kodama, "Properties of Fine Size Fractions in Relation to the Distribution of Humic-Inorganic Matter Complexes in Athabasca Oil Sands", AOSTRA J. Res., 4 (1988) 277.
6. L.S. Kotlyar, B.D. Sparks and K.H. Chung, "Organic Rich Solids from Oil Sands: Properties and Role in Processing", Rev. Process Chem. and Eng., 1 (1998) 81.
7. K. Takamura, "Microscopic Structure of Athabasca Oil Sand", Can. J. Chem. Eng., 60 (1982) 538.
8. J.E. Zajic, D.G. Cooper, J.A. Marshall and D.F. Gerson, "Microstructure of Athabasca Bituminous Sands by Freeze-Fracture Preparation and Transmission Electron Microscopy", Fuel, 60 (1981) 619.
9. F.W. Camp, "A Description and Reserve Estimate of the Oil Sands of Alberta", Oil & Gas Conservation Board of the Province of Alberta, 1963.
10. M.A. Carrigy and D. Wallace, "New Analytical Results on Oil Sands from Deposits Throughout the World", *Third Int'l Conf. on Heavy Crude and Tar Sands*, Long Beach, CA, July 22-31, 1985, Vol. 1, Alberta Oil Sands Technology and Research Authority, Edmonton, AB, 1985, p. 231.
11. D. Wallace, D. Henry and K. Takamura, "A Physical Chemical Explanation for Deterioration in the Hot Water Processability of Athabasca Oil Sand Due to Aging", Fuel Sci. Technol. Int., 7 (1989) 699.
12. G. Faure, *Inorganic Geochemistry*, Macmillan, New York, N.Y., 1991, pp. 474-485.
13. J.D. Payzant, T.W. Mojelsky, T.D. Cyr, D.S. Montgomery and O.P. Strausz, "The Identification of 9-*n*-Alkyl Fluoren-9-ols in the Alberta Oil Sands", Org. Geochem., 8 (1985) 177.
14. T.W. Mojelsky and O.P. Strausz, "Detection of Methyl Fluorenones in Athabasca Oil Sand Bitumens", Org. Geochem., 9 (1986) 31.
15. T.D. Cyr and O.P. Strausz, "The Structures of Tricyclic Terpenoid Carboxylic Acids and Their Parent Alkanes in the Alberta Oil Sands", J. Chem. Soc. Chem. Commun., (1983) 1028.
16. J.D. Payzant, D.S. Montgomery and O.P. Strausz, "Novel Terpenoid Sulfoxides and Sulfides in Petroleum", Tetrahedron Lett., 24 (1983) 651.
17. E.C. Sanford, "Interrelationship Between Oil Sand Fines Solids, Process Aids, Mechanical Energy and Oil Sand Age After Mining", Can. J. Chem. Eng., 61 (1983) 554.
18. L.L. Schramm and R.G. Smith, "Two Classes of Anionic Surfactants and Their Significance in Hot Water Processing of Oil Sands", Can. J. Chem. Eng., 65 (1987) 799; *idem*, "Some Observations on the Aging Phenomenon in the Hot Water Processing of Athabasca Oil Sands. Part 1. The Nature of the Phenomenon", AOSTRA J. Res., 3 (1987) 195; *idem*, "Some Observations on the Aging Phenomenon in the Hot Water Processing of Athabasca Oil Sands. Part 2. The Mechanism of Aging", AOSTRA J. Res., 3 (1987) 215.
19. a) Ref. 1b, p. 15. b) J. Drelich, K. Bukka, J.D. Miller and F.V. Hanson, "Surface Tension of Toluene-Extracted Bitumens from Utah Oil Sands as Determined by Wilhelmy Plate and Contact Angle Techniques", Energy & Fuels, 8 (1994) 700. c) C.W. Bowman, "Molecular and Interfacial Properties of Athabasca Tar Sands", in *Seventh World Petroleum Congress*, Mexico, 1967, Vol. 3, Elsevier, Amsterdam, 1967, p. 583. d) E.E. Isaacs and K.F. Smolek, "Interfacial Tension Behaviour of Athabasca Bitumen/Aqueous Surfactant Systems", Can. J. Chem. Eng., 61 (1985) 233. e) Z.M. Potoczny, E.I. Vargha-Butler, T.K. Zubovits and A.W. Neumann, "Surface Tension of Bitumen. I. Temperature Dependence", AOSTRA J. Res., 1 (1984) 107.
20. K. Darcovich, L.S. Kotlyar, W.C. Tse, J.A. Ripmeester, C.E. Capes and B.D. Sparks, "Wettability Study of Organic-Rich Solids Separated From Athabasca Oil Sands", Energy & Fuels, 3 (1989) 386.
21. K. Takamura and E.E. Isaacs, "Interfacial Properties", in *AOSTRA Technical Handbook on Oil Sands, Bitumens and Heavy Oils*, L.G. Hepler and C. Hsi, Eds., Alberta Oil Sands Technology and Research Authority Technical Publication Series No. 6, Edmonton, AB, 1989, p. 99.

22. a) K.C. Khulbe, V. Hornof and G. Neale, "Interfacial Activity of Heavy Oil and its Maltene Constituents Against Caustic Solutions", AOSTRA J. Res., 2 (1985) 95. b) Y. Xu, "Dynamic Interfacial Tension Between Bitumen and Aqueous Sodium Hydroxide Solutions", Energy & Fuels, 9 (1995) 148.

23. E.E. Isaacs and D.N. Morrison, "Interfacial Films at the Athabasca Bitumen/Water Interface", AOSTRA J. Res., 2 (1985) 113.

24. A. Yeung, T. Dabros, J. Czarnecki and J. Masliyah, "On the Interfacial Properties of Micrometer-Sized Water Droplets in Crude Oil", Proc. Roy. Soc. London, A, 455 (1999) 3709.

25. K. Bhattacharyya, "Photophysical Probes for Organized Assemblies", in *Org. Mol. Photochem.*, Vol. 3, V. Ramamurthy and K.S. Schanze, Eds., Marcel Dekker, N.Y. 1997, p. 283.

26. K. Moran, A. Yeung and J. Masliyah, "Measuring Interfacial Tensions of Micrometer-Sized Droplets: a Novel Micromechanical Technique", Langmuir, 15 (1999) 8497.

27. E.E. Isaacs, H. Huang, A.J. Babchin and R.S. Chow, "Electroacoustic Method for Monitoring the Coalescence of Water in Oil Emulsions", Colloids and Surfaces, 46 (1990) 177.

28. C.W. Bowman, "Mining the Athabasca Tar Sands", Science J., 5A (1969) 28.

29. J. Leja and C.W. Bowman, "Application of Thermodynamics to the Athabasca Tar Sands", Can. J. Chem. Eng., 46 (1968) 479.

30. E.Y. Sheu, M.M. DeTar, D.A. Storm and S.J. DeCanio, "Aggregation and Kinetics of Asphaltenes in Organic Solvents", Fuel, 71 (1992) 299.

31. S.E. Taylor, "Use of Surface Tension Measurements to Evaluate Aggregation of Asphaltenes in Organic Solvents", Fuel, 71 (1992) 1338.

32. S.I. Andersen, S.M. del Rio, D. Khvostitchenko, S. Shakir and C. Lira-Galeana, "Interaction and Solubilization of Water by Petroleum Asphaltenes in Organic Solution", Langmuir, 17 (2001) 307.

33. J.H. Masliyah, *Electrokinetic Transport Phenomena*, Alberta Oil Sands Technology and Research Authority Technical Publication Series No. 12, Edmonton, AB, 1994.

34. D.J.A. Williams and K.P. Williams, "Electrophoresis and Zeta Potential of Kaolinite", J. Colloid Interface Sci., 65 (1978) 79.

35. P.C. Hiemanz, *Principles of Colloid and Surface Chemistry*, Marcel Dekker, New York, 1977; L.L Schramm, "Suspensions", *Advances in Chemistry Series 251*, L.L. Schramm, Ed., American Chemical Society, Washington, DC, 1992, p. 729.

36. I.E. Melton and B. Rand, "Particle Interactions in Aqueous Kaolinite Suspensions", J. Colloid Interface Sci., 60 (1977) 331.

37. a) The theory on which the computation of disjoining pressure is based neglects any consideration of entropic and steric stabilization and specific adsorption of ions and hydration effects as well as the possible role of the oscillatory hydration/hydrophobic forces (*cf.* Israelachivili et al.), etc. Consequently, the shape of the disjoining pressure functions in Figure 3.38 is only a first approximation of the true functions. b) J.N. Israelachvili and G.E. Adams, "Measurement of Forces Between two Mica Surfaces in Aqueous Electrolyte Solutions in the Range 0–100 nm", J. Chem. Soc. Faraday Trans. I, 75 (1978) 975; *Intermolecular and Surface Forces*, 2nd ed., Academic Press, New York, N.Y.,1992.

38. K. Takamura and R.S. Chow, "A Mechanism for Initiation of Bitumen Displacement From Oil Sand", J. Can. Petrol. Technol., 22 (Nov.–Dec. 1983) 22.

39. K. Takamura and D. Wallace, "The Physical Chemistry of the Hot Water Process", J. Can. Petrol. Technol., 27 (1988) 98.

40. Qi Dai and K.H. Chung, "Hot Water Extraction Process Mechanism Using Model Oil Sands", Fuel, 75 (1996) 220.

41. R.S. Chow, "The Stability of Kaolinite-in-Water Dispersions", Colloids and Surfaces, 61 (1991) 241.

42. W. Jazrawi, "Dredging and Cold Water Extraction Process for Oil Sands", AOSTRA Oil Sands 2000, Session 2, Paper 4, March 26–28, 1990, Edmonton, AB.

43. L.L. Schramm, Ch. 1 in *Emulsions. Fundamentals and Applications in the Petroleum Industry*, L.L. Schramm, Ed., Advances in Chemistry Series 231, American Chemical Society, Washington, DC, 1992.

Appendix 3.1

The optimum basicity for the hot water separation is at about pH 8.5 where the surface carboxylic groups are nearly completely dissociated, Figure 3.30, and the maximum occurs in the pH function of the zeta potential, Figure 3.27 and in the bitumen-water interfacial tension, Figure 3.14. Above pH 8.5 the negative zeta potential decreases and the electric double layer and diffuse layer, Figure 3.25 collapses with increasing ion concentration in the aqueous phase. Above pH 8.5 the interfacial tension also decreases and steeply drops down to the ultra low region around pH 12–12.4, resulting in an oil-in-water emulsion. In this pH region some chemical alterations also take place especially at elevated temperatures involving the hydrolysis of carboxylic acid esters producing more *n*-alkanoic acids along with more complex carboxylic acids and alcohols. Some of these materials have low MW like the *n*-alkanoic acids and *n*-alcohols (*cf.* Chapter 13) and some are anchored to the asphaltene. The carboxylic acids liberated produce additional quantities of carboxylate surfactants and the alcohols especially asphaltene core-anchored series induce H-bonded aggregation of the asphaltene molecules. Parallel to these processes and even at lower pH values some of the acids are leached from the maltene and oil sands solids (*cf.* Chapter 13) into the aqueous phase as free acids and carboxylates.

The major role of the carboxylate surfactants created by caustic addition is to maintain high negative charges on the sand and bitumen surface and create an energy barrier for fines-fines interaction and thereby prevent fines coagulation while at the same time keeping down the energy barrier for oil coagulation which is a desirable process, Figure 3.43. Additionally the carboxylates promote oil filming and occlusion of air bubbles in slurrying.

Organic Chemistry: Nomenclature and Some Basic Concepts

4

The purpose of this brief chapter is to refresh the reader's memory of some of the basic tenets of organic chemistry and the principles applied to the naming of those organic compounds pertaining to bitumen chemistry.

Petroleum is composed primarily of two elements, carbon and hydrogen, along with lesser amounts of "heteroatoms"—nitrogen, oxygen and sulfur—as well as trace concentrations of metals (V, Ni, Fe, *etc.*) and minerals:

C	79–87%	O	0–2%
H	9.5–14%	N	trace–1.7%
S	trace–8%	metals	trace–0.1%

The bulk of conventional oils comprises hydrocarbons, molecules composed of carbon and hydrogen only. Heavy oils and bitumens contain elevated levels of heteroatoms and they are correspondingly rich in NOS-containing compounds. Light, paraffinic crude oils may have combined carbon + hydrogen contents up to 98% with H-to-C atomic ratios, $(H/C)_a$, up to 2.0 and, in exceptional cases, as high as 2.3. Such oils may contain up to about 80% by weight hydrocarbons. In heavy oils and particularly bitumens with high heteroatom contents, the $(H/C)_a$ values are low, around 1.45–1.6. In such cases, the hydrocarbon content of the oil is usually low as well; in Athabasca bitumen with 4.5% sulfur, 1% oxygen and 0.4% nitrogen, the hydrocarbon content is estimated to be 35–45%. The rest of the bitumen is then made up of molecules which, in addition to carbon and hydrogen, also contain one or more heteroatoms.

The important types of hydrocarbons which are found in copious quantities in petroleum are :

- alkanes (acyclics, or paraffins): open-chain aliphatic hydrocarbons;
- cycloalkanes (alicyclics, or naphthenes): cyclic aliphatic hydrocarbons, also called "naphthenes" by petroleum chemists because they are found in the "naphtha" fraction of petroleum and are isomeric with "alkenes", and
- aromatics: cyclic hydrocarbons with three alternating single–double bonds as well as their combination products such as alkylaromatics, naphthenoaromatics and alkyl naphthenes.

Alkenes (olefins) with double-bonded carbons are found only in trace quantities and alkynes (acetylenes) with triple-bonded carbons are altogether absent.

1.0 Acyclic Alkanes

Acyclic alkanes are one of the groups of hydrocarbons constituting the saturate fraction of petroleum. They contain only single, sigma bonds, joining carbon to carbon and to hydrogen. The simplest alkane molecule is methane

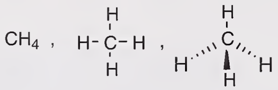

in which the four hydrogen atoms define the apexes of a tetrahedron surrounding the central tetravalent carbon atom.

Substitution of a CH_3 group for a hydrogen atom leads to ethane,

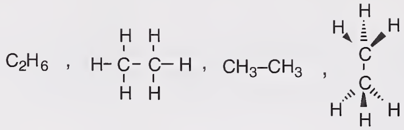

and further substitutions to

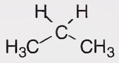
propane

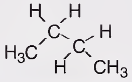
butane

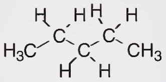
pentane

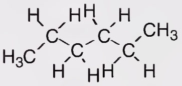
hexane, *etc.*

From the tetrahedral symmetry of the carbon valences it follows that all bond angles in the molecules are 109.5°. Series of molecules, the members of which differ in the number of CH_2 (methylene) groups in the chain, are called homologous series and the members of the series are the homologs of one another. Carbon has the ability to bond to itself, forming extremely long chains, as in the alkanes, with series formula C_nH_{2n+2} where n is the number of carbon atoms in the molecule. Alkane molecules with as many as 100 carbon atoms have been synthesized. The alkane molecule is termed *normal*-alkane (*n*-alkane) if its carbon skeleton is unbranched. The members of the homologous series of *n*-alkanes beyond the first four members are named according to the standard nomenclature established by the International Union of Pure and Applied Chemistry, IUPAC, as pentane, hexane..., decane, *etc.* In naming these compounds the "alk" stem in the generic name "alkanes" is replaced by the Greek prefix indicating the number of carbon atoms in the molecule, *e.g.*, pent for five, giving pent + ane = pentane, hexane,...heptadecane, *etc.*, Table 4.1.

Table 4.1 Nomenclature of simple alkanes

No. of C	Alkane	No. of isomers	Radical
C_5	pentane	3	pentyl
C_6	hexane	5	hexyl
C_7	heptane	9	heptyl
C_8	octane	18	octyl
C_9	nonane	35	nonyl
C_{10}	decane	75	decyl
C_{11}	undecane	159	undecyl
C_{15}	pentadecane	4,347	pentadecyl
C_{20}	eicosane	366,319	eicosyl
C_{25}	pentacosane	36,797,588	pentacosyl
C_{30}	triacontanes	4,111,846,763	triacontyl
C_{40}	tetracontane	6.25×10^{13}	tetracontyl

Homologous series of compounds are important constituents of petroleum and in conventional crude oils *n*-alkanes are often the most abundant homologs.

Alkanes having four or more carbon atoms may exist in different spacial arrangements in which the sequence of bondings is different:

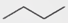
n-butane
B.P. –0.5°C

*iso*butane
B.P. –12°C

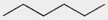
n-hexane
B.P. 68.7°C

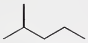
*iso*hexane
60.2°C

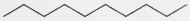
n-decane
174.1°C

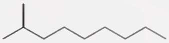
*iso*decane
167.1°C

These molecules are called isomers of one another. If the methyl branching is from the carbon second from the end of the chain, they are called *iso*alkanes and if it is from the carbon third from the end of the chain, *anteiso*alkanes.

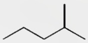
*iso*hexane

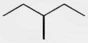
*anteiso*hexane

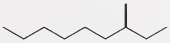
*anteiso*decane

Branched alkanes, according to IUPAC convention, are considered to be derivatives of the longest single carbon chain present in the molecule. The carbon atoms are numbered from one end to the other in the chain,

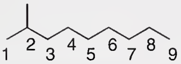

and therefore this *iso*decane molecule is considered to be a substituted nonane, 2-methylnonane, because the end carbon which is chosen as number 1 is the one that gives the smaller number at the point of branching. The names of the alkyl radicals are derived from their parent alkanes, Table 4.1. On multiple substitution the prefixes di-, tri-, tetra-, *etc.*, are used:

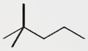
2,2-dimethylpentane

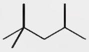
2,2,4-trimethylpentane
(incorrectly called *iso*octane,
used for grading gasoline)

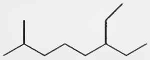
6-ethyl-2-methyloctane

The last example illustrates another rule for naming an alkane, specifically, that the alkyl substituents must be listed in alphabetical order: hence 6-ethyl-2-methyloctane and not 2-methyl-6-ethyloctane. (This molecule could also be called 3-ethyl-7-methyloctane; however, the next rule that applies here states that the substituent should be on the chain carbon bearing the lowest number possible: $6,\underline{\underline{2}}$ is lower than $\underline{\underline{3}},7$.)

Carbon atoms to which one carbon and three hydrogens are attached, such as the terminal methyl carbons of alkanes, *e.g.*,

$$\overset{*}{C}H_3\text{–}CH_2\text{–}CH_2\text{–}CH_2\text{–}\overset{*}{C}H_3,$$

are called primary carbons and radicals derived from them by the removal of a hydrogen atom, *e.g.*

$$\overset{*}{C}H_3\text{–}CH_2\text{–}CH_2\text{–}CH_2\text{–}\overset{*}{C}H_2\bullet\ ,$$

1-pentyl radical

are primary alkyl radicals. Similarly, carbon atoms to which two carbons and two hydrogen atoms are attached are called secondary carbons and the radicals derived from them by the removal of a hydrogen atom, *e.g.*,

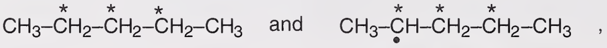

$CH_3-\overset{*}{C}H_2-\overset{*}{C}H_2-\overset{*}{C}H_2-CH_3$ and $CH_3-\underset{\bullet}{\overset{*}{C}}H-\overset{*}{C}H_2-\overset{*}{C}H_2-CH_3$,

2-pentyl radical

are secondary alkyl (pentyl) radicals. Lastly, the central carbon in isobutane

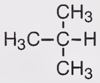

$$H_3C-\overset{\displaystyle CH_3}{\underset{\displaystyle CH_3}{C}}-H$$

is a tertiary carbon and the radical derived from it by the removal of the hydrogen atom is a tertiary alkyl (butyl) radical.

Homologous series of compounds like *n*-alkanes show gradual incremental changes in their physical properties, boiling point, density, gas chromatographic retention times (Kovats' indices) *etc.*, and values for individual members can be predicted by interpolation or extrapolation. The variation in these properties can be attributed to changes in the London dispersion forces which, owing to the correlated motion of electrons within the molecules, produce a net attractive force between molecules, the magnitude of which depends on the area of contact of two molecules. The greater the contact area, the greater the attractive force and, since each additional methylene group provides an additional area of contact that increases the total attractive force, the boiling point is increased. The dispersion forces are even greater in solids and the melting point increases gradually with increasing chain length. As a result of different packing requirements in the crystal for odd and even zigzag chains,

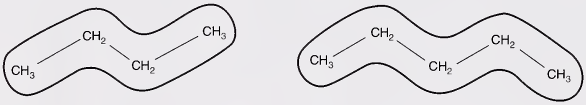

there is an alternation in melting points with growing chain length.

n-Alkanes are the only group of hydrocarbons capable of forming mixed crystals and therefore in *n*-alkane-rich petroleums and petroleum products such crystals often occur, with the effect of greatly increasing the viscosity of the petroleum. In industry, mixed crystals of *n*-alkanes are called "paraffins". There are no other substances in petroleum which crystallize, even if their melting points are much above the temperature of the oil. The reason for this is that individual compounds are usually found only in low concentrations and, since they do not form mixed crystals with their homologs, the depression of the freezing point is so large that crystallization of a single substance cannot take place.

With increasing number of carbon atoms in the molecule the number of possible isomers increases, in the beginning at a moderate rate, but above C_{10} the rate accelerates—the $C_{40}H_{82}$ alkane may exist in 6.25×10^{13} different isomeric forms! Of course, only few of the possible homologs have been isolated. In nonbiodegraded petroleum, usually the *n*-alkanes are the dominant alkanes in concentrations of up to 64% or so, followed by the isoprenoid and then the higher branched isomers. *Iso*- and *anteiso*-alkanes are present in relatively low concentrations.

Isoprenoids are methyl-branched alkanes produced biosynthetically from five-carbon isoprene units

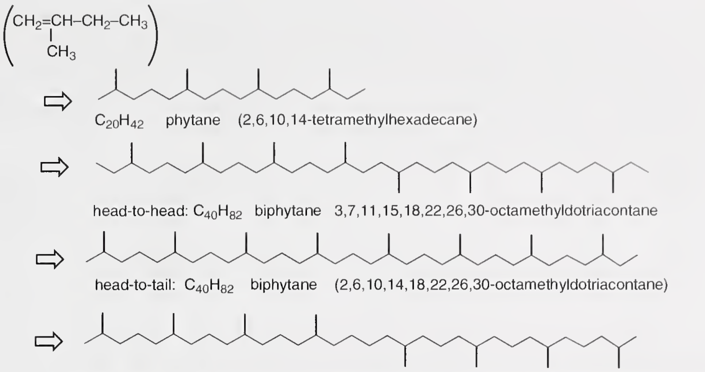

$(CH_2{=}CH{-}CH_2{-}CH_3$ with CH_3 on C-2$)$

$C_{20}H_{42}$ phytane (2,6,10,14-tetramethylhexadecane)

head-to-head: $C_{40}H_{82}$ biphytane 3,7,11,15,18,22,26,30-octamethyldotriacontane

head-to-tail: $C_{40}H_{82}$ biphytane (2,6,10,14,18,22,26,30-octamethyldotriacontane)

tail-to-tail: $C_{40}H_{82}$ biphytane, lycopane (2,6,10,14,19,23,27,31-octamethyldotriacontane)

and occur in petroleum, along with their degradation products:

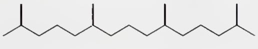

$C_{19}H_{40}$ pristane
2,6,10,14-tetramethylpentadecane

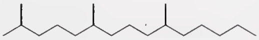

$C_{18}H_{38}$ norpristane
2,6,10-trimethylpentadecane

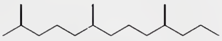

$C_{16}H_{34}$
2,6,10-trimethyltridecane

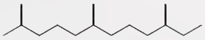

$C_{15}H_{32}$ farnesane
2,6,10-trimethyldodecane

In alkane molecules the alkyl moieties rotate relatively freely about the carbon-carbon bond and, although some energy barrier for rotation exists, it is too small to arrest rotation at room temperature. Therefore, alkanes do not exhibit isomerisms due to differences in molecular geometry (conformation) alone; instead the rotationally different species of the molecule are in an equilibrium distribution. For example, *n*-butane at room temperature exists as a mixture of two rotameric forms, the *anti* and somewhat less stable *gauche*,

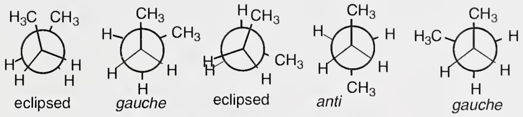

while the eclipsed forms represent energy barriers for rotation.

2.0 Cycloalkanes

The carbon chain skeleton of alkanes can close to form rings, *e.g.*,

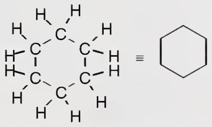

C_6H_{12}, cyclohexane

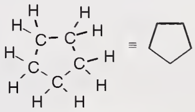

C_5H_{10}, cyclopentane

with series formula C_nH_{2n}. The ring size may vary from a three-membered ring to very large rings, but the only important ring sizes in petroleum chemistry are the five- and six-membered rings, cyclopentanes and cyclohexanes. The radicals derived from cycloalkanes are the cycloalkyls: cyclopentyl, cyclohexyl, *etc.* The physical properties of cycloalkanes are similar to those of the alkanes but, in general, the melting points and boiling points are slightly higher than those of the comparable acyclic analogs. In many respects the chemistry of cycloalkanes is also similar to that of alkanes but differences arise from conformation and stability effects.

In alkanes, all bond angles are equal to the tetrahedral angle 109.5° whereas in a cyclic system the ring imposes a bond angle different from 109.5° and therefore the ring is strained, that is, its energy is higher than that of the acyclic system. In a planar cyclopentane molecule the C–C bond angles would be 108°, not much different from the tetrahedral angle, and therefore the ring strain should be small. There is, however, another important effect contributing to ring strain to consider, namely, the one due to the nonbonding repulsive interactions between pairs of hydrogen atoms on adjacent carbons and carbons across the ring. As a result, cyclopentane has a nonplanar geometry

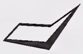

in which the total ring strain is at a minimum, 25.1 $kJ\cdot mol^{-1}$. For cyclohexane, the most stable geometry is a chair conformation

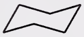

which is essentially strain free. This is one of the reasons why six-membered rings are so ubiquitous in nature and why they occur abundantly in petroleum. It is a consequence of the chair conformation that the hydrogens occupy two distinctly different types of positions within the cyclohexane molecule,

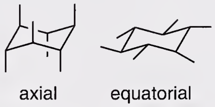

axial and equatorial. In both cyclopentane and cyclohexane the conformations are dynamic and the conversion from one chair form into another involves rotation about C–C bonds with an energy barrier of 45.2 $kJ\cdot mol^{-1}$ and a frequency of 100,000 s^{-1} at room temperature. Thus when a substituent such as a methyl group is present two conformations exist, in one the methyl group occupies an axial and, in the other, an equatorial position,

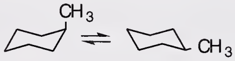

the double arrow symbol " $\rightleftharpoons$ " indicating equilibrium. As it turns out there is a significant difference in stability between the two conformers, the equatorial being more stable, Table 4.2. At room temperature both conformers are present, but the equatorial conformer is more abundant, 95%, than the axial conformer, 5%. For bulkier substituents such as a *t*-butyl group the energy difference between the two conformers is even larger. When two substituents are present on the ring they can be positioned on the same side of the ring (both above or both below) or one above and the other one below the average plane of the ring,

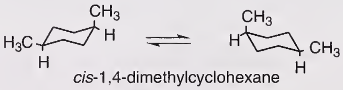

cis-1,4-dimethylcyclohexane

Table 4.2 Thermochemistry of cyclic alkanes

Ring strain		Conformational energies in monosubstituted cyclohexanes:	
Compound	ΔG^0, kJ·mol^{-1}	$-\Delta G^0$ (axial $\rightleftharpoons$ equatorial), kJ·mol^{-1}	
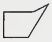	26.8	CH_3	7.1
	209	CH_3CH_2	7.5
	110	$CH(CH_3)_2$	8.8
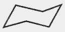	1.7	$C(CH_3)_3$	~20.9-25.1
		phenyl	13.0

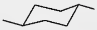	7.9 kJ·mol^{-1} more stable than	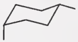
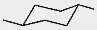	14.2 kJ·mol^{-1} more stable than	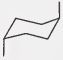
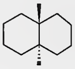	8.4 kJ·mol^{-1} more stable than	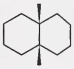

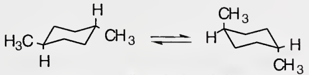

trans-1,4-dimethylcyclohexane

the two being geometrical isomers and designated as *cis*- and *trans*-isomers. In the *cis*-isomer one methyl is always axial and the other equatorial. However, in the *trans*-isomer both methyls can be equatorial and since this is the more stable conformation the *trans*-isomer is considerably more stable than the *cis*-isomer. The difference in energy between the *cis*- and *trans*-isomers becomes even greater when the substituents are bulkier and in the case of 1-*t*-butyl-4-methylcyclohexane the equilibrium is shifted completely in favor of the *trans*-isomer.

Cycloalkanes also exist in condensed form having two or more rings in which at least two carbon atoms are part of at least two rings:

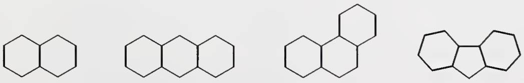

, *etc.*

In bicyclic structures there are two bridgehead atoms common to both rings and there are three arms connecting the two bridgehead atoms:

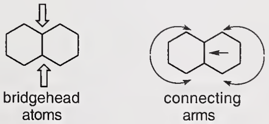

Bicycloalkanes are considered as derivatives of the alkanes having the same number of carbon atoms and therefore the above bicyclic compound is a bicyclodecane. In naming the compound, the number of carbon atoms in each of the three connecting arms (starting with the longest arm, then the next longest, and so on, ending with the shortest) is inserted in square brackets after the term “bicyclo”. Thus, the compound

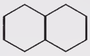

is named bicyclo[4.4.0]decane (but is commonly called decalin). It can exist in two geometric forms,

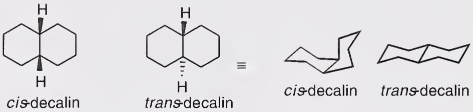

where the symbols (▬) and (ıııı) indicate hydrogen atoms positioned above and below the plane.

In both isomeric decalins, each of the two cyclohexane rings is in the chair conformation. In *cis*-decalin the rings are fused together in such a way that each ring represents an axial and an equatorial substituent on the other while in *trans*-decalin each ring comprises two equatorial substituents on the other. Consequently, *trans*-decalin is more stable than *cis*-decalin. The *cis-trans* isomers cannot interconvert unless a C–C bond is broken. The *trans* form is rigid and the two rings cannot flip from one chair form to another like cyclohexane can. Consequently, the orientation of the substituent is fixed in the chair-chair conformation. In contrast, the chair-chair forms of *cis*-decalin are relatively flexible and inversion of both rings at once occurs fairly easily with a barrier of 58.6 kJ·mol^{-1}. A substituent therefore can interconvert between axial and equatorial positions.

Cycloalkanes are important constitutents of petroleum and the saturate fractions of oil sand bitumens consist mainly of cycloalkanes ranging from one ring to six fused rings.

3.0 Aromatics

This class of cyclic organic molecules contains, in addition to single bonds, double bonds forming especially stable electron systems stabilized by quantum mechanical resonance phenomena. The prototype aromatic molecule is benzene, a cyclic planar C_6H_6 compound with a regular hexagonal geometry:

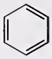

However, the hexagonal geometry is inconsistent with alternating single and double bonds as illustrated above in the benzene ring, because the double bonds should have a shorter bond distance than the single bonds, causing a distortion of the regular hexagon to a distorted hexagon:

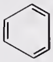

From the measurement of the heat of hydrogenation required to convert benzene to cyclohexane, the benzene molecule turns out to be more stable than expected for a molecule with alternating single-double bonds. This extra stability, amounting to 150.6 kJ·mol^{-1}, is called the empirical resonance energy of benzene and its origin, according to wave mechanical considerations, lies in the special stability of the bonds formed by the delocalization of the six electrons (representing the second bonds in the three double bonds) to a uniform 1.5 bonds between each of the neighbouring carbon atoms in the molecule. This aromatic stability explains the relative chemical inertness and unique chemical behaviour of benzene and aromatic molecules. Thus, the structure of benzene is characterized by delocalized bonds extending to all the ring carbons which may be symbolized by writing the structure as

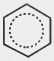

indicating the complete equivalence of all C–C bonds and distances. Nevertheless, it is still customary to write the structures of benzene and other aromatic compounds in terms of alternating single-double bonds

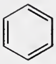

or by indicating aromaticity by a circle inside the ring:

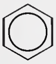

The radical derived from benzene by the removal of a hydrogen atom is the phenyl radical. Replacing the hydrogen atom by an alkyl group produces alkylbenzenes or poly-alkylbenzenes.

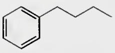

n-alkylbenzene

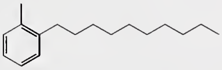

ortho-decylmethylbenzene

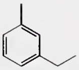

meta-ethylmethyl-benzene

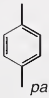

para-dimethyl-benzene

The benzene ring may be fused to a cycloalkane or another aromatic ring,

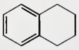

cyclohexanebenzene
(common name: tetralin)

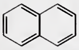

naphthalene

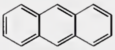

anthracene

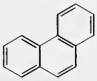

phenanthrene

In polynuclear aromatic molecules, the aromaticity in general decreases and the chemical reactivity of the molecule increases as the number of aromatic rings increases. This is reflected by the magnitude of the empirical resonance energy which has values of 150.6, 255.2, 351.5 and 387.0 $kJ \cdot mol^{-1}$ for benzene, naphthalene, anthracene and phenanthrene, showing that the second ring contributes less than the first, and the third ring slightly more or slightly less than the second, depending on molecular geometry, the linearly condensed anthracene being less stable than its angularly condensed isomer, phenanthrene.

All the aromatic compounds mentioned above and their higher polybenzenoid hydrocarbon derivatives listed below, along with a multitude of known and unknown structures, occur in petroleum and have some role in petroleum chemistry. According to IUPAC convention the nomenclature of aromatic compounds includes a numbering system for the aromatic carbon and an alphabetical designation of the sides around the periphery of the aromatic rings (using lower case italic letters) as illustrated below:

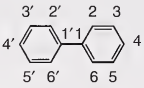
3′ 2′ 2 3
4′ 1′1 4
5′ 6′ 6 5

biphenyl

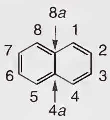
8a
8 1
7 2
6 3
5 4
4a

naphthalene

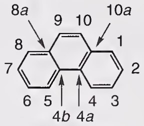
8a 9 10 10a
8 1
7 2
6 5 4 3
4b 4a

phenanthrene

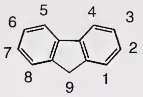

fluorene

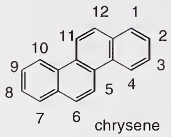
12 1
11 2
10 3
9
8 5 4
7 6

chrysene

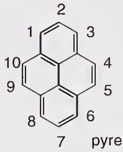
2
1 3
10 4
9 5
8 6
7

pyrene

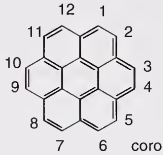
12 1
11 2
10 3
9 4
8 5
7 6

coronene

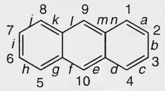
8 9 1
j k l m n a
7 i 2 b
6 h g f e d c 3
5 10 4

anthracene

Some of the higher benzenoid hydrocarbons are named as the "benz-" derivatives of simpler hydrocarbons. The position of fusion is represented by the letter designating the side of the molecule.

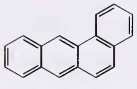

benz[*a*]anthracene

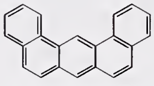

dibenz[*a,j*]anthracene

In some polycyclic aromatic systems some of the C–H bonds may become quite acidic. Outstanding examples are indene and fluorene,

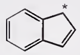

indene

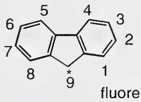

fluorene

the asterisks indicating the position of acidity and high reactivity. These compounds are oxidized readily and 9-alkylfluorenes, 9-alkylfluoren-9-ols and alkylfluoren-9-ones are significant constituents of oil sand bitumens.

4.0 Heteroatom-Containing Compounds

The bulk of sulfur and nitrogen in petroleum and bitumen is present as members of the rings of cyclic, mainly aromatic molecules. Reported to be present are: series of alkylthiophenes, a), alkylbenzo[*b*]thiophenes, b), alkyldibenzo[*b,d*] thiophenes, c), as well as higher benzo- and cycloalkanobenzothiophenes, d),

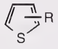

a

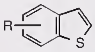

b

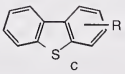

c

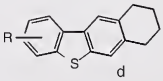

d

alkylthiolanes, e) and alkylthianes, f),

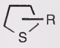

e

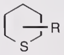

f

, *etc.*,

where R is an alkyl group. Lesser amounts of sulfur are also present in the form of open-chain sulfides, R–S–R. Among nitrogen compounds the most common ones are: alkylcarbazoles, g), alkylpyridines, h), alkylquinolines, i), and alkylmetalloporphyrins, j).

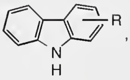

g

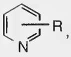

h

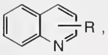

i

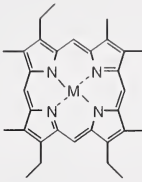

j

M = Ni $^{2+}$, VO $^{2+}$

Some of these nitrogen compounds are neutral, some are weakly acidic and others are slightly basic. Their acid-base properties and ability to form complexes with certain transition metals are exploited for their isolation from the oil. The porphyrins are intensely colored in their free forms as well as in their metal complexes.

Oxygen is present mainly in the form of carboxylic acid groups, alcoholic hydroxyl groups, carbonyl groups of ketones, esters and ethers, rather than in the rings of cyclic compounds.

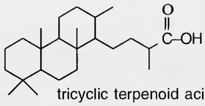

tricyclic terpenoid acid

CH_3–$(CH_2)_{14}CH_2OH$

n-hexadecanol

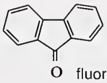
fluoren-9-one

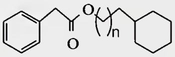

,

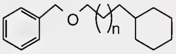

etc.

Relatively few compounds have been identified containing more than one heteroatom. These include the carboxylic acids, some sulfoxides and, of course, the porphyrins, among others.

The groups

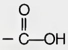

$-\overset{O}{\overset{\|}{C}}-OH$

carboxy

, R–OH

hydroxyl

,

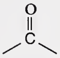

carbonyl

, *etc.*,

are functional groups. Their reactivity is not much altered when they are transferred from one carbon atom to another and they dominate the chemistry of the molecule. The C–S–C bonds in sulfides, the mercapto –SH group in thiols, and the alkylcarboxy group (–C(O)–OR) in esters are some other functional groups.

5.0 More About Isomerism in Carbon Compounds

Structural and geometric isomerism results from differences in the structural arrangement of atoms, *e.g.*

C_6H_{12}

and

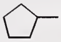
C_6H_{12}

structural isomers

or the orientation of an atom or groups of atoms with respect to a plane in the molecule, *e.g.*, *cis*- and *trans*-1,4-dimethylcyclohexane

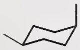
and

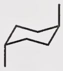
geometrical isomers

A third kind of isomerism may arise from differences in the spatial arrangement of atoms or groups of atoms in the molecule. This can be simply illustrated by analogy with the non-superimposable mirror image symmetry relationship between the left hand and right hand:

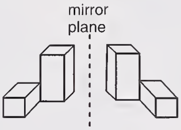

This general symmetry property involving mirror images is called chirality and two compounds that differ in chirality only, are called enantiomers. An example is 2-iodobutane, $CH_3CHICH_2CH_3$,

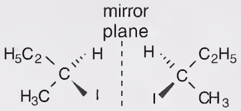

These two enantiomeric 2-iodobutane molecules are said to be stereoisomers. They owe their chirality to the asymmetry of the central carbon atom which has four different substituents attached to it.

The physical properties of the two enantiomeric 2-iodobutanes are identical except with respect to the way they interact with polarized light and thus the two molecules are optically active. Both isomers rotate the plane of plane polarized light passing through them. On facing the beam, one enantiomer rotates it clockwise (dextrorotatory, +) and the other one, counter-clockwise (levorotatory, –). To designate the absolute configuration of the enantiomers, the letters R (latin rectus, right) and S (latin sinister, left) are used according to standard nomenclature. In this way the enantiomer

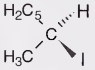

is assigned the letter S and called (S)-2-iodobutane and the enantiomer

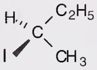

is assigned the letter R and is called (R)-2-iodobutane. The process of changing an asymmetric center from R to S or *vice versa* is called inversion. In general, inversions require the breaking of carbon-substituent bonds and therefore require a high activation energy.

In organic geochemistry the R and S designations are restricted to carbon atoms which are not part of a ring structure; for asymmetric carbon atoms in ring structures, the designations α and β are employed to indicate positions below and above the average plane of the polycyclic molecule. In structural formulas the use of a small circle on the asymmetric carbon indicates the position of a hydrogen atom, an open circle for α(H) and a filled circle for β(H), *e.g.*:

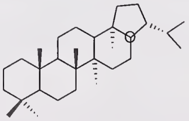

17α(H),21β(H)hopane

An equimolar mixture of two enantiomers is called a racemic mixture or racemate and can be specified by the (±) symbol, for example (±)-2-iodobutane. The physical properties of racemates are not necessarily the same as those of the pure enantiomers. Racemic mixtures may crystallize to give separate crystals of the (+) and (–) forms or crystals of a racemic compound containing equal numbers of (+) and (–) molecules.

Compounds containing more than one asymmetric carbon may possess a larger number of stereoisomers. For example, 2-chloro-3-iodobutane has four stereoisomers

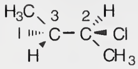

(2S,3R)-2-chloro-3-iodobutane

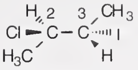

(2R,3S)-2-chloro-3-iodobutane

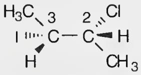

(2R,3R)-2-chloro-3-iodobutane

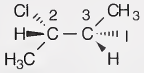

(2S,3S)-2-chloro-3-iodobutane

forming two pairs of enantiomers, the (2S,3R)–(2R,3S) and the (2R,3R)–(2S,3S) pairs. Stereoisomers which are not enantiomers (mirror images) are said to be diastereomers:

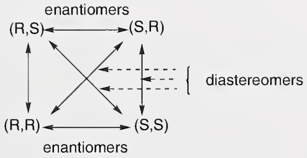

Stereoisomerism also exists in cyclic compounds. 1,4-Dimethylcyclohexane does not contain asymmetric carbon centers

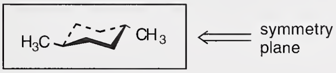

and *cis*-1,3-dimethylcyclohexane contains two asymmetric carbons,

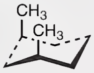

but the molecule has a plane of symmetry and optical rotation by one of the centers is perfectly balanced by the optical rotation of the other center. Such molecules are called “meso” molecules and they are optically inactive. The *trans*-isomer does not contain a plane of symmetry

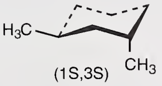

(1S,3S)

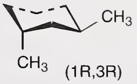

(1R,3R)

and exists as a pair of enantiomers.

In molecules containing more than one chiral center, inversion of a single asymmetric center yields an epimer. Inversion of one or more asymmetric centers yields a diastereomer.

An important question relating to stereoisomerism is its interrelationship with chemical reactions. In this connection a basic tenet is that achiral reactants produce only achiral or racemic products. When at least one chiral center is present in one of the reagents, racemic and diastereomeric products may result and the yields of the latter are not necessarily identical. Enantiomers show equal reactivity toward achiral reagents, but when they react with another chiral compound, the two enantiomers generally do not react at equal rates.

Chiral molecules synthesized by living organisms are produced only in a single, specific stereoisomer form which is usually not the most thermodynamically stable of the possible isomers. In an organic sediment such a biological isomer undergoes isomerization to the more stable geological isomer and the extent of isomerization can yield information on the evolutionary history of the sediment.

Crude oils display a mild optical rotatory power owing to their chiral molecular content. This rotatory power is usually concentrated in the cyclic terpenoid hydrocarbon fraction of the oil containing drimane, cheilanthane, sterane and hopane type biomarker hydrocarbons, the chemistry and organic geochemical significance of which will be discussed in Chapters 13 and 14.

6.0 Chemical Structures of the Bioorganic Precursor Source Materials of Petroleum

In general, five major compound classes of bioorganic molecules are considered as precursor source materials of petroleum. They are the lipids, proteins, carbohydrates, lignins and pigments. These materials were originally synthesized by the living organisms (bacteria, phytoplankton, zooplankton and higher plants) which are the main contributors of organic matter in sediments.

Lipids are the biomolecules that are insoluble in water but soluble in chlorinated methanes, ethers, aliphatic and aromatic hydrocarbons and acetone. They include fats, oils, waxes and related substances.

Fats and oils are esters of mostly even carbon number, straight-chain carboxylic acids and the triol glycerine:

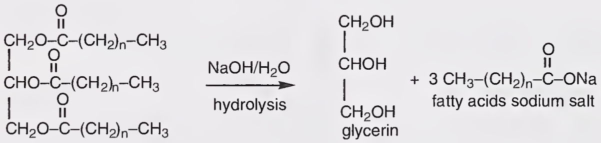

$$\begin{array}{l} CH_2O\text{–}\overset{O}{\overset{\|}{C}}\text{–}(CH_2)_n\text{–}CH_3 \\ CHO\text{–}\overset{O}{\overset{\|}{C}}\text{–}(CH_2)_n\text{–}CH_3 \\ CH_2O\text{–}\overset{O}{\overset{\|}{C}}\text{–}(CH_2)_n\text{–}CH_3 \end{array} \xrightarrow[\text{hydrolysis}]{NaOH/H_2O} \begin{array}{c} CH_2OH \\ CHOH \\ CH_2OH \\ \text{glycerin} \end{array} + 3\ CH_3\text{–}(CH_2)_n\text{–}\overset{O}{\overset{\|}{C}}\text{–}ONa$$

fatty acids sodium salt

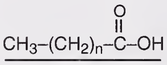

$$CH_3\text{–}(CH_2)_n\text{–}\overset{O}{\overset{\|}{C}}\text{–}OH$$

	n
lauric acid	12
myristic acid	14
palmitic acid	16
stearic acid	18

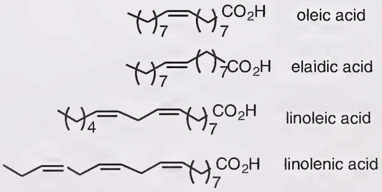

Carboxylic acids readily undergo decarboxylation on thermolysis to form *n*-alkanes:

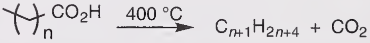

Alkanes and other hydrocarbons, mainly of the isoprenoid and terpenoid types along with their simple derivatives, which are synthesized by living organisms and found abundantly in organic sediments, also satisfy the solubility requirements for lipids. Some examples of the biological precursors of these hydrocarbons are the following:

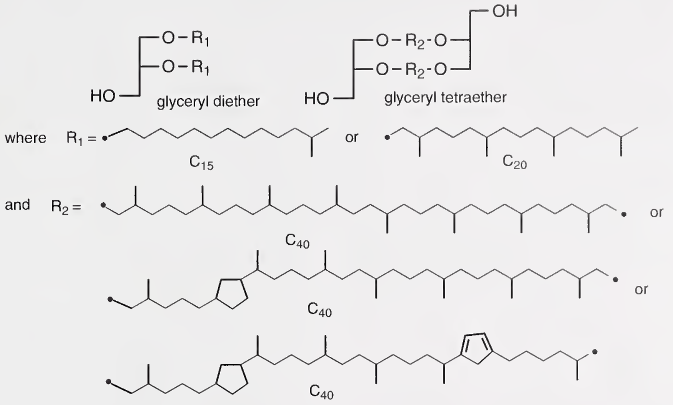
OH
O–R₁
O–R₁
HO
glyceryl diether
O–R₂-O
O–R₂-O
HO
glyceryl tetraether
where R₁ =
or
C₁₅
C₂₀
and R₂ =
or
C₄₀
or
C₄₀
C₄₀

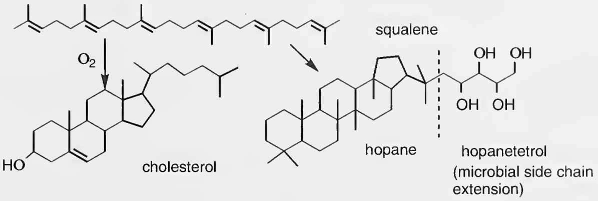
squalene
O₂
OH OH
OH OH
HO
cholesterol
hopane
hopanetetrol
(microbial side chain
extension)

among many others.

Proteins are essential components of the living cell. They serve varied biological functions as structural materials, catalysts, energy stores and the transporting agents of various materials throughout the organism. They are polymeric materials with molecular weights ranging from 6,000 to tens of millions g·mol^{-1}. The structural units of the protein molecule are the amino acids joined by peptide linkages which, on hydrolysis, release an amine and a carboxylic acid:

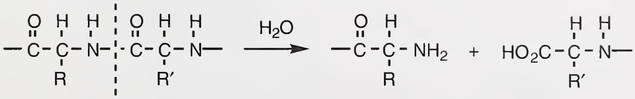

$$-\overset{O}{\overset{\|}{C}}-\underset{R}{\overset{H}{C}}-\overset{H}{N}-\overset{O}{\overset{\|}{C}}-\underset{R'}{\overset{H}{C}}-\overset{H}{N}- \xrightarrow{H_2O} -\overset{O}{\overset{\|}{C}}-\underset{R}{\overset{H}{C}}-NH_2 + HO_2C-\underset{R'}{\overset{H}{C}}-\overset{H}{N}-$$

Protein precursors account for most of the nitrogen compounds in petroleum.

Carbohydrates constitute the family of sugars, the mono-, di-, oligo- and polysaccharides. Monomeric sugars are pentacyclic and hexacyclic ethers

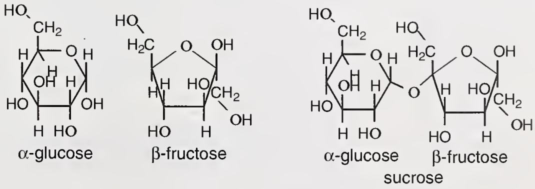
HO
CH₂
H
O
H
H
OH
H
HO
OH
H HO
α-glucose
HO
H₂C
O
OH
H
HO
CH₂
OH
HO H
β-fructose
α-glucose
β-fructose
sucrose

which can combine through an ether linkage to form di- to polysaccharides containing up to 8,000 monomeric units. Carbohydrates are the most abundant constituents of plants and animals.

They provide the supporting tissues of plants and certain animals, store energy, and constitute essential portions of the genetic materials deoxyribonucleic acid (DNA) and ribonucleic acid (RNA). Some of the important polysaccharides are:

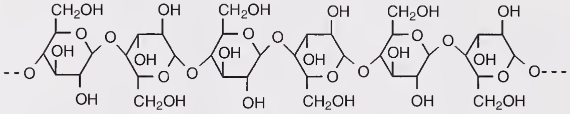

cellulose

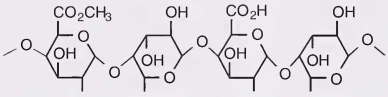

pectin

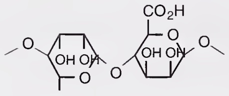

alginic acid

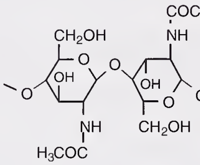

chitin

Like proteins, carbohydrates are hydrolyzed and converted into monomers which are largely decomposed before incorporation into the kerogen macromolecule would occur.

Lignin is a random polymeric macromolecule built from phenyl-propyl alcohol derivatives as monomeric units. It occurs between the cellulose micelles of supporting woody tissues of plants. Lignins show phylogenetic differentiation and different plants have lignins of different composition. Structural segments of hypothetical lignin molecules are shown below.

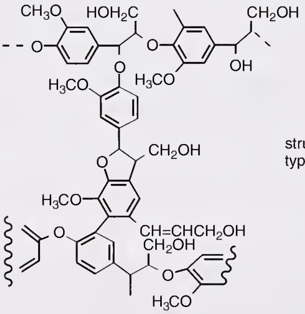

structural segment showing typical linkages in lignin

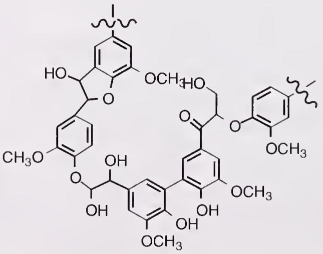

structural segment showing typical linkages in softwood lignin

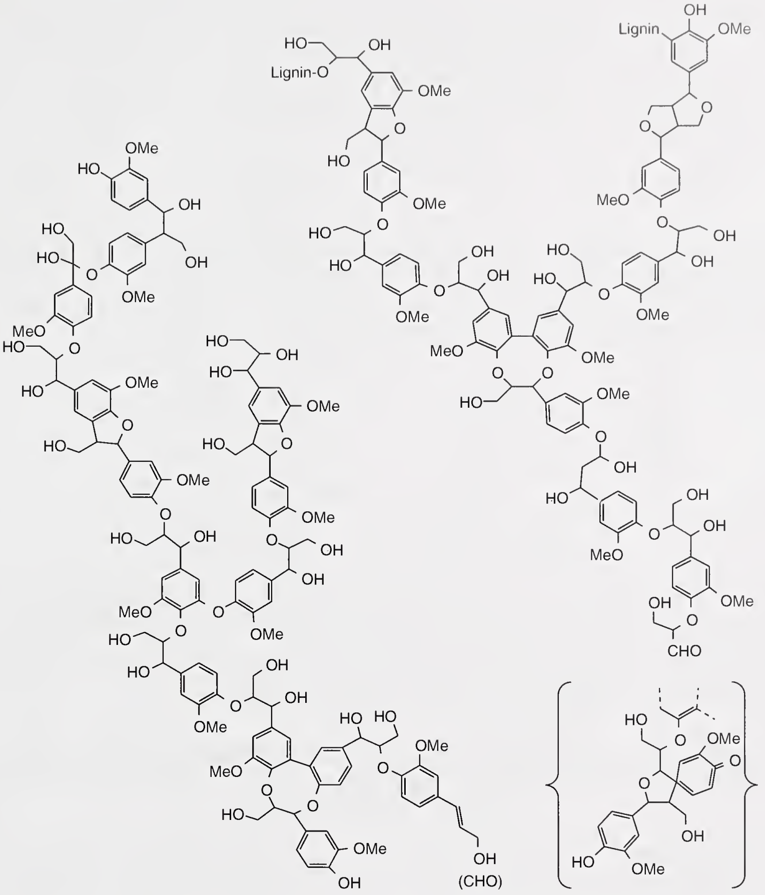

(After L.A. Lucia and Ki-Oh Hwang, The Spectrum, 14 (2) (2001) 9.)

Lignin is the only precursor source material whose structure is dominated by aromatics and it is rich in phenolic and alcoholic hydroxyl, methoxy and ether moieties as well.

Pigments are highly colored substances of which the most important ones, in the context of petroleum composition, are the various chlorophylls and, to a much smaller extent, the hemins:

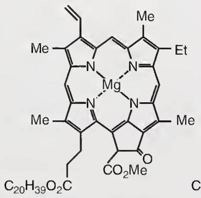

chlorophyll-*a*

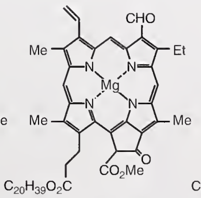

chlorophyll-*b*

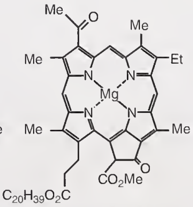

bacteriochlorophyll

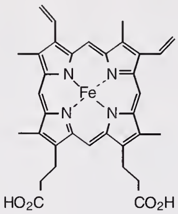
hemin

Chlorophylls occur in the green parts of plants and are responsible for their green color; they act as the photosynthetic pigments absorbing sunlight and converting it to chemical energy. In the sediments they undergo chemical transformation to porphyrins which form stable metalloporphyrin complexes with Ni^{2+} and VO^{2+} ions

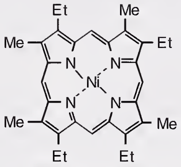
Nickel ETIO porphyrin

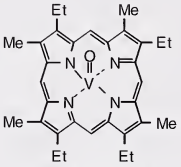
Vanadyl ETIO porphyrin

and these are the molecular forms of the chorophyll residues found in petroleum. The role of hemins as the source material of petroporphyrins is uncertain but is considered to be quite minor compared to that of chlorophylls. Hemins are the red pigments in animal blood and muscle and are the principal agents for the transport of oxygen.

7.0 Types of Functional Groups and Chemical Structures in Alberta Bitumens

Aside from hydrocarbons, the more important types of functional groups and chemical structures detected in Alberta bitumens and heavy oils are listed in Table 4.3. The cyclic molecules are far more important than the acyclics, although open-chain alkyl groups attached to ring structures represent a significant weight percent of the bitumen. The "R" substituents in the structures may represent either an open-chain hydrocarbon radical, an alicyclic hydrocarbon radical, or an aromatic hydrocarbon radical. Most of the ring structures, including pure hydrocarbons, bear at least one alkyl substituent.

Table 4.3 Some types of functional groups and chemical structures in Alberta bitumens

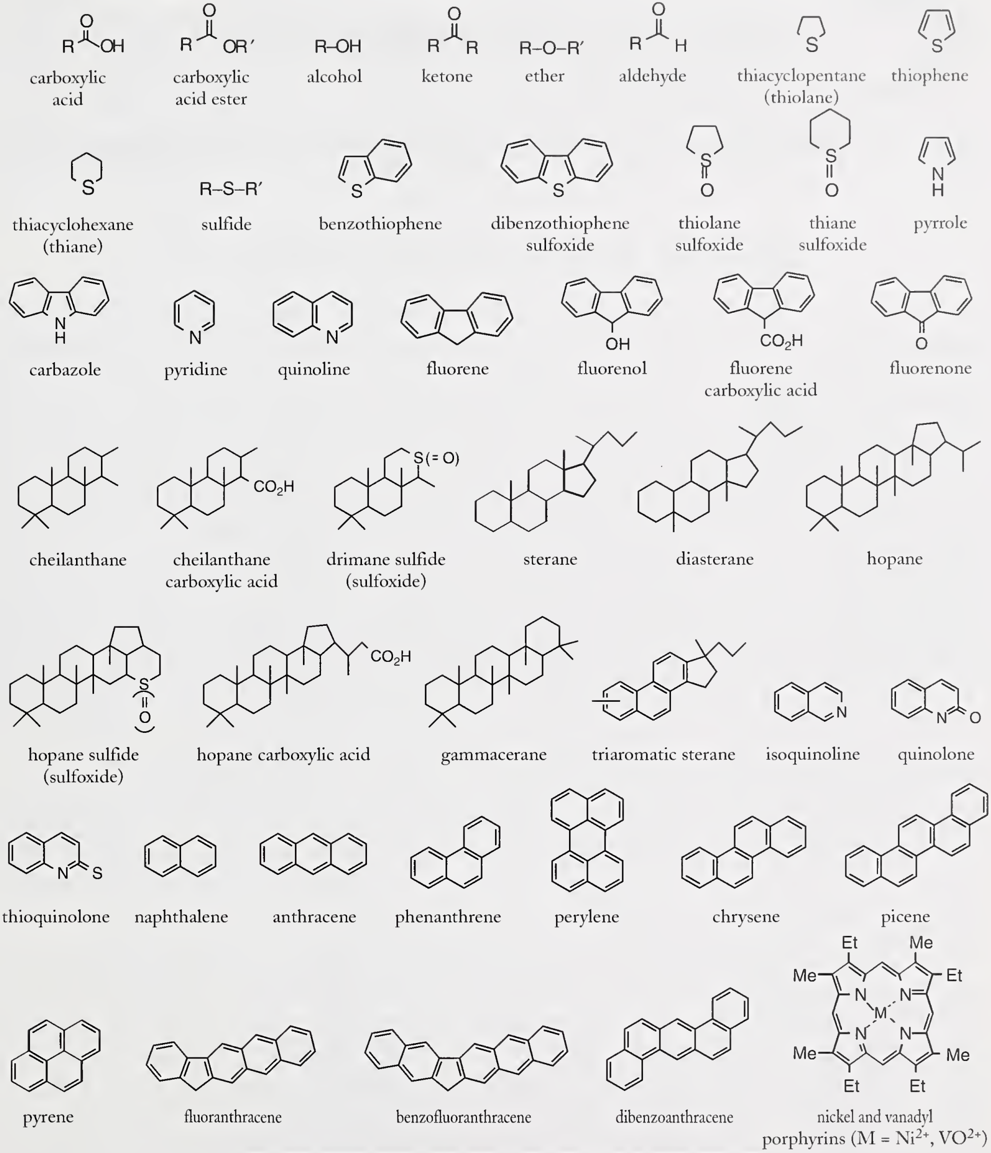
carboxylic acid
carboxylic acid ester
alcohol
ketone
ether
aldehyde
thiacyclopentane (thiolane)
thiophene
thiacyclohexane (thiane)
sulfide
benzothiophene
dibenzothiophene sulfoxide
thiolane sulfoxide
thiane sulfoxide
pyrrole
carbazole
pyridine
quinoline
fluorene
fluorenol
fluorene carboxylic acid
fluorenone
cheilanthane
cheilanthane carboxylic acid
drimane sulfide (sulfoxide)
sterane
diasterane
hopane
hopane sulfide (sulfoxide)
hopane carboxylic acid
gammacerane
triaromatic sterane
isoquinoline
quinolone
thioquinolone
naphthalene
anthracene
phenanthrene
perylene
chrysene
picene
pyrene
fluoranthracene
benzofluoranthracene
dibenzoanthracene
nickel and vanadyl porphyrins (M = Ni2+, VO2+)

n-Alkanes: may be dominated by the even carbon number or odd carbon number members, depending on the origin and history of the sediment. Therefore, the odd to even ratio may be used as a biomarker indicator giving information about the origin and history of the oil. The Carbon Preference Index, CPI, defines the ratio, by weight of the odd to even molecules as $\mathrm{CPI} = \frac{1}{2}\left[\frac{C_{25}+C_{27}+C_{29}+C_{31}+C_{33}}{C_{24}+C_{26}+C_{28}+C_{30}+C_{32}} + \frac{C_{25}+C_{27}+C_{29}+C_{31}+C_{33}}{C_{26}+C_{28}+C_{30}+C_{32}+C_{34}}\right]$ for the higher members of the series and the Odd-Even Preference, $\mathrm{OEP} = \frac{(C_{17}+6C_{19}+C_{21})}{(4C_{18}+4C_{20})}$ for the lower homologues.

Composition and Properties of Bitumen

5

1.0 Definition, Characterization, Separation

Bitumen is the heaviest form of petroleum. It is a dark brown-to-blackish, dense, slightly viscoelastic, semisolid hydrocarbon which, in general, is rich in heteroatoms, nitrogen, oxygen, sulfur (NOS) and various metals. It occurs in nature in association with unconsolidated and loosely consolidated sandstones and carbonate rocks as oil sand and oil carbonate accumulations and various types of "migrabitumens" (bitumens that have undergone secondary alterations). The latter materials which, in smaller quantities, can be found in many places worldwide, are classified according to their solubility in carbon disulfide, fusibility, hydrogen to carbon ratio, *etc.*, and include mineral waxes, natural asphalts, asphaltites and pyrobitumens. Another type of bitumen also occurs in finely divided form as a companion of kerogen, the precursor of most petroleums. Kerogen, the most abundant form of organic carbon on earth, can be found in all sedimentary rocks, usually in small quantities and in association with up to 10% (but usually less) bitumen. This bitumen has a different origin and chemical composition from pooled bitumen and may be called rock bitumen. Rock bitumen, after kerogen, is probably the second most abundant form of organic carbon on earth.

Bitumen, according to most recent classification schemes, is defined as petroleum having a viscosity greater than 10^4 mPa·s and a density greater than 1.000 $g \cdot cm^{-3}$, corresponding to an American Petroleum Institute (API) gravity of less than 10 degrees, Table 5.1. Such viscous liquids do not flow readily and therefore oil sand bitumens cannot be recovered by conventional recovery technology.

Petroleum comprises mainly hydrocarbon compounds, that is, molecules composed of only carbon and hydrogen. The three principal types of hydrocarbons present in petroleum are the paraffins (acyclic alkanes with generic formula C_nH_{2n+2}), the naphthenes (cycloalkanes, C_nH_{2n+Z} where $Z = 0, |-2| - |-12|$) and the aromatics (benzene and its derivatives, C_nH_{2n+Z} where $Z = -6$ and less). Their proportions vary from crude oil to crude oil and, depending which one of them predominates, we differentiate between paraffinic, naphthenic (asphaltic), and aromatic crude oils. Most of the constituent hydrocarbon molecules, especially in the higher-boiling (> 200℃) fractions, are not purely paraffinic, naphthenic or aromatic but contain a combination of groups belonging to two or even all three types of hydrocarbons. For example, alkylbenzenes,

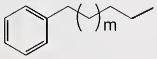

C_nH_{2n-6}

The API gravity scale is a modification of the earlier Baumé scale. In the API gravity scale the gravity of water has a value of 10° and that of liquid methane (at its saturation pressure), 340°. The API scale is defined as:

$$°API = \frac{141.5}{\begin{array}{c}\text{specific gravity}\\ (15.6 / 15.6\ ℃)\end{array}} - 131.5 \qquad (1)$$

Table 5.1 Classification of crude oils according to grade[1]

Grade of oil	Specific gravity	API gravity ° API	Viscosity mPa·s	
Conventional light oil	< 8.76	>30		⬜
Conventional medium oil	0.934–0.876	20–30		░
Heavy oil	1.00–0.934	10–20	$\leq 10^3$	▒
Extra heavy oil	> 1.00	< 10	$\leq 10^4$	▓
Bitumen	> 1.00	< 10	$> 10^4$	█

contain a paraffinic group (the side chain) and an aromatic group (the benzene ring) and alkyltetralins

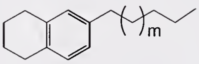

C_nH_{2n-8}

contain a paraffinic, an aromatic and a naphthenic (cyclohexeno) group. For this reason and also because of the gradation in the concentration distribution of the different constituent classes (paraffins, naphthenes, aromatics) in the whole oil and in its various fractions, we can have intermediate paraffinic–naphthenic, paraffinic–naphthenic–aromatic, *etc.* class crude oils. Depending on density, each class can exist as light and heavy crude. Aromatic crudes usually tend to be heavier than paraffinic crudes.

Oil sand and carbonate bitumens are heavy and, as a rule of thumb, microbiologically degraded petroleums. The microorganisms causing the biodegradation of petroleum preferentially metabolize straight-chain paraffinic hydrocarbons and therefore bitumens are devoid of, or strongly depleted in, their paraffinic complement and belong to the naphthenic–aromatic class heavy crude oil family.

Since the early days of the petroleum industry there has existed a need for the characterization and classification of crude oils in terms of simple, readily obtainable physical and chemical parameters, in order to determine their commercial value, composition, recovery and refining requirements and product yields. Historically, the parameters that have been most useful in this respect are the density or API gravity, refractive index, molecular weight, viscosity, boiling point of fractions and distribution according to volatility, color, *etc.* Of the many suggestions that have been made for the characterization of crude oils in terms of one or more simple physical properties, the ones listed in Table 5.1 are useful for quick orientation and classification. One of the simplest, for example, of the many correlations developed between class composition and physical parameters is the viscosity–gravity constant, defined for viscous oils as

$$\text{vgc} = \frac{d - 0.240 - 0.022\log(v - 35.5)}{0.755} \tag{2}$$

where d is the specific gravity (15.6/15.6°C) and v is the Saybolt viscosity at 99°C (see Section 2.2). For Athabasca (Syncrude, Suncor) bitumen with $d = 1.025$ and $v = 513$, the value of vgc is computed to be 0.962. For paraffinic oils, the value of vgc is lower, around 0.8, and therefore the high value of the index for bitumen is consistent with its known low paraffinic content. Yet another characterization factor is the Universal Oil Product, UOP, or Watson characterization factor, defined as

$$K = \frac{T_b^{1/3}}{\text{spec. grav.}} \qquad (3)$$

where T_b is the average boiling point on the Rankin scale (degrees Fahrenheit + 460). This factor was invented to reflect the thermal cracking properties of heavy oils and its value ranges from < 10 to 15 for aromatic < naphthenic < paraffinic materials.

Since petroleum, including bitumen, is a highly complex and variable mixture of thousands and thousands of hydrocarbon, hydrocarbon-based and other types of molecules, some of which are present as real solutions and others as colloidal dispersions, the formulation of universal characterization–classification schemes in terms of a few bulk physical properties is not a readily accomplishable task. Quite the contrary, the precise definition of petroleum even with modern chemical methods, as will be shown in later chapters, represents a challenge to the petroleum chemist. Nevertheless, it should be pointed out that with modern instrumental methods like, for example, high-field nuclear magnetic resonance (NMR), Fourier transform infrared (FTIR) spectroscopy, capillary gas chromatography–mass spectrometry (GC–MS) and high-pressure liquid chromatography–mass spectrometry (HPLC-MS), in combination with wet chemical methods, powerful insight into the chemical composition of petroleum can be obtained in routine type analyses. For instance with NMR spectroscopy it is a relatively simple task to obtain precise values for the relative proportions of the alkyl, naphthenic and aromatic carbon contents and the relative proportions of the hydrogen atoms attached to alkyl, naphthenic and aromatic carbons.

The chemical composition and colloidal structure of the bitumen are the primary factors that determine the nature of the products that can be obtained from the upgrading of the bitumen; they also set the requirements for the technologies necessary to achieve optimum process economy. Ultimately, these same intrinsic properties are also responsible for the observable physical and chemical properties which are monitored during process operations. Some of these physical properties, along with elemental compositions, will be reviewed in the sections below. Details of the chemical composition will be the subject of subsequent chapters.

In order to investigate the properties of bitumen, the bitumen first has to be separated from the associated mineral matter in the oil sand. This can be achieved by a number of means, including solvent extraction, centrifugation, and water displacement. The means of separation may have a mild effect on the quantity, composition and properties of the produced bitumen. By definition, bitumen is the benzene- or toluene-soluble organic matter present in the rock or the rock matrix having a density and viscosity as indicated in Table 5.1. As noted in Chapter 3, there are small quantities of other organic materials present in oil sands (and in oil carbonates) which have compositions and origins different from those of the bitumen and which are not soluble in benzene, toluene or in nonpolar organic solvents. Employing solvents other than benzene, toluene or simple chlorinated hydrocarbons (for example, methylene chloride), small amounts of these non-bitumen organic materials may be solubilized and extracted with the bitumen.

The precise analytical determination of the bitumen content of oil sands is of great importance with regard to the assessment of the extent of bitumen reserves present in a deposit. The analytical method that has been developed specifically for Athabasca oil sand by Syncrude Canada Ltd.[2] employs "a blend of 74% toluene and 26% isopropyl alcohol, which extracts both the bitumen and the water from the solids, producing a homogeneous liquid phase. The bitumen is determined gravimetrically on an aliquot of this solution. A Karl Fischer titration is used to measure the water concentration. Solids are measured gravimetrically." This method has been accepted by the oil sand industry as the reference procedure for the determination of bitumen content.

From comparative laboratory studies on solvent extraction it was reported that:[3]

- the extraction efficiency and mineral content of the extract depend on the solvent, the extractor and filter employed;
- the extraction efficiencies of toluene, pyridine, methylene chloride, *etc.*, are equally high but the bitumen from the methylene chloride extraction contains a higher level of chloride (850 ppm) than that from the toluene extraction (100 ppm). This has been attributed to a slight decomposition of methylene chloride by hydrolysis, producing hydrogen chloride;
- the percentage amount of residual organic carbon left on the sand after solvent extraction is small and follows the order 0.15:0.16:0.21 for toluene, pyridine and methylene chloride in the particular procedure employed in these studies; and
- grinding of the oil sands prior to solvent extraction produces bitumen with an enhanced inorganic content.

In practical terms, either of the above solvents can be used for laboratory studies. However, in other respects, methylene chloride[4] offers the following advantages over toluene or pyridine:

- low toxicity;
- no flash point (no fire or explosion hazard); and
- low boiling point, 39.8°C (*versus* 110.6°C for toluene and 115.5°C for pyridine) along with low heat of vaporization, which reduce the loss of light ends.

For these reasons, methylene chloride is the solvent of choice for laboratory extraction of the bitumen.

The centrifugation method[5] (70°C, spun at 3,000 rpm (1,780 g) for 2–2.5 hours) is reported to give a yield of only 65% of the bitumen from a high-grade (15.8% bitumen-containing) oil sand. The properties (°API, MW, C, H, N, O, S, V, Ni contents, class composition, simulated distillation) of centrifuged and benzene-extracted bitumens were practically identical except that the viscosity of the centrifuged sample was somewhat lower than that of the extracted sample. This is a consequence of the combined effect of the loss of the high-viscosity, heavy fraction of the bitumen (35%) in the centrifugation and the low-viscosity light end in the benzene extraction procedure. That light end losses can indeed occur was proven in unrelated experiments[6,7] by removing and collecting the light oil (which amounted to ~0.6%) by vacuum distillation at 90–100°C and 0.1 torr pressure and measuring the viscosity of the bitumen with and without the light oil added. The result indicated a nearly two-fold decrease in viscosity at 60°C upon addition of the light oil back to the bitumen. The conclusion from these studies on the centrifugation separation of bitumen from the oil sand is that any advantage offered over solvent extraction is offset by the uncertainty introduced by the low recovery.

Lastly, the separation in the industrial hot water process is carried out at a basic *pH* of about 8.5 and around 82°C. Under these conditions some acidic (carboxylic acids) and other water-soluble materials (alcohols, organic sulfides and sulfoxides, hydrocarbons, *etc.*) may be removed from the bitumen and transferred to the aqueous phase as a real or colloidal solution. At the same time a variety of carboxylic acids, humic acids, fulvic acids, ketones, alcohols and other substances are solubilized by the hydrolytic reactions of chemisorbed and humic matter and these freshly liberated materials may be introduced into the bitumen. It should be noted here that salts of carboxylic acids (formic, acetic, propionic, butyric, *etc.*) are regular constituents of the connate water solids[8] and C_{14}–C_{30} *n*-alkanoic acids[9a] as well as C_2–C_5 α, ω–di–*n*–alkanoic acid[9b] anions have been isolated from petroleum-associated waters and from the industrial process water.

Both laboratory solvent-extracted and industrial hot-water-separated bitumens have solid (ash) contents of the order 0.4–1.0%, which can be reduced (but not readily eliminated) by centrifuging the bitumen solution—except when the procedure is carried out in super high speed ultracentrifuges (at $\geq$50 k gravity).[10]

Some analytical results reported on the bitumen, water and solids contents of Syncrude[11,12] and Suncor[3] oil sands are given in Table 5.2. The necessity of using small samples in the analysis introduces considerable variability among replicate sample analyses performed on any given bulk quantity of oil sand, owing to subsampling uncertainty. For instance, it has been shown[11] that for bulk samples of the order 325 kg, as many as twenty 120-g subsamples must be collected and analyzed so that sampling uncertainties become less than three times the analytical standard deviation.

Table 5.2 Precision of oil–water–solids analyses

Syncrude:[a]		Oil sand grade		
		High	Medium	Low
% Bitumen	Mean	14.64	11.62	8.87
	RSD (%)[b]	2.2	1.7	4.7
% Water	Mean	1.45	3.63	4.65
	RSD (%)	11.7	7.2	5.8
% Solids	Mean	84.22	84.96	86.72
	RSD (%)	0.4	0.6	0.3
% Mass Balance	Mean	100.31	100.21	100.24
	SD	0.36	0.47	0.42
Suncor:[c]				
% Bitumen	15.29 ± 0.72			
% Water	1.76 ± 0.84			

[a] From J.K. Liu, Ref. 12. These values were determined from an interlaboratory round-robin in which each laboratory analyzed 10 replicate samples of each grade of oil sand. The standard deviation includes the variance due to subsampling the oil sand. [b] RSD = relative standard deviation. [c] From L.D.L. Vorndran *et al.*, Ref. 3. 21 analyses.

2.0 Elemental Composition

The oldest and simplest means of chemical characterization of petroleum is in terms of elemental composition. Bitumen and petroleum in general are composed (to the extent of about 99.4–99.9%) of five elements: carbon and hydrogen (over 90%) and nitrogen, oxygen and sulfur (in a combined amount of up to about 9.9%). The rest (up to about 0.6%) is made up of metals in the form of organometallics such as vanadium and nickel porphyrins, carboxylic acid salts, oxides, carbonates, sulfides, silicates, fine clay particles, clay organics and heavy minerals.

While considering the physical properties and elemental compositional data which are reviewed below it should be kept in mind that most of the published data either do not refer to, or do not describe in sufficient detail, the method used to prepare the bitumen samples. Also, some of the data represent a single measurement, and others, multiple measurements. In some analyses oxygen was determined by direct measurement while in others it is given as the difference between the cumulative CHNS percent composition of bitumen and heavy oils and 100%, with or without appropriate corrections for ash and solid contents. Lastly, it should also be pointed out that considerable differences in the results may occur from laboratory to laboratory owing to the differences in analytical procedures or materials employed.

As seen from the data collected in Tables 5.3 and 5.4 the elemental compositions of most Alberta bitumens vary between narrow limits:

carbon	83.1 ± 0.5%
hydrogen	10.3 ± 0.3%
nitrogen	0.4 ± 0.1%
oxygen	1.1 ± 0.3%
sulfur	4.6 ± 0.5%

Variations in the existing data on oil sand bitumens from all sources are not extensive either. When the sulfur content is low, as, for example, 0.5% in Sunnyside bitumen, the carbon and hydrogen contents are correspondingly higher. It should be noted that the range given above for Alberta bitumens is commensurate with the range of scatter that emerged from round robin comparison of data.

Another important parameter derived from the hydrogen and carbon content is the atomic ratio of these two major elemental constituents, $(H/C)_a$. For Alberta bitumens this ratio hovers around 1.51 ± 0.03 but for low-sulfur bitumens the values are somewhat higher, 1.54–1.65.

Table 5.3 Elemental compositions of some bitumens and heavy oils

	C	H	N	O	S	$(H/C)_a$
Athabasca	83.31	10.59	0.41	0.88	4.78	1.53
Athabasca Suncor lease	83.86	10.44	0.45	1.30	4.62	1.49
Athabasca Suncor lease	82.40	10.20	0.56	1.41	4.48	1.49
Athabasca Suncor lease	83.23	10.7	0.46	~0.9	4.54	1.54
Athabasca Suncor lease	82.99	10.5	0.42	0.8	5.23	1.52
Athabasca Suncor lease	83.1	10.6	0.4	1.1	4.8	1.53
Athabasca Mildred–Ruth Lakes	83.18	10.4	0.45	2.25	3.5	1.50
Athabasca Bitumont	83.3	10.45	0.4	1.05	4.8	1.50
Athabasca Ells River	83.3	10.4	0.4	1.3	4.6	1.50
Athabasca Clearwater River	83.6	10.3	0.4	0.2	5.5	1.48
Athabasca Wabasca–McMurray	83.1	10.6	0.40	1.1	4.8	1.53
Lloydminster	83.23	10.50	0.31	0.9	4.2	1.51
Lloydminster	82.83	10.66	0.35	1.05	4.39	1.54
Cold Lake	83.12	10.73	0.34	1.42	4.17	1.55
Wabasca	83.30	11.30	0.36	0.74	4.07	1.63
Peace River	82.69	10.18	0.51	1.61	5.90	1.48
Carbonate	82.17	10.08	0.24	1.31	5.36	1.47
Asphalt Ridge	85.6	11.5	0.80	1.73	0.45	1.61
Asphalt Ridge	85.3	11.7	1.02	1.1	0.59	1.65
P.R. Springs	84.4	11.1	1.00	2.2	0.75	1.58
Tar Sand Triangle	84.0	10.1	0.46	1.1	4.4	1.44
Sunnyside	86.3	11.7	0.9	0.6	0.5	1.63
Bemolange	87.1	11.2	0.7	1.2	0.5	1.54

Table 5.4 General characterization and distillation data for Suncor coker feed bitumen[a]

Characterization

Property	Historical data		Sample 1	Sample 2
	Max.	Min.		
API gravity	11.3	8.6	11.3	10.6
Density	0.991	1.010	0.991	0.9952
Viscosity (cp)				
15°C	371,000	18,000	42,600	17,960
25°C	113,000	6,090	13,500	6,087
60°C	1,240	459	610	459
100°C	119	72	88	72
Ramsbottom carbon residue (wt%)	12.7	10.1	11.5	10.1
Ash (wt%)	0.65	0.44	0.51	0.58
Carbon (wt%)	83.86	82.38	83.86	82.40
Hydrogen (wt%)	10.84	10.00	10.44	10.20
Nitrogen (wt%)	0.68	0.33	0.45	0.56
Sulfur (wt%)	4.98	4.43	4.62	4.48
Oxygen (wt%)	1.42	0.84	1.30	1.41
Vanadium (ppm wt)	200	151.1	190	167
Nickel (ppm wt)	87.2	49	72.7	49
Asphaltene (wt%)	16.2	13.9	14.4	13.9
Acid number	2.61	2.03	2.03	2.11

Distillation data

Cut temp. (°C)	Cumulative vol. (%)		Cut temp. (°C)	Cumulative vol. (%)	
	Sample 1	Sample 2		Sample 1	Sample 2
144	–	–	343	21.4	23.41
150	–	–	375	26.8	28.12
175	–	–	400	31.3	31.78
195	–	4.83	425	35.4	28.12
225	6.9	8.88	450	39.4	39.52
250	9.7	11.65	475	43.5	43.29
275	12.5	14.41	500	47.6	47.07
300	15.2	17.17	524	51.5	50.46
325	18.4	20.74			

[a] Courtesy of Suncor. Field: Athabasca. Stratigraphic unit: McMurray. Location: 23-92-10-W4M. Method of production: hot water separation

The $(H/C)_a$ ratio is an important property of crude oils. The higher the ratio, the more valuable the crude. In conventional oils this ratio varies considerably; it may be as high as 2.0–2.3 in very light oils and as low as 1.4 in very heavy oils. The values of the $(H/C)_a$ ratios of the main types of hydrocarbons comprising the oil are characteristically different, as illustrated by the following typical compound types in the oil:

Paraffins:		$(H/C)_a$
CH_4	methane	4
C_2H_6	ethane	3
$CH_3CH_2CH_3$	propane	2.67
$CH_3(CH_2)_{14}CH_3$	hexadecane	2.125
in general for paraffins		> 2.0

Naphthenes:			
perhydro- phenanthrene	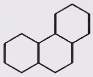	$C_{14}H_{24}$	1.714
in general for naphthenes			$1.0 < (H/C)_a \leq 2.0$
Aromatics:			
phenanthrene	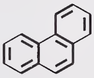	$C_{14}H_{10}$	0.714
in general for aromatics			≤ 1.0

Thus, the value of $(H/C)_a$ of 1.51 for bitumens is in agreement with their naphthenic–aromatic and low paraffinic character.

For gasoline the $(H/C)_a$ value is in the 1.9–1.95 range and this dictates the strategy for bitumen upgrading: the $(H/C)_a$ ratio must be increased. This can be accomplished either by addition of hydrogen, rejection of carbon, or both. It follows that the cost of upgrading and hence the commercial value of the bitumen is dependent on the $(H/C)_a$ ratio. Moreover, the $(H/C)_a$ value reflects the relative abundance of the less desirable, condensed, higher-molecular-weight asphaltic aggregates with a high propensity for coke formation, which limits upgrading options and the type of products obtainable. Many of the physical properties of bitumen also correlate with the $(H/C)_a$ ratio, for example, gravity, viscosity, distillation curve, pour point, etc.

The heteroatom and metal atom contents of bitumen are generally higher than those of conventional crude oils.

The oxygen content of bitumen, 1.1 ± 0.3%, is well above the few tenths of a percent found in light oils. This elevated oxygen content can be attributed to the microbial and associated water washing history of the bitumen. During the degradation of the precursor oil by aerobic microorganisms, some oxygen incorporation into the bitumen takes place either biologically or abiogenically from the oxygen dissolved in the surface-derived formation water flowing through the deposit. This mild, partial oxidation renders the bitumen more reactive and capable of taking up even more oxygen upon air exposure.

In contrast to oxygen incorporation, the incorporation of sulfur into the bitumen and crude oil is thought to occur in the early stages of diagenesis from the sulfur and hydrogen sulfide produced by sulfate-reducing bacteria, as will be discussed in Chapter 13.

The nitrogen in the bitumen and crude oil is derived partly from the transformation of pigment materials (chlorophylls, hemoglobins) and partly from that of amino acids and amides (from proteins, RNA, DNA, nucleic acids, cell walls of algae, *etc.*).

The heteroatoms are not distributed uniformly over the compound classes in the bitumen. The saturated (least polar) hydrocarbon fraction contains little in the way of heteroatoms, followed by the monoaromatic fraction with a quite low heteroatom content, and the di- and polyaromatic fractions with increasing heteroatom contents. The highest percentage oxygen is usually found in the most polar subfractions of the polars, followed by the asphaltene fraction. Similarly, the nitrogen is concentrated in the most polar and heaviest fractions, the polars and the asphaltene, while the less polar fraction (40–50%) of the bitumen is nearly devoid of nitrogen.

Most bitumens, including all the major reservoirs of the world, contain elevated levels of sulfur, up to ~6%, distributed in the aromatic, polar and asphaltene fractions. Without exception the asphaltene fraction has the highest sulfur content—in the case of Alberta bitumens, about 8.0–9.5%.

All crude oils contain trace metal constituents and bitumens are more abundant in trace metals than are lighter crude oils. The metals occur as oil-soluble porphyrin complexes and carboxylic acid salts, structural units in the asphaltene as well as components in the fine heavy minerals, silts, clays and clay organics which are suspended in the oil.

The distribution pattern of heteroatoms with class composition and polarity is paralleled by the distribution pattern with boiling points of the fractions: the heteroatom, V and Ni contents progressively increase with increasing boiling point.[13,14]

Trace metal distributions in Athabasca oil sand bitumen, fines and centrifuged bitumen as determined by neutron activation analysis[15] are given in Table 5.5. It is evident that all the

Table 5.5 Measured trace element concentrations (in $\mu g\ g^{-1}$) in Athabasca oil sand bitumen, fines and mineral-free bitumen[a]

Element	Athabasca I			Athabasca II	
	Bitumen (10.75%)[b]	Fines (2.23%)[b]	Bitumen mineral-free[b]	Bitumen (10.98%)[b] mineral-free	Fines (0.21%)[b]
Al	3190±300[c]	11300±7100	<1000	274±16	133000±9200
As	0.56±0.06	6.3±0.4	0.341±0.061	0.146±0.014	15.4±0.05
Ba	8.4±2.7	472±2	<6	2.9±1.2	464±76
Ce	2.50±0.34	91.8±2.0	<0.9	0.22±0.03	102±12
Cl	23.3±3.1	109±3	19.4±3.2	13.8±2.9	<20
Co	4.39±0.20	34000±280	3.19±0.22	0.24±0.03	22.9±3.1
Cr	4.60±0.37	93.1±1.3	1.31±0.45	0.85±0.07	117±18
Cs	0.23±0.02	5.9±0.1	<0.05	0.02±0.001	5.9±0.8
Eu	0.04±0.005	1.4±0.05	<0.02	0.007±0.001	1.4±0.2
Fe	1030±70	26600±180	<200	242±17	27500±4100
Ga	1.30±0.2	20.1±0.5	0.58±0.18	0.360±0.051	28.7±1.9
Hf	0.39±0.02	7.72±0.02	0.12±0.03	0.046±0.007	8.8±1.2
K	594±45	16800±30	0	<44.3±2.9	17200±64
La	1.64±0.12	49.2±1.2	<0.4	0.17±0.02	62.3±0.8
Mn	18.4±1.6	520±74	<7	4.76±0.21	733±19
Mo	n.d.[d]	n.d.	n.d.	7.2±1.8	<20
Na	149±10	2750±7	52±12	21.2±3.0	2110±13
Ni	68.1±8.0	52.0±7.7	66.3±8.0	71±16	69±17
Rb	5.7±1.1	57±14	3.71±1.2	1.72±0.13	65±22
Sb	0.05±0.009	0.58±0.05	0.03±0.01	0.025±0.002	1.0±0.3
Sc	0.48±0.02	12.7±0.2	<0.1	0.19±0.01	14.1±0.2
Se	0.61±0.06	27.1±0.3	0.51±0.06	0.34±0.03	3.1±0.7
Sm	0.20±0.03	5.82±0.09	<0.07	0.03±0.06	8.4±0.5
Sr	5.0±0.5	160±19	<3	3.0±0.2	183±3
Ta	0.22± 001	15.6±0.3	<0.04	0.004±0.001	1.5±0.2
Tb	0.023±0.008	0.71±0.12	<0.02	0.007±0.001	0.68±0.5
Th	0.56±0.04	12.7±0.2	<0.1	0.11±0.01	14.0±2
Ti	183±37	6830±580	<100	<80	9690±2200
V	144±19	142±16	139±19	170±5	194±24
Zr	9.80±3.4	219±9	<7	2.81±0.78	254±83

[a] From F.S. Jacobs and R.H. Filby, Ref. 15. [b] Weight percent of oil sand. [c] Mean ± standard deviation. [d] Not determined.

elements present in the bitumen are also present—and in significantly higher concentrations—in the fines. Some of the trace elements in the bitumen are present as fine mineral suspensions. When the fines are removed by centrifugation of the bitumen suspension, only about two thirds of the original 30 elements—Al, As, Ba, Cl, Co, Cr, Fe, Ga, Hf, Mn, Mo, Na, Ni, Rb, Sb, Se, Ti, V and Zr—remain measurable in the mineral-free bitumen. Therefore, it can be concluded that the rest of the elements—Ce, Cs, Eu, K, La, Sc, Sm, Sr, Ta, Tb, Th—detected in the uncentrifuged bitumen are present mainly in the inorganic particulate phase of the extracted bitumen. When the whole oil sand is ground prior to extraction, the metal content of the "mineral-free" bitumen shows an increase, suggesting that it may contain finely dispersed minerals that centrifugation (3,000 rpm for 30 minutes) does not remove. Comparison[16,17] of the average metal compositions of Syncrude coker feed and laboratory toluene-extracted bitumens with those of light Western Canadian oils, Table 5.6 and Appendix 5.1, points to the enhanced levels of trace metals in the bitumens relative to those of conventional crude oils—an observation which is valid for bitumens in general and can be taken as an indication of the existence of a genetic continuum between conventional oils, heavy oils and solid bitumens. Some of the metals, V and Ni, play the role of a biological marker, yielding information about the origin and depositional environment of the oil. Thus, high concentrations of V and Ni and high V/Ni ratios are characteristic of marine carbonate or siliclastic oils having moderate to high sulfur and low wax contents. A large percentage of the vanadium and nickel in petroleum occurs as porphyrin complexes.

In addition to the metal species detected by neutron activation analysis in Athabasca oil sands and bitumens, Tables 5.5 and 5.6, trace quantities of Nb, Y, La, Nd and U were detected in the fines by X-ray fluorescence spectroscopy.[18] For further relevant information *cf.* Appendix 5.1.

Table 5.6 Comparison of Athabasca bitumen trace element concentrations with Western Canada crude oil averages

Element	Concentration (ppm)			
	Syncrude coker feed[a]		Syncrude toluene extract[a]	Western Canada Oils mean[b]
	Sample 1	Sample 2		
V	n.d.[c]	177	140	13.6
Ni	74.1	71.9	30.1	9.38
Fe	142	254	127	10.8
Co	1.35	2.00	0.481	0.0537
Cr	1.01	1.68	0.719	0.0933
Mn	n.d.	3.85	1.40	0.100
Zn	n.d.	n.d.	0.615	0.459
Cu	n.d.	n.d.	0.725	n.d.
As	0.400	0.321	0.286	0.111
Se	0.286	0.517	0.167	0.052
Sb	0.031	0.028	0.013	0.0062
Hg[d]	n.d.	n.d.	0.686	50.9
Br	0.155	0.104	0.194	0.491
Cl	n.d.	8.00	7.53	39.3
Ti	n.d.	n.d.	50.5	n.d.
Na	40.3	20.9	32.7	3.62

[a] From F.S. Jacobs and R.H. Filby, Ref. 16. [b] From B. Hitchon *et al.*, Ref. 17. [c] Not determined.
[d] Values for Hg are in ppb.

Some of the metal compounds, including portions of the vanadyl and nickel porphyrins, have sufficient volatility to appear in the distillate of the crude, but the bulk of the metal concentrates in the residue. Iron, copper, and especially vanadium and nickel, can cause corrosion in the processing equipment and act as poisons to the catalyst in catalytic cracking, reducing product yield and increasing gas and coke production. Also, the ash from the burning of metal-containing oils is detrimental to engines and for this reason gasoline must be free of nickel, vanadium and metals in general.

3.0 Physical Properties

The physical properties of a substance are determined by its chemical composition and physical state and, in the case of a colloidal system like bitumen, its colloidal state. Therefore, physical properties are reflections of deeper, more fundamental properties. It follows that they are not independent of one another and their interdependence can be used advantageously in the prediction of one property from other measured properties. The scheme for the characterization of crude oils listed in Table 5.1, for example, is based on the existence of an indirect relationship between density or API (American Petroleum Institute) gravity and viscosity. Both the density and viscosity of a crude oil are strongly affected by the quantities of polar and higher-molecular-weight fractions present, the polars (or resins) and asphaltenes. This is illustrated by the example of a Prudhoe Bay oil and an Athabasca bitumen:

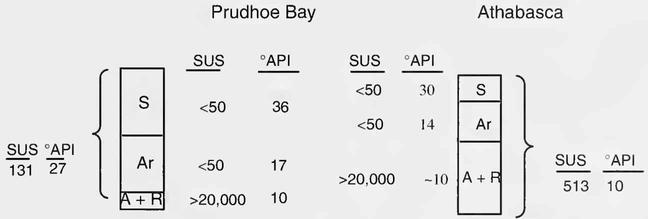

S = saturates, Ar = aromatics, R = resins, A = asphaltene

(SUS viscosities measured at 99°C)

In both cases the viscosity of the whole oil is derived from the high viscosities of the solid resin and asphaltene fractions of the oil. In turn, the densities and viscosities of the resin and asphaltene fractions are determined by the nature and number of functional groups and the types of bonds they contain, along with their size, shape and spatial orientation. The polar groups may be acidic (carboxylic acids) or basic (nitrogen bases) and their carrier molecules may be acidic, basic, amphoteric or neutral with a high propensity to undergo molecular aggregations. The aggregates can have molecular weight distributions ranging from several hundred to tens of thousands (as measured by vapor pressure osmometry). At the molecular level, the potential for diversity is enormous; nevertheless, the bulk properties of these substances are, with surprising uniformity, fairly well predictable from their elemental composition and other simple properties. This provides the basis for the many correlations known to exist between the various properties of crude oils.

3.1 Density and specific gravity

Three related quantities are involved here:

- **density**, grams per cubic centimeter ($g{\cdot}cm^{-3}$ or $kg{\cdot}m^{-3}$; its reciprocal is the specific volume);
- **specific gravity**, the ratio of the mass of a volume of the substance to the mass of the same

volume of water. This quantity depends on the temperatures at which the masses of the sample and the water are measured. The standard temperatures for this widely-used quantity in the petroleum industry are 15.6/15.6°C (60/60°F);

- **API gravity**, which is the preferred property, defined in Eq. 1. Values of API gravity range from about 5° for dense (1.0337 $g{\cdot}cm^{-3}$) bitumens to about 45° for very light (0.8 $g{\cdot}cm^{-3}$) crudes.

Density–gravity is probably the simplest single property that best characterizes a crude oil and its numerical value depends on many parameters. Aromaticity in general tends to increase density and paraffinicity tends to decrease density. In general, increases in molecular weight, polarity, contents of asphaltene, resins, sulfur, nitrogen, oxygen, vanadium and nickel, correlate with an increase in density of the crude as do the vanadium to nickel ratio, viscosity, carbon residue, etc.

API gravity values for selected bitumens and heavy oils are listed in Table 5.7. It should be noted that bitumen properties, including density, change slightly during extraction owing to the loss of volatile and water-soluble components and the presence of residual solvent, water and varying amounts of fine solids in the extracted material. Therefore, values quoted could be slightly different from values for the in-place virgin bitumen. Bitumen density is dependent on temperature and for Athabasca bitumens it is well described by the expression

$$d_2 = d_1 + 0.62\ (t_1 - t_2) \tag{4}$$

where d_1 is the density at temperature t_1 (°C) and d_2 is the density at temperature t_2. From Figure 5.1 it is seen that for bitumens with API values ≥ 9°, the density of water exceeds that of bitumen in the temperature range $40 < t < 130$°C.[19] The maximum difference occurs around 82°C, the temperature used in the hot water separation process, and this provides the physical basis for the rise of the bitumen to the top of the aqueous slurry in the primary separator.

Table 5.7 API gravities and viscosities of some bitumens and heavy oils

	API gravity, °	Viscosity (mPa·s)	
Peace River	6.7–9.0	$1.25–1.55 \times 10^5$	(24°C)
Athabasca	5.4–11.3	$7–265 \times 10^3$	(24°C)
Cold Lake	9.3–11.4	$2–17.6 \times 10^4$	(24°C)
Wabasca:			
Grand Rapids	8–13		
Wabiskaw	11–18.1	$0.4–27 \times 10^3$	(24°C)
Carbonate:			
Grosmont	5.3–7.0	$5.1–8.3 \times 10^3$	(65°C)
Lloydminster	10–18	$2.6–8.9 \times 10^3$	(24°C)
Asphalt Ridge	10.4 (–14.4)	$2.5–6.4 \times 10^4$	(60°C)
Sunnyside	10.4	1.65×10^6 cSt	(38°C)
P.R. Spring	10.3		
Tar Sand Triangle	4.1(–11)	7.6×10^{10} cSt	(98°C)
Bemolonga	10.1		
Trinidad	–2		
Utah		$3.6–3.8 \times 10^5$	(60°C)
Boscan	10.3	2×10^4 cSt	(38°C)
Arroyo Grande	2.6	1.3×10^6 cSt	(98°C)

Density is a function of pressure as well and tends to slowly increase with pressure. Raising the pressure from ca 0.1 to 100 MPa increases the density of bitumens by about 4%.

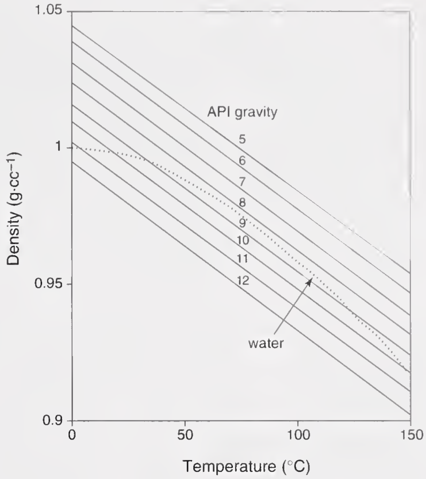

Figure 5.1 Density of Athabasca bitumen as function of temperature. From D.R. Prowse, Ref. 19.

Many of the chemical and physical properties of crude oil exhibit some form of functional dependence on the API gravity. A number of these relationships are shown diagrammatically in Figure 5.2. In order to understand the root of such relationships one has to turn to the organic geochemistry and biomarker chemistry of petroleum. According to the theory of petroleum formation derived from organic geochemistry and biomarker chemistry, the character of a crude oil is determined by its origin: its biotic source material, its source rock and their depositional environment.[20] Thus, the chemical properties of a crude oil will depend on whether its precursor sediment was deposited in a marine, lacustrine or terrestrial setting in a carbonate or clay rock in a reducing or oxic environment, *etc.* Marine, carbonate sediments in a strongly reducing, sulfate-rich environment produce high sulfur medium grade crude oils. The processes promoting sulfur incorporation into the sediments are also promoting the incorporation of vanadium and to a lesser extent nickel (*cf.* Chapter 13). Consequently high sulfur content of an oil is more often than not supplemented by high vanadium and nickel contents and high ratios of vanadium to nickel. Hence, is the interrelationship between S, V, Ni and V/Ni.

Now, the primary character of the oil is further modified throughout its history; during migration from the source rock to the reservoir rock by chromatographic effects and in the reservoir by microbiological, thermal, thermocatalytic, water washing, chemical and gas precipitation caused fractionation processes. Some of these processes may proceed parallel others in a counter parallel fashion. For example, as was illustrated above on the example of Prudhoe Bay and Athabasca oils microbial degradation destroys preferentially the lighter oily components including *n*-alkanes and lower cycloalkanes leaving behind a heavy residue with a lower API gravity and higher NOS, V, Ni content and viscosity. Hence, is the relationship between S content, asphalt content and API gravity.

As seen in Figure 5.2 API gravity increases with increasing depth of burial. The data points represented by the plots of Figure 5.2 are too few and scattered for individual presentation. Therefore, the data were divided into three depth zones and the averages within these zones are plotted.

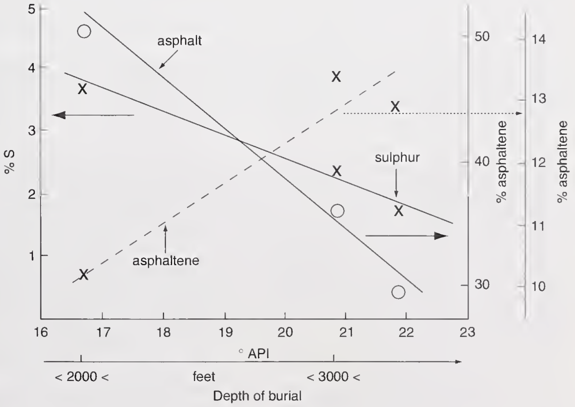

Figure 5.2 Correlation of API gravity, sulfur, asphalt and asphaltene content with depth of burial for Alberta heavy oils.

These indicate that:

- API gravity increases with increasing depth of the reservoir owing to rising geothermal temperature and increasing cracking reactions;
- sulfur content decreases with increasing API values;
- asphaltene content decreases with increasing API values; but
- the asphaltene content increases with rising API values, which can be due to the combination of a number of simultaneous steps—chromatographic effect involving increased adsorption of the rising oil column on the reservoir rock, and formation of asphaltene from the increased decomposition of the resins, overcompensating for the decomposition of asphaltene.

The variation in oil properties with depth of burial is primarily due to the geothermal gradient, created by the outflowing heat from the interior of the earth, resulting in an approximately +1°C temperature change with each 40 m depth. This gradient is not uniform and affected by among other circumstances the spatial redistribution of heat by flowing groundwater. In the Western Canada sedimentary basin large flow systems extending from the Rockies to the Canadian Shield are known to exist (*cf.* Chapter 7.1). Descending water movement in recharge areas causes geothermal lows and upward water motion in discharge areas brings heat toward the surface[21] and produces geothermal gradient “highs”. It then follows that burial depth alone is not a precise measure of the thermal stress of a sediment and that can at least in part account for the scatter in the data in Figure 5.2. Also the data in the figure was not from a single vertical column, but from the different deposits in the Western Canada sedimentary basin. Available data from vertical column will be discussed in section 5.1 of this chapter.

General correlation functions for various properties of heavy oils with API gravity are shown in Figure 5.3.

3.2 Viscosity

The frictional resistance that a moving fluid offers to an applied shearing force is a measure of its viscosity. Therefore, viscosity is the most important single physical property in any process involving the movement of fluids—oil, bitumen and water. The relative viscosities of different phases govern the flow of fluids through the pore structure of oil-bearing formations and can be the limiting factors determining the rate and amount of oil production from a reservoir. When the frictional resistance is independent of the shearing force applied, the material is said to exhibit Newtonian behavior. Bitumen is mildly non-Newtonian and viscoelastic and, like most non-Newtonian liquids, its frictional resistance decreases slightly with increasing shear force. Colloidal water accentuates non-Newtonian flow characteristics and where it does so, it increases viscosity considerably.

The extremely high viscosity of Alberta (and other) bitumens makes it impractical to attempt the recovery of bitumen by conventional oil recovery technologies or to transport bitumen by pipeline. However, as it happens, the viscosity of bitumen is strongly temperature dependent and tends to decline rapidly with rising temperature. Thus, raising the temperature offers, in principle, a simple means of reducing viscosity and rendering the bitumen more mobile. An alternative way of reducing the viscosity is by dilution with a solvent or a pressurized gas, by colloidal dispersion in a low-viscosity immiscible medium or by partial upgrading.

Viscosity is defined by Newton’s law of viscous flow as the frictional force, f, restricting the relative motion of two adjacent layers of a fluid. This force is proportional to the area of the interface and the velocity gradient between them and is given by

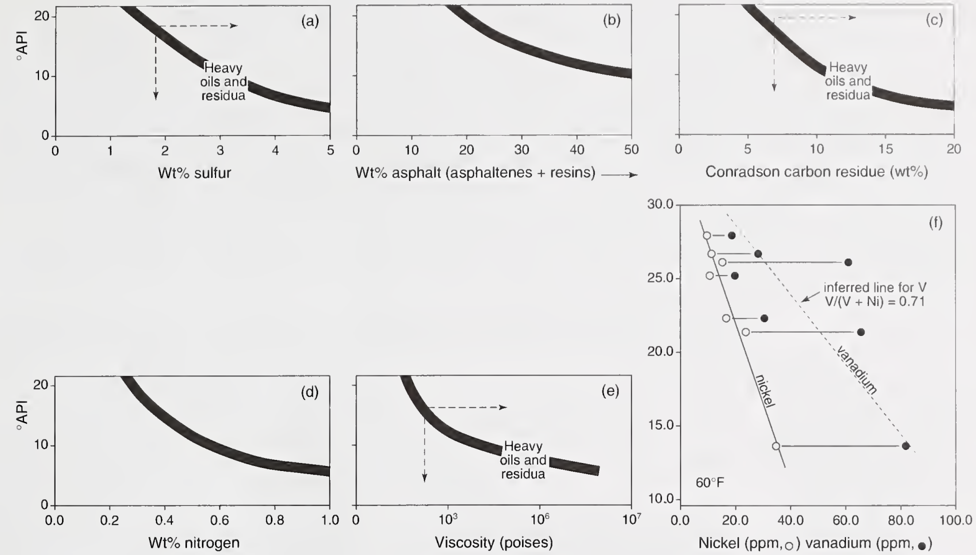

Figure 5.3 Generalized correlations of API gravity with sulfur, nitrogen, asphalt, nickel and vanadium contents, carbon residue and viscosity of crude oils. a)–e), after J.G. Speight, Ref. 1; f), from J.A. Curiale, Ref. 20b, © 1987, American Chemical Society.

$$f = \eta S(dV/dR) \tag{5}$$

where S is the interfacial area, dV/dR is the velocity gradient and η is the coefficient of viscosity. The viscosities most often used in the oil sand industry are:

- **dynamic (absolute) viscosity**, the unit of which is the poise in the cgs system and Pa·s in the SI system of units:
  1 poise (P) = 1 dyn·s·cm^{-2} = 0.1 Pa·s = 10^{-5} N·s·cm^{-2};
  1 centipoise (cP) = 0.01 P = 0.001 Pa·s = 1 mPa·s = 10^{-3} kg·m^{-1}·s^{-1};
- **kinematic viscosity**, the units of which are
  1 stokes (St) = 1 poise/density (cm^2·s^{-1});
  1 centistokes (cSt) = 0.01 St

The Saybolt universal viscosity (seconds) (SUS)* is used less frequently in the oil sand industry. Appropriate conversion factors between SUS and kinematic viscosity in tabulated form for various temperature and viscosity ranges are available in the literature.

Reported ranges for the viscosities of various bitumens and heavy oils are listed in Table 5.7 and are plotted as a function of temperature in Figures 5.4 and 5.5. As the plots show, the logarithm of viscosity exhibits a nearly linear relationship with temperature.

Several equations have been proposed relating viscosity to temperature, *e.g.*,

$$\log\eta = \frac{8.91}{(1 + t/135)^{1.645}}\ 1.2 \ \text{(Briggs)} \tag{6}$$

---

*SUS is defined as the time in seconds required for the flow of 60-mL petroleum through a calibrated orifice from a container at a constant temperature. Saybolt universal second = cSt × 4.635 at 38°C (100°F) and cSt × 4.667 at 99°C (210°F).

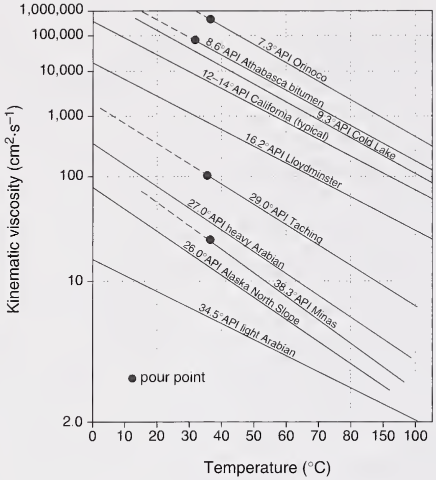

Figure 5.4 Crude oil and bitumen viscosity data. From D.R. Prowse, Ref. 19.

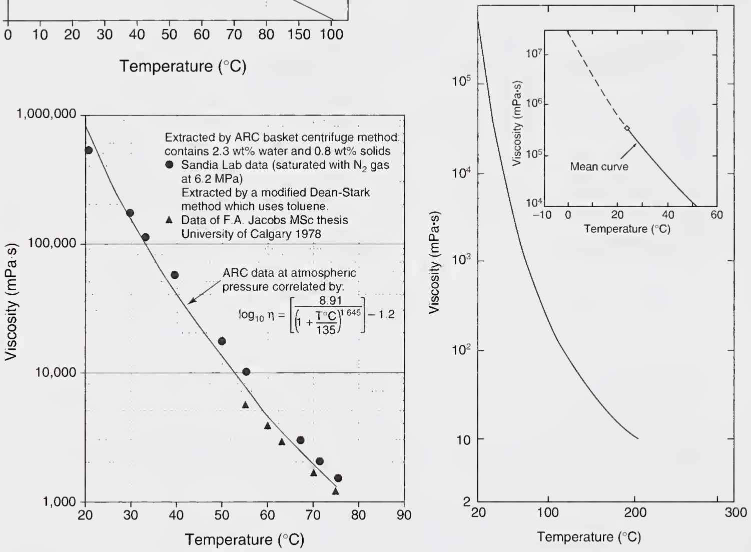

Figure 5.5 Viscosity of surface-mined Suncor Athabasca bitumen and mean viscosity of Athabasca bitumen as a function of temperature. From D.R. Prowse, Ref. 19.

where η = viscosity (mPa·s) at atmospheric pressure and t = temperature (°C);

$$\log\eta = \frac{A}{T} + B \quad \text{(Andrade, after deGurman Carrancio)} \tag{7}$$

where T = temperature (K) and A, B are constants; and

$$\log\log(\eta + 0.8) = -n\log(T/T_x) + \log\log(\eta_x + 0.8) \quad \text{(Walther)} \tag{8}$$

where η = kinematic viscosity (centistokes) at temperature T, (K), and η_x is the kinematic viscosity at T_x ; n is a constant.

Detailed studies[22,23] on the temperature dependence of the viscosity of Athabasca bitumen yielded the data tabulated in Table 5.8, which could be reproduced by the Andrade equation:

$$\eta\ (\text{mPa·s}) = 1.0 \times 10^{-10} \exp[1.01 \times (10^4/T)]. \tag{9}$$

Another variation of the Andrade equation published recently[24] was derived from a more extensive database:

$$\eta \text{ (mPa·s)} = (4 \pm 3) \times 10^{-10} \exp[(1.01 \pm 0.1) \times (10^4/T)]. \quad (10)$$

This equation was claimed to apply well at temperatures up to nearly 100°C. Additional data on the temperature dependence of the viscosity of bitumens are collected in Table 5.9.[25a]

From Figure 5.4 it is apparent that temperature affects the viscosity of heavy oils more than that of light oils. This can be attributed to the increased role of colloidal micellar association equilibria in heavy oils and especially bitumens. The temperature coefficient *A* in the Andrade

Table 5.8 Variation of viscosity with temperature for various bitumens

	Temperature (°C)	Viscosity (mPa·s)		Temperature (°C)	Viscosity (mPa·s)
Athabasca[a]	15	3.8×10^5	Suncor	15	1.7×10^5
Athabasca	25	8.4×10^4	Suncor	25	4.23×10^4
Athabasca	40	1.4×10^4	Suncor	60	1.19×10^3
Athabasca	50	4.7×10^3	Suncor	100	1.19×10^2
Athabasca	60	2.0×10^3	Lloydminster heavy oil	15	1.15×10^4
Athabasca	70	9.3×10^2	Lloydminster heavy oil	25	4.13×10^3
Athabasca	80	5.0×10^2	Lloydminster heavy oil	60	2.80×10^2
Syncrude[b]	15	$> 8 \times 10^5$	Lloydminster heavy oil	100	5.5×10^1
Syncrude	25	2.9×10^5	Utah	20	$1.3–1.7 \times 10^8$
Syncrude	60	4.15×10^3	Utah	38	$6.8–7.7 \times 10^6$
Syncrude	100	2.76×10^2	Utah	60	$3.58–3.82 \times 10^5$

[a] From L.L. Schramm and J.C.T. Kwak, Ref. 22. [b] From D. Wallace and D. Henry, Ref. 23.

Table 5.9 Variation of viscosity with shear rate[a]

Sample[b]	Temperature (°C)	Viscosity at infinitely low shear (Pa·s)	Viscosity at infinitely high shear (Pa·s)
1	27.5	172	168
1	42.5	17.5	16.6
1	72.5	3.1	2.1
2	27.5	170	167
2	42.5	22.3	21.0
2	57.5	7.3	6.65
2	72.5	2.65	2.40
3	27.5	1.96	1.68
3	42.5	0.56	0.485
3	57.5	0.36	0.28
4	27.5	43.7	36.3
5	27.5	57.6	46.8
6	27.5	302	273
7	27.5	51.8	46.8
7	40.0	12.7	12.2
7	57.5	3.55	2.84
1[c]	27.5	286	269
6[d]	27.5	103	90
6[e]	27.5	1,050	<650

[a] From J.M. Dealy, Ref. 25a. [b] Sample 1 = Athabasca CS_2-extracted bitumen; 2 = Cold Lake cold-bailed bitumen; 3 = Lloydminster primary production heavy oil; 4 = Cold Lake cold-bailed bitumen; 5 = Cold Lake steam-stimulated bitumen; 6 = Athabasca toluene-extracted bitumen; 7 = Cold Lake cold-bailed bitumen (8.4% water). [c] Sample aged at 80°C for 48 h. [d] 2% toluene added. [e] 5% asphaltenes added.

equation (7) is related to the strength of the various intermolecular forces causing the association (and hence the high viscosity).

The above equations are for Newtonian liquids, where the viscosity is a single constant at a given temperature and pressure. For crude oils, departure from Newtonian behaviour occurs near the cloud point, where wax precipitation commences, and near the boiling point, where vaporization begins to take place. However, bitumens are inherently non-Newtonian and can be described by the Bingham model obeying the relation

$$\tau = \tau_0 + \mu\varepsilon \qquad (11)$$

where μ = viscosity, τ = shear stress, ε = shear rate and τ_0 = shear stress required to initiate flow. This means that the measured viscosity value is somewhat dependent on the shear rate, as can be seen from the data listed in Table 5.9.

Pressure has a mild—but under some circumstances significant—influence on viscosity. With increasing pressure, viscosity increases linearly up to a few thousand atmospheres, beyond which the increase reportedly becomes exponential. There are several equations described in the literature relating viscosity to both temperature and pressure, *e.g.*[25b]

$$\log\eta(\text{Pa·s}) = 2.30259[b/(1 + (t - 30)/303.15)^S + C] + B_oP\exp(dt) \qquad (12)$$

where t = °C, C = –3.002 and B_o, d and S are related to b, which is evaluated from known viscosity ($\eta_{30°C}$) at 30.0°C;

$$\log\eta = \exp(a_1)\, T^{a_2} + a_3P, \qquad (13)$$

where a_1, a_2 and a_3 are constants.[26]

Viscosity can be correlated with density and the schematic viscosity *versus* density plot in Figure 5.6 indicates a rapid exponential increase in viscosity with density (at atmospheric pressure). This correlation provides the basis for the characterization of crude oils depicted in Figure 5.1. Viscosities of various bitumens and fractions thereof have also been correlated with molecular weights.[27] Figure 5.7 indicates that, at high viscosities ($\eta > 1.83 \times 10^4$ mPa·s, MW $\geq$ 483), the logarithm of viscosity is a linear function of the MW and is represented by the equation ln η = 0.0482MW – 13.44. At lower viscosities an equation third-order in MW approximates the relationship.

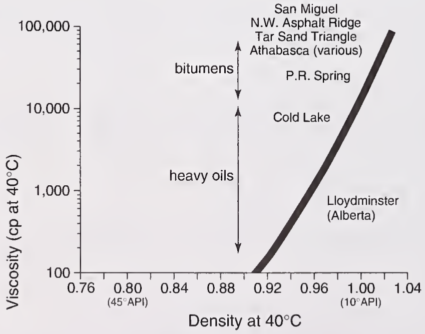

Figure 5.6 Relationship between density and viscosity for various bitumens and heavy oils. After J.G. Speight, Ref. 1.

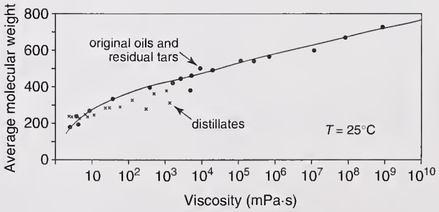

Figure 5.7 Relationship between viscosity and molecular weight for various bitumens and bitumen fractions. From F.A. Seyer and C.W. Gyte, Ref. 27.

The variation in the kinematic viscosity and density along with other relevant properties of the various process streams from the upgrading of Athabasca bitumen in the Syncrude plant are given in Table 5.10. In general, the molecular weight (and with it, the extent of molecular association by intermolecular forces) increases with increasing boiling point, and so do density and viscosity. Hydrotreatment of the stocks reduces heteroatom contents, density, boiling point and viscosity. The final product of the upgrading operation, Athabasca synthetic crude, has a straw color with a density of 0.85 $g \cdot cm^{-3}$ and a viscosity of 5–6 $mm^2 \cdot s^{-1}$ compared to bitumen with its viscosity of about 130,000 $mm^2 \cdot s^{-1}$ and black color. Some additional relevant viscosity data are listed in Table 5.11.

The connection between viscosity and other physical and chemical properties will be discussed in a later chapter.

3.3 Thermal properties

3.3.1 Liquid-solid transition

Phase transitions of crude oils (including bitumens), unlike those of pure chemicals, do not occur at sharply-defined temperatures but rather in more or less narrow temperature ranges. This is a direct consequence of the well-recognized complexity of the chemical composition of crude oils, each constituent compound having its own transition temperature and each compound class its own characteristic phase transition behavior. For example, *n*-alkanes in the C_5–C_{16} range are liquids at room temperature while above C_{16} they are solids. Being regular constituents of crude oils up to at least C_{33} (M.P. 71°C), the solid higher members are present as solutes in the liquid portion of the crude. Therefore, on cooling, highly paraffinic crudes tend to lose their paraffins by precipitation, forming mixed crystals. The temperature at which paraffin precipitation begins to take place under standardized conditions is the **cloud point**. Upon further cooling, the oil begins to solidify at a certain temperature. When the test is carried out under standardized conditions the lowest temperature at which the oil pours or flows is the **pour point**. There are a number of practical consequences of cloud point and pour point characteristics. Below the cloud point or pour point the oil becomes non-Newtonian and a high pour point oil may not be transportable in pipeline at room temperature. A high pour point with a high API gravity is an indication of high paraffinicity. For example, the saturate fraction of a Prudhoe Bay oil (27° API) has a pour point of +1°C and API gravity of 36° compared to the saturate fraction of Athabasca bitumen (10° API) with a pour point of –55°C and API gravity of 30°. This can be attributed to the fact that the saturate fraction of the bitumen is devoid of *n*-alkanes and has a very low paraffinicity whereas branched alkanes and short-chain alkyl cycloalkanes, the latter being the major components of bitumen saturates, have low melting points*

		MP (°C)			MP (°C)
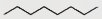	*n*-octane C_8H_{18}	–56.5		*n*-pentane C_5H_{12}	–132
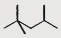	2,2,4-trimethylpentane	–107.8		2-methylbutane	–161
	cyclohexane	6.2			
	methylcyclohexane	–126.9			

---

*Deviation from this trend occurs in cases where the molecule has high symmetry with a compact geometry, *e.g.* neopentane, M.P.–20°C; 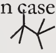 2,2,3,3-tetramethylbutane, M.P. 101°C.

Table 5.10 Properties of distillates derived from Athabasca bitumen and their hydrotreated products[a]

	Coker LGO	Coker CGO	Coker HGO	Hydrotreated LGO	Hydrotreated HGO
Feeds					
Density, 20°C ($g\cdot cm^{-3}$)	0.9447	0.9830	1.0045	0.8686	0.9402
Refractive ind., 20°C	1.5302	1.5547	1.5718	1.4854	1.5288
Sulfur (wt%)	3.67	4.29	4.64	0.66	1.52
Nitrogen (mg·kg)	1,443	2,915	3,910	1,355	2,850
Carbon (wt%)	85.07	84.63	84.16	87.41	86.70
Hydrogen (wt%)	10.88	10.15	9.88	12.38	11.37
Kinematic viscosity					
20°C ($mm^2\cdot s^{-1}$)	17	191	1,768	4.7	109
40°C ($mm^2\cdot s^{-1}$)	7.9	50	249	2.9	3.4
ASTM D2887					
IBP	175	194	230	142	291
5%	236	260	309	182	319
10%	255	283	334	202	330
30%	292	341	385	245	359
50%	317	385	423	276	382
70%	344	429	461	303	408
90%	393	480	508	334	448
95%	425	499	528	347	469
FBP	501	529	567	378	522
Hydrotreated products, typical operating conditions					
Density, 20°C ($g\cdot cm^{-3}$)	0.8891	0.9027	0.9233	0.8479	0.9091
Refractive ind., 20 °C	1.4949	1.5013	1.5162	1.4691	1.5051
Sulfur (mg·kg)	1,120	479	1,430	35	936
Nitrogen (mg·kg)	102	173	798	4.6	501
Carbon (wt%)	87.16	87.82	88.10	87.45	87.63
Hydrogen (wt%)	12.53	12.39	11.62	13.16	12.32
Kinematic viscosity					
20°C ($mm^2\cdot s^{-1}$)	10	24	67	4.3	56
40°C ($mm^2\cdot s^{-1}$)	5.1	11	23	2.7	20
ASTM D2887					
IBP	123	87	100	127	132
5%	201	190	213	174	282
10%	224	230	261	193	307
30%	272	299	335	236	345
50%	302	345	380	267	371
70%	331	393	424	295	399
90%	384	456	482	328	441
95%	421	482	507	341	463
FBP	519	530	555	372	524

[a] From F.A. Seyer and C.W. Gyte, Ref. 27.

Table 5.11 Additional relevant viscosity data

	Temperature (°C)	Viscosity (mPa·s)
Suncor distillates[a]		
kerosene	38	1.7
	58	1.3
gas oil	38	20.4
	58	3.6
hydrotreated products		
kerosene	25	2.8
gas oil	25	52.0
heavy naphtha	38	1.1
synthetic crude	26	4.6
pentane	20	0.24
methylene chloride	20	0.47
benzene	20	0.67
	40	0.52
toluene	20	0.60
	40	0.48
xylene	20	0.62
naphthalene	100	0.78
water	20	1.01
	40	0.67
ethanol	25	1.08
1,2-ethanediol	15	26.09
glycerol	25	945

[a] From F.A. Seyer and C.W. Gyte, Ref. 27.

resulting in the low pour point of bitumen saturates. Thus, the API gravity of the Prudhoe Bay saturate fraction after removal of the paraffins was found to be unchanged, but its pour point had dropped to –35°C.

In general, the higher the gravity of an oil, the lower its pour point. Violation of this trend is an indication of a high paraffinic character for the oil. Examples of this are seen in Figure 5.4 where the Taching (29°) and Minas (38.3°) crudes have much higher pour points (> 30°C) than would be expected on the basis of their gravity, indicating highly paraffinic crudes.

3.3.2 Liquid-vapor transition

Vaporization and condensation are two essential steps in the distillation fractionation of crude oils. Volatility, governed by the vapor pressure and latent heat of vaporization, is the property that determines the distillation characteristics of a pure liquid. In multicomponent systems, however, cohesional forces and specific chemical interactions among the component molecules may make volatility a very complicated function of composition (azeotropy, immiscibility). Experimentally, the distillation characteristics of crude oils are determined by the distillation curve in which either the volume of distillate is plotted as a function of temperature at regular intervals or the temperature is plotted as a function of volume of distillate at regular intervals.

For homologous series of compounds the boiling point of a liquid is a smooth, logarithmic type function of the number of carbon atoms in the molecule and varies with the types of bonds and functional groups present, Figures 5.8a and b. For compounds with the same number of carbon atoms the boiling point follows the order aromatics > naphthenics > *n*-alkanes > isoalkanes and can be estimated for the compounds in Figure 5.8b from the equation

$$t\,^{\circ}\mathrm{C} = 364.4 \times \ln(N_A^{1.122} + N_N^{1.065} + N_P + 5.476) - 836.3 \qquad (14)$$

where t ℃ is the boiling point and N_A, N_N and N_P are the numbers of aromatic, naphthenic and paraffinic carbon atoms in the molecule. Correspondingly, the distillation curve—temperature versus volume percent of crude distilled—is a function of gravity and shifts to the right with increasing API gravity as seen from Figures 5.9 and 5.10. In other words, lighter oils give more light distillates and, since hydrocracking increases the API gravity, it causes the distillation curve of the bitumen to shift to the right, Figure 5.10.

Average boiling points obtained from distillation curves generally correlate better with many physical and chemical properties. The boiling points that best correlate with molecular weights, the "mean average boiling points", can be calculated from the equation

$$\text{m.b.p.}(^{\circ}\mathrm{R}) = 0.5\left[\sum_{i=1}^{n} x_i T_{bi} + \left(\sum_{i=1}^{n} xv_i T_{bi}^{1/3}\right)^3\right] \qquad (15)$$

where x_i and xv_i are the mole fraction and volume fraction of component i and T_{bi} is the normal boiling point of component i in °R.

The maximum temperature to which heavy petroleum hydrocarbons can be exposed during a distillation process without the danger of decomposition is about 250℃, which corresponds to the boiling point of molecules up to C_{20}. There have been many attempts to raise the limiting molecular size in distillation. The molecular size can be increased up to C_{40}–C_{45} by conducting the distillation under vacuum. In modern analytical laboratory practice, throughout the industry the true boiling point distillation sequence has been replaced by low-resolution packed column gas chromatographic analysis which is faster and less laborious and allows for minimal sample consumption. The method relies on the experimental observation that hydrocarbons are eluted from a nonpolar adsorbent according to their boiling points, which makes it possible to relate elution time to the atmospheric equivalent boiling point of the hydrocarbon components. With the availability of highly automated computer-operated gas chromatographs, simulated distillation by gas chromatography is a standardized routine procedure widely applied for obtaining true boiling point distributions of crude oils, bitumens, and distillates. The distillation data in Table 5.4 and Figures 5.9 and 5.10 were obtained by the simulated distillation method up to an atmospheric equivalent boiling point of 567℃. Analogous data published by Syncrude Research on the vacuum distillation of bitumen in an automatic vacuum distillation apparatus are tabulated in Table 5.12.

For illustrative purposes, general characterization data for Athabasca Suncor coker feed bitumen are also given in Table 5.4.

3.3.3 Carbon residue

On distillation, petroleum and petroleum products as a rule leave some non-distillable residue behind which, on further heating, decomposes to release some additional distillable material and a carbon residue. The original distillable fraction of the oil, depending on the temperature and other characteristics of the distillation, may also partially decompose and ultimately add to the carbon residue. This carbon residue is a measure of the coke-forming propensity of the oil and, when obtained under appropriate experimental conditions, can be related to the amount of

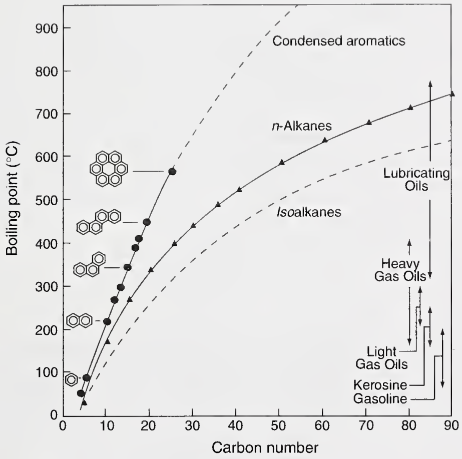

Figure 5.8a Relationship between boiling point and carbon number for aromatics, *n*-alkanes and iso-alkanes. After N. Berkowitz, "Fossil Hydrocarbons", p. 126, Academic Press, New York, N.Y. 1997.

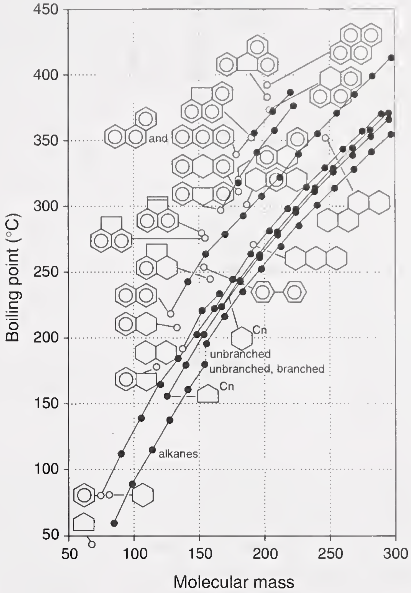

Figure 5.8b Boiling points of hydrocarbons and their homologous series as a function of molecular weight. From H.-J. Neumann *et al.,* Ref. 28.

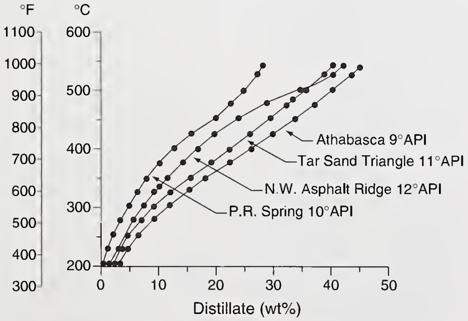

Figure 5.9 Simulated distillation data for Athabasca and Utah bitumens and a conventional crude oil. After J.G. Speight, Ref. 1.

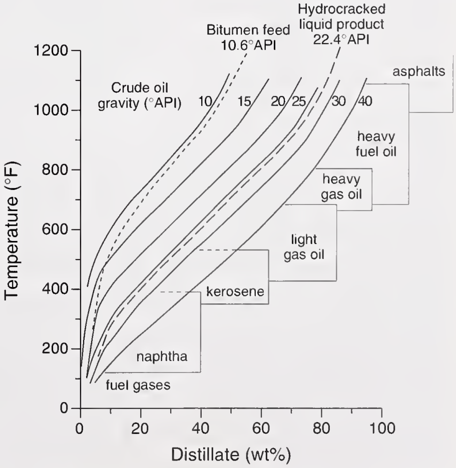

Figure 5.10 Average crude oil, Athabasca bitumen and Athabasca hydrocracked product oil distillation curves. From H.H. Chen *et al,* Ref. 29. © 1990, Elsevier.

Table 5.12 Automated distillation of bitumen[a]

Volume % off	Average atmospheric equivalent temperature °C	Standard deviation (ls, n = 7) °C
IBP	248.5	20.5
5	321.6	2.9
10	348.8	3.4
15	373.3	1.9
20	399.3	1.8
25	424.9	1.5
30	449.5	1.3
35	475.0	1.8
40	501.1	1.6
45	526.9	1.2
Cracking	532.3	1.2

[a] From J.K. Liu and H.E. Gunning, Ref. 31.

coke that would be formed in the refining or upgrading operation. In the upgrading of bitumen, the produced coke is used for power generation to cover the energy requirement of the plant and coke formed in excess of that amount is an undesired product. Excessive coke formation may also limit the production capacity of the coker.

The carbon residue is determined in the laboratory by heating the sample to 500–550°C under prescribed conditions. There are three test procedures in current use, the Ramsbottom carbon residue (RCR), the Conradson carbon residue (CCR) and the microcarbon residue (MCR) tests, each of which yields slightly different results, Table 5.13 and Figure 5.11. The correlation between the CCR and MCR values is good, but reportedly sample dependent; however, the correlation between the RCR and CCR values is less satisfactory.

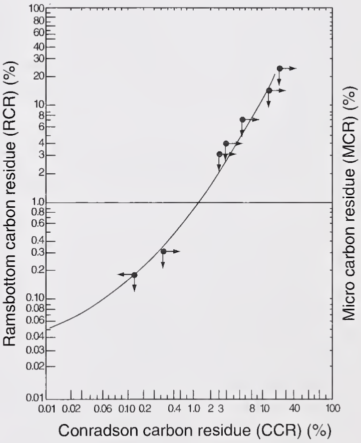

Figure 5.11 Correlations between MCR, RCR and CCR. From J. Cooley *et al.*, Ref. 32.

Before proceeding further it should be added that, as with all tests, the results are substantially influenced by the details of how the experiments are conducted and depend on such factors as the material of the test crucible (glass, platinum), temperature and the atmosphere present (air, nitrogen), etc. Another important factor to consider is the mineral matter content of the bitumen because, in the course of the carbon residue test, it ends up in the residue. Correction for this can be made by measuring the ash content of the carbon residue after removing the carbon by combustion at around 540°C.

Because light oils and distillates have low values for the carbon residue, it is customary to measure carbon residues from their 10% distillation residues (topped oils). In some cases it may be desirable to measure carbon residues even for bitumens and heavy oils on topped stocks which are prepared as distillation residues at a specified temperature, for example, the Cold Lake and Pembina samples in Table 5.13.

Table 5.13 Comparison of MCR, CCR and RCR data (%) for some bitumens, maltenes and heavy oils

Sample	MCR	CCR	RCR
Cold Lake		13.6	
	12.5	13.2	11.3
Cold Lake 565+ °C	24.6	24.2	
Athabasca			12.1
"		13.2	
" (Syncrude)		11.8	
Athabasca maltene			5.4
Wabasca	8.4	8.6	7.6
Tar Sand Triangle			21.6
Pembina 445+ (°C)	5.5	5.5	
Lloydminster		10.4	
		9.1	
Fort Kent	9.9	9.8	9.0
Blackfoot	11.2	11.4	9.0
Battrum	11.0	11.0	10.0
Morgan	12.2	12.8	10.4
Westmin	12.2	12.4	11.2
Primrose	12.4	12.9	11.2
Lindbergh	12.5	13.0	11.2
Fort Kent	13.0	12.6	11.2
Sunnyside		14.2	
" maltene		8.2	
N.W. Asphalt Ridge			3.5
Asphalt Ridge			9.0
" maltene			6.8
Jobo		14	
P.R. Spring			12.5
California	9.8	9.4	9.0
Maya	11.7	11.1	10.7
Boscan		14.0	14.0

The data collected in Table 5.13 show that for native heavy oils and bitumens the carbon residue varies between about 5 and 14%. Light oils leave carbon residues much smaller than those from heavy oils and there is a broad correlation between API gravity and carbon residue: the lower the gravity, the higher the carbon residue from the oil. Through this correlation with API gravity, the carbon residue in native oils is related to the contents of hydrogen, sulfur, nitrogen, vanadium, nickel and metals as well as to the $(H/C)_a$ ratio, viscosity, and other properties.

Most, but not all, of the carbon residue comes from the asphaltene in the oil, Table 5.14, and therefore the higher the asphaltene content the higher, in general, will be the carbon residue from the oil. Since the maltene (*i.e.* the deasphalted bitumen) content of bitumen is 5 to 11 times higher than its asphaltene content, the partial contribution of the maltene (even though it produces a much lower specific carbon residue than asphaltene) is not negligible. Hence, the relationship between the asphaltene content of the bitumen and its carbon residue will be modified by the carbon residue from the maltene which, in the above cases, varied between 5.4 and 8.2%. The carbon residue from the maltene originates mainly from the resins, and the saturates and aromatics give the least amount of carbon residue. It is important to note that the carbon residues of the bitumen fractions are not additive properties and that the carbon residue from the asphaltene is

Table 5.14 Carbon residues of bitumens, maltenes and asphaltenes

Sample	Carbon residue (%)
Athabasca	RCR (%)
bitumen	12.1
maltene	5.4
asphaltene	42.3 (calculated)
Asphalt Ridge	RCR (%)
bitumen	9.0
maltene	6.8
asphaltene	31.8 (calculated)
Sunnyside	CCR (%)
bitumen	14.2
maltene	8.2
asphaltene	37.4 (calculated)

influenced by the presence of the maltene and vice versa. Therefore, the RCR values for asphaltene in Table 5.14, calculated as the difference of the RCR values of the bitumen and maltene, apply for the asphaltene-in-bitumen solution. Neat asphaltene would give higher RCR values.

3.3.4 Specific heat and latent heat

Knowledge of thermochemical and thermodynamic properties and the availability of accurate data are necessary requirements for the design and operation of petroleum processing units and internal combustion engines. Some of the important properties involved here are the specific heat, heat of vaporization and heat of combustion.

a) Specific heat

Specific heat is defined as the quantity of heat required to raise the temperature of a unit mass of material by one degree of temperature. For hydrocarbons the specific heat is inversely proportional to the specific gravity and directly proportional to the temperature. A rough estimate of the specific heat, c, of crude oils can be made from the specific gravity, *d* (15.6/15.6℃), and F, the temperature in Fahrenheit degrees, using the equation

$$c = (1/d) \times (0.388 + 0.00045\mathrm{F})\ \mathrm{cal{\cdot}{}^{\circ}F{\cdot}\,g^{-1}} \quad (16)$$

Accurate determination of specific heat depends on whether it is measured at a constant volume or a constant pressure. High-precision specific heat values at constant pressure, c_p, have been reported for heavy oils, bitumens, asphaltenes and cokes.[33] It has also been shown that the measured values can be represented accurately by equations of the forms

$$c_p = a + bT + cT^2 \quad (17)$$

$$c_p = a' + b'T + c'T^{-2} \quad (18)$$

in the temperature range 300–600K, Tables 5.15–17. Equations of type 17 are better for extrapolating to temperatures lower than the specified range whereas equations of type 18 are better for extrapolating to temperatures higher than the specified range.

Table 5.15 Specific heats ($J \cdot K^{-1} \cdot g^{-1}$) of bitumens/heavy oils according to the constants in the relation $c_p = a + bT + cT^2$.[a]

Source	a	b	c
Athabasca	0.055	6.818×10^{-3}	-4.464×10^{-6}
Cold Lake, Esso Resources	−0.007	7.410×10^{-3}	-5.279×10^{-6}
Cold Lake, BP[b]	−0.067	7.232×10^{-3}	-4.260×10^{-6}
Eyehill-Lloydminster	0.404	5.294×10^{-3}	-2.644×10^{-6}
Primrose[b]	0.537	4.595×10^{-3}	-1.638×10^{-6}
Peace River, early production	0.239	5.901×10^{-3}	-3.663×10^{-6}
Peace River, later production	−0.018	7.361×10^{-3}	-5.213×10^{-6}
Grosmont[b]	0.223	5.820×10^{-3}	-2.972×10^{-6}
Asphalt Ridge	0.032	6.967×10^{-3}	-4.027×10^{-6}
Malagasy	0.036	6.870×10^{-3}	-4.259×10^{-6}
Nigeria	−0.078	7.375×10^{-3}	-4.933×10^{-6}
Zaire	0.141	7.678×10^{-3}	-5.532×10^{-6}
Venezuela	0.256	6.087×10^{-3}	-3.536×10^{-6}

[a] From R. Cassis *et al.*, Ref. 33. Unless otherwise noted, the temperature range is 300–600 K [b] Temperature range: 320–600 K.

Table 5.16 Specific heats ($J \cdot K^{-1} \cdot g^{-1}$) of bitumens/heavy oils according to the constants in the relation $c_p = a' + b'T + c'T^{-2}$.[a]

Source	a'	b'	c'
Athabasca	1.763	1.542×10^{-3}	-4.884×10^{4}
Cold Lake, Esso Resources	2.055	1.108×10^{-3}	-6.021×10^{4}
Cold Lake[b], BP	1.655	2.068×10^{-3}	-5.301×10^{4}
Eyehill-Lloydminster	1.383	2.218×10^{-3}	-2.704×10^{4}
Primrose[b]	1.181	2.635×10^{-3}	-1.929×10^{4}
Peace River, early production	1.634	1.581×10^{-3}	-3.973×10^{4}
Peace River, later production	1.980	1.196×10^{-3}	-5.725×10^{4}
Grosmont[b]	1.379	2.286×10^{-3}	-3.436×10^{4}
Asphalt Ridge	1.596	2.175×10^{-3}	-4.539×10^{4}
Malagasy	1.659	1.848×10^{-3}	-4.619×10^{4}
Nigeria	1.817	1.535×10^{-3}	-5.441×10^{4}
Zaire	1.961	1.161×10^{-3}	-5.969×10^{4}
Venezuela	1.623	1.887×10^{-3}	-3.951×10^{4}

[a] From R. Cassis *et al.*, Ref. 33. Unless otherwise noted, the temperature range is 300–600 K [b] Temperature range: 320–600 K.

b) Latent heats of vaporization and fusion

The latent heat of vaporization (ΔH_V) is the amount of heat necessary to vaporize a unit mass of liquid at its atmospheric boiling point. Latent heat of vaporization data are needed for the design of distillation and other equipment.

The latent heat of fusion (ΔH_F) is the amount of heat required to convert a unit mass of solid to a liquid without any temperature change.

The latent heat of vaporization for hydrocarbons in general decreases with increasing molecular weight, from 514 $J \cdot g^{-1}$ for methane to about 205 $J \cdot g^{-1}$ for eicosane (n-$C_{20}H_{42}$). The latent heat of fusion increases from about 63 $J \cdot g^{-1}$ for methane to over 226 $J \cdot g^{-1}$ for long-chain ($C_{>32}$) *normal* alkanes.

For aromatic compounds some values of ΔH_F and ΔH_V are shown in Table 5.18.

Table 5.17 Specific heats ($J{\cdot}K^{-1}{\cdot}g^{-1}$) of asphaltenes and cokes according to the constants in the relation $c_p = a + bT + cT^{\pm 2}$.[a]

Substance	Temperature range (K)	a	b	c
$c_p = a + bT + cT^2$				
Asphaltenes[b]	280–620	–5.93	8.079×10^{-3}	-5.353×10^{-6}
Syncrude coke	280–720	–0.141	3.918×10^{-3}	-2.108×10^{-6}
Suncor coke	280–720	–0.286	4.930×10^{-3}	-2.733×10^{-6}
$c_p = a + bT + cT^{-2}$				
Asphaltenes[b]	280–620	1.444	1.748×10^{-3}	-5.609×10^{4}
Syncrude coke	280–720	–0.778	1.239×10^{-3}	-2.739×10^{4}
Suncor coke	280–720	–0.921	1.424×10^{-3}	-3.647×10^{4}

[a]From. R. Cassis *et al.*, Ref. 33. [b] Values listed are averages of Athabasca, Cold Lake, Peace River and Nigeria asphaltenes.

Table 5.18 Latent heats of vaporization and fusion of some aromatic compounds

Compound	ΔH ($J{\cdot}g^{-1}$)		Compound	ΔH ($J{\cdot}g^{-1}$)	
	Fusion	Vaporization		Fusion	Vaporization
Benzene	127.6	394.4	Ethylbenzene	86.6	335.5
Naphthalene	148.9	337.7	Propylbenzene	77.2	318.7
Anthracene	162.0		Butylbenzene	84.0	292.9
Phenanthrene	92.5	331.3	Hexamethylbenzene	127.2	—
Toluene	72.1	360.7	Coronene	64.0	
o-Xylene	122.6	341.9	Thiophene	59.2	374.8
m-Xylene	107.9	336.4			
p-Xylene	159.4	336.5			

c) Heat of combustion

The heat of combustion is the amount of heat evolved when a unit mass of combustible material is burnt completely to specified products under specified conditions. It is a direct measure of the heating value of petroleum, petroleum products and other fuel materials. In addition, most of the standard enthalpies of formation (heats of formation at constant pressure, ΔH_f^0), constituting the backbone of thermal data, are derived from heats of combustion. Values of heats of combustion for selected fuels are listed in Table 5.19.

Table 5.19 Heats of combustion for selected fuels

Fuel	Heats of combustion ($kJ{\cdot}g^{-1}$)
Anthracite	57.7–64.7
Bituminous coal	43.7–61.2
Sub-bituminous coal	31.5–48.9
Lignite	22.7–31.5
Charcoal	50.7
Gasoline	46.4–47.9
Kerosene	43.4–46.8
Fuel oil	39.9–46.6
Crude oil	41.8–48.4

The heat of combustion is, of course, related to composition and for a precise expression it is necessary to specify whether the value is obtained at a constant pressure (ΔH) or constant volume (ΔU) and whether the produced water is in the form of liquid water or vapor at the temperature of the measurement. Heats of combustion at a constant volume for the combustion process

$$\text{combustible} + O_2(g) \longrightarrow CO_2(g) + H_2O(l) + SO_2(g) + N_2(g) + \text{ash} \quad (19)$$

for bitumens, crude oils and bitumen products are tabulated in Tables 5.20 and 5.21 along with their elemental composition. The experimental values ($kJ \cdot g^{-1}$) have been found to be fairly accurately or at least satisfactorily calculable from the expression

$$\Delta U^0 = -0.347(\%C) - 1.1696(\%H) - 0.1507(\%S) + 0.1927(\%O + \%N) \quad (20)$$

Table 5.20 Heats of combustion and compositions of bitumens/heavy oils. ΔU° values are constant-volume heats of reactions represented by Equation (20), T = 298.15 K, and all substances are in their thermodynamic standard states. Compositions are expressed as wt%.[a]

Source of bitumen/heavy oil	ΔU° ($kJ \cdot g^{-1}$)	%C	%H	%S	%N	%O	%Ash
Athabasca	–41.46	83.44	10.45	4.19	0.48	1.24	0.28
Peace River	–40.55	81.20	9.92	5.88	0.36	1.89	0.71
Cold Lake	–41.60	83.50	10.50	4.16	0.46	0.80	0.94
Madagascar	–42.73	86.29	11.33	0.61	0.73	1.66	0.08
Nigeria	–42.22	85.98	10.72	0.84	0.69	1.73	0.04
Asphalt Ridge, Utah	–42.68	85.75	11.43	0.49	0.88	1.82	0.05

[a] From H.-K. Yan *et al.*, Ref. 34.

Table 5.21 Heats of combustion and compositions of substances from bitumen/heavy oil. ΔU° values are constant volume heats of reactions represented by Equation (20), T = 298.15 K, and all substances are in their thermodynamic standard states. Compositions are expressed as wt%.[a]

Source of bitumen/heavy oil	ΔU° ($kJ \cdot g^{-1}$)	%C	%H	%S	% (N+O)	%Ash
Syncrude gas oil #1	–44.50	87.46	11.91	0.28	0.35	
Syncrude gas oil #2	–44.52	87.51	11.78	0.35	0.36	
Syncrude synthetic crude oil #1	–45.81	87.36	12.05	0.42	0.17	
Syncrude synthetic crude oil #2	–45.54	86.90	12.56	0.36	0.18	
Syncrude naphtha #1	–44.71	85.59	13.38	0.15	0.18	
Syncrude naphtha #2	–44.65	85.80	13.21	0.17	0.82	
Syncrude naphtha #3	–46.11	83.45	13.79	0.29	2.32	
Syncrude naphtha #4	–46.41	83.70	13.92	0.21	2.03	
Syncrude H-oil pitch	–38.65	82.67	8.14	4.56	2.18	2.09
Asphaltenes from Athabasca bitumen, medium-grade ore	–37.02	78.52	7.83	7.62	2.87	2.32
Asphaltenes from Athabasca bitumen, high-grade ore	–36.82	78.71	8.12	7.75	3.74	0.86
Asphaltenes from Cold Lake	–37.79	80.83	7.79	7.54	2.84	1.04
Maltenes from Athabasca	–42.17	83.33	10.90	4.20	1.46	0.25
Suncor coke	–33.53	83.93	3.70	5.78	3.34	2.85
Syncrude coke #1	–29.70	78.72	1.76	6.55	3.68	8.53
Syncrude coke #2	–29.43	78.21	1.69	6.36	4.32	9.18
Syncrude coke #3	–28.91	76.49	1.66	6.59	5.82	8.57
Syncrude coke #4	–29.13	77.52	1.66	6.54	4.63	8.26

[a] From L.G. Hepler *et al.*, Ref. 35.

4.0 Optical Properties

The color of crude oil (*e.g.* asphaltene: dark brown–black; resins: deep reddish–brown) is primarily due to the heavy constituents and thus it is the simplest indicator of oil quality. All bitumens have a dark brown–black color indicating high asphaltene and resins contents.

From the standpoint of chemical characterization of crude oils and crude oil products the most valuable optical properties are the infrared and visible–ultraviolet spectral properties. These properties will be discussed in connection with the chemical characterization studies of specific fractions of the bitumen while here we will consider only the refractive and optical rotatory properties.

4.1 Refractive index

The refractive index n is the ratio of the velocity of the propagation of light in vacuum to that in a given medium. The use of the refractive index in the characterization of petroleum fractions is made possible by the changes in the refractive index with molecular structure for narrowly separated subfractions of petroleum fractions having similar molecular weights. The refractive index is not an additive property but in various functional forms, for example as molar refraction R_M,

$$R_M = \frac{n^2 - 1}{n^2 + 2} \times \frac{M}{\rho} \tag{21}$$

or the temperature-independent expression $(n^{2/3} - 1) \times M/\rho$ (where M is the molecular mass and ρ the density), it can be employed as an additive quantity with structure-dependent increments. Nonetheless, n itself exhibits broad trends, varying with molecular size and structure. Its value increases in the order paraffins < naphthenes < aromatics, Table 5.22, and, in the latter

Table 5.22 Refractive indices of hydrocarbons, organosulfur compounds, bitumens and Syncrude process streams

Hydrocarbon	$[n]_D^{20}$ [a]	Hydrocarbon	$[n]_D^{20}$ [a]
Pentane	1.3579	Toluene	1.4961
Hexane	1.3749	n-Octyltoluene	1.4920
Heptane	1.3876	Styrene	1.5468
Nonane	1.4054	Tetralin	1.5461
Decane	1.4119	Decalin	1.4811
Eicosane	1.4425	Phenanthrene[b]	1.5943
Cyclopentane	1.4064	Thiophene	1.5289
Cyclohexane	1.4266	n-Amyldisulfide	1.4889
Cycloheptane	1.4449	1-Dodecanethiol	1.4589
Cyclohexene	1.4465	Bitumen (Ath., Syncrude)	1.57
1-Heptene	1.3999	Syncrude coker LGO[c]	1.5302
cis -1,3-Pentadiene	1.4329	Hydrotreated LGO	1.4854
trans -1,3-Pentadiene	1.4267	" , second time	1.4691
Bicyclohexane	1.4800	Syncrude coker HGO[d]	1.5718
Benzene	1.5011	Hydrotreated HGO	1.5288
Naphthalene	1.5898	" , second time	1.5051
Cyclohexylbenzene	1.5263		

[a] $[n]_D^{20}$ = Refractive index at 20°C at the wavelength of the sodium D line (589.08–589.6 nm).
[b] Temperature not specified. [c] Light gas oil. [d] Heavy gas oil.

two cases, with the number of rings in the molecule. Within a given structural series the refractive index also increases with molecular size. Small values of the refractive index indicate the presence of paraffinic compounds and high values, of aromatic compounds. Thus, the measurement of the refractive index, which can be done simply and quickly on small quantities of samples, can provide useful information on the composition of petroleum. This explains its widespread use in the petroleum industry.

As seen from the data in Tables 5.10 and 5.22, the refractive indices of upgraded bitumen products progressively decrease upon successive upgrading steps as more and more aromatic compounds are converted to naphthenic, and naphthenic to paraffinic compounds. Therefore, along with other parameters, the refractive index can be used as an indicator of the degree of upgrading.

The reliability of characterization methods based on the refractive index can be improved by combination with simultaneous density measurements. This then leads to the refractivity intercept method (ASTM D-2159) or to the temperature-independent specific refraction method:

$$C = \frac{n-1}{(n^2+2)d} \tag{22}$$

In yet another variation of the refractive-index-based characterization, the dispersion of the refractive index rather than the index itself is applied. Thus, in the highly useful specific dispersion method the refractive index is measured at two wavelengths of visible light (the C 656.3 nm red and the F 486.1 nm blue lines of the hydrogen atom spectrum are commonly used), from which the specific dispersion is calculated as $(n_F - n_C)/d$. The particular usefulness of the specific dispersion comes from its independence of the molecular weight; the values for saturated hydrocarbons are much lower than those for aromatics and those for alkenes are intermediate.

4.2 Optical rotation

Optical rotation (or optical activity) is the ability of a molecule possessing one or more asymmetric centers to alter the orientation of the plane of polarized light. If a compound causes the plane of polarization to rotate in a clockwise (positive) direction on facing the beam, it is called dextrorotatory and in a counterclockwise (negative) direction, levorotatory. Most petroleums show optical activity and are usually dextrorotatory, but levorotatory petroleums are also known.

Optical activity in crude oils is concentrated in the 250–300°C distillation cut which corresponds to the molecular weight range of many steroid and triterpenoid compounds known to occur in petroleum. Many of these types of compounds are found in the saturate fraction of crude oils and bitumens, for instance Prudhoe Bay crude oil and Athabasca bitumen saturate fractions contain significant concentrations of steranes and triterpanes and they are optically active with specific rotations $[\alpha]_{400}^{100°C}$ of +1.45 and +3.50. (The difference is due entirely to dilution effects arising from the higher percentage saturate content in the Prudhoe Bay (50%) than in the Athabasca (20%) sample.) The specific rotation, [α], is the angle of rotation per $g{\cdot}mL^{-1}$ concentration over a one-mm-long optical path. The temperature of the measurement is given as a superscript and the wavelength of the light as a subscript; the letter "D" signifies the sodium D lines (589.0 and 589.6 nm). The optical activity of petroleum constitutes strong evidence that petroleum originates at least in part from organic matter which was produced by living organisms. Isomerization reactions during the course of thermal maturation of the oil leads to gradual loss of the optical rotatory power with the accumulated thermal history of the oil. Hence there is a broad inverse relationship between the age of the oil and its optical activity.

A kind of optical rotation is based on the magneto–optical effect, according to which all liquids (and solids) become optically active when placed in a magnetic field. This is called the Faraday effect and it obeys the relation $\Theta = VlH$, where Θ is the angle of rotation, H the magnetic field strength, l the light pass and V is the "Verdet" constant (minutes·oersted^{-1}·cm^{-1}). The value of V is an intrinsic property of the substance. The Faraday effect has been used in compositional studies of hydrocarbons.

5.0 Class Composition

Bitumen is recognized as being an extremely complex natural material but, in spite of its complexity, it would be wrong to surmise that it could—or that it should—contain every imaginable compound on earth. For example, a sizeable fraction of bitumen contains molecules with 40 or more carbon atoms, and the number of possible isomers of the $C_{40}H_{82}$ paraffin tetracontane, which is only a mid-size hydrocarbon molecule and only one of the many possible types of C_{40} hydrocarbons, is an astronomical figure, 6.25×10^{13}. This number increases rapidly with increasing number of carbon atoms or with the introduction of heteroatoms in the molecule. Thus, while the number of compounds represented in bitumen has not been counted, thousands of compounds have been identified and thousands more have been noted to be also present. Still, their number would probably not exceed, at the most, a few hundred thousands, a mere trifle when contrasted to the number theoretically possible. Why is it, then, that bitumen is only a "moderately" complex substance? The answer lies in the origin and history of petroleum, as will be briefly referred to in subsequent chapters and more exhaustively discussed in Chapter 13.

It is convenient to divide the constituents of petroleum into four broad compound classes (*cf.* Chapter 14.6.8) which can be separated from one another and gravimetrically measured. The relative proportions of these compound classes, the asphaltene, polars, aromatics and saturates, impart unique characteristics to the crude oil and the compositions of each of these compound classes will be discussed in detail in forthcoming chapters. Here we only concern ourselves with the distribution and determination of compound classes in bitumens and heavy oils.

- Separation of the asphaltene is the first step in the class separation of bitumen and heavy oil. It is accomplished by solvent precipitation using a low-molecular-weight alkane as precipitant (see Chapter 14). Asphaltene is the highest-molecular-weight fraction of petroleum; it is rich in heteroatoms, polyaromatic moieties and in polar functional groups and has a strong propensity for molecular aggregation. Consequently, its solubility properties are different from those of the rest of the bitumen and asphaltene can be precipitated from a concentrated benzene or toluene solution of the bitumen by the addition of *n*-pentane or *n*-heptane. In effect, the definition of asphaltene is given in terms of this solubility criterion and, accordingly, asphaltene is that portion of the bitumen (crude oil) which is soluble in toluene but insoluble in *n*-pentane or *n*-heptane. More recently, *n*-heptane has become the choice of precipitant used, and the asphaltene so precipitated is designated as *n*-heptane asphaltene (*n*-C_7-asphaltene *vs.* *n*-C_5-asphaltene. The apparent solubility of asphaltene in *n*-heptane is considerably higher than in *n*-pentane and therefore, from a given bitumen, the weight of the *n*-heptane asphaltene is less than that of the *n*-pentane asphaltene. This is largely due to the smaller amount of co-precipitated polar material in the *n*-heptane asphaltene; in the *n*-pentane asphaltene this material is measured as asphaltene. In addition to the nature of the precipitant, the percentage asphaltene precipitated is also dependent on the experimental conditions of precipitation, to be discussed in detail in Chapter 14 along with other relevant problems. The deasphaltened bitumen is called the maltene. Elemental analytical data, Table 5.23, show that maltene is a lighter material with more favorable properties—higher $(H/C)_a$, lower heteroatom content, lower molecular weight—than those of bitumen.

Table 5.23 Representative analytical data for Alberta bitumens and bitumen fractions[a]

Fraction	Source	Wt %					$(H/C)_a$	MW
		C	H	N	O	S		
Whole bitumen	Ath.	83.98	10.22	0.65	1.97	4.57	1.46	620
	Cold Lake	83.93	10.46	0.23	0.94	4.70	1.49	490
	Peace R.	81.68	9.98	0.14	2.08	5.60	1.46	520
	Wabasca	82.44	10.32	0.42	0.82	5.51	1.49	600
Asphaltene	Ath.	81.31	7.88	1.06	2.79	7.53	1.16	5,920
	Cold lake	80.54	7.39	1.15	1.78	6.51	1.10	8,140
	Peace R.	79.87	8.15	0.78	2.08	8.82	1.21	3,500
	Wabasca	80.46	8.20	0.99	1.16	8.40	1.21	5,760
Maltene	Ath.	84.38	10.63	0.07	0.85	3.91	1.51	435
	Cold Lake	84.19	11.01	0.27	0.61	3.89	1.54	430
	Peace R.	82.89	10.61	0.08	1.27	5.41	1.53	440
	Wabasca	82.99	10.74	0.28	1.04	5.25	1.54	530

[a] From Ref. 36.

- The "resin" fraction of petroleum was originally also defined in terms of solubility properties; however, today the definition is exclusively in terms of adsorption properties, specifically, resins constitute that portion of the maltene that is adsorbed on a clay (Attapulgus clay, Fuller's earth) or, alternatively, as that portion of the maltene that is eluted from silica gel by polar eluants (*e.g.*, methanol in benzene) but not by *n*-pentane or benzene. In the latter case it has become common practice to denote the fraction as "polars" rather than "resins". It should be borne in mind that the two definitions are not equivalent and this discrepancy is the source of some of the scatter in the class compositional data one finds in the literature.
- The saturates and aromatics are eluted from the adsorbent (Attapulgus clay, silica gel) with *n*-pentane or benzene prior to elution of the resins and constitute the oily fraction of the bitumen or crude oil. The saturates are then separated from the aromatics on an alumina column: the saturates are eluted with *n*-pentane and the aromatics with benzene. The saturates may contain small amounts of contaminants from the other fractions which may be removed by silver-ion-on-silica-gel chromatography.

Details of some class separation procedures are given in the flow charts shown in Figures 5.12–14.

Thus, as can be deduced from the preceding paragraphs, the class compositions are given as operational definitions, although the saturates and (to a somewhat lesser degree) the aromatics represent true compound class families. For this reason the results of a class analysis are strongly dependent on the conditions employed. Therefore, strict adherence to the adopted protocol is a prime condition for reproducibility, and the validity of the data is restricted to the particular analytical procedure followed and the types and qualities of the solvents employed.

Many class fractionation procedures have been described in the literature. From the standpoint of bitumen chemistry, the two notable ones are the SARA[2] (saturates, aromatics, resins, asphaltene) and the USBM-API-60[37] methods, schematic flow charts for which are

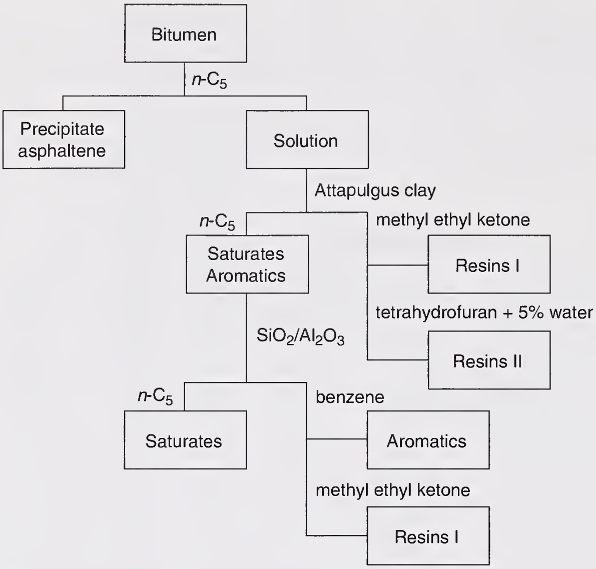
Bitumen
n-C5
Precipitate asphaltene
Solution
Attapulgus clay
n-C5
methyl ethyl ketone
Saturates Aromatics
Resins I
tetrahydrofuran + 5% water
SiO2/Al2O3
Resins II
n-C5
benzene
Saturates
Aromatics
methyl ethyl ketone
Resins I

Figure 5.12 Flow diagram for the SARA class composition procedure used at Syncrude Canada Ltd.

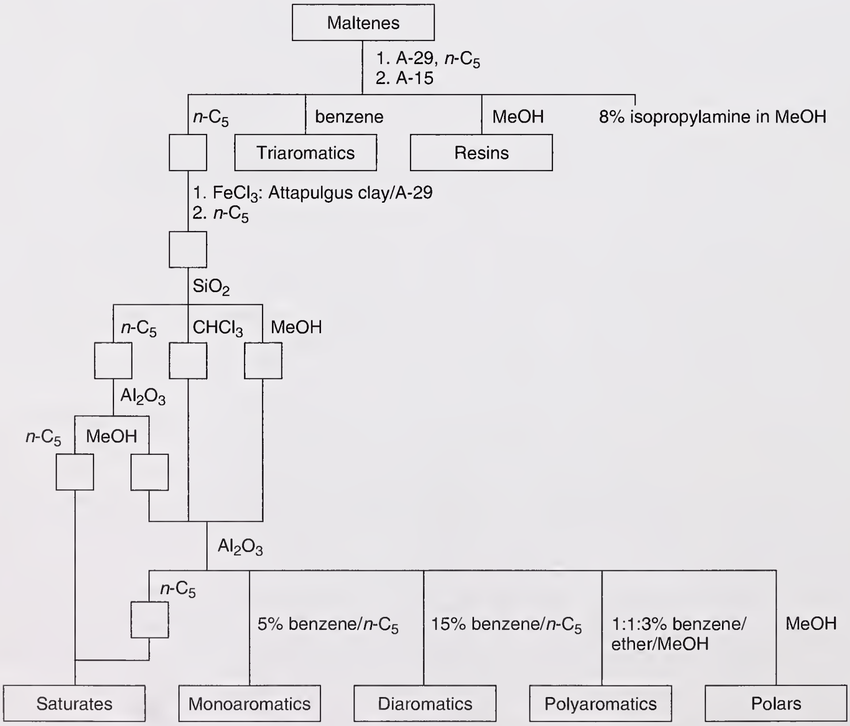
Maltenes
1. A-29, n-C5
2. A-15
n-C5
benzene
MeOH
8% isopropylamine in MeOH
Triaromatics
Resins
1. FeCl3: Attapulgus clay/A-29
2. n-C5
SiO2
n-C5
CHCl3
MeOH
Al2O3
n-C5
MeOH
Al2O3
n-C5
5% benzene/n-C5
15% benzene/n-C5
1:1:3% benzene/ether/MeOH
MeOH
Saturates
Monoaromatics
Diaromatics
Polyaromatics
Polars

Figure 5.13 Flow diagram for the USBM-API-60 class composition procedure.

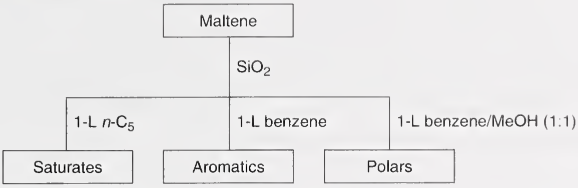

Figure 5.14 Flow diagram for the SAPA class composition procedure.

shown in Figures 5.12 and 5.13. Either method can be applied to the analysis of the whole bitumen, the maltene or their distillate fractions. Since the percentage of asphaltene as obtained by solvent precipitation is an important quality parameter of the bitumen feedstock, it is preferably separated from the bitumen and measured gravimetrically prior to the chromatographic analyses.

The USBM-API-60 procedure, which is the most involved procedure of the schemes shown in Figures 5.12–14, yields more, although not necessarily needed, information. In this procedure the sample is applied to an anion exchanger column to remove the acidic components of the sample, then to a cation exchanger column to remove the basic components, followed by coordination chromatographic removal of the neutral nitrogen compounds on a $FeCl_3$-on-Attapulgus-clay column. Next, the saturates and aromatics are separated by adsorption chromatography on silica gel and alumina columns as indicated in the flow chart in Figure 5.13.

The results of USBM-API-60 analyses of four Alberta bitumen samples[36,38–41] are given in Table 5.24; results of a SARA analysis of Athabasca bitumen as reported by Syncrude Canada Ltd. are given in Table 5.25. The agreement between the two sets of data is satisfactory and from these results it appears that the class compositions of Alberta oil sand bitumens vary within the following limits:

saturates	15–21%
aromatics	18–19%
resins	44–48%
asphaltene	14–20%

The saturate fractions obtained, containing one- to six-ring hydrocarbons, are quite clean and the levels of aromatic or heteroatom contamination are low. Also, the recovery of the saturated hydrocarbons is good. The aromatic fraction contains heteroatoms, mainly sulfur in the form of thiophenes and cyclic sulfides. Resins, comprising the largest class fraction, consist of acidic, basic, amphoteric and neutral constituents. The "acidic" fraction is about twice the weight percent of the basic fraction. This, at least in part, is due to the presence of amphoteric compounds which also adsorb on the ion exchanger column applied first in the analytical sequence. The data in Table 5.24 were obtained from analyses in which the anion exchanger column was applied first and the cation exchanger column, second. Thus, the anion exchanger column adsorbed and removed from the solution not only the acids but also the amphoteric compounds. If the order of the column application had been reversed, that is, if the cation exchanger had been used first, then this column would adsorb not only the bases but the amphoterics as well. The amount by which the percentage of bases would increase would then be the same as that by which the percentage of acids + amphoterics would decrease. Thus, the sum of the acids + amphoterics + bases would remain unchanged, as was found in the ion exchanger analysis of Athabasca asphaltene.[39]

Table 5.24 Class composition of Alberta oil sand bitumens using the USBM-API-60 procedure

Component	Weight %			
	Peace River	Wabasca	Athabasca	Cold Lake
Hydrocarbons:	34	33	36	40
saturated	15	15	18	21
aromatic	19	18	18	19
Asphaltene	20	19	17	16
Resins:	44	48	46	44
acids + amphoterics	12	10	14	15
bases	7	6	7	7
neutral N-compounds	1	3	1	1
neutral (others)	24	29	24	21
Total	98	100	99	100

Table 5.25 Class analysis of Athabasca Syncrude and Utah bitumens using the SARA method[a]

Athabasca[a]

Component	Mean value[b]	Standard deviation[b]
Saturates	16.87	± 0.10
Aromatics	18.27	± 0.58
Resins I	38.99	± 0.77
Resins II	5.85	± 0.25
Asphaltene	17.18	± 0.19
Overall recovery	97.16	± 0.82

[a] From J.T. Bulmer and J. Starr, Ref. 2. [b] Six determinations.

Utah[c]

Component	Whiterocks	Sunnyside	PR Spring	Asphalt Ridge	Circle Cliff
Saturates	29.5	24.9	26.6	32.4	23.8
Aromatics	22.2	18.1	25.7	22.4	19.2
Resins	42.4	30.0	31.7	37.6	28.8
Asphaltene	3.3	23.7	16.0	7.3	28.1
Gravity, °API	12.7	5.5	7.8	14.4	14.3
$(H/C)_a$	1.60	1.45	1.57	1.56	1.37

[c] Cited in Ref. 22, Chapter 3.

The neutral nitrogen compounds isolated comprise about 1% of the bitumen, except in the Wabasca sample where they amount to 3%. The rest of the neutral resins includes thiophenes, cyclic sulfides and sulfoxides, fluorenols and fluorenones, alkanols, cycloalkanols, carbazoles, pyridines, quinolines and vanadyl and nickel porphyrins, among many other polar compounds; however, some of these compounds tend to elute with the aromatic fraction when the separation of aromatics and polars is grossly incomplete as in the SAPA method of class analysis and, to a smaller extent, in the SARA method as well. On the other hand, some of the higher condensed and most of the high-molecular-weight aromatic hydrocarbons elute with the neutral polars and this may reduce the error in the gravimetry that arises from the contamination of the isolated aromatic fraction by heterocycles.

The n-C_5 (n-pentane precipitated) asphaltene content of the samples reported in Tables 5.4 and 5.25 is in the 14–20% range, which is representative of Alberta bitumens.

The results from the single analyses of the four bitumen samples naturally do not provide a database from which conclusions may be drawn vis-à-vis the possible existence of compositional trends; nonetheless, it will be noted that the lowest asphaltene and highest saturate contents obtain for the Cold Lake bitumen, which is in agreement with the incompletely biodegraded status of this bitumen and the more severely biodegraded status of the other three bitumens listed in Table 5.24.

The USBM-API-60 analysis is time-consuming and, since not all the information it yields is required in an industrial operation, class analyses of bitumen at the Syncrude oil sand plant are carried out by the SARA method, Figure 5.12, which is less time- and cost-intensive. And, while the results from the two methods agree reasonably well, not all the class analytical methods published in the literature provide comparable results. For example, the SAPA method is fraught with the most common error in class analysis, the overestimation of the hydrocarbon fraction. In the SAPA (saturates, aromatics, polars and asphaltene) method, Figure 5.14, incomplete separation of the saturates–aromatics–polars leads to quite different values for Athabasca bitumen, 33, 36, 15 and 17% for the saturates, aromatics, polars and asphaltene. The "saturate" fraction here contains about 50% aromatics + heterocompounds and the "aromatic" fraction, about 50% polar material, as indicated by their lower $(H/C)_a$ values and higher NOS contents, compared to the silica–alumina separated fractions.

The above comparison of the three methods for the class analysis of bitumen demonstrates the need for caution when reviewing analytical data from different laboratories without appropriate reference to the particular procedure employed. Because of these inconsistencies in the class analysis arising from the lack of universally accepted standards, comparison of data for various bitumens from different laboratories is not strictly meaningful unless sufficient experimental details of the analyses are provided. It is probably better to rely on a few, well-measured properties such as asphaltene content, API gravity, and sulfur content when comparing bitumen qualities. The values of these properties for Alberta oil sand bitumens cover the same range as those for bitumens from other worldwide sources, with a few notable exceptions, Table 5.26.

Table 5.26 Properties of bitumens from Alberta and other worldwide sources

Source	Asphaltene content wt%	°API gravity	Sulfur content wt%
Alberta oil sands and carbonates, and worldwide ranges	11–20	6–24	1–5
Exceptions			
Trinidad Lake	33	0.7	6
Bermuda Lake	35	2	4
Selenitra	45		7
Brasilian	28	11	2
Tar Sand Triangle (U.S.)	26	11	4

In the separation of the bitumen from the sand by either the water flotation or a solvent extraction process, significant amounts of inorganic matter, of the order of 0.5–1.0% of the bitumen, remain in the crude bitumen. This inorganic residue, referred to as ash, is associated with the polar fractions of the bitumen (the asphaltene and the resins) while the hydrocarbon fractions contain quite low levels of ash. The ash content of the asphaltene from benzene-extracted Athabasca bitumen may be as high as 3.2–3.5%, in the polar resins, 1.8%, and in the less polar resins, 0.5–0.6%. In bitumen, produced industrially by water flotation the ash level is 0.5–0.7%. The ash level can be reduced to 0.1–0.2% by centrifugation of the diluted bitumen but the ash cannot be completely removed except by centrifugation in super-high-speed ultracentrifuges.

The main precursors of ash are the clay minerals and thus the aluminum, iron and silicon contents of the bitumen are correctly reflected by the ash content; however, the vanadium and nickel contents are relatively independent of the ash level, suggesting that these metal species are present mainly in oil-soluble form. This is in agreement with the isolation of oil-soluble nickel and vanadyl (VO^{2+}) porphyrin complexes from the bitumen which, however, would account for only a fraction of the metals.

5.1 Distribution in the reservoir

The composition and temperature in the reservoir change, as has been discussed above with depth of burial. However, reliable data on these parameters in the open literature are few and far between.

With respect to temperature variance, the surface layers of the Athabasca deposit experience frost penetration during winter months to a depth of 3 m or more, and seasonal temperature changes have been measured 14 m below the surface. Below 14 m the reservoir temperature increases with depth from about 10°C at 67 m to about 18°C at 334 m.[42]

For the near-surface Athabasca deposit, compositional variations have been reported[43] to occur within a given formation with vertical depth and, along with an increase in the bitumen content towards the base of the formation, the asphaltene, resin and heteroatom contents as well as the percentage amount of distillation residue have been reported to increase. However, the statistical significance of these data has not been validated.[44]

In a subsequent study[45] on Athabasca and Cold Lake oil sands an increase in the asphaltene content with vertical depth was recorded, Table 5.27, but an increase in the bitumen content was not confirmed. More recently, in a single set of experiments,[46] it has been found that the bitumen content in the vertical depth of a 28-m payzone below a 400-m burial depth shows a nearly monotonic decline with depth. When the data were corrected for free pore space in the reservoir rock, the data became somewhat scattered but the trend remained. The percentage asphaltene content of the bitumen, while also displaying considerable scatter, showed a distinctly higher average value in the lower half of the payzone than in the upper half. This trend may be attributed to the upward migratory pathway of the precursor oil in the sand rock formation. Along its migratory path, the oil loses some of its asphaltene to the rock through a chromatographic effect. This should not only reduce the asphaltene content of the migrating oil, but also cause a change in the composition of the residual asphaltene owing to the preferential retention by the rock of the higher-MW and more polar components of the asphaltene. Thus, all three studies cited concordantly point to a compositional change in the bitumen, which is consistent with and provides evidence for an upward migratory pathway of the oil in the reservoir rock. This tentative conclusion needs further validation by additionai data.

Table 5.27 Variability in Asphaltene Content[a] in Single Cores

Depth (m)	Cold Lake Bitumen[b] Asphaltene Content (wt%)	Depth (m)	Athabasca Bitumen Asphaltene Content Neighboring Samples (wt%)		Mean
420	16.0	170	16.7	18.6	17.7
	15.6	177	19.9	18.4	19.2
	16.4	178	20.2	19.5	19.9
	–	186	20.6	20.0	20.3
	16.9	187	20.0	20.7	20.4
	–	196	20.6	21.2	20.9
430	17.2	201	21.0	20.2	20.6
	17.9	209	22.0	20.3	21.2
	16.8	215	18.9	20.1	19.5
	17.4	223	19.2	23.0	21.1
	–	231	20.5	19.5	20.0
	18.3				
	–				
440	18.4				
	–				
	–				
	18.3				
	18.8				
	–				
450	18.4				

[a] Asphaltenes were precipitated from 40:1:1 pentane:benzene:bitumen. Unless otherwise noted, data are from Ref. 45. [b] J. Starr and D. Wallace, "The Evaluation of Data for the Initial Characterization of an Oil Sand Deposit," paper presented at the Int. Symp. on the Characterization of Heavy Crudes and Residues, Lyon, France, 1984.

6.0 Summary

Bitumen represents the heaviest form of petroleum,with densities ≥ 1,000 kg·m^{-3} (API gravities ≤ 10°) and viscosities ≥ 10,000 mPa·s. The major deposits of pooled bitumen occur in sandstone and some in carbonate rock beds. When rock bitumen, the frequent companion of kerogen, is taken into account bitumen constitutes (after kerogen) the second most abundant form of organic carbon on earth. The common denominator determining the physical and chemical characteristics of most pooled bitumens is their microbiological origin *via* a secondary microbiological degradation of pooled conventional oils. This process is selective and preferentially removes the acyclic and other low-MW hydrocarbon constituents of the oil, leaving behind a viscous, heavy residue enriched in high-MW components, resins and heteroatoms. The shared microbiological history is then the overriding cause responsible for the well-known common physical and chemical properties characterizing bitumens, such as high density, viscosity, MW, refractive index, NOS/metal, $(C/H)_a$ ratio, boiling point, aromatic and naphthenic content, among others. Each of these properties varies with the degree of microbiological degradation that the bitumen experienced and the variation is in the same direction, i.e. more degradation means higher density, higher viscosity, higher MW, etc. Consequently all these, along with other properties, appear to be interrelated and vary in parallel directions.

The separation of bitumen from the rock matrix is carried out industrially by water flotation and in the laboratory by solvent extraction. In either case some mineral fines remain in the bitumen and can only be removed completely by very high-speed centrifugation (*e.g.* at 366 k gravity). The characterization of the bitumen should then be done on material from which the fines have been removed as completely as possible. In any event, some of the properties of bitumen are altered during the extraction process and, for example, density (API gravity) and viscosity can be affected significantly. The elemental composition of Alberta bitumens follows the order C >H> S > O > N with narrow ranges in percentage concentration. The $(H/C)_a$ ratio indicates a weak correlation with the degree of microbiological degradation and samples from the most degraded deposits, the Carbonate, Athabasca and Peace River deposits, show lower values, 1.48–1.53, than the less degraded Lloydminster, Cold Lake, Wabasca deposits, 1.54–1.55.

Density is a linear function of temperature and for an API gravity $\geq 9°$ it shows a maximum drop below the density of water around 82℃. Therefore, this temperature is the most suitable one for the hot water separation of the bitumen. Viscosity, on the other hand, is an approximately inverse exponential function of temperature and several functions have been proposed and are in use. Bitumen being non-Newtonian, its measured viscosity is somewhat dependent on shear rate. Viscosity varies with density, pressure and MW and increases—in some cases exponentially—with the value of these parameters. In the Syncrude plant upgrading process the density of bitumen decreases from approximately 1.0 $kg{\cdot}m^{-3}$ to 0.85 $kg{\cdot}m^{-3}$ in the final synthetic crude and the viscosity, from 130,000 $mm^2{\cdot}s^{-1}$ to 5–6 $mm^2{\cdot}s^{-1}$.

Vaporization and condensation are essential steps in the processing of petroleum and are governed by the vapor pressure and latent heat of vaporization. The boiling point is a function of class composition; it varies in the order aromatics > naphthenics > *n*-alkanes > isoalkanes and can be estimated from the composition. Distillation characteristics are expressed in terms of distillation curves in which temperature is plotted against percentage distillate. The shape of the curves is a function of gravity and shifts to the right with increasing gravity (lighter oil).

In order to avoid cracking during distillation it may be conducted under vacuum or in laboratory tests substituted by simulated distillation using gas chromatography—a widely-accepted practice to obtain true boiling point distribitions.

On distillation, bitumens leave substantial amounts of nondistillable residues which are a measure of the coke-forming propensity of the bitumen. There are three test procedures to measure this, of which the microcarbon residue (MCR) and Conradson carbon residue (CCR) are the superior ones. The amounts of these residues correlate inversely with the API gravity and thus bitumens give higher residue numbers than do conventional oils. The residue number from asphaltene is higher than that from the deasphaltened fraction (maltene) of the oil and it is important to note that these values are not additive for the whole oil.

Specific heats, latent heats of vaporization and fusion, and heats of combustion have been measured for various bitumens, bitumen fractions and related materials, and equations to estimate them as functions of density, temperature or elemental composition are available in the literature.

Of the optical properties, the refractive index or its temperature-independent forms (*e.g.* molar refraction) is employed as a simple and useful method to indicate class composition. High values of "n" obtain for aromatic compounds, low values for paraffins and intermediate values for naphthenes. In combination with density measurements or as the dispersion measured at two wavelengths, the method becomes independent of temperature or MW. Most crude oils exhibit optical acivity, which provides important supplementary evidence for their biological origin. The rotatory power resides in the di- through pentacyclic portion of the saturate fraction.

Compound class distributions of crude oils are severely affected by microbiological degradation. Thus, the microbiologically severely degraded Carbonate, Athabasca and Peace River bitumens are completely devoid of *n*-alkanes but the less degraded Cold Lake bitumen still contains small amounts and the related Lloydminster heavy oil contains even more. The dominant class fraction in all these bitumens is the resins/polars, and the asphaltenes, aromatics and saturates are present in about equal concentrations. Of these, the saturates can be cleanly isolated as mixtures of one- to six-ring hydrocarbons. The aromatics, along with the pure hydrocarbons, contain thiophenes, cyclic sulfides and carbazoles, as well as other resinous substances. The resins comprise carboxylic acids, alcohols, sulfoxides, along with some sulfides, ketones, carbazoles, pyridines, quinolines, porphyrins, etc. Their constituents are mainly neutrals followed by acids > bases > amphoterics. The asphaltenes also comprise acids > bases > neutrals > amphoterics.

Bibliography

1. a) J.G. Speight, *The Chemistry and Technology of Petroleum*, 3rd Edition, Marcel Dekker, Inc., New York, 1999. b) R.F. Meyer, Proceedings, 15th World Petr. Congr. 2, (1998) 459. c) UNITAR Centre for Heavy Crude and Tar Sands: Definitions.
2. *Syncrude Analytical Methods for Oil Sand Bitumen Processing*, J.T. Bulmer and J. Starr, Eds., Alberta Oil Sands Technology and Research Authority Technical Publication Series No. 1, Edmonton, AB, 1979.
3. L.D.L. Vorndran, A.J. Serres, J.K. Donnelly, R.G. Moore and D.W. Bennion, "Bitumen Separation for Experimental Use", Can. J. Chem. Eng., 58 (1980) 580.
4. G. Gimber, K. Groves, M. Heschke, J. Lastovica and G. Rademacher, "Oil Sand Processing Using Methylene Chloride" in *Challenges and Innovations: Heavy Oil and Oil Sands Technical Symposium*, University of Calgary, Calgary, AB, February, 1985.
5. D. Wallace, M. Polikar and F. Ferracuti, "Preparation of Bitumen From Oil Sand by Centrifugation", Fuel, 63 (1984) 862.
6. H.H. Chen, T.W. Mojelsky, J.D. Payzant, E.M. Lown, D. Henry, D. Wallace and O.P. Strausz, "Chemical Changes in Alberta Oil Sands During Steam Treatment", AOSTRA J. Res., 7 (1991) 17.
7. I. Rubinstein, D. Henry, D. Hoover, K.P. Thomas, A.L. Pickard and I. Taylor, "Viscosity", Ch. 10 in *A Review of Analytical Methods for Bitumens and Heavy Oils*,.D. Wallace, Ed., Alberta Oil Sands Technology and Research Authority Technical Publication Series No. 5, Edmonton, AB, 1988, p. 89.
8. W.D. Gunter and G.W. Bird, "Inorganic Geochemistry" in *AOSTRA Technical Handbook on Oil Sands, Bitumens and Heavy Oils*, L.G. Hepler and C. Hsi, Eds., Alberta Oil Sands Technology and Research Authority Technical Publication Series No. 6, Edmonton, AB, 1989, p. 203.
9. (a) J.E. Cooper, "Fatty Acids in Recent and Ancient Sediments and Petroleum Reservoir Waters", Nature, 193 (1962) 744; (b) D.B. MacGowan and R.C. Surdarn, "Difunctional Carboxylic Acid Anions in Oilfield Waters", Org. Geochem., 12 (1988) 245.
10. L.S. Kotlyar, B.D. Sparks, J.R. Woods, S. Raymond, Y. LePage and W. Shelfantok, "Distribution and Types of Solids Associated with Bitumen", Petr. Sci. Technol., 16 (1998) 1.
11. D. Wallace and B. Kratochvil, "Sampling Uncertainty in the Determination of Major Components in Athabasca Oil Sand", AOSTRA J. Res., 1 (1984) 31; B. Kratochvil, J.K. Taylor and D. Wallace, "Sampling", Ch. 2 in *A Review of Analytical Methods for Bitumens and Heavy Oils*, D. Wallace, Ed., Alberta Oil Sands Technology and Research Authority Technical Publication Series No. 5, Edmonton, AB, 1988.
12. J.K. Liu, "Analytical Methods" in *AOSTRA Technical Handbook on Oil Sands, Bitumens and Heavy Oils*, L.G. Hepler and C. Hsi, Eds., Alberta Oil Sands Technology and Research Authority Technical Publication Series No. 6, Edmonton, AB, 1989, p. 11.

13. N.M. Boduszynski, "Composition of Heavy Petroleums .1.", Energy & Fuels, 1 (1987) 2.

14. M.R. Gray, *Upgrading Petroleum Residues and Heavy Oils,* Marcel Dekker, Inc., New York, 1994.

15. F.S. Jacobs and R.H. Filby, "Solvent Extraction of Oil Sand Components for Determination of Trace Metals by Neutron Activation Analysis", Anal. Chem., 55 (1983) 74.

16. F.S. Jacobs and R.H. Filby, "Trace Element Composition of Athabasca Tar Sands and Extracted Bitumen", in *Atomic & Nuclear Methods in Fossil Energy Research,* R.H. Filby, Ed., Plenum Press, New York, 1982.

17. B. Hitchon, R.H. Filby and K.R. Shaw, "Geochemistry of Trace Elements in Crude Oils, Alberta, Canada", Preprints, Am. Chem. Soc. Div. Petrol. Chem., 18 (1973) 623.

18. J.T. Purdham and O.P. Strausz, unpublished results.

19. *Some Physical Properties of Bitumens and Oil Sands,* D.R. Prowse, Ed., Alberta Research Council, 1983.

20. a) K.E. Peters and J.M. Moldowan, *The Biomarker Guide*, Prentice Hall, Englewood Cliffs, N.J. 1993, p. 140. b) J.A. Curiale, "Distribution of Transition Metals in North Alaskan Oils", Ch. 8 in *Metal Complexes in Fossil Fuels*, R.H. Filby and J.F. Branthaver, Eds., ACS Symposium Series 344, American Chemical Society, Washington, D.C. (1987) p. 135.

21. F.W. Jones and J.A. Majorowicz, "Some Aspects of the Thermal Regime and Hydrodynamics of the Western Canadian Sedimentary Basin", in *Fluid Flow in Sedimentary Basins and Aquifers*, J.C. Goff and B.P.J. Williams, Eds., Geol. Soc. Special Publication No. 34 (1987) 79.

22. L.L. Schramm and J.C.T. Kwak, "The Rheological Properties of an Athabasca Bitumen and Some Bituminous Mixtures and Dispersions", J. Can. Petrol. Technol., 27 (1988) 26.

23. D. Wallace and D. Henry, "A Correlation for Correcting the Viscosity of Solvent-Extracted Bitumen to a Solvent-Free Basis", AOSTRA J. Res., 3 (1987) 239.

24. L.G. Hepler and R.G. Smith, *The Alberta Oil Sands: Industrial Procedures for Extraction, and Some Recent Fundamental Research*, Alberta Oil Sands Technology and Research Authority Technical Publication Series No. 14, Edmonton, AB, 1994.

25. a) J.M. Dealy, "Rheological Properties of Oil Sand Bitumens", Can. J. Chem. Eng, 57 (1979) 677. b) V.R. Puttagunta, B. Singh and A. Miadonye, "Correlation of Bitumen Viscosity with Temperature and Pressure", Can. J. Chem. Eng., 71 (1993) 447, 988.

26. A.K. Mehrotra, Can. J. Chem. Eng., 72 (1994) 763 and references therein.

27. F.A. Seyer and C.W. Gyte, "Viscosity" in *AOSTRA Technical Handbook on Oil Sands, Bitumens and Heavy Oils*, L.G. Hepler and C. Hsi, Eds., Alberta Oil Sands Technology and Research Authority Technical Publication Series No. 6, Edmonton, AB, 1989, p. 154.

28. H.-J. Neumann, B. Paczynska-Lahme and D. Severin, "Composition and Properties of Petroleum" in *Geology of Petroleum*, Vol. 5, H. Beckmann, Ed., Halsted Press, New York, N.Y., 1981.

29. H.H. Chen, D.S. Montgomery, O.P. Strausz and Z.M. George, "Hydrocracking of Athabasca Bitumen Using Oil-Soluble Organometallic Catalysts" in *Catalysts in Petroleum refining 1989*, D.L. Trimm, S. Akashah, M. Absi-Halabi and A. Bishara, Eds., Elsevier Science Publishers, Amsterdam, 1990 p. 439.

30. J.B. Maxwell, *Data Book on Hydrocarbons*, Van Nostrand, Princeton, N.J.; *Am. Petr. Inst. Technical Data Book—Petr. Refining*, 4th ed., American Petroleum Institute, Washington, D.C., 1981; for boiling point–molecular weight relations see, for example, K.H. Altgelt and M.M. Boduszynski, "Composition of Heavy Petroleums. 3. An Improved Boiling Point Molecular Weight Relation", Energy & Fuels, 6 (1992) 68.

31. *Syncrude Analytical Methods Manual for Bitumen Upgrading*, J.K. Liu and H.E. Gunning, Eds., Alberta Oil Sands Technology and Research Authority Technical Series No. 11, Edmonton, AB, 1991.

32. J. Cooley, S. Noel, A.L. Pickard, I. Rubinstein, E.R. Hoffman, K.P. Thomas, S.E. Litka and R. Wasel, "Carbon Residue", Ch. 12 in *Review of Analytical Methods for Bitumens and Heavy Oils*, D. Wallace, Ed., Alberta Oil Sands Technology and Research Authority Technical Series No. 5, Edmonton, AB, 1988, p. 113.

33. R. Cassis, N. Fuller, L.G. Hepler, R.J.C. McLean, A Skauge, N.S. Srinivasan and H.-K. Yan, "Specific Heat Capacities of Bitumens and Heavy Oils, Reservoir Minerals, Clays, Dehydrated Clays, Asphaltenes and Cokes", AOSTRA J. Res., 1 (1985) 163.

34. H.-K. Yan, Y. Zhou and L.G. Hepler, "Heats of Combustion of Light and Heavy Oils", Oilfield Chemistry (People's Republic of China), 5 (1988) 218.

35. L.G. Hepler, "Thermochemical and Thermodynamic Properties" in *AOSTRA Technical Handbook on Oil Sands, Bitumens and Heavy Oils*, L.G. Hepler and C. Hsi, Eds., Alberta Oil Sands Technology and Research Authority Technical Series No. 6, Edmonton, AB, 1989; H-K. Yan and L.G. Hepler, "Combustion of Light and Heavy Oils", in *China-Canada Heavy Oil Technology Symposium Proceedings*, Alberta Oil Sands Technology and Research Authority, Edmonton, AB, 1987.

36. O.P. Strausz, "The Chemistry of the Alberta Oil Sand Bitumen", Can. Inst. Min. Metall. Special Volume, 17 (1977) 146.

37. U.S. Bureau of Mines, API RP-60, 1974; W.E. Haines and C.J. Thompson, "Separating and Characterizing High-Boiling Petroleum Distillates: the USBM-API Procedure".

38. O.P. Strausz, "Specific Problems in the Upgrading of Alberta Oil Sand Bitumen—An Overview of its Characteristic Composition and Structure", J. Japan. Petrol. Inst., 27 (1984) 89.

39. M.L. Selucky, S.S. Kim, F. Skinner and O.P. Strausz, "Structure-Related Properties of Athabasca Asphaltenes and Resins as Indicated by Chromatographic Separation", in *Chemistry of Asphaltenes*, J.W. Bunger and N.C. Li, Eds., Adv. Chem. Ser. 195, American Chemical Society, Washington, D.C., 1981, p. 83.

40. M.L. Selucky, Y. Chu, T. Ruo and O.P. Strausz, "Chemical Composition of Athabasca Bitumen", Fuel, 56 (1977) 369.

41. M.L. Selucky, Y. Chu, T. Ruo and O.P. Strausz, "Chemical Composition of Cold Lake Bitumen", Fuel, 57 (1978) 9.

42. M.A. Carrigy, "The Physical and Chemical Nature of a Typical Tar Sand: Bulk Properties and Behavior", in *Proceedings, 7th World Petroleum Congress*, Elsevier, Amsterdam, 1967, Vol. 3 p. 573.

43. R. Schutte, paper presented at the 25th Annual Meeting, Petroleum Society of the Canadian Institute of Mining and Metallurgy, Calgary, AB, May 7–10, 1974, quoted in Ref. 1 p. 69.

44. R. Schutte, private communication, 1995.

45. M.A. Carrigy and D. Wallace, "New Analytical Results on Oil Sands From Deposits Throughout the World", in *Proceedings, Int. Conf. on Heavy Crudes and Tar Sands*, Long Beach, CA, July 22–31, 1985, Vol. 1, Alberta Oil Sands Technology and Research Authority, Edmonton, AB, 1985, p. 231.

46. O.P. Strausz, E.M. Lown and T. Mojelsky, unpublished results.

Appendix 5.1

Inorganic Constituents of Petroleums

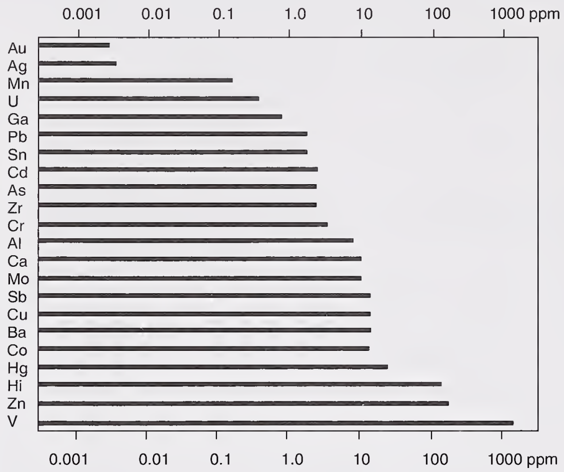

Figure 1. Maximum values reported for selected elements in petroleum. Data from P. Jones, "Trace Elements and Other Elements in Crude Oil—a Literature Review", Report of British Petroleum Research Centre, Sunbury, U.K., 1975. Reproduced from D.A.C. Manning and A.P. Gize, "Organic Matter and Metalliferous Deposits", in *Organic Geochemistry, Principles and Applications*, M.H. Engle and S.A. Macko, Eds., Plenum Press, New York, N.Y. 1993, p. 547.

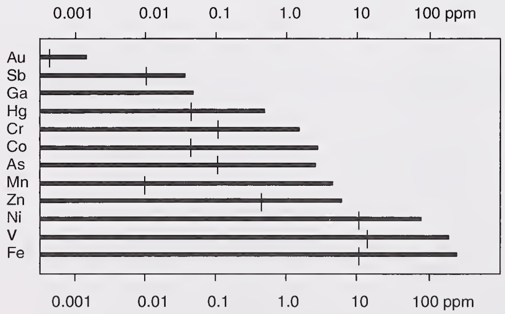

Figure 2. Maximum values of metal contents in oils from the Western Canada Basin. The vertical bar on each line marks the mean value. Data from B. Hitchon, R.H. Filby and K.R. Shah, "Geochemistry of Trace Elements in Crude Oils, Alberta, Canada", in *The Role of Trace Metals in Petroleum,* T.F. Yen, Ed., Ann Arbor Science Publishers, 1975, p. 111 and B. Hitchon and R.H. Filby, "Geochemical Studies—1. Trace Elements in Alberta Crude Oils", Alberta Research Council Open File Report 1983–02. Reproduced from D.A.C. Manning and A.P. Gize, "Organic Matter and Metalliferous Deposits", in *Organic Geochemistry, Principles and Applications*, M.H. Engle and S.A. Macko, Eds., Plenum Press, New York, N.Y. 1993, p. 547.

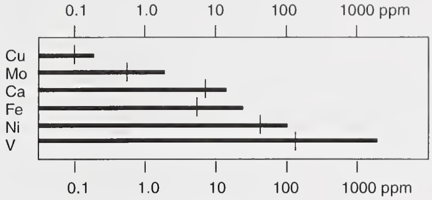

Figure 3. Maximum values of metal contents of oils from Venezuela. The vertical bar on each line marks the mean value. Data from R. Simoza, N. Carrión de Rosa–Brussin, R.J. Torres and C.L. Eyzaguirre, "Distribution de V, Ni, Zn, Mo, Ca, K, Fe y Cu en los Crudos de la Región sur de La Cuenta Oriental de Venezuela" in *Proceedings, 6th Venezuelan Geological Congress*, Sociedad Venezolana de Geologos, Caracas, 1985, Vol. 3 p. 2088. Reproduced from D.A.C. Manning and A.P. Gize, "Organic Matter and Metalliferous Deposits", in *Organic Geochemistry, Principles and Applications*, M.H. Engle and S.A. Macko, Eds., Plenum Press, New York, N.Y. 1993, p.547.

Minerals

6

Inorganic minerals constitute at least 80% of oil sands. The major component of all Alberta oil sands is sand, comprising mostly α-quartz (SiO_2). In the surface-mineable Athabasca deposit it occurs mainly as clastic, unconsolidated grains in which the crystals are no longer distinct. In some of the larger crystals colorless inclusions of either liquid or gas have been reported. Some fine-grained crystalline quartz of very angular shape, referred to as chert, is also present. Quartz aggregation through silicification does not occur to any large extent and sandstone formation is more common, involving the cementing together of quartz grains with minerals other than silica.[1]

Most of the formations have mature and stable mineralogy; even though the bulk of the solids (silica, silicates, aluminum silicates and oxides) are relatively inert materials they can undergo various reactions—in the reservoir during *in-situ* thermal recovery and in the plant during hot water separation—that would interfere with the production of bitumen. Small quantities of carbonates, sulfides and heavy minerals, and the interaction of the polyvalent ions Ca^{2+}, Mg^{2+}, Fe^{3+}, *etc.*, with the sand/bitumen interface may significantly affect bitumen separation, as discussed in Chapter 3. In steam displacement, hydrothermal reactions may lead to the dissolution of kaolinite and dolomite and the growth of analcime, calcite, chlorite, smectite, *etc.* In *in-situ* combustion the hydrothermal–geochemical reactions may be even more complicated and could lead to adverse effects, for instance loss of permeability, or to beneficial effects, for example provision of a conduit for steam and water injection by the dissolution of thin carbonate-rich zones in the formation.[2]

The major groups of mineral constituents of various Alberta oil sand deposits are listed in Table 6.1 and the ranges and mean concentrations of some of them are given[3] in Table 6.2. In the McMurray Formation kaolinite and illite are the two major clay minerals, potash, feldspar, dolomite and mica the major light minerals, and siderite and pyrite/marcasite are the main heavy minerals. The chemical formulas of the important minerals in oil sands are given in Table 6.3.

According to elemental analytical data the main constituent of the mineral solid is, of course, silicon (and oxygen, not measured) followed by aluminum, iron, calcium, magnesium, titanium, zirconium, *etc.*, Table 6.4, along with a host of trace constituents[4–6] (*cf.* Tables 5.5 and 5.6 as well), comprising more than half of the stable elements.

The total heavy minerals may amount to up to one percent of the solids. These minerals are concentrated in the fines fraction of the mineral solids. In the course of the hot water separation of the bitumen the heavy minerals accumulate in the froth as a result of a spontaneous flotation process. The froth concentrate contains 28-30% TiO_2, 10–20% $ZrO_2{\cdot}SiO_2$, 7–9% Al_2O_3 and 16–18% Fe_2O_3. Another process whereby mineral solids and trace metals are concentrated is the burning of the coke produced in the upgrading of bitumen, which produces mineral-rich ash containing high concentrations of Al_2O_3, V_2O_5, TiO_2, NiO and $ZrSiO_4$. Commercial exploitation of these mineral resources has not materialized, although with increasing

Table 6.1 Minerals in Alberta oil sands[a]

A. Light minerals ($d < 2.96$ g·cm^{-3}; ~99% of total minerals)

1. Quartz is the most abundant (~60–90+,%)
2. Clay minerals: kaolinite and illite (variable)
3. Feldspar (small content with quartz)
4. Micas: muscovite, sericite, biotite
5. Chlorite
6. Carbonates: siderite, dolomite, calcite, magnesite, *etc.*, variable
7. Chalcedony: grains observed in larger-mesh fractions

B. Heavy minerals: $d > 2.96$ g·cm^{-3}

1. Major:	
a) Oxides:	titanium: leucoxene and ilmenite iron: hematite, magnetite , and limonite
b) Silicates:	tourmaline, zircon, epidote and staurolite
c) Sulfides:	pyrite/marcasite and sphalerite
d) Carbonates:	siderite
2. Minor:	
a) Oxides:	corundum, cassiterite and rutile
b) Silicates:	garnet, kyanite, chloritoid, zoisite, amphiboles, pyroxenes, sillimanite, spinel, zircon
c) Sulfides:	chalcopyrite, bornite
d) Carbonates:	dolomite, calcite (magnesite and rhodochnosite in mixed carbonates)

C. Possible minerals present:

Uranitite or carnotite, apatite, sphene, pentlandite, pyrrhotite, cordierite, molybdenite, manganite, pyrolusite, psilomelane

[a] From Ref. 1.

levels of production of bitumen by the hot water process it may become feasible in the not-too-distant future.

The size distribution of mineral particles is an important property of oil sands and profoundly affects the processability of bitumen in the hot water separation process and in *in-situ* thermal recovery. As was pointed out in Chapter 3, the size distribution of the mineral particles is directly related to the water and bitumen contents and thus defines the grade of the oil sand ore.

For the classification of grain size the Wentworth scale, which is a logarithmic scale in which neighboring grade sizes are separated by a factor of two, is in common use. The ϕ (phi) scale expresses grain size as the negative of the power, x, of the number 2 in the equation 2^x = grain size (mm); $-x = \phi$, as seen from Table 6.5. In the Wentworth scale silt and clay are defined as the 62.5–2 μm and < 2 μm particles (regardless of composition), which is somewhat different from the size definition used in the oil sand industry, 45–5 μm and < 5 μm.

Grain size distributions are characteristically different in different grades of oil sands. This is illustrated by the examples of low-grade, medium-grade and high-grade Athabasca Suncor oil sands taken from different geographic locations, Table 6.6. The high-grade ore is characterized by a very low silt and clay content, about 2% (in general, < 10%) and particle diameters in the 150–250 μm range (Group I sands) typical of the bottom of the McMurray

Table 6. 2 Means and ranges of the principal minerals in Alberta oil sand deposits[a]

Deposit	Athabasca				Peace River		Wabasca				Cold Lake		Lloydminster	
Formation	McMurray		Clearwater		Bluesky/ Gething		Wabiskaw		Grand Rapids "A"		Clearwater/ Grand Rapids		Dina	
No. of samples	247		15		32		15		6		15		13	
	Mean	Range	Mean	Range	Mean	Range	Mean	Range	Mean	Range	Mean	Range	Mean	Range
Percent of total minerals														
Quartz	80.0	41–97	63.0	21–87	69.0	17–92	81.0	57–96	66.0	55–87	75.0	30–98	83.0	56–95
Potash feldspar	2.0	0–16	6.0	0–42	2.0	0–7	4.0	T–20	10.0	0–30	7.0	0–19	3.0	0–23
Plagloclase	0.1	0–8	3.0	0–11	n.d.[b]		1.0	0–6	12.0	0–41	7.0	0–27	2.0	0–8
Calcite	0.2	0–28	4.0	0–12	0.5	0–5	0.9	0–9	0.3	0–2	0.1	0–2	0.1	0–1
Dolomite	0.4	0–9	4.0	0–13	5.0	0–24	1.0	0–7	N		0.6	0–5	1.0	0–16
Siderite	1.0	0–20	2.0	0–4	n.d.		0.3	0–2	3.0	0–15	N		N	
Pyrite/marcasite	0.4	0–10	5.0	0–45	6.0	0–62	1.0	0–4	1.0	0–8	0.1	0–2	N	
Kaolinite	9.0	1–27	5.0	0–19	15.0	4–27	7.0	2–18	4.0	2–7	3.0	0–11	6.0	1–15
Mica	1	0–8	T	0–2	0.3	0–4	0.8	0–2	0.2	0-1	0.5	0–3	2.0	0–8
Illite	4	tr[c]–10	6.0	1–15	3.0	tr–11	3.0	tr–9	3.0	1–10	3.0	tr–13	2.0	tr–7
Chlorite	n.d.		0.3	tr–4	N		0.1	0–1	n.d.		1.0	tr–7	n.d.	
Montmorillonite	n.d.		1.0	tr–7	N		n.d.		n.d.		3.0	0–17	n.d.	
Percent of total clay minerals														
Kaolinite	65.0	28–90	39.0	0–67	85.0	47–94	74.0	57–85	54.0	40–78	52.0	0–91	67.0	20–96
Illite	31.0	7–54	44.0	29–66	13.0	6–35	24.0	14–38	36.0	16–60	25.0	7–42	26.0	4–60
Chlorite	0.8	0–18	6.0	1–15	0.9	0–18	2.0	0–5	5.0	0–9	8.0	2–25	4.0	0–17
Montmorillonite	0.2	0–7	11.0	2–26	0.3	0-3	0.6	0–5	5.0	0-11	15.0	0–42	3.0	0–27
Mixed-layer	3.0	0–26	N		0.7	0–4	N		N		N		N	
Kaolinite/illite ratio	2.0	0.2–11	0.9	0–2	7.0	1–15	3.0	2-6	2.0	0.7–5	2.0	0–9	3.0	0.6–13

[a] From P. Bayliss and A.A. Levinson, Ref. 3. © 1976, Canadian Society of Petroleum Geologists. T=Trace; N=not detected

Table 6.3 Chemical formulas for some of the major mineral constituents of Alberta oil sands

analcite	$NaAlSi_2O_6 \cdot H_2O$	manganite	$MnO(OH)$
apatite	$Ca_5(PO_4)_3(OH,F,Cl)$	molybdenite	MoS_2
biotite	$[(Mg,Fe^{2+})(Si_3Al)O_{10}(OH)_2] \cdot K$	montmorillonite[a]	
bornite	Cu_5FeS_4	muscovite	$[(Al_2)(Si_3Al)O_{10}(OH)_2]K,Na$
calcite	$CaCO_3$	potash feldspar	$K_2O \cdot Al_2O_3 \cdot 6SiO_2$
cassiterite	SnO_2		
chalcopyrite	$CuFeS_2$	pyrite/marcasite	FeS_2
chlorite	$[(Mg,Fe^{2+})_3(Al,Si)_4O_{10}(OH)_2]$ $(Mg,Al)_3(OH)_6$	pyrolusite	MnO_2
chloritoid	$(Fe,Mg)_2(Al_4Si_2O_{10})(OH)_4$	pyrrhotite	FeS
clinozoisite	$Ca_2Al_3Si_3O_{12}(OH)$	quartz	SiO_2
cordierite	$(Mg,Fe)_2Al_4Si_5O_{18}$	rutile	TiO_2
corundum	Al_2O_3	siderite	$FeCO_3$
dolomite	$CaMg(CO_3)_2$	sillimanite	Al_2SiO_5
epidote	$Ca_2Fe^{3+}Al_2O(Si_2O_7)(SiO_4)(OH)$		
garnet	$(Mg,Fe,Ca)_3Al_2(SiO_4)_3$	sphalerite	ZnS
hematite	Fe_2O_3	sphene	$CaTiSiO_5$
illite	$[(Al_2,Fe_2,Mg_2,Mg_3)(Si_{4-x}Al_x)$ $O_{10}(OH)_2 \cdot K_x$ $(x = 0.5–0.75)$		
kaolinite	$Al_2Si_2O_5(OH)_4$	spinel	$MgAl_2O_4$
kyanite	Al_2SiO_5	staurolite	$Fe_2Al_9Si_4O_{23}(OH)$
leucoxene & ilmenite	$FeTiO_3$	tourmaline	$Na(Mg,Fe,Al)_3Al_6Si_6O_{18}$ $(BO_3)_3(OH,F)_4$
limonite	$FeO(OH)$	uranitite	UO_2
magnesite	$MgCO_3$	zircon	$ZrSiO_4$
magnetite	Fe_3O_4	zoisite	$Ca_2Al_3(SiO_4)_3(OH)$

[a] Example of a montmorillonite reported: $[(Al_{1.77}Mg_{0.20})(Si_{3.74}Al_{0.26})O_{10}(OH)_2] \cdot Ca_{0.16} \cdot Na_{0.07} \cdot Mg_{0.04}$

Table 6.4 Elemental composition of oil sand mineral solids

Element[a]	Wt%
Si	43–50
Al	0.4–2.5
Fe	0.07–0.54
Ca	0.00–0.36
Ti	0.05–0.21
Mg	0.04–0.14
C	0.08
H	0.18
S	0.14
Zr	0.05
Mn	0.05
Cu	0.0025

[a] In addition, trace amounts of the following metals have been detected: As, B, Ba, Br, Ca, Ce, Cl, Cr, Co, Cu, Eu, Ga, Hf, I, K, La, Li, Mo, Na, Nb, Ni, O, P, Pb, Rb, Sb, Sc, Se, Sm, Sn, Ta, Tb, Th, U, V, Zn, Y.

Table 6.5 Wentworth scale for grain size classification[a]

U.S. standard sieve mesh #	Grain diameter		Phi (ø)	Wentworth size class	
	mm	μ			
use	4096		−12		
wire	1024		−10	Boulder (−8 to −12ø)	
squares	256		−8		GRAVEL
	64		−6	cobble (−6 to −8ø)	
	16		−4	pebble (−2 to −6ø)	
5	4		−2		
6	3.36		−1.75		
7	2.83		−1.5	granule	
8	2.38		−1.25		
10	2.00		−1.0		
12	1.68		−0.75		
14	1.41		−0.5	very coarse sand	
16	1.19		−0.25		
18	1.00		0.0		
20	0.84		0.25		
25	0.71		0.5	coarse sand	
30	0.59		0.75		
35	0.50	500	1.0		SAND
40	0.42	420	1.25		
45	0.35	350	1.5	medium sand	
50	0.30	300	1.75		
60	0.25	250	2.0		
70	0.210	210	2.25		
80	0.177	177	2.5	fine sand	
100	0.149	149	2.75		
120	0.125	125	3.0		
140	0.105	105	3.25		
170	0.088	88	3.5	very fine sand	
200	0.074	74	3.75		
230	0.0625	62.5	4.0		
270	0.053	53	4.25		MUD
325	0.044	44	4.5	coarse silt	
analyzed	0.037	37	4.75		
by	0.031	31	5.0		
pipette	0.0156	15.6	6.0	medium silt	
or	0.0078	7.8	7.0	fine silt	
hydrometer	0.0039	3.9	8.0	very fine silt	
analyzed	0.0020	2.0	9.0		CLAY
by	0.00098	0.98	10.0		
pipette	0.00049	0.49	11.0		
or	0.00024	0.24	12.0		
hydrometer	0.00012	0.12	13.0		
	0.00006	0.06	14.0		

[a] From Ref. 4.

Table 6.6 Particle size distributions in Athabasca oil sands[a]

Particle size		Cumulative wt%		
ø	µm	Low grade	Medium grade	High grade
0.00	1000	18.3	0.5	0.1
0.50	710	21.7	0.8	0.2
1.00	500	24.3	1.3	0.5
1.50	350	26.7	1.8	3.5
2.00	250	29.0	2.4	48.0
2.50	177	32.0	16.9	89.0
3.00	125	41.2	67.2	94.7
3.50	88	66.9	91.6	97.2
4.00	62	78.5	96.2	98.1
4.50	44	89.0	98.4	98.9
4.75	37	90.7	98.4	98.9
>4.75	<37	100.0	100.0	100.0
Median grain size (µm)	182	136	244	

[a] From Ref. 4.

Formation. The medium-grade ore has a fines content (silt + clay) of about 5% (in general, 2–10%) and grain sizes of 85 to 180 µm (Group II sands) and is typical of the middle of the McMurray Formation. Lastly, the low-grade ore has a very high fine sand and fines content, nearly 60% (in general, 10–60%) and average grain sizes 44–110 µm (Group III sands); it is typical of the top of the McMurray Formation.

FTIR and X-ray diffraction studies of the clay minerals have shown that the composition, crystal structure and affinity of the clay toward organic matter vary with particle size.[7,8] Clays separated from bitumen and asphaltene by centrifugation contain kaolin-group minerals, illite and quartz. On going from coarse to finer and finer particles, the relative proportion of well-crystallized, ordered kaolinite to disordered kaolinite progressively diminishes. In addition to the kaolin-group minerals, illite is also present, showing signs of interstratification, probably as a mixed illite–smectite layer. With decreasing particle size significant deterioration in the illite crystallinity can also be observed.

In addition to the spectrum of kaolin, the FTIR spectrum of the clays isolated from bitumen and asphaltene features a distinct absorption in the spectral region 2,800–3,000 cm^{-1} which is attributed to some humic material chemisorbed to the clay (see Chapter 8). The relative amount of this organic material, as well as the relative proportion of noncrystalline to crystalline clay in the complex, shows an increasing trend as the severity of the centrifugation required to separate the clay from the asphaltene increases. With decreasing crystallinity the clay has an increasing affinity toward organic matter and this makes the removal of clay from asphaltene progressively more difficult.

Further discussion of the clay–organic matter will follow in Chapter 8.

Bibliography

1. *Oil Sands Composition and Behavior Research: the Research Papers of John A. Bichard 1957–1965*, Alberta Oil Sands Technology and Research Authority, Edmonton, AB, 1987.

2. W.D. Gunter and G.W. Bird, “Inorganic Chemistry”, Ch. 9 in *AOSTRA Technical Handbook on Oil Sands, Bitumens and Heavy Oils,* L.G. Hepler and C. Hsi, Eds., Alberta Oil Sands Technology and Research Authority Technical Publication Series No. 6, Edmonton, AB, 1989, p. 203.
3. P. Bayliss and A.A. Levinson, “Mineralogical Review of the Alberta Oil Sands Deposits (Lower Cretaceous, Mannville Group)”, Bull. Can. Petrol. Geol., 24 (1976) 82.
4. *Some Physical Properties of Bitumens and Oil Sands*, D.R. Prowse, Ed., Alberta Research Council, 1983.
5. F.S. Jacobs, F.W. Bachelor and R.H. Filby, “Determination of Trace Elements in GPC Fractions of Oil-Sand Asphaltenes by INAA”, *Proc. Fifth Int. Conf. Nuclear Methods in Environmental and Energy Research,* University of Missouri, April, 1984, U.S. Dept. of Energy, p. 438.
6. F.S. Jacobs and R.H. Filby, “Solvent Extraction of Oil-Sand Components for Determination of Trace Elements by Neutron Activation Analysis”, Anal. Chem., 55 (1983) 74.
7. T.M. Ignasiak, L. Kotlyar, F.J. Longstaffe, O.P. Strausz and D.S. Montgomery, “Separation and Characterization of Clay from Athabasca Asphaltene”, Fuel, 62 (1983) 353.
8. F.J. Longstaffe, “Clay Mineral Characteristics of Different Types of Oil Sands”, AOSTRA Report, 1983.

7

Reservoir Water

Reservoir water, a ubiquitous component of reservoir fluids, is generally believed to have its ultimate origin in the ancient seawater in which the source sediments were deposited and migrated to the reservoir rock along with the oil. In the case of the Alberta oil sands deposits, however, the reservoir water most closely associated with the bitumen, the connate—or irreducible—water (Chapter 3) is believed to be inherited from the water-saturated sand rock which presumably contained the water of the sea in which the reservoir sands were deposited.

A second source of reservoir water is the surface-derived meteoric water from rain, rivers and lakes. This water is fresh water that often contains microbes and oxygen and acts primarily to dilute the seawater. The dissolved oxygen can react with the crude oil or the rock minerals causing their oxidation either directly, catalytically or microbiologically. Mobile waters, induced either by hydrodynamism or by compaction of the sediment, can also cause water washing of the crude oil by carrying away the more water-soluble lower MW and polar components of the oil.

The ionic (and isotopic) composition of sea water which originally contained 3.5% total solids[1] undergoes alterations, Table 7.1, as a result of various controlling influences involving dilution by meteoric water recharge, concentration changes by membrane filtration, ion exchange, salt diffusion and other processes generally believed to have taken place during migration of the oil/water slurry from the source rock to the reservoir rock. As a result, salt concentrations may increase up to 35%. How these considerations would apply to Alberta oil sand reservoir waters is not without ambiguity, in view of the absence of a comprehensive, self-consistent theory to unravel the history of these reservoir waters. In any event, the one aspect of the history of the Alberta oil sand reservoir waters, for reasons to be discussed in Chapter 13, is the involvement of huge volumes of meteoric water percolating through the reservoirs as part of the large flow systems propelled by hydrostatic pressures[2] extending from The Rocky Mountains to the Canadian Shield, Figure 7.1.

The dominant ionic species (Table 7.1) in seawater and reservoir waters are the sodium and chloride ions, followed, in seawater, by the sulfate and magnesium ions, and in reservoir waters, by the calcium and bicarbonate ions. The Mg^{2+}/Ca^{2+} ratio in seawater is about three, whereas in reservoir waters this ratio is inverted with a magnitude depending on burial depth.

In oil sand deposits the reservoir water may be present in various structural arrangements[3], Figure 7.2, such as:

i) connate water—or irreducible water—defined as the water trapped in the oil-saturated zones at the time the oil migrated into the formation;
ii) shale stringers, in which water is isolated;
iii) shale bed waters which, like the bottom water, can be in hydraulic contact with water sources beyond the confines of the reservoir and are not necessarily related to the composition of the water within the oil-saturated zone (*v.i.*);

Table 7.1 Compositions ($mg{\cdot}L^{-1}$) of sea water and formation waters (mean) from the Western Canada Sedimentary basin[a]

Component	Sea water	Formation water
Li	0.17	10.7
Na	10,760	14,340
K	387	561
Rb	0.12	0.88
Mg	1,290	317
Ca	413	2,210
Sr	8	108
Mn	0.002	0.32
Zn	0.01	0.30
Cl	19,350	26,920
Br	67	114
I	0.06	9
HCO_3^-	142	1,500
SO_4^{2-}	2,710	350
TDS[b]	35,100	46,400

[a] From B. Hitchon *et al.*, Ref.1. [b] Total dissolved solids.

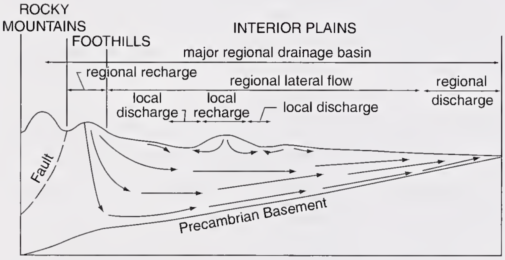
ROCKY
MOUNTAINS
FOOTHILLS
INTERIOR PLAINS
major regional drainage basin
regional recharge
regional lateral flow
regional
discharge
local
discharge
local
recharge
local discharge
Fault
Precambrian Basement

Figure 7.1 A Schematic model for the relation of the hydrodynamic situation in the basin. From J.A. Majorowicz *et al.*, Ref. 2. © 1985, Geophysical Press Ltd.

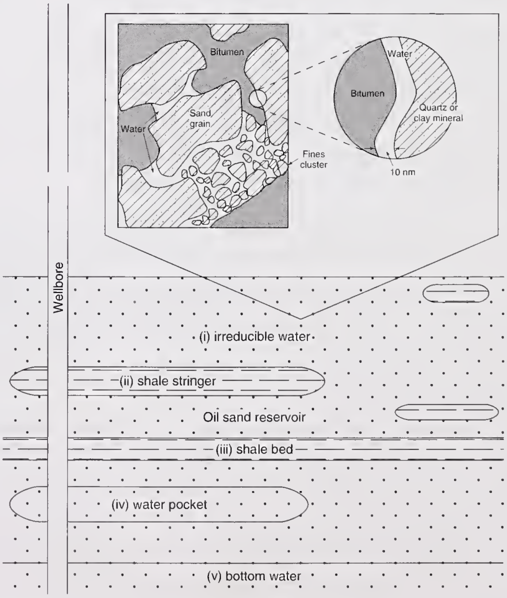
Bitumen
Sand
grain
Water
Fines
cluster
Water
Bitumen
Quartz or
clay mineral
10 nm
Wellbore
(i) irreducible water
(ii) shale stringer
Oil sand reservoir
(iii) shale bed
(iv) water pocket
(v) bottom water

Figure 7.2 Illustration of the five different types of water in an oil sand reservoir. From W.D. Gunter and G.W. Bird, Ref. 3. The oil sand microstructure at the top is from K. Takamura, Can. J. Chem. Eng., 60 (1982) 538. © 1982, Canadian Society for Chemical Engineering.

iv) water pockets, which occur as isolated pockets of high water saturation within the oil-saturated zone, and

v) bottom water, a water accumulation within a zone such as the one found at the base of the Peace River oil sand deposits.

The dissolved solids contents of the five types of formation waters can vary and, in general, differ from one another. The composition and properties of connate water are important with regard to the water displacement separation of the bitumen, and the composition of all formation waters may be an important parameter with regard to the geochemical processes taking place during *in-situ* thermal recovery.

As has been discussed in Chapter 3, one important property of Alberta oil sands distinguishing them from most of the oil sands in the United States is their water-wet condition resulting from the presence of a thin film of connate water surrounding each mineral grain. Even though the total amount of water tied up in these surface films is quite small, only a few percent of the 2–10% connate water in the oil sand, its technological significance in rendering the separation of bitumen by the water flotation process facile cannot be over-stressed. The bulk of the connate water is trapped within pore spaces and fines clusters by capillary forces.

The chemical analysis of connate water, which is the only formation water that will be considered here, is complicated by the difficulties associated with the isolation of representative samples. This is due to the complexity of the sand–oil–water structure and the presence of water-dissolved salts, water-soluble but solid salts, colloidally dispersed soluble and insoluble salts in the water, the host of minerals which are in contact with the water and which have although small but, under certain conditions, significant solubility, fine suspensions of clay particles capable of undergoing cation exchange and various adsorption reactions with the dissolved cations, and dissolved oil or oil components such as carboxylic acids, carboxylate ions, nitrogen bases and cations, water-soluble hydrocarbons, *etc.*, all of which influence one another's solubility. The *pH* is a critical property of the connate water that can profoundly affect the solubility of ions and minerals and the behavior of the oil sand in the hot water process. Consequently, the composition and the results of analyses are significantly dependent on the mode of sample preparation.

Analytical data for a Cold Lake oil sand core obtained from three different methods of analysis, Table 7.2, reveal that the major dissolved solid is sodium chloride along with appreciable amounts of sulfate and carbonate/bicarbonate. The results from the different methods of analysis show considerable deviations, manifesting the complexity of the system and the difficulties in defining representative samples. The "solvent only" procedure involves extraction of bitumen with carbon tetrachloride followed by centrifugation separation of the connate water; the "solvent plus water" method consists of shaking of the sample with cold water/carbon tetrachloride and separation of the water phase; in the "hot water" procedure hot water is mixed with the sample and then separated. The difference between the "solvent only" and the two water extraction results has been attributed to the incomplete extraction of the connate water in the latter two cases; however, this in itself cannot account for all the differences, for example, the much higher sodium and carbonate/bicarbonate, potassium, magnesium, aluminum, iron, boron and propionate ion concentrations in the presence of added water and especially hot water.

Data for connate water analyses from a Cold Lake McMurray location along with one analysis from outside the Cold Lake area are listed in Table 7.2 and ion concentrations for different grades of Athabasca oil sands are listed in Table 7.3. In every case sodium (up to

Table 7.2 Connate water analyses ($mg \cdot L^{-1}$) of Alberta oil sands[3]

	Cold Lake (Clearwater)			Cold Lake McMurray	Other McMurray
	solvent only	solvent + water	hot water		
pH (25°C)	8.13	8.84	8.79	8.22	7.62
Lithium	<1	<2	NR[a]	<1	2.7
Sodium	2,650	3,498	3,907	4,010	16,000
Potassium	32	43	58.8	50	166
Magnesium	11	8.8	13.1	51	281
Calcium	18	10.5	14.0	25	160
Strontium	<1	<2	<2	4	224
Barium	<1	<2	<2	7	9.5
Manganese	<1	<2	<2	<0.1	0.2
Iron	<1	33.4	57.7	<0.1	0.18
Aluminum	<3	31.6	37.7	<2	<2
Fluoride	<20	19.7	21.7	NR	NR
Chloride	3,165	2,634	2,761	5,130	26,600
Bromide	<20	<18	<18	NR[b]	NR
Nitrate	<20	<18	<18	NR	NR
Phosphate	<20	<18	<18	NR	NR
Sulfate	668	628	677	208	56
T. bicarbonate[b]				1,411	136
T. carbonate				53.4	3
T. inorganic carbon	56	643	834	291	28.1
T. Si/SiO_2	<2/4.28	65.9/140	77.2/165	3/6.42	6.1/13
T. B/H_3BO_3	11/62.9	38.7/221	43.9/251	7/40	3.1/17.7
T. alk. (as HCO_3^-)				1,525	NR
TDS[c]				10,990	43,547
T. sulfur				108	26
T. Phosphorous				<1	2.1
Formate	<20	<18	<18	NR	NR
Acetate	<21	<18	19.3	NR	NR
Propionate	<20	126	173	NR	NR
Butyrate	<20	<18	<18	NR	NR
Calc. charge bal. (%)	8.27	5.83	3.92	4.35	–2.92

[a] NR = not reported. [b] T. = total. [c] TDS = total dissolved solids.

Table 7.3 Ion concentrations ($mg \cdot L^{-1}$) in the connate waters of Athabasca oil sands[a]

	Na^+	K^+	Ca^{2+}	Mg^{2+}	Cl^-	SO_4^{2-}
High grade	2,758	194	288	91		
	5,880	200	38	25		
	1,476	57	10	<10		
	6,063	806	318	300		
	5,500	357	33	<33		
Medium grade	2,000	158	302	110		
	1,717					
Low grade	3,947					
	2,744	140	177	65		
	4,444	150	113	51		
High grade	482		73	18	218	727

[a] From the publications of Dean Wallace, Alberta Research Council.

16,000 mg·L^{-1}) and chloride (up to 26,600 mg·L^{-1}) are the dominant ions, the average ranges being 2,000–5,000 mg·L^{-1} for sodium and 2,500–4,000 mg·L^{-1} for chloride ions. Total dissolved solids range up to 44,000 mg·L^{-1}. High levels of calcium, magnesium and sulfate ions are indicative of an oxidative history of the sample according to the mechanisms considered in Chapter 3. The sulfuric acid produced directly from the oxidation of iron sulfides and from the hydrolysis of the iron sulfate product dissolves the calcium carbonate and magnesium carbonate minerals present and may also undergo ion-exchange reactions with clays containing exchangeable calcium and magnesium to release more of these ions:

$$H^+ + \text{clay·Ca} \rightleftharpoons Ca^{2+} + [\text{clay·H}]^- \quad (1)$$

$$H^+ + \text{clay·Mg} \rightleftharpoons Mg^{2+} + [\text{clay·H}]^- \quad (2)$$

The presence of these ions and polyvalent ions in general, causes binding between bitumen and sand, the efficiency of which increases exponentially with the valence of the cations and is therefore detrimental to the separability of bitumen. The divalent ions could also consume the sodium hydroxide added to the oil sand slurry in the hot water extraction process to produce carboxylate surfactants and could react with the surfactants as well to produce precipitate (*cf.* Chapter 3).

$$2\,OH^- + Ca^{2+} \rightleftharpoons Ca(OH)_2\downarrow \quad (3)$$

$$2\,OH^- + Mg^{2+} \rightleftharpoons Mg(OH)_2\downarrow \quad (4)$$

$$2R\text{–}COOH + Ca^{2+} \rightleftharpoons Ca(R\text{–}COO)_2\downarrow + 2\,H^+ \quad (5)$$

$$2\,R\text{–}COOH + Mg^{2+} \rightleftharpoons Mg(R\text{–}COO)_2\downarrow + 2\,H^+ \quad (6)$$

It has been shown that not all the water-soluble salts are in solution in the connate water and the solid salts may be assumed to be in equilibrium with their solution and the bitumen and minerals.[3] This conclusion was derived from experiments in which samples of oil sands were successively washed 12 times with 1:1 water, yielding increasing cummulative amounts of dissolved salts. In a good oil sand, for example, the first washing afforded 0.042 wt% salt. After the 12th washing the accumulated amount of salt that went into solution was 0.060 wt%. The difference, 0.018 wt%, represents solid salts in equilibrium with their saturated aqueous solution*.The increase in the sodium, potassium and other cation concentrations reported in Table 7.2 using the analytical methods with added water could be explained if it is assumed that solid water-soluble salts are present in the oil sand.

The salt content of an oil sand is dependent on the freshness of the sample; fresh oil sands with *pH* ~ 8 have lower total salt contents than weathered oil sands by as much as a factor of ten and the composition of the salts present is also affected, the salts from the latter oil sand being richer in Ca^{2+}, Mg^{2+} and Fe^{3+}.

The solubilities of the various minerals present at neutral *pH*'s are small, but may drastically increase at low or high *pH* values and would also vary with temperature. Solubility and equilibrium curves for quartz in water, Figures 7.3 and 7.4 for example, demonstrate the

---

* It has been reported[4] that, from Athabasca oil sands, "Under a microscope the dried and heated soluble salt appears to be a mixture of bright-red amorphous forms admixed with more predominantly clear needle-shaped crystals. This varies from tar sand to tar sand and frequently black crystal forms are observed."

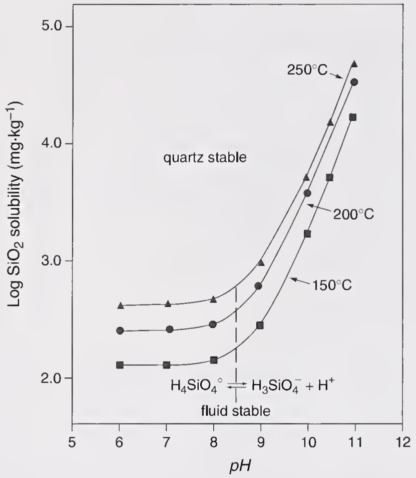

Figure 7.3 Variation of the solubility of quartz with temperature and *pH*. From W.D. Gunter and G.W. Bird, Ref. 3.

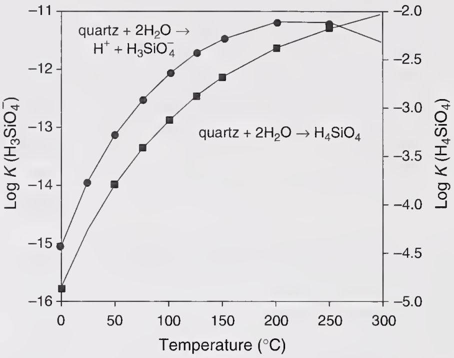

Figure 7.4 Quartz equilibria in aqueous solutions. From W.D. Gunter and G.W. Bird, Ref. 3.

dramatic rise in the solubility of quartz with increasing temperature and with *pH* above 8. Silicic acid and the silicate ion, H_4SiO_4 and $H_3SiO_4^-$, could precipitate to form colloidally suspended amorphous silica when the temperature is lowered and can react with aluminum, iron and other ions in the solution to form various minerals. These reactions between silicic acid and metal ions may lead to highly complicated hydrogeo-chemical reactions which become increasingly important with rising temperature. For example, the colloidal "salts" (< 0.2 µm) reported to have been found in connate waters and containing the elements Fe:Si:Al in an atomic proportion of 1:10:5 were probably the precipitated products of the reactions of dissolved silicic acid.

It has also been suggested that colloidally suspended polysilicic acids are also involved with hydroxy ions of iron and aluminum in various geochemical processes, *e.g.*,

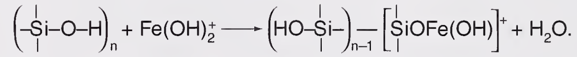

$$\left(-\overset{|}{\underset{|}{Si}}-O-H\right)_n + Fe(OH)_2^+ \longrightarrow \left(HO-\overset{|}{\underset{|}{Si}}-\right)_{n-1} - \left[\overset{|}{\underset{|}{Si}}OFe(OH)\right]^+ + H_2O. \qquad (7)$$

The ability of polysilicic acids to undergo such reactions diminishes as the polymerization of the acid progresses.

The *pH* of most oil sands (connate water) is slightly basic with values of 8 ± 0.8 and with a considerable buffer capacity. Both of these properties are associated with the presence of carbonate minerals, the water-soluble carbonates and the carboxylates: formate, acetate, propionate and butyrate. The carboxylates are derived from the corresponding carboxylic acids, which represent the most water-soluble fraction of the carboxylic acid content of the bitumen. The occurrence of longer-chain C_{14}–C_{30} *n*–alkanoic acids in petroleum-associated formation waters has also been reported[5] and in oil field brines even an abundance of α, ω-di-*n*-alkanoic acids ranging from C_2 to C_5 have also been identified[6].

The organic constituents of connate water, aside from the carboxylic acids, have not been investigated in depth but would be expected to contain some water-soluble bitumen components in an equilibrium distribution. Low-MW polar organic molecules (sulfoxides, thiophenes, quinolines, pyridines, etc.) and even hydrocarbons like benzene, toluene and alkanes have considerable water solubility. Moreover, the carboxylic acids activated by the nitrogen bases would also act as surfactants to promote the micellar colloidal dissolution of otherwise insoluble organic molecules. As was discussed in Chapter 3, during the course of the hot water separation of bitumen the slightly alkaline extraction water contains a full complement of organic biomarkers including alkanes, cyclic terpanes, steranes, carboxylic acids, alcohols and other constituents of the bitumen and associated humic materials.

Low *pH* values of the connate water, like those of natural waters in general, are an indication of the presence of free sulfuric acid from the oxidation of heavy metal sulfides, as has been mentioned before.

Bibliography

1. B. Hitchon, G.K. Billings and J.E. Klovan, "Geochemistry and Origin of Formation Waters in the Western Canada Sedimentary Basin — III. Factors Controlling Chemical Composition", Geochim. Cosmochim. Acta, 35 (1971) 567.
2. J.A. Majorowicz, F.W. Jones, H.L. Lam and A.M. Jessop, "Terrestrial Heat Flow and Geothermal Gradients in Relation to Hydrodynamics in the Alberta Basin, Canada", J. Geodynamics, 4, (1985) 265.
3. W.D. Gunter and G.W. Bird, "Inorganic Chemistry", Ch. 9 in AOSTRA Technical Handbook on Oil Sands, Bitumens and Heavy Oils, L.G. Hepler and C. Hsi, Eds., Alberta Oil Sands Technology and Research Authority Technical Publication Series No. 6, Edmonton, AB, 1989, p. 203.
4. *Oil Sand Composition and Behaviour. The Research Papers of John A. Bichard 1957–1965*, Alberta Oil Sands Technology and Research Authority, Edmonton, AB, 1987.
5. J.E. Cooper, "Fatty Acids in Recent and Ancient Sediments and Petroleum Reservoir Waters", Nature, 193 (1962) 744.
6. D.B. MacGowan and R.C. Surdam, "Difunctional Carboxylic Anions in Oil Field Waters", Org. Geochem., 12 (1988) 245.

Methylene Chloride–Insoluble Organic Matter

8

As has been briefly mentioned in Chapter 3, oil sands (and oil carbonates) contain varying concentrations of organic matter which is not extracted by boiling methylene chloride or toluene. According to its origin, this organic matter can be divided into two main groups: in one group are compounds which are related to the bitumen either by origin or by chemical and/or microbiological evolution and in the other, compounds such as humic substances which are foreign to the bitumen and probably preexisted in the host rock prior to the invasion of the precursor oil. These materials, or portions thereof, can be mobilized and partially extracted with polar solvents (methanol, pyridine) or aqueous sodium hydroxide, pyrophosphate, *etc.*[1] Sodium hydroxide reportedly[2] extracts only humic substances that are either free or associated with nonsilicate forms of Fe_2O_3 and Al_2O_3, but mixtures of NaOH and $Na_4P_2O_7$ extract calcium-associated humic substances as well. In the latter case the metals Ca, Al and Fe are precipitated as the pyrophosphates and the humic acid is converted to soluble sodium humates. With sodium hydroxide alone, up to about 30% of the insoluble organic carbon could be solubilized as a complex mixture of carboxylic, fulvic and humic acids from a methylene chloride-preextracted Athabasca oil sand sample.

The aggregate amount of methylene chloride-insoluble organic matter in the oil sand bears an approximate relationship to the quality of the ore, inasmuch as low bitumen content (*i.e.* low-grade) ores have, at least in the Athabasca deposit, higher concentrations of these substances than do high-grade ores. Thus, in a (marine) Syncrude Beach oil sand (SBS) with 6.1–6.9% bitumen content the methylene chloride-insoluble organic carbon content was 1.5%, corresponding to about 2% or more organic matter, that is, nearly as much as one-third of the bitumen content.[3] In high-grade (estuarian) Syncrude oil sands (SHG) with bitumen contents of 11.8–12.7% on the other hand, the methylene chloride-insoluble organic carbon content was found to be lower, only 0.3%, and in an oil sand containing 15.3% bitumen it was even lower, 0.2%. The amount of residual (insoluble) carbon is somewhat dependent on the solvent employed[4] for the extraction of bitumen and for a good solvent it varies between 0.12 and 0.24% of the extracted sand, Table 8.1. It has also been established that the insoluble organic content is not evenly distributed across the size scale of the mineral particles but that in both the high- and low-grade oil sands it is concentrated in the < 44-μm fraction.

1.0 Bitumen-Related Organic Matter

Samples from the Athabasca, Peace River, Wabasca and Cold Lake deposits have been examined. Saponification of the methylene chloride-extracted medium-high-grade ore sands with 1.0*M* KOH in $MeOH/C_6H_6/H_2O$ under reflux conditions yields organic material comprising up to 0.2% of the oil sand, or about 1–5% of the bitumen.[5] Following the separation scheme in Figure 8.1 the yields of the neutral, monocarboxylic acid methyl ester and polar fractions were determined. The percentage yields, Tables 8.2 and 8.3, exhibit no apparent trends either with

Table 8.1 Extraction efficiencies of solvents[a]

Solvent	B.P. (℃)	% Residual C in sand
Carbon tetrachloride	76.7	0.123
Chloroform	61	0.148
Trichloroethylene	86.9	0.164
Tetrachloroethylene	121.1	0.161
Methylene chloride	40.7	0.207
o-Xylene	143.6	0.251
Toluene	110.8	0.154
Benzene	80.2	0.228
Benzene/methanol (9:1 V:V)		0.175
Pyridine	115.5	0.159
Carbon disulfide	46.4	0.242
Acetone	56.2	3.10
Hexane	68.8	3.85

[a] From L.D.L. Vorndran *et al.*, Ref. 4. © 1980, Canadian Society for Chemical Engineering.

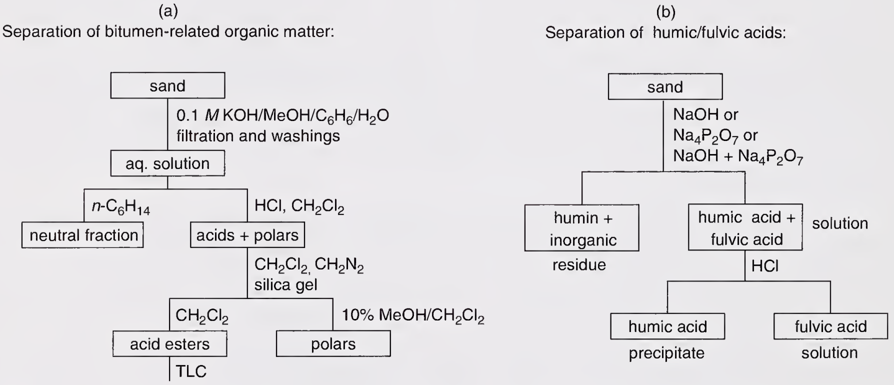
(a)
Separation of bitumen-related organic matter:
sand
0.1 *M* KOH/MeOH/C_6H_6/H_2O
filtration and washings
aq. solution
n-C_6H_{14}
neutral fraction
HCl, CH_2Cl_2
acids + polars
CH_2Cl_2, CH_2N_2
silica gel
CH_2Cl_2
acid esters
TLC
10% MeOH/CH_2Cl_2
polars
(b)
Separation of humic/fulvic acids:
sand
NaOH or
$Na_4P_2O_7$ or
NaOH + $Na_4P_2O_7$
humin +
inorganic
residue
humic acid +
fulvic acid
solution
HCl
humic acid
precipitate
fulvic acid
solution

Figure 8.1 Procedures for isolating the bound monocarboxylic acids (a) and the humic and fulvic acids (b) from Athabasca oil sand.

Table 8.2 Samples studied and wt% (× 10^{-3}, of the whole oil sand) of products from the saponification of preextracted Alberta oil sands[a]

Sample (burial, m)	Bitumen (wt%)	Monocarboxylic methyl esters	Neutral material	Polar material	Total products
Ath. (18)[b]	12.71	1.06	8.33	83.6	93.0
Ath. (5–7)[c]	6.86	5.43	73.3	57.8	136.5
P.R. (579.1)	4.27	22.9	37.3	147.3	207.5
P.R. (577.6)	6.92	16.6	36.8	68.9	122.3
P.R. (567.2)	6.60	12.4	12.0	98.6	123.0
P.R. (562.9)	7.69	14.1	24.6	119.6	158.3
Wab. (237)	11.50	26.8	20.2	130.0	177.0
C.L. (500)	11.61	0.58	43.9	25.2	69.7

[a] From T.D. Cyr and O.P. Strausz, Ref. 5. © 1984, Elsevier Science Ltd. [b] High-grade ore from the Syncrude quarry (SHG). [c] Low-grade ore from the Syncrude quarry (SBS).

Table 8.3 Yields of methyl esters[a] from the saponification of preextracted Alberta oil sands[b]

Type	Peace River (558 m)	Wabasca (237 m)	Athabasca 1 (52 m)[c]	Athabasca 2 (30 m)[c]	Athabasca 3 (surface)[c]	Athabasca 4 (surface)[c]
Normal saturated						
n-12	144	50	20	151	339	133
n-13	90	22	–[d]	–	24	30
n-14	112	50	64	212	93	203
n-15	68	34	14	91	36	48
n-16	513	272	271	796	442	565
n-17	54	–	6	–	23	–
n-18	157	72	55	179	88	281
CPI[e]	6.3	2.5	54.3	11.3	23	–
Iso saturated						
i-15	130	–	14	–	204	320
i-16	419	–	–	–	245	54
Anteiso saturated						
ai-15	370	–	41	–	259	47
ai-17	418	–	48	–	159	75
10-Me 16	148	–	–	–	57	–
Normal unsaturated						
n-16	153	–	137	338	169	138
n-18: vaccenate	378	72	73	179	88	136
n-18: oleate	247	–	60	177	280	120
n-18: linoleate	130	–	–	–	43	–
Cyclopropyl						
C_{17}	102	–	63	67	194	107
C_{19}	83	72	40	–	420	329
Concentrations in ppm based on bitumen-free preextracted sand						
Total esters	52.3	159[f]	2.5	8.1	44.2	45.8
Polars	599	1003	25.8	92.7	293	371
Neutrals	13.6	83	16.5	32.4	200	119

[a] From D.D. McIntyre *et al.*, Ref. 6. [b] Yields of individual components are expressed in ppb based on bitumen-free preextracted sand. [c] Athabasca 1 = Tarry Water Sand; 2 = Syncrude high grade; 3 = Cities Service (severely weathered); 4 = Abasand (severely weathered). [d] Trace. [e] Carbon Preference Index (see Chapter 13). [f] This sample contained a complex, unresolved mixture of methyl esters.

respect to depth of burial or to the bitumen content of the ore. In nearly every case the most abundant fraction, up to 0.15%, is the polar fraction; the concentration of the monocarboxylic acid ester fraction ranges from 1 to 27 ppm. Only the latter fraction of the extract was subjected to detailed analyses and the following types of acids, Figures 8.2–8.6, were identified:[5,6] C_{12}–C_{32} *normal*, *iso*, *anteiso* and 10-methyl alkanoic acids, C_{16}–C_{20} mono- and diunsaturated *normal* alkanoic acids, 2-methyl monounsaturated C_{16} and C_{18} alkanoic acids, C_{17} and C_{19} cyclopropyl *normal* alkanoic acids and di- and tricyclic terpenoid acids, in the form of their methyl esters. The individual acids identified and their carbon ranges are listed in Table 8.4. They comprise 1–15% of the total insoluble organic carbon.

In considering the chemical state of these monocarboxylic acids in the oil sand, we have to remember that C_{12}–C_{32} monocarboxylic acids are soluble in methylene chloride, the solvent

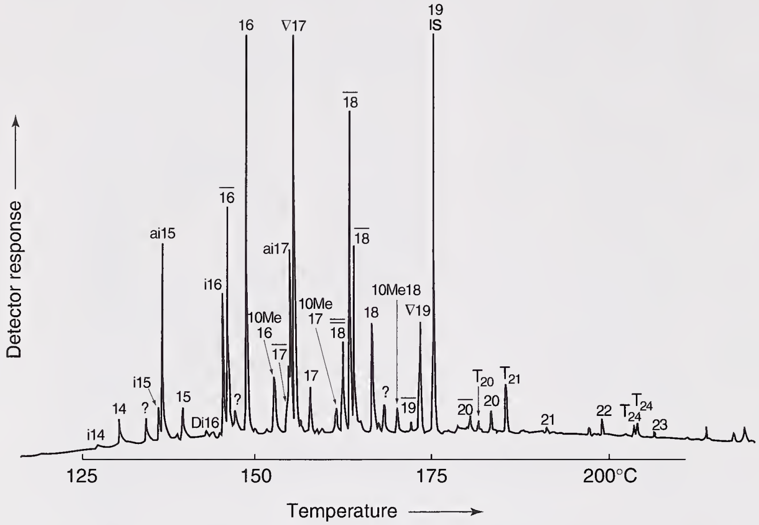

Figure 8.2 Capillary gas chromatogram of the methylene chloride-insoluble mono-carboxylic acid methyl esters from Athabasca (Syncrude high grade) oil sands. The carbon numbers are indicated and where there is no other label the peak corresponds to a *normal* saturated ester. i = iso; ai = anteiso; single and double bars indicate mono- and diunsaturation; ∇ = cyclopropyl acid esters; Di = dicyclic; T = tricyclic; IS = internal standard. From T.D. Cyr and O.P. Strausz, Ref. 5. © 1984, Elsevier Science Ltd.

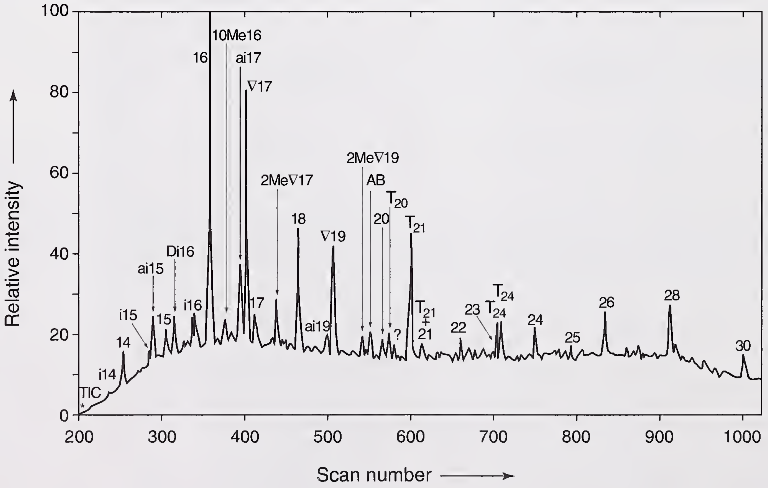

Figure 8.3 Total ion current from the capillary GC–MS of the methylene chloride-insoluble saturated monocarboxylic acid methyl esters from Athabasca (Syncrude Beach Sand, low grade) oil sands. Symbols as in Figure 8.2; AB = methyldehydroabietic acid methyl ester. From T.D. Cyr and O.P. Strausz, Ref. 5. © 1984, Elsevier Science Ltd.

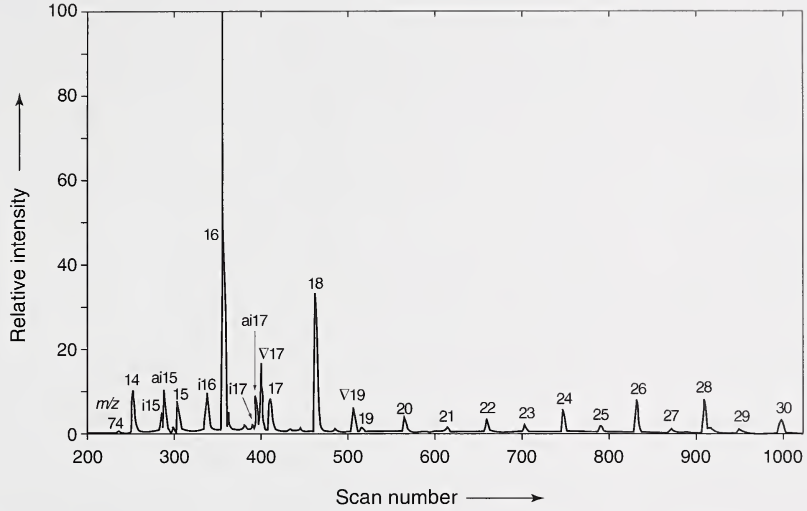

Figure 8.4 *m/z* = 74 Cross scan of the capillary GC–MS of the methylene chloride-insoluble monocarboxylic acid methyl esters from Athabasca (Syncrude Beach Sand, low grade) oil sands showing the distribution of the saturated acyclic components. From T.D. Cyr and O.P. Strausz, Ref. 5. © 1984, Elsevier Science Ltd.

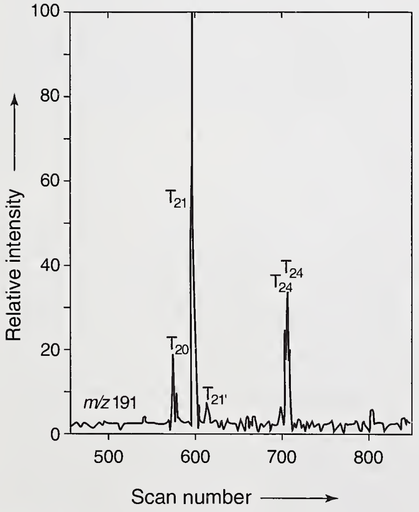

Figure 8.5 *m/z* = 191 Cross scan of the capillary GC–MS of the methylene chloride-insoluble monocarboxylic acid methyl esters from Athabasca (Syncrude Beach Sand, low grade) oil sands showing the distribution of the tricyclic components. From T.D. Cyr and O.P. Strausz, Ref. 5. © 1984, Elsevier Science Ltd.

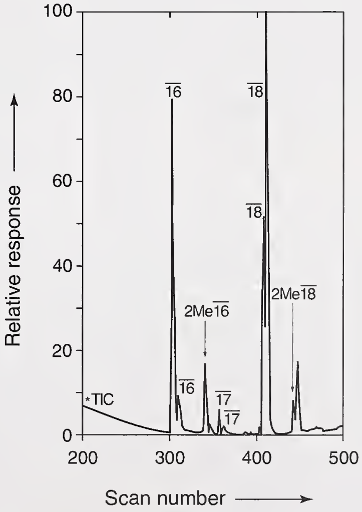

Figure 8.6 Total ion current from the capillary GC–MS of the methylene chloride-insoluble monocarboxylic acid methyl esters from Athabasca (Syncrude Beach Sand, low grade) oil sands showing the distribution of the unsaturated acyclic components. From T.D. Cyr and O.P. Strausz, Ref. 5. © 1984, Elsevier Science Ltd.

Table 8.4 Bound acyclic and cyclic aliphatic monocarboxylic acids identified in Alberta preextracted oil sands

Type	Structure and carbon range	
Normal, saturated	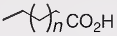	n = 8–30
Iso, saturated	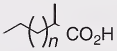	n = 7–13
Anteiso, saturated	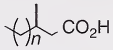	n = 8, 10, 12, 14
10-Methyl, saturated	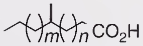	n =7, m = 4–6
Normal, monounsaturated	$C_{\overline{16}} - C_{\overline{20}}$	
Normal, unsaturated	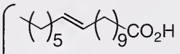	C_{18} vaccenic acid
	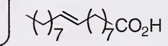	C_{18} elaidic acid
	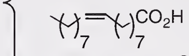	C_{18} oleic acid
	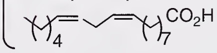	C_{18} linoleic acid
2-Methyl, monounsaturated	2-CH_3-C_{16} and C_{18}	
Cyclopropyl	C_{17} and C_{19}	
Cyclic terpenoid	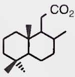 Bi16 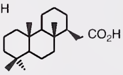 T20 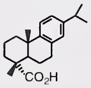 dehydroabietic acid 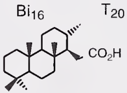 T21 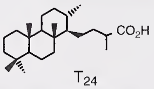 T24	

used for the extraction of the bitumen; therefore, had they been present as free acids, they should have been removed from the oil sand together with the bitumen. On the other hand, if they had been present as sodium or potassium salts, they should have been readily removed by the connate water, refluxing as an azeotropic mixture with the solvent. Therefore, the very presence of these acids in the solvent-extracted sand is a strong indication that they were chemically bound or chemisorbed to the surfaces of some of the components of oil sand solids or that they were present as calcium and magnesium salts. As far as active surfaces are concerned, possible candidates would be the carbonate minerals, calcite, magnesite, dolomite, siderite and the negatively-charged fines or sand surfaces. The modes of association could be in the form of monocarboxylates, hydrogen bonding, polyvalent metal ion bridging or ion-exchange mechanisms, as will be discussed in more detail later. The low-MW C_1–C_4 fatty acid salts present in the connate water (*cf.* Chapter 7) could have been formed from the reaction of these highly water-soluble acids with the carbonate or clay minerals. The water solubility of the carboxylic acids becomes progressively lower with increasing carbon number and this lack of solubility, coupled with the presence of active sites on the surfaces, makes them more closely associated with the surfaces.

Some of the fatty acids could also be bound to the humic substances *via* ester linkages, as has been suggested before,[7] or they could be mechanically trapped in the interior cavities of the macromolecular structures.

Detailed consideration of the composition and origin of the chemisorbed acids as well as their geochemical significance will be postponed until Chapter 13, which deals with the biomarker chemistry of Alberta bitumens. Here, it will only be remarked that the straight-chain and cyclopropyl acids were probably produced during relatively recent microbial processes which were responsible for the degradation of the precursor oil and its conversion to bitumen. Small quantities of free, straight-chain carboxylic acids are also present in the bitumen at concentrations of approximately 100 ppb (based on the bitumen), which is about two to three orders of magnitude less than the total amount of the same acids in the chemisorbed material. Originally, the concentration of these acids in the bitumen was probably much higher but in time it declined, owing to the combined effects of chemical (catalytic decomposition, reactions with the minerals), physical (water washing) and microbiological processes. In the chemisorbed state, however, the acids were protected against such effects and were preserved intact as tell-tale messengers of the past history of the formation.

The low-grade SBS oil sand (and low-grade oil sands in general) release more monocarboxylic acids and total organic saponification products than the SHG oil sand (and high-grade oil sands in general).

The more immediate practical significance of the chemisorbed acids is related to their potential beneficial impact as natural surfactants in the currently used industrial hot water separation of the bitumen. As mentioned above, the amount of straight-chain and cyclopropyl alkyl carboxylic acids in the methylene chloride-insoluble portion of the whole oil sands is about two to three orders of magnitude higher than that present in free form in the bitumen. Moreover, since they are chemisorbed onto the water-wet mineral surface, they are immersed in the connate water film separating the bitumen from the minerals. Upon treatment with base, this strategic location—within the interface where it is needed for interfacial action— should render the chemisorbed acids more effective as surfactants than the acids in the bulk of the bitumen since the latter would have to move to the interfacial region by the slow process of diffusion. During the alkaline hot water separation carboxylate ions are also produced in the

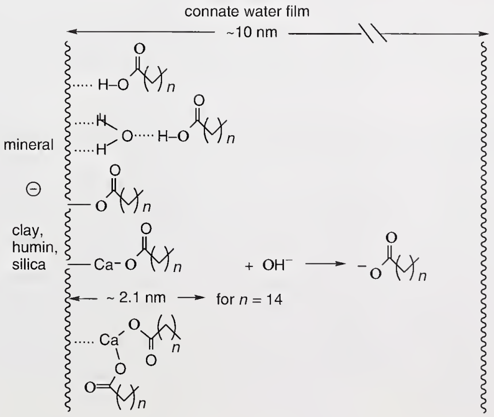

Scheme 8.1

bulk bitumen, as manifested by the observation that the interfacial tension between water and toluene solutions of coker feed bitumen is lower than that of toluene solutions of solvent-extracted bitumen.[8]

If the coating of the mineral surfaces by the carboxylic acids becomes excessive it may render the surfaces hydrophobic, thereby creating an impedance to water displacement of the bitumen.

2.0 Bitumen-Unrelated Organic Matter

All organic sediments contain organic solvent-insoluble organic matter which is related to humus, the family of organic compounds (with the exception of undecayed cells and the biomass) in soil. The main constituents of humus, Figure 8.1, have been defined by soil scientists according to their solubility characteristics as humin, humic acids and fulvic acids: the acids are soluble in dilute aqueous sodium hydroxide or metal-precipitating agents such as $Na_4P_2O_7$, or chelating agents such as acetone/H_2O/HCl solutions, *etc.*, while humin is completely insoluble. Fulvic and humic acids are differentiated by their solubility in HCl, fulvic acid being soluble and humic acid, insoluble. Humic substances in subaerial soils are formed from the polycondensation of lignin and cellulose-derived and microorganism-synthesized building blocks involving quinones and polyphenols. In subaquatic sediments humic substances may arise from the polycondensation of mainly plankton-synthesized protein, carbohydrate and lipid derivatives, along with land-derived lignin and cellulose. The structures of humic and fulvic acids are dependent on their origin; humic acids formed in subaquatic sediments in general have higher $(H/C)_a$ ratios, 1.00–1.50, compared with values of 0.50–1.00 in soil or coal humic acids.

The bulk of the bitumen-unrelated organic matter in oil sands comprises humic materials (humin, humic acid and fulvic acid) along with lesser amounts of resinous material consisting of bound carboxylic acids, hydrogen-bonded ketones, ketones chelated to Lewis acids forming acetone-soluble complexes upon treatment with HCl, and other unidentified, inorganic-bound organic complexes.

Many fine studies on the bitumen-unrelated organic matter in Alberta oil sands have been published in the last 15 years or so, but the salient features of only a few can be mentioned here.

2.1 Characterization of bitumen-unrelated organic matter

The methylene chloride-extracted sands from Syncrude high-grade (SHG) and low-grade (SBS) ores studied having bitumen contents of 12.7 and 6.9% were found to contain 0.3 and 1.5% organic carbon.[3] Of this organic carbon, 61% in the high-grade and 66% in the low-grade ores were associated with the < 44-μm fines (which amounted to 8.3 and 35.7% of the methylene chloride-extracted sand). From these results it can be calculated that the concentrations of organic carbon in the fines from the two oil sands are commensurate, being 2.2 and 2.8%, and therefore the higher amount of organic carbon in the low-grade sand is mainly due to the higher amount of fines present.

Syncrude oil sand	$C_{org.}$	Fines	$C_{org.}$ in fines	$C_{org.}$ in >150-μm sand
low grade (SBS)	1.5%	35.7%	2.8%	0.4%
high grade (SHG)	0.3%	8.3%	2.2%	<0.1%

In contrast, the coarse sand (>150 µm in size) from the low-grade ore contains 0.4% organic carbon whereas that from the high-grade ore, only < 0.1%. This finding indicates a possible difference in the origin and thus in the composition of the organic compounds associated with the coarse sands on the one hand and the fines on the other.

An examination of the mineralogy of the sand[3a,b] revealed that the > 44-µm size fraction is composed mainly of quartz with lesser amounts of feldspar and trace amounts of clay (54% kaolinite and 46% illite). In the < 44-µm fraction, however, clay becomes a main component along with quartz, and feldspar is still a trace component, Table 8.5. Kaolinite is, in general, the main component of the clay, followed by illite, a few percent chlorite and, occasionally, trace amounts of smectite.

Compositional data for fractions of humic and resinous materials from methylene chloride-extracted SBS according to the extraction sequence illustrated in Figure 8.7 are given

Table 8.5 Mineral composition of preextracted Athabasca (Syncrude) oil sands[a]

Ore type[b]	Sand size µm	Concentration[c]			Relative % of clay			
		Quartz	Feldspar	Clay	Kaolinite	Illite	Chlorite	Smectite
SHG	53	M	m	t	63	37	n.d.[d]	n.d.
SBS	53	M	m	t	54	46	n.d.	n.d.
SHG	44	M	m	t	40	60	n.d.	n.d.
SBS	44	M	m	t	54	46	n.d.	n.d.
SHG	<44	M	t	M	72	24	2	t
SBS	<44	M	t	M	64	32	4	n.d.

[a] From T.M. Ignasiak *et al.*, Ref. 3a. [b] SHG = Syncrude high grade, SBS = Syncrude low grade. [c] M = major, m = minor to moderate, t = traces. [d] Not detected.

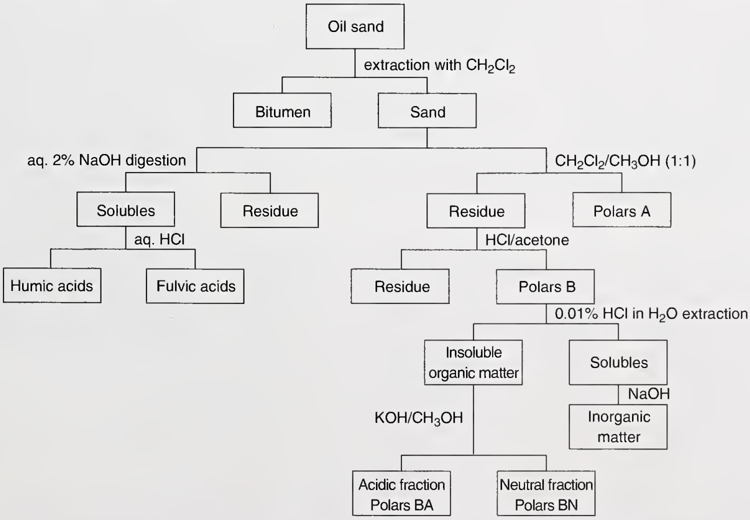
Oil sand
extraction with CH_2Cl_2
Bitumen
Sand
aq. 2% NaOH digestion
CH_2Cl_2/CH_3OH (1:1)
Solubles
Residue
Residue
Polars A
aq. HCl
HCl/acetone
Humic acids
Fulvic acids
Residue
Polars B
0.01% HCl in H_2O extraction
Insoluble organic matter
Solubles
NaOH
KOH/CH_3OH
Inorganic matter
Acidic fraction Polars BA
Neutral fraction Polars BN

Figure 8.7 Procedure for fractionating the methylene chloride-insoluble material from Athabasca (Syncrude) oil sands. From T.M. Ignasiak *et al.*, Ref. 3a.

in Table 8.6. Both humic acids and fulvic acids are present, the former being more abundant. The chemical natures of the two classes of acids are vastly different, as manifested by their elemental compositions: the fulvic acids are extremely rich in NOS atoms and have a higher $(H/C)_a$ ratio and a much lower molecular weight (400) than the humic acids (the molecular weight of the humic acids was not measured in this study but it generally lies in the 10^4–10^6 range). Of the five groups of compounds listed in Table 8.6, humic acids have the lowest $(H/C)_a$ ratio (0.70), although higher values (around 1.1) have been obtained in other studies.

Table 8.6 Chemical composition of the dichloromethane-insoluble material in Syncrude Beach Sand oil sands[a]

Fraction	Yield,[b] wt% of		% d.a.f.[c]					% Ash by diff.	$(H/C)_a$	MW[d] g·mol^{-1}
	sand	$C_{org.}$	C	H	N	S	O			
Humic acids	0.4	18.3	68.6	4.0	1.8	2.5	23.1	1.9	0.70	–
Fulvic acids[e]	0.1	3.0	44.1	5.0	8.4	8.0	34.5	–	1.36	400
Polars A	0.1	5.0	76.0	8.5	1.1	6.7	7.7	1.0	1.34	740
Polars BN	0.4	21.8	81.6	9.4	0.4	0.9	7.7	1.7	1.38	550
Polars II[f]	0 .1	5.1	75.9	8.5	1.2	6.2	8.2	1.5	1.35	1,300

[a] From T.M. Ignasiak *et al.*, Ref. 3a. [b] Based on a standard 24-h digestion. [c] Dry ash free. [d] By VPO in benzene. [e] Calculated from the methyl esters. [f] Fraction extracted from the tailings.

The data in Table 8.6 were obtained for materials from a standard 24-hour digestion. After more exhaustive extraction the low-grade sand released 0.86% humic acids and the high-grade sand, 0.11%. The yields of fulvic acids, on the other hand, were similar for the two grades of oil sand and did not exceed 0.13%. The carbon in the humic and fulvic acids accounts for about 43% of the organic carbon in the sand.

Soil fulvic acids contain up to 2% sulfur and 1–3% nitrogen and soil humic acids contain up to 2% sulfur and <1–3% nitrogen. As much as one-half of the total nitrogen in humic substances can be accounted for as amino acid nitrogen. Additional amounts of nitrogen are present as amides, slightly modified amino acids, amino sugars, purine and pyrimidine bases, ammonia, and others. Sulfur-containing amino acids have also been isolated from soil, suggesting that the sulfur in the humic and fulvic acids may be present in these forms.

Humic materials are considered to be the precursors of kerogen, the geomacromolecular precursor of petroleum, and fulvic acid, humic acid, humin and kerogen represent progressively increasing maturity stages in the diagenetic evolution of organic sediments. The ratio fulvic acid:humic acid:(humin + kerogen) for a given deposit is a function of the depth of burial and decreases with depth as seen in Figure 8.8. These ratios for the SHG and SBS oil sands are approximately 1:10:20 and 1:1:2.5 and would

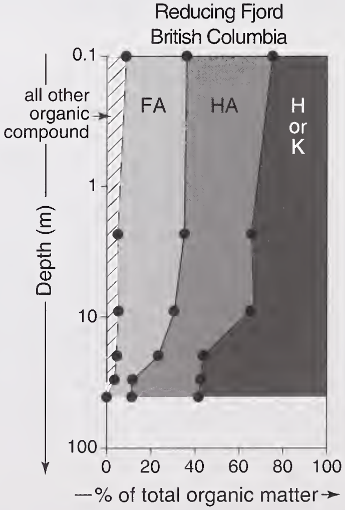

Figure 8.8 Evolution of fulvic acids (FA), humic acids (HA), humins (H) and kerogen (K) as a function of depth of burial. From B.P. Tissot and D.H. Welte, Ref. 7. © 1984, Springer-Verlag.

correspond to a burial depth in recent sediments of 10–100 m. Below 100 m fulvic acids tend to disappear.

The chemical composition as well as the IR absorption spectra of the humic and fulvic acids obtained from the two oil sands were similar. In general, the IR spectra resemble those of typical humic acids present in soil, peat and lignite, which are described as heteropolycondensates whose reactivity is attributed largely to the oxygen-containing functional groups COOH, phenolic OH, alcoholic OH, quinone C=O, ketone C=O and OCH_3.

The FTIR spectrum of SBS humic acid, Figure 8.9a, suggests the presence of bound carboxylic acids (the broad band at 3,600–2,000 cm^{-1} and the strong absorptions at 1,710 and 1,220 cm^{-1}). In fact, upon methylation with diazomethane, about 10% of the humic acids become soluble in ether and this portion displays the absorptions typical of methyl esters (at 1,730, 1,435 and 1,250 cm^{-1}), Figure 8.9b. (The presence of polymeric phenols, alcohols and chelated ketones in the structural framework of oil sand humic acids is also suggested.) Treatment of the SBS humic acids with 1% concentrated hydrochloric acid in acetone removed 20% of them. The extract, which is readily soluble in acetone, has a composition similar to that of the total acids and its FTIR spectrum, Figure 8.9c, shows a distinct reduction in the intensity of the 1,600 cm^{-1} band attributed to α,β-unsaturated ketones and/or strongly H-bonded conjugated ketones.

Additional, valuable structural information on humic acids has been obtained from recent ^1H and ^{13}C NMR studies[9] which will be considered later.

The FTIR spectrum of the fulvic acids, Figure 8.10a, indicates that the oxygen functionalities of these acids consist mainly of phenolic and/or alcoholic and carboxylic groups. Upon methylation of this material the phenols, whose characteristic OH stretching absorption was obscured by the water of hydration, are converted to the corresponding methyl ethers. This is reflected in the appearance, Figure 8.10b, of the characteristic bands at 2,850 and bands at 1,400, 1,200–1,250 and 1,000 cm^{-1}, while the carboxylic acids (1,710 cm^{-1}) and carboxylates (1,580, 1,405 cm^{-1}) were converted to esters with absorptions at 1,730, 1,435 and 1,200–1,250 cm^{-1} indicating a weak residual aromatic carbon (or ketone/quinone) resonance.

The ^1H NMR spectrum of the methylated fulvic acids, Figure 8.11, which accounted for 65% of the fulvic acids extracted from the sand, demonstrated that during methylation roughly five methoxy groups (with resonances at 3.7 ppm) were formed in an average molecule described by the formula $C_{15}H_{20}N_2SO_9$. Here, the intensities of the aromatic proton resonances appear to be weak and the hydroxyl groups may be mainly alcoholic rather than phenolic.

The nonhumic substances were extracted from the sand with 1:1 CH_2Cl_2/CH_3OH and fractionated according to the scheme outlined in Figure 8.7.

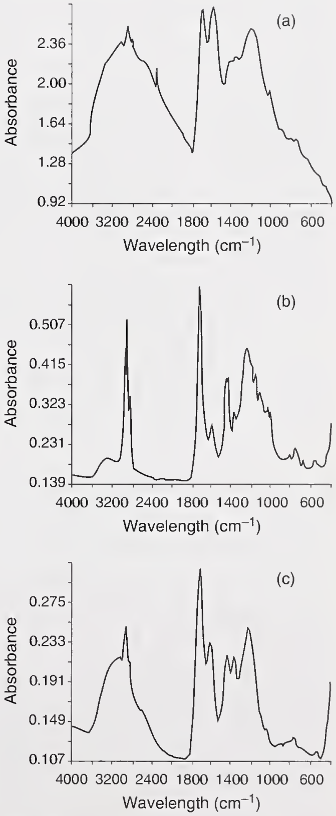

Figure 8.9 FTIR spectra of the Athabasca (Syncrude Beach Sand) humic acids. a, total acids; b, methylated acids; c, HCl/acetone extract.[3a]

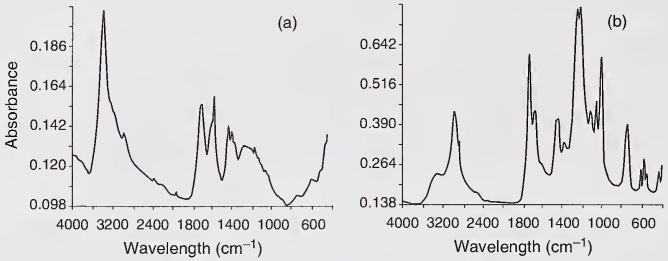

Figure 8.10 FTIR spectra of the Athabasca (Syncrude Beach Sand) fulvic acids. a, total acids; b, methylated acids. From T.M. Ignasiak *et al.*, Ref. 3a.

The FTIR spectrum of the Polars A fraction, Figure 8.12, clearly shows the presence of free alkanoic acids (3,500–2,500, 1,710 and 1,200 cm^{-1}, and the 2,925, 2,850, 1,470 and 1,380 cm^{-1} CH_2 and CH_3 absorptions) and these acids were shown to be the same types as those isolated by saponification of the sand.[5] Since esters and carboxylic acid salts could not have been hydrolyzed by the extraction solvent used (1:1 CH_2Cl_2/CH_3OH) it appears that some of the chemisorbed acyclic acids listed in Table 8.4 are bound by weak hydrogen bonds to the negatively charged mineral surfaces as indicated in Scheme 8.1. Sulfoxides and phenols are probably also present in Polars A (1,000–1,040 cm^{-1}).

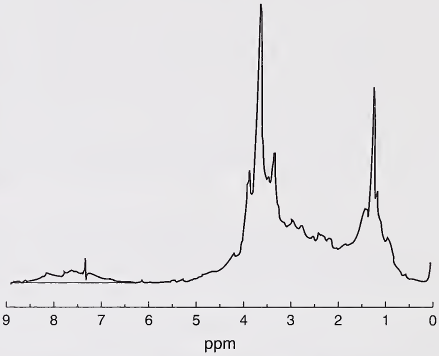

Figure 8.11 ^1H NMR spectrum of the Athabasca (Syncrude Beach Sand) methylated fulvic acids. From T.M. Ignasiak *et al.*, Ref. 3a.

After removal of Polars A, subsequent extraction with acetone acidified with concentrated HCl (99:1) generated Polars B. The FTIR spectrum of this fraction, Figure 8.13a, features an unusual infrared pattern with prominent bands at 3,400, 1,600, 1,450 and 1,380 cm^{-1}. The first two absorptions can be readily identified with stretching OH and C=O or C=C bonds, respectively; however, the intensities of the bands at 1,450 and 1,380 cm^{-1}, which are within the region of the deformation vibrations of the CH_2 and CH_3 groups, are much higher than those of the C–H stretching vibrations that occur at 2,800–3,000 cm^{-1}; this is not normally observed in hydrocarbons.

On combustion, the Polars B fraction yielded 41% ash, revealing the presence of inorganic matter other than the fines (which had been previously removed by centrifugation of the extract).

A material, free of inorganic matter was readily obtained, however, by washing Polars B with 0.01% aqueous HCl. After washing, the organic residue became completely soluble in methylene chloride and the yield of the fraction was reduced from 1.0 to 0.4% of the extracted sand. The organic residue was then treated with alkaline methanol and two subfractions were obtained, Polars BN and Polars BA, comprising the neutral and acidic components (Figure 8.7).

The neutral fraction, Polars BN (90% of the organic portion of Polars B), is characterized by low nitrogen and sulfur contents (Table 8.6). The infrared spectra of Polars BN and Polars BA, Figure 8.14, show a drastic reduction in the intensities of the peaks at 1,600, 1,450 and 1,380 cm^{-1} which were highly prominent in the spectrum of Polars B, Figure 8.13, along with

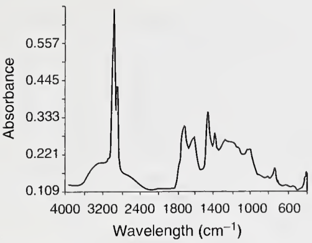

Figure 8.12 FTIR spectrum of the Polars A extract (*cf.* Figure 8.7) from the Athabasca (Syncrude Beach Sand) methylene chloride-insoluble material. From T.M. Ignasiak *et al.*, Ref. 3a.

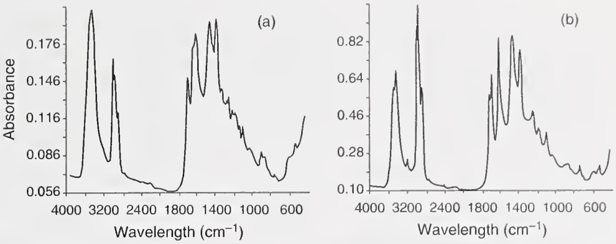

Figure 8.13 FTIR spectrum of a) the Polars B extract (*cf.* Figure 8.7) from the Athabasca (Syncrude Beach Sand) methylene chloride-insoluble material and b) the Polars BN extract to which $FeCl_3$ had been added. From T.M. Ignasiak *et al.*, Ref. 3a.

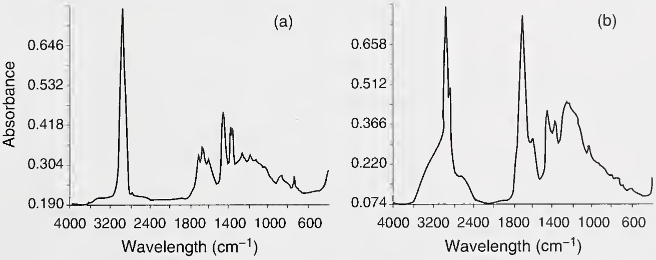

Figure 8.14 FTIR spectra of the Polars BN (a) and BA (b) extracts (*cf.* Figure 8.7) from the Athabasca (Syncrude Beach Sand) methylene chloride-insoluble material. From T.M. Ignasiak *et al.*, Ref. 3a.

the disappearance of the 3,400 cm^{-1} band. The spectrum of Polars BA shows absorptions typical of those of carboxylic acids.

The aqueous solution obtained from washing Polars B was treated with NaOH. This resulted in the precipitation of inorganic hydroxides (0.3% of the sand). After drying, it was found that about 75% of the precipitate consisted of Fe_2O_3.

The changes in the IR spectrum of Polars B before and after water washing, along with the substantial amounts of iron found in this fraction, strongly imply that most of the Polars B fraction was extracted from the sand in the form of $FeCl_3$ complexes. This conclusion was further substantiated by comparing the FTIR spectrum of Polars B (Figure 8.13a) with that of a sample prepared by mixing Polars BN with anhydrous $FeCl_3$ in acetone, followed by evaporation of the solvent (Figure 8.13b). As seen from Figure 8.13 the two spectra are very similar, indicating that complexation had taken place between some basic carbonyl functionality and the $FeCl_3$ Lewis acid. The shifts and number of bands in the carbonyl absorption region are indicative of ligands with diketone and/or α,β-unsaturated ketone functionalities existing in several different structural arrangements involving chelation with Fe^{3+} and perhaps other metal ions. Therefore, the desorption mechanism of the specific water-insoluble group of ketones which adhere strongly to the mineral surface is attributed to a donor–acceptor interaction, where the acceptor is the Lewis acid formed *in situ* by the action of hydrochloric acid on the metal in the (mainly iron-containing) minerals present. From this it follows that the solubilization of the complexes in the solvent used for extraction is a necessary condition for this separation to occur.

An industrially important process where iron is thought to play an active role is the chain of interactions that promote adsorption of the organic matter on the clay in the clay sludges from oil sand.[10,11] The mechanism of interaction of carbonyl-bearing species is thought to involve chelation of metal ions with carbonyl groups, facilitated by the formation of protonated clay[10] along with a number of other adsorption mechanisms utilizing broadly defined van der Waals forces.[12,13] The iron engaged in the adhesion of the organic matter in the oil sands may, in the form of exchangeable cations, be an integral part of the clay structure or may, in the form of positively charged oxides, attract anions either by itself or through bridging with clays.

2.2 Distribution of the bitumen-unrelated organic matter in the oil sand tailing fractions

To determine the distribution of the closely bound organic matter in the mineral matrix and to evaluate the capacity of this material to retain bitumen on the mineral surfaces after wet sieving, SHG and SBS samples were subjected to the Syncrude Batch Extraction Test (SBET). In the SBET, which is a laboratory simulation of the industrial hot water extraction process, the high-grade ore gave 96% recovery of bitumen while the SBS ore gave about 24%.

The tailings from the hot water separation of the SBS sample were then subjected to wet sieving. After removing the residual bitumen with dichloromethane, each particle size fraction was subjected to a series of extractions as illustrated in Figure 8.15. The results are summarized in Table 8.7. Here we see, first of all, that (with the exception of the coarsest sand fraction) the percentage amount of extracts increases with decreasing particle size and reaches 1.56% in the < 44-µm fraction: this corresponds to over 60% of the total recovered chemisorbed organic matter.

The total amount of Polars I extracted from each particle size fraction of the SBS tailings using 1:1 CH_3OH/CH_2Cl_2 (0.41% of the extracted sand) is higher than the Polars A fraction (0.1% of the extracted sand, Table 8.6) obtained by extracting the whole methylene chloride-extracted sand with the same solvent. Apparently, digestion of the oil sand with aqueous base in the course of the SBET separation led to the desorption of the highly polar ketones (capable of forming soluble complexes with $FeCl_3$ in acetone/HCl) from the sand and rendered them soluble in CH_2Cl_2/CH_3OH.

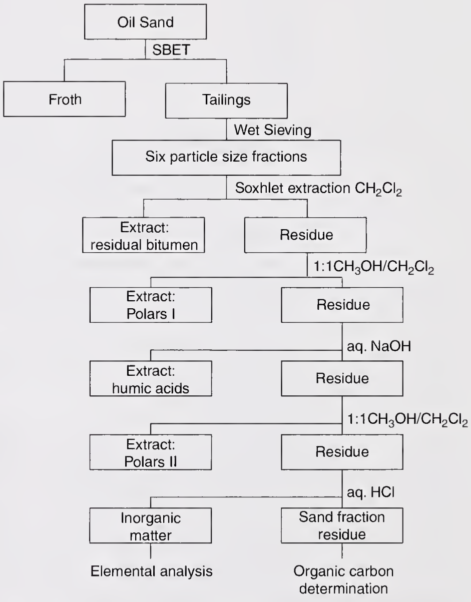
Oil Sand
SBET
Froth
Tailings
Wet Sieving
Six particle size fractions
Soxhlet extraction CH_2Cl_2
Extract: residual bitumen
Residue
1:1 CH_3OH/CH_2Cl_2
Extract: Polars I
Residue
aq. NaOH
Extract: humic acids
Residue
1:1 CH_3OH/CH_2Cl_2
Extract: Polars II
Residue
aq. HCl
Inorganic matter
Sand fraction residue
Elemental analysis
Organic carbon determination

Figure 8.15 Procedure for fractionating the methylene chloride-insoluble material in the tailing sands from the Syncrude Batch Extraction Test of Beach Sand oil sands. From T.M. Ignasiak *et al.*, Ref. 3a

The yields of Polars I and humic acids from the particle size sand fractions were comparable, while Polars II accounted for < 10% of the total material extracted from each fraction. On average, only about one-third of the organic carbon of the closely bound organic matter was extractable and hence the remainder was present in the form of insoluble humins.

Table 8.7 Distribution of organic matter in the Syncrude Beach Sand tailings[a]

		Wt% in tailing fraction					
Sand		Extracted					Unextracted
Particle size, μm	Wt% of tailings	Residual bitumen	Polars I	Humic acids	Polars II	Total $C_{org.}$	$C_{org.}$
150	19.4	2.5	0.25	0.27	0.047	0.43	0.83
106	16.9	1.2	0.10	0.10	0.010	0.16	0.20
75	11.6	1.4	0.12	0.14	0.024	0.22	0.59
53	9.4	1.8	0.16	0.16	0.029	0.26	0.75
44	8.5	5.6	0.39	0.27	0.062	0.55	1.15
<44	34.2	7.3	0.76	0.67	0.134	1.17	2.00

[a] From T. Ignasiak *et al.*, Ref. 3a.

The chemical characteristics of Polars I and humic acids are the same as those of Polars A and B and the humic acids obtained from the whole methylene chloride-extracted sand.

As demonstrated by the above data, the fines—that is, the ≤44-μm fraction—have the greatest capacity to retain organic matter. In both the SHG and SBS oil sands the fines, independently of their concentration in the sand tailings, accumulated over 60% of the residual bitumen in the tailings and contained more than 60% of the closely bound organic carbon. Nonetheless, it should be noted that even the coarsest particle size (150 μm) fraction retains organic matter, both chemisorbed and bitumen, in significant relative and absolute amounts. Also, as with the chemisorbed organic matter (with the exception of the 150+ μm fraction) the percentage of bitumen retained on the fraction is inversely proportional to the particle size of the fraction.

In exploring the cause of the poor separability of the SBS ore in the conventional hot water separation process, a significant relationship that appears to have emerged from this study is the dependence of the amount of bitumen retained in the SBET and wet-sieved particle size fractions on the chemisorbed organic carbon content. Thus, as shown in Figure 8.16, the percentage of bitumen in the particle size fractions varies in an approximately linear fashion with the percentage of organic carbon content after methylene chloride extraction of the fraction, and seems to extrapolate to zero bitumen content at 0% organic carbon content. Direct support for the assignment of the quality of the methylene chloride-extracted sand as the property responsible for the poor separability of the SBS ore came from auxiliary studies in which an oil sand reconstituted from Beach Sand + water + high-grade bitumen was shown to display poor separability in the SBET test.

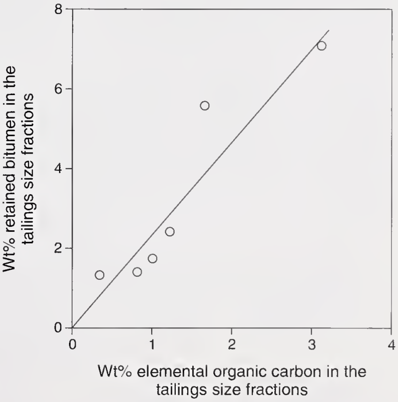

Figure 8.16 Relation between the weight percent retained bitumen and the weight percent organic carbon in the various SBS tailings size fractions from the SBET of SBS ore. From T.M. Ignasiak *et al.*, Ref. 3a.

All of the above results then lead to the important conclusion that, in the case of the SBS ores, the poor separability is due to the presence of the methylene chloride-insoluble materials—Polars A, BN, BA, humic acids, fulvic acids and humins—across all the size fractions of the sand, forming a hydrophobic film on the mineral surfaces. This organic film, taking the place of the thin aqueous film which is present on the clean sand surface in the case of high-grade ores, is bound to the high-energy, negatively charged quartz, clay and other mineral surfaces by a variety of bonds. As a result, the surface is now oil-wettable, with the potential of establishing a bond of far greater wet strength than that between bitumen and silica.

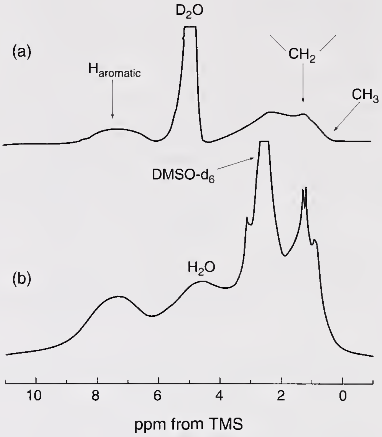

Figure 8.17 Typical 300-MHz ^1H NMR spectra of humic acids from oil sands and oil sand overburdens dissolved in (a) NaOD; (b) DMSO-d_6. From A. Majid and J.A. Ripmeester, Ref. 14. © 1990, Butterworth-Heinemann.

Additional structural information on the chemisorbed organic matter in Athabasca oil sand and related materials comes from comparative chemical and ^1H as well as ^{13}C NMR spectroscopic studies[9,14] of the isolated humic acids and nonhumic organic matter. The ^1H NMR spectra of the humic acids are shown in Figure 8.17. From the data in Table 8.8 it is evident that the total chemisorbed organic matter concentrations in the overburdens are higher than in the oil sands whereas the fractional amount of humic acid concentrations is lower. The ^1H aromaticities in the oil sands and overburdens, 0.20–0.30, appear to lie in the range reported for terrestrial humic acids, 0.17–0.35, and are significantly higher than the range reported for aquatic humic acids, 0.02–0.07. The difference in the chemical compositions of the humic acids in the overburden and the oil sands seems to suggest that, in the overburdens, secondary alterations that caused a chemical differentiation in the humic acids have taken place. Being closer to the surface, the humic acids in the overburden are more susceptible to the effects of climatic conditions (oxidation, water washing, microbes) while in the oil sand, after being exposed to the influence of the microbes that caused the biodegradation of the precursor oil, the humic acids became sealed under a protective bitumen layer. In general, as was noted before (from the distinct preference for even carbon number members in the fatty acid series, the relatively high fulvic acid content and the low reflectance[15] value of the associated coals), the humic and nonhumic materials are thermally immature, indicating that during their history they have not been buried deeply.

Table 8.8 Comparison of some compositional properties of chemisorbed organic material in oil sands, oil sand fractions and overburdens[a]

Sample[b]	Fines	Bitumen	$C_{org.}$[c]	IOM[d]	Humic acids	
	wt% of dry sample				wt% of IOM	^1H aromaticity
SOS-1	32	3.5	1.0	1.3	25.4	0.25
SOS-2	22	8.3	0.9	1.2	30.0	0.30
SBS	11	10.0	0.09	0.12	16.7	–
SOB-1	70	2.3	2.9	4.0	4.8	0.20
SOB-2	64	3.6	1.5	2.1	6.2	–
SCT	15	5.5	11.1	18.0	16.1	0.49
OPS	0	–	19.3	32.5	20.9	0.48

[a] From A. Majid and J.A. Ripmeester, Ref. 14. [b] SOS = Suncor oil sand; SBS = Syncrude Beach Sand; SOB = Suncor overburden; SCT = Syncrude centrifuge tailings; OPS = oil phase solid consisting of heavy minerals from oil sand tailings. [c] $C_{org.}$ = insoluble organic carbon. [d] IOM = insoluble organic matter.

The solution phase ^{13}C NMR spectra of humic acids from the oil sands and overburdens, Figure 8.18, are similar and confirm the presence of carboxylic, phenolic and carbonyl groups, monocyclic aromatic and naphthenic rings and paraffinic carbons. The aromaticity values calculated from the ^{13}C NMR spectra, 0.4–0.69, are higher than those reported for soil and aquatic humic acids, again pointing to a large terrestrial contribution from vascular plants (lignin, tannin, *etc.*).

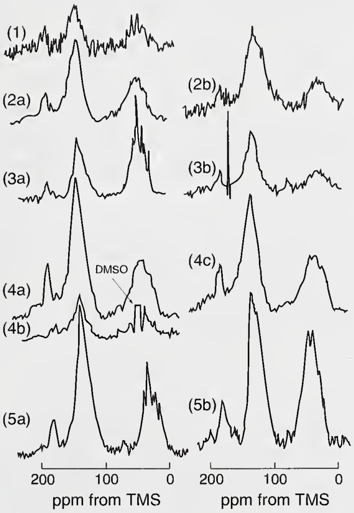

ppm	assignment
0-70	aliphatic carbons (paraffinic, naphthenic)
50-110	aliphatic C–OH, C–OR, carbohydrate, C–N
110-145	aromatic C–H, aromatic C–C, aromatic C–R
145-160	aromatic C–OH, C–OR
160-190	acid, ester (COOH, COOR)
190-230	aldehyde, ketone
~75	carbohydrate
168	carbonate
~175	COOH, COOR, CONHR

Figure 8.18 Solution-phase (NaOD) ^{13}C NMR spectra of humic acids from (1) SOS-1; (2) a), SOS-2 b), toluene-extracted SOS-2; (3) a), SOB-1, b), toluene-extracted SOB-1; (4) a), SCT, b), SCT in DMSO-d_6, c) 2nd extract of SCT; (5) a), 1st extract from OPS, b), 2nd extract from OPS. See Table 8.8 for sample designations. From A. Majid and J.A. Ripmeester, Ref. 14. © 1990, Butterworth-Heinemann.

All the spectra feature sizeable resonances around 175 ppm corresponding to carboxylic carbon and weak (if any) resonances around 75 ppm, characteristic of carbohydrates. From the data on the oil sand and overburden samples the following estimates for the relative amounts of oxygen-bearing carbon can be made:

aliphatic –C–O–	4.8–8.8%
aromatic –C–O–	5.1–8.1%
carbonyls 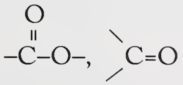 $-\overset{\overset{\displaystyle O}{\|}}{C}-O-,\ \rangle C=O$	5.5–16.1%

Examination of the nonhumic acid portions of the chemisorbed organic matter after removal of the bulk of the inorganic matrix by HCl/HF acid digestion indicated that the differences in elemental and trace metal compositions and in the ^{13}C NMR spectra between the materials from the overburden and the oil sands were sufficiently large to indicate that they probably had different origins as well as diagenetic histories.

The distribution of the insoluble organic matter in the oil sands is not uniform even in a given particle size fraction, and it would appear to be concentrated in a relatively small fraction of hydrophobic, oil-wet minerals.[16] This can be seen from Figure 8.19. Here, in Figure 8.19a the percentage of solids separated from two toluene-extracted medium-grade Athabasca oil

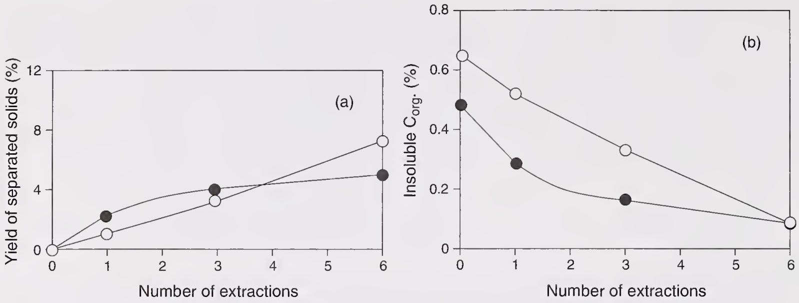

Figure 8.19 Yields of a) solids suspended in aqueous phase and b) insoluble organic carbon in the sand as a function of number of extraction steps for two Athabasca medium-grade oil sands.[16]

sands in the form of an aqueous suspension (upon agitation in the presence of a 0.1% sodium pyrophosphate solution with a high-intensity (Spex) mixer) is plotted as a function of the number of repeated extraction steps. In Figure 8.19b the percentage of insoluble organic carbon in both sands is also plotted as a function of the extraction steps. According to the figures up to 85% of the insoluble organic carbon may be concentrated in 5–6% of the oil sand solids.

Moreover, in a study[17] of Athabasca tailings pond sludge, it was found that a substantial amount of the chemisorbed organic matter was present in association with that fraction of solids which existed largely as aggregates (globules) of fine particles probably originating from (marine) oil sands displaying poor bitumen recovery. Noncrystalline inorganic–organic complexes and skin-forming solids were also shown to be present in the oil sands.

2.3 Bonding between humic and inorganic substances

The mineral substances in oil sands, by virtue of their surface properties, have the capacity of forming bonds of various types and strengths with the large array of different kinds of functional groups that occur in the organic compounds that are indigenous to oil sand deposits. The three most abundant types of minerals in oil sands are silica (α-quartz), carbonates and clays. It is widely recognized that clays, owing to their chemical composition, crystal structure, large surface area and cation exchange capacity, Table 8.9, are much better adsorbents than silica or carbonates.

The two important clay minerals in Athabasca oil sands are kaolinite (30–70%) and illite (30–50%). Chlorites and mixed-layer clays each may comprise up to 7–8% and there are only trace-to-small amounts of smectites present.

Table 8.9 Surface areas and cation exchange capacities of clay minerals

Clay	Specific surface area, $m^2 \cdot g^{-1}$	Cation exchange capacity, meq·100 g^{-1}
Kaolinite	25–50	3–15
Illite	75–112	10–40
Vermiculite	500–700	100–150
Montmorillonite	700–800	80–150
SHG < 44 mm	11.3	–
SBS < 44 mm	10.3	–

Kaolinite is a two-layer phyllosilicate (platy) clay with generic formula $Al_4(Si_4O_{10})(OH)_8$, consisting of alternating layers of silicon oxides and aluminum hydroxides, the former being tetrahedral and the latter, octahedral. The Al^{3+} ions in the octahedral layers can be partly substituted by Fe^{3+}, Cr^{3+}, Fe^{2+}, Mg^{2+}, *etc.*, and the Si^{4+} ions in the tetrahedral layers, by Al^{3+}. The extent of substitution of either Al or Si in kaolinite and in two-layer clays in general, is small.

Illite (named after the state of Illinois) is a three-layer clay which consists of an aluminum oxyhydroxide layer sandwiched between two silicon oxide layers. A given crystal consists of several sheets of these three-layer arrangements. The excess negative charges resulting from isomorphous substitutions (of Si^{4+} by Al^{3+}) in the lattice are neutralized by cations adsorbed on the grain surfaces and on the outer surfaces of the tetrahedral layers. The ions adsorbed on the interlamellar surfaces bond the lamellae together. These adsorbed ions are exchangeable and are responsible for the cation exchange capacity of the clay. In certain clay minerals the interlamellar cations can be replaced by polar molecules such as water, in which case one cation can be replaced by several water molecules. As a result, the interlayer distances increase and the clay expands (*e.g.*, montmorillonite, vermiculite). In the case of illite, the interlamellar cation is potassium, K^+, which binds exceptionally strongly, and the clay structure is stabilized to such a degree that the clay becomes nonexpandable. Thus, illite is an example of a nonswelling, three-layer clay.

In addition to the surface charges, the broken crystal edges may acquire a *pH*-dependent negative or positive charge (unlike the lattice charges which are *pH*-independent) resulting from the dissociation of the SiO–H and Al–OH surface groups:

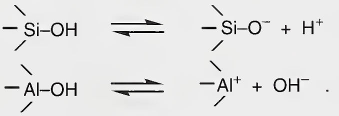

$$\text{Si–OH} \rightleftharpoons \text{Si–O}^- + H^+ \; ; \qquad \text{(a)}$$

$$\text{Al–OH} \rightleftharpoons \text{Al}^+ + OH^- \; . \qquad \text{(b)}$$

At *pH* values around 8, as usually encountered in Alberta oil sands, reaction (a) predominates and consequently silica is negatively charged while the hydrous sesquioxide (Al_2O_3 and Fe_2O_3) surfaces are positively charged.

The high interfacial reactivity of clays and minerals in general is derived primarily from their electric charge and this may lead to several mechanisms[1] for the adsorption of humic matter. The most important of these mechanisms include hydrogen bonding, electrostatic attraction or chemical adsorption and coordination complexing. Physical adsorption involves only weak van der Waals forces which play a significant role in the adsorption of nonpolar molecules; however, in the highly polar humic materials and resins the role of van der Waals forces is of only minor importance relative to polar interactions.

The **hydrogen bond** is a weak linkage (up to ~ 80 kJ) between two small, electronegative atoms—usually oxygen (fluorine) and nitrogen—*via* a single H atom and represents an important mechanism for the adsorption of water, carboxylic acids, phenols, alcohols, basic carbonyl, basic nitrogen and other compounds to the negatively charged clay and quartz mineral surfaces, Figure 8.20. As seen from the diagram, the prime sites for H-bonded adsorption are surface oxygens or OH's while other possibilities include adsorbed water and protons of cation hydration water.

Electrostatic bonding of organic cations occurs through cation exchange

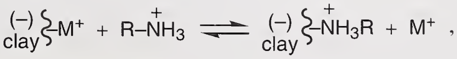

$$\underset{\text{clay}}{(-)}\text{–}M^+ + \text{R–}\overset{+}{N}H_3 \rightleftharpoons \underset{\text{clay}}{(-)}\text{–}\overset{+}{N}H_3R + M^+ \; ,$$

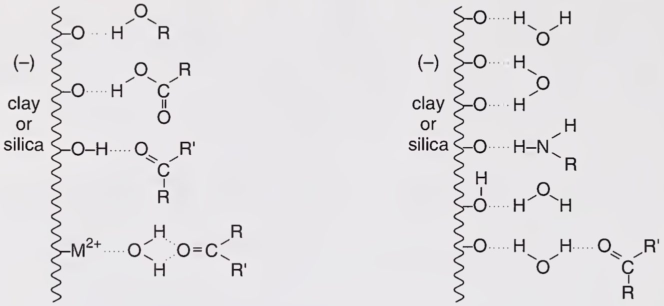

Figure 8.20 Hydrogen bonding of oxygen and nitrogen compounds to negatively charged clay or silica surfaces.

where the organic cation is formed by the protonation of weak nitrogen bases,

$$R\text{–}NH_2 + H^+ \rightleftharpoons R\text{–}NH_3^+ .$$

Coordination complexing is important when polyvalent ions, mainly Al^{3+} and Fe^{3+}, are present. In this type of bonding the metal ion essentially forms a bridge between the clay and the organic ligand,

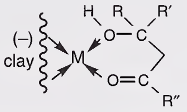

,

where the arrows represent electron pairs donated by the ligands to the metal or the coordination bonds.

Analysis of the < 44-μm fraction of the mineral matter in the tailings and especially in the froth of the SBS oil sand, Table 8.10, indeed shows relatively high concentrations of Al, Fe and Ti; therefore, coordination complexing through these metals is probably of major importance in bonding the humic matter to the SBS clays. In soil chemistry it has been generally recognized

Table 8.10 Elemental composition (wt%) of SHG and SBS bitumen-free oil sands and SBS bitumen-free fractions

Element	SHG[a]	SBS[a]	SBS fines[b]	SBS froth[c]
Ca	0.05	0.15	0.06	0.19
Mg	0.04	0.15	0.16	0.24
K	0.19	0.38	1.05	1.02
Al	1.09	2.71	4.15	4.70
Fe	0.34	0.72	0.76	1.32
Ti	0.21	0.27	0.40	0.58
Mn	0.02	0.02	0.01	0.01
P	0.01	0.04	0.03	0.05
S	0.02	0.03	0.02	0.15
Si	43.40	35.95	38.65	34.40

[a] Wt% of total bitumen-free sand. [b] Wt% of fines fraction of tailings obtained from the Hot Pot Test and Soxhlet-extracted with CH_2Cl_2 to remove bitumen. The fines constitute 35.7 wt% of the sand tailings and lack the water-soluble salts. The sand tailings amount to 80.4% of the oil sand. [c] The froth constitutes 7.0% of the oil sand and contains 17.8% fines.

that Fe^{3+} and Al^{3+} are the main cations responsible for the binding of humic and fulvic acids to clays. In such cases the bonding is strong and displacement of the bound metal is difficult, requiring a strong chelating agent. This ties in with the observation that about one-half of the organic carbon in SBS fines cannot be separated from the clays.

For Athabasca oil sands it has been reported that 50–75% of the grains from the tailing sands are stained with a film of iron oxide[12] and it is known that the surface reactions of hydrous oxide-coated clays are dominated by these oxides. Therefore, the possibility exists for strong bonding to stained silica and clay surfaces through coordination (ligand exchange) as well as simple anion exchange mechanisms, examples of which are

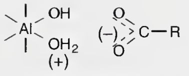

(anion exchange)

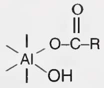

(ligand exchange)

The anion exchange complex can be broken more readily than the ligand exchange complex, releasing the anion (*i.e.*, the humic matter) from the surface.

A model proposed for a clay–humate complex in soil[1] is shown in Figure 8.21. The salient features of the complex are the multitude of bonds between the clay and humic matter, including several hydrogen bonds with the participation of surface-adsorbed water molecules and metal ions serving as bridges with coordination bonds, as well as metal carboxylates. Although some of the individual bonds may be weak, their sum total is such that they constitute extremely strong binding. Some of the adsorbed humic material is hydrophobic and thus, in the oil sand, when it replaces the aqueous film around the clay particle separating the bitumen from the clay surface, it provides a hydrophobic layer capable of forming strong bonding to the bitumen. The fatty acids and other monocarboxylic acids in the chemisorbed organic matter can form carboxylates with the surface metal ions and thus can contribute substantially to the hydrophobization of the clay surface. In soil chemistry, several examples of calcium and magnesium salts of soil fatty acids causing hydrophobization of the soil are known.[1]

Negatively charged clean silica surfaces can also adsorb humic materials and carboxylic acids by means of hydrogen bonding, van der Waals forces and, to a lesser extent, by the participation of metal ion bridges. Some fungi-produced fulvic acids, for example, have been found to cause the hydrophobization of soil.

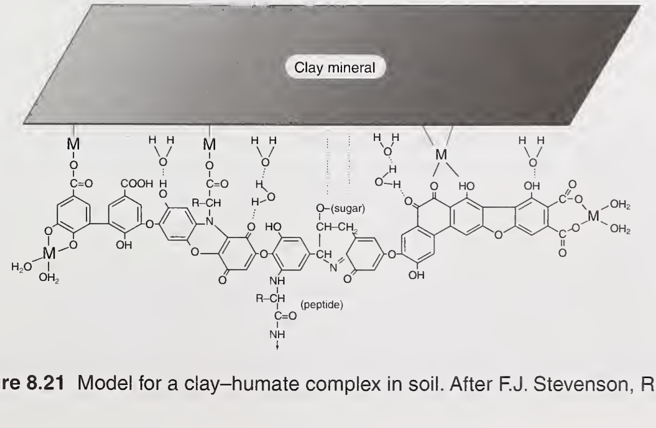

Figure 8.21 Model for a clay–humate complex in soil. After F.J. Stevenson, Ref. 1.

In the oil sand ore at *pH* values of 7–8 the carbonate rocks $CaCO_3$, $MgCO_3$ and $CaMg(CO_3)_2$ have a positive surface charge while $FeCO_3$ has a small negative surface charge.

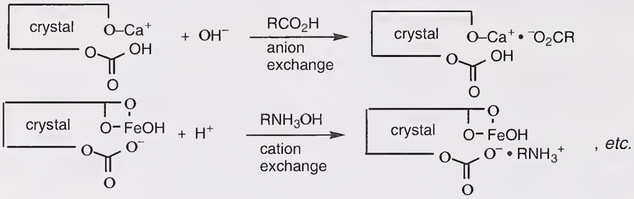

These types of interactions explain the observation[18] made in the hot water separation of Utah (Uinta Basin) oil sands that the carbonate minerals preferentially report with the bitumen stream rather than the tailings stream. The adsorption of carboxylic acids (and other polar molecules) by the anion exchange mechanism renders the carbonate mineral surfaces hydrophobic and thereby bitumen wettable, and thus the minerals float along with the bitumen.

Molecules of humic acids and humins contain many polar functional groups which, for various reasons (steric hindrance, nonavailability of proper surface sites, *etc.*), may not all be bound to the mineral surface. Depending on the nature and number of unbound polar groups the surface property may vary from strongly hydrophobic to strongly hydrophilic, which could markedly affect the processability of the oil sand ore. A strongly hydrophilic organic coating has been identified as the main cause of water retention, resulting in high-water-content products in the hot water separation of the bitumen. Surface coating by the monocarboxylic acids could also lead to the hydrophobization of the mineral surfaces.

Properties of oil sand solids have been shown to correlate and vary progressively with particle size. Thus, the percentage amounts of

- polars I, II; humic acids;
- total extractable $C_{org.}$ and unextractable $C_{org.}$;
- precipitate by NaOH from the HCl extract and the concentrations of Al, K, Fe, Ti, S in the extract and in the solids

all appear to increase with decreasing particle size (<150 μm) of the wet sieved size fractions, Table 8.7, and the advancing process streams, Table 8.10. Scanning electron microscopy—X-ray fluorescence determinations of iron, titanium and sulfur also indicate increased concentrations of these elements in the smaller particle size fractions,[19] Figure 8.22.

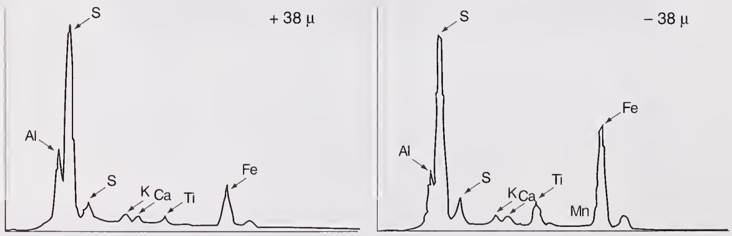

Figure 8.22 X-ray fluorescence spectra of the +38 μ and –38 μ minerals from a high-water-content extraction. After R.J. Mikula *et al.*, Ref. 19.

^{13}C NMR spectra of plant process streams solids,[19] Figure 8.23, suggest increased concentrations of polysaccharides, carboxylic acids and esters, as well as carbonyl carbons (relative to aliphatic carbons) in the smaller particle size fractions and in those oil sands that show poor separability and a high water content in the separation products.

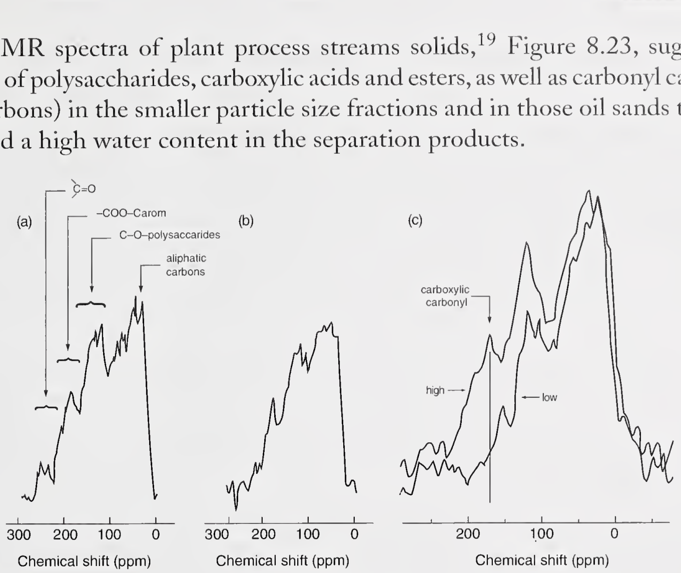

Figure 8.23 ^{13}C NMR spectra of the solids in a) high-water-content and b) low-water-content feedstocks prior to first-stage centrifugation. c) ^{13}C NMR spectra of the solids in high-water-content and low-water-content feedstocks after first-stage centrifugation. Most of the minerals have been removed, leaving only very small particles. After R.J. Mikula *et al.*, Ref. 19.

Another property of oil sand solids that correlates with particle size is surface tension. As shown in Figure 8.24, the surface tension (determined by the freezing front method) of Athabasca (Suncor) centrifuged plant feed solids decreases with decreasing particle size of the fractions and therefore the fraction becomes increasingly hydrophilic and capable of retaining more water. In agreement with this observation it was found that the surface tension of the corresponding solids from high-water-content oil sands is lower than that from low-water-content oil sands (< 29 mJ·m^{-2} *vs* 60 mJ·m^{-2}) and thus the former are more hydrophilic than the latter.

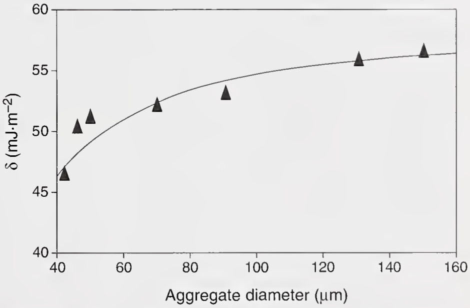

Figure 8.24 Variation in the freezing front surface tension with particle size for centrifuged feed solids. After R.J. Mikula *et al.*, Ref. 19.

In the industrial hot water process most of the insoluble organic matter ends up in the tailing pond sludge. The ^{13}C cross polarization/magic angle spinning NMR spectrum of this sludge from one of Syncrude's tailing ponds, Figure 8.25,[20] shows features in common with the spectrum of the insoluble organic matter separated from the Syncrude oil sand feed, except that the aliphatic portion of the spectrum is more intense here relative to the aromatic portion, indicating a higher relative solubility of the aromatic components in the alkaline process water. In turn, both spectra are quite similar to the spectrum of humic acids (Figure 8.18). In this connection it should be noted that organic-rich solids, as well as humic acids, have also been detected in Utah oil sands by ^{13}C NMR spectroscopy, Figure 8.26. All the humic acid and

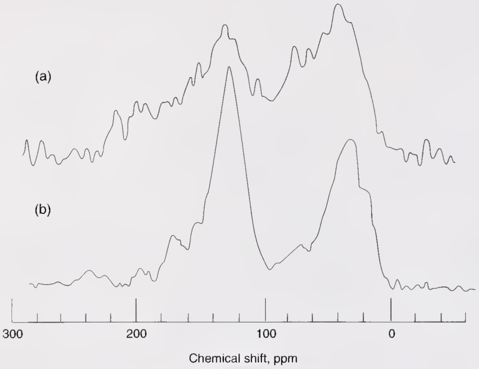

Figure 8.25 Solid-state CP/MAS ^{13}C NMR spectra of insoluble organic matter from sludge (a) and oil sand feed (b). From L.S. Kotlyar *et al.*, Ref. 20. © 1990, Butterworth-Heinemann Ltd.

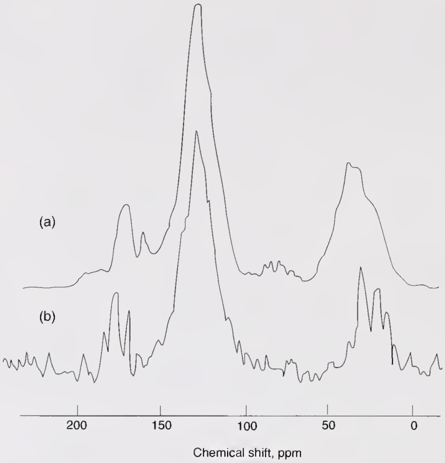

Figure 8.26 Solution ^{13}C NMR spectra of humic acid derived from Athabasca (a) and Utah (b) oil sands. From L.S. Kotlyar *et al.*, Ref. 21. © 1988, Butterworth-Heinemann Ltd.

insoluble organic matter spectra exhibit resonances corresponding to paraffinic/naphthenic carbons, aromatic and heteroaromatic carbons, aliphatic C–O, C–N, carbohydrate, carboxylic acid (ester, amide) and carbonyl (carbonate) carbons in various proportions.

From the above discussion it is seen that essentially all mineral surfaces can bind, with varying bond strengths, polar molecules and that the surface properties of the minerals can thereby be drastically altered—for example, from hydrophilic to hydrophobic. Minerals with strongly hydrophobic surfaces tend to adhere to the bitumen while minerals with strongly hydrophilic surfaces (probably also possessing some hydrophobic sites) tend to retain water in the bitumen during the hot water separation step. Also, chemisorption exerts a protective influence against any chemical alteration of organic matter, as has been observed in petroleum[22] and soil[1] chemistry, and can be credited with the preservation of biologically, chemically and thermocatalytically reactive compounds which otherwise would have been destroyed. From a study of the insoluble organic–inorganic complexes in a Utah oil sand it was concluded that the presence of these complexes is a common feature of oil sands, even from different deposits.[23]

Other compounds tentatively identified in the hot water extracts of Athabasca oil sands, which are extraneous to the bitumen and therefore must have been originally present in the methylene chloride-insoluble fraction, include carbohydrates, amyrins, fridelanone, inositols, *etc.*[24]

3.0 Summary

All Alberta oil sands contain CH_2Cl_2/toluene-insoluble organic components which, according to their origin, are related either to the bitumen or to humic substances such as humins, humic acids and fulvic acids. These humic substances are of terrestrial origin and in all probability preexisted in the sand rock prior to the invasion of the sand by the oil. A portion of the insoluble organic matter is intimately associated with the mineral contents of the host rock, forming strongly-bound complexes. Some of this organic matter can be mobilized by extraction with polar organic solvents (ether, acetone, pyridine), some with aqueous bases or polyphosphates, while others remain insoluble.

The quantity of the insoluble organic matter as well as its composition vary significantly not only from deposit to deposit but also with depth of burial within one deposit. However, it is difficult to correlate them with any given property or known historical feature of the deposit other than the particle size distribution of its mineral content and, specifically, the amounts of fines and clays present. Accordingly, the amount of insoluble organic matter is approximately proportional to the amount of fines present. Even within the fines, the bulk of the insoluble organic matter has been shown to be concentrated in a few percent of the oil sand solids.

Among the bitumen-related compounds identified were suites of acyclic carboxylic acids dominated by their even-carbon-number members. This can be considered to be a clear proof for the occurrence of intense microbiological activities in the deposit in the not-too-distant past. These and other carboxylic acids are present as solutes in the connate water, chemisorbed to sand, clay and mineral surfaces, sparingly-soluble solid salts, ester-bound to humic matter or trapped within the internal cavities of macromolecular structures. All carboxylic acids can be mobilized by sodium hydroxide as carboxylate ions in the connate water, thereby producing a natural surfactant which can promote the separation of the bitumen in the hot water process, as was discussed in Chapter 3. Their strategic location, insofar as being present in the connate water, explains their efficacy in acting as surfactants. Minor components of bitumen-related carboxylic acids are the cyclic terpenoid acids which represent a principal group of carboxylic acids isolated from the bitumen. In addition to carboxylic acids, some polar and nonpolar neutral substances were also isolated.

The bulk of the insoluble organic matter comprises humic substances, humins > humic acids > fulvic acids. Overburdens with low bitumen contents also contain varying amounts of humins along with some humic acids. The humins:humic acids:fulvic acids ratios in the SHG (7 m) and SBS (18 m) samples indicate a very low thermal maturity for these humic substances. With respect to the geothermal maturity status of these sediments, another indicator, in addition to the distribution of the humic materials and the carbon number distribution of the *n*-alkanoic acids, is the vitrinite reflectance of the coal occasionally found in the sand deposits. The reflectance values of the coal specimens found near the Syncrude quarry and in the deeper-lying Peace River deposit both imply a low geothermal maturity status for the sediments, the former corresponding to lignite and the latter to a sub-bituminous rank coal.

The humic materials are strongly bound to the mineral matter in the oil sand rock and only a relatively small fraction would be expected to be mobilized under the relatively mild conditions of the hot water extraction operation. Consequently, they may not play a significant role as natural surfactants. On the other hand, high concentrations of firmly-bound organic matter might affect the separability of the bitumen in a negative way by coating the fine mineral surfaces with a hydrophobic film possessing a high affinity for bitumen. The iron oxide coating reportedly present on the grains of the tailing sands may facilitate the adhesion of the organic matter to the clay as well as to the larger sand particles.

Another large fraction of the insoluble organics recovered comprises the polar neutrals. Its propensity to undergo complexation with $FeCl_3$ (and perhaps with other metal salts), together with its IR spectrum, are indicative of the presence of diketone and/or α,β-unsaturated ketone functionalities. These ketones may be responsible for the active role that iron is thought to play in the mechanism of adsorption of the organic matter on the clay.

In general, the most important mechanisms responsible for the adsorption of insoluble organic matter on electrically-charged clay and mineral particle surfaces are thought to be hydrogen bonding, electrostatic or chemical adsorption, coordination complexing (ligand exchange) and anion exchange. The adsorption of humic matter containing many polar functionalities may change the character of the mineral surface from strongly hydrophobic to strongly hydrophilic, markedly affecting the processability of the oil sand ore: a hydrophobic coating results in the retention of bitumen and a hydrophilic coating may result in water retention.

The complex chemistry associated with the insoluble organic matter is further complicated by the variation of the surface properties of the clays and minerals, owing to cation exchange and dissociation phenomena resulting from changes in the *pH* and salt contents of the process water.

Bibliography

1. F.J. Stevenson, *Humus Chemistry*, John Wiley & Sons, New York, N.Y., 1st Ed., 1982, 2nd Ed., 1994.
2. M.M. Kononova, *Soil Organic Matter*, 2nd Ed., Pergamon, Oxford, U.K., 1966.
3. a) T.M. Ignasiak, Q. Zhang, B. Kratochvil, C. Maitra, D.S. Montgomery and O.P. Strausz, "Chemical and Mineral Characterization of the Bitumen-Free Athabasca Oil Sands Related to the Bitumen Concentration in the Sand Tailings from the Syncrude Batch Extraction Test", AOSTRA J. Res., 2 (1985) 21; b) F.J. Longstaffe, "Clay Mineral Characteristics of Three Different Types of Oil Sand", Report to AOSTRA, Edmonton, AB, 1983; c) T.M. Ignasiak, L. Kotlyar, F.J. Longstaffe, O.P. Strausz and D.S. Montgomery, "Separation and Characterization of Clay From Athabasca Asphaltene", Fuel, 62 (1983) 353.
4. L.D.L. Vorndran, A.J. Serres, J. K. Donnelly, R.G. Moore and D.W. Bennion, "Bitumen Separation for Experimental Use", Can. J. Chem. Eng., 58 (1980) 580.
5. T.D.Cyr and O.P. Strausz, "Bound Carboxylic Acids in the Alberta Oil Sands", Org. Geochem., 7 (1984) 127.
6. D.D. McIntyre, D.S. Montgomery and O.P. Strausz, "Carboxylic Acids Bound to the Mineral Matter in Heavy Cretaceous Oils of Alberta", AOSTRA J. Res., 2 (1986) 223.
7. B.P. Tissot and D.H. Welte, *Petroleum Formation and Occurrence*, Springer-Verlag, Berlin, 1984.
8. L.G. Hepler and R.G. Smith, *The Alberta Oil Sands: Industrial Procedures for Extraction and Some Recent Fundamental Research,* Alberta Oil Sands Technology and Research Authority, Edmonton, AB, 1994.
9. A. Majid, B.D. Sparks and J.A. Ripmeester, "Characterization of Solvent-Insoluble Organic Matter Isolated From Alberta Oil Sands", Fuel, 70 (1991) 78; *idem,* "Characterization of Sedimentary Organic Matter Associated With Inorganic Matrix of Overburden From Alberta Oil Sand Deposits", AOSTRA J. Res., 7 (1991) 111.
10. G. Fritschy and E. Papirer, "Interactions Between a Bitumen, its Components and Model Fillers", Fuel, 57 (1978) 701.
11. M.A. Kessick, "Structure and Properties of Oil Sands", J. Can. Petrol. Technol., 18 (1979) 49; *idem,* "Complex Acids and Their Role in the Stability of Clay Sludges From Oil Sands", Clays Clay Min., 27 (1979) 301.
12. T.J. McLaws, "Silica Sands in the Fort McMurray Area, Alberta", Economic Geology Report 6, Alberta Research Council, 1980, pp. 11, 14.
13. L.G. Morrill, B.C. Mahilum and S.H. Mohinddin, *Organic Compounds in Soils, Sorption, Degradation and Persistence*, Ann Arbor Science Publishers, 1982, p. 38.
14. A. Majid and J.A. Ripmeester, "Isolation and Characterization of Humic Acids From Alberta Oil Sands and Related Materials", Fuel, 69 (1990) 1527.

15. We thank Dr. B.N. Nandi, Department of Energy, Mines and Resources, CANMET, Ottawa, Canada, for this information communicated to us through Dr. D.S. Montgomery.

16. L.S. Kotlyar, B.D. Sparks, H. Kodama and P.E. Grattan-Bellew, "The Distribution of Inorganic Matter–Humic Complexes During a Solvent Extraction–Spherical Agglomeration Process for Bitumen Recovery from an Athabasca Oil Sand", AOSTRA J. Res., 2 (1985) 121.

17. L.S. Kotlyar, B.D. Sparks and H. Kodama, "Isolation and Characterization of Organic-Rich Solids Present in Athabasca Tailings Pond Sludge", AOSTRA J. Res., 6 (1990) 41.

18. K. Bukka, J.D. Miller, F.V. Hansen and A.G. Oblad, "Mineral Matter Distribution During the Hot Water Processing of Utah Tar Sand", AOSTRA J. Res., 7 (1991) 101.

19. R.J. Mikula, D.E. Axelson and D. Sheeran, "Mineral Matter and Clay–Organic Complexes in Oil Sands Extraction Processes", Fuel Sci. Technol. Int'l, 11 (1993) 1695.

20. L.S. Kotlyar, J.A. Ripmeester and B.D. Sparks, "Isolation and Characterization of Various Types of Organic Matter in Oil Sands Tailings Sludge", Fuel, 69 (1990) 1522.

21. L.S. Kotlyar, J.A. Ripmeester, B.D. Sparks and J. Woods, "Comparative Study of Organic Matter Derived from Utah and Athabasca Oil Sands", Fuel, 67 (1988) 1529.

22. P. Peng, A. Morales-Izquierdo, A. Hogg and O.P. Strausz, "Molecular Structure of Athabasca Asphaltene: Sulfide, Ether and Ester Linkages", Energy & Fuels, 11 (1997) 1171; I. Rubinstein, C. Spyckerelle and O.P. Strausz, "Pyrolysis of Asphaltenes: A Source of Geochemical Information", Geochim. Cosmochim. Acta, 43 (1979) 1.

23. L.S. Kotlyar, B.D. Sparks, H. Kodama and P.E. Grattan-Bellew, "Isolation and Characterization of Organic-Rich Solids Present in Utah Tar Sand", Energy & Fuels, 2 (1988) 589.

24. A. Morales, N. Kazmi, E.M. Lown and O.P. Strausz, unpublished results.

9

Reservoir Gases

Oil sand deposits are continuously undergoing slow chemical changes in the reservoir as a result of catalytic and microbiological oxidation, and various other thermocatalytic effects. These chemical changes are accompanied by the evolution of gases and as a consequence, occasional gas pockets can be found in the formation. Thus, the Athabasca deposit is known to contain thin gas zones near the top and zones that once contained gas but now are water-bearing. Some of the gases produced are quite reactive and readily undergo secondary reactions re-converting them to liquid or solid materials. Other components of the gases produced are inert and accumulate in the formation to a stationary concentration, the level of which is governed by their rates of formation, the available void space, and their solubilities and rates of diffusion in the oil sand. Most of the produced gases ultimately escape through the overburden into the atmosphere. Because of the slowness of the process, the occurrence of chemical transformations is difficult to detect by analysis of the bulk composition of the bitumen. It can, however, be readily monitored by measuring the gaseous and low-molecular-weight, volatile materials which are released. Although the total amount of gases present in the oil sands is small, of the order of several parts per million, the gases can be readily measured and can have an influence on the hot water separation of the bitumen by aiding the flotation of the bitumen.

The presence of gases in the oil sands can be visually demonstrated by placing small lumps of fresh oil sands under water and evacuating the flask.[1] Bubbles appear at the surface of the sands and in the beginning they are uncontaminated with oil. However, as more gas evolves, the bubbles become covered with a thin film of oil, which is carried to the water surface. This oil represents volatiles which can be distilled out from the oil sands under reduced pressure at slightly elevated temperatures. Clean sand breaks from the lumps and accumulates at the bottom of the flask. As the pressure is further reduced, gas evolution becomes very rapid and the lumps float. On restoring the pressure

> "the evolution of gases ceases and the lumps sink to the bottom of the flask. If the tar sands are pre-mixed with water and then subjected to a vacuum, particles of oil can be observed to float to the surface by virtue of 'dissolved' gas bubbles, which are held at the surface of these oil particles by a thin film. On breaking the vacuum, these bubbles collapse and the oil particles sink."[1]

In the hot water industrial separation of bitumen, degassing is caused by raising the temperature (to 82°C, which is accompanied by the breakup of the oil sand structure) rather than by pressure reduction.

In quantitative studies the gaseous materials can be collected in a high-vacuum apparatus and analyzed by gas chromatography.

All the oil sand samples studied to date have been found to contain fairly large concentrations of nitrogen along with some argon, neither of which were measured. These gases may be attributed to air trapped in the formation from which the oxygen has been removed by reaction with the bitumen.

The composition of gases (and highly volatiles) from some of the Alberta oil sand reservoirs, namely the Athabasca, Cold Lake and Peace River reservoirs, has been studied.[2–5] The compounds detected were C_1–C_7 hydrocarbons, carbon dioxide, carbon monoxide, carbonyl sulfide, carbon disulfide, hydrogen sulfide, sulfur dioxide, methanol and acetaldehyde. The quantitative results for Athabasca, Cold Lake and Peace River oil sands are given in Tables 9.1–9.4. Measurements were done between 5 and 210°C and from the data it would appear that quantitative degassing of the oil sands by applying vacuum alone cannot be accomplished at room temperatures and that temperatures of 50–60°C are required to liberate the gases trapped in the oil sands. At higher temperatures, on the other hand, thermolysis of the oil sands commences and produces all the gases and highly volatiles which were present at reservoir temperature, 5°C, and therefore it is not possible to differentiate precisely between the quantity of gases which were originally present in the reservoir and those which evolved from thermolysis during the degassing of the samples.

The above results, which are qualitatively similar for all the samples studied, show that the gases originally present in the oil sands were formed from the slow partial thermocatalytic and probably microbial oxidation of the oil sands and the subsequent slow decomposition of the oxidized materials. The occurrence of these processes confers an apparent high degree of thermal reactivity to the virgin oil sands.

Under all conditions the most important gaseous component is carbon dioxide. However, some of the carbon dioxide originates from air, as an artifact of the sample preparation procedure, and some from the carbonate minerals (if present), as has been shown in hydrous pyrolysis experiments. An even smaller portion of the carbon dioxide can come from the disproportionation reaction of carbonyl sulfide[6]

$$2\,COS \rightleftharpoons CS_2 + CO_2 \qquad (1)$$

which forms in the reaction of hydrogen sulfide with carbon monoxide, and with CO_2

$$H_2S + CO \rightleftharpoons H_2 + COS \qquad (2)$$

$$H_2S + CO_2 \rightleftharpoons H_2O + COS \qquad (3)$$

catalyzed by the minerals in the sand.

There are two unusual components of the gases, neopentane, $C(CH_3)_4$, and acetaldehyde, $CH_3C(O)H$. Neopentane is unique among C_5 hydrocarbons in that it has generally been found as only a minor component in crude oils, ranging from 0.1 to 0.7% of the total C_5 hydrocarbons present. Therefore, the presence of neopentane as the major or sole C_5 hydrocarbon in Athabasca and Cold Lake oil sands is thought to be related to the microbiological histories of these oil sand deposits since there are no known thermal processes occurring in petroleum leading to a predominance of neopentane among isomeric C_5 hydrocarbons. In the Peace River deposit, where neopentane is absent, the other C_5 hydrocarbons were more abundant than in the Cold Lake and Athabasca samples.

The other unusual component, acetaldehyde (which is not a regular constituent of petroleum), is a highly reactive molecule and would not be expected to survive significant time periods in the oil sands deposits. The presence of this compound (a characteristic product of the oxidation of hydrocarbons) in Alberta oil sands provides direct evidence for the slow oxidation

Table 9.1 Composition of gases[a] (10^{-8} mol·(kg oil sand)$^{-1}$) evolved from Athabasca (Saline Creek) oil sand at 5 and 25°C[b]

Sample # (depth, m)	1 (9.1)		2 (21.3)	3 (27.4)	4 (32.0)	
Temp., °C	5	25	25	25	5	25
Methane	103	79.7	636	110	678	1,322
Ethylene	0.6	0.7	n.d.[c]	n.o.[d]	n.o.	n.o.
Ethane	90.4	47.2	423	5.6	498	553
Acetaldehyde	198	448	10.0	127	16.1	4.8
Propylene	18.7	17.9	50.0	3.6	12.4	33.6
Propane	11.7	13.6	18.5	1.3	18.9	17.6
i-Butane	65.0	112	208	50.4	122	165
i-Butene	9.4	18.0	22.7	17.8	8.2	11.9
n-Butane	0.6	10.3	3.6	4.0	14.0	24.1
Neopentane	889	1,620	1,860	716	964	1,700
Pentanes + pentenes[e]	5.3	88.7	69.3	67.1	35.4	46.0
C_6	84.1	426	403	225	150	293
C_7	149	271	300	181	162	332
Carbon monoxide	41.8	217	n.o.	47.9	19.9	26.3
Carbon dioxide	8,700	37,100	7,600	6,700	24 ,600	21, 600
Carbonyl sulfide	3.0	4.6	0.7	2.1	0.8	0.9

[a] From O.P. Strausz, Ref. 2. [b] Gases were collected for 5.5 h from each sample. [c] Not determined. [d] Not observed. [e] Exclusive of neopentane.

Table 9.2 Composition of gases[a] (10^{-8} mol·h^{-1}·(kg oil sand)$^{-1}$) evolved from Athabasca oil sand as function of temperature[b]

	Temperature (°C)					
	5	70	95	130	170	210
Methane	20.7	22.6	28.2	45.8	151	540
Ethylene	<0.01	0.06	1.53	2.70	25.3	32.2
Ethane	<0.01	0.57	1.68	3.00	10.8	20.6
Acetaldehyde	0.51	2.36	23.3	30.4	37.5	5.53
Propylene	0.05	0.35	0.93	6.60	32.9	49.1
Propane	0.20	0.43	0.76	6.73	20.2	37.5
i-Butane	<0.01	0.08	0.21	n.d.[c]	1.31	1.98
i-Butene	<0.01	0.13	0.81	0.80	1.24	3.04
n-Butane	<0.01	0.31	1.00	3.47	15.1	12.2
Butenes	<0.01	1.43	n.d.	2.80	9.8	n.d.
Neopentane	24.4	n.d.	32.9	45.5	56.2	81.3
Pentanes + pentenes[d]	<0.01	1.19	13.4	78.2	102	153
Carbon monoxide	<0.01	54.7	113	331	1,160	1,950
Carbonyl sulfide	<0.01	0.38	1.11	n.o.	20.0	18.9
Carbon disulfide	<0.01	<0.01	10.7	9.6	10.0	5.16
Hydrogen sulfide	<0.01	<0.01	<0.01	<2.95	<425	<427
Sulfur dioxide	<0.01	<0.01	0.60	n.d.	66.4	860

[a] From K.N. Jha *et al.*, Ref. 3. [b] Each sample was heated for 5.5 h. [c] Not determined. [d] Exclusive of neopentane.

Table 9.3 Composition of gases[a] (10^{-8} mol·h^{-1}·(kg oil sand)$^{-1}$) evolved from Cold Lake oil sand as function of temperature[b]

	Temperature (°C)					
	5	70	95	130	170	210
Methane	2.20	6.75	11.4	34.8	104.0	691
Ethylene	n.o.[c]	0.58	1.76	7.24	35.0	81.6
Ethane	n.o.	1.30	2.45	4.78	5.16	82.2
Acetaldehyde	1.64	9.9	26.7	15.3	3.42	1.31
Propylene	n.o.	0.75	2.18	12.4	n.d.[d]	89.8
Propane	0.63	1.85	3.04	27.9	n.d.	n.d.
i-Butane	0.63	1.00	1.21	1.53	2.53	n.d.
i-Butene	4.65	6.35	6.95	11.3	23.1	18.9
n-Butane	n.o.	11.6	13.0	14.5	23.7	44.8
Butenes	n.o.	16.4	26.8	27.7	27.7	94.8
Neopentane	12.0	n.d.	n.d.	38.2	n.d.	n.d.
Pentanes + pentenes[e]	0.24	0.97	2.92	6.65	11.3	42.0
C_6	520	687	749	809	840	900
Carbon monoxide	n.o.	13.5	42.0	160	335	871
Carbonyl sulfide	n.o.	0.66	1.85	5.04	9.18	35.5
Hydrogen sulfide	n.o.	n.o.	n.o.	<15.5	<29.1	<351

[a] From K.N. Jha *et al.*, Ref. 3. [b] Each sample was heated for 5.5 h. [c] Not observed. [d] Not determined. [e] Exclusive of neopentane.

Table 9.4 Composition of gases (10^{-8} mol·h^{-1}·(kg oil sand)$^{-1}$) evolved from Peace River oil sand as function of temperature[a]

	Temperature, °C/heating time, h							
	5/5.5	25/5.5	50/5.5	70/5.2	92/3.0	115/2.0	130/2.0	150/1.0
Methane	0.62	0.85	1.4	7.6	20.7	80.1	165	577
Ethylene	n.o.[b]	0.10	10.2	12.7	7.9	24.3	35.8	43.4
Ethane	n.o.	0.03	0.58	6.1	3.2	8.9	20.1	50.5
Methanol	n.o.	n.o.	n.o.	0.11	4.3	11.7	11.6	16.1
Acetaldehyde	0.03	0.18	12.2	26.4	80.2	126	101	155
Propylene	0.10	0.11	10.9	11.6	15.6	37.2	62.6	156
Propane	n.o.	n.o.	1.8	4.2	22.2	12.6	34.7	357
i-Butane	n.o.	n.o.	0.09	0.9	11.6	7.9	20.8	151
i-Butene	n.o.	n.o.	6.3	6.2	8.7	27.5	50.3	124
n-Butane + butenes	n.o.	0.13	0.78	3.0	7.4	17.0	21.8	86.7
Pentanes + pentenes	17.7	26.4	6.7	13.0	65.8	112	170	609
C_6	7.3	9.8	2.7	6.2	10.9	24.9	38.0	119
Carbon monoxide	0.24	0.54	14.4	20.3	483	261	548	2 050
Carbon dioxide	143	500	3,260	6,820	24,300	13,400	26,800	101,000
Carbonyl sulfide	0.03	0.04	0.59	1.30	11.5	20.3	31.8	105

[a] From K.N. Jha *et al.*, Ref. 4. [b] Not observed.

reaction taking place in the deposits. Of the hydrocarbons present, the alkenes are more reactive than the alkanes and in petroleum they are usually found in much lower concentrations than their saturated counterparts; however, in the oil sand gases, the concentrations of the C_2–C_4 alkanes and alkenes are commensurate.

The relative concentrations (taken as the rate of evolution) of neopentane and methane in the samples studied appear to correlate with the depth of burial of the sample,

Sample	Burial depth	Methane*	Neopentane*
Athabasca	9–32 m	20.7–100	24.4–300
Cold Lake	376 m	2.2	12
Peace River	563–573 m	0.6	0

$^{*}10^{-8}$ mol·h^{-1}·(kg oil sand)$^{-1}$

but not with the extent of the biodegradation of the bitumen, which follows the order Athabasca >Peace River > Cold Lake.

As the temperature is raised, thermolysis of the oil sands produces the same gases as originally found to be present at room temperature in progressively increasing quantities, the only exception being acetaldehyde which, not unexpectedly, was found to undergo partial decomposition while being formed and its yield was a maximum at temperatures between 70 and 170℃. The decomposition of acetaldehyde produces carbon monoxide and methane,

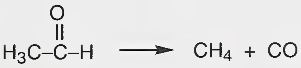

$$H_3C\text{–}\overset{\overset{\displaystyle O}{\|}}{C}\text{–}H \longrightarrow CH_4 + CO \qquad (4)$$

and a fraction of the CH_4 and CO present in the oil sands must have arisen from reaction (4).

In repeated low-conversion thermolysis experiments using the same sample over and over again,[5] Tables 9.5–9.7 and Figure 9.1, it is seen that the yields of each product rapidly decline with thermolysis time, revealing that the precursor of the gaseous products is not the bulk bitumen but some much more reactive components of the oil sand present in quite low concentrations, and that as these precursors are depleted, the gas yields fall. Furthermore, as the data in Table 9.6 indicate, when small quantities of air were accidentally leaked into the sample, the subsequent thermolysis tended to give high yields for all the products, especially for the typical oxidation products acetaldehyde, carbon monoxide and carbon dioxide, along with the appearance of additional oxidation products—methanol, acetone and propionaldehyde. This observation was confirmed by thermolysis experiments[7] carried out at 130℃ in the presence of 150 torr added oxygen, Table 9.8, and varying the oxygen pressure, Figure 9.2. Here we can see increases in the yields not only of the oxygenated but all the hydrocarbon products as well. Consequently, in the light of these results, it is evident that the precursor of the low-temperature decomposition products is not the bulk bitumen but a small quantity of a mildly oxidized fraction of the bitumen and perhaps of chemisorbed organic matter (the humin and the humic and fulvic acids) as well. The oxidation could have occurred, at least partly, microbiologically but as the above data suggest, the nonbiological oxidation by molecular oxygen is very efficient and gives the right products. The efficiencies of both the oxidation and the decomposition reactions are due to the catalytic effects exerted by the mineral components of the oil sand, as will be evident from the results of other experiments to be discussed in a later chapter.

The supply of oxygen may come directly from air through exposure of the oil sand to the atmosphere or, more often, through exposure to surface-derived oxygen-containing meteoric

Table 9.5 Composition of gases (10^{-8} mol·(kg oil sand)$^{-1}$) evolved from Athabasca oil sand as function of time and temperature[a]

	Sample 1 (210°C)			Sample 2 (5.5 h at each successive temp.)			
	0–5.5 h	5.5–12.5 h	12.5–18.0 h	5°C	70°C	95°C	210°C
Methane	2,470	1,440	1,700	114	29.7	36.4	4,240
Ethylene	265	60.9	46.0	<0.1	2.5	5.6	57.6
Ethane	101	86.3	70.1	<0.1	7.1	5.9	165
Acetaldehyde	60.0	5.6	1.3	2.8	90.4	57.6	8.4
Propylene	311	73.6	55.8	0.3	4.3	7.0	413
Propane	196	77.9	60.4	1.1	6.5	4.0	405
i-Butane	2.3	20.1	16.3	<0.1	1.2	<0.1	100
i-Butene	237	113	71.9	<0.1	<1.0	0.7	116
n-Butane	102	70.9	45.3	<0.1	5.0	3.2	282
1-Butene	n.o.[b]	n.o.	n.o.	<0.1	<0.1	0.9	n.o.
2-Butene	n.o.	n.o.	n.o.	<0.1	<0.1	n.o.	n.o.
Neopentane	331	51.4	23.3	134	419	n.d.[c]	392
Pentanes + pentenes[d]	184	96.8	72.1	<0.1	<0.1	8.4	218
Carbon monoxide	10,700	2,600	1,540	n.o.	261	445	14,500
Carbon dioxide	271,000	18,600	11,400	5,860	33,400	12,800	109,000
Carbonyl sulfide	92.3	10.3	16.0	n.o.	4.1	3.0	208
Carbon disulfide	21.9	7.7	9.0	n.o.	<0.1	8.1	19.8
Hydrogen sulfide	<431	<949	<802	n.o.	n.o.	n.o.	<1,400
Sulfur dioxide	n.d.	n.d.	n.d.	n.o.	n.o.	n.o.	1 370
Oxygen	3,350	2,020	3.53	11,000	1,080	5.54	3.75
Nitrogen	20,200	12,400	115	16,600	6,090	179	165

[a] From O.P. Strausz *et al.*, Ref. 5. © 1977, Butterworth-Heinemann. [b] Not observed. [c] Not determined.
[d] Exclusive of neopentane.

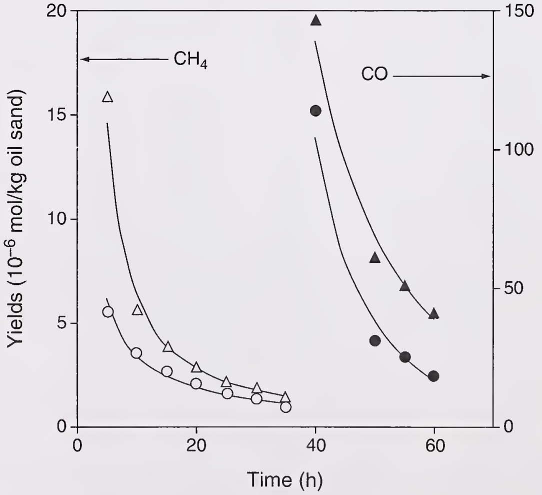

Figure 9.1 Yields of products as a function of successive heating time for an Athabasca oil sand sample. O, ●, CH$_4$ at 150 and 200°C; Δ, ▲, CO at 150 and 200°C.

Table 9.6 Composition of gases (10^{-8} mol·(kg oil sand)$^{-1}$) evolved from an Athabasca oil sand sample as a function of time at 130°C[a]

Time interval (h)	0–5.5	5.5–11.0	11.0–16.5	16.5–22.0	22.0–27.5	27.5–33.0	33.0–38.5	38.5–44.0	44.0–49.5
Methane	262	106	89.5	26.6	38.9	Air leaked in	40.2	16.5	38.1
Ethylene	14.8	13.5	15.3	5.4	8.0		9.0	3.5	7.7
Ethane	16.5	7.0	6.0	2.2	2.7		12.2	2.2	2.2
Acetaldehyde	167	59.7	37.2	8.1	12.0		155	29.5	23.2
Propylene	36.3	23.9	24.4	5.8	9.5		12.1	5.5	7.5
Propane	37.0	63.5	16.0	9.1	8.0		8.2	3.7	5.2
i-Butane	n.o.[b]	n.o.	n.o.	n.o.	n.o.		n.o.	n.o.	n.o.
i-Butene	4.4	n.o.	n.o.	n.o.	0.4		1.8	0.3	0.6
n-Butane	19.1	10.8	11.0	2.7	4.1		7.7	4.2	3.7
Butenes	15.4	7.9	5.8	1.6	1.1		9.6	4.2	2.4
Neopentane	250	61.8	14.5	10.9	14.5		29.4	3.2	5.0
Pentanes + pentenes[c]	430	102	17.3	4.4	3.5		64.6	5.3	8.2
Carbon monoxide	1,820	778	622	172	223	Air leaked in	688	185	247
Carbon dioxide	78,500	21,100	9,640	2,200	2,330		8,890	2,200	2,390
Carbonyl sulfide	n.o.	n.o.	n.o.	n.o.	n.o.		4.2	2.3	n.o.
Carbon disulfide	n.o.	n.o.	n.o.	5.0	4.6		29.3	n.o.	n.o.
Hydrogen sulfide	<16.2	<30.5	<41.5	<8.9	<7.2		<1.4	<8.4	<2.7
Sulfur dioxide	n.o.	n.o.	n.o.	n.o.	n.o.		35.4	49.4	27.2
Oxygen	5,930	114	96	151	213		446	3.0	<1
Nitrogen	15,200	543	412	712	822		15,800	56.5	12.5

[a] From O.P. Strausz *et al.*, Ref. 5. © 1977, Butterworth-Heinemann. [b] Not observed. [c] Exclusive of neopentane.

Table 9.7 Composition of gases (10^{-8} mol·((kg oil sand)$^{-1}$) evolved from an Athabasca oil sand sample as function of time at 170°C[a]

Time interval (h)	0–5.5	5.5–11.0	11.0–16.5	16.5–22.0	22.0–27.5
Methane	832	588	756	296	311
Ethylene	139		74.1	18.1	19.0
Ethane	59.6		39.5	14.3	10.6
Acetaldehyde	206		17.5	92.3	3.2
Propylene	181		62.2	17.3	16.0
Propane	111		42.9	12.0	10.8
i-Butane	7.2		n.o.[b]	0.6	1.5
i-Butene	6.8		7.4	1.8	2.2
n-Butane	82.8		18.6	9.9	8.9
Butenes	53.7		40.3	11.4	13.4
Neopentane	309		164	69.5	24.7
Pentanes + pentenes[c]	55.3		66.0	11.3	14.3
Carbon monoxide	6,360	3,260	2,800	756	774
Carbon dioxide	229,000		25,600	7,250	5,850
Carbonyl sulfide	110		18.6	7.2	4.9
Carbon disulfide	55.1		43.2	8.8	n.o.
Hydrogen sulfide	<2 340		<345	<161	<230
Sulfur dioxide	365		316	124	48.9
Oxygen	8,770	9.6	4.9	23.5	14.6
Nitrogen	18,900	222	300	372	1,120

[a] From O.P. Strausz, *et al.*, Ref. 5. © 1977, Butterworth-Heinemann. [b]Not observed. [c] Exclusive of neopentane.

Table 9.8 Composition of gases (10^{-8} mol·(h^{-1}·((kg oil sand)$^{-1}$) from the oxidation of Athabasca oil sand at 130°C[a,b]

	Oxygen			Oxygen	
	nil	6 mmol		nil	6 mmol
Methane	4.97	81.8	C_5	34.8	37.0
Ethylene	0.82	57.0	C_6	2.74	148
Ethane	1.14	21.6	C_7	3.68	11.5
Propylene	1.95	67.9	Acetaldehyde	5.50	1,640
Propane	0.73	20.1	Acetone	n.o.[c]	459
i-Butane	0.20	1.74	Carbon monoxide	11.1	5,920
i-Butene	0.72	25.7	Carbon dioxide	2,830	56,400
Butane	14.5	29.5	Carbonyl sulfide	0.41	42.2
Butenes	0.35	7.70	Hydrogen sulfide	35.7	n.o.
Neopentane	20.0	n.d.[d]	Sulfur dioxide	n.o.	23.4

[a] From K.N. Jha *et al.*, Ref. 7. © 1978, American Chemical Society. [b] Reactor volume 500 cm^3, 130-g oil sand, O_2 pressure 150 torr. [c] Not observed. [d] Not determined due to the large interfering peak of acetone. Other oxidation products detected were methanol and propionaldehyde.

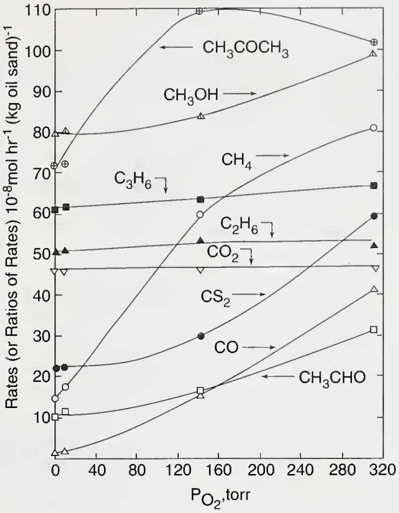

Figure 9.2 Rates or ratios of rates (based on the rate in the absence of O_2) in the thermolysis of 200-g Athabasca oil sands at 130°C as a function of initial oxygen pressure: O, CH_4 (rates); Δ, CO (rate ratios); ❒, CH_3CHO (rate ratios + 10); ●, CS_2 (rates + 20); ▲, C_2H_6 (rates + 50); ■, C_3H_6 (rates + 60); ⊕, CH_3COCH_3 (rates + 70); ◬, CH_3OH (rates + 80). From K.N. Jha *et al.*, Ref. 7.

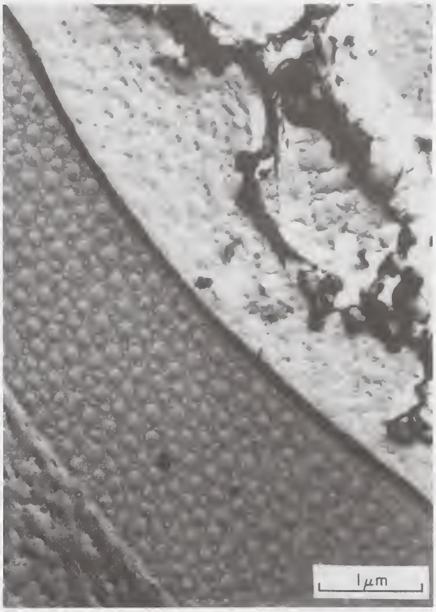

Figure 9.3 A bituminous sand fracture replica of a bitumen emulsion. From J.E. Zajic *et al.*, Ref. 8. © 1981, Butterworth–Heinemann.

water flowing through the deposit. In all cases, parallel to the oxidation of the organic components of the oil sand, the metal sulfides present may experience oxidation as well, as was discussed in Chapter 3, resulting in the formation of sulfate ions and elemental sulfur; however, oxidation of sulfur-containing organic components *via* abiogenic reactions at temperatures below 50°C is quite slow.

We recall here the brief remarks made in Chapter 3 concerning the electron microscopy of freeze-fractured Athabasca oil sands, revealing the presence of densely-packed globular structures in some regions.[8] As the replicated electron micrograph in Figure 9.3 shows, the globules might have been created by the occlusion of some colloidally-dispersed fluid, originally suggested to be the connate water. However, in light of the discussion of the microstructure of oil sands in Chapter 3, it is much more likely that the globules are gas bubbles present or formerly present in the bitumen component of the oil sands.

An important conclusion derived from the above studies on the nature and amounts of gases present in the oil sands is that these gases come from partially oxidized materials in the bitumen. These constituents endow the bitumen with an apparent reactivity which, in earlier days, was inadvertently thought to be an inherent property of the whole bitumen and this reactivity was construed as evidence for a young, thermally immature age and hence an *in-situ* origin for the bitumen.

Bibliography

1. *Oil Sands Composition and Behaviour Research. The Research Papers of John A. Bichard 1957–1965*, Alberta Oil Sands Technology and Research Authority, Technical Publication Series #4, Edmonton, AB, 1987.
2. O.P. Strausz, Final Report, AOSTRA/University Agreement #29, "Determination of Light Gases Present and Those Produced by Thermolysis of Alberta Oil Sands and Components", December, 1979.
3. K.N. Jha, D.S. Montgomery and O.P. Strausz, "Chemical Composition of Gases in Alberta Bitumens and in Low-Temperature Thermolysis of Oil Sand Asphaltenes and Maltenes" in *Oil Sand and Oil Shale Chemistry*, O.P. Strausz and E.M. Lown, Eds., Verlag Chemie, New York, N.Y., 1977, p. 33.
4. K.N. Jha, D.S. Montgomery and O.P. Strausz, "Thermolysis and Oxidation of the Alberta Oil Sand Bitumen", Preprints, Am. Chem. Soc., Div. Fuel Chem., 24 (1979) 260.
5. O.P. Strausz, K.N. Jha and D.S. Montgomery, "Chemical Composition of Gases in Athabasca Bitumen and in Low-Temperature Thermolysis of Oil Sand, Asphaltene and Maltene", Fuel, 56 (1977) 114.
6. F. Faraji, I. Safarik, O.P. Strausz, E. Yildirim and M. Torres, "The CO-Catalyzed Conversion of H_2S to H_2 + Sulfur. Part 2. The Thermal Decomposition of COS", Can. J. Chem. Eng., 77 (1999) 78; F. Faraji, I. Safarik, O.P. Strausz, E. Yildirim and M. Torres, "The Direct Conversion of Hydrogen Sulfide to Hydrogen and Sulfur", Int. J. Hydrogen Energy, 23 (1998) 451.
7. K.N. Jha, P.M. Rao and O.P. Strausz, "Oxidation of the Athabasca Oil Sand and its Fractions", Preprints, Am. Chem. Soc. Div. Fuel Chem., 23 (1978) 91 and unpublished results.
8. J.E Zajic, D.G. Cooper, J.A. Marshall and D.F. Gerson, "Microstructure of Athabasca Bituminous Sands by Freeze-Fracture Preparation and Transmission Electron Microscopy", Fuel 60 (1981) 619.

Chemical Composition of the Saturate Fraction

10

The bulk of crude oil comprises acyclic and cyclic saturated hydrocarbons and aromatic hydrocarbons. Unsaturated hydrocarbons such as alkenes are present only in trace quantities, although a recently published study[1] on the occurrence of alkenes in a large number of Russian crude oils may necessitate revision of this view, and alkynes are altogether absent. The origin of the alkenes in Russian crude oils was attributed to the radiolytic dehydrogenation of the saturated hydrocarbons, due to natural radioactivity. However, in the case of Alberta bitumens and a Lloydminster heavy oil, a careful ^{1}H NMR study indicated an upper limit of only 100 ppm for the concentration of alkenes.[2] The saturated hydrocarbons as a class usually can be quite neatly separated from the rest of the oil by column chromatography on silica gel and alumina followed by silver ion chromatography to remove the small amount of alkenes and aromatic or heteroaromatic compounds which would have co-eluted with the saturates.

This chromatographically separated saturate fraction usually contains only small concentrations of heteroatoms and is almost a pure hydrocarbon mixture. Alberta bitumens and bitumens in general do not contain a high concentration of saturates. This is understandable since bitumens are the residues of the microbiological degradation of crude oils and crude oil-consuming microbes are noted for their selective tastes, having preference for alkanoic hydrocarbons, especially *normal* alkanes. Once *normal* alkanes have been consumed the branched alkanes are attacked, with decreasing preference for increasing extent of branching. Some of the cyclic saturates and aromatics, particularly the monocyclic members, can also be destroyed by microbes, causing the degradation of petroleum in the reservoir. Therefore, since what is left behind is usually the nonbiodegradable portion of the saturates, it does not come as a surprise that the saturate contents of bitumens are low and that the *normal* alkane complement is more or less missing, depending on the extent of degradation the oil has experienced.

Unlike bitumens, conventional crude oils may be quite rich in saturates. Thus, for example, a crude oil from the Turner Valley Formation, southwestern Alberta (Mississippian M2 limestone, depth 2,700 m) was found to contain 64% *n*-alkanes and 82% total saturates. Another light crude from Leduc, central Alberta (Devonian D3 Formation, depth 1,600 m) contained 63.5% *n*-alkanes and 76% total saturates. Such paraffinic oils, if subjected to severe biodegradation, could therefore lose over two-thirds of their mass. The saturate fraction of their residue, which would be similar to a bitumen, would be highly enriched in branched alkanes and naphthenics.

The saturate fractions of bitumens, like the saturate fractions of crude oils, contain some hydrocarbon molecules in unaltered form or in altered but still recognizable forms which are characteristic of life processes. These molecules were produced by living organisms whose bodies provided the biotic source material of the oil either directly or through secondary alterations or by the microorganisms which were associated at one time or another with the sediment containing the original source material. Such fossil molecules are called biological markers and include hydrocarbons such as the acyclic isoprenoids, phytane and pristane, mono-, di- and tricyclic terpenoid hydrocarbons, tetracyclic steranes and the pentacyclic triterpanoids, the hopanes, along with many others. The origin, composition, alterations and organic geochemical significance of biomarkers in general will be discussed in Chapter 13. Here it is only noted that the cyclic terpenoid hydrocarbon biomarkers are, for the most part, much more resistant against microbial attack than the acyclic alkanes and therefore, during microbial degradation of the oil, their relative concentrations will generally be enhanced in the residual bitumen. Consequently, the saturate fractions of Alberta bitumens are fairly concentrated in biomarkers and their biomarker complement—as will be shown later—has a special significance with respect to their overall compositions.

The total saturate contents of Alberta bitumens vary between 14 and 22% as determined gravimetrically by the USBM API–60 or the Syncrude SARA separation procedure.[3,4] Owing to its high H/C atomic ratio, low heteroatom content, Table 10.1, low molecular weight and high volatility (90% distillable at 240℃ and 10^{-3} torr), the saturate fraction is the most valuable fraction of the bitumen.

Table 10.1 Elemental compositions of the saturate fractions of Athabasca and Cold Lake bitumens[a]

	Wt%						MW	H/C
	of maltene	C	H	N	O	S	(g·mol^{-1})	atomic
Athabasca	24.8	85.0	12.9	0.00	0.0	0.15	365	1.82
Cold Lake	29.4	86.6	12.8	0.06	0.0	0.18	n.d.[b]	1.77

[a] From M.L. Selucky *et al.*, Refs. 3 and 4. [b] Not determined.

Since the major compound classes of the bitumen or crude oil comprise a large number of molecules with innumerable individual components, the detection, identification and semiquantitative estimation of these constituent molecules is not a trivial pursuit. In addition to the most common separation methods such as solvent precipitation, vacuum distillation, silica and alumina column chromatography and silver ion thin-layer chromatography, it may be advantageous to employ further adduction chromatographic separations of the various molecular structural types prior to the principal instrumental method of analysis, mass spectrometry. In the case of large, complex molecules and molecular aggregates, it may be necessary to resort to chemical functionalization or thermal and chemical degradative alterations in order to facilitate mass spectral analysis.

1.0 Athabasca Bitumen Saturates

The chemical composition of Athabasca Syncrude high-grade (SHG) maltene (the deasphaltened portion of the bitumen) has been investigated by field ionization mass spectrometry[5–7] (FIMS), Appendix 10.A.1, in the earliest stages of the application of the FIMS method to the investigation of the composition of bitumen and crude oil, pointing to the outstanding utility of this method. FIMS is a powerful analytical tool to probe into the composition of complex hydrocarbon mixtures, owing to the ability of the field ionization process to ionize cyclic hydrocarbon molecules without causing their significant fragmentation. Acyclic hydrocarbons, however, undergo somewhat more extensive fragmentation. Therefore, in the FIMS spectrum of most hydrocarbon molecules essentially only the parent molecular ions appear, which greatly simplifies its evaluation and the identification of component molecules by their elemental formula C_nH_{2n+Z}. Also, the ion yield for cyclic molecules is quite uniform over a broad range of structures and, as a result, the signal intensities, as a first approximation, can be taken to be directly proportional to the sum of the concentrations of the contributing molecules. This strength of the FIMS method is also the source of its weakness, namely, that it can provide the molecular mass of the sample molecules but no further information with regard to the molecular structure, and thus all isomeric molecules present contribute to their common molecular ion signal. An exception is represented by the family of acyclic alkanes, where some limited structural information may be derived from the FIMS spectrum.

Prior to FIMS analysis, the maltene was subjected to a series of chromatographic separations on a silica gel column (2.5 cm × 1 m) resulting in 15 subfractions which were then molecularly distilled at 240°C and 10^{-3} torr pressure. The combined yields of the distillates comprised 66% of the maltene, fractions of which are displayed in Figure 10.1. The elution sequence employed and the yields of the subfractions obtained are listed in Table 10.2. The most volatile of the subfractions (90% distillable) was subfraction 1, comprising mainly saturates and monoaromatics. After molecular distillation, subfraction 1 was rechromatographed on a silver ion on silica gel thin layer plate into four subfractions, Table 10.3. Subfraction 1a, comprising 15.1% (16.8% after correction for nondistillable residue) of the bitumen was found to be composed of saturated hydrocarbons and subfractions 1c and 1d, of monoaromatic hydrocarbons. Subfraction 1b, amounting to only 0.4% of the bitumen, was not analyzed further.

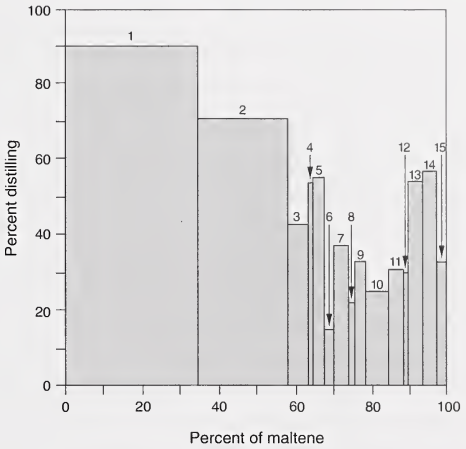

Figure 10.1 Fractionation of Athabasca maltene and distillation data (240°C, 10^{-3} Torr) for the 15 subfractions eluted from silica gel. Compounds heavier than C_{50} do not distill under these conditions. From J.D. Payzant *et al.*, Ref. 5.

The capillary gas chromatogram of subfraction 1a, shown in Figure 10.2, is characterized by a broad unresolved hump superimposed by a large number of sharp peaks corresponding to individual constituent molecules, and is, with some variations, representative of the saturate fractions of all Alberta bitumens. As it happens, the sharp peaks are nearly all due to terpenoid-type biological marker molecules, nearly all of which are cyclic. The designations over the peaks

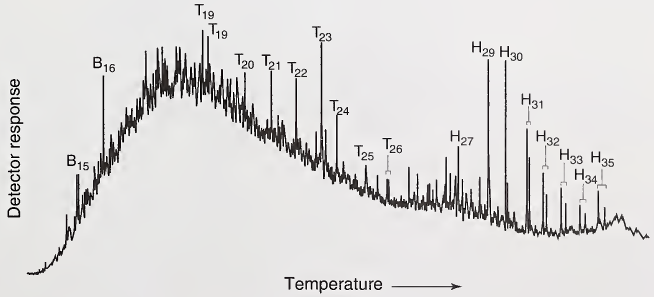

Figure 10.2 Capillary gas chromatogram of subfraction 1a (Table 10.2). The peaks labelled D, T and H are the bicyclic and tricyclic terpenoid hydrocarbons and the hopanes, respectively, and the subscript numbers indicate the number of carbon atoms in the molecule. From J.D. Payzant *et al.*, Ref. 5.

Table 10.2 Chromatography of the maltene fraction of Athabasca bitumen on silica gel[a]

Subfraction	Solvent	Volume (mL)	Wt (g)	% of Maltene	% Distillate	Distillable as % maltene	Color of distillate	Comments
1	*n*-C_5	750	1.7885	35.8	~90	32.2	pale yellow	saturates + monoaromatics
2	10% Bz /*n*-C_5	750	1.1554	23.1	76	17.5	yellow	diaromatics + benzo- and dibenzothiophenes
3	15% Bz /*n*-C_5	750	0.2909	5.8	43	2.5	orange	triaromatics + sulfides
4	10% CH_2Cl_2/*n-C_5*	1,000	0.0501	1.0	54	0.5	orange	nitrogen compounds
5	25% CH_2Cl_2/*n-C_5*	750	0.1573	3.1	55	1.7		nitrogen compounds
6	50% CH_2Cl_2/*n-C_5*	75	0.1259	2.5	15	0.38		nitrogen compounds
7	50% CH_2Cl_2/*n-C_5*	625	0.1987	4.0	37	1.5		mixture of nitrogen compounds and fluorenones
8	100% CH_2Cl_2	100	0.0734	1.5	22	0.33	bright red	fluorenones
9	100% CH_2Cl_2	650	0.1153	2.3	33	0.76	dull red	mixture of fluorenones and fluorenols
10	10% ethyl acetate/CH_2Cl_2	75	0.3235	6.5	25	1.63		fluorenols
11	10% ethyl acetate/CH_2Cl_2	675	0.2089	4.2	31	1.3		complex mixture
12	1% *i*-propanol/CH_2Cl_2	600	0.0253	0.5	–	–		
13	2% CH_3OH/CH_2Cl_2	1,000	0.2145	4.3	54	2.3		carboxylic acids
14	2% CH_3OH/CH_2Cl_2	1,000	0.1898	3.8	57	2.2		carboxylic acids and sulfoxides
15	15% CH_3OH/CH_2Cl_2	650	0.1451	2.9	33	0.96		sulfoxides
Total				101.3		65.76		

[a] From J.D. Payzant *et al.*, Ref. 5.

Table 10.3 Refractionation of the saturate subfraction 1 using Ag⁺–TLC chromatography[a]

Subfraction	*Rf* range	% of subfraction 1	maltene	bitumen	Color
1a	0.85–1.0	56.4	18.2	15.1	colorless
1b	0.6–0.85	1.6	0.5	0.4	colorless
1c	0.3–0.6	25.0	8.1	6.7	colorless
1d	0.0–0.3	17.0	5.5	4.5	pale yellow
		100.0	32.3	26.7	

[a] From J.D. Payzant *et al.*, Ref. 5.

indicate bicyclic (B), tricyclic (T), and pentacyclic (hopanoid, H) terpenoid hydrocarbons with carbon numbers indicated in the subscript. The nature and distribution of biological markers in the saturate fraction will be briefly discussed later in this chapter and more extensively in Chapter 13.

The FI mass spectrum of subfraction 1a is shown in Figure 10.3. The height of any given peak may be taken to be directly proportional to the sum of the concentrations of the individual compounds with the same molecular mass responsible for the peak. Therefore, since the individual compounds are recognized and distinguished by their molecular mass only, all isomeric compounds appear in a single peak. Since this fraction contains only saturated hydrocarbons the "n" and "Z" numbers in the empirical formula C_nH_{2n+Z} identify a compound by its carbon number and number of rings. For example, in the inset enlargement of Figure 10.3 the set of peaks clustered around mass 456 are all C_{33} compounds with varying numbers of hydrogens: mass 452 with elemental formula $C_{33}H_{56}$ (C_nH_{2n-10}), mass 454 with elemental formula $C_{33}H_{58}$ (C_nH_{2n-8}) and likewise 456, $C_{33}H_{60}$ (C_nH_{2n-6}); 458, $C_{33}H_{62}$ (C_nH_{2n-4}); 460, $C_{33}H_{64}$ (C_nH_{2n-2}); 462, $C_{33}H_{66}$ (C_nH_{2n}). The number of rings in the molecule can be obtained from the value of Z: $Z = 0$ indicates a monocyclic hydrocarbon, $Z = -2$ a bicyclic hydrocarbon, *etc.* For an acyclic paraffin, Z would be +2. Thus, we can see that the C_{33} compounds of the

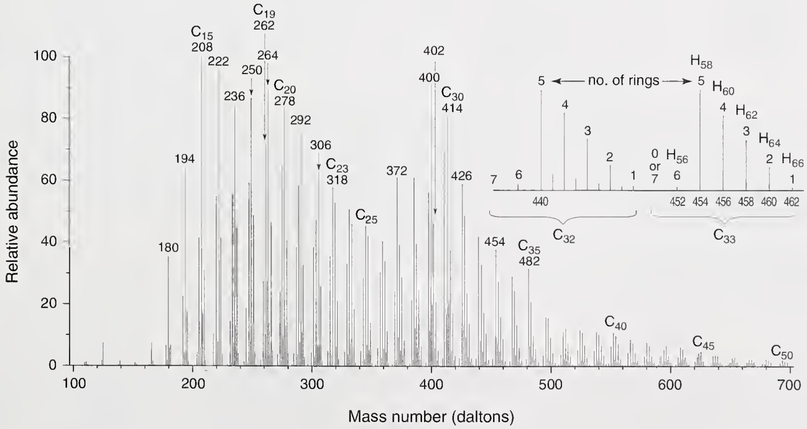

Figure 10.3 Field ionization mass spectrum of subfraction 1a (Table 10.2). The peaks at $m/z = 208, 222, 236$, *etc.*, correspond to C_nH_{2n-2} (bicyclic) compounds with maxima at $n = 15$, 16 and 17; at $m/z = 262, 318, 402$, *etc.*, to C_nH_{2n-4} (tricyclic) compounds with maxima at $n = 19$, 23 and 29; at $m/z = 372, 400, 414$, *etc.*, to C_nH_{2n-6} (tetracyclic) compounds with maxima at $n = 27$, 29 and 30; and at $m/z = 426, 454, 482$, *etc.*, to C_nH_{2n-8} (pentacyclic) compounds with maxima at $n = 31$, 33 and 35. The inset of the C_{32} cluster peaks includes the odd-mass-numbered peaks to illustrate that cracking, which produces mainly odd-mass-numbered fragments with mass values lower than the mass of the parent molecule, does occur to a small extent. Also, a fraction of the odd-mass-numbered peaks appearing are due to the natural abundance of the ^{13}C isotope. From J.D. Payzant *et al.*, Ref. 5.

saturate fraction comprise mono- through hexacyclic alkanes and that acyclic and heptacyclic alkanes are practically absent. At this carbon number the most abundant cyclic compounds are the pentacyclics followed by, in decreasing order of importance, the tetra-, tri-, bi-, hexa- and monocyclics. At a different carbon number the relative order of abundance by the number of rings may be different. In the C_{20} cluster for example, the 278 mass peak corresponding to $C_{20}H_{38}$ bicycloalkanes is the most intense, followed by the mass 276, 280 and 274 peaks representing the tricyclic, monocyclic and tetracyclic alkane series, respectively. Acyclic and pentacyclic hydrocarbons are present but in very small quantities at this carbon number, and hexacyclic hydrocarbons are absent.

Alternatively, the data in Figure 10.3 can be replotted in such a way that they display the relative abundance of the member compounds in each C_nH_{2n+Z} series with respect to their carbon number. These displays of the data are shown for the mono-, bi- and tricycloalkanes in Figure 10.4 and for the tetra- and pentacyclic series in Figure 10.5. The concentration maxima occur at C_{18}, C_{15}, C_{19}, C_{29}, C_{30} and C_{40} for the mono-, bi-, tri-, tetra-, penta- and hexacyclic series, with local maxima as summarized in Table 10.4. This trend by and large follows the one established for hydrocarbon biomarker molecules in the saturate fraction, as will be discussed

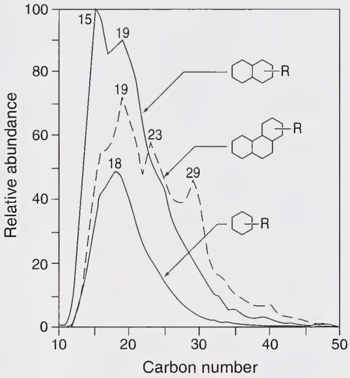

Figure 10.4 Relative abundances of the mono-, bi- and tricyclic hydrocarbons in the saturates, subfraction 1a, as a function of carbon number. From J.D. Payzant *et al.*, Ref. 5.

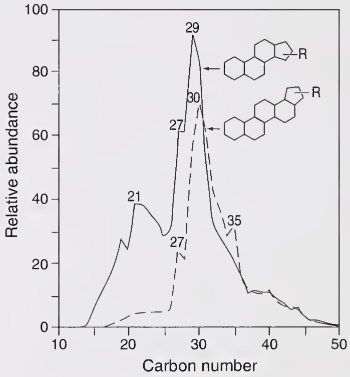

Figure 10.5 Relative abundances of the tetra-and pentacyclic hydrocarbons in the saturates, subfraction 1a, as a function of carbon number. From J.D. Payzant *et al.*, Ref. 5.

Table 10.4 Gravimetric composition of Athabasca saturate subfraction 1a as determined by FIMS[a]

Formula	Series	C_{max}	Relative abundance (%) in subfraction 1a	% of maltene	% of bitumen
C_nH_{2n+2}	acyclic	19	0.3	0.05	0.04
C_nH_{2n}	monocyclic	18	11.1	2.02	1.68
C_nH_{2n-2}	bicyclic	15, 19	28.3	5.15	4.27
C_nH_{2n-4}	tricyclic	19, 23, 29	24.6	4.48	3.72
C_nH_{2n-6}	tetracyclic	29, 27, 21, 19	21.4	3.89	3.23
C_nH_{2n-8}	pentacyclic	30, 35, 27	12.7	2.31	1.92
C_nH_{2n-10}	hexacyclic	40	1.5	0.27	0.23
Total			99.9	18.2	15.1[b]

[a] From J.D. Payzant *et al.*, Ref. 5. [b] After correction for nondistillable residue, the saturate content of the bitumen becomes 16.8%.

shortly, and suggests the existence of a close genetic relationship between the bulk saturates and the saturated hydrocarbon biomarkers in the bitumen. The most abundant biomarkers identified were all cyclic terpenoid, along with some steroid, hydrocarbons.

The weight percent distribution of the saturates according to the number of rings in the Athabasca bitumen can also be determined from the data in Figure 10.3 and the results are given in Table 10.4. The most abundant are the bicyclics followed by, in decreasing order of importance, the tri-, tetra-, penta-, mono-, hexa- and acyclics in an aggregate amount of 15.1(16.8)% in terms of the bitumen.

While FIMS provides invaluable information on the carbon number distribution of the individual C_nH_{2n+Z} series, it says nothing about the structures of the individual isomers. To obtain this information it is necessary to concentrate desired fractions by chromatographic procedures and to analyze the fractions by GC–MS. Individual peak assignments are then made by comparison of the MS and GC retention time data with those of authentic standards if such standards are available. Some of the components of the saturate fraction of petroleum can be selectively removed from the mixture by adduction chromatography, Appendix 10.A.2, as indicated in Figure 10.6[8] to yield completely separated or highly enriched fractions.

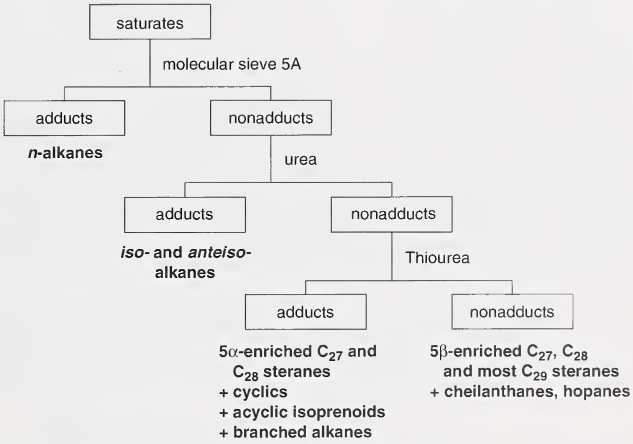

Figure 10.6 Chromatographic separation scheme for the components of the saturate fraction.

By analogy to the adduction of *n*-alkanes to 5A molecular sieve, molecular sieve 1310 (zeolite Na10) with a larger pore diameter of 9–10 Å is capable of removing bi-, tri- and pentacyclic terpanes from the saturate fraction by adsorption or adduction.[9] The diameters of these cyclic terpenoid molecules are commensurate with the pore diameters of the zeolite Na10 and therefore their adsorption energy is relatively large compared to the smaller or larger diameter member molecules of the saturate fraction.

The zeolite adduct (ZA) fraction from Athabasca saturates, as seen from the comparison of its gas chromatogram (Figure 10.7) with that of the total saturate fraction (Figure 10.2), is essentially composed of the skimmed-off biomarkers of the saturate fraction.

At this point we digress a little, to very briefly explain the different gas chromatographic–mass spectrometric (GC–MS) methods of analysis with respect to data aquisition and manipulation. When the data aquisition is performed by fully scanning the complete operational mass range, the total ion current (TIC) is recorded as a function of the retention time of the chromatographic eluate. The TIC chromatogram contains all the ion intensities produced and measured in each scan; in other words, a complete mass spectrum is recorded in every scan, allowing structural identifications to be made for those chromatographic peaks which are sufficiently clean and intense. Now, if one is searching for a particular compound class, for which a fragment ion is known to be characteristic and intense, the scans having that specific

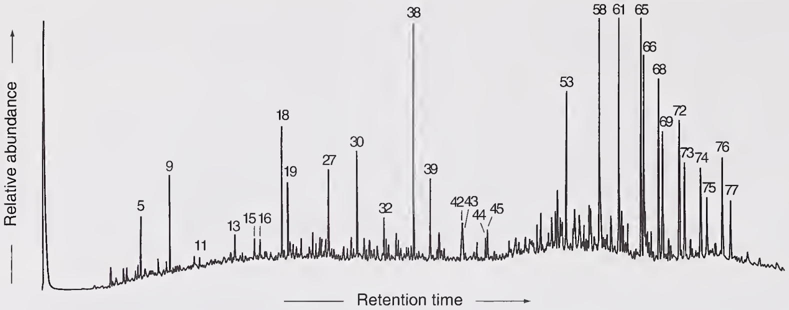

Figure 10.7 Capillary gas chromatogram of the zeolite 1310 adduct fraction of the Athabasca saturate fraction. The peak assignments are listed in Table 10.5. From A. Dimmler *et al.*, Ref. 8. © 1984, Elsevier Science Ltd.

fragment ion can be extracted from the TIC chromatogram with the proper software to produce a single ion chromatogram (also called a "cross scan" chromatogram) containing only the chromatographic peaks that show that particular ion in their mass spectra. This allows the assignment of carbon number distributions in homologous and speudo-homologous series. Another way to accomplish the same goal, provided that the specific fragment ions of the target compounds are known, is to acquire the data by monitoring the fragment ion intensities as a function of GC retention time rather than scanning the complete mass spectrum for the whole run time. The information provided by the full mass spectrum is lost but the relative sensitivity is increased because the signal-to-noise ratio for the target compounds is improved and the chromatogram obtained is usually very clean. This approach is known as selected-ion monitoring (SIM) or single-ion recording (SIR).

The usefulness of single-ion chromatograms can be readily seen by the examples of the mass spectra of compounds containing the (bicyclic) drimane ring system

Bicyclic I

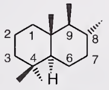

1, $C_{15}H_{28}$
8β(H)-drimane

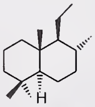

2, $C_{16}H_{30}$

which feature a base peak at *m/z* = 123

m/z = 123

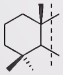

and those of tricyclic triterpanes which feature a base peak at *m/z* = 191:

Tricyclic II

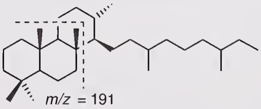

The drimane molecule is a member of the terpane family of hydrocarbons which are derived by the combination of isoprene units. Drimane is built from the "head-to-tail" combination of three isoprene units followed by cyclization:

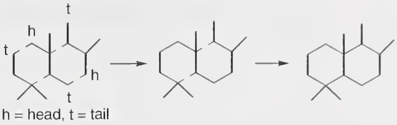

The *m/z* = 123 and 191 chromatograms of the ZA fraction are shown in Figure 10.8 and the assignments of the peaks labeled 1–77 are given in Table 10.5. The compounds denoted as bicyclic I contain an 8β(H)-drimane ring system and an isoprenoid alkyl group at C_9, and range from C_{15} to C_{24}. Among the bicyclic compounds, those represented by peak 5 (drimane **1**) and peak 9 (its methyl derivative **2**) are the most prominent. The tricyclic II peaks range from C_{19} to C_{30} with the C_{23} member

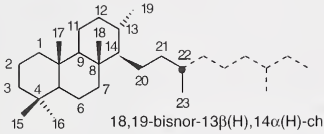

18,19-bisnor-13β(H),14α(H)-cheilanthane

being the most abundant.[10,11] From C_{25} on the series members occur as diastereomer pairs owing to the presence of the C_{22} chiral center. There are also other isomers with unidentified structures present in lesser quantities. The largest number of isomers, five, occurs at C_{19}. Altogether 27 tricyclics have been detected, 16 of which belong to the tricyclic II series. The latter all-head-to-tail hexaprenoid triterpane series were first identified in Athabasca saturates and subsequently found to be identical with the ubiquitous tricyclic hydrocarbon biomarkers (whose structure had not been previously identified) present in all petroleums.

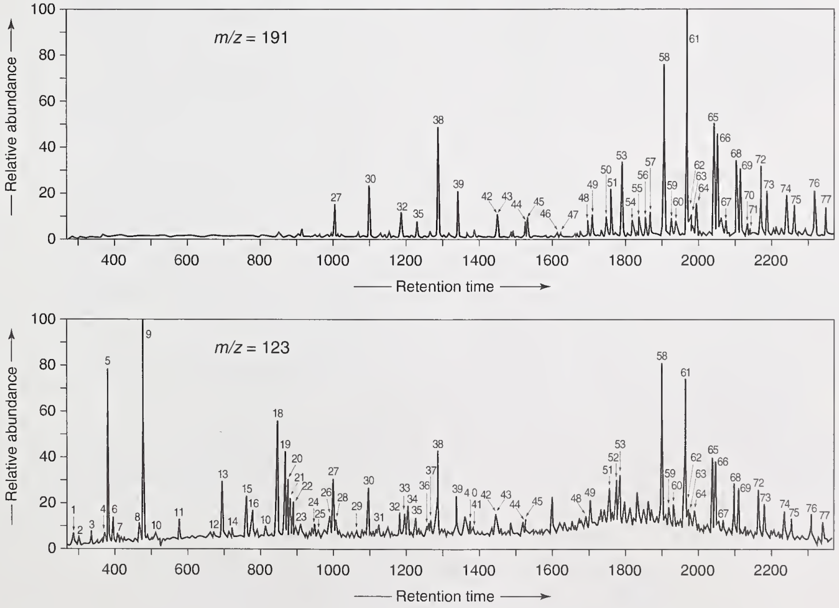

Figure 10.8 GC–MS chromatograms of the zeolite 1310 adduct fraction from Athabasca bitumen showing the *m/z* = 191 and 123 cross scans. The peak assignments are listed in Table 10.5. From A. Dimmler *et al.*, Ref. 8. © 1984, Elsevier Science Ltd.

Table 10.5 Peak assignments for the chromatogram shown in Figure 10.7[a]

Peak No.	Assignment	Peak No.	Assignment
1	C_{16} bicyclic	40	C_{23} tetracyclic
2	C_{16} bicyclic	41	C_{24} tricyclic
3	C_{15} bicyclic	42	C_{25} tricyclic, II
4	C_{15} bicyclic	43	C_{25} tricyclic, II
5	C_{15} bicyclic, I	44	C_{26} tricyclic, II
6	C_{15} bicyclic	45	C_{26} tricyclic, II
7	C_{15} bicyclic	46	C_{27} tricyclic, II
8	C_{16} bicyclic	47	C_{27} tricyclic, II
9	C_{16} bicyclic, I	48	C_{28} tricyclic, II
10	C_{17} bicyclic	49	C_{28} tricyclic, II
11	C_{17} bicyclic, I	50	C_{29} tricyclic, II
12	C_{18} bicyclic	51	C_{29} tricyclic, II[b]
13	C_{18} bicyclic, I	52	C_{29} sterane[c]
14	C_{19} bicyclic	53	C_{27} hopane
15	C_{19} bicyclic, I	54	C_{28} hopane[c]
16	C_{19} tricyclic	55	C_{30} tricyclic, II[c]
17	C_{19} bicyclic	56	C_{30} tricyclic, II
18	C_{19} tricyclic, II	57	C_{28} hopane[c]
19	C_{19} tricyclic	58	C_{29} hopane
20	C_{19} tricyclic	59	C_{30} hopane-like
21	C_{20} bicyclic	60	C_{29} moretane
22	C_{20} bicyclic, I	61	C_{30} hopane
23	C_{19} tricyclic	62	C_{30} hopane-like
24	C_{20} tricyclic	63	C_{30} hopane-like
25	C_{20} tricyclic	64	C_{30} moretane
26	C_{20} tricyclic	65	C_{31} 22S-hopane
27	C_{20} tricyclic, II	66	C_{31} 22R-hopane
28	C_{21} bicyclic, I	67	C_{31} moretane
29	C_{21} tricyclic	68	C_{32} 22S-hopane
30	C_{21} tricyclic, II	69	C_{32} 22R-hopane
31	C_{21} tricyclic	70	C_{32} moretane
32	C_{22} tricyclic, II	71	C_{32} moretane
33	C_{23} bicyclic, I	72	C_{33} 22S-hopane
34	C_{23} bicyclic, I	73	C_{33} 22R-hopane
35	C_{23} tricyclic	74	C_{34} 22S-hopane
36	C_{24} bicyclic, I	75	C_{34} 22R-hopane
37	C_{24} bicyclic, I	76	C_{35} 22S-hopane
38	C_{23} tricyclic, II	77	C_{35} 22R-hopane
39	C_{24} tricyclic, II		

[a] From A. Dimmler *et al.*, Ref. 8. © 1984, Elsevier Science Ltd. [b] Plus 18α(H)-22,29,30-trisnorhopane. [c] A second component was also present.

The pentacyclic hopanoid hydrocarbons which also have a base peak at *m/z* = 191, *e.g.*,

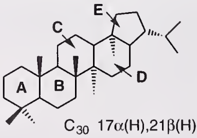

C_{30} 17α(H),21β(H)-hopane

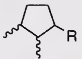

R = H, CH_3, C_2H_5, i-C_3H_7, ...to i-C_8H_{17}

are well-known biomarker components of petroleum and their distribution in Athabasca and Alberta oil sand bitumens in general is typical of their distribution in mature oil,[10] ranging from C_{27} to C_{35} (and less often to C_{37}). Owing to the presence of the chiral center at C_{22},

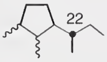

the C_{31}–C_{35}(C_{37}) members of the series appear as diastereomer pairs, the biologic 22R epimer eluting somewhat after the geologic (thermally produced) 22S epimer, featuring the typical mature hopane pattern as seen in Figures 10.2, 10.7 and 10.8. The most abundant in the series are the C_{29}, C_{30} and C_{31} members.

Another important series of cyclic biomarkers comprises the tetracyclic steranes:

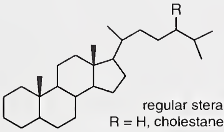

regular sterane
R = H, cholestane $C_{27}H_{48}$

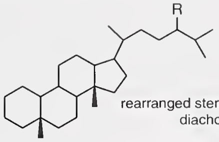

rearranged sterane (diasterane), diacholestane

The distribution of the steranes can be severely affected by biodegradation[12] and indeed, Athabasca and other Alberta bitumen samples contain only small amounts of C_{27}–C_{29} regular steranes. Most of the steranes are rearranged diasteranes which are little affected by biodegradation, and their maximum concentration occurs at C_{21} and in the C_{27}–C_{29} range,[13] Figure 10.9.

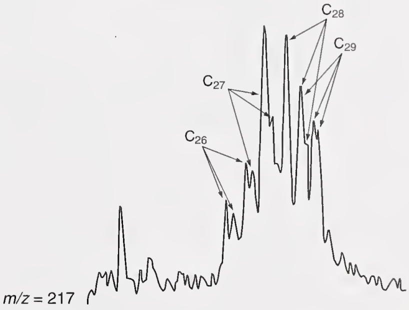

Figure 10.9 GC–MS $m/z = 217$ cross scan of the steranes in the Athabasca TUNA fraction. From I. Rubinstein and O.P. Strausz, Ref. 13. © 1979, Elsevier Science Ltd.

The concentration maxima of the bicyclic (C_{15} and C_{16}), tricyclic (C_{19} and C_{23}), and pentacyclic (C_{29} and C_{30}) terpanes as well as those of the tetracyclic C_{21}, C_{27}–C_{29} steranes isolated from the saturate fraction of Athabasca bitumen closely correspond to the concentration maxima in the distribution of the di-, tri- , tetra- and pentacyclic components of the saturate fraction, Figures 10.4 and 10.5. This correlation between the concentration distribution of the biological marker series and the series of cyclic components of the saturate fraction of the bitumen cannot be coincidental and it is taken as a manifestation of their genetic relationship. From this, it is concluded that the saturate fraction of the bitumen is mainly composed of a complex mixture of cyclic terpenoid and steroid biomarker molecules and their isomerization and degradation products which survived the thermal and microbial degradation of the precursor oil, along with lesser quantities of alkylcyclohexanes, alkyldecalins, *etc.*

Monocyclic terpenoid hydrocarbons have not been detected in Athabasca or any other Alberta saturates. The absence of this class of terpenoid compounds in the saturates is puzzling since, as will be shown in Chapter 11, a monocyclic terpenoid hydrocarbon framework is present in the maltene in functionalized form as a series of bicyclic sulfides.[14] Along with this series of sulfides there are also series of tri-, tetra- and hexacyclic sulfides corresponding to the bi-, tri- and pentacyclic terpenoid hydrocarbons present in the saturate fraction. The most abundant of the cyclic terpenoid sulfide series is the bicyclic series, which, on hydrodesulfurization, is converted to monocyclic terpane, yet this is the only one which does not appear to occur in hydrocarbon form in the saturate fraction.

2.0 Other Alberta Bitumen Saturates

The saturate fractions of essentially all the oil sands and carbonate bitumens and Cretaceous heavy oils of the Western Canada Sedimentary Basin show quite similar distributions of biological markers. The differences in the distributions of these markers and those of the *n*-alkane and cycloalkane contents of the saturates are more related to the extent of their biodegradation than to the differences in their original composition.

FIMS studies on Cold Lake saturates[15] yielded the data on the concentration versus the number of rings in the molecules listed in Table 10. 6 for the thiourea adduct (TUA) and nonadduct (TUNA) and their sum. The total amount of the TUA is about 7–12% of the saturates and that of TUNA is 88–93% (the corresponding values for Athabasca saturates are 5 and 95%). The distribution here is similar to that determined for Athabasca saturates with the exception of the relatively higher abundance of the acyclic and monocyclic series, in agreement with the generally held view of the less biodegraded status of the Cold Lake bitumen. The distribution according to ring number follows the order di- > mono- > tri- > tetra- > penta- > acyclic > hexacyclic in a total amount about 3–4% higher than in the case of the Athabasca material.

Table 10.6 Gravimetric composition of the Cold Lake saturate fraction as determined by GC–FIMS[a]

Formula	Series	Relative abundance (%) in		Total, % of bitumen
		TUA[b]	TUNA[c]	
C_nH_{2n+2}	acyclic	5	3	0.66
C_nH_{2n}	monocyclic	27	23	4.82
C_nH_{2n-2}	bicyclic	36	28	5.94
C_nH_{2n-4}	tricyclic	17	19	3.85
C_nH_{2n-6}	tetracyclic	9	15	2.92
C_nH_{2n-8}	pentacyclic	4	9	1.72
C_nH_{2n-10}	hexacyclic	2	3	0.59
Total		100	100	20.5

[a] From J.D. Payzant *et al.*, Ref. 15. © 1980, Elsevier Science B.V. [b] Thiourea adduct fraction. [c] Thiourea nonadduct fraction.

The Cold Lake saturates contain small quantities of *n*-alkanes displaying a smooth unimodal distribution[4] up to at least C_{33}, Figure 10.10, and a series of acyclic isoprenoids, Figure 10.11. The latter are dominated by the phytane (C_{20})–pristane (C_{19}) pair

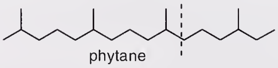

phytane
m/z = 183

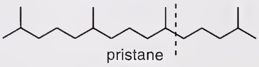

pristane
m/z = 183

and they present a curious pattern of pairs of peaks at C_{24}/C_{25}, C_{29}/C_{30}, C_{34}/C_{35}, C_{39}/C_{40} and probably C_{14}/C_{15},[15] resembling the distribution of C_{18}–C_{40} isoprenoid hydrocarbons found in conventional crude oils and assigned to the head-to-head and head-to-tail linked C_{40} isoprenoids

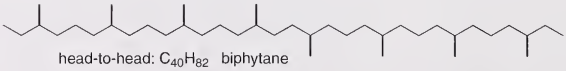

head-to-head: $C_{40}H_{82}$ biphytane

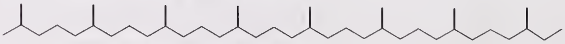

head-to-tail: $C_{40}H_{82}$ biphytane

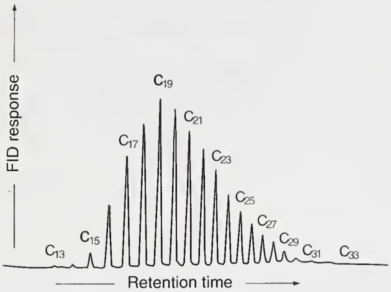

Figure 10.10 Gas chromatogram of the *n*-alkane fraction of Cold Lake bitumen. From M.L. Selucky *et al.*, Ref. 4. © 1978, Butterworth-Heinemann.

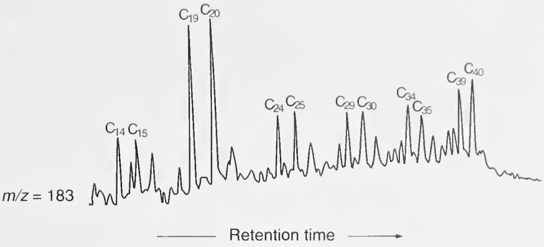

Figure 10.11 GC–MS $m/z = 183$ cross scan of the acyclic isoprenoids in the TUA fraction of Cold Lake bitumen. From J.D. Payzant *et al.*, Ref. 15. © 1980, Elsevier Science B.V. A similar series has also been detected in the TUA fraction of Leduc conventional oil.[6]

along with their diagenetic debris, indicative of archaebacterial lipid input in the biotic source material of the crude oil.[16,17] Additionally, the isomeric lycopane, featuring a tail-to-tail linked biphytane

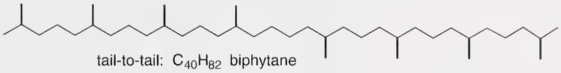

and the cyclic $C_{40}H_{80}$ and $C_{40}H_{78}$ isoprenoids

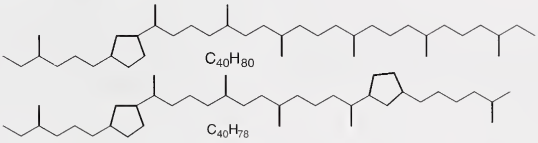

may also be present.

Further studies on Cold Lake saturates were carried out using a FIMS instrument interfaced with a gas chromatograph (GC–FIMS) to permit a limited resolution of the isomeric species. This instrument was one of the first of its kind reported in the literature and the first one introduced into petroleum chemistry.[6,7,15,18] The FI mass chromatograms showing the distribution of the mono-, bi- and tricyclic alkanes in the TUA fraction are given in Figures 10.12–10.14 which show the scans for only every third carbon number (*n*) series for visual clarity and ease of interpretation. In each figure at each value of *n* the presence of several isomers is revealed. The number of isomers increases with increasing *n* and number of rings. Thus, in the case of the C_{16} monocyclics, Figure 10.12, eight isomers are discernible, while for the C_{14} tricyclics, Figure 10.14, 12 or more isomers are in evidence. For the monocyclics, the cross scans for $m/z = 83$ and 97, which are the major fragment ions in the mass spectra of alkylcyclohexane and alkylmethylcyclohexane,

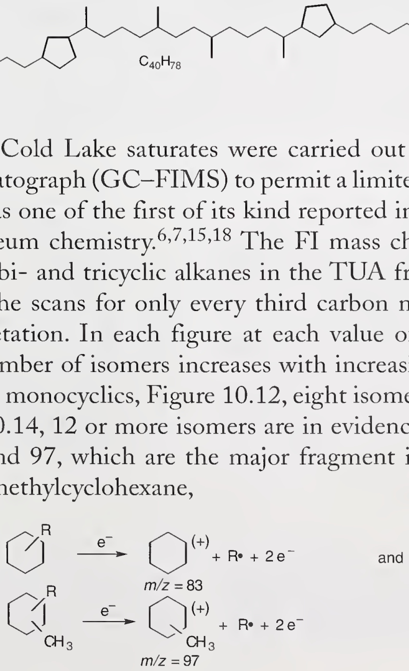

indicate that two of the isomeric series are alkyl- and methylalkyl cyclohexanes. The other isomers are probably terpane-derived species. Similarly, there are two isomeric bicyclic series, the *m/z* = 137 and 151 fragmentograms of which are shown in Figure 10.15. By analogy with the *m/z* = 83 and 97 fragments due to the cyclohexyl and methylcyclohexyl ions, as was observed in the monocyclic series, the *m/z* = 137 and 151 fragments were believed to signal the presence of the decalyl and methyldecalyl ions:

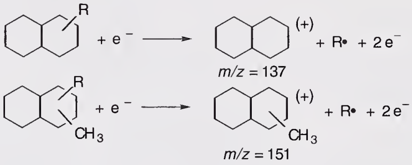

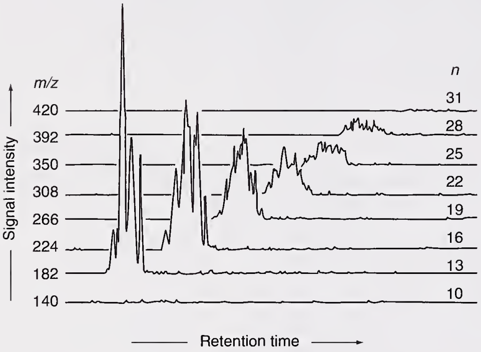

Figure 10.12 GC–FIMS scan of the molecular ions of the C_{10}, C_{13}, C_{16}, C_{19}, C_{22}, C_{25}, C_{28} and C_{31} monocyclic components of the TUA fraction of Cold Lake bitumen. From J.D. Payzant *et al.,* Ref. 15. © 1980, Elsevier Science B.V.

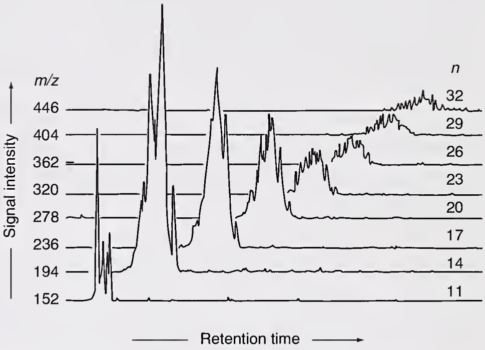

Figure 10.13 GC–FIMS scan of the molecular ions of the C_{11}, C_{14}, C_{17}, C_{20}, C_{23}, C_{26}, C_{29} and C_{32} bicyclic components of the TUA fraction of Cold Lake bitumen. From J.D. Payzant *et al.,* Ref. 15. © 1980, Elsevier Science B.V.

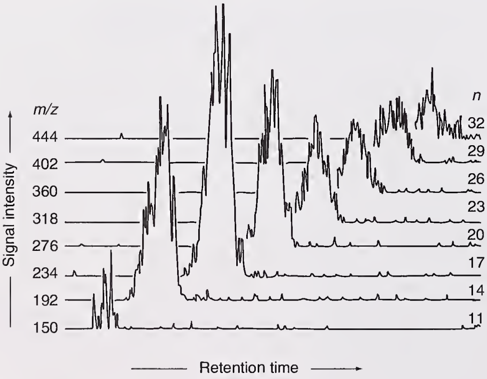

Figure 10.14 GC–FIMS scan of the molecular ions of the C_{11}, C_{14}, C_{17}, C_{20}, C_{23}, C_{26}, C_{29} and C_{32} tricyclic components of the TUA fraction of Cold Lake bitumen. From J.D. Payzant *et al.,* Ref. 15. © 1980, Elsevier Science B.V.

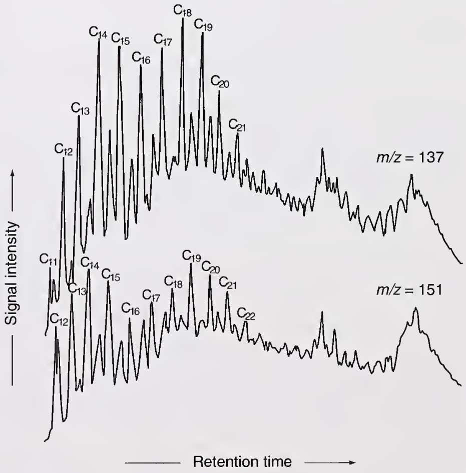

Figure 10.15 GC–MS *m/z* = 137 and 151 cross scans of the TUA fraction of Cold Lake bitumen showing the bicyclic components. From J.D. Payzant *et al.*, Ref. 15. © 1980, Elsevier Science B.V.

The shorter-retention-time isomer gave the m/z = 151 peak and the longer-retention-time isomer gave the m/z = 137 peak. Therefore, it was proposed that these two series consist of the alkyldecalin and methylalkyldecalin series.

Tricyclic compounds are present in the TUA fraction in relatively low concentrations. Figure 10.14 illustrates the FI mass chromatogram in the n = 11–32 range. A regular series of multiple peaks similar to those observed in the mono- and bicyclic series is evident.

Lastly, the sterane distribution in the small quantity of tetracyclic components of the TUA fraction as determined by GC–EIMS and FIMS is depicted in Figure 10.16. The major components are the 5α(H)-C_{27} and -C_{28} members.

Similar data have also been obtained for the TUNA fraction and are reproduced for the mono-, di- and tricyclic components in Figures 10.17–10.19. Evidently, the number of isomers present at each carbon number is greater and each of the series extends to somewhat higher carbon numbers, up to and beyond C_{33}, than in the TUA fraction. This increased complexity is due to the restricted selectivity involved in removing certain compound classes in the thiourea adduction process. The tricyclic series (Figure 10.19) exhibits an interesting feature, namely, that the last-eluting major peaks in the C_{20}–C_{29} isomer cross scans are especially intense, particularly for the case of the C_{23} isomers. These peaks represent a series of compounds in the C_{19}–C_{30} range which is also present in Athabasca saturates, as discussed above: they are the

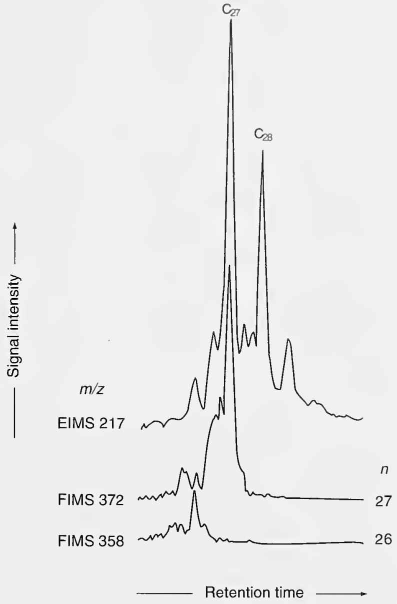

Figure 10.16 GC–MS m/z = 217 cross scan and FIMS cross scans of the molecular ions of the 5α(H)-C_{27} and -C_{28} steranes in the TUA fraction of Cold Lake bitumen. From J.D. Payzant *et al.*, Ref. 15. © 1980, Elsevier Science B.V.

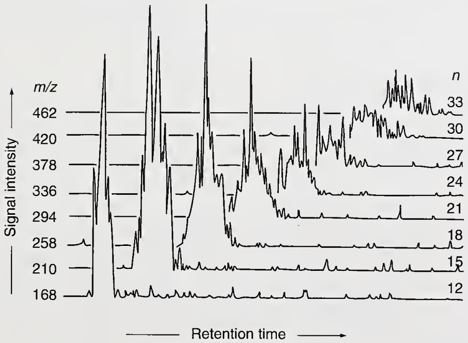

Figure 10.17 GC–FIMS scans of the molecular ions of the C_{12}, C_{15}, C_{18}, C_{21}, C_{24}, C_{27}, C_{30} and C_{33} monocyclic components of the TUNA fraction of Cold Lake bitumen. From J.D. Payzant *et al.*, Ref. 15. © 1980, Elsevier Science B.V.

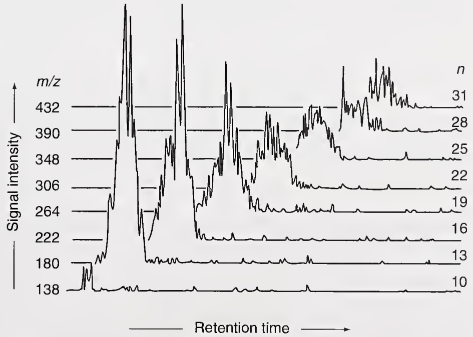

Figure 10.18 GC–FIMS scans of the molecular ions of the C_{10}, C_{13}, C_{16}, C_{19}, C_{22}, C_{25}, C_{28} and C_{31} bicyclic components of the TUNA fraction of Cold Lake bitumen. From J.D. Payzant *et al.*, Ref. 15. © 1980, Elsevier Science B.V.

homologous series of tricyclic II compounds, 18,19-bisnor-13β(H),14α(H)-cheilanthane, and its derivatives.

Most of the steranes are found in the tetracyclic component of the TUNA fraction and their GC–EIMS and FIMS scans as obtained by separation on a packed column display a complex distribution, Figure 10.20, dominated by the C_{27}–C_{29} members. With the high theoretical plate capillary columns available today the resolution obtainable is much higher (*cf.* Chapter 13). Nevertheless, it is instructive to compare the resolution obtained by monitoring the parent *m/z* = 386 peak intensities in FIMS which indicates the presence of more than a dozen C_{28} isomeric tetracyclic hydrocarbons, most of which are most likely steranes.

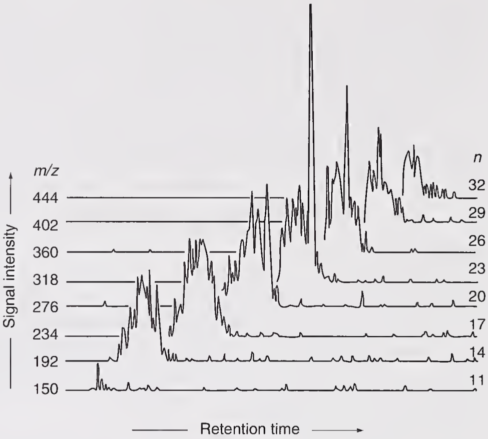

Figure 10.19 GC–FIMS scans of the molecular ions of the C_{11}, C_{14}, C_{17}, C_{20}, C_{23}, C_{26}, C_{29} and C_{32} tricyclic components of the TUNA fraction of Cold Lake bitumen. From J.D. Payzant *et al.*, Ref. 15. © 1980, Elsevier Science B.V.

Comparative compositional FIMS data for the TUA and TUNA fractions of the Lloydminster Cretaceous heavy oil and the Athabasca and Cold Lake oil sand bitumens[7] are shown in Figures 10.21 and 10.22, respectively. The composition of both fractions of the Lloydminster oil is dominated by acyclic alkanes while the oil sand bitumens contain only small concentrations of acyclics which, in the Athabasca TUA fraction, appear to show a high preference for the even carbon number members. This latter feature of the Athabasca alkanes is an indication of their recent secondary origin. The distribution of the components according to ring number in the molecule is as follows:

Lloydminster: acyclics > mono ~ bi- > tricyclics
Cold Lake: bi- ~ mono- > tricyclics > acyclics
Athabasca: bi- > tri- > mono- > tetracyclics > acyclics.

These distributions, along with the *n*-alkane contents (Lloydminster >> Cold Lake > Athabasca), establish that the effect of biodegradation is the least severe for the Lloydminster heavy oil followed by the Cold Lake bitumen, and lastly, most severe, for the Athabasca bitumen. Several samples of Wabasca saturates have also been examined and were found to contain, along with the suites of hopanes and cheilanthanes, pristane, phytane, and C_{15} and C_{16} isoprenoids, but little—if any—*n*-alkanes. Thus, with respect to the severity of biodegradation, they appear to lie between the Cold Lake and Athabasca bitumens.

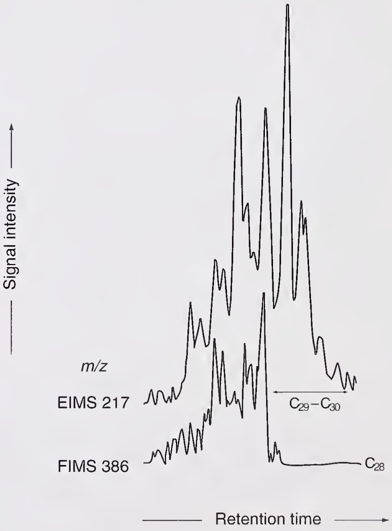

Figure 10.20 GC–MS *m/z* = 217 cross scan and FIMS scans of the molecular ions of the C_{28} steranes in the TUNA fraction of Cold Lake bitumen. From J.D. Payzant *et al.*, Ref. 15. © 1980, Elsevier Science B.V.

Some information is also available on the composition of the saturate fraction of a Carbonate Trend[19] and a Peace River[20] bitumen as well as a Venezuelan crude oil core sample

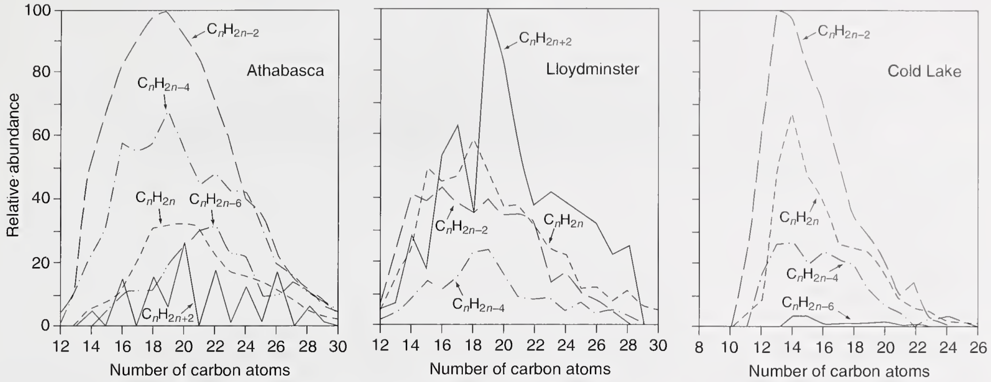

Figure 10.21 Relative concentration *versus* carbon number as determined by FIMS for the TUA fraction of Lloydminster, Cold Lake and Athabasca saturates. From J.D. Payzant *et al.*, Ref. 7. © 1979, Elsevier Science Ltd.

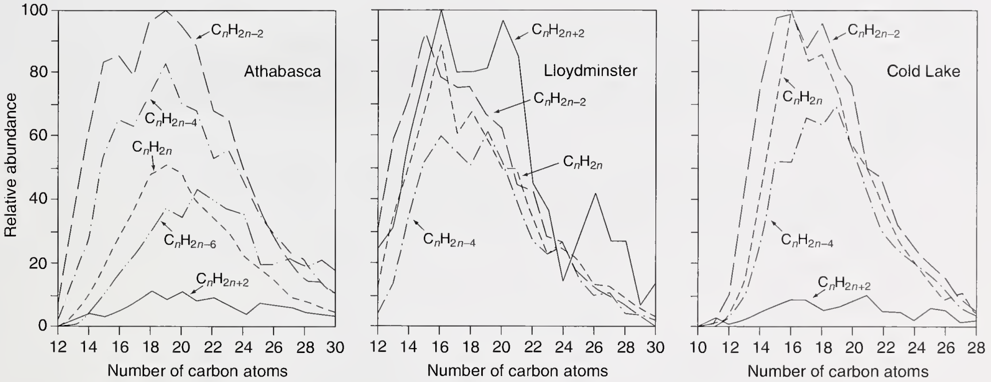

Figure 10.22 Relative concentration *versus* carbon number as determined by FIMS for the TUNA fraction of Lloydminster, Cold Lake and Athabasca saturates. From J.D. Payzant *et al.*, Ref.7. © 1979, Elsevier Science Ltd.

(asphaltene 0.74%, sulfur 1.9%). The FIM spectra of the Carbonate Trend bitumen saturates and Athabasca bitumen saturates are shown in Figure 10.23 and the capillary gas chromatograms of the Peace River core saturates (molecular sieves 1310 adducts) and the saturates from a steam-treated well head, in Figure 10.24.

As will be noted, the FIMS of Athabasca saturates in Figure 10.23 is strikingly different from the FIMS we saw in Figure 10.3. The inconsistency is attributable to the different experimental procedures employed for the isolation of the saturate fractions for the FIMS analyses. In Figure 10.23 the FIMS analysis was done on the crude saturates as obtained from the silica/alumina column chromatography, whereas in Figure 10.3 the crude n-C_5 eluent from the silica gel column was subjected to vacuum distillation and subsequent silver ion on silica gel thin layer chromatography for the quantitative removal of alkene, aromatic, nitrogen and sulfur compound impurities. The presence of such impurities would significantly alter the FIMS by producing mass peaks identical with the various saturated hydrocarbon mass peaks, *e.g.*

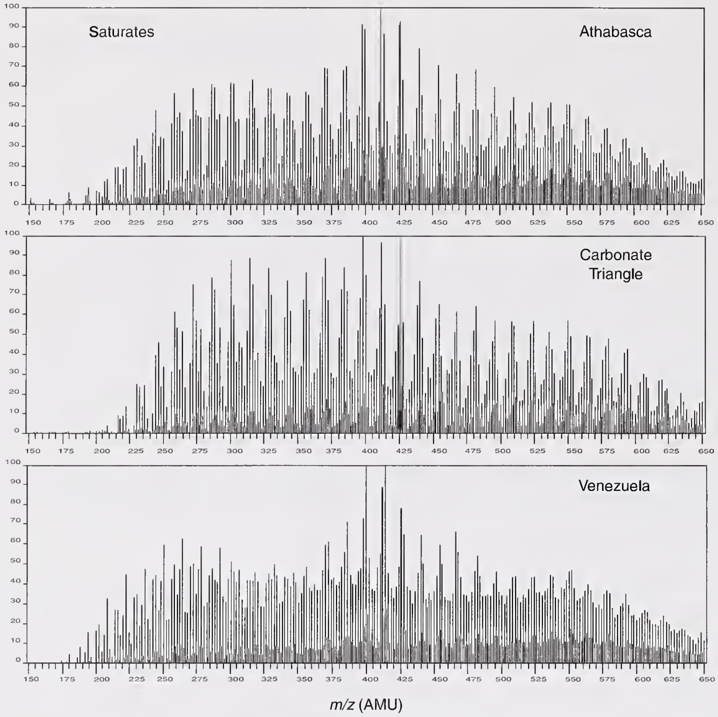

Figure 10.23 FIMS spectra of the saturate fractions from Athabasca and Carbonate Trend bitumens and a Venezuelan crude.[19]

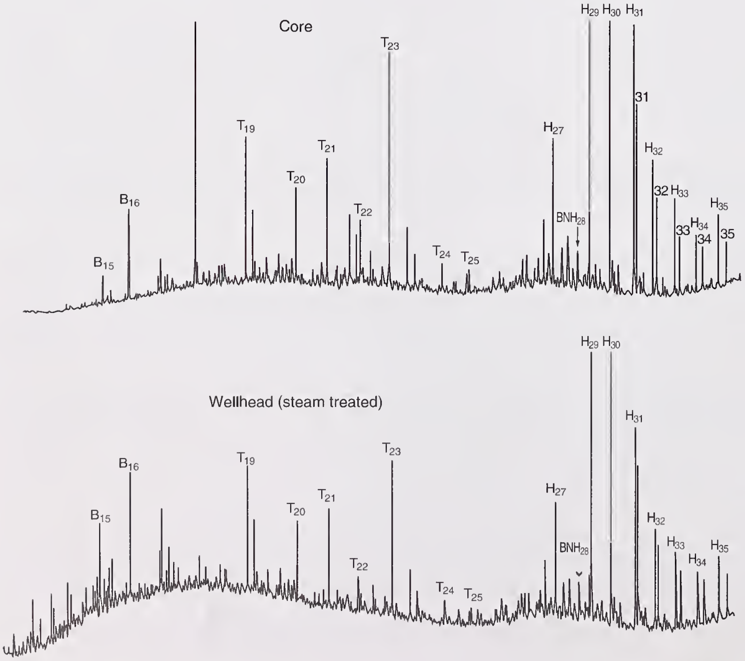

Figure 10.24 Gas chromatograms of the molecular sieve 1310 adducts of Peace River core and wellhead (steam treated) saturates. D = bicyclic, T = tricyclic, H = hopane, BNH = 28,30-bisnorhopane.[20] The subscripts refer to the number of carbon atoms in the molecule.

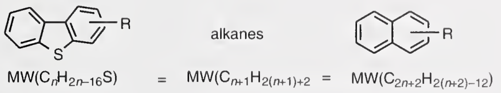
R
S
alkanes
R
MW(C$_n$H$_{2n-16}$S) = MW(C$_{n+1}$H$_{2(n+1)+2}$ = MW(C$_{2n+2}$H$_{2(n+2)-12}$)

Consequently, the spectrum in Figure 10.3 is devoid of alkane peaks whereas in Figure 10.23 *apparent* alkane peaks due to impurities abound.

The spectra of the Athabasca and Carbonate Trend samples in Figure 10.23 are quite similar. Both possess rather prominent series of materials represented by the formula C_nH_{2n-6}, C_nH_{2n-8} and C_nH_{2n-10} or their equivalent sulfur compound analogs. In the spectrum of the Venezuelan crude oil saturates these series are still distinct but the distribution with respect to z number is rather flat. This is understandable since this crude oil is not biodegraded and its paraffinic and mono- and bicyclic complement is not depleted. In all three samples the maximum concentration occurs in the C_{29}–C_{31}, m/z = 396–424 range and in all the FIMS the concentration of the odd m/z species is low, indicating that fragmentation of the molecular ions is of no great significance.

Figure 10.24 shows the gas chromatogram of the molecular sieve 1310 adduct of the saturate fraction of the Peace River bitumen extracted from a core sample and that for a wellhead bitumen sample obtained from the Shell Peace River *in-situ* pilot project in the core area using the "huff and puff" steam drive process. First, we note the close similarity between the Peace River and Athabasca samples, Figures 10.24 (top) and 10.7. In effect, the two native samples give nearly identical gas chromatograms. Secondly, we note that exposure of the Peace River bitumen to heat caused a general maturation of the saturates, in the sense that the higher members of the various series tended to convert to lower members of the series. Thus the ratios

$$H_{31}/H_{29}, T_{23}/T_{19}, H_{31}/H_{27}, T_{19}/D_{16}, \textit{etc.}$$

have all declined during heat exposure owing to the degradation reactions:

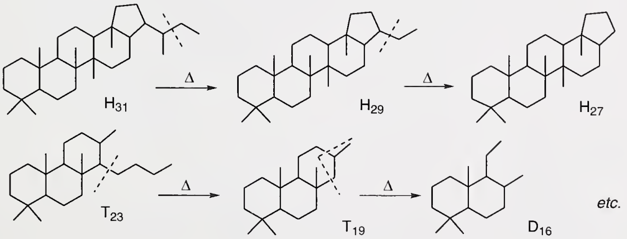

These changes appear to be manifestations of chemical alterations of the bitumen during its *in-situ* recovery.

An interesting and unique class of molecules found in the Peace River bitumen and Lloydminster heavy oil, but not found in other Alberta bitumens, is adamantane[20] and its methyl, propyl and butyl derivatives.

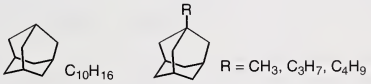

Adamantane has a strain-free, rigid, three-dimensionally fused tricyclic ring structure and a high thermodynamic stability and for these reasons all tricyclic alkanes containing 10 carbon atoms are converted to adamantane under thermal stress in the presence of strong Lewis acids.

Adamantane is a member of the family of diamondoid hydrocarbons which have diamond-like structures. If the substrate contains an alkyl substituent then alkyl-substituted adamantanes result. Adamantanes have been reported earlier to be present in various East European heavy oils^{21}, Ponca City oil^{22} and more recently in some highly mature Chinese crude oils,^{23} and in effect they have been proposed for geochemical application as maturity indices.

3.0 The Nondistillable Portion of Athabasca Saturates

Sections 1.0 and 2.0 of this chapter dealt with the chemical composition of the distillable portion of the saturate subfractions, comprising ≥90% of the saturates. The remaining ≤10% of the fraction does not distill at 240°C and 10^{-3} torr pressure. This nonvolatility may be due to either a high molecular weight, a difference in molecular composition, or both. In order to gain some insight into this question the ^{13}C NMR spectra of the distillable and nondistillable portions of Athabasca saturates were taken and compared.

The 500-MHz inverse-gated decoupled ^{13}C NMR spectra of the nondistillable and distillable portions of Athabasca saturates shown in Figures 10.25 and 10.26, are revealing. They display significant differences in chemical composition involving the alkyl substituents on ring structures and possibly free alkanes, as well as in the degree of aromatic contamination present in the two fractions. The aromatic resonances (110–150 ppm) appear as a broad, unresolved hump which is more important relative to the aliphatic and alicyclic region (10–60 ppm) in the nondistillable than in the distillable portion of the saturates. Moreover, the differences in the aliphatic region lie primarily in the relative intensities of the terminal and ring methyls

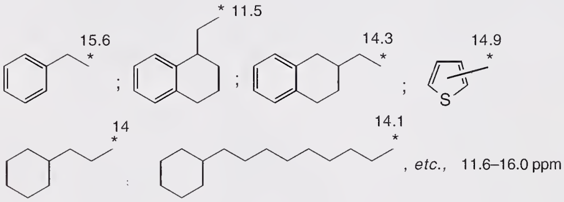

to the midchain and certain α-methylenes:

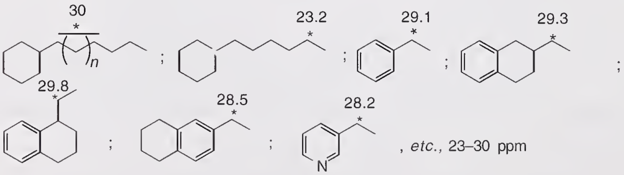

Thus, it is seen that the terminal methyl resonance intensity relative to the mid-chain methylene resonance intensity is much higher in the distillable than in the nondistillable portion. *This reveals the absence of sizeable quantities of long alkyl chains in the distillable portion of the saturates and their presence in the nondistillable portion,* in agreement with the conclusions drawn from the mass spectrometric studies described above, namely, that the distillable portions of the Alberta bitumen saturates are, by and large, derived from terpenoid hydrocarbon biomarkers. On the other hand, the NMR spectrum of the nondistillable portion of the saturates resembles that of the asphaltenes except that its aromatic carbon content is lower than that of asphaltene which, as will be shown in Chapter 14, is rich in long *n*-alkyl chain substituted alicyclics, aromatics and

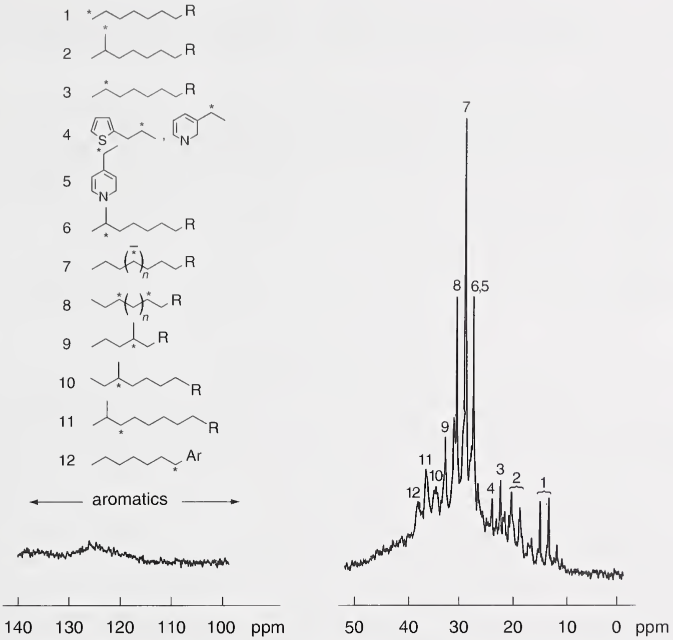

Figure 10.25 500-MHz inverse-gated decoupled ^{13}C NMR spectrum of the nondistillable (240°C, 10^{-3} torr) portion of Athabasca saturates.

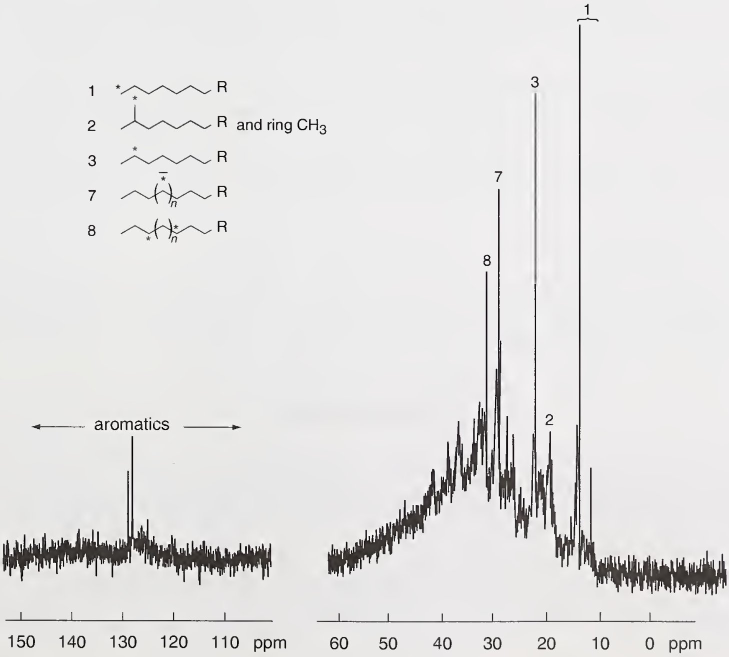

Figure 10.26 500-MHz inverse-gated decoupled ^{13}C NMR spectrum of the distillable (240°C, 10^{-3} torr) portion of Athabasca saturates.

heterocyclics. This similarity between the two NMR spectra is a strong indication that the nondistillable portion of the saturates is genetically related to the asphaltene and had similar biotic source materials.

The nondistillable portion of the saturate fraction was also subjected to thermolysis and at 375°C yielded, among other products, a homologous series of *n*-alkanes and terminal *n*-alkenes with carbon number distribution up to C_{28} and with a maximum at C_{18}. The appearance of these products proves their presence in the nondistillable portion of the saturates and confirms the assignment of the ^{13}C NMR spectrum.

Additional details of the chemistry of the saturates will be discussed in Chapter 13.

4.0 Summary

As has been shown in this chapter, it is possible to separate, in nearly quantitative yields, fairly clean saturate fractions from Alberta bitumens, which comprise a complex mixture of mono- through hexacyclic alkanes, with small quantities of acyclic and trace amounts of *n*-alkanoic hydrocarbons. This saturate fraction, with a $(H/C)_a$ of > 1.8, MW < 400 $g \cdot mol^{-1}$ and only trace amounts of heteroatom contamination, represents the most valuable portion of the bitumen. Apart from a few hundred biological marker molecules accounting for a small weight percentage of the saturate fraction, the bulk of the fraction cannot be resolved into individual components by GC. The best resolution was achieved by FIMS and GC–FIMS methods, which showed that the most abundant constituents are the bicyclics followed by either the tri- and tetracyclics, or the mono-, tri- and tetracyclics, depending on the extent of biodegradation the precursor oil experienced. From these results it is possible to compare the bulk concentration distributions according to carbon number in the molecule for each ring number series with the distributions of the cyclic terpenoid hydrocarbon biological marker molecules in the saturates.

From this comparison it has been concluded that the bulk of the distillable portion of the saturates is composed of rearranged and partly degraded cyclic terpenoid biological marker hydrocarbons along with smaller quantities of nonterpenoid cyclic hydrocarbons which survived microbial degradation because of their resistance to biodegradation. As will be evident from the next chapter, these conclusions are reinforced by studies on the composition of the aromatic fraction of the bitumen.

In contrast, the nondistillable portion (≤10%) of the saturates consists of long-chain *n*-alkyl substituted aromatics and naphthenics which are structurally and genetically related to the asphaltene fraction of the bitumen.

Bibliography

1. E.B. Frolov and M.B. Smirnov, "Unsaturated Hydrocarbons in Crude Oils", Org. Geochem., 21 (1994) 189.
2. O.P. Strausz, Final Report, AOSTRA/University Agreement #428, "Characterization of Olefins Present in Athabasca Bitumen and the Cretaceous Heavy Oils of Alberta", January, 1988; H.K.J. Choi, D.D. McIntyre, D.S. Montgomery and O.P. Strausz, "Investigation of Alkenes in Heavy Oils by Hydroboration and Nuclear Magnetic Resonance Spectroscopy", AOSTRA J. Res., 3 (1987) 125.
3. M.L. Selucky, Y. Chu, T.C.S. Ruo and O.P. Strausz, "Chemical Composition of Athabasca Bitumen", Fuel, 56 (1977) 369.
4. M.L. Selucky, Y. Chu, T.C.S. Ruo and O.P. Strausz, "Chemical Composition of Cold Lake Bitumen", Fuel, 57 (1978) 9.

5. J.D. Payzant, A.M. Hogg, D.S. Montgomery and O.P. Strausz, "A Field Ionization Mass Spectrometric Study of the Maltene Fraction of Athabasca Bitumen. Part I — The Saturates", AOSTRA J. Res., 1 (1985) 175.
6. O.P. Strausz, I. Rubinstein, A.M. Hogg and J.D Payzant, "Advances in the Chemistry of Alberta Tar Sands: Field Ionization Gas Chromatographic/Mass Spectrometric Studies" in *Atomic and Nuclear Methods in Fossil Energy Research,* R.H. Filby, B.S Carpenter and R.C Ragaini, Eds., Plenum Press, New York, N.Y., 1982, p. 409.
7. J.D. Payzant, I. Rubinstein, A.M. Hogg and O.P. Strausz, "Field Ionization Mass Spectrometry: Application to Geochemical Analysis", Geochim. Cosmochim. Acta, 43 (1979) 1187.
8. A. Dimmler, T.D. Cyr and O.P. Strausz, "Identification of Bicyclic Terpenoid Hydrocarbons in the Saturate Fraction of Athabasca Oil Sand Bitumen", Org. Geochem., 7 (1984) 231.
9. A. Dimmler and O.P. Strausz, "Enrichment of Polycyclic Terpenoid, Saturated Hydrocarbons From Petroleum by Adsorption on Zeolite Na10", J. Chromatogr., 270 (1983) 219.
10. C.M. Ekweozor and O.P. Strausz, "18,19-Bisnor-13β(H),14α(H)-Cheilanthane: A Novel Degraded Tricyclic Sesterterpenoid-Type Hydrocarbon From the Athabasca Oil Sands", Tetrahedron Lett., 23 (1982) 2711.
11. C.M. Ekweozor and O.P. Strausz, "Tricyclic Terpanes in the Athabasca Oil Sands: Their Geochemistry", in *Advances in Organic Geochemistry* 1981, M. Bjøroy et al., Eds., Wiley Heyden, London, England, 1983, p. 746.
12. K.E. Peters and J.M. Moldowan, *The Biomarker Guide*, Prentice Hall, Englewood Cliffs, N.J. 1993.
13. I. Rubinstein and O.P. Strausz, "Geochemistry of the Thiourea Adduct Fraction From an Alberta Petroleum", Geochim. Cosmochim. Acta, 43 (1979) 1387.
14. O.P. Strausz, E.M. Lown and J.D. Payzant, "Nature and Geochemistry of Sulfur-Containing Compounds in Alberta Petroleums", Ch. 22 in *Geochemistry of Sulfur in Fossil Fuels*, ACS Symposium Series 429, W.L. Orr and C.M. White, Eds., Am. Chem. Soc., Washington, D.C., 1990, p. 366.
15. J.D. Payzant, I. Rubinstein, A.M. Hogg and O.P. Strausz, "Analysis of Cold Lake Bitumen Hydrocarbons by Combined GLC–Field Ionization Mass Spectrometry and GLC–Electron Impact Mass Spectrometry", Chem. Geol., 29 (1980) 73.
16. J.M. Moldowan and W.K. Seifert, "Head-to-Head Linked Isoprenoid Hydrocarbons in Petroleum", Science, 204 (1979) 169.
17. B.P. Tissot and D.H. Welte, *Petroleum Formation and Occurrence*, 2nd Ed., Springer-Verlag, Berlin, 1984, pp. 114–116.
18. A.M. Hogg, J.D. Payzant, I. Rubinstein, and O.P. Strausz, "Application of GC/FIMS to Hydrocarbon Analysis", 27th Annual Conference on Mass Spectrometry and Allied Topics, Seattle, WA, 1979.
19. I. Rubinstein, D.S. Montgomery and O.P. Strausz, unpublished results, 1980.
20. D.D. McIntyre, AOSTRA Postdoctoral Fellowship Report, Department of Chemistry, University of Alberta, October, 1984.
21. Al. A. Petrov, O.A. Arefjev and Z.V. Yakubson, "Hydrocarbons of Adamantane Series as Indices of Petroleum Catagenesis Processes" in *Advances in Organic Geochemistry*, Paris Technip, 1973, p. 518.
22. Ref. 17, p. 392.
23. J. Chen, J. Fu, G. Sheng, D. Liu and J. Zhang, "Diamondoid Hydrocarbon Ratios: Novel Maturity Indices for Highly Mature Crude Oils", Org. Geochem., 25 (1996) 170.

Appendix 10.1

Field Ionization, GC–FI Mass Spectrometry

Field ionization is the phenomenon whereby an electron tunnels from atoms or molecules under the action of an intense electrical field with field gradients of the same order of magnitude as that experienced by the electrons outermost from the nucleus, which is about $(2\text{–}5) \times 10^8$ $V{\cdot}cm^{-1}$. This results in molecular ion formation with little excess internal energy content in the ion. Therefore, the primary molecular ions do not fragment to smaller ions before analysis and direct molecular weight determination can be accomplished in the mass spectrometer.

The emitter source used in the field ionization mass spectroscopic studies[1–8] described in this and in subsequent chapters was the high-efficiency carbon needles on tungsten wire type. The relative sensitivities of component molecules with respect to ionization in mixtures of various compound classes have been investigated under various experimental conditions employing various emitter types and found to be, within certain experimental parameters, nearly equal.

Since FI produces essentially only molecular ions—with the notable exception of acyclic alkanes (see below)—the concentration of a given hydrocarbon may be assumed to be proportional to the measured intensity of that ion at the appropriate mass. This feature of the process dispenses with the necessity of calibration for individual components for the quantitative study of a complex mixture, which is a huge advantage of the FIMS over other MS methods. Also, in the analysis of petroleum fractions at sufficently high resolution ($M/\Delta M \sim 10{,}000$) many sulfur-containing species and hydrocarbon types (C_nH_{2n-2}, C_nH_{2n-12}, C_nH_{2n-26}, or C_nH_{2n-6} and $C_nH_{2n-10}S$, etc.) can be resolved.

In addition to these attractive features, the GC–FIMS combination offers a number of advantages, including the following

- different isomeric molecules with identical molecular weights can be resolved without interference from coeluting molecules with different molecular weights and furthermore, in the case of acyclic alkanes, fragmentation can be recognized, corrected for, and used for quantitative analysis and structural correlations; and
- different homologous series (C_nH_{2n}, C_nH_{2n-14} or C_nH_{2n-6} and $C_nH_{2n-10}S$, etc.) can be resolved without resorting to very high resolution analysis.

Indeed, these features and the general utility of the GC–FIMS method, especially when it is applied in combination with GC–electron impact MS, are amply demonstrated by the results obtained from the very first studies on petroleum and petroleum fractions. Specific examples are shown in Figures 10.1.1 and 10.1.2 for the TUA fraction of a Leduc conventional oil.[3] The molecular ion intensities monitored in Figure 10.1.1 are for the parent series C_nH_{2n+2}, along with the most important fragment ions $m/z = 29$, 43 and 47. The mechanism of formation of the fragment ions here is quite different from that in electron impact fragmentation where it is the result of excess internal, mainly vibrational, energy. Here, on the other hand, the fragmentation is thought to be the consequence of electrostatic interactions. In order to understand this, it is necessary to consider the polarizability of the molecules under analysis. In an acyclic saturated hydrocarbon, the polarizability is considerably higher along the carbon chain than across it. Consequently, the molecule will approach the emitter end-on.[9] When FI occurs, the resulting positive charge will be localized, at least initially, at that end of the molecule nearest to the emitter. Experimentally, it is observed that the major (>90%) fragment ion from an *n*-alkane is the $m/z = 29$ ion. A small amount of $m/z = 28$ is also present. Bond rupture

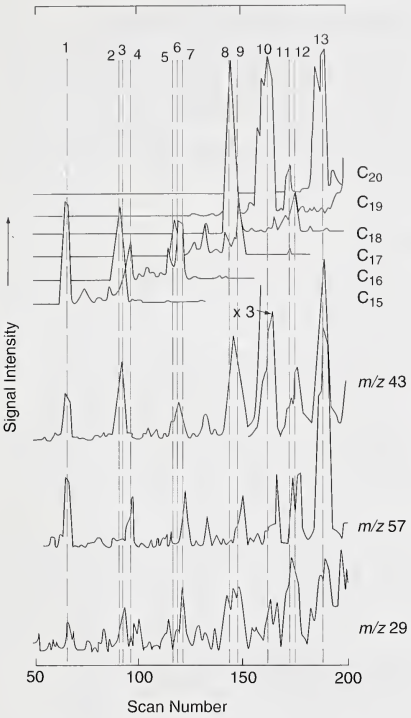

Figure 10.1.1 Thiourea adduct fraction of Leduc conventional oil. Expanded display of the molecular ion intensities from $n = 15$ to 20 in the formula C_nH_{2n+2} and the fragment ion intensities corresponding to $m/z = 29$, 43 and 57. From O.P. Strausz *et al.*, Ref. 3. © 1982, Plenum Press. See Table 10.1.1.

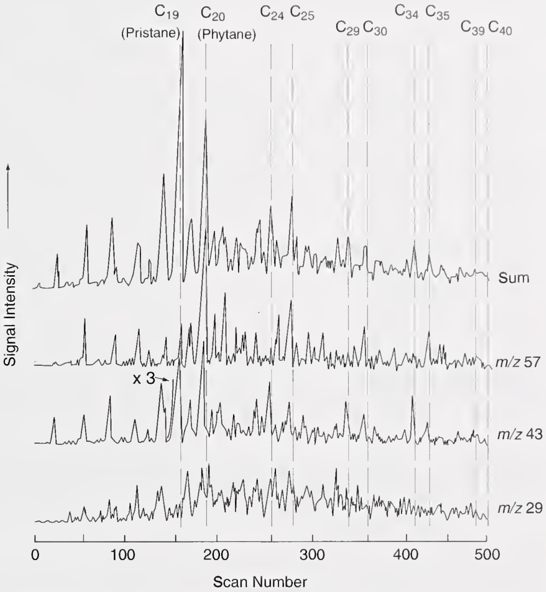

Figure 10.1.2 Thiourea adduct fraction of Leduc conventional oil. Sum of the molecular ion intensities for the series C_nH_{2n+2} and the fragment ions $m/z = 29$, 43 and 57. From O.P. Strausz *et al.*, Ref. 3. © 1982, Plenum Press.

therefore occurs between the second and third carbon atoms in the chain. The relative abundance of the fragment ion $m/z = 29$ increases proportionally with the number of carbon atoms in the molecule. This phenomenon has been explained[9] as follows. After ionization, the end of the ion where the electric charge is localized nearest to the emitter is repelled from the emitter by the intense electrical field. The amount of strain placed on the weakened bond causing its rupture is dependent on the mass and inertia of the remaining part of the molecule. In the case where the mass of the remainder of the molecule is large, compared to the fragment, the degree of extension of the weak bond and the inertia of the remainder will be considerably greater than in the case where the fragment ion and the remainder of the molecule are of comparable mass. Therefore, the amount of fragmentation within a homologous series increases with increasing number of carbon atoms.

In the case where there is branching at the end of the alkane, such as in pristane,

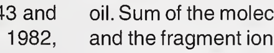

the amount of fragmentation is greater than in the corresponding *n*-alkane since the resulting fragment ion is thermodynamically more stable. For pristane the $m/z = 43$ ion comprises >

Table 10.1.1 Structures of acyclic alkanes in the thiourea adduct of Leduc oil[a]

Peak no.[b]	*n*[c]	Proposed structure	Fragment ions observed
1	15	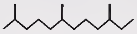	43, 57, 29 (?)
2	16	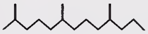	43, 29
3	15	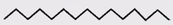	29
4	16	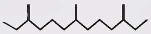	57
5	17	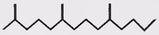	43
6	16	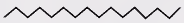	
7	17	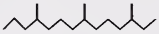	57, 29
8	18	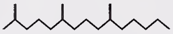	43
9	17	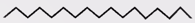	
10	19	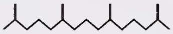	43
11	19	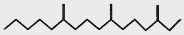	57, 29
12	18	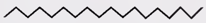	
13	20	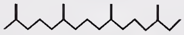	43, 57, 29

[a]From O.P. Strausz et al., Ref. 3. © 1982, Plenum Press. [b] Peak numbers as in Figure 10.A.1.
[c]Value of *n* in the formula C_nH_{2n+2}.

90% of the fragment ions and $m/z = 42$ accounts for most of the remainder; $m/z = 29$ and 57 are quite small.

The phytane molecule,

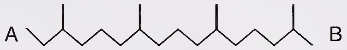

yields two fragment ions $m/z = 43$ and 57, with small amounts of $m/z = 42$ and 56, corresponding to the fragments from each end of the molecule. Also, $m/z = 29$ is observed at very low intensity, Figure 10.A.2. The $m/z = 43$ ion intensity is larger than that of the $m/z = 57$ ion by a factor of about two, suggesting that the greater distance of the methyl branch from end A reduces the amount of fragmentation from this end since the almost symmetrical molecule would not be expected to display a strong preference for orienting itself one way or the other in the electric field.

This interpretation of FI spectra was confirmed by a model study[4] involving standard mixtures of eicosane, pristane and dodecylcyclohexane. Eicosane affords mainly $m/z = 29$ and pristane, mainly $m/z = 43$. Alkylcyclohexane does not fragment significantly. It was found that the ratios of the respective molecular ions in this mixture varied by a factor of five, with extremes of emitter temperatures. Importantly, however, the ratios of the sums of molecular ions and the aggregate fragment ions remained constant within experimental error.

Alkylcyclohexane and saturated hydrocarbons possessing rings generally do not fragment appreciably under FI conditions since their most easily polarizable moiety is the ring which, even if undergoes C–C bond rupture, would not fragment because a rupture in the ring results in ring opening without fragmentation.

Because of its unique manner of generation, the nature of the fragment ion from acyclic alkanes conveys information about the terminal moiety of the molecule. Thus, in GC–MS studies the structure of the terminal moiety, along with the carbon number in the molecule, can be deduced from the FI spectrum and information on the mode of branching, from the GC elution time. FI can be applied for solid state samples as well and has been used for the MS studies of asphaltene and other solid state petroleum components and products.

Bibliography

1. J.D. Payzant, I. Rubinstein, A.M. Hogg and O.P. Strausz, “Field-Ionization Mass Spectrometry: Application to Geochemical Analysis”, Geochim. Cosmochim. Acta, 43 (1979) 1187.
2. A.M. Hogg, J.D. Payzant, I. Rubinstein and O.P. Strausz, “Application of GC/FIMS to Hydrocarbon Analysis”, paper presented at the 27th Annual Conference on Mass Spectrometry and Allied Topics, Seattle, WA, 1979.
3. J.D. Payzant, I. Rubinstein, A.M. Hogg and O.P. Strausz, “Analysis of Cold Lake Bitumen Hydrocarbons by Combined GLC–Field Ionization Mass Spectrometry and GLC–Electron Impact Mass Spectrometry”, Chem. Geol., 29 (1980) 73.
4. O.P. Strausz, I. Rubinstein, A.M. Hogg and J.D. Payzant, “Advances in the Chemistry of Alberta Tar Sands: Field Ionization Gas Chromatographic/Mass Spectrometric Studies”, in *Atomic and Nuclear Methods in Fossil Energy Researh*, R.H. Filby, B.S. Carpenter and R.C Ragaini, Eds., Plenum Press, New York, 1982, p. 409.
5. J.D. Payzant, A.M. Hogg, D.S. Montgomery and O.P. Strausz, “Field Ionization Mass Spectrometric Study of the Maltene Fraction of Athabasca Bitumen. Part I. The Saturates”, AOSTRA J. Res., 1 (1985) 175.
6. J.D. Payzant, A.M. Hogg, D.S. Montgomery and O.P. Strausz, “Field Ionization Mass Spectrometric Study of the Maltene Fraction of Athabasca Bitumen. Part II. The Aromatics”, AOSTRA J. Res., 1 (1985) 183.
7. J.D. Payzant, A.M. Hogg, D.S. Montgomery and O.P. Strausz, “Field Ionization Mass Spectrometric Study of the Maltene Fraction of Athabasca Bitumen. Part III. The Polars”, AOSTRA J. Res., 1 (1985) 203.
8. A.M. Hogg and J.D. Payzant, “Design of a Field Ionization/Field Desorption Electron Impact Ion Source and its Performance on a Modified MS9 Mass Spectrometer”, Int. J. Mass Spectrosc. Ion Phys., 27 (1978) 291.
9. H.D. Beckly and G. Wagner, “Analytische Anwendungsmöglichkeiten des Fieldionen–Massenspektrometers”, Z. Anal. Chem., 197 (1963) 58.

Appendix 10.2

Adduction Chromatography

In modern chemistry a special class of compounds is recognized that features weaker-than-covalent bonding. A subgroup of such compounds is represented by the "inclusion compounds", characterized by the inclusion of certain specific molecules, the guest molecules, into the internal cavities of a crystalline compound, the host compound. There is no bonding between the host and the guest, except by weak van der Waals forces. There are two main types of inclusion compounds distinguished according to the shape of the cavity in the host crystal. The ones with a crystal lattice forming long tunnels or channels are generally called inclusion compounds whereas the ones with spaces that are completely enclosed are referred to as cage compounds or clathrates. In both instances the guest molecule must satisfy certain size and shape requirements in order to fit into the space of the host crystal for inclusion.

Among the host inclusion compounds most used in the fractionation of petroleum products we find zeolites (molecular sieves), urea and thiourea.

Molecular sieves come in various pore sizes (channel diameters). The most frequently-used molecular sieve is the 5 Å (S115) for the adduction of *n*-alkanes (cross-sectional diameter 4 Å) ≥ C_6 and their separation from other alkanes. In this case the alkane molecule must be fully inserted into the channel in order to effect good separation. "Silicates", which have two pore size channels, circular channels with 6 Å and elliptical channels with 5.1–5.7 Å diameters on the major axes, have been employed for the separation of *n*-alkanes, monomethylalkanes, branched and cyclic fractions.[1] Molecular sieve X10 has been utilized for the isolation of pentacyclic triterpanes[2] from a thiourea nonadduct fraction and X13 with a pore diameter of 9–10 Å for the isolation of bicyclic and tricyclic terpanes and hopanes from saturate fractions.[3]

Urea and thiourea form, through an extensive network of hydrogen bonds, slightly distorted hexagonal channels much like a honeycomb, which are stable only when a guest molecule is present.[4] The dimension of the channel depends on the nature of the guest molecule. For example, the dimensions of the channels in the urea adduct of *n*-hexadecane are 4.1 × 4.8 Å and in thiourea adducts, generally, 5.8 × 6.8 Å. In the complexes, the molar ratio is usually non-integral (*e.g.* octane/urea = 1:6.73) but by chance it may be integral (*e.g.* 1,5-cyclooctadiene/thiourea = 1:3.0). In the latter adduct the planar thiourea molecules are tilted by 10° from the channel axis; thus, the walls of the channels are not flat but have a corrugated appearance.

In urea and thiourea adduction it is not required that the guest molecule be entirely inside the channel of the host. This makes it possible to adduct molecules whose cross-sectional dimensions exceed the dimensions of the channels, *e.g.* branched and cyclic hydrocarbons with long *n*-alkyl chains which adduct by the chains, fatty acids, iso- and anteisoalkanes, etc.

As can be surmised from the above discussions, adduction chromatography plays a highly useful role in the biomarker chemistry of fossil fuels, Table 10.2.1.

Among the other types of inclusion compounds, gas hydrates have potential significance in fossil fuel chemistry. These are stable, crystalline, snow-like solids, clathrates. The components of natural gas (CH_4, C_2H_6, C_3H_8, C_4H_{10}, i-C_4H_{10}) and a few inorganic gases (N_2, CO_2, H_2S) are known to form clathrates with water. They are called gas hydrates. Through hydrogen bonding, the water molecules can create metastable skeleton structures with interstitial, molecular-size

Table 10.2.1 Partial list of hydrocarbons adducted to thiourea

stigmastane	β-carotane	cyclopentane and methylated cyclopentanes
sitostane	lycopane	bi(cyclopentyl) *cis*-(0,3,3)-bicyclooctane
ergostane	adamantane	1,3-bicyclopentylcyclopentane
cholestane	5α-steranes[1]	4-methylsteranes
phytane	acyclic isoprenoids	nuclear methylated rearranged steranes
pristane	naphthalene	anthracenes
n-alkylcyclohexane tricycloheptanes	1,5-cyclopentadiene	various [2,2,1]bicycloheptanes

[1] But not 5β-steranes

cavities that can accomodate these low-MW gas molecules. Each of the cavities can accomodate a single gas molecule and, through interaction with the host water molecules by van der Waals forces, the gas molecules stabilize the gas hydrate. The crystal structure of the gas hydrate will depend on the geometry of the gas molecule. X-ray structural investigations[5] revealed that a gas hydrate may have two different structural forms: structure I and structure II. The former has two small and six large cavities formed by 46 water molecules per unit cell. Each of these cavities can be occupied by one gas molecule and thus when methane is the guest molecule the maximum number of methane molecules for each occupied cavity is eight, per 46 water molecules per unit cell. Therefore, the empirical formula for this methane hydrate is $CH_4 \cdot 5.75H_2O$ which corresponds to 13.41 wt% CH_4 and 86.59 wt% H_2O. From the value of the density, 0.897 $g \cdot cm^{-1}$, it follows that 1 m^3 of $CH_4 \cdot 5.75H_2O$ has a weight of 897 kg, *i.e.* 120.3 kg CH_4 and 776.7 kg H_2O. Methane hydrates are only formed in structure I. The standard enthalpy change for the decomposition of methane hydrate into liquid water and methane gas is 12.95 $kcal \cdot mol^{-1}$.

The equilibrium of a gas hydrate depends on the gas pressure and temperature, and high pressure and low temperature favor hydrate formation. The presence of electrolytes and polar solvents like alcohols (methanol), on the other hand, suppress gas hydrate formation.

Now there are at least three aspects that make the chemistry of gas hydrates relevant to the fossil fuel industry:

- reportedly, there are such large quantities of methane hydrates in the sea floor that its total energy content would surpass all the world's fossil fuel reserves combined. The potential amount of carbon in oceanic methane hydrates has been estimated to be about 4.2×10^{14} tons[6] and 1×10^{13} tons.[7] These values may be compared to the value of 5×10^{12} tons of carbon estimated to be present in all fossil fuels. If only a fraction of this resource could be harnessed, it could extend the age of our fossil fuel-based civilization quite significantly. On the other hand, these methane hydrate deposits are fragile and could discharge gas into the atmosphere, thereby causing global climate changes by enhancing the greenhouse effect.
- in search of methods to lower the rate of carbon dioxide accumulation in the atmosphere, the possibility of sequestering carbon dioxide and storing it on the sea floor at least temporarily in the form of a gas hydrate, $CO_2 \cdot 5.75H_2O$, are being experimentally explored. Rapid hydrate formation in the sea is thought to occur in the depth range 2,700–4,500 m.
- gas hydrate formation may occur in pipelines under high pressure, low temperature conditions causing corrosion problems and solid coatings to deposit on the walls, impeding the pipeline flow. Therefore, such operating conditions that would minimize gas hydrate formation need to be maintained.

Bibliography

1. T.C. Hoering and D.H. Freeman, "Shape-Selective Sorption of Monomethylalkanes by Silicate, a Zeolite Form of Silica", J. Chromatogr., 316 (1984) 333; N. West, R. Alexander and R.I. Kagi, "The Use of Silicate for Rapid Isolation of Branched and Cyclic Alkane Fractions of Petroleum", Org. Geochem., 15 (1988) 499.
2. E.V. Whitehead, "The Structure of Petroleum Pentacyclanes" in *Advan. Org. Geochem. 1973,* B.Tissot and F. Biemer, Eds., Editions Technip, Paris, France, p. 225.
3. A. Dimmler and O.P. Strausz, "Enrichment of Polycyclic Terpenoid Saturated Hydrocarbons from Petroleum by Adsorption on Zeolite NaX", J. Chromatogr., 270 (1983) 219.
4. I. Garneau, S. Raymond and F. Brisse, "A Thiourea-1,5-Cyclobutadiene Clathrate at 173K", Acta Cryst., C51 (1995) 538.
5. K.S. Pederson, Aa. Fredenslund and P. Thomassen, *Properties of Oils and Natural Gas*, Gulf Publishing Co., Houston, TX, 1989.
6. G.R. Dickens, "The Potential Volume of Oceanic Methane Hydrates with Variable External Conditions", Org. Geochem. 32, (2001) 1179.
7. E. Suess, G. Bohrmann, F. Greinert and E. Lausch, "Flammable Ice", Scientific American, p. 76, Nov. 1999.

Chemical Composition of the Aromatic Fraction

11

Aromatic compounds ranging from alkylbenzenes to large condensed polyaromatic and heteroaromatic molecules are abundant in bitumens and heavy oils. They are usually alkyl- and naphthenic-substituted and some of them can be recognized as the partially or fully aromatized derivatives of the cyclic terpenoid hydrocarbons of the saturate fraction of the bitumen with which we have become acquainted in Chapter 10. Owing to the broad variations in the size and chemical and physical properties of this class of molecules, an aromatic fraction of bitumen cannot be as simply defined, either conceptually or experimentally, as can a saturate fraction. Nonetheless, by a combination of various column chromatographic methods it is possible to isolate an aromatic fraction and separate it into monoaromatic, diaromatic, triaromatic and polyaromatic subfractions. Both the composition and the quantity of the aromatic fraction and its subfractions are greatly dependent on the method used for their isolation (Chapter 5), and this explains the large variations in the percentage of aromatic contents reported in the literature for a given oil or bitumen. Thus, for example, the aromatic content of Athabasca bitumen has been reported[1–4] to have values ranging from 18 to 38 wt% of the bitumen, Table 11.1. The Cold Lake, Peace River and Wabasca bitumens contain concentrations of monoaromatic and diaromatic hydrocarbons similar to those in Athabasca bitumen, but their polyaromatic contents are somewhat higher and increase in the order Cold Lake < Peace River < Wabasca.

The monoaromatic subfraction has the lowest heteroatom content, Table 11.2, the highest (H/C) atomic ratio and the lowest molecular weight of the subfractions. With increasing aromaticity of the subfractions their (H/C) atomic ratios decrease and heteroatom contents increase. The monoaromatic subfraction contains only a small amount of sulfur and is colorless or pale yellow, but the rest of the fractions contain benzo-, dibenzo- and higher condensed thiophenes along with other sulfur compounds and have a yellow or orange color.

Detailed compositional studies of an aromatic fraction have been carried out only on Athabasca bitumen.[3,4] The method of investigation employed was a combination of chromatographic fractionations followed by FIMS and high-resolution EIMS studies.

Table 11.1 Aromatic contents of Alberta oil sand bitumens (wt% of bitumen)

Sample	Mono-	Di-	Polyaromatic	Total	Total by Syncrude
Athabasca	8.3[a]	3.8[a]	23.8[a]	35.9[a]	18–19[b]
	8.0[c]	3.6[c]	23.9[c]	35.5[c]	18–19[b]
	>12.5[d]	7.5[d]	16.4[d]	36.5[d]	
Cold Lake	8.1[a]	3.6[a]	24.4[a]	36.1[a]	–
Peace River	8.6[a]	3.3[a]	30.2[a]	42.1[a]	–
Wabasca	7.6[a]	2.5[a]	35.1[a]	45.2[a]	–

[a] USBM API-60 separation.[1] [b] Syncrude method of separation.[2] [c] Silica/alumina separation.[1] [d] Silica/alumina and FIMS/high-resolution EIMS.[3,4]

Table 11.2 Elemental composition of aromatic subfractions[a]

Fraction	Sample	wt%					(H/C) atomic	MW $g \cdot mol^{-1}$
		C	H	N	O	S		
Monoarom.	Athabasca	87.7	11.7	–	0.6	0.26	1.60	340
	Cold Lake	87.8	11.8	–	0.65	0.74	1.60	
Diarom.	Athabasca	87.6	10.6	–	0.6	2.4	1.46	380
	Cold Lake	87.6	10.7	–	0.8	2.2	1.46	
Polyarom.	Athabasca	81.3	9.8	0.13	2.0	7.1	1.44	490
	Cold Lake	81.6	9.6	0.16	2.5	6.7	1.41	

[a] USBM API-60 separation.[1]

1.0 Monoaromatic Subfraction

1.1 Subfraction 1c

The FI mass spectrum of the aromatic subfraction 1c (Figure 10.1 and Table 10.3) of Athabasca bitumen is shown in Figure 11.1. The molecular weight of this material is fairly broad, extending to $m/z \approx 700$ with a maximum at $m/z \approx 244$. This subfraction has been examined by high-resolution EIMS and, up to ~C_{40}, no sulfur-containing species were noted. The EIMS mass measurement confirmed the Z number* assignments listed in Table 11.3 where the FIMS results for the composition of this fraction by Z number are summarized. Most prominent are the series with $Z = -8$ and -10 corresponding to a series of alkyl aromatics with one and two naphthenic rings:

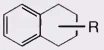

C_nH_{2n-8}

R=C $_8H_{17}$: $m/z = 244$

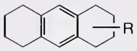

C_nH_{2n-10}

R=C $_4H_9$: $m/z = 242$

Figure 11.2 displays the concentration distribution with respect to carbon number for the $Z = -6$

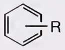

C_nH_{2n-6}

and –8 series. Both curves indicate a fairly smooth distribution between C_{12} and C_{50} with a maximum at C_{18}. The small blips appearing on the curves may indicate branching on the alkyl chains or the presence of more than one *n*-alkyl chain in the molecule. Figure 11.3 displays the corresponding plots for the tri- through pentacyclic monoaromatics in Fraction 1c. The tricyclic series has a maximum at C_{19}, the tetracyclics have maxima at C_{22}, C_{27} and C_{29} and the pentacyclics (C_nH_{2n-14}) have a flat plateau from ~C_{30} to ~C_{43}, showing a good correlation with the concentration distribution of the corresponding series of the saturate fraction, Figures 10.4 and 10.5.

1.2 Subfraction 1d

The FI mass spectrum of subfraction 1d is reproduced in Figure 11.4. The concentration distributions of the various series are plotted against carbon number in the molecule in Figures

---

*The term m/z is the mass/charge ratio, where z is the charge on the ion. In the series formula C_nH_{2n+Z} Z is a measure of the hydrogen deficiency.

Table 11.3 Composition of subfraction 1c by Z number[a]

Z in C_nH_{2n+Z}	Relative abundance (%) in subfraction 1c	%	
		Maltene	Bitumen
−6	13.7	1.11	0.92
−8	33.2	2.69	2.23
−10	27.8	2.25	1.87
−12	13.7	1.11	0.92
−14	7.0	0.57	0.47
−16	3.4	0.28	0.23
−18	1.2	0.10	0.08
	100.0	8.11	6.72[b]

[a] From Ref. 4. [b] 7.47% after correction for nondistillable residue.

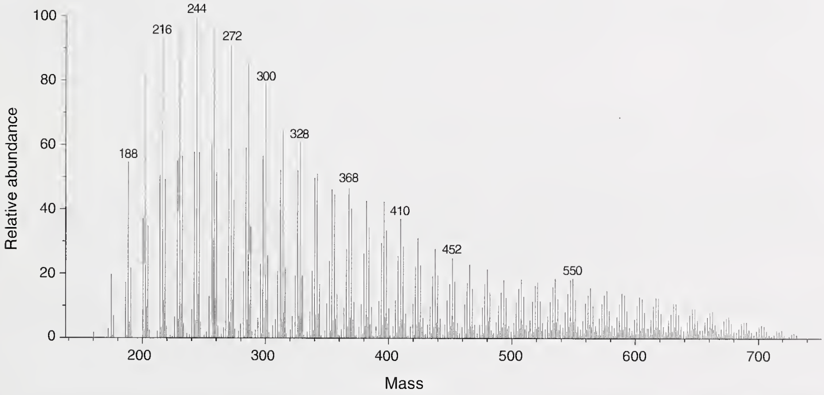

Figure 11.1 Field ionization mass spectrum of subfraction 1c. The prominent series of peaks spaced by 14 daltons at m/z = 216, 230, 244 *etc.* corresponds to a homologous series of compounds of formula C_nH_{2n-8} (tetralins) with maxima around n = 16, 17 and 18; peaks at 2 daltons less, 214, 228, 242, *etc.*, to compounds of formula C_nH_{2n-10} with maxima around n = 16, 17 and 18 and peaks at 218, 232, 246, *etc.*, to compounds of formula C_nH_{2n-6}(alkylbenzenes) with maxima around n = 16, 17 and 18.[4] The value of "n" extends to over 50.

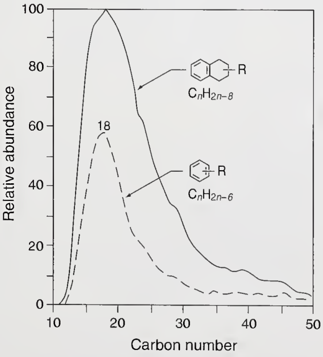

Figure 11.2 Z-Plots for the homologous series of monoaromatic hydrocarbons C_nH_{2n-6} and C_nH_{2n-8}, derived from the data of Figure 11.1, subfraction 1c. The plots display the relative abundance of the alkylbenzenes (Z = −6) and tetralins (Z = −8) in subfraction 1c as a function of carbon number.[4]

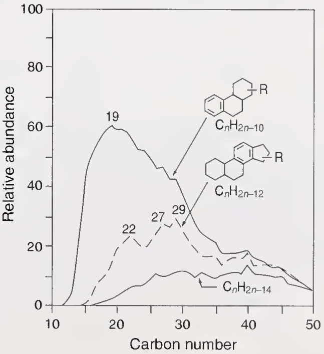

Figure 11.3 Z-Plots for the homologous series of tri-, tetra and pentacyclic monoaromatic hydrocarbons C_nH_{2n-10}, C_nH_{2n-12} and C_nH_{2n-14} derived from the data of Figure 11.1, subfraction 1c. The polymodality and broadness of the Z = −12 plot contrast with the distributions in Figure 11.2.[4]

11.5 and 11.6 and listed in Table 11.4 according to ring number. Here the correlation with the corresponding saturated series, Figures 10.4 and 10.5, Table 10.4, appears to be more pronounced and suggests the possibility of a genetic relationship between these monoaromatic series and the appropriate saturated hydrocarbon series. Indeed, this view will be reinforced later by additional results. The molecular weight distribution in Figure 11.4 is broad and extends to beyond $m/z = 700$ with a maximum at $m/z = 274$. A high-resolution EIMS study of subfraction 1d revealed that the $Z = -6$ and -8 series contain, in addition to hydrocarbons, homologous series of benzothiophenes, $C_nH_{2n-10}S$, and benzothiophenes with one naphthenic ring, $C_nH_{2n-12}S$. It will be noted here that the MWs of the C_n benzothiophene compounds coincide with the MWs of the C_{n+2} alkylbenzene compounds:

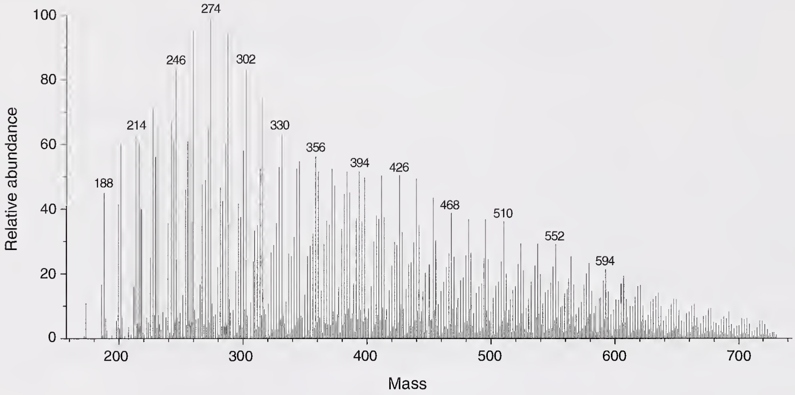

Figure 11.4 Field ionization mass spectrum of subfraction 1d. The prominent series of peaks at m/z = 246, 260, 274, *etc.* corresponds to a homologous series of alkylbenzenes of formula C_nH_{2n-6} with maxima around n = 18, 19 and 20.[4]

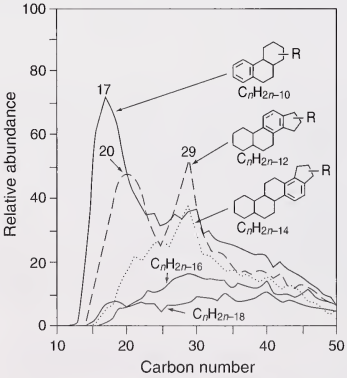

Figure 11.5 Z-Plots for the homologous series of monoaromatic hydrocarbons C_nH_{2n-10}, C_nH_{2n-12} and C_nH_{2n-14} derived from the data of Figure 11.4, subfraction 1d. Note the prominent maxima at $n = 20$ and 29 on the $Z = -12$ trace and at $n = 29$ on the $Z = -14$ trace.[4]

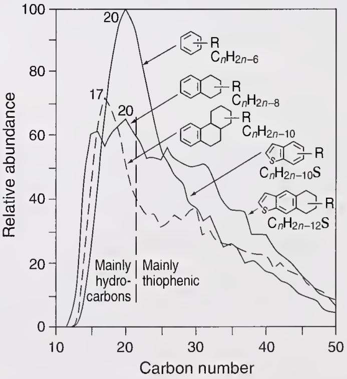

Figure 11.6 Z-Plots for the remaining homologous series derived from the data of Figure 11.4, subfraction 1d. The traces corresponding to $Z = -8$ and -10 have been shown by high-resolution EIMS to be mainly the hydrocarbon series C_nH_{2n-8} and C_nH_{2n-10} below n = 22. Above this carbon number the series are dominated by alkylbenzo[b]thiophenes and alkylcycloalkylbenzo[b]thiophenes of formula $C_nH_{2n-10}S$ and $C_nH_{2n-12}S$.[4]

Table 11.4 Composition of subfraction 1d by Z number[a]

Z in C_nH_{2n+Z}[b]	Relative abundance (%) in subfraction 1d	% Maltene	% Bitumen
−6 and $C_nH_{2n-10}S$	22.4	1.23	1.02
−8 and $C_nH_{2n-12}S$	24.7	1.35	1.13
−10	18.5	1.01	0.84
−12	14.3	0.78	0.65
−14	9.8	0.54	0.45
−16	6.2	0.34	0.28
−18	4.0	0.22	0.18
	99.9	5.47	4.55[c]

[a] From Ref. 4. [b] About two-thirds of the $Z = -6$ and -8 series comprise sulfur compounds and the rest, hydrocarbons. For $n \leq 20$ the hydrocarbon series are more abundant, while for $n \geq 20$ the sulfur-containing series becomes dominant. [c] 5.06% after correction for nondistillable residue.

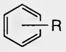
C_nH_{2n-6} ($C_{20}H_{34}$)

R = $C_{14}H_{29}$: $m/z = 274$

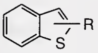
$C_nH_{2n-10}S$ ($C_{18}H_{26}S$)

R = $C_{10}H_{21}$: $m/z = 274$

Differentiation is, however, possible by the determination of the MWs by high-resolution EIMS. Thus, for example, the MW of the $C_{12}H_{14}S$ molecule is 190.303 amu and that of the $C_{14}H_{22}$ molecule is 190.328 amu.

The monoaromatic material in subfraction 1c, Table 11.3, comprises 6.72 wt% of the bitumen. It is a clear, colorless liquid almost free from sulfur and other heteroatoms. The heavier cyclic material, subfraction 1d, reported in Table 11.4, is a clear, pale yellow liquid which contains significant quantities of sulfur and comprises 4.55 wt% of the bitumen. Thus, the combined monoaromatic subfractions 1c and 1d amount to 11.3 wt% and, after correction for the presence of nondistillables, 12.5 wt% of the bitumen. Comparing this value with those derived by conventional chromatographic methods, 8.0 and 8.3 wt%, Table 11.1, it is evident that the latter tend to underestimate the amount of monoaromatics present in the bitumen. The concentration distribution with respect to ring number in the molecule has maxima at two and three rings, as was found for the saturate fraction of the bitumen, Table 10.4.

2.0 Diaromatic Subfraction

The next fraction in the primary separation of the maltene, subfraction 2 (Figure 10.1 and Table 10.2), amounted to 23.1% of the maltene or 19.2% of the bitumen. Of this, 76% was distillable as a yellow oil which was further fractionated on an alumina column into seven subfractions with individual yields as listed in Table 11.5 in a total amount of 14.5% of the bitumen. The small sizes of subfractions 2f and 2g prevented further analysis of these fractions and therefore only subfractions 2a through 2e were examined by FIMS and high-resolution EIMS.

2.1 Subfraction 2a

The FIMS mass intensity data for subfraction 2a are shown in Figure 11.7. The distribution by molecular weight is bimodal with maxima centered at $m/z = 230$ and 390. At the low mass end of the distribution, the large peaks at $m/z = 224$ and 238 are due to the homologous series C_nH_{2n-14} with $n = 17$ and 18. Interspersed between the C_nH_{2n-14} peaks is a series of

Table 11.5 Chromatographic separation of subfraction 2 on alumina[a]

Subfraction	Eluent	% of bitumen		Color
		Distillate	Distillate corrected for nondistillable residue	
2a	3% Bz/C_5[b]	6.27	8.25	colorless
2b	6% Bz/C_5	2.89	3.8	pale yellow
2c	12% Bz/C_5	2.79	3.7	light yellow-green
2d	25% Bz/C_5	1.90	2.5	yellow-green
2e	50% Bz/C_5	0.52	0.7	yellow-green
2f	100% Bz	0.10	0.13	
2g	CH_3OH/CH_2Cl_2	0.07	0.09	brown
	Total	14.5	19.2	

[a] From Ref. 4. [b] Benzene/*n*-pentane.

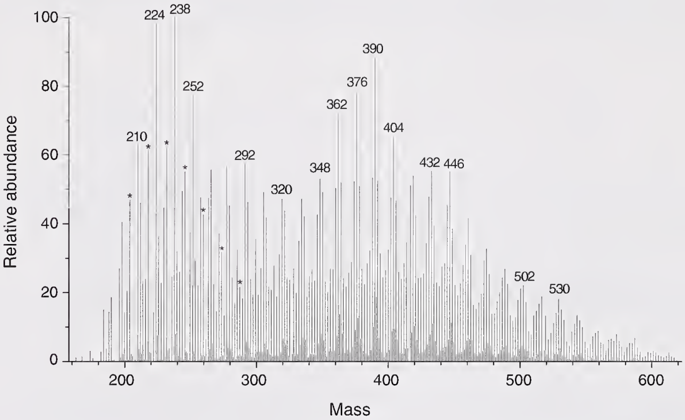

Figure 11.7 Field ionization mass spectrum of subfraction 2a. The prominent series of peaks at $m/z = 224$, 238, 252, *etc.*, correspond to a homologous series of diaromatic hydrocarbons of formula C_nH_{2n-14} with maxima around $n = 17$, 18 and 19. The peaks marked with an asterisk correspond to a homologous series of benzothiophenes, $C_nH_{2n-10}S$ with the peak at $m/z = 232$ corresponding to $C_{15}H_{20}S$. The peaks at 376, 390, 404, *etc.*, correspond to a homologous series of diaromatic hydrocarbons of formula C_nH_{2n-16} with maxima around $n = 28$, 29 and 30. The peaks 2 daltons above and below these major peaks correspond to compounds of formula C_nH_{2n-14} and C_nH_{2n-18} which have one less or one more saturated ring, respectively, than the C_nH_{2n-16} series. The maximum around $n = 29$ suggests that these series are related to the steranes and hopanes in the saturate fraction.[4]

benzothiophene peaks, marked with asterisks, with a maximum at $n = 16$. Benzothiophenes are only minor components of this fraction. At the high mass end of the distribution around $m/z = 390$, the large peaks are due to a series of hydrocarbons corresponding to the $Z = -14, -16$ and -18 series with a maximum at $n = 29$.

Molecules of formula C_nH_{2n-14} may be monoaromatic compounds containing four additional saturated rings or diaromatic compounds with one additional saturated ring. However, the lower MW ($n \approx 16$–19) members of the C_nH_{2n-14} series must contain two aromatic rings due to the low value of n. Moreover, monoaromatic compounds containing three or four saturated rings are in abundance in subfractions 1c and 1d and thus are not expected to be present in subfraction 2a. The low-MW $Z = -14$ compounds of subfraction 2a possess only a few methylene groups external to the ring system. Their distribution with respect to n is smooth and covers only a narrow range of n.

In contrast, the high-MW $Z = -14$ to -18 series exhibit a maximum at $n = 29$. They must be diaromatic compounds with one to three additional saturated rings:

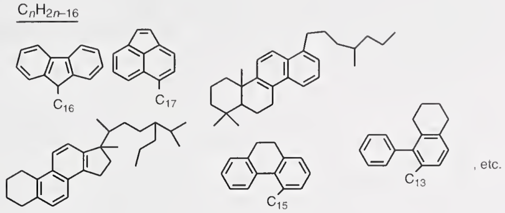

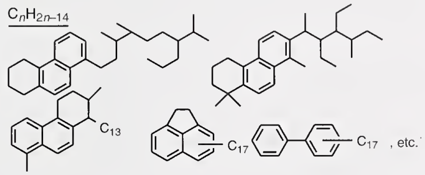

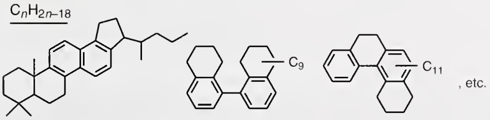

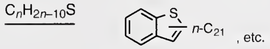

The distribution of these compounds with respect to n (maximum at $n = 29$ with shoulders at $n = 27$ and 31–33) is a somewhat smoother version of the distribution of the saturated hydrocarbons possessing four and five rings. Like the saturate subfraction 1a (16.8%), aromatic subfraction 2a is an abundant fraction (8.3%) of the bitumen. The percentage distribution of the various Z series of compounds in subfraction 2 is listed in Table 11.6.

2.2 Subfraction 2b

The FIMS mass intensity data for subfraction 2b are shown in Figure 11.8. This fraction is dominated by the C_nH_{2n-14} series with maxima at $n = 16, 17, 18$ ($m/z = 210, 224$ and 238). On comparing this distribution with that for the $Z = -14$ series in Figure 11.7 it will be noted that subfraction 2a has a second maximum at $n = 29$ whereas subfraction 2b does not. The $Z = -14$ series has either two aromatic and one naphthenic rings or one aromatic and four naphthenic rings. However, since—as with subfraction 2a—the maximum occurs at low n values, 16, 17, 18, these molecules cannot contain five rings and therefore they must be diaromatic with one naphthenic ring. Also present are benzothiophenes $C_nH_{2n-10}S$:

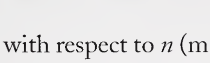

The peaks marked with an asterisk are mainly n-alkyl substituted benzothiophenes, on the basis of their smooth distribution.

The $m/z = 184$ peak is the $n = 14$ member of the naphthalene, C_nH_{2n-12}, series:

Table 11.6 Percentages of various *Z* series of compounds present in subfraction 2[a]

Mass series "*Z*"	Possible elemental compositions	% in subfraction[b]				
		2a	2b	2c	2d	2e
−6	C_nH_{2n-6} C_nH_{2n-20} $C_nH_{2n-10}S$	14.1	14.8	14.7	18.0	15.1
−8	C_nH_{2n-8} C_nH_{2n-22} $C_nH_{2n-12}S$	12.6	9.0	6.0	8.2	14.3
−10	C_nH_{2n-10} C_nH_{2n-24}	8.7	3.4	3.5	4.4	8.5
−12	C_nH_{2n-12} $C_nH_{2n-16}S$	11.1	14.5	36.0	23.4	17.0
−14	C_nH_{2n-14} $C_nH_{2n-18}S$	20.9	31.8	19.5	13.1	5.8
−16	C_nH_{2n-16}	19.7	18.1	10.7	12.2	6.6
−18	C_nH_{2n-18} $C_nH_{2n-22}S$	12.8	8.4	9.6	20.6	32.7

[a] From Ref. 4. [b] The percentage of a given *z* series in a subfraction was obtained by first summing the ion intensities of the compounds in a given homologous series indicated in the first column on the left over the range from *n* = 10 to 50. This sum is then divided by the total number of ions summed over all the series from–6 to–18 multiplied by 100. Possible elemental compositions associated with the various *z* series are given in the second column on the left. Only the major elements, C, H, and S, present in the fractions are considered.

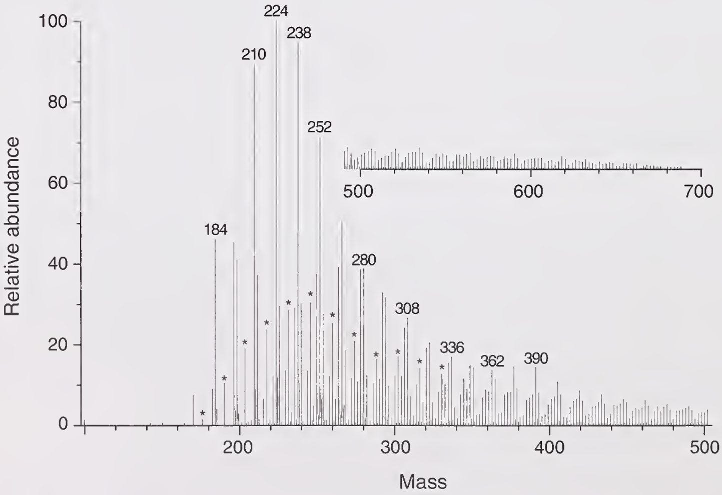

Figure 11.8 Field ionization mass spectrum of subfraction 2b. The prominent series of peaks at *m/z* = 210, 224, 238, *etc*., correspond to a homologous series of diaromatic hydrocarbons of formula C_nH_{2n-14} with maxima around *n* = 16, 17 and 18. The peaks marked with an asterisk are benzothiophenes $C_nH_{2n-10}S$.[4]

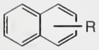

C_nH_{2n-12}

High-resolution EIMS has shown that higher members of this series consist of a mixture of naphthalenes and dibenzothiophenes, $C_nH_{2n-16}S$, which are the most abundant compounds in the next subfraction 2c.

2.3 Subfraction 2c

The FIMS data for subfraction 2c are shown in Figure 11.9. The spectrum is dominated by a long series of *n*-alkyldibenzothiophenes, $C_nH_{2n-16}S$,

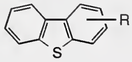

$C_nH_{2n-16}S$

with a maximum at $n = 16$, $m/z = 240$. The homologous series of compounds with an apparent Z value of -6 is actually a mixture of a series of hydrocarbons with $Z = -20$ (≈75%) and benzothiophenes, $C_nH_{2n-10}S$ (25%). The minor series of peaks corresponding to C_nH_{2n-14} is a mixture again and, in addition to the hydrocarbon series, contains $C_nH_{2n-18}S$, dibenzothiophenes with an additional cyclohexane ring.

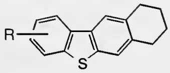

$C_nH_{2n-18}S$

The mixture is dominated by the $Z = -14$ components at the low molecular weight end of the distribution, while the $C_nH_{2n-18}S$ components dominate the high molecular weight end.

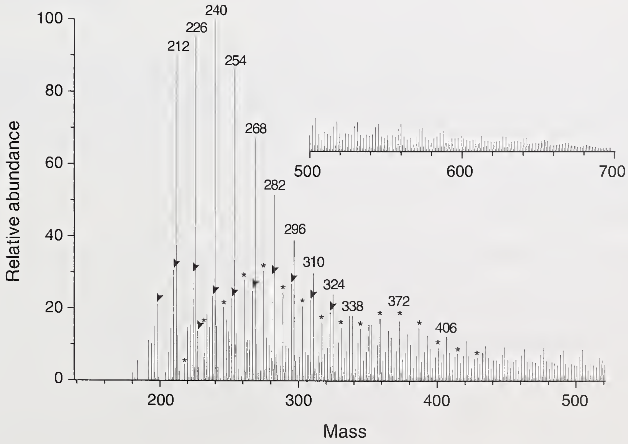

Figure 11.9 Field ionization mass spectrum of subfraction 2c. The prominent series of peaks at m/z = 212, 226, 240, *etc.*, correspond to a homologous series of alkyldibenzo[b,d]thiophenes, $C_nH_{2n-16}S$, with maxima around n = 14, 15 and 16. The peaks labelled with an asterisk represent mixtures of C_nH_{2n-20} and $C_nH_{2n-10}S$ and those labelled with an arrowhead, mixtures of C_nH_{2n-14} hydrocarbons and $C_nH_{2n-18}S$ alkylcycloalkyldibenzo[b,d]-thiophenes.[4]

2.4 Subfraction 2d

The FI mass spectrum of subfraction 2d is reproduced in Figure 11.10. The compounds in greatest abundance at *m/z* = 206 and 220 belong to the C_nH_{2n-18} series

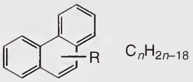

with a maximum at n = 16 and 17. The molecules of this series contain three fused aromatic rings, in contrast to the C_nH_{2n-18} series of subfraction 2a which possesses only two fused aromatic rings and three saturated rings. The maximum in n in the diaromatic series in subfraction 2a occurs at $n \approx 29$ but in the triaromatic series here the maximum is at n = 17. In addition to the triaromatic $Z = -18$ series, subfraction 2d contains substantial quantities of dibenzothiophenes. In subfraction 2c the maximum in the $C_nH_{2n-16}S$ series was at n = 16 while in subfraction 2d it is at n = 15.

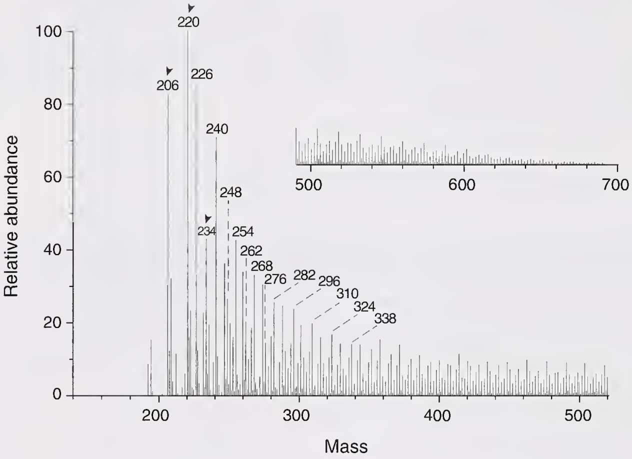

Figure 11.10 Field ionization mass spectrum of subfraction 2d. The series of peaks at *m/z* = 206, 220, 234, *etc.*, correspond to a homologous series of triaromatic hydrocarbons of formula C_nH_{2n-18} with maxima around n = 16, 17 and 18 and those at *m/z* = 226, 240, 254, *etc.*, to a homologous series of dibenzothiophenes of formula $C_nH_{2n-16}S$ with maxima around n = 15, 16 and 17.[4]

2.5 Subfraction 2e

The FI mass spectrum of subfraction 2e is presented in Figure 11.11. This fraction is dominated by a series of peaks which have the nominal masses of the $Z = -18$ series. The lowest molecular weight (220 and 234) members of this series are mainly C_nH_{2n-18} as in subfraction 2d. However, the major peaks at *m/z* = 262 and 276 belong to the tribenzothiophene series, $C_nH_{2n-22}S$:

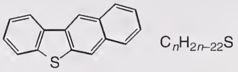

A summary of composition, including the percentage distribution of the various Z series in subfractions 2a through 2e, is given in Table 11.6. The most important constituents are the ones having Z values of −12, −14 and −16 and the least abundant are the ones with Z = −10 and −8.

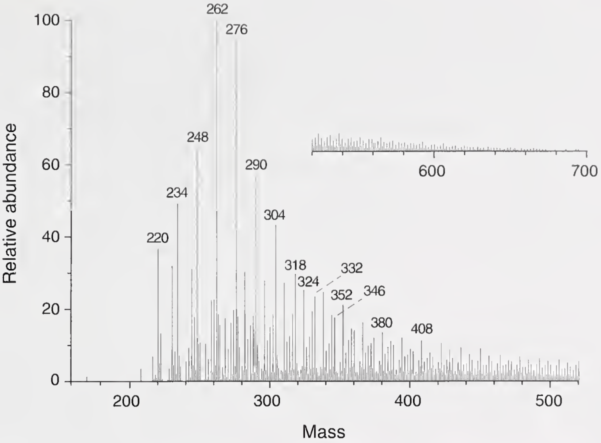

Figure 11.11 Field ionization mass spectrum of subfraction 2e. The series of peaks at $m/z = 220, 234$, *etc.* have the nominal mass of the $Z = -18$ series. High-resolution EIMS shows that the $m/z = 220$ and 234 members are mainly C_nH_{2n-18} as in subfraction 2d. The peaks at $m/z = 262$ and 276 are mainly $C_nH_{2n-22}S$ with $n = 18$ and 19. The peaks at $m/z = 324, 352, 380$ and 408 are mixtures of C_nH_{2n-12} and $C_nH_{2n-16}S$.[4]

3.0 Triaromatic Subfraction

Subfraction 3 in the primary separation of the maltene, Figure 10.1 and Table 10.2, amounted to 4.8 wt% of the bitumen. On distillation, it yielded an orange oil corresponding to 43% of the subfraction, or 2.1 wt% of the bitumen. This oil was then further separated chromatographically on an alumina column into seven subfractions, Table 11.7, and five of these subfractions were investigated with FIMS and high-resolution EIMS.

3.1 Subfraction 3b

The FIMS mass intensity data for subfraction 3b are shown in Figure 11.12. The large isolated peaks are due to cyclic sulfides belonging to the following series:

- $Z = -2$ with maximum abundance at $m/z = 212$, elemental formula $C_{13}H_{24}S$;
- $Z = -4$ with maximum abundance at $m/z = 252$, elemental formula $C_{16}H_{28}S$;
- $Z = -6$ with maximum abundance at $m/z = 348$, elemental formula $C_{23}H_{40}S$; and
- $Z = -10$ with maximum abundance at $m/z = 456$, elemental formula $C_{31}H_{52}S$.

Concentration *versus* carbon number plots for these series are shown in Figure 11.13.

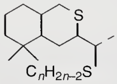

$C_nH_{2n-2}S$

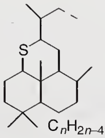

$C_nH_{2n-4}S$

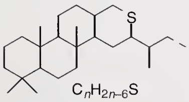

$C_nH_{2n-6}S$

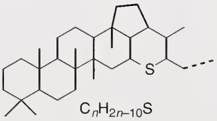

$C_nH_{2n-10}S$

The sulfides detected here show a striking resemblance in their elemental composition and concentration distribution to a group of sulfoxides detected in the polar fraction of the bitumen,[5] Chapter 12, indicating a genetic relationship between these two classes of constituents of the bitumen. As their elemental composition indicates, the sulfides and sulfoxides have cyclic

Table 11.7 Chromatographic separation of subfraction 3 on alumina[a]

Subfraction	Eluent	% of bitumen		Color
		Distillate	Distillate corrected for nondistillable residue	
3a	3% Bz/C_5[b]	0.05	0.12	colorless
3b	6% Bz/C_5	0.26	0.60	colorless
3c	12% Bz/C_5	0.31	0.72	faint yellow
3d	25% Bz/C_5	0.44	1.02	pale yellow
3e	50% Bz/C_5	0.39	0.91	yellow
3f	100% Bz	0.24	0.56	yellow
3g	CH_3OH/CH_2Cl_2	0.38	0.88	brown
	Total	2.07	4.81	

[a] From Ref. 4. [b] Benzene/*n*-pentane.

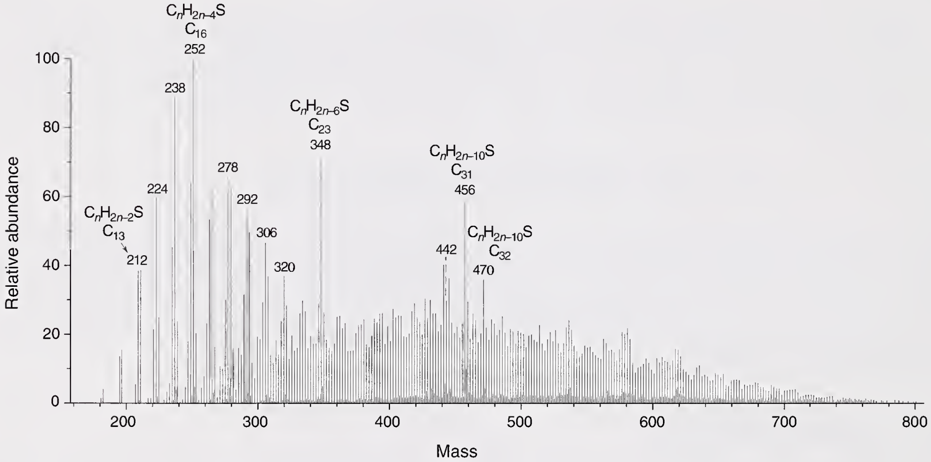

Figure 11.12 Field ionization mass spectrum of subfraction 3b. The series of peaks at $m/z = 198$, 212, 226, *etc.*, corresponds to bicyclic sulfides $C_nH_{2n-2}S$ with a maximum at n = 13; peaks at $m/z = 224$, 238, 252, *etc.*, to tricyclic sulfides $C_nH_{2n-4}S$ with a maximum at $n = 16$; peaks at 334, 348, 362, *etc.*, to tetracyclic sulfides $C_nH_{2n-6}S$ with a maximum at $n = 23$ and peaks at 442, 456, 470, *etc.*, to hexacyclic sulfides $C_nH_{2n-10}S$ with a maximum at $n = 31$.[4]

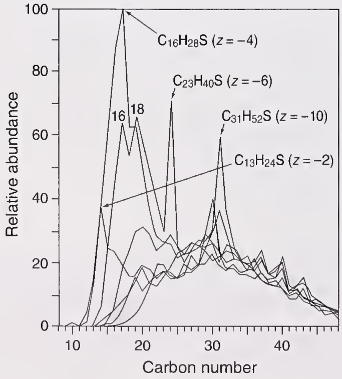

Figure 11.13 *Z*-Plots for the homologous series of saturated sulfides derived from the data of Figure 11.12, subfraction 3b. The elemental formulae of the prominent peaks were confirmed by high-resolution EIMS.[4]

structures ranging from two to six rings. This genetic relationship can be further extended to their parent hydrocarbon molecules (obtained upon hydrodesulfurization), the corresponding series of bi-, tri- and pentacyclic terpanes identified in the saturate fraction of the bitumen. These compounds were first detected[4] in Athabasca bitumen and their structures were subsequently established.[6] They represented the first examples of families of sulfur-containing biomarkers discovered in petroleum and they have since been shown to be ubiquitous constituents of sulfur-containing petroleums.

As can be seen from Figure 11.12, the possibility of the presence of pentacyclic and even heptacyclic sulfides, *e.g.*

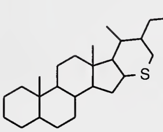

and

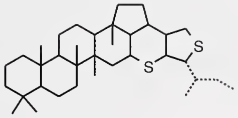

as well as some of their partially aromatized derivatives, *e.g.*

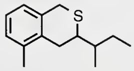

,

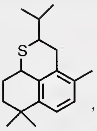

,

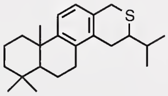

, etc.

cannot be excluded; on the contrary, it appears quite likely.

The structures, possible origins and geochemical significance of these sulfur compounds will be discussed in detail in Chapters 12 and 13.

3.2 Subfraction 3c

The FI mass intensity data for subfraction 3c are shown in Figure 11.14. In contrast to the previous subfraction, the principal homologous series present in this subfraction consist mainly of aromatic compounds. The main series present are the C_nH_{2n-20}, C_nH_{2n-22}, C_nH_{2n-24} and C_nH_{2n-26} hydrocarbons and the $C_nH_{2n-24}S$ sulfide series.

The $z = -20$ series features three fused aromatic rings and one naphthenic ring, as in triaromatized steranes,

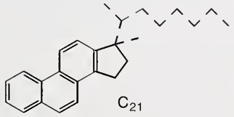

which have been detected among the biomarkers in the bitumen, Chapter 13. The carbon number in the series covers the range 17–26 with a maximum at C_{20}.

The $z = -22$ series may correspond to the ring-opened "secohopane" structure,

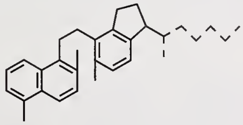

and the series extends from C_{25} to about C_{31}.

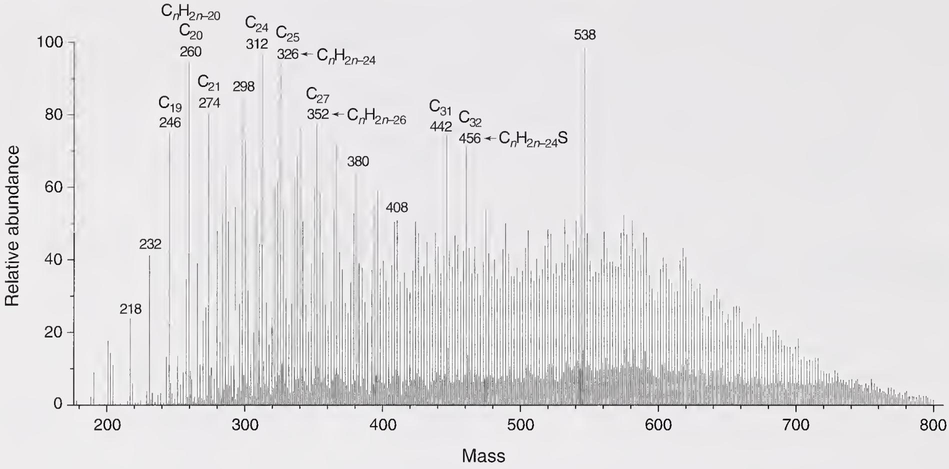

Figure 11.14 Field ionization mass spectrum of subfraction 3c. The series of peaks at m/z = 246, 260, 274, *etc.*, correspond to a series of aromatic hydrocarbons of formula C_nH_{2n-20} with maxima at n = 19, 20 and 21; those at m/z = 298, 312, 326, *etc.*, to a series of aromatic hydrocarbons of formula C_nH_{2n-24} with maxima around n = 23, 24 and 25, and those at m/z = 352, 366, 380, *etc.*, to a series of aromatic hydrocarbons of formula C_nH_{2n-26} with maxima around n = 27, 28 and 29. The peaks at m/z = 442 and 456 were shown by high resolution EIMS to be $C_nH_{2n-24}S$ with n = 31 and 32. A satisfactory mass measurement could not be obtained for the peak at m/z = 538.[4]

In the $Z = -24$ series the four-fused-aromatic-ring structure could have arisen from the aromatization and dealkylation of rings A–D and the opening of the E ring in hopanes:

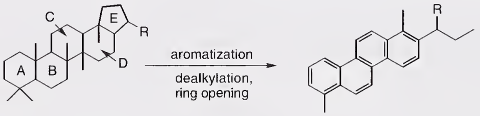

The most abundant (C_{24}) member may have the structure

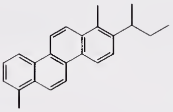

and the series range may go up to about C_{31}.

Likewise, the $Z = -26$ series could have arisen from the aromatization and dealkylation of hopanes without E ring opening:

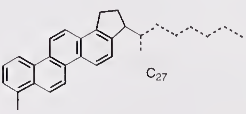

with a carbon range of C_{23}–C_{30} and a maximum at C_{27}.

Finally, the two large peaks at m/z = 442 and 456 with n = 31 and 32 in the $C_nH_{2n-24}S$ series could be tentatively assigned to the hexacyclic sulfides detected in subfraction 3b, in which three of the rings are now aromatized:

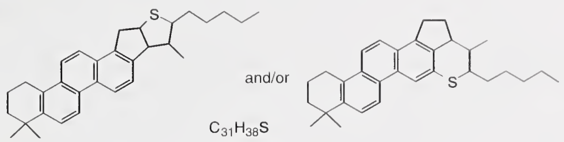

$C_{31}H_{38}S$

The partial or full aromatization of alicyclic structures invoked above in the correlation of aromatic structures to alicyclic structures is known to occur readily during the maturation of petroleum.

3.3 Subfraction 3d

The FIMS mass intensity data for subfraction 3d are reproduced in Figure 11.15. The homologous series in this fraction giving rise to the peaks at *m/z* = 288, 302, 316, 330, *etc.* belong to some unidentified $C_nH_{2n-24}S$ series. The second prominent homologous series at *m/z* = 350, 364, 378, *etc.*, is apparently a mixture of two homologous series which were not resolved sufficiently to permit a high-resolution EIMS determination of the atomic composition.

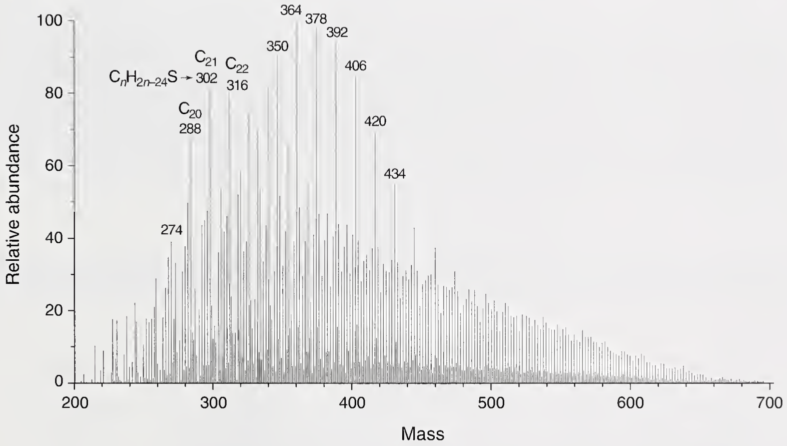

Figure 11.15 Field ionization mass spectrum of subfraction 3d. The series of peaks at *m/z* = 288, 302, 316, *etc.*, belong to the $C_nH_{2n-24}S$ series with maxima around $n = 20$, 21 and 22. The prominent series of peaks at *m/z* = 364, 378 and 392 could not be resolved sufficiently by high-resolution EIMS to unambiguously determine the atomic composition.[4]

3.4 Subfraction 3e

Subfraction 3e, according to its FI mass spectrum, Figure 11.16, consists of a mixture of numerous classes of compounds. At the low mass end, the series of odd mass number peaks 235, 249, 263, *etc.*, are nitrogen-containing compounds belonging to the homologous series $C_nH_{2n-17}N$ with a maximum at *m/z* = 263 which corresponds to the elemental formula $C_{19}H_{21}N$. These series of compounds could then be either benzoquinolines or the isomeric carbazoles with an additional naphthenic ring,

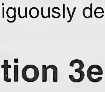

benzoquinoline

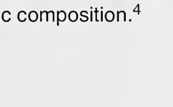

cyclohexanecarbazole

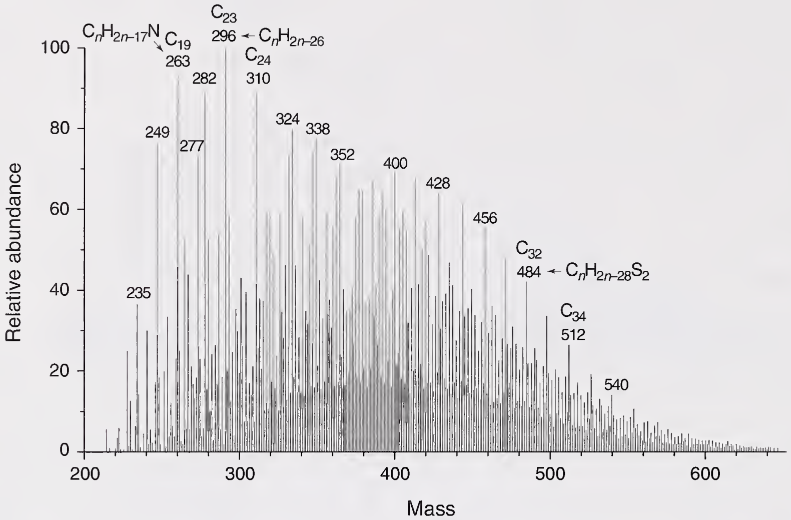

Figure 11.16 Field ionization mass spectrum of subfraction 3e. The series of peaks at *m/z* = 249, 263, 277, *etc.*, corresponds to the nitrogen-containing series $C_nH_{2n-17}N$ with maxima around n = 18, 19 and 20, and those at *m/z* = 282, 296, 310, *etc.*, to the polyaromatic series C_nH_{2n-26} with maxima around n = 22, 23 and 24. The high-mass series of compounds at *m/z* = 456, 470, 484, *etc.*, corresponds to $C_nH_{2n-28}S_2$ with maxima around n = 30, 31 and 32.[4]

However, quinolines are quite basic compounds and therefore would have long retention times on silica gel. Consequently, the compounds in question must belong to the carbazole series with R = C_1–C_4.

The hydrocarbon peaks at *m/z* = 282, 296, 310, *etc.* are members of the homologous series C_nH_{2n-26}, a series isomeric with the C_nH_{2n-26} series present in subfraction 3c. The maximum of this series in subfraction 3c appeared at C_{27}, Figure 11.14, while here it occurs at C_{23} and its carbon numbers cover the approximate range 22–27.

The major high-mass series compounds in the spectrum at *m/z* = 456, 470, 484, *etc.*, have the formula $C_nH_{2n-28}S_2$ and thus for the *m/z* = 484 member, an elemental formula of $C_{32}H_{36}S_2$. These compounds are the only molecules in the maltene which have been found to contain more than one sulfur atom. Their structures have not been elucidated, but they appear to be related to the $C_nH_{2n-24}S$ series in subfraction 3c. The fully aromatized hopanoid disulfide, *e.g.*

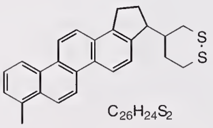

$C_{26}H_{24}S_2$

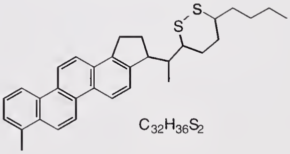

$C_{32}H_{36}S_2$

may be a plausible structural candidate. This would also be consistent with the detection of hopanes bound to asphaltene molecules in the bitumen by two sulfide bridges in the alkyl side chain (Chapter 14). The approximate carbon range for this series is 26–36.

3.5 Subfraction 3f

The FIMS mass intensity data for subfraction 3f are reproduced in Figure 11.17. Two series, a hydrocarbon series with elemental formula C_nH_{2n-24} and a maximum at $n = 21$,

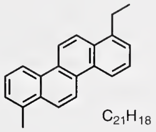

and a sulfide or thiophene series with elemental formula $C_nH_{2n-28}S$ and maximum at C_{22}, dominate the subfraction. For the latter molecule, a possible structure would be:

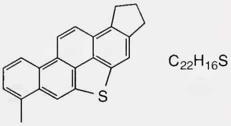

High-resolution EIMS showed that the composition changes abruptly, the peak at $m/z = 270$ having an elemental formula $C_{21}H_{18}$ and the peak at $m/z = 312$ an elemental formula $C_{22}H_{16}S$, in spite of the two series appearing to be a single homologous series whose members' molecular weight changes by mass 14 corresponding to a CH_2 group. A thiophene molecule, structurally analogous to the above $C_{22}H_{16}S$ compound,

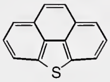

corresponding to the series formula $C_nH_{2n-20}S$, has been identified in a coal sample.[7]

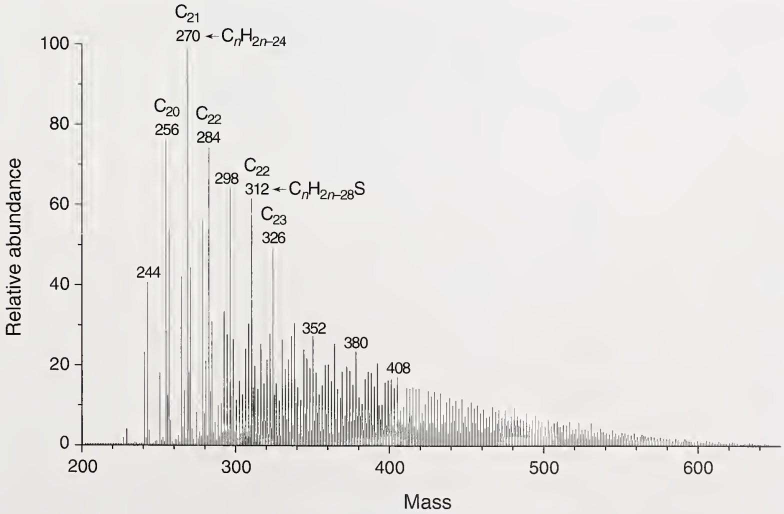

Figure 11.17 Field ionization mass spectrum of subfraction 3f. The prominent series of peaks at $m/z = 256, 270, 284$, *etc.* corresponds to the series C_nH_{2n-24} with a maximum at $n = 21$. The peak at $m/z = 312$ belongs to the series $C_nH_{2n-28}S$ with $n = 22$.[4]

4.0 General Properties of Distillable Aromatics

Up to this point, we have been concerned with the chemical composition of that portion of the aromatic fraction of Athabasca maltene which was distillable at 240℃ and at 10^{-3} torr. This comprises about 90% of subfraction 1 (saturates + monoaromatics), 76% of subfraction 2 (diaromatics), and 43% of subfraction 3 (triaromatics), Table 10.2. Thus, as expected, the monoaromatic subfraction is the most volatile and the triaromatic subfraction is the least volatile. Also, the color becomes more pronounced as we go from the mono- to the triaromatic subfraction, and this is largely due to the increasing content of aromatic sulfur compounds.

Subfractions 1c and 1d consist of monoaromatics ranging from alkylbenzenes to alkylbenzenes with up to six naphthenic rings, Table 11.8, in a combined amount of 11.3% distillable and 12.6% total if one includes the nondistillable portion of the bitumen. This is an approximate figure because it may include some diaromatic molecules and, moreover, it was made with the questionable assumption that the relative monoaromatic content of the nondistillable portion of the bitumen is the same as that of the distillable portion. On the other hand, to determine the total monoaromatic content of the bitumen, the monoaromatic content of subfraction 2 would have to be taken into consideration and therefore the 12.6% value representing the losses and gains in error may be considered to be a reasonable estimate. According to ring number distribution, the largest subfraction is the bicyclic series followed by the tricyclic series, together accounting for over 50% of the combined subfractions 1c and 1d. The concentration distribution follows the order bi- > tri- > mono- > tetra- > penta > hexa- > heptacyclics, which is similar to that found for the saturates: bi- > tri- > tetra- > penta- > mono- > hexacyclics or acyclics. The concentration distributions as a function of carbon number, Figures 11.2–11.6, are again quite similar to what we have encountered in the saturates, that is, the maxima occurred at the following carbon numbers:

Table 11.8 Distribution of compound types in the monoaromatic subfractions 1c and 1d

Compound type	Wt% of bitumen			Total dist. + nondist.[a]
	Subfraction 1c	Subfraction 1d	Total	
	0.92	1.02	1.94	2.16
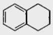	2.23	1.13	3.36	3.73
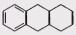	1.87	0.84	2.71	3.01
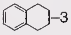 [b]	0.92	0.65	1.57	1.74
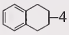	0.47	0.54	1.01	1.12
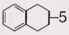	0.23	0.28	0.51	0.57
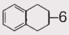	0.08	0.18	0.26	0.29
Total	6.7	4.6	11.3	12.6

[a]Total of 1c and 1d including nondistillable residue. [b] Number of naphthenic rings.

	Monoaromatics	Saturates
monocyclics	18, 20	18
bicyclics	18, 20 (15)	15 (19)
tricyclics	17, 19	19 (23,29)
tetracyclics	29 (20, 22)	29 (21)
pentacyclics	29	30

The close analogy between the concentration distributions (by both ring number and carbon number) in the monoaromatics and the saturates again points to a genetic relationship between the two fractions, suggesting that the aromatic fraction was formed mainly by aromatization of the saturates.

Subfraction 2 is another major aromatic fraction of the bitumen comprising 19.2% or, after molecular distillation, 14.5% of the bitumen. It consists mainly of diaromatic hydrocarbons, lesser amounts of monoaromatic hydrocarbons and even lesser amounts of triaromatic hydrocarbons, along with copious quantities of sulfur compounds including alkylbenzothiophenes, dibenzothiophenes and their naphtheno and higher benzo derivatives, Tables 11.6 and 11.9. The concentration distribution with respect to ring number follows the order tri- > bi- > mono- > tetracyclics. This pattern of distribution is different from that of the monoaromatics; nonetheless the fraction on the whole also exhibits a definite correlation with the saturates within the same ring number class and the prominent hydrocarbon members of the fraction listed in Table 11.9 can be, in principle at least, derived from the known biomarkers in the saturates. The following examples may serve as illustrations:

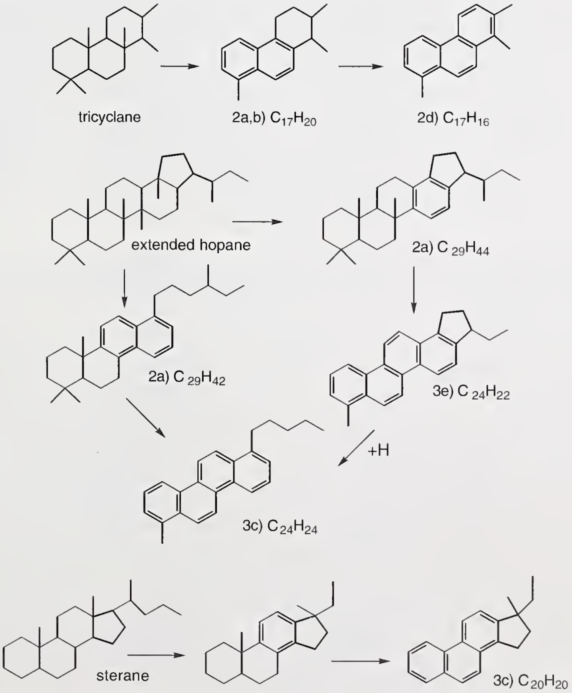

Table 11.9 Structures of the most abundant component types of subfraction 2

Subfraction	Compound type
2b	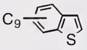 $C_{17}H_{24}S$ 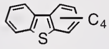 $C_{16}H_{16}S$ 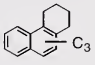 $C_{17}H_{20}$
2c	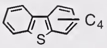 $C_{16}H_{16}S$ 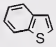 C_8H_6S 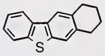 $C_{16}H_{14}S$ 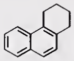 $C_{14}H_{14}$
2d	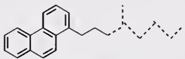 $C_{17}H_{16}$ 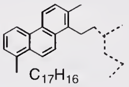 $C_{17}H_{16}$ 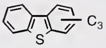 $C_{15}H_{14}S$
2e	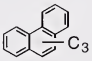 $C_{17}H_{16}$ 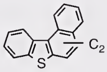 $C_{18}H_{14}S$

Starting with a saturated cyclic biomarker, as the aromatization progresses, dealkylation and ring opening will take place as well, and the maximum in the concentration *versus* the carbon number in the series plots will shift to smaller carbon numbers, Figures 11.18 and 11.19. Thus, in Figure 11.18 the maximum concentration in the saturated tetracyclic series occurs at C_{29} with a secondary maximum around C_{21} which is due to the loss of part of the isoprenoid side chain. As the aromatization progresses, the maximum shifts first from C_{29} to C_{21} and then to C_{19}, owing to simultaneous dealkylation. Also, the pentacyclic series in the saturate fraction has its maximum at C_{30} which, similarly to the tetracyclic series, shifts to C_{23} in the tetraaromatic series, again because of the loss of the methyl groups and part of the alkyl side chain from the ring structure (Figure 11.19). The existence of these correlations lends strong support to the proposition that the bulk of the polycyclic aromatic hydrocarbons in subfractions 1c and d, subfraction 2, and, as will be discussed below, in subfraction 3, originated from the aromatization, ring cleavage and dealkylation of saturated, mainly cyclic terpenoid, hydrocarbon-type biomarkers in the oil during thermal maturation.

The aromatic sulfur compounds in fraction 2, alkylbenzothiophenes and alkyldibenzothiophenes, may be in part related to the asphaltene fraction, as will be seen in Chapter 14.

Subfraction 3 is a medium-size fraction in the bitumen, amounting to 5.8% of the bitumen. However, its volatility is low, only 43% being distillable (corresponding to 2.5% of the bitumen). This subfraction, Table 11.10, contains several series of saturated cyclic sulfides ranging from two to six rings. They were first identified in Athabasca and other Alberta bitumens and oils and later shown to be ubiquitously present in all sulfur-containing petroleums. Their structure will be discussed in the next chapter which deals with the chemical composition of the polar fraction. The rest of this subfraction appears to be composed of a large number of alkyl-substituted tri- and tetraaromatic compounds involving triaromatic steroid and tetraaromatic hopanoid hydrocarbons, some novel condensed thiophenes with structures related to hopanes, aromatized hexacyclic sulfides and possibly disulfides with structures related to the hexacyclic sulfides found in subfraction 3b, and some carbazoles with a condensed naphthenic ring, corresponding to the series formula $C_nH_{2n-17}N$. The bulk of the carbazoles is concentrated in the more polar fractions, as will be seen in Chapter 12.

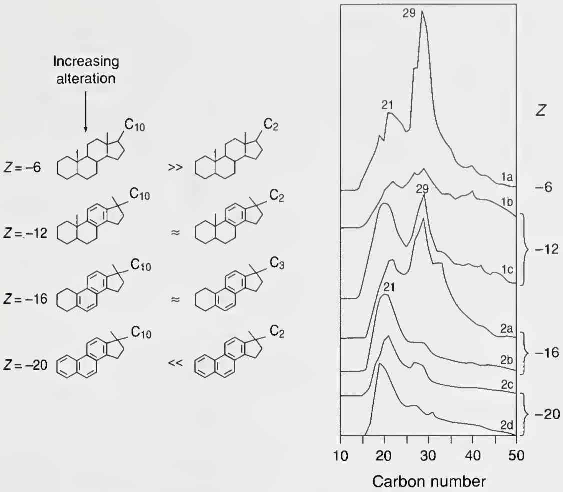

Figure 11.18 Composite *Z*-plot of tetracyclic molecules in various subfractions, where C_x is the carbon number in the side chains. Subfraction numbers and *Z* numbers are indicated on the right. Fully saturated $Z = -6$ compounds show a maximum at $n = 29$ and a shoulder at $n = 21$ corresponding to the loss of the long side chain from the original steroid precursor molecule. As the degree of alteration increases the position of the maximum intensity shifts from C_{29} to C_{21}, reflecting the increased probability of losing the side chain as aromatization increases.[4]

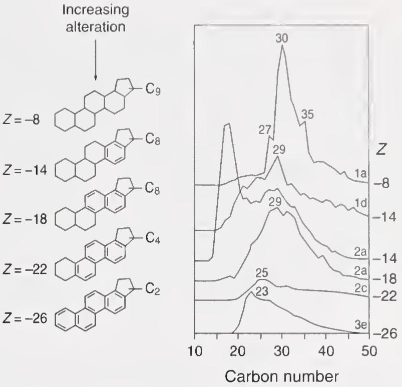

Figure 11.19 Composite *Z*-plot of pentacyclic molecules in various subfractions, where C_x is the carbon number in the side chains. Subfraction numbers and *Z* numbers are indicated on the right. The $Z = -8$ trace has maxima around $n = 27$, 30 and 35, characteristic of the pentacyclic hopanes. As these pentacyclic materials are increasingly altered, the maximum shifts gradually to lower *n*. The maximum at low *n* on the $Z = -14$ trace for subfraction 2a is due to the presence of tricyclic diaromatics which were not removed chromatographically from the pentacyclic monoaromatics.[4]

Table 11.10 Structures of the most abundant component types of subfraction 3

Subfraction	Compound type
3b	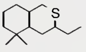 $C_{13}H_{24}S$ 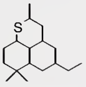 $C_{17}H_{28}S$ 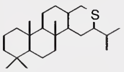 $C_{23}H_{40}S$ 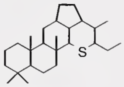 $C_{26}H_{52}S$
3c	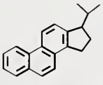 $C_{20}H_{20}$ 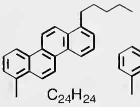 $C_{24}H_{24}$ 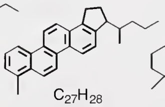 $C_{27}H_{28}$ 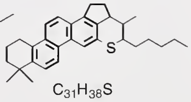 $C_{31}H_{38}S$
3d	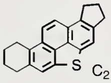 $C_{21}H_{18}S$
3e	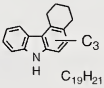 $C_{19}H_{21}N$ 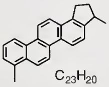 $C_{23}H_{20}$ 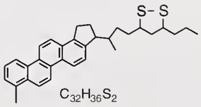 $C_{32}H_{36}S_2$
3f	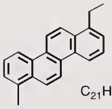 $C_{21}H_{18}$ 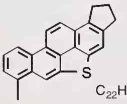 $C_{22}H_{16}S$

To summarize, a great variety of compounds have been detected in the aromatic fraction of Athabasca bitumen. Many of the compound series gave prominent peaks in the FI mass spectra and their elemental formulas were confirmed by high-resolution EIMS. In each of the FI spectra, however, there are still a large number of other peaks representing different types of molecules whose concentrations, while smaller than those of the compounds specifically mentioned above, are still significant, but no effort has yet been made to identify them. Further adding to the complexity is the fact that each mass signal represents the sum of isomeric molecules. In spite of this, it can clearly be recognized that a sizeable portion of the aromatic fraction of the bitumen has originated from the aromatization, isomerization, dealkylation and ring opening of the cyclic terpenoid and steroid hydrocarbons present in the saturate fraction of the bitumen.

5.0 Composition of the Nondistillable Aromatics

The mass spectrometric studies discussed thus far were performed on the distillable portion of the aromatics. The total aromatic content in the bitumen amounts to 36.4 wt% of the bitumen, of which 76.4%, that is, 27.8 wt% of the bitumen, is distillable. (This includes the non-aromatic cyclic sulfides which chromatographically report with the aromatic fraction.) The remaining 23.6% of the aromatics, accounting for 8.6 wt% of the bitumen, were nondistillable. Elemental analysis of this material gave results similar to those listed in Table 11.2 for the polyaromatic subfraction: C, 82.5%; H, 9.6%; N, 0.53%; O, 1.44%; S, 6.3%, $(H/C)_a$, 1.40 and MW 825 g·mol^{-1}.

5.1 NMR studies

As with the case of the saturates, valuable information about the composition and structure of the nondistillable aromatics was obtained by ^{13}C NMR spectroscopy. The 400-MHz ^{13}C NMR spectrum of the nondistillable polyaromatic fraction is shown in Figure 11.20 and its attached proton test (APT) spectrum, in Figure 11.21.[8] The APT spectrum aids the assignments of the aliphatic resonances of the spectrum since quaternary C and CH_2 feature positive absorption and CH and CH_3, negative absorption (at 45° pulse). The 500-MHz NMR spectrum of the whole nondistillable aromatic Athabasca sample is shown in Figure 11.22. This spectrum is similar to the one in Figure 11.20 and both show the presence of long *n*-alkyl moieties attached to cyclic systems. Both these spectra also closely resemble the spectrum of the nondistillable saturates (Figure 10.25) and that of the asphaltene,[9] as will be seen in Chapter 14. On the other hand, both spectra are distinctly different from the spectrum of the distillable portion of the aromatics, Figure 11.23. Here the

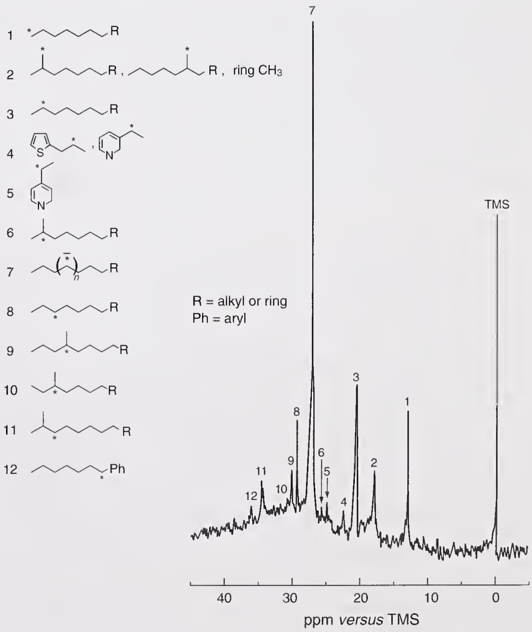

Figure 11.20 Aliphatic portion of the 400 MHz ^{13}C NMR (in the FT mode with a 45° pulse) spectrum of a nondistillable Athabasca polyaromatic subfraction.[8]

intense, sharp, mid-chain methylene resonance absorption at 30 ppm is missing and the total aliphatic signals in the 10–40 ppm region appear to be markedly reduced, relative to the aromatic absorptions in the 110–150 ppm range and the unresolved hump absorption of naphthenic carbons in the 10–60 ppm range. The terminal methyl intensities in the 12–16 ppm region, however, remained unsuppressed. This spectrum is in line with, and thus lends further support to, the suggestion made above, that is, that the distillable aromatics are derived from the cyclic terpenoid alkanes (comprising the saturate fraction of the bitumen) which do not possess long alkyl side chains. Thus, here as with the saturates, we come to the conclusion that the distillable and nondistillable portions of the hydrocarbon fractions of the bitumen are structurally different, the former being related to the cyclic terpenoid biomarkers in the bitumen and the latter to the asphaltene.[9,10]

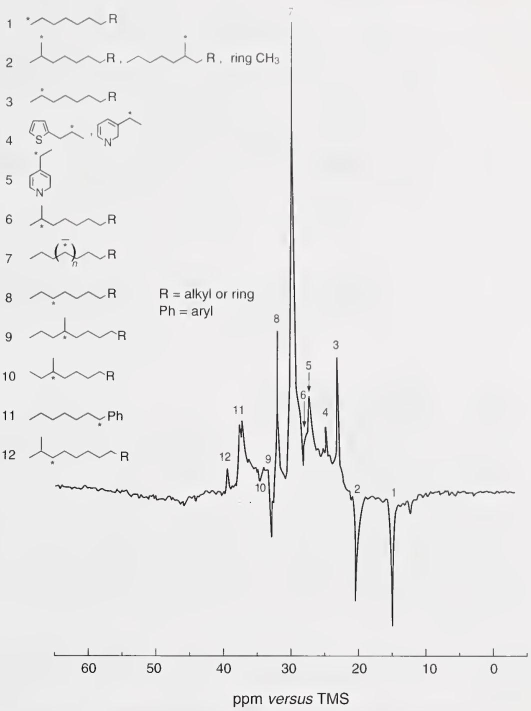

Figure 11.21 The 400 MHz attached proton test (APT) ^{13}C NMR spectrum of the same sample as in Figure 11.20. Positive absorption corresponds to quaternary C and CH_2, and negative absorption to CH and CH_3.[9]

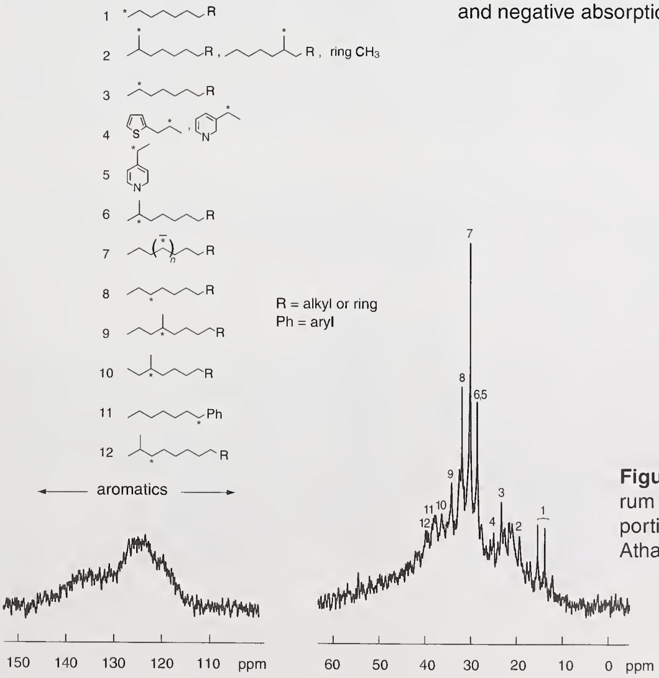

Figure 11.22 500-MHz ^{13}C NMR spectrum of the nondistillable (240°C, 10^{-3} torr) portion of the whole aromatic fraction of Athabasca maltene.

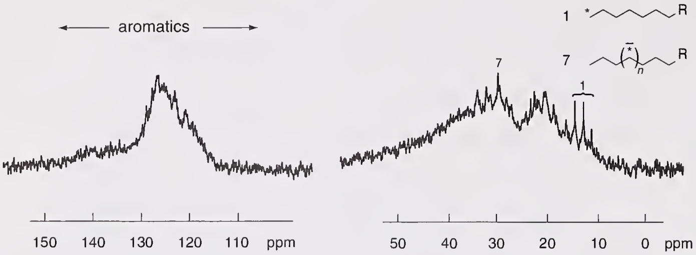

Figure 11.23 500-MHz ^{13}C NMR spectrum of the distillable portion of the whole aromatic fraction of Athabasca maltene.

5.2 Thermolysis

Flash thermolysis of 6-g nondistillable aromatics[11] was carried out in a toluene solution at 430°C in a flow of nitrogen with residence times of 10–15 seconds, as will be described in more detail in Chapter 12, and yielded 2.82-g brown oily distillate (47% yield). This pyrolysis oil was separated by silica gel chromatography into 0.81-g saturate, 1.77-g aromatic and 0.081-g polar fractions (relative proportions 30.5, 66.5 and 3.0%). Each of these fractions was examined separately by chromatographic and chemical methods, as illustrated in Figure 11.24.

5.2.1 The *n*-pentane eluent of the pyrolysis oil

The gas chromatogram of the *n*-pentane eluent, Figure 11.25, shows that it consists mainly of *n*-alkanes and 1-*n*-alkenes up to ~C_{31} in an amount corresponding to about 1.3% of the nondistillable aromatics. The eluent was treated with *m*-chloroperbenzoic acid (MCPBA) to remove alkenes and condensed thiophenes and, after subsequent chromatographic separations, an aromatic subfraction was obtained in 2.5% yield, the gas chromatographic–mass spectrometric–total ion current (GC–MS–TIC) chromatogram of which is shown in Figure 11.26. On the basis of their mass spectra, three of which are shown in Figure 11.27, each of the peaks appearing in the TIC chromatogram could be assigned to one of the following series:

- alkylbenzenes up to 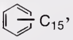,
- C_{15}–C_{22} *n*-alkanes,
- alkylnaphthalenes up to 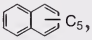,
- alkyltetrahydronaphthalenes up to 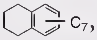,
- alkyltetrahydrophenanthrenes (or anthracenes) up to 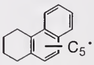.

Owing to the mild conditions of the thermolysis, it may be assumed that the thermolysis products were liberated from the nondistillable matrix by the cleavage of one, or perhaps two, covalent bonds and that they did not undergo further structural changes. Thus, they can be viewed as being part of the original nondistillable molecules in the form of structural units. Therefore, these product molecules probably arose *via* the following type of reactions:

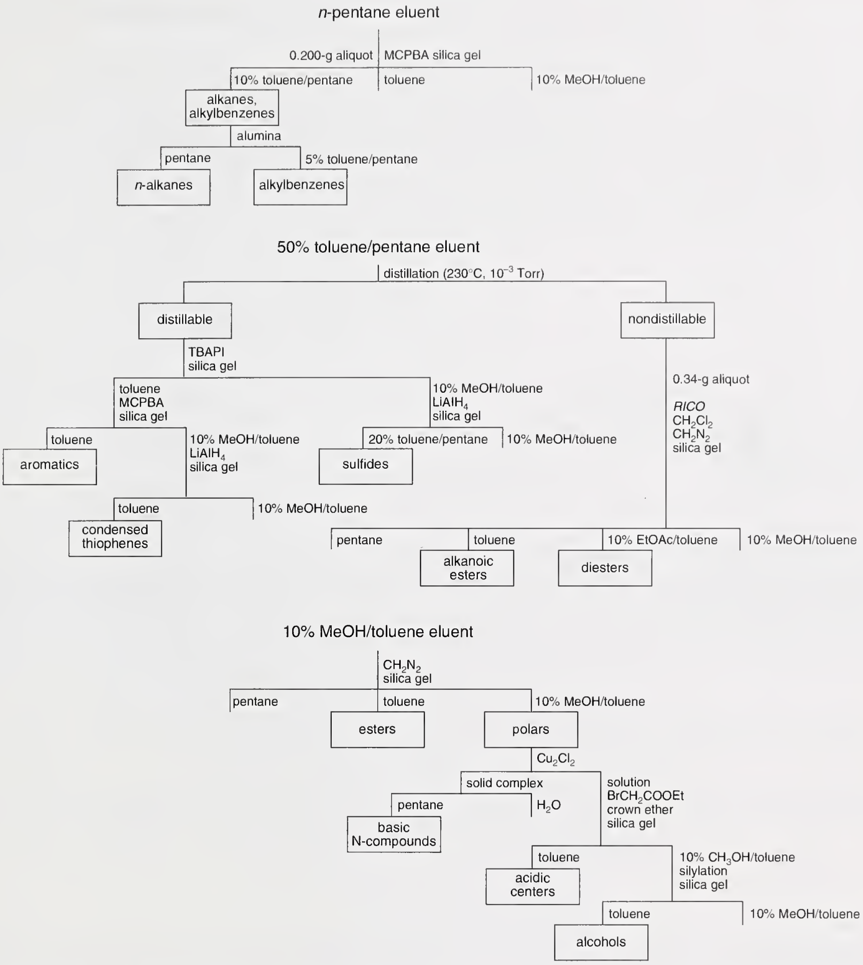
n-pentane eluent
0.200-g aliquot
MCPBA silica gel
10% toluene/pentane
toluene
10% MeOH/toluene
alkanes, alkylbenzenes
alumina
pentane
5% toluene/pentane
n-alkanes
alkylbenzenes
50% toluene/pentane eluent
distillation (230°C, 10^{-3} Torr)
distillable
nondistillable
TBAPI silica gel
toluene MCPBA silica gel
10% MeOH/toluene $LiAlH_4$ silica gel
0.34-g aliquot
RICO CH_2Cl_2 CH_2N_2 silica gel
toluene
aromatics
10% MeOH/toluene $LiAlH_4$ silica gel
20% toluene/pentane
10% MeOH/toluene
sulfides
toluene
condensed thiophenes
10% MeOH/toluene
pentane
toluene
alkanoic esters
10% EtOAc/toluene
diesters
10% MeOH/toluene
10% MeOH/toluene eluent
CH_2N_2 silica gel
pentane
toluene
esters
10% MeOH/toluene
polars
Cu_2Cl_2
solid complex
pentane
H_2O
basic N-compounds
solution $BrCH_2COOEt$ crown ether silica gel
toluene
acidic centers
10% CH_3OH/toluene silylation silica gel
toluene
alcohols
10% MeOH/toluene

Figure 11.24 Chromatographic and chemical steps used to separate the *n*-pentane, toluene and methanol eluents of the pyrolysis oil of the nondistillable Athabasca aromatic fraction. TBAPI = tetrabutylammonium periodate; MCPBA = *m*-chloroperbenzoic acid; RICO = ruthenium-ions-catalyzed oxidation.

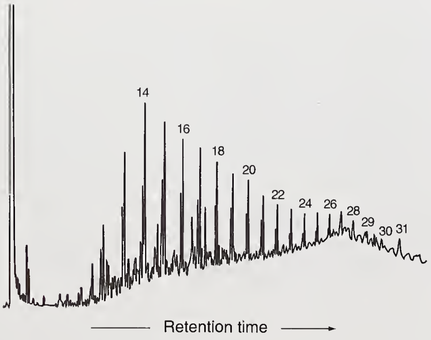

Figure 11.25 Gas chromatogram of the *n*-pentane eluent (Figure 11.24) of the nondistillable aromatics pyrolysis oil. The numbers above the peaks correspond to the number of carbon atoms in the *n*-alkanes. The corresponding *n*-1-alkenes are the smaller peaks to the left of the *n*-alkanes.

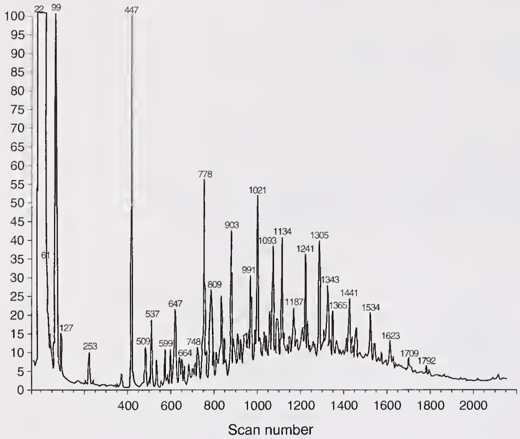

Figure 11.26 GC–MS–TIC chromatogram of the aromatic subfraction of the *n*-pentane eluent (Figure 11.24) of the nondistillable aromatics pyrolysis oil.

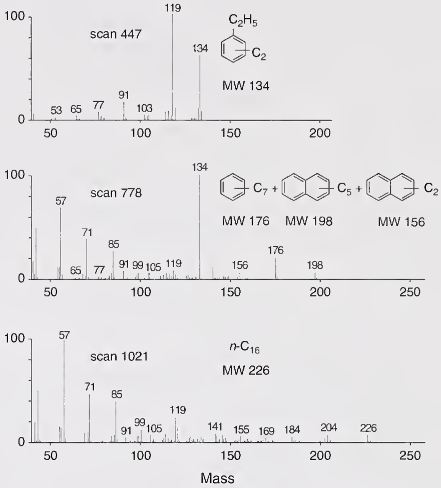

Figure 11.27 High-resolution mass spectra of scans 447, 778 and 1021 of Figure 11.26.

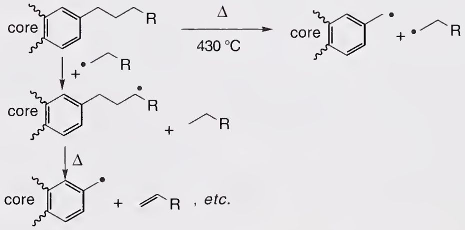

and

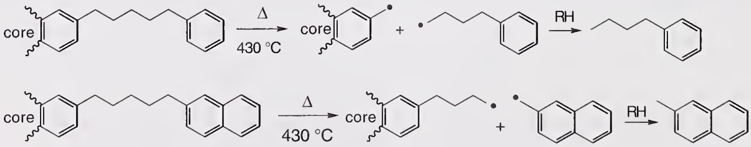

thereby providing unambiguous, direct evidence for their pre-existence in the nondistillable molecules.

5.2.2 The 50% toluene/*n*-pentane eluent of the pyrolysis oil

This fraction was further separated into a distillable (24% at 230°C and 10^{-3} torr) and a nondistillable (70%) subfraction.

a) Distillable subfraction

i) Hydrocarbons

The distillable subfraction (7.3%), after oxidation with TBAPI to remove sulfides and with MCPBA to remove thiophenes,[12] gave the TIC chromatogram shown in Figure 11.28. Again, based on the mass spectrum of the individual components, three of which are shown in Figure 11.29, this material (comprising 6.3% of the nondistillable aromatics) consists of:

- alkylbenzenes, 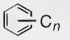

, where $n \leq 22$
- alkylnaphthalenes, 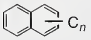

, where $n \leq 6$
- alkyldecahydronaphthalenes, 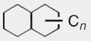

, where $n \leq 5$
- alkyltetrahydronaphthalenes, 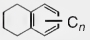

, where $n \leq 7$
- alkylphenanthrenes (anthracenes), 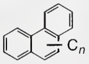

(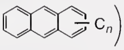

), where n = 1–10.

ii) Sulfides

The thiophenes and cyclic sulfides both elute with the aromatics in silica gel chromatography. Therefore, the distillable aromatic subfraction was oxidized with tetrabutylammonium periodate (TBAPI) which selectively converts sulfides to sulfoxides. The sulfoxides, being much more polar than the rest of the aromatics present, can be readily separated by silica gel chromatography and reduced back to sulfides with $LiAlH_4$.

$$\begin{matrix}\text{sulfides}\\ \text{in}\\ \text{aromatics}\end{matrix} \xrightarrow{\text{TBAPI}} \begin{matrix}\text{sulfoxides}\\ \text{in}\\ \text{aromatics}\end{matrix} \xrightarrow[\text{chromatography}]{\text{silica gel}} \text{separated sulfoxides} \xrightarrow{\text{LiAlH}_4} \text{isolated sulfide fraction}$$

GC–MS–SIR chromatograms of the sulfides are shown in Figures 11.30 and 31, displaying homologous series of 2-*n*-alkyl- and 2,5-di-*n*-alkylthiolanes and thianes

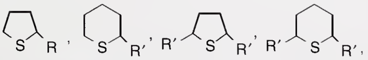

where R and R′ are (up to) 6-methyl-2-dodecyl and octadecyl groups, respectively. The concentration distributions in the thiolane and thiane series are probably distorted as a result of increasing losses of the lower molecular weight components due to increasing volatility, and the true concentration maxima should occur at lower carbon numbers than is apparent in the chromatograms.

The thiolanes and thianes are all *n*-alkyl substituted (in the 2- or 2,5-positions), as can be deduced from the constancy of the GC retention times within a series and the more or less smooth concentration distributions. The bicyclic terpenoid sulfides, however, (Figure 11.31b) appear to have variable retention times and concentration distributions in the C_{13}–C_{24} range, indicative of an isoprenoid side chain. This series is structurally identical to the bicyclic terpenoid sulfides detected by FIMS in the distillable portion of the aromatic fraction, *cf.* Figure 11.13. In contrast, the *n*-alkylthiolane and thiane series found here in the nondistillable portion of the aromatics (0.4%) do not occur in the distillable portion but are present in copious quantities as structural units in the asphaltene molecules.[13]

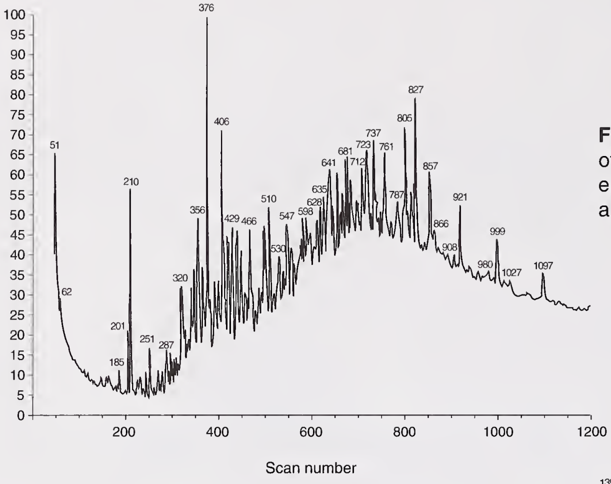

Figure 11.28 GC–MS–TIC chromatogram of the aromatic subfraction of the toluene eluent (Figure 11.24) of the nondistillable aromatics pyrolysis oil.

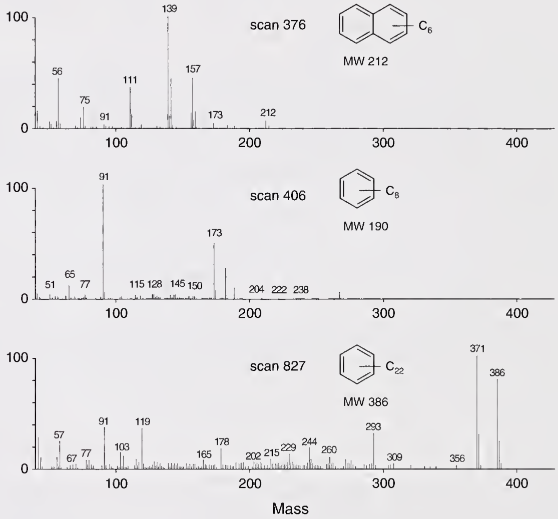

Figure 11.29 High-resolution mass spectra of scans 376, 406 and 827 of Figure 11.28.

iii) Thiophenes

Following the removal of the sulfides, the aromatic subfraction from which the sulfides were removed was oxidized with *m*-chloroperbenzoic acid (MCPBA) to convert the slightly polar thiophenic compounds to their strongly polar sulfones for chromatographic separation:

$$\begin{array}{c}\text{aromatics}\\\text{(–sulfides)}\end{array} \xrightarrow{\text{MCPBA}} \begin{array}{c}\text{thiophene}\\\text{sulfones}\end{array} \xrightarrow[\text{chromatography}]{\text{silica gel}} \begin{array}{c}\text{isolated}\\\text{sulfones}\end{array} \xrightarrow{\text{LiAlH}_4} \begin{array}{c}\text{isolated}\\\text{thiophenes}\end{array}$$

GC analysis showed that the thiophenes isolated (comprising 0.4% of the nondistillable aromatics) were a complex mixture in which only dibenzothiophene, 1-methyl, 4-methyl, 3- and 2-methyl, an ethyl, and a cluster of dimethyl dibenzothiophenes could be identified, but other higher condensed dibenzothiophenes were noted.

b) Nondistillable subfraction

The nondistillable subfraction of the toluene eluent could not be analyzed by mass spectrometry. Therefore, it had to be degraded to smaller molecules which were amenable to chemical analysis.

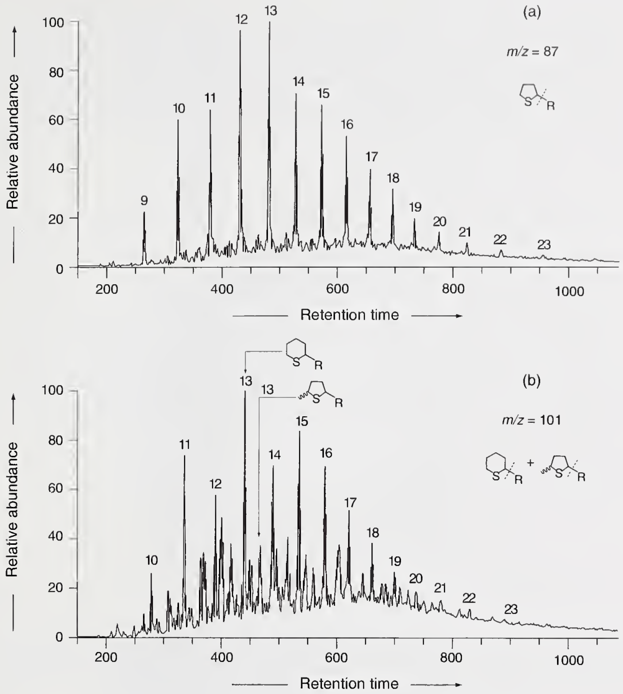

Figure 11.30 GC–MS cross-scan chromatograms of the monocyclic sulfide products from the 430°C flash thermolysis of the nondistillable aromatic fraction. a): m/z = 87, 2-*n*-alkylthiolanes; b): m/z = 101, 2-*n*-alkylthianes and 2-methyl-5-*n*-alkylthiolanes. The numbers above the peaks correspond to the number of carbon atoms in the molecule.

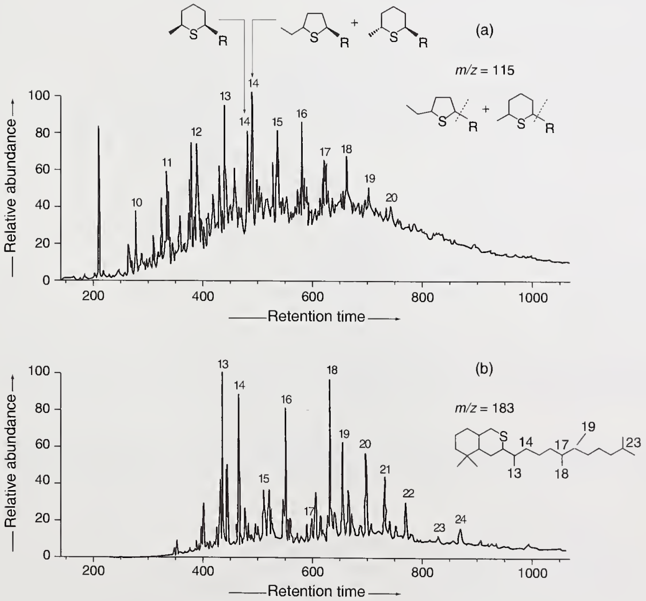

Figure 11.31 GC–MS cross-scan chromatograms of the mono- and bicyclic sulfide products from the 430°C flash thermolysis of the nondistillable aromatic fraction. a): m/z = 115, 2-ethyl-5-*n*-alkylthiolanes and 2-methyl-6-*n*-alkylthianes; b): m/z = 183, bicyclic terpenoid sulfides. The numbers above the peaks correspond to the number of carbon atoms in the molecule.

This was accomplished by chemical means using ruthenium ions-catalyzed oxidation (RICO).[14] The method is based on the ability of the Ru^{8+} ion to selectively oxidize aromatic carbon to carbon dioxide or carboxylic acids while leaving aliphatic and alicyclic saturated carbons essentially intact. Thus, an alkylbenzene is oxidized to carbon dioxide and an alkylcarboxylic acid

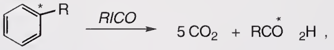

the site of attachment of the alkyl group to the aromatic ring becoming the carboxylic carbon. The identification of the carboxylic acids produced can then establish the nature of the alkyl side chains and their relative concentration distribution in the original parent molecules. Analysis of the produced acids (after diazomethane treatment to convert them to their methyl esters), Figures 11.32 and 11.33, show that the major components are *n*-alkanoic acid esters and the minor peaks are due to α-methyl and β-methyl branching in a total amount of about 0.8%. Thus, for example, scan 1369 is due to the methyl ester of an *n*-alkanoic acid exhibiting two main modes of fragmentation:

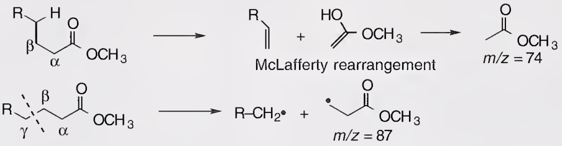

Scan 1301, showing intense peaks at *m/z* = 88 and 101, represents an α-methylpentadecanoic acid methyl ester

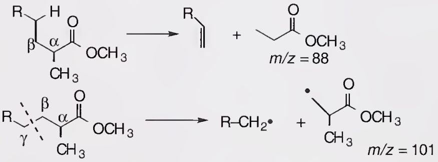

and scan 1101 features intense *m/z* = 74 and 101 peaks, which suggests a β-methylpentadecanoic acid methyl ester structure:

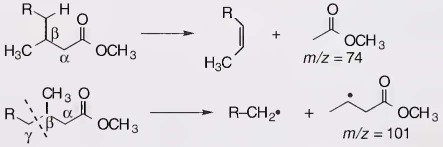

The other minor peaks visible in the spectrum probably represent higher α-branched (ethyl, propyl, *n*-butyl) *n*-alkanoic acid methyl esters, as was found in the RICO of the asphaltene (Chapter 14).

Also detected were α,ω-di-*n*-alkanoic acid methyl esters from the polymethylene bridges connecting two aromatic units,

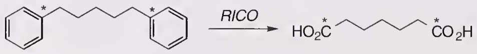

along with some benzenedicarboxylic acid methyl esters in a combined amount of 3.2%.

From this it follows that the original parent molecules were rich in *n*-alkyl substituted aromatic structures with some contribution by α- and β-methyl and α-ethyl, propyl and

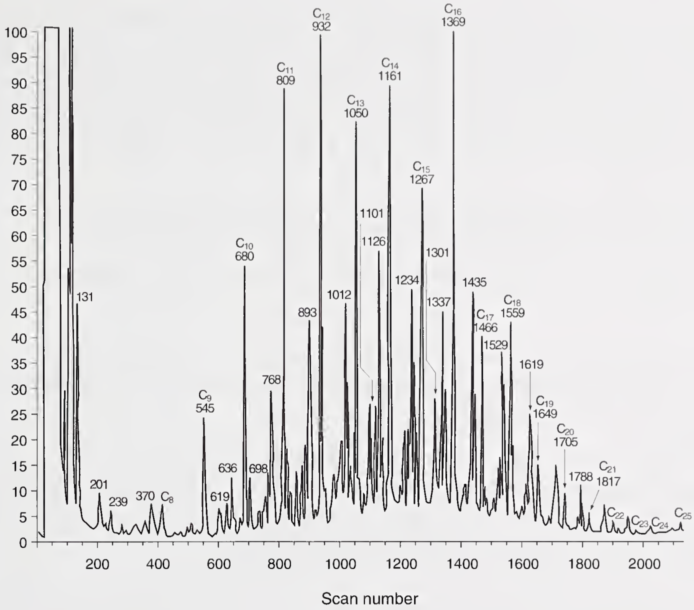

Figure 11.32 GC–MS–TIC chromatogram of the *n*-alkanoic acid methyl esters produced from the ruthenium ions-catalyzed oxidation of the nondistillable portion of the toluene eluent (Figure 11.24) of the nondistillable aromatics pyrolysis oil.

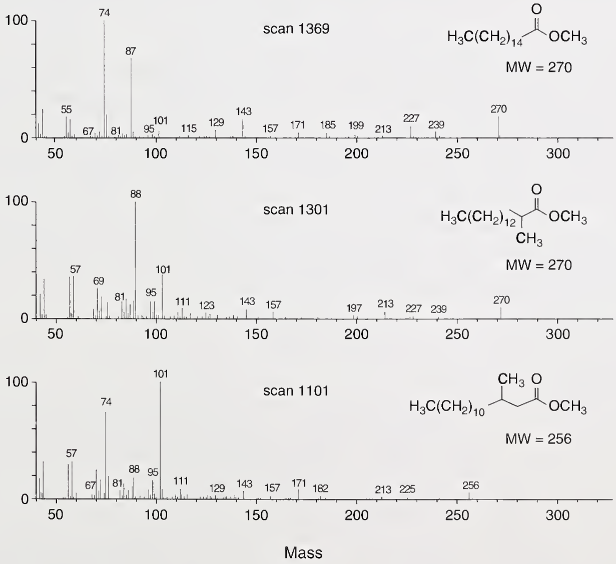

Figure 11.33 High-resolution mass spectra of scans 1369, 1301 and 1101 of Figure 11.32.

n-butyl groups. Thus, the overall composition of the nondistillable subfraction of the aromatics conforms to, and further generalizes what has been concluded before, namely, that the dominant structural units are alkyl-substituted and alkyl-bridged benzenes, naphthalenes, phenanthrenes and their partially hydrogenated derivatives, bearing a significant number of alkyl side chains, the latter being mainly of the *n*-alkyl type with modest contributions from C_1–C_4 branching, mainly in the α-position.

5.2.3 The 10% methanol/toluene eluent of the pyrolysis oil

This fraction should contain basic nitrogen compounds, carboxylic acids, ketones and alcohols, if present.

Therefore, the fraction was first treated with diazomethane to convert any carboxylic acids to their methyl esters and the fraction containing the esters was chromatographically separated, but no ester could be detected.

Next, the basic nitrogen compounds were complexed with $CuCl_2 \cdot 2H_2O$ and the complexes were isolated from the rest of the polars. Detected were a series of alkylquinolines with C_3–C_9 side chains and one alkylpyridine; these compounds were also isolated, and in greater quantities, from the polar fraction of the bitumen.[15]

The solution remaining after the $CuCl_2 \cdot 2H_2O$ complexation was treated to isolate molecules with acidic centers, such as fluorenes and carbazoles. Although this class constituted 0.8% of the nondistillables, it proved to be exceedingly complex and only one peak could be identified, *viz.*

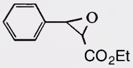

Following this, the residual polar material was treated with *t*-butyldimethylsilylchloride to convert alcohols to silyl ethers which, being nonpolar compounds, could be isolated from the rest of the polar material by chromatography. After separation, the ether fraction was analyzed by GC–MS and the TIC chromatogram and mass spectra of three selected peaks are reproduced in Figures 11.34 and 11.35. A variety of alcohols are in evidence, the most prominent series of which comprises *n*-alkanols from ~C_{10} to ~C_{26} dominated by the even-carbon-number homologs, the most abundant of which are the $C_{18} > C_{12} > C_{10} > C_{16}$ members. Scan 762 is consistent with a decahydronaphthalene alcohol structure,

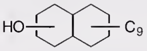

,

while scan #969 could be

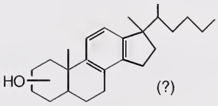

since some sterols have been detected in the polar fraction of the bitumen (*cf.* Chapter 12). Definitive structural identifications of these molecules have not been made. The EIMS spectra also suggest that this fraction contains, in addition to the above-mentioned alcohols, significant concentrations of other polycondensed naphthenic alcohols. These alcohols can be present in the original parent molecules either as alcohol or ethers which, on pyrolysis, decompose to yield

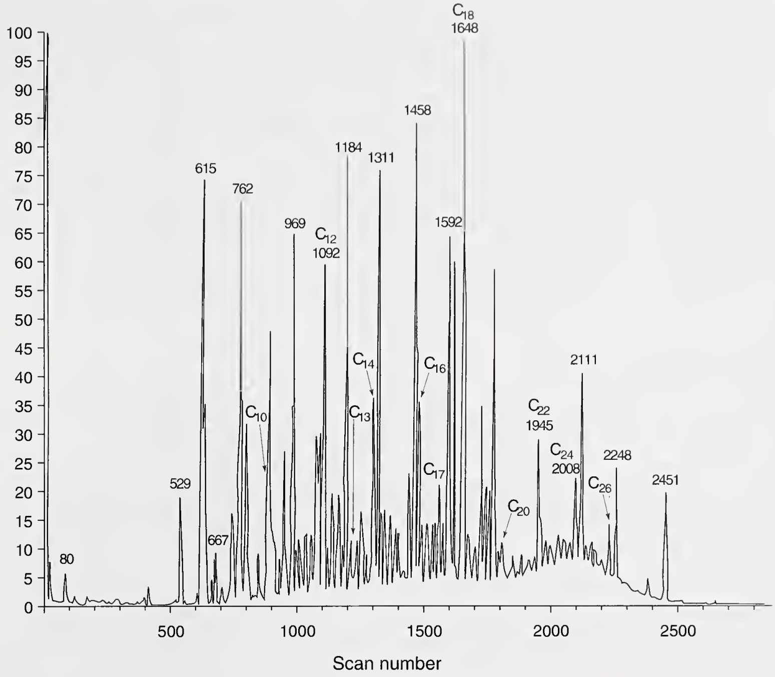

Figure 11.34 GC–MS–TIC chromatogram of the silylethers of the alcohols in the 10% methanol/toluene eluent (Figure 11.24) of the nondistillable aromatics pyrolysis oil. The carbon numbers refer to the *n*-alkylalcohol series.

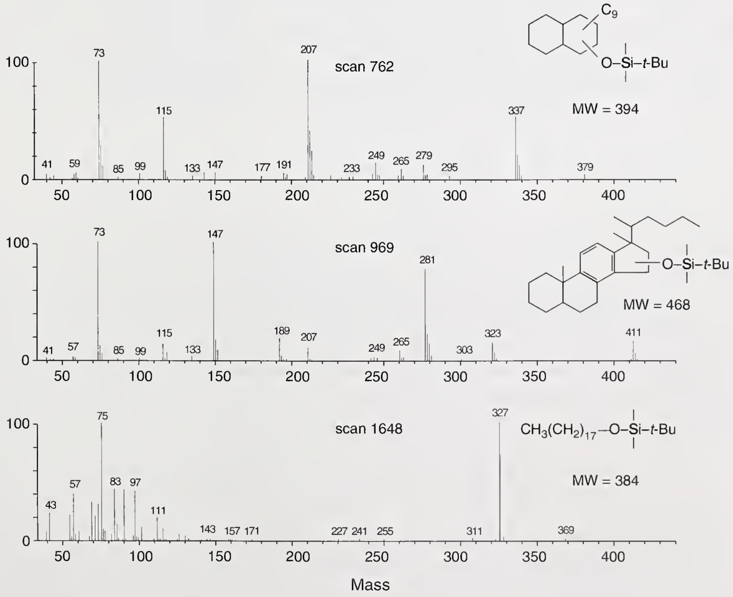

Figure 11.35 High-resolution mass spectra of scans 762, 969 and 1648 of Figure 11.34.

alcohols. The FTIR spectrum of the nondistillable aromatic fraction of the maltene contains a broad absorption centered at ~3,300 cm^{-1} which is probably due to O–H stretching vibrations. Therefore, at least some of the alcohols detected were present as such in the original material.

In summary, detailed chemical studies of the composition of the nondistillable aromatic portion of Athabasca maltene revealed the presence of:

- large amounts of *n*-alkyl-substituted aromatics including benzenes, naphthalenes, phenanthrenes and their partially or wholly hydrogenated derivatives, which is in full agreement with the NMR spectrum of the fraction;
- *n*-alkyl-substituted thiolanes and thianes along with lesser quantities of bicyclic terpenoid sulfides;
- alkyldibenzothiophenes;
- alkylquinolines and a pyridine;
- a broad variety of alcohols including *n*-alkyl types and a complex mixture of condensed alicyclic alcohols, probably containing monoaromatic and possibly other sterols.

Thus, it is clear that *n*-alkyl moieties are one of the dominating elements in the structures of the molecules comprising the nondistillable portion of the aromatics, in sharp contrast to the dominance of the terpenoid elements and the absence of *n*-alkyl moieties in the distillable portion of the aromatics. As will be shown in Chapter 14, the main characteristic features of the molecules making up the asphaltene fraction are the dominance of *n*-alkyl moieties and the presence of *n*-alkylthiolanes, thianes and thiophenes. This similarity between the structural elements of the asphaltene and those of the nondistillable aromatics, as we found before for the nondistillable saturates, points to a genetic relationship between the asphaltene and the nondistillable portions of the saturates and aromatics.

5.3 Ruthenium ions-catalyzed oxidation

Additional insight into the structural details of the nondistillable aromatics comes from RICO experiments on the **whole** nondistillable aromatics which, in addition to the *n*-alkanoic acid series, also yielded a suite of α,ω-di-*n*-alkanoic acids in the C_8–C_{17} range, Figure 11.36, from the reaction

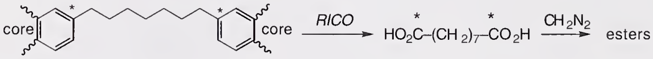

thereby establishing the existence of *n*-alkanoic bridges between aromatic units in the nondistillable aromatic fraction. Phthalic acid along with its monomethyl, dimethyl and ethyl derivatives were also present in the oxidation products, Figure 11.36. The formation of these products is the consequence of the deactivating effect of the carboxylic group on the reactivity of the benzene ring with respect to RICO which, in the case of two carboxylic groups on a benzene ring, arrests further oxidation of the ring:

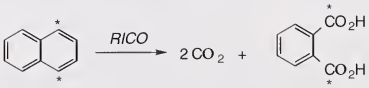

Thus, the formation of phthalic acids is the manifestation of the existence of condensed aromatic ring systems in the nondistillables. Higher benzenecarboxylic acids up to hexacarboxylic acids are produced in the RICO of asphaltene (Chapter 14) where condensation of the aromatic structure is much more extensive than in the nondistillable aromatics.

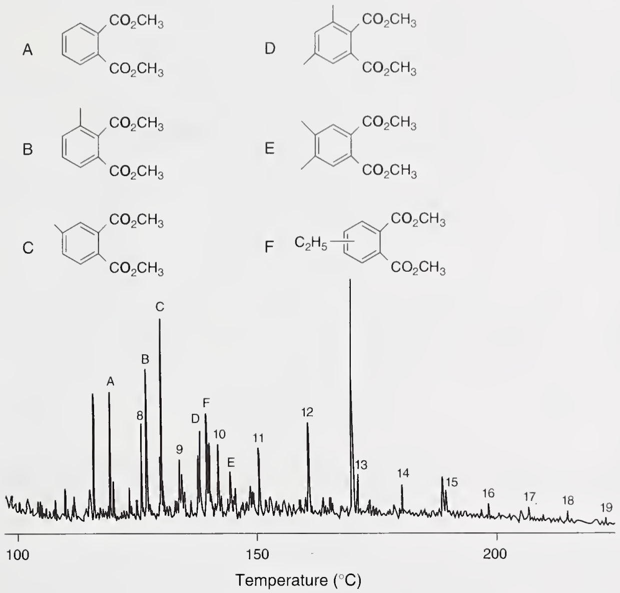

Figure 11.36 Gas chromatogram of the methyl esters of benzenepolycarboxylic and α,ω-di-*n*-carboxylic acids following the ruthenium ions-catalyzed oxidation of the nondistillable aromatic fraction. The numbers above the peaks correspond to the number of carbon atoms in the α,ω-diesters.

From the RICO studies, we conclude that *n*-alkyl side chains and bridges attached to aromatic units are important structural elements in the nondistillable aromatics. The high yields of *n*-alkanes and 1-*n*-alkenes from the pyrolysis of the nondistillable residue of the RICO products suggest that *n*-alkyl chains and bridges may also be attached to naphthenic units:

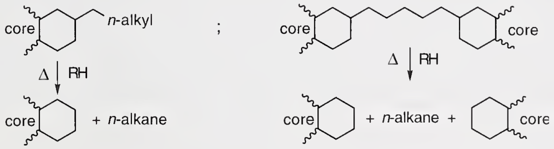

This structural feature also pertains to asphaltene and will be discussed again in Chapter 14.

6.0 Aromatics in Other Alberta Bitumens

Comparative data have been reported from FIMS studies of Cold Lake and Athabasca bitumen and Lloydminster heavy oil on the distribution of some of the aromatic series in the whole aromatic fraction, along with distribution of the cyclic terpenoid sulfides and thiophenes.[16]

From the plots of the relative concentration *versus* the number of carbon atoms in the molecule shown in Figure 11.37, the concentration maxima in the various series of distillable alkylaromatic compounds range from C_{10} to C_{18} and the concentrations drop to near zero around C_{28}–C_{32}. The maximum in the monoaromatic C_nH_{2n-6} series occurs at C_{20} in the Athabasca, C_{15} in the Cold Lake and C_{10} in the Lloydminster oil. This series, as well as the series of alkylbenzenes detected by FIMS analysis of subfraction 1d (Figure 11.4) could be, at

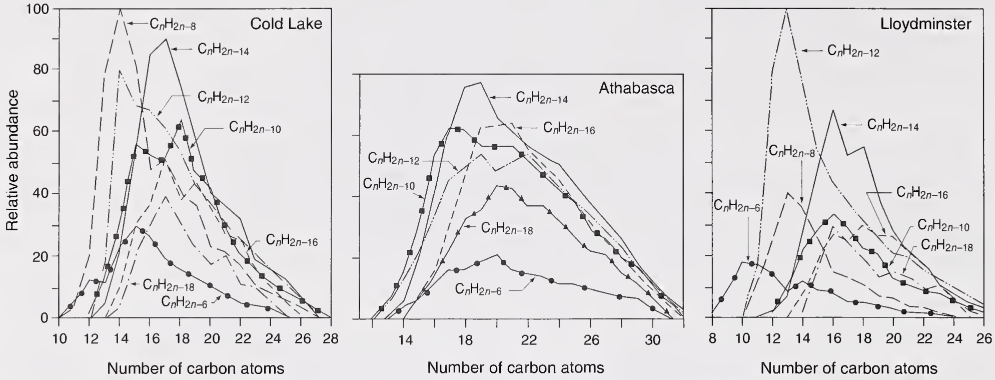

Figure 11.37 Distribution of aromatic hydrocarbons in Cold Lake and Athabasca bitumens and Lloydminster heavy oil as determined by FIMS. From J.D. Payzant *et al.*, Ref. 16. © 1979, Elsevier Science Ltd.

least partly, composed of homologous series of methylphenylisoprenoids which have been found to be present in the C_{13}–C_{31} range in source rock bitumens and oils from numerous Paleozoic-age petroleum systems in the Western Canada Basin.[17] For the diaromatic C_nH_{2n-12} series the maxima occur at C_{19}, C_{14} and C_{13}, respectively, in the three oils and for the triaromatic C_nH_{2n-18} series at C_{20}, C_{17} and C_{16}. The apparent trend is as expected since, as the extent of biodegradation increases in the order Lloydminster < Cold Lake < Athabasca, the positions of the maxima tend to gradually shift to higher carbon numbers as the lower ring number series become depleted.

In other respects, the three oils show similar compositional characteristics and the differences that exist in their composition can be attributed to differences in their paleolithographic and microbial history.

Similar distribution plots for some of the alkylthiophenic compounds are shown in Figure 11.38. The upper limit of the carbon range is 24–30 with maxima at C_{14}–C_{16} for the Lloydminster, C_{14}–C_{17} for the Cold Lake, and C_{17}–C_{19} for the Athabasca samples. In every case the benzothiophene series, $C_nH_{2n-10}S$, is more abundant than the dibenzothiophene series, $C_nH_{2n-16}S$.

The data discussed here for Athabasca and Cold Lake bitumens and Lloydminster heavy oil are characteristic of and generally applicable to most Alberta bitumens and heavy oils.

7.0 Aromatic Compounds Identified

There are a number (albeit a small number) of other aromatic hydrocarbons and some heterocyclic molecules which elute from the silica gel column with the aromatics, whose molecular structures have been identified. These include some methylated phenanthrenes, chrysenes, picenes, pyrenes, perylenes, fluoranthanes, naphthalenes, suites of C_{20}–C_{22} and C_{26}–C_{29} monoaromatic and triaromatic steranes and some aromatized hopanes (which will be discussed among the biomarkers in Chapter 13), homologous series of cyclic terpenoid sulfides and thiophenes (which will be considered in detail in Chapter 12), along with series of alkylfluorenes, alkylfluorenols and alkylfluorenones.

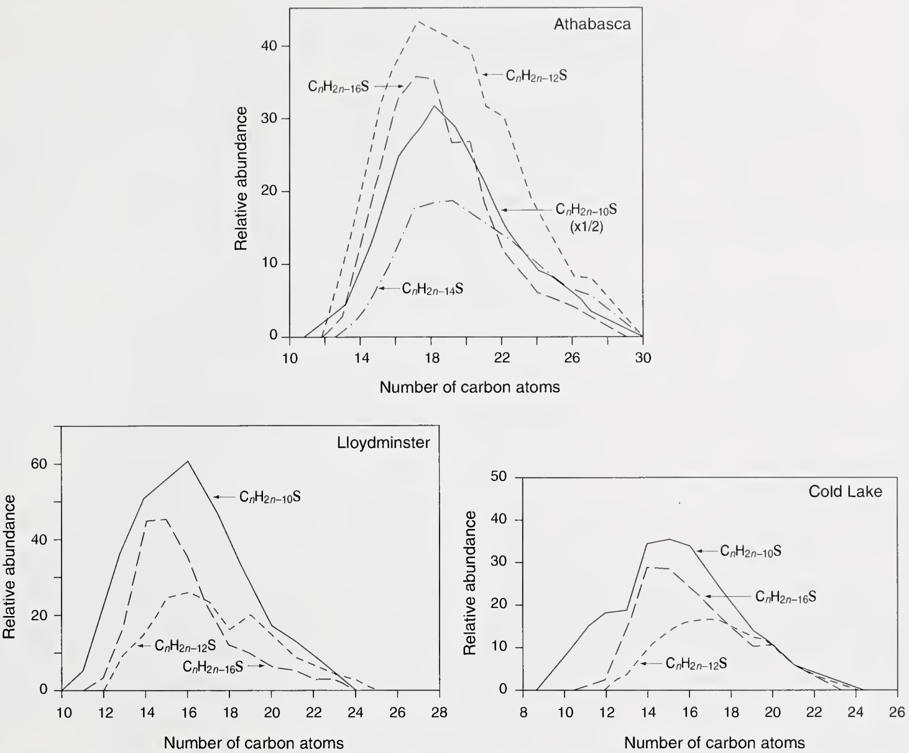

Figure 11.38 Distribution of thiophenic compounds in the aromatic fractions of Athabasca and Cold Lake bitumens and Lloydminster heavy oil as determined by FIMS. From J.D. Payzant *et al.*, Ref. 16. © 1979, Elsevier Science Ltd.

A few members of the family of tricyclic aromatic molecules with series formula C_nH_{2n-16} corresponding to fluorenes have reported to be minor components of the aromatic hydrocarbons in crude oil[18] and bitumen,[19] but in general fluorenes were considered to be only trace constituents of petroleums until the discovery of relatively large concentrations of fluorenes and their derivatives in Alberta bitumens. This was made possible by the high acidity of fluorene and its exploitation for the isolation of these classes of molecules through a series of chemical transformations and GC–SIR MS analyses.

The high acidity of the fluorene molecule resides in the 9-position, which causes a marked weakening in the strength of the C(9)–H bond. Consequently, the 9-position of the fluorene molecule is considerably more reactive than the other carbon centers and undergoes facile oxidation to the corresponding fluoren-9-one. In 9-alkylfluorenes the oxidation leads to 9-alkyl fluoren-9-ols:

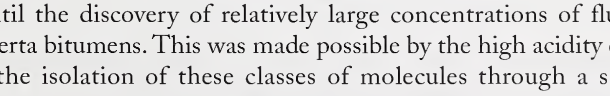

Quantitative conversion of fluorenes to fluorenones and fluorenols can be achieved in the base-catalyzed oxidation with molecular oxygen by the agency of a phase transfer catalyst such as 18-crown-6-ether. This oxidation reaction has been exploited for the isolation and GC analysis of the fluorenes in Athabasca bitumen[20]:

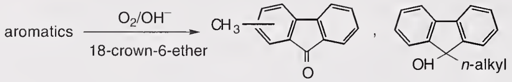

The reaction yielded a mixture of methylated fluorenones, 9-*n*-alkylfluoren-9-ols and nuclear methylated 9-*n*-alkylfluoren-9-ols, which were separated by silica gel column chromatography. The fraction eluted with CH_2Cl_2 contained the fluorenones (>C=O 1703 cm^{-1}) and the more polar fraction eluted with 10% EtOAc in CH_2Cl_2 contained the alcohols (OH 3380 cm^{-1}).

TIC and cross-scan mass chromatograms for the isolated fluorenone fractions of two samples of bitumens, one from a depth of 18 m and the other from 35 m, are shown in Figures 11.39 and 11.40. The latter sample was taken directly from the deposit and placed immediately under an argon atmosphere where it was stored until processing, and was considered to be "fresh", as opposed to the former, "aged" sample for which no precautions were taken during storage. From the mass spectra of peaks which corresponded to the retention times of authentic samples of 1,4-dimethylfluoren-9-one, 3,4-dimethylfluoren-9-one, 2,4-dimethylfluoren-9-one, and 2,3-dimethylfluoren-9-one it could be determined that the aged sample contained 1,4-, 3,4- and 2,4- but not 2,3-dimethylfluoren-9-ones. The fresh sample, on the other hand, contained all four A-ring substituted dimethylfluoren-9-ones as well as 1,2,3,4-tetramethylfluoren-9-one. Apparently the aging process tends to remove the small amounts of 2,3-dimethylfluorene and 1,2,3,4-tetramethylfluorene from the bitumen. Both samples contained trace amounts of the parent fluoren-9-one and the relative concentrations for the dimethyl compounds were: 1,4 > 3,4 > 2,4 > 2,3. The overall concentration distributions in the gas chromatograms of the two samples indicate that both samples contained mono-, di-, tri- and tetramethyl substituted fluorenes and that the fresh sample contained fewer isomers than the aged sample.

The more polar fraction of the fresh sample containing the fluorenols gave the TIC and cross-scan mass chromatograms shown in Figure 11.41. The *m/z* = 181 fragmentogram shows the presence of a series of 9-*n*-alkylfluoren-9-ols with R = methyl to octyl

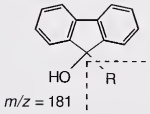

and the *m/z* = 195, 209 and 223 fragmentograms show the distribution of the nuclear mono-, di- and trimethyl derivatives. Based on the fluorenols isolated, the corresponding fluorenes must be present in the bitumen, *i.e.*, a series of 9-*n*-alkylfluorenes with the alkyl group extending from C_1 to at least C_8. In addition, a corresponding series of nuclear monomethylated fluorenes bearing a series of *n*-alkyl groups in the 9 position is present in the aromatic fraction. Corresponding nuclear dimethylated and trimethylated fluorenes are present in much lower concentration and the nuclear tetramethylated fluorenes are present only in trace amounts. The major component of the whole series is 9-methylfluorene which has been detected in several heavy oil and bitumen samples.

The oxidized forms of fluorenes, the fluorenones and fluorenols, are also present in the bitumen[21,22] and, being polar compounds, they form part of the polar fraction in class separation. As will be discussed in Chapter 12, the concentration distribution of the oxidized fluorenes in the resins of the bitumen is quite similar to the distribution of their parent hydrocarbons, the fluorenes. Moreover, the fresh sample, taken from a greater depth (35 m) than the aged sample (18 m), and kept under argon until commencement of the analysis, was found to contain only

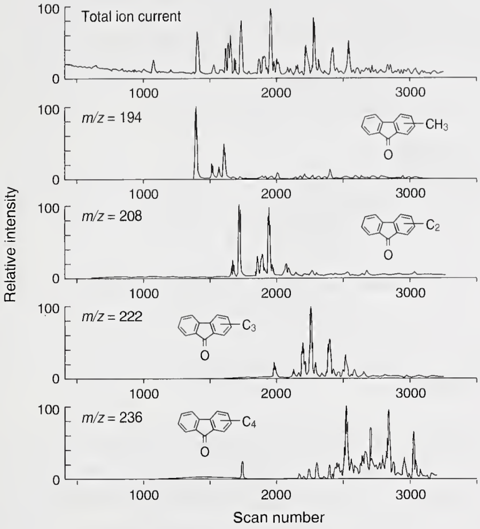

Figure 11.39 GC–MS cross-scan chromatograms of the molecular ions of fluorenones from the oxidation of the aromatic fraction of a fresh Athabasca sample. From T.W. Mojelsky and O.P. Strausz, Ref. 20. © 1986, Elsevier Science Ltd.

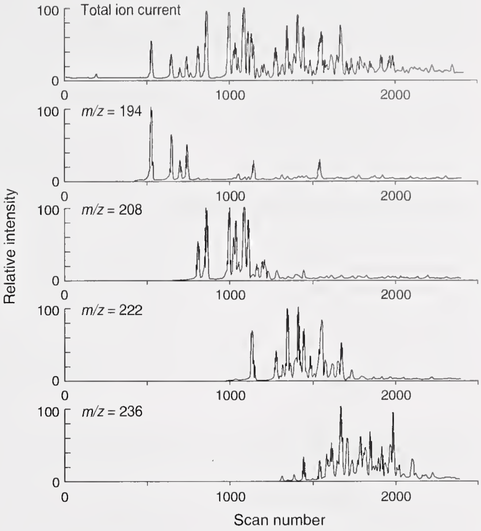

Figure 11.40 GC–MS cross-scan chromatograms of the molecular ions of fluorenones from the oxidation of the aromatic fraction of an aged Athabasca sample. From T.W. Mojelsky and O.P. Strausz, Ref. 20. © 1986, Elsevier Science Ltd.

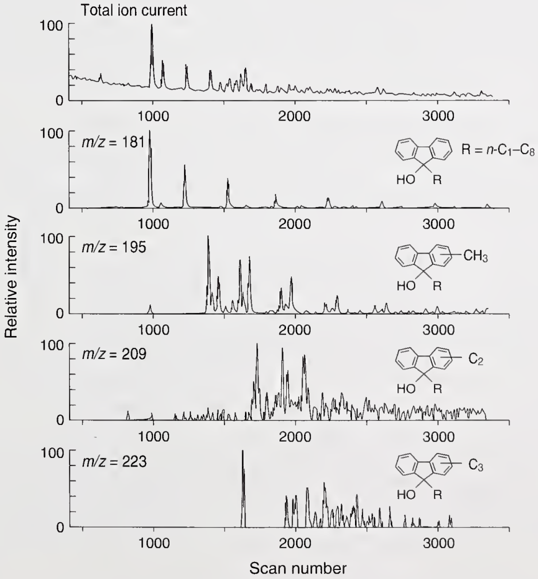

Figure 11.41 GC–MS cross-scan chromatograms of the molecular ions of 9-*n*-alkylfluoren-9-ols from the oxidation of the aromatic fraction of a fresh Athabasca sample. From T.W. Mojelsky and O.P. Strausz, Ref. 20. © 1986, Elsevier Science Ltd.

low concentrations of fluorenols and no detectable fluorenones, indicating that the fluorenones and fluorenols were formed by the partial oxidation of fluorenes and that the relative concentrations of the fluorenes, fluorenones and fluorenols can serve as an indicator of the oxidative state of the bitumen. The composition of the weathered sample clearly demonstrates that oxidation of fluorenes is one of the principal processes taking place under oxidative conditions in Athabasca oil sand.

The cyclic terpenoid sulfides are also susceptible to oxidation to form sulfoxides and the relative amounts of sulfoxides to sulfides can also be utilized as a marker for determining the oxidative state of the bitumen (*cf.* Chapter 12).

The question of the geochemical origin of fluorene in petroleum will be discussed in Chapter 13.

8.0 Summary

The Athabasca bitumen sample described in Chapter 10 was found to contain 36.5% aromatics which are defined in terms of a silica gel column and an Ag^+ ion on silica gel thin layer plate chromatographic separation scheme; 76.4% of this aromatic fraction is distillable at 240℃ and at 10^{-3} torr pressure. After further fractionation by alumina column chromatography, FIMS and high-resolution EIMS investigations of this distillable aromatic fraction revealed a complex mixture of mono- through tetraaromatic, along with some pentaaromatic hydrocarbons and nitrogen and sulfur aromatics (carbazoles and thiophenes) with a total number of aromatic and naphthenic rings of up to six. In addition, novel series of naphthenic sulfides in the C_{12}–C_{35} range with two to six rings featuring isoprenoid side chains were also found to be present. Structurally, these are saturated compounds and are unrelated to aromatics; however, their chromatographic properties make them elute with the diaromatics and hence they are mentioned here. The most abundant components of the aromatic fraction are the bi- and tricyclics and the bi- and triaromatics.

Most of the hydrocarbons, the sulfides and a portion of the sulfur aromatics are genetically related to the cyclic terpenoid hydrocarbons which make up the bulk of the saturate fraction of the bitumen. They probably were formed by aromatization, isomerization, dealkylation, partial ring opening and sulfur incorporation reactions. The genetic relationship with the saturates is revealed by the correlation that exists between the concentration distributions with respect to the carbon number in the molecule for the various ring number series and their trend with respect to the number of total rings (aromatic + naphthenic) in the molecule. In agreement with this conclusion, the NMR spectrum of the distillable aromatics shows that long-chain *n*-alkyl moieties are not dominant structural elements and that the total alkyl content is low. The origin of the nitrogen heteroaromatics, the carbazoles, is less certain.

The nondistillable aromatics amount to about 8.6% of the bitumen. They are richer in heteroatoms and have a higher MW than the distillable aromatics. The NMR spectrum of the nondistillable aromatics is markedly different from that of the distillable aromatics and shows that long-chain *n*-alkyl groups are principal structural elements and that the nondistillable portion of the aromatic fraction, like the nondistillable portion of the saturate fraction, is structurally related to asphaltene and may be considered to be degraded, low-molecular-weight asphaltenes. Indeed, thermolysis of the nondistillable aromatics produces a series of *n*-alkanes and terminal alkenes up to C_{28} along with series of *n*-alkylthiolanes and thianes, a diagnostic proof for a close correlation with asphaltene structure, along with *n*-alkyl-substituted mono-, di- and triaromatics and hydroaromatics. The RICO oxidation yields a series of n-alkanoic acids from the aromatic side chains, α,ω-di-n-alkanoic acids from the n-alkyl bridges between aromatics, and phthalic acids from the condensed aromatic nuclei, in close analogy with the behavior and structure of asphaltene.

Bibliography

1. M.L. Selucky, Y. Chu, T.C.S. Ruo and O.P. Strausz, "Chemical Composition of Cold Lake Bitumen", Fuel, 57 (1978) 9; also, unpublished results.
2. J.T. Bulmer and J. Starr, *Syncrude Analytical Methods for Oil Sand and Bitumen Processing*, Syncrude Canada Ltd., Edmonton, AB, 1979.
3. J.D. Payzant, A.M. Hogg, D.S. Montgomery and O.P. Strausz, "A Field Ionization Mass Spectrometric Study of the Maltene Fraction of Athabasca Bitumen. Part I — The Saturates", AOSTRA J. Res., 1 (1985) 175.
4. J.D. Payzant, A.M. Hogg, D.S. Montgomery and O.P. Strausz, "A Field Ionization Mass Spectrometric Study of the Maltene Fraction of Athabasca Bitumen. Part II — The Aromatics", AOSTRA J. Res., 1 (1985) 183.
5. J.D. Payzant, D.S. Montgomery and O.P. Strausz, "Novel Terpenoid Sulfoxides and Sulfides in Petroleum", Tetrahedron Lett., 24 (1983) 651.
6. O.P. Strausz, E.M. Lown and J. D. Payzant, "Nature and Geochemistry of Sulfur-Containing Compounds in Alberta Petroleums", Ch. 22 in *Geochemistry of Sulfur in Fossil Fuels*, ACS Symposium Series 429, W.L. Orr and C.M. White, Eds., Am. Chem. Soc., Washington, D.C., 1990, p. 366.
7. A.L. Chaffee, D.S. Hoover, R.B. Johns and F.K. Schweighardt, "Biological Markers Extractable From Coal", in *Biological Markers in the Sedimentary Record*, R.B. Johns, Ed., Elsevier, Amsterdam, 1986, p. 335.
8. T.W. Mojelsky, D.S. Montgomery and O.P. Strausz, "The Side Chains Associated With the Undistillable Aromatic and Resin Components of Athabasca Bitumen", AOSTRA J. Res., 2 (1986) 177.
9. N. Cyr, D.D. McIntyre, G. Toth and O.P. Strausz, "Hydrocarbon Structural Group Analysis of Athabasca Asphaltene and its GPC Fractions by ^{13}C NMR", Fuel, 66 (1987) 1709.
10. O.P. Strausz, T.W. Mojelsky and E.M. Lown, "The Molecular Structure of Athabasca Asphaltene: An Unfolding Story", Fuel, 71 (1992) 1355.
11. O.P. Strausz, E.M. Lown and T.W. Mojelsky, unpublished results.
12. O.P. Strausz, E.M. Lown and J.D. Payzant, "Isolation of Sulfur Compounds From Petroleum", Ch. 5 in *Geochemistry of Sulfur in Fossil Fuels*, ACS Symposium Series 429, W.L. Orr and C.M. White, Eds., Am. Chem. Soc., Washington, D.C., 1990, p. 83.
13. J.D. Payzant, D.S. Montgomery and O. P. Strausz, "The Identification of Homologous Series of Benzo[b]thiophenes, Thiophenes, Thiolanes and Thianes Possessing a Linear Carbon Framework in the Pyrolysis Oil of Athabasca Asphaltene", AOSTRA J. Res., 4 (1988) 117.
14. T.W. Mojelsky, T.M. Ignasiak, Z. Frakman, D.D. McIntyre, E.M. Lown, D.S. Montgomery and O.P. Strausz, "Structural Features of Alberta Oil Sand Bitumen and Heavy Oil Asphaltenes", Energy & Fuels, 6 (1992) 83.
15. T.W. Mojelsky, D.S. Montgomery and O.P. Strausz, "The Basic Nitrogen Compounds in Athabasca Maltene", AOSTRA J. Res., 3 (1986) 25.
16. J.D. Payzant, I. Rubinstein, A.M. Hogg and O.P. Strausz, " Field-Ionization Mass Spectrometry: Application to Geochemical Analysis", Geochim. Cosmochim. Acta, 43 (1979) 1187.

17. A.G. Requejo, J. Allan, S. Creaney, N.R. Gray and K.S. Cole, "Alkyl Isoprenoids and Diaromatic Carotenoids in Paleozoic Source Rocks and Oils from the Western Canada and Williston Basins", Org. Geochem., 19 (1991) 245.

18. D.J. Hallett, F.I. Onuska and M.E. Comba, "Aliphatic and Polyaromatic Compounds of Weathered and Unweathered Southern Louisiana Crude Oil", Marine Environ. Res., 8 (1983) 73.

19. M.A. Poirier and B.S. Bas, "Characterization of Polynuclear Aromatic Hydrocarbons in Bitumen, Heavy Oil Fractions Boiling Above 350° by Gas Chromatography–Mass Spectrometry", Fuel, 63 (1984) 361.

20. T.W. Mojelsky and O.P. Strausz, "Detection of Alkylated Fluorenes in Athabasca Oil Sand Bitumens", Org. Geochem., 9 (1986) 39.

21. T.W. Mojelsky and O.P. Strausz, "Detection of Methyl Fluorenones in Athabasca Oil Sand Bitumens", Org. Geochem., 9 (1986) 31.

22. J.D. Payzant, T.W. Mojelsky, T.D. Cyr, D.S. Montgomery and O.P. Strausz, "The Identification of 9-n-Alkyl Fluoren-9-ols in the Alberta Oil Sands", Org. Geochem., 8 (1985) 177.

Chemical Composition of the Polar Fraction

12

The residue remaining behind after removal of the saturate and aromatic fractions from the maltene constitutes (depending on the mode of separation) the "polar" or "resin" fraction of the bitumen. The term "resin" is a misnomer and has a historical origin. In the early days of petroleum chemistry little was known about the chemical composition of this fraction of petroleum and the term was adopted on the basis of its physical resemblance to natural resins, to which it has no chemical connection.

In the past, resins have been variously defined as that fraction of petroleum which:

- is soluble in *n*-pentane but insoluble in propane,
- is adsorbed and therefore can be separated from the maltene on Attapulgus clay, and
- in the USBM-60 procedure, can be separated from the maltene on anion/cation exchangers to remove the acids and bases and then on Fe^{3+}-impregnated Attapulgus clay to remove the neutral nitrogen compounds;

whereas polars are the fraction that stays back on silica gel after elution of the saturate and aromatic fractions of the maltene with hydrocarbon solvents.

Quantities of polars or resins determined by the various methods may not be the same and, depending on the method used for their isolation, the polar or resin content of a given bitumen may vary between 15 and 45%. This variation is largely due to the gradual transition between the more polar components of the aromatic fraction and the less polar portion of the polar/resin fraction itself and the "fuzziness" of the dividing line between them. The apparent polar/resin content is also dependent on the method followed in the precipitation of the asphaltene: the maltene from which the asphaltene was removed by *n*-heptane precipitation will have a higher polar/resin content than the maltene from which the asphaltene was removed by *n*-pentane precipitation. Here again the difference is due to the difficulties in drawing a sharp dividing line between low-MW asphaltene and high-MW polar/resin components. Polar/resin molecules, especially those with highly polar functional groups, tend to complex, adsorb and/or chemisorb to asphaltene and integrate themselves into the asphaltene micelles or aggregates in the bitumen.

Bitumen polars/resins, like petroleum polars/resins in general, consist of a mixture of acidic, basic, amphoteric and other polar but otherwise neutral molecules. They are rich in heteroatoms and have a lower (H/C) atomic ratio and a higher MW than the hydrocarbon fractions, the saturates and aromatics. For example, for the most polar fraction (30%) of Athabasca (Syncrude high grade) maltene the number average MW is of the order 800–900 $g \cdot mol^{-1}$. The MW distribution is broad, representing a highly polydispersed system which extends from about 300 $g \cdot mol^{-1}$ to over 6,000 $g \cdot mol^{-1}$, well into the MW range of asphaltene.

Since most of the results to be discussed in this chapter come from silica gel fractionations, the term "polars" will be used to designate the "polars/resins" fraction.

Some analytical data on polar subfractions from Athabasca bitumen are tabulated in Table 12.1. The less polar Polar I subfraction was cut arbitrarily from the polyaromatic + nonspecific less polar fraction, giving 8.8% for this subfraction and 22.5% for the more polar Polar II subfraction. Their combined amount, 31.3% of the bitumen, may be compared to the USBM API–60 results giving 13.7% acids + amphoterics, 6.5% bases, and 1.4% neutral nitrogen compounds for a total of 21.6% of the bitumen. The continuous nature of the transition between the high-MW and more polar end of the polyaromatic + nonspecific polar constituents of the bitumen and the low-MW and less polar end of its polar fraction introduces an unavoidable measure of arbitrariness in the separation of these fractions and this is responsible for the apparent scatter in the reported values for the polar (and the difference between the polar and resin) contents of crude oils and bitumens.

Table 12.1 Elemental composition of Athabasca polar subfractions[a]

Subfraction	Solvent	Wt% of bitumen	C	H	N	O	S	MW	$(H/C)_a$	Ash
			wt%					$(g \cdot mol^{-1})$		%
Polar I	benzene	8.8	82.4	9.5	0.70	1.51	5.9	830	1.39	0.56
Polar II	40% CH_3OH /CH_2Cl_2	22.5	79.6	10.0	0.64	4.12	5.7	910	1.50	1.77

[a] Separated on silica gel from n-C_5-deasphaltened bitumen. MW by VPO.

The Athabasca Polar subfractions I and II were further fractionated by adsorption and gel permeation (GPC) chromatographic methods[1] into narrower subfractions, as outlined in Figures 12.1 and 2. The elemental compositions of the collected subfractions are given in Tables 12.2–12.4.

From Table 12.2 it is seen that the MW range is broader in the more polar subfraction II and that the variations in composition, NOS contents and $(H/C)_a$ with MWs of the GPC fractions are different in the two subfractions. These compositional trends can be illustrated as follows:

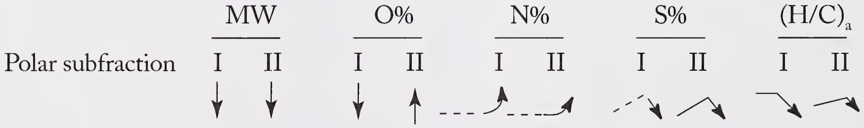

The picture, however, changes considerably when the number of heteroatoms, rather than their percentage composition in the molecule, is considered, Figure 12.3. In this correlation all three heteroatoms exhibit a monotonic decline with decreasing MW of the GPC fraction.

Separation of Polar I by adsorption chromatography on an alumina column, Table 12.3, suggests a clear polarity effect leading to a general increase in the oxygen and nitrogen contents and $(H/C)_a$ ratios as the polarity of the subfraction increases. The sulfur content, on the other hand, varies according to a maximum curve. In further alumina chromatographic separation of one of the subfractions, Polar I–4, this subfraction also appears to display analogous trends.

It will be noted that during the time-consuming separation procedures some oxygen uptake occurs since the combined oxygen content of the fractions exceeds the oxygen content of the whole initial Polar I material. A similar slow oxidation is also apparent from the corresponding data for Polar II separated on a silica column, listed in Table 12.4. Here, the trend in oxygen content is similar to that observed for the Polar I subfractions, but the sulfur

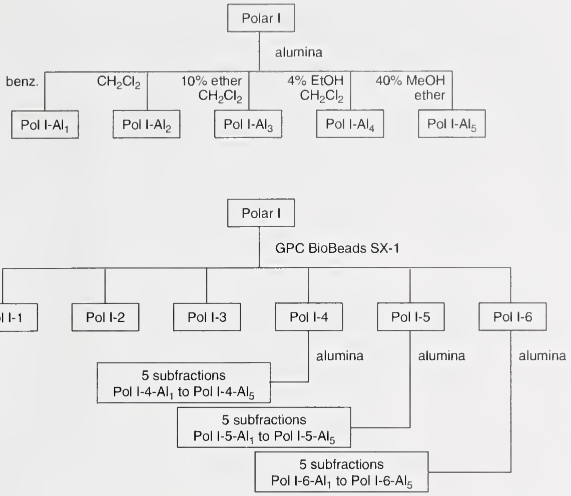
Polar I
alumina
benz.
CH_2Cl_2
10% ether CH_2Cl_2
4% EtOH CH_2Cl_2
40% MeOH ether
Pol I-Al_1
Pol I-Al_2
Pol I-Al_3
Pol I-Al_4
Pol I-Al_5
Polar I
GPC BioBeads SX-1
Pol I-1
Pol I-2
Pol I-3
Pol I-4
Pol I-5
Pol I-6
alumina
alumina
alumina
5 subfractions Pol I-4-Al_1 to Pol I-4-Al_5
5 subfractions Pol I-5-Al_1 to Pol I-5-Al_5
5 subfractions Pol I-6-Al_1 to Pol I-6-Al_5

Figure 12.1 Fractionation schemes for Athabasca Polar I fraction.[1]

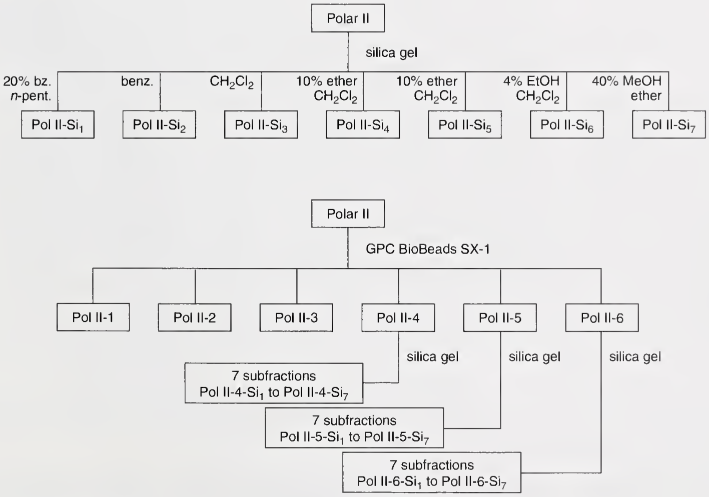
Polar II
silica gel
20% bz. *n*-pent.
benz.
CH_2Cl_2
10% ether CH_2Cl_2
10% ether CH_2Cl_2
4% EtOH CH_2Cl_2
40% MeOH ether
Pol II-Si_1
Pol II-Si_2
Pol II-Si_3
Pol II-Si_4
Pol II-Si_5
Pol II-Si_6
Pol II-Si_7
Polar II
GPC BioBeads SX-1
Pol II-1
Pol II-2
Pol II-3
Pol II-4
Pol II-5
Pol II-6
silica gel
silica gel
silica gel
7 subfractions Pol II-4-Si_1 to Pol II-4-Si_7
7 subfractions Pol II-5-Si_1 to Pol II-5-Si_7
7 subfractions Pol II-6-Si_1 to Pol II-6-Si_7

Figure 12.2 Fractionation schemes for Athabasca Polar II fraction.[1]

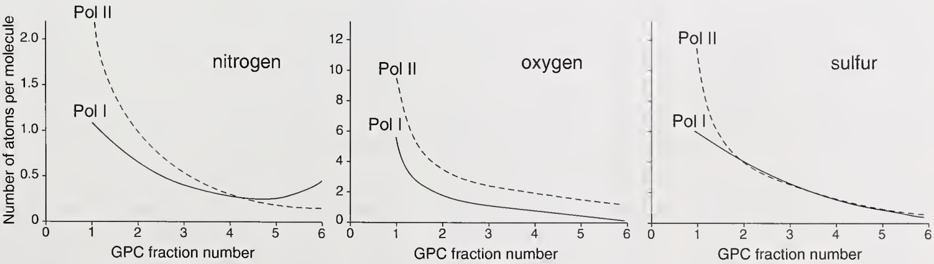

Figure 12.3 Distribution of heteroatoms per molecule in the GPC subfractions of Athabasca Polars I and II.[1]

Table 12.2 Elemental compositions of Athabasca polar GPC subfractions[a]

Polar subfraction	Wt%	C	H	N	O	S	MW (g·mol^{-1})	(H/C)$_a$
		wt% d.a.f.[b]						
Polar I–1	5.5	82.01	9.77	0.44	2.49	5.29	3,630	1.43
Polar I–2	14.4	82.24	10.07	0.36	1.31	6.02	2,220	1.47
Polar I–3	21.9	82.33	9.88	0.44	1.50	5.85	1,460	1.44
Polar I–4	27.8	82.32	9.60	0.42	1.16	6.50	1,000	1.40
Polar I–5	23.6	82.50	8.73	0.97	1.10	6.70	490	1.27
Polar I–6	6.2	83.99	7.84	2.16	1.10	4.91	350	1.12
Polar II–1	14.5	81.08	9.56	0.65	2.51	6.20	6,100	1.42
Polar II–2	17.7	80.43	10.12	0.62	2.55	6.28	2,220	1.51
Polar II–3	20.8	80.13	10.08	0.58	2.82	6.39	1,400	1.51
Polar II–4	25.0	78.97	9.97	0.55	4.05	6.46	770	1.52
Polar II–5	18.4	78.81	9.37	0.59	5.45	5.78	460	1.43
Polar II–6	2.8	81.37	7.55	0.83	5.47	4.78	310	1.11

[a] In all the fractions ash (determined by difference) was < 0.5%. [b] Dry ash free.

Table 12.3 Elemental compositions of Athabasca Polar I alumina adsorption and gel permeation chromatographic subfractions

Polar subfraction	Wt%	C	H	N	O	S	MW (g·mol^{-1})	(H/C)$_a$
		wt% d.a.f.[a]						
Polar I–Al$_1$	4.9	84.69	8.80	0.00	1.00	5.51	–	1.25
Polar I–Al$_2$	23.6	82.26	8.98	0.46	1.45	6.85	860	1.31
Polar I–Al$_3$	27.8	80.27	9.31	0.42	2.60	7.40	790	1.39
Polar I–Al$_4$	20.2	81.56	9.28	0.61	3.07	5.48	960	1.36
Polar I–Al$_5$	14.5	81.08	9.43	0.63	3.98	4.88	900	1.40
Polar I–4–Al$_1$	5.7	85.36	9.25	0.24	1.45	3.70	–	1.30
Polar I–4–Al$_2$	23.2	82.07	9.00	0.35	1.53	7.22	–	1.32
Polar I–4–Al$_3$	27.7	80.12	9.35	0.51	2.50	7.52	950	1.40
Polar I–4–Al$_4$	21.7	81.53	9.31	0.75	3.10	5.31	–	1.37
Polar I–4–Al$_5$	13.1	80.97	9.38	0.30	4.00	5.35	–	1.39

[a] Dry ash free.

Table 12.4 Elemental compositions of Athabasca Polar II silica gel adsorption and gel permeation chromatographic subfractions[1]

Polar subfraction	Wt%	C	H	N	O	S	Ash[a]	MW (g·mol^{-1})	(H/C)$_a$
		wt%							
Polar II–Si$_1$	6.0	80.62	9.53	0.59	3.65	5.61	0.2	–	1.42
Polar II–Si$_2$	9.3	80.80	9.38	0.63	4.20	4.99	1.6	–	1.39
Polar II–Si$_3$	6.3	81.24	9.61	0.50	4.20	4.45	6.0	–	1.42
Polar II–Si$_4$	16.3	79.95	9.72	0.52	4.45	5.36	0.2	850	1.46
Polar II–Si$_5$	17.3								
Polar II–Si$_6$	30.9	77.41	10.09	0.22	4.78	7.49	2.2	680	1.56
Polar II–Si$_7$	9.2	73.78	9.76	0.32	7.48	8.66	4.0	–	1.59
Polar II–5–Si$_4$	13.3	79.80	8.86	1.26	6.30	3.75	0.84	500	1.33
Polar II–5–Si$_5$	7.0	78.72	10.03	0.86	6.15	4.24	0.00	530	1.53
Polar II–5–Si$_6$	43.2	74.91	9.93	0.43	6.07	8.66	0.00	460	1.59
Polar II–5–Si$_7$	10.6	70.99	9.20	0.62	10.07	9.12	1.62	470	1.55

[a] By difference.

content varies according to a minimum curve and the nitrogen content decreases as the polarity of the subfraction increases. In one GPC fraction, Polar II–5, which was subsequently refractionated on silica gel, the trends are again somewhat different in that the sulfur content monotonically increased with increasing polarity of the fraction.

The general conclusion from these data is that correlations between heteroatom content, MW and polarity are difficult to predict and that the assumption that increasing polarity means increasing MW requires revision. Indeed, it will be shown in Chapter 14 that the polarities of Athabasca asphaltene subfractions, graded according to their elution order from a silica gel column, are actually an inverse function of their MWs and that in GPC-separated asphaltene subfractions the NOS contents change only slightly with MW.

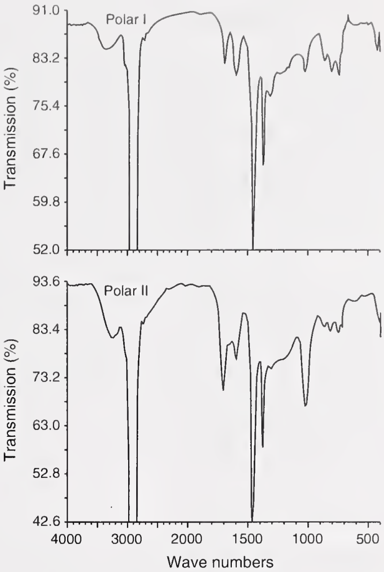

Figure 12.4 Infrared spectra of Athabasca Polars I and II fractions.[1]

The infrared spectra of Polar I, Polar II and their GPC subfractions are shown in Figures 12.4 and 12.5. The Polar I and Polar II spectra both feature intense CH_2 and CH_3 absorptions (2860, 2925, 2960 and 2870 cm^{-1}; 1460 and 1380 cm^{-1}), weak aromatic absorptions (3030, 1600, 880, 850 and 740 cm^{-1}), hydrogen bonding absorptions (alcoholic, phenolic and carboxylic –OH; 2300–3500 cm^{-1}), free carboxylic carbonyl (1710 cm^{-1}) and sulfoxide (1040 cm^{-1}) absorptions. According to the IR spectra Polar II contains less aromatics than Polars I and more sulfoxides, carboxylic acids and alcohols, in agreement with their elemental composition. In Polars I the aromaticity of the last fraction is higher than that of the previous fraction due to the accumulation of aromatic amines (3480, 1325 and 1600 cm^{-1}), probably carbazoles. In Polars II there are more carboxylic acids and sulfoxides in the lower MW fractions and the Polars II–5 fraction is particularly rich in sulfoxides while the Polars II–6 fraction is rich in carboxylic acids and aromatics: specifically, sulfoxides increase from subfractions 1 to 5 then decrease in subfraction 6, while the acids increase on going from subfractions 1 to 6.

1.0 Mass Spectroscopic Studies on the Lower Molecular Weight Components of Athabasca Polars

Detailed compositional studies on the polar fractions of bitumen have been reported for Athabasca bitumens only. In the continuation of the combined chromatographic fractionation/FIMS/high-resolution EIMS studies on the saturate and aromatic fractions, the polars were fractionated into 12 subfractions, (numbers 4 to 15 in Table 10.2 and Figure 10.1) and 10 of these subfractions were studied using FIMS/high-resolution EIMS. As will be noted from the data in Table 10.2, the volatility of the polar fractions is lower than that of the hydrocarbon fractions, and the NMR spectra, in agreement with elemental analysis, indicate structural differences between the distillable portions (which were analyzed by mass spectrometry) and the nondistillable residues.

1.1 Subfractions 4 to 7

Subfractions 4–7 in Table 10.2 and Figure 10.1 are rich in neutral nitrogen compounds, as indicated by the strong N–H IR absorption of the polar subfractions I-5 and I-6, Figure 12.5. Basic nitrogen compounds are present in the maltene (see below) but they would not be expected to be present in subfractions 4–7 (Table 10.2) because they are known to adsorb very strongly onto silica gel and can be eluted only with difficulty. The FI mass spectra[2] of subfractions 4–6 are shown in Figures 12.6–12.8.

Figure 12.6 features two prominent homologous series of nitrogen compounds, one of them appearing at $m/z = 251, 265, 279$ (max.), 293, ...*etc.*, represented by series formula $C_nH_{2n-15}N$ with a maximum at $n = 20$ and the other at $m/z = 277, 291, 305, 319, 333$ (max.), 347, ...*etc.*, represented by series formula $C_nH_{2n-17}N$ with a maximum at $n = 24$. The lower members of the latter series, $n = 18, 19$ (max.), 20, *etc.*, already appeared in subfraction 3e. The $C_nH_{2n-15}N$ series are alkylcarbazoles,

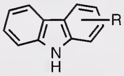

and the smooth distribution pattern suggests that R is an *n*-alkyl group of varying length. The $C_nH_{2n-17}N$ series are alkylcarbazoles with a condensed naphthenic ring:

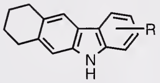

Each of the series may contain several different isomers, *e.g.*

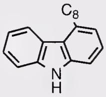

,

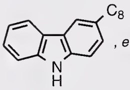

, *etc.*, and

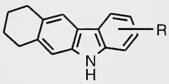

,

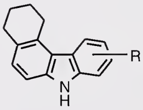

, *etc.*

Figure 12.7 shows that the main components of subfraction 5 are the same two series in a somewhat different distribution, along with lesser amounts of the $C_nH_{2n-19}N$ and $C_nH_{2n-21}N$ series appearing at $m/z = 303, 317, 331, 345$, and 301, 315, 357, 399, *etc.*, respectively, corresponding to an alkylcarbazole with two naphthenic rings and an alkylbenzocarbazole

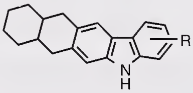

and

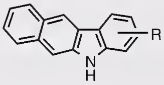

.

From Figure 12.8 it is seen that subfraction 6 is still mainly composed of nitrogen compounds such as alkylcarbazoles, alkylbenzocarbazoles, alkylcyclohexanecarbazoles and alkylcyclohexanebenzocarbazoles, $C_nH_{2n-23}N$, $m/z = 341, 355, 369, 383, 397, 411, 425, 439$, *etc.*,

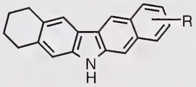

along with small quantities of even higher condensed alkylcarbazoles featuring benzocarbazoles with two naphthenic rings, dibenzocarbazoles and dibenzocarbazoles with one and two naphthenic rings, all alkyl-substituted, forming homologous series.

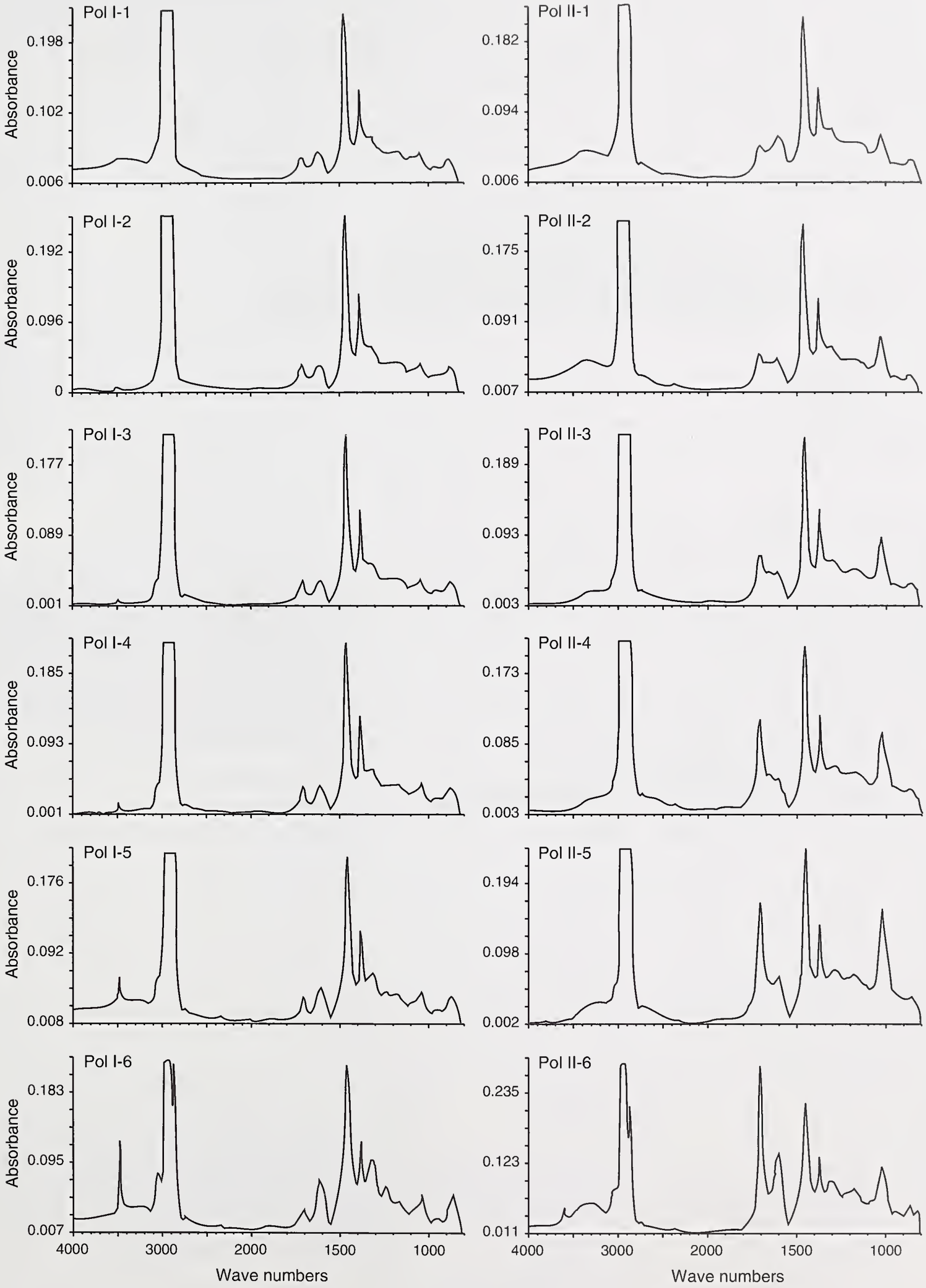

Figure 12.5 Infrared spectra of the six GPC subfractions of Athabasca Polars I and II.[1]

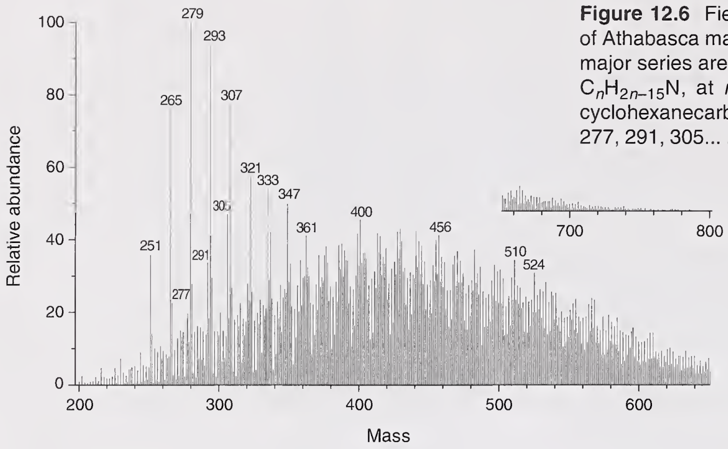

Figure 12.6 Field ionization mass spectrum of Athabasca maltene subfraction 4.[2] The two major series are alkyl-substituted carbazoles, $C_nH_{2n-15}N$, at *m/z* = 251, 265, 279... and cyclohexanecarbazoles, $C_nH_{2n-17}N$, at *m/z* = 277, 291, 305... .

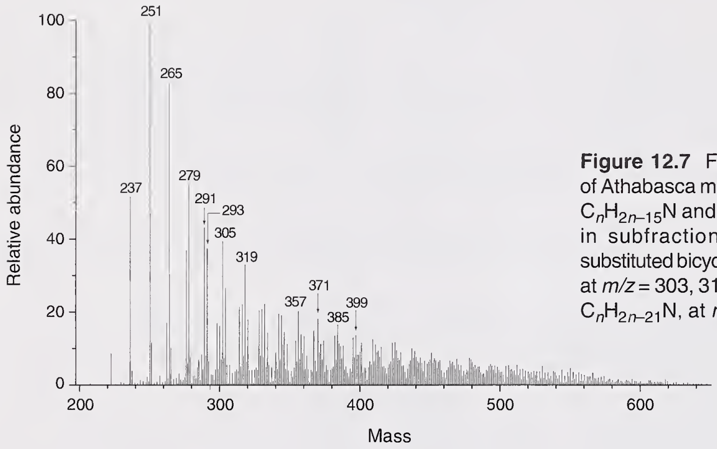

Figure 12.7 Field ionization mass spectrum of Athabasca maltene subfraction 5.[2] The same $C_nH_{2n-15}N$ and $C_nH_{2n-17}N$ series dominate as in subfraction 4. Also present are alkyl-substituted bicyclohexanecarbazoles $C_nH_{2n-19}N$, at *m/z* = 303, 317, 331... and benzocarbazoles, $C_nH_{2n-21}N$, at *m/z* = 287, 30l, 315, 329, ...

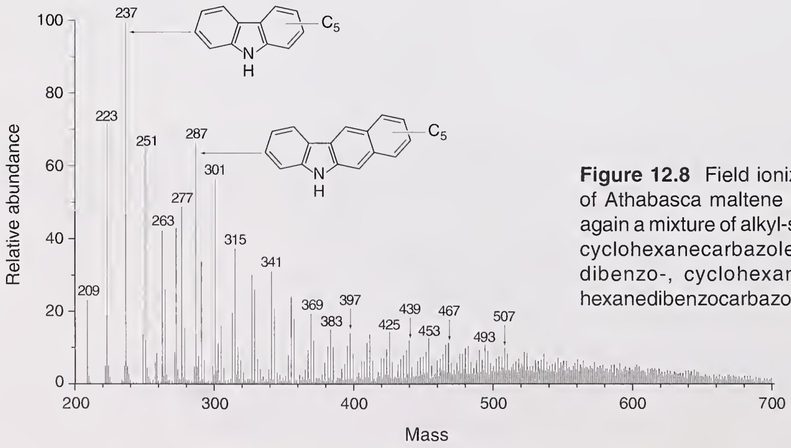

Figure 12.8 Field ionization mass spectrum of Athabasca maltene subfraction 6.[2] This is again a mixture of alkyl-substituted carbazoles, cyclohexanecarbazoles, benzocarbazoles, dibenzo-, cyclohexanedibenzo-, dicyclohexanedibenzocarbazoles, *etc.*

Plots of relative concentrations *versus* carbon number for the more abundant series of carbazoles in subfraction 6 are shown in Figure 12.9. The most abundant nitrogen compounds are the carbazoles followed by, in decreasing order of abundance, benzocarbazoles, cyclohexanecarbazoles, cyclohexanebenzocarbazoles and dicyclohexanecarbazoles. The elemental formula in each series has been confirmed by high-resolution EIMS and, in some cases, by chromatographic elution behaviour.

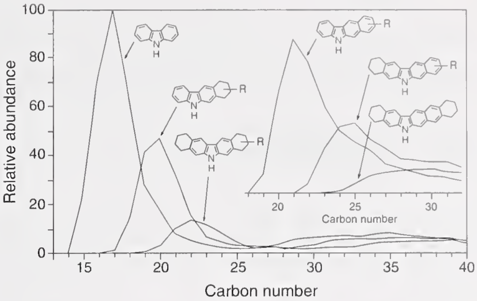

Figure 12.9 Relative concentrations *versus* carbon number in the molecule, for the five carbazole series in Athabasca maltene subfraction 6.

The FI mass spectrum of subfraction 7 still indicated the presence of residual carbazoles; in effect carbazoles are quite spread out and members of the carbazole compound class can be found in the aromatic fraction and in the *n*-pentane precipitated asphaltene fraction of the bitumen. In the latter case the carbazoles, along with a host of other compounds, can be separated from the asphaltene by acetone extraction and concentrated by a series of chromatographic steps, as will be discussed later in this chapter.

Comparison of the carbon number at which the maximum concentration occurs in the various series of alkylcarbazoles in subfractions 4–7 reveals a regular pattern, Table 12.5, according to which the *n*-value at which the maximum concentration in a given series occurs in a fraction decreases with increasing fraction number or retention time. Thus, for example, the maximum concentration in the $C_nH_{2n-15}N$ series is found at $n = 20, 18, 17$ and 16 in subfractions 4, 5, 6 and 7. This behaviour may be understood in terms of the group adsorption energies. To a first approximation the adsorption energy of a molecule should be equal to the sum of the adsorption energies of its individual constituent groups. This assumes that the adsorption of a group, *i*, is not affected by the simultaneous adsorption of another group, *j*, in the same molecule. While this is not always the case, in practice it is an effective approximation in many cases. The group adsorption energies of amines on silica gel have large positive values (+20.9 to +41.8 kJ for tertiary, primary amino and amide groups) and aromatic –CH= groups have small positive values, +1.0 kJ, contributing positively to the molecular adsorption energy and thereby to the lengthening of the retention time. The adsorption energy of methylene on silica gel, on the other hand, has a small negative value, –0.2 kJ, and therefore the adsorption energy and the retention time for the molecule will decrease with increasing number of methylene groups present in the molecule within a given $C_nH_{2n+z}N$ series, in agreement with the data compiled in Table 12.5. Conversely, the greater the number of aromatic rings in the molecule, the greater the adsorption energy and the retention time, and therefore molecules in the $z = -15$ series elute before molecules in the $z = -21$ series.

Table 12.5 Carbon numbers and masses of the most abundant components of three of the homologous series of carbazoles in the silica gel polar subfractions 4–7.

Subfraction number	$C_nH_{2n-15}N$		$C_nH_{2n-17}N$		$C_nH_{2n-21}N$	
	n	*m/z*	*n*	*m/z*	*n*	*m/z*
4	20	279	23	319		
5	18	251	21	291	23	315
6	17	237	21	291	21	287
7	16	223	20	277		

The main compound class present in subfraction 7 is dominated by a series of peaks at *m/z* = 208, 222 (max.), 236, 250, etc, and another series at *m/z* = 244, 258, 272 (max.), 286, ...*etc.*, which correspond to the series formulas $C_nH_{2n-18}O$ and $C_nH_{2n-24}O$.

1.2 Subfraction 8

The same $C_nH_{2n-18}O$ and $C_nH_{2n-24}O$ series of peaks seen in the FI spectrum of subfraction 7 also appear in the FI mass spectrum of subfraction 8, Figure 12.10. The distillable portion of this fraction comprises only 0.27% of the bitumen but it is highly enriched in alkylfluoren-9-ones

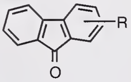

and their higher condensed derivatives. It has a bright red color and features a characteristic carbonyl absorption in the infrared at 1710 cm^{-1}. The series with $Z = -18$ consists of alkylfluorenones and the one with $Z = -24$ of alkylbenzofluorenones:

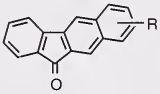

In confirmation of these assignments, a series of methylfluoren-9-ones (mono- to tetramethyl) from Athabasca polars were isolated as their β-hydroxy ester derivatives and their chemical structures confirmed. One of the major dimethyl derivatives present was the 1,4 isomer:

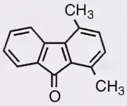

The chemistry of these fluorenones will be considered later in this chapter.

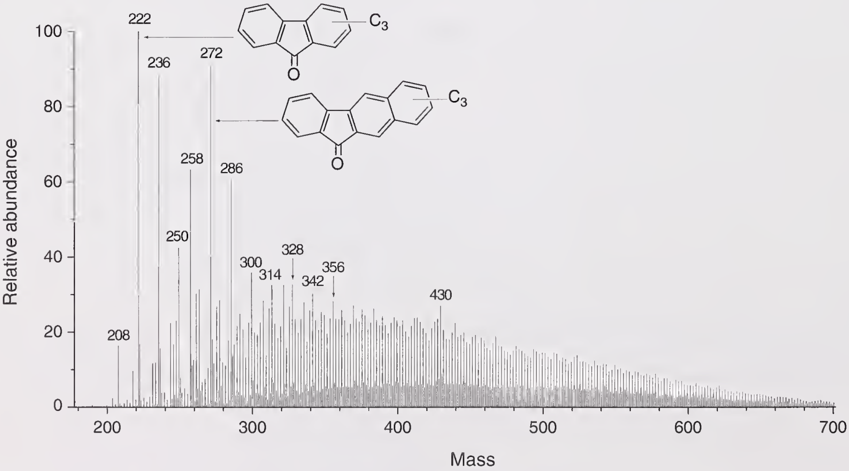

Figure 12.10 Field ionization mass spectrum of Athabasca maltene subfraction 8.[2] The alkyl-substituted fluoren-9-ones, $C_nH_{2n-18}O$, appear at *m/z* = 208, 222, 236... and the benzofluoren-9-ones, $C_nH_{2n-24}O$, at *m/z* = 258, 272, 286... .

1.3 Subfractions 9 and 10

Subfraction 9 consists of a mixture of fluorenones and a series of compounds giving peaks at *m/z* = 210, 224, 238, 252 (max.), 266, ...*etc.*, in the FI mass spectrum. The latter series of peaks are the dominant feature of the FI mass spectrum of the next fraction, subfraction 10, Figure 12.11, and they were shown by high-resolution EIMS to have the series formula $C_nH_{2n-16}O$ representing 9-*n*-alkylfluoren-9-ols.

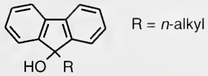

As will be described later, fluorenols have been separated from the maltene and their structures identified spectroscopically by comparison with authentic standards. The *n*-alkyl chain extends to at least C_9 and, in addition, parallel series with nuclear alkylated centers

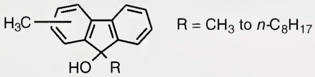

have also been detected. Fluorenols with branched alkyl chains were not detected.

Also detected in fraction 10 were series of alkylquinolines and alkylquinolones, as will be discussed later in this chapter.

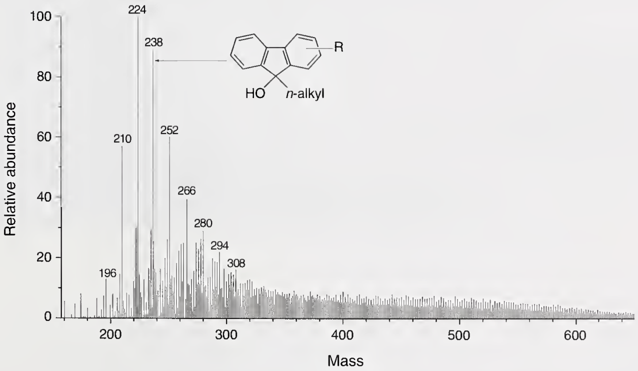

Figure 12.11 Field ionization mass spectrum of Athabasca maltene subfraction 10.[2] The series at *m/z* = 210, 224, 238... corresponds to 9-*n*-alkylfluoren-9-ols, $C_nH_{2n-16}O$.

1.4 Subfraction 11

This subfraction consists of a complex mixture of even-mass-numbered aromatic hydrocarbons and odd-mass-numbered nitrogen compounds forming a broad, featureless hump extending to *m/z* ≈ 800 with a maximum at around *m/z* = 576–620. This fraction was not examined under high resolution and thus the series formulae for the compounds in the FI mass spectrum could not be established.

1.5 Subfraction 13

Subfraction 13 gave the FI mass spectrum shown in Figure 12.12. This subfraction appeared to be a mixture of primarily aliphatic carboxylic acids. Therefore, it was methylated with diazomethane and rechromatographed to give the subfractions listed in Table 12.6. Subfractions 13-II to 13-IV were analyzed by FIMS giving the spectra shown in Figures 12.13–12.15.

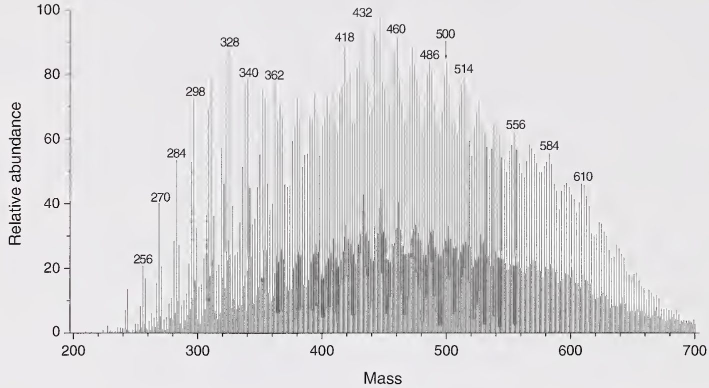

Figure 12.12 Field ionization mass spectrum of Athabasca maltene subfraction 13, a mixture of primarily naphthenic carboxylic acids.

Table 12.6 Chromatographic separation of subfraction 13 after methylation

Subfraction number	Solvent	Volume (mL)	Weight (mg)	%
13–I	n-C_5	250	–	–
13-II	CH_2Cl_2	250	25.6	27
13-III	10% EtOAc in CH_2Cl_2	125	26.6	28
13-IV	5% CH_3OH in CH_2Cl_2	150	43.0	45
Total			95.2	100

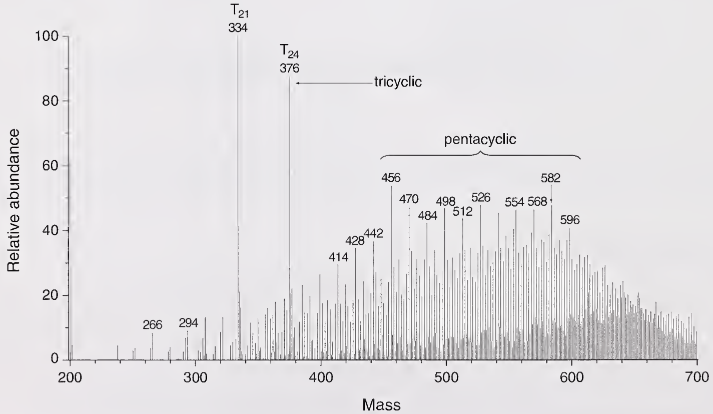

Figure 12.13 Field ionization mass spectrum of Athabasca maltene subfraction 13–II, the methyl esters of carboxylic acids.[2] The peaks at $m/z = 334$ and 376 correspond to tricyclic esters with $n = 21$ and 24, and the series of peaks at $m/z = 456, 470, 484...$, to pentacyclic esters with $n = 30, 31, 32$.... The bulk of the fraction consists of methyl esters of cyclic monocarboxylic acids along with small amounts of acyclic acids.

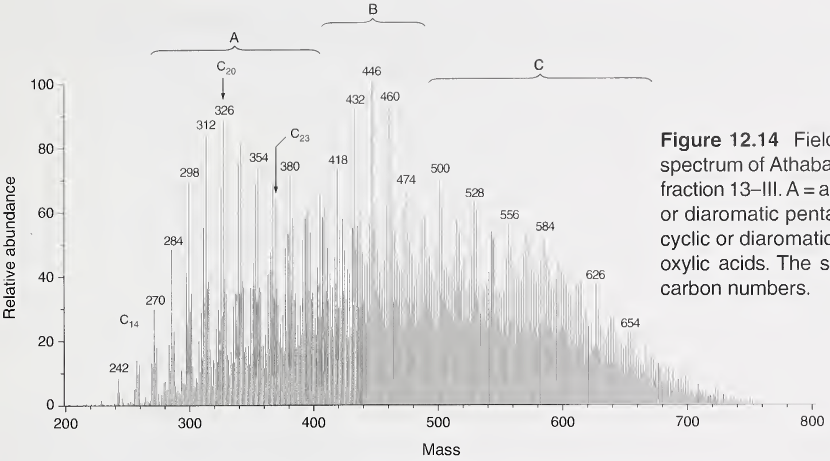

Figure 12.14 Field ionization mass spectrum of Athabasca maltene subfraction 13–III. A = acyclic, B = tricyclic or diaromatic pentacyclic, C = tetracyclic or diaromatic hexacyclic carboxylic acids. The subscripts are the carbon numbers.

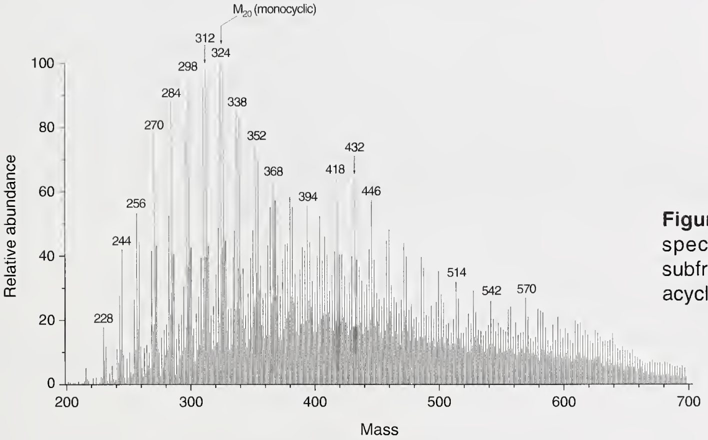

Figure 12.15 Field ionization mass spectrum of Athabasca maltene subfraction 13–IV, also a mixture of acyclic to hexacyclic acids.

The two dominant peaks, one at m/z = 334 and the other at 376 in Figure 12.13, correspond to the tricyclic acid methyl esters of series formula C_nH_{2n-5} CO_2CH_3 with n = 20 and 23. As will be discussed later, the structures of the corresponding acids have been shown to be

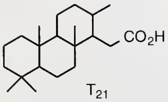

T_{21}

and

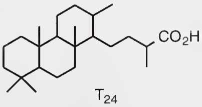

T_{24}

The series, and some isomers thereof, appears to extend to quite high carbon numbers. In addition to the methyl esters of the tricyclic acids, a long series of pentacyclic carboxylic acid methyl esters are present, giving the peaks at m/z = 456, 470, 484, ...*etc*., up to at least 596 corresponding to carbon numbers in the acids from about 30 to 40 and more likely from ~25 to ~48. These pentacyclic acids represent hopanoic acids, or some analogues, for example,

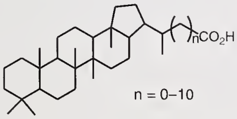

and their demethylated and side-chain extended derivatives. The presence of the tricyclic carboxylic acids in the polars explains the observation that on thermolysis, the polar fraction of the bitumen releases the entire series of tricyclic terpanes

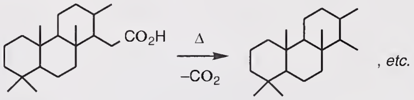

from C_{19} to C_{30} which have been identified among the saturated biomarkers in the bitumen, along with some hopanes formed from the hopanoic acids.

The bulk of subfraction 13-II is a mixture of saturated cyclic monocarboxylic acid methyl esters. The small amounts of acyclic esters present are mainly of the *n*-alkanoic type. Above m/z = 400 a considerable proportion of the esters possesses some degree of aromaticity.

Subfractions 13-III and 13-IV (Figures 12.14 and 12.15) were not studied with high-resolution EIMS and therefore, in the absence of exact mass measurements, elemental formulas cannot be deduced. Nonetheless, it is probable that here again, the methyl esters of various acyclic, alicyclic and partially aromatized cyclic carboxylic acids comprise the bulk. Thus, for example, the series of peaks at m/z = 418, 432, 446, 460, ...*etc.* prominent in the spectra of both fractions could be due to the diaromatized analogues of the pentacyclic acid series appearing at m/z = 456, 470, ...*etc.*, in subfraction 13-II. A number of aromatic carboxylic acids have indeed been identified in that portion of Athabasca polars which is complexed to the asphaltene (see below) and can be separated from the asphaltene by acetone extraction. Also, the major peaks at m/z = 242, 270, 284, 298, 312, 326, 354... most likely represent *n*-alkanoic acids from C_{19} to C_{27} and beyond. The entire range may extend from C_{14} to well over C_{40}.

1.6 Subfraction 14

Subfraction 14 is a mixture of cyclic carboxylic acids and cyclic sulfoxides. The FI mass spectrum showed the presence of the same series of pentacyclic carboxylic acids which appeared in subfraction 13, m/z = 456, 470, 484, ...*etc.*

In order to remove the acids from the sulfoxides the fraction was methylated and rechromatographed on silica gel. Subfraction 14-IV, Table 12.7, (65%) gave the FI mass spectrum shown in Figure 12.16, which shows the presence of homologous series of cyclic saturated sulfoxides with two through six rings:

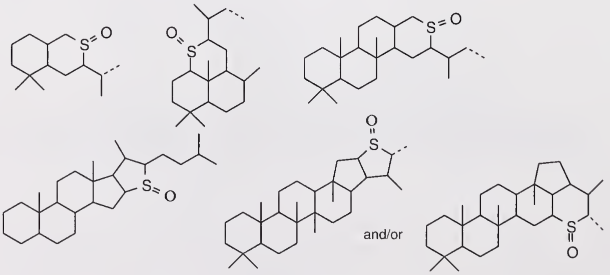

The most intense peaks at m/z = 228, 242, 256, 270, ...*etc.*, represent saturated bicyclic sulfoxides; 226, 240, 254, ...*etc.*, tricyclic sulfoxides; 364, 378, 392, ...*etc.*, tetracyclic sulfoxides; 418, 432, 446, 460, ...*etc.*, pentacyclic sulfoxides, and 458, 472, 486, ...*etc.*, hexacyclic sulfoxides. The

Table 12.7 Chromatographic separation of subfraction 14 after methylation

Subfraction number	Solvent	Volume (mL)	%
14–I	Skelly B	250	1.3
14-II	CH_2Cl_2	250	23.1
14-III	10% EtOAc in CH_2Cl_2	125	11.0
14-IV	5% CH_3OH in CH_2Cl_2	150	64.5
Total			99.9

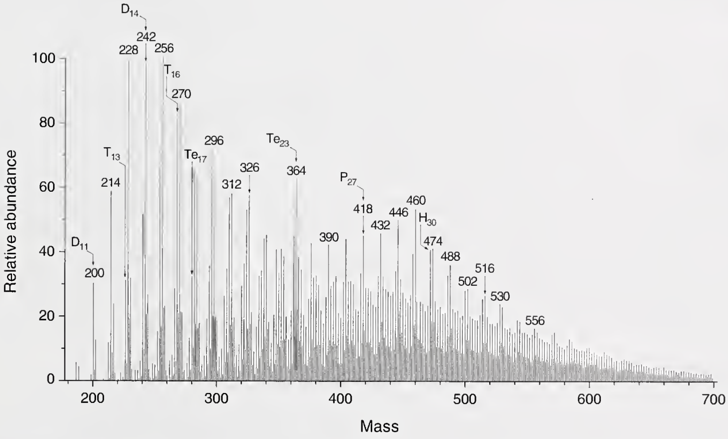

Figure 12.16 Field ionization mass spectrum of Athabasca maltene subfraction 14–IV. The bicyclic sulfoxides appear at $m/z = 200, 214, 228, \ldots$; the tricyclics at $m/z = 226, 240, 254, \ldots$; the tetracyclics at $m/z = 336, 350, 364, \ldots$; the pentacyclics at $m/z = 390, 404, 418, \ldots$; and the hexacyclics at $m/z = 458, 472, 486, \ldots$.

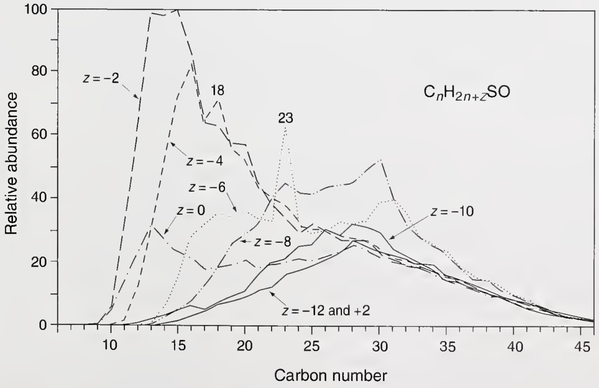

Figure 12.17 Relative concentration, *versus* carbon number in the molecule, of the mono- through heptacyclic sulfoxides in subfraction 14–IV.[2]

concentration distribution for each series as a function of carbon number is plotted in Figure 12.17, from which it is seen that the maximum in each series occurs at a different carbon number which happens to coincide with the maximum in the parent hydrocarbon series in the saturate fraction of the bitumen. Some of these sulfoxide molecules may contain a partially aromatized ring structure.

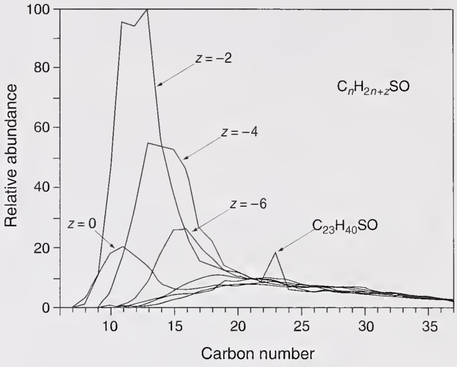

Figure 12.18 Relative concentration, *versus* carbon number in the molecule, of the mono- through heptacyclic sulfoxides in subfraction 15.

1.7 Subfraction 15

Subfraction 15 is a minor one and consists again primarily of the same sulfoxides as subfraction 14, the most intense *m/z* peaks at 200, 214, 228 belonging to the bicyclic sulfoxide series, the ones at 226, 240, 254, ...*etc.* to the tricyclic, *etc.* The concentration distribution plots for this fraction, Figure 12.18, are somewhat different from those shown in Figure 12.17 because the fraction is dominated by the lower-MW members of the di-, tri- and tetracyclic sulfoxides, in agreement with the expected chromatographic behavior of alkyl-substituted cyclic series of compounds.

1.8 Comments on the mass spectroscopic studies

The FIMS studies on Athabasca polars, as were the FIMS studies on the saturates and aromatics, have been highly instructive and brought to light the existence of many new types of molecules in the bitumen which have not been described before in the chemical literature, such as the tricyclic terpenoid hydrocarbons in the saturates, the cyclic sulfides in the aromatics, and the cyclic carboxylic acids and sulfoxides in the polars. Also discovered was the presence of series of molecules, the principal members of which were known in the chemical literature but not recognized before as regular constituents of bitumen or crude oil. Examples of these are the alkylfluorenones and fluorenols and their many condensed derivatives. The results are also informative with regard to the relative concentration distribution of the members within compound types and they should be helpful in attempts to genetically correlate compound series occurring in the same or different fractions of the bitumen.

Mass spectroscopic data alone, however, cannot reveal the precise structure of molecules and therefore the mass spectroscopic studies had to be complemented by other instrumental and chemical investigations. Moreover, no information has been gained through these studies on the composition of the nondistillable portion of the bitumen fractions. In the case of the polars, this is a more serious problem than in the case of the saturates or aromatics because the polars are less volatile than either the saturates or the aromatics and less than 50% of them are distillable. The polars comprise 36% of the maltene or 30% of the bitumen and therefore the proportion of polars that has been investigated by FIMS/EIMS amounts to less than 15% of the bitumen, leaving the rest unaccounted for. This nondistillable polar portion has been studied by instrumental methods involving FTIR and NMR spectroscopy and by chemical degradative methods, as will be described below.

In the following sections of this chapter, the chemical composition of Athabasca polars will be examined separately for each compound type.

2.0 Chemical Studies on Athabasca Polars

2.1 Sulfur-containing components

2.1.1 Saturated sulfides and sulfoxides

All Alberta heavy oil and bitumen polars are rich (5–6%) in sulfur. Most of the sulfur is present in the nondistillable portion of the polar fraction, and in the distillable portion the sulfur is mainly present as sulfoxides. These sulfoxides are structurally related to the cyclic sulfides which were detected in the aromatic fraction of the maltene, and therefore the structures of the two compound classes will be discussed together in this chapter.

The observation that the sulfur in some petroleums readily oxidizes to the sulfoxide in air, whereas in others the sulfur does not undergo this reaction, was reported over 25 years ago. It was also reported that oil taken directly from the wellhead contained no sulfoxides whereas a sample of this oil, after prolonged storage in the laboratory, showed the presence of sulfoxides. Oil sand bitumens are known to undergo chemical changes upon extended storage in air and, in view of their high sulfur content, one of the processes responsible for the chemical changes may well be the reaction of the sulfide constituents with atmospheric oxygen to form sulfoxides. It is also possible that sulfoxides are naturally present in native oil sand bitumens, in which case their concentration in the bitumen could be an indicator of the redox conditions that prevailed in the deposit.

Sulfoxides are chemically reactive and interfacially active molecules. Their properties are related to the polar character of the sulfoxide functionality

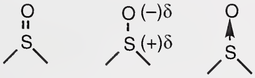

which in turn is the result of the large difference between the electronegativities of the sulfur and oxygen atoms and the nature of the S–O bond. Sulfoxides, together with portions of the carboxylic acids and nitrogen bases, are the last-eluting compounds from the silica gel column in the fractionation of the polars by elution chromatography (subfractions 14 and 15 in the silica gel separation scheme, Table 10.2). The bulk of the sulfoxides in the polars, Figures 12.17 and 12.18 and Table 12.8, are saturated cyclic molecules and, like the cyclic sulfides in subfraction 3b, they show maxima in their concentration distribution at C_{13} for the bicyclic series, at C_{18} for the tricyclic series, at C_{23} for the tetracyclic series, around C_{30} for the pentacyclic series and around C_{28}–C_{30} for the hexacyclic series.[3–6] This similarity is a clear indication that a close structural and genetic relationship may, and probably does, exist between these two compound classes in the maltene if the sulfoxides were indeed produced by the oxidation of sulfides. In order to learn more about the structures, genetic and geologic backgrounds of the sulfoxides and their relationship with the sulfides, it is necessary to separate the sulfoxides from the rest of the maltene.

The outline of the strategy for the separation of the sulfoxide class of compounds from the bitumen and their subsequent reduction to sulfides and hydrocarbons[7,8] is illustrated in Figure 12.19. Reduction to the sulfides is a necessary first step because sulfoxides would be difficult to analyze by GC owing to their very polar nature while their corresponding sulfides are readily amenable to such analyses. This reduction is also necessary for structural comparison of the sulfoxides and sulfides in the maltene. Furthermore, the reduction or hydrodesulfurization

Table 12.8 Mass measurements of sulfoxides[a]

Formula	Measured	Difference × 10^{-4} [b]	Z[c]
$C_{10}H_{18}SO$	186.1074	−4	−2
$C_{10}H_{20}SO$	188.1232	−3	0
$C_{11}H_{20}SO$	200.1230	−5	−2
$C_{13}H_{24}SO$	228.1545	−3	−2
$C_{14}H_{28}SO$	244.1864	+3	0
$C_{15}H_{28}SO$	256.1865	+5	−2
$C_{17}H_{30}SO$	282.2012	−6	−4
$C_{17}H_{32}SO$	284.2181	+8	−2
$C_{18}H_{32}SO$	296.2170	−4	−4
$C_{19}H_{36}SO$	312.2494	+7	−2
$C_{23}H_{40}SO$	364.2807	+7	−6

[a] From J.D. Payzant *et al.*, Ref. 3. © 1983, Elsevier Science Ltd.
[b] Obs. – calc. [c] Value of Z in $C_nH_{2n+Z}SO$.

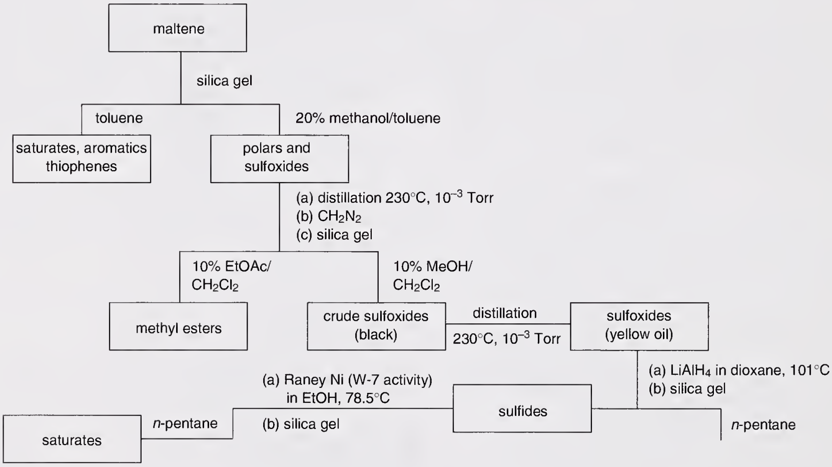
maltene
silica gel
toluene
20% methanol/toluene
saturates, aromatics thiophenes
polars and sulfoxides
(a) distillation 230°C, 10^{-3} Torr
(b) CH_2N_2
(c) silica gel
10% EtOAc/ CH_2Cl_2
10% MeOH/ CH_2Cl_2
methyl esters
crude sulfoxides (black)
distillation
230°C, 10^{-3} Torr
sulfoxides (yellow oil)
(a) $LiAlH_4$ in dioxane, 101°C
(b) silica gel
(a) Raney Ni (W-7 activity) in EtOH, 78.5°C
(b) silica gel
sulfides
n-pentane
saturates
n-pentane

Figure 12.19 Flow chart illustrating the separation and isolation of sulfoxides in the maltene and the sulfoxides → sulfides → saturates conversions.

of sulfides and sulfoxides to hydrocarbons is an important step in the derivation of the molecular structure of the sulfides and sulfoxides.

Employing the analytical procedure as outlined in Figure 12.19, the sulfoxide components of a number of bitumens and oils have been isolated. The IR spectra of the sulfoxides and of the sulfides prepared by the reduction of the sulfoxides from Athabasca maltene are shown in Figure 12.20. The sulfoxide spectrum features the characteristic, intense absorption band of the sulfoxide group at 1040 cm^{-1} (and some weak absorptions around 1700 and 3300 cm^{-1} which are due to the presence of residual carboxylic acids and their methyl esters). The absorption bands common to both the sulfoxide and sulfide spectra are due to methyl and methylene bending (1380 and 1470 cm^{-1}) and stretching (2970, 2920 and 2860 cm^{-1}) vibrations. The IR spectra of the sulfoxides from various sources show little variance, as can be seen from comparison with the IR spectrum of the sulfoxides in Lloydminster heavy oil, Figure 12.21. These IR spectra were obtained on molecularly distilled materials. If the distillation step in the separation of the sulfoxides (Figure

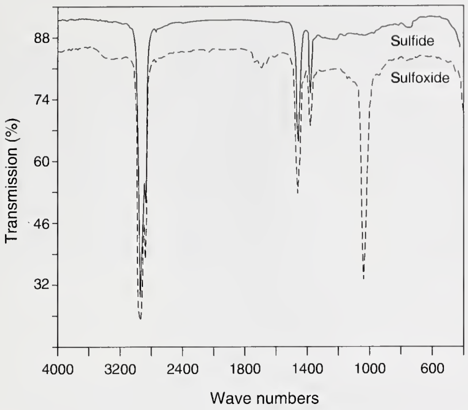

Figure 12.20 IR spectra of the sulfoxides and their corresponding sulfides (obtained by reduction with $LiAlH_4$) from Athabasca maltene. From J.D. Payzant *et al.*, Ref. 3. © 1983, Elsevier Science Ltd.

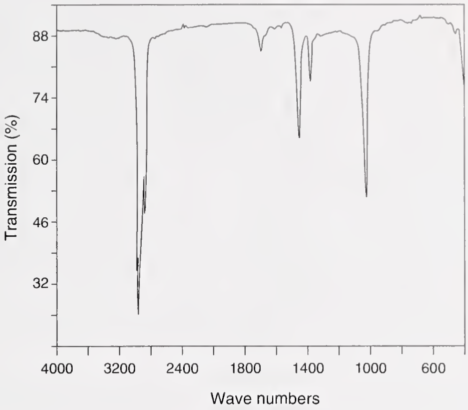

Figure 12.21 IR spectrum of the sulfoxides from Lloydminster heavy oil.

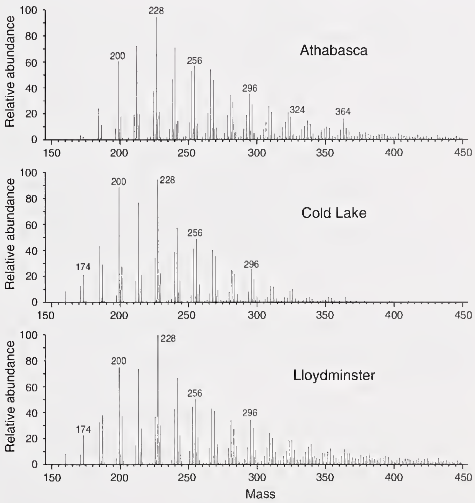

Figure 12.22 Field ionization mass spectra of the distillable (230°C, 10^{-3} Torr) sulfoxide fractions of Athabasca and Cold Lake bitumens and Lloydminster heavy oil.

12.19) is omitted then the spectrum shows the presence of more (acid, ester, aromatic) contaminants. The volatile portion of the sulfoxides comprises about one-third of the weight of the whole crude sulfoxide fraction and the FI spectra of these distillable sulfoxides from the Athabasca and Cold Lake bitumens and Lloydminster heavy oils, Figure 12.22, are nearly identical: in each case the most intense peak is at m/z = 228, followed by m/z = 200 and beyond m/z = 228 the intensities exhibit a gradual, monotonic decline. The exact values of the MWs measured for some of the component molecules are tabulated in Table 12.8 and the elemental compositions of the volatile sulfoxides along with those of the corresponding sulfides resulting from the reduction of the sulfoxides with $LiAlH_4$/THF are given in Table 12.9. (The average empirical formulas that can be estimated from the data are $C_{18}H_{34}SO$ for the sulfoxides and $C_{16}H_{26}S$ for the sulfides, corresponding to an average bicyclic structure for the sulfoxides and a tetracyclic one for the sulfides.)

For a few crude oils the results of the gravimetric measurements of the distillable sulfoxide fraction are compiled in Table 12.10. All of the few oils examined were found to contain small quantities of sulfoxides, ranging from 0.02 to 0.9% of the bitumen. Of course, each of these oils also contained alicyclic sulfides, and in considerably higher quantities than sulfoxides. The sulfoxide content (as well as that of the sulfides) shows a broad, but not a simple, correlation with depth of the deposit and the highest sulfoxide contents (0.7–0.9%) were obtained in

Table 12.9 Elemental compositions of the volatile sulfoxides and the corresponding sulfides in Athabasca Syncrude high-grade maltene

	Sulfoxide wt%	Sulfide[a] wt%
C	71.97	75.43
H	10.93	10.43
N	0.70	0.25
S	11.67	12.89
O	5.90	0.91
Total	101.17	99.91
$(H/C)_a$	1.82	1.66
$(O/S)_a$	1.01	0.14

[a] Sulfides from $LiAlH_4$/THF reduction of the volatile sulfoxide mixture.

Table 12.10 Distillable sulfoxide contents of some bitumens and oils

Source	Depth (m)	Sulfoxide content,[a] wt%	
		of maltene	of bitumen
Athabasca (McMurray)	5	1.06	0.88
	18	0.88	0.73
	37	0.1	0.08
Cold Lake (Clearwater)	500	0.24	0.20
Lloydminster (Sparky)	670	0.42	0.36
Nordegg (Jurassic)	1,423	0.021	0.017

[a] Distillable sulfoxides after separation of methyl esters of carboxylic acids, *cf.* Figure 12.19.

bitumens nearest to the surface (5–18 m) and the lowest (0.02%), in the most deeply buried deposit. The total sulfoxide contents, which would include the nondistillable sulfoxides, would be higher than the values listed by about a factor of three.

In order to correlate the sulfoxides with the sulfides and to establish their molecular structures, it is necessary, as a first step, to subject them to GC analysis. Since, as mentioned above, sulfoxides are too polar for GC analysis, they are first converted to their sulfides which are less-polar compounds. This can be accomplished by reduction with $LiAlH_4$/*p*-dioxane under reflux condition (101.5°C). The capillary mass chromatogram of the sulfoxide-derived sulfides of Athabasca (Syncrude Beach Sand) maltene is shown in Figure 12.23. The peaks labelled 1–11 are alicyclic sulfides whose mass spectra are shown in Figures 12.24 and 12.25. Peak #1 corresponds to a sulfide with MW 184 and elemental formula $C_{11}H_{20}S$, and therefore it has two naphthenic rings. All the other mass spectra, with the exception of the ones corresponding to peaks 1 and 3, have m/z = 183 as their base peak

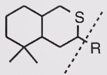

m/z = 183

and compounds 1, 2, 4, 6, 8, 10 and 11 form a homologous series of bicyclic sulfides with a progressively increasing alkyl side chain and elemental formulas

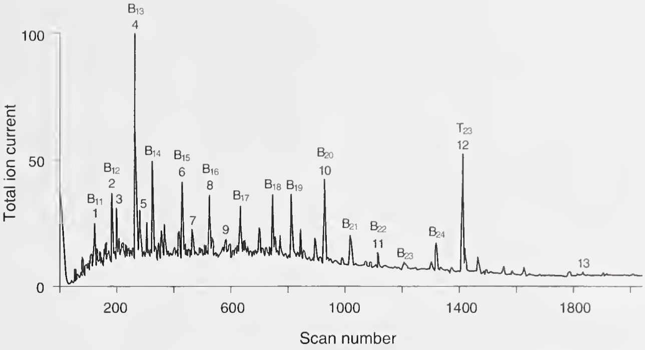

Figure 12.23 Total ion current mass chromatogram of the sulfoxide-derived sulfides in Athabasca (Syncrude Beach Sand) maltene. Peaks labelled B are bicyclic sulfides with carbon numbers as indicated by the subscripts. The peak labelled T_{23} is a C_{23} tetracyclic sulfide.

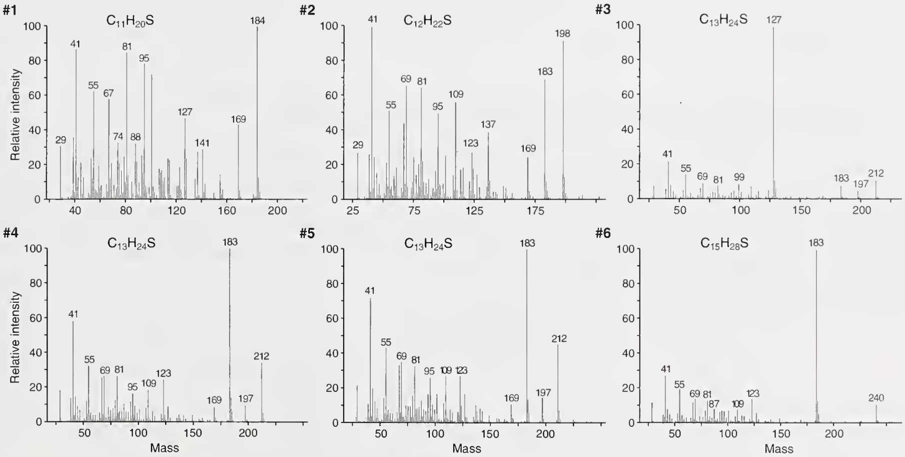

Figure 12.24 EIMS of peaks 1 to 6 of Figure 12.23.

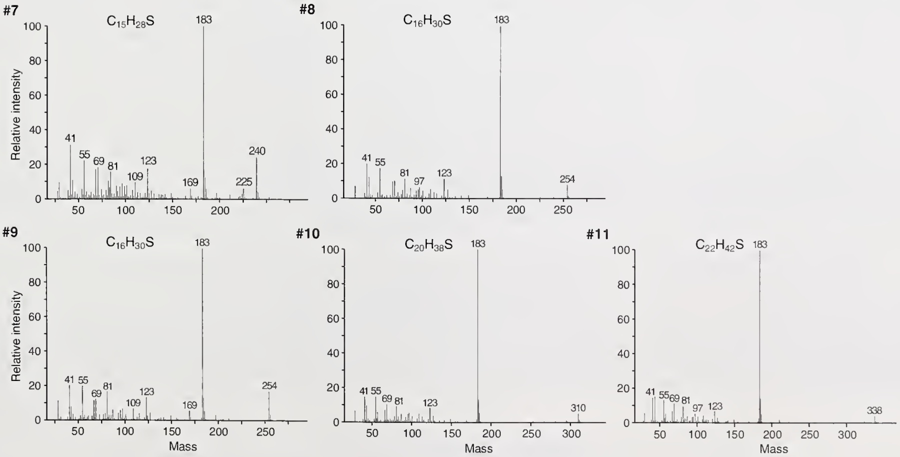

Figure 12.25 EIMS of peaks 7 to 11 of Figure 12.23.

1	$C_{11}H_{20}S$	8	$C_{16}H_{30}S$
2	$C_{12}H_{22}S$	10	$C_{20}H_{38}S$
4	$C_{13}H_{24}S$	11	$C_{22}H_{42}S$, *etc.*
6	$C_{15}H_{28}S$		

Compounds 3, 5, 7 and 9 are isomers of the appropriate members of the main series, that is, 3 and 5 are isomers of 4, 7 is an isomer of 6 and 9 is an isomer of 8. On this basis the peaks labelled "D" in Figure 12.23 are assigned to a homologous series of bicyclic sulfides having carbon numbers as indicated by the subscripts.

A comparison between the capillary mass chromatogram and the GC–MS of the sulfoxide-derived sulfides with those of the sulfides isolated from the aromatic fraction of Athabasca maltene reveals that the two series are identical. This observation is also valid for the higher cyclic sulfides. Therefore, from here on the identification and structural elucidation of the sulfides which originally were present as sulfoxides in the oil and of the sulfides in the oil will be pursued as a single problem.

a) *Bicyclic terpenoid sulfides and sulfoxides*

The cyclic sulfides present in the maltene elute with the aromatic fraction upon class separation of the maltene fractions. The sulfides can then be isolated from the aromatic fraction by first oxidizing them to the sulfoxides using tetra-*n*-butylammonium periodate (TBAPI) in toluene/methanol solvent under reflux, separating the polar fractions on a silica gel column, and then following the procedure outlined in the flow diagram in Figure 12.19. Alternatively, the above procedures can be applied to the whole maltene which then will yield the sum of the sulfides and sulfoxides which were originally present in the maltene. (With regard to the step involving the oxidation of the sulfides, the TBAPI method is superior to the photooxidation method which was used in early studies on the sulfides.) Illustrative *m/z* = 183 cross-scan mass chromatograms of bicyclic sulfides from the whole maltene, representing the combined sulfoxides and sulfides, are shown in Figure 12.26. Now, comparing the separate data from the sulfoxides and the sulfides with the data representing the combined sulfoxides + sulfides, we observe a striking similarity which reveals that the sulfoxides are the oxidized derivatives of the same sulfides which constitute the sulfide fraction of the maltene.

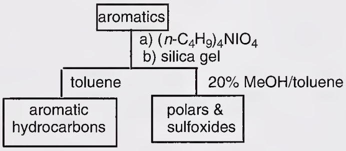

Each peak labelled "B" in Figure 12.23 and all the numbered peaks in the cross-scan mass chromatograms in Figure 12.26 represent a bicyclic sulfide molecule with an alkyl side chain ranging from C_1 in the C_{12} sulfide to C_{16} in the C_{27} sulfide. The minima appearing in the concentration distribution at the C–12, –17 and –23 positions suggest isoprenoid branching in the side chain,

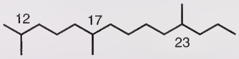

since, to obtain the C_{12}, C_{17} or C_{23} members from the higher homologs, two carbon-carbon bonds have to be broken, an event less likely than the cleavage of a single carbon-carbon bond.

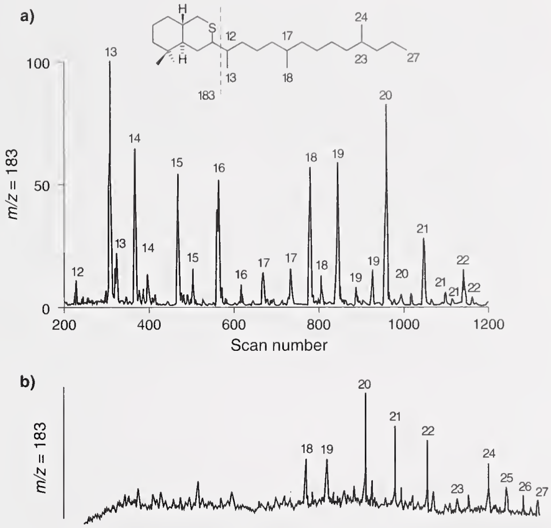

Figure 12.26 *M/z* = 183 cross-scan mass chromatograms of the bicyclic sulfides in Athabasca maltene. The numbers above the peaks refer to the number of carbon atoms in the molecule. a) Sulfoxide-derived sulfides from Syncrude Beach Sand maltene. From O.P. Strausz *et al.*, Ref. 6. © 1990, American Chemical Society. b) Sulfides from Syncrude Fluvial maltene, showing the extended members of the series. From J.D. Payzant *et al.*, Ref. 9. © 1986, Elsevier Science Ltd.

This isoprenoid branching assignment, based on intensity variation, is also supported by the alterations in retention times on the GC column. If the chains were linear, the spacing between successive members of the homologous (or rather, pseudo-homologous) series—represented by the addition of another CH_2 group—would be nearly uniform (in reality, gradually declining with increasing chain length), indicating a nearly constant difference in the time of elution. The major peaks from C_{14} to C_{18} are, in effect, approximately equally spaced since the side chain is *normal* over this range. However, the spacing between the main C_{13} and C_{14} members, the C_{18} and C_{19} members and the C_{24} and C_{25} members, is less than it is for the average incremental increases in the side chain from C_{14} to C_{18}. This is in accord with the expected behavior of a molecule with the above branching pattern since *iso*alkanes elute from a GC column before *n*-alkanes of the same carbon number. The small spacing between the main C_{13} and C_{14} members suggests a branch point at C–12, and those between the main C_{18} and C_{19} and C_{24} and C_{25} members suggest branch points at C–17 and C–23. This represents a head-to-tail connection between the C–11 to C–15 and C–16 to C–20 isoprene units and a tail-to-tail connection between the C–16 to C–20 and C–21 to C–25 isoprene units:

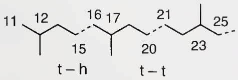

More structural information on the bicyclic sulfides came from the hydrocarbons produced by their Raney nickel reduction. Thus, for example, on reduction the B_{13} sulfide yielded *trans*-2-butyl-1,3,3-trimethylcyclohexane

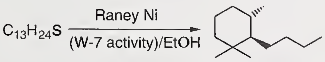

Combining this information with the mass spectrometric fragmentation pattern of the bicyclic sulfide series which features the intense *m/z* = 183 base peak for each member, two structures are possible:

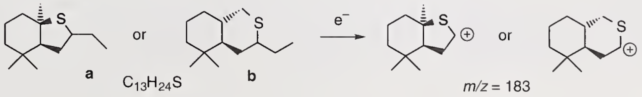

Distinction between the two structures was made possible on the basis of NMR spectroscopic data. Using preparative scale chromatography and a C_8-bonded silica gel column it was possible to obtain a sample of the main $C_{13}H_{24}S$ isomer from Lloydminster heavy oil in 55–60% purity. The 400-MHz ^1H NMR spectrum of this material,[10] Figure 12.27, reveals the presence of only three methyl groups in the molecule, two singlets due to the geminal methyls and one triplet due to the chain-end methyl. This result clearly settles the question in favor of a six-membered ring structure:

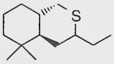

Additional confirmation of a six-membered ring structure came from deuterium exchange experiments on the oxidized (HOAc/30% H_2O_2, 25°C, 16 h) C_{13} sulfide, the sulfone

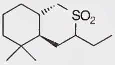

the ^1H NMR spectrum of which is shown in Figure 12.28. The signals arising from the resonances of the hydrogen atoms on the carbons adjacent to the sulfur (H_2, H_3, H_4) are significantly shifted, while the rest of the signals remain much the same as before. The acidic protons on the carbon atoms adjacent to the sulfur in the sulfones may be exchanged for deuterium (*n*-BuLi/CD_3SOCD_3, 25°C, 16 h, D_2O quench) which permits the determination of the number of hydrogen atoms on carbons α to the sulfur by mass spectrometry. This is illustrated by the mass spectra of the undeuterated and deuterated sulfones, Figure 12.29, which show that indeed three deuterium atoms were incorporated into the molecule, as expected on the basis of the structure derived from the NMR spectrum of the sulfide. Thus, the sulfonation/deuteration experiment confirms structure **b** above. In addition, the mass and NMR spectra of synthetically prepared compound **a** are quite different from those of the natural material in the oil, and the mass spectrum features an m/z = 197 base peak rather than the m/z = 183 observed for the natural material.

The structure established above applies to the main series of bicyclic sulfides from C_{11} to about C_{27}:

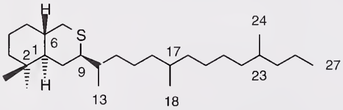

1α(H),6β(H)-2,2-dimethyl-9-alkylbicyclo-[4,4,0]-8-thiadecane

The stereochemistry of the side chain has not been established but was tentatively assigned the 9β geometry. Each member of the main series has one or more other, minor isomers which elute from the GC column after the main series member. The terpenoid nature of the molecule is readily recognized:

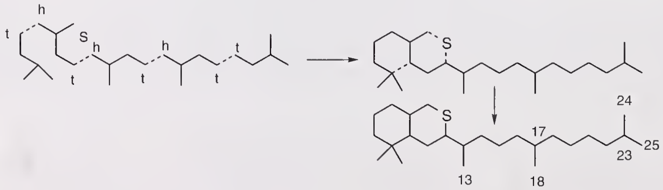

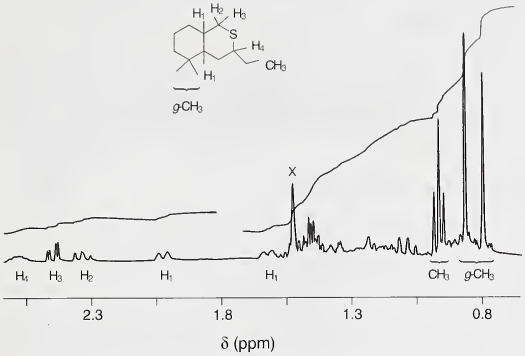

Figure 12.27 400-MHz ^{1}H NMR spectrum of the $C_{13}H_{24}S$ bicyclic sulfide from Lloydminster heavy oil. X denotes some extraneous products. From J.D. Payzant *et al.*, Ref. 10. © 1988, Harwood Academic Publishers.

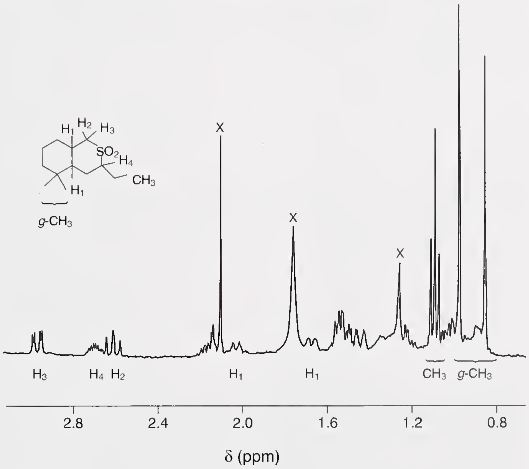

Figure 12.28 400-MHz ^{1}H NMR spectrum of the $C_{13}H_{24}SO_2$ bicyclic sulfone. X denotes some extraneous products. From J.D. Payzant *et al.*, Ref. 10. © 1988, Harwood Academic Publishers.

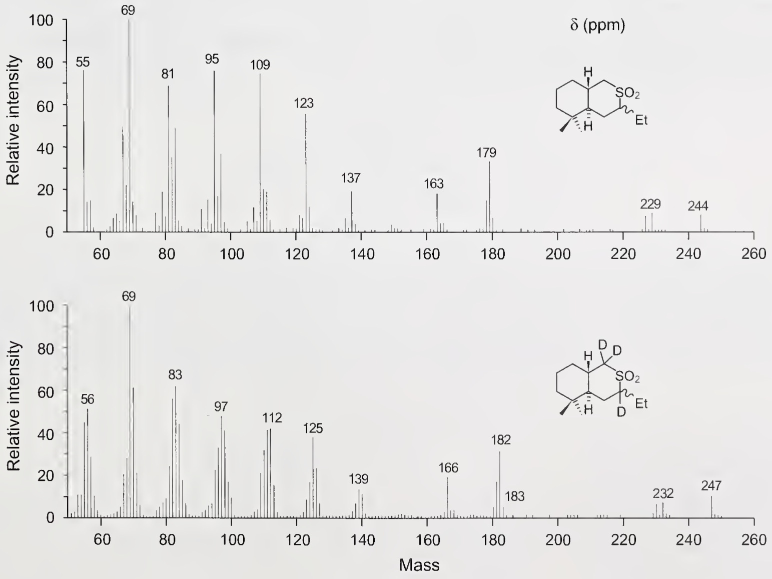

Figure 12.29 Mass spectra of the $C_{13}H_{24}SO_2$ bicyclic sulfone (upper panel) and its corresponding deuterated sulfone (lower panel), showing the incorporation of three deuterium atoms. From J.D. Payzant *et al.*, Ref. 10. © 1988, Harwood Academic Publishers.

The first four isoprene units are joined together in a head-to-tail configuration and the fifth is attached to the side chain in a tail-to-tail configuration.

These bicyclic terpenoid sulfides were later found to be ubiquitous components of all sulfur-containing crude oils and they constitute the most abundant terpenoid sulfide series therein. After the bicyclics, the next most abundant terpenoid sulfide series is the tetracyclics.

b) Tetracyclic terpenoid sulfides and sulfoxides

The most abundant member of this series of sulfides in the maltene, Figure 12.30, is the C_{23} compound, with a MW of 348 and base peak of *m/z* = 319 in the mass spectrum. This leads to an elemental formula $C_{23}H_{40}S$, corresponding to a tetracyclic sulfide with an ethyl side chain. The carbon range of the series extends from C_{21} to C_{40} or possibly to C_{41}, Figure 12.31, and the concentration distribution suggests methyl branching in the side chain at C–22, C–27, C–32 and C–37:

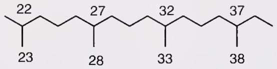

The variations in retention times, as with the bicyclic sulfides, support this assignment.

Raney nickel reduction yields the same series of tricyclic terpanes, for example,

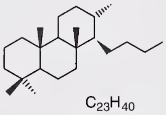
, etc.

$C_{23}H_{40}$

as was isolated from the saturate fraction of the maltene, with the C_{23} member as the major component. This observation, in conjunction with the *m/z* = 319 base peak in the mass spectrometric fragmentation of the sulfides, requires the bridgehead position for the sulfur to be analogous to that in the bicyclic sulfides:

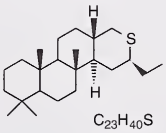

$C_{23}H_{40}S$

If this structure is correct, then on oxidation to sulfone and deuterium exchange, three deuterium atoms should be incorporated into the molecule. Indeed, the mass spectra of the sulfone and deuterated sulfone shown in Figure 12.32 confirm the above structure. The MW of the C_{23} sulfone on deuteration increased from 380 to 383, but the masses of the fragmentations

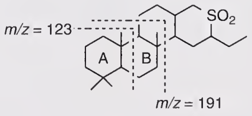

did not change, and therefore none of the three deuterium atoms resides on the A or B rings. Therefore, the series formula corresponds to the all head-to-tail structure

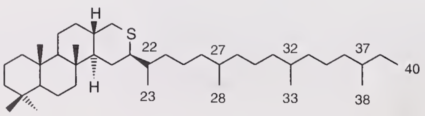

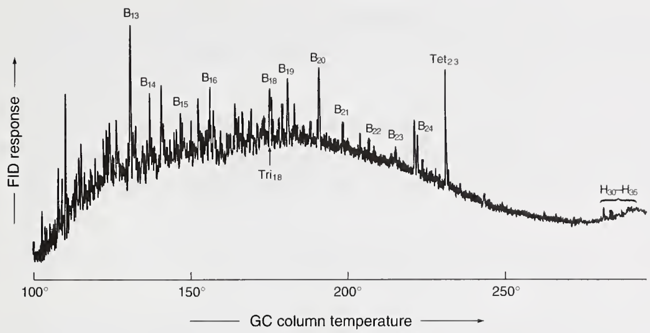

Figure 12.30 Capillary gas chromatogram of the sulfides isolated from the whole maltene fraction of Athabasca (Syncrude) bitumen. Peaks labelled B_n correspond to bicyclic terpenoid hydrocarbons with n carbon atoms. The tricyclic terpenoid C_{18} sulfide (Tri_{18}) is not resolved from the D_{18} sulfide. The tetracyclic C_{23} and hexacyclic (hopanoid) sulfides, H, are also labelled. From J.D. Payzant *et al.*, Ref. 9. © 1986, Elsevier Science Ltd.

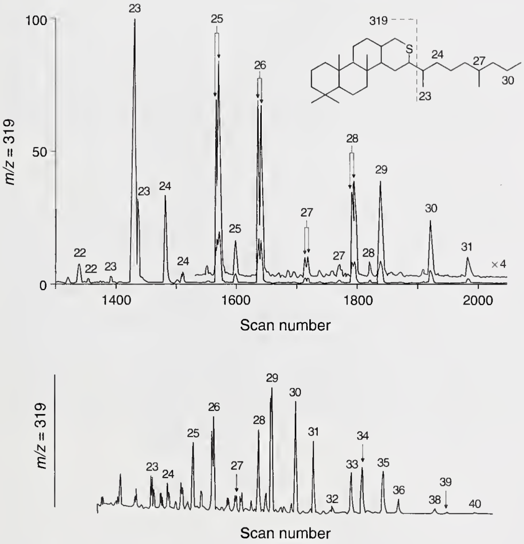

Figure 12.31 M/z = 319 cross-scan mass chromatograms of the tetracyclic sulfides produced from the reduction of the sulfoxides in Athabasca (Syncrude Beach Sand) maltene (top) and the tetracyclic sulfides in Cold Lake (Wolf Lake) maltene (bottom).

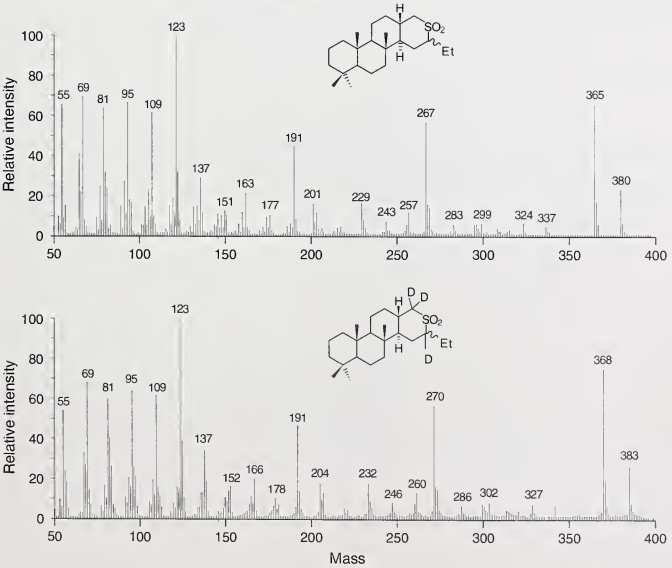

Figure 12.32 Mass spectra of the $C_{23}H_{40}SO_2$ tetracyclic sulfone (upper panel) and its corresponding deuterated sulfone (lower panel), showing the incorporation of three deuterium atoms. From J.D. Payzant *et al.*, Ref. 10. © 1988, Harwood Academic Publishers.

The diastereomers around the C–22 asymmetric carbon in the C_{25}–C_{28} members of the main series are partially resolved in the m/z = 319 cross-scan mass chromatogram, Figure 12.31, lending additional support to the above structure.

As will be noted here, in the case of the tricyclic terpenoid hydrocarbons the series ends at C_{30}, whereas in the case of the tetracyclic sulfides the series extends to C_{40} and possibly to C_{41}. The difference appears to suggest a stabilizing effect of the sulfur moiety in the molecule against cleavage of the side chain.

c) Tricyclic terpenoid sulfides and sulfoxides

This class of sulfides normally represents a less important constituent of the sulfides than either the bicyclic or tetracyclic sulfides. However, in the sulfoxides the relative order of concentration may change to bi > tri > tetra > penta. The carbon number distribution of the tricyclic sulfide series, Figure 12.33, covers the C_{17}–C_{31} range and again, as with the bi- and tetracyclic series, the presence of a number of minor isomers is in evidence. The concentration distribution and retention time spacing of the members in the main series both suggest methyl branchings at the C–17, C–23 and C–28 positions

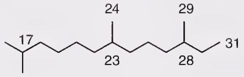

and the maximum in the concentration at m/z = 280 corresponds to a $C_{18}H_{32}S$ tricyclic sulfide. Figure 12.34 shows the mass spectrum of the C_{18} member. The intense m/z = 251 peak becomes a base peak for the higher members of the series, corresponding to the loss of the alkyl side chain. Raney nickel reduction of the sulfide yielded a homologous series of alkylated 8β(H)-drimanes, the bicyclic alkanes detected in the saturate fraction of the maltene, the most abundant member of which was the C_{18} homolog:

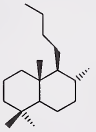

$C_{18}H_{34}$

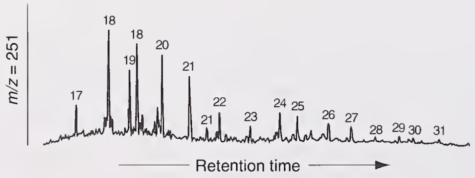

Figure 12.33 *M/z* = 251 cross-scan mass chromatograms of the tricyclic sulfides in Athabasca (Syncrude, Trench) maltene. The numbers above the peaks correspond to the total number of carbon atoms in the molecule. From J.D. Payzant *et al.*, Ref. 9. © 1986, Elsevier Science Ltd.

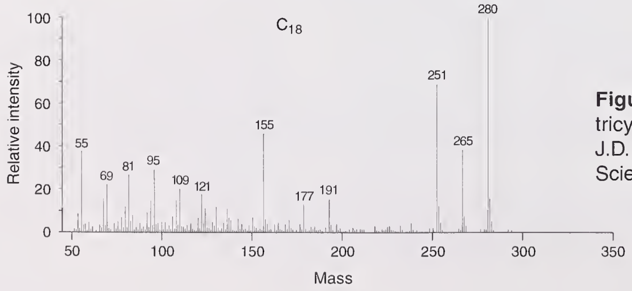

Figure 12.34 Mass spectrum of the C_{18} tricyclic sulfide in Athabasca maltene. From J.D. Payzant *et al.*, Ref. 9. © 1986, Elsevier Science Ltd.

Since, in the mass spectrometer, electron impact causes the loss of an ethyl group, the sulfur must be attached to the third carbon from the end of the chain

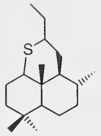

and this gives rise to two possible tricyclic systems:

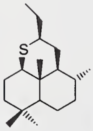

or

a

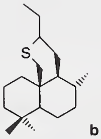

b

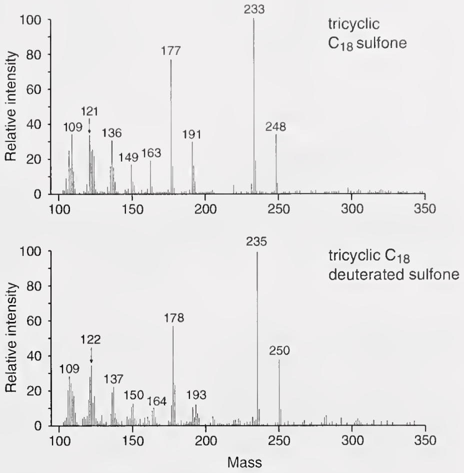

Figure 12.35 Mass spectra of the tricyclic C_{18} sulfone and deuterated sulfone. EIMS does not yield molecular ions, nevertheless it indicates that two deuterium atoms have been incorporated. Chemical ionization involving NH_4Cl^-, however, does yield intense $(M + 18)^+ = 330$ and 332 ions, unequivocally showing the incorporation of two deuterium ions.

Support for the tricyclic **a** structure comes from the mass spectra of the C_{18} sulfone and the deuterated C_{18} sulfone, Figure 12.35, showing the incorporation of two deuterium atoms in the molecule as required by structure **a**. Structure **b** should have incorporated three deuterium atoms. Thus, the structure of the main tricyclic terpenoid sulfide series is

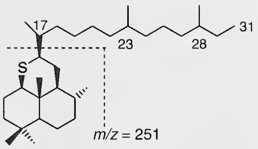

Pairs of diastereomers appear in the GC mass chromatograms of the C_{20}–C_{25} members of the main isomeric series because of the C–17 carbon becoming asymmetric at $\geq C_{20}$, in line with the proposed structure.

d) Hexacyclic terpenoid sulfides and sulfoxides

At the far end of the gas chromatogram in Figure 12.30, a cluster of small peaks is discernible. The molecular ion cross-scan mass chromatograms of these materials, Figure 12.36, revealed that they are C_{30}–C_{35} hexacyclic sulfides—undoubtedly related to the hopanoid hydrocarbons present in the saturates. As is apparent from the mass chromatograms of each carbon number, one major and several minor isomers are present. The mass spectra of the sulfides, sulfones and deuterated sulfones of the major C_{30} member are shown in Figure 12.37 where it is seen that these are hexacyclic compounds and that, in the case of the sulfides, the most intense peak after the molecular ion is the $m/z = 191$ peak; in the case of the sulfones the base peak is the $m/z = 191$ peak, as in the case of the hopanoid hydrocarbons. On deuteration three deuterium atoms were incorporated into the C_{30} molecule and two in the higher-MW members of the series.

On Raney nickel reduction a series of hopanes could be detected among the hydrocarbon products. These hopanes had a distribution pattern different from that of the hopanes in the

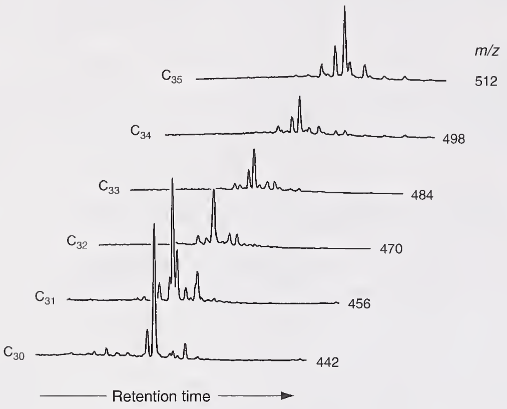

Figure 12.36 Molecular ion mass chromatograms of the hopane sulfides in Athabasca maltene. From T.D. Cyr *et al.*, Ref. 5. © 1986, Elsevier Science Ltd.

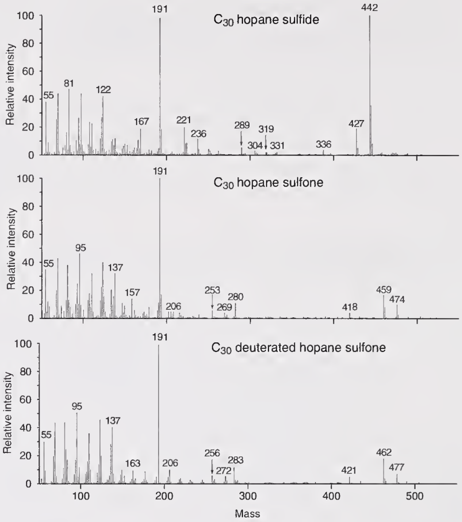

Figure 12.37 Mass spectra of the most abundant C_{30} hopane sulfide, sulfone and deuterated sulfone showing two hydrogen atoms attached to the carbon atoms adjacent to the sulfur. From T.D. Cyr *et al.*, Ref. 5. © 1986, Elsevier Science Ltd.

saturate fraction of the maltene: the hopanes derived from the sulfides extend from C_{30} to C_{35} and display a 22R/22S ratio of about two, whereas the hopanes from the saturate fraction extend from C_{27} to C_{35} and typically have a 22R/22S ratio of about 0.7, which is close to the thermal equilibrium value for these epimers. Therefore, it appears that the cyclic structure slows considerably the rate of the 22R → 22S isomerization.

Interpretation of the above information requires that the sulfur be attached to C_{30} in the hopane (in hopanes the ring carbons are numbered first, followed by the ring-attached carbons):

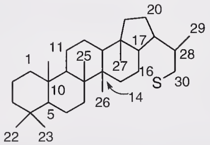

Molecular models show that the second valence of sulfur may be attached without much strain to either carbon 16, 17 or 20 but attachment to carbon 17 does not satisfy the deuterium exchange experiments. Attachment at either carbon 16 or 20,

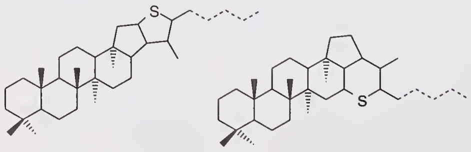

however, is in accord with the deuteration results and both structures are relatively strain free. Consequently, the available data do not discriminate against one or the other structure and, in effect, both may be present. Indeed, the mass chromatograms in Figure 12.36 indicate in each case the presence of one major, one minor and some trace isomers.

These hopanoid sulfides represent the least abundant family of cyclic terpenoid sulfides in bitumen and crude oil, and their presence cannot always be detected where the other families are clearly present.

e) Monocyclic sulfides and sulfoxides

Monocyclic terpenoid sulfides have not been detected in Alberta bitumen. Monocyclic *n*-alkyl-substituted thianes and thiolanes,

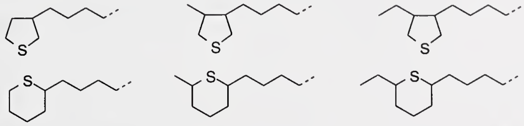

, *etc.*,

however, do occur in all nonbiodegraded or incompletely degraded sulfur-containing petroleums along with the cyclic terpenoid sulfides discussed above. The *n*-alkyl chains render the *n*-alkyl thianes and thiolanes susceptible to microbial attack resulting in their destruction,[11] while the terpenoid-type sulfides are evidently resistant against such attacks and survive the microbial degradation of the oil. The two types of sulfides, namely the *n*-alkyl thianes and thiolanes on the one hand, and the terpenoid sulfides on the other, can be separated from one another by adduction chromatography using thiourea. This is illustrated with the example[12] of Bellshill Lake petroleum sulfides in Figure 12.38. The upper panel shows the gas chromatogram of the whole sulfide fraction isolated as described above. The middle panel shows the gas chromatogram of the thiourea adduct and the lower panel, that of the thiourea nonadduct fractions. The latter is quite similar to those obtained from bitumen and heavy oil maltenes; the sharp peaks overlying the continuum are due to the cyclic terpenoid and steroid sulfides.

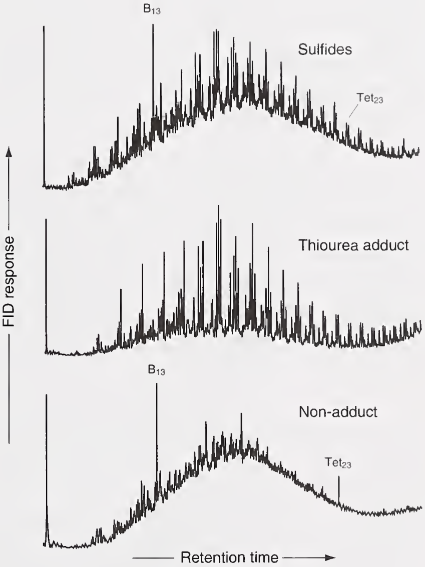

Figure 12.38 Gas chromatograms of the sulfides in Bellshill Lake petroleum. Upper panel: total sulfides. Middle panel: thiourea adduct of the sulfides. Lower panel: thiourea non-adduct of the sulfides. B_{13} and Tet_{23} correspond to the bicyclic C_{13} sulfide and the tetracyclic C_{23} sulfide. From J.D. Payzant *et al.*, Ref. 12. © 1989, Elsevier Science Ltd.

The Wabasca bitumen contains thiolanes and thianes derived from aliphatic isoprenoids as manifested by the appearance of phytane, pristane and C_{15}–C_{18} isoprenoids in the hydrocarbons produced from their Raney nickel reduction.[13] Some Wabasca sulfide-derived hydrocarbons also contain *n*-alkanes,[14] indicating the presence of *n*-alkyl thiolanes and thianes, and suggesting that the bitumens were not completely biodegraded. Athabasca sulfides, when reduced with low-efficiency Raney nickel, yield a series of *n*-alkanes apparently from the selective hydrodesulfurization of the small amounts of n-alkyl thiolanes and thianes present. When the reduction is done with W–7 activity Raney nickel, however, the terpenoid hydrocarbons produced swamp the trace amounts of *n*-alkanes and thus the latter would escape detection.

The saturate fraction of the Bellshill Lake maltene bears a close resemblance to the hydrocarbons produced by the Raney nickel hydrodesulfurization of the total sulfide fraction,

Figure 12.39. Both are dominated by *n*-alkanes forming a smooth series up to at least C_{34} with a maximum at C_{16} and in the latter case with a slight preference for the even carbon number members at C_{16} and above C_{23}. The small peaks eluting between the *n*-alkane peaks are mainly due to acyclic isoprenoids (*e.g.* pristane and phytane), cyclic terpenoid as well as steroid biomarkers, and they again bear close resemblance in the two samples, except for their relative proportions. For example, the values of the pristane-to-phytane ratio are different, 1.2 and 0.4 in the saturate fraction of the maltene and the sulfide-derived hydrocarbons. The significance of this will be examined in Chapters 13 and 14.

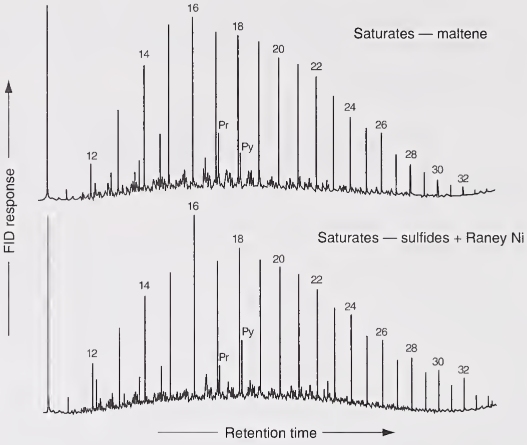

Figure 12.39 Gas chromatograms of alkanes derived from Bellshill Lake petroleum. Upper panel: alkanes separated from the maltene fraction. Lower panel: alkane products of the Raney nickel reduction of the sulfides. From J.D. Payzant *et al.,* Ref. 12. © 1989, Elsevier Science Ltd.

Cross-scan mass chromatograms for the Bellshill Lake sulfides are shown in Figure 12.40. In the Bellshill Lake oil, thiolanes are present in a slightly higher concentration than the thianes, but in other oils, the thiolanes are usually much more prevalent. A common important characteristic of these cyclic sulfides is the specificity of their alkyl substitution. As seen from their structure, the alkyl group is always present on the carbon α to the sulfur.

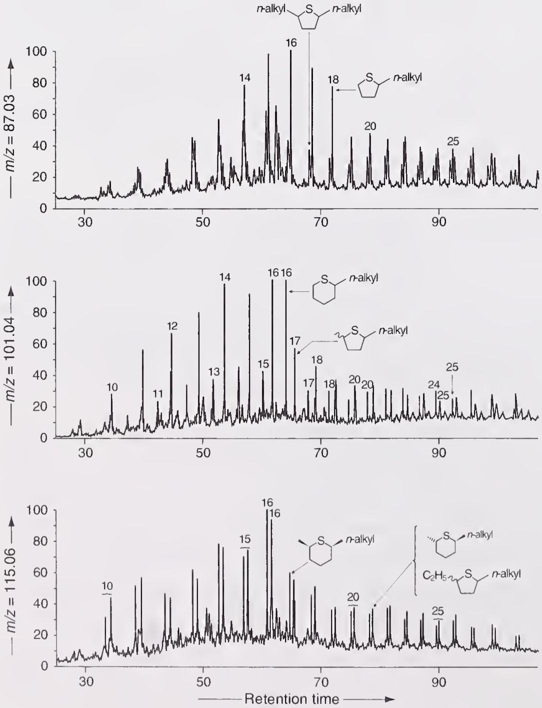

Figure 12.40 *M/z* = 87, 101 and 115 cross-scan chromatograms of the sulfides from Bellshill Lake petroleum. The mass fragmentograms for *m/z* = 87.03 (upper panel) represent 2-*n*-alkylthiolanes and 2,5-di-*n*-alkylthiolanes; *m/z* = 101.04 (middle panel), 2-*n*-alkylthianes and 2-methyl-5-*n*-alkylthiolanes; and *m/z* = 115.06 (lower panel), 2-methyl-6-*n*-alkylthianes and 2-ethyl-5-*n*-alkylthiolanes. Each fragmentogram is normalized to the most abundant peak. The relative intensities of the *m/z* = 87, 101 and 115 fragmentograms are 0.58 to 1.0 and 0.52, respectively. The structures of the various sulfides are as indicated and the numbers above the peaks correspond to the total number of carbon atoms in the molecule except for the 2,5 di-*n*-alkylthiolanes (upper panel) which have one fewer carbon atom than the 2-*n*-alkylthiolanes from which they are incompletely resolved. From J.D. Payzant *et al.,* Ref. 12. © 1989, Elsevier Science Ltd.

As was noted above, only trace amounts of *n*-alkyl thiolanes and thianes are present in biodegraded oils and bitumens, and only small concentrations are present in incompletely degraded oils like some Wabasca bitumen samples. On the other hand, they appear to be always present in sulfur-containing nonbiodegraded oils. In contrast, the terpenoid sulfides are always present in sulfur-containing oils regardless of their microbial history.

More consideration will be given to *n*-alkyl thiolanes and thianes in petroleum in Chapters 13 and 14.

f) Pentacyclic terpenoid sulfides and sulfoxides

Both the sulfide and sulfoxide classes of compounds in Alberta bitumens contain pentacyclic terpenoids which have been detected directly by FIMS and by the appearance of various steranes in their reduced hydrocarbon mixture. The FIMS data indicate that the concentration maximum occurs around C_{30} in both the sulfides and sulfoxides. Most of these pentacyclic compounds are probably derived from steranes and are related to the sterane-type sulfides which have been detected in other oils.[15] One sterane-derived sulfide, the structure of which has been elucidated, is lanostane sulfide

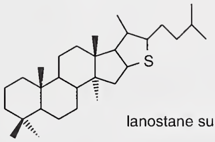

lanostane sulfide $C_{30}H_{52}S$

isolated from an immature Chinese crude oil. The sterane sulfides in Athabasca bitumen presumably have analogous structures.

g) Terpenoid sulfides and sulfoxides complexed to asphaltene

Oil sand asphaltenes precipitated from a methylene chloride or toluene solution of bitumen with *n*-pentane, contain up to 21–22% weight percent low-to-medium MW, by and large pentane-soluble polar material complexed to asphaltene, which can be separated from the asphaltene by extraction with a polar solvent such as acetone. The acetone extract can then be further fractionated into subfractions of increasing polarity, as will be described later in Section 2.2.1 d) of this chapter. The most polar of these subfractions displayed an intense absorption at 1040 cm^{-1}, characteristic of sulfoxides, and, after methylation and chromatographic fractionation to remove the acids present, the isolated sulfoxides were reduced to the sulfides, affording the gas chromatogram[16] reproduced in Figure 12.41. These are the same terpenoid cyclic sulfides which have been isolated from the aromatic fraction and from the whole maltene. GC–MS showed that the concentration distributions in the complexed hexacyclic sulfides are, however, different, ranging from C_{27} to C_{35} with C_{30} (two isomers) > C_{31} (two isomers) > C_{29} (one isomer) >> $C_{28} \sim C_{27}$. In the sulfides isolated from the maltene, only the C_{30}–C_{35} members were detected. This result again illustrates the variance in the distribution of a given biomarker depending on the fraction analyzed.

h) Conclusion

Four series of cyclic terpenoid sulfides and their sulfoxide analogues, namely bi-, tri-, tetra- and hexacyclic series:

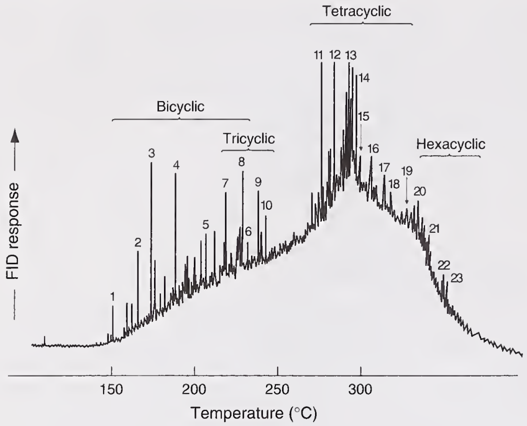

Figure 12.41 Gas chromatogram of the reduced sulfoxides complexed to Athabasca asphaltene. Peaks 1–6, bicyclic, 7–10, tricyclic, 11–19, tetracyclic, 20–23, hexacyclic sulfides. From Z. Frakman *et al.*, Ref. 16. © 1990, American Chemical Society.

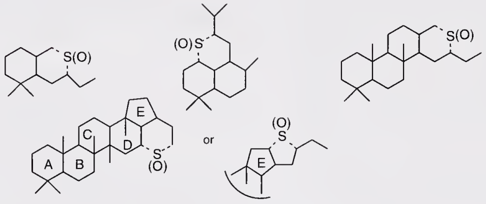

have been detected in Alberta bitumens and their molecular structure established. They are all derived from cyclic, terpenoid hydrocarbon biomarkers by the incorporation of a sulfur atom in a bridgehead position, attached on one side to the second carbon in the side chain and to a carbon in the hydrocarbon ring or to a ring-attached methyl carbon on the other side to form a six-membered (or, in the case of the hexacyclic series, perhaps a five-membered) sulfide ring. Pentacyclic sulfides, most of them derived from steranes, are also present along with trace to small quantities of *n*-alkyl-substituted thiolanes and thianes, and also thiolanes and thianes derived from acyclic isoprenoids such as phytane, pristane and others.

The combined amount of thiolanes and thianes characterized is small compared to the total amount of cyclic terpenoid sulfides and the ratio of the areas under the GC-resolved peaks and under the unresolved hump is about the same as that of the peaks representing the cyclic terpenoid biomarkers and the underlying continuum in the saturate fraction of the bitumen. Undoubtedly, the rest of the cyclic sulfides can be related to the steroid, acyclic and cyclic terpenoid-type hydrocarbons forming the unresolved continuum in the saturate fraction of the bitumen since the identified sulfides are related to the terpenoid biomarkers in the saturates.

The sulfoxides are genetically related to the sulfides and in all probability were formed by the slow, *in-situ* oxidation of the latter. Their concentration is always small relative to the sulfides and tends to decrease with burial depth of the deposit; it can be taken as a cumulative measure of the redox conditions in the deposit. The cyclic terpenoid sulfides, ranging from about 4 to 16% of Alberta bitumen maltenes, Table 12.11, are regular constituents of not only bitumens but all sulfur-containing petroleums. Their quantities and concentration distributions can give information about the thermal, microbiological, water washing and redox history of the oil (see Chapter 13). Unlike the *n*-alkyl-substituted thiolanes and thianes, the cyclic terpenoid sulfides are resistant to microbiological attack and would survive the secondary microbiological degradation of the oil which removes the *n*-alkyl-substituted thiolanes and thianes.

Table 12.11 Sulfide and thiophene contents of various petroleums

Sample	Depth (m)	Wt% of maltene		S/Th
		Sulfides (S)	Thiophenes(Th)	
Athabasca	0	6.9	6.4	1.1
Athabasca Suncor coker feed	0	3.8	4.4	0.86
Peace River	500	4.3	11.8	0.36
Cold Lake	~500	4.6	6.1	0.75
Wolf Lake	~500	3.6	2.9	1.2
Peace River	558	16	7.6	2.1
Lloydminster	670	2.6	5.7	0.47
Lloydminster	~700	3.9	6.7	0.46
Bellshill Lake	920	3.1[a]	5.5	0.56
Pembina	1,080	0.2[a]	0.9	0.22
Leduc	1,580	0.3[a]	1.1	0.27

[a] In these samples the sulfides are mainly *n*-alkyl-substituted thianes and thiolanes with some cyclic terpenoid sulfides; in contrast, in the rest of the samples the latter are the only components.

Sulfides may contain additional functional groups having considerable polarity (*e.g.* carboxylic, carbonyl, alcoholic OH, nitrogen functionalities), in which case they would not be measured using the method applied here. Also, they may be complexed to asphaltene, or covalently attached to large molecules in the polar and asphaltene fractions of the bitumen, and again they would not be measured. Consequently, the total concentration of sulfides present in the bitumen is considerably higher than the values reported above.

2.1.2 Thiophenes

The average concentration of sulfides in Athabasca maltene is about 7% which, with a 13% sulfur content, represents about 1% sulfur in the maltene, whereas the sulfur content of the maltene is about 4%. Even if a 25% allowance is made for complex sulfides, still two-thirds of the sulfur is present primarily as alkylbenzo- and higher condensed thiophenes; thiophenes without one or more condensed aromatic rings are apparently absent. On class separation of the maltene, most of the thiophenic compounds are found in the aromatic fraction. The sulfur content of the polars is higher than that of the aromatics but in the polars the sulfur is mainly present as structural units of N, O or N,O-containing high-MW sulfur compounds.

The distribution of thiophenic compounds present in the aromatic fractions of Athabasca and Cold Lake bitumens and Lloydminster heavy oil as determined by FIMS was plotted in Figure 11.38 where it was seen that the most abundant series was the alkylbenzothiophene series followed by the alkyldibenzothiophene series, and alkylbenzothiophene series with one and with two condensed naphthenic rings. The carbon range for these compounds extends from the number of ring carbons to 23–29 carbons with maximum concentrations around C_{14}–C_{18}.

Like the sulfides, the thiophenic compounds can be separated as a compound class from the maltene or the aromatic fraction of the maltene by a procedure similar to that applied for the separation of the sulfides. Thiophenes are mildly polar molecules with small dipole moments, the sulfur being at the negative end of the dipole:

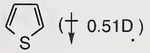

They can be converted to their sulfones by oxidation, *e.g.*,

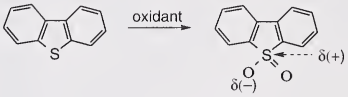

using different oxidants, the recommended one being *m*-chloroperbenzoic acid (MCPBA) according to the scheme shown in Figure 12.42. The separated sulfones then can be reduced with $LiAlH_4$ back to thiophenes.

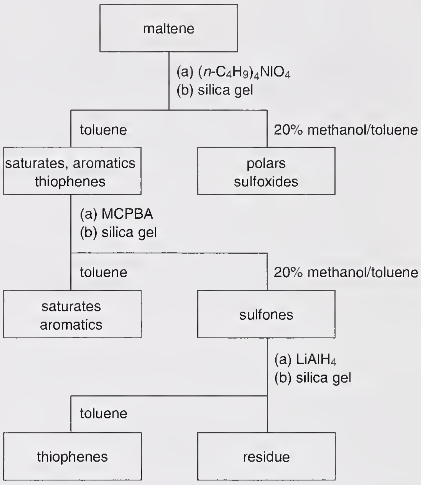

Figure 12.42 Separation scheme for the thiophenes in the maltene.

Following the above procedure, for which restrictions similar to the method employed for the determination of the sulfide content apply, the total thiophenic contents of a number of maltenes have been determined and the data, along with the sulfide contents of the maltenes, are given in Table 12.11. In the case of conventional oils, the content of thiophenic compounds is always higher than that of the sulfides, but in the case of the bitumen, the ratios vary between 0.5 and 2. The ratios are apparently sensitive to alterations caused by biodegradation as well as by lithostratigraphic conditions and can be significantly affected even when the samples are from the same borehole but from somewhat different depths, as in the case of Peace River samples in Table 12.11. It should also be kept in mind that the composition of the sulfides may also change and the relative proportions of the two different structural classes of molecules, the *n*-alkyl substituted thiolanes and thianes on the one hand, and the cyclic terpenoid sulfides on the other, may fluctuate. The bitumen sulfides are essentially free of *n*-alkyl substituted thiolanes and thianes whereas the nonbiodegraded crude oil sulfides always consist of both types of sulfides in varying proportions. Not only the structures of these sulfides but also their origins and biotic source materials are different.

Gas chromatograms of thiophenic compound classes from Alberta bitumens and Bellshill Lake crude oil are shown in Figure 12.43. The thiophenes from the bitumens display a broad, unresolved hump on which are superimposed a large number of sharp peaks representing individual constituent thiophenic compounds. In contrast, the gas chromatogram of the Bellshill Lake conventional oil thiophenes does not feature such a degree of complexity and only a modest number of relatively low-MW compounds appear to comprise the fraction, without a major contribution from any unresolved hump. This may signify a trend in distribution with depth since the Bellshill Lake sample originated from the greatest depth, 920 m. The peaks corresponding to dibenzothiophene and its monomethyl derivatives are identified in the gas chromatograms. They are minor components of the Syncrude sample but, along with dimethyldibenzothiophenes, they dominate the Bellshill Lake sample. Many of the peaks and much of the unresolved hump represent polyalkylated dibenzothiophenes and the early-eluted peaks are polyalkylated benzothiophenes which are converted to a limited number of dibenzothiophenes and benzothiophenes with short side chains on increasing thermal maturation (depth of burial). The abundance of benzothiophenes relative to dibenzothiophenes seems to decline with increasing depth of burial, along with the ratios of 1-methyldibenzothiophene to the 2-, 3- and 4-methyldibenzothiophenes.

The ratio (2-methyl + 3-methyl)/2(1-methyl) dibenzothiophenes has been suggested as a dibenzothiophene maturity index (DBTI). The value of this index increases with thermal maturation because the 1-methyl isomer, which seems to be the primary isomer, converts to the thermodynamically more stable 2-, 3- and 4-methyl isomers. Consequently, the value of DBTI increases with the depth of burial of the deposit, Table 12.12.

In addition to the monomethyldibenzothiophenes, all samples contain a complex mixture of isomeric C_2- and C_3- dibenzothiophenes as shown in the m/z = 197 cross-scan mass chromatograms in Figure 12.44, along with a series of 1-n-alkyldibenzothiophenes with side-chain lengths ranging from C_1 to n-C_7 in the bitumen maltenes and up to n-C_{12} in the Lloydminster maltene.[17] The latter oil is only moderately biodegraded and the variation in the length of the side chain may be due to the extent of biodegradation experienced by the oil. Severe biodegradation can metabolize members of the series with chain lengths exceeding n-C_7 but not the shorter-chain members. It is known that certain microorganisms attack n-alkylated aromatic molecules when the n-alkyl side chain exceeds a critical length.[18,19] Aerobic bacteria thought to be responsible for the degradation of the

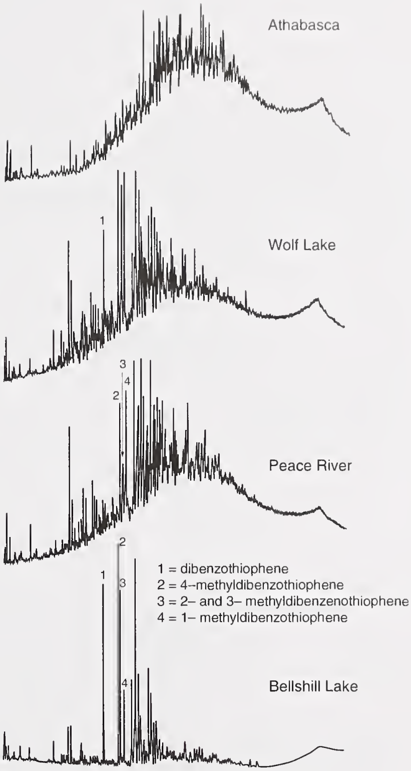

Figure 12.43 Gas chromatograms of the thiophenic compound fractions in Alberta petroleums. From J.D. Payzant *et al.*, Ref. 7. © 1989, American Chemical Society.

Table 12.12 Dibenzothiophene maturity indices (DBTI) for petroleums at different depths

Sample	Depth (m)	% Thiophenes[a]	DBTI
Athabasca (Suncor coker feed)	0	2.7	0.43
Wolf Lake	500	2.9	0.47
Cold Lake	500	2.4	0.73
Peace River	558	7.6	0.35
	500	0.56	–
Bellshill Lake	920	5.5	1.17
Pembina	1080	0.91	0.85
Leduc	1580	1.1	1.59
Beaverlodge (North Dakota)	4050	0.33	4.25

[a] As % of maltene.

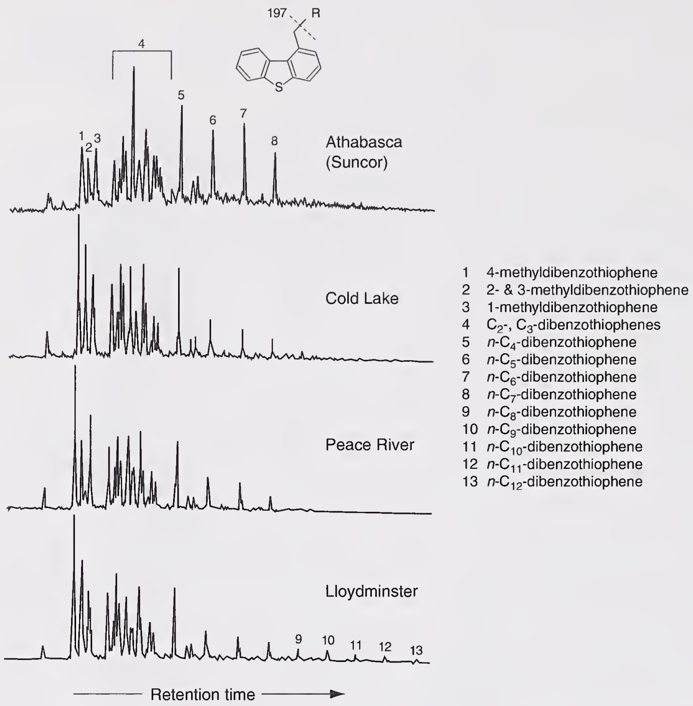

Figure 12.44 *M/z* = 197 cross-scan mass chromatograms for the condensed thiophene fractions in Alberta petroleums. The samples are arranged in order of increasing depth of burial. From J.D. Payzant *et al.*, Ref. 17. © 1991, American Chemical Society.

oil do not attack n-C_8 or shorter-chain alkanes,[20] and this selectivity appears to apply even when the n-alkane forms a side chain on an aromatic carbon. The question of side-chain length will be considered again in Chapter 14 in connection with the pyrolysis products of asphaltene where it will be seen that 1-n-alkyldibenzothiophene compounds are major structural units of the asphaltene molecules.

2.2 Oxygen-containing components

After sulfur, the most important heteroatom in Alberta bitumens and heavy oils is oxygen. Bitumens contain 1–2% oxygen, asphaltenes 1–3% and maltenes 0.6–1.3%. Most of the oxygen in the maltene is concentrated in the most polar portion of the polar fraction where it can reach a concentration as high as 10%. IR and FIMS studies on Athabasca polars show that in the most polar portion the oxygen is mainly present in cyclic carboxylic acids, along with lesser amounts of acyclic acids and esters, and in sulfoxides. In the less polar portion of the polar fraction and in the polyaromatics, oxygen is present as carbonyls in fluorenones and perhaps in quinolones, as hydroxyls in n-alcohols, sterols, fluorenols and other cyclic alcohols. A sizeable fraction of these functional groups is attached to biomarker-type hydrocarbon molecules. The carboxylic acids occur mainly in free form and, to a lesser extent, as esters and salts. They are partitioned between the aromatic, polar and also the asphaltene fraction. Moreover, a rich variety of carboxylic acids can also be found in the non-bituminous organic matter present in most oil sands, chemically bound to the sand.

2.2.1 Carboxylic acids and esters

The FIMS studies of the polars have already shown the presence of acyclic through hexacyclic carboxylic acids in the most polar portion. Prominent among these were the tricyclic, pentacyclic and acyclic alkanoic acid series. The tricyclic acids occur in the C_{20}–C_{26} range and they feature two dominant components at C_{21} and C_{24}. The pentacyclic acids comprise a long series ranging from C_{30} to at least C_{40}, but more likely from C_{23} to C_{43}. On chromatographic and solvent precipitation fractionation of the bitumen these acids are partitioned between the aromatic, polar and asphaltene fractions and the concentration distributions of these acids vary from fraction to fraction. Thus, in the sand-bound organic matter, as discussed in Chapter 8, it is the acyclic acids that dominate while in the maltene and asphaltene, the cyclic acids are in excess. In the maltene, FIMS reveals that the pentacyclic acids are preponderant, yet their presence outside the C_{30}–C_{33} range could not be detected by chromatographic methods. A few hopanoic acids have also been detected by GC–MS analysis of the polars complexed to asphaltene.

a) Tricyclic acids and esters

The tricyclic acids were isolated from the polar fraction of Athabasca bitumen as a concentrate by a series of chromatographic steps involving alumina column, GPC (Sephadex LH-20), and finally reversed phase (C_{18}-bonded silica gel) chromatography, following saponification of the polars. The isolated concentrate was, after methylation, subjected to GC–MS analysis yielding the *m/z* = 191 mass chromatogram reproduced in Figure 12.45. The carbon number of the series is in the range 20–26 with one of the C_{21} isomers and an unresolved mixture of two C_{24} isomers comprising about 75% of the total tricyclic acids. The mass spectra of some of the individual members of this series, shown in Figure 12.46, display an intense, dominating *m/z* = 191 base peak, the hallmark of the terpenoid A/B ring systems:

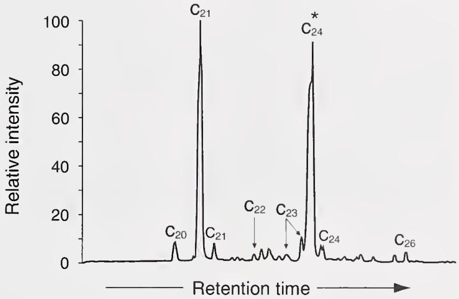

Figure 12.45 *M/z* = 191 cross-scan mass chromatogram of the tricyclic carboxylic acid methyl ester concentrate from Athabasca bitumen.[20]

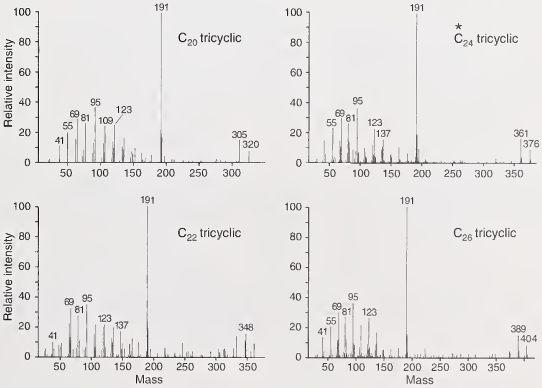

Figure 12.46 Mass spectra of the tricyclic carboxylic acid methyl esters shown in Figure 12.45.[20, 22]

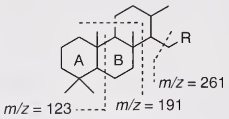

Following GC–MS analysis, the ester mixture was reduced to the alcohol stage with $LiAlH_4$ and the alcohols, after mesylation, were further reduced to alkanes with $LiAlH_4$ or mono-deuterated alkanes with $LiAlD_4$:

$$C_{23}H_{41}CO_2CH_3 \xrightarrow{LiAlH_4} C_{23}H_{41}CH_2OH \xrightarrow{\text{mesyl sulfate}} C_{23}H_{41}CH_2Omesyl \xrightarrow[LiAlD_4]{LiAlH_4} \begin{matrix} C_{24}H_{44} \\ C_{24}H_{43}D \end{matrix}$$

The resultant hydrocarbon mixture, after concentration of the cyclic terpenoid components by molecular sieve 13X adduction, can be compared to the terpenoid hydrocarbon molecular sieve 13X adducts from the saturate fraction of the bitumens, Figure 12.47. From the GC retention times and mass spectral data, Figure 12.48, it can be concluded that the components of the reduced hydrocarbon mixture correspond to the respective members in the saturate fraction of the bitumen.

The identification of the hydrocarbon framework, however, still does not clarify the position of the carboxyl group in the original acid molecules. That information is contained in the position of the deuterium atom in the $LiAlD_4$-reduced hydrocarbon molecules, since the deuterium atom will be attached to what was the carboxylic carbon in the original acid molecules.[20,22] The position of the deuterium atom in the hydrocarbon molecules can be inferred from the mass spectra, Figure 12.49, which show that neither the m/z = 191 fragment peak from the A/B bicyclic ring fragment nor the m/z = 261 fragment peak from the loss of the C_5 side chain in the C_{24} tricyclane are affected by deuteration:

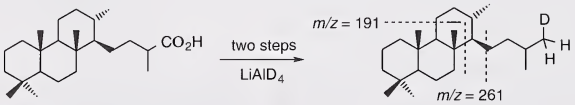

Combining this structural information with the appearance of ill-resolved doublets in the gas chromatogram of the C_{24}, C_{25} and C_{26} members but not the lower, C_{21}, C_{22}, C_{23} members of the acid series, Figure 12.45, it follows that the carboxylic group is attached to the side chain in the terminal position:

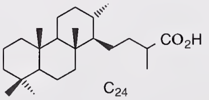

C_{24} ;

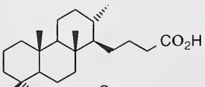

C_{23}

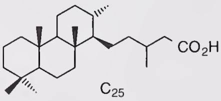

C_{25} ;

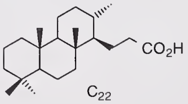

C_{22}

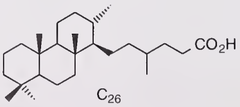

C_{26} ;

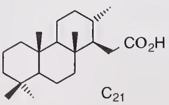

C_{21}

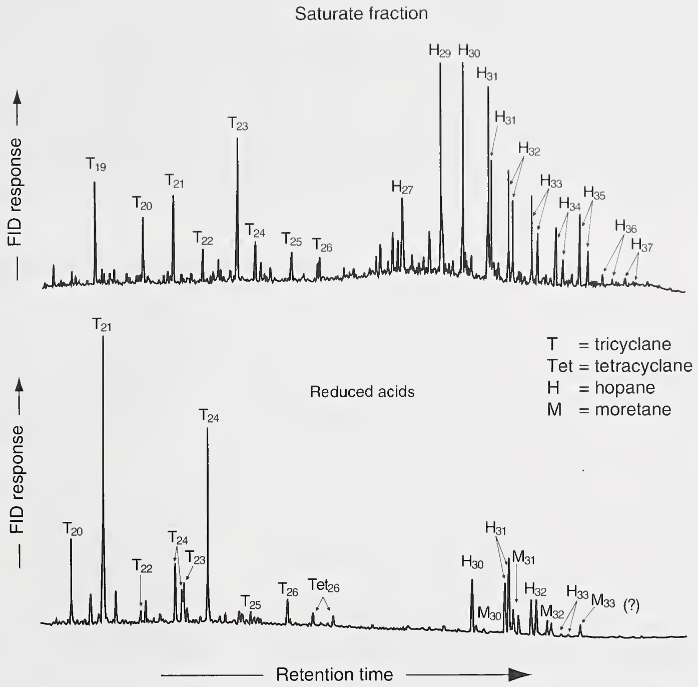

Figure 12.47 Gas chromatogram of the zeolite-adducted saturates from the saturate fraction of Athabasca maltene (top) and from the reduced carboxylic acid methyl esters (bottom). Subscripts refer to the number of carbon atoms in the molecule.[20]

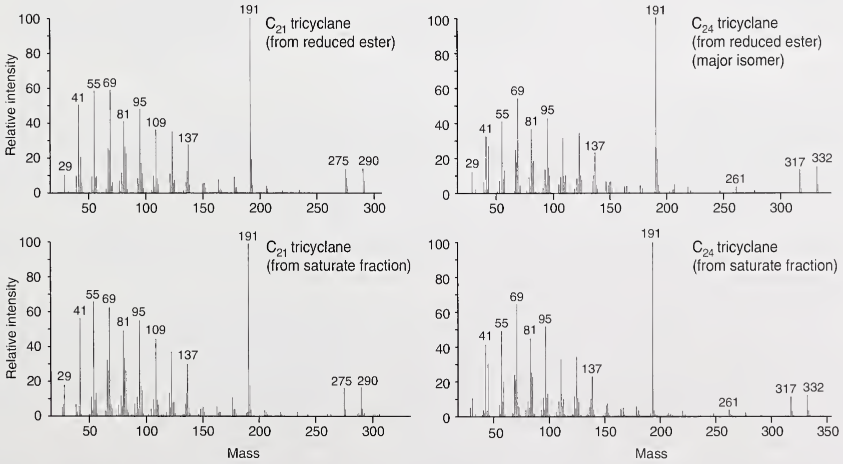

Figure 12.48 Mass spectra of the C_{21} and C_{24} tricyclanes from the reduced esters and the C_{21} and C_{24} tricyclanes isolated from the saturate fraction.[20]

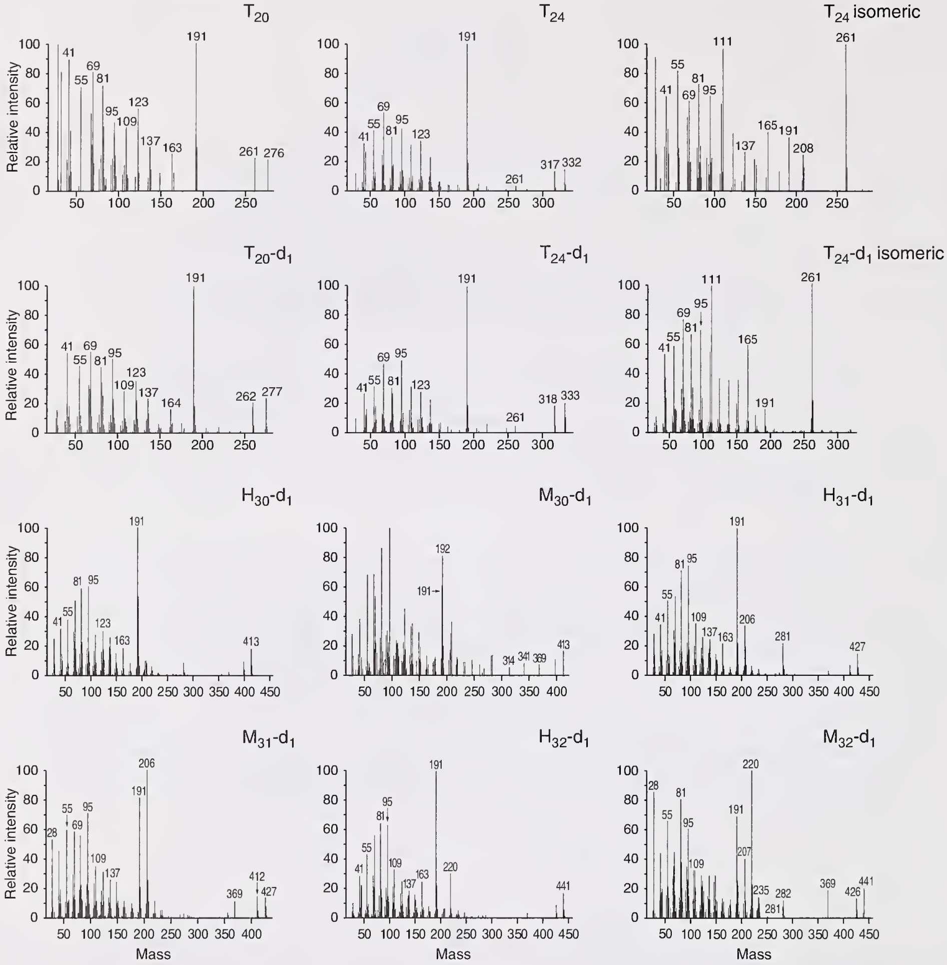

Figure 12.49 Mass spectra of the C_{21} and C_{24} tricyclanes obtained from the $LiAlH_4$ reduction of the corresponding esters (T) and of their monodeuterated isotopomers from $LiAlD_4$ reduction (T-d_1) and of the monodeuterated C_{30}–C_{32} hopanes (H-d_1) and moretanes (M-d_1) from the $LiAlD_4$ reduction of their carboxylic acid methyl esters.[22]

The structure for C_{24} is also in agreement with the observation that the reduction of the carboxyl diastereomers produces a single isomer.

The tricyclic alkanes above C_{24} from the saturate fraction of the bitumen consist of pairs of diastereomers of approximately equal concentration, as is the case for the C_{24} and C_{25} tricyclic esters; however, for the C_{26} tricyclic ester, the ratio of diastereomers is 7 to 1, suggesting that the CO_2H functionality slows down isomerization three carbons away.

The relative concentration distributions of the homologs within a given compound class of the structurally related tricyclic acids, tetracyclic sulfides, tetracyclic sulfoxides and tricyclic alkanes, all having the same hydrocarbon framework, are somewhat different and the geochemical significance of this point will be discussed in Chapter 13.

When the acids were extracted from the bitumen with aqueous potassium carbonate, presumably only the free acids and any acid anhydride present were extracted, whereas upon saponification with aqueous methanolic potassium hydroxide, the free, esterified and salt-bound acids are all extracted. On this basis it was found that in Athabasca bitumen approximately one-half of the C_{21} tricyclic acid is present as free acid while essentially all of the C_{24} tricyclic acids are present in free form. Some of the carboxylic acids in the maltene must be present as salts since pyridine, quinoline and even stronger bases have been shown to be present in small quantities[21] and the colloidal clay content may comprise fine particles of calcium and magnesium carboxylates.

b) Pentacyclic acids and esters

Of the extended series of $C_nH_{2n-8}CO_2$ acids with $n = 23$–43 observed in the most polar portion of the Athabasca polar fraction by FIMS, Figure 12.13, only the C_{30}–C_{32} along with traces of the C_{33} homologs could be detected by GC analysis of the reduced hydrocarbons, Figure 12.47. The rest of the series must comprise isomeric forms of the hopanoic acids, the reduced parent hydrocarbons of which are not adducted by molecular sieve 13X used in the analytical fractionation process. The total amount of hopanoic acids as revealed by GC analysis of the reduced esters comprises a small fraction of the total cyclic carboxylic acids. The individual members of the reduced pentacyclic acid series were identified on the basis of their GC retention times (which, on nonpolar columns, are higher for moretanes than for hopanes) and their mass spectra, Figure 12.49.[20] Designating isomerism at the C_{17} and C_{21} positions as $\alpha\beta$ (hopanes) and $\beta\alpha$ (moretanes) and at the C_{22} position as S and R, the relative abundance of the series components $\alpha\beta$R, $\alpha\beta$S, $\beta\alpha$R, $\beta\alpha$S turns out to be markedly different from the distribution found in the saturate fraction of Athabasca bitumen. Thus, the carboxylic acids-derived hydrocarbons have a relatively higher concentration of moretanes and of the 22R isomers, suggesting an apparent lower degree of thermal maturity. Hopanes and moretanes may be differentiated by comparing the intensities of their mass spectral fragments A and B:

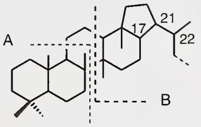

Fragment A is $m/z = 191$, while fragment B is $m/z = 149$ (C_{27}), 177 (C_{29}), 191 (C_{30}), 205 (C_{31}) and 219 (C_{32}). In the case of the hopanes the intensity of fragment A is always higher than that of fragment B, whereas in the $\beta\beta$ series, fragment B is about as intense as fragment A for the C_{29} and C_{31} members; for moretanes the ratio of fragment B to A is 1.4 and 1.2 for the C_{29} and C_{31} members. These ratios cannot be determined for C_{30} members because both fragments A and B have a mass of 191. For the monodeuterated C_{30} compounds formed in reduction with $LiAlD_4$ however, fragment B has mass $m/z = 192$ and thus fragments A and B can be differentiated. The fragment ratio data are compiled in Table 12.13.[20,23,24]

The relative concentration distributions of the homologs and isomers of the hydrocarbon molecular core of a given kind—tricyclic or pentacyclic—show considerable variance, as discussed above for the case of the tricyclic terpenoid compound class, depending on the nature of their molecular functionality, *i.e.* whether they are in hydrocarbons, carboxylic acids, sulfides or sulfoxides. Moreover, even within a given functionality class some variation may exist with the analytical origin of a fraction; for example, we have seen that the sulfoxides in the polar fraction and the sulfoxides in the acetone extract of the asphaltene show different distributions. Another

Table 12.13 Mass spectral differentiation of hopanes, moretanes and β,β-hopanes in the pentacyclic acid-derived hydrocarbons[20,23,24]

Compound	$\frac{A}{B}\left(\frac{m/z = 191}{m/z = 149 + n\,14}\right)^a$ Hopane		Moretane		β,β-Hopane
C_{29}	2.6	(2.3^b)	1.2	(0.7^b)	(0.5^b)
C_{30}	2.4	–	0.8	–	–
C_{31}	2.9	(2.0^b)	0.8	(0.8^b)	(0.5^b)
	($2.20–2.30^c$)		($1.00–1.20^c$)		($0.65–0.75^c$)

[a] n = number of carbon atoms in side chain attached to C–21. [b] From Ref. 23. [c] From Ref. 24.

example is seen from the chromatograms shown in Figures 12.50, displaying the concentration distributions of the tricyclic and pentacyclic acids isolated from the acetone extract of Athabasca asphaltene. Here, we observe the dominance of the cyclic acids by the C_{21} and, to a lesser extent, by the C_{24} acid as before, and a minor contribution from the hopanoic acids. In the latter however, the distribution of the α,β hopanoic acids C_{29} (one isomer) > $C_{30}R$ > $C_{30}S$ > $C_{31}S$ > $C_{31}R$ with minor amounts of the β,α isomers is significantly different from that of the hopanes obtained from the reduced acids following the saponification of the whole polar fraction, Figure 12.47. The data also show that, in the hydrocarbon series, the R/S isomer ratio is lower than in any of the functionalized derivatives and that in the carboxylic acids, the moretanes/hopanes ratio is exceptionally high. The geochemical significance of these findings will be examined more closely in Chapter 13.

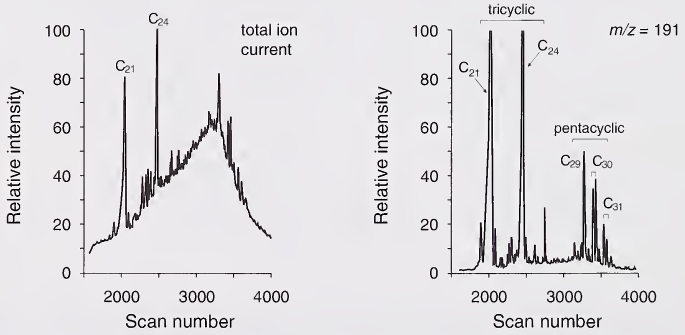

Figure 12.50 GC–MS chromatograms of the tricyclic and pentacyclic acid methyl esters in Fraction C of the Athabasca n-C_5-asphaltene acetone extract. From Z. Frakman *et al.*, Ref. 16. © 1990, American Chemical Society.

c) Acyclic acids and esters

The third largest class of acids present in Athabasca bitumen is the series of *n*-alkanoic acids along with small quantities of *n*-alkenoic acids. These acids and their salts (formed with the native basic nitrogen compounds in the polar fraction, the pyridines and quinolines and with calcium and magnesium) as well as their esters are distributed across the aromatic, polar and asphaltene fractions in the bitumen. The distribution of *n*-alkanoic acids is characterized by a carbon range of about 8–28 and a strong preference for the even-carbon-number members, in particular, the C_{16} and then the C_{18} members. Above C_{18} the acid concentration drops to a trace level. Some samples also contained small amounts of oleic (*cis*-9-octadecenoic), elaidic (*trans*-9-octadecenoic) acids as well as 8-octadecenoic acids.

In the series isolated from the acetone extract of Athabasca *n*-C_5-asphaltene there is also a maximum at C_{16} and C_{18}, and in the organic matter chemically bound to the sand, aside from the maximum at C_{16} and C_{18}, a slight maximum also occurs at C_{26}–C_{28}. In the bitumen the straight-chain acids are minor constituents relative to the cyclic terpenoid acids, amounting to about one-tenth of the latter. In the solid-bound organic matter, the relative concentrations are reversed and the dominant acids are the acyclic acids.

The presence of small quantities of *n*-alkanoic and *n*-alkenoic acids in bitumen[25] is generally considered to be related to the microbial processes that have taken place in the deposit and the distribution of these acids can give some indications about the microbial history of the deposit.

d) Miscellaneous carboxylic acids

The rest of the carboxylic acids detected in the polar fraction are aromatic acids, with the exception of two tetracyclic C_{26} acids which are apparent in the GC of the hydrocarbons from the reduction of the acid methyl esters, Figure 12.47. Their structures have not been elucidated but they are thought to be either steroid or one-ring-opened hopanoic acid derivatives. Another acid that was noted was a tetracyclic monoaromatic C_{23} acid which, on the basis of the mass spectrum of its methyl ester, appears to be a steroid acid.

Detailed chromatographic separation along with IR and MS studies on the acetone extract of Athabasca *n*-C_5-asphaltene (which, as mentioned before, contains components of the polar fraction) revealed the presence of a variety of aromatic monocarboxylic acids as well.

The acetone extract was prepared by refluxing 10-g asphaltene with 500-mL acetone for 24 h to give a reddish-brown extract in 18% yield (N, 0.96; O, 4.4; S, 7.9; ash, 0.36 wt%). The extract was subjected to chromatographic separation, first by GPC on Bio-Beads SX–2 and then on silica gel, as indicated in the flow diagram shown in Figure 12.51. Of the four fractions (A–D) taken for further studies, the IR spectra, Figure 12.52, indicated that fraction A contained aromatic nitrogen compounds (carbazoles) and small amounts of carbonyl compounds; fraction B appeared to be composed of aromatic carbonyl compounds; fraction C, aromatic alcohols, carbonyls and carboxylic acids; and fraction D, saturated carboxylic acids and sulfoxides. The carbonyl compounds in fraction A were isolated by alumina chromatography and combined with fraction B to give fraction B–1, which was examined for carbonyl compounds as will be discussed in the next section of this chapter.

The IR spectrum of fraction C displayed free and bonded OH stretching bands at 3600–2800 cm^{-1}, a strong carbonyl stretching band at 1705 cm^{-1} and aromatic absorption at 1600 cm^{-1}. To separate the acids, the fraction was esterified with diazomethane and the esters were isolated chromatographically. The eluate contained the same tricyclic and pentacyclic terpenoid acids that were found in the polar fraction (Section 2.2.1.a),b)) in an aggregate amount of 400 ppm of the bitumen.

Fraction D, besides having a high oxygen content (9.5%), also contained large amounts of sulfur (8.6%) and its principal IR absorption bands are assigned to carboxylic acids (1710 and 3600–2800 cm^{-1}) and naphthenic sulfoxides (1040 cm^{-1}). In order to isolate the acids from the sulfoxides, the fraction was methylated with diazomethane and the esters were separated on a silica gel column using IR spectroscopy to monitor the separation. Seven subfractions were taken, but only four were investigated further. The IR spectra of these four fractions are shown in Figure 12.53.

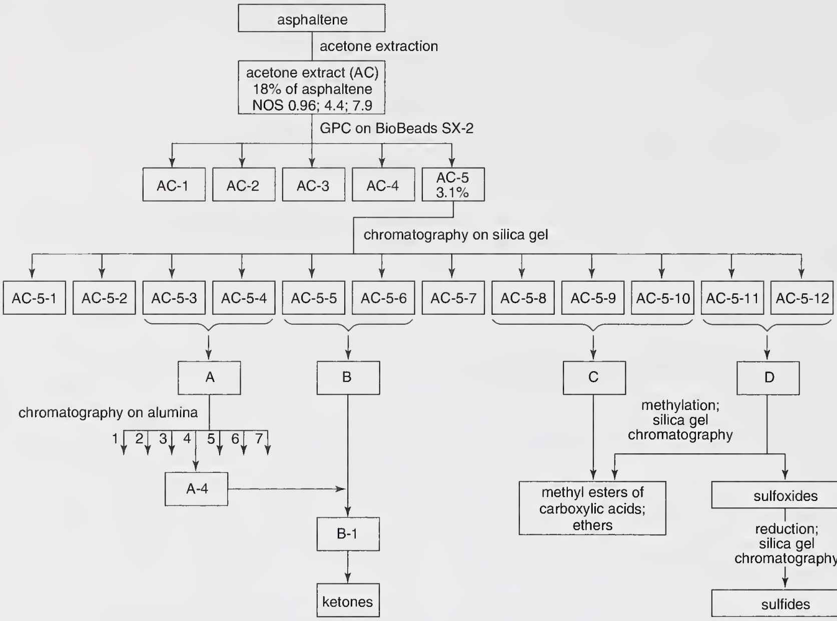
asphaltene
acetone extraction
acetone extract (AC)
18% of asphaltene
NOS 0.96; 4.4; 7.9
GPC on BioBeads SX-2
AC-1
AC-2
AC-3
AC-4
AC-5
3.1%
chromatography on silica gel
AC-5-1
AC-5-2
AC-5-3
AC-5-4
AC-5-5
AC-5-6
AC-5-7
AC-5-8
AC-5-9
AC-5-10
AC-5-11
AC-5-12
A
B
C
D
chromatography on alumina
1
2
3
4
5
6
7
A-4
B-1
ketones
methylation;
silica gel
chromatography
methyl esters of
carboxylic acids;
ethers
sulfoxides
reduction;
silica gel
chromatography
sulfides

Fraction	Wt%[a]	MW	C[b]	H[b]	N[b]	S[b]	O[b]	H/C
AC-1	2.05	2920	77.07	9.07	0.79	9.09	3.98	1.41
AC-2	2.46	1790	77.38	8.87	0.87	8.79	4.09	1.37
AC-3	5.06	1210	77.76	8.59	0.88	8.04	4.73	1.33
AC-4	3.30	670	77.95	7.98	1.10	7.59	5.38	1.23
AC-5	3.10	450	80.10	7.05	1.24	6.05	5.56	1.06
A	1.10	495			2.51	4.49	1.94	0.96
B	0.02	555			0.81	5.04	5.26	0.93
C	0.81	480			0.97	4.17	7.79	1.09
D	0.85	450			0.95	8.60	9.54	1.20

[a] Based on original asphaltene. [b] Wt%, d.a.f., of the acetone extract AC.

Figure 12.51 Separation scheme for the isolation of oxygen-, sulfur- and nitrogen-containing compounds complexed to asphaltene.

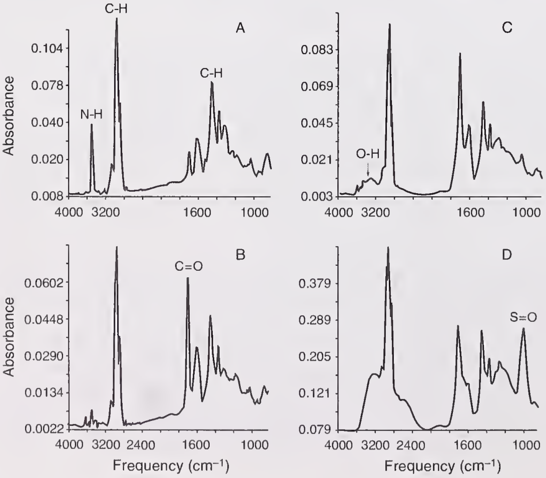

Figure 12.52 Infrared spectra of fractions A–D (*cf.* Figure 12.51) of the acetone extract of *n*-C_5-asphaltene. From Z. Frakman *et al.*, Ref. 16. © 1990, American Chemical Society.

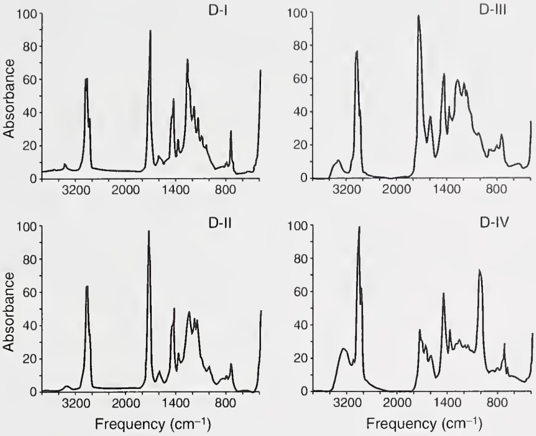

Figure 12.53 Infrared spectra of subfractions D-I to D-IV of the carboxylic acid methyl esters in the acetone extract of *n*-C_5-asphaltene.

Subfraction D-I, eluted with 10% CH_2Cl_2 in benzene, displays a sharp carbonyl absorption in the IR at 1717 cm^{-1}, together with peaks at 1600, 1454, 1435 and 1276 cm^{-1}, suggesting that it contains methyl esters associated with alkyl groups and with aromatic moieties. GC–MS analysis showed that subfraction D-I contained the methyl esters of *n*-alkanoic acids, and of the several other components, only a few were identified, including a series with formula $C_nH_{2n-18}SO_2$. Since the sulfone group absorption is absent in the IR spectrum, the compounds in this series were identified as the methyl carboxylate derivatives of dibenzothiophene:

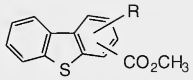

where R = C_1–C_4. The mass spectra of the C_{15} and C_{16} members of the series are given in Figure 12.54, **1** and **2** and the data are tabulated in Table 12.14. These acids appear to be the end-products of the biodegradation of long-chain *n*-alkyldibenzothiophenes,[18] a principal structural element of the asphaltene molecules and their degradation products, the nondistillable portion of maltene. The C_{17} member of the group occurs in eight isomeric forms and altogether 20 different species have been detected.

Other compounds identified in this fraction were members of the series with formula $C_nH_{2n-20}O_2$. The bulk of this series appeared in the next subfraction.

Subfraction D-II was eluted with CH_2Cl_2. Its IR spectrum featured a strong ester carbonyl band at 1736 cm^{-1} and the symmetric and asymmetric vibrations of the C–O–C linkage at 1300–1050 cm^{-1}. In addition to *n*-alkanoic acid methyl esters, it consisted of compounds with series formula $C_nH_{2n-20}O_2$. The mass spectra of the C_{17} and C_{18} members of the series are shown in Figure 12.54, **3** and **4**. This series has been identified as alkyl-substituted methyl carboxylates of anthracene and/or phenanthrene:

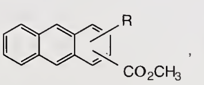

,

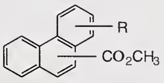

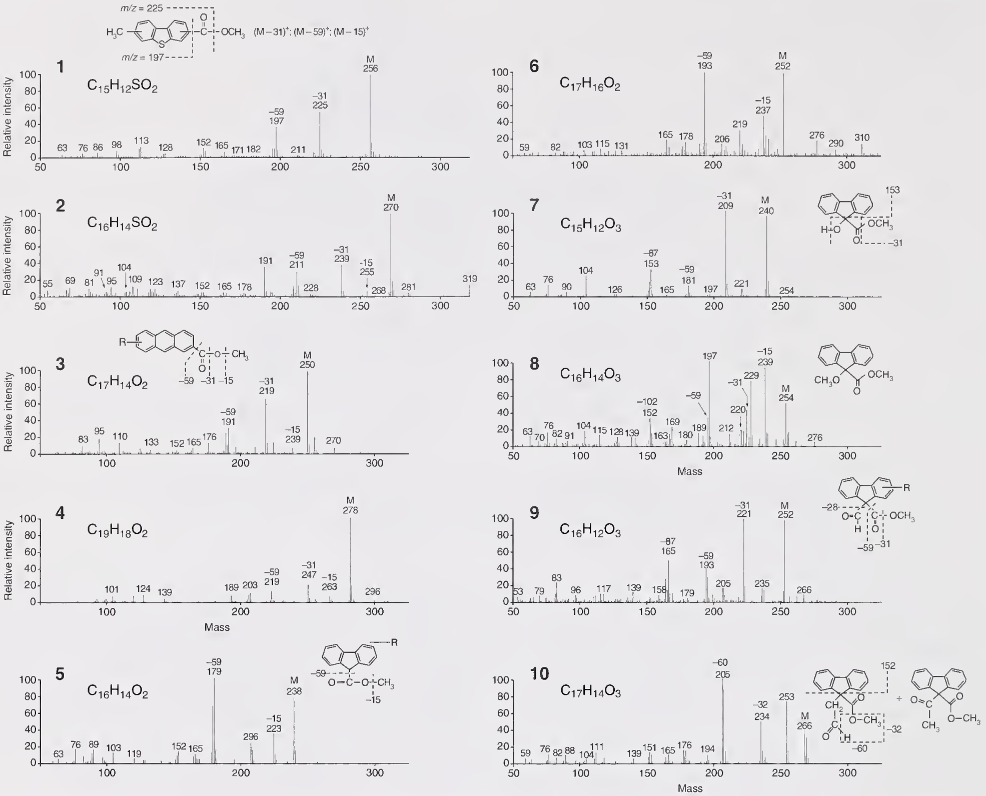

Figure 12.54 EIMS of the methyl carboxylates of the following compounds in the asphaltene acetone extract: **1** and **2**—dibenzothiophene, C_{15} and C_{16}, $C_nH_{2n-18}SO_2$; **3** and **4**—anthracene/phenanthrene, C_{17} and C_{19}, $C_nH_{2n-20}O_2$; **5** and **6**—fluorene-9, C_{16} and C_{17}, $C_nH_{2n-18}O_2$; **7**—9,9-hydroxyfluorene, C_{15}, $C_nH_{2n-18}O_3$; **8**—9,9-methoxyfluorene, C_{16}, $C_nH_{2n-18}O_3$; **9**—9,9-formylfluorene, C_{16}, $C_nH_{2n-20}O_3$; **10**—9,9-acetylfluorene, C_{17}, $C_nH_{2n-20}O_3$; **10**—9,9-acetaldehydefluorene, C_{17}, $C_nH_{2n-20}O_3$; (9,9-1-hydroxyethylfluorene, C_{17}, $C_nH_{2n-18}O_3$).

where R = C_1–C_4. As seen from the data listed in Table 12.14, one member occurs in up to six different isomeric forms. This series, like the dibenzothiophene carboxylic acid series in subfraction D-I and the other aromatic carboxylic acid series in the more polar fraction to be discussed below, probably were formed from the biodegradation of the long-chain *n*-alkyl-substituted parent aromatic core, in the present instance anthracene or phenanthrene.

Another, short series of aromatic carboxylic acids detected in subfraction D-II is represented by the series formula $C_nH_{2n-18}O_2$ which, on the basis of the mass spectra of the C_{16} and C_{17} methyl carboxylates, Figure 12.54, 5 and 6, corresponds to the methyl carboxylates of fluorene:

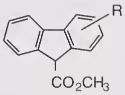

where R = C_1–C_5 and CO_2CH_3 is probably attached to C_9.

Table 12.14 High-resolution mass spectral data on the methyl esters of the carboxylic acids in the acetone extract of n-C_5-asphaltene

Nominal mass	Measured mass	Formula	No. of isomers	No. of C in side chain	Yield, % of asphaltene
		$C_nH_{2n-18}SO_2$[a]			
256	256.0558	$C_{15}H_{12}SO_2$	5	1	0.03
270	270.0714	$C_{16}H_{14}SO_2$	6	2	
284	284.0872	$C_{17}H_{16}SO_2$	8	3	
298	298.0103	$C_{18}H_{18}SO_2$	1	4	
		$C_nH_{2n-20}O_2$[b]			
250	250.1036	$C_{17}H_{14}O_2$	1	1	0.10
250	250.0986	$C_{17}H_{14}O_2$	4	1	
264	264.1140	$C_{18}H_{16}O_2$	6	2	
264	264.1157	$C_{18}H_{16}O_2$	3	2	
278	278.1289	$C_{19}H_{18}O_2$	1	3	
292	292.1426	$C_{20}H_{20}O_2$	1	4	
		$C_nH_{2n}O_2$[c]	C_{12}–C_{28}		
		$C_nH_{2n-18}O_2$[d]			
238	238.0986	$C_{16}H_{14}O_2$	2	1	
252	252.1136	$C_{17}H_{16}O_2$	2	2	
294	294.1608	$C_{20}H_{22}O_2$	1	5	
		$C_nH_{2n-6}O_2$[e]	C_{20}–C_{25}		0.41
		$C_nH_{2n-10}O_2$[f]	C_{28}–C_{31}		
		$C_nH_{2n-18}O_3$[g]			
240	240.0775	$C_{15}H_{12}O_3$	2	0	0.15
254	254.0929	$C_{16}H_{14}O_3$	11	1	
268	268.1088	$C_{17}H_{16}O_3$	1	2	
		$C_nH_{2n-20}O_3$[h]			
252	252.0999	$C_{16}H_{12}O_3$	3	0	
266	266.0939	$C_{17}H_{14}O_3$	4	1	
280	280.1105	$C_{18}H_{16}O_3$	2	2	

[a–f]: Methyl esters of the carboxylic acids of: [a] dibenzothiophenes; [b] anthracenes and/or phenanthrenes; [c] *n*-alkanes; [d] fluorenes; [e] tricyclic terpanes; and [f] pentacyclic terpanes; [g] 9-hydroxyfluorenes and 9-methoxyfluorene; [h] 9-formylfluorene; 9-acetylfluorene and 9-acetaldehydefluorene along with 9-1-hydroxyethylfluorene, $C_nH_{2n-18}O_3$.

The next subfraction, D-III, eluted with 10% ethyl acetate in CH_2Cl_2, was found to contain two series of aromatic acids, one with series formula $C_nH_{2n-18}O_3$ and the other, $C_nH_{2n-20}O_3$.

On the basis of the IR spectrum of the fraction, Figure 12.53, which displays prominent absorptions at 1737 (>C=O) and 3300 cm^{-1} (O–H), and the mass spectra of some of the series members, Figure 12.54, 7, the $C_nH_{2n-18}O_3$ series is tentatively identified as 9-carbomethoxy-9-hydroxyfluorenes

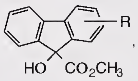

where R = H, CH_3 or C_2H_5 and 9-carbomethoxy-9-methoxyfluorene, **8**.

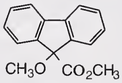

In the $C_nH_{2n-20}O_3$ series at least three isomers are present, as represented by 9-carbomethoxy-9-formylfluorene, **9**,

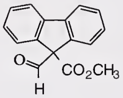

9-carbomethoxy-9-acetylfluorene, **10**,

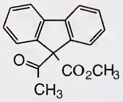

and 9-carbomethoxy-9-acetaldehydefluorene, **10**,

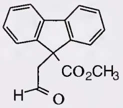

In spectrum **10**, along with the two $C_nH_{2n-20}O_3$ isomers, one $C_nH_{2n-18}O_3$ compound with MW 268 g·mol^{-1} is apparent. This compound appears to be the reduced alcohol from the 9-carbomethoxy-9-acetylfluorene, *i.e.* 9-carbomethoxy-9-1-hydroxyethylfluorene:

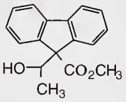

The data on the aromatic carboxylic acids discussed in this section are summarized in Table 12.14 and the total ion mass chromatograms of the acids are displayed in Figure 12.55. The aromatic cores in the identified acids such as

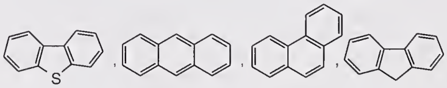

are all of common occurrence in the asphaltene molecules and their degradation products.

The aggregate amount of acids identified in Fraction D was 0.69% of the asphaltene. The IR spectra of Fractions B and C (Figure 12.52) show intense carboxylic carbonyl absorptions and these fractions have high oxygen contents. Therefore, the combined carboxylic content of Fractions A–D = Fraction AC-5 (3.1%) would be much higher and would account for a sizeable portion of Fraction AC-5. For comparison, the total amount of acids isolated by saponification of the bitumen from a low-grade Athabasca (Syncrude Beach Sand) ore was 1.9%.

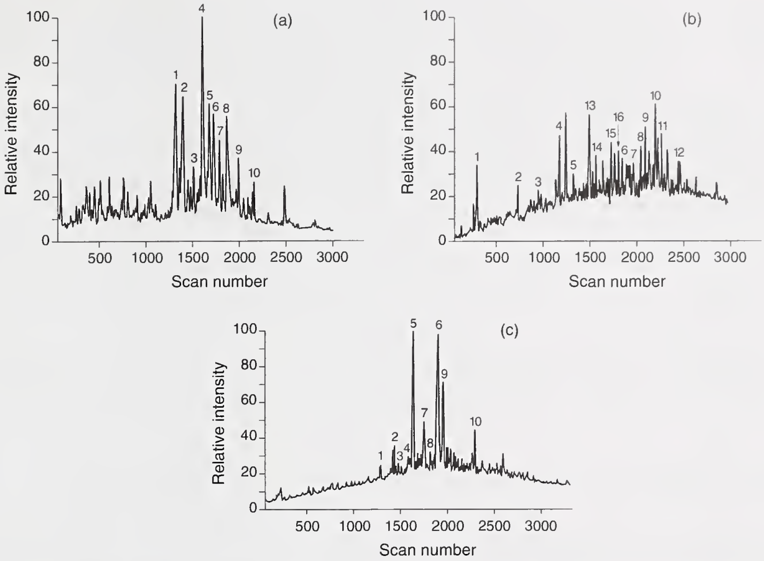

Figure 12.55 Total ion current chromatogram of the aromatic methylated acids in Fraction D of the acetone extract of n-C_5-asphaltene. a) Esters eluted with 10% CH_2Cl_2 in benzene. Peaks 1–10 correspond to the series $C_nH_{2n-18}SO_2$. b) Esters eluted with CH_2Cl_2. Peaks 1–5 correspond to n-alkanoic acids; 6–12, to the series $C_nH_{2n-20}O_3$; 13–16, $C_nH_{2n-18}O_2$. c) Esters eluted with 10% ethyl acetate in CH_2Cl_2. Peaks 1–6 correspond to the series $C_nH_{2n-18}O_3$; 7–10, $C_nH_{2n-20}O_3$. From Z. Frakman *et al.*, Ref. 16. © 1990, American Chemical Society.

2.2.2 Acid anhydrides and esters

In carboxylic acid anhydrides the IR absorption of the O=C–O–C=O chromophore falls into the distinctive frequency range 1760–1820 cm^{-1} (which is a transparent window for all but a few chromophores) and is characterized by a doublet band separated, on the average, by 60 cm^{-1}. The higher frequency band is stronger in acyclic and the lower, in cyclic anhydrides. Such twin bands located around 1780 and 1725 cm^{-1} have been reported in the IR spectrum of the most polar 16% fraction of Athabasca maltene,[26] Figure 12.56. These bands may be due to a single carrier (anhydride) or to different carriers such as a ketone or a carboxylic acid (the 1725 cm^{-1} band) and a lactone, *e.g.*

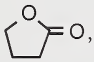

, (the band around 1780 cm^{-1}).

Differentiation between these possibilities can be made by chemical means. Specifically, anhydrides can be hydrolyzed upon treatment with an alkali bicarbonate whereas lactones are not. Such hydrolysis studies in which Fuller's Earth-separated Athabasca resins were treated with potassium bicarbonate and the consequent chemical changes taking place monitored by IR have been reported.[27] Figure 12.57 shows the FTIR spectrum of the original sample and those recorded after various treatments. Four prominent bands are visible in the spectra, the 1775 cm^{-1} band which may be due to anhydrides or lactones, the 1727 cm^{-1} band which may be due to anhydrides or esters, the 1702 cm^{-1} band due to acids or perhaps ketones, and the band centered at 1600 cm^{-1} which could be due to aromatic or carboxylate ion absorption. Upon treatment with bicarbonate, spectrum (a), the 1775 cm^{-1} band disappeared with a simultaneous decrease in the intensity of the 1725 cm^{-1} band and an increase in the 1702 cm^{-1} and

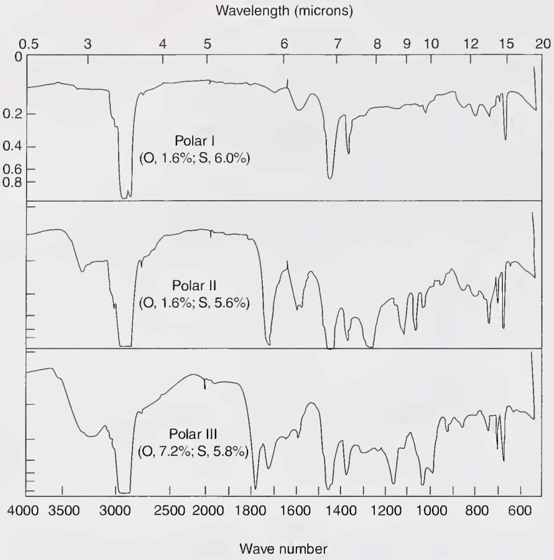

Figure 12.56 IR spectra of the three subfractions of the Athabasca polar fraction. From M.L. Selucky *et al.*, Ref. 26. © 1978, American Chemical Society.

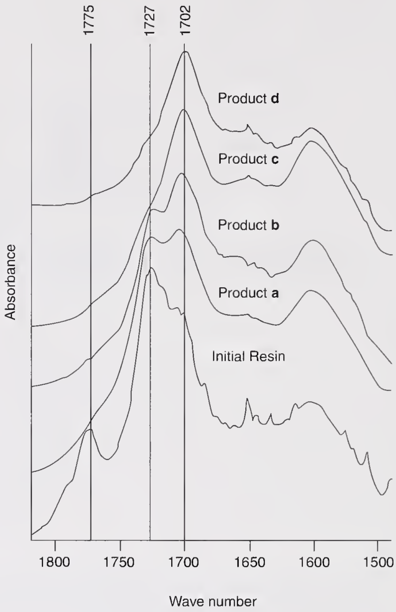

Figure 12.57 Specular reflectance FTIR spectra of Athabasca polar fraction and polar hydrolysis products. From K. Bukka *et al.*, Ref. 27b. © 1994, Butterworth-Heinemann.

1600 cm^{-1} carboxylate absorption bands. These spectral changes are consistent with the 1775 cm^{-1} and part or all of the 1727 cm^{-1} band being due to anhydride carriers.

In a second step, product **a** was subjected to mild treatment with sodium hydroxide solution at 25°C to hydrolyze the esters. This reaction resulted in a reduction of the absorption intensity at 1727 cm^{-1}, relative to the band at 1702 cm^{-1}, spectrum **b**. Further treatment of product **b** with sodium hydroxide under reflux conditions to hydrolyze the more intractable, residual esters, gave spectrum **c** from which the 1726 cm^{-1} band is almost completely gone. Also, the intensity of the band around 1600 cm^{-1} is strongest in product **c** but the absorption band of the free acids at 1702 cm^{-1} is intense as well, indicating that even under reflux conditions not all the acids were converted to salts or that the initial absorption was due to some cyclic or aromatic ketones or imides. Lastly, product **c** was converted to free acids with hydrochloric acid treatment yielding spectrum **d** in which the 1600 cm^{-1} absorption band is reduced (to its initial intensity), compared to that in product **c**, confirming that some of the absorption around 1600 cm^{-1} was due to carboxylate ions produced in the chemical treatments.

As is evident from the spectra of Polar I, II and III (Figure 12.56), the anhydrides are concentrated in the Polar III fraction and the intensity of their 1780 cm^{-1} band here is considerably higher than that of their 1725 cm^{-1} band. This means that the anhydride carriers have an acyclic, rather than a cyclic structure:

R–C(O)–O–(O)C–R

acyclic

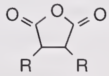

cyclic

The open structure is also supported by the presence of the intense 1170 cm^{-1} band due to the C–O–C stretching vibration. The range for this vibration in acyclic anhydrides is 1045–1175 cm^{-1} whereas in cyclic anhydrides it is 1210–1310 cm^{-1}.

Free carboxylic acids in the resin fraction of bitumens have been credited with the ability to impact the viscosity of bitumen.[27b] It has been shown that increasing concentrations of the acids like increasing concentration of the asphaltenes are accompanied by elevated viscosities. The effect was attributed to increased hydrogen bondings of the asphaltene.

Other major components of this fraction are the cyclic sulfoxides, as shown by the appearance of the intense 1040 cm^{-1} sulfoxide band, and carboxylic acids, as indicated by the broad, intense chelated OH band at *ca* 2300–3600 cm^{-1}.

The Polar II fraction contains some acids and ketones (1715 cm^{-1}), aromatics (3030, 1600 cm^{-1}) and alcohols (1040–1270 cm^{-1} and 2500–3500 cm^{-1}). The Polar I fraction comprises mainly hydrocarbons.

The acid anhydrides in the resins could have originated from the thermolysis of the acids, which is known to afford anhydrides,

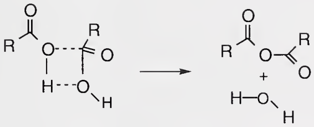

or from the catalytic effect of some superacidic mineral surfaces naturally present in the oil sand:

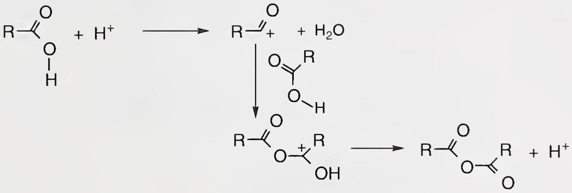

It should be noted that resins of other oil sand bitumens investigated exhibited either no absorptions at 1775 cm^{-1} (Whiterocks, Asphalt Ridge, Sunnyside, Alabama) or only very weak ones (Oklahoma).[27]

2.2.3 Ketones

Fluorenones and their reduced forms, the fluorenols, rarely occur in nature. The most concentrated and abundant natural sources of these families of aromatic ketones and alcohols appear to be the polar fractions of bitumens and crude oil, as was first discovered in Athabasca bitumen.[2] The detection of fluorenones by FIMS and the observation of the carbonyl chromophore by FTIR spectroscopy in the polar fraction of Athabasca bitumen led to a more detailed chemical study of fluorenones.

The fluorenone concentrate, obtained after chromatographic separation of the maltene and molecular distillation (230°C, 10^{-3} Torr) of the crude fraction, comprised 0.33% of the maltene and showed a weak carbonyl absorption at 1710 cm^{-1}, where fluoren-9-one absorbs. Isomeric carbonyl compounds with the same series formula ($C_nH_{2n-18}O$) as fluorenone such as anthrone and phenalen-1-one,

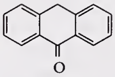
anthrone

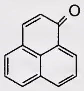
phenalen-1-one

absorb at 1680 and 1640 cm^{-1}, respectively. Alkyl groups on the aromatic nuclei would not be expected to shift significantly the frequency of the ketone stretch vibration. Therefore, on the basis of the FTIR and mass spectra, which exhibit fragmentation patterns similar to those of 9-carbomethoxy-9-hydroxy fluorene as discussed below, the fluoren-9-one structure is assigned to the ketones detected.

The fluorenones in the concentrate were selectively reduced to their ethyl-9-(9-hydroxy)fluorenylacetates (β-hydroxy esters) by treatment with Zn powder in the presence of ethyl bromoacetate:[16,28]

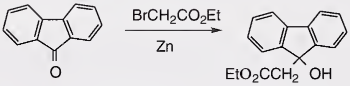

Product yields were essentially quantitative for fluoren-9-one and similar, near-quantitative results were obtained for other model ketones of diverse structures. The introduction of the hydroxy group greatly facilitated the GC resolution of the derivatized ketones from the other polar components of the concentrate.

The capillary GC mass chromatograms of the isolated β-hydroxyesters of the fluorenones are shown in Figure 12.58. The dominant mode of fragmentation for the mono-, di-, tri- and tetramethyl nuclear methylated derivatives of the β-hydroxy esters is loss of the ester group (m/z = 87):

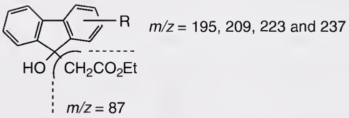

The total ion current and the m/z = 195, 209, 223 and 237 cross-scan spectra of the β-hydroxy esters of fluorenones are shown in the figure. The parent compound, ethyl 9-(9-hydroxy) fluorenylacetate, was not detected. Of the four possible nuclear monomethylated β-hydroxy esters only two appeared, and of the di-, tri- and tetra-nuclear methylated derivatives, fewer than half the number of possible isomers showed up. The most abundant members of the series are the trimethyl followed by the di-, tetra- and monomethyl compounds, as determined from GC retention time measurements of spiked samples of synthetically-prepared standards. In the dimethyl series the 1,4-, 2,4-, and 3,4- isomers are most abundant and the 2,3 isomer may be missing, as can also be seen from the gas chromatograms and the mass spectra in Figure 12.59. The methyl groups, of course, do not need to be located in one of the rings in the molecule and probably are distributed over both aromatic rings. Alkyl-substituted fluoren-9-ones longer than C_1 were not detected but could have been present.

Fluorenones are also present in the acetone extract of Athabasca n-C_5 asphaltene where series of fluorenones, benzofluorenones, dibenzofluorenones and acenaphthylenofluorenones (?) or their isomers have been identified in the form of their β-hydroxyesters.[16] Figure 12.60 shows the TIC chromatogram and the high-resolution mass spectrum of the four series:

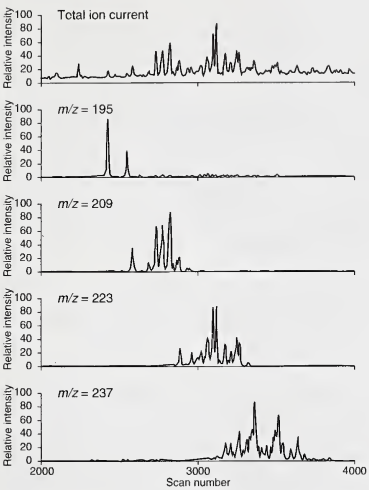

Figure 12.58 GC–MS cross-scans of the β-hydroxy esters of fluorenones. From T.W. Mojelsky and O.P. Strausz, Ref. 28. © 1986, Elsevier Science Ltd.

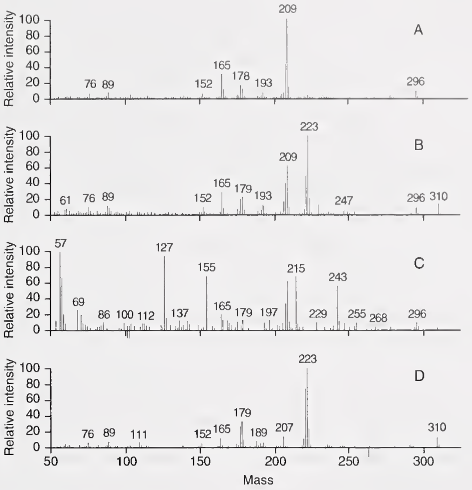

Figure 12.59 Mass spectra of scans corresponding to the retention times of compounds A–D from the capillary gas chromatogram of the–β-hydroxy esters of fluorenones: (A) 1,4-dimethylfluoren-9-one; (B) 3,4-dimethylfluoren-9-one; (C) 2,4-dimethylfluoren-9-one; (D) 2,3-dimethylfluoren-9-one. From T.W. Mojelsky and O.P. Strausz, Ref. 28. © 1986, Elsevier Science Ltd.

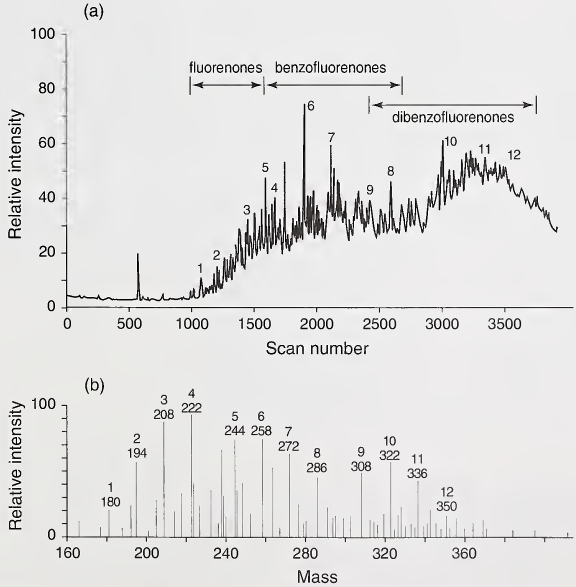

Figure 12.60 GC–MS analysis of the β-hydroxy esters in fraction B–1 (Figure 12.51). a) Total ion current chromatogram; b) high-resolution mass spectrum. Peaks 1–4 correspond to C_0–C_3 alkylfluorenones; 5–8, to C_1–C_4 alkylbenzofluorenones; 9–12, to C_2–C_5 alkyldibenzofluorenones. From Z. Frakman *et al.*, Ref. 16. © 1990, American Chemical Society.

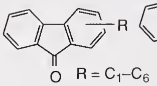

$C_nH_{2n-18}O$
(16 species)

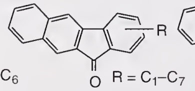

$C_nH_{2n-24}O$
(28 species)

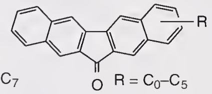

$C_nH_{2n-30}O$
(19 species)

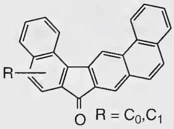

$C_nH_{2n-34}O$
(7 species)

The number of species detected reflects the number of isomers present.

The total quantity of fluorenones in the acetone extract was estimated to be about 0.16% of the asphaltene or 0.03% of the bitumen, from which the total quantity in the bitumen[29] is estimated to be about 0.3%.

As was shown in Chapter 11, Section 7.0, fluorenes present in the aromatic fraction of the bitumen are readily oxidized with molecular oxygen under appropriate conditions to fluoren-9-ones and 9-alkylfluorenes to 9-alkylfluoren-9-ols and either this or microbial oxidation during the biodegradation of the precursor oil must be the source of the fluorenones and the fluorenols (*v.i.*) in the polars. The distribution of the fluoren-9-ones in the polars is similar to that in the oxidation products from the aromatics[30] and the ratio of the concentration of fluoren-9-ones to that of nuclear alkylated fluorenes is an indicator of the cumulative redox history of the deposit.

2.2.4 Alcohols

A variety of alcohols are known to be present in Athabasca bitumen, equipartitioned between the polars, the asphaltene-complexed polars, and the aromatics. Most of the alcohols occur as free alcohols and a portion is bound in esters and ethers. The alcohols differ in type, quantity and relative abundance depending upon whether their source is the asphaltene, polar or aromatic fraction. They can be detected in the form of acetates, trimethylsilylethers or, after selective reduction, as hydrocarbons, by GC analysis following chromatographic enrichment of the concentrates.

Primary *n*-alcohols are of widespread occurrence in the bitumen and can be found in the aromatics, polars, asphaltene-bound polars, and in chemically bound form in the asphaltene. They show a strong even-carbon-number preference and in the polars they are dominated by the $C_{22} > C_{28} > C_{30}$ members, Figure 12.61. The shorter-chain members from C_{10} to C_{22} can be found in the acetone extract of the asphaltene and whole series up to C_{34} is liberated in the saponification of asphaltene. The even-carbon preference is maintained in the acetone extract as well.

In the aromatic fraction, primary *n*-alcohols have been found to be chemically bound to the nondistillable portion from which they could be liberated by mild thermolysis. These primary *n*-alcohols also exhibit strong, even-carbon preference and the C_8–C_{28} series is dominated by the C_{18} member. In the polar fraction several bicyclic alcohols were detected, the C_{15} member of which was present in different isomeric forms. In the aromatic fraction, benzyl alcohol and a suite of cyclic alcohols like

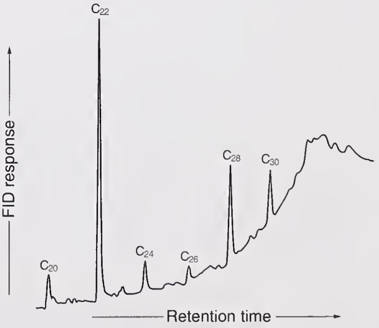

Figure 12.61 Gas chromatogram of the *n*-alcohols (in the form of their acetates) in the polar fraction of Athabasca bitumen.

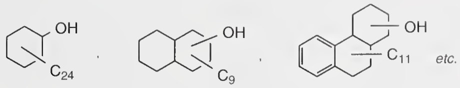

have been tentatively identified.

Among the nonsaponifiable products following saponification of asphaltene and the aromatics, several sterols and steroidols were found. The only biological alcohol positively identified in the polars is β-sitosterol:

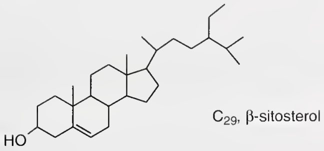

From the aromatic fraction, stigmasterol and sitosterol were tentatively identified and a C_{29} ($Z = -12$) alcohol was detected.

The most abundant and, also for geochemical information content, significant type of alcohol in Alberta maltene is a suite of fluorenols, including fluoren-9-ol and 9-*n*-alkyl fluorene-9-ols along with their nuclear methylated derivatives, and higher condensed benzo- and dibenzo-counterparts, which are structurally related to the 9-*n*-alkyl fluorene series found in the aromatic fraction[2,30] and the 9-hydroxy- and 9-methoxy carboxylic acid series identified in the acetone extract of asphaltene.

The 9-*n*-alkyl fluorene-9-ols were isolated from Athabasca polars employing an involved chromatographic procedure.[31] The FI mass spectrum of the concentrate, Figure 12.62, reveals that it comprises a series of fluorenols with alkyl side chains ranging from C_1 up to C_{13} along with lesser quantities of benzo-, dibenzo-, cyclohexane- and bicyclohexanefluorenols. The identities of the structures were established by comparison with the properties of synthetically prepared standards using FTIR, mass spectroscopy, and retention times on three different polarity GC columns. The mass spectra shown in Figure 12.63 are straightforward and fully consistent with the structures proposed:

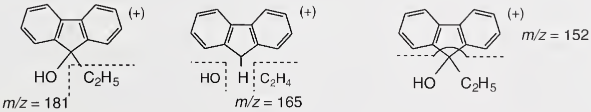

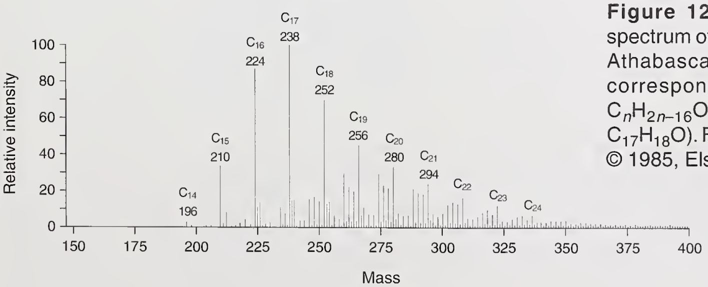

Figure 12.62 Field ionization mass spectrum of the fluorenol concentrate from Athabasca bitumen. The major peaks correspond to the elemental formula $C_nH_{2n-16}O$ (for example, $m/z = 238$ is $C_{17}H_{18}O$). From J.D. Payzant *et al.*, Ref. 31. © 1985, Elsevier Science Ltd.

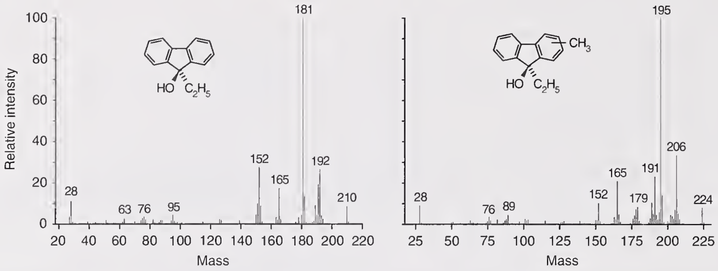

Figure 12.63 High-resolution mass spectra of two of the fluorenols in Athabasca bitumen. Peak 206 = ethylanthracene, 192 = methylanthracene and 191 = 206 –Me (*m/z* = 15). From J.D. Payzant *et al.*, Ref. 31. © 1985, Elsevier Science Ltd.

The TIC and cross-scan mass spectra in Figure 12.64 reveal that the concentration of the 9-*n*-alkyl series members declines monotonically with increasing length of the side chain from C_1 to n-C_8 and beyond, and that there are three isomeric nuclear monomethyl series showing the same trend in concentration distribution.

Between the main peaks of the alkylfluorenols in the FI mass spectrum in Figure 12.62 there are weaker signals which signify the presence of benzofluorenols, cyclohexanefluorenols, dicyclohexanefluorenols and even smaller quantities of dibenzofluorenols with series formulas

- $C_nH_{2n-16}O$ fluorenols
- $C_nH_{2n-22}O$ benzofluorenols
- $C_nH_{2n-28}O$ dibenzofluorenols
- $C_nH_{2n-18}O$ cyclohexanefluorenols
- $C_nH_{2n-20}O$ bicyclohexanefluorenols

Fluorenols, benzofluorenols and dibenzofluorenols were also identified in the acetone extract of asphaltene where the following compounds have been detected:

	No. of species	*x+y* in side chain	MW
fluorenols			
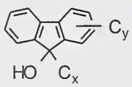		6	266.3822
		7	280.409
benzofluorenols			
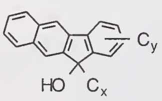	3	1	246.308
	2	2	260.3294
	1	3	274.3616
	1	5	302.4152
dibenzofluorenols			
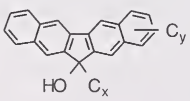	2	0	282.341
	2	1	296.3678
	1	4	338.4482

Here, as with the parent hydrocarbons, we observe a selectivity in the pattern of substitution: the alkyl group is *normal* alkyl and it is attached to the same carbon, namely, C–9. The significance of this structural specificity and the origin and geochemistry of the fluorene structure will be discussed in Chapter 13. As mentioned before, these fluorenols must have been produced from the parent hydrocarbons by *in-situ* oxidation processes.

2.3 Nitrogen-containing components

In Alberta bitumens, nitrogen is the least abundant of the heteroatoms, with a concentration range of 0.3–0.7%. In general, the nitrogen contents of crude oils are usually low and about 90% of crudes contain less than 0.2% of nitrogen. Owing to a relative minimum in the frequency distribution, close to 0.25%, one can distinguish the high-nitrogen crude oils (N > 0.25%) from the normal, nitrogen-poor petroleums (N < 0.25%). The highest concentrations of nitrogen are found in oil sand bitumens (*e.g.*, Alberta 0.7%, Asphalt Ridge 1.14%) and in certain crude oils from California (*e.g.*, Wilmington 0.65% and Gato Ridge 0.75%).

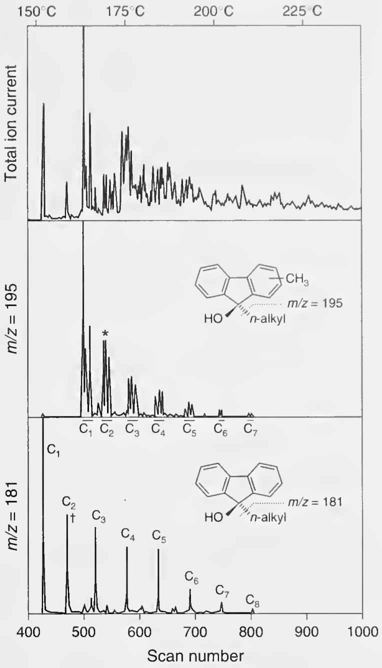

Figure 12.64 GC–MS data for the fluorenol concentrate from Athabasca bitumen. The mass spectra of the peaks labelled * and † in the middle and bottom panels are shown in Figure 12.63. From J.D. Payzant *et al.*, Ref. 31. © 1985, Elsevier Science Ltd.

As with oxygen, the concentration distribution of nitrogen in Athabasca polars varies with MW: the highest nitrogen contents obtain in the lowest MW GPC polar subfractions (Polar I–5, I–6 and II–6, Table 12.2). Of the bitumen class fractions, the highest nitrogen content obtains for asphaltene, followed by the polars, maltene and oils (saturates + aromatics). For Athabasca bitumen one reported concentration distribution for nitrogen was: asphaltene, 1.26%; maltene, 0.50%; polars, 0.58%, and oils, 0.22%. When a Cold Lake polar fraction was separated by ion exchange chromatography, the nitrogen content was higher in the basic than in the acidic fractions and tended to increase progressively with polarity and MW.[32] Upon ion exchange chromatographic fractionation of Athabasca maltene, polars, oils and asphaltene, the most nitrogen-enriched fractions were persistently the most basic fractions isolated.

Ever since Treibs' discovery of petroporphyrins in 1934,[33] nitrogen-containing compounds have played a historic role in the evolution of the theory of petroleum formation and have since been the subject of continuing interest. This interest is due to their geochemical significance, of their large structural variety widespread occurrence in petroleum and other fossil fuels and, from the refiner's point of view, to their impact on refining technology and product quality as well as toxicities.

Nitrogen compounds have the potential for providing information with regard to the source material of petroleum and act as indicators of thermal maturity, the migrational and water washing history of the crude, in addition to providing a tool for oil correlation. Even at low concentrations, nitrogen compounds can adversely affect the quality of untreated but distilled liquid fuels, causing gum and tar formation, the source of which is believed to be polymerized pyrrole. The elimination of nitrogen-containing compounds requires more severe hydrogenation conditions than for compounds containing sulfur or oxygen and therefore the concentrations and types of nitrogen compounds present determine the degree of difficulty of refining. The reason why carbon-bound nitrogen is more difficult to remove from the crude lies in the strength of the C–N bond and the inherent chemical reactivity of nitrogen. Oxygen is present in bitumen primarily as $-CO_2H$, $>C{=}O$ and $-C{-}OH$ functionalities, and since $-CO_2H$ and $>C{=}O$ are good leaving groups, moderate heating readily extrudes CO_2 and CO. Also, alcohols can eliminate water to yield alkenes. Sulfur, being a third-row atom, forms a weaker bond with carbon than either oxygen or nitrogen, has larger and more polarizable valence orbitals and, owing to the availability of low-lying *d*-orbitals, has a tendency to undergo valence shell expansion resulting in facile displacement reactions with hydrogen atoms and free radicals, *e.g.*,

$$R{-}SH + H\bullet \longrightarrow R\bullet + H_2S$$

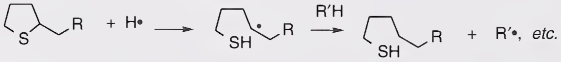

In contrast, the C–N bond is strong, the nitrogen atom does not readily undergo valence shell expansion and, in turn, therefore displacement reactions; moreover, being trivalent, one more bond has to be broken for removal in the form of NH_3 than for the case of divalent oxygen or sulfur atoms. Also, nitrogen can participate in an aromatic ring system and form highly stable aromatic molecules more efficiently than either oxygen or sulfur.

Basic, pyridinic compounds have a tendency to react with acid catalysts, poisoning catalytic sites, and adversely affecting catalyst performance. Thus, in the manufacture of high-octane gasoline, in order to protect the acid catalyst used, the nitrogen compounds are generally removed by catalytic hydrogenation prior to catalytic cracking.

Another undesirable aspect of the nitrogen compounds is related to the mutagenic activity of some of the carbazole derivatives.

The nitrogen-containing compounds present in bitumens may be classified according to MW. The lower-MW members are volatile and amenable to GC and MS investigations while the higher-MW members, like those in the asphaltenes, consist of complex polyaromatic structures involving other heteroatoms as well. The majority of the low- and medium-MW nitrogen compounds identified consist of alkyl-substituted mono- through tetraaromatic mononitrogen azaarenes involving pyridine and pyrrole derivatives, some of them with one or two additional condensed cyclohexane rings. The pyridine-based alkyl azaarenes are weak bases with pK_a values from 7 to 9; the alkylindoles, some alkylacridines, amides and alkylhydroxypyridines are very weak bases with pK_a values from 2 to 7; and the carbazoles and some of the alkylindoles and amides are nonbasic. All crudes and bitumens also contain small concentrations of metalloporphyrins.

In the silica gel chromatography of nitrogen compounds, the order of elution follows the order of the basicity of the molecules: the least basic, neutral molecules elute first. Accordingly, in the fractionation of the polars in the FIMS study of the Athabasca maltene, the alkylcarbazoles, alkylcyclohexan-, benzo-, dicyclohexan- and cyclohexanbenzocarbazoles eluted first from the column (Figures 12.6–12.8). The basic nitrogen compounds, pyridines, quinolines, *etc.*, elute later, and in effect the most basic portion of the nitrogen compounds, accounting for about 22–25% of the nitrogen in the maltene, was reported[21] not to elute at all with the solvents commonly used for elution in silica gel chromatography. This portion of the nitrogen compounds can be recovered only with elution using hot pyridine.

In subfraction 6 of the silica gel fractionation (Figure 12.8) the relative importance of the five series of carbazoles represented by the series formula $C_nH_{2n-15}N$, $C_nH_{2n-17}N$, $C_nH_{2n-19}N$, $C_nH_{2n-21}N$, and $C_nH_{2n-23}N$, as can be seen from Figure 12.9, is in the order: carbazole (3 rings) > benzo- (4 rings) > cyclohexan- (4 rings) > cyclohexanbenzo- (5 rings) > dicyclohexan-carbazoles (5 rings). Thus, by ring number, the order is 3 > 4 > 5. As for aromaticity, the ones that are more aromatized within a given ring number are present in slightly greater quantities. The distribution curve for each of the five series exhibits a maximum occurring at carbon numbers for the various Z series as follows:

Z	-15	-17	-21	-19	-23
n	17	20	21	22	25

All these features in the distribution of the series could be rationalized if it were assumed that the additional rings in the higher cyclic carbazoles were formed by the cyclization and subsequent aromatization of the alkyl side chains in the alkyl carbazoles. Such processes have been suggested to explain the presence of benzo[*h*]quinolines in petroleum,[34,35] presumably from the cyclization and aromatization of 8-alkylquinolines and, in turn, benzo[*h*]phenanthridine from benzo[*h*]quinolines.

The aggregate amount of carbazoles present in Athabasca maltene can be estimated from the FI mass spectra to be ≥ 1.6% of the maltene.

Indoles,

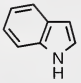

$C_nH_{2n-9}N$

have not been specifically detected in the FIMS study; however, it has to be kept in mind that some of the Z-series detected and identified coincide with the indole series (*e.g.*, $C_nH_{2n-23}N$ and $C_{n-1}H_{2(n-1)-9}N$) and therefore small amounts of alkylindoles and cyclohexanindoles, *etc.*, could have been present in the samples analyzed.

2.3.1 Carbazoles in the acetone extract of asphaltene

The acetone extract of asphaltene is rich in polar materials and, among them, nitrogen-containing molecules. The carbazoles in the acetone extract of Athabasca asphaltene[36] have been isolated by a series of chromatographic steps, Figure 12.51, involving GPC–silica gel chromatography (fraction A) followed by alumina chromatography and have then been subjected to elemental, FTIR and GC–MS analyses. The composition of the GPC fractions shows a clear, gradual trend with MW in that the oxygen and nitrogen contents increase whereas the sulfur content and saturation (H/C ratio) decrease with decreasing MW, Figure 12.51. Only fraction AC-5, which constituted approximately 20% of the acetone extract (or 3.1% of the asphaltene) appeared to be sufficiently volatile to be examined by capillary GC–MS. This fraction was chromatographed on silica gel to give subfractions AC–5–1 to AC–5–12, using a series of solvent polarities. Elemental analysis showed that subfractions AC–5–3, AC–5–4 and AC–5–7 were enriched in nitrogen, containing over 2%. Fraction AC–5–7 was found to contain porphyrins and its composition will be discussed in a later section. The combined fractions AC–5–3 and AC–5–4 constitute fraction A in Figure 12.51, which was rechromatographed on alumina. The IR spectra of the nitrogen-enriched alumina separated subfractions shown in Figure 12.65 exhibit distinct absorption bands at 3480 and 1325 cm^{-1}, assigned for the most

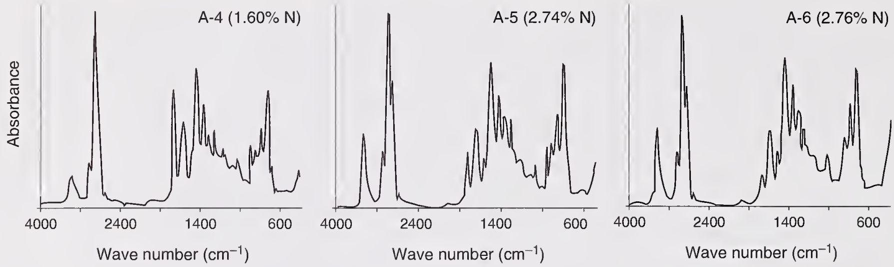

Figure 12.65 Infrared spectra of nitrogen-enriched fractions A–4 to A–6 of the asphaltene acetone extract.[36]

part to the stretching vibrations of the pyrrole type N–H and C–N bonds. In addition, strong absorption bands at 3030, 1600, 860, 800 and 750 cm^{-1}, characteristic of aromatic compounds, were present. The particularly strong absorption at 750 cm^{-1} indicated that the aromatic rings were not highly substituted.

Fractions A–4 through A–6 were examined by GC–MS and the ion peaks associated with nitrogen compounds were cross scanned and also identified by high-resolution EIMS.

The TIC chromatogram of Fraction A–4 is shown in Figure 12.66 and the mass spectra of three of the compound groups are given in Figure 12.67. Peaks 1–4 all represent mass 223.1345 isomeric C_4 alkyl-substituted carbazoles; peaks 5–8, (mass 237.1508) and 9–12 (mass 251.1669), isomeric C_5 and C_6 substituted carbazoles, with series formula $C_nH_{2n-15}N$.

The TIC chromatogram, Figure 12.68, and the high-resolution mass spectrum of Fraction A–5 indicated that three homologous series of nitrogen-containing compounds were present. The most prominent series of peaks belong to the alkylbenzocarbazole series $C_nH_{2n-21}N$ with the largest number of isomers, eight, occurring at C_4 substitution, Table 12.15. The cross-scan mass chromatograms seen in Figure 12.69 show that peaks 27–30, 31–33 and 35–37 of Figure 12.68 belong to a series of cyclohexanbenzocarbazoles with series formula $C_nH_{2n-23}N$ in the C_{21}–C_{24} range. The remaining peaks belong to the dibenzocarbazole series, $C_nH_{2n-27}N$, with two to six carbons in the side chains.

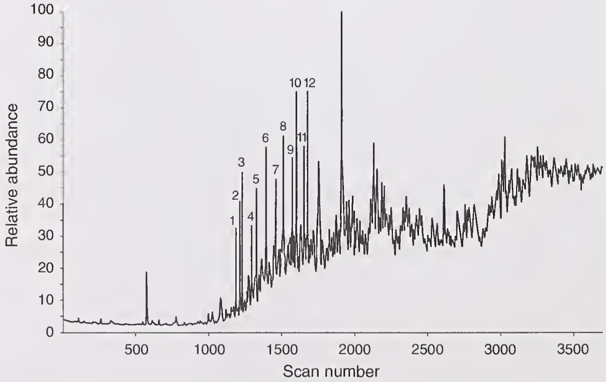

Figure 12.66 Total ion current chromatogram of Fraction A--4 of the asphaltene acetone extract.

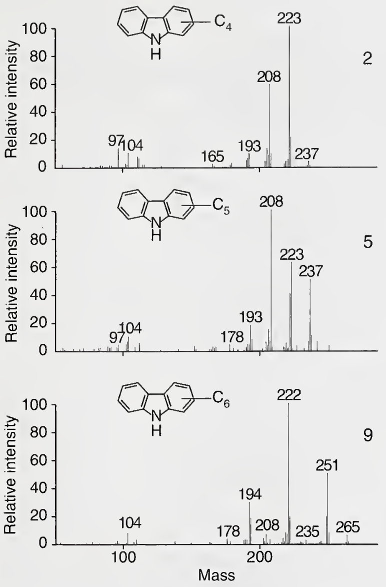

Figure 12.67 EIMS of peaks 2 ($m/z = 223$), 5 ($m/z = 237$) and 9 ($m/z = 251$) in Figure 12.66.

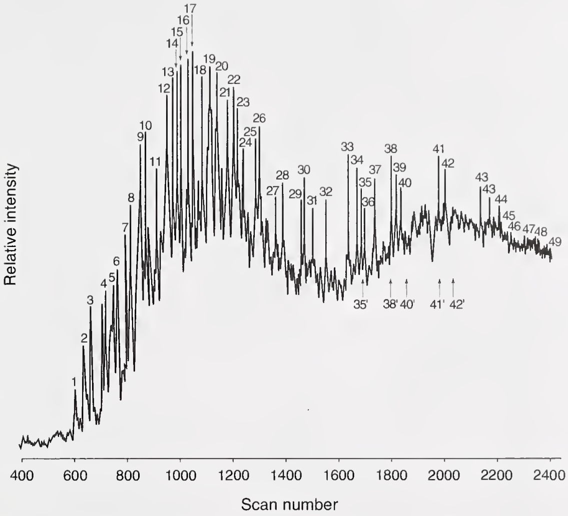

Figure 12.68 Total ion current chromatogram of Fraction A–5 of the asphaltene acetone extract. See Table 12.15 for some of the peak assignments.

The cross-scan chromatograms of fraction A–6 are shown in Figure 12.70. The peaks represent alkyldibenzocarbazoles with series formula $C_nH_{2n-27}N$ in the C_{20}–C_{24} range.

Instead of acetone extraction, the asphaltene-complexed polars can also be separated from the asphaltene by GPC on Bio-Beads SX–1 followed by GPC on Bio-Beads SX–2 and silica gel chromatography. The cross-scan mass chromatograms of one of the fractions, Figure 12.71, reveals the presence of a series of alkylbenzocarbazoles even more abundant than the one found in Fraction A–5, for example, there are 11 C_{20}, 11 C_{19} and 8 C_{18} isomeric alkylbenzocarbazoles.

The data on asphaltene-complexed carbazoles are summarized in Table 12.16. Altogether, 92 different carbazoles have been detected in the acetone extract of asphaltene. Their concentration distribution is different from that of the free carbazoles in the polar fraction and, not unexpectedly, is shifted toward the more aromatic direction. In the polar

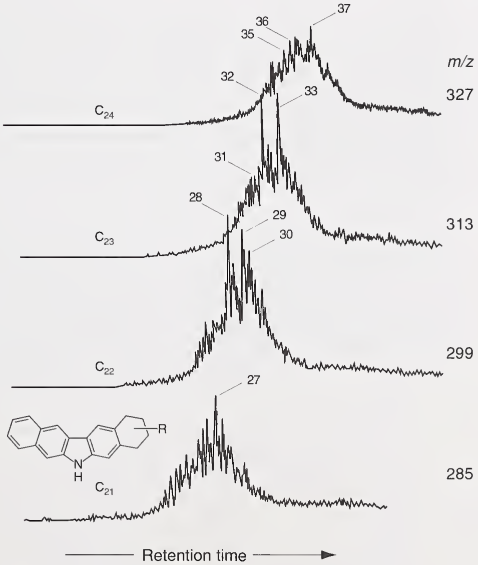

Figure 12.69 $M/z = 285$, 299, 313 and 327 cross-scan chromatograms corresponding to the cyclohexanebenzocarbazole series $C_nH_{2n-23}N$ in Fraction A–5 of the asphaltene acetone extract. The peak numbers correspond to the labeled peaks in Figure 12.68.

Table 12.15 Mass spectroscopic data for the alkylbenzocarbazole and alkyldibenzocarbazole series in chromatographic subfractions A–5 and A–6 and a GPC subfraction

Mass	R[a] = C_nH_{2n+1}	Formula	
Alkylbenzocarbazoles			
Subfraction A-5			Peak no. in Figure 12.68
245.1192	C_2H_5	$C_{18}H_{15}N$	1, 2, 3, 4[b], 5, 7
259.1354	C_3H_7	$C_{19}H_{17}N$	6, 8, 9[b], 10, 11, 12, 13
273.1513	C_4H_9	$C_{20}H_{19}N$	14, 15, 16, 17[b], 18, 19, 20, 21
287.1669	C_5H_{11}	$C_{21}H_{21}N$	22, 23[b], 24, 25, 26
301.1828	C_6H_{13}	$C_{22}H_{23}N$	34[b]
315.1977	C_7H_{15}	$C_{23}H_{25}N$	38, 39[b], 40
329.4851	C_8H_{17}	$C_{24}H_{27}N$	41, 42[b]
GPC subfraction AC–5[c]			Peak no. in Figure 12.71[c]
231	CH_3	$C_{17}H_{13}N$	1,2[b]
245	C_2H_5	$C_{18}H_{15}N$	3,4,5,6[b],7,8,9,10
259	C_3H_7	$C_{19}H_{17}N$	11,12,13,14,15[b],16,17,18,19,20,21
273	C_4H_9	$C_{20}H_{19}N$	22,23,24,25[b],26,27,28,29,30,31,34
287	C_5H_{11}	$C_{21}H_{21}N$	32,33[b],35,38,41
Alkyldibenzocarbazoles			
Subfraction A-6			Peak no. in Figure 12.70
267	H	$C_{20}H_{13}N$	1[b],1′
281	CH_3	$C_{21}H_{15}N$	2[b],3,4,5
295	C_2H_5	$C_{22}H_{17}N$	6,7[b],8,9,10
309	C_3H_7	$C_{23}H_{19}N$	11,12,13,14,15[b],16
323	C_4H_9	$C_{24}H_{21}N$	17,18[b]

[a] External to the aromatic ring. [b] Major component. [c] Not listed are the C_{22}–C_{25} members of the series, corresponding to C_6H_{13} (two isomers), C_7H_{15} (two isomers), C_8H_{17} (two isomers), and C_9H_{19} (three isomers) substituents.

Table 12.16 Distribution of carbazoles in the acetone extract of Athabasca asphaltene

Substituents	Carbazoles $C_nH_{2n-15}N$	Benzocarbazoles $C_nH_{2n-21}N$	Cyclohexanbenzocarbazoles $C_nH_{2n-23}N$	Dibenzocarbazoles $C_nH_{2n-27}N$
	Number of alkyl-substituted species			
H				2
C_1		2	4	4
C_2		8	6	5
C_3		11	4	6
C_4	4	11		2
C_5	4	5		
C_6	4	2		
C_7		3		
C_8		2		
C_9		3		
Total	12	47	14	19

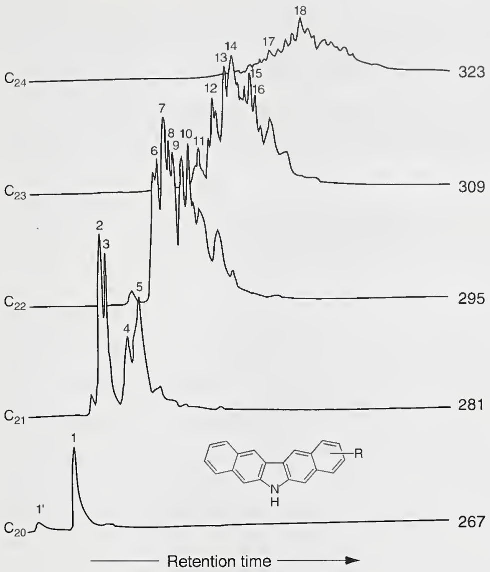

Figure 12.70 *M/z* = 267, 281, 295, 309 and 323 cross-scan chromatograms corresponding to the alkyldibenzocarbazole series $C_nH_{2n-27}N$ in Fraction A–6 of the asphaltene acetone extract. See Table 12.15 for some of the peak assignments.

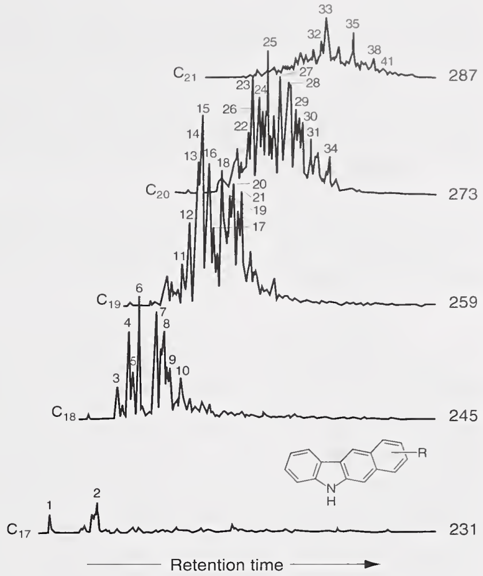

Figure 12.71 *M/z* = 231, 245, 259, 273 and 287 cross-scan chromatograms corresponding to the alkylbenzocarbazole series $C_nH_{2n-21}N$ present in a chromatographic subfraction of GPC-separated asphaltene. See Table 12.15 for some of the peak assignments.

fraction the most abundant free carbazole species are the alkylcarbazoles (Figure 12.9) while in the asphaltene-complexed carbazoles, the most abundant are the alkylbenzocarbazole species. Further differences are the presence of C_2–C_7 alkylcyclohexan- and C_1–C_5 alkyldicyclohexancarbazoles in the polar fraction and their nonappearance in the asphaltene-complexed material.

Over a hundred different carbazole species have been detected by GC–MS. Their mass spectra have been determined, but the exact structure has not been established for any of them. The number of isomers varies with the carbazole species and with the number of carbon atoms in the alkyl side chains. The largest number of isomers, 11, was found in the C_3- and C_4-substituted benzocarbazole species where the concentration maximum occurred. If it is assumed that the dibenzocarbazoles and the cyclohexanbenzocarbazoles were formed by the cyclization of the C_5 and higher alkyl benzocarbazoles, for example by the reactions

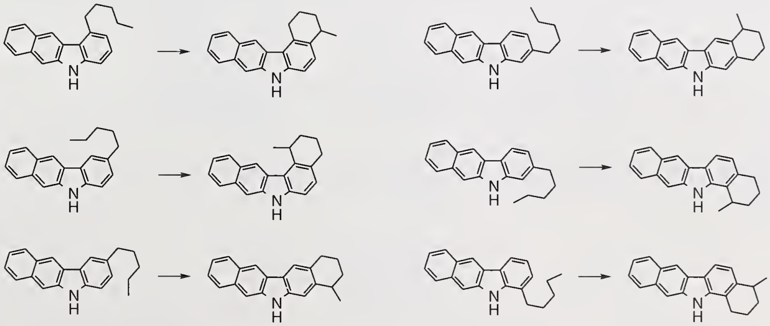

then the drop from 11 to 5 in the number of isomers in going from C_4- to C_5-alkylbenzocarbazole may be due to the cyclization reactions producing an additional ring in the molecule in the form of six isomeric C_1-alkylcyclohexanbenzo- or dibenzocarbazoles. If this is so, then the C_4-alkyl benzocarbazoles would not seem to have any propensity for cyclization (which would involve the terminal methyl group of the *n*-butyl side chain), but the C_5, C_6 and C_7 alkyl side chains would readily cyclize.

The total concentration of the carbazole species (including the carbazoles complexed to asphaltene) may be estimated, from the combined FIMS and GC–MS results, to lie in the range 2.5–3.0% of Athabasca maltene.

From a study[37] of the distribution of carbazoles in hydrocracked Athabasca gas oil using ^{13}C NMR, GC–FTIR and FIMS methods, it was concluded that alkylcarbazoles substituted with up to 15 carbons were the major series of nitrogen compounds present. The important species were the mono-, di- and trialkyl-substituted carbazoles, with substitution in the 4-position dominating. This was attributed to the high reactivity of the 1-substituted isomers which were absent in the hydrocracked product and had presumably been removed in the hydrocracking process. To explain the apparent resistance of the 4-alkyl homologs towards destruction, it was considered that during the hydrocracking process these isomers could have undergone parallel destruction and formation via the opening of condensed saturated rings, *e.g.*,

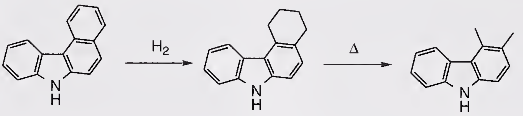

The absence of aromatic and naphthenic condensed carbazoles (which are abundant in the maltene) in the hydrocracked product is an indication of the higher reactivity of these molecules (because of their less aromatic character and the ease of benzylic carbon–carbon cleavage in the condensed naphthenic rings) and their consequent efficient removal in the hydrocracking operation.

2.3.2 Basic nitrogen compounds

Basic nitrogen compounds, or azaarenes, together with accompanying polyaromatic hydrocarbons, are ubiquitous in nature and occur in petroleum[34,35,38–40] although usually in less than 0.5% concentration. The number of aromatic rings in the petroleum-based azaaromatics identified varies from one to four and they are usually alkyl-substituted with up to nine carbon atoms in the side chain. Few azaarenes have been specifically identified, among which are the following:

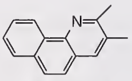

2,3-dimethylbenzo-[*h*]quinoline[41]

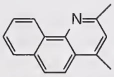

2,4-dimethylbenzo-[*h*]quinoline[41]

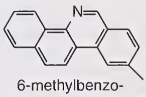

6-methylbenzo-[*c*]phenanthridine[34]

The substitution pattern reported for quinoline featured the presence of a methyl group at position 2 in every case

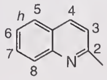

and the presence of other alkyl groups at positions 3, 4 and 8, but none at 5, 6 or 7. Alkyl groups larger than ethyl were found only at position 8. The distribution was found to be dominated by methyl and 8-isopropyl substitution.[39]

Of the triaromatic nitrogen bases identified, all have the benzo[*h*]quinoline structure and the parent molecule, as for all azaarenes, is either absent or present in only very small concentrations.

The basic nitrogen compounds in Athabasca and Cold Lake maltenes were examined using $CuCl_2 \cdot 2H_2O$ complexation for isolation. Two preliminary enrichment methods were applied, one involving deactivated basic alumina chromatography and the other, $TiCl_4$ complexation, Figure 12.72.

The fractionation results using the former method are given in Table 12.17 and show a basic nitrogen compound concentrate comprising 0.5% of the maltene for both the Athabasca and Cold Lake samples and, for the Athabasca concentrate, a nitrogen content of 1.72% corresponding to about 0.15% basic nitrogen compounds. The gas chromatogram of the Athabasca material is shown in Figure 12.73 and the tentative peak assignments are listed in Table 12.18. Three series of nitrogen bases, alkylpyridines, alkylquinolines and alkylbenzoquinolines

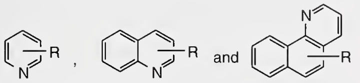

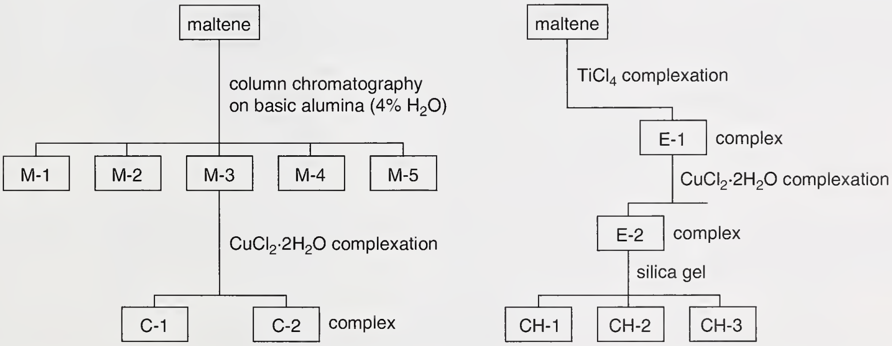
maltene
column chromatography
on basic alumina (4% H2O)
M-1
M-2
M-3
M-4
M-5
CuCl2·2H2O complexation
C-1
C-2
complex
maltene
TiCl4 complexation
E-1
complex
CuCl2·2H2O complexation
E-2
complex
silica gel
CH-1
CH-2
CH-3

Figure 12.72 Two schemes for the separation of the basic nitrogen compounds in Athabasca maltene.

Table 12.17 $CuCl_2 \cdot 2H_2O$ complexation of basic nitrogen fractions from Athabasca and Cold Lake maltenes

Fraction	Wt% of maltene	Elemental analysis (wt %)				
		C	H	N	O	S
Athabasca						
C–1(NB)[a]	21.7	82.69	9.16	0.72	1.19	6.24
C–2(B)[b]	0.51	83.13	8.48	1.72	1.45	5.22
Cold Lake						
C–1(NB)	17.7					
C–2(B)	0.50					

[a] NB = nonbasic.[b] B = basic.

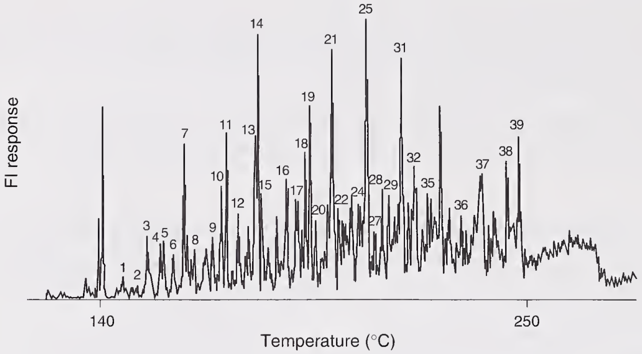

Figure 12.73 Gas chromatogram of the complexed Athabasca residue C–2 (Figure 12.72). The peak assignments are listed in Table 12.18.

with series formula $C_nH_{2n-5}N$, $C_nH_{2n-11}N$, and $C_nH_{2n-17}N$ were identified. Except for a few compounds that have an isopropyl, *n*-propyl or ethyl group, most of the polyalkylated nitrogen bases exhibit only a parent ion and a base peak in their mass spectrum, as illustrated by the example of the spectra in Figure 12.74. Nonetheless, in some cases it is still possible to extract information from the fragmentation pattern with regard to the nature of the alkyl substituents and their location on the ring structure.

In Figure 12.74b, for example, the C_6-alkylquinoline isomer exhibits as its dominant fragmentation the characteristic benzylic cleavage of an ethyl substituent losing a methyl group. Alkyl groups attached to position 8 of quinoline, on the other hand, undergo a unique fragmentation[42] involving the loss of a hydrogen atom and the formation of a five-membered ring:

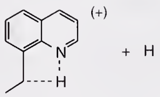

An example of this is seen in Figure 12.74c where the ethyl group in the 8-ethyl-C_4-alkylquinoline undergoes this type of process:

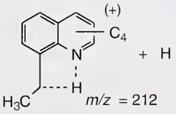

A similar fragmentation pattern appears in the case of the C_5-alkylquinoline, the mass spectrum of which, Figure 12.74a, indicates the presence of an isopropyl group in position 8 (8-isopropyldimethylquinoline).

In addition to the three series of aromatic nitrogen bases with *z* values of –5, –11 and –17 and the single C_{15} species with $z = -15$ assigned to a C_3-alkylazafluorene, other short series of nitrogen bases were detected when, instead of alumina, a silica gel column was employed for the enrichment prior to $CuCl_2 \cdot 2H_2O$ complexation. These included C_2-, C_3- and C_4-alkylazapyrenes,

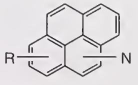

Table 12.18 Basic nitrogen compounds tentatively identified in Athabasca maltene following chromatographic separation and $CuCl_2{\cdot}2H_2O$ complexation[43]

Peak number[a]	Formula	Structural Assignment
1	$C_{14}H_{17}N$	8-isopropyldimethylquinoline
2	$C_{14}H_{23}N$	C_9-alkylpyridine
3	$C_{15}H_{25}N$	C_{10}-alkylpyridine
4	$C_{15}H_{19}N$	C_6-alkylquinoline
5	$C_{15}H_{19}N$	C_6-alkylquinoline
6	$C_{15}H_{19}N$	ethyl-C_4-alkylquinoline
7	$C_{15}H_{19}N$	8-ethyl-C_4-alkylquinoline
8	$C_{15}H_{19}N$	8-isopropyl-2,3,4-trimethylquinoline
9	$C_{16}H_{21}N$	8-isopropyltetramethylquinoline
10	$C_{16}H_{21}N$	C_7-alkylquinoline
11	$C_{15}H_{15}N$	C_3-alkylazafluorene
12	$C_{15}H_{19}N$	C_6-alkylquinoline
13	$C_{15}H_{13}N$	C_2-alkylbenzoquinoline
14	$C_{15}H_{13}N$	C_2-alkylbenzoquinoline
15	$C_{15}H_{13}N$	C_2-alkylbenzoquinoline
16	$C_{16}H_{15}N$	C_3-alkylbenzoquinoline
17	$C_{16}H_{15}N$	ethylmethylbenzoquinoline
18	$C_{16}H_{15}N$	C_3-alkylbenzoquinoline
19	$C_{16}H_{15}N$	C_3-alkylbenzoquinoline
20	$C_{17}H_{23}N$	C_8-alkylquinoline
21	$C_{16}H_{27}N$	C_{11}-alkylpyridine
22	$C_{17}H_{17}N$	ethyl-C_2-alkylbenzoquinoline
23	$C_{18}H_{19}N$	C_5-alkylbenzoquinoline
24	$C_{18}H_{19}N$	C_5-alkylbenzoquinoline
25	$C_{17}H_{29}N$	C_{12}-alkylpyridine
26	$C_{17}H_{29}N$	C_{12}-alkylpyridine
27	$C_{17}H_{29}N$	C_{12}-alkylpyridine
28	$C_{18}H_{31}N$	C_{13}-alkylpyridine
29	$C_{18}H_{31}N$	C_{13}-alkylpyridine
30	$C_{18}H_{31}N$	C_{13}-alkylpyridine
31	$C_{18}H_{31}N$	C_{13}-alkylpyridine
32	$C_{18}H_{31}N$	C_{13}-alkylpyridine
33	$C_{19}H_{27}N$	C_{10}-alkylquinoline
34	$C_{19}H_{33}N$	C_{14}-alkylpyridine
35	$C_{19}H_{33}N$	C_{14}-alkylpyridine
36	$C_{19}H_{21}N$	C_6-alkylbenzoquinoline
37	$C_{20}H_{23}N$	C_7-alkylbenzoquinoline
38	$C_{21}H_{25}N$	C_8-alkylbenzoquinoline
39	$C_{21}H_{25}N$	C_8-alkylbenzoquinoline

[a] Peak numbers correspond to those in Figure 12.73. Also detected were: C_0-tetrahydrodibenzoquinoline, C_1-alkyltetrahydrobenzoquinoline, C_2-alkyltetrahydrodibenzoquinoline, C_3-alkylazafluoranthrene (ethyl substituent) and C_6-alkyloctahydrobenzoquinoline.

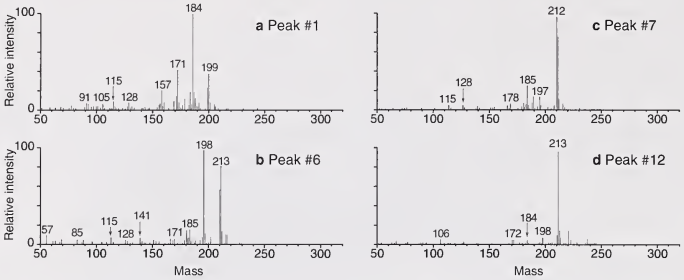

Figure 12.74 EIMS of peaks 1, 6, 7 and 12 of Figure 12.73. 1 = 8-isopropyl-dimethyl- quinoline; 6 = ethyl-C_4-alkylquinoline; 7 = 8-ethyl-C_4-alkylquinoline; 12 = C_6-alkylquinoline.

or azafluoranthrenes ($Z = -21$),

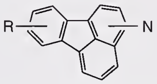

C_0-, C_1-, C_2- and C_3-alkyltetrahydrodibenzoquinolines ($Z = -19$),

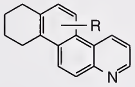

and C_1-, C_2-, C_3-and C_4-alkyldibenzoquinolines ($Z = -23$):

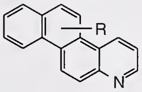

Cross-scan mass chromatograms for these azaarenes are shown in Figure 12.75 from which it is seen that the dominant members in their respective series are the C_3-alkylazapyrenes, C_0-alkyltetrahydrodibenzoquinolines and the C_3-alkyldibenzoquinolines.[43a]

The azaarenes from the Cold Lake maltene were preconcentrated prior to $CuCl_2 \cdot 2H_2O$ treatment with $TiCl_4$ complexation. The individual bases detected with the GC–MS technique, Table 12.19, are also present in Athabasca maltene, but here they are restricted to the alkylpyridine and alkylquinoline series; the alkylbenzo- and alkyldibenzoquinoline series, with one exception, were not detected.

When the $TiCl_4/CuCl_2 \cdot 2H_2O$-separated nitrogen bases from Athabasca maltene were subjected to silica gel chromatographic separation into three fractions according to polarity, the first-eluting, least-polar fraction consisted of alkylpyridines, followed, in turn, by alkylbenzo-quinolines and, the most polar fraction, alkylquinolines, Figure 12.72 and Table 12.20. This elution order probably represents the relative basicities of the fractions, according to which the weakest bases are the pyridines and the strongest, the quinolines. The C_7-alkylquinoline and the ethylmethylbenzoquinoline which eluted with the pyridines are probably sterically hindered around the nitrogen and thus are less strongly adsorbed onto the chromatographic column.[44]

Alkylquinolines were also detected in Athabasca maltene by FIMS. Here, the series of alkylquinolines starts at m/z = 227, corresponding to $C_{16}H_{21}N$, a C_7-alkylquinoline, and

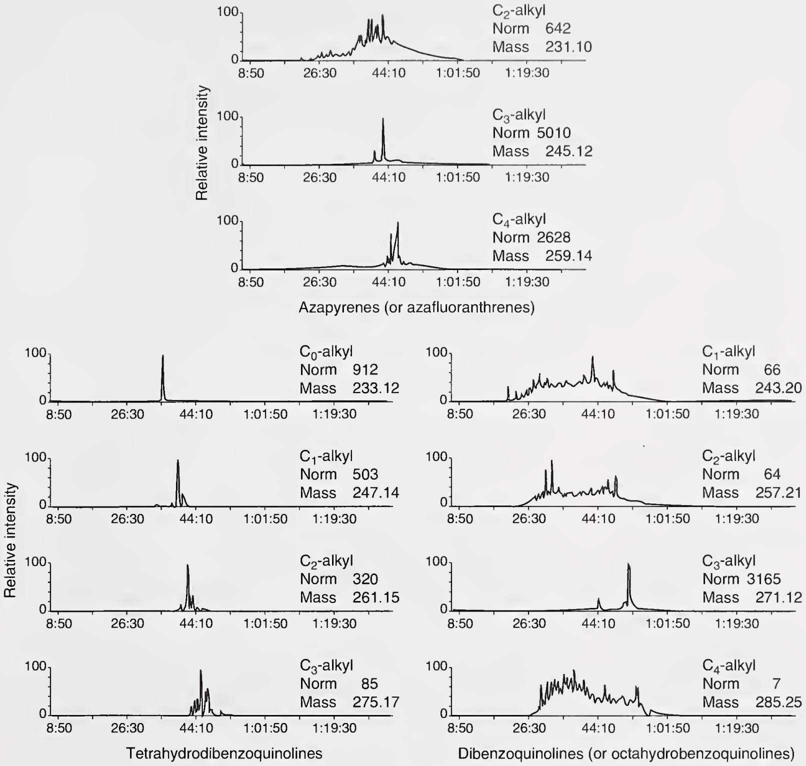

Figure 12.75 Cross-scan chromatograms of the molecular ions of some of the basic nitrogen compounds in Athabasca maltene.[43]

Table 12.19 Basic nitrogen compounds identified in Cold Lake maltene following $TiCl_4$ and $CuCl_2 \cdot 2H_2O$ complexations[43]

Formula	Structural Assignment
$C_{14}H_{17}N$	8-isopropyldimethylquinoline (two isomers)
$C_{15}H_{19}N$	8-isopropyl-2,3,4-trimethylquinoline
$C_{16}H_{21}N$	8-isopropyltetramethylquinoline (three isomers)
$C_{17}H_{23}N$	C_8-alkylquinoline (three isomers)
$C_{18}H_{25}N$	C_9-alkylquinoline
$C_{16}H_{15}N$	C_3-alkylbenzoquinoline
$C_{16}H_{21}N$	C_7-alkylquinoline
$C_{16}H_{27}N$	C_{11}-pyridine
$C_{17}H_{29}N$	C_{12}-pyridine (two isomers)
$C_{18}H_{31}N$	C_{13}-pyridine
$C_{19}H_{27}N$	C_{10}-alkylquinoline
$C_{19}H_{33}N$	C_{14}-pyridine

Table 12.20 Basic nitrogen compounds in Athabasca maltene following $TiCl_4$ and $CuCl_2 \cdot 2H_2O$ complexations and silica gel chromatography of the basic nitrogen residue[43]

Fraction	Formula	Structural Assignment
CH–1	$C_{16}H_{21}N$	C_7-alkylquinoline
	$C_{16}H_{15}N$	ethylmethylbenzoquinoline
	$C_{16}H_{27}N$	C_{11}-alkylpyridine
	$C_{17}H_{29}N$	C_{12}-alkylpyridine
	$C_{18}H_{31}N$	C_{13}-alkylpyridine
	$C_{19}H_{33}N$	C_{14}-alkylpyridine
CH–2	$C_{14}H_{11}N$	C_1-alkylbenzoquinoline
	$C_{15}H_{15}N$	C_3-alkylcyclopentenylbenzoquinoline
	$C_{15}H_{13}N$	C_2-alkylbenzoquinoline (two isomers)
	$C_{16}H_{15}N$	ethyl-methylbenzoquinoline
	$C_{16}H_{15}N$	C_3-alkylbenzoquinoline
CH–3	$C_{14}H_{17}N$	8-isopropyl-2,4-dimethylquinoline
	$C_{14}H_{17}N$	8-ethyl-C_3-alkylquinoline
	$C_{15}H_{19}N$	8-isopropyl-2,3,4-trimethylquinoline
	$C_{15}H_{19}N$	8-ethyl-C_4-alkylquinoline
	$C_{15}H_{19}N$	8-isopropyltrimethylquinoline
	$C_{16}H_{21}N$	8-isopropyltetramethylquinoline(two isomers)
	$C_{17}H_{23}N$	8-isopropyl-C_5-alkylquinoline

continues at m/z = 241, 255, 269, 283, 297...395, *etc.*, corresponding to extended homologs up to C_{27}. Along with the alkylquinolines, a series of $C_nH_{2n+z}N$ with $z = -13, -15, -17, -19, -21, -23$ compounds are also present with maximum concentrations at m/z = 267, 321, 333, 345, 371, 383. These peaks correspond to the following compound types:

Series formula	Carbon range	Structure considered
$C_nH_{2n-11}N$	C_{16}–C_{27}	quinoline
$C_nH_{2n-13}N$	C_{17}–C_{28}	tetrahydrobenzoquinoline
$C_nH_{2n-15}N$	C_{17}–C_{28}	azafluorene, octahydrodibenzoquinoline
$C_nH_{2n-17}N$	C_{18}–C_{28}	azaphenanthrene
$C_nH_{2n-19}N$	C_{17}–C_{28}	tetrahydrodibenzoquinoline
$C_nH_{2n-21}N$	C_{18}–C_{28}	azapyrene, azafluoranthrene
$C_nH_{2n-23}N$	C_{18}–C_{28}	dibenzoquinoline

Comparison of the data at hand reveals that the fraction of azaarenes isolated by complexation is depleted in the higher-MW members of the series while the silica gel-separated fraction appears to have lost its low-MW members. Thus, the concentration distribution of azaarenes can be distorted by the method employed for their separation and therefore this aspect of the published material on azaarenes should be viewed with caution.

FIMS studies also showed the presence of alkylhydroxyquinolines or alkylquinolones,

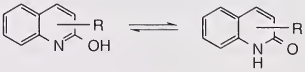

as the only series with an additional heteroatom. These series of compounds, eluting with the sulfoxides on a silica gel column, were detected in the residue of the cyclic sulfoxides of Athabasca resins after $LiAlH_4$ reduction (Figure 12.19). The IR spectrum of the fraction features a strong absorption at 1644 cm^{-1} owing to the carbonyl stretching vibration and weak absorptions at 1100 and 1040 cm^{-1}, the latter being due to the sulfoxides. The FIMS spectrum of the quinolone concentrate isolated by chromatographic and chemical methods is shown in Figure 12.76. This spectrum, like that of the azaarenes, is dominated by the odd-mass-numbered peaks; the minor, even-mass-numbered peaks are due to cyclic terpenoid sulfoxides. It should be noted here that the relative amounts of quinolines and azaarenes may vary abruptly with depth of burial even within the same deposit. For example, a maltene sample from the Syncrude quarry at a depth of 18 m below the surface which had been exposed to air was found to contain only small quantities of azaarenes or quinolones relative to fluorenols or sulfoxides, compared to another maltene sample from the same quarry but at a depth of 32 m, which had been protected from exposure to air.

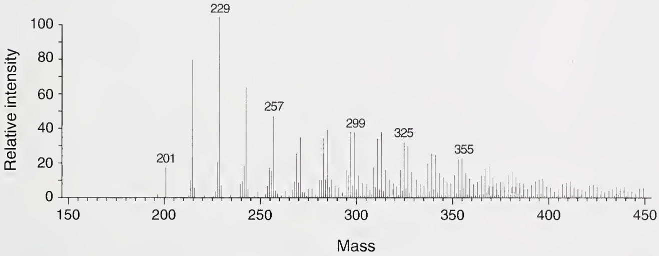

Figure 12.76 Field ionization mass spectrum of quinolones and related compounds in Athabasca maltene. This series elutes with the residue of the cyclic sulfoxides after $LiAlH_4$ reduction (*cf.* Figure 12.19).

The maximum concentration in the quinolone series occurs at *m/z* = 229, corresponding to the structure

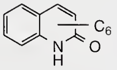

$C_{15}H_{19}NO$; $Z = -11$.

The length of the alkyl side chain in this series varies from C_4 to C_{21}. From *m/z* = 243 on, other major odd-mass-numbered peaks become apparent, the largest of which are two mass units less than the quinolone peaks, *e.g.*, *m/z* = 241, 255, 269, 283, *etc.* These could be either quinolones[44] with one condensed naphthenic ring, *e.g.*,

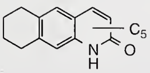

$C_{18}H_{23}NO$; $Z = -13$

with *m/z* = 269, or azadibenzothiophenes

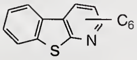

$C_{17}H_{19}NS$; $Z = -15$

with *m/z* = 269 as well. It is probable that both of these classes of compounds are present. The maximum concentration in these series occurs at *m/z* = 297. Beyond *m/z* = 250, peaks can be seen at every odd mass number throughout the spectrum (up to 450 daltons). The series of peaks immediately to the right of the quinolone peaks at two mass units higher could be dibenzo derivatives of the quinolone series or azadibenzothiophenes. Alternatively, it is possible that these series of peaks are at least partly due to thioquinolones *e.g.*

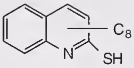

$C_{17}H_{23}NS$; $Z = -11$

with *m/z* = 273. The maximum concentration in this series is found around *m/z* = 315. Both thioquinolones and azadibenzothiophenes have been reported on various occasions to be present in crude oils, bitumens, shales, *etc.*[45]

All nitrogen base compound types found in Alberta maltenes have been reported to be present in other bitumens and crude oils from a variety of sources and, as in Alberta maltenes, the aggregate amount of pyridinic (basic) nitrogen is always less than the amount of pyrrolic (nonbasic) nitrogen, together amounting to about 18–20% of the total nitrogen, regardless of the source of the oil.

Utah (Northwest Asphalt Ridge) bitumen and produced oils, for example, have been reported[46] to contain pyridine-based alkylaromatics in the same Z-value range, from −5 to −23, as found in Athabasca and Cold Lake bitumens. Also detected were *n*-alkylcarbazoles, alkylindoles, alkylhydroxypyridines, amides, alkylcarboxamides and traces of alkylamines.

Like aromatic nitrogen molecules in general, alkylpyridines and their aromatic and naphthenic condensed derivatives are highly stable compounds and are quite resistant to catalytic hydrodenitrogenation. ^{1}H and ^{13}C NMR, IR and MS studies[47] have revealed that pyridine bases comprise a sizeable fraction of the residual nitrogen bases in synthetic crude oil produced from the upgrading of Athabasca bitumen. These pyridine bases—mostly pyridine and quinoline derivatives—possess a less aromatic and more naphthenic condensed character and they are more alkyl substituted than their counterparts in the original maltene. Evidently, a fraction of the pyridine bases survives the coking step, presumably with somewhat shortened side chains and with some of the naphthenic rings opened, and, as it turns out, the fate of this fraction during subsequent hydrodenitrogenation depends on the position of the alkyl substituents in the molecule. Thus, if alkyl substituents are absent in the hetero-ring, that is, in the 2-, 3- and 4-positions of quinoline, then this ring is the one that is hydrogenated. Accordingly, unsubstituted quinoline has been reported[48] to yield 100% 1,2,3,4-tetrahydroquinoline on catalytic hydrogenation:

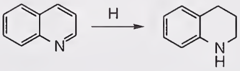

On the other hand, if the hetero-ring is alkyl substituted then it is the benzene ring of the quinoline that is preferentially hydrogenated. This shift in selectivity has been demonstrated with 2,4-dimethylquinoline which, on catalytic hydrodenitrogenation, yielded 80% 5,6,7,8-tetrahydroquinoline.

The naphthenic rings created by the catalytic hydrodenitrogenation of the aromatic rings can undergo ring opening creating dialkyl-substituted pyridines and quinolines

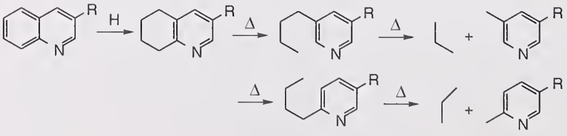

which, on being subjected to alkyl chain shortening cracking reactions, leave behind highly stable substituted pyridine and quinoline derivatives in the hydrotreated gas oil.

From ^{1}H, ^{13}C NMR, IR and MS studies of the residual basic nitrogen compounds after hydrodenitrogenation of Athabasca gas oil,[37] it was concluded that most of the residue comprised pyridine and quinoline derivatives with condensed cyclohexane rings, most of which were derived from the hydrogenation or partial hydrogenation of condensed aromatic rings. These saturated rings then underwent, to some extent, ring opening and alkyl chain shortening cracking reactions, leaving behind highly stable substituted pyridine and quinoline derivatives in the hydrotreated gas oil.

2.3.3 Porphyrins

Porphyrins (Greek “porphura”, purple) are highly-coloured, naturally-occurring pigments, ubiquitously present in protoplasms. The well-known, biologically important pigments chlorophyll, and hemes of hemoglobin, are metalloporphyrins. The porphyrin nucleus comprises four pyrrole units linked together by methine bridges. The peripheral positions are numbered according to the older, Fischer nomenclature and the newer, revised nomenclature as shown below:

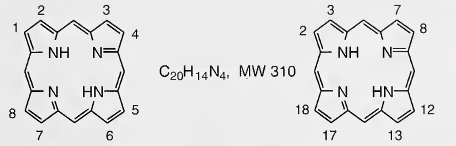

Fischer nomenclature

Modern nomenclature

The porphyrin molecule is amphoteric, the two amide hydrogens being acidic and the two tertiary nitrogens basic. Porphyrin and its derivatives can form complex salts with just about any metal, but only two metals, vanadium as vanadyl, VO^{2+}, and nickel as Ni^{2+}, are of importance in petroporphyrins, although copper porphyrins have been detected in immature oils:[49]

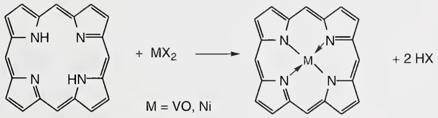

Free-base porphyrins occur in petroleum only in minute quantities.

The existence of metalloporphyrins in petroleum and other fossil fuels was discovered in the early 1930s by Treibs.[50] This discovery was a milestone in the evolution of the theory of petroleum formation since it provided the first definitive evidence for the biological origin of fossil fuels and was the first example of the group of constituent molecules later to become known as biological markers or biomarkers.

Porphyrins[51a] are planar, highly stable molecules having aromatic character and characteristic electronic spectra in the near-UV and visible regions. The near-UV Soret band, occurring around 400–410 nm, is intense and therefore useful for the detection of small amounts of porphyrins in a sample, but is not sensitive to peripheral substitution. The visible part of the spectrum, 450–700 nm, consists of four bands which are so sensitive to substitution that they have been classed as four distinct spectral series corresponding to four compound classes designated as “etio” (unsubstituted methine bridgeheads), “phyllo” (alkyl-substituted methine bridges), “rhodo” (electron-withdrawing substituents, carboxyl or benzo), and “DPEP” (exocyclic ring), Figures 12.77[51a] and 12.78[52]. Representative structures for better-known examples of each of these series are shown below.

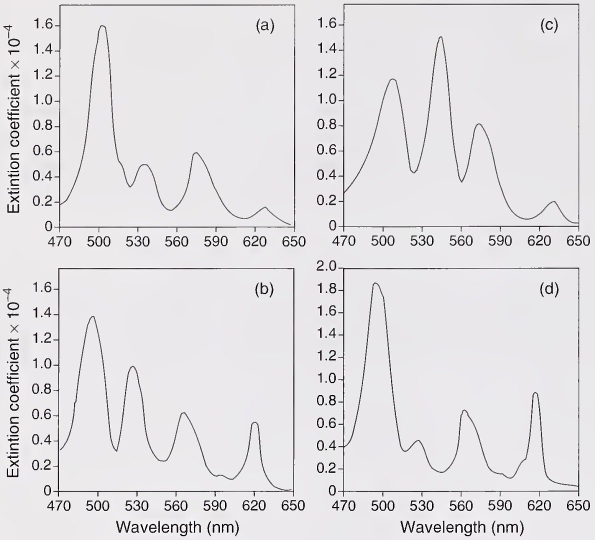

Figure 12.77 Visible spectra of porphyrins. (a) γ-phylloporphyrin XV; (b) etioporphyrin I; (c) rhodoporphyrin XV; (d) deoxophylloerythroporphyrin. The Roman numerals designate a particular set of substituents, see text. From E.W. Baker and S.E Palmer, Ref. 51a. © 1978, Academic Press.

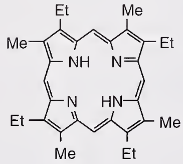

etioporphyrin I
(etio type)

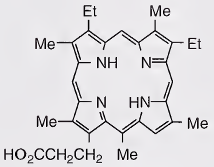

phylloporphyrin XV
(phyllo type)

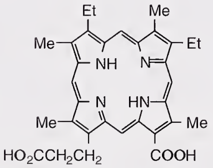

rhodoporphyrin XV
(rhodo type)

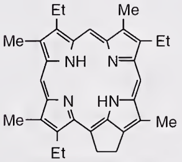

deoxophylloerythroetioporphyrin
(DPEP)

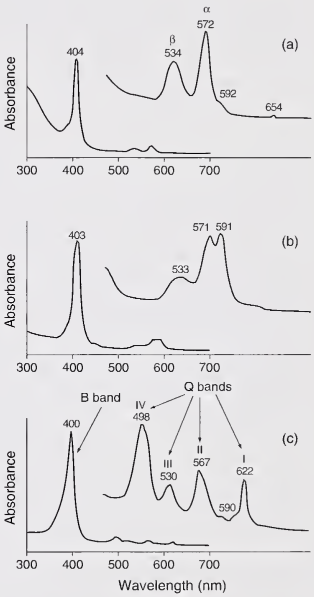

Figure 12.78 UV-visible spectra of porphyrins complexed to Athabasca asphaltene.[52b] a) vanadyl porphyrins in GPC fraction AC–5 (Figure 12.84); b) vanadyl rhodo–etio porphyrins in GPC fraction AC–4; c) free porphyrin bases after demetalation.

In metalloporphyrins the Soret bands are split in two and the four visible bands of the free porphyrins, Figures 12.77 and 12.78, reduce to two, designated as α and β, and these are not sensitive to substitution. The positions of the Soret, α, and β bands for the vanadium and nickel porphyrins are sufficiently different to allow differentiation between the two types, Table 12.21.

All spectra discussed represent π→π* transitions between the two highest HOMO and two lowest LUMO orbitals of the free porphyrine base. The four bands in the visible are termed Q bands and the Soret band in the near-UV, the B band. The QI and QIII bands are fundamental vibronic bands and bands II and IV are the (1, 0) harmonics of bands I and II, respectively.

The petroporphyrins occur as homologous series of the nickel and vanadium chelates of DPEP and etio porphyrins and a number of less abundant skeletal type porphyrins, ranging

Table 12.21 Positions of the Soret, α and β bands of vanadyl and nickel porpyrins[51]

Band	Vanadyl	Nickel
Soret	408/410 nm^a	390/395 nm^b
β	531 nm^a	514 nm^b
α	570 nm^a	550 nm^b
α/β intensity ratio	2^b; 1.3^a	3^b; 2.0^a

[a] For the etio porphyrin complexes.[b] For the DPEP complexes.

in carbon number from 20 to >50. Some of their structures are shown in Figure 12.79. Depending on the substitution, the particular members of each series may be designated by a Roman numeral, for example:

etioporphyrin I: R_1, R_3, R_5, R_7 = CH_3; R_2, R_4, R_6, R_8 = C_2H_5;
etioporphyrin II: R_1, R_4, R_5, R_8 = CH_3; R_2, R_3, R_6, R_7 = C_2H_5;
etioporphyrin III: R_1, R_3, R_5, R_8 = CH_3; R_2, R_4, R_6, R_7 = C_2H_5, *etc.*

The origin of the members with carbon numbers exceeding 32 is attributed to transalkylation (alkylation–dealkylation) reactions and kerogen binding. The ionization potentials of porphyrins are quite low and thus they are suited to low-voltage (12–15 eV) mass spectrometric analysis whereby only the parent molecular ions are detected. Table 12.22 lists the MWs of some homologous series of porphyrins.

The etio porphyrins in petroleum were derived from chlorophylls *via* oxidative opening (rather than thermal scission) of the exocyclic ring of the DPEP-type precursors, as will be discussed in Chapter 13. Inasmuch as the predominance of the nickel(II) and vanadyl(II) porphyrins in sediments is concerned, it has been suggested that it is the consequence of the availability of good ion carriers for these metals, which can bind to porphyrins to form complexes with high stability indices and stable metal-nitrogen bonds.

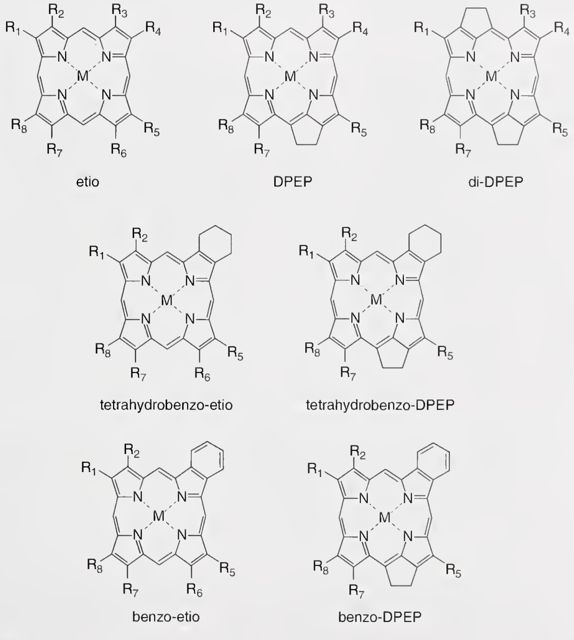

etio

DPEP

di-DPEP

tetrahydrobenzo-etio

tetrahydrobenzo-DPEP

benzo-etio

benzo-DPEP

Figure 12.79 Structures of some of the most common petroporphyrins. In many cases the positions of the tetrahydrobenzo and benzo substituents have not been established.

The elemental and porphyrin-bound vanadium and nickel contents increase with the sulfur content of crude oils,[49] Figure 12.80 and the ratio of vanadyl to nickel porphyrins has been shown to exhibit a weak correlation with the sulfur and asphaltene content, the higher the sulfur/asphaltene content, the higher the ratio. This is in line with the high values for these ratios in the oil sand bitumens and heavy oils of Alberta,[53] Table 12.23. This trend is related to the mechanism by which nickel and vanadium incorporate into the porphyrin structure during

Table 12.22 Molecular weights of homologous series of porphyrins[a]

n or *m*[b]	Etio and phyllo series 310 + 14*n*	DPEP series 308 + 14*m*	Rhodo series (benzo DPEP) 316 + 14*n*
8	422	420	428
9	436	434	442
10	450	448	456
11	464	462	470
12	478	476	484
13	492	490	498
14	506	504	512
15	520	518	526
16	534	532	540

[a] For vanadyl porphyrins the peaks would be 65 mass units higher. [b] Number of carbon atoms attached to the porphyrin nucleus.

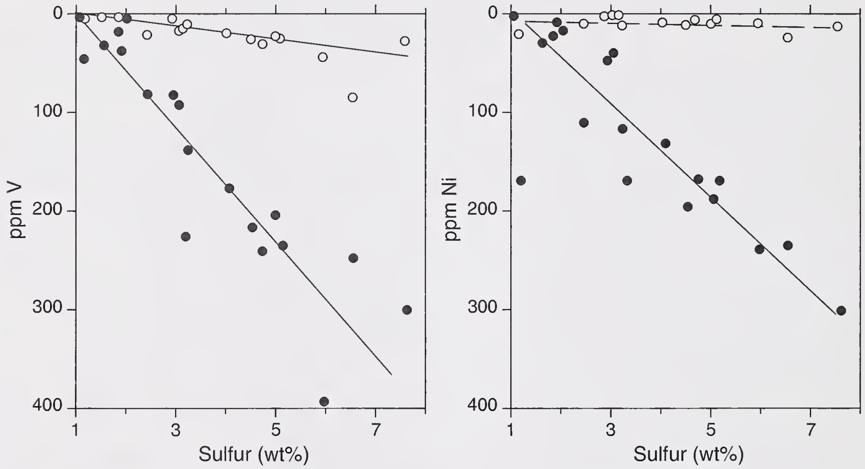

Figure 12.80 Elemental (●) and porphyrin (O) vanadyl and nickel contents as a function of weight percent sulfur from two U.S. crude oils. From E.W. Baker and J.W. Louda, Ref. 49. © 1986, Elsevier Science Publishers.

Table 12.23 Geochemical, V, Ni and vanadyl porphyrin data for the Athabasca, Peace River and Cold Lake oil sands[a]

Property	Athabasca	Peace River	Cold Lake
Present depth of reservoir (m)	0	169	444
V concentration (μg/g)	196 ± 3	180 ± 3	191 ± 3
Ni concentration (μg/g)	74.8 ± 3	62.4 ± 1	62.6 ± 5
V/Ni[b]	2.6 ± 0.1	2.9 ± 0.1	3.1 ± 0.2
VOP (μg V/g)[c]	92.5	92.0	76.8
Extractable VOP[c]	47.2%	51.1%	40.1%

[a] From D. Strong and R.H. Filby, Ref. 53. [b] Demetalated weight ratio. [c] Vanadyl porphyrin contents are estimated to have a relative error of ±10–15%.

early diagenesis. It has been proposed that in marine sediments Ni^{2+} and VO^{2+} cations in the pore water solution compete for chelation to the free-base porphyrins.[54] Under oxic conditions nickel, because of its higher equilibrium constant value, is favoured. However, under anoxic conditions, the higher sulfide concentration from the hydrogen sulfide generated by sulfate-reducing bacteria causes the precipitation of Ni^{2+} as nickel sulfide. Under such conditions the VO^{2+} ion would remain in solution and be available for complexation with porphyrins. Similarly, oils that are associated with source rocks deposited under highly reducing, H_2S-rich conditions, feature higher vanadium-to-nickel ratios than those generated from source rocks of more oxic environments.[55]

The composition of the porphyrins in a given crude oil changes with its geothermal history. With increasing thermal stress the DPEP/etio and Ni/V porphyrin ratios decrease as a consequence of the order of their relative thermal stabilities:

$$\text{V-etio} \geq \text{Ni-etio} \geq \text{V-DPEP} > \text{Ni-DPEP.}$$

The average length of the alkyl substituents also tends to decrease with increasing thermal stress. In addition, new skeletal-type porphyrins appear, such as benzo, tetrahydrobenzo, di-DPEP and butano, along with higher-MW porphyrins.

The presence of metalloporphyrins and other organically bound metals, mainly carboxylates, has a deleterious effect on the upgrading of bitumens and heavy oils.[56] During operations where a catalyst is used, the metals liberated by the decomposition of the metalloporphyrins deposit on the catalyst causing a reduction in catalyst performance and lifetime. Nickel and vanadium porphyrins have long been noted for their ability to poison and foul the catalysts used in fluid catalytic cracking and hydrodesulfurization. When the zeolite catalysts in fluid cracking are coated with a nickel deposit there is extensive coke and hydrogen production but the nickel coating does not lower catalyst activity. Vanadium is also harmful to zeolite catalysts. During catalyst regeneration vanadium deposited on the alumina–silica matrix can be converted to vanadium pentoxide (MP 690°C) which causes the migration of vanadium to the zeolite particle, bringing about the destruction of its crystallinity and catalytic activity. Many studies have been reported on the mechanisms of metalloporphyrin decomposition, hydrodemetalation and catalyst poisoning occurring in the hydrodesulfurization of petroleum fractions. The catalysts employed here are alumina-supported Co-Mo, Ni-Mo or Ni-W. In the hydrodesulfurization process the metalloporphyrins are gradually hydrogenated and the bonding of the metal in the hydrogenated porphyrins becomes weaker; ultimately, the porphyrin is demetalated. The metals react with the hydrogen sulfide produced and are converted to metal sulfides. Metal and metalloporphyrin deposition at the mouth of the pore of the catalyst has been reported to take place, causing plugging of the pores and a decrease in catalyst performance.

Early studies[57,58] of the porphyrins in Athabasca bitumen showed the porphyrins to consist for the most part of the two major DPEP and etio types and minor amounts of the benzo type. Also, the vanadyl complexes predominated over the nickel complexes. The concentration of porphyrins was reported to be 21–45 ppm for the nickel and 222–500 ppm for the vanadyl complexes. The homologous series of DPEP and etio porphyrins were also detected in the asphaltene fraction of Athabasca bitumen.

Relatively recent studies on Alberta oil sand porphyrins cover the following topics:

- the distribution of vanadyl porphyrins in the bitumen, maltene and asphaltene fractions of Athabasca, Peace River and Cold Lake oil sands;[53]

- the distribution of the etio–DPEP porphyrin ratios in the vanadyl porphyrins of the Athabasca oil sand and Grosmont carbonate maltenes,[59]
- the observation[52a] and distribution[52b] of porphyrins complexed to Athabasca asphaltene, and
- distribution of V, Ni, VO-porphyrins in GPC separated fraction of Cold Lake asphaltene.[60]

In an early spectroscopic study of Athabasca asphaltene it was shown that the vanadyl porphyrins are present not exclusively in the maltene but also, and in detectable concentrations, in the asphaltene fraction of the bitumen. This conclusion was deduced from the observation of the characteristic Soret band of porphyrins in the absorption, fluorescence and excitation spectra of the asphaltene.[52a] Moreover, it was also found that the porphyrins are not evenly distributed over the bulk of the *n*-C_5-asphaltene but are concentrated up to about 80% in the lowest-MW 22% fraction prepared by GPC separation. Thus, it followed that the porphyrins were present in free, and not chemically-bound, form. This was later confirmed by the isolation of a suite of porphyrins from the asphaltene.[52b] Subsequent studies[53] on various asphaltenes led to similar findings.

The asphaltene-associated porphyrins can be isolated from asphaltene using various solvent extraction (*n*-pentane, acetone, acetone-methanol azeotrope) as well as gel permeation chromatography.

The fractions—bitumen, maltene, *n*-pentane extract of asphaltene, methanol/acetone extract of asphaltene—were subjected to chromatographic separation according to the scheme shown in Figure 12.81 and the porphyrin-enriched chromatographic fractions were analyzed by MS for vanadyl porphyrins. An example of a corrected, reconstructed ion intensity–ion mass distribution plot is reproduced in Figure 12.82. The numerical data derived for the various vanadyl porphyrin ratios are tabulated in Table 12.24. In addition to the more abundant DPEP and etio-vanadyl porphyrins, smaller quantities of tetrahydrobenzo-DPEP, benzo-etio and benzo-DPEP porphyrins were detected, all in the C_{27}–C_{40} range with maxima at C_{32} and in relative concentrations

DPEP > etio > THBD > benzo-etio > benzo-DPEP.

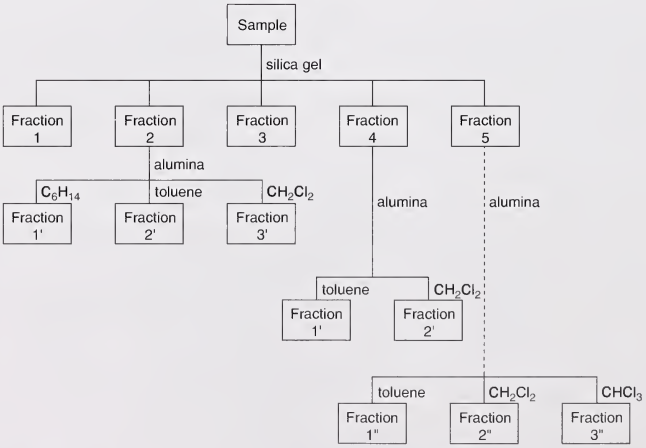

Figure 12.81 Scheme for the chromatographic separation of porphyrins from bitumen components. The vanadyl porphyrins are concentrated in Fraction 4 (silica gel) and purified on alumina, eluting with CH_2Cl_2 (Fraction 2′). Nickel porphyrins elute in Fraction 2. From D. Strong and R.H. Filby, Ref. 53. © 1987, American Chemical Society.

Table 12.24 Vanadyl porphyrin ratios[a] for Athabasca (A), Peace River (PR), and Cold Lake (CL) oil sands[b]

Component	Etio/DPEP[c]			Etio/THBD			Etio/benzo-ETIO			Etio/benzo-DPEP			THBD/benzo-DPEP		
	A	PR	CL	A	PR	CL	A	PR	CL	A	PR	CL	A	PR	CL
Whole bitumen[d]	0.56	0.61	0.72	1.71	2.62	3.14	1.99	3.35	3.51	2.40	4.55	5.92	1.40	1.74	1.88
Maltenes	0.65	0.77	0.84	3.75	5.22	6.29	6.00	7.66	11.3	7.73	12.77	13.5	2.06	2.45	2.15
n-Pentane extract of asphaltenes	0.60	0.66	0.70	2.40	3.82	4.20	3.23	4.81	5.22	3.53	5.36	5.51	1.47	1.40	1.31
Methanol-acetone extract of asphaltenes	0.34	0.39	0.68	1.28	1.52	2.58	1.41	1.74	3.25	1.94	2.47	5.76	1.51	1.62	2.23

[a] Etio/other porphyrin ratios were calculated from averaged MS scans and over the entire carbon number range of the envelope. [b] From D. Strong and R.H. Filby, Ref. 53. © 1987, American Chemical Society. [c] DPEP intensities include not only true DPEP species (*i.e.*, cycloethano) but also identical mass species of possible alternative cycloalkano porphyrins. [d] Whole bitumen porphyrins extracted in porphyrin aggregate.

The concentration ratios of the two major porphyrin components (etio/DPEP) in the three deposits are similar, displaying a slightly increasing trend with the depth of burial of the oil. This trend is also observed for the etio/other porphyrins ratio. Also, the presence of the cycloalkano or benzo group increases the relative concentration of asphaltene-complexed vanadyl porphyrins, probably as a result of increased polarity, charge transfer complexation capacity and solubility parameter changes in the porphyrin molecule. From their chromatographic behavior, the polarity of each class of porphyrins has been inferred to vary inversely with carbon number in the molecule and, in agreement with this, the higher carbon number homologs of both the DPEP and etio series were found to be more abundant in the mass spectra of the less-polar maltenes than in the methanol-acetone extracts of the asphaltenes.

The total amounts of vanadyl porphyrin and the vanadium and nickel contents of the three bitumens were also measured and from the reported values, Table 12.23, it is seen that only about 45–50% of the vanadium in the bitumen is present as vanadyl porphyrin and a similarly small fraction of the nickel is present in the form of nickel porphyrin. The remainder of the metals is still in unknown form. Some of the unaccounted-for metals are suspected to be present as carboxylic acid salts and high-MW porphyrin derivatives, as well as inorganic salts.

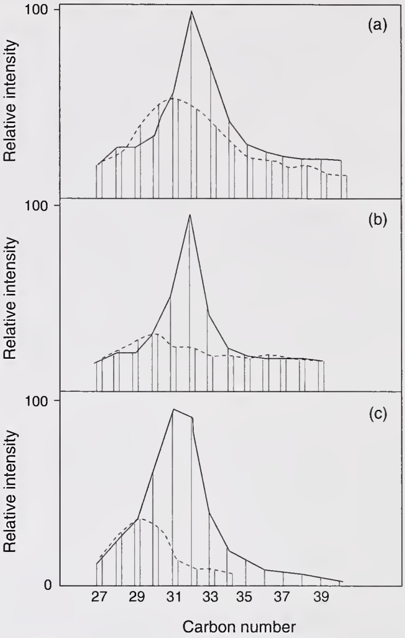

Figure 12.82 Molecular ion histograms of etio (---) and DPEP (—) vanadyl porphyrins isolated from Athabasca a) maltenes, b) *n*-pentane extract of asphaltene, and c) methanol–acetone extract of asphaltene. From D. Strong and R.H. Filby, Ref. 53. © 1987, American Chemical Society.

In another contemporary study, the vanadyl porphyrin distributions were determined in the maltene fractions of the Athabasca oil sands and Grosmont carbonate deposits.[59] In this study, the vanadyl porphyrins were chromatographically separated and subjected to demetalation by treatment with methanesulfonic acid. The demetalated porphyrins were isolated by chromatography and analyzed by GC to yield the distribution plots shown in Figure 12.83. Again, the two distribution plots are quite similar and, in turn, they resemble the ones obtained in the above study, Figure 12.82. However, as will be shown below, the methane sulfonic acid demetalation step is fraught with problems and results in significantly distorted etio/DPEP ratios.

In the study of polar compounds complexed to Athabasca asphaltene, the Bio-Beads SX-2 separated acetone extract, Figure 12.51, was examined for porphyrins.[52b] Porphyrins were detected in the four lower MW fractions (with over 80% being concentrated into the two lowest MW fractions (450, 670 g·mol^{-1})). These fractions were each separately fractionated by column chromatography on silica gel as shown in the flow diagram in Figure 12.84 followed by TLC.

The concentration of vanadyl porphyrins complexed to asphaltene was determined to be 325 ppm and the carbon range was considerably broader than found before,[52b] extending from C_{20} to C_{53}, with an etio/DPEP ratio of 0.95. It was also found that in the overall

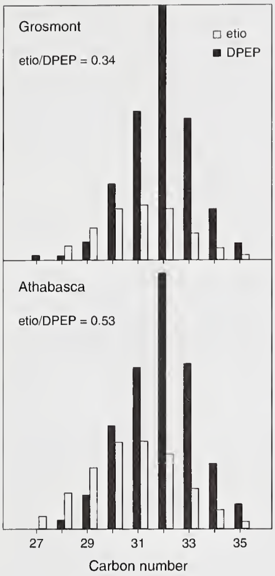

Figure 12.83 Distribution of vanadyl porphyrins in Athabasca and Grosmont (Carbonate Triangle) bitumen samples. From C.F. Hoffman and O.P. Strausz, Ref. 59. © 1986, American Association of Petroleum Geologists.

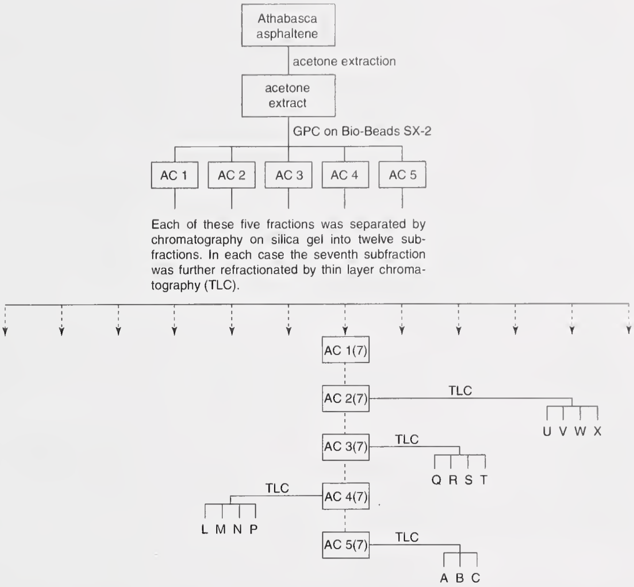
Athabasca asphaltene
acetone extraction
acetone extract
GPC on Bio-Beads SX-2
AC 1
AC 2
AC 3
AC 4
AC 5
Each of these five fractions was separated by chromatography on silica gel into twelve subfractions. In each case the seventh subfraction was further refractionated by thin layer chromatography (TLC).
AC 1(7)
AC 2(7)
TLC
U V W X
AC 3(7)
TLC
Q R S T
TLC
AC 4(7)
L M N P
AC 5(7)
TLC
A B C

Figure 12.84 Scheme for the chromatographic separation of vanadyl porphyrins complexed to Athabasca asphaltene.[52b]

separation procedure the tail ends of the carbon range were easily lost, and this had an influence on the etio/DPEP ratios.

One of the TLC isolates from fractions AC-3 and AC-4 displayed a UV-Vis spectral pattern typical of rhodoporphyrins, Figure 12.85. The low-resolution mass spectrum of a TLC subfraction of AC-4, Figure 12.86, indeed shows the presence of another series of porphyrins belonging to the $360 + 14n$ series, ranging from C_{34} to C_{48}. High-resolution mass measurements confirmed the benzoporphyrin series formula $C_nH_{2n-34}N_4VO$. This minor series amounts to about 7 ppm of the asphaltene.

Up to about 1988, demetalation with methanesulfonic acid was a widely used method to obtain analyzable porphyrin concentrates from petroleum because it is much simpler and faster than chromatographic separation. However, it was found that treatment of one of the chromatographic fractions using methane sulfonic acid had demetalated only 50% of the sample, as indicated by the UV-Vis spectra of the products, Figure 12.87. The free-base porphyrins consisted largely of the DPEP series, Figure 12.88, with a maximum at C_{32}. This series was accompanied by small amounts, ~10%, of a series characterized by the $m/z = 524, 538, 552, 566, 580$ peaks which, on the basis of high-resolution MS results, was assigned the formula $C_nH_{2n-24}N_4O_8$. The presence of peripheral oxygen was confirmed by the IR spectrum of the free porphyrins, which displayed a distinct carbonyl absorption band at 1727 cm^{-1}, Figure 12.89.[61] Geoporphyrins containing up to six oxygen atoms—four in carboxylic groups and two in carbonyl or alcohol groups—are known. The carboxylic groups in these porphyrin carboxylic acids in their native state are assumed to bond to the same kind of metal as the porphyrin base. It should be noted here that nickel porphyrins were not detected in the asphaltene acetone extract.

The direct extraction of free-base porphyrins from the Athabasca asphaltene acetone extract with methanesulfonic acid proceeded with an efficiency of 38% with the loss of the

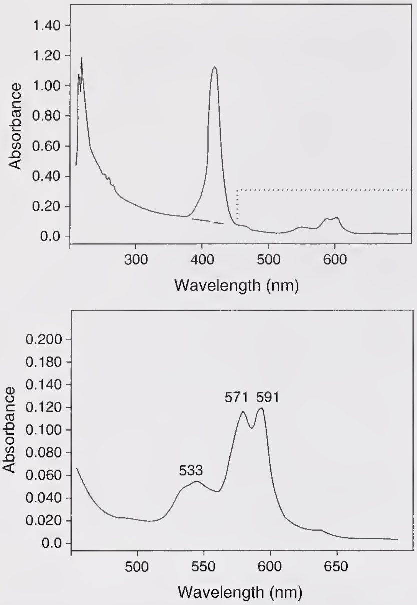

Figure 12.85 UV spectrum of one of the silica gel chromatographic fractions of band N (Figure 12.84), showing the spectral pattern containing the 591-nm band typical of benzoporphyrins. The spectrum above shows the Soret band and the visible portion of the spectrum is enlarged in the lower panel.[52b]

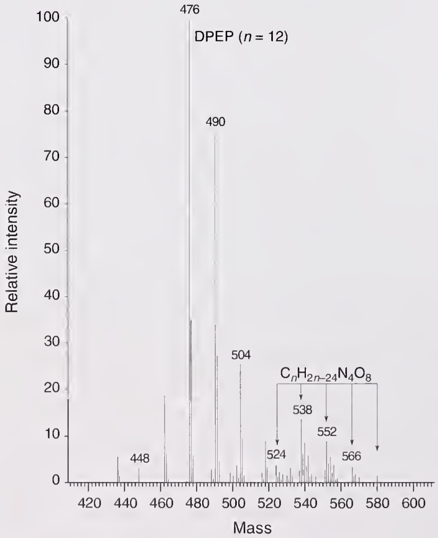

Figure 12.88 Low-resolution mass spectrum of the demetalated DPEP and $C_nH_{2n-24}N_4O_8$ porphyrin series present in band B (Figure 12.84).

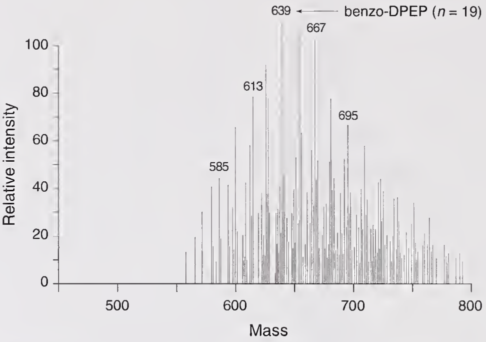

Figure 12.86 Low-resolution mass spectrum of the benzo DPEP vanadyl porphyrins present in Fraction AC–4, Figure 12.84.[52b]

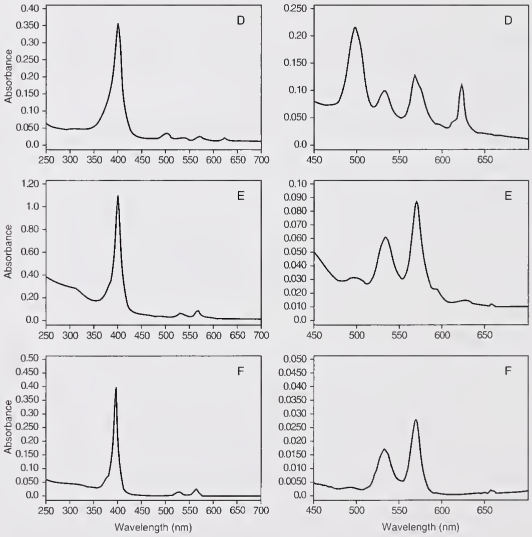

Figure 12.87 UV-visible spectra (scale expansions of the 500–650 nm regions on the right) of three TLC-separated fractions of the product of the methanesulfonic acid-treated silica gel subfraction of band B (Figure 12.84). Spectrum D corresponds to demetalated porphyrins, E and F to vanadyl porphyrins.[52b]

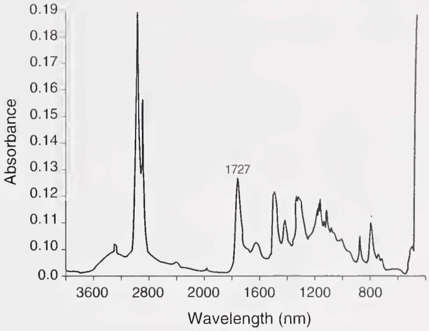

Figure 12.89 Infrared spectrum of TLC Fraction D of Figure 12.87.

homologs below C_{28} and above C_{34}, giving an etio/DPEP ratio of 0.60. Thus, the free-base porphyrins obtained are depleted in the etio type and also in the homologs of the DPEP and etio series at both ends of the MW distribution.

In the bitumen, 47% of the vanadium was estimated to be present in the form of vanadyl porphyrin. In the case of the asphaltene, the corresponding percentage is much lower. The vanadium content of the asphaltene is 630 ppm while the vanadium present in vanadyl porphyrins is, at most, 10 wt% of the vanadyl porphyrins which, for the 325-ppm vanadyl porphyrins present, amounts to 33 ppm or about 5% of the total vanadium. The rest of the vanadium in the asphaltene is then probably either in inorganic minerals, carboxylic acid salts or chelates in partially degraded, high-MW porphyrins covalently bound to the asphaltene core. It also follows that, in contrast to this distribution, practically 100% of the vanadium in the maltene is present as vanadyl porphyrin.

An examination of the distribution of vanadyl porphyrins* in GP-separated fractions of Cold Lake asphaltene[60] led to results similar to those reported for Athabasca asphaltene.[52a] Specifically, it was found that some 80% of the porphyrins were associated with the lowest-MW 12% (800 g·mol^{-1}) fraction of the asphaltene, Table 12.25, and the highest accumulation, 51%, occurred in the 200–450 g·mol^{-1} MW range, representing 3% of the asphaltene. It was also observed that the highest accumulation of V and vanadyl porphyrins also occurred in the same fractions and, in agreement with other studies, only about 12% of the 820-ppm vanadium present in the asphaltene was bound to porphyrins. Interestingly, the nickel distribution was

Table 12.25 V, Ni and Porphyrin Distribution in Cold Lake Asphaltene[a] [60]

Fraction	Wt%	MW	Porphyrin		V	Ni	V in Porphyrin
			μg·g^{-1}	wt%	μg·g^{-1}		μg·g^{-1}
Whole	100	2,000	1,200	100	820	320	100
1	14	5,000	200	3	740	330	17
2	35	4,000	130	4	740	320	11
3	25	3,000	250	5	710	310	21
4	16	1,800	590	8	660	270	50
5	12	800	7,000	80	1,500	310	600
5–1	50	1,200	2,100	11	870	250	180
5–2	25	700	5,600	18	1,400	290	480
5–3	16	450	15,600	29	2,800	330	1,300
5–4	8	200	22,000	22	3,200	550	1,900
5–5	0.5	100	–	–	180	420	0

[a] Precipitated by n–C_5.

---

*Although the porphyrins were isolated from n-C_5-asphaltene, the lowest-MW fraction of this asphaltene, like that of Athabasca asphaltene, is soluble in acetone and properly belongs to the resin/polar fraction of the bitumen.

found to be fairly uniform across the fractions except the lowest MW 1% fraction where it showed a slight enhancement.

To conclude this section on porphyrins it will be noted that there is good agreement among the results reported from various laboratories on the nature, overall occurrence and distribution of porphyrins, vanadium and nickel in crude oil and bitumen.

Differentiation between inorganic and organically bound vanadium is, at least in principle, possible with the aid of electron spin resonance (ESR) spectroscopy.[62] The vanadium atom in its tetravalent state, like in the vanadyl ion, VO^{2+}, having a $3d^1$ electron configuration, is paramagnetic. The hyperfine interaction arising from the coupling of the $^1/_2$ spin of the unpaired electron to the $^7/_2$ nuclear spin (I) of the vanadium atom gives rise to a hyperfine spectrum of 2I + 1 lines. The central portion of the ESR spectrum of asphaltenes indeed shows the eight-line hyperfine spectrum and in fact two sets of an eight-line spectrum. The doubling of the spectrum is due to the axial symmetry of the vanadyl porphyrin molecule. Such paramagnetic systems, when randomly oriented in a powder, exhibit two characteristic line components due to the orientation of the symmetry axis parallel and perpendicular to the magnetic field. Some examples of the vanadyl ESR spectra are shown in Figure 12.90. The two asphaltene spectra are due to vanadyl etio porphyrin and the mineral fine spectrum is attributed to vanadyl ions in a clay or mineral matrix.

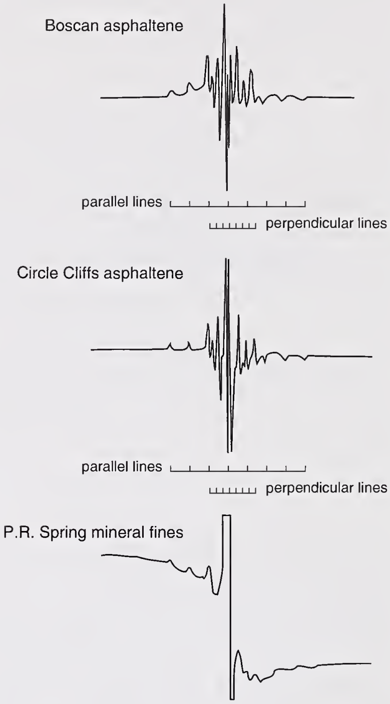

Figure 12.90 ESR spectra of VO^{2+} from Boscan and Circle Cliffs asphaltene and mineral fines extracted from P.R. Spring bitumen. From W.R.M. Graham, Ref. 62. © 1987, American Chemical Society.

The ESR spectra of asphaltenes and of the fines are different, thus giving different values for the magnetic constants, the g-factor and A (the hyperfine splitting constant); presumably this would make it possible to differentiate the V^{4+} ion in the porphyrin from the V^{4+} ion in the mineral matrix.

3.0 Composition of the Nondistillable Polars

For this study, a modified class separation procedure was used, involving large samples and solvent volumes and a long silica gel column. The polar fraction thus obtained (from repeated fractionation of fresh maltene) comprised 16% of the maltene, of which 14% was nondistillable at 230°C and 10^{-3} Torr. As with the saturate and aromatic fractions, the composition of the nondistillable polar portion is significantly different from that of the distillable portion. The nondistillable polars (C: 79.6%; H: 9.5%; N: 1.25%; O: 2.14% and S: 8.2% with $(H/C)_a = 1.46$ and MW = 1156 $g{\cdot}mol^{-1}$) contain a higher percentage of sulfur and nitrogen and a lower percentage of oxygen than even the most polar Polar II fraction (Table 12.1) and have a higher MW. Interestingly, in spite of the high MW, the $(H/C)_a$ ratio is relatively high, suggesting the presence of a high proportion of aliphatic carbon. The FTIR spectrum, Figure 12.91, indeed

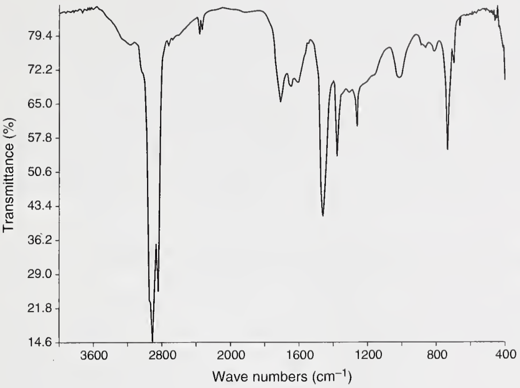

Figure 12.91 FTIR spectrum of the nondistillable polar fraction of Athabasca maltene.

shows intense methyl and methylene absorptions, 2930, 2860, 1460, 1380 cm^{-1}; weak absorptions which appear to be due to the presence of aromatic carbon (1600 and 3030 cm^{-1}); an intense 740 cm^{-1} absorption indicating C–H$_{\text{arom.}}$ out-of-plane vibrations of sparingly substituted aromatic rings; and strong carbonyl (1610, 1650 cm^{-1}), carboxylic C=O (1710 cm^{-1}), hydroxyl (~3200, 1260, 1020 cm^{-1}) and sulfoxide group (1030 cm^{-1}) absorptions.

3.1 NMR studies

The 500-MHz ^{13}C NMR spectrum of the nondistillable polars,[63] Figure 12.92, shows features similar to those of the nondistillable aromatics (Figure 11.22) and saturates (Figure 10.25) and the asphaltene (*cf.* Chapter 14) in the sense that the mid-chain methyl resonances around 29.5 ppm are significantly stronger than that of the terminal methylene absorption around 14.1 ppm, revealing the presence of long-chain *n*-alkyl groups. Comparison of this spectrum with that of the distillable portion of the polars is instructive. The latter spectrum, Figure 12.93, displays essentially the same resonances in the aliphatic (10–40 ppm) region as the former, but here the 14.1-ppm methyl resonance is more intense relative to the 29.5-ppm mid-chain methylene resonances than in the nondistillables and in effect the terminal methyl resonances are more intense than the mid-chain methylene resonances. Also, the sharp peak intensities superimposed on the broad hump are lower relative to the hump, which represents naphthenic carbon. This is a clear manifestation that, in the distillable polars, both the relative proportion of long alkyl chains to naphthenic carbon and the average chain length are lower than in the nondistillable portion of the polars. These results are in agreement with conclusions arrived at before in the examination of the NMR spectra of the aromatic and saturate fractions, namely, that the nondistillable portion of the polars and indeed of all fractions of the maltene bears a resemblance to the asphaltene, suggesting that the heavier, nondistillable portions of the maltene are structurally and genetically related to asphaltene. Another significant difference between the two polars spectra is that in the distillables spectrum the resonances due to aromatic carbon appear as a narrow continuum in the 115–145 ppm region whereas these resonances are broader in the nondistillable spectrum, 115–165 ppm, indicating a more extensive condensation of the aromatic and a higher proportion of heteroaromatic structures. The distillables spectrum also displays weak resonances at 178.34 and around 182 ppm. These are due to the presence of carboxylic acid groups,

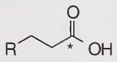

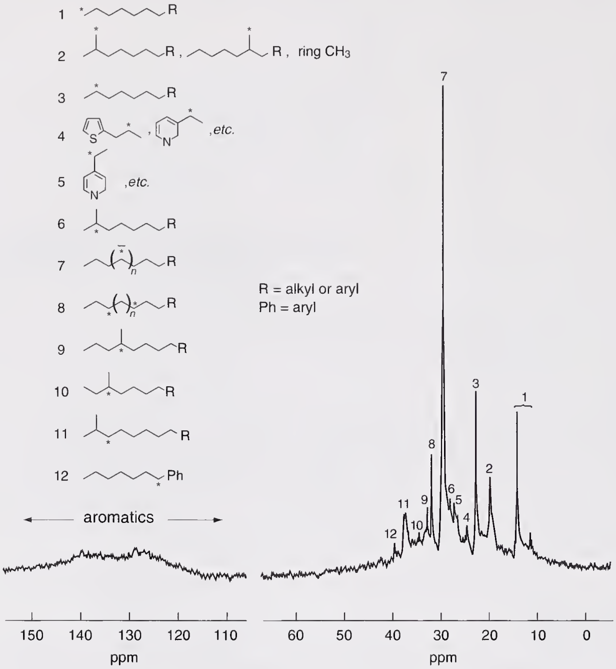

Figure 12.92 500-MHz ^{13}C NMR spectrum of the nondistillable polar fraction of Athabasca maltene.

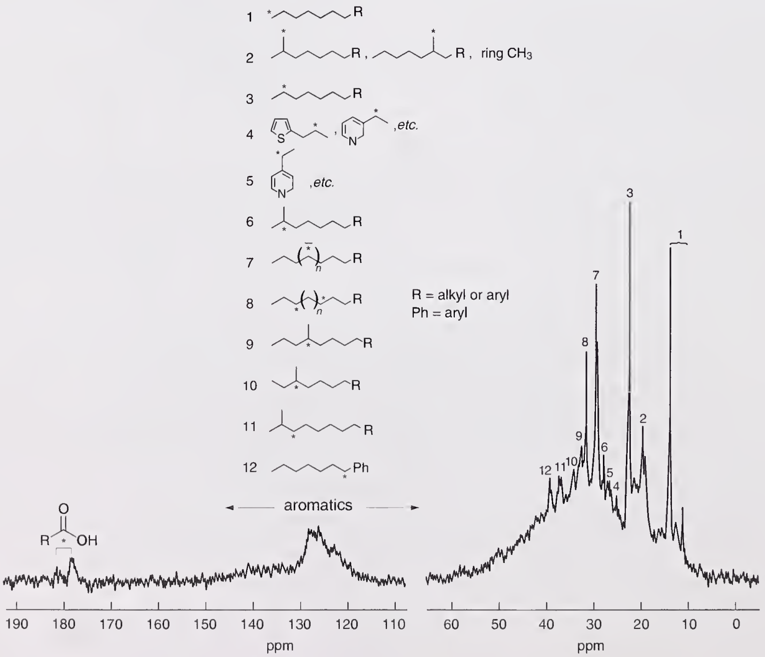

Figure 12.93 500-MHz ^{13}C NMR spectrum of the distillable polar fraction of Athabasca maltene.

in agreement with the isolation of free tricyclic, hopanoic, *n*-alkanoic and aromatic acids in the distillable polars and their lower concentrations in the nondistillable polars.

The composition and structure of nondistillable resins were further investigated using—as before—thermal and chemical degradation methods followed by detailed analytical examination of the products using capillary GC–MS and GC–FIMS. First the thermal degradative studies will be considered and then the chemical studies.

3.2 Flash pyrolysis of the nondistillable polars

The chemical composition of the nondistillable polars was explored using flash pyrolysis to degrade the polar molecules to chemically analyzable fragments. The same flash pyrolysis technique was applied as in the cases of the nondistillable aromatics and the asphaltene. The pyrolysis oil was initially fractionated according to the scheme illustrated in Figure 12.94; 57.2% of the pyrolysis oil was collected as a distillate and 5.2% as a nondistilling oil remaining in the reaction flask. Flow diagrams outlining the analytical procedures used to treat each eluent are shown in Figures 12.95–12.97.

3.2.1 The *n*-pentane eluent of the distillate

GC analysis revealed the presence of a series of *n*-alkanes and 1-*n*-alkenes, up to ~C_{31}, Figure 12.98, superimposed on a broad continuum. MCPBA oxidation, Figure 12.95, was employed to remove sulfur compounds and alkenes. The oxidized residue was then subjected to silica gel chromatography, yielding a colorless oil (25%) and a yellow oil (75%). The colorless oil was further fractionated by alumina chromatography giving an *n*-pentane (60%) and a 10% toluene–*n*-pentane (40%) eluent.

The gas chromatogram of the *n*-pentane eluent, shown in Figure 12.99, indicates that this fraction consists mainly of *n*-alkanes up to about C_{32}.

Examination of the total ion current chromatogram of the toluene/*n*-pentane eluent shown in Figure 12.100 suggests that it comprises alkylbenzenes with up to C_{15} side chains, naphthalenes and tetrahydronaphthalenes along with alkylthiophenes. The full mass spectra of a few representative alkylbenzenes and a naphthalene in the sample are shown in Figure 12.101 and tentative peak assignments for Figure 12.100 are listed in Table 12.26. The $m/z = 97$ cross-scan chromatogram of the eluent, Figure 12.102, revealed that the thiophene series consisted of the methyl *n*-alkyl homologs to which the 2-methyl-5-*n*-alkylthiophene structure is assigned, by analogy with the *n*-alkylthiophene series identified in the pyrolysis oil of asphaltene (*cf.* Chapter 14) and in various native, nonbiodegraded conventional oils.

The yellow oil from the MCPBA oxidation of the *n*-pentane eluent was reduced by $LiAlH_4$ and the reduced oil was chromatographed on silica gel into a condensed thiophene and an alcohol fraction.

The $m/z = 198$, 212 and 226 cross-scan chromatograms of the thiophene fraction, showing the distribution of the mono-, di-, and trimethyldibenzothiophenes, are shown in Figure 12.103. The value of the DBTI index here, 0.26, is similar to that of the distillable portion of the maltene, 0.43 and the nondistillable portion of the aromatics, 0.41. Mass spectrometric analysis of this fraction showed that the dominant components are benzo[*b*]-thiolanes, probably generated during the $LiAlH_4$ reduction treatment:

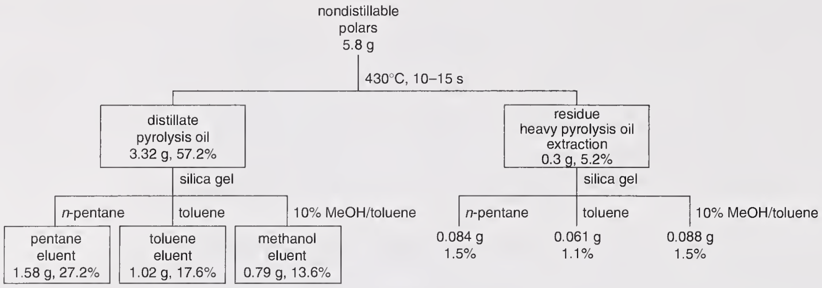
nondistillable polars 5.8 g
430°C, 10–15 s
distillate pyrolysis oil 3.32 g, 57.2%
residue heavy pyrolysis oil extraction 0.3 g, 5.2%
silica gel
n-pentane
toluene
10% MeOH/toluene
pentane eluent 1.58 g, 27.2%
toluene eluent 1.02 g, 17.6%
methanol eluent 0.79 g, 13.6%
silica gel
n-pentane
toluene
10% MeOH/toluene
0.084 g 1.5%
0.061 g 1.1%
0.088 g 1.5%

Figure 12.94 Flow diagram showing the chromatographic fractionation steps used for the primary separation of the pyrolysis oil from the nondistillable polars.

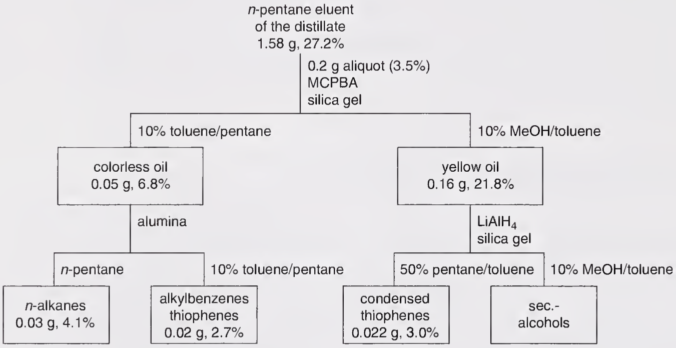
n-pentane eluent of the distillate 1.58 g, 27.2%
0.2 g aliquot (3.5%)
MCPBA
silica gel
10% toluene/pentane
10% MeOH/toluene
colorless oil 0.05 g, 6.8%
yellow oil 0.16 g, 21.8%
alumina
LiAlH4
silica gel
n-pentane
10% toluene/pentane
50% pentane/toluene
10% MeOH/toluene
n-alkanes 0.03 g, 4.1%
alkylbenzenes thiophenes 0.02 g, 2.7%
condensed thiophenes 0.022 g, 3.0%
sec.-alcohols

Figure 12.95 Chromatographic/chemical procedures used to separate the components of the pentane eluent of the pyrolysis oil of the nondistillable polars. MCPBA = *m*-chloroperbenzoic acid; $LiAlH_4$ = lithium aluminum hydride. The percentage yields are in terms of the total nondistillable polar fraction.

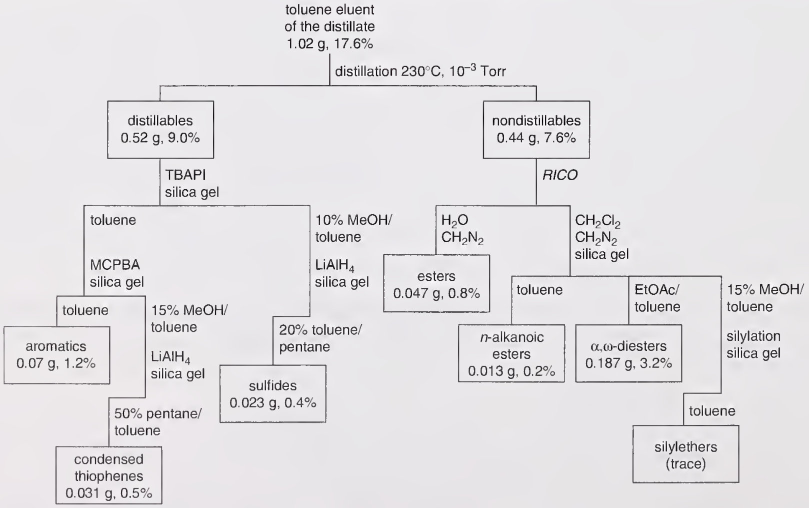
toluene eluent of the distillate 1.02 g, 17.6%
distillation 230°C, 10⁻³ Torr
distillables 0.52 g, 9.0%
nondistillables 0.44 g, 7.6%
TBAPI
silica gel
RICO
toluene
10% MeOH/ toluene
H2O CH2N2
CH2Cl2 CH2N2 silica gel
MCPBA silica gel
LiAlH4 silica gel
esters 0.047 g, 0.8%
toluene
EtOAc/ toluene
15% MeOH/ toluene
toluene
15% MeOH/ toluene
aromatics 0.07 g, 1.2%
LiAlH4 silica gel
20% toluene/ pentane
n-alkanoic esters 0.013 g, 0.2%
α,ω-diesters 0.187 g, 3.2%
silylation silica gel
sulfides 0.023 g, 0.4%
50% pentane/ toluene
toluene
condensed thiophenes 0.031 g, 0.5%
silylethers (trace)

Figure 12.96 Chromatographic/chemical procedures used to separate the components of the toluene eluent of the pyrolysis oil of the nondistillable polars. MCPBA = *m*-chloroperbenzoic acid; TBAPI = *t*-butylammoniumperiodate; $LiAlH_4$ = lithium aluminum hydride; *RICO* = ruthenium ions-catalyzed oxidation. The percentage yields are in terms of the total nondistillable polar fraction.

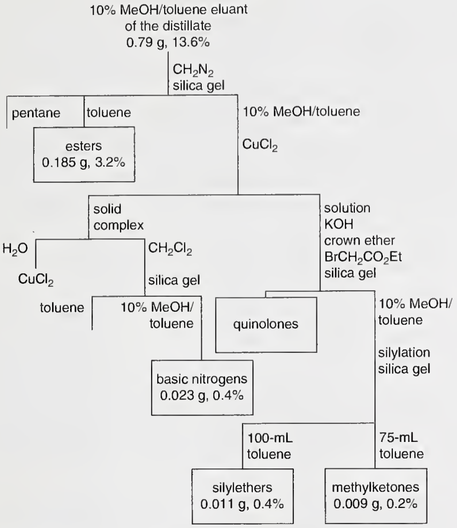
10% MeOH/toluene eluant of the distillate 0.79 g, 13.6%
CH_2N_2 silica gel
pentane
toluene
10% MeOH/toluene
esters 0.185 g, 3.2%
$CuCl_2$
solid complex
solution
KOH
crown ether
$BrCH_2CO_2Et$
silica gel
H_2O
$CuCl_2$
CH_2Cl_2
silica gel
toluene
10% MeOH/toluene
quinolones
10% MeOH/toluene
silylation silica gel
basic nitrogens 0.023 g, 0.4%
100-mL toluene
75-mL toluene
silylethers 0.011 g, 0.4%
methylketones 0.009 g, 0.2%

Figure 12.97 Chromatographic/chemical procedures used to separate the components of the methanol eluent of the pyrolysis oil of the nondistillable polars. The percentage yields are in terms of the total undistillable polar fraction.

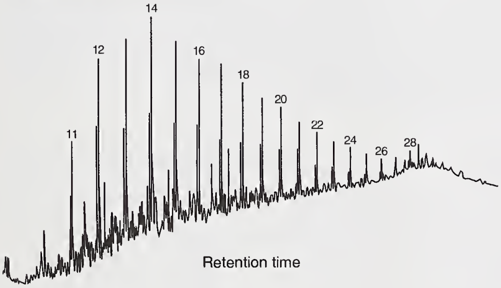

Figure 12.98 Gas chromatogram of the *n*-pentane eluent of the nondistillable polars pyrolysis oil. The numbers above the peaks correspond to the number of carbon atoms in the *n*-alkane. The peaks immediately preceding the *n*-alkanes are the 1-*n*-alkenes.

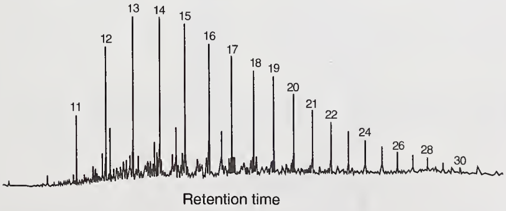

Figure 12.99 Gas chromatogram of the *n*-alkane subfraction of the *n*-pentane eluent (Figure 12.95). The numbers above the peaks correspond to the number of carbon atoms in the alkane.

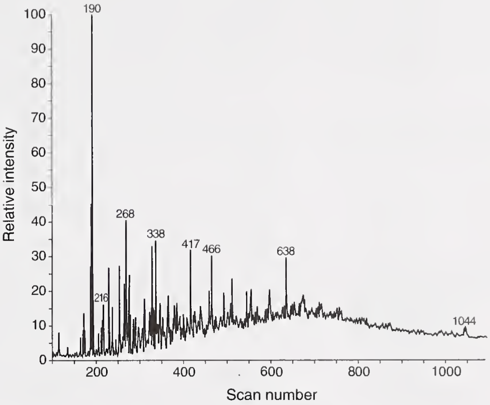

Figure 12.100 GC–MS total ion chromatogram of the aromatic subfraction (10% toluene/pentane eluent, Figure 12.95) of the *n*-pentane eluent.

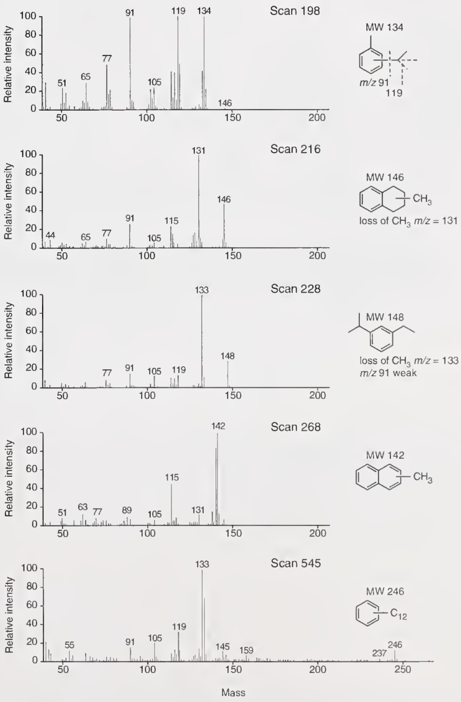

Figure 12.101 High-resolution mass spectra of scans 198, 216, 228, 268 and 545 of Figure 12.100.

Table 12.26 Structural assignments for some of the peaks in Figure 12.100

Scan no. (MW)	Structure	Scan no. (MW)	Structure	Scan no. (MW)	Structure
638 (274)	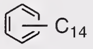	366 (196)	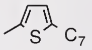	264 (146)	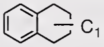
599 (266)	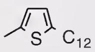	354 (190)	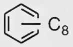	253 (168)	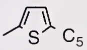
557 (252)	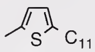	338, 336 (156)	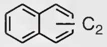	237, 228 (120)	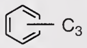
545 (246)	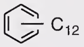	329, 325 (176)	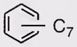	216 (146)	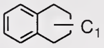
512 (232)	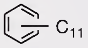	311 (182)	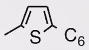	193 (154)	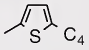
466, 459, 440 (218)	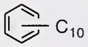	289 (160)	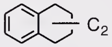	187 (132)	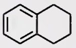
417 (204)	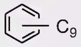	277, 268 (142)	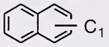	171 (134)	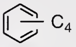

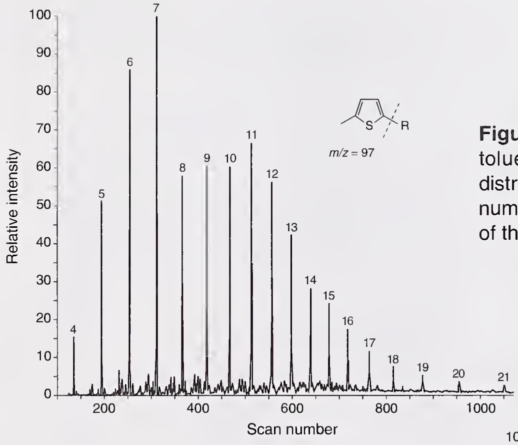

Figure 12.102 *M/z* = 97 cross-scan chromatogram of the toluene/*n*-pentane eluent (Figure 12.95) showing the distribution of the 2-methyl-5-*n*-alkylthiophene series. The numbers above the peaks indicate the carbon numbers of the *n*-alkyl side chains.

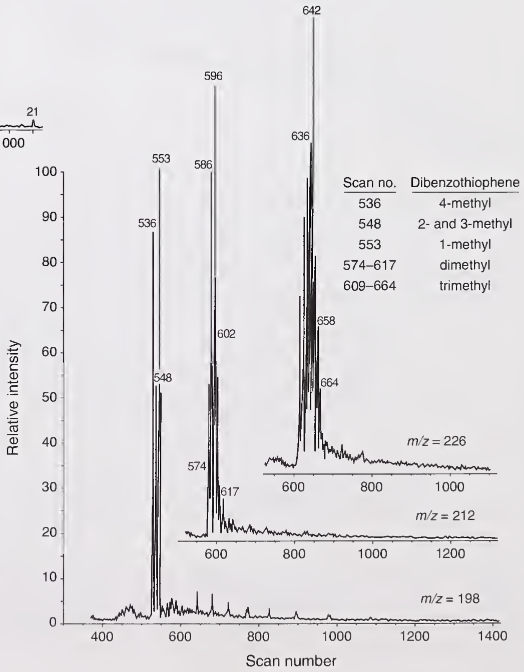

Scan no.	Dibenzothiophene
536	4-methyl
548	2- and 3-methyl
553	1-methyl
574–617	dimethyl
609–664	trimethyl

Figure 12.103 *M/z* = 198, 212 and 226 cross-scan chromatograms of the alkyldibenzothiophenes in the yellow oil of the *n*-pentane eluent (Figure 12.95).

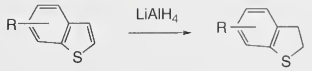

2-*n*-Butylbenzothiophene does not reduce to the corresponding 2,3-dihydro compound. Therefore, the reduced compounds probably have their alkyl substituents in positions other than the 2-position and the alkylbenzothiophenes which survived the $LiAlH_4$ treatment without undergoing reduction had their alkyl substituents in the 2-position.

The polar chromatographic fraction following $LiAlH_4$ reduction comprises alcohols from the oxidation of the 1-alkenes:

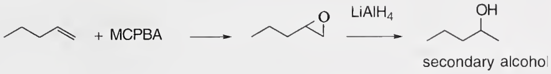

The gas chromatogram in Figure 12.104 displays a series of secondary *normal* alcohols derived from the 1-*n*-alkene series which was formed in the thermal cleavage of the *n*-alkyl chains

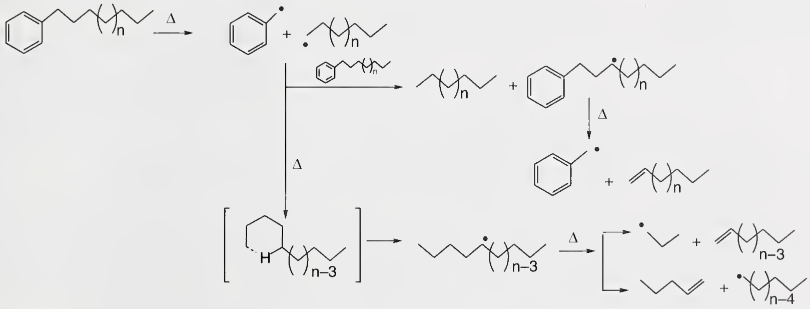

The carbon range lies in the 9–31 region. There are a multitude of unassigned peaks which (as with the *n*-alkanes) belong to branched and cyclic alcohols.

The approximate yields of the chromatographic fractions of the *n*-pentane eluent (Figure 12.95) are as follows:

alkanes	~4.1%
alkylbenzenes/thiophenes	~2.7%
condensed thiophenes	~3.0%

The yield of the alcohol fraction, representing the yield of alkenes, was not measured, but can be estimated to be about two-thirds of the alkane fraction, about 2.7%. Thus, the total yield of the analyzable fractions recovered from the *n*-pentane eluent is about 46% of the *n*-pentane eluent or 12.5% of the nondistillable resins.

3.2.2 The toluene eluent of the distillate

a) Distillable toluene eluent

The distillable (230℃, 10^{-3} Torr) portion of the toluene eluent was subjected to TBAPI oxidation to convert the nonpolar sulfides to the strongly polar sulfoxides for chromatographic separation on silica gel (Figure 12.96). The polar fraction containing the sulfoxides was treated with $LiAlH_4$ to reduce the sulfoxides back to the sulfides for GC analysis and the nonpolar fraction was subjected to oxidation with MCPBA and separated into a nonpolar, aromatic fraction and a polar fraction containing the sulfones from the oxidation of the condensed thiophenes. The latter fraction was also treated with $LiAlH_4$ to reduce the sulfones back to the condensed thiophenes for GC–MS analysis.

The *m/z* = 87, 101, 115, 183 and 319 cross-scan chromatograms of the sulfides separated as described above are shown in Figures 12.105–109.

The *m/z* = 87 cross-scan (Figure 12.105) represents 2-*n*-alkylthiolanes:

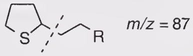

The recovered range extends from C_9 to C_{24} with a maximum at C_{11-12} but the observed distribution is distorted by losses due to volatility in the analytical procedures and the true maximum should lie at lower carbon numbers. This applies to all the sulfides and to all the series of compounds detected.

The *m/z* = 101 cross scan representing the distribution of the *cis*- and *trans*-2-methyl-5-*n*-alkylthiolanes (the first-eluting peaks) and the 2-*n*-alkylthianes (the second-eluting peaks)

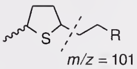

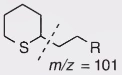

is shown in Figure 12.106. The unlabelled peaks are mainly bicyclic sulfides.

The *m/z* = 115 cross-scan showing the distribution of the *cis*- and *trans*-2-methyl 6-*n*-alkyl thianes and *cis*- and *trans*-2-ethyl-5-*n*-alkyl thiolanes is reproduced in Figure 12.107. The resolution of the various isomers is poor and there are peaks appearing which belong to *n*-alkylthiolanes, *n*-alkylthianes, methyl-*n*-alkylthiolanes and bicyclic sulfides.

The distribution of the bicyclic terpenoid sulfides observed here, Figure 12.108, is similar to that found in the pyrolysis oil of the undistillable aromatics and differs from that found in the distillable aromatics in that the C_{18} member is the most abundant and there is a dip in the concentration at C_{15}. The shift is attributable to thermal effects and the increased cleavage rate of the weaker tertiary carbon bonds between C–17 and C–16 and C–17 and C–19 in the side chain. It should also be taken into consideration that the sulfide molecules are chemically bound to the high-MW core material and the nature and position of attachment can also affect the side chain length distribution in the products. The minima occurring at C–17 and C–23 owing to isoprenoid branching are evident in all the distributions regardless of the source of the series.

Lastly, small quantities of tetracyclic terpenoid sulfides are present as well, Figure 12.109, in a concentration distribution similar to that in the maltene.

Returning to the separation scheme shown in Figure 12.96, the other fraction isolated by silica gel chromatography of the TBAPI-oxidized toluene extract containing the aromatics and condensed thiophenes was subjected to MCPBA oxidation and the aromatics were separated from the polar sulfones by silica gel chromatography. The sulfones then were reduced back to the thiophenes with $LiAlH_4$. The total ion current chromatogram of the condensed thiophenes is shown in Figure 12.110 and the mass spectra of three of the scans, corresponding to C_2-, C_3- and C_7-benzo[*b*]thiolanes are shown in Figure 12.111. Table 12.27 lists some of the peak assignments for Figure 12.110. The fraction consists mainly of series of alkylbenzo- and

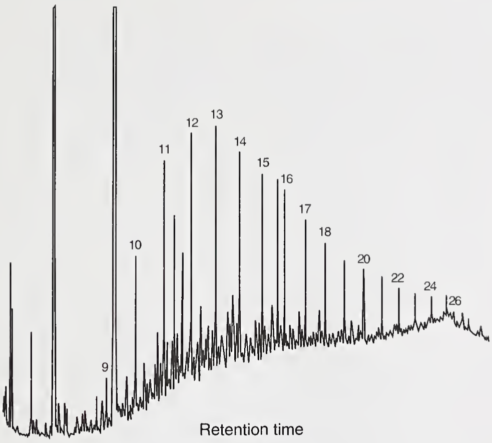

Figure 12.104 Gas chromatogram of the secondary alcohols, *n*-alkan-2-ols, derived from the 1-*n*-alkenes in the *n*-pentane eluent (Figure 12.95). The numbers above the peaks correspond to the carbon number of the alcohol.

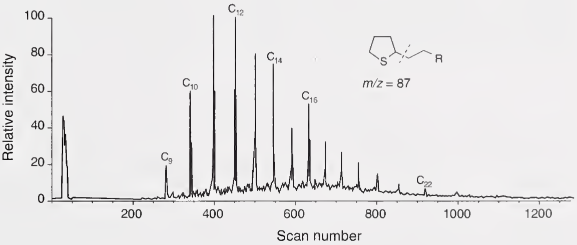

Figure 12.105 *M/z* = 87 cross-scan chromatogram of the sulfide subfraction of the toluene eluent showing the total carbon number distribution of 2-*n*-alkylthiolanes.

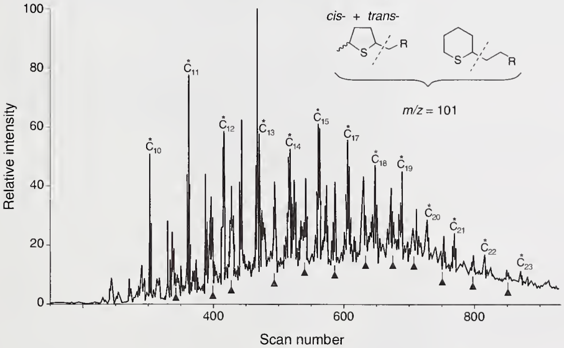

Figure 12.106 *M/z* = 101 cross-scan chromatogram of the sulfide subfraction of the toluene eluent showing the carbon number distributions of the 2-methyl-5-*n*-alkylthiolanes (*) and 2-*n*-alkylthianes (▲).

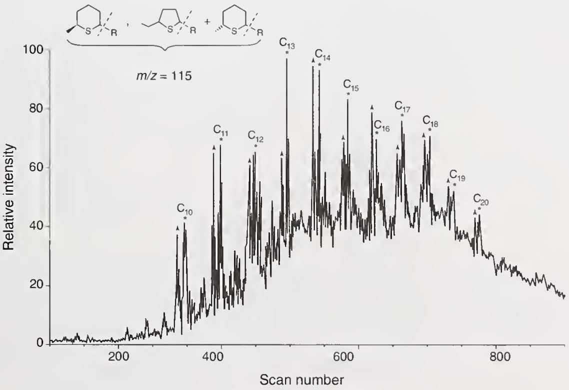

Figure 12.107 *M/z* = 115 cross-scan chromatogram of the sulfide subfraction of the toluene eluent showing the carbon number distributions of the *cis*-2-methyl-6-*n*-alkylthianes (▲) and 2-ethyl-5-*n*-alkylthiolanes + trans-2-methyl-6-*n*-alkylthianes (*).

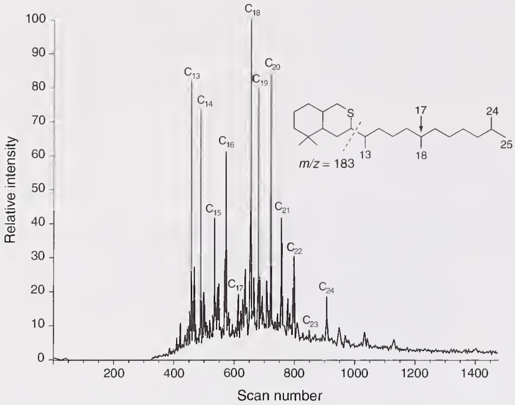

Figure 12.108 M/z = 183 cross-scan chromatogram of the sulfide subfraction of the toluene eluent showing the carbon number distribution of the bicyclic sulfides.

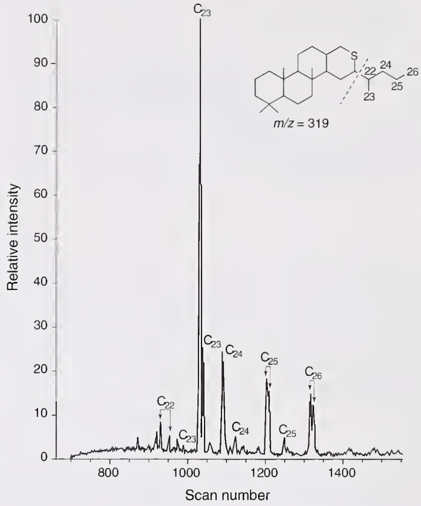

Figure 12.109 M/z = 319 cross-scan chromatogram of the sulfide subfraction of the toluene eluent, showing the carbon number distribution of the tetracyclic sulfides.

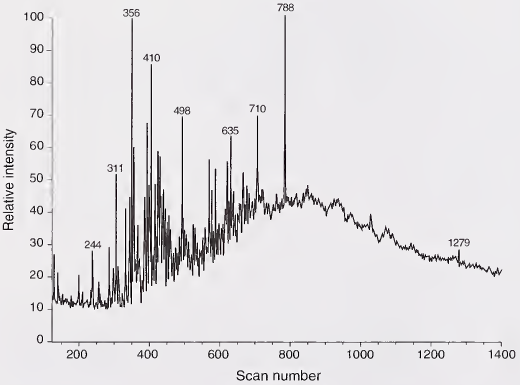

Figure 12.110 GC–MS total ion current chromatogram of the benzo- and dibenzothiophenes and benzothiolanes in the toluene eluent (Figure 12.96). See Table 12.27 for peak assignments.

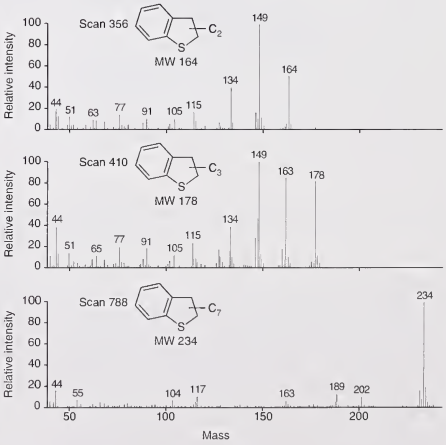

Figure 12.111 Mass spectra of peaks 356, 410 and 788 of Figure 12.110.

Table 12.27 Structural assignments for some of the peaks in Figure 12.110

Scan no. (MW)	Compound	Scan no. (MW)	Compound
244 (134)	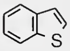	574 (198)	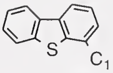
311 (148)	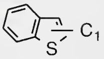	582 (198)	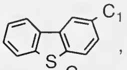, 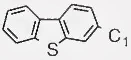
356 (164)	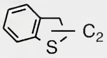	591 (198)	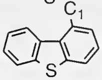
410 (178)	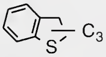	625–647 (212)	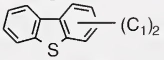
529 (184)	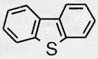	*ca* 660–690 (226)	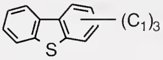
		788 (234)	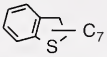

alkyldibenzothiophenes, alkylbenzothiolanes and related structures with *Z* values in their series formulas of –8 to –18 and carbon number of 8–20.

The above structural assignments were supported by field ionization studies, Figure 12.112. Table 12.28 lists some of the possible structures consistent with the observed field ionization molecular ions. These compounds are represented by the series formula $C_nH_{2n+Z}S$, where the values of *Z* range from –8 to –18 and the total number of carbon atoms in the side chain ranges from 8 to 20.

The aromatic subfraction of the toluene eluent was also examined by GC–MS and GC–FIMS. The GC–MS total ion current chromatogram is shown in Figure 12.113 and some illustrative mass spectra of individual members are reproduced in Figure 12.114. Some of the structural assignments are listed in Table 12.29. The GC–FIMS total ion current chromatogram of this material is presented in Figure 12.115 and illustrative FI mass spectra in Figure 12.116, showing the presence of benzene homologs up to pentadecyl. A number of isomers of each homolog are clearly in evidence. In summary, the main series of aromatic hydrocarbons detected are:

• alkylbenzenes with up to C_{15} side chains	C_nH_{2n-6}
• alkyltetrahydronaphthalenes with up to C_{11} side chains	C_nH_{2n-8}
• alkyloctahydrophenanthrenes with up to C_6 side chains	C_nH_{2n-10}
• alkylnaphthalenes with up to C_{11} side chains	C_nH_{2n-12}
• alkyldiphenyl or α,ω-diphenylalkane with up to C_6 side chains	C_nH_{2n-14}
• alkylfluorenes with up to C_9 side chains	C_nH_{2n-16}
• alkylphenanthrenes with up to C_7 side chains	C_nH_{2n-18}
• alkyltetrahydrochrysenes with up to C_3 side chains	C_nH_{2n-20}
• alkylpyrenes with up to C_3 side chains	C_nH_{2n-22}

Thus, hydrocarbons with carbon numbers up to 22 which are described by the series formula C_nH_{2n+Z}, where *Z* varies from –6 to –22, were detected. There appears to be little difference between the composition of the aromatics in the *n*-pentane eluent and that in the toluene eluent of the pyrolysis oil except that the former is leaner in higher-condensed molecules.

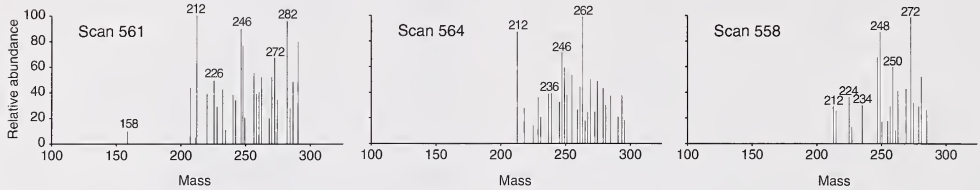

Figure 12.112 Illustrative FIM spectra of three different scans of the condensed thiophene fractions in the toluene eluent. Several molecules are eluting at the same time from the column. (Figure 12.96). See Table 12.28 for peak assignments.

Table 12.28 Probable structures for some of the components of the condensed thiophenes from FIMS

Scan no.[a] (MW)	Compound	Scan no.[a] (MW)	Compound
443 (218)	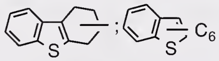	564 (240)	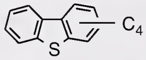
469 (224)	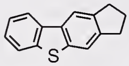	585 (246)	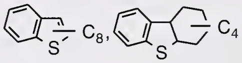
483 (232)	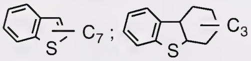	588 (286)	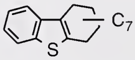
528 (242)	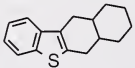	614 (244)	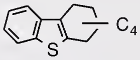
534 (256)	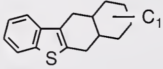	623 (258)	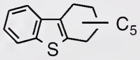
546 (248)	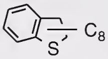	623 (270)	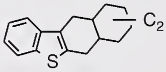
548 (212)	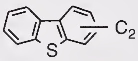	629 (296)	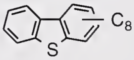
548 (262)	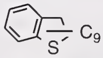	638 (274)	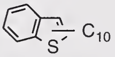
558 (226)	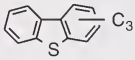	649 (282)	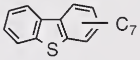
564 (306)	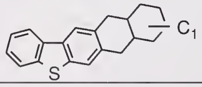		

[a] Figure 12.112

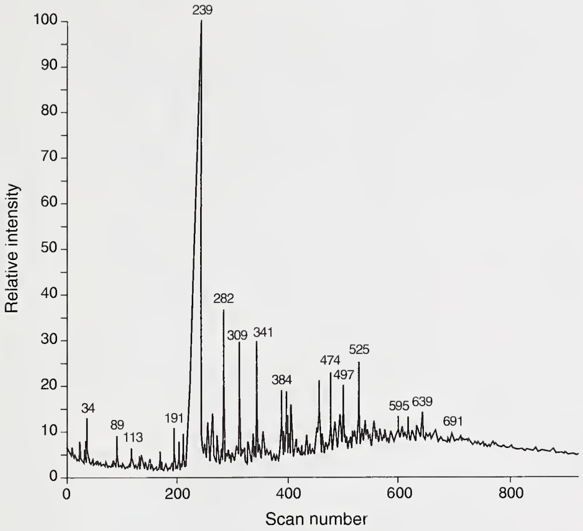

Figure 12.113 GC–MS total ion current chromatogram of the aromatic subfraction of the toluene eluent of the nondistillable resin pyrolyzate.

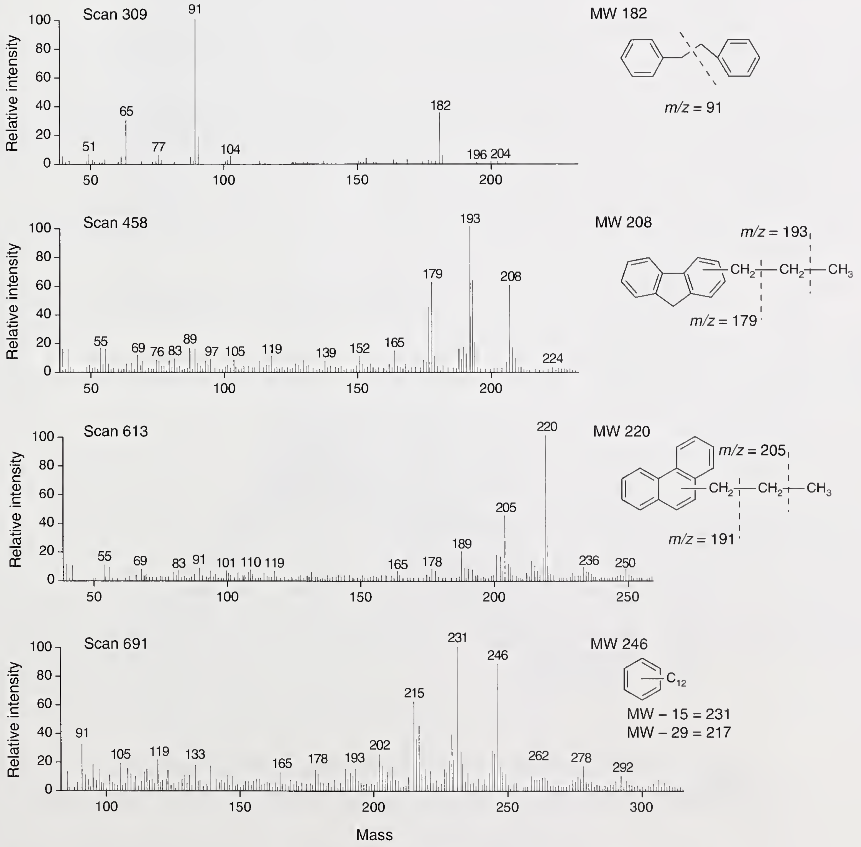

Figure 12.114 High-resolution mass spectra of scans 309, 458, 613 and 691 in Figure 12.113.

Table 12.29 Structural assignments for some of the peaks in Figure 12.113

Scan no. (MW)	Structure	Scan no. (MW)	Structure
113 (134)	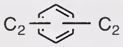	415 (210)	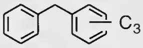
151 (148)	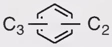	435 (196)	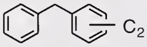
191 (142)	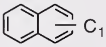	451 (208)	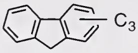
239	...artifact	480, 482 (192)	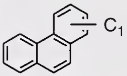
262 (156)	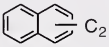	530, 541 (206)	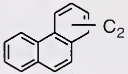
384 (202)	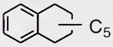	613 (220)	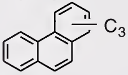
395 (180)	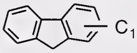	621 (218)	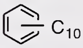
403 (194)	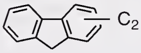	639 (232)	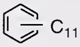
		691 (246)	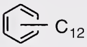

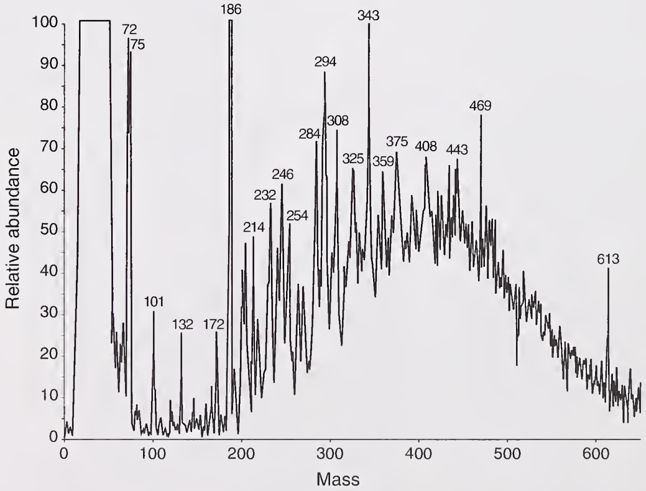

Figure 12.115 GC–FIMS total ion current chromatogram of the aromatic subfraction of the toluene eluent.

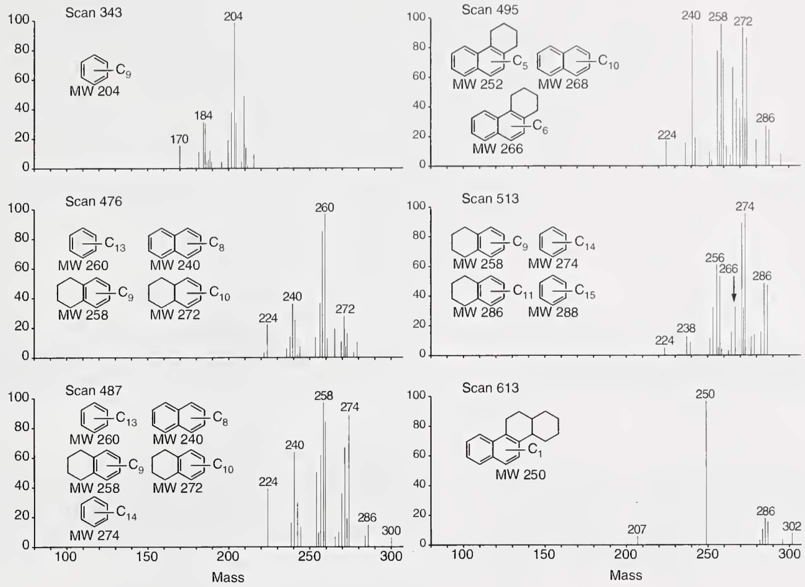

Figure 12.116 FI mass spectra of some of the peaks of Figure 12.115.

This completes the analysis of the distillable portion of the toluene eluent. The weight percentages of the fractions analyzed were: aromatic, 1.2%; condensed thiophenes, 0.5%; and sulfides, 0.4%, in terms of the nondistillable polars.

A portion of the toluene extract did not distill at 230°C and 10^{-3} Torr and was studied separately.

b) Nondistillable toluene eluent

This fraction was subjected to RICO and the resulting acids were partitioned into organic-soluble and water-soluble components. Each of these fractions was esterified with diazomethane.

The organic-soluble acid esters were chromatographed and the separated *n*-alkanoic acid methyl esters were analyzed by GC yielding the chromatogram shown in Figure 12.117. The distribution by carbon number is smooth and extends from C_7 to C_{26}. Here again the location of maximum concentration is affected by the losses, mainly due to volatility, and the true maximum would be at lower carbon numbers, perhaps as low as C_2. Elution of the organic phase with 15% EtOAc/toluene gave a fraction which afforded the total ion current mass chromatogram seen in Figure 12.118 displaying a series of α,ω-di-*n*-alkanoic acids esters from C_6 to C_{17}. These acids arise from the oxidation of *n*-alkanoic bridges connecting two aromatic ring systems in the molecules:

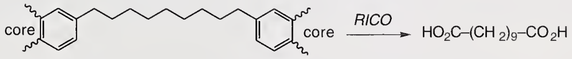

The dominance of the C_6 acid points to the abundance of hydroaromatic moieties,

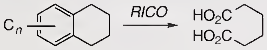

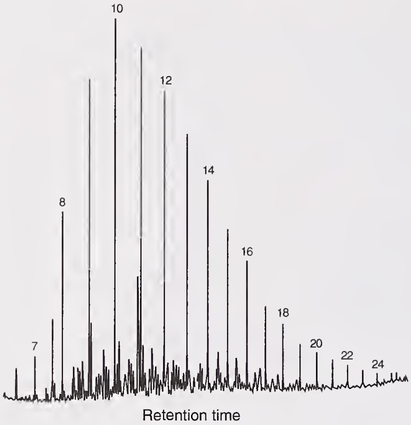

Figure 12.117 Gas chromatogram of the *n*-alkanoic acid esters from the ruthenium ions-catalyzed oxidation of the nondistillable toluene eluent. The numbers above the peaks correspond to the carbon number of the acid.

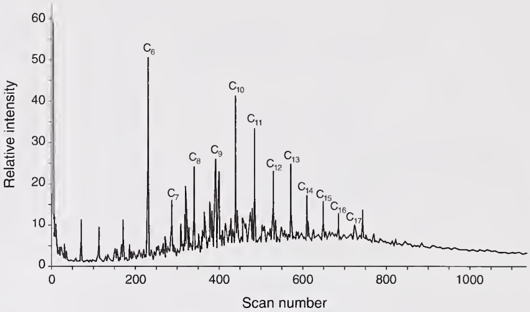

Figure 12.118 GC–MS total ion current chromatogram of the α,ω-di-*n*-alkanoic acid esters from the ruthenium ions-catalyzed oxidation of the nondistillable toluene eluent. The numbers above the peaks correspond to the carbon number of the acid.

in agreement with the GC–MS and GC–FIMS results indicating the presence of the types of hydroaromatic molecules:

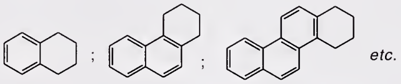

Following removal of the mono- and diesters, the residue was silylated with dimethyl *t*-butylsilylchloride and the resultant silyl ethers were analyzed by GC–MS, Figure 12.119. These ethers would form from the alcohols produced in the RICO reaction by the conversion of carbon-hydrogen bonds in activated alkanes to hydroxyl groups.^{64} Indeed, the major peaks are due to silyl ethers (except scan 192 which is disilyl ether) with unknown structures. Scan 319 could be due to benzylsilyl ether

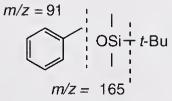

showing the major fragmentations: loss of *t*-Bu (*m/z* = 165), of methyls and *t*-Bu (*m/z* = 135) and of siloxyl (*m/z* = 91). The peaks above scan 643 are not due to silyl ethers.

The gas chromatogram of the methyl esters appearing in the aqueous phase of the RICO reaction mixture is shown in Figure 12.120. The major peaks in the series, Table 12.30, belong to benzenedi- through hexacarboxylic acid esters arising from the RICO of the condensed aromatic nuclei, *e.g.*

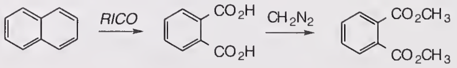

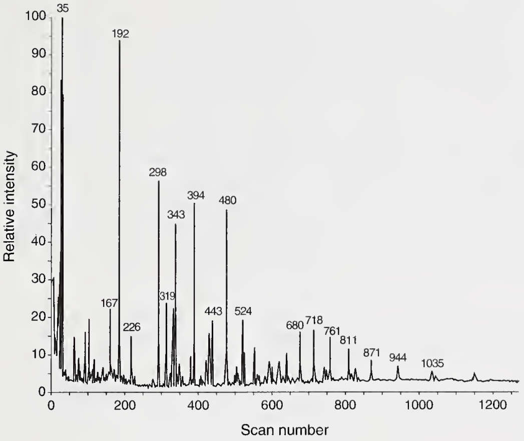

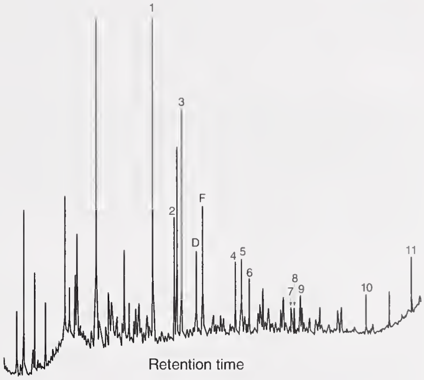

Figure 12.119 GC–MS total ion current chromatogram of the silyl ethers derived from the alcohols produced in the ruthenium ions-catalyzed oxidation of the nondistillable toluene eluent.

Figure 12.120 Gas chromatogram of the benzenepolycarboxylic acid esters produced in the ruthenium ions-catalyzed oxidation of the nondistillable toluene eluent. Peak assignments are given in Table 12.30.

Table 12.30 Structural assignments for some of the peaks in Figure 12.120 ($R = CO_2CH_3$)

Peak no.	Structure	Peak no.	Structure	Peak no.	Structure
1	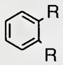	2	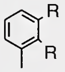	3	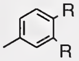
4	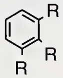	5	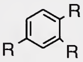	6	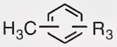
7	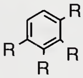	8	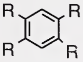	9	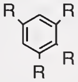
10	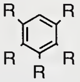	11	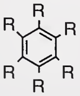	D	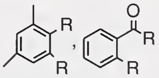
F	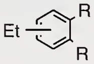				

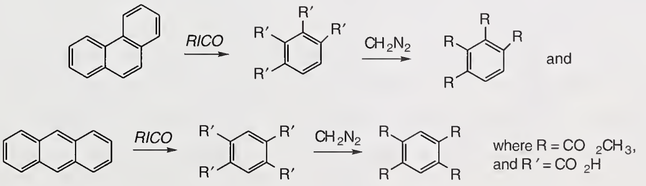

where $R = CO_2CH_3$, and $R' = CO_2H$

The distribution of these benzenecarboxylic acid esters is not too different from that found in the asphaltene fraction of the bitumen and its significance will be discussed in Chapter 14. Here, it will suffice to say that the most abundant of these acids are the 1,2-diacids and that their abundance decreases with the number of carboxylic groups in the molecule. Moreover, the extent of polycondensation in the nondistillable polars appears to be somewhat smaller than that in asphaltene which is in line with expectations based on the VPO MWs of the fractions, about 6,000 $g\cdot mol^{-1}$ for asphaltene and 1,100 $g\cdot mol^{-1}$ for the nondistillable polars.

The approximate amounts of the compound classes in the various subfractions from the nondistillable toluene eluent are: aqueous esters, 0.8%; *n*-alkanoic acid esters, 0.2%; and α,ω-acid diesters, 3.2%, in terms of nondistillable polars. The presence of the *n*-alkanoic and α,ω-diacid esters shows that dealkylation of the alkylaromatic moieties in the polars during the pyrolysis is incomplete and that relatively large amounts of *n*-alkyl bridges are left intact in the pyrolysis products.

3.2.3 The polar (CH_3OH/toluene) eluent of the distillate

Carboxylic acids, azaarenes, alcohols, carbonyl compounds and other polar substances can be expected to be present in this fraction of the pyrolysis oil.

The fraction was first treated with diazomethane (Figure 12.97) which converts carboxylic acids to their methyl esters, then was chromatographed on silica gel to separate the slightly polar esters from the rest of the fraction. The total ion current chromatogram of the esters is seen in Figure 12.121 and some illustrative mass spectra are shown in Figure 12.122. Identified were a series of tricyclic terpenoid acids and series of *n*-alkanoic acids dominated by the C_{16} and C_{18} members and showing a preference for the even-carbon-number homologs. There are a number of unidentified molecules including a major series which are evidently structurally related and have similar, nondescript mass spectra. The tricyclic terpenoid acids are probably the same molecules which were identified in the most polar fraction of the polars. These acids could, in principle, have been attached to the polar molecules either at their hydrocarbon ends or through an ester linkage since the thermolysis of the esters may afford the carboxylic acids:

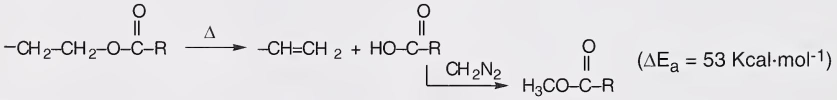

$$-CH_2-CH_2-O-\overset{O}{\overset{\|}{C}}-R \xrightarrow{\Delta} -CH=CH_2 + HO-\overset{O}{\overset{\|}{C}}-R \xrightarrow{CH_2N_2} H_3CO-\overset{O}{\overset{\|}{C}}-R \qquad (\Delta E_a = 53\ Kcal\cdot mol^{-1})$$

However, their carbon distribution, indicating a strong even carbon preference and dominated by the C_{16} and C_{18} members, clearly points to the above ester decomposition as the source of the acids. Indeed, a similar series of *n*-alkanoic acid esters was shown to be present in Athabasca asphaltene (see Chapter 14).

Following removal of the acids, the basic nitrogen compounds were separated by complexation with $CuCl_2\cdot 2H_2O$ and analyzed by GC–MS, Figure 12.123. According to the tentative structural assignments, Table 12.31, the mixture consists of the same types of basic nitrogen compounds as found in the distillable polars, namely alkylated pyridines, quinolines, azafluorenes and azaphenanthranes, each of which occur in a number of isomeric forms.

The residual polar eluent was reacted with a mixture of KOH, crown ether and ethylbromoacetate to test the mixture for the presence of acidic centers such as quinolones.

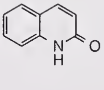

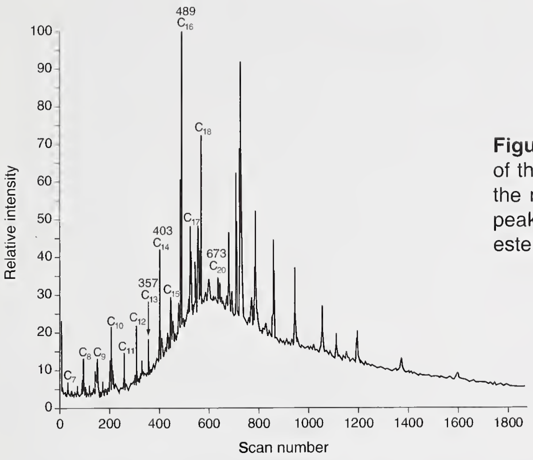

Figure 12.121 GC–MS total ion current chromatogram of the methyl esters of the carboxylic acids present in the methanol/toluene eluent. The numbers above the peaks correspond to the carbon numbers of the acid esters.

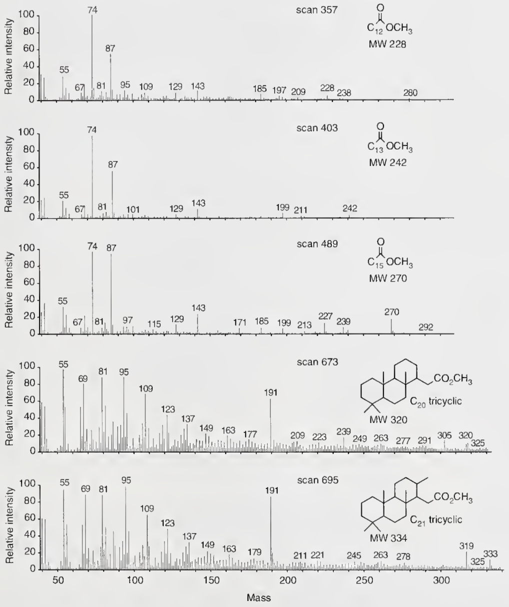

Figure 12.122 EIMS spectra of scans 357, 403, 489, 673 and 695 of Figure 12.121.

Table 12.31 Structural assignments for some of the peaks in Figure 12.123

Scan no. (MW)	Structure	Scan no. (MW)	Structure	Scan No. (MW)	Structure
341 (157)	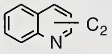	410 (177)	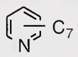	608 (207)	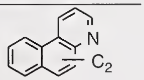
378 (171)	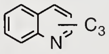	429 (227)	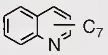	655 (227)	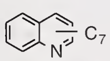
383 (177)	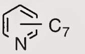	469 (185)	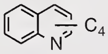	812 (279)	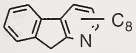
398 (171)	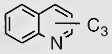	579 (213)	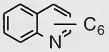		

The GC–MS total ion current and mass spectra, Figures 12.124 and 12.125, indeed suggest that alkylquinolones may be present, *e.g.* scan 725 could indicate

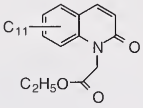

,

and scan 576

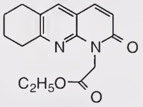

, *etc.*

Also present are a series of peaks which have the correct MWs for alkylindenes and carbazoles. Such compounds, however, should have eluted before in the toluene eluent and would not be expected to be present in the polar eluent.

The next group of compounds tested for were the alcohols using, as before, *t*-butyldimethylsilylchloride to derivatize them. The silyl ethers were separated chromatographically and analyzed by GC and GC–MS. The gas chromatogram, Figure 12.126, indicated the presence of alkylated benzyl alcohols, tetralin alcohols, decanol and possibly a phenanthranol. Some tentative peak assignments are listed in Table 12.32.

During elution of the silyl ethers, a red band was observed on the column. This was eluted with additional toluene to yield a reddish oily material giving the total ion current chromatogram in Figure 12.127. The series identified here is that of methyl *n*-alkyl ketones,

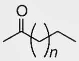

where n = 7–11 or possibly 16. The mass spectrum of these ketones is characterized by a strong m/z = 58 ion which arises from the Norrish-type fragmentation

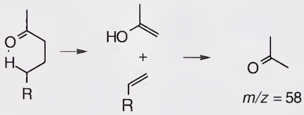

In Figure 12.128, scan 320 of Figure 12.127 is compared with the mass spectrum of authentic 2-dodecanone. The similarity of the two spectra is convincing and appears to confirm the structural assignment. The ketones, like the quinolones and fluorenones which were identified after derivatization with ethylbromoacetate, should have eluted with toluene and their presence in the polar fraction is puzzling.

The most polar residue left behind after removal of ketones contained, according to its FTIR spectrum, compounds with OH, CO, CH_2, CH_3 and aromatic carbon functionalities. GC–MS analysis of this material was inconclusive, but it would appear to be consistent with the presence of alkylated compound types such as

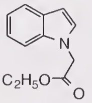

,

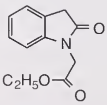

,

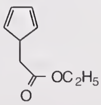

,

and others. The $-CH_2COOC_2H_5$ group originated from the ethyl bromoacetate treatment.

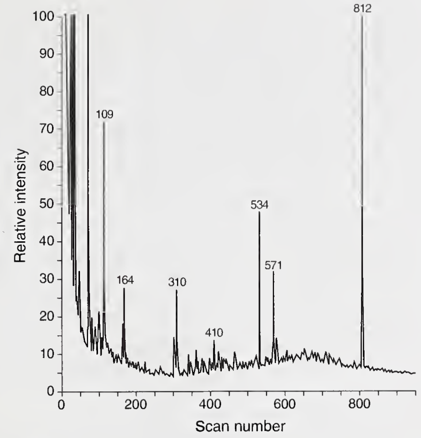

Figure 12.123 GC–MS total ion current chromatogram of the basic nitrogen compounds in the methanol/toluene eluent. Tentative peak assignments are listed in Table 12.31.

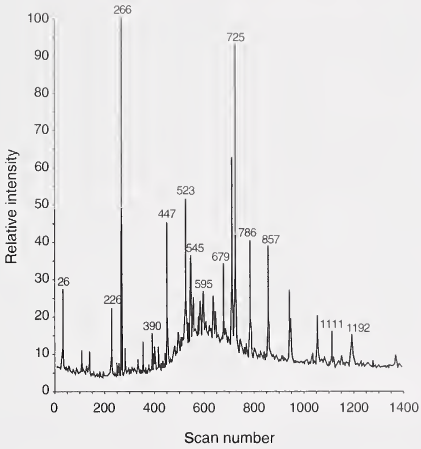

Figure 12.124 GC–MS total ion current chromatogram of the quinolones in the methanol/toluene eluent.

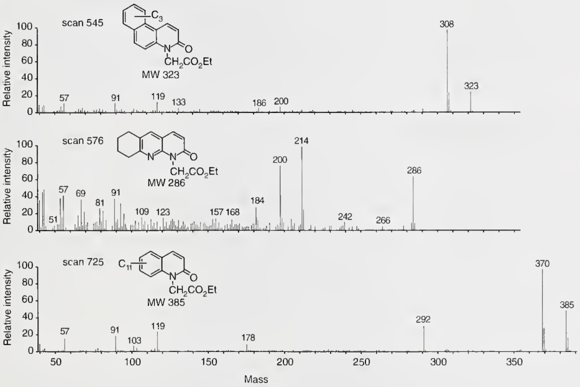

Figure 12.125 High-resolution mass spectra of scans 545, 576 and 725 of Figure 12.124.

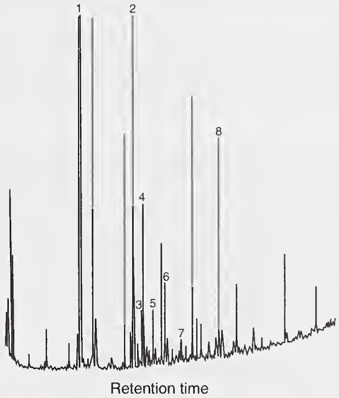

Figure 12.126 Gas chromatogram of the silyl ethers of the alcohols present in the methanol/toluene eluent. Tentative peak assignments are listed in Table 12.32.

Table 12.32 Structural assignments for some of the peaks in Figure 12.126[a]

Peak no.	Structure	Peak no.	Structure
1	(*t*-Bu)Si–R	5	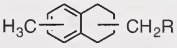
2	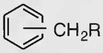	6	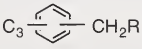
3	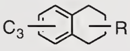	7	$CH_3-(CH_2)_8CH_2R$
4	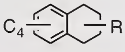	8	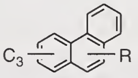 (tentative)

[a] R = –O–Si(*t*-Bu)

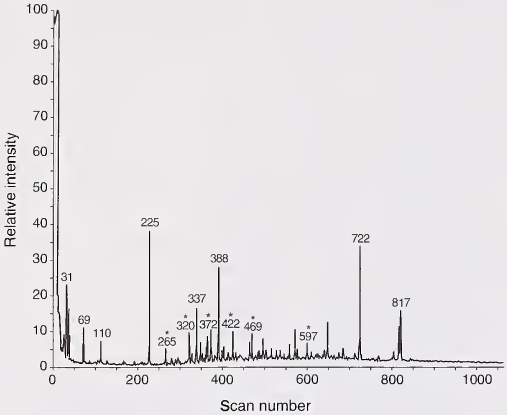

Figure 12.127 GC–MS total ion current chromatogram of the methyl-*n*-alkylketones (marked *) in the methanol/toluene eluent.

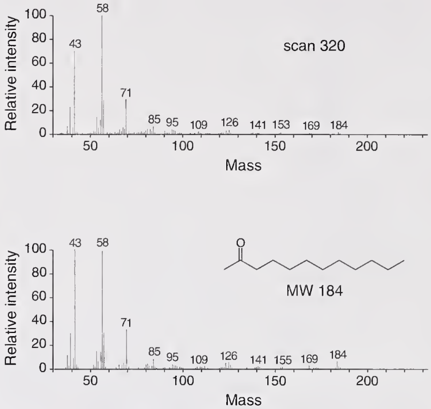

Figure 12.128 High-resolution mass spectra of scan 320, Figure 12.127, and authentic 2-dodecanone.

The fractions isolated from the polar eluent comprised a small weight percentage of the nondistillable polars with the exception of the ester fraction, which amounted to 3.2%. The percentages of the other fractions were: basic nitrogens, 0.4; alcohols and ketones, 0.2 each.

3.2.4 Pyrolysis oil recovered from the reactor

At the conclusion of the pyrolysis, the char in the reactor was extracted with methylene chloride. The extract, which amounted to 5.2 wt%, was fractionated by solvent extraction, using the same solvent system as with the distillate, into a pentane, a toluene and a polar extract (1.5, 1.1 and 1.5% of the nondistillable polar fraction). The pentane eluent gave the gas chromatogram shown in Figure 12.129. It reveals the presence of *n*-alkane/*n*-alkene series (C_{11}–C_{32}) along with other hydrocarbons as indicated by the broad, unresolved continuum. No further analysis has been done on this material but it may be assumed that it has a composition similar that of the distillable portion of the pyrolysis oil.

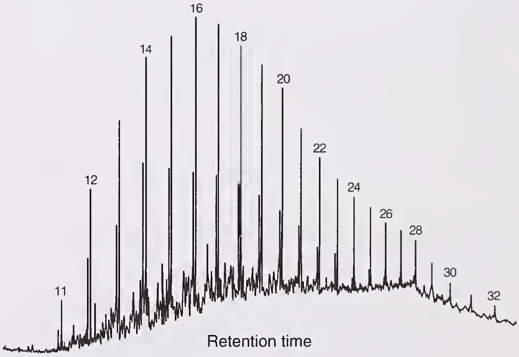

Figure 12.129 Gas chromatogram of the *n*-pentane eluent of the pyrolysis oil extracted from the residue. The numbers above the peaks correspond to the carbon number of the *n*-alkane. The corresponding 1-*n*-alkenes are the smaller peaks immediately to the left of the *n*-alkanes.

3.3 Summary and conclusions

On pyrolysis the nondistillable polars gave an oil (62.4%) and a charry residue. About 10% of the polar material in the pyrolysis oil has been identified at the molecular level. It consisted of many homologous series and a large number of individual compounds which were covalently bonded by one (and not more than two) bonds to other polar molecules. Assuming that these compounds are primary cleavage products, they give information about the structural elements of the polar molecules. From this it appears that the global composition of the nondistillable polars is fundamentally different from that of the distillable polars, and this is most explicitly manifested by their ^{13}C NMR spectra. The nondistillable polars are rich in *n*-alkyl moieties which are primarily present as long side chains and bridges attached to aromatics and, to a lesser extent, naphthenic carbons. The distinction between distillable and nondistillable polars is reminiscent of that of the aromatics and in both cases, the nondistillable portions bear close structural relationships to the asphaltene fraction, as will be seen in Chapter 14, while the distillable portions, being rich in terpenoid and terpenoid-derived structures, are more similar to the saturate fraction of the maltene. The compounds and homologous series of compounds identified in the pyrolysis products of the nondistillable polars are also produced, with a few exceptions, in the pyrolysis of the asphaltene.

4.0 Thermolysis of the Polars

On the basis of the above descriptions of the chemical composition of the distillable polars subfraction and the flash pyrolysis products of the nondistillable polar subfraction, it can be surmized that the thermal decomposition of the whole polar fraction must be a complex process comprising many parallel, simultaneous and sequential reactions. Some of these reactions are independent of one another while others are interrelated and interdependent. These interactive properties extend to the components of other compound class fractions, if present, and indeed it is widely recognized that the thermolysis properties of given fractions of bitumen are interdependent and that the thermolysis properties of the bitumen itself are not simple additive properties of the constituent fractions. In other words, the thermolysis properties of the whole bitumen cannot be estimated as an arithmetic or molar mean of those of the compound class fractions constituting the bitumen.

Polars impact the thermolysis properties of bitumen in a major way, partly because of their high concentrations and partly because of their compositional and MW distributional variance. The thermal decomposition reactions of the saturate fraction and the alkylaromatic hydrocarbons are simpler because in all the different molecules they are restricted to the cleavage of relatively few types of bonds. They have also been more extensively investigated and are better understood.

Thermogravimetric results on Athabasca polar fractions feature a faster weight loss at lower temperatures for the more polar, higher-MW Polar II than the Polar I fraction, Figure 12.130. This apparent anomaly can be attributed to differences in MW distribution. From Table 12.2 it can be seen that the overall higher MW of Polar II is due to the higher MW and higher concentration of subfraction

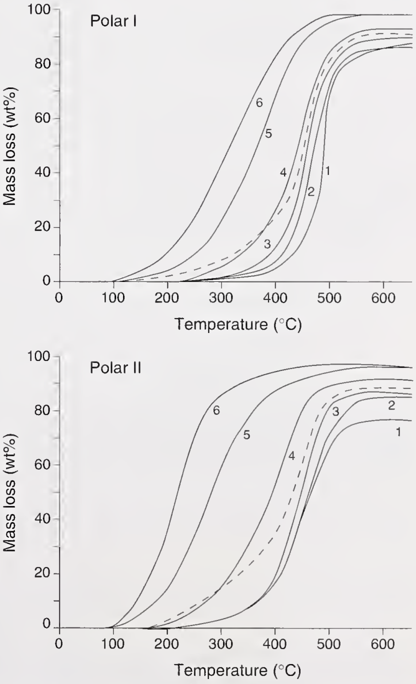

Figure 12.130 Thermogravimetric percentage weight losses of Polars I and II (Table 12.1) and their GPC fractions (Table 12.2).

II–1 as well as the higher concentration of subfraction II–2 since the MWs of subfractions Polar II–3–6 are the same or slightly less than those of the corresponding subfractions of Polar I. For both fractions the amount of >600°C residue increases with increasing MW—a trend which is in line with general experience in petroleum chemistry.

Thermolysis of the Polar I and II GPC fractions at constant temperature (390°C, near the threshhold of thermal decomposition) in a stream of nitrogen shows opposite trends in the distillate yields as a function of fraction number (*i.e.* MW), Figure 12.131: the distillate yields from the Polar I subfractions decrease, whereas those from the Polar II subfractions increase, with increasing fraction number. The gas chromatograms of the saturate fractions of the distillates are shown in Figure 12.132 where it is seen that in both cases the predominance of *n*-alkanes seen in subfractions 1 gradually decreases with decreasing MW and, in the cases of the lightest subfractions, 5, *n*-alkanes appear to be absent altogether. Although the thermolyses of GPC subfractions 6 were not investigated it is reasonable to assume that *n*-alkanes would not have been produced either. GPC subfractions 5 and 6 comprise 30 and 20% of Polar I and Polar II.

These results are in agreement with the ^{13}C NMR results on the low-MW distillable and high-MW nondistillable portions of the polars, reinforcing the conclusion that the former is structurally and probably genetically related to the low-MW distillable portion of the hydrocarbons and the latter, to the asphaltene fraction of the bitumen.

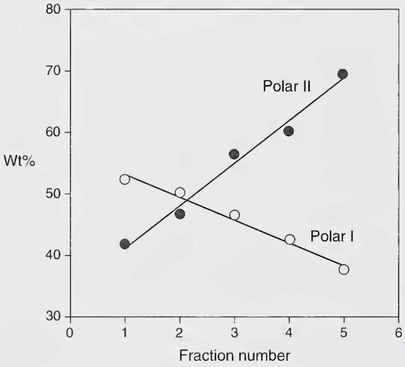

Figure 12.131 Yields of distillates from the thermolysis (1 h, 390°C) of the GPC fractions of Polars I and II.

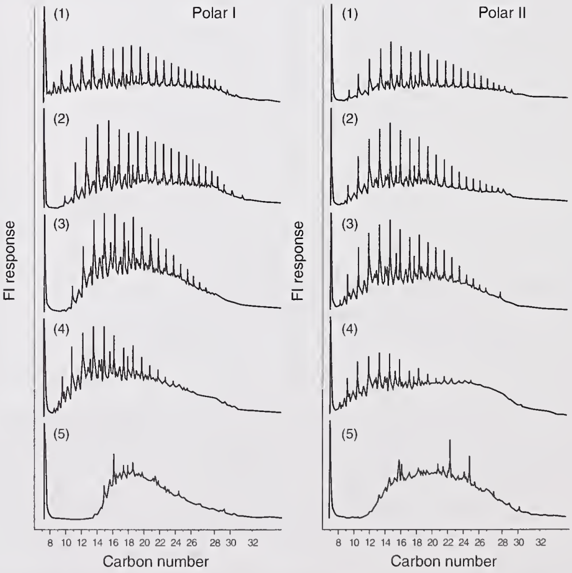

Figure 12.132 Gas chromatograms of the saturated hydrocarbons produced in the thermolysis of the Polars I and II GPC fractions.

Bibliography

1. O.P. Strausz, S. Berlozecki and T. Ignasiak, Progress Report to AOSTRA, "Chemical Studies on Resins", Agreement #142, May 26, 1981–June 30, 1982.
2. J.D. Payzant, A.M. Hogg, D.S. Montgomery and O.P. Strausz, "A Field Ionization Mass Spectrometric Study of the Maltene Fraction of Athabasca Bitumen. Part III – The Polars", AOSTRA J. Res., 1 (1985) 203.
3. J.D. Payzant, D.S. Montgomery and O.P. Strausz, "Novel Terpenoid Sulfoxides and Sulfides in Petroleum", Tetrahedron Lett., 24 (1983) 651.
4. J.D. Payzant, T.D. Cyr, D.S. Montgomery and O.P. Strausz, "The Synthesis of 1β(H),6β(Me)-2,2,6-Trimethyl-8-Ethylbicyclo-[4,3,0]-7-Thianonane and the Structure of the Isomeric Bicyclic Terpenoid Sulfides Occurring in Petroleum", Tetrahedron Lett., 26 (1985) 4175.
5. T.D. Cyr, J.D. Payzant, D.S. Montgomery and O.P. Strausz, "A Homologous Series of Novel Hopane Sulfides in Petroleum", Org. Geochem., 9 (1986) 139.
6. O.P. Strausz, E.M. Lown and J.D. Payzant, "Nature and Geochemistry of Sulfur-Containing Compounds in Alberta Petroleums", Ch. 22 in *Geochemistry of Sulfur in Fossil Fuels*, ACS Symp. Series 429, W.L. Orr and C.M. White, Eds., American Chemical Society, Washington, D.C., 1990, p. 366.
7. J.D. Payzant, T.W. Mojelsky and O.P. Strausz, "Improved Methods for the Selective Isolation of the Sulfide and Thiophenic Classes of Compounds from Petroleum", Energy & Fuels, 3 (1989) 449.
8. O.P. Strausz, E.M. Lown and J.D. Payzant, "Isolation of Sulfur Compounds from Petroleum", Ch. 5 in *Geochemistry of Sulfur in Fossil Fuels*, ACS Symp. Series 429, W.L. Orr and C.M. White, Eds., American Chemical Society, Washington, D.C., 1990, p. 83.
9. J.D. Payzant, D.S. Montgomery and O.P. Strausz, "Sulfides in Petroleum", Org. Geochem., 9 (1986) 357.
10. J.D. Payzant, T.D. Cyr, D.S. Montgomery and O.P. Strausz, "Studies on the Structures of the Terpenoid Sulfide Type Biological Markers in Petroleum" in *Geochemical Biomarkers*, T.F. Yen and J.M. Moldowan, Eds., Harwood Academic Publishers, Chur, Switzerland, 1988, p. 133.
11. P.M. Fedorak, J.D. Payzant, D.S. Montgomery and D.W.S. Westlake, "Microbial Degradation of *n*-Alkyl Tetrahydrothiophenes Found in Petroleum", Appl. Environ. Microbiol., 54 (1988) 1243.
12. J.D. Payzant, D.D. McIntyre, T.W. Mojelsky, M. Torres, D.S. Montgomery and O.P. Strausz, "The Identification of Homologous Series of Thiolanes and Thianes Possessing a Linear Carbon Framework from Petroleums and Their Interconversion Under Simulated Geological Conditions", Org. Geochem., 14 (1989) 461.
13. H.H. Chen, T.W. Mojelsky, J.D. Payzant, E.M. Lown, D. Henry, D. Wallace and O.P. Strausz, "Chemical Changes in Alberta Oil Sands During Steam Treatment", AOSTRA J. Res., 7 (1991) 17.
14. O.P. Strausz, "Oil Fingerprinting", Final Report to Alberta Energy Co., February 1989.
15. M.E.L. Kohnen, J.S. Sinninghe Damsté, A.C. Kock-van Dalen and J.W. DeLeeuw, "Di- or Polysulphide Bound Biomarkers in Sulphur-Rich Geomacromolecules as Revealed by Selective Chemolysis", Geochim. Cosmochim. Acta, 55 (1991) 1375; P. Peng, A. Morales–Izquierdo, J. Fu, G. Sheng, J. Jiang, A. Hogg and O.P. Strausz, "Lanostane Sulfides in an Immature Oil", Organic Geochem., 28 (1998) 125.
16. Z. Frakman, T.M. Ignasiak, E.M. Lown and O.P. Strausz, "Oxygen Compounds in Athabasca Asphaltene", Energy & Fuels, 4 (1990) 263.
17. J.D. Payzant, E.M. Lown and O.P. Strausz, "Structural Units of Athabasca Asphaltene: The Aromatics with a Linear Carbon Framework", Energy & Fuels, 5 (1991) 445.
18. P.M. Fedorak and D.W.S. Westlake, "Fungal Metabolism of *n*-Alkylbenzenes", Appl. Environ. Microbiol., 51 (1986) 435; "Degradation of Sulfur Heterocycles in Prudhoe Bay Crude Oil by Soil Enrichments", Water, Air, Soil Pollut., 21 (1984) 225.
19. K.M. Scow, "Rate of Biodegradation", Ch. 9 in *Handbook of Chemical Property Estimation Methods*, W.J. Lyman, W.F. Reehl and D.H. Rosenblatt, Eds., American Chemical Society, Washington, D.C., 1990, p. 58.

20. T.D. Cyr and O.P. Strausz, "The Structures of Tricyclic Terpenoid Carboxylic Acids and Their Parent Alkanes in the Alberta Oil Sands", J. Chem. Soc., Chem. Commun. (1983) 1028; "Bound Carboxylic Acids in the Alberta Oil Sands", Org. Geochem., 7 (1984) 1271; T.D. Cyr, Postdoctoral Fellowship Report to AOSTRA, October 1983.

21. V.N. Aiyar, O.H. Houwen and F.W. Bachelor, "Distribution of Nitrogen in Fractions of Athabasca Bitumen", Fuel, 59 (1980) 276.

22. T.D. Cyr, "Carboxylic Acids in the Bitumen and Bound to the Mineral Matter of Alberta Oil Sands", AOSTRA Fellowship Report, June, 1982.

23. W.K. Seifert and J.M. Moldowan, "The Effect of Thermal Stress on Source Rock Quality as Measured by Hopane Stereochemistry", in *Advances in Organic Geochemistry* 1979, A.G. Douglas and J.R. Maxwell, Eds., Pergamon Press, Oxford, U.K., 1980, p. 229.

24. J.M. Schmitter, P. Arpino and G. Guichoss, "Investigation of High Molecular Weight Carboxylic Acids in Petroleum by Different Combinations of Chromatography (Gas and Liquid) and Mass Spectrometry (Electron Impact and Chemical Ionization)", J. Chromatogr., 167 (1978) 149.

25. A.S. Mackenzie, G.A. Wolff and J.R. Maxwell, "Fatty Acids in Some Biodegraded Petroleums. Possible Origins and Significance", in *Advances in Organic Geochemistry* 1981, M. Bjorøy *et al.*, Eds., Wiley-Heyden, London, 1983, p. 637.

26. M.L. Selucky, T. Ruo, Y. Chu and O.P. Strausz in *Analytical Chemistry of Liquid Fuel Sources: Tar Sands, Oil Shale, Coal and Petroleum*, S. Siggia and H.B. Jensen, Eds., Advan. Chem. Ser. 170, American Chemical Society, Washington, D.C., (1978) p. 117.

27. (a) J.G. Speight and S.E. Moschopedis, "Anomalous Effects in the Character of the Carbonyl Absorption (ca 1700 cm^{-1}) in the Infrared Spectra of Petroleum Resins and Asphaltenes", Prepr., Am. Chem. Soc., Div. Petrol. Chem., 26 (1981) 907. (b) K. Bukka, J.D. Miller, F.V. Hanson, M. Misra and A.G. Oblad, "The Influence of Carboxylic Acid Content on Bitumen Viscosity", Fuel, 73 (1994) 257.

28. T.W. Mojelsky and O.P. Strausz, "Detection of Methyl Fluorenones in Athabasca Oil Sand Bitumens", Org. Geochem., 9 (1986) 31.

29. J.D. Payzant, A.M. Hogg, D.S. Montgomery and O.P. Strausz, "A Field Ionization Mass Spectrometric Study of the Maltene Fraction of Athabasca Bitumen. Part I – The Saturates", AOSTRA J. Res., 1 (1985) 175.

30. T.W. Mojelsky and O.P. Strausz, "Detection of Alkylated Fluorenes in Athabasca Oil Sand Bitumens", Org. Geochem., 9 (1986) 39.

31. J.D. Payzant, T.W. Mojelsky, T.D. Cyr, D.S. Montgomery and O.P. Strausz, "The Identification of 9-n-Alkyl Fluoren-9-ols in the Alberta Oil Sands", Org. Geochem., 8 (1985) 177.

32. M.L. Selucky, S.S. Kim, F. Skinner and O.P. Strausz, "Structure-Related Properties of Athabasca Asphaltenes and Resins as Indicated by Chromatographic Separation", in *Chemistry of Asphaltenes*, Advan. Chem. Ser. 195, American Chemical Society, Washington, D.C., 1981, p. 83.

33. A. Treibs, "Organic Minerals. III. Chlorophyll and Hemin Derivatives in Bituminous Rocks, Petroleums, Mineral Waxes and Asphalts. Origin of Petroleum", Justus Liebigs Ann. Chem., 510 (1934) 42.

34. J.M. Schmitter, P. Garrigues, I. Ignatiadis, R. DeVazelhes, F. Perin, M. Ewald and P. Arpino, "Occurrence of Tetraaromatic Azaarenes in Petroleum", Org. Geochem., 6 (1984) 579.

35. J.M. Schmitter and P. Arpino, "Possible Origin and Fate of α-Methylquinolines and α-Methylbenzo[*h*]quinolines From Crude Oils", in *Advances in Organic Geochemistry 1981*, M Bjorøy, *et al.*, Eds., Wiley-Heyden, London, 1983, p. 808.

36. Z. Frakman, T.M. Ignasiak, D.S. Montgomery and O.P. Strausz, "Nitrogen Compounds in Athabasca Asphaltene: The Carbazoles", AOSTRA J. Res., 3 (1987) 131.

37. P.L. Jokuty and M.R. Gray, "Resistant Nitrogen Compounds in Hydrocracked Gas Oil From Athabasca Bitumen", Energy & Fuels, 5 (1991) 791.

38. H.L. Lochte, " Petroleum Acids and Bases", Ind. Eng. Chem., 44 (1952) 2597.

39. J.M. Schmitter, I. Ignatiadis and P.J. Arpino, "Distribution of Diaromatic Nitrogen Bases in Crude Oils", Geochim. Cosmochim. Acta, 47 (1983) 1975.

40. J.M. Schmitter, H. Colin, J.L. Excoffier, P. Arpino and G. Guichon, "Identification of Triaromatic Nitrogen Bases in Crude Oils", Anal. Chem., 54 (1982) 769.

41. L.M. Schenck and J.R. Bailey, "The Nitrogen Compounds in Petroleum Distillates. XXIII. Isolation of 2,3-Dimethylbenzo[*h*]quinoline (I) and 2,4-Dimethylbenzo[*h*]quinoline (II) from California Petroleum", J. Am. Chem. Soc., 63 (1941) 2331.

42. P.M. Draper and D.B. MacLean, "Mass Spectra of Alkylquinolines", Can. J. Chem., 46 (1968) 1487.

43. a) T.W. Mojelsky, D.S. Montgomery and O.P. Strausz, "The Basic Nitrogen Compounds in Athabasca Maltene", AOSTRA J. Res., 3 (1986) 25. b) Yuezhu Chen, University of Petroleum, China and Department of Chemistry, University of Alberta. Unpublished results.

44. S. Imamichi, T. Kodama, F. Morishita and T. Kojima, "Analysis of Azaarenes in Coal Liquids", Bunseki Kagaku (Anal. Chem.), 34 (1985) 282.

45. M. Yamamoto, K. Taguchi and K. Sasaki, "Basic Nitrogen Compounds in Bitumen and Crude Oils", Chem. Geol., 93 (1991) 193.

46. S.A. Holmes, "Nitrogen Functional Groups in Utah Tar Sand Bitumen and Produced Oil", AOSTRA J. Res., 2 (1986) 167.

47. P.L. Jokuty and M.R. Gray, "Nitrogen Bases Resistant to Hydrodenitrogenation: Evidence Against Using Quinoline as a Model Compound", Ind. & Eng. Chem. Res., 31 (1992) 1445.

48. P.A. Claret and A.G. Osborne, "Alkylquinolines and Arylquinolines", in *Quinolines*, G. Jones, Ed., Wiley, New York, N.Y., 1982, Part II.

49. E.W. Baker, "Mass Spectrometric Characterization of Petroporphyrins", J. Am. Chem. Soc., 88 (1966) 2311; E.W. Baker, T.F. Yen, J.P. Dickie, R.E. Rhodes and L.F. Clark, "Mass Spectrometry of Porphyrins II. Characterization of Petroporphyrins", J. Am. Chem. Soc., 89 (1967) 3631; E.W. Baker and J.W. Louda, "Porphyrins in the Geological Record", Ch. 4 in *Biological Markers in the Sedimentary Record*, R.B. Johns, Ed., Elsevier, Amsterdam, 1986, p. 125; *cf.* also H.J. Callot and R. Ocampo, "Geochemistry of Porphyrins" in *The Porphyrin Handbook*, Vol. 1. Synthesis and Organic Chemistry, Ch. 7, p. 349, Eds., K.M. Kadish, K.M. Smith and R. Guillard, Academic Press, 2000.

50. A. Treibs, "Organic Mineral Substances. II. Occurrence of Chlorophyll Derivatives in an Oil Shale of the Upper Triassic", Justus Liebigs Ann. Chem., 509 (1934) 103; "Chlorophyll and Hemin Derivatives in Organic Mineral Substances", Angew. Chem., 49 (1936) 682.

51. a) E.W. Baker and S.E. Palmer, "Geochemistry of Porphyrins", Ch. 11 in *The Porphyrins, Part A, Structure and Synthesis*, D. Dolphin, Ed., Academic Press, New York, N.Y., 1978, p. 485. b) N. Zh. Mamardashvili and O.A. Golubchikov, "Spectral Properties of Porphyrins and Their Precursors and Derivatives", Russ. Chem. Revs., 70 (2001) 577; c) I. Baraldi, A. Carnevali, G. Ponterini and D. Vanossi, "Electronic Spectrum of Porphyrins. CS INDO CI Study", J. Mol. Structure (Theochem.) 333 (1995) 121.

52. a) T. Yokota, F. Scriven, D.S. Montgomery and O.P. Strausz, "Absorption and Emission Spectra of Athabasca Asphaltene in the Visible and Ultraviolet Regions", Fuel, 65 (1986) 1142. b) Z. Frakman, T.M. Ignasiak, D.S. Montgomery and O.P. Strausz, "Nitrogen Compounds in Athabasca Asphaltene: The Vanadyl Porphyrins", AOSTRA J. Res., 4 (1988) 171.

53. D. Strong and R.H. Filby, "Vanadyl Porphyrin Distribution in Athabasca Oil Sand Bitumens", in *Metal Complexes in Fossil Fuels*, R.H. Filby and J.F. Branthaver, Eds., ACS Symposium Series 344, American Chemical Society, Washington, D.C., 1987, p. 154.

54. M.D. Lewan, "Factors Controlling the Proportionality of Vanadium to Nickel in Crude Oils", Geochim. Cosmochim. Acta, 48 (1984) 2231.

55. K.E. Peters and J.M. Moldowan, *The Biomarker Guide*, Prentice Hall, Englewood Cliff, N. J., 1993, p. 206.

56. J.F. Branthaver, "Influence of Metal Complexes in Fossil Fuels on Industrial Operations", in *Metal Complexes in Fossil Fuels*, R.H. Filby and J.F. Branthaver, Eds., ACS Symposium Series 344, American Chemical Society, Washington, D.C., 1987, p. 188.

57. J.B.F. Champlin and H.N. Dunning, "A Geochemical Investigation of the Athabasca Bituminous Sands", Econ. Geol., 55 (1960) 797.

58. G.W. Hodgson and B.L. Baker, "Vanadium, Nickel and Porphyrins in Thermal Geochemistry of Petroleum", Am. Assoc. Petrol. Geol. Bull., 41 (1957) 2413; G.W. Hodgson, E. Peake and B.L. Baker, "Origin of Petroleum Porphyrins — Position of the Athabasca Oil Sands", in *The Karl A. Clark Volume, A Collection of Papers on the Athabasca Oil Sands*, Research Council of Alberta, Edmonton, Alberta, 1963, p. 75.

59. C.F. Hoffman and O.P. Strausz, "Bitumen Accumulation in Grosmont Platform Complex", Am. Assoc. Petrol. Geol. Bull., 70 (1986) 1113.

60. K.M. Sample, N. Cyr, Ph.M. Federak and D.W.S. Westlake, "Characterization of Asphaltenes from Cold Lake Heavy Oil: Variation in Chemical Structure and Composition with Molecular Weight", Can. J. Chem., 68 (1990) 1092.

61. R.H. Filby and G.J. Van Berkel, "Geochemistry of Metal Complexes in Petroleum, Source Rocks, and Coals: An Overview", in *Metal Complexes in Fossil Fuels*, R.H. Filby and J.F. Branthaver, Eds., ACS Symposium Series 344, American Chemical Society, Washington, D.C., 1987, p. 2; M.I. Chicarelli, S. Kaur and J.R. Maxwell, "Sedimentary Porphyrins: Unexpected Structures, Occurrences, and Possible Origins", *ibid.*, p. 40; R. Ocampo, H.J. Callot and P. Albrecht, "Evidence for Porphyrins of Bacterial and Algal Origin in Oil Shale", *ibid.*, p. 68.

62. W.R.M. Graham, "Analysis of Metal Species in Petroleum and Tar Sands Using the Electron Paramagnetic Resonance and Fourier Transform Infrared Techniques", in M*etal Complexes in Fossil Fuels*, R.H. Filby and J.F. Branthaver, Eds., ACS Symposium Series 344, American Chemical Society, Washington, D.C., 1987, p. 358.

63. T.W. Mojelsky, I. Safarik, E.M. Lown and O.P. Strausz. To be published.

64. J.M. Bakke and M. Lundquist, "The RuO_4 Oxidation of Cyclic Saturated Hydrocarbons. Formation of Alcohols", Acta Chem. Scand., Ser. B40 (1986) 430.

Biomarkers in Bitumens

13

The terms biomarkers, biological markers and molecular fossils refer to ancient molecules synthesized by living organisms which gave rise to the formation of sedimentary organic matter or which became associated with the sedimentary organic matter at a later stage of its evolutionary history and retained their structural integrity in the sediments over geological times. The first biomarkers discovered in petroleum by Treibs[1] were the porphyrins, the geochemical degradation products of chlorophylls, hemes and related biomolecules. Their detection provided the first direct evidence for the organic origin of petroleum and led to the concept of carbon cycles.

Porphyrin biomarkers have been continually studied with undiminishing interest since Treibs' time and much is being learned from them about the evolution of sedimentary organic matter. The porphyrins are just one of the many compound classes representing biomarkers. The most important biomarker class, corresponding to the bulk of known biomarkers, is the hydrocarbon class, specifically the saturated hydrocarbon type, which has been extensively investigated over the last four decades or so. In the 1970s, attention turned to oxygen-containing biomarkers, primarily carboxylic acids and alcohols, while the chemistry of sulfur-containing biomarkers, predominantly alkylated cyclic sulfides and thiophenic compounds, emerged during the 1980s.

Biomarker chemistry has brought to light an impressive body of knowledge related to organic sediments and a fascinating view, rich in intricate details, of how petroleum was formed and evolved to the state in which we find it today.[2–8] This has laid the foundation for the scientific theory of petroleum formation and led to a better understanding of the interrelationships between the formation and evolution of organic sediments and the evolution of life on earth, and their effects on the atmosphere and hydrosphere. Also, studies of biomarkers have helped to elucidate many aspects of the chemical compositions and molecular structures of bitumens, their past history, and the mystery surrounding their origin.

Biomarker chemistry has not only matured during the last few decennia, but in recent years it has also gained importance in practical applications as a tool to investigate oil correlations (with oils, source-rocks, *etc.*), providing a valuable aid to oil exploration.

The first biomarker study on Alberta oil sand bitumens, involving porphyrins, was reported in 1954 and was followed by a series of papers through the 1960s[9] and then again in the 1980s.[10–12] However, the most informative biomarkers studied belong to the class of saturated hydrocarbons and they consist of bi-, tri- and pentacyclic terpanes and tetracyclic steranes together with their partially or fully aromatized derivatives.[13–18] The study of saturated and aromatic biomarkers can give information on the biotic source material of the oil,[2–8] and, in many cases, makes it possible to infer the biological class or even the species of organism responsible for their formation. Valuable information can also be obtained regarding the depositional environment and nature of the source rocks. By selecting related precursor-product pairs and connecting them with feasible thermal, chemical and biological alterations, small changes in biomarker structure (*e.g.*, isomeric distribution, degree of aromatization, side chain length, ring opening, *etc.*) can be correlated with thermal maturity, microbial activity, water-washing history of the oil and the redox conditions during deposition.

Among the most important oxygen-containing biomarkers in Alberta bitumens are the acids (tricyclic terpenoid, *n*-alkanoic and some pentacyclic carboxylic acids) and *n*-alcohols.[19–22] Sulfur-containing biomarkers were originally discovered in Alberta bitumens[23,24] and subsequently found to be ubiquitous constituents of all sulfur-containing oils.[25,26] A broad variety have also been found in many different kinds of organic sedimentary matter.[27] The main sulfur-containing biomarkers in Alberta bitumen consist of the di-, tri-, tetra- and hexacyclic terpenoid sulfides present in the maltene fraction of the bitumen as was discussed in previous chapters and the *n*-alkyl substituted thiolanes, thianes, thiophenes, benzo- and dibenzothiophenes which represent structural elements in the asphaltene. The latter can be liberated from the asphaltene upon thermolysis, *cf.* Chapter 14.

In the following, the biomarker chemistry of Alberta oil sand will be discussed in two parts. The first deals with the biomarkers in the bitumen using conventional methods for the preparation of biomarker-enriched fractions in organic solvents and the second, with the isolation of biomarker concentrates using a novel method, namely, the aqueous alkaline extraction of the whole oil sand or the bitumen. In both cases each class of biomarkers will be examined separately and the information obtained from these studies will be discussed.

PART I. BIOMARKERS IN THE BITUMEN

1.0 Hydrocarbon-type Biomarkers

Most hydrocarbon-type biomarkers are derived from isoprene subunits,

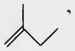

and belong to the so-called isoprenoid or terpenoid family of hydrocarbons. They occur in acyclic and cyclic forms and, depending on the number of isoprene subunits from which they are biosynthesized, are named according to the following nomenclature:

monoterpanes	from two isoprenes, C_{10};	sesterterpanes	from five isoprenes, C_{25}
sesquiterpanes	from three isoprenes, C_{15};	triterpanes	from six isoprenes, C_{30}
diterpanes	from four isoprenes, C_{20};	tetraterpanes	from eight isoprenes, C_{40}

1.1 Cyclic terpenoid biomarkers

A partial list of the more important cyclic terpenoid hydrocarbons detected in Alberta bitumens and heavy oils is shown in Table 13.1. The empty and filled circle notation introduced in Chapter 4 designates α and β hydrogens, *i.e.* hydrogens lying below and above the average plane of the rings or, in the case of an alkanoic carbon, below or above the plane of the paper.

The gas chromatograms of cyclic terpenoid hydrocarbon biomarkers present in Athabasca and Peace River bitumens were reproduced in Figures 10.2, 7, 8 and 24 and the structural assignments were listed in Table 10.5. The prominent series are the C_{27}–C_{35} hopanes, C_{24}–C_{27} tetracyclic terpanes, C_{21}–C_{29} steranes, C_{19}–C_{30} cheilanthane-type tricyclic terpanes, and C_{15}–C_{23} bicyclic drimanes along with some of their isomers. The hopanes and tricyclanes show a

Table 13.1 Some of the most important cyclic terpenoid hydrocarbons found in Alberta bitumens and heavy oils

Bicyclics:

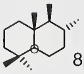

$C_{15}H_{28}$
8β(H)-drimane

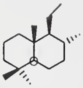

$C_{16}H_{30}$
8β(H)-14-methyldrimane

Tricyclics:

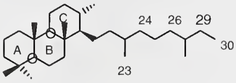

C_{23} = 18,19-bisnor-13β(H),14α(H)-cheilanthane
$C_{19} – C_{30}$ tricyclic terpanes

Tetracyclics:

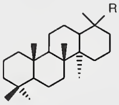

R = H, CH_3, C_2H_5, C_3H_7
17,21-secohopanes

C_{21}:

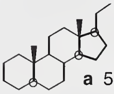

a 5α(H),14α(H),17α(H)-pregnane

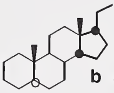

b 5α(H),14β(H),17β(H)-pregnane

C_{22}:

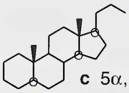

c 5α,14α,17α-bisnorcholane

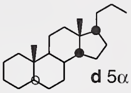

d 5α,14β,17β-bisnorcholane

C_{27}:

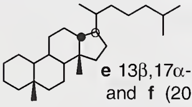

e 13β,17α-diacholestane (20S)
and **f** (20R)

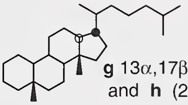

g 13α,17β-diacholestane (20S)
and **h** (20R)

C_{28}:

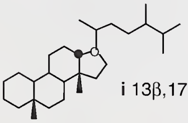

i 13β,17α–24-methyldiacholestane (20S) and **j** (20R)

C_{27}, C_{28}:

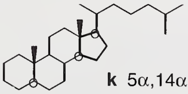

C_{27}
k 5α,14α,17α-cholestane (20S)

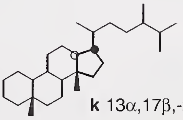

C_{28}
k 13α,17β,-24-methyldiacholestane (20S)

C_{27}, C_{29}:

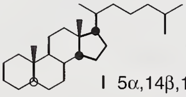

C_{27}
l 5α,14β,17β-cholestane (20R)

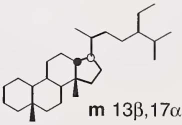

C_{29}
m 13β,17α–24-ethyldiacholestane (20S)

Table 13.1 (continued)

C_{27}: n 5α,14β,17β-cholestane (20S)
C_{28}: n 13α,17β-24-methyldiacholestane (20R)
C_{27}: o 5α,14α,17α-cholestane (20R)
C_{29}: p 13β,17α,-24-ethyldiacholestane (20R)
C_{28}: q 5α,14α,17α-24-methylcholestane (20S)
C_{28}: r 5α,14β,17β–24-methylcholestane (20R) + 13α,17β-24-ethyldiacholestane (20S)
C_{28}: s 5α,14β,17β-24-methylcholestane (20S)
C_{29}: t 13α,17β,-24-ethyldiacholestane (20R)
C_{28}: u 5α,14α,17α-24-methylcholestane (20R)
C_{29}: v 5α,14α,17α-24-ethylcholestane (20S)
C_{29}: w 5α,14β,17β-24-ethylcholestane (20R)
C_{29}: x 5α,14β,17β-24-ethylcholestane (20S)
C_{29}: y 5α,14α,17α-24-ethylcholestane (20R)

Pentacyclics:

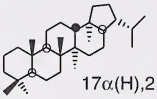
17α(H),21β(H)-hopane

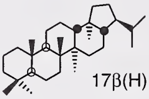
17β(H),21α(H)-hopane ≡ moretane

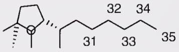

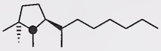

C_{31}:	17α(H),21β(H)-homohopane	homomoretane
	α,β-homohopane	β,α-homohopane
C_{32}:	α,β-bishomohopane	β,α-bishomohopane
C_{33}:	α,β-trishomohopane	β,α-trishomohopane
C_{34}:	α,β-tetrakishomohopane	β,α-tetrakishomohopane
C_{35}:	α,β-pentakishomohopane	β,α-pentakishomohopane

C_{29}:

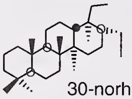
30-norhopane

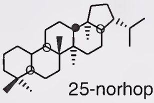
25-norhopane

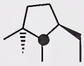
30-normoretane

C_{28}:

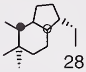
28,30-bisnorhopane

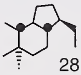
28,30-bisnormoretane

C_{28}:

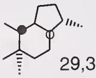
29,30-bisnorhopane

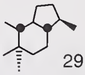
29,30-bisnormoretane

Table 13.1 (continued)

C_{27}:

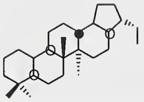

25,28,30-trisnorhopane

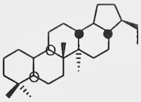

25,28,30-trisnormoretane

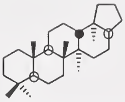

17α(H)-22,29,30-trisnorhopane
T_m – less stable isomer

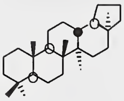

18α(H)-22,29,30-trisnorneohopane
T_s –more stable isomer

C_{30}:

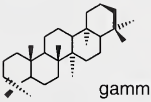

gammacerane

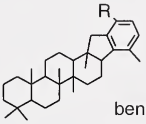

benzohopanes

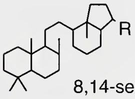

8,14-secohopanes

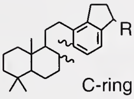

C-ring monoaromatic 8,14-secohopanes

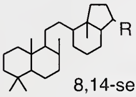

8,14-secohopanes

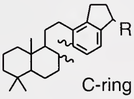

C-ring monoaromatic 8,14-secohopanes

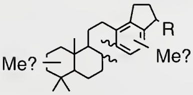

methylated C-ring
monoaromatic 8,14-secohopanes

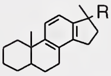

C-ring monoaromatic
steranes

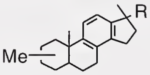

methylated C-ring
monoaromatic steranes

Acyclics:

diterpanes:

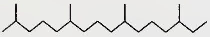

phytane, C_{20}

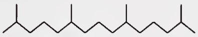

pristane, C_{19}

triterpane:

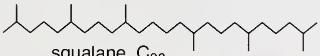

squalane, C_{30}

...head-to-head

tetraterpanes:

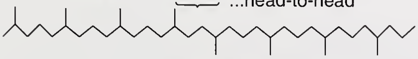

bis-phytane, C_{40}

...head-to-tail

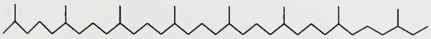

regular C_{40} isoprenoid

...tail-to-tail

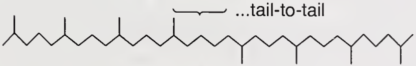

lycopane, C_{40}

characteristic base peak in their mass spectra at *m/z* = 191 corresponding to the cleavage of the AB ring system and a somewhat weaker signal at *m/z* = 123 corresponding to the cleavage of the A ring.

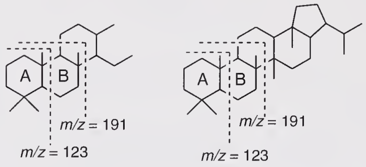

The bicyclic terpanes have base peaks at *m/z* = 123 corresponding to the cleavage off the A ring:

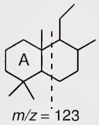

The characteristic fragment ion from the decomposition of 14α(H)- or 14β(H)-steranes is the ABC ring structure

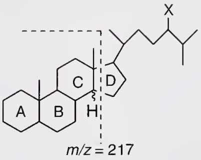

with *m/z* = 217.

The distribution of the main classes of these biomarkers can then be conveniently studied by capillary gas chromatography and GC–MS, monitoring their characteristic base peaks. In more advanced varieties of GC–MS, softer modes of ionization such as chemical or field ionization may be used instead of electron impact. The resolution and specificity can be greatly increased by the use of tandem or triple-stage mass spectrometers, GC–MSMSMS.[8]

1.1.1 Pentacyclic terpenoid hydrocarbons

The pentacyclic hopane molecule possesses nine asymmetric carbon atoms (at the 5,8,9,10,13, 14,17,18, and 21 positions),

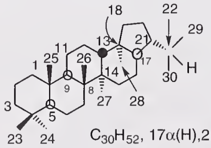

$C_{30}H_{52}$, 17α(H),21β(H)-hopane

and therefore can exist in many different isomeric forms. The stereochemistry, however, is geochemically important only at the 17 and 21 positions and, in the case of extended hopanes with an alkyl side chain from C_4 to C_8,

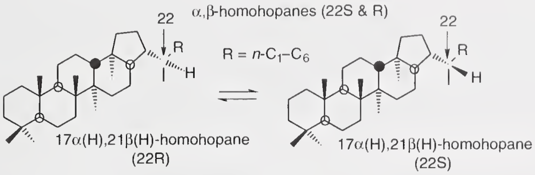
α,β-homohopanes (22S & R)
22
R
H
R = n-C1–C6
22
R
H
17α(H),21β(H)-homohopane (22R)
17α(H),21β(H)-homohopane (22S)

at the 22 position as well. These extended side chain hopanes are called homohopanes.

Hopanes and hopanoids are produced in nature primarily by prokaryotic bacteria where they serve the same biological function as the sterols in eukaryotes, that is, they provide the building material for the reinforcement of the cell membrane.[4] C_{30}, but no higher, hopanoids are also produced in some higher plants, ferns, a few fungi, *etc.* The homohopanes, even though they extend in carbon number up to 35 (with less frequent variants of C_{36} and C_{37} and beyond), are still triterpanes and the five extra carbon atoms are added to the C_{30} molecule as a C_5 sugar molecule (a ribose or arabinose unit) in the biosynthetic mechanism of the bacteria.

Hopane-type triterpenoids are abundant in nature. In organic sedimentary matter their content is estimated to be of the order of 10^{12} tons and they are one of the most abundant classes of complex organic molecules in the geosphere.[4]

Of the many different possible homohopane isomers, living organisms produce only one, namely the β,β-22R (biological) isomer

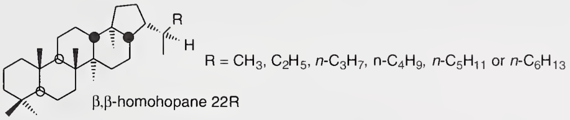

which, being thermodynamically less stable than the β,α isomer (called moretane) and the β,α isomer in turn being less stable than the α,β isomer, undergoes thermal isomerization in the sediment to produce the α,β epimer:

$$\begin{tikzcd}
\beta,\beta \arrow[r] \arrow[rr, bend left] & \beta,\alpha \arrow[r] & \alpha,\beta
\end{tikzcd}$$

Therefore, the ratio β,α/α,β decreases with increasing thermal maturity from 0.8 in immature source bitumens down to ~0.05 in mature oils. Parallel to the β,α → α,β conversion, the biologically-produced 22R epimer of the homohopanes isomerizes to the more stable 22S epimer, resulting in a mixture of the 22R and 22S stereoisomers. Ultimately, in mature oils the two epimers reach an equilibrium concentration distribution corresponding to a value of about 0.6 for the 22S/(22S + 22R) ratio. Hence, these two isomeric ratios for hopanes and the homohopanes are used as maturity indicators in the oil.[8]

During the course of thermal maturation, other changes take place in the hopane molecules as well, the most conspicuous of which is the shortening and ultimately the loss of the entire alkyl side chain on C_{21}. This is responsible for the appearance of the homologous series of hopanes from C_{27} to C_{35}.

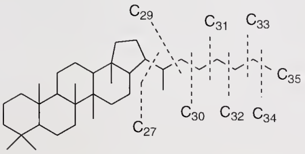

In a mature distribution, characteristic of the Alberta oil sand bitumens, Figure 13.1a and Table 13.2, the most abundant member is C_{29} (after correction for the sensitivity difference in the m/z = 191 peak for C_{30} and C_{29}) followed by $C_{31} > C_{30} > C_{32} > C_{27} > C_{33} > C_{35} > C_{34} > C_{28}$.

The demethylated hopanes with carbon numbers less than 30 are the norhopanes. The carbon numbers of the methyl groups lost are given as prefixes and the number of methyl groups lost is indicated by the designations norhopane, bisnorhopane and trisnorhopane for one, two, and three methyl groups. Thus, the two isomeric bisnorhopanes seen in the GC–MS of Athabasca saturates, Figure 13.1a, have the structures:

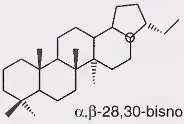

α,β-28,30-bisnorhopane

and

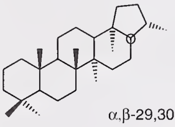

α,β-29,30-bisnorhopane

The low concentrations of the bisnorhopanes in the bitumen are consistent with the severe mechanistic requirements for their formation, involving the cleavage of not one, but two C–C bonds. Of the two isomeric trisnorhopanes present in the bitumen,

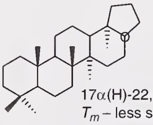

17α(H)-22,29,30-trisnorhopane
T_m – less stable

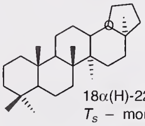

18α(H)-22,29,30-trisnorneohopane
T_s – more stable

formation of the 17α requires the cleavage of a single C–C bond in the precursor while the 18α hopane, in addition to C–C bond cleavage, requires the migration of a methyl group from C–18 to C–17, and it therefore occurs in a lower concentration compared to the 17α isomer.

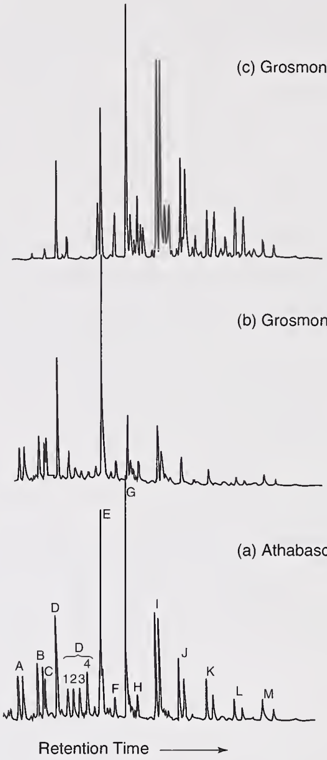

Figure 13.1 GC–MS m/z = 191 cross-scan chromatograms showing the tricyclic terpanes and hopanes in: (a), Athabasca, (b), Grosmont, and (c), Grosmont-B (bound) oil sand bitumens. The peak assignments are listed in Table 13.2. From C.F. Hoffmann and O.P. Strausz, Ref. 16. © 1986, American Association of Petroleum Geologists.

Homohopanes and norhopanes are rich in geochemical information. For example, the T_m isomer of the above trisnorhopanes is less stable and therefore decomposes faster on thermal maturation than the T_s isomer. Hence the $T_s/(T_s + T_m)$ ratio increases with thermal maturation and consequently can serve as an indicator of the thermal maturity status of the oil.

The distributions of triterpanes and steranes have been investigated[17] in a comparative study of some 72 samples from Lloydminster heavy oil; Provost, Cold Lake, Peace River, Wabasca-Wabiskaw, Wabasca-Grand Rapids and Athabasca oil sand; and Grosmont carbonate bitumens. Illustrative examples of the m/z = 191 mass chromatograms shown in Figure 13.2 indicate close similarities in the hopane distributions, with minor, characteristic differences. These mass chromatograms agree with those obtained from other studies, Figures 10.7, 8 and 24, except with respect to the appearance (in the former study) of one peak due to the presence of gammacerane:

Table 13.2 Structural assignments of the peaks in Figure 13.1[a]

Compound		Elemental composition	Structure[b]	
A	C_{28} tricyclic terpane (22S + R)	$C_{28}H_{52}$	I,	$R' = CH_3$, $R'' = C_9H_{19}$
B	C_{29} tricyclic terpane (22S + R)	$C_{29}H_{54}$	I,	$R' = CH_3$, $R'' = C_{10}H_{21}$
C	18α(H)-22,29,30-trisnorneohopane	$C_{27}H_{46}$	II,	$R^{\bullet} = H$
D	17α(H)-22,29,30-trisnorhopane	$C_{27}H_{46}$	III,	$R^{\bullet} = H$
D-1	17α(H),21β(H)-29,30-bisnorhopane	$C_{28}H_{48}$	III,	$R^{\bullet} = CH_3$
D-2,3	C_{30} tricyclic terpane (22S + R)	$C_{30}H_{56}$	I,	$R' = CH_3$ $R'' = C_{10}H_{21}$
D-4	17α(H),21β(H)-28,30-bisnorhopane +17β(H),21α(H)-28,30-bisnorhopane	$C_{28}H_{48}$	IVa IVb	
E	17α(H),21β(H)-30-norhopane	$C_{29}H_{50}$	III,	$R^{\bullet} = C_2H_5$
F	17β(H),21α(H)-30-norhopane	$C_{29}H_{50}$	V,	$R^{\bullet} = C_2H_5$
G	17α(H),21β(H)-hopane	$C_{30}H_{52}$	III,	$R^{\bullet} = CH(CH_3)_2$
H	17β(H),21α(H)-hopane	$C_{30}H_{52}$	V,	$R^{\bullet} = CH(CH_3)_2$
I	17α(H),21β(H)-homohopane[c]	$C_{31}H_{54}$	III,	$R^{\bullet} = CH(CH_3)C_2H_5$
J	17α(H),21β(H)-bishomohopane[c]	$C_{32}H_{56}$	III,	$R^{\bullet} = CH(CH_3)C_3H_7$
K	17α(H),21β(H)-trishomohopane[c]	$C_{33}H_{58}$	III,	$R^{\bullet} = CH(CH_3)C_4H_9$
L	17α(H),21β(H)-tetrakishomohopane[c]	$C_{34}H_{60}$	III,	$R^{\bullet} = CH(CH_3)C_5H_{11}$
M	17α(H),21β(H)-pentakishomohopane[c]	$C_{35}H_{62}$	III,	$R^{\bullet} = CH(CH_3)C_6H_{13}$

[a] From C.F. Hoffmann and O.P. Strausz, Ref. 16. © 1986, American Association of Petroleum Geologists.

b

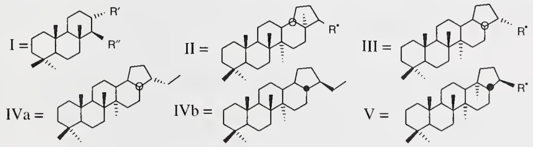

[c] 22S + R

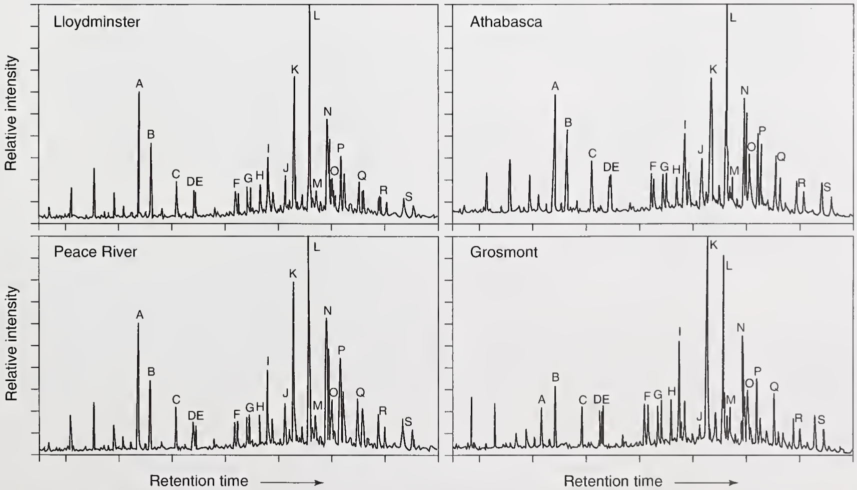

Figure 13.2 GC–MS *m/z* = 191 cross-scan chromatograms showing the tri- and pentacyclic terpane distributions in Lloydminster, Athabasca, Peace River and Grosmont heavy oils and oil sand bitumens. The peak assignments are listed in Table 13.3. From P.W. Brooks *et al.*, Ref. 17. © 1988, Elsevier Science Ltd.

Table 13.3 Compounds identified in the $m/z = 191$ fragmentograms shown in Figures 13.2, 13.3 and 13.4[a]

Peak	Compound	Peak	Compound
A	C_{23} tricyclic terpane	N	17α(H),21β(H)-homohopanes (20S + 20R)
B	C_{24} tricyclic terpane	O	gammacerane
C	C_{25} tricyclic terpane	P	17α(H),21β(H)-bishomohopanes (20S + 20R)
D	C_{24} tetracyclic terpane	Q	17α(H),21β(H)-C_{33} hopanes (20S + 20R)
E	C_{26} tricyclic terpane isomers	R	17α(H),21β(H)-C_{34} hopanes (20S + 20R)
F	C_{28} tricyclic terpane isomers	S	17α(H),21β(H)-C_{35} hopanes (20S + 20R)
G	C_{29} tricyclic terpane isomers	T	17α(H)-25 norhopane
H	18α(H)-trisnorhopane (T_s)	U	17α(H)-25,30 bisnorhopane
I	17α(H)-trisnorhopane (T_m)	V	17α(H)-25 norhomohopanes
J	28,30-bisnorhopanes	W	17α(H)-25 norbishomohopanes
K	17α(H),21β(H)-norhopane	X	17α(H)-25 nor C_{32} hopanes
L	17α(H),21β(H)-hopane	Y	17α(H)-25 nor C_{33} hopanes
M	17β(H),21α(H)-moretane	Z	17α(H)-25 nor C_{34} hopanes

[a] From Ref. 17. © 1988, Elsevier Science Ltd.

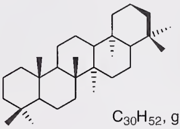

$C_{30}H_{52}$, gammacerane

The appearance of gammacerane in one series of analyses and the absence in another must be due to the variation in the GC resolution of the α,β-C_{31} 22R homohopane and gammacerane. If the resolution is insufficient, the two molecules coelute on the column.

The more important pentacyclic terpane ratios determined from the heights of the capillary GC $m/z = 191.1794$ peaks and expressed as percentages were as follows:

- β,α-C_{30}/(α,β-C_{30} + β,α-C_{30}): in the range 7–20% with an average value of ~10% (except where affected by biodegradation), indicating mature oils. Severe biodegradation may destroy the α,β-C_{30} hopane but the β,α-C_{30} hopane (moretane) or the α,β- and β,α-C_{29} norhopane/normoretane in some cases are more resistant against microbial attack and not so readily destroyed, *cf.* Figure 13.1. The percentages of β,α-C_{29} in terms of α,β-C_{29} + β,α-C_{29} for Athabasca , Peace River and Grosmont bitumens are ~ 9, 8, and 8.
- $T_s/(T_s + T_m)$: in the range ~23–58% with an average value of ~40%. These ratios are not supposed to be affected by biodegradation and the narrowness of the range points to the similarities in the biomarker compositions of all the sand and the carbonate bitumens and to a similar or common origin. The values all appear to be low and, according to the published biomarker maturity scale, would indicate low levels of maturity. Interestingly, the two heavy oil samples examined, Lloydminster and Lloydminster–Provost, which were collected at the greatest burial depths, had values of $T_s/(T_s + T_m)$ distinctly higher than those of the bitumens.
- 22S-C_{31}/(22S-C_{31} + 22R-C_{31}) and 22S-C_{32}/(22S-C_{32} + 22R-C_{32}): 60 ± 5%, which indicates a mature oil. In some cases severe biodegradation preferentially removes the biological R-epimers but leaves the 22S-C_{31}–C_{35} distribution unaffected, thereby shifting considerably the 22S/22R ratios. In other cases biodegradation removes the C_{29}–C_{34} hopanes but leaves the C_{35} members behind.

- gammacerane, Gm/α,β-C_{30}: in the range 0.1–0.27 except for the severely biodegraded oils in which case values may be as high as 0.72. The narrowness of the range is in agreement with the observations described above with regard to the close similarities of the biomarker compositions.
- α,β- and β,α-28,30-bisnorhopane/α,β-C_{30}: in the range 0.14–0.26 except when severe biodegradation has taken place, in which case the value increases up to 0.45.
- 25-norhopanes were detected in the Wabasca Grand Rapids A and Carbonate Trend bitumen samples. In the *m/z* = 191 mass chromatogram of hopanes, only the C_{29} member of the 25-norhopane series would appear

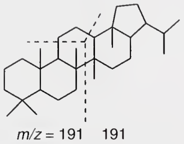

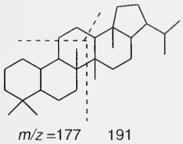

and the rest of the series can be detected[17] by *m/z* = 177 cross scanning, Figures 13.3 and 13.4. In most of the samples from these two deposits, smaller or larger concentrations of 25-norhopanes were detected and they showed a direct correlation with the extent of biodegradation that the bitumen had undergone. More specifically, the concentrations of 25-norhopanes were directly proportional to the quantity of hopanes destroyed by biodegradation. In some samples the C_{30}–C_{34} hopanes were found to be nearly completely destroyed, with the simultaneous appearance of the full C_{29}–C_{33} complement of the 25-norhopanes. The C_{35} hopanes are metabolized slowly and, in some cases, the rate of destruction of the C_{29} hopane is slower than those of the others (Figures 13.1b, 13.3 and 13.4). These findings show that hopanes can be microbiologically converted to 25-norhopanes in the reservoired oil and that hopanes and 25-norhopanes are related as precursor and product, respectively. The specificity of the reactions that occur in the course of biodegradation is highly dependent on the types of bacterial populations causing the alteration of the oil, and other factors which can be substrate-, organism- or environment-related. It has been suggested that demethylated hopanes, like 25-norhopanes, are not paleodegradation products of hopanes but rather are indigenous biomarkers of source rocks and, like hopanes, they may be derived from demethylated hopanoidal precursors. The data on 25-norhopanes in Alberta bitumens[17,18] (Ref. 8, pp 258–262) suggest that this is not the case.

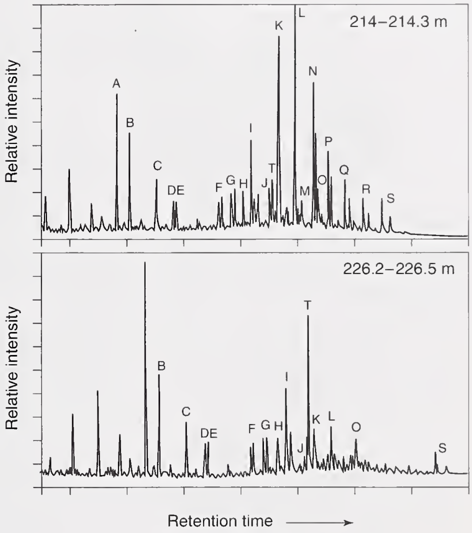

Figure 13.3 GC–MS *m/z* = 191 cross-scan chromatograms showing the tri- and pentacyclic terpane distributions in Wabasca Grand Rapids Formation A oil sand bitumen at depths of 214–214.3 and 226.2–226.5 m. The peak assignments are listed in Table 13.3. From P.W. Brooks *et al.*, Ref. 17. © 1988, Elsevier Science, Ltd.

In the biodegraded bitumen where the hopane concentrations are depleted, the apparent relative concentrations of bisnorhopanes, trisnorhopanes, gammacerane or tricyclic terpanes

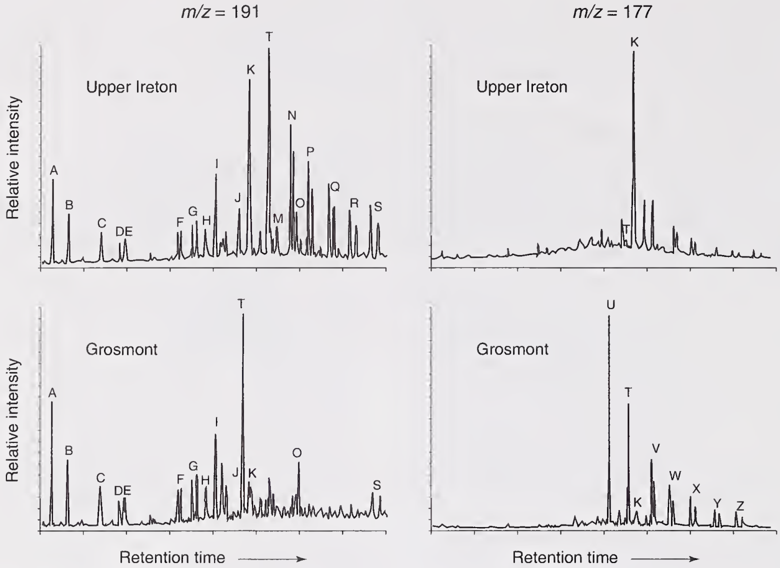

Figure 13.4 GC–MS m/z = 191 and 177 cross scan-chromatograms showing the tri- and pentacyclic terpane distributions in two Carbonate Triangle oil sand bitumens, Upper Ireton and Grosmont.[18] The peak assignments are listed in Table 13.3.

remain unaltered. These molecules are more resistant against microbial attack and would be by and large unaffected by biodegradation.

In the study of one of the Grosmont carbonate bitumen samples,[16] the crushed, solvent-extracted inorganic matrix was found to contain some bitumen (~1.6% of the total organic matter) which could only be isolated *via* the destruction of the rock matrix by dissolution in hydrochloric acid. This bitumen (with an asphaltene content of ~86%) was quite unlike the solvent-extracted bitumen and it contained pristane and phytane (in a ratio of ~0.4) and some *n*-alkanes with a bimodal distribution centered at n-C_{24} and n-C_{31} and a significant predominance of odd carbon members above n-C_{28} (the latter feature being indicative of a higher, terrestrial plant origin). A series of bicyclic terpenoid hydrocarbons (C_{15}–C_{24}) which had been identified in relatively high abundance in Athabasca and other oil sand bitumens was also observed here, in a distribution dominated by the C_{15} and C_{16} components. However, these same compounds could only be detected in trace amounts in the solvent-extracted bitumen. The distribution of hopanes (Figure 13.1) and the presence of *n*-alkanes here suggests a somewhat lower degree of thermal maturity and the absence of biodegradation. Moreover, significant differences can be seen in the distribution of the steranes in the bound bitumen compared to all other sand or carbonate bitumens, Figure 13.5, in that it contains more α,α,α-cholestane and α,α,α-ethylcholestane, indicating less extensive biodegradation. Evidently, this bound bitumen was protected during the biodegradation of the in-place oil by its host mineral matrix, resulting in the preservation of its biodegradable hydrocarbon content.

On the basis of the biomarker content, the origin of the strongly-bound bitumen in the carbonate sample could be related to the small concentrations of indigenous organic sedimentary matter associated with the reservoir rock. After making allowance for the difference in biodegradation, the bound bitumen is somewhat less thermally mature but in other respects it

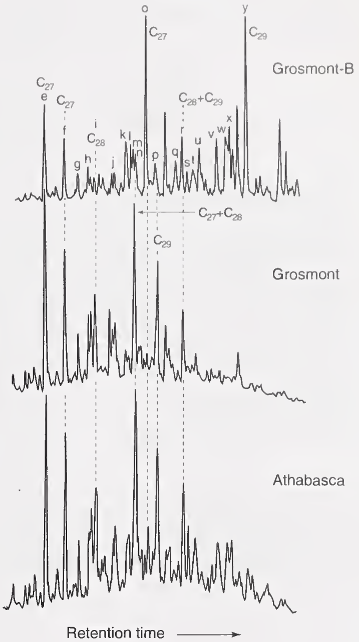

Figure 13.5 GC–MS m/z = 217.2 cross-scan chromatograms showing the C_{27}–C_{29} steranes in Athabasca and Grosmont (B = bound) oil sand bitumens. The structures of peaks e–x are listed in Table 13.1. From C.F. Hoffmann and O.P. Strausz, Ref. 16. © 1986, American Association of Petroleum Geologists.

is, in general, similar to the solvent-extractable bitumen and the sand and carbonate bitumens of Alberta. Militating against a genetic relationship with the latter, however, is the absence of tricyclanes.

Studies of the saturated pentacyclic terpenoid hydrocarbon biomarkers have revealed that all bitumens from the Alberta sand and carbonate deposits are mature and that biodegradation, with the exception of the carbonate and the Wabasca Grand Rapids A bitumens, was not severe enough to affect the distribution of hopanes. However, in the latter two bitumens, biodegradation was severe and effected the conversion of α,β-hopanes to 25-norhopanes. The close similarity found here between all Alberta bitumens extends to other biomarkers and points to a close compositional and genetic relationship between the bitumen accumulations in the Western Canada Sedimentary Basin.

1.1.2 Tetracyclic terpenoid hydrocarbons

a) Saturated steroids

The precursors of steranes in sediments and petroleum are the sterols from eukaryotic organisms. Sterols have the same biological precursor as hopanoids, namely the acyclic hexaprenoid biomolecule, squalene:

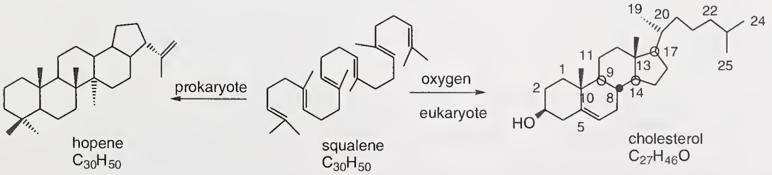

The conversion of squalene to hopane is an anaerobic process involving an unsaturated hopane, possibly hop-22(29)-ene which is converted in bacteria to β,β-bacteriohopanetetrol (22R) by the addition of a d-ribose derivative:

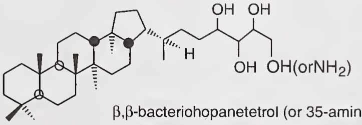

β,β-bacteriohopanetetrol (or 35-aminotriol)

During diagenesis β,β-bacteriohopanetetrol is reduced to β,β-hopane (22R):

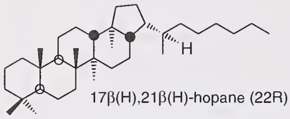
17β(H),21β(H)-hopane (22R)

The conversion of squalene to cholesterol or sterols generally follows an oxidative route and the sterols may undergo dehydration and dehydrogenation during diagenesis to form monoaromatic and ultimately triaromatic steranes as outlined in Figure 13.6.[28] Alternatively, through several steps involving hydrogenation, dehydration, dehydrogenation, backbone rearrangement, *etc.*, they may form rearranged steranes—diasteranes, or non-rearranged regular steranes.

The hopanes and steranes are formed initially in their thermodynamically unstable, flat conformation, *e.g.*,

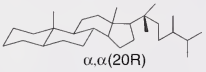
α,α(20R)

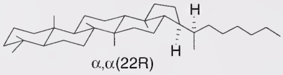

α,α(22R)

corresponding to their conformation in the cell membrane, Appendix 13.1. Steranes, like the hopanes, undergo epimerization reactions in the sediment during diagenesis:

$$\begin{tikzcd}
\alpha,\alpha(20R) \arrow[rr, shift left] \arrow[dr, shift left] & & \beta,\beta(20R) \arrow[ll, shift left] \arrow[rr, shift left] \arrow[dl, shift left] & & \beta,\beta(20S) \arrow[ll, shift left] \\
& \alpha,\alpha(20S) \arrow[ul, shift left] \arrow[ur, shift left] & & &
\end{tikzcd}$$

From the standpoint of geochemical information content, the important asymmetric centers in steranes are at the C–14, –17 and –20 positions. Theoretically, stereoisomerism is also possible at the C–8, –9, –10, –13 and –5 positions. However, at the first four sites, because of kinetic or thermodynamic limitations, only one of the isomers occurs in nature. As for the C–5 position, most sterols contain a double bond at this carbon and hydrogenation of the double bond favors the α isomer by a factor of 2–10. In addition, the position of equilibrium connecting the α and β isomers is shifted so far to the side of the α-isomer that the β-isomer becomes vanishingly small in all except very immature oils. With regard to the 20S/20R distributions, eventually, thermal equilibrium is reached at

$$20S/(20S + 20R) \sim 0.50$$

and for α,αR-α,αS-β,βR-β,βS in the proportion 1:1:3:3.

The other geochemically important isomeric forms of steranes are represented by the backbone-rearranged diasteranes in which the carbon number of the original sterols, as in the regular steranes, remains preserved:

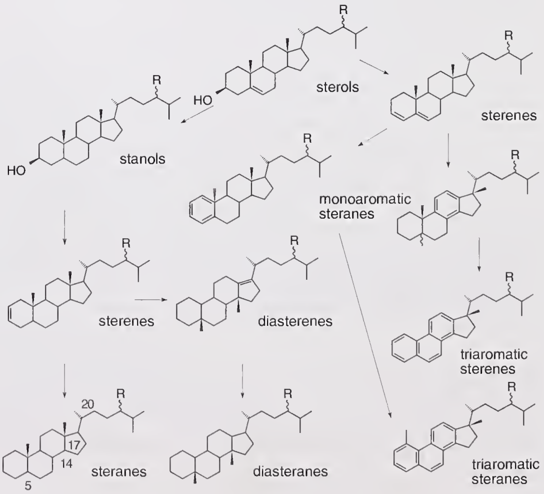

Figure 13.6 Sterol–sterene–sterane conversions taking place during maturation of an oil. From R.P. Philp, Ref. 28. © 1986, American Chemical Society.

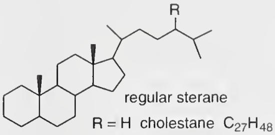

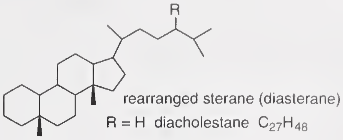
R
rearranged sterane (diasterane)
R = H diacholestane $C_{27}H_{48}$

Diasteranes, regular steranes, and aromatic steranes serve as useful biomarkers in petroleum.

The relative importance of diasteranes compared to steranes in an oil depends on the nature of the source rocks, the thermal maturity of the oil and its microbiological history. Thus, low diasterane/sterane ratios indicate anoxic, clay-poor, carbonate source rocks. On the other hand, high ratios are characteristic of oils derived from source rocks containing abundant clays. High diasterane/sterane ratios may also result from high thermal maturity and/or extensive biodegradation. Thermal maturity may favor the formation of diasteranes or may preferentially accelerate the destruction of steranes. Severe biodegradation can lead to selective destruction of the steranes relative to the diasteranes.

Alberta heavy oils and bitumens, being more or less biodegraded petroleums, contain reduced amounts of steranes and exhibit elevated diasterane/sterane ratios. Representative examples of m/z = 217.2 cross-scan mass chromatograms of Athabasca and Grosmont bitumens are shown in Figures 13.5 and 13.7.

All oils and bitumens investigated contained C_{21} and C_{22} ($\alpha\alpha$- and $\beta\beta$-pregnane, $\alpha\alpha$- and $\beta\beta$-bisnorcholane) steranes. In addition, steranes in the C_{27}–C_{29} range were detected[17] in the Lloydminster and Provost heavy oils and Cold Lake, Wabasca and Peace River bitumens, Figure 13.8 and Table 13.4. Athabasca bitumen samples showed either low levels of C_{27}–C_{29} steranes or none at all; 22 of the 25 Carbonate Trend bitumen samples analyzed were found to be devoid of C_{27}–C_{29} steranes. All samples investigated, with the exception of four of the Grosmont bitumen samples, were found to contain diasteranes.

The main features of the sterane distributions along with their geochemical significance may be summarized as follows:[17]

- The measured diasteranes/steranes ratio, 0.6–2.9 for C_{27}-diasterane/α,αR, correlates with the extent of biodegradation the oil had experienced, as also inferred from other biomarker and nonbiomarker properties of the oil. The absence of steranes indicates severe biodegradation, and the absence of both steranes and diasteranes, extremely severe biodegradation. From the data it can be concluded that the heavy oils are the least, and the Athabasca bitumen the most, biodegraded representatives of the Cretaceous heavy oil–oil sand bitumen accumulations of the Western Canada Sedimentary Basin.

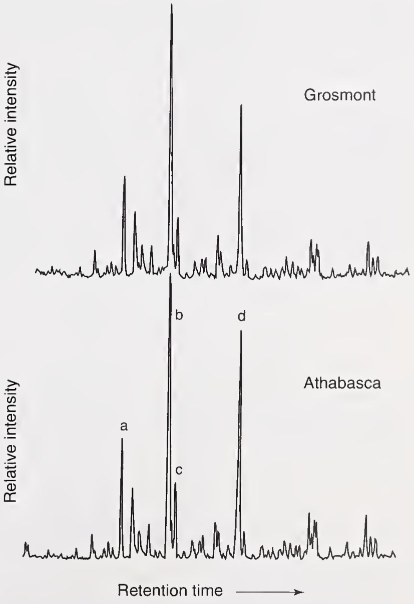

Figure 13.7 GC–MS m/z = 217.2 cross-scan chromatograms showing the C_{21}–C_{22} steranes in Athabasca and Grosmont oil sand bitumens. The structures of peaks a–d are listed in Table 13.1. From C.F. Hoffmann and O.P. Strausz, Ref. 16. © 1986, American Association of Petroleum Geologists.

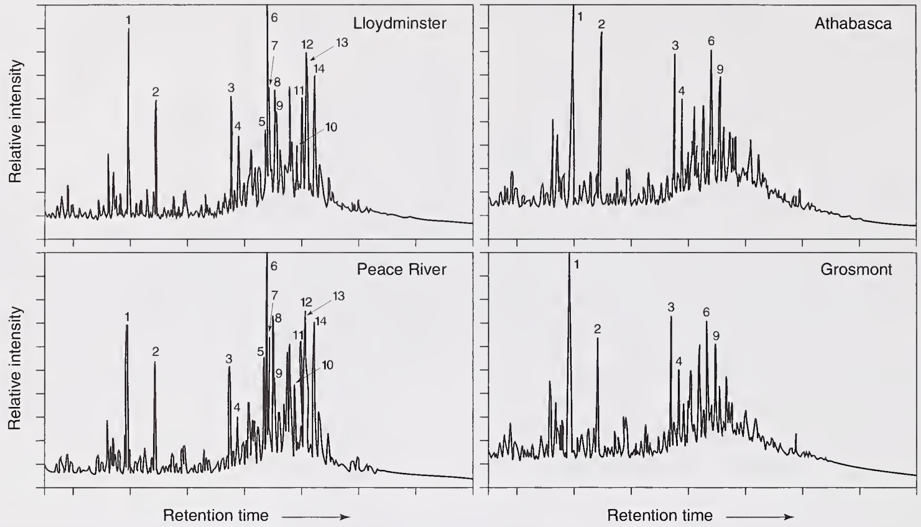

Figure 13.8 GC–MS $m/z = 217.2$ cross-scan chromatograms showing the sterane distributions in Lloydminster heavy oil and Athabasca, Peace River and Grosmont bitumens. The peak assignments are listed in Table 13.4. From P.W. Brooks *et al.*, Ref. 17. © 1988, Elsevier Science Ltd.

Table 13.4 Compounds identified in the $m/z = 217.2$ fragmentograms shown in Figure 13.8

Peak	Compound
1	C_{21} sterane
2	C_{22} sterane
3	13β(H),17α(H)-diacholestane (20S)
4	13β(H),17α(H)-diacholestane (20R)
5	5α(H),14α(H),17α(H)-cholestane (20S)
6	5α(H),14β(H),17β(H)-cholestane (20R) + 24-ethyl-13β(H),17α(H)-diacholestane (20S)
7	5α(H),14β(H),17β(H)-cholestane (20S)
8	5α(H),14α(H),17α(H)-cholestane (20R)
9	24-ethyl-13β(H),17α(H)-diacholestane (20R)
10	24-methyl-5α(H),14α(H),17α(H)-cholestane (20R)
11	24-ethyl-5α(H),14α(H),17α(H)-cholestane (20S)
12	24-ethyl-5α(H),14β(H),17β(H)-cholestane (20R)
13	24-ethyl-5α(H),14β(H),17β(H)-cholestane (20S)
14	24-ethyl-5α(H),14α(H),17α(H)-cholestane (20R)

[a] From P.W. Brooks *et al.*, Ref. 17. © 1988, Elsevier Science Ltd.

The Paleozoic carbonate bitumens from which the steranes have been removed by biodegradation, and especially the Grosmont and Nisku Formation bitumens from which even the diasteranes have been removed, are the most severely biodegraded bitumens in the Western Canada Sedimentary Basin. The C_{21}–C_{22} region, which is apparently resistant towards biodegradation, is dominated by the regular steranes (Figure 13.7) and this suggests that the diasterane/sterane ratio in the original oil was probably low. This conclusion is further corroborated by studies on asphaltene-bound steranes, as will be discussed in Chapter 14.

- The carbon number distribution of steroidal alkanes involving βα-C_{27}, -C_{28} and -C_{29} diasteranes lies within a narrow range (C_{27}:C_{28}:C_{29} ~39:19:42) for all Cretaceous and carbonate heavy oils and bitumens, pointing to a close genetic relationship between them and consequently a common source or sources for these materials. When all the C_{27}, C_{28} and C_{29} diasteranes are considered, Figure 13.5, the order of abundance seems to be $C_{27} > C_{28} \sim C_{29}$. These distributions lie within the range predicted for marine, carbonate oils, as will be discussed below. The C_{29} steranes were thought to be derived from higher plants and thus to represent terrestrial input. However, evidence is accumulating for the presence of C_{29} steranes or sterane precursors in diatoms and algae and therefore the validity of C_{29} steranes as terrestrial markers is questionable. Consequently, the observed sterane distributions may be interpreted as signifying a marine origin with possible minor contribution from terrestrial sources.
- The relative abundance of the 20S geological isomers was determined using the α,α-C_{29}-20S and α,α-C_{29}-20R sterane components. The values obtained, 41–52%, are characteristic of early-mature to mature petroleum. On the whole, the diasteranes in the samples appeared to be unaffected by biodegradation (with the exception of some of the Grosmont and Nisku Formation bitumens, where they are absent) and therefore analogous parameters for Athabasca and Grosmont bitumens were determined using the 20S and 20R components of β,α-diacholestane. The values derived were slightly higher, 55 and 58%, than the values obtained from the measurements of the sterane components.
- The maturity parameters ββ/(ββ + αα) were determined from the C_{29} steranes. The values ranged from 59 to 84% compared to the equilibrium value of 70% for mature oils. Parameters for Athabasca and Grosmont samples—which are practically devoid of regular C_{27}–C_{29} steranes—were obtained from the equivalent C_{21} components (Figure 13.7). These yielded values of 70% and 72%. Thus, here again, the thermal maturity indices for the heavy oils and bitumens ranged from early-mature to mature.

In contrast to the distributions of steranes found in the heavy oils and bitumens corresponding to mature, biodegraded petroleums, the steranes in the bound bitumen from the Grosmont Formation displayed a distribution characteristic of an immature, nonbiodegraded oil. The biological 20R epimers in the α,α-steranes, which are more abundant than the geological 20S isomers, along with the low relative abundance of β,β-steranes, point to a marginal maturity at most for the bound bitumen. These features again parallel those found in asphaltene-bound steranes.

b) Aromatic steroids

Monoaromatic steroids (MA) are gradually converted to triaromatic steroids (TA) in the course of thermal maturation (Figure 13.6):

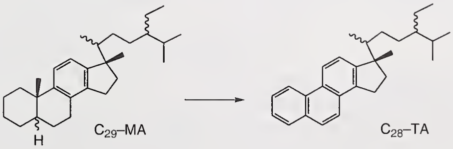

The transformation is accompanied by the loss of methyl from C–10 and loss of the asymmetric center at C–5. Monoaromatic steroids with the C–10 methyl group rearranged to C–5 also generate triaromatic steroids in the course of thermal maturation:

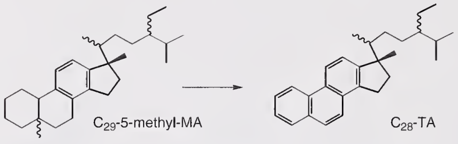

Parallel to aromatization, side-chain shortening also takes place:

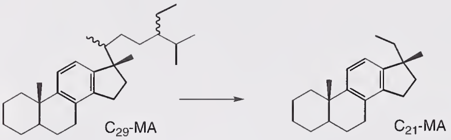

The distributions of monoaromatic and triaromatic steroid hydrocarbons in Athabasca and Grosmont bitumens are shown in the *m/z* = 253.20 and 231.12 cross-scan mass chromatograms of Figures 13.9 and 10 and the geochemically significant biomarker ratios derived therefrom are summarized in Table 13.5. The ratios (expressed as percentages) for the Athabasca

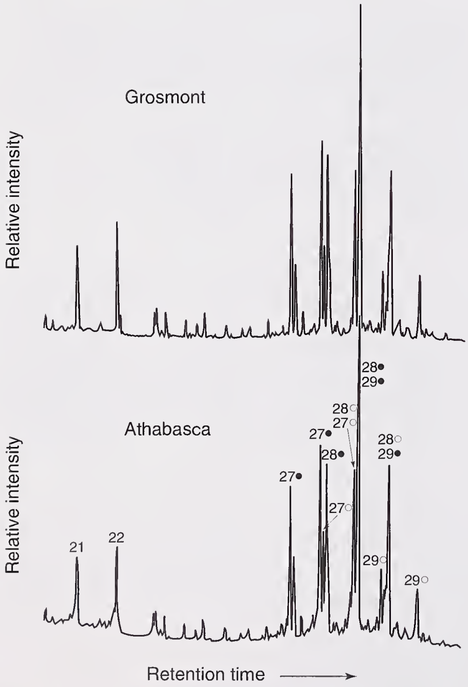

Figure 13.9 GC–MS $m/z = 253.2$ cross-scan chromatograms showing the distribution of C_{21}–C_{29} monoaromatic steroid hydrocarbons in Athabasca and Grosmont bitumens. Carbon numbers and stereochemistry are indicated. The open and filled circles refer to 5α(H) and 5β(H) isomers. For peaks having the same carbon number the 20S components elute before the 20R components. From C.F. Hoffmann and O.P. Strausz, Ref. 16. © 1986, American Association of Petroleum Geologists.

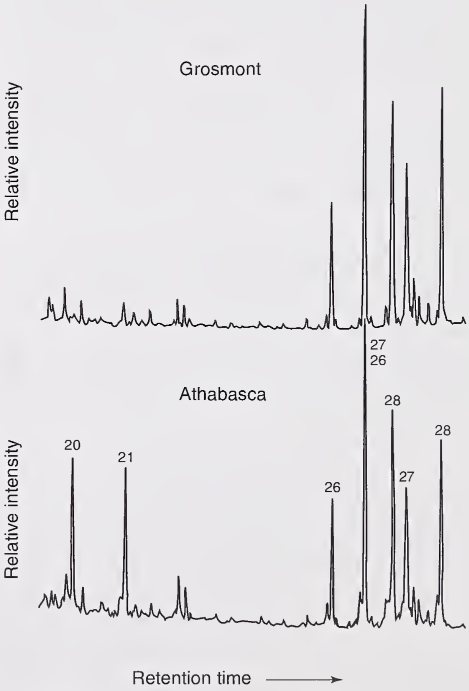

Figure 13.10 GC–MS $m/z = 231.12$ cross-scan chromatograms showing the distribution of C_{20}–C_{28} triaromatic steroid hydrocarbons in Athabasca and Grosmont bitumens. Carbon numbers are indicated. For peaks having the same carbon number the 20S components elute before the 20R components. From C.F. Hoffmann and O.P. Strausz, Ref. 16. © 1986, American Association of Petroleum Geologists.

Table 13.5 Biomarker ratios[16] for aromatic hydrocarbons in Athabasca and Grosmont bitumen samples[a]

Sample	Triaromatic[b]	C_{26} Triarom.[c]	C_{20} Triarom.[d]	C_{21} Monoarom.[e]	20S[f]
Athabasca	35	43	26	11	52
Grosmont	38	44	n/a	13	47
Grosmont (bound)	10	7	12	8	47

[a] All values are percentages.

[b] Σ (C_{26}–C_{28} triarom.)/(Σ C_{26}–C_{28} triarom. + Σ C_{27}–C_{29}-monoarom.) [c] (C_{26} + C_{27} triarom.)/(C_{26} + C_{27} triarom. + C_{28} + C_{29}-monoarom.) [d] (C_{20} + C_{21} triarom.)/(Σ C_{20}–C_{28} triarom.) [e] (C_{21} + C_{22} monoarom.)/(Σ C_{21}–C_{29} monoarom.) [f] 20S/(20S + 20R) C_{28} triarom.

and Grosmont bitumens have similar values, indicating a similar early mature-to-mature state. The Grosmont bound bitumen, as found before, corresponds to an immature thermal state and, unlike the steranes where the C_{27} (C_8 side chain) components dominate, the aromatic steroid hydrocarbons are dominated by components with C_{10} side chains.

c) Secohopanes

Tetracyclic terpanes arising from the cleavage of a ring in hopane molecules are termed secohopanes and the position of ring cleavage is indicated by specifying the carbon positions of the cleavage in the molecule. Thus, 17,21-secohopane designates a hopane molecule in which the bond between C–17 and C–21 has been cleaved. 17,21-Secohopanes with carbon numbers ranging from 24 to 27 occur in most oils and bitumens,

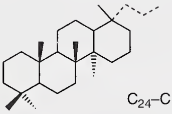

C_{24}–C_{27}-17,21-secohopanes

and the C_{24} member of the series is the most prevalent. The series has been detected in low abundance in the Athabasca and Grosmont bitumens, with the C_{24} member dominating. The concentration of the C_{24} member amounted to about 25, 24 and 15% of the trisnorhopanes, $T_s + T_m$ in the Athabasca, Grosmont and Grosmont-bound bitumens. This percentage concentration is an indicator of the thermal maturity of the oil and tends to increase with increasing thermal maturity. Therefore, once again the Athabasca and Grosmont bitumens have the same thermally mature status and the bound Grosmont bitumen, an immature status.

A short series of 8,14-secohopanes has also been detected in the aqueous alkaline extract of the Athabasca oil sand, as will be shown in Part II of this chapter.

1.1.3 Tricyclic terpenoid hydrocarbons

Tricyclic terpenoid hydrocarbons in the C_{19}–C_{30} range (and occasionally extending beyond C_{30}, *e.g.* up to C_{45} in a California crude[29a] and up to C_{54} in Early to Late Cretaceous Brazilian oil and rock samples[29b]*; also the same hydrocarbon framework can be recognized in the tetracyclic terpenoid sulfides[29c] up to C_{36} and occasionally to C_{40} (*v.i.*) which are ubiquitous trace components of crude oils, bitumens and rock extracts. Up to C_{30} they are thought[30] to arise from bacterial or algal lipids with tricyclohexaprenol from prokaryotic membranes as the immediate precursor. Tricyclic diterpanes (C_{19}, C_{20}) in petroleum have been suggested to be derived from diterpenoids, an example of which is abietic acid, a product of vascular plants. Also known is a sesterterpenoid plant product, a cheilanthatriol, occurring in ferns.

---

* The latter were reported to have originated from lacustrine saline water and a marine carbonate environment.

The structure of these cheilanthane-type hydrocarbon biomarkers has been discussed in Chapter 10. In mature oils and in Alberta oils and bitumens the 13β(H),14α(H)-isomers predominate. The maximum in concentration typically occurs at C_{23}, Table 13.6, and the members below C_{27} comprise ~90% of the total. (The C_{27} and C_{22} members are present in very small concentrations because of isoprenoid branching at these positions.) This type of distribution is typical for all Alberta bitumens and many other oils and is considered to be indicative of carbonate source rocks. Tricyclic terpanes are strongly resistant to microbial attack and even where the regular steranes and hopanes are degraded, as in the Grosmont bitumen, the distribution of tricyclic terpanes does not appear to be affected by biodegradation. Nonetheless, biologically demethylated tricyclic terpanes have been observed[31] in some bitumens from the Orinoco Tar Belt and elsewhere. In these series of tricyclic terpanes, the methyl group is removed from the C–10 position and the characteristic base peak in their mass spectrum, like that of the C–10 demethylated hopanes, becomes the m/z = 177 instead of the 191 peak,

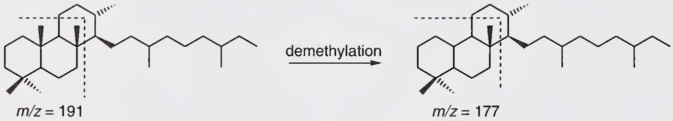

mimicking the distribution of the original tricyclic terpanes. In the Paleozoic carbonate bitumens from Alberta, however, no evidence has been found for the presence of demethylated tricyclic

Table 13.6 Tricyclic terpanes in Athabasca bitumen

Carbon number	Saturates	Pyrolyzate[a] Maltene	Pyrolyzate[a] Polar	Pyrolyzate[a] Asphaltene
	Concentration, $\mu g \cdot g^{-1}$ bitumen in the pyrolyzate			
19	95.0	136.6	5.8	150.6
20	48.3	105.0	33.3	404.8
21	100.0	85.0	4.2	240.7
22	40.8	40.0	–	45.8
23	23.3	26.7	14.2	83.3
23	334.9	220.7	44.1	625.6
24	221.7	129.1	1.6	105.0
25	147.8	100.8	0.8	15.8
26	26.7	24.2	–	21.7
26	31.6	25.0	–	–
28	79.1	–	–	–
29	29.2	–	–	–
30	21.7	–	–	–
Total	1,200	893	104	1,693
$\frac{\Sigma(C_{19}–C_{22})}{\Sigma(C_{24}–C_{26})}$	0.66	1.3	18	5.9

[a] 300°C, 72 h

terpanes and the $m/z = 177$ mass chromatograms show no sign of demethylated tricyclic terpanes even when the hopanes are completely demethylated (Figures 13.3 and 13.4).

Because tricyclic terpanes survive even severe biodegradation relatively intact, the ratio

$$\Sigma \text{ tricyclics}/(\Sigma \text{ tricyclics} + \text{hopanes})$$

(where tricyclics = C_{28} + C_{29}(22R + S) and hopanes = C_{29}–C_{33} hopanes) has been used as a reliable maturity indicator for the mature and post-mature range (for oils from the same source rock materials). Oils derived from carbonate source rocks contain low concentrations of the tricyclic terpanes above C_{26} and therefore tend to give low values for this ratio. In most Alberta heavy oils and bitumens (with the exception of the Paleozoic carbonate samples) the value of this ratio is about 0.2, indicating carbonate source rocks for these oils and bitumens.

As will be recalled here, many of the hydrocarbon-type biological markers present in the saturate fraction of the bitumen are also present in functionalized form distributed over the aromatic (*e.g.*, cyclic terpenoid sulfides), polar (*e.g.*, tricyclic and pentacyclic carboxylic acids, cyclic terpenoid sulfoxides) and asphaltene fractions. Portions of these functionalized biomarkers can be converted to hydrocarbons upon thermolysis. Parallel to their liberation, the hydrocarbon biomarkers thus produced also undergo decomposition. From Table 13.6 it is seen that the total concentration of tricyclic hydrocarbons in the saturate fraction of Athabasca bitumen is ~1200 ppm. On pyrolysis (300°C, 72 h) the polar fraction affords 104 ppm tricyclic terpanes. Therefore, on thermolysis of the maltene, at least 1,304 ppm tricyclic terpanes should be produced, but only 893 ppm is actually found. This result indicates that under the conditions of thermolysis, about one-third of the tricyclic terpanes involved decompose. Thermolysis of the asphaltene produces 1,693 ppm tricyclic terpanes, significantly more than are present in the saturate fraction, 1,200 ppm. If, during thermolysis of the asphaltene, one-third of the tricyclic hydrocarbons are again lost through decomposition, then the amount of tricyclic hydrocarbons originally produced in the asphaltene thermolysis was probably around 2,500 ppm. From this, it can be concluded that the tricyclic terpenoid hydrocarbons present in free form in Athabasca bitumen, ~1,200 ppm, represent only about one-third of the total free-plus-functionalized tricyclic hydrocarbon structures, *i.e.* 1,200 + 156 + 2,500 ≈ 3,856 ppm.

The total amount of tricyclic terpenoid hydrocarbons in the saturate fraction is commensurate with, but distinctly less than that of the hopanes, which is estimated to be of the order of 1,800 ppm, Figures 13.11 and 10.2, about the same as the value reported for hopanes in a Hamilton Dome Wyoming crude oil, 1,773 ppm (Ref. 8 p. 41). Values reported in the literature for the absolute concentration of tricyclic terpanes are sparse.

The concentration distribution of individual tricyclic terpanes in the saturate fraction (Table 13.6) follows the order $C_{23} > C_{24} > C_{25} > C_{21} > C_{19} > C_{20}$. In the maltene, polar and asphaltene pyrolyzates the C_{23} member is still the most abundant but the order is altered and, from the asphaltene, the distribution is in the sequence $C_{23} > C_{20} > C_{21} > C_{19} > C_{24}$. The dominant trend is that on thermolysis the relative importance of the lower members (C_{19}, C_{20}, C_{21}) of the series increases compared to that of the higher members ($\geq C_{24}$). This trend can be attributed to the shortening and loss of side chains on thermolysis

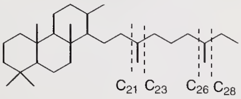

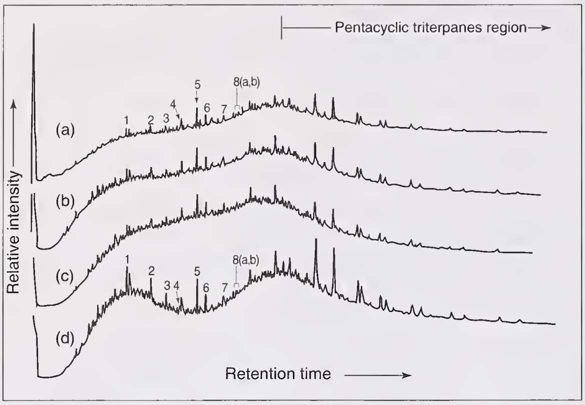

Figure 13.11 Gas chromatograms of the branched and cyclic alkanes in Athabasca oil sand 300°C pyrolyzates: a) 6 h; b) 12 h; c) 24 h; d) 72 h pyrolysis. The molecular formulas of the numbered peaks are $C_{19}H_{34}$ (1), $C_{20}H_{36}$ (2), $C_{21}H_{38}$ (3), $C_{22}H_{40}$ (4), $C_{23}H_{42}$ (5), $C_{24}H_{44}$ (6), $C_{25}H_{46}$ (7) and $C_{26}H_{48}$ (8a,b). From C.M. Ekweozor and O.P. Strausz, Ref. 14. © 1983, Wiley Heyden.

and to the nature of decomposing precursors and their decomposition reactions. The important reactions in the latter context appear to be:

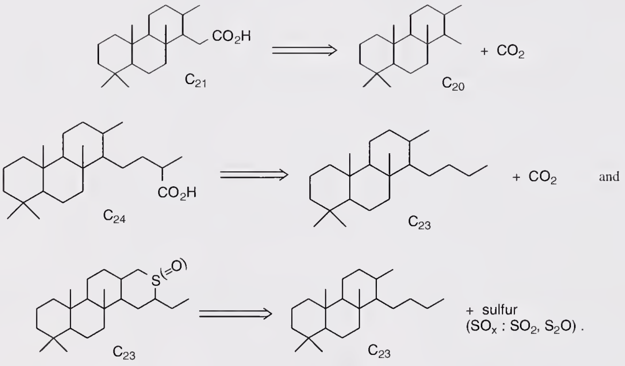

As will be seen in Chapter 14, tricyclic and pentacyclic terpenoid hydrocarbons are attached to the asphaltene molecules by sulfide, ether, ester and C_{arom}–C bonds which, upon thermolysis, release their terpanes with truncated side chains as well.

In the side chain, C–22 becomes an asymmetric center in the C_{25} and higher members which then appear as doublets in the gas chromatograms. The earlier-eluting C_{23} isomer is thought to have the 14β(H) configuration which is less stable than the 14α(H) configuration and this may explain the relatively high concentration of the 14α(H) epimer in the thermolysis products. A minor isomeric series of tricyclic hydrocarbons are also present in the C_{19}–C_{24} range, the mass spectra of which show intense m/z = 123 peaks but no m/z = 191 peaks. On this basis, it is assumed that these are C–13-alkylated tricyclic terpanes lacking an alkyl substituent on C–14. These compounds are known to give m/z = 123

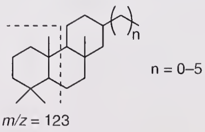

but not 191 peaks.

As the example of the tricyclic terpenoid hydrocarbons demonstrates, any given hydrocarbon type biomarker in the oil and especially in the bitumen may also be present in functionalized or bound forms in the aromatic, polar (and asphaltene) fractions of the oil. In effect, the concentration of a biomarker series with a given carbon skeleton in the asphaltene may exceed (as happens to be the case in the above example) its concentration in the saturates fraction of the oil. These functionalized and bound biomarkers may (and mostly do) have distributions different from those of their hydrocarbon counterparts and carry valuable supplementary geochemical information.

1.1.4 Bicyclic terpenoid hydrocarbons

Some of the bicyclic terpanes, like the hopanes, secohopanes and tricyclic terpanes, originate from bacterial (prokaryotic) membrane lipids. The prominent series of prokaryotic bicyclic terpanes, drimanes,

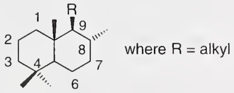

are thought to have formed from the unsaturated Δ11(12)*-bacteriohopanetetrol during diagenesis. They are of widespread occurrence in sediments and crude oil. Others, like eudesmane,

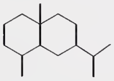

are believed to be terrogenic indicators.

Drimanes, along with other bicyclic terpanes, are quite common in Alberta bitumens.[15] In Athabasca saturates 23 bicyclic terpanes, 11 of which belong to the drimane series, have been detected. These bicyclic terpanes have 15–24 carbon atoms, the most abundant being the C_{15} and C_{16} drimanes, *cf.* Figure 10.2. As can be determined from the mass spectra, the non-drimane members do not form a single series of a particular structure. Four members show base peaks at *m/z* = 137 instead of 123, as do the drimanes. There are a number of bicyclic terpanes known which show a strong signal at *m/z* = 137 in their mass spectrum. Some examples are:

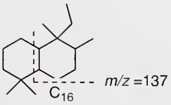

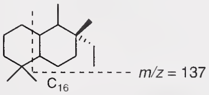

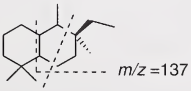

Drimanes have also been shown to be present in at least one functionalized form, namely, as tricyclic sulfides,[25]

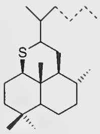

---

*The designation Δ11(12) indicates that the double bond is located between C–11 and C–12.

in Alberta bitumens and oils and in sulfur-containing oils in general. The hydrocarbon skeleton of these drimanes, however, do not appear to be the derivatives of hopanoid or cheilanthanoid type progenitors, as indicated by their methyl branchings in the side chains. In the sulfide molecules the 4th and 5th isoprene units in the side chains are joined in a tail-to-tail configuration, whereas in the hopanoid and cheilanthanoid molecules all the isoprene units are joined in a head-to-tail configuration.

1.1.5 Monocyclic terpenoid hydrocarbons

Monocyclic hydrocarbons in the C_{10}–C_{30} range are present in Athabasca saturates, but the structural identification of individual compounds has not been reported. The presence of monocyclic terpanes, however, can be invoked on the basis of the experimental observation that bicyclic terpenoid sulfides,

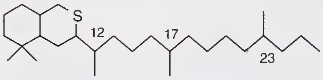

which contain a monocyclic terpenoid carbon skeleton,

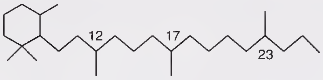

are present in the maltene in prodigious amounts. Other cyclic terpenoid sulfides in the maltene, the tricyclic, tetracyclic and hexacyclic sulfides, all contain cyclic terpenoid carbon skeletons corresponding to the cyclic terpanes known to be present in the maltene;

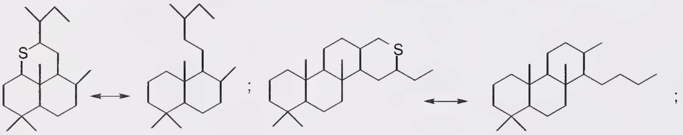

and

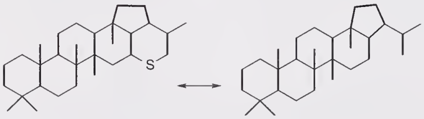

These monocyclic terpanes in the C_{12}–C_{27} range could have formed from the 9,10-ring opening of drimanes. Alternatively, they could have formed from the cleavage of β-carotane, *v.i.* It will be noted that here again the 1st to 4th isoprene units are joined together in a head-to-tail configuration whereas the 4th and 5th units are in a tail-to-tail configuration.

1.2 Acyclic terpenoid biomarkers

Acyclic isoprenoids found in petroleum usually range in carbon number from C_{15} (farnesane) to C_{40} (bisphytane, lycopane). The most commonly occurring acyclic isoprenoids in petroleum are the C_{19} and C_{20} diterpenoids, pristane and phytane. These diterpenoids are the diagenetic products of phytol, the hydrolytic product of chlorophyll-*a*, chlorophyll-*b*, bacteriochlorophyll-*a*, α and β-tocopherols, carotenoid pigments and archaebacterial membranes.

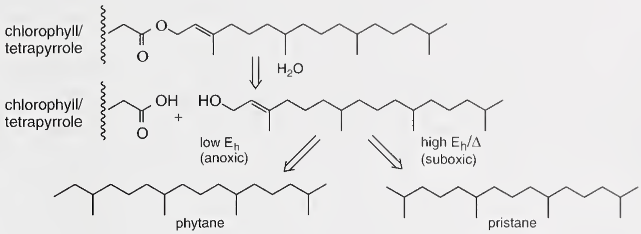

Under highly reducing conditions through a number of steps, phytol is reduced to phytane. Conversely, under strongly oxidizing conditions, the hydroxyl group of phytol is oxidized to a carboxylic group which subsequently may undergo decarboxylation to yield pristane. For this reason, a low pristane/phytane ratio, < 0.6, signifies an anoxic (< 0.1-mL oxygen/L water), commonly hypersaline (brines with > 35 parts per thousand salts) environment during source rock deposition; a high value, > 3.0, indicates terrestrial organic matter input under oxic conditions.

Similarly, farnesane

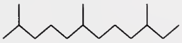

can arise from the hydrolysis of bacteriochlorophylls-*d* (from *chlorobium* group photosynthetic bacteria).

When higher acyclic terpenoids are present in petroleum, the pristane/phytane ratio may be altered by the degradation of the higher terpenoids, which also produces pristane and phytane, and thus the ratio becomes unreliable as a depositional environment indicator. Among the higher acyclic isoprenoids, the $C_{40}H_{82}$ isomeric tetraterpanes, bisphytane (head-to-head), regular tetraterpane (head-to-tail) and lycopane (tail-to-tail) appear to have relevance to Alberta oils.

Pristane, phytane, C_{15}, C_{16} and smaller quantities of other acyclic isoprenoids have been detected in Lloydminster heavy oil and Cold Lake and Wabasca[32] bitumens, Figures 13.12 and 10.11. As seen from the figures, the pristane/phytane ratio is ~ 0.8 – 1.05. In the case of the Cold Lake sample, thiourea adduction separation followed by m/z = 183 cross-scan analysis (the m/z = 183 peak, resulting from the cleavage of the tertiary C–C bond, is characteristic of long-chain isoprenoid hydrocarbons)

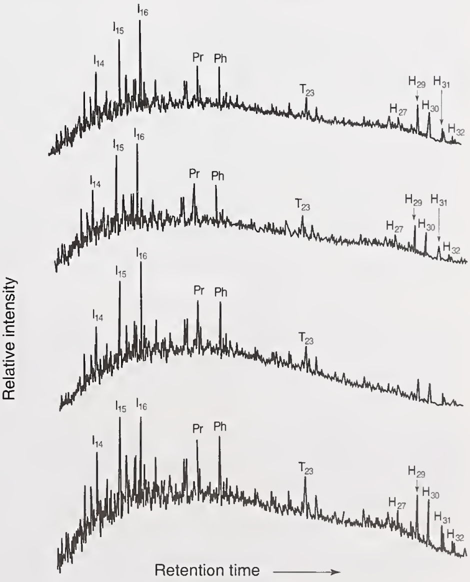

Figure 13.12 Gas chromatograms of the saturate fractions from a less severely biodegraded Alberta oil. Each sample was taken from different depths between about 450 and 500 m. I_{14}, I_{15} and I_{16} are C_{14}, C_{15} and C_{16} isoprenes; Pr and Ph, pristane and phytane; T_{23}, a C_{23} tricyclic hydrocarbon; H, hopanes with varying numbers of carbon atoms.

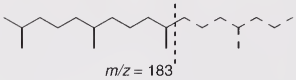

revealed the presence of a series of acyclic isoprenoids occurring in pairs up to C_{40}, one carbon apart and separated by one isoprene unit. These compound(s) can be either one of the three isomeric tetraterpanes listed in Table 13.1 and the lower MW compounds, including pristane and phytane, can be the thermal degradation products of the C_{40} parent compound(s). All three $C_{40}H_{82}$ compounds—bisphytane, regular isoprenoid and lycopane—are thought to be derived from archaebacterial lipids and their presence in the bitumen is a signature of archaebacterial contribution to the biotic source material of the bitumen. Therefore, under such conditions the pristane/phytane ratio, even if it can be determined, is not a reliable geochemical indicator unless it is ascertained that higher isoprenoids are absent.

These early biomarker studies on Alberta bitumens reported in the period 1977–1988 which centered primarily on steroid and terpenoid hydrocarbons have led to useful information regarding the source rock, depositional environment, diagenetic, catagenetic and microbiological history of the various bitumen deposits and their interrelationship. They were then substantially expanded during the intervening period. The results from these early periods will be summarized in the following section of this chapter and the more recent results will be examined in Section 7.0 dealing with the source and migration of the precursor oil to the bitumen.

1.3 Geochemical conclusions from early studies on hydrocarbon biomarkers

In this subsection we examine the geochemical significance of the hydrocarbon-type biomarkers which have been identified in the hydrocarbon fraction of the maltene. The conclusions reached from these considerations will then be supplemented later with those obtained in more recent studies on biomarkers, in studies on the whole oil sand and various other fractions thereof.

The study of biomarkers in a crude oil provides a fingerprint of the oil for comparison with other oils, source rock bitumen, kerogen, *etc.*, at the molecular level, involving trace-to-small quantities of constituent molecules. The terpane fingerprint, as discussed in the preceding sections, offers the most useful fingerprint for such correlations. Beyond empirical correlations, the nature of the biomarkers present in the oil and their concentration distributions contain invaluable information regarding the origin of the oil, its biotic source materials, the nature and paleoenvironmental conditions of its source rock deposition, and its diagenetic, catagenetic, migrational, water washing and biodegradational history.

Perhaps the most striking aspect of the results of terpane fingerprinting studies of the vast Lower Cretaceous sand and Paleozoic carbonate oil and bitumen accumulations of the Western Canada Sedimentary Basin is the very close similarities of the terpenoid biomarker contents after allowance is made for the extent of biodegradation. Nearly all heavy oil and bitumen deposits in the Basin show signs of biodegradation of varying severity. The facility of aerobic bacteria to catabolize hydrocarbons has been shown to follow the order: *n*-alkanes > acyclic isoprenoids > steranes > hopanes > diasteranes > tricyclic terpanes > aromatic steroids. Using the relative concentrations of these particular types of hydrocarbons in the oil, the extent of biodegradation of the various deposits follows the order: Lloydminster < Cold Lake < Provost < ~ Peace River ~ Wabasca (Wabiskaw) < Athabasca < Wabasca (Grand Rapids Formation A sand) ~ Carbonate Triangle (Upper Ireton, Shunda, Debolt) << Carbonate Triangle (Nisku) < Carbonate Triangle (Grosmont).

The Lower Cretaceous Bellshill Lake crude oil is thought to be a prototype of the original oil, the biodegradation of which resulted in the formation of the heavy oil and bitumen accumulations of the Western Canada Sedimentary Basin.[33,34] The Bellshill Lake oil, as was seen in Figures 12.39 and 12.40, does not show signs of biodegradation and contains a full complement of *n*-alkanes, *n*-alkylthiolanes and *n*-alkylthianes.[35] The ranking of biodegradation as given above should be viewed as an indication of broad trends only, although intra-reservoir variations among samples are minor. On the whole, in the southeastern part of the Basin, biodegradation is milder than in the northwestern part and the carbonate bitumens are more severely degraded than the sand bitumens.

The Lloydminster heavy oils contain some *n*-alkanes, isoprenoids and higher branched alkanes, *cf.* Figures 10.21 and 22, and relatively low concentrations of asphaltenes. Trace amounts of *n*-alkanes can be found in Cold Lake and some of the Wabasca bitumens, but bitumens from the other reservoirs are practically—if not completely—devoid of *n*-alkanes. Acyclic isoprenoids can also be found in the Cold Lake and some Wabasca bitumens. Regular steranes can be found up to the Wabasca bitumen in the biodegradation ranking list but only in small concentrations or none at all in the Athabasca and carbonate bitumens. Diasteranes are present in all bitumens except in four samples of the most severely biodegraded Grosmont Carbonate bitumen, and the C_{27} diacholestane/cholestane ratio generally increases down the list. Hopanes are present in all samples but in some regions of the Wabasca, Grosmont and Nisku formations the hopane concentrations are diminished, in which case the 25-norhopanes appear. The 25-norhopanes evidently were formed by the microbial demethylation of hopanes.

The distribution of hopanes, when not affected by biodegradation, features C_{29}/C_{30} ratios in m/z = 191 cross scans of up to unity or even slightly higher. Such high relative concentrations of the C_{29} norhopane have been associated with petroleums from organic-rich evaporite-carbonate rocks. This hypothesis is also supported by the presence of 28,30-bisnorhopane, 29,30-bisnorhopane and the partial preservation of the C_{35}-homohopanes. (Strong preservation of the C_{35}-homohopanes is taken to imply a carbonate source rock in an anoxic basin.) A sizeable peak for gammacerane in the m/z = 191 cross scan may signify hypersaline water during deposition of the source rock. Such information, as derived from the distribution of biomarkers in the bitumen, can be useful when exploring for the source rocks of the bitumen.

The thermal maturity of the bitumen is reflected by the following average geochemical parameter values for hopanes, as can be read from the oil generation curve,[8] Figure 13.13,

• $\beta,\alpha\text{-}C_{30}/(\alpha,\beta\text{-}C_{30} + \beta,\alpha\text{-}C_{30})$	10%
• $\beta,\alpha\text{-}C_{29}/(\alpha,\beta\text{-}C_{29} + \beta,\alpha\text{-}C_{29})$	~8–9%
• $T_s/(T_s + T_m)$	~40%
• 22S–C_{31}/(22S–C_{31} + 22R–C_{31}) and 22S–C_{32}/(22S–C_{32} + 22R–C_{32})	~60%

concordantly pointing to an early-mature to mature status.

The values indicated are maximum values beyond which the ratios remain constant, except for 18β/(18α + 18β)-oleane, βα/(αβ + βα)-hopanes (C_{30}) and ββ/(ββ + αβ + βα)-hopanes, where the numbers 10, 5, 0 are minimum values.

The geochemical parameter values derived from steroidal biomarkers,

• 20S/(20S + 20R) of $\alpha,\alpha\text{-}C_{29}$	~41–52%

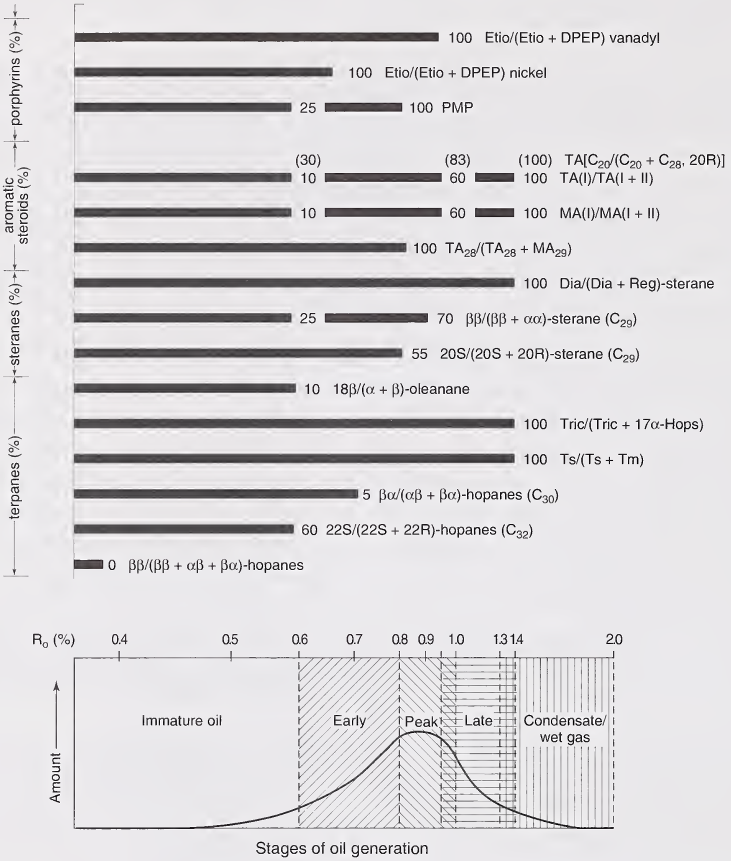

Figure 13.13 Approximate ranges of biomarker maturity parameters in correlation with vitrinite reflectance and an oil generation curve. After K.E. Peters and J.M. Moldowan, Ref. 8.

• 20S/(20S + 20R) of β,α-diacholestane	~55–58%
• β,β/(β,β + α,α) of C_{29} steranes	~59–84%
• β,β/(β,β + α,α) of C_{21} steranes	~70–72%

- and the values for mono- and triaromatic steranes as summarized in Table 13.5

are all in agreement with the hopane-derived values, suggesting an early-mature to mature state for the bitumen.

The relative abundance of secohopanes in the bitumen compared to (T_s + T_m) ~ 25% lends additional support to the thermally early-mature to mature state for the bitumen.

The distributions of mono- and triaromatic steroids, like those of other, microbiologically unaffected biomarkers, are very similar in the Athabasca and Grosmont bitumens (Figures 13.9 and 10). The one exception in this regard is the presence of the triaromatic C_{20} and C_{21} steroids in Athabasca and their conspicuous absence in the Grosmont bitumen. This may be interpreted as being due to water washing effects which could have preferentially removed the triaromatic hydrocarbons. That the Grosmont deposit has been severely water washed was shown by the distribution of its terpenoid sulfoxides, to be discussed in the following section.

Biomarker chemistry, as is evident from the material covered in this section, has achieved a high level of sophistication during the past three decades or so and today it is capable of providing reliable information with regard to the origin and history of petroleum. Thus, since about the mid-1980s it has become possible to delineate three broad groups of petroleums according to the nature and origin of their source material as marine, terrestrial or lacustrine, and to assign the nature of their source rocks as shales or carbonates,[8] Table 13.7. Further subdivisions according to particular details of depositional conditions (*e.g.* marine—evaporatic, carbonate, deltaic, calcareous, siliceous, *etc.*) and the nature of source materials (*e.g.*, algal, bacterial, vascular plants, *etc.*) have been made, but they will not be considered here. No single characteristic listed in Table 13.7 can serve as a valid basis for the classification of the oil or its source rock, but taken together they are thought to be reliable geochemical indicators. Many of the characteristic parameters employed in these classifications are affected, and some of them quite severely, by biodegradation. Therefore, in attempting to draw conclusions about the geochemistry of the heavy oil and bitumen accumulations of the Western Canada Sedimentary Basin it is necessary to take into consideration the effects of biodegradation. Along with the biomarker parameters, some nonbiomarker bulk properties of Alberta bitumens are also listed in Table 13.7 together with some relevant data for the Bellshill Lake oil.

The high sulfur and thiophenic contents of the bitumens may be thought of as a result of the biodegradation of the precursor oil since biodegradation is known to be capable of enhancing the sulfur content in the bitumen end product. In laboratory biodegradation experiments[36] this enhancement was found to be only ~4% for the case of Prudhoe Bay crude, but for the case of Bellshill Lake crude, it amounted to 43%, Table 13.8. Therefore, in order to rationalize the origin of the very high sulfur content of bitumen, about 4.5%, one must assume that the precursor oil had an elevated sulfur content. This conclusion is in accord with the high sulfur content, 1.9%, of the presumed stereotype of the bitumen precursor, the Bellshill Lake oil. The high thiophenic sulfur content is synonymous with a high total sulfur content since most of the sulfur in petroleum is present in the form of thiophenic compounds.

API gravity is another property affected by biodegradation and therefore the API gravity of the bitumen cannot be directly related to its geochemistry. The API gravity of the precursor oil can be estimated, on the basis of the API gravity of the Bellshill Lake oil, to have been somewhat less than 27° which, after biodegradation, water washing and abiogenic oxidation, could have dropped to the present-day values of 6–10°.

The *n*-alkane, pristane and phytane distributions, even if there is enough material left after biodegradation, cannot be related to the source material or source rock of the oil. Here again, the Bellshill Lake oil is used as a prototype of the original precursor oils. For the Bellshill Lake oil the n-C_{21}–C_{35} content is low and the pristane/phytane ratio has a value of 1.2; however, in the alkanes from the reduction of the cyclic sulfides—which are thought to better represent the oil before it had experienced secondary alterations—the ratio is 0.4. The pristane/n-C_{17} ratio is low, 0.26, and it is even lower, 0.14, in the sulfide-derived alkanes; the values for the phytane/n-C_{18} ratios are similarly low, 0.23 and 0.27. The CPI of the Bellshill Lake oil is 1.0 and 0.86 in the sulfide-derived alkanes.

The concentrations of steranes in the bitumens are reduced and their distributions altered by biodegradation. However, the C_{27}, C_{28} and C_{29} distributions in the regular steranes and diasteranes are in the range of marine, carbonate oils. The sterane/17α(H)-hopane ratios are low, even in cases where the biodegradation appears to be mildest, and the diasterane/sterane

Table 13.7 Characteristics of petroleum according to source materials and source rocks[8]

Characteristics	Shales	Carbonate	Marine	Terrestrial	Lacustrine	Alberta bitumens	Bellshill Lake oil
	Source rocks		Source materials				
API gravity	med./high	low/med.	—	—	—	low[a]	27° med.
Sulfur wt%	variable	high	high	low	low	high[b]	high (1.9%)
Thiophenic S	low	high	—	—	—	high[b]	high
C_{21}–C_{35} *n*-alkanes	—	—	low	high	high	n.a.[c]	low
Saturates/aromatics	med./high	low/med.	—	—	—	n.a.[c](low)	low
Naphthenes/paraffins	med./low	med./high	—	—	—	n.a.[c](high)	high
CPI (C_{22}–C_{32})[d]	≥1	≤1	—	—	—	n.a.[c]	1.0 (0.86)[e]
Pristane/phytane	high (≥1)	low (≤1)	≤2	≤3	~1–3	n.a.[c](low)	1.2 (0.4)[e]
Phytane/*n*-C_{18}	low (≤0.3)	high (≥0.3)	—	—	—	n.a.[c](low)	0.2 (0.3)[e]
Pristane/*n*-C_{17}	—	—	low (<0.5)	high (>0.6)	—	n.a.[c](low)	0.3 (0.2)[e]
Steranes	$C_{27}<C_{29}$	$C_{27}>C_{29}$	high C_{28}	high C_{29}	low C_{28}	within marine carbonate oil range	
Steranes/17α-hopanes	high	low	high	low	low	low (in mildly degraded bitumen)	
Diasteranes/steranes	high	low	—	—	—	low (in mildly degraded bitumen)	
C_{29}/C_{30}-hopanes	low	high	—	—	—	high (≥1)	
C_{35}-homohopanes	low	high				high	
$T_s/(T_s+T_m)$	high	low				low	
C_{29}-MA-steroids	low	high				high (within marine carbonate oil range)	
V/(V + Ni)	low	high	high/low	low/absent	low/absent	high	

[a] Lowered by biodegradation.

[b] Increased by biodegradation. [c] Not applicable.

[d] $\mathrm{CPI} = \left[\dfrac{C_{25}+C_{27}+C_{29}+C_{31}+C_{33}}{C_{26}+C_{28}+C_{30}+C_{32}+C_{34}} + \dfrac{C_{25}+C_{27}+C_{29}+C_{31}+C_{33}}{C_{24}+C_{26}+C_{28}+C_{30}+C_{32}}\right] \Big/ 2$ where C_x is the GC peak height of the C_x *n*-alkane

[e] The numbers in brackets are the ratios in the alkanes produced from the reduction of sulfides.

Table 13.8 Microanalytical data for the biodegradation of Prudhoe Bay and Bellshill Lake oils[36]

Sample[a]	%				
	C	H	N	O	S
PB	84.31	11.66	0.23	0.82	1.52
PB168	85.01	11.14	0.33	1.93	1.58
BH	84.51	12.00	0.14	0.87	1.91
BH168	82.81	10.73	0.17	2.27	2.73

[a] PB = Prudhoe Bay; BH = Bellshill Lake; 168 = time (h) of incubation.

ratios could not have been high in the original nonbiodegraded oils either. The distribution of monoaromatic steroids is within the range for marine carbonate oils.

As seen from the data in Table 13.7 a correlation (at the present level of understanding of biomarker chemistry and organic geochemistry) between the bulk properties and biomarker compositions of the bitumens (heavy oils, Bellshill Lake oil, *etc.*) and the possible source rocks and organic source materials points concordantly and unambiguously to a marine carbonate origin for the bitumen (and associated oil) accumulations of the Western Canada Sedimentary Basin. This conclusion has importance to the elucidation of the origin of these hydrocarbon accumulations and the identification and location of their source rocks. In Table 13.7 the term "carbonate rocks" refers to fine-grained sedimentary rocks containing 50% or more of carbonate minerals.[8] In the literature various authors at various times have suggested a number of different source rocks, mostly shales, for the precursor oils of the bitumens. However, in light of recent developments in the interpretive biomarker–organic geochemical investigations of petroleum[8] and advancements discussed above in the biomarker chemistry of Alberta bitumens,[13–14,16–18] it has become increasingly evident that carbonate- rather than shale-based source rocks are required for the bitumens and heavy oils of the Western Canada Sedimentary Basin.

The major types of hydrocarbon biomarkers found in Alberta oil sand thus far are the saturates, accompanied by lesser amounts of aromatics. Because of their higher chemical reactivities and their capacity to take up hydrogen in a reducing environment until they become fully saturated, unsaturated hydrocarbon biomarkers are, in general, much less abundant than the saturated or aromatic types and occur only in trace quantities in petroleum. The only alkenic biomarker identified in significant quantity in Athabasca maltene and asphaltene is the all-important ubiquitous hexaprenoid biomolecule squalene,[37] the *in-vivo* precursor of the steroids and hopanoids. However, since the average lifetime of such a reactive molecule in the deposit under either reducing or oxic conditions should be short, squalene had to be formed in the recent past. It is known that live (dormant) bacteria and other microbes are present in the oil sand deposits down to a depth of 700 m and since only a small fraction of the squalene can be separated from the asphaltene chromatographically while the bulk can only be separated by combined thermolysis–chromatography, it is possible that some or perhaps most of the squalene is bound in live or dead organisms.

2.0 Sulfur-Containing Biomarkers

All Alberta heavy oils and bitumens and indeed all of the few dozens[23-26] of sulfur-containing petroleums examined thus far have been found to contain cyclic terpenoid sulfides.[29c,35,38,40,41] The distribution of the sulfides is basically determined by the distribution of the hydrocarbons in the early evolutionary stages of the sediment and subsequently modified by thermal maturation, biodegradation, oxidation, water washing and migrational alteration of the oil.[27] The different series of the sulfides, *i.e.* the bi-, tri-, tetra- and hexacyclic terpenoid and the pentacyclic—assumed to be mainly steroid—sulfides and their individual members, are affected to different extents by the above processes. Nonbiodegraded petroleums contain, in addition to the cyclic terpenoid sulfides, 2-*n*-alkyl and 2,5-di-*n*-alkyl-substituted thiolanes and thianes[23–26,35,41] which, as has been shown in laboratory experiments,[42] are apparently readily attacked by the bacteria causing the degradation of the oil:

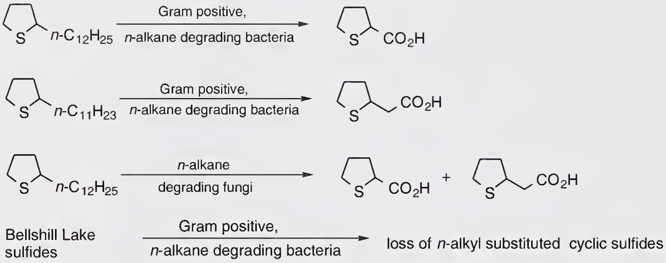

The formation of the thiolane carboxylic acids is accompanied by the formation of lesser amounts of the sulfoxide and sulfone derivatives of the starting thiolane. On prolonged microbial action, the thiolane carboxylic acids are also destroyed, to yield unspecified products.

The terpenoid sulfides are more resistant to microbial attack and survive the biodegradation of the oil. Consequently, biodegraded oils contain only the terpenoid sulfides.[26]

When both *n*-alkyl-substituted thiolanes/thianes and terpenoid sulfides are present in the oil, the two classes of sulfides can be separated from one another by thiourea adduction, *cf.* Figure 12.38. The terpenoid sulfides separated this way from the Bellshill Lake conventional oil show a close similarity to the distribution of the terpenoid sulfides in bitumens and heavy oils. As will be shown below, this distribution is not highly specific since the distributions of terpenoid sulfides in all petroleums studied[25,26,41]—involving a variety of conventional and heavy oils of various ages as well as bitumens—are quite similar after appropriate allowance is made for the various secondary alterations (water washing, thermal maturation) the oil has undergone. However, what is truly striking is the similarity in the distribution of the saturate fraction of a given oil and that of the hydrocarbon products from the reduction of its sulfide fraction as illustrated in Figures 12.39, 13.12 and 13.14 for the alkane and reduced sulfide components of Bellshill Lake oil and Wabasca bitumens. For the latter, the major difference between the sulfide-derived and the native alkanes is the higher relative abundance of the C_{23} tricyclic in the former. Among the more subtle but persistent and characteristic differences, one recognizes the generally lower I_{15}/I_{16}, Pr/Ph, H_{29}/H_{30} and H(22S)/H(22R) ratios in the sulfide-derived material. It is then tempting to postulate that the hydrocarbons "locked up" in the sulfide molecules correspond to a more appropriate representation of the hydrocarbon distribution as it existed in the young oil, prior to exposure to secondary thermal, biological and other effects than do the hydrocarbon distributions found today in the oil. This conjecture appears to be

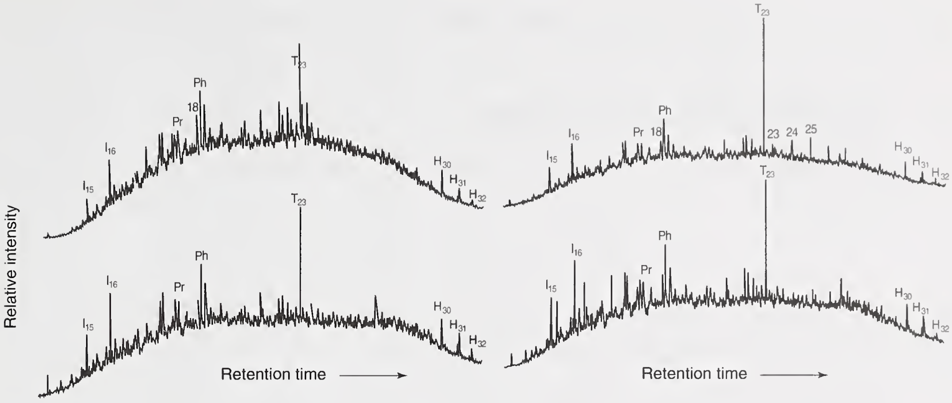

Figure 13.14 Gas chromatograms of the hydrocarbons obtained after Raney nickel reduction of the sulfides in Wabasca bitumens. I_{15} and I_{16} are C_{15} and C_{16} isoprenes; Pr and Ph, pristane and phytane; T_{23}, C_{23} cheilanthane; 18, 23, 24, 25, *n*-alkane chain length; H, hopanes with varying numbers of carbon atoms.

supported by the general absence of norhopanes and the higher abundance of *n*-alkanes in the sulfide-derived hydrocarbons, a feature reminiscent of that observed for the distribution of carboxylic acids as well.

2.1 Origin of sulfides and incorporation of sulfur into the sedimentary organic matter

According to current understanding, sulfur incorporation into the sedimentary organic matter takes place during the early stages of diagenetic evolution.[27] The source of the sulfur is the sulfate ion which, in highly reducing-to-anoxic marine sediments, is microbiologically reduced (by sulfate-reducing bacteria, *e.g., Desulfovibrio*) to sulfide ion in equilibrium with dissolved hydrogen sulfide or polysulfides. These sulfide species can react with organic matter and with metals (primarily iron) and if both are present, in parallel, competing processes. Scavenging of sulfur by iron (to ultimately form pyrite) is efficient and if a sufficient quantity of iron is present, sulfur incorporation into the organic matter will not be extensive. Lime anhydrites muds with low clay content do not possess sufficient iron or other metals to scavenge all the available sulfide and thus, under these conditions much of the sulfide becomes incorporated into the organic matter to produce high-sulfur kerogens or bitumens. Clay-poor (carbonate or anhydrite) marine rocks deposited under highly reducing-to-anoxic conditions are the source rocks of many high-sulfur kerogens and oils.

Marine, clay-containing siliclastic rocks (including most shales) are sufficiently rich in iron and other metals to remove most of the reduced sulfur from the sediments and become source rocks for low-sulfur kerogens and oils.

The special requirements regarding the sedimentary environment for the generation of high-sulfur kerogens and oils are reflected in the distribution of biomarkers carried over to the oils. The carbonate source rocks and anoxic depositional conditions result in a relatively high concentration of the C_{35} homohopanes compared to the other homohopane members and low values for the pristane/phytane, diasteranes/steranes, tricyclanes above C_{26}/tricyclanes below C_{26}, *etc.* ratios. These biomarker characteristics can therefore be used to extract information with regard to the nature of the source rock and the depositional environment of the oil. As we have seen thus far, all the available data on Alberta heavy oils and bitumens favor carbonate source rocks for the precursor oils.

2.2 Bicyclic terpenoid sulfides

The main C_{12}–C_{27} series of these sulfides corresponds to the structure

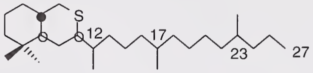

with minima in the concentration distribution at C–12, –17 and –23. The carbon skeleton appears to be directly related to a fragment of carotene:

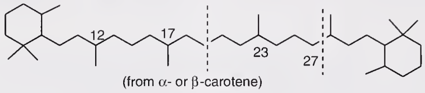

(from α- or β-carotene)

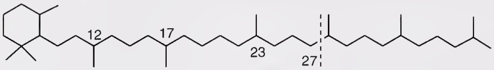

(from γ-carotene)

Neither acyclic nor cyclic fragments of carotene have been identified in any Alberta bitumen or oil but it will be recalled that a series of acyclic isoprenoids up to C_{40} has been detected in Cold Lake bitumen saturates.

Bicyclic terpenoid sulfides have been found to be present in every sulfur-containing petroleum examined and thus, their carbon skeleton, the monocyclic terpanes,

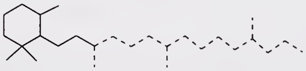 ,

must be ubiquitous trace components of petroleum. The distribution of bicyclic sulfides, displaying concentration maxima at C_{13} and C_{20}, appears to suggest multiple sources for these monocyclic terpanes. One of these could be α-, β- or γ-carotene or their precursors and the other one could be the diterpane corresponding to the saturated carbon skeleton of vitamin A. (β-Carotene is known to undergo hydrolytic cleavage at the central bond with two molecules of water in the liver and intestines of animal organisms to yield two molecules of vitamin A: hence the well-known provitamin A role of β-carotene.) It should also be mentioned that β-carotene has been detected in lacustrine and marine oils and has been associated with anoxic, saline deposition of algal organic matter.

Bicyclic terpenoid sulfides are useful geochemical indicators of thermal maturity and water washing. Thermal maturation has the effect of lowering the concentration of the sulfides as a whole (Table 13.9), reducing not only the relative proportion of the bicyclic terpenoid sulfides compared to the total sulfide fraction but also the concentration of the longer-side-chain members of the bicyclic sulfides compared to the C_{13} (and C_{14}) member, Figure 13.15. The apparent maturities increase with depth of burial, as expected, and also with age. The two most mature oils are the Leduc and Utikuma Lake oils which are of Devonian age, while the rest of the oils are of Cretaceous origin.

Water washing also has the effect of lowering the concentration of the sulfides as a whole and through differential removal of the more soluble members of the series, progressively

Table 13.9 Sulfide contents of various oil sand bitumens, heavy and conventional oils[a]

Sample	Depth (m)	Grade °API	Asph.	Sulfides[b]	Biode-graded	Water-washed
			%			
Alberta						
Trench[c]	0	3.7	15.7	7.0	yes	no
Beach Sand I[c]	3	7.4	n.d.	n.d.	yes	no
Beach Sand II[c]	0	8.8	17.7	n.d.	yes	yes
Test Pit[c]	5	14.5	17.0	5.2	yes	slight
Auger[c]	15	14.1	22.0	5.2	yes	yes
High Grade[c]	30	15.1	17.0	5.5	yes	yes
Fluvial[c]	43	11.9	20.0	5.7	yes	yes
Tarry Water[c]	45	5.4	19.0	2.2	yes	extreme
Abasand	d	15.5	57.0	1.1	yes	yes
Carbonate T.	245	n.a.	20.7	5.6	extreme	extreme
Wabasca	?	e	11.6	3.0	yes	extreme
Lloydminster	670	f	13.6	3.0	no	no
Peace River	558	10.6	20.4	16.1	yes	no
Wolf Lake	427	e	16.3	3.9	yes	extreme
Bellshill Lake	920	f	n.d.	2.7	no	no
Thompson Lake	926	f	n.d.	2.1	no	no
Pembina	1400	f	n.d.	0.8	no	no
Niton B	1985	f	n.d.	0.98	no	no
Leduc	1580	f	n.d.	1.3	no	no
Utikuma Lake	1726	f	n.d.	1.0	no	no
Rainbow Lake	1795	f	n.d.	0.3	no	yes
Foreign						
Llanganello	925	n.a.	14.1	7.7	–	–
Cerro Negro	?	n.a.	19.4	5.0	yes	no
Orinoco	?	n.d.	12.4	3.4	yes	extreme
Prudhoe Bay	?	f	n.d.	6.3	no	no

[a] All samples except Carbonate Trend, Leduc, Utikuma Lake and Rainbow Lake (Devonian) are from the Cretaceous period. [b] In the maltene. [c] From the Syncrude (Athabasca) mining site. [d] Outcrop. [e] Cold bailed. [f] Oil.

lowers the relative concentrations of the shorter-side-chain members. The latter effect alters the distribution in the opposite direction compared to that of thermal maturation and therefore one effect can cancel the alteration brought about by the other. The degree of alteration brought about by water washing varies between the bi-, tri- and tetracyclic sulfide series, the bicyclic series being the most susceptible to water washing.

Similarly, the sulfoxides in the polar fraction of the oil can be used as geochemical indicators. The sulfoxides, after separation from the oil, have been reduced to the sulfides by $LiAlH_4$ and analyzed as above. Figure 13.16 shows the m/z = 183.12 cross-scan mass chromatograms of the sulfides obtained from the reduction of the sulfoxide subfractions from Athabasca and Grosmont bitumens. The spectrum of the Athabasca sample is quite similar to that obtained from the sulfides themselves, Figure 13.15, showing that the sulfides and sulfoxides in the oil have the same distributions. The spectrum of the Grosmont sample indicates extensive water washing.

The effect of water washing has been experimentally demonstrated in the laboratory on a crude concentrate of terpenoid sulfoxides isolated from Athabasca bitumen by exposing it to a water flow (of Edmonton city tap water) at room temperature for about 3 months. The water

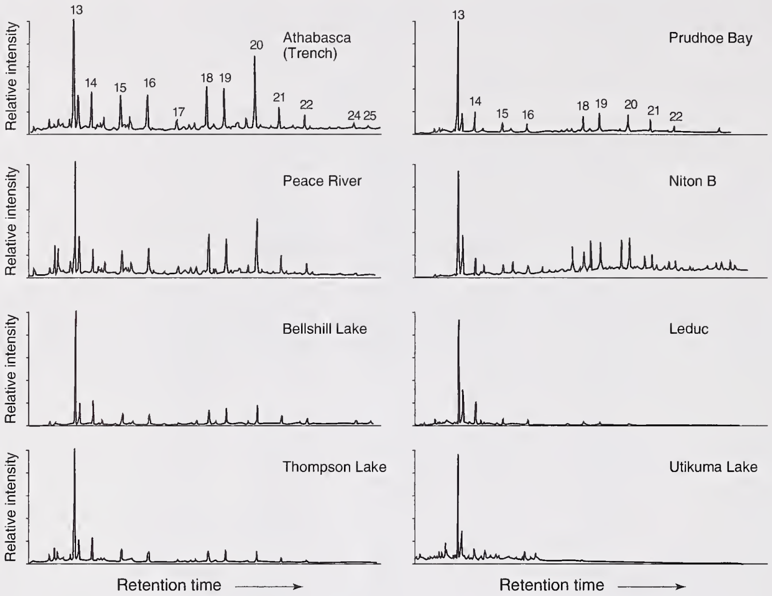

Figure 13.15 GC–MS *m/z* = 183 cross-scan chromatograms showing the bicyclic terpenoid sulfide distributions in Athabasca (Trench) and Peace River bitumens, and Bellshill Lake, Thompson Lake, Prudhoe Bay, Niton B, Leduc and Utikuma Lake conventional oils.[25] The numbers above the peaks correspond to the number of carbon atoms in the molecule. The samples are progressively more deeply buried, *cf.* Table 13.9.

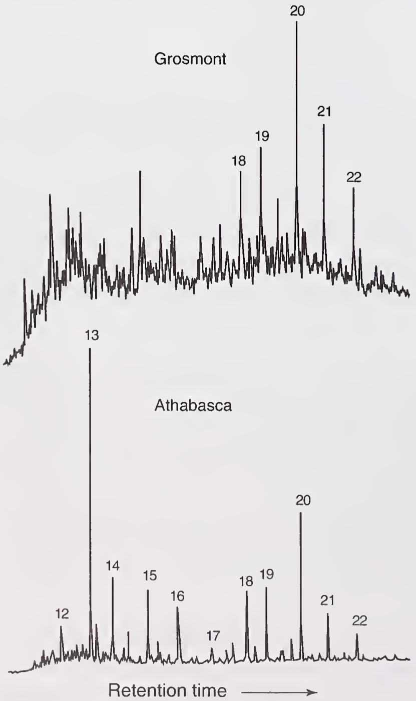

Figure 13.16 GC–MS *m/z* = 183 cross-scan chromatogram of the bicyclic terpenoid sulfides obtained by the $LiAlH_4$ reduction of the bicyclic terpenoid sulfoxides in Grosmont and Athabasca bitumens. The number above each peak corresponds to the number of carbon atoms in the molecule. From C.F. Hoffmann and O.P. Strausz, Ref. 16. © 1986, American Association of Petroleum Geologists.

wash preferentially removed the C_{12}–C_{17} bicyclic components and significantly reduced the abundance of the C_{17}–C_{20} tricyclic components. The distribution of the tetracyclic sulfoxides was only slightly altered under these conditions, with approximately a 10% reduction in the abundance of the C_{22} and C_{23} components. The three series of terpenoid sulfides therefore seem to provide three different grades of geochemical indicators for mild, extensive and severe water washing. Complications arising from biodegradation of the oil and other effects (differences in the original distributions of the sulfides, oxidation, contact with catalytic minerals, *etc.*) may distort the original distribution of the sulfides, although the terpenoid sulfides appear to be resistant to mild biodegradation. Nonetheless, severe biodegradation, like that experienced by the Grosmont bitumen, could conceivably affect their distribution.

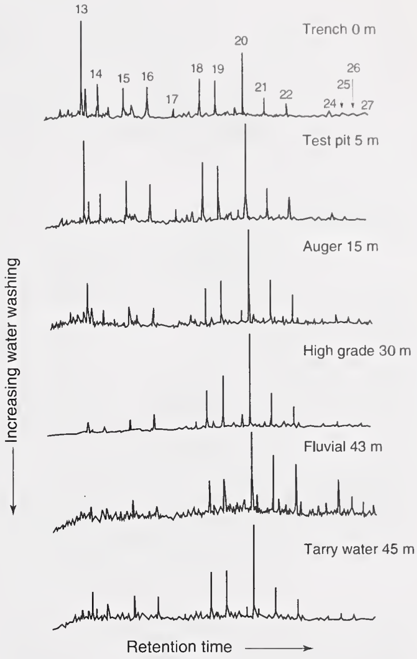

Figure 13.17 GC–MS *m/z* = 183 cross-scan chromatograms of the bicyclic terpenoid sulfides in five samples from the Athabasca (Syncrude mining site) deposit as a function of depth of burial (the samples are not in a vertical column). All traces are normalized to the most abundant peak. "Zero" means the top of the sand formation after removal of the overburden. The number above each peak corresponds to the number of carbon atoms in the molecule. From J.D. Payzant *et al.*, Ref. 25. © 1986, Elsevier Science Ltd.

The usefulness of terpenoid sulfides as indicators of the water washing history of crude oils is illustrated using the various strata of a Syncrude mine pit in Figure 13.17. The bitumen in the pit shows increasing levels of water washing with increasing depths, as manifested by the gradual increase in the ratio of the C_{18}–C_{22} components to the C_{12}–C_{16} components due to increased water solubility and therefore increased removal of shorter-side-chain members. The bottom spectrum for the Tarry Water sample appears to be less washed than the two samples immediately above it. However, the tri- and tetracyclic sulfide distribution suggests otherwise, indicating that minor differences in the ratios are not always meaningful, in a quantitative sense, as water washing indicators.

Bicyclic terpenoid sulfide distributions for various bitumens and oils indicating their water washing status are shown in Figure 13.18. Of the six samples shown in the figure, four, namely the California, Wolf Lake, Orinoco and Abasand samples display clear evidence of water washing. (The Abasand sample was taken from the surface and was exposed to weathering for about 50 years.)

2.3 Tricyclic terpenoid sulfides

The tricyclic terpenoid sulfides are present in minor amounts, compared to the other terpenoid sulfide series, in all the samples examined except the Devonian petroleum from the Rainbow field in northwestern Alberta and the Peace River samples. The Rainbow field severely water washed oil contains the lowest amount of sulfides, 0.3%, and the highest relative amount of tricyclic sulfides, exceeding the concentration of either the di- or tetracyclic sulfides. The distribution by carbon number of the tricyclic terpenoid sulfides, Figure 13.19, displays only

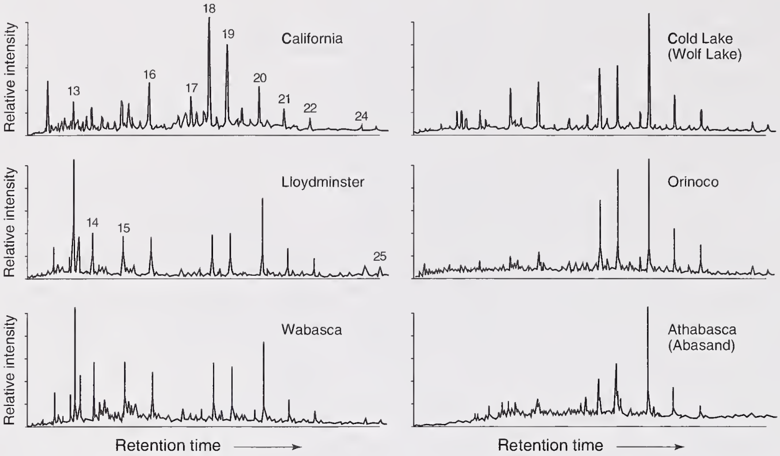

Figure 13.18 GC–MS $m/z = 183$ cross-scan chromatograms of the bicyclic terpenoid sulfides in various oil sand bitumens, heavy oils and conventional oils.[25] The number above each peak corresponds to the number of carbon atoms in the molecule.

minor variations with respect to thermal maturation or water washing of the oil. In non-water-washed samples, the carbon range of the main isomeric series extends from 17 to 31 with the C_{18} member being the most abundant. Minima in distribution are apparent at C_{17}, C_{23} and C_{28}. With increasing thermal maturation, a slight decrease in the concentration of the longer side chain members occurs relative to the shorter side chain members but this decrease is not as pronounced as with the bi- and tetracyclic sulfide series. Water washing can remove the C_{17} member and reduce the C_{18} and C_{19} homologs to such an extent that the concentration maximum is shifted to C_{20}. In general, the tricyclic sulfides appear to be less water soluble and are chemically less reactive than their bi- or tetracyclic counterparts; for example, their Raney nickel reduction to the hydrocarbons requires more severe conditions (200 *vs* 100°C for the di- and tetracyclic sulfides).

The main series of tricyclic sulfides has the structure

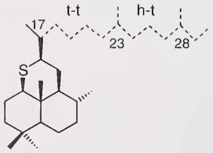

which, on Raney nickel reduction, can be converted to the bicyclic terpanes, the extended drimanes,

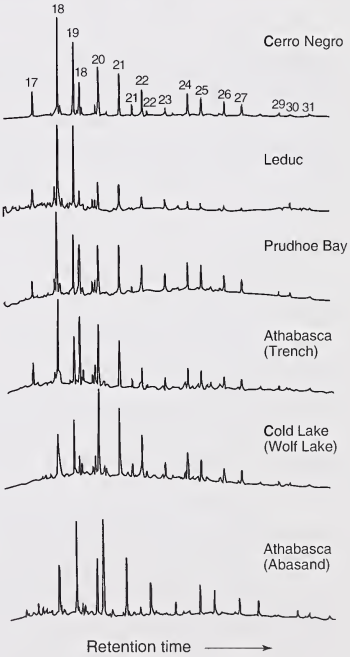

Figure 13.19 GC–MS $m/z = 251$ cross scan-chromatograms of the tricyclic terpenoid sulfides in various oil sand bitumens and conventional oils. All traces are normalized to the most abundant peak. The number above each peak corresponds to the number of carbon atoms in the molecule. From J.D. Payzant *et al.*, Ref. 25. © 1986, Elsevier Science Ltd.

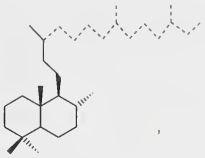

which are present in the saturate fraction of the oil. However, the carbon range of the drimanes detected was C_{15} to C_{24} only, compared to the C_{17}–C_{31} range for the sulfides.

Returning to Figure 13.19, the top four mass chromatograms do not indicate exposure to water washing, while the bottom two—as with the bicyclic sulfides—clearly bear the marks of extensive water washing of the oils: thus the C_{17}-member was removed and the C_{18} and C_{19} members reduced, shifting the maximum in concentration to C_{20}. The top four mass chromatograms, in spite of the vastly different origins of the oils they represent, show a common pattern for the carbon number distribution—a feature which applies to all oils investigated. Thus, the tricyclic sulfides appear to be relatively inert under geological conditions compared to the other cyclic terpenoid sulfides. This is consistent with their resistance to reduction with Raney nickel and their exceptionally high relative concentration in the severely water washed Rainbow oil where the sulfur concentration is the lowest of all samples studied.

2.4 Tetracyclic terpenoid sulfides

On Raney nickel reduction, tetracyclic terpenoid sulfides are reduced to the cheilanthane-type tricyclic terpanes

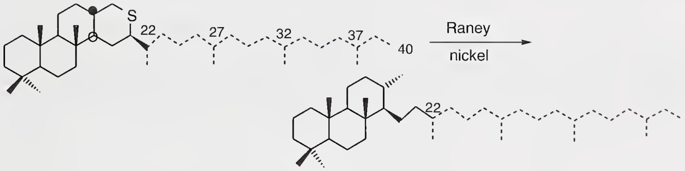

present in the saturate fraction of the oil, but the carbon number distribution of the terpanes from the reduced tetracyclic sulfides, as with the case of the tricyclic sulfides, extends to a broader range, C_{22}–C_{40}, than that of the hydrocarbons, C_{20}–C_{30}. This shows that the cheilanthanes originate at least in part from a tetraterpane precursor[25,29,30] in which the isoprene units are all joined in a head-to-tail configuration.

The tetracyclic terpenoid sulfide carbon number distribution patterns exhibit few trends with maturity. All oils which appear to be mature by other criteria, for example, Bellshill Lake and Leduc, show low intensities for members higher than C_{24} and the C_{23} member is by far the most abundant in the mass chromatograms, Figure 13.20a, when the oil lacks a water washing history. However, even when the oil is less mature and has not been exposed to water washing or only to mild water washing, it may display a similar distribution pattern, Figure 13.20b. After excessive water washing, however, the C_{23} member abundance may be greatly reduced and the concentration maximum shifted to C_{29} or C_{30}, Figure 13.21.

The sum of the concentration ratio of the tricyclic terpenoid hydrocarbons above C_{25} and below C_{26}, $\Sigma{>}C_{25}/\Sigma{<}C_{26}$, as has been discussed above, has been related to the origin of the oil. Thus, this ratio is low for oils from carbonate source rocks, while it is near unity for oils from

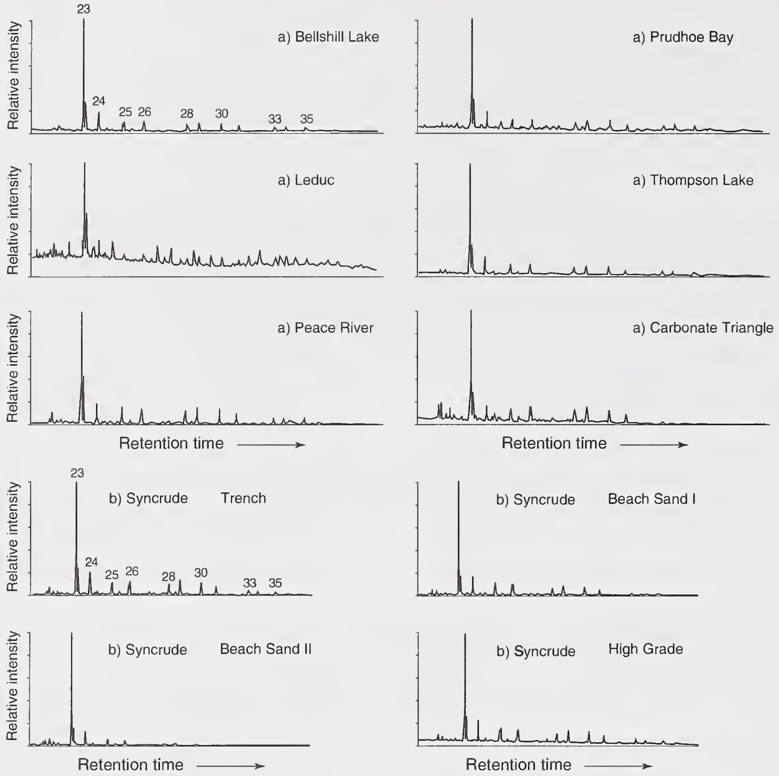

Figure 13.20 GC–MS *m/z* = 319 cross-scan chromatograms of the tetracyclic terpenoid sulfides in a) various oil sand bitumens and conventional oils which have not experienced waterwashing and b) four samples from the Syncrude mining site.[41] All traces are normalized to the most abundant peak. The number above each peak corresponds to the number of carbon atoms in the molecule.

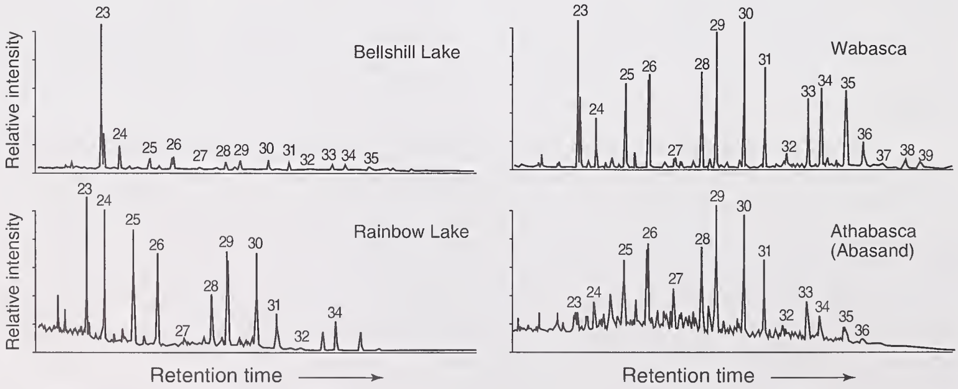

Figure 13.21 GC–MS *m/z* = 319 cross-scan chromatograms of the tetracyclic sulfides in two conventional oils and two waterwashed oil sand bitumens.[41] All traces are normalized to the most abundant peak. The number above each peak corresponds to the number of carbon atoms in the molecule.

other sources. The ratios for the hydrocarbons of Alberta oils and bitumens are all low and those for $\Sigma{>}C_{25}$ (tetracyclic sulfides)/$\Sigma{<}C_{26}$ (tetracyclic sulfides) from all the non-water-washed oils studied were also found to be quite low, as can be seen from Figure 13.21; moreover, the concentration distributions of the hydrocarbons and sulfides are, in general, quite similar except that the carbon number in the latter extends to higher values. Therefore, it may be concluded that the distributions of tetracyclic terpenoid sulfides are indicative of a carbonate source rock for the oils and bitumens shown in Figure 13.20.

2.5 Pentacyclic steroid sulfides

The FIMS seen in Figures 12.16 and 12.17 suggest the existence of a series of pentacyclic sulfides as well in Athabasca bitumen. The concentration of this pentacyclic series, maximum in the C_{23}–C_{30} range, is commensurate with the concentration of the tetracyclic series. Although the structure of this series has not been explored, the series is believed to comprise primarily sterane sulfides, *e.g.*

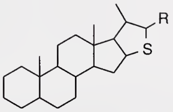

and lesser amounts of secohopane sulfides. Sterane sulfides of the above general structure have been identified[43–46] in various crude oils and in lieu of more detailed information it may be assumed that the bulk of the pentacyclic sulfides in Athabasca bitumen conform to this structure.

2.6 Hexacyclic terpenoid sulfides

Small concentrations of hexacyclic sulfides and sulfoxides having C_{30}–C_{35} hopanoid carbon skeletons

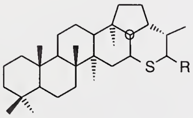

and/or

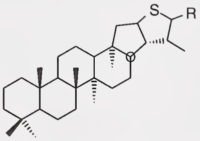

have also been detected in Athabasca, Wabasca and other bitumens.[29c] Their concentration distribution, Figure 12.36, is characteristically different from the distribution of the hopanes (C_{27}–C_{35}) in the saturate fraction of the bitumen, indicating an early incorporation of sulfur into the organic matter during diagenesis. The difference is threefold:

i) there is no norhopane skeleton in the sulfide molecules;

ii) in the sulfides the 22R biological isomer is more abundant than the 22S geological isomer whereas in the hydrocarbons the reverse is true;

iii) the C_{35} hopane sulfide is more abundant than either the C_{34}, C_{33} or C_{32} members, of the series and in the case of the sulfoxides the C_{35} member is the most abundant, Figure 13.22. This is in contrast to the distribution in the case of the hydrocarbons where the relative order of importance is $C_{32} > C_{33} > C_{35} \geq C_{34}$. This relatively high concentration of the C_{35} member of the sulfide series is again consistent with, and thus lends additional support to, the overall conclusion that these bitumens originated from carbonate source rocks.

Raney nickel reduction of the distillable sulfides yields C_{30}–C_{35} hopanes in which the 22R isomers are more abundant than the 22S isomers—22R/22S ≈ 2.0 as compared to a value of 0.7 in the hopanes from the saturate fraction.

2.7 Cyclic terpenoid sulfoxides

Exposure of oil sand to oxidizing water or air would oxidize the more reactive hydrocarbons (*e.g.*, fluorenes) to alcohols, carbonyls and acids, and the sulfides would be partially converted to sulfoxides. Also, as mentioned above, microbial degradation of the oil may produce low concentrations of sulfoxides. Indeed, most Alberta oil sand contain small concentrations of sulfoxides, usually amounting to only a fraction of the concentration of the sulfides.

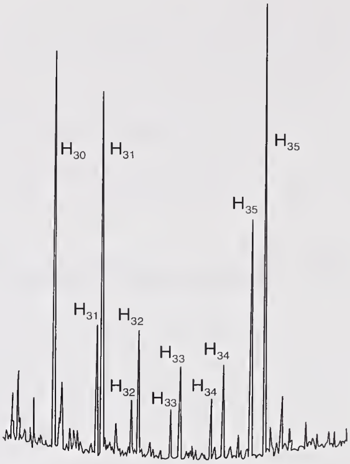

Figure 13.22 Gas chromatogram showing the distribution of hopanes in the molecular sieves 13X adducts from the reduction of sulfoxides and sulfides in the nondistillable Athabasca resins.[39]

The distribution of the individual members in the sulfoxides is sufficiently similar, even if not necessarily identical, to that of the sulfides and consequently the sulfoxides—after chromatographic separation from the resins and reduction by $LiAlH_4$ to the sulfide state—can be used as an alternative to the sulfides for geochemical purposes. This method has been exploited for the study of the water washing history of the Grosmont bitumen (Figure 13.16). In some cases, the heavily biodegraded and water-washed Carbonate Trend bitumens contain such low concentrations of terpenoid sulfides that their analysis becomes difficult. It has been found, however, that the sulfoxide concentrations in such bitumens are still substantial (probably as a result of chemisorption to high-molecular-weight polar and asphaltene components) and sufficient for geochemical analysis.

The sulfoxides, in the few instances where they were measured quantitatively, comprised 1–13% of the sulfides, *cf.* Table 12.10. The highest concentrations occurred near the surface of the deposit and decreased with depth of burial. The percentage amount of sulfoxides, in terms of sulfides in the bitumen, is a semiquantitative measure of the oxidative history of the bitumen and, in conjunction with the concentration of fluorenones and fluorenols relative to that of fluorenes could be used for assessing the oxidative state of the bitumen or crude oil.

2.8 Thiophenes

Benzothiophenes and alkyldibenzothiophenes in crude oils have been associated with carbonate/evaporite source rocks. All Alberta Cretaceous oils, and especially bitumens, contain significant concentrations of alkylbenzo- and alkyldibenzothiophenes. Moreover, 2-*n*-alkyl and 2,5-*n*-alkylthiophenes, 2-*n*-alkyl-, 4-*n*-alkyl- and 2,4-di-*n*-alkylbenzothiophenes along with 1-*n*-alkyldibenzothiophenes have been shown to be abundantly present as structural units in the asphaltene fraction of bitumens indicating, once again, carbonate source rocks for these oils and bitumens. From near-edge X-ray absorption spectroscopy studies[47] it has been concluded that high-sulfur oils feature high thiophene/sulfide ratios, as had been found[26] for all Alberta bitumens and the Bellshill Lake oil, and are related to carbonate source rocks.

The isomeric distribution of monomethyldibenzothiophenes has been known to be related to the depth of burial of petroleum.[48] 1-Methyldibenzothiophene, the dominant isomer present in low-maturity oils, isomerizes to the thermodynamically more stable 2-, 3- and 4-methyl-dibenzothiophene with increasing depth of burial. A maturity index involving isomeric methyldibenzothiophenes has been defined[48] as

$$\text{DBTI} = \frac{\text{2-methyl-} + \text{3-methyl-}}{2(\text{1-methyl-})}$$

Values of the DBTI have been determined, *e.g.*, Figure 13.23, for a few bitumens and oils and are plotted in Figure 13.24 as a function of burial depth. The figure shows that the DBTI is an approximately linear function of the burial depth and increases as the burial depth increases. On this scale, Athabasca, Cold Lake and Wabasca bitumens are all low-maturity oils.

The dominance of *n*-alkyl substituents in specific locations in the benzo- and dibenzothiophene structural units in the maltene and in the asphaltene, along with *n*-alkylthiophenes, point to the *n*-alkanoic—probably *n*-alkanoic acid—origin of these sulfur compounds in the bitumens of the Western Canada Sedimentary Basin and in other oils, as will be discussed in Chapter 14. As such they are highly useful biomarkers, especially in degraded petroleums where the *n*-alkane complement of the oil has been destroyed, identifying the principal original source materials of the oil and the reaction pathways for their conversion to the sulfur compounds as they are found today.

3.0 Biodegradation of Petroleum

A variety of microorganisms, including bacteria, fungi, yeasts, protozoa and actinomycetes, are known to mineralize hydrocarbons. Both aerobic and anaerobic bacteria can be active, but sub-

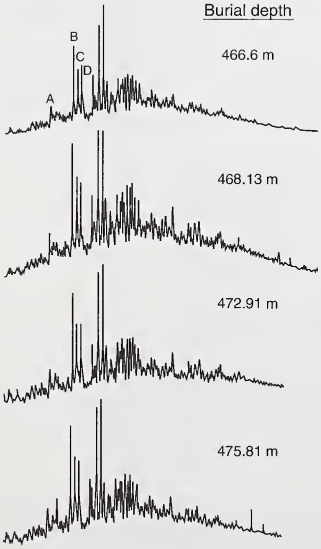

Figure 13.23 Gas chromatograms of dibenzothiophenes in four Wabasca core samples of different burial depths.[41] A = dibenzothiophene; B = 4-methyldibenzothiophene; C = 2-methyl- and 3-methyldibenzothiophene; D = 1-methyldibenzothiophene.

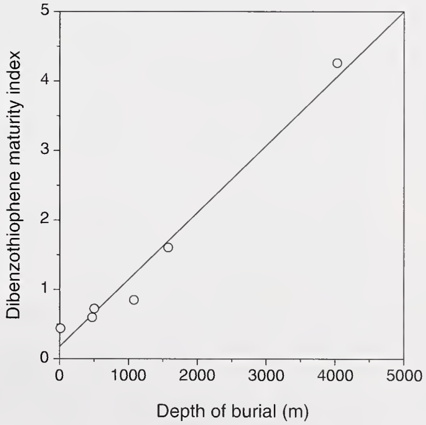

Figure 13.24 Dibenzothiophene maturity index as a function of depth of burial for Athabasca (Suncor coker feed, surface), Wabasca (470 m), Cold Lake (500 m), Pembina (1080 m), Leduc (1580 m) and Beaverlodge (4050 m) bitumens and oils. From J.D. Payzant, T.W. Mojelsky and O.P. Strausz, "Improved Methods for the Selective Isolation of the Sulfide and Thiophenic Classes of Compounds from Petroleum", Energy & Fuels, 3 (1989) 449. © 1989, American Chemical Society.

surface secondary microbial degradation of petroleum is generally attributed to the action of aerobic bacteria. Therefore, a necessary condition to biodegradation is the presence of oxygen supplied as a solute in surface-derived meteoric formation water. This establishes a link between biodegradation and water washing of the oil and, as we saw above, most biodegraded oils show signs of having experienced various degrees of water washing. The involvement of dissolved oxygen can also bring about the slow and, in the case of sand and carbonate bitumens, probably catalytic oxidation of reactive hydrocarbons (*e.g.*, diphenylmethanes, fluorenes, *etc.)* to alcohols, carbonyls and carboxylic acids. Sulfides and thiophenes can be oxidized to sulfoxides and sulfones, *etc.* Thus, biodegradation, water washing and oxidative chemical alterations of petroleum are complementary processes which, in general, occur simultaneously and in parallel.

Biodegradation caused by anaerobic bacteria may be important under certain conditions. Sulfate-reducing bacteria, for example, may utilize the oxygen in the sulfate ion and produce reduced sulfur as a byproduct under anaerobic conditions. The sulfur in turn may react with the oil to generate sulfur-rich oil or bitumen.

In Alberta, most biodegraded petroleums are found 0–700 meters below the surface. At much greater depths, higher temperatures may inhibit microbial growth, which is thought to have an upper temperature limit of 65–80°C. At 700 m the geothermal temperature is still below 65°C, the limiting temperature for bacterial activity. Temperature, however, is only one of the many parameters (including availability of nutrients, *pH*, salinity, microbial population, quality of the oil/water interface, presence of H_2S, *etc.*) that affect microbial activity. Availability of oxygen may also be a limiting factor. Thus, the Lloydminster oil from a depth of 670 m is only mildly biodegraded and mildly water washed. The next stratigraphic zone in the available data bank is at a depth 920 m below the surface, represented by Bellshill Lake and Thompson Lake oils, which are neither biodegraded nor water washed. In effect, none of the oils from 900 m or deeper strata is waterwashed with the exception of the Rainbow Lake oil which is from the greatest depth (1,795 m) in the sample suite: it is severely water washed, has a sulfide content of only 0.3%, and is not biodegraded. This observation may suggest that when water washing does occur at great depths, the water may be oxygen-free, having lost its oxygen content on its way down to the deeper strata.

Hydrocarbon-type biomarkers are known to be biodegradable according to the following order: *n*-alkanes > acyclic isoprenoids > steranes > hopanes > diasteranes ≤ tricyclic terpanes > aromatic steroids. Therefore, these classes of hydrocarbons are removed from the oil during its biodegradation approximately in the sequence in which they are written above, that is, *n*-alkanes first, isoprenoids second, *etc.* Gross features of the compositional changes caused by biodegradation are seen from the results of experiments done on the biodegradation of Prudhoe Bay oil, shown in Figures 1.8 and 13.25. The process, as seen from Figure 13.25, is not strictly sequential and some polycyclic alkanes (and aromatic compounds) are destroyed before the removal of the *n*-alkanes is

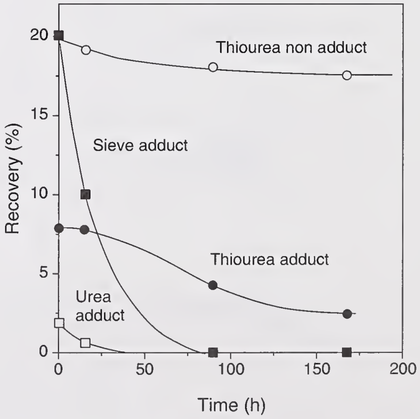

Figure 13.25 Biodegradation of the saturate fraction of Prudhoe Bay oil. The sieve adduct contains *n*-alkanes; the urea adduct, *iso-* and *ante-iso* alkanes; the thiourea adduct, steranes and acyclic isoprenoids; the thiourea nonadduct, steranes, hopanes, cheilanthanes and other cycloalkanes. From I. Rubinstein *et al.,* Ref. 36. © 1977, Elsevier Science Ltd.

complete. The overall biodegradation, especially the initial phase, is a remarkably fast process and consumes about 15% of the oil in the first 16 hours of incubation and about 51% after 168 hours. After 168 hours, no further change in composition of the oil could be observed and the biodegradation was essentially complete. At this stage the saturate fraction had been reduced by 64%, the aromatic fraction by 50%, and the polar fraction showed a slight increase from about 10 to 12% (Figure 1.8). The final degradation product of the 27.3° API gravity crude oil was a 10° API gravity bitumen-like substance.[36]

The actual chemical changes taking place in an oil deposit and their rates depend on the circumstances and conditions such as oxygen and nutrients supply, temperature, *pH*, E_h, salinity of water, *etc.* Indeed, it has been reported that the biodegradation of Orinoco bitumen in the near- or at-surface regions follows a pathway different from that in the subsurface region.[31] Superimposed on the biodegradation-induced changes are the alterations caused by water washing and chemical oxidation.

Various scales have been proposed for assessing the extent of biodegradation that an oil has experienced. One such scale,[8] shown in Figure 13.26, is based on the removal of hydrocarbon-type biomarkers from the oil as discussed above. On this scale of 1 to 10 for mild to severe biodegradation, Lloydminster heavy oil would rank about 4; Wabasca, Cold Lake, Peace River bitumens about 5–6; Athabasca bitumen about 7, and Grosmont bitumen about 8–9.

With regard to the origin of the biodegraded oils and bitumens of the Western Canada Sedimentary Basin and other major bitumen accumulations worldwide, it is now generally accepted that they are the residues of the microbial degradation of conventional petroleums. The possibility that the heavy oils and bitumens may be related to the Lower Cretaceous pooled oils found in the general area has been considered and subsequently substantiated by chemical

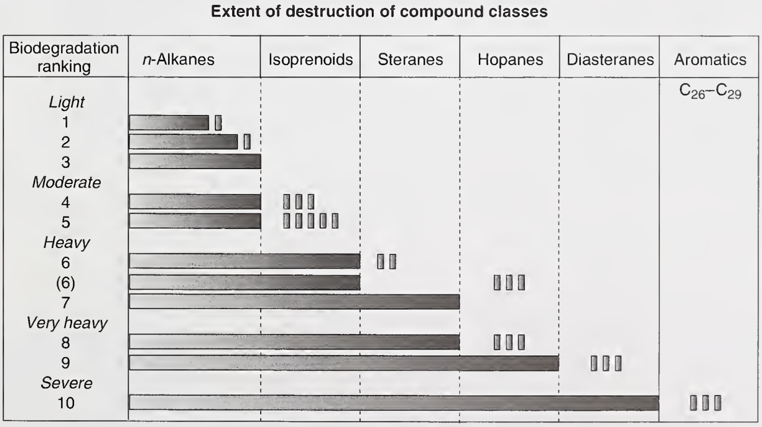

1. lower homologs of *n*-alkanes depleted
2. general depletion of *n*-alkanes
3. only traces of *n*-alkanes remain
4. no *n*-alkanes, acyclic isoprenoids intact
5. acyclic isoprenoids absent
6. steranes partially degraded
7. steranes degraded, diasteranes intact
8. hopanes partially degraded
9. hopanes absent, diasteranes attacked
10. C_{26}–C_{29} aromatic steroids attacked

Figure 13.26 Effects of various levels of biodegradation (on a scale of 1 to 10) on a typical mature oil. After K.E. Peters and J.M. Moldowan, Ref. 8.

and microbiological studies.[33,34,49–51] The fact that subsurface pooled oils may be altered by bacterial action to produce high-density crudes was clearly recognized in the late 1950s.[52]

The Lower Cretaceous Bellshill Lake oil (which is similar to the Prudhoe Bay oil) has been suggested as a prototype of the precursor oils of the bitumens and heavy oils of Alberta.[33,34] A gradual degradation sequence starting with this 26°API gravity oil from the Mannville Formation and ending with the severely degraded Pelican heavy oil from the Wabiskaw Formation is illustrated in Figure 13.27. According to these data, the *n*-alkanes and acyclic isoprenoids gradually diminish, but the relative distribution of the cycloalkanes is unaffected. A schematic illustration of the geological setting for the Western Canada Sedimentary Basin showing the oil and bitumen deposits is reproduced in Figure 13.28. A similar correlation has been suggested to exist among the various light oil, heavy oil and bitumen deposits of the Eastern Venezuelan Sedimentary Basin. In both cases, the highest API gravity oil lies deepest and as the burial depth decreases, the API gravity also progressively decreases.

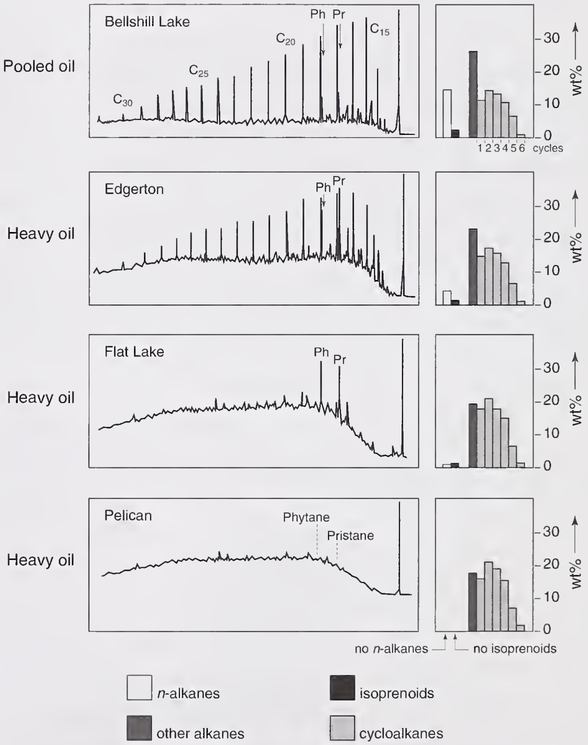

Figure 13.27 Biodegradation of *n*-alkanes, isoprenoid and other branched alkanes and cycloalkanes in the Western Canada Sedimentary Basin. From G. Deroo *et al.*, Ref. 33. © 1984, Canadian Society of Petroleum Geologists.

If the oil sand bitumen is the biodegradation end product of a conventional oil, then laboratory biodegradation of conventional oils should leave a bitumen or bitumen-like end product. Conversely, Athabasca or other highly degraded bitumens should not be biodegradable and should undergo only minor changes during incubation with microbial cultures which have been shown to cause the conversion of a conventional oil to an oil sand bitumen-like substance. The results of such experiments,[36] shown in the form of block diagrams, Figure 13.29, confirm both of these tenets. The weight losses in the Prudhoe Bay and Bellshill Lake oils after 168 hours' incubation were 51 and 47%, whereas in the Lloydminster oil, only about 9%. Peace River bitumen did not show any weight loss during attempted biodegradation. The weight decrease in the conventional oils is due to the complete destruction of the *n*-, *iso*- and *anteiso*- alkane and isoprenoid contents and a large decrease in the aromatic content. The acyclic branched alkanes and cycloalkanes (thiourea nonadduct) decreased slightly and the polars increased slightly in the Prudhoe Bay oil while in the Bellshill Lake oil they both decreased slightly. The Lloydminster oil lost its *iso*- and *anteiso*-alkanes and a fraction of its isoprenoid and branched alkane and cycloalkane contents. Peace River bitumen did not undergo any class compositional change.

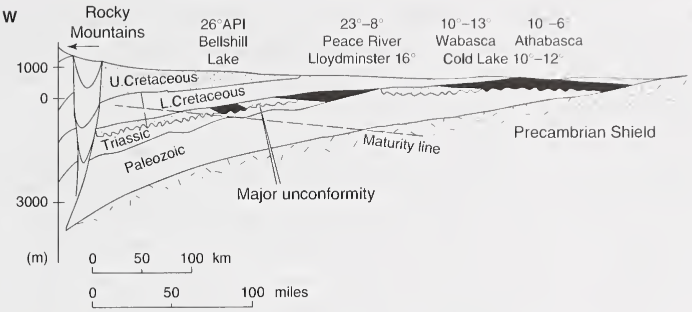
W
Rocky Mountains
26°API Bellshill Lake
23°–8° Peace River Lloydminster 16°
10°–13° Wabasca Cold Lake 10°–12°
10°–6° Athabasca
E
1000
0
3000
(m)
U.Cretaceous
L.Cretaceous
Triassic
Paleozoic
Maturity line
Precambrian Shield
Major unconformity
0 50 100 km
0 50 100 miles

Figure 13.28 Schematic cross section of the Western Canada Sedimentary Basin. The numbers indicate the ranges of API gravity of the various accumulations. From B.P. Tissot and D.H. Welte, Ref. 6. © 1984, Springer-Verlag.

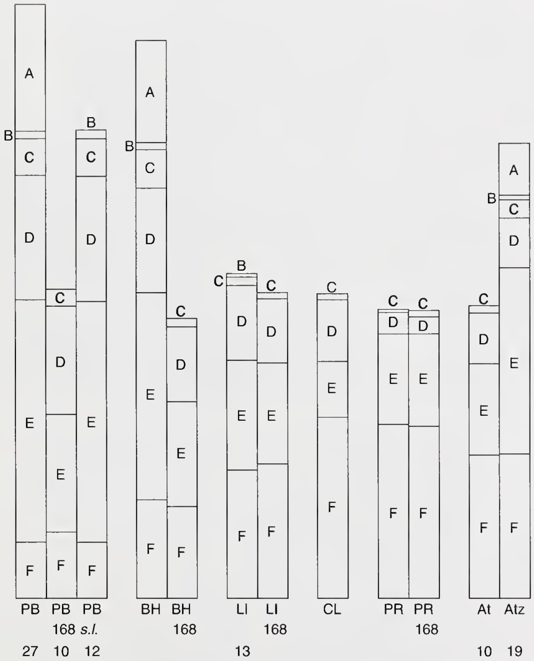

Figure 13.29 Gravimetric analyses of various oils and bitumens. PB = Prudhoe Bay; BH = Bellshill Lake; LI = Lloydminster; CL = Cold Lake; PR = Peace River; At = Athabasca; Atz = synthetic Athabasca crude produced from Syncrude materials. The suffix 168 means after incubation for 168 h with either pure or mixed cultures; *s.l.*, after incubation for 21 days with *saccharomyces lipolytica*. The numbers along the abscissa refer to the API gravities. A = molecular sieve adduct; B = urea adduct; C = thiourea adduct; D = thiourea nonadduct; E = aromatic fraction; F = polar fraction.[36]

In all the above experiments, biodegradation of the sample materials was brought about by a mixture of six different species of bacteria consisting of approximately 90% Gram-negative rods and 10% of a Gram-positive coryneform type rod. One experiment was also carried out on Prudhoe Bay oil using the yeast *Saccaromyces lipolytica* in a 21-day incubation. The yeast completely removed the *n*-alkane fraction while leaving the rest of the oil virtually unchanged.

Comparing the class compositions of the final bacterial biodegradation products among themselves and with the bitumens, it is seen that there is a good deal of resemblance among all these materials. The bitumens differ from the laboratory degraded products with respect to their elevated polar contents. This may be due to the higher heteroatom and polar contents of the bitumen precursor oils compared to the Prudhoe Bay or Bellshill Lake oils, Table 13.8 (*cf.* Table 5.3 and Figure 13.29), mechanistic differences in the biodegradation processes, exposure of the oil to simultaneous water washing and catalytic oxidation processes during reservoir biodegradation, and other unknown causes. Also, the Bellshill Lake and original precursor oils were younger and less mature at the time of the secondary biodegradation processes and therefore probably contained more polar material than they do today.

There have been many studies reported in the past three decades or so on the microbial degradation of hydrocarbons and petroleum. Degradability and mechanistic pathways involving individual hydrocarbon (and other organic) compounds, crude oils, bitumens and their fractions, and various microbes in mixed-species or single-species cultures have been studied. The effects of in-reservoir microbial activity on the bulk composition and properties of crude oils and their biomarker distributions have also been extensively explored. The ramifications of these investigations to bitumen chemistry may be summarized as follows:

- **the overall quality** of the oil declines with biodegradation and its properties vary with increasing biodegradation as follows:
  - API gravity: ↓
  - density: ↑
  - (H/C) atomic ratio: ↓
  - heteroatom content: ↑
  - viscosity: ↑
  - asphaltene content: ↑

- ***n*-alkanes** in the C_8–C_{20} range degrade the fastest. Below C_8 or above C_{20}, *n*-alkanes are not degraded so efficiently by aerobic bacteria. This may explain the observation that the *n*-alkyl side chains in the 1-*n*-alkyldibenzothiophenes isolated from the maltenes of bitumens extend to octyl only, while in the 1-*n*-alkyldibenzothiophenes from the pyrolysis of asphaltenes they extend to at least tridecyl. The alkyl groups in the large asphaltene molecules were protected against biodegradation by the supramolecular aggregate structure of the asphaltene but in the maltene such protection was minimal. Longer chains are degraded faster than shorter chains. The yeast *Saccaromyces lipolytica*, and presumably other yeasts, degrade *n*-alkanes and only *n*-alkanes from (Prudhoe Bay) crude oil. Sulfate-reducing (anaerobic) bacteria metabolize *n*-alkanes in the C_8–C_{31} range.

  These observations explain the near or complete absence of *n*-alkanes in the sand and carbonate bitumens and heavy oils of Alberta. The small quantities of *n*-alkanes detected in the Cold Lake bitumen have their maximum shifted to C_{19} compared to the C_{16} maximum in the Bellshill Lake *n*-alkanes, in agreement with the greater degradability of the $< C_{21}$ *n*-alkanes relative to the $>C_{20}$ members of the series.

- **acyclic isoprenoids** degrade at a somewhat slower rate than *n*-alkanes. The variation in acyclic isoprenoids with progressive biodegradation as indicated by the $m/z = 113$ ($C_8H_{17}^+$) and 183 ($C_{13}H_{27}^+$) ions in their mass chromatogram is illustrated in Figure 13.30 for the Prudhoe Bay oil in comparison with Bellshill Lake, Lloydminster, Cold Lake and Athabasca oils and bitumens.[53] The mass chromatograms indicate that in nonbiodegraded oils (Prudhoe Bay and Bellshill Lake) and mildly biodegraded oils (PB16 and Lloydminster) the pristane to phytane ratios are greater than unity while in more biodegraded oils (PB90 and Cold Lake, which are essentially free of *n*-alkanes) the pristane to phytane ratio is unity or less and in the severely biodegraded oils (PB168 and Athabasca) the isoprenoids are absent. (The pristane to phytane ratio in the hydrocarbons from the Raney nickel reduction of the isolated sulfides of the Bellshill Lake oil, thought to be more representative of the original hydrocarbon distribution in the oil, is about 0.4, indicating carbonate source rocks. Also, it should be noted that the Cold Lake oil contains acyclic isoprenoids up to C_{40} and their gradual degradation would affect the pristane/phytane ratios.)

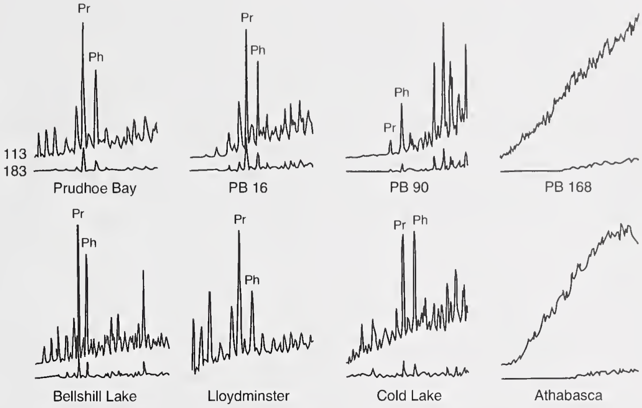

Figure 13.30 GC–MS *m/z* = 113 ($C_8H_{17}^+$) and 183 ($C_{13}H_{27}^+$) cross-scan chromatograms showing the changes in the acyclic isoprenoids in Prudhoe Bay oil before and after biodegradation for 16, 90 and 168 h; the bottom traces show the *m/z* = 113 chromatograms for the nonbiodegraded Bellshill Lake, Lloydminster and Cold Lake oils and the biodegraded Athabasca bitumen. Pr = pristane, Ph = phytane. From R.J. Crawford *et al.,* Ref. 53. © 1978, Verlag Chemie Int.

- **unsaturation** increases and branching decreases biodegradability. A quaternary alkyl carbon retards biodegradation more if it is present in the penultimate position in the chain.
- **cycloalkanes**, as a rule of thumb, are less biodegradable than acyclic alkanes and pristane, phytane and other acyclic isoprenoids are completely degraded before any significant change in polycyclic markers would occur.

  The cheilanthane-type tricyclic terpanes are extremely resistant to biodegradation and they can be detected in all Alberta bitumens and heavy oils.

  Steranes, in general, are degraded with decreasing efficiency in the order ααα20R > ααα20S > αββ20R > αββ20S > diasteranes, that is, the ααα20R epimers with the biological configuration are more susceptible to microbial attack than the other epimers. Diasteranes are highly resistant to biodegradation and are present in all Alberta oils and bitumens. Regular steranes are present in the Lloydminster and Provost heavy oils and Cold Lake, Wabasca, Peace River bitumens, but are absent in most of the more severely biodegraded Athabasca and Carbonate Trend bitumens. In the Athabasca and Grosmont bitumens the C_{21} and C_{22} regular steranes, ααα-C_{21} and C_{22} as well as αββ-C_{21} and C_{22}, survived biodegradation, indicating a high level of resistance to microbial attack.

  Hopanes are present in all nonbiodegraded and moderately biodegraded Alberta oils with the exception of the severely biodegraded Wabasca Grand Rapids Formation A and Grosmont bitumens in which the hopanes are partially or fully degraded to the 25-norhopanes.

  The class compositional block diagram in Figure 13.29 reveals that biodegradation affects the alicyclic class the least, aside from the polar fraction, in the Prudhoe Bay and Bellshill Lake oils. In both cases the alicyclic content declines slightly after 168 hours of incubation. A similarly slight decrease also appears in the 168-hour biodegraded Lloydminster oil. Therefore, one principal difference between the mechanism and ultimate result of the biodegradation of acyclic and cyclic alkanes is that the former are nearly completely mineralized and the latter are only structurally modified by biodegradation: *n*-alkanes $\rightarrow CO_2 + H_2O$ while hopane → 25-norhopane, *etc.*

- the **aromatics**, as seen from Figures 1.8 and 13.29, are highly susceptible to biodegradation. Indeed, mononuclear aromatics with alkyl or carboxyalkyl side chains and naphthalenes with alkyl side chains are known to be attacked by bacteria and the latter by at least one fungus, Figure 13.31. Comparison of the mass chromatograms for naphthalene and methylnaphthalenes indicates a close similarity between the Prudhoe Bay and Bellshill Lake oils on the one hand and the PB168 and Athabasca bitumens on the other, where the naphthalene contents have been drastically reduced. Similar data for polymethylphenanthrenes and anthracenes, Figure 13.32, suggest again that the two oils are similar and that only the less substituted triaromatics, having none, one and two methyl groups, underwent biodegradation.[53]

  Polycyclic aromatics with more than three rings are not biodegraded. This is seen from the mass chromatograms of the dimethyl aromatics (naphthalenes, phenanthrenes plus anthracenes, chrysenes and picenes) for the Prudhoe Bay oil and the PB168 and Athabasca bitumens, Figure 13.33. Comparison shows that biodegradation removed the dimethylnaphthalenes and reduced the concentration of dimethylphenanthrenes relative to those of the chrysenes and picenes. The similarities in the PB168 and Athabasca mass chromatograms are noteworthy.

  Thus, from the preceding discussion we can conclude that the large, approximately 50%, reductions in the aromatic contents of the Prudhoe Bay and Bellshill Lake oils after 168 hours incubation is largely due to the loss of the mono- and diaromatic complements of the oil.

  Aromatic steroids in petroleum are known to be resistant to biodegradation. The distributions of monoaromatic and triaromatic steroids have been determined for Athabasca and Grosmont bitumens (Figures 13.9 and 10), and they were found to be identical (except for the C_{20} and C_{21} triaromatics) even though the two bitumens appear to have different biodegradation rankings, the Grosmont bitumen being more degraded. This observation, along with the distribution patterns established, suggests that the aromatic steroids in neither of the two bitumens were affected by biodegradation. The difference that exists in the triaromatic steroids distribution, namely the presence of substantial concentrations of C_{20} and C_{21} triaromatic steroids in the Athabasca and their absence from the Grosmont bitumen, is thought to be due to the difference in the water washing history of the two formations. According to their bicyclic terpenoid sulfoxide distributions, Figure 13.16, the Athabasca sample is not (or is only mildly) waterwashed while the Grosmont sample is severely waterwashed. Thus, it appears reasonable to assume that the C_{20} and C_{21} members are more soluble in water than the higher carbon number members of the series and therefore they were removed from the Grosmont oil during the severe water washing.

- the **polar fraction** (including the asphaltene) of the bitumen is the largest class fraction present. In laboratory-degraded oils, however, the polar fractions, while being significant, amounted to a smaller proportion of the biodegradation end product. The absolute amount of the polar fraction does not change substantially during the course of biodegradation; in the Prudhoe Bay oil it increased slightly, while in the Bellshill Lake oil it decreased slightly. This apparent relative constancy may be misleading and can be the result of a balance between destruction and production of polar materials during biodegradation. It is known that terpenoid sulfides can at least partly be converted to sulfoxides, *n*-alkyl thiolanes to thiolane carboxylic acids, *n*-alkyl thiophenes to thiophene carboxylic acids, fluorenes and 9-alkyl fluorenes to fluorenones and fluorenols (also in abiogenic processes accompanying biodegradation), benzene to phenol or 1,2-dihydroxybenzene, naphthalene to dihydroxydihydronaphthalene, tri- and pentacyclic terpanes (possibly) to their carboxylic acid derivatives, *etc.* On the other hand, fatty acids,

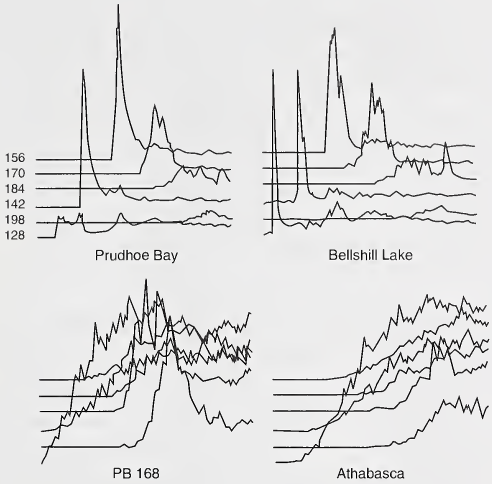

Figure 13.31 GC–MS $m/z = 128, 142, 156, 170, 184$ and 198 cross-scan chromatograms showing the naphthalene, mono-, di-, tri-, tetra- and pentamethylnaphthalene distributions in nonbiodegraded (Prudhoe Bay and Bellshill Lake) and biodegraded (PB168 and Athabasca) oils. From R.J. Crawford *et al.*, Ref. 53. © 1978, Verlag Chemie Int.

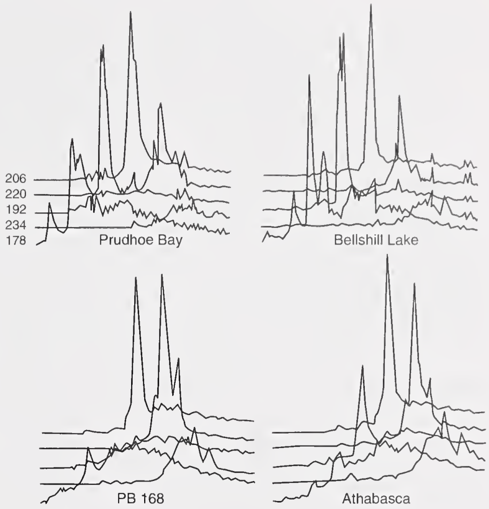

Figure 13.32 GC–MS $m/z = 178, 192, 206, 220$ and 234 cross-scan chromatograms showing the distributions of polymethylphenanthrenes and polymethylanthracenes in nonbiodegraded (Prudhoe Bay and Bellshill Lake) and biodegraded (PB168 and Athabasca) oils. From R.J. Crawford, *et al.*, Ref. 53. © 1978, Verlag Chemie Int.

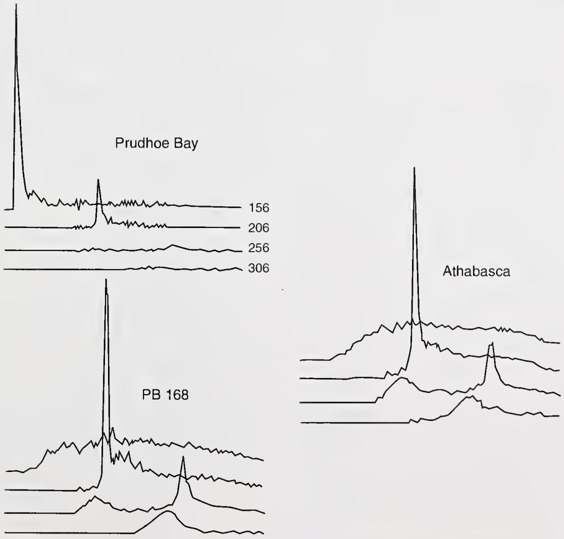

Figure 13.33 GC–MS cross-scan chromatograms showing $m/z = 156$ (dimethylnaphthalenes), 206 (dimethylphenanthrenes and anthracenes), 256 (dimethylchrysenes) and 306 (dimethylpicenes) in nonbiodegraded (Prudhoe Bay) and biodegraded (PB168 and Athabasca) oils. From R.J. Crawford, *et al.*, Ref. 53. © 1978, Verlag Chemie Int.

isoprenoid acids, alcohols, phenylalkanoic acids and some other polar molecules can be mineralized completely and thus removed from the biodegradation residue.

Biodegradation has been shown to have little effect on the distribution of vanadyl porphyrins but nickel porphyrins might be selectively destroyed.

To conclude this section, it should be pointed out that the microbial degradations of crude oil and its individual biomarker components have been the subject of many investigations in recent times. These studies have covered microbiological degradation processes in the field and in laboratory environments using various cultures and nutrients under a variety of conditions. They brought to light a wealth of information and focussed attention on the complex nature of these processes.

The microbial "degradation" of crude oil as it occurs in the reservoir leads to a deterioration of the oil quality. It has, however, long been realized that at least in principle, the reverse should also be possible and extensive research is being conducted worldwide by microbiologists to realize this possibility. The potential for success in developing useful microbiologial technologies for the improvement of some select properties of crude oil is considered to be promising. Among recent examples to illustrate the point one can cite the ring opening reaction of dibenzothiophene and phenanthrene[54a] along with the viscosity reduction *via* selective cleavage of aliphatic sulfide bonds[54b] in crude oil. Also, the feasibility of bringing about significant reduction in NOS and metal content accompanied by a highly favorable redistribution of the SARA fractions has been demonstrated.[55]

4.0 Water Washing of Petroleum

Water washing, as was discussed in connection with its effect on the sulfides distribution in Section 2 of this chapter, is—after thermal maturation and biodegradation—the third major factor causing the subsurface alteration of petroleum. Low MW (C_{15-}) hydrocarbons, contrary to intuitive expectation, are quite soluble in water, Figure 13.34 and Table 13.10,[56] and their solubility, in general, increases with rising temperature[56]. The C_{15-} polar compounds, carboxylic acids, sulfides, sulfoxides, carbonyls, alcohols, pyridines, quinolines, *etc.*, would have even higher solubilities and therefore all these molecules would be susceptible to dissolution in, and partial or complete removal by, water flowing past crude oil. Surface recharge formation water driven by a hydraulic head loses its dissolved oxygen and becomes warmer as it penetrates deeper strata, Figure 13.35. Thus, below a certain depth (*ca* two km below the surface) biodegradation and biogenic oxidation cease to be operative and water washing becomes the major cause of the alteration of petroleum. The transition between water washed and nonwashed zones—especially in the oil sand deposits—can be quite abrupt, as demonstrated by the data on the distribution of cyclic terpenoid sulfides, depending on lithostratigraphic conditions.

Water washing may occur during migration of the oil from the source rocks to the reservoir rocks through the water-saturated pores of the carrier bed; however, there are indications suggesting that water washing of the accumulated oil in the reservoir is the more important process with regard to chemical alteration.

Regarding the water solubilities of the various types of hydrocarbons, Figure 13.34 and Table 13.10 show that in general, small molecules are more soluble than larger molecules and polar molecules are more soluble than nonpolar molecules. For a given carbon number the order is heteroaromatics > aromatics > alicyclics > branched alkanes > *n*-alkanes, as determined for binary mixtures of pure compounds. In the water washing of petroleum, however, what

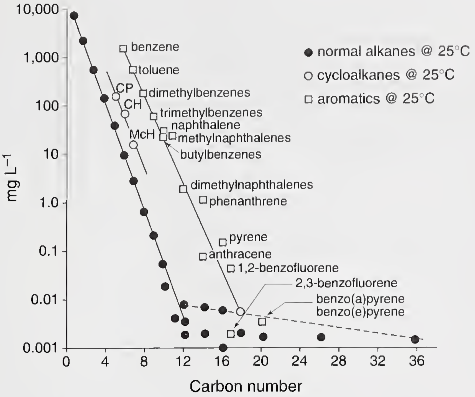

Figure 13.34 Solubilities of *n*-alkanes, cycloalkanes and aromatics in water at 25°C as a function of carbon number. From E. Lafargue and C. Barker, Ref. 56. © 1988, American Association of Petroleum Geologists.

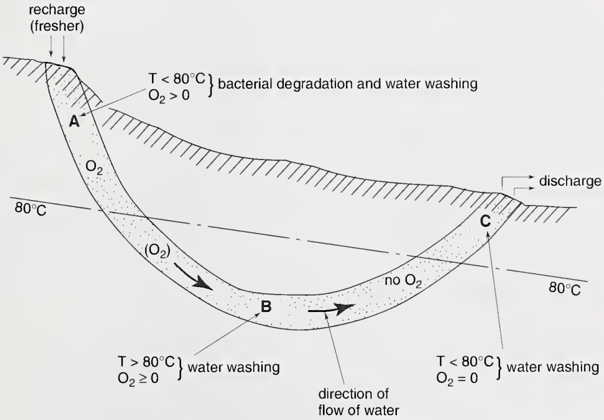
recharge
(fresher)
T < 80°C
$O_2 > 0$
bacterial degradation and water washing
A
O_2
80°C
(O_2)
B
no O_2
C
discharge
80°C
T > 80°C
$O_2 \geq 0$
water washing
direction of
flow of water
T < 80°C
$O_2 = 0$
water washing

Figure 13.35 Schematic geological setting for water washing of crude oils in the absence and presence of biodegradation. From E. Lafargue and C. Barker, Ref. 56. © 1988, American Association of Petroleum Geologists.

Table 13.10 Solubilities of selected petroleum constituents in water

Compound	S[a]	Compound	S[a]
benzene	0.178	methane	0.00227
cyclohexane	0.0058	ethane	0.00568
cyclohexene	0.016	ethylene	0.01336
n-hexane	0.0011	propane	0.00669
1-hexene	0.0053	propene	0.0200
toluene	0.053	*n*-butane	0.00724
1-heptene	0.032	*n*-pentane	0.0041
cycloheptane	0.0030	*n*-heptane	0.00024
n-decane	0.0000015	methylcyclohexane	0.00151
1-decene	0.00057	2,3-dimethylpentane[b]	0.0052
naphthalene	0.0031	anthracene	0.0000062
phenanthrene	0.00011	1-methylnaphthalene	0.0028
2-methylnaphthalene	0.0025	pentylbenzene	0.00105
isopentane	0.0048	indole	0.187
carbazole	0.000120	quinoline	0.6
furan	1	dibenzofuran	0.000656
thiophene[b]	0.302	benzo[b]thiophene	0.013
fluorene	0.00019		

[a] $S = 100 \times (m_{su})/(m_{su} + m_{sv})$ where m_{su} = mass of solute and m_{sv} = mass of solvent. [b] in ppm.

determines the apparent solubilities is not the absolute solubility of the pure compound but its relative solubilities in the water containing other hydrocarbons and in the oil. Also, colloidal processes may be operative. For example, the increased solubilities of small alkanes in aqueous micellar solutions[57] compared to their solubilities in pure water are attributed to the transfer of the small alkane molecules from the water to the interior of the micelle.[58] Furthermore, the observation that *n*-alkanes are more soluble in water during water washing than are the cycloalkanes which, in the pure state, have higher solubilities in water, is also ascribable to colloidal processes. Pure water and warmer water are more efficient in removing hydrocarbons from the oil than are saline water or colder water,[56] Figures 13.36 and 13.37. The effects of carbon number and isoprenoid branching in the alkane molecules, and the amount of water passing through the oil on the extent of water washing is illustrated by the plots for *n*-alkanes and isoprenoids in Figure 13.38. The plots for both series of hydrocarbons demonstrate that above C$_{15}$ the effect of water washing on the composition of the oil tends to diminish. Thus, severe water washing can remove most of the C$_{15-}$ complement of the oil and thereby reduce its API gravity (for example from 37 to 27°) and overall quality without much affecting the relative distribution of the biomarkers present in the oil, and therefore invalidating any geochemical conclusions drawn from the biomarker distributions.

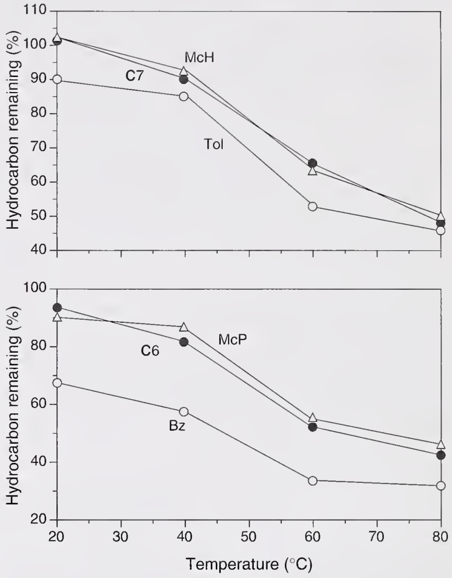

Figure 13.36 Effect of water temperature on the removal of *n*-hexane (C6), *n*-heptane (C7), methylcyclopentane (McP), methylcyclohexane (McH), benzene (Bz) and toluene (Tol) from a Misener Formation oil. From E. Lafargue and C. Barker, Ref. 56. © 1988, American Association of Petroleum Geologists.

Because the oil has to experience a flow of ground water through it in the reservoir in order to undergo biodegradation or water washing, most biodegraded oils show signs of water washing as manifested by their cyclic terpenoid sulfide/sulfoxide distributions (Figures 13.16–13.19 and 13.22). Severe water washing not only affects the quality of the oil by decreasing its API gravity, but at the same time may also influence its processability because some of the low-MW polar compounds having high water solubilities might have acted as effective surfactants needed for the efficient separation of the bitumen from the sand and fines in the water flotation process.

Evaluation of the water washing status of an oil would be a difficult task[59]—especially in the case of a biodegraded oil—without the cyclic terpenoid sulfide/sulfoxide concentration

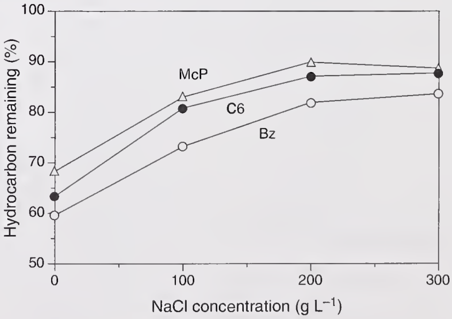

Figure 13.37 Effect of water salinity on the removal of *n*-hexane (C6), methyl-cyclopentane (McP) and benzene (Bz) from a Misener Formation oil with 250-mL water. From E. Lafargue and C. Barker, Ref. 56. © 1988, American Association of Petroleum Geologists.

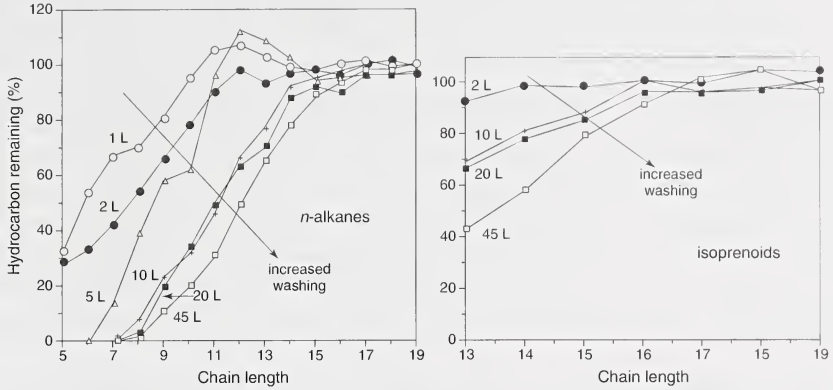

Figure 13.38 Extent of *n*-alkane and isoprenoid removal during water washing of Bolivar Coastal Field oil with 1–45 L fresh water. From E. Lafargue and C. Barker, Ref. 56. © 1988, American Association of Petroleum Geologists.

distribution data which, as illustrated by Figures 13.16–13.19 and 13.22, provide a valuable water washing indicator system with practical utility.

5.0 Oxygen-Containing Biomarkers

In the oxygen-containing compounds identified in oil sand bitumens the oxygen is present primarily as free carboxylic acids, carboxylic acid esters and anhydrides, perhaps carboxylic acid salts, alcohols, ethers, carbonyls, and sulfoxides. In many cases the oxygen functionality is attached to clearly recognizable biomarker frameworks. In such cases then, it may be surmised that the oxygen was introduced in the molecule by microbial or abiogenic catalytic oxidation processes utilizing the oxygen of surface-derived formation waters. Indeed, it has been shown[42,60] that the microbial degradation of sulfides and dibenzothiophenes containing long *n*-alkyl chains results—through a chain-end-attack—in the formation of a carboxylic acid in which the carboxylic group is attached either directly, or through a methylene group, to the original ring structure, *e.g.*

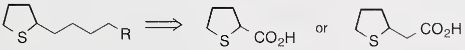

The aromatic carboxylic acids shown in Figure 12.54 and listed in Table 12.14 are probably the residues of such microbial oxidation of the corresponding alkylaromatics. Similarly, alcohol or carbonyl groups may arise from the oxidation of reactive C–H bonds in the hydrocarbon biomarker molecules. Alternatively, some of the carboxylic acids present in the bitumen and in the organic matter chemisorbed to the sand may be thought of as having been synthesized and introduced into the oil by the same microbes that caused the alteration of the original oil.

5.1 Carboxylic acids

The dominant carboxylic acids identified in Alberta oil sand maltenes are the C_{21} and C_{24} tricyclic terpenoid acids,

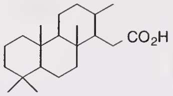

and

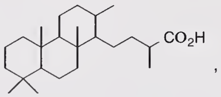

,

whose structures correspond to the main isomers of the C_{21} and C_{24} tricyclic terpenoid hydrocarbons in the saturate fraction. On decarboxylation these acids would convert to the C_{20} and C_{23} members of the cheilanthane hydrocarbons and this process could be a major route to the formation of the C_{20} and C_{23} members of the hydrocarbon series. The C_{21} and C_{24} acids are accompanied by small quantities of the C_{20}–C_{26} members of the tricyclic terpenoid acids, bicyclic terpenoid acids, two C_{26} tetracyclic terpenoid acids, C_{14}–C_{28} *n*-alkanoic acids, C_{28}–C_{32} hopanoic, moritanoic acids, traces of *cis*-, *trans*-9-octadecenoic and $C_{\overline{\overline{18}}}$-9-12-*cis*, *cis* acids[22] along with various aromatic carboxylic acids,[21] and other yet unidentified carboxylic acids (*cf.* Chapter 12).[19–22]

The nature and distribution of carboxylic acid biomarkers have been studied in a number of petroleums and led to the following conclusions:

- the total acid content expressed as the acid number, *i.e.* the number of milligrams KOH needed to neutralize the acids in one gram oil, increases with the extent of biodegradation of the oil. The acid number in general lies in the range 0.5–2.6 mg KOH/g oil for biodegraded oils and < 0.5 mg KOH/g oil for nonbiodegraded oils. The acid number of Athabasca bitumen is 2.0–2.6 mg KOH/g bitumen, in agreement with its known biodegraded state.
- in biodegraded oils, *n*-alkanoic acids are present in low concentration and in biodegraded marine oils the concentration of the $\leq C_{19}$ members is high compared to the $> C_{19}$ members. In Alberta bitumens the dominant components of the series are the C_{16} and C_{18} members with a CPI strongly favoring the even carbon number members. This feature of the acids distribution in the oil sand bitumens is again in line with the above geochemical conclusions, namely that the bitumens are the biodegradation products of marine oils. These acids have been postulated to be also produced by the microorganisms responsible for the biodegradation of the precursor oil *via* the aerobic pathway of biosynthesis.[22]
- biodegraded marine oils contain high concentrations of the C_{21} and C_{24} members of the tricyclic terpenoid acids along with small concentrations of the C_{20}, isomeric C_{21}, C_{24} and C_{26} homologs. In Athabasca bitumen, in addition to the above homologs, a C_{22}, two C_{23}, and a C_{25} homolog were also detected.
- pentacyclic acids in the C_{30}–C_{33} range have been reported to be present in nonbiodegraded and biodegraded oils and the ratio Σ(tricyclic terpenoid acids)/Σ(pentacyclic terpenoid acids) has been shown to be a function of the extent of biodegradation the oil has experienced, the ratio increasing with the extent of biodegradation. The value of this ratio for Athabasca maltene is ~16, in agreement with the literature values of 5–30 for biodegraded oils. C_{32} hopanoic acid has been reported to form from the oxidation of bacteriohopanetetrol, the progenitor of the extended hopanes,

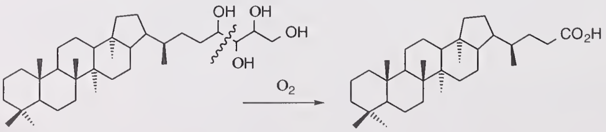

under an oxic depositional environment.

- the distribution of hopanoic acids in the oil sand bitumen indicates a less mature distribution (higher $\beta\alpha/\alpha\beta$ and R/S ratios) than in the hydrocarbons, as has been found in other oils. The shift in the maturity distribution of the pentacyclic acids compared to that of the hydrocarbons has been interpreted in terms of the washing of rocks by the oil during its migration from source to reservoir, during which immature acid components are picked up. If this interpretation is correct, then the hopanoic acids in the bitumen are associated with the secondary migrational rather than the biodegradational history of the precursor oil. It is, however, more likely that the functionalized and chemically-bound hydrocarbon biomarkers in general undergo stereoisomerization (R/S, α/β) reactions less readily than the free parent hydrocarbon molecules and therefore appear to be less thermally mature. This applies to all functionalized and chemically-bound biomarkers.
- The aromatic carboxylic acids identified in the polar fractions:

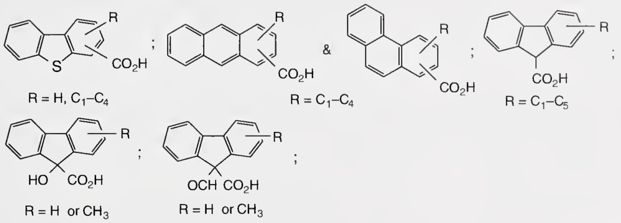

are all compounds which would be expected to result from the microbial degradation of *n*-alkyl substituted tricycloaromatics, dibenzothiophenes, anthracenes, phenanthrenes and fluorenes. As has been discussed before, *n*-alkyl substituted dibenzothiophenes up to *n*-C_8 and fluorenes up to *n*-C_9 have been detected in oil sand maltenes. In mildly biodegraded maltenes or in the structural units of asphaltenes, the alkyl chain lengths in the dibenzothiophenes are greater and extend to *n*-C_{13}. The non-occurrence of longer than *n*-C_8 substituted dibenzothiophenes in the biodegraded oil sand maltenes can be attributed to biodegradation, in agreement with laboratory experiments[60] showing that longer than *n*-C_8 chain *n*-alkyldibenzothiophenes can be biodegraded when incubated with oil-degrading microorganisms.

In light of this information, it would then appear reasonable to assume that at least portions of the tri- and pentacyclic terpenoid acids were also formed from their parent hydrocarbons and perhaps from the corresponding sulfides during the biodegradation of the precursor oil.

5.2 Ketones

Two kinds of ketones have been positively identified in the maltenes, the fluorenones and quinolones:

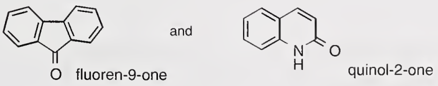

Small quantities of acetaldehydes together with trace amounts of acetone and other carbonyls have also been detected in some oil sand.

Fluorene is a slightly acidic hydrocarbon (with a pK_a value of 25), the acidic hydrogens being the ones in the 9-position. These hydrogens are relatively weakly bound and they can be oxidized by air around room temperature to yield fluoren-9-one. Similarly, 9-alkylfluorenes would oxidize to 9-alkylfluoren-9-ols. Therefore, fluorenes, nuclear methylated fluorenes and their 9-*n*-alkyl derivatives, along with some unidentified alkylfluorenes and higher condensed analogs which are naturally present in bitumen, are expected to be readily oxidized to fluorenones and fluorenols during the microbial and/or catalytic degradation of the precursor oil. This would explain the presence of nuclear methylated fluoren-9-ones, 9-*n*-alkylfluoren-9-ols and nuclear methylated 9-*n*-alkylfluoren-9-ols and some of their more condensed analogs in the oil sand maltene, displaying distributions similar to those of their parent hydrocarbons. Fluoren-9-ones contain mono- through tetra- and possibly higher methyl-substituted derivatives, but longer alkyl substituents were not detected.

The origin of the second most important class of carbonyl compounds identified in bitumens, the alkylquinolones with C_4–C_{21} alkyl side chains, is less certain. The observation that their concentration in air-exposed bitumen containing elevated levels of fluorenols and sulfoxides was low compared to non-air-exposed bitumen would superficially militate against a formation mechanism involving the oxidation of quinolines. However, it is possible that on air exposure the rate of destruction of quinolones is faster than their rate of formation from quinolines.

The presence and concentration distribution of fluorenones and fluorenols, as those of the sulfides, can serve as a useful redox indicator reflecting the oxidative history of the reservoired oil.

5.3 Alcohols

Acyclic, naphthenic and aromatic alcohols have been identified in oil sand bitumens, but phenolic hydroxyl groups have not been positively detected.

n-Alcohols from C_8 to C_{30} with a strong even carbon number preference and maxima at C_{16} and C_{18}, some free and some chemically bound, appear to have originated from the same microbial processes that gave rise to the formation of the *n*-alkanoic acids and caused the biodegradation of the precursor oil. It should be noted, however, that long-chain alcohols have been observed in marine sediments and even-carbon-number *normal* alcohols in the C_8 to C_{26} range occur in higher plant waxes and therefore their presence can possibly (but not likely) be an indication of some terrestrial contribution to the original oil.

Many cyclic alcohols ranging from mono- through tetracyclic are present in the bitumen. Among the saponification products of the asphaltene and aromatic fractions, several sterols have been detected. They are dominated by the C_{29} ($Z = -8$ through -12) members which indicates the possibility that they were terrestrial, derived from higher plants. β-sitosterol (C_{29}, $Z = -8$) was positively identified and stigmasterol (C_{29}, $Z = -10$) was tentatively identified.

The most abundant alcohols present in the bitumen are the nuclear methylated fluoren-9-ols, 9-*n*-alkylfluoren-9-ols and their nuclear methylated derivatives, along with their higher condensed (benzo-, dibenzo-, cyclohexano-, and dicyclohexano-) analogs. The oxidation of 9-*n*-alkylfluorenes is even more facile than the oxidation of fluorene and therefore the relative concentration of 9-*n*-alkylalcohols is higher than their parent hydrocarbons.

The presence of the *n*-alkyl group only or predominantly in the 9-position provides additional important support for the formation of the fluorene family of compounds in oil from the cyclization and aromatization of *n*-alkanoic chains

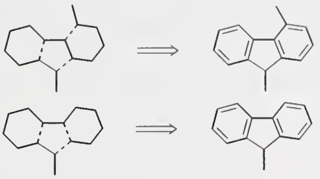

and for the contribution of such processes to the formation of the aromatic and asphaltenic structures of the oil.

6.0 Nitrogen-Containing Biomarkers

Nitrogen compounds in petroleum originate from at least two sources. The less important, but better understood of these, are the chlorophylls, the progenitors of porphyrins, while the quantitatively more important but incompletely understood ones are represented by ultralaminae, the result of selective preservation of biomacromolecular membranes. In transmission electron microscopic studies of numerous marine and lacustrine source rocks, it has been discovered that the apparently amorphous kerogens contain abundant bundles, 10–30 nm lamellae, called ultralaminae.[61] A material derived from ultralaminae is algaenan, a polymethylenenic aliphatic polymer containing amides in highly sterically-protected positions. Ultralaminae appear to be the dominant component of many Type II kerogens, representing the thin outer cell walls of green algae. Algaenan of an extant alga (*scenesdesmus quadricanda*) contains about 2.5% nonhydrolyzable nitrogen by weight, which has been postulated to lead to a fairly constant atomic C/N ratio of 40.8 in the derived kerogen.[62] The occurrence of bacterans, analogous cell wall polymers in bacteria and cyanobacteria, has also been reported.

As has been discussed above, sulfur content is an important parameter in petroleum classification. A high sulfur content indicates carbonate source rocks and a low sulfur content, clastic, shale source rocks. However, it has been pointed out[62] recently that an assignment solely based on sulfur content can be erroneous because of the effect of maturation and it has been suggested that a better assignment could be made by exploiting the relative constancy of the C/N ratios in kerogens and daughter oils and using the nitrogen concentration in the form of S/N weight ratios as an internal standard. The classifications of bitumens on this basis are listed in Table 13.11. The S/N ratios for Alberta bitumens lie in the 10–20 range, indicating marine carbonate source rocks deposited under hypersaline, sulfate-rich conditions, as concluded before on the basis of sulfur concentration alone.

Of the nitrogen-containing compounds in the oil, the geochemistry of only the porphyrins[63] is well understood. Treibs,[1] on discovering the petroporphyrins, recognized their

Table 13.11 Classification of petroleum on the basis of S/N ratios[62]

S/N wt ratio	Provenance/source rock type
<1	freshwater, lacustrine, paludal
1.0–3	shales rich in reactive iron
3.0–5	marine shales
5.0–15	carbonates and pelagic sediments
15.0–25	carbonates, marine, with sulfate-rich, hypersaline depositional conditions
>25	effect of thermochemical sulfate reduction

genetic relationship with chlorophylls and proposed a pathway involving a number of intermediates for the transformation of chlorophyll *a* to DPEP petroporphyrin. Since then, there have been several modifications proposed to the Treibs transformation pathway; the one[64] shown in Figure 13.39 was suggested to carry more weight than the earlier ones because it is based on the experimental study of tetrapyrrole distributions in selected sediments and features a minimum number of intermediates necessary for the conversion. The free porphyrin base produced in the sequence is then metalated to yield the metallopetroporphyrin. In addition to chlorophyll *a*, the diagenetic alteration in the sediment of chlorophyll *b*, c_1, c_2, c_3, bacteriochlorophyll *a-d*, hemes and possibly other types of tetrapyrroles, produce a broad array of petroporphyrins which, by 1990, was shown to give rise to the occurrence of at least 78 petroporphyrins belonging to 49 basic carbon frameworks.[65] The variations within a framework are due to the nature of the metal present, level of oxidation and alkyl side chain lengths. By 1998 the number of basic frameworks had increased to over 70.[66]

Petroporphyrins can give information on the origin and nature of the biotic source material, the maturity status of the oil and the redox conditions of the source rock depositional environment. Vanadyl porphyrins are not affected by biodegradation and thus they are useful maturity indicators in severely biodegraded oils.[67]

For the total metalloporphyrin content of Athabasca bitumen, values up to 880 ppm have been reported and for Lloydminster heavy oil, 240 ppm (and an earlier value of 500 ppm). The highest metalloporphyrin content reported in the literature is for Boscan bitumen at 3,500 ppm. The elemental V and Ni contents in Athabasca, Peace River and Cold Lake bitumens have similar values of around 190 and 73 ppm. Of the 190 ppm V only about half could be isolated as VO–porphyrin and an even smaller fraction of the 73 ppm Ni in the Athabasca bitumen as Ni porphyrins. The discrepancy could be attributed to experimental errors due to difficulties in the estimation of the metalloporphyrins and to the existence of other, organically-bound forms of these metals—primarily as carboxylates and perhaps dimeric or covalently asphaltene-bound partially reduced metalloporphyrins in the bitumen. Also, soluble clay-complexed or oxygenated metalloporphyrins, if present, would not necessarily report with the porphyrins depending on the analytical method used. Free porphyrins are present in oil in minute quantities only and the metals and metalloporphyrins are distributed between the maltene and the asphaltene, the latter presumably in an equilibrium or quasi-equilibrium state. In Athabasca maltene, all the V appears to be porphyrin-bound whereas only a fraction of the Ni, about 13–29%, is present as nickel porphyrins.[10] In the asphaltene, the picture is different. Of the 630–710 ppm V reported to present in the asphaltene, only about 5% could be accounted for in terms of the 332-ppm VO-porphyrins that could be isolated from the asphaltene, and in the extracted asphaltene the VO-porphyrin Soret band became barely noticeable.[12] Thus, in asphaltene only a small fraction of the V and Ni is in the form of metalloporphyrins and the bulk of the metals is either bound in carboxylic acids, degraded porphyrins not showing the Soret band, or in clay organic and other minerals. High-MW asphaltene-bound porphyrins have been referred to in the literature[68] but their characterization was incomplete and it is not clear whether the porphyrins were truly covalently-bound or only chemisorbed to the asphaltene.

Vanadyl porphyrins with oxygen functionalities have also been reported in the vanadyl porphyrin extracts from Athabasca bitumen. These included a carbonyl[69] and four carboxylic groups[12] adjacent to the porphyrin nucleus. The former molecules were detected in the maltene and the latter in the asphaltene-adsorbed phase of the bitumen.

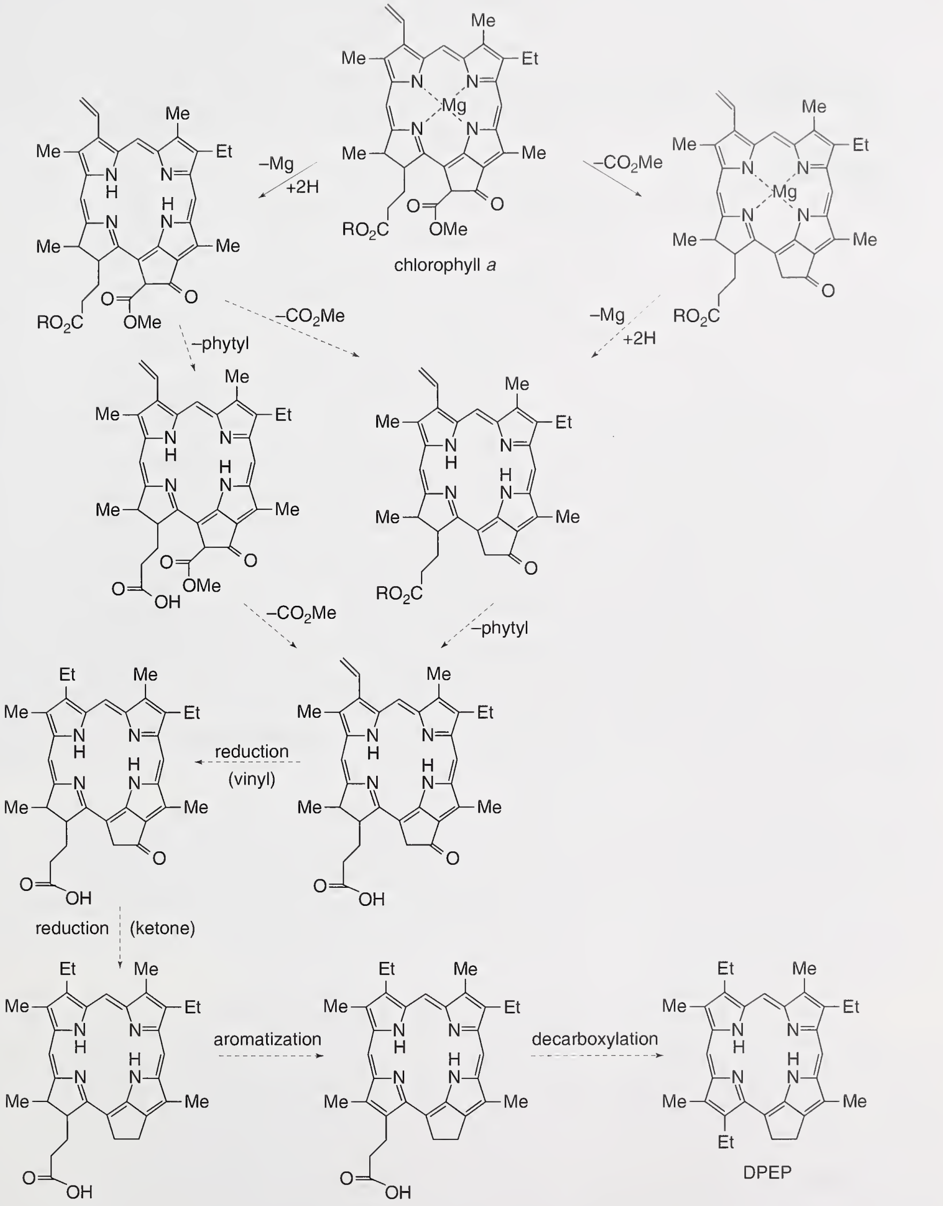
chlorophyll *a*
−Mg
+2H
−CO2Me
−phytyl
reduction
(vinyl)
reduction
(ketone)
aromatization
decarboxylation
DPEP
Me
Et
RO2C
OMe
OH
Mg

Figure 13.39 Modified Treibs scheme for the conversion of chlorophyll *a* to DPEP porphyrin based on components isolated from the sediment of a eutrophic freshwater lake in Cumbria (U.K.). The dotted arrows indicate possible pathways. From B.J. Keely *et al.*, Ref. 64. © 1990, American Chemical Society.

The high V, Ni and metalloporphyrin contents and the V/Ni ratios in Alberta oil sand bitumen,[10] in agreement with other characteristics of the bitumen, point to a marine origin, Table 13.7, for the precursor oil.

The etioporphyrin is formed from the thermal or oxidative cleavage of the exocyclic ring in the DPEP porphyrin. If ring opening were a purely thermal process, the etio/DPEP ratio could

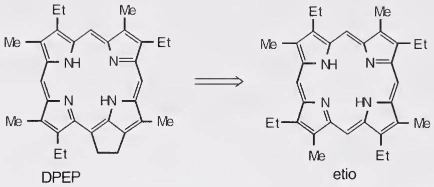

be regarded as a maturity parameter. Since this is not the case, and oxidative, catalytic and other processes which also alter the ratio do occur, the ratio is not a reliable maturity parameter. The value of the ratio is also dependent on the phase and is always smaller in the asphaltene-chemisorbed material than in the material dissolved in the maltene, Table 12.24. This is an additional consequence of the protection afforded by adsorption against catalytic, microbial and chemical attack on adsorbed molecules in the aggregate phase of asphaltene. Moreover, the ratio and the carbon range of the porphyrin series depend on the method of analysis. Thus, demetalation of Athabasca asphaltene vanadyl porphyrins with methanesulfonic acid gave etio/DPEP = 0.60 and C_{28}–C_{34} while direct measurement as vanadyl porphyrin gave etio/DPEP = 0.95 and C_{20}–C_{53}. The vanadyl porphyrin ratios for Athabasca, Peace River and Cold Lake bitumens have similar values and they appear to exhibit a slightly decreasing trend which apparently correlates with the extent of biodegradation (and presumably with the depth of the original oil formation).

A more reliable porphyrin maturity parameter (PMP)[8] is the [C_{28} etio/(C_{28} etio + C_{32} DPEP)] ratio which is supposed to correlate with oil generation from the kerogen. Thus, PMP values of 0.2 indicate the beginning of oil generation. The values for PMP that can be obtained from the mass spectrometric analysis of vanadyl porphyrins in Athabasca, Peace River and Cold Lake bitumen are 0.21, 0.19 and 0.29, once again signalling an early-mature thermal maturity status for these bitumens.

Thus, from the study of the porphyrins in Alberta bitumens one arrives at the same conclusions as from the study of the hydrocarbon, sulfur- and oxygen-containing biomarkers, reinforcing the validity of those conclusions, namely, that Alberta bitumens are the residue of marine oils deposited in a strongly reducing environment in the presence of an excess of sulfide ions in carbonate source rocks.

Additional nitrogen compounds with some relevance to geochemical applications include certain members of the alkylquinoline and alkylcarbazole families[70,71] and, more recently, benzo[a]carbazole and benzo[c]carbazole, the ratios [a]/[c] and [a/(a + c)], of which have been suggested to be a maturity-independent indicators of secondary oil migration distances.[72]

7.0 Secondary Migration of Petroleum

Secondary migration, Figure 13.40,[6] is defined as the movement of petroleum compounds on their way from the source rocks to the reservoir rocks through porous and permeable carrier rocks under the influence of buoyant rise, capillary pressures and hydrodynamic forces. Identification and delineation of secondary migration pathways are of paramount economic importance: in the search for new petroleum resources information is required about the route and distance traveled by the migrating oil, and with respect to the search for the source rocks of Alberta bitumens such information may be of extreme value for the identification of the source rocks.

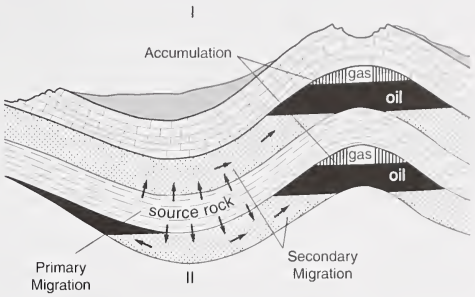

Figure 13.40 Illustration of primary and secondary migration. From Tissot and Welte, Ref. 6. © 1984, Springer-Verlag.

During migration the oil experiences profound chemical alterations (*cf.* Figure 1.4). The most intensive changes in chemical composition are probably due to "geochromatographic" effects, whereby the rock surface selectively adsorbs components of the migrating oil according to the polarity, size and shape of the oil molecules. Various clay minerals have been implicated as active adsorbers. Some of the biomarker concentrations may be altered as well, and on its passage through organically-coated rock pores the moving oil may even desorb some (usually younger) biomarkers, thus endowing the oil with contradicting distributions of thermal maturity indicators. Differential dissolution in the aqueous phase of the constituent molecules of the oil may also be a factor in the chemical alteration of the oil. On the other hand biodegradation, according to generally-held beliefs, does not play a significant role in the chemical alteration of the migrating oil relative to the potential magnitude of this effect observable in the reservoir.

The benzocarbazole method developed recently[72] for the determination of secondary oil migration distances is based on the difference in the adsorptive property of the two isomeric benzocarbazoles present in crude oils with respect to solid organic matter and clay minerals, owing to the differences in their molecular geometry, dipole moments, molecular electrostatic potentials and partial charges. The preferential sorption of the rod-shaped [a] isomer relative to the sub-spherical [c] isomer results in a secondary migrational distance-dependent decrease in the [a/c] and [a/(a + c)] ratios in the moving oil. Early results indicate that the fractional [a/(a + c)] ratio decreases approximately linearly when plotted against the logarithm of the secondary migration distance of the oil, Figure 13.41.[70] Laboratory studies yielded results consistent with the field data.[72]

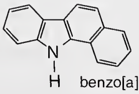
benzo[a]carbazole

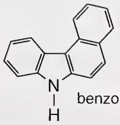
benzo[c]carbazole

The benzocarbazole method could be applied for the reliable determination of the lateral distance the pooled bitumen precursor oils had traveled from the source rock to the present-day location of the bitumen, provided biodegradation did not alter the distribution of the isomeric benzocarbazole molecules. A consideration of the general characteristics of secondary oil migration, however, dictates that the microbiological degradation of the precursor oils to Alberta

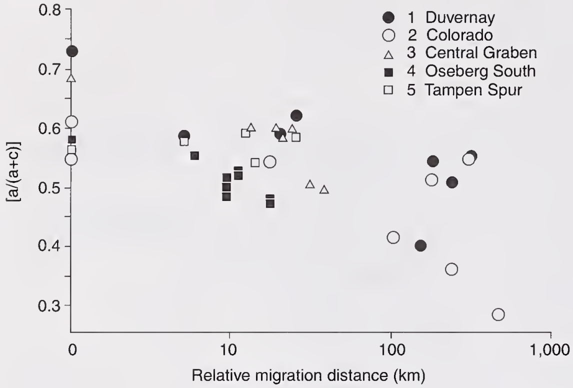

Figure 13.41 Benzocarbazole [a/(a + c)] ratios vs. log (migration distance). From S.R. Larter *et al.*, Ref. 72. © 1996, Nature Publishing Group.

bitumens could not have taken place during the secondary migration of the precursor oils. Naturally, it could not have occurred in the course of primary migration either. This identifies the locale of the biodegradation as the present-day reservoir rocks. If, indeed, degradation of the oils had taken place in the reservoir where they are found today, then the time when the degradation occurred can be identified since it had to be contemporaneous with the transport of the oil into the reservoir.This sequence of events follows from the fact that the biodegradation process is accompanied by at least a 50% weight loss of the oil and since the specific gravity of an oil is lower (~0.9 g·cm^3) than that of the bitumen (~1.0 g·cm^3) and the pore volume of the sand is about 30%, the maximum oil saturation at a minimum 2% water content could not have exceeded about 6% had the degradation occurred after completion of the migration. In effect, in the majority of the Alberta deposits, the bitumens are present in concentrations exceeding 6%, up to about 18%. Thus, the high oil saturation of the oil sands provides convincing evidence for the contemporaneous occurrence of the invasion of the oil into the reservoir rock and its microbiological degradation to bitumen.

PART II. BIOMARKERS IN THE ALKALINE PROCESS WATER

1.0 Hydrocarbon-type biomarkers

In the course of the investigation of the organic content of Alberta oil sand process waters it was discovered[73] that dilute aqueous alkaline extraction of the oil sands or components thereof is an excellent way of preparing concentrates of hydrocarbons, carboxylic acids, alcohols and other oxygen and sulfur compounds, all of them recognized biological marker molecules, for analytical studies. The method is applicable to the whole oil sand or any of its components, and offers certain advantages which include the following:

- experimental simplicity and speed of preparation of the concentrate;
- easy preparation of large-scale sample material, and
- opening a new window on biomarker content, rendering possible the detection of additional species.

In broad terms, the method consists of treating the sample (*e.g.* 300-g oil sands) with aqueous sodium hydroxide (~0.01*N*, 600 mL) at temperatures between 80℃ and reflux temperature of the aqueous slurry, from 10 minutes to 48 hours, followed by the separation of the floating bitumen and bottom-settled sand from the aqueous phase. The latter is then acidified, extracted with methylene chloride and the organic solution is dried over sodium sulfate. In the studies to be described, several variations of this scheme have been employed.

It is not clear whether the organic solutes form a true solution in the water or whether they are colloidally dispersed, owing to the surfactant action of the soap formed from the carboxylic acids and sodium hydroxide. The solubilities of the hydrocarbons present ($>C_{15}$) are vanishingly small and it is not likely that they would form a true solution in water under the circumstances.

The GC–mass chromatograms in Figures 13.42 and 13.43 reveal the presence of a fairly broad series of *n*-alkanes in the whole oil sands and a narrower series in the solvent-extracted sand in the ranges C_{17}–C_{36} and C_{22}–C_{30}. The difference in range is largely due to the difference in the time of duration and in the temperature of the extraction step, 48 hours *vs.* 15 minutes, and 100° *vs.* 80°. The presence of mineral matter-associated *n*-alkanes, which were not mobilized and solubilized after 48 hours methylene chloride extraction of the oil sand seems to suggest that they were trapped in the mineral-bound humic matter. However, an alternative explanation may be as follows. It is well established that there exists in the oil sand a significant dormant population of bacteria (and possibly other microorganisms) capable of metabolizing crude oils, down to a depth of 700–800 m.[74] Their presence is confirmed by the minor but manifest biodegradation processes that are presently ongoing and that are responsible for the production of C_1–C_7 hydrocarbons and unusual products such as neopentane (which, in some cases, is the only C_5H_{12} hydrocarbon present), acetaldehyde, carbon monoxide, *etc.*, *cf.* Chapter 9. Important additional evidence can be found in the presence of small but readily detectable amounts of squalene in the bitumen[37] arising from bacterial detritus, and the composition of mineral-bound acids, Figures 8.2–8.6. This explanation could perhaps also account for the appearance of *n*-alkanes and other hydrocarbon biomarkers in the products of the various mild chemical degradations of asphaltene.[75]

The GC–mass chromatograms shown in Figures 13.44 and 13.45 display the distributions of the di-, tri- and pentacyclic terpanes in the extract. Evidently, they are similar to those obtained by the conventional method of concentration except for the presence of trace quantities of C_{36} and C_{37} hopanoids, Figure 13.46, each of which features three isomers. These species have not been seen in Alberta bitumens before although extended homohopanes up to C_{40} have been mentioned in the literature.[76] The species at retention times 46.4, 48.2 and 50.3, 52.4 minutes, appear to be the extended members of the R and S homohopane series.

The m/z = 372 cross scan of C_{27} 8,14-secohopane isomers is reproduced in Figure 13.47. The 8,14-secohopanes form a short series ranging from C_{27} to C_{31}, each member occurring in a number of different isomeric forms. 8,14-Secohopanes have not been detected in Athabasca bitumen by conventional methods of biomarker assaying.

The distributions of steranes and C-ring monoaromatic steranes found here, Figures 13.48 and 13.49, are very similar to those found by the conventional method of separation but in addition to these, a new, previously undetected C-ring monoaromatic, A-ring methylated sterane series ranging from C_{20} to C_{29}, Figure 13.50, was also identified.

The triaromatic steranes were also found to show a distribution very similar to the one found before in the C_{26}–C_{28} range, Figure 13.51, but the C_{20} and C_{21} members were severely depleted—as in the case of the Grosmont carbonate bitumen. (There, the absence of the C_{20} and C_{21} members was attributed to water washing effects.)

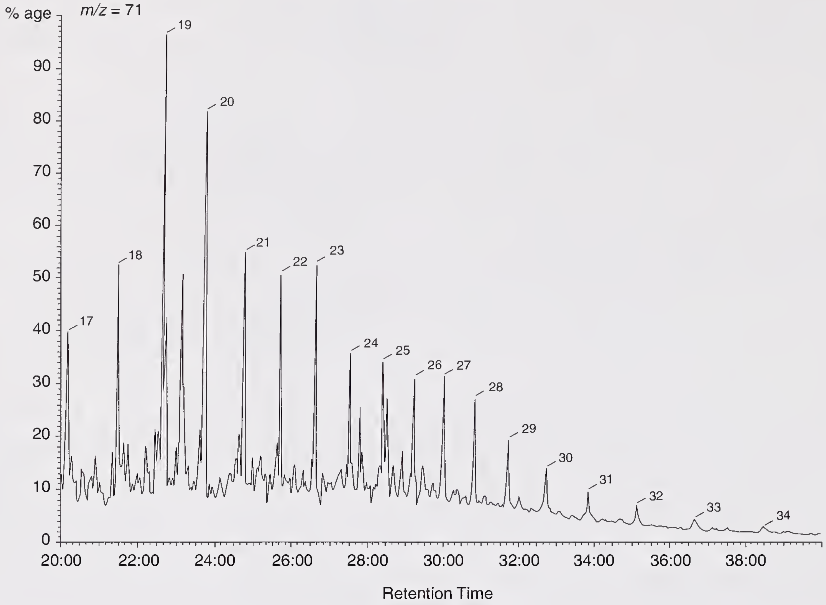

Figure 13.42 GC–MS $m/z = 71$ cross scan of the aqueous extract of Athabasca oil sands (300 g) + NaOH (0.5 g) extracted in a Soxhlet apparatus with H_2O (600 mL) for 48 h, showing the C_{17}–C_{34} *n*-alkanes.[73]

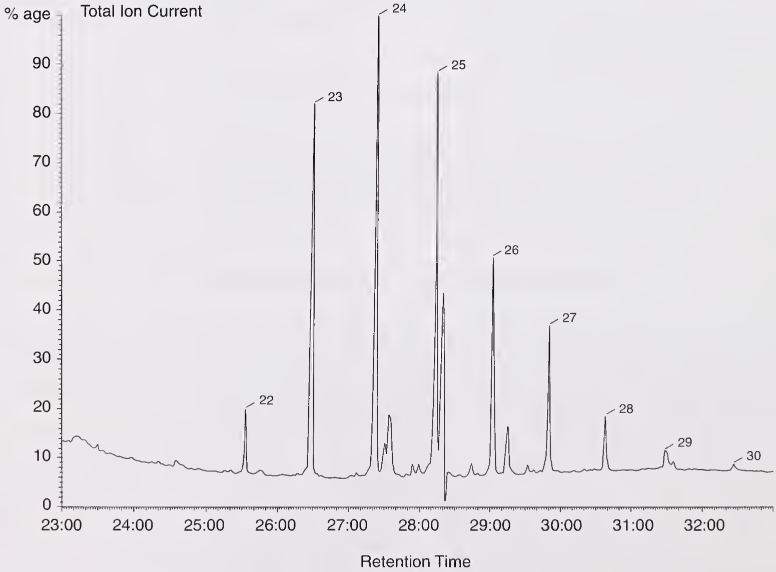

Figure 13.43 GC–MS total ion current chromatogram of CH_2Cl_2 Soxhlet-extracted oil sands (300 g) treated with 0.01 *N* NaOH (600 mL) 15 min at 80°C, showing the C_{22}–C_{30} *n*-alkanes.[73]

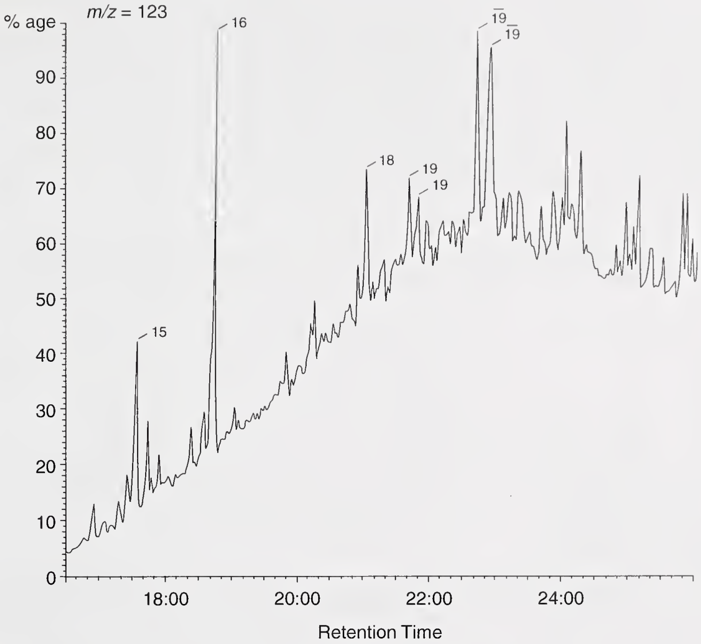

Figure 13.44 GC–MS m/z = 123 cross scan of the saturate fraction of the aqueous extract from Athabasca oil sands (500 g) + 0.01 *N* NaOH (800 mL) Soxhleted 15 min at 80°C, showing the C_{15}–C_{19} bicyclic terpenoid hydrocarbons.

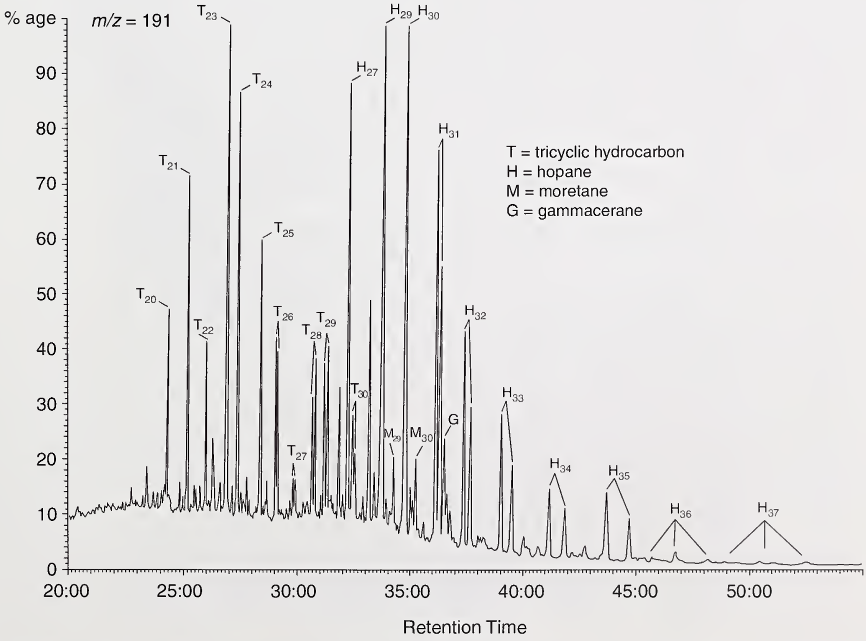

Figure 13.45 GC–MS m/z = 191 cross scan of the Figure 13.42 extract, showing the distribution of the tricyclic and pentacyclic terpenoid hydrocarbons.

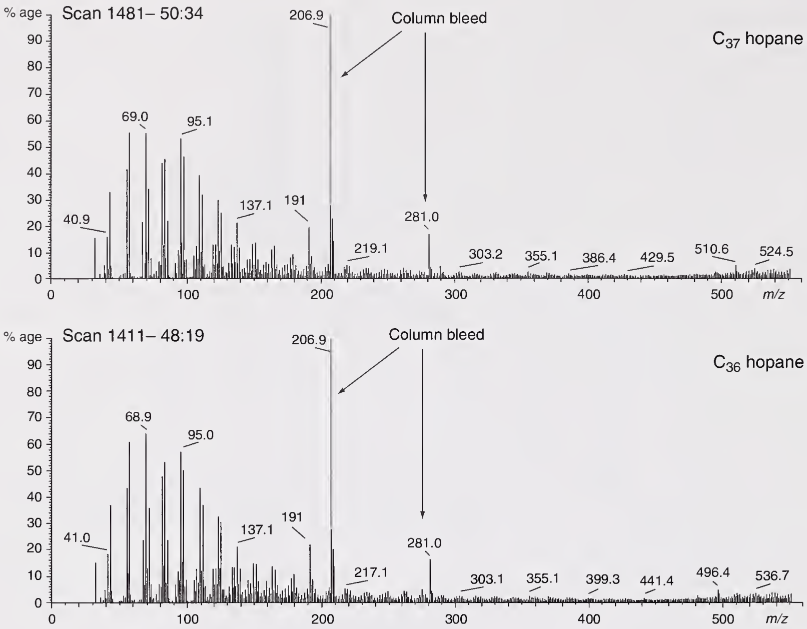

Figure 13.46 EIMS of the C_{36} and C_{37} hopanes in the Figure 13.42 extract.

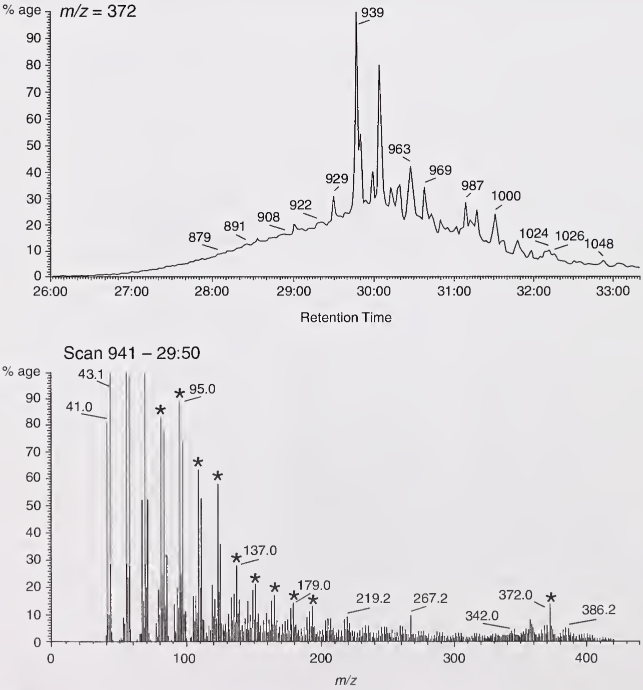

Figure 13.47 GC–MS $m/z = 372$ cross scan of the Figure 13.42 extract, showing the presence of C_{27} 8,14-secohopane.

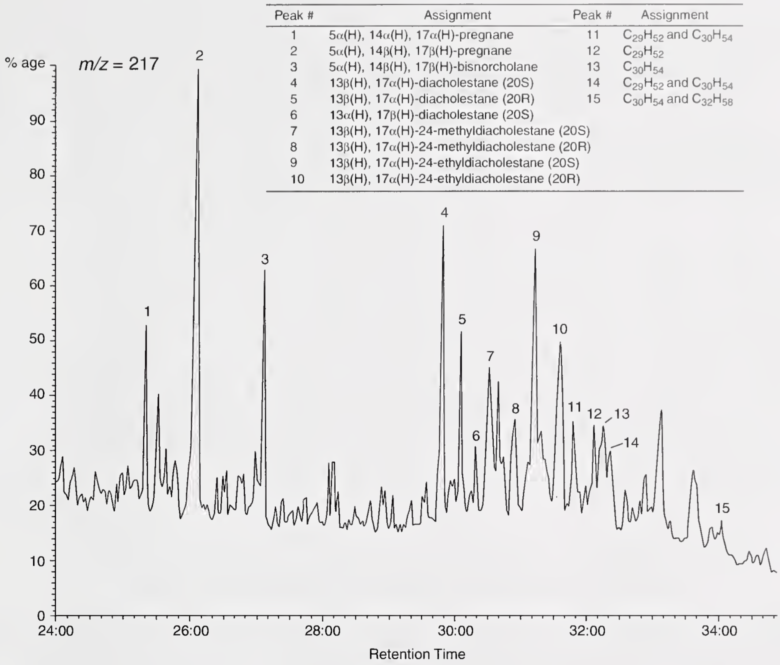

Peak #	Assignment	Peak #	Assignment
1	5α(H), 14α(H), 17α(H)-pregnane	11	$C_{29}H_{52}$ and $C_{30}H_{54}$
2	5α(H), 14β(H), 17β(H)-pregnane	12	$C_{29}H_{52}$
3	5α(H), 14β(H), 17β(H)-bisnorcholane	13	$C_{30}H_{54}$
4	13β(H), 17α(H)-diacholestane (20S)	14	$C_{29}H_{52}$ and $C_{30}H_{54}$
5	13β(H), 17α(H)-diacholestane (20R)	15	$C_{30}H_{54}$ and $C_{32}H_{58}$
6	13α(H), 17β(H)-diacholestane (20S)		
7	13β(H), 17α(H)-24-methyldiacholestane (20S)		
8	13β(H), 17α(H)-24-methyldiacholestane (20R)		
9	13β(H), 17α(H)-24-ethyldiacholestane (20S)		
10	13β(H), 17α(H)-24-ethyldiacholestane (20R)		

Figure 13.48 GC–MS $m/z = 217$ cross scan of the Figure 13.42 extract, showing the distribution of steranes.

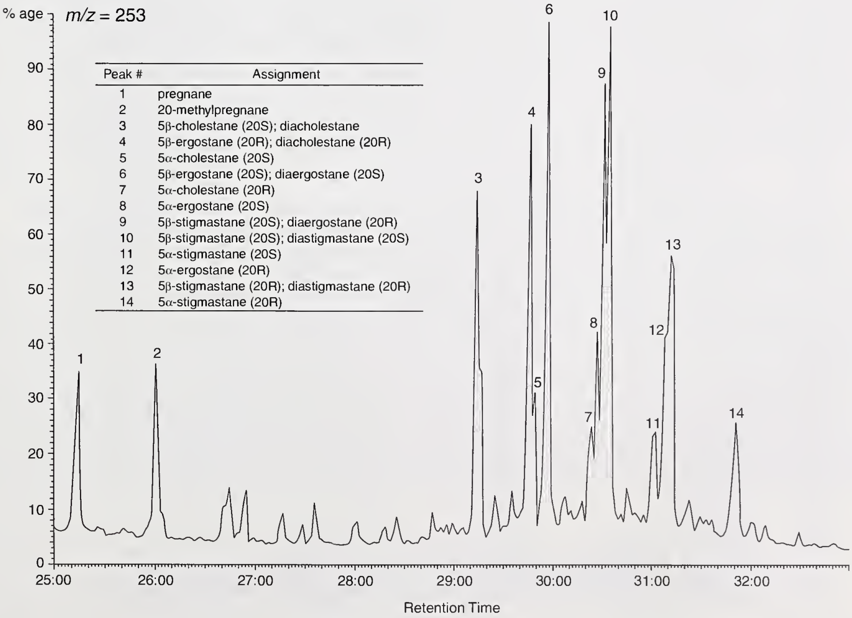

Peak #	Assignment
1	pregnane
2	20-methylpregnane
3	5β-cholestane (20S); diacholestane
4	5β-ergostane (20R); diacholestane (20R)
5	5α-cholestane (20S)
6	5β-ergostane (20S); diaergostane (20S)
7	5α-cholestane (20R)
8	5α-ergostane (20S)
9	5β-stigmastane (20S); diaergostane (20R)
10	5β-stigmastane (20S); diastigmastane (20S)
11	5α-stigmastane (20S)
12	5α-ergostane (20R)
13	5β-stigmastane (20R); diastigmastane (20R)
14	5α-stigmastane (20R)

Figure 13.49 GC–MS $m/z = 253$ cross scan of the Figure 13.42 extract, showing the C-ring aromatic steranes distribution.

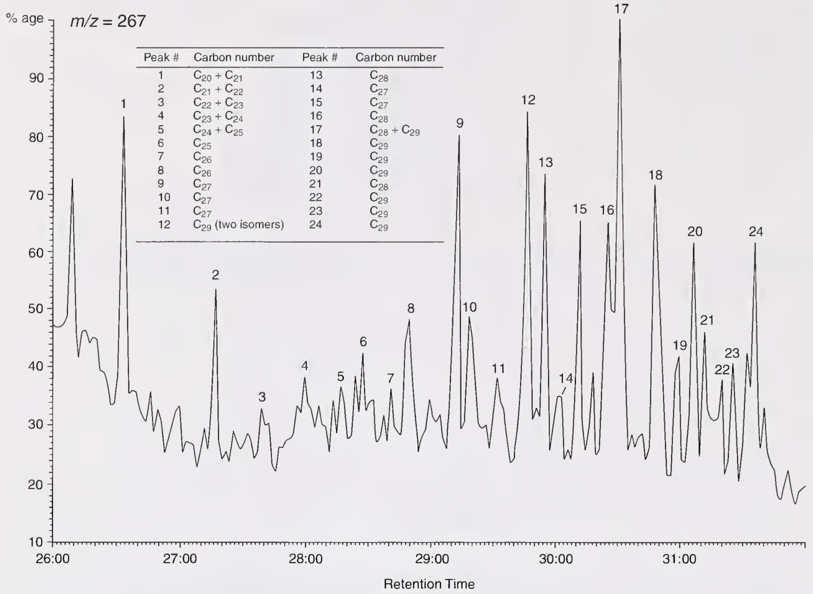

Peak #	Carbon number	Peak #	Carbon number
1	$C_{20} + C_{21}$	13	C_{28}
2	$C_{21} + C_{22}$	14	C_{27}
3	$C_{22} + C_{23}$	15	C_{27}
4	$C_{23} + C_{24}$	16	C_{28}
5	$C_{24} + C_{25}$	17	$C_{28} + C_{29}$
6	C_{25}	18	C_{29}
7	C_{26}	19	C_{29}
8	C_{26}	20	C_{29}
9	C_{27}	21	C_{28}
10	C_{27}	22	C_{29}
11	C_{27}	23	C_{29}
12	C_{29} (two isomers)	24	C_{29}

Figure 13.50 GC–MS *m/z* = 267 cross scan of the Figure 13.42 extract, showing the C-ring monoaromatic, A-ring methylated steranes distribution.

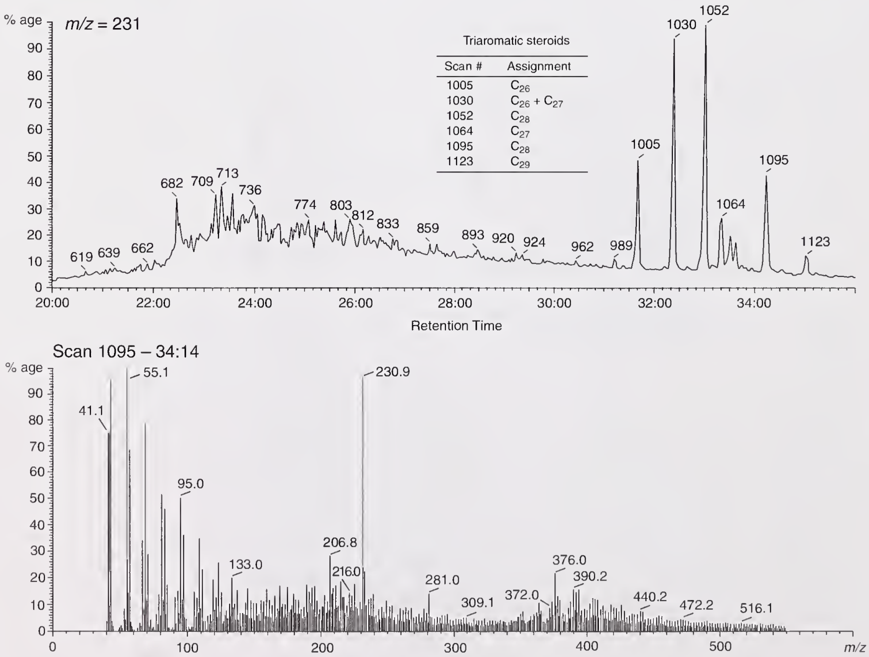

Triaromatic steroids

Scan #	Assignment
1005	C_{26}
1030	$C_{26} + C_{27}$
1052	C_{28}
1064	C_{27}
1095	C_{28}
1123	C_{29}

Figure 13.51 GC–MS *m/z* = 231 cross scan of the Figure 13.42 extract, showing the triaromatic steranes distribution. Also shown is the mass spectrum of scan 1095, a C_{28} member of the series.

Additional new series of biomarkers not found before in the maltene fraction of Athabasca bitumen comprise a C_{27}–C_{31} series of D-ring monoaromatic 8,14-secohopanes, Figure 13.52, two C_{29} methylated D-ring monoaromatic 8,14-secohopanes, Figure 13.53, and a series of C_{32}–C_{35} benzohopanes, Figure 13.54.

All the previously-unidentified biomarkers identified in the water extraction procedure are in agreement with the previously-established marine, carbonate source character of the bitumen and lend further support to this classification.

As is evident from the foregoing discussion, the water extract from the hot, aqueous alkaline extraction of oil sand is a superior source for the hydrocarbon-type biomarkers in the oil sand because while it contains essentially all the previously-detected hydrocarbon type biomarkers, it permits the detection of biomarkers not detected in Athabasca bitumen using conventional methods of analyses. One minor drawback with the method is that it is not immediately clear if the particular molecules identified originated from the bitumen, or a fraction of the oil sand, or the sand-chemisorbed organic matter. This problem can be resolved by subjecting the bitumen-extracted sand to the same hot, aqueous alkaline extraction followed by analysis of the extract.

2.0 Oxygen-Containing Biomarkers

Two series of oxygen-containing compounds were detected and identified by GC–MS. These were the C_8–C_{36} *n*-alkanoic acids and the C_{13}–C_{20} *n*-alkanols.

GC–MS $m/z = 74$ cross scan chromatograms of the alkanoic acid methyl esters obtained by the alkaline extraction of the oil sand and those from conventional chromatographic separation from the maltene are shown for comparison in Figures 13.55 and 13.56. The two spectra show similarity in featuring a strong even-to-odd preference, the location of maximum intensity at hexadecanoic acid, and an unusually intense peak for nonanoic acid. However, they differ in the breadth of distribution (C_8–C_{28} *vs.* C_8–C_{18}) and the relative concentration distributions of the common members. This difference indicates a sizeable contribution to the *n*-alkanoic acid complement here from the sand-bound organic matter, in agreement with the data discussed in Chapter 8.

The acid composition was also investigated using fast atom bombardment mass spectroscopy, FAB–MS. In this mode of ionization the acid fraction is bombarded by high-velocity xenon atoms in the presence of triethylamine, causing the removal of H-atoms and ionization yielding M–1 ions without any fragmentation. Although the intensities of the M–1 ions could then hypothetically be related to the concentrations of the parent carboxylic acids in the sample, the relative sensitivity of the ionization is apparently structure and molecular size dependent. and the resulting FAB mass spectrum does not reliably reflect the relative concentration distribution of the carboxylic acids. Moreover, the FAB–MS measures only MW and consequently very different structures with identical MW could register as single peak, *e.g.*

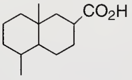

MW = 210

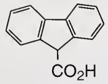

210

$C_{13}H_{27}CO_2H$

228

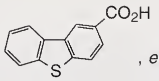

228

, *etc.*

Since we know that aside of saturated alkanoic acids there are some unsaturated alkanoic acids (Chapters 8 and 12), various naphthenic acids as well as a gamut of aromatic carboxylic acids

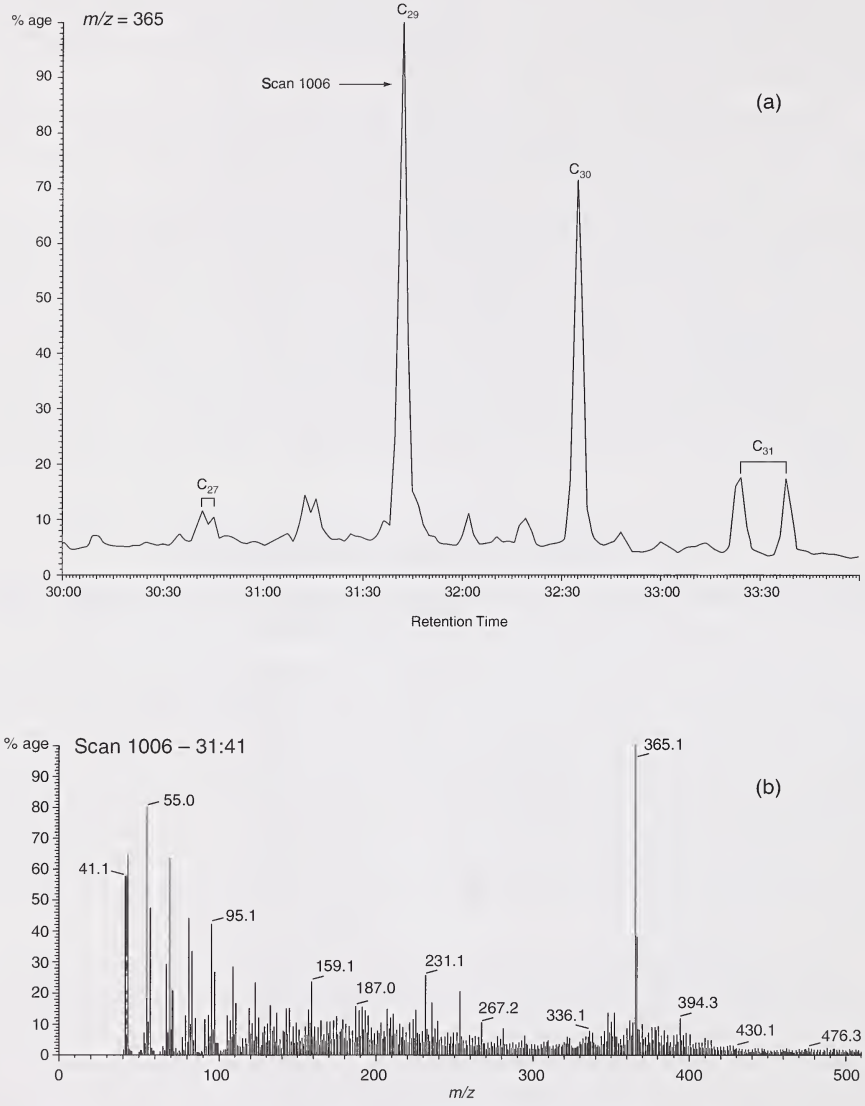

Figure 13.52 GC–MS *m/z* = 365 cross scan of the Figure 13.42 extract, showing a) the D-ring monoaromatic 8,14-secohopanoids distribution. Also shown b) is the mass spectrum of scan 1006, a C_{29} member of the series.

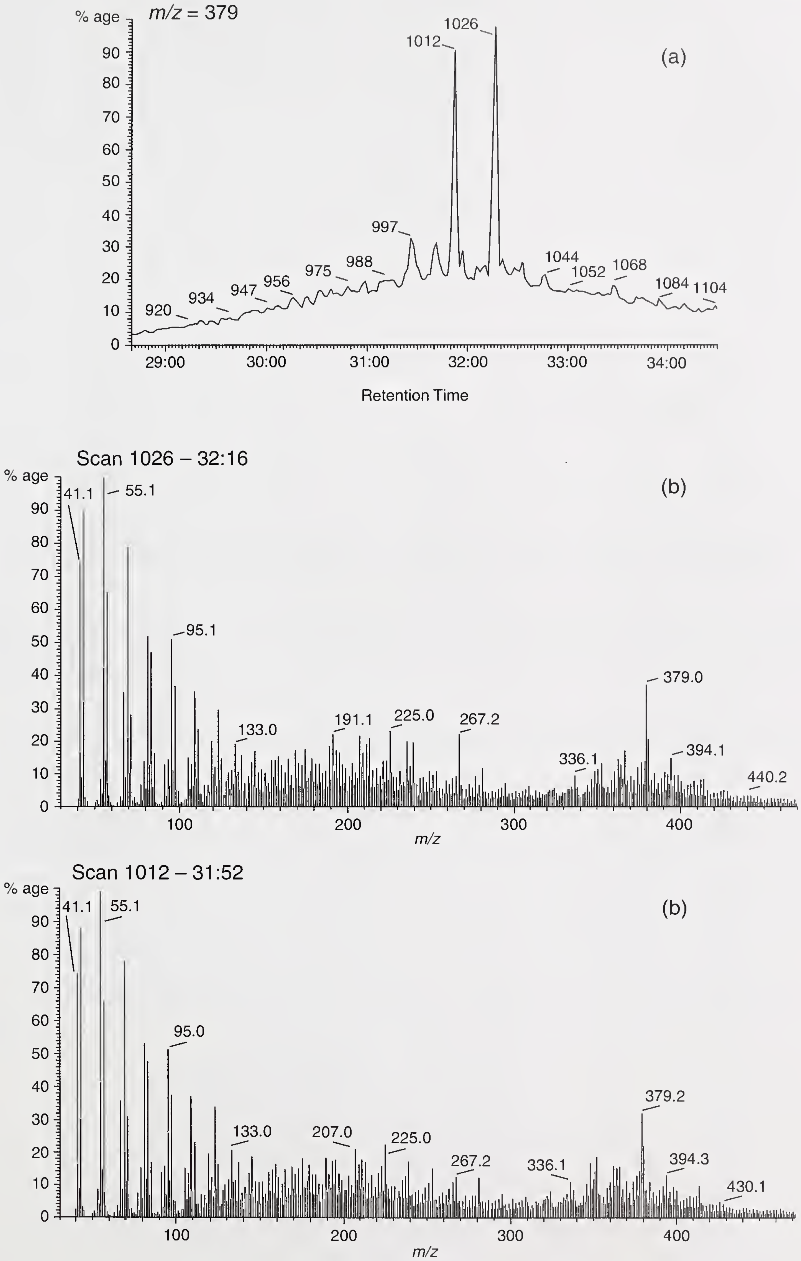

Figure 13.53 GC–MS $m/z = 379$ cross scan of the Figure 13.42 extract showing a) the presence of two members of monoaromatic secohopanoids containing a methyl group and b) the EIMS of the two isomers.

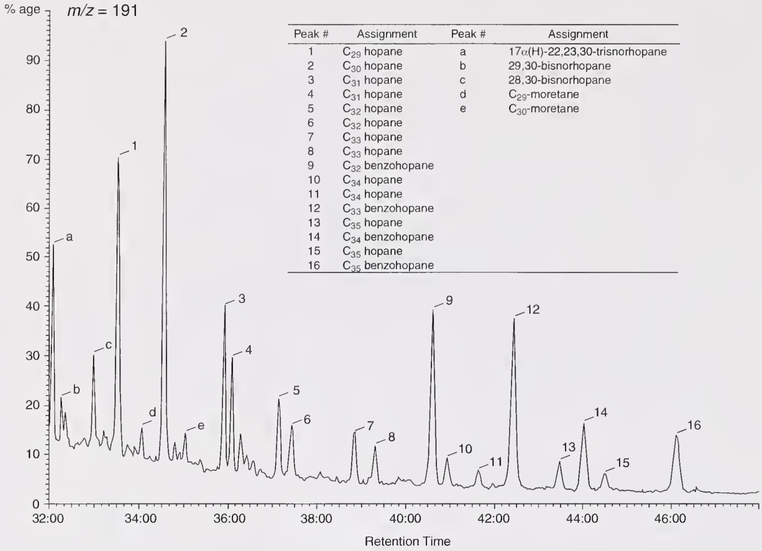

Peak #	Assignment	Peak #	Assignment
1	C_{29} hopane	a	17α(H)-22,23,30-trisnorhopane
2	C_{30} hopane	b	29,30-bisnorhopane
3	C_{31} hopane	c	28,30-bisnorhopane
4	C_{31} hopane	d	C_{29}-moretane
5	C_{32} hopane	e	C_{30}-moretane
6	C_{32} hopane		
7	C_{33} hopane		
8	C_{33} hopane		
9	C_{32} benzohopane		
10	C_{34} hopane		
11	C_{34} hopane		
12	C_{33} benzohopane		
13	C_{35} hopane		
14	C_{34} benzohopane		
15	C_{35} hopane		
16	C_{35} benzohopane		

Figure 13.54 GC–MS $m/z = 191$ cross scan showing the C_{29}–C_{35} hopanes and a short series of benzohopanes in the alkaline process water.

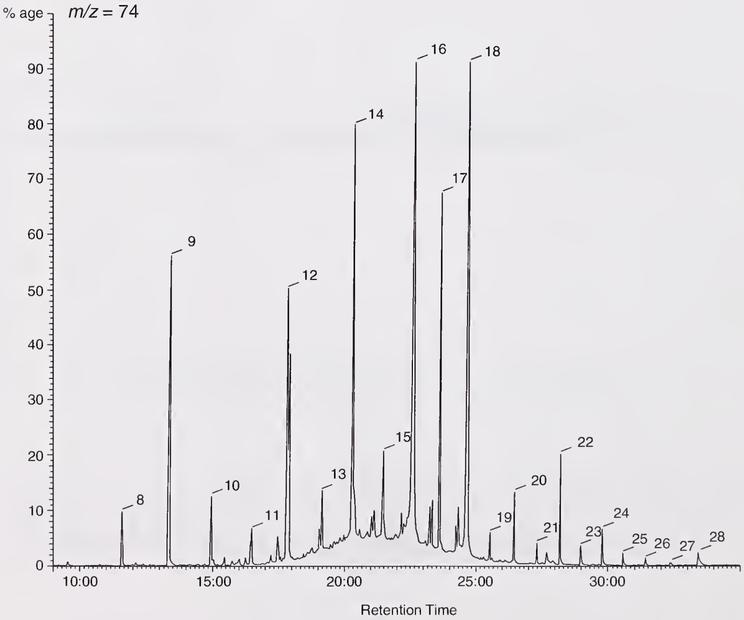

Figure 13.55 GC–MS $m/z = 74$ cross scan of the total organic extract from the alkaline process water showing the *n*-alkanoic carboxylic acids. The numbers are the carbon numbers of the acids in the methyl esters of the analysate.

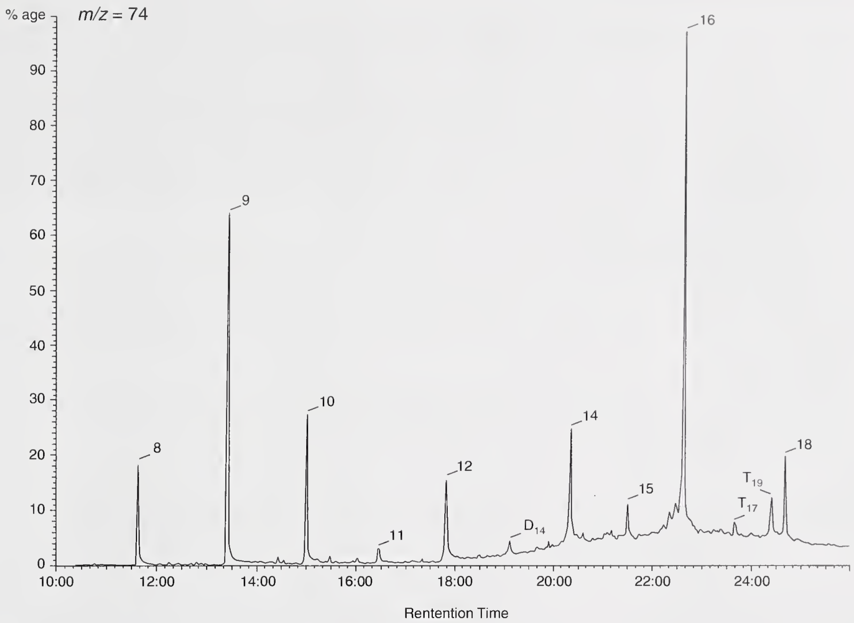

Figure 13.56 GC–MS $m/z = 74$ cross scan showing the *n*-alkanoic carboxylic acids in the maltene fraction of the bitumen. The numbers indicate the acid carbon numbers in the methyl esters of the analysate.

present in the bitumen, the interpretation of the FAB mass spectra is not possible in the absence of other information.

Some time ago, a study[77] on the acid content of Athabasca oil sand slurry concluded that the major acid components of the slurry were sulfonic acids. However, a specific search for sulfonic acids in the work described above[73] unequivocally showed the absence of sulfonic acids. The most probable explanation for the discrepancy should be sought in the quality of the oil sand used in the two studies. It is known that when oil sands are stored in air at (or above) room temperature any pyrite and other sulfide minerals that may be present are oxidized to produce sulfate ions (*cf.* Chapter 3) and that organic sulfides and thiophenes may be oxidized to sulfoxides and sulfones:

$$FeS_2 \xrightarrow{O_2} SO_4^{2-}$$

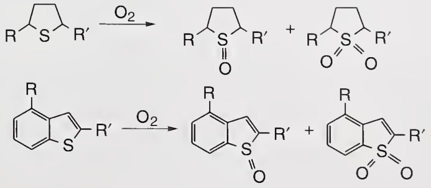

The formation of sulfonic acids may then be envisioned *via* the intermediacy of the sulfones:

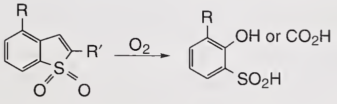

We therefore conclude that the earlier study[77] was probably done on oxidized oil sands whereas in the more recent study[73] the oil sand was fresh, not extensively exposed to aerobic oxidation.

The significance of the data on the acid component of the alkaline extract is that it clearly establishes that only one major natural surfactant is present in the oil sand slurry, namely, the even-carbon-number dominated C_8–C_{28} *n*-alkanoic acid series. It appears that the cyclic terpenoid and aromatic acids are not as readily extractable as the *n*-alkanoic acids which are more inclined to micelle formation than the cyclic acids.

The *n*-alkanols present in the C_{13}–C_{20} range are also strongly dominated by the even-carbon-number members, especially the C_{18}, C_{16} and C_{20} members are abundant, reinforcing their relatively recent origin, along with the *n*-alkanoic acids, from secondary microbiological processes in the reservoir.

In addition to the compound classes described above, a host of additional molecules were also tentatively identified some of which are listed in Table 13.12.

Table 13.12 Compounds detected and tentatively identified in the alkaline extracts of Athabasca oil sands

dodecenol	C_8–C_{14} alkanethiols
tetradecenol	C_8 and C_{11} thioethers
hexadecenol	C_{11}–C_{22} bicyclic sulfoxides
octadecenol	glycerol
α-amyrin	carbohydrate
β-amyrin	nonanal
inositol	decanal
3-fridelanone	C_{22}, C_{24}, C_{28} monounsat. alkanols
9-methylfluoren-9-ol	propylene glycol
cholesterol	γ-sitosterol

3.0 The Origin of Alberta Oil Sands and Their Secondary Migration

Early geologists and geochemists exploring the Western Canada Sedimentary Basin were astounded by the realization of the vastness of the oil accumulation, the origin of which challenged their imagination. (Excellent, brief reviews of these early studies of the Basin are found in references 78 and 79.) Several conflicting schools of thought emerged and the arguments centered around questions like:

- are the bitumen deposits young, immature oils which have not yet turned into conventional oils or are they the remnants of some ancient oils which somehow had lost their light, oily complement?
- were the bitumens or their precursor oils deposited in their present-day reservoir rocks or did they get there by secondary migration?
- if the oils migrated to their present-day reservoirs, what types of rocks—shale or carbonate sourced them; and where are these source rocks located?
- if the oils did migrate to their present-day reservoirs from their source rocks, where and how did this migration take place?
- if the bitumen is indeed the remnant of some precursor oil how was its oily complement lost?

Today, we know the answer to most of these questions. But, what still remains to be elucidated is the origin, source rocks, time of migration and the migrational fairways of the oil from the source rocks to the reservoir rocks. These problems have not been fully resolved in spite of the extensive detailed research carried out in the past 15–20 years or so.

Currently there are two views[79–85] regarding the possible source rocks of the bitumens and associated heavy oils (which amount to only about two percent of the bitumens). According to one view[78,82,84,85] the huge deposit is "a mixture of oils leaking from the immediately underlying section with principal contributions coming from the Jurassic (Nordegg and possibly younger Jurassic) as well as the Mississippian" (Exshaw/Bakken), Figure 13.57 and *cf.* Figure 2.6. In contrast, the other "most likely scenario[79–83] proposed is that "all the tar sands/heavy oils both in Cretaceous and Paleozoic rocks have a similar source rock which is the same as that of the majority of the Mississippian and Lower Cretaceous conventional oils. The source rock with the closest biomarker characteristics to these bitumens and oils is the Exshaw Formation."[79] It was further stated that the Exshaw Formation is the only major source rock with the areal extent to source oils or biodegraded oils with similar characteristics observed in reservoirs from northeast British Columbia to northern Montana.

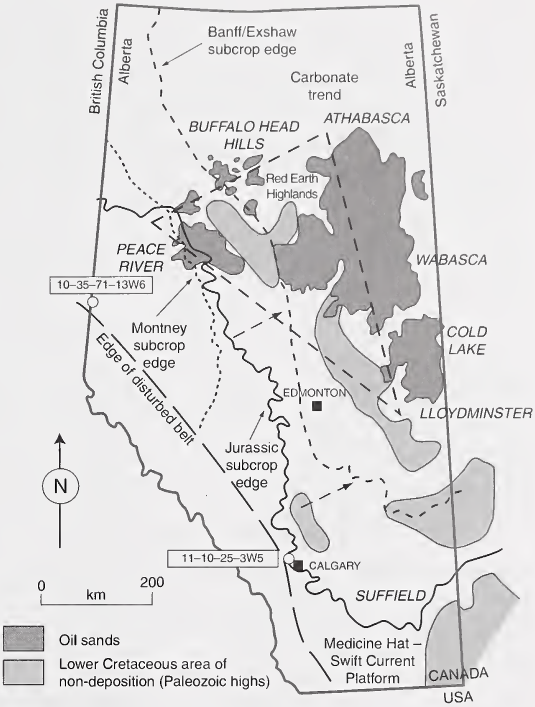
British Columbia
Alberta
Banff/Exshaw subcrop edge
Carbonate trend
Alberta
Saskatchewan
BUFFALO HEAD HILLS
ATHABASCA
Red Earth Highlands
PEACE RIVER
WABASCA
10–35–71–13W6
Montney subcrop edge
Edge of disturbed belt
COLD LAKE
EDMONTON
LLOYDMINSTER
N
Jurassic subcrop edge
11–10–25–3W5
CALGARY
0
km
200
SUFFIELD
Oil sands
Lower Cretaceous area of non-deposition (Paleozoic highs)
Medicine Hat – Swift Current Platform
CANADA
USA

Figure 13.57 Map showing relavent subcrop edges and Paleozoic highs. – – → general direction of oil migration. After D. Barson, R. Bartlett, F. Hein, M. Fowler, S. Grasby and C. Riedigers, "Hydrogeology of Heavy Oil and Tar Sands Deposits" Water Flow and Supply, Migration and Degradation", Proceedings, GeoCanada 2000, Calgary, AB. May 2000.

It should be noted that both these views are based on extensive hydrocarbon-type biomarker correlation studies in which measured were, among others, the C_{27}–C_{35} pentacyclic triterpanes, steranes, aromatized steranes and aryl isoprenoids distributions.

Interestingly, the nature of the source rock identified—shale or carbonate—was not specified in either case.

3.1 Timing of hydrocarbon generation and migration

There is general agreement that the Mannville Group has acted as a major regional collector for oil draining from thermally mature, pre-Mannville source rocks. This has resulted in the focussing of the bulk of the oils of the Basin in an easterly migration into the Peace River, Athabasca-Wabasca, Cold Lake and Lloydminster reservoirs.

From the burial history of the region it has been concluded that peak hydrocarbon generation from the Exshaw Formation occurred earlier in west-central Alberta in the Peace

River region (between about 1.07 × 10^8 and 0.87 × 10^8 years ago), than in the southern region of Alberta, where peak hydrocarbon generation from the Exshaw Formation was not achieved until about 0.56 × 10^8 years ago.[79] An implication of this temporal sequence is that the Exshaw oils in the Mississippian reservoirs below the Peace River oil sands and Grosmont reservoirs below Athabasca oil sands could have been biodegraded prior to, and/or during Lower Mannville deposition. This then may explain the higher degree and differing nature of biodegradation relative to the Mannville oil sands bitumens. It also follows that the Mannville cannot have been very deep when filled by the oil and biodegradation must have taken place contemporaneously with the placement of the oil as required by the high degree of oil saturation and also indicated by the loose uncemented nature of the reservoir sand.

In southern Alberta hydrocarbon generation from the Exshaw Formation did not commence until about 0.56 × 10^8 years ago.[79,83] The oils generated migrated at least as far as Provost and possibly as far as Lloydminster (eastern Alberta) and Aberfeldy (western Saskatchewan). This later occurrence of hydrocarbon generation and migration may account for the generally lower levels of biodegradation found in these fields and it is also consistent with the more consolidated nature of the host reservoir rocks.

The initial quantity of the generated oils in the Basin can be estimated on the basis of model biodegradation studies on Bellshill Lake and Prudhoe Bay, both about 27° API conventional oils and taking into account losses due to water washing and oxidations as being not less than twice the quantity of the residual biodegraded bitumen, about 3.6 trillion barrels.

Bibliography

1. A. Treibs, "The Occurrence of Chlorophyll Derivatives in an Oil Shale of the Upper Triassic", Ann., 517 (1934) 103.
2. G. Eglinton and M. Calvin, "Chemical Fossils", Sci. Am., 216 (1967) 32.
3. G. Eglinton, "Organic Geochemistry. The Organic Chemist's Approach", in *Organic Geochemistry: Methods and Results*, G. Eglinton and M.T.J. Murphy, Eds., Springer-Verlag, Berlin, 1969, p. 20.
4. G. Ourisson and P. Albrecht, "Hopanoids. I. Geohopanoids: The Most Abundant Natural Products on Earth?", Accounts Chem. Res., 25 (1992) 398; G. Ourisson and M. Rohmer, "Hopanoids. II. Biohopanoids: A Novel Class of Bacterial Lipids", *ibid.*, p.403.
5. G. Ourisson, P. Albrecht and M. Rohmer, "The Microbial Origin of Fossil Fuel", Sci. Am., 251 (1984) 44.
6. B.P. Tissot and D.H. Welte, *Petroleum Formation and Occurrence*, 2nd Ed., Springer-Verlag, Berlin, 1984.
7. *Biological Markers in the Sedimentary Record*, R.B. Johns, Ed., Elsevier, Amsterdam, 1986.
8. K.E. Peters and J.M. Moldowan, *The Biomarker Guide*, Prentice Hall, Englewood Cliff, N.J., 1993.
9. G.W. Hodgson, "Vanadium, Nickel and Iron Trace Metals in Crude Oils of Western Canada", Bull. Am. Assoc. Petrol. Geol., 38 (1954) 2537; G.W. Hodgson, B.L. Baker and E. Peake, "The Role of Porphyrins in the Geochemistry of Petroleum", Proc., 7th World Petrol. Congr., 9 (1967) 117.
10. R.H. Filby and D. Strong, "Nickel(II) and Vanadium(IV) Complexes in Alberta Oil-Sand Bitumens", in *Tar Sand and Oil Upgrading Technology*, S.S. Shih and M.C. Oballa, Eds., AIChE Symp. Series No. 282 (1991).
11. D. Strong and R.H. Filby, "Vanadyl Porphyrin Distribution in Alberta Oil Sand Bitumens", in *Metal Complexes in Fossil Fuels*, R.H. Filby and J.F. Branthaver, Eds., ACS Symposium Series 344, American Chemical Society, Washington, D.C., 1987, p. 154.
12. Z. Frakman, T.M. Ignasiak, D.S. Montgomery and O.P. Strausz, "Nitrogen Compounds in Athabasca Asphaltene: The Vanadyl Porphyrins", AOSTRA J. Res., 4 (1988) 171; T. Yokota, F. Scriven, D.S.

Montgomery and O.P. Strausz, "Absorption and Emission Spectra of Athabasca Asphaltene in the Visible and Near Ultraviolet Regions", Fuel, 65 (1986) 1142.

13. C.M. Ekweozor and O.P. Strausz, "18,19-Bisnor-13β(H),14α(H)-Cheilanthane: A Novel Degraded Tricyclic Sesterterpenoid-Type Hydrocarbon from the Athabasca Oil Sands", Tetrahedron Lett., 23 (1982) 2711.

14. C.M. Ekweozor and O.P. Strausz, "Tricyclic Terpanes in the Athabasca Oil Sands: Their Geochemistry", in *Advances in Organic Geochemistry 1981*, M. Bjorøy *et al.*, Eds., Wiley Heyden, London, England, 1983, p. 746.

15. A. Dimmler, T.D. Cyr and O.P. Strausz, "Identification of Bicyclic Terpenoid Hydrocarbons in the Saturate Fraction of Athabasca Oil Sand Bitumen", Org. Geochem., 7 (1984) 231.

16. C.F. Hoffmann and O.P. Strausz, "Bitumen Accumulation in the Grosmont Platform Complex, Upper Devonian, Alberta, Canada", Am. Assoc. Petrol. Geol. Bull., 70 (1986) 1113.

17. P.W. Brooks, M.G. Fowler and R.W. Macqueen, "Biological Markers and Conventional Organic Chemistry of Oil Sands/Heavy Oils, Western Canada Basin", Org. Geochem., 12 (1988) 519.

18. P.W. Brooks, M.G. Fowler and R.W. Macqueen, "Biomarker Chemistry of Cretaceous Oil Sands/Heavy Oils and Paleozoic Carbonate Trend Bitumens, Western Canada Basin", Proc., Fourth UNITAR/UNDP Conference on Heavy Crude and Tar Sands, Edmonton, AB, Aug. 7–12, 1988, Alberta Oil Sands Technology and Research Authority, Edmonton, AB, Vol. 2, p. 593.

19. T.D. Cyr and O.P. Strausz, "The Structures of Tricyclic Terpenoid Carboxylic Acids and Their Parent Alkanes in the Alberta Oil Sands", J. Chem. Soc., Chem. Commun., (1983) 1028.

20. T.D. Cyr and O.P. Strausz, "Bound Carboxylic Acids in the Alberta Oil Sands", Org. Geochem., 7 (1984) 127; D.D. McIntyre, D.S. Montgomery and O.P. Strausz, "Carboxylic Acids Bound to the Mineral Matter in Heavy Cretaceous Oils of Alberta", AOSTRA J. Res., 2 (1986) 223.

21. Z. Frakman, T.M. Ignasiak, E.M. Lown and O.P. Strausz, "Oxygen Compounds in Athabasca Asphaltene", Energy & Fuels, 4 (1990) 263.

22. A.S. Mackenzie, G.A. Wolff and J.R. Maxwell, "Fatty Acids in Some Biodegraded Petroleums. Possible Origins and Significance", in *Advances in Organic Geochemistry 1981*, M. Bjorøy *et al.*, Eds., Wiley Heyden, London, England, 1983, p. 637.

23. J.D. Payzant, D.S. Montgomery and O.P. Strausz, "Novel Terpenoid Sulfoxides and Sulfides in Petroleum", Tetrahedron Lett., 24 (1983) 651.

24. J.D. Payzant, T.D. Cyr, D.S. Montgomery and O.P. Strausz, "The Synthesis of 1β(H),6β(Me)-2,2,6-Trimethyl-8-Ethylbicyclo-[4,3,0]-7-Thianonane and the Structure of the Isomeric Bicyclic Terpenoid Sulfides Occurring in Petroleum", Tetrahedron Lett., 26 (1985) 4175.

25. J.D. Payzant, D.S. Montgomery and O.P. Strausz, "Sulfides in Petroleum", Org. Geochem., 9 (1986) 357.

26. O.P. Strausz, E.M. Lown and J.D. Payzant, "Nature and Geochemistry of Sulfur-Containing Compounds in Alberta Petroleums" in *Geochemistry of Sulfur in Fossil Fuels*, ACS Symposium Series 429, W.L. Orr and C.M. White, Eds., American Chemical Society, Washington, D.C., 1990, p. 366.

27. W.L. Orr and J.S. Sinninghe Damsté, "Geochemistry of Sulfur in Petroleum Systems" in *Geochemistry of Sulfur in Fossil Fuels*, ACS Symposium Series 429, W.L. Orr and C.M. White, Eds., American Chemical Society, Washington, D.C., 1990, p. 2; Ref. 8, p. 137.

28. R.P. Philp, "Geochemistry in the Search for Oil", Chem. Eng. News, (Feb. 10, 1986) 28.

29. a) J.M. Moldowan, W.K. Seifert, E. Arnold and E.J. Gallegos, "Identification of an Extended Series of Tricyclic Terpanes in Petroleum", Geochim. Cosmochim. Acta, 47 (1983) 1531; b) S.M.B. DeGrande, F.R. Aquino Neto and M.R. Mello, "Extended Tricyclic Terpanes in Sediments and Petroleums", Org. Geochem., 30, 1039 (1993); c) T.D. Cyr, J.D. Payzant, D.S. Montgomery and O.P. Strausz, "A Novel Series of Hopane Sulfides in Petroleum", Org. Geochem., 9 (1986) 139.

30. D. Heissler, R. Ocampo, P. Albrecht, J.-J. Riehl and G. Ourisson, "Identification of Long-Chain Tricyclic Terpene Hydrocarbons (C_{21}–C_{30}) in Geological Samples", J. Chem. Soc. Chem. Commun., (1984) 496.

31. F. Cassani and G. Eglinton, "Organic Geochemistry of Venezuelan Extra-Heavy Crude Oils. 2. Molecular Assessment of Biodegradation", Chem. Geol., 91 (1991) 315.

32. O.P. Strausz, "Oil Fingerprinting", Final Report to Alberta Energy Company, February, 1989.

33. G. Deroo, B. Tissot, R.G. McCrossan and F. Der, "Geochemistry of the Heavy Oils of Alberta" in *Oil Sands Fuel of the Future*, Memoir 3, Can. Soc. Petrol. Geol., 148 (1984), 184.

34. G. Deroo, T.G. Powell, B. Tissot, R.G. McCrossan and P.A. Hacquebard, "The Origin and Migration of Petroleum in the Western Canadian Sedimentary Basin, Alberta", Geol. Surv. Can. Bull. 262 (1977); G. Deroo and T.G. Powell, "The Oil Sands Deposits of Alberta: Their Origin and Geochemical History", in *Oil Sand and Oil Sale Chemistry*, p. 11. O.P. Strausz and E.M. Lown, Eds., Verlag Chemie N.Y. 1978.

35. J.D. Payzant, D.D. McIntyre, T.W. Mojelsky, M. Torres and O.P. Strausz, "The Identification of Homologous Series of Thiolanes and Thianes Possessing a Linear Carbon Framework from Petroleums and their Interconversion Under Simulated Geological Conditions", Org. Geochem., 14 (1989) 461.

36. I. Rubinstein, O.P. Strausz, C. Spyckerelle, R.J. Crawford and D.W.S. Westlake, "The Origin of the Oil Sand Bitumens of Alberta: A Chemical and a Microbiological Simulation Study", Geochim. Cosmochim. Acta, 41 (1977) 1341; I. Rubinstein and O. P. Strausz, "Thermal Treatment of Athabasca Oil Sand Bitumen and its Component Parts", Geochim. Cosmochim. Acta, 52 (1979) 171.

37. N. Samman, T. Ignasiak, C.-J. Chen, O.P. Strausz and D.S. Montgomery, "Squalene in Petroleum Asphaltenes", Science, 213 (1981) 1381.

38. J.D. Payzant, T.D. Cyr, D.S. Montgomery and O.P. Strausz, "Studies on the Structures of the Terpenoid Sulfide Type Biological Markers in Petroleum" in *Geochemical Biomarkers*, T.F. Yen and J.M. Moldowan, Eds., Harwood Academic Publishers, Chur, Switzerland, 1988, p. 133.

39. T.D. Cyr, "Bicyclic, Tricyclic and Pentacyclic Terpanes", AOSTRA Fellowship Report, University of Alberta, October, 1983.

40. J.D. Payzant, D.S. Montgomery, A.M. Hogg and O.P. Strausz, "A Field Ionization Mass Spectrometric Study of the Maltene Fraction of Athabasca Bitumen. Part II—The Aromatics", AOSTRA J. Res., 1 (1985) 175.

41. O.P. Strausz, Progress Report, "The Role of Sulfur in Alberta Heavy Crude Oils, as Related to Production, Upgrading and Oxidation", AOSTRA/University Agreement 530, July 1, 1986 – December 31, 1986.

42. P.M. Fedorak, J.D. Payzant, D.S. Montgomery and D.W.S. Westlake, "Microbial Degradation of *n*-Alkyl Tetrahydrothiophenes Found in Petroleum", Appl. Environ. Microbiol., 54 (1988) 1243.

43. P. Peng, A. Morales-Izquierdo, J. Fu, G. Sheng, J. Jiang, A. Hogg and O. P. Strausz, "Lanostane Sulfides in an Immature Crude Oil", Org. Geochem., 28 (1998) 125.

44. P. Schaeffer, C. Reiss and P. Albrecht, "Geochemical Study of Macromolecular Organic Matter from Sulfur-Rich Sediments of Evaporitic Origin (Messinian of Sicily) by Chemical Degradation", Org. Geochem., 23 (1995) 567.

45. J.S. Sinninghe Damsté, J.W. de Leeuw, D.A.C. Kock-van, M.A. de Zeeuw, F. de Lange, W.I.C. Rijpstra and P.A. Schenck, "The Occurrence and Identification of Series of Organic Sulfur Compounds in Oils and Sediment Extracts. I. A Study of Rozel Point Oil (USA)", Geochim. Cosmochim. Acta, 51 (1987) 2369.

46. J.C. Schmidt, "Marqueurs Biologiques Souffrés dans les Pétroles", PhD Dissertation, Université Louis Pasteur de Strasbourg, France (1986).

47. G.S. Waldo, R.M.K. Carlson, J.M. Moldowan, K.E. Peters and J.E. Penner-Hahn, "Sulfur Speciation in Heavy Petroleums: Information from X-Ray Absorption Near Edge Structure", Geochim. Cosmochim. Acta, 55 (1991) 801.

48. a) J. Albaigés, J. Albaga, E. Clavell and J. Grimalt, "Petroleum Geochemistry of the Tarragona Basin (Spanish Mediterranean) Off-Shore", Org. Geochem., 10 (1986) 441; b) A. Chakhmakhchev, M. Suzuki and K. Takayama, "Distribution of Alkylated Dibenzothiophenes in Petroleum as a Tool for Maturity Assessments", Org. Geochem., 26, 483 (1997).

49. C.R. Evans, M.A. Rogers and N.J.L. Bailey, "Evolution and Alteration of Petroleum in Western Canada", Chem. Geol., 8 (1971) 147.

50. N.J.L. Bailey, A.M. Jobson and M.A. Rogers, "Bacterial Degradation of Crude Oil; Comparison of Field and Experimental Data", Chem. Geol., 11 (1973) 2203.

51. N.J.L. Bailey, H.H. Krouse, C.R. Evans and M.A. Rogers, "Alteration of Crude Oil by Waters and Bacteria — Evidence from Geochemical and Isotope Studies", Am. Assoc. Petrol. Geol. Bull., 57 (1973) 1276; J. Connan, "Origin of Severely Biodegraded Oils: A New Approach Using Biomarker Patterns of Asphaltene Pyrolyzates" in *Applied Petroleum Geochemistry*, M.L. Bodenave, Ed., Editions Technip, Paris, France, 1993, p. 455.

52. A.A. Kartsev, Z.A. Tabasaranskii and G.A. Mogilevskii, *Geochemical Methods of Prospecting and Exploration for Petroleum and Natural Gas*, Engl. transl. P.A. Witherspoon and W.O. Romey, University of California Press, Berkeley, CA, 1959.

53. R.J. Crawford , C. Spyckerelle and D.W.S. Westlake, "Biodegradation of Oil Reservoirs" in *Oil Sand and Oil Shale Chemistry*, O.P. Strausz and E.M. Lown, Eds., Verlag Chemie, N.Y., 1978, p. 163.

54. a) Q. Wu, M.R. Gray, M.A. Pickard, P.M. Fedorak and J.M. Foght, "Biocatalytic Ring Opening of Dibenzothiophene and Phenanthrene as Model Substrate Dissolved in Crude Oil," A.C.S. Petr. Chem. Div. Preprints 48 (1) (2003) 47. b) K.M. Kirkwood, S. Ebert, D. Kharbanda, J.M. Foght, P.M. Fedorak and M.R. Gray, "Bioprocessing for Heavy Crude Oil Viscosity Reduction", A.C.S. Petr., Chem. Div., Preprints 48 (1) (2003) 50.

55. E.T. Premuzic, M.S. Lin, M. Bohenec and W.M. Zhou, "Bioconversion Reactions in Asphaltenes and Heavy Crude Oils", Energy and Fuels, 13 (1999) 297.

56. E. Lafargue and C. Barker, "Effect of Water Washing on Crude Oil Compositions", Am. Assoc. Petrol. Geol. Bull., 72 (1988) 263.

57. A. Wishnia, "The Hydrophobic Contribution to Micelle Formation: the Solubility of Ethane, Propane, Butane and Pentane in Sodium Dodecyl Sulfate Solution", J. Phys. Chem., 67 (1963) 2079.

58. C. Tanford, *The Hydrophobic Effect: Formation of Micelles and Biological Membranes*, Wiley, New York, 1973.

59. S.E Palmer, "Effect of Biodegradation and Water Washing on Crude Oil Composition", Ch.23 in *Organic Geochemistry*, M.H. Engel and S.A Macko, Eds., Plenum Press, New York, 1993, p. 551; "Effect of Biodegradation and Water Washing on Crude Oil Composition", Ch. 4 in *Source and Migration Processes and Evaluation Techniques*, R.K. Merril, Ed., American Association of Petroleum Geologists, Tulsa, OK, 1991.

60. P.M. Fedorak and D.W. S. Westlake, "Degradation of Soil Heterocycles in Prudhoe Bay Crude Oil by Soil Enrichments", Water, Air, Soil Pollut., 21 (1984) 225.

61. C. Largo and S. Derenne, "Non-Hydrolyzable Macromolecules of Microbial Cell Walls. Geochemical Importance", Abstracts, Am. Chem. Soc. Div. Geochem., 204th Nat'l Meeting, Chicago, Ill., paper 39 and references therein.

62. K.F.M. Thompson, "A Classification of Petroleum on the Basis of the Ratio of Sulfur to Nitrogen", Org. Geochem., 21 (1994) 877.

63. E.W. Baker and J. W. Louda, "Porphyrins in the Geological Record" in *Biological Markers in the Sedimentary Record,* R.B. Johns, Ed., Elsevier, Amsterdam, 1986, p. 125.

64. B.J. Keely, W.G. Prowse and J.R. Maxwell, "The Treibs Hypothesis: An Evaluation Based on Structural Studies", Energy & Fuels, 4 (1990) 628.

65. H.J. Callot, R. Ocampo and P. Albrecht, "Sedimentary Porphyrins: Correlations with Biological Precursors", Energy & Fuels, 4 (1990) 635.

66. H.J. Callot and R. Ocampo, "Geochemistry of Porphyrins" in *The Porphyrin Handbook, Vol. 1 Synthesis and Organic Chemistry*, Ch. 7, p. 349, K.M. Kadish, K.M. Smith and R. Guillard, Eds., Academic Press, 2000.

67. P. Sundaraman and R.J. Hwang, "Effect of Biodegradation on the Vanadyl Porphyrin Distribution", Geochim. Cosmochim Acta, 57 (1993) 2283.

68. M. Blumer and M. Rudrum, "High Molecular Weight Fossil Porphyrins. Evidence for Monomeric and Dimeric Tetrapyrroles of about 1100 Molecular Weight", J. Inst. Petrol. Technol., 56 (1970) 99.

69. M.F. Millson, D.S, Montgomery and S.R. Brown, "An Investigation of the Vanadyl Porphyrin Complexes of the Athabasca Oil Sands", Geochim. Cosmochim. Acta, 30 (1966) 207.

70. M. Yamamoto, "Fractionation of Azaarenes during Oil Migration", Org. Geochem., 19 (1992) 389.

71. M. Li, S.R. Larter, D. Stoddart and M. Bjorøy, "Liquid Chromatographic Separation Schemes for Pyrrole and Pyridine Nitrogen Aromatic Heterocycle Fractions from Crude Oils Suitable for Rapid Characterization of Geochemical Samples", Anal. Chem., 64 (1992) 1337.

72. S.R. Larter, B.F.J. Bowler, M. Li, M. Chen, D. Brincat, B. Bennett, K. Noke, P. Donohoe, D. Simmons, M. Kohnen, J. Allan, N. Telnaes and I. Horstad, "Molecular Indicators of Secondary Oil Migration Distances", Nature, 383 (1996) 593.

73. N. Kazmi, A. Morales-Izquierdo, E.M. Lown and O.P. Strausz, to be published.

74. D.W. Westlake, University of Alberta, private communication.

75. C.M. Ekweozor, "Characterization of the Non-Asphaltene Products of Mild Chemical Degradation of Asphaltene", Org. Geochem., 10 (1986) 1053.

76. J. Rullkotter and R.P. Philp, "Extended Hopanes up to C_{40} in Thornton Bitumen", Nature, 292 (1981) 616.

77. L.H. Ali, "Surface-Active Agents in the Aqueous Phase of the Hot Water Flotation Process for Oil Sands", Fuel, 57 (1978) 357.

78. S. Creaney and J. Allen, "Petroleum Systems in the Foreland Basin of Western Canada", in Foreland Basins and Fold Belts, Am. Assoc. Petrol. Geologists Memoir 55. Eds. R.W. Macqueen and D.A. Leckie (1992) 279.

79. M. Fowler and C. Riediger, "Origin of Athabasca Tar Sands", in *Hydrogeology of Heavy Oil and Tar Sand Deposits: Water Flow and Supply, Migration and Degradation*. Eds. D. Barson, R. Bartlett, F. Hein, M. Fowler, S. Grosby and C. Riediger Field Trip Guidebook No. 14. GeoCanada 2000, Calgary, 01 May 2000.

80. M.G. Fowler, C.L. Riediger and J. Obermajer, "New Insights into the Origin of the Alberta Tar Sands of the Werstern Canada Basin, the World's Largest Hydrocarbon Deposit", Abstract of Papers, 20th International Meeting on Organic Geochemistry, Sept. 10–14, 2001, Nancy, France.

81. C.L. Riediger, R. MacDonald, M.G. Fowler, L.R. Snowdon and M.D. Sherwin, "Origin and Albertion of Lower Creaceous Mannville Group Oils from the Provost Oil Field, East Central Alberta, Canada", Bull. Can. Petrol. Geology, 47 (1999) 43.

82. S. Creaney, J. Allan, K.S., K.S. Cole, M.G. Fowler, P.W. Brooks, K.G. Osadetz, R.W. MacQueen, L.R. Snowdon and C.L. Riediger, "Petroleum Generation and Migration in the Western Canada Sedimentary Basin", in Geological Atlas of the Western Canada Sedimentary Basin, Eds. G.D. Mossop and I. Shetsen, Can. Soc. Petrol. Geologists and Alberta Research Council, 31 (1994) 455.

83. C.L. Ridiger, "Migration of "Nordegg" Oil in the Western Canada Basin. How Much and How Far?", Bull., Can. Petrol. Geology, 42 (1994) 63.

84. J. Allan and S. Creaney, "Oil Families of the Western Canada Basin", Bull. Can. Petrol. Geology, 39 (1991) 107.

85. S. Creaney and J. Allan, "Hydrocarbon Generation and Migration in the Western Canada Sedimentary Basin", in Classic Petroleum Provinces, Ed. J. Brooks, Geol. Soc. Spec. Publ. No. 50 (1990) 189.

Appendix 13.1

Sterols are important biological molecules with many biological roles. In eukaryotes one of these roles is to increase the rigidity of cell membranes. Cholesterol has many possible stereo isomers, but living organisms synthesize only one of them, which is designated as 14α(H), 17α(H), 20R. The sterol molecules contain polar and nonpolar ends and this amphipathic character, combined with the flat molecular geometry, enables them to fit into the lipid membrane structure. In prokaryotic organisms the counterpart of sterols in the reinforcing the rigidity of the cell membranes is the hopanetetrol (and related molecules). These two molecules have similar sizes and shapes and they both are amphipathic.

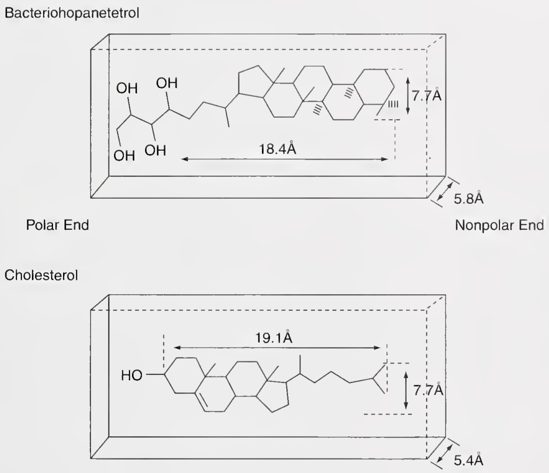
Bacteriohopanetetrol
OH
OH
OH
OH
18.4Å
7.7Å
5.8Å
Polar End
Nonpolar End
Cholesterol
19.1Å
HO
7.7Å
5.4Å

This explains the ubiquitous occurrence of hopanes and steranes in crude oils and sedimentary organic matters.[8]

Chemical Composition of Asphaltene

14

1.0 Introduction

Petroleum and bitumen, as stated before, comprise a highly complex mixture of organic and organometallic compounds as well as clay-organic complexes and their aggregates, the individual components of which exhibit wide variations in elemental composition, structure and size, and consequently in their chemical and physical properties. Many of the constituent molecules are polar; some may even carry electric charges, unpaired electrons, or both, and have a tendency to aggregate under the influence of the intermolecular forces acting among them. The loose aggregates of various sizes formed with internal structures are then colloidally suspended in the liquid portion of the oil. This agglomeration introduces additional layers of structure in petroleum and especially in bitumen, which may have a significant impact on the macroscopic properties of these materials. It is, then, not surprising that the constituent molecules of various compound classes and polydispersed aggregates exhibit a broad variety of solubility characteristics with respect to the oily portion of petroleum and organic solvents, which is further complicated by various adsorption phenomena. This property has been exploited for the fractionation of the oil according to molecular size, polarity and structural type.

Asphaltene is a friable, amorphous, thermolabile, dark solid which, upon heating, decomposes with intumescence without a sharp melting point, while giving off first water vapor and then gases and other vapors. When it is separated from the crude by solvent precipitation, which today is the generally accepted method for the isolation of this material, asphaltene has a dark brown color. After removal of the chemisorbed resins and low-MW asphaltene fragments, the residual asphaltene left behind after evaporation of the solvent is black and the chemisorbed material is deep reddish-brown. In solution asphaltene has a dark color, the intensity of which varies with concentration, but it does not turn red or any other spectrally clean color at any concentration. It is, however, possible to isolate from the crude asphaltene small quantities of colored individual components of the chemisorbed material (*e.g.* fluorenones—bright red; polycondensed aromatics and condensed thiophenes—yellow/orange; various vanadyl porphyrins—violet, green, yellow, *etc.*). The amounts of these foreign substances in the precipitated asphaltene vary with the particulars of the parent crude and the precipitation process.

For petroleum chemists the term “asphaltene” is generally applied in the narrow sense of petroleum asphaltene. There are, however, other asphaltenes, some of which are related while others are unrelated to petroleum, such as shale oil asphaltene, asphalt asphaltene, coal tar asphaltene, coal liquid asphaltene, *etc.* There is, of course, no compelling reason why all these asphaltenes should have the same chemical composition or why they should bear more than a casual resemblance in their chemical composition or structure; they are grouped together solely on the basis of their solubility characteristics.[1] They may be chemically distinctly different materials and, as has been aptly remarked,”the similarity between coal and petroleum-derived asphaltenes begins and ends at the definition of the separation procedure”.[1] Coal asphaltenes, for example, have lower MWs and hydrogen and sulfur contents, and higher aromaticity and oxygen contents—mainly in phenolic OH and carbonyl forms—than petroleum asphaltenes.

Another type of asphaltene is the one that is associated with "rock bitumen", a constant companion of kerogen in sedimentary rocks. The asphaltene found in sedimentary rocks, oil sands, carbonate bitumens and crude oils is probably the second most abundant form of organically-bound carbon on earth, after kerogen. This adds an epistemological dimension to the occurrence and chemistry of asphaltene.

Petroleum asphaltene itself falls into different groups according to molecular structure as well as chemical and physical properties and we also have to distinguish between native asphaltenes and processed asphaltenes (in atmospheric residues, vacuum residues, cracked and hydrocracked oils, *etc.*) because of substantial differences in their compositions, molecular sizes and other properties. Regrettably, this is not always done in practice and can be a source of confusion in the literature.

The "definition" of asphaltene can be formulated on two levels—the level of operational formalism and the level of molecular structural compound class type. In operational terms, asphaltene was originally defined by Boussingault in 1837 as the distillation residue of a bitumen.

The term "asphaltene" was first coined by the French chemist J.B. Boussingault in 1837 (Ann. Chim. Phys., V. 64 p. 141), some two decades antecedent to the birth of the petroleum industry marked by the discovery of petroleum in Pennsylvania in 1859. In his studies on an oil sand bitumen from eastern France and asphalts from Peru, he observed that the bitumen sample, on distillation, gave a volatile, oily liquid soluble in ether, that he named "petrolene" (after petroline for paraffin wax) and a brittle, shiny solid residue insoluble in alcohol and soluble in essence of turpentine which he named "asphaltene".[*]

Led by his observation of a broad range of distillation temperatures for "petrolene", Boussingault recognized that petrolene is not a single compound but rather a mixture of many different compounds and he suggested that the ratio of the two basic constituents of bitumen, "petrolene" and "asphaltene", can vary continuously from sample to sample. Boussingault's original definition of asphaltene as the nondistillable residue of bitumen has since been changed to a solubility-based definition, although, until quite recently in some cases, reported data on asphaltene still referred to whole vacuum residues.

At the time of the first isolation of asphaltene, molecular sciences were in an embryonic state of development. Few organic compounds had been isolated in relatively pure state and the structure of even the simplest molecules was still a matter of controversy. Atomic weights were in an array of confusion; for example, most chemists used six for the ratio of atomic weights of carbon and hydrogen and others, 12.25 (the current value is 11.92). Laboratory techniques and equipment were equally rudimentary. Yet, rather remarkably, Boussingault's determination of the elemental composition of Bechelbronn (eastern France) oil sand "petrolene" in 1837 gave C 88.3% and H 12.0% resulting in an H/C value of 1.62, which falls in the mean range of ~1.6–1.7 for the distillable part of oil sand maltenes. Boussingault recognized "petrolene" to be a mixture of hydrocarbons and, from his results on asphaltene, C 75.0%, H 9.9%, O 14.8%, asphaltene appeared to be an oxidized hydrocarbon.

Much later, in the early part of this century, Marcusson[2] introduced a solvent precipitation method using petroleum naphtha. The use of *n*-pentane precipitant was suggested by Strieter in 1941[3] and its use for the isolation of Athabasca asphaltene was first reported by Pasternak and Clark in 1951.[4] In current practice, the choice of precipitant is usually *n*-heptane and asphaltene is defined as that portion of the crude oil that is soluble in toluene (or organic solvents having solubility parameter values in the 17.5–22.2 MPa$^{1/2}$ range) and insoluble in *n*-

---

[*] From the word "asphaltum", that probably originated from the Akkadian and came into the English and French vocabularies through the Greek "asphaltos", since it resembled asphalt in most respects.

heptane. The difference in yield (and composition) between *n*-pentane and *n*-heptane asphaltene varies from sample to sample (between the extremes of 10–98%), the *n*-heptane precipitate always being the smaller. But even the *n*-heptane precipitate always contains adsorbed resinous and other maltene materials (carboxylic acids, fluorenones, fluorenols, polycyclic aromatized terpenoids, thiolane- and thiane-derived and acyclic sulfoxides, carbazoles, quinolines, vanadyl porphyrins, *etc.*), hydrocarbons, as well as low-MW asphaltene fragments. Thus, the solubility-based definition encompasses not only all the various groups of asphaltene, but all those materials which are foreign to the bulk of the asphaltene in size, chemical composition and properties; in the conceptual "definition" of asphaltene they are not considered to belong to asphaltene.

From the standpoint of industrial recovery and transportation of crude oil and crude oil products, it is the operational definition that is paramount in most instances whereas in the upgrading of bitumen and refining of heavy crudes the molecular structural property-based definition is equally important. Conceptually, petroleum asphaltenes are soluble, polydisperse, random organic geomacromolecules with a strong tendency to form supramolecular aggregates. Small molecules such as, for example, a bicyclic terpenoid sulfoxide,

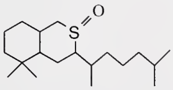

even though tending to come down with asphaltene on precipitation, do not belong to asphaltene from a compositional point of view: they are merely coprecipitated or adsorbed foreign substances, the bulk of which can be readily removed from the asphaltene. In scientific studies conducted for the elucidation of the covalent molecular structure or other fundamental chemical or physical properties of asphaltene, it is imperative that all foreign substances be removed from the asphaltene proper as completely as possible without significant loss of the asphaltene itself. The task of structural elucidation of the polydispersed, random asphaltene macromolecule is arduous enough in itself without having to deal with the presence of interfering foreign substances. This self-evident principle is often overlooked in practice.

Apart from solvent extraction–solvent precipitation, asphaltene may be separated by chromatographic methods. During the 1930s much work was done in Germany on refining Marcusson's solvent precipitation method and on developing new elution chromatographic methods for the isolation of asphaltenes. Coal asphaltenes, for example, were separated from coal hydrogenation products by elution chromatography over either Fuller's earth (a mixture of montmorillonite, kaolinite and halloysite) or Terrana earth. The methods were reported to give reproducible results. More recently gel permeation, high-performance liquid adsorption, ion exchanger and thin-layer chromatographic methods for the separation of asphaltene have also been developed.

The fundamental properties of asphaltene, as of other substances, are determined by chemical composition, molecular structure, molecular conformation, colloidal structure and size. Recent studies have revealed an unexpected close compositional and structural similarity among native petroleum asphaltenes from a variety of sources with relatively small and characteristic variations, reflecting differences in origin (biotic source materials), source rock, depositional environment and conditions, diagenetic, migrational and thermal history of their formation. Because of its thermal reactivity, during the thermal maturation of the deposit asphaltene may undergo profound chemical alterations.

Until not long ago asphaltene was considered by many to have an intractable and undecipherable molecular structure. True, the asphaltene molecule presents a most formidable challenge to the structural chemist, but progress is being made and ultimately it will lead to a satisfactory understanding of the complex and intricate covalent structure of this molecule. Presently, asphaltene may be thought of as not-so-random covalently-bound assemblages of small to mid-size alkyl- and naphthenoaromatic hydrocarbons and their sulfur and, to a lesser extent, nitrogen, derivatives. Some of these structural units are linked together by, in addition to C–C linkages which can extend to quite long-chains, C–S (and C–O) hetero linkages.

The "not-so-random" -ness requires comments. This term simply reflects the recognition that, hidden under the apparent randomness, some clear molecular structural principles prevail and, aside from some relatively minor characteristic variances, they apply to most of the asphaltenes studied regardless of age, origin, burial depth (within limits) or geographical and even continental location.

Early indications that petroleums and asphaltenes in petroleums are colloidal systems were reported[5] at the beginning of the century. In the period 1923 to 1933 Nellensteyn,[6] through his studies of the surface tension and rheological properties of bitumen, arrived at the conclusion that bitumens are micellar colloidal systems. According to Nellensteyn the nucleus of the micelles comprises micro-crystalline graphite* and high-MW organic particles of asphaltene surrounded by protective bodies (resin molecules) bound to the asphaltene particles by adsorptive forces. Nellensteyn's original ideas were subsequently further developed by Pfeiffer (1950).[7] According to the Nellensteyn-Pfeiffer theory the asphaltenes in asphaltic bitumens are "the centers of micelles which are formed by adsorption and perhaps partly by absorption of part of the maltenes on the surfaces or in the interiors of the asphaltene particles". This micellar model was believed to be consistent with the existing data on solubility, surface tension, viscosity and other known rheological properties of bitumens and the strong dependence of molecular weight values on the method used for their determination. Pfeiffer and Saal[8] also recognized that graphite cannot be an integral component of asphaltene and stated that "asphaltenes in all probability consist of high-molecular hydrocarbons of a predominantly aromatic character", with "some oxygen, some sulfur and a still smaller quantity of nitrogen" in them. Determining the molecular weights of several asphaltenes using Langmuir's monomolecular film method, Pfeiffer and Saal obtained values that ranged from 9,000 to 140,000 $g \cdot mol^{-1}$ which they identified with the approximate molecular weights of the micelles. Methods for molecular weight determination based on colligative properties—vapor pressure lowering or freezing point depression—gave much smaller values, in the 1,500–4,500 $g \cdot mol^{-1}$ range. These early investigations on the "micellar" properties of asphaltenes laid the foundation for more recent studies from the mid-1950s on.

Since the early work of Nellensteyn and Pfeiffer in the 1930s, the enigma of the chemical composition of petroleum asphaltene and asphaltenes in general has yielded slowly, reluctantly, and not without controversy, to the determined enquiries of petroleum and coal chemists. Another property of the asphaltene which has hampered molecular structural studies of this complex-enough substance is its tendency to form molecular complexes with a broad variety of nonasphaltene molecules normally present in petroleum. Nonetheless, progress in our conceptual understanding of the molecular architecture of asphaltene has lately accelerated and led to important advances. This has been made possible by the development of high-performance, high-resolution chemical instrumentation with advanced data processing capabilities (such as computerized capillary GC and capillary GC/mass spectrometry, ^{1}H and ^{13}C NMR spectroscopy, capillary GC/FTIR, UV spectroscopy, electron paramagnetic resonance (EPR) spectroscopy, instrumental neutron activation analysis (INAA), X-ray absorption near edge structure (XANES) spectroscopy, *etc.*), improvements in chromatographic and chemical separation techniques, and progress in petroleum chemistry, organic geochemistry, biomarker chemistry and colloid chemistry. In the latter field, advances in the areas of scattering sciences—small-angle neutron scattering (SANS), small-angle X-ray scattering (SAXS), scanning tunneling microscopy (STM), high-resolution transmission microscopy (HRTEM), ultracentrifugation, microfiltration, flocculation and various aggregation phenomena studies, *etc.*—permitted significant strides in investigations of the colloidal states of asphaltenes.

---

*This conclusion, derived from an ill-conceived experiment, was based on the appearance of the graphite diffraction pattern in the diffractogram of an asphaltene sample that he had subjected to ether extraction over a period of a year and as a consequence it became partly insoluble in CS_2 (since it was partly converted to carboid).

Lastly, advances in the experimental methods are now being supplemented by chemical computational approaches within the framework of molecular mechanics. This method permits the calculation of the most stable conformation of molecules and their aggregates both in vacuum and in solution.[9] Analytical functions are used to represent bond stretching, bending and torsional as well as nonbonded (electrostatic interactions, dispersion attraction and exchange repulsion) energies of molecules. To start, an initial configuration is specified and the interatomic distances and bond angles are adjusted, employing an iterative computational method until the minimum energy configuration is obtained. In order to distinguish between local minima and true minima, several different starting configurations are used. If the same minima are obtained, then one can assume that the minima are representative of the conformations of interest. For meaningful computational results, detailed knowledge of the covalent molecular structures of asphaltene and resin molecules would be required and this can be obtained only from experimental studies. Parallel to the above studies, better descriptions of the solubility characteristics of asphaltene have also been developed, most of which are based on thermodynamical approximations.

The presence of colloidally-dispersed asphaltene in petroleum affects the viscosity, density (specific gravity) and elemental composition of the crude, which properties are of paramount importance in determining the commercial value of the oil and the technology required for its recovery and refining. Heavy oils contain more asphaltene (and heavy ends) than light oils, and bitumens contain more asphaltene than heavy oils. Asphaltene is also the primary precursor of coke, the solid carbonaceous by-product of the coking step in the upgrading of bitumen to synthetic crude oil.

Among the physical properties of asphaltene from a technological point of view, one of the most important ones is its solubility because the undesired spontaneous precipitation of asphaltene can cause severe operational difficulties in every stage of the processing and handling of petroleum. Heavy oils and bitumens have high asphaltene contents and as a first guess one may conclude that these oils are more prone to precipitate their asphaltenes than are lighter oils with lower or very low asphaltene contents. However, one has to remember that asphaltene is thermolabile and light oils with low asphaltene contents often come from deep reservoirs with high geothermal temperatures. Owing to their extensive geothermal history, the asphaltene fractions of these oils are cracked in reactions not unlike those in upgrading operations. As a result, the alkyl side chains, bridges and other appendages are lost, and this leads to an increase in aromatic condensation and an increase in the alkane and aliphatic content of the maltene fraction: each of these changes negatively affects solubility and together they may effect a strong reduction in the solvent power of the maltene and the solubility of the residual asphaltene in the oil. Also, it is possible that asphaltene precipitation takes place in the reservoir and that the supernatant oil becomes saturated with asphaltene. In a deep reservoir the temperature and pressure are both high and during the passage of the oil to the surface as the values of these parameters decline, the solubility of the asphaltene will decrease and this may cause further precipitation.

Heavy oils, on the other hand, have experienced as a rule only mild exposure to geothermal heat, their asphaltene's alkyl complement is intact and the high aromatic and resin contents of their maltene fraction makes this maltene an excellent solvent for asphaltene, capable of peptizing large amounts of it.

As the preceding discussions demonstrate, solubility—as are other properties—is determined by molecular composition, structure, size, conformation and colloidal structure. The same parameters determine chemical reactivity as well.

Asphaltene has the least favorable composition of the crude oil fractions: it has the highest NOS, metal and ash contents, the lowest H/C ratios and the highest MW and aggregation state. Also, asphaltene is known to be the most important source of coke during the cracking and refining operations. The residual asphaltenes from these operations, aside from their solubility-based operational definition, may have little in common with their predecessor, the native asphaltene. Their MW is much reduced, alkyl, sulfide and other bridges broken and appendages largely removed, and at the same time their aromaticity increased.

Athabasca oil sand asphaltene is one of the most extensively investigated asphaltenes. Instrumental and, in particular, chemical studies have brought to light many structural features of this material and led to the detection and identification of a host of constituent molecules. Some of the architectural principles of this asphaltene have also been elucidated and the roles of C–C, C–S (and C–O) bridges and side-chain appendages demonstrated.

2.0 Solubility Characteristics and Precipitation of Asphaltenes

The solubility of asphaltene in the maltene of crude oil and the stability of the asphaltene solution with respect to precipitation are of considerable interest to all phases of the petroleum industry—recovery, transportation, storage, refining, upgrading—where asphaltene precipitation can cause troublesome operational difficulties. When conditions under which the asphaltene solution is stable are changed, asphaltene precipitation may take place. Asphaltene solubility may be affected by composition (addition and mode of addition of a miscible solvent, chemical reactions), temperature, pressure, contact with surfactants, metal or hydrogen ions (*pH*), exposure to an electrical potential differential such as that generated by moving charges when the oil flows in a conduit (electrokinetic effect), frictional electricity (triboelectric effect), mechanical shear (shaking, acoustic vibration), *etc.*

Asphaltene precipitation may occur spontaneously in the reservoir as a result of petroleum gas buildup. In a pooled reservoir the precipitated asphaltene may settle to the bottom resulting in an improvement in the quality of the supernatant crude (lower density, viscosity and heteroatom content). Troublesome asphaltene precipitation may take place in the near-wellbore region where asphaltene deposition can block pore throats resulting in a reduction of permeability, changes in wettability and a reduction in the cross-sectional area for flow during the oil recovery operation. The asphaltene particles in the oil have been postulated to carry some positive surface charge and therefore preferentially deposit on pores containing kaolinite, which is negatively charged. (This could also occur in interfaces with acidic media[10] at *pH* values ≤ 6.5 (*v.i.)*.) In the course of thermal processing of the oil or upgrading of the bitumen, asphaltene precipitation leads to coke formation and enhanced coke yields. Another occurrence of asphaltene precipitation is in the laboratory during the analytical determination of the asphaltene content of oil samples.

The separation of asphaltene can be achieved by either digestion of the sample with a precipitant (n-C_5 or n-C_7) or precipitation with a precipitant from a concentrated solution of the sample in a diluent. The quantities and properties of the precipitated asphaltene depend on the temperature, nature and quantities of diluent and precipitant used. (For this reason, in data reporting it is desirable to indicate the precipitant used in the isolation of the asphaltene by a prefix, *e.g.* n-C_5-asphaltene, n-C_7-asphaltene, *etc.*) The solvent power and precipitate-forming efficiency of many hydrocarbon liquids have been investigated and compared. Some results, showing the variation in the percentage amount of precipitate formed from Athabasca bitumen and from an Arabian light atmospheric residue diluted with an equal volume of benzene upon addition of 40 volumes of the specified solvent at room temperature as a function of the carbon number of various types of hydrocarbons,[11,12] are shown in Figure 14.1. The precipitate yield in both cases is highest with the smallest alkane used, propane, and decreases rapidly at first and then more gradually with increasing carbon number in the three most efficient series of precipitating agents, 2-methyl-alkanes, n-alkanes and terminal alkenes. The efficiency of bringing about precipitation for these three series of hydrocarbons follows the order of listing. Cycloalkanes, on the other hand, are relatively good solvents for petroleum asphaltene, although not for coal asphaltene, and therefore are inefficient precipitating agents. The ability of a solvent to solubilize asphaltene or, in general, to dissolve a solid or to form a homogeneous solution with another liquid, may be expressed in terms of solubility parameters.

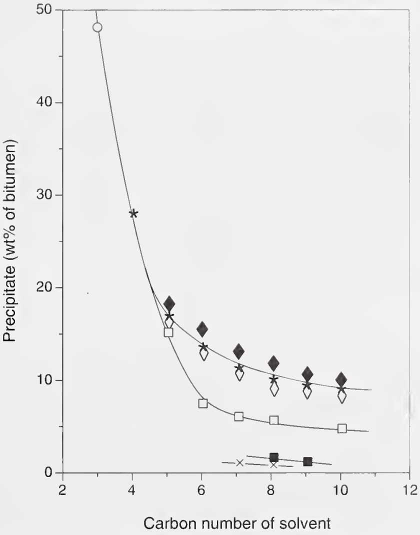

Figure 14.1 Precipitate yield from Athabasca bitumen and Arabian light atmospheric residues as a function of carbon number of the precipitant. Athabasca: ⋆, n-alkanes; ◆, 2-methyl paraffins; ◊, 1-alkenes; ×, cycloparaffins; ■, methylcyclo-paraffins. Data from Ref. 11. Arabian: □, n-paraffins. Data from Ref. 12.

2.1 Solubility parameters

Solubility parameters are molecular properties which are defined either in terms of the cohesion energy density or the internal pressure of the solvents, which are assumed to be nonpolar liquids. Thus, Hildebrand[13] defined a solubility parameter which is related to internal pressure as the ratio of the surface tension and the cubic root of the molar volume,

$$\delta_1 = \gamma V^{-1/3} \tag{1}$$

$$(\mathrm{dyn \cdot mol^{1/3} \cdot cm^{-2} = 0.1\ N \cdot mol^{1/3} \cdot mm^{-2} = 10^5\ J \cdot mol^{1/3} \cdot m^{-3}})$$

where δ_1 is the solubility parameter, γ is the surface tension and V is the molar volume.

Subsequently, Hildebrand, Prausnitz and Scott[14] designated the energy of vaporization per cubic centimeter as the cohesion energy density and defined its square root as another solubility parameter,

$$\delta_2 = \left(\frac{\Delta E_v}{V}\right)^{1/2} = \left(\frac{\Delta H_v - RT}{V}\right)^{1/2}$$

(hildebrand = $\text{cal}^{1/2}\cdot\text{cm}^{-3/2}$ = $(\text{MPa}^{1/2})/2.04$)

where ΔE_v and ΔH_v are the energy and the enthalpy of vaporization, R is the universal gas constant and T is the temperature (K). The more widely-used parameter, $\delta_{2,}$ is important in the estimation of the heat of mixing for two nonpolar liquids a and b:

$$\Delta H_m \approx \Delta E_m = \phi_a\phi_b(x_a V_a + x_b V_b)(\delta_a - \delta_b)^2 \tag{3}$$

where the ϕ's are the volume fractions of the liquids and the x's are their mole fractions. From the free energy equation

$$\Delta G_m = \Delta H_m - T\Delta S_m, \tag{4}$$

where ΔG_m is the free energy and ΔS_m the entropy of mixing, it is evident that, in order to obtain a negative value for ΔG_m, which is necessary for mixing to occur, ΔH_m must be reduced. This can be achieved if δ_a and δ_b have similar values. The entropy of mixing, ΔS_m, usually has positive values and thus, the important conclusion we have arrived at is that, for mixing of two nonpolar liquids or dissolution of a nonpolar solid in a nonpolar solvent to occur, the components should have similar δ values. Liquids differing by two hildebrands in their δ values are generally incompletely miscible, since the internal pressure (holding a unit volume of liquid together) exerted by the liquid with the higher internal pressure (*i.e.* higher solubility parameter) will "extrude" the molecules of the liquid with the lower internal pressure (lower solubility parameter) out of the solution matrix.

The solubility parameter theory was derived for regular solutions, which are defined as solutions for which the entropy change on mixing, $\Delta S_{m,}$ equals the ideal value and the volume change on mixing, $\Delta V_{m,}$ is zero, but no restriction is imposed on the enthalpy of mixing. These criteria are usually satisfied by solutions of nonpolar solutes in nonpolar solvents where the primary intermolecular forces are London dispersion forces (instantaneous dipole-induced dipole interactions). However, the above criteria are not satisfied when: a) the solute and solvent molecules are polar (in which case dipole-dipole, dipole-induced-dipole, charge transfer and hydrogen bonding interactions may become important); b) specific molecular orientation effects are operative; c) the solvent and solute molecules have rather different sizes; and d) the low density of one of the liquids is near its critical point. Therefore, the solubility parameter theory would not be expected to be applicable for colloidal aggregate solutions of polar, random, polydispersed macromolecules like asphaltenes. Yet, as will be seen from the data available, the correlation between the solubility of asphaltene and solvent solubility parameter is quite good for nonpolar and low-polarity solvents.[15]

Nellensteyn[16] was the first to relate solvent power for asphaltene to physical properties of the solvents. He found that, for simple hydrocarbons, the percentage yield of asphaltene precipitate from bitumen decreases with increasing surface tension of the solvent. The validity of this relationship follows from the relative constancy of the cubic root of the molar volumes of saturated hydrocarbons in the expression for δ_1, Eq. (1). Subsequently, Labout[17] correlated asphaltene solubility with the δ_1 value of solvents and showed that the percentage amount of precipitate tends to decrease with increasing values of the solubility parameter δ_1 of the solvent and that precipitate formation ceases altogether above a certain value (~4.6 dyn·mol$^{1/3}$·cm^{-2}), Figure 14.2.

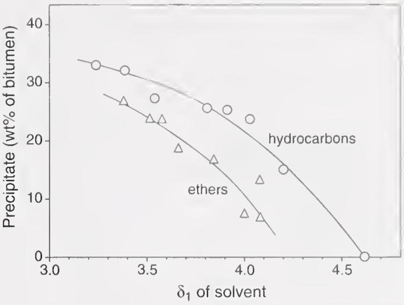

Figure 14.2 Relation of amount precipitated from a Mexican bitumen upon dilution with a 100-fold quantity of precipitant to solubility parameter δ_1. From J.W.A. Labout, Ref. 17. © 1950, Elsevier, Amsterdam.

A more exhaustive study of the correlation between asphaltene solubility and precipitation from bitumen solutions on one hand, and the solubility parameters δ_1 and δ_2 on the other, has been reported[11] on Athabasca bitumen. The yield of precipitate from a concentrated benzene solution of the bitumen upon addition of a 40-fold volume excess of a series of hydrocarbons and other liquids is tabulated in Table 14.1 and plotted as a function of the solubility parameters δ_1 and δ_2 of the precipitant in Figure 14.3, where it is seen that the yield of precipitate increases with decreasing δ_1 or δ_2. Precipitate formation ceases when δ_2 reaches a value of about 17.1 MPa$^{1/2}$ because the asphaltene becomes completely soluble in hydrocarbons with $\delta_2 \geq 17.1$ MPa$^{1/2}$. A δ_2 value can be assigned to asphaltene as well. From the observation that asphaltene becomes completely soluble in solvents with $\delta_2 = 17.1$ MPa$^{1/2}$, and since toluene, benzene, methylene chloride, pyridine and nitrobenzene with δ_2 values of 18.2, 18.9, 20.2, 21.7 and 22.5 MPa$^{1/2}$, respectively, are all excellent solvents for petroleum asphaltene, the value for δ_2 of asphaltene can be established as not less than 19.6 MPa$^{1/2}$. Thus, liquids with $\delta_2 < 17.1$ MPa$^{1/2}$ do not interact sufficiently strongly with asphaltene to break up the bonds between the asphaltene molecules by solvation and therefore would not effect complete solubilization. On the other hand, the solvation energy of the solvents with δ_2 in the 17.1–22.1 MPa$^{1/2}$ range is sufficiently large to overcome the cohesion energy of asphaltene and cause solubilization. From detailed solubility studies a value of 23.0 MPa$^{1/2}$ has been reported for a "purified" asphaltene and a significantly lower value of 20.0 MPa$^{1/2}$ for the same asphaltene in its parent oil.[18] Other values (in MPa$^{1/2}$) reported for a variety of different asphaltenes using different methods of measurement include:

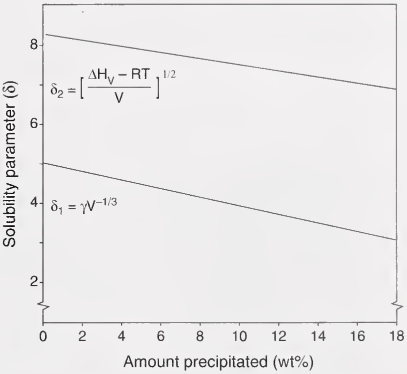

Figure 14.3 Relation of amount precipitated from Athasbasca bitumen to solubility parameters, δ_1 and δ_2, using pure solvents and solvent blends. After D.L. Mitchell and J.G. Speight, Ref. 11. © 1973, Butterworth-Heinemann, Oxford, U.K.

20.5[19]
20.60–20.92 (crude oil)[21]
20.7 (δ_D, δ_P, δ_H: 20.2, 2.0, 4.0)[22]
20[24]
21.9–21.5[20]
21.15–21.90 (n-C$_7$ asphaltene)[21]
19.50; 20.04 ($1-1.07 \times 10^{-3}$T°C)[23]

Figure 14.3 also features data on binary benzene–*n*-pentane solvent mixtures, the δ values of which are additive and can be calculated from the molar compositions of solvents a and b:

Table 14.1 Yields of precipitate from Athabasca bitumen using various solvents[a]

Solvent	Solubility parameter, δ			Precipitate
	$gV^{-1/3}$	$[(\Delta H_V - RT)/V]^{1/2}$		wt% bitumen[b]
	(dyn·mol$^{1/3}$·cm^{-2})	(cal$^{1/2}$·cm$^{-3/2}$)	MPa$^{1/2}$	
normal hydrocarbons				
pentane	3.2	7.0	14.4	16.9
hexane	3.5	7.3	14.9	13.5
heptane	3.8	7.5	15.3	11.4
octane	3.9	7.6	15.4	9.8
nonane	4.0	7.7	15.6	9.4
decane	4.1	7.7	15.8	9.0
2-methyl hydrocarbons				
*iso*pentane	3.1	6.8	13.8	17.6
*iso*hexane	3.4	7.1	14.4	15.3
*iso*heptane	3.7	7.2	14.8	12.8
*iso*octane	3.8	7.4	15.0	11.5
*iso*nonane	3.9	7.5	15.4	10.0
*iso*decane	3.9	7.6	15.5	9.8
terminal alkenes				
pentene	3.4	7.1	14.6	16.2
hexene	3.6	7.3	15.0	13.0
heptene	3.8	7.5	15.4	10.9
octene	4.0	7.6	15.6	9.0
nonene	4.1	7.7	15.8	8.6
decene	4.1	7.8	16.0	8.5
cycloparaffins				
cyclopentane	5.0	8.2	16.8	1.0
methylcyclopentane	4.6	7.9	16.2	1.4
ethylcyclopentane	4.6	9.0	18.5 (?)	1.9
cyclohexane	5.3	8.2	16.8	0.7
methylcyclohexane	4.7	7.9	16.2	1.0
ethylcyclohexane	4.9	8.1	16.6	1.4
decalin	5.5	8.6	17.6	0
aromatics				
benzene	6.5	9.2	18.9	0
toluene	6.0	8.9	18.2	0
o-xylene	6.1	9.0	18.5	0
m-xylene	5.8	8.8	18.0	0
p-xylene	5.7	8.8	18.0	0
ethylbenzene	5.9	8.8	18.0	0
n-propylbenzene	5.6	8.7	17.8	0
n-butylbenzene	5.4	8.6	17.6	0
miscellaneous hydrocarbons				
2,2,4-trimethylpentane				
*iso*octane	3.4	6.9	14.1	15.8
*neo*pentane	2.4	6.2	12.7	21.5
*neo*hexane	3.2	6.7	13.7	17.9
cyclohexene	6.0	8.5	17.4	0
other solvents				
pyridine	8.6	10.6	21.7	0
nitrobenzene	9.3	10.8	22.1	0
chloroform	6.3	9.2	18.9	0
carbon tetrachloride	5.8	8.6	17.6	0
methylene chloride	7.1	9.8	20.1	0

[a] After D.L. Mitchell and J.G. Speight, Ref. 11. © 1973, Butterworth-Heinemann; used in the construction of plots in Figure 14.3. [b] Bitumen was diluted with an equal volume of benzene before precipitation with a 40-fold volume of *n*-pentane.

$$\delta_{ab} = \frac{x_a V_a \delta_a + x_b V_b \delta_b}{x_a V_a + x_b V_b} \tag{5}$$

where xs and Vs are the mole fractions and molar volumes.

The observed variation in the quantities of precipitate formed as a function of the δ_1 values of the solvents in Table 14.1 and Figure 14.3 is closely similar to that using δ_2 values.[11] From the limiting δ_1 values at which precipitation ceases, for example, with cyclohexane having $\delta_1 = 5.3$ dynes·mol$^{1/3}$·cm^{-2} and a precipitate yield of only 0.7%, the maximum value of the surface tension of the solvent at which precipitation still takes place can be estimated. Thus, taking the molar volume of cyclohexane, 108.7 cm^3·mol^{-1}, and multiplying its cubic root, 4.8 cm·mol$^{-1/3}$, by $\delta_1 = 5.3$ dynes·mol$^{1/3}$·cm^{-2}, we obtain for γ, the surface tension of the liquid at which precipitation still occurs, 25.4 dynes·cm^{-1}. All good solvents for asphaltene, such as benzene, for which $\gamma = 29.3$ dynes·cm^{-1}, have surface tensions greater than 25 dynes·cm^{-1} and poor solvents causing precipitation of asphaltene from its solution have surface tensions lower than 25 dynes·cm^{-1}, *e.g.* *n*-pentane, $\gamma = 15.7$ dynes·cm^{-1}.

More advanced theoretical treatments of solubility parameters have led to the extension of the range of their applicability to include polar molecules. In one such treatment the effective solubility parameter is the sum of three independent components:

$$\delta = \sqrt{\delta_D^2 + \delta_P^2 + \delta_H^2} \tag{6}$$

δ_D is included to take into consideration the dispersion forces which nearly correspond to the δ_2 values listed in Table 14.1, δ_P to take into consideration the polar, and δ_H, the hydrogen bonding interactions. This so-called three-dimensional solubility parameter theory is capable of giving satisfactory accounts of the solubility behavior of many weakly polar molecules and may explain, Table 14.2, why pyridine, quinoline and nitrobenzene, for example, are better solvents for asphaltene than carbon disulfide. In the latter molecule only dispersion forces are operative, but in the former solvents, moderate-strength polarization and hydrogen bonding interactions are also operative in addition to strong dispersion forces. Nonetheless, the intermolecular force dominating the solubility of asphaltene is the dispersion force and the interaction energy arising from this force is proportional to the product of the polarizabilities of the asphaltene and the solvent (*v.i.*). The polarizabilities of aromatic compounds are, in general, higher than those of paraffinic compounds and this explains their higher solvent power.

The closest match of the δ_D, δ_P and δ_H values with Athabasca asphaltene occurs for the case of naphthalene (Table 14.2), α-methylnaphthalene, (anthracene, phenanthrene), *o*-dichlorobenzene and methylene chloride; these compounds are probably the best pure solvents for asphaltene.

There are several treatments of the solubility of polymers reported in the literature. By applying thermodynamic, statistical, statistical thermodynamic and statistical mechanical models as well as fractal aggregation kinetics and, more recently, molecular mechanics calculations, various theories have been developed for homogeneous and heterogeneous polymers and asphaltenes. For asphaltene solubility and precipitation point calculations, the most notable treatment is in terms of the simple solution thermodynamic model-based equation[23] which relates the solubility of asphaltene to a combination of the solubility parameter with the Flory–Huggins entropy of mixing for polymer solutions.

In order to understand this we need to consider the equation for the energy of mixing for one mole of solution, given by the Hildebrand-Scatchard (H–S) equation

Table 14.2 Three-dimensional solubility parameters of various liquids at 25℃[15a]

Solvent	Molar volume V	Parameters ($MPa^{1/2}$)			
		δ_D	δ_P	δ_H	δ(total)
benzene	89.4	18.4	0	2.0	18.5
methyl chloride	55.4	15.3	6.1	3.9	16.9
methylene chloride	63.9	13.4	11.7	9.6	20.2
chloroform	80.7	17.8	3.1	5.7	19.0
carbon tetrachloride	97.1	17.8	0	0.6	17.8
tetrahydrofuran	81.7	16.8	5.7	8.0	19.5
diethyl ether	104.8	14.5	2.9	5.1	15.6
acetone	74.0	15.5	10.4	6.9	19.9
acetophenone	117.4	19.6	8.6	3.7	21.7
methyl *iso*butyl ketone	125.8	15.3	6.1	4.1	17.0
methyl *iso*amyl ketone	142.8	15.9	5.7	4.1	17.4
nitrobenzene	102.7	17.6	14.0	0.0	22.5
pyridine	80.9	19.0	8.8	5.9	21.8
aniline	91.5	19.4	5.1	10.2	22.5
quinoline	118.0	19.4	6.9	8.9	22.4
carbon disulfide	60.0	20.4	0	0.6	20.4
dimethyl sulfoxide	71.3	18.4	16.3	10.2	26.6
dimethyl sulfone	75.0	19.0	19.4	12.2	29.8
benzyl alcohol	103.6	18.4	6.3	13.7	23.8
cyclohexanol	106.0	17.4	4.1	13.5	22.4
o-dichlorobenzene	112.8	18.0	9.8	0.0	20.5
water[b]	18.0	15.5	15.9	42.2	47.7
asphaltene[c]		20.2	2.0	4.0	20.7
asphaltene					20.3
naphthalene		19.2	2.0	3.9	19.7
α-methylnaphthalene		20.6	0.8	4.7	21.2
phenanthrene					20.0
anthracene					20.3
pentene–1		13.9	4.1	–	14.5
hexene–1		14.4	3.9	–	15.0
heptene–1		14.6	3.6	2.7	15.3
octene–1		15.0	3.5	2.3	15.5
none–1		15.4	3.4	–	15.8
decene–1		15.7	3.3	1.3	16.0
cyclopentene		15.3	5.8	4.1	16.9
methylcyclopentane		15.7	3.5	0.0	16.0
ethylcyclopentane		15.9	3.3	0.0	16.2
ethylcyclohexane		16.1	2.6	0.0	16.3
undecane		16.0	0.0	0.0	16.0
dodecane		16.2	0.0	0.0	16.2

[a] Solid, treated as supercooled liquid. [b] Values uncertain. [c] Athabasca asphaltene with a molar mass 3, 920 g·mol^{-1} (from Ref. 22).

$$\Delta_m U_v = (x_L V_L + x_A V_A)(\delta_L - \delta_A)^2 \phi_L \phi_A,$$

where $m = V_A/V_L$, $\phi_L = x_L/(mx_A + x_L)$, $\phi_A = m\,x_A/(mx_A + x_L)$, is the molar volume and x is the mole fraction.

The most important derived molar property from the H–S equation is the activity coefficient, f_A

$$RT\ln(f_A) = RT\ln(a_A/x_A) = V_A\,\phi_A^2(\delta_L - \delta_A)^2$$

where "a" is the activity. The infinitely dilute solution where $V_A x_A << V_L\,x_L$, $RT\ln(a_A/x_A) = V_A(V_L x_L/V_A x_A + V_L x_L)^2(\delta_L - \delta_A)^2 = V_A(\delta_L - \delta_A)^2$. These equations are valid for the binary mixtures of species *A* and *L* where *n*, the molecular sizes, are not too different. If this condition is not met the inclusion of a correction term, the Flory-Huggins size effect term is necessary. This involves replacing $-R\ln x_A$ in the entropy of mixing with $-R[\ln x_A + \phi_L(1 - V_L/V_A)]$. Various modifications of the resulting equation led to different results as illustrated by Eqs. (7–9):

$$f_{VA} = \exp\left\{\frac{V_A}{V_L}\left[1 - \frac{V_L}{V_A} - \frac{V_L}{RT}\left(\delta_A - \delta_L\right)^2\right]\right\} \tag{7}$$

Here, f_{VA} is the volume fraction of asphaltene soluble in the crude oil (liquid), V_A and V_L are the molar volumes of asphaltene and crude oil (liquid) and δ_A and δ_L are the respective solubility parameters.

The Flory-Huggins term appended activity coefficient function has been used with various modifications with lesser or greater success for "molecularly dispersed" asphaltene solutions in pure solvents or solvent mixtures and in deasphaltened crude oil. Another example[22,25] of this is Eq. (8)

$$K_i = \exp\left\{1 - \frac{V_i^L}{V_m} + \ln\left(\frac{V_i^L}{V_m}\right) + \frac{V_i^L}{RT}\left(\delta_i - \delta_m\right)^2\right\} \tag{8}$$

and its three-dimensional variant, Eq. (9)

$$K_i = \exp\left\{1 - \frac{V_i^L}{V_m} + \ln\left(\frac{V_i^L}{V_m}\right) + \frac{V_i^L}{RT}\left[\left(\delta_{Di} - \delta_{Dm}\right)^2 + b\left[\left(\delta_{Pi} - \delta_{Pm}\right)^2 + \left(\delta_{Hi} - \delta_{Hm}\right)^2\right]\right]\right\} \tag{9}$$

where K_i is the equilibrium ratio x_i^s/x_i^l (x_i^s and x_i^l are the solid- and liquid-phase mole fractions of component *i*), V_i^L and V_m are the liquid-phase molar volumes of component *i* and the solvent, and the variable *b* is a weighting factor. The expression containing the squared differences of the solubility parameters in Eq. (9) is the distance between the solvent solubility "sphere" and the solubility sphere of asphaltene component *i*. The closer the two spheres, the more likely the asphaltene to be dissolved.

Eq. (7) gave good results for precipitation point predictions when nonassociated asphaltenes were treated as homogeneous substances, but predictions for the amount of precipitated asphaltene were less satisfactory. In recent studies on Athabasca asphaltene, the molar mass distribution was determined experimentally and correlations were developed for the physical properties required for the solubility calculations: molar volume and the solubility parameter. Solubility curves calculated this way for Eqs. (8) and (9) in comparison with experimental measurements are shown in Figures 14.4 and 14.5. It is seen that both the one-dimensional and the three-dimensional solubility parameter models correctly predict the solubility of asphaltene in nonpolar and slightly polar solvents including *normal* and branched alkanes, aromatics, dichloromethane, 1-hexene and decalin. In slightly more polar media the three-dimensional model gives better results for the solubility of asphaltene than the one-dimensional

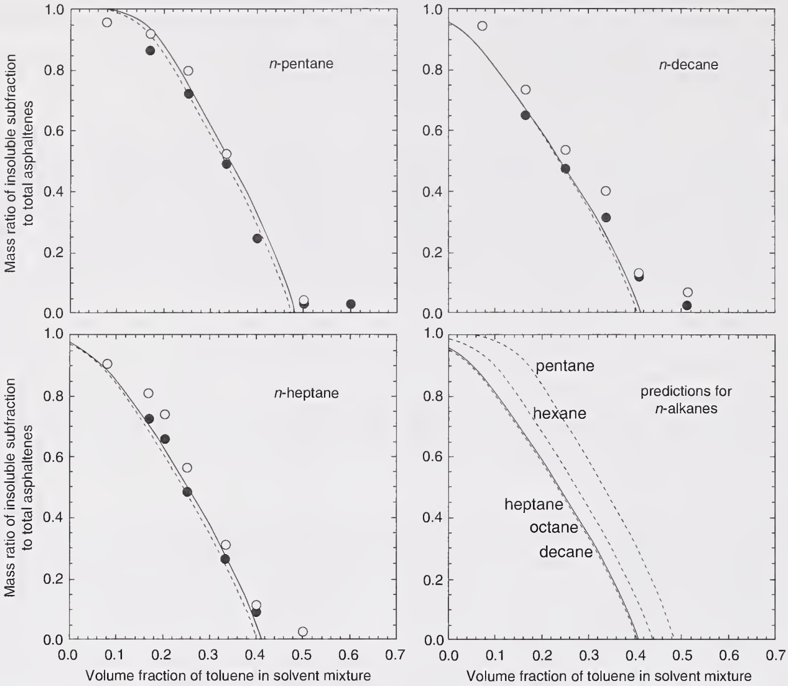

Figure 14.4 Solubility of asphaltenes in solutions of toluene/*n*-alkanes. ●, precipitation method, O, solubility method; —, one-dimensional model, Eq. (8), - - -, three-dimensional model, Eq. (9). From K.D. Mannistu, *et al.*, Ref. 22. © 1997, American Chemical Society.

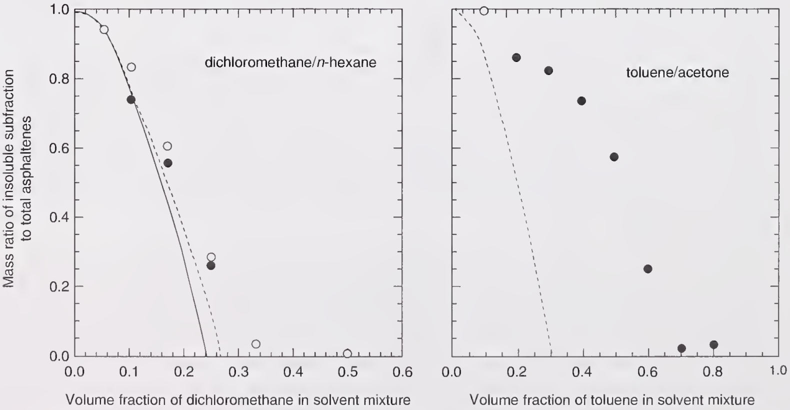

Figure 14.5 Solubility of asphaltenes in solutions of dichloromethane/*n*-hexane and toluene/acetone. ●, precipitation method, O, solubility method; —, one-dimensional model, Eq. (8), - - -, three-dimensional model, Eq. (9). From K.D. Mannistu *et al.*, Ref. 22. © 1997, American Chemical Society.

model. For highly polar solvents the one-dimensional model fails, while the three-dimensional model gives results of limited validity.*

It has also been observed[22,25,26] that the amount of asphaltene precipitate is greater when the asphaltene is dissolved from a solid form than when it is precipitated from solution. This behavior is not consistent with the solubility model for asphaltene considered thus far, and the reasons for the observed "hysteresis" will be discussed later in this chapter.

None of the solubility models discussed above takes into consideration the presence of electrical charges or free spins on asphaltene (or the stream electrical charges in a flow of oil through a pipe).

A diagrammatic approach to the solubility of asphaltene employs a two-dimensional solubility parameter field in which a closed area representing the complete solubility domain of a petroleum fraction is mapped out. The two solubility parameters used are the complexing solubility parameter δ_C and the field force solubility parameter δ_{FF}. The former is considered to be the measure of the "interaction energy that requires a specific orientation between an atom of one molecule and a second atom of a different molecule" (essentially the vectorial sum of δ_P and δ_H, *i.e.* $\delta_C = \sqrt{\delta_P^2 + \delta_H^2}$) and the latter to be the measure of "the interaction energy of the liquid that is not destroyed by changes in the orientation of the molecules". Hydrogen bonding and donor–acceptor interactions are part of the complexing solubility parameter component and van der Waals and dipole interactions are part of the field force solubility parameter component. The solvent power of each liquid is represented by a vector from the origin to a point on these diagrams, Figure 14.6, with the magnitude of the vector being the overall solubility parameter $\delta_O = \sqrt{\delta_C^2 + \delta_{FF}^2}$.

In the plots of Figure 14.6[27] the residue fractions are divided according to whether they are completely soluble, partially soluble or insoluble. This defines solubility polygon areas based on the fact that mixtures of solvents are solvents. Even nonsolvents on one side of the solubility domain can be mixed with nonsolvents on the other side to form solvents. Examples are seen in Figure 14.6D for 50–50% by volume of methyl ethyl ketone and *n*-hexane and tetrahydroquinoline with cyclohexane and with decalin.

This method, aside from its simplicity, offers the advantage that solubility is not defined by a single point—a single solubility parameter value—but instead by a visual image of a closed domain in a solubility parameter field. In the example provided by the Cold Lake residue fractions it is seen that the saturate fraction has low solubility, even in moderately-complexing liquids. The large solubility area of the aromatics is attributed to the low molecular mass of this fraction, the lowest among the fractions. Asphaltene, as seen, requires high δ_{FF} and low δ_C values for maximum solubility. It is noted that solvents for coke represent a subset of solvents for asphaltene, asphaltene for resins, resins for aromatics meaning that solvents for asphaltene are solvents for resins, *etc.* and neither these fractions can be solvent extracted but can readily be precipitated.

---

* It is interesting to note the linear relationship in Figure 14.3 between measured asphaltene solubility and the solubility parameter ($q = \alpha\,(\delta - 8.5)$, where q is the amount of precipitate formed and α is a proportionality factor) in contrast to the exponential character of Eqs. (7–9) as well as that of the equation $\ln x_a = -M_a / RT\rho_a\,[(\delta_s - \delta_a)^2]$ (where x_a is the mole fraction solubility of the asphaltene, δ_s and δ_a are the solubility parameters of the solvent and the asphaltene, M_a is the molecular weight and ρ_a is the density of asphaltene) derived from the activity coefficient function without the Flory-Huggins correction term. J.G. Speight, The Chemistry and Technology of Petroleum, Third Edition, 1999, Marcel Dekker, N.Y. p. 452.

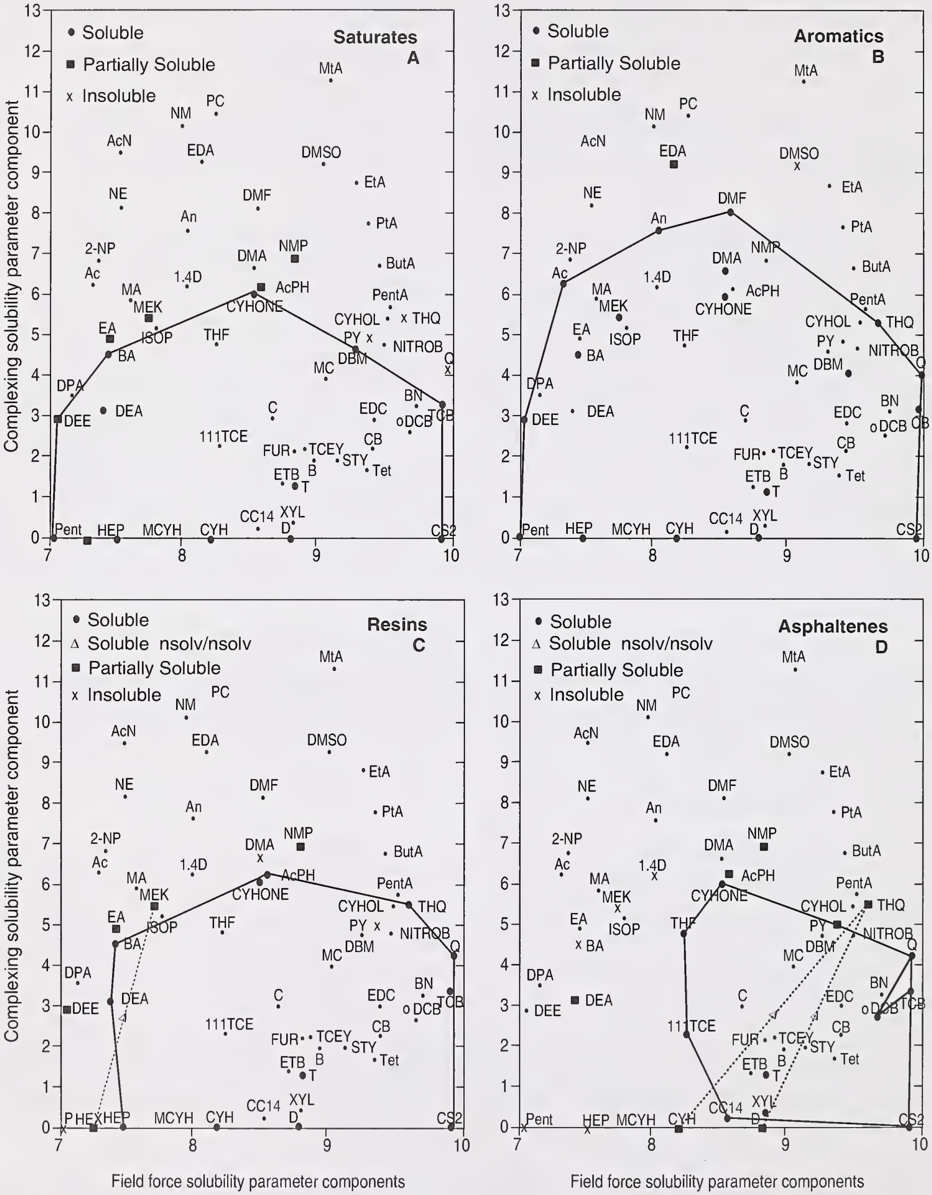

Figure 14.6 Two-dimensional solubility parameter diagrams for Cold Lake saturates, aromatics, resins and asphaltenes at concentrations 0.1 g/25 mL. The dark triangle in the asphaltenes diagram represents coke. From I.A. Wiehe and S.K. Liang, Ref. 27. © 1996, Elsevier.

The method is clearly an empirical one and the diagrams in Figure 14.6 would have to be determined for each asphaltene (fraction) sample over the entire solubility range.

A simple schematic approach to the solubility of asphaltene[28] is based on a phase diagram representation in terms of polarity and MW. In the schematic MW *versus* polarity plot shown in Figure 14.7 the diagonal line for *n*-heptane indicates the phase distribution between precipitated asphaltene, above and to the right of the diagonal line, and the *n*-heptane solution of the asphaltene below and to the left of the line. As seen from the diagram, less-polar materials of higher MW and more-polar materials of lower MW both precipitate as asphaltene. With *n*-pentane as the precipitating agent the diagonal line shifts to the left including both less-polar and lower-MW materials in the precipitate and therefore increasing the total amount of precipitate.

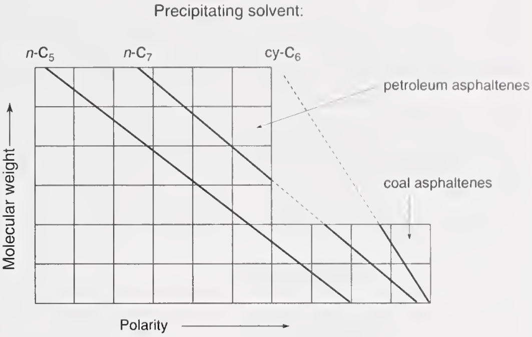

Figure 14.7 Comparison of petroleum and coal asphaltenes precipitation. Adapted from R.B. Long, Ref. 28. © 1981, American Chemical Society.

The extension at the lower right of the diagram depicts the phase distribution for coal liquids. Coal asphaltenes have lower MWs and, on account of their high phenolic oxygen content, a higher polarity than petroleum asphaltenes. In the diagram, both *n*-heptane and *n*-pentane are shown to cause asphaltene precipitation from either petroleum residua or coal liquid solutions, but cyclohexane does not cross through the polarity–MW field of the petroleum asphaltene, only that of coal liquids. This representation illustrates the fact that coal asphaltenes are not soluble in cyclohexane while petroleum asphaltenes are.

Thus, even if such a diagrammatic representation does not advance the theory of asphaltene solubility, it may serve as a simple educational aid.

A measure of the solvent-solute interaction is the enthalpy of solution, but only a few measurements of enthalpies of solution have been reported for asphaltene. These include the heats of solution of Athabasca asphaltene[29] in toluene and xylene to form 1.0% solutions at 25°C:

Substance dissolved	Solvent	ΔH/J (g substance dissolved)$^{-1}$
bitumen	toluene	18.39
asphaltene	toluene	–6.94
maltene	toluene	8.87
bitumen	xylene	13.20
asphaltene	xylene	–8.88
maltene	xylene	5.14
bitumen	methylene chloride	18.2

From these data and the asphaltene content of the bitumen, 17%, it can be calculated that upon dissolution of 1.0-g asphaltene in 4.98-g maltene the heat of dissolution will be –73.2 J, which is an order of magnitude larger than the heat of solution in toluene or xylene. Further dilution with the maltene to give 1.0% solution of the asphaltene would be accompanied by even more heat evolution. The exothermicity of these processes is a manifestation of solvent strengths, indicating that the order of solvent strength for asphaltene in toluene ~ xylene << maltene, in agreement with the values of the solubility parameters from direct measurements, Tables 14.1, 14.3 and 14.4. Also the high exothermicity explains the good solubility of Athabasca asphaltene in the maltene fraction of its bitumen.

Table 14.3 Cot θ and δ_2 solubility parameters[30a]

Solubility parameter	Cot θ_v	Cot θ	δ_2, MPa$^{1/2}$ (literature)
Pure hydrocarbons			
n-heptane	–1.00	–1.00	15.3
1-heptene	–0.35	–	–
cyclohexane	+0.48	+0.35	16.8
1,2-dimethylcyclohexane	+0.38	–	–
xylene	+2.14	+1.73	18.0
benzene	+2.38	+1.38	18.8
decalin	+1.79	–	–
tetralin	+2.14	+1.96	19.4
Hydrocarbon mixtures			
deodorized varsol	–0.21	–	–
coker gas oil	+0.18	–	–
virgin gas oil	+0.18	–	–
Athabasca coker gas oil	+0.82	–	–
hydrotreated A.C.G.O.	+0.91	–	–
Athabasca natural gas oil	+0.99	–	–
steam cracked gas oil	+1.12	–	_
cracked gas oil	+1.28	–	–
Solvesso + 150	+2.37	+2.41	17.3
heavy aromatic naphtha	+2.75	–	–
Other pure solvents			
*iso*butylheptylketone	+1.41	+0.80	15.9
pyridine	+2.41	+1.30	21.8
tetrahydrofuran	+2.41	–	19.5
carbon tetrachloride	+1.94	+1.19	17.7
trichloroethylene	+2.41	+1.46	19.0
o-dichlorobenzene	+4.13	+2.90	20.8

Table 14.4 Solubility parameter and compositional data for Athabasca bitumen compound class fractions[30a]

Oil fraction	Solubility parameter Cot θ_v	H/C ratio	Wt%	
			sulfur	nitrogen
Saturates	1.1	1.65	1.9	<0.02
Aromatics	3.2	1.38	5.9	0.2
Resin 1	4.0	1.53	5.4	0.7
Resin 2*	4.5	1.46	5.1	0.9
Asphaltene	–	1.23	8.2	1.2
Maltene	2.4	–	–	–

* More polar.

The endothermicity of the dissolution in maltene is due in part to the low affinity of the aromatic solvents for the saturate fraction of the maltene and in part to the much higher cohesion energy density of the resin fraction of the maltene compared to that of the aromatic solvents (*v.i.* and Tables 14.3 and 14.4).

As has been discussed above, in solubility parameter theory, solubility—that is, the maximum amount of solute that a given quantity of solvent under a given condition is capable of keeping in solution—is related to the total cohesion energy or internal pressure, *i.e.*, solubility parameters of the solvent and solute. Solubility parameters can be calculated from a variety of different physical properties of a substance; however, direct measurement of solubility yields the most reliable data. For this reason, other empirical methods for solubility parameter measurements and comparisons have been proposed. The one employed at the Imperial Oil research department in Sarnia[30a] in the late 1950s–early 1960s is based on incompatibility arising from the insolubility of the least-soluble asphaltene components of the oil.[30] This critical solubility point—precipitation point or flocculation threshold— of asphaltenes was determined by titrating oil in solution with different solvents against a reference titrant, such as *n*-heptane, using microscopic observations of the precipitation end point.

The method is illustrated schematically in Figure 14.8. The volumes of solvent per weight of oil are plotted as a function of the volume of titrant per weight of oil. Good solvents give positive slopes, Figure 14.8A. If the line is vertical, Figure 14.8B, the asphaltenes are critically soluble in the solvent. If the line has a negative slope, Figures 14.8C and D, it represents a poor solvent. When the solvent and titrant are the same the slope of the line is −45° with the *x*-axis. The smaller the positive slope the better the solvent, Figure 14.8E. Thus, the slope of the line described for a given solvent-titrant system is a measure of the solvent power of the solvent and cot θ, Figure 14.8F, is a practical measure of the solvent power for hydrocarbon mixtures. The experimental procedure is relatively quick and gives reproducible results which are transposable from one solvent system to the other. Some examples of the results are shown in Figures 14.9 and 14.10 where the characteristic nature of the *x*-axis intercept for a particular precipitant is illustrated for pure and industrial hydrocarbons, and the characteristic nature of the y-axis intercept for a particular solvent.

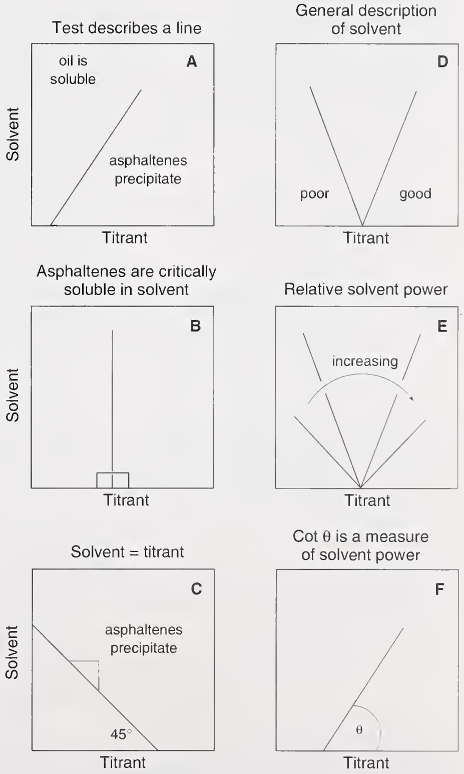
Test describes a line
oil is soluble
A
asphaltenes precipitate
Solvent
Titrant
General description of solvent
D
poor
good
Titrant
Asphaltenes are critically soluble in solvent
B
Solvent
Titrant
Relative solvent power
E
increasing
Titrant
Solvent = titrant
C
asphaltenes precipitate
45°
Solvent
Titrant
Cot θ is a measure of solvent power
F
θ
Titrant

Figure 14.8 Interpretation of the cot θ solubility parameter. From Ref. 30a.

Values of cot θ_v (volume) and cot θ (molar) solubility parameters relative to *n*-heptane are given in Table 14.3 along with their δ_2 values. The higher the solvent power, the larger the positive value cot θ will acquire. A poor solvent

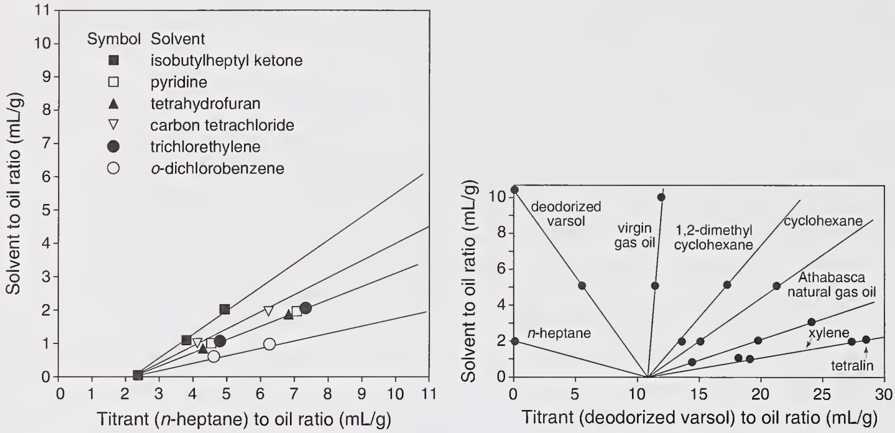

Figure 14.9 Experimental titration plots for the cot θ solubility parameter. From Ref. 30(a).

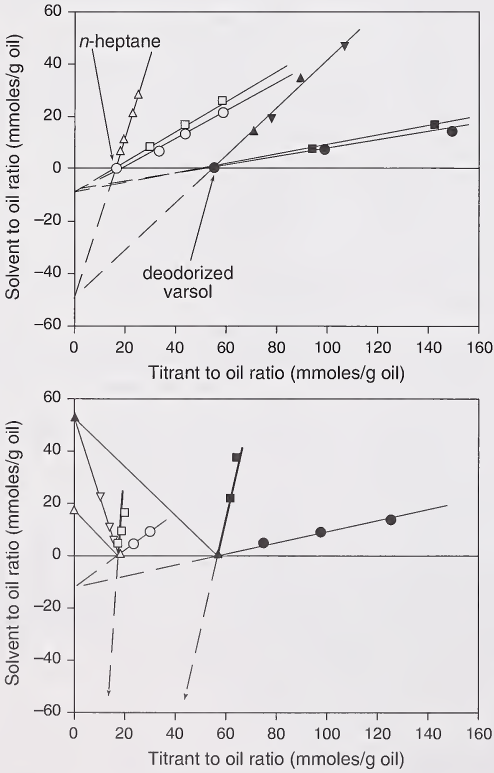

solvent	titrant	
	n-heptane	deodorized varsol
1,2-dimethylcyclohexane	△	▲
cyclohexane	▽	▼
xylene	□	■
tetralin	○	●

solvent	titrant	
	n-heptane	deodorized varsol
	△	▲
deodorized varsol	▽	▼
virgin gas oil	□	■
Athabasca natural gas oil	○	●

Figure 14.10 Experimental titration plots for the cot θ solubility parameter for pure and industrial hydrocarbon solvents showing *y*-axis intercepts. From Ref. 30(a).

has a negative value and the titrant has a value of −1.0. Solvents with values below −1 are poorer solvents than the titrant and solvents in which asphaltenes are just critically soluble have a cot θ value of zero.*

Cot θ solubility parameters for the low-hydrogen-bonding hydrocarbons with $\delta_2 \leq 19.4$ MPa$^{1/2}$ correlate well with δ_2 but polar solvents like pyridine and ketones do not.

At the critical solubility point the interfacial tension between the immiscible phases changes from zero to a positive value. Also, cot θ is zero at the critical solubility point and hence

$$\sum_{x=1}^{x=n} \cot \theta \, m_x = 0, \tag{10}$$

where m is the mole fraction of the solvent component x. From this equation cot θ values can be calculated for a single component of solvent mixtures. If the solubility parameter of the titrant is known the solubility parameter of the solvent can be calculated and *vise versa*.

Cot θ values for the silica gel separated class fractions of a bitumen, along with some compositional data, are presented in Table 14.4. The data predict increasing solvent powers for asphaltene in the order saturates < aromatics < resin 1 < resin 2. Moreover, the resins 2 ($\cot \theta_v = 4.5$) are far superior solvents to any pure solvent ($\cot \theta_v$ (max) ≈ 4.13).

Following these earlier studies, since the early 1980s various other methods for the determination of the flocculation threshold have been developed (or reported as being under development) and employed in the oil industry. These incorporate more advanced detection techniques, overcoming the drawbacks of visible light/visual microscopic detection systems. They include, among others, the following:

i) infrared laser light/variable length fiber optics/photodetector;
ii) capillary viscometry;
iii) electrical conductivity measurements;
iv) optical fluorescence spectroscopy/cross-polarization microscopy;
v) differential scanning calorimetry;
vi) refractive index measurement. This method is based on the correlation between the Hildebrand solubility parameter and the cohesion parameter "a" in the van der Waals equation of state (which is a different measure of the internal pressure):

$$\delta_2 \approx \frac{a^{1/2}}{V} \tag{11}$$

The correlation can be shown,[31] with some assumptions, to lead to the following expression for δ_2 in terms of the refractive index n:

$$\delta_2 = \left(\frac{\sqrt{3}\pi h \upsilon}{384\, \sigma^3}\right)^{1/2} \frac{\sigma^3}{V/N} \; \frac{n^2 - 1}{(n^2 + 2)^{3/4}} \tag{12}$$

where σ is the hard sphere diameter of the molecule, h is Planck's constant, υ is the UV absorption frequency and N is Avogadro's number;

vii) laser photon correlation spectroscopy;
viii) particle size analysis;
ix) heat transfer analysis, *etc.*

---

* θ is characteristic for the solvent relative to the titrant; the x-axis intercept is a characteristic of the oil and it is a measure of the stability of the asphaltene solution in the oil; the y-axis intercept is a characteristic of the solvent, independent of the titrant used and is a measure of solvent power.

Employing a flocculation threshold point apparatus, the design of which was based on technique "i", a "precipitation potential" scale has been established[32] for a set of solvents/precipitants. On this scale, Figure 14.11, precipitants have positive precipitation potentials and solvents negative precipitation potentials. The rankings (according to solvent power) reported correlate well with the cot θ values.

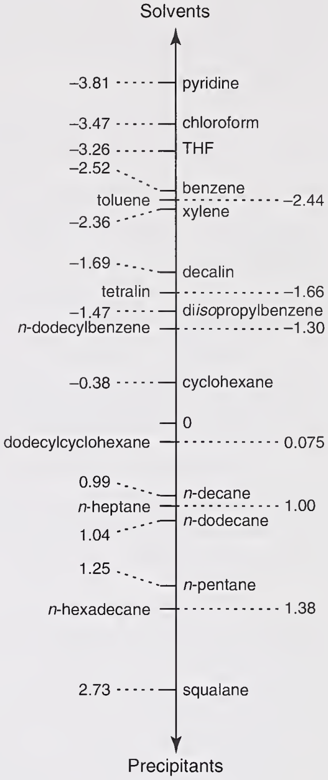

Figure 14.11 Precipitation potential scale. From G. Hotier and M. Robin, Ref. 32. © 1983, Inst. Franc. Petr.

Returning to Figure 14.1, we note that the difference in yields between the *n*-heptane and the *n*-decane precipitate is quite small, but the *n*-pentane precipitate yield is about 1.5–2.5 times greater than the *n*-heptane precipitate yield. The higher alkanes precipitate only the least-soluble portions of the asphaltene which, in general, have a different composition and MW from the lower-alkane-precipitated asphaltenes. The yield of the material corresponding to the difference between *n*-pentane and propane precipitation is quite large and this material was defined in the early days of petroleum chemistry as the resin fraction of the oil.

The material corresponding to the difference between the *n*-pentane and *n*-heptane precipitates represents low-MW asphaltene fragments and maltene molecules adsorbed to the asphaltene. These materials are analogous to what used to be called the "difference asphaltene", the material which is removable from n-C_5-asphaltene by ether extraction. The quantities of the "difference asphaltenes" for a number of Athabasca oil sand and conventional crude oil asphaltenes have been reported to comprise 30–35% of the n-C_5-asphaltene. Sequential extraction of Athabasca n-C_5-asphaltene[33] having an initial number average (VPO) molecular weight of 3350 $g \cdot mol^{-1}$ with *n*-pentane, ethanol, acetone and ethyl acetate removed 37% of the asphaltene and the molecular weight of the residual asphaltene increased to 6320 $g \cdot mol^{-1}$. The color of the isolated asphaltene varies with the mode of separation. Thus the native, Athabasca n-C_5-asphaltene has a dark brown color. After acetone extraction, which removes 21–22% material, the extract has a deep reddish-brown color and the extracted asphaltene is black.

The shapes of the curves in Figure 14.1 are probably representative of most native bitumens and petroleum vacuum residua but conventional crude oils may show considerable departure from these curves. Examples of such departures are provided by the Rengiu, Zhongyuan and Shengly crudes from China[34] with 10–15% n-C_5-asphaltene and less than 0.2% n-C_7-asphaltene contents. Thus, some 98% of these n-C_5-asphaltenes should be considered to be resins.

2.1.1 General solvency and chemistry

It has been known for some time that the intermolecular forces between hydrocarbons and nonpolar, non-hydrogen-bonded molecules are, in general, dominated by London dispersion forces. The interaction energy, ε, generated between molecule A and molecule B by dispersion forces is given by the equation

$$\varepsilon_{AB} = \frac{3}{2}\left(\frac{I_A I_B}{I_A + I_B}\right)\alpha_A\alpha_B \tag{13}$$

where I's and α's are the ionization potentials and polarizabilities. The polarizability, in turn, is $\alpha \sim 2Ze^2r^2/\varepsilon_0 I$, where Z is the number of electrons, r the radius, e the electron charge and ε_0 the vacuum permittivity. Thus, the polarizability of a molecule is proportional to the number of electrons in it and its size, and inversely proportional to its ionization potential. The ionization potentials for hydrocarbons follow the general order alkanes > alkenes > aromatics and therefore their polarizabilities follow the reverse order.

Polarizability is also related to the refractive index, n, by the equation

$$\frac{n^2-1}{n^2+2} = \frac{4}{3}\pi n\alpha \tag{14}$$

where n is the number of molecules per cubic centimeter; therefore, the polarizability is related through Eq. (12) to the solubility parameter.

A plot showing a linear relationship between the solubility parameter and the refractive index function, $(n^2-1)/(n^2+2) \equiv (F_{RI})$, for hydrocarbons[21] is displayed in Figure 14.12. The linearity of the plot is an indication that the 3/4 power of the $(n^2+2)^{3/4}$ term in the denominator of Eq. (12) can be approximated by a power of unity. The relationship between δ, n, $(n^2-1)/(n^2+2)$ and the volume fraction of a binary mixture of a crude oil and a precipitant can then be exploited to determine the value of n and $(n^2-1)/(n^2+2)$ where precipitation of the least-soluble fraction of the asphaltene in the oil commences[31], Figure 14.13. Here, the initial portion of the plot, from neat crude oil to the precipitation point, open circles, is linear and the straight line shown is a least-squares fit to the F_{RI} data for the same crude oil, pure n-heptane and asphaltene-free mixtures of the two. Measured and extrapolated values of n for this oil (1.470) were indistinguishable.

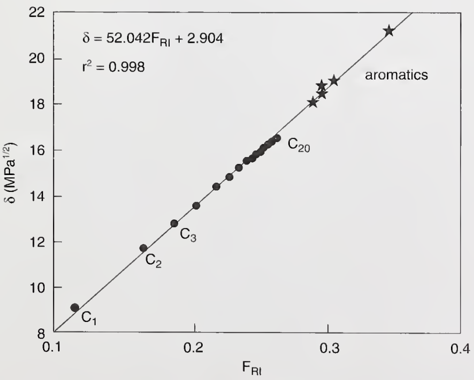

Figure 14.12 Solubility parameter as a function of the refractive index function. From F.X. Wang and J.S. Buckley, Ref. 21. © 2001, American Chemical Society.

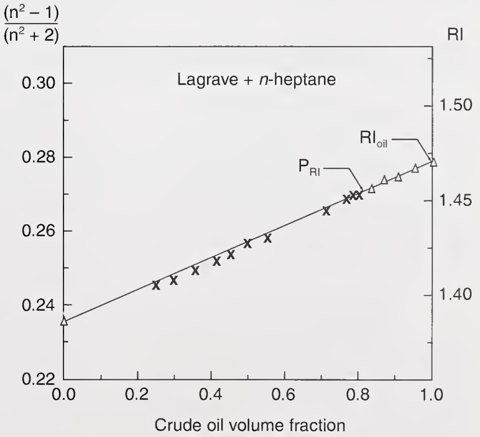

Figure 14.13 Refractive index function and refractive index as a function of the volume fraction of a crude oil in crude oil/*n*-heptane solutions. Δ: no precipitate; **X**: precipitate. After J.S. Buckley, *et al.*, Ref. 31.

The measured refractive indices of crude oils vary in the interval 1.47–1.57 and the n (precipitation onset) values range from 1.40 to 1.49.[20,30] (The refractive index of Athabasca bitumen is 1.57.) The refractive index of one asphaltene sample was determined to have a somewhat uncertain value of 1.72 at a density of 1.2 $g \cdot mL^{-1}$ and 1.70 if the value of the density were 1.0.[31]

Recently a new, elegant asphaltene solubility model, reportedly without the need to invoke simplifying assumptions or approximations has been developed.[21] The method permits the calculation of compositional ranges over which asphaltenes are stable, metastable or unstable.

With regard to solvent power, the order according to molecular type varies as follows: branched alkanes < *n*-alkanes < 1-alkenes < cycloalkanes < condensed cycloalkanes < aromatics < condensed naphthenoaromatics < condensed aromatics. An increase in the chain length of alkanes monotonically increases solvent power. Aromatic compounds are highly polarizable and have high dispersion forces and negative heats of solution; hence their superior solvent power. In agreement with this, molecular mechanics calculations on model asphaltenes have shown[35] that a fully relaxed isolated Athabasca asphaltene molecule reacts with a benzene molecule first at the center of the largest aromatic moiety as expected, and the first solvent molecule interacts with the asphaltene most energetically and with subsequent solvent molecules the interaction energy decreases rapidly.

Chlorine substitution in a hydrocarbon results in strong dispersion forces with weak, but substantial dipoles (except CCl_4) and hydrogen bonding ability, with $\delta_D \sim 15–20$, $\delta_P \sim 0–8$ and $\delta_H \sim 0–8$ $MPa^{1/2}$; bromine substitution leads to $\delta_D \sim 16–22$, $\delta_P \sim 3–5.6$ and $\delta_H \sim 3.5–8$ $MPa^{1/2}$. Acyclic alcohols, ethers and ketones have low solvent power because of their low δ_D and/or high δ_H values. Among the best solvents for asphaltene, along with naphthalene, α-methylnaphthalene, phenanthrene and anthracene, are *o*-dichlorobenzene and the aromatic nitrogen bases aniline, quinoline, pyridine and nitrobenzene, and the resins from the same crude oil or bitumen as the asphaltene. Resins from other crude oils or bitumens have been reported to be less efficient solvents than the resins taken from the same crude oil or bitumen as the asphaltene, suggesting a role for molecular recognition.

2.1.2 Solubility—precipitation

All the above treatments of the solubility–precipitation phenomena of asphaltene are based on thermodynamic or other bulk considerations, without regard to the chemistry involved. Earlier, it was shown that acetone extraction of *n*-C_5-Athabasca asphaltene removed up to 22% material comprising resins (aliphatic and aromatic carboxylic acids, cyclic terpenoid sulfoxides, alkyl naphtheno- and benzocarbazoles, quinolines, vanadyl porphyrins, alkylfluorenones, fluorenols, *etc.*) along with some other maltene components and low-MW asphaltene fragments.

The same resin molecules have also been detected in the maltene fraction of the bitumen. The question then is whether or not the distribution of the resin molecules observed represents an equilibrium (quasi equilibrium) partitioning between the maltene solution and the asphaltene aggregate phase, or, alternatively, whether the resin compounds found in the precipitated asphaltene represent mechanically occluded material which does not correspond to a thermodynamic equilibrium distribution. In order to elucidate this question, a series of dissolution/reprecipitation steps were carried out[36] on Athabasca *n*-C_5-asphaltene using *n*-pentane as the precipitant and the method of precipitation (40-fold volume excess of *n*-pentane over the methylene chloride solvent) recommended for the precipitation of asphaltene from the crude oil. The results, depicted in Figure 14.14, reveal that the precipitated asphaltene, washed on a filter with *n*-pentane until the washings became completely colorless, keeps releasing (deep reddish-brown) resins up to at least six reprecipitations. The aggregate amount of resins released after six reprecipitations was 21.9% of the asphaltene, or about the same as was obtained after one week of acetone Soxhlet extraction[37] (21.2%, VPO MW ~ 1200 g·mol^{-1}) or isolated as the lowest-molecular-weight 20.8% fraction (VPO MW 1200 g·mol^{-1}) in Bio-Beads SX-1 gel permeation chromatographic fractionation[38] of Athabasca asphaltene. Thus, the composition of the resins removed from the asphaltene by each of the three methods may be assumed to be similar, but not exactly identical. Now, if the resins released upon sequential reprecipitation had been occluded into the asphaltene, the resin content should have dropped to nearly zero after just one reprecipitation. Therefore, the plot in Figure 14.14 is an indication that the equipartitioning is not due to occlusion but to an equilibrium phenomenon. This conclusion was confirmed by observations made in further experiments as follows:

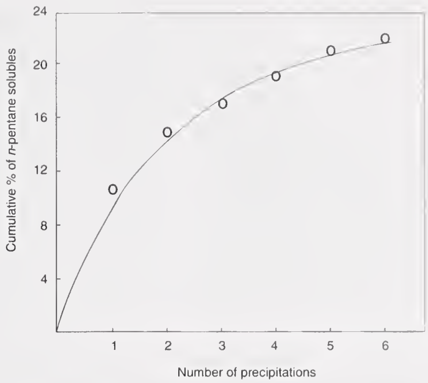

Figure 14.14 Athabasca asphaltene precipitate yield as a function of number of re-dissolutions/re-precipitations using *n*-pentane.[36]

i) 76.4% of the combined extract (1.10 g) from the six reprecipitation experiments was soluble in 40:1 *n*-pentane/dichloromethane (600 mL); and

ii) when the soluble portion of the extract (0.84 g) was dissolved in 600 mL *n*-pentane/methylene chloride (40:1) to which was added the total 3.9-g residual asphaltene left behind after the sixth reprecipitation step, the solid asphaltene showed a weight gain corresponding to adsorption of 57.2% of the dissolved resins from the solution. Undoubtedly, adsorption of solubles would be even more extensive if the asphaltene + solubles had been dissolved in the methylene chloride prior to the addition of the *n*-pentane precipitants to the solution.

Experiments using *n*-heptane as precipitant gave entirely analogous results except that the *n*-C_7-solubles after six successive reprecipitations contained less insolubles, only 10%, than the *n*-C_5 solubles (23.6%).

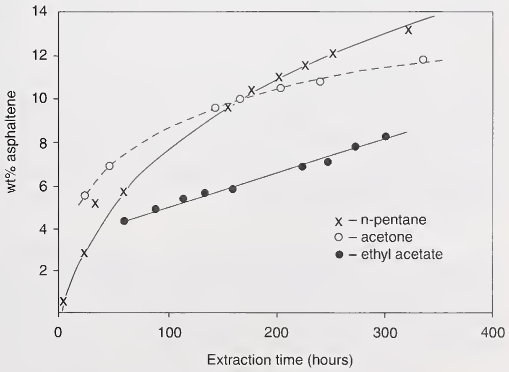

Figure 14.15 Successive extraction of Athabasca Syncrude high-grade asphaltene with various solvents. Cumulative extract, wt% of asphaltene obtained with each solvent *vs.* extraction time with each solvent.[33]

Here, it should also be noted that Athabasca asphaltene is not entirely insoluble in *n*-pentane. At slightly elevated temperature (36°C) under prolonged reflux conditions *n*-C_5 asphaltene slowly releases low-MW substances, Figure 14.15 and Table 14.5[33], composed mainly of resinous materials along with hydrocarbons representing occluded biomarkers, di-, tri- and pentacyclic terpanes and steranes. At the same time, the maltene left in the *n*-pentane solution after precipitation of the asphaltene contains low concentrations of asphaltenic

Table 14.5 Yields and elemental analysis of fractions obtained by successive Soxhlet extraction

Fraction	Wt% , d.a.f.[a]			Ash (by diff.)	$(H/C)_a$	MW	Extract yield[b]
	N	S	O				
initial asphaltene	1.46	7.61	3.22	2.00	1.24	3350	
pentane extract	0.86	7.28	3.56	0.00	1.30	860	16.6
acetone extract	1.40	7.35	5.51	0.00	1.33	1180	9.9
ethyl acetate extract	0.95	7.39	4.21	0.00	1.32	1270	8.2
residual asphaltene	1.35	7.89	2.72	3.00	1.20	6320	65.2

[a] Dry, ash-free. [b] Wt%, in terms of initial asphaltene.

materials distributed over all the compound class fractions of the maltene and these can be detected in the nondistillable (240°C, 1 Torr) residue of each fraction by ^{13}C NMR spectroscopy, as was discussed in previous chapters. Thus, the initial step of the class separation of asphaltene by precipitation, like the initial step in the chromatographic separation of the lower MW compound class fractions, is fraught by cross-contamination problems, namely, some asphaltene is left in the maltene fraction and some maltene becomes incorporated into the asphaltene fraction. Therefore, in scientific investigations it is more practical and expedient to study the low-MW resinous portion and the remaining high-MW portion of the asphaltene separately. The bulk of the adsorbed resinous material from Athabasca *n*-C_5 asphaltene can be separated by acetone Soxhlet extraction for one week. The resulting two fractions manifest differences not only in their chemical composition but in their thermal maturity status and possibly biotic source materials[37] as well.

After *n*-pentane extraction (Figure 14.15 and Table 14.5) successive extraction with ethanol, acetone and ethyl acetate yielded additional quantities of extracts. Extraction with ethanol was the least efficient, yielding only 0.9% extract after 120 hours. Compound class fractionation of the *n*-pentane, acetone and ethyl acetate extracts revealed that only the *n*-pentane extract contained some hydrocarbon subfractions (saturates, mono- and diaromatics); the acetone extract contained only polars; and the ethyl acetate extract contained a small quantity of diaromatics, the bulk being polars. The extracts all show lower nitrogen contents and (VPO) MWs and higher oxygen and $(H/C)_a$ ratios than the initial asphaltenes and the MWs tend to increase in the order of successive extraction. Also, the MW of the extracted asphaltene increased nearly twofold, relative to that of the original asphaltene.

The FTIR spectra of the extracts revealed the presence of carboxylic acids (1700–1710, 2800–3500 cm^{-1}), sulfoxides (1030 cm^{-1}), especially intense in the ethanol extract, and various C–O and OH functionalities (1018–1600 cm^{-1}). In the extracted asphaltene the carboxylic absorption is weak and absorptions at 1040, ~3600 and ~3700 cm^{-1} appear to indicate the presence of clay minerals.

Compounds that have been reported to be adsorbed to Athabasca asphaltene or observed to be adsorbed in laboratory experiments include carbazoles,[39] vanadyl porphyrins,[40] sulfoxides, various carboxylic acids and alcohols[41], squalene,[42], α-cholestane,[43–45] molybdenum acetylacetonate,[46] hydrocarbon biomarkers,[37] and others.

Returning to the reprecipitation experiments discussed above, a puzzling feature to explain is the observation that the freshly-precipitated asphaltene containing 22% adsorbed substances soluble in *n*-pentane at room temperature can be washed with *n*-pentane at room temperature without affecting the adsorbate. This is possible only if the adsorbate is located in the interior of the asphaltene particle which is surrounded with an *n*-pentane insoluble outer layer protecting the interior. The insoluble surface layer is formed by the extraction of its *n*-pentane-soluble components by the precipitant solvent (40:1 *n*-pentane:methylene chloride) and the subsequent exposure to the neat precipitant (*n*-pentane) washing solvent. Once the precipitant (*n*-pentane) solubles are removed the solubility of the layer is lowered, thereby creating a barrier in the equilibrium process involving the interior of the solid asphaltene particles and the bulk of the precipitant/solvent liquid. This insoluble outer layer may be so densely packed that the *n*-pentane molecule could not penetrate it, or, more likely, that the *n*-pentane molecule could pass through it but the passageways are too narrow for the *n*-pentane-solvated maltene molecules to exit through them.

This explanation also applies to the phenomenon referred to as "hysteresis", whereby precipitation and dissolution of asphaltene under similar conditions yields incongruent results, the solids from dissolution being always larger, Figure 14.16.[26] There again, formation of a rigid insoluble or less soluble outer layer on the asphaltene particles surfaces acts as a barrier to the complete dissolution of the resins in the interior of the particles necessary to achieve equilibrium.

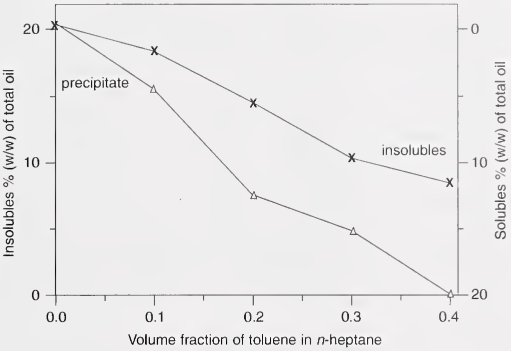

Figure 14.16 Insolubles and precipitates *vs.* solvent composition. Δ: dissolution; **X**: precipitate. After S.I. Andersen, Ref. 26.

In closing this section it should be pointed out that adsorption of resinous substances—and even of saturated and aromatic hydrocarbons—from the solution phase by dissolved or dispersed solid asphaltene has now been convincibly documented and will be considered again later in this chapter. Here it is important to note that:

- asphaltene, precipitated either from a solution of the bitumen or from neat bitumen, contains substantial amounts of resins;
- the main cause of the gradual loss of resins from the asphaltene upon sequential reprecipitation is not the liberation of resins mechanically occluded into the asphaltene during the precipitation process but an equilibrium equipartitioning of the resins between the solution phase and the adsorbed phase in the dissolved asphaltene;
- the capacity of asphaltene to adsorb maltene components may exceed the initial maltene content of the asphaltene (21–22%) and the asphaltene could conceivably adsorb additional amounts of maltenes from a concentrated precipitant (*n*-pentane/methylene chloride, 40:1) solution of the maltene; in effect, extrapolation back to zero precipitation would appear to indicate a much higher concentration of adsorbed maltene in the asphaltene of the whole bitumen;
- washing of the precipitated asphaltene with neat precipitant (*n*-pentane) removes the maltene molecules present as surface-adhered material and as components of the surface layer of the asphaltene particles, thereby endowing the surface with a low-solubility coating which hinders or arrests the dissolution of the particle's interior; the adsorptive properties of solid and dissolved asphaltenes are quite different, those of the latter being stronger;
- the phenomenon of asphaltene "hysteresis" is a manifestation of the presence of an insoluble or sparingly-soluble surface coating on the asphaltene particles which slows down or prevents dissolution of the resins in the particle interior to reach equilibrium with the solution phase.

The above statements should be of general validity and apply to all petroleum asphaltenes.

These phenomena impact the solubility properties of asphaltene and should be taken into consideration in solubility/precipitation equilibrium calculations. They also illustrate the conceptual error associated with the interpretation of low temperature (≤ 112℃) asphaltene MW determination, where the "correct" value of the MW is obtained from extrapolation to zero concentration dilution in the customary belief that the decrease in MW with decreasing concentration is caused by the dissociation of the asphaltene molecular aggregates. In reality, it is primarily the release of resins that lowers the apparent MW of the asphaltene and this effect should be enhanced upon dilution. Thus, the average MW of resin-free asphaltene aggregates should be larger—and by a considerable amount—than that measured at any concentrations generally used in vapor pressure osmometry or other colligative property determinations. This conclusion is clearly supported by the large, approximately twofold, increase in the MW of Athabasca n-C_5-asphaltene upon acetone (or other low-solvent-power solvent)[33,37,39–41] extraction (or removal of chemisorbed resins by other means). In effect, there is no physical evidence to support the notion of dissociation of asphaltene aggregates upon dilution at temperatures below ~112℃ and in the concentration range employed in VPO measurements and it may even be possible that removal of the chemisorbed resins leads to a slight increase in aggregation. Dissociation of the asphaltene aggregates, however, becomes important at low concentrations, around a few hundreds of one percent and of course at elevated temperatures (>112℃).

The acetone extracts have been shown to contain a broad spectrum of individual compounds, ranging from simple small hydrocarbon and resin molecules with MWs ~180 $g{\cdot}mol^{-1}$ to asphaltene fragments with VPO MWs >1200 $g{\cdot}mol^{-1}$. These asphaltene fragments are distinctly different from the acetone-insoluble asphaltene in terms of MW, physical appearance and chemical composition (*v.i.*).

More detailed treatments of the problem of MW, MW distribution, nature of the aggregates and related topics will follow later in this chapter.

2.1.3 Fractionation effects in precipitation

The yield of precipitate is dependent on the precipitant and precipitation conditions employed, and increases as the carbon number in the n-alkane precipitant decreases from C_{10} to C_3, Figure 14.1. The effect is due to the variation of precipitation potential which, according to theory, should lead to a fractionation in the MW of the precipitate: n-C_{10}-asphaltene should have a higher MW than the n-C_5-asphaltene, since n-C_{10} precipitates only the least-soluble, highest-MW fraction of the asphaltene while keeping the rest in solution. The variation in MW with precipitant chain length[47,48] seen in Table 14.6 may appear to be inconsistent with previous conclusions, but it is not, and can be explained as follows: extraction of the n-C_5-asphaltene with n-C_6 removes part of the adsorbed low-MW resins, not unlike the extraction with acetone, and further extraction of the C_6-insoluble asphaltene with n-C_7 removes more resins which now have somewhat higher MW; extraction of the C_7-insoluble asphaltene with n-C_8 removes the last of the resins—if any were still left—and primarily a portion of the more soluble, lower-MW asphaltene, leaving behind a less soluble, higher-MW asphaltene residue.

Along with the MW changes, variations occur in the chemical compositions as well. Also, the n-C_{10}-asphaltene is richer in inorganic materials and has a higher ash content than the lower n-alkane precipitated fractions. The changes in MW distribution are illustrated by the size

Table 14.6 Molecular weight of asphaltene fractions of n-C_{4-8} precipitated oils

Fraction	MW(VPO)		
	Brazilian[47]	Arabian light[47]	North Sea recombined[48]
i^aC_5	1520	1360	n-C_4 2716
iC_5–s^bC_6	480	340	n-C_5 1962
iC_6–sC_7	1095	560	n-C_6 1099
iC_7–sC_8	2795	810	
iC_8	3710	2360	

[a] i = insoluble.[b] s = soluble

exclusion chromatograms,[49] Figure 14.17, which show a shift in the size distribution envelope to higher values for the less soluble portion of the asphaltene.

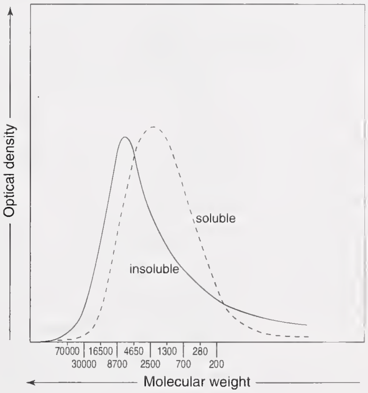

Figure 14.17 Gel permeation chromatograms of fractions of Bati Raman asphaltene soluble and insoluble in dioxane-toluene (70:30 v:v). From J.C. Monin and R. Pelet, Ref. 49. © 1983, Wiley Heyden.

Theoretically calculated MW distribution curves[50] are shown in Figure 14.18 for various scenarios. Figure 14.18a shows the MW distributions for the precipitated and non-precipitated asphaltene upon addition of 5.0 mL n-C_7 to 1 g of oil and Figure 14.18b, upon addition of 20.0 mL n-C_7. As seen from the figures, the yield of precipitated asphaltene is higher with 20 mL precipitant and the size distribution envelopes are shifted to even lower MW values. The distribution curves for the precipitated asphaltene upon addition of 10 mL each of n-C_5, n-C_7 and n-C_{10} are shown in Figure 14.18c and, for the asphaltene that remained in solution, in Figure 14.18d. The trends manifested are as discussed above; that is, the amount of precipitated asphaltenes decreases in the order n-C_5 > n-C_7 > n-C_{10} and the size distribution envelopes are shifted to higher MW values in the case of the solid relative to what was left in solution, and the gap between solid and solution distribution maxima is largest for n-C_{10} and smallest for n-C_5 precipitant.

2.2 Precipitation procedures

There are several analytical procedures described in the literature for the determination of the asphaltene contents of various native and processed feedstocks, *e.g.* for *n*-heptane UOP 614-68, ASTM D4124, IP 143; for *n*-pentane, Syncrude Analytical Method 5.1. The separation of the asphaltene can be achieved either by digestion with a precipitant (n-C_5 or n-C_7) or by precipitation with a precipitant from a concentrated solution (in a diluent) of the sample. When precipitation, which is the preferred method for oil sand bitumens, is used rather than digestion, the precipitating agent should be added to the asphaltene solution slowly and with continuous stirring to ensure a "dry", easily filterable precipitate that will not adhere to the walls.

2.2.1 Volume ratio of precipitant to feedstock

The results, obtained in digestion, on the relationship between the yield of asphaltene and volume ratio of *n*-pentane to Athabasca bitumen[51] are plotted in Figure 14.19. The data indicate the requirement of a 20–25-fold excess volume of *n*-pentane for the precipitation of asphaltene

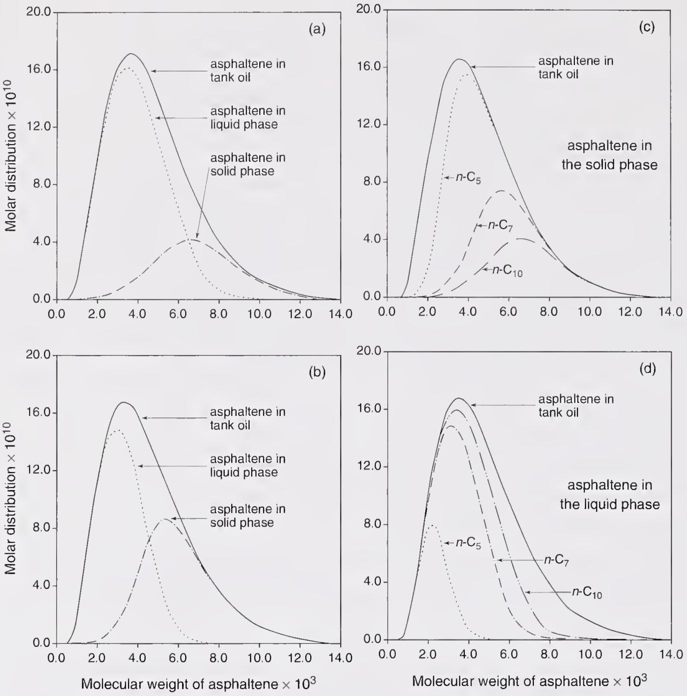

Figure 14.18 Computed molecular weight distribution curves for precipitated and nonprecipitated asphaltenes. a. 5.0-mL *n*-heptane to 1-g tank oil; b. 20-mL *n*-heptane to 1-g tank oil; c, d. 10.0-mL precipitating solvent. From S. Kawanaka *et al.,* Ref. 50. © 1991, American Chemical Society.

from the bitumen. When a diluent such as benzene is present as in the precipitation mode, a correspondingly higher excess of *n*-pentane would be required. Thus, for example, for 1.0 mL of bitumen containing 0.83-mL maltene, at least 20 mL of *n*-pentane is required. If 1.0 mL of benzene is present then (1.83/0.83) × 20 = 44 mL of *n*-pentane would be needed since the benzene is as good a solvent for asphaltene as the maltene (*cf.* Tables 14.3 and 14.4). The recommended value is 40-mL *n*-pentane. With *n*-heptane as the precipitating agent the alkane-to-feedstock ratio requirement, at least with some asphalt feedstocks, may be higher than with *n*-pentane, as can be seen from the plots in Figure 14.20.

Similar data for the precipitation mode are displayed by the plots in Figure 14.21 for the solvent pairs *n*-heptane/toluene and *n*-heptane/pyridine. Here the circles and crosses represent experimental data points, and the solid lines, theoretically calculated solubilities. Both the experimental and calculated solubilities for pyridine lie above those for toluene, indicating that pyridine is a better solvent for asphaltene than toluene, in

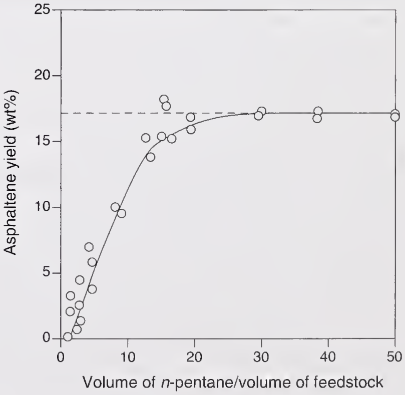

Figure 14.19 Relationship of asphaltene yield to *n*-pentane/feedstock ratio. Time, 16 h, T = 25°C. From J.G. Speight *et al.*, Ref. 51. © 1984, Butterworth-Heinemann.

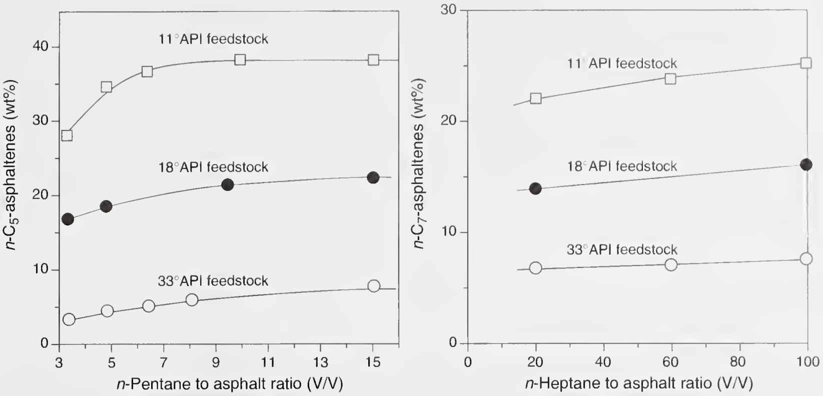

Figure 14.20 Effect of n-pentane and n-heptane to asphalt ratio on percent of n-C_5-asphaltenes and n-C_7-asphaltenes from 90 penetration straight reduced asphalts. T = 25°C. From L.W. Corbett and U. Petrossi, Ref. 12. © 1978, American Chemical Society.

agreement with their solubility parameter values, *cf.* Table 14.2.

The onset of precipitation, the critical ratio of precipitant to crude oil, also varies with MW of the precipitant and keeps increasing with MW, as indicated by the experimental data and theoretically-predicted plot, Figures 14.22[48] and 14.23.[53]

The reversibility of the precipitation step has been tested and a significant degree of hysteresis has been reported here as well.[53] Using an Iranian light tank oil, precipitation of asphaltene was carried out by the addition of about 2.7 cm^3 n-hexane (b.p. 68.7°C) per gram tank oil at 60°C. Sixty hours after precipitation, when the n-hexane was presumed to be distilled out of the solution, the precipitate was expected to be quantitatively dissolved had the process been fully reversible. This was not the case, however, and some 27% of the precipitate remained behind. In order to settle the issue, more rigorous tests would be desirable.

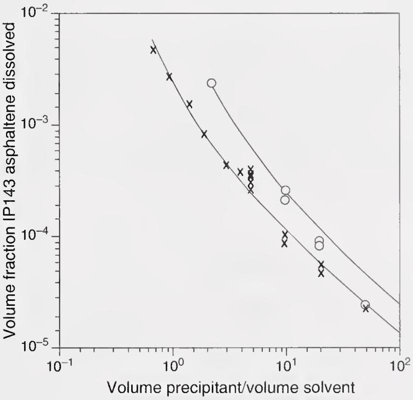

Figure 14.21 Experimental (data points) and theoretical (solid lines) solubilities of asphaltene in n-heptane/toluene (×) and n-heptane/pyridine (O). From A. Hirschberg and L. Hermans, Ref. 52. © 1984, Institut Français du Pétrole.

2.2.2 Contact time

The quantity of asphaltene precipitated depends on the contact time, *i.e.* the time elapsed between the addition of the alkane to the bitumen and the separation of the asphaltene. A plot showing the reported variation in the yield of insolubles *versus* contact time in the digestion mode of separation, Figure 14.24, reveals that the asphaltene yield reaches a constant value at 12 hours and remains essentially unchanged between 12 and 24 hours. The shape of this curve is determined primarily by the kinetics of solubilization and diffusion rate of the maltene fraction of the bitumen while in the precipitation mode the time required to reach a stable and reproducible

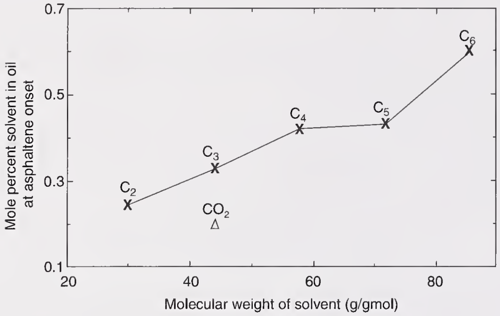

Figure 14.22 Concentration of titrant at asphaltene onset as a function of solvent molecular weight at 100°C and 29.9 MPa. After A. Hammami *et al.*, Ref. 48.

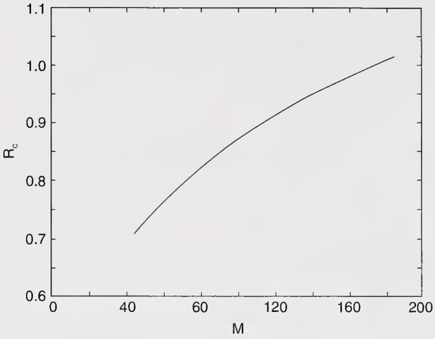

Figure 14.23 Predicted onset of precipitation R_c as a function of molecular weight M of the solvent. From H. Rassamdana, *et al.*, Ref. 53. © 1996, American Institute of Chemical Engineering.

yield of precipitate would presumably be governed by the kinetics of precipitation and equilibration of the polar constituents between the asphaltene aggregates or micelles and the solution. The latter is a relatively slow process, as will be discussed later along with other relevant processes involved in micellization, aggregation and dissolution phenomena.

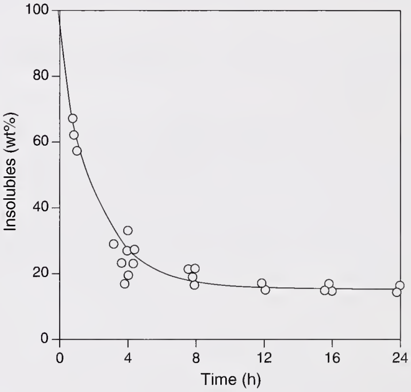

Figure 14.24 Relationship of asphaltene yield to feedstock/paraffin contact time. T = 25°C; 30-mL *n*-pentane per gram bitumen. From J.G. Speight *et al.*, Ref. 51. © 1984, Butterworth-Heinemann.

2.2.3 Temperature

The effect of temperature on the solubility of asphaltene is paramount. Temperature affects the solubility of asphaltene in the maltene fraction of the oil and in the precipitating solvent. It also changes the degree of dissociation of the asphaltene. When asphaltene in laboratory experiments is precipitated from the solution of the parent oil in a solvent by the addition of a precipitant, the precipitation potential value and the quantity of precipitate formed is usually determined by the solubility parameter of the precipitant because of its large excess concentration, and the maltene of the oil and solvent used contribute a small correction term only. Therefore, variations with temperature in the precipitation potential or quantity of precipitate formed are characteristic parameters for the precipitant and not the oil. Early studies[17] indicated that the amount of asphaltene precipitate formed in three aromatic-free gasoline fractions with boiling points 75, 113 and 163°C decreased as the temperature was raised, Figure 14.25, manifesting increased solubility with rising temperature. More recently, similar results were also obtained[48,54–56] with n-$C_{5\text{-}8}$ as the precipitants, Figure 14.26 and Tables 14.7 and 14.8. Disregarding variation in the entropy term with temperature in the free energy expression, this trend suggests, in line with expectations, a positive value for the heat of solution in low-solvent-power solvents. For precipitants, no direct measurements of heat of solution appear to be available. In contrast, for good solvents like toluene xylene and maltene, the heat of solution is negative and consequently a rise in temperature would be expected to

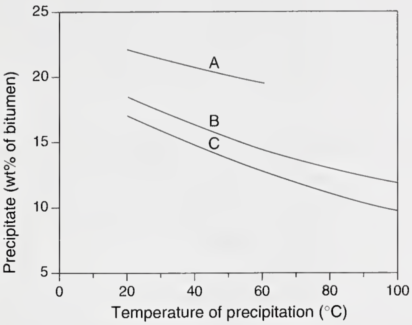

Figure 14.25 Relation between the quantity of precipitate obtained by dilution of a Mexican bitumen with 100-fold quantities of aromatic-free gasoline fractions boiling at about 75 (A), 113 (B), and 163 (C) °C. From J.W.A. Labout, Ref. 17. © 1950. Elsevier.

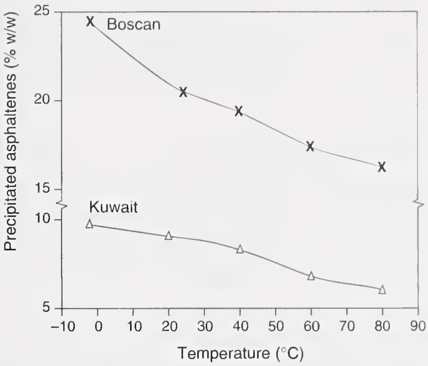

Figure 14.26 Amount of asphaltenes precipitated from Boscan and Kuwait crude oils by *n*-heptane as a function of temperature. After S.I. Andersen, Ref. 54.

Table 14.7 Asphaltene yield* and molecular weight as a function of precipitation temperature[54]

Crude	T °C	Asph. %(w/w)	MW (VPO)
Boscan	-2	24.49	2700
	25	20.45	2000
	40	19.29	3700
	60	17.23	5800
	80	15.92	7300
Kuwait	-2	9.75	3700
	20	9.01	4300
	40	8.25	3500
	60	6.29	5900
	80	5.97	6800

* Precipitant: n-C_7

Table 14.8 Asphaltene yield from Kirkuk[55] light and North Sea[56] waxy oil as a function of temperature with different precipitants

T, °C	Asphaltene, wt% of oil			
	n-C_5	n-C_6	n-C_7	n-C_8
0[55]	9.2	6.4	6.3	
23[55]	8.4	5.7	5.1	
reflux[55]	7.7	4.3	4.2	
33[56]	1.48	1.30	0.82	0.90
54[56]			0.79	
58[56]		0.69		0.66
84[56]			0.49	
100[56]				0.51

have a suppressing effect on solubility. Also, rising temperature causes gradual dissociation of aggregates or micelles, promoting dissolution. Indeed, as seen from the data in Table 14.7, the precipitation temperature affects not only the quantity of asphaltene but, as we have seen before, its MW as well. With rising temperature, the progressively smaller quantities of asphaltene precipitated have progressively higher MWs indicating that the lower MW fractions tend to increasingly remain in solution with rising temperature. It is also possible that the high MW molecules liberated from the asphaltene·resin complexes undergo aggregation yielding higher MW asphaltene·asphaltene complexes. Evidence for this has been observed in GPC studies on highly diluted Athabasca asphaltene solutions as will be discussed in section 6.7 of this chapter and more recently in temperature studies on Kuwait and Boscan asphaltenes.[55]

From the above discussions and the enthalpies of solutions data (on p. 475) it follows that the solubility of n-C_5 asphaltene in the parent maltene should increase as the temperature is lowered. On the other hand, paraffinic crude oils with a 60–70% paraffin content and low aromatic and polar contents may behave differently. In such oils, the presence of high concentrations of precipitating solvents (C_1–C_{30} paraffins) may turn the dissolution of the asphaltene in the maltene into an endothermic process with an increase in solubility as the temperature rises.

2.2.4 Pressure

When solid asphaltene is exposed to the vapor of a solvent it will absorb solvent and swell. On dissolution in the liquid solvent the swelling process will continue and, according to viscosity data, will produce a "rheological volume" which, in the solution, is larger than the dry volume of the asphaltene itself. The swelling of asphaltene in solution has been recently confirmed by low-angle X-ray scattering that will be considered in section 8.0 of this chapter. From chemical composition measurements in early studies it was also inferred that, as would be predicted, the volume of the asphaltene micelle or aggregate in the bitumen is significantly larger than the volume of the asphaltene itself, owing to the uptake of chemisorbed resin and aromatic molecules. Since in the aggregate the solvent and resin molecules are more closely packed than in the intermicellar phase, the combined volume of maltene molecules plus asphaltene molecules in the micelle would be expected to occupy a smaller volume than the sum of the net asphaltene volume and net solvent volume. Therefore, the process of aggregate formation should be accompanied by a net volume contraction. From Le Chatelier's principle, it then follows that the solubility of asphaltene in general should increase with rising pressure.

There are indeed experimental data that verify this prediction. In Figure 14.27 are plotted the amounts of asphaltene precipitated from a 2:1 mixture of crude oil with propane at room temperature as a function of pressure.[57a] As the pressure rises the amount of precipitate decreases because of the increased solubility. Similar results were reported for C_5H_{12}, C_6H_{14} and C_7H_{16} at 25 and 80°C. In each case the amount of asphaltene precipitated was higher by a factor of 1.2–1.6 at atmospheric pressure than at 350 atmospheres under otherwise identical conditions. Figure 14.28 shows analogous data for a Venezuelan live oil.[57b] Above the bubble point, where the system is only affected by changes in pressure, the solubility increases

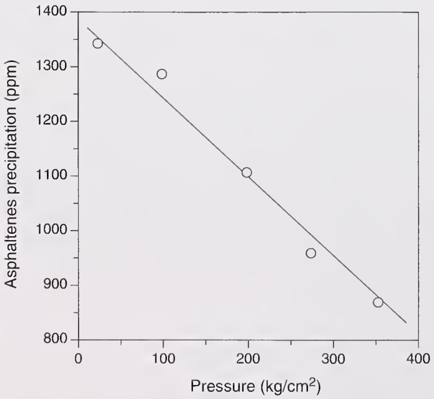

Figure 14.27 Effect of pressure on asphaltene precipitation by propane (oil: propane = 2:1). From C. Lhioreau *et al.*, Ref.57a. © 1967, Institut Français du Pétrole.

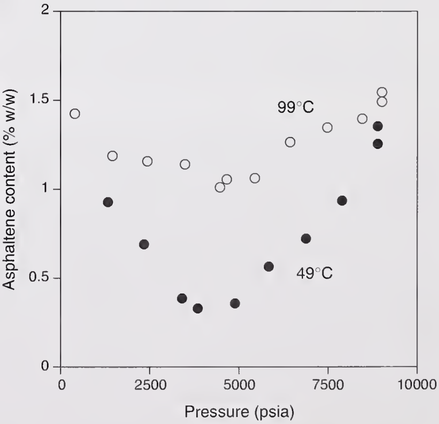

Figure 14.28 Asphaltene content of a Venezuelan crude oil as a function of pressure at T = 49 and 99°C. R. Angulo *et al.*, Ref. 57b.

monotonically with pressure. Below the bubble point, compositional changes are also taking place and evidently override the effects of pressure changes. (*cf.* Section 8.0 and reference 191)

2.2.5 Exposure to oxygen and light

Asphaltene is known to react with atmospheric and solvent-dissolved oxygen. The rate of the reaction is slow at room temperature but increases fairly rapidly with increasing temperature. Some of the reactive resin components are also readily oxidizable and are thus converted to asphaltene. The result of the combined effect is then an increase in both asphaltene content and asphaltene MW. Light exerts a catalytic effect on the oxidation reaction and therefore both light and temperature accelerate the rate of oxidation.[58] At or near room temperature and in the time frame of laboratory testings the oxidation reaction is slow and causes barely detectable effects, but on prolonged exposure of the sample to air the changes become noticeable.

Indicators of the oxidative history of an asphaltene are the IR absorption bands (1020–1030 cm^{-1}) of the sulfoxide groups formed from the oxidation of sulfide linkages, the carbonyl absorption bands (~1600 cm^{-1}) from the oxidation of reactive H–C-9 bond as in fluorene, increased carboxylic absorption bands (~1705 cm^{-1}) from the oxidation of carbonyl groups, *etc.*

3.0 Elemental Composition of Asphaltenes

3.1 C, H, N, O and S

The chemical compositions of all asphaltenes, regardless of their origin, differ significantly from those of their source materials. They are, without exception, characterized by decreased H/C atomic ratios and elevated concentrations of the common heteroatoms, nitrogen, oxygen and sulfur as well as of trace metals, solids and inherent ash contents, relative to their source materials, the crude oil, bitumen, asphalt, *etc.* The elemental compositions of native petroleum asphaltenes, examples of which are compiled from the literature in Table 14.9, show little variation in their hydrogen-to-carbon ratios and nitrogen contents. The oxygen and especially the sulfur contents are, however, more variable. In Table 14.10 are listed approximate mean values and ranges for the CHNOS contents of native petroleum asphaltenes from various sources, along with their atomic ratios. The data for Alberta bitumen and heavy oil asphaltenes fall into narrower ranges. Of course, there are asphaltenes which would have elemental compositions outside the ranges given here. The elemental composition is also somewhat dependent on the nature of the solvent used for the precipitation of the asphaltene and, unless indicated otherwise, the data in Tables 14.9 and 14.10 refer to n-C_5-asphaltene. Comparative data for n-C_5- and n-C_7-asphaltenes are listed in Table 14.11.

When viewing these data one must bear in mind that, unless they originated from the same laboratory, the asphaltene samples may not have been prepared by the same analytical procedure and therefore they would not be directly comparable in composition. Moreover, not all analyses reported in the literature are normalized to 100% CHNOS content, and oxygen is frequently reported by difference. All these factors, taken together with the differing levels of accuracy in the analyses, especially in the case of single determinations, could have introduced sizeable errors in the data and broadened the ranges. All the data listed in Table 14.9 are normalized to 100% CHNOS content.

The narrow ranges of the compositional variances in native petroleum asphaltenes in conjunction with the constancy of the H/C atomic ratios imply comparatively subtle differences

Table 14.9 Elemental compositions of various asphaltenes (solids-free)

Source	Wt%					$(H/C)_a$	MW[a]
	C	H	N	O	S		
Alberta							
Athabasca	80.6	7.9	1.1	2.8	7.5	1.16	4500
	81.3	7.9	1.1	2.8	7.5	1.16	4800
	79.9	8.3	1.2	3.2	7.6	1.24	3600
Syncr. (30 m)	81.7	8.1	1.3	1.4	7.5	1.19	3180
Cities Service (4 m)	79.4	8.2	1.0	3.4	7.9	1.24	3200
Abasand (5 m)[b]	75.4	7.8	0.7	9.3	6.8	1.24	<~2240
Tarry water sand	80.5	8.2	1.2	2.4	7.6	1.21	–
Syncr. (35 m)	80.3	8.0	1.1	2.9	7.6	1.20	3180
	81.4	8.3	1.2	1.2	7.9	1.22	–
	80.0	8.1	1.2	2.0	8.6	1.22	7464
	80.4	8.1	1.2	2.3	8.7	1.21	4698
Cold Lake	82.7	7.6	1.2	1.8	6.7	1.10	8140
	81.5	8.0	1.1	1.7	7.9	1.18	4767
	82.0	7.9	1.2	1.7	7.7	1.16	–
Peace River	80.2	8.2	0.8	2.1	8.8	1.22	3500
(558 m)	78.6	8.4	1.1	3.1	8.6	1.28	2300
steam produced	80.3	7.9	1.2	1.9	8.7	1.18	–
	80.4	8.0	1.1	2.1	8.4	1.19	3948
Wabasca	80.5	8.2	1.0	1.2	8.4	1.21	5760
(237 m)	80.7	8.3	1.0	2.2	7.7	1.23	–
	79.8	8.4	1.0	2.0	8.8	1.23	3981
Lloydminster	81.7	8.2	1.0	1.5	7.5	1.20	–
	81.9	7.7	1.1	1.3	7.9	1.13	6108
Carbonate Triangle	79.7	7.9	1.1	2.7	8.6	1.19	–
	81.9	8.3	1.1	2.4	7.3	1.22	3554
Utah							
Sunnyside	84.4	9.2	1.6	4.2	0.6	1.3	8000
Asphalt Ridge	83.8	9.4	1.9	3.9	0.9	1.3	4547
Arabian							
"heavy"	82.7	7.6	1.0	0.8	7.9	1.10	–
Venezuela							
Tia Juana n-C_6	83.9	7.4	1.5	4.4[c]	2.8	1.06	–
Cerro Negro n-C_7	81.2	7.7	2.1	1.9[c]	5.5	1.14	–
Boscan n-C_6	80.3	7.7	1.8	5.4[c]	4.9	1.15	–

[a] Vapour pressure osmometry in benzene. [b] Surface outcrop, severely weathered. [c] By difference. For a more extensive compilation see J.G. Speight, *The Chemistry and Technology of Petroleum*, Marcel Dekker, Inc. , New York, 2nd ed., 1999.

Table 14.10 Ranges of composition and atomic ratios for petroleum asphaltenes

	Composition (Wt%)			Atomic ratios	
	Alberta	Total		Alberta	Total
C	80.5 ± 3.5	81.5 ± 4.0	H/C	1.20 ± 0.04	1.17
H	8.1 ± 0.4	8.0 ± 1.2	N/C	0.01	0.01
N	1.1 ± 0.3	1.4 ± 0.8	O/C	0.02	0.03
O	2.5 ± 1.2	2.8 ± 1.2	S/C	0.04	0.03
S	7.9 ± 1.1	6.3 ± 2.5			

Table 14.11 Elemental compositions of asphaltene fractions precipitated by different solvents[59]

Source	Precipitant[a]	Composition (wt%)					Atomic ratios			
		C	H	N	O	S	H/C	N/C	O/C	S/C
Canada	1	79.5	8.0	1.2	3.8	7.5	1.21	0.013	0.036	0.035
	2	78.4	7.6	1.4	4.6	8.0	1.16	0.015	0.044	0.038
Iran	1	83.8	7.5	1.4	2.3	5.0	1.07	0.014	0.021	0.022
	2	84.2	7.0	1.6	1.4	5.8	1.00	0.016	0.012	0.026
Iraq	1	81.7	7.9	0.8	1.1	8.5	1.16	0.008	0.010	0.039
	2	80.7	7.1	0.9	1.5	9.8	1.06	0.010	0.014	0.046
Kuwait	1	82.4	7.9	0.9	1.4	7.4	1.14	0.009	0.014	0.034
	2	82.0	7.3	1.0	1.9	7.8	1.07	0.010	0.017	0.036

[a] 1 = *n*-pentane, 2 = *n*-heptane.

in the relative proportions of the main structural elements, the aromatic, naphthenic and aliphatic types present in native petroleum asphaltenes. The nitrogen content is also fairly constant, seldom lying outside the 0.9–1.8% range, which is nearly an order of magnitude higher than the nitrogen content of the maltene fraction of the oil. More variable are the oxygen and especially the sulfur contents with ranges of 1–3% and up to 9%, respectively.

The oxygen content can be affected by such factors as the integrated redox conditions, weathering and water washing history of the reservoir. An extreme example of these influences is seen in the Abasand sample where over 50 years of surface exposure to weathering has caused an increase in the oxygen content from 3% to 9% along with some decreases in the nitrogen and sulfur contents.

The sulfur content of the asphaltene is determined by the sulfur content of its source material, the crude oil or bitumen, and varies nearly in direct proportion with it. The sulfur content of the asphaltene is always higher than that of its source material and, in the case of oil sand bitumens, the ratio may be as high as two.

For a given asphaltene the elemental composition shows minor changes with molecular weight when the asphaltene is fractionated according to molecular weight, Table 14.12, or when different precipitating agents are used. In general, the data show that as the carbon number of the *n*-alkane precipitant increases, the H/C atomic ratio drops and the molecular weight rises (Table 14.6). Also, in agreement with these trends, the H/C atomic ratios are persistently lower and the N/C and S/C atomic ratios higher for the n-C_7-asphaltenes which, in general have higher molecular weights than the n-C_5-asphaltenes. The slight compositional changes in the gel permeation chromatography (GPC) separated fractions are also in overall agreement with the above trends.

3.2 Trace metals

The trace metals and the heteroelements NOS in petroleum tend to accumulate in the resin and especially the asphaltene fraction. The available data for worldwide crude oils and bitumens[60] show that V, Ni and Fe are present in highest concentration and that the elements V, Ni, Cd, Cr and Mo exhibit a weak negative correlation with API gravity and, with the exception of Cd, a positive correlation with the asphaltene content. For the elements Co, Cu, Mn, Zn and Fe no correlations are reported to exist with either API gravity or asphaltene content. The highest concentrations of Ni and V are known to occur in the Mara and West Mara fields of the

Table 14.12 Analyses of Athabasca asphaltene and its GPC fractions[38]

Athabasca [38a]

GPC fraction	1	2	3	4	5	Whole asphaltene
Yield (wt%)	22.5	30.5	13.6	11.1	20.8	
MW (VPO)	16,900	13,700	7,100	3,400	1,200	3,600
Elemental analysis (wt% daf basis)						
C	79.8	79.8	80.1	80.0	79.8	79.9
H	8.1	8.2	8.3	8.6	8.2	8.3
N	1.2	1.2	1.1	1.1	1.1	1.2
S	7.9	8.0	7.9	7.4	7.0	7.6
O	3.0	2.8	2.6	2.9	3.9	3.2
$(H/C)_a$	1.22	1.23	1.24	1.29	1.23	1.24
Number of carbon atoms per 100 C atoms of major carbon types (solution state results)						
C aliphatic	65	66	61	59	52	57
C aromatic	35	34	39	41	48	43

Cold Lake [38b]

GPC fraction	1	2	3	4	5	Whole asphaltene
Yield (wt%)	14	33	25	16	12	
MW $(\mathrm{GPC}_{\max})$	5,000	4,000	3,000	1,800	800	2,000
Elemental analysis						
C	81.2	80.9	80.8	81.0	80.6	79.9
H	7.8	7.8	7.8	8.1	7.2	7.5
N	1.3	1.2	1.5	1.3	1.4	1.3
S	7.8	7.4	7.3	7.3	6.3	7.6
$(H/C)_a$	1.14	1.15	1.15	1.15	1.06	1.12

Maracaibo Basin, Venezuela, up to concentrations of 1,000 and 100 ppm in the oil and 5,300 and 360 ppm in the asphaltene,[61] showing a positive correlation with sulfur content.

The concentrations of trace elements in Athabasca bitumen and their distribution between the maltene and asphaltene fractions have been reported[62] and, from the data compiled in Table 14.13, it is seen that indeed, V, Fe and Ni are by far the most abundant trace metals. Moreover, the concentration of every trace element is much higher in the asphaltene than in the maltene, by as much as one order of magnitude or more in some cases. The sums of the concentrations for some of the elements in the maltene and the asphaltene do not agree with the concentrations of these elements in the bitumen, indicating some degree of inaccuracy in the figures.

The data in Table 14.13 include the trace metals that are present in the bitumen and its components in organically bound oil-soluble form but not those that are entrained as finally divided mineral matter, probably colloidal illite and kaolinate with some silica. The geochemical classification of the elements in Table 14.13, that is, the assignment to predominantly organic or predominantly inorganic forms, is given in Table 14.14. As seen, all the four major constituents—Ni, V, Fe and Mo—are present in both the bitumen and the asphaltene predominantly as organic complexes and Ni and V are thought to be present totally in organically bound form.

Table 14.13 Trace element concentration ($\text{mg}\cdot\text{g}^{-1}$) in Athabasca bitumen, maltene and asphaltene[62]

Element	Bitumen[a]	Maltene	Asphaltene	Element	Bitumen[a]	Maltene	Asphaltene
Al	<80	2	<2	Mo	7.2	0.20	22
As	0.11	0.09	0.357	Na	15.8	2.3	37
Ba	<3	<0.01	8 ± 2	Ni	70.3	22	192
Ce	<0.1	<0.005	<0.5	Rb	1.55	<0.003	6.5
Cl	13.8	n.d.[b]	n.d.	Sb	0.022	<0.001	0.08
Co	0.18	0.056	1.02	Sc	0.16	0.19	0.87
Cr	0.55	0.17	3.0	Se	0.33	0.297	0.94
Cs	<0.01	<0.001	<0.03	Sm	<0.01	0.0034	0.04
Eu	<0.004	0.002	0.020	Sr	2.5	<1	–
Fe	171	139	720	Ta	<0.004	<0.04	<0.02
Ga	0.296	<0.04	1.11	Tb	0.004	0.004	0.04
Hf	0.02	<0.001	0.12	Th	0.07	0.046	0.32
K	0	0	0	Ti	n.d.	n.d.	n.d.
La	<0.04	0.008	<0.2	V	170	53.8	630
Mn	2.87	2.71	10.4	Zr	<2	<0.01	<10

[a] Mineral free. [b] Not determined.

Table 14.14 Geochemical classification of trace elements in Athabasca bitumen and asphaltene[62]

% Organically bound	Geochemical classification	Element in	
		Asphaltene	Bitumen
0–40	predominantly inorganic	Al, Ce, Cs, K, Mn, Sm, Sr, Ta, Zr	Al, Ba, Ce, Cs, Eu, K, Sm, Sr, Ta, Zr
60–100	predominantly organic	As, Ba, Co, Fe, Ga, Mo, Na, Ni, Rb, Sb, Sc, Se, Tb, Th, V	As, Co, Cr, Fe, Ga, Mn, Mo, Na, Ni, Rb, Sb, Sc, Se, Rb, Th, V

A study of the concentration distribution of trace metals in Athabasca and Cold Lake asphaltene as a function of the MW of gel permeation chromatographic (GPC) separated fractions of the whole asphaltene revealed[63] that the metal concentrations are related to the MW of the fractions and the higher the MW, the higher the concentrations of the metals. The highest-MW fraction, comprising ~58% of the asphaltene, accounts for up to 90% of the metals present in the asphaltene. Most of these non-removable metals are strongly complexed to the heteroatoms of the organic molecules and even the colloidal clay minerals are probably bound to the organic matter. X-ray diffraction used to characterize the clay minerals shows that the crystallinity decreases as the particle size diminishes.

The mineral content of C_5-asphaltene can be quite high. In the case of benzene-extracted Athabasca bitumen, the crude asphaltene can have an ash level of 3.5 wt%. The ash content can be reduced by centrifugation of the asphaltene solution to a level of 0.5 wt%, which is the "inherent" ash content of the asphaltene. Most of this inherent ash comprises oxides of V, Ni and Fe along with the other trace metal oxides, and small amounts of SiO_2 and PO_4 (as metal phosphates).

Recently, it has been shown[64] that by the use of super-ultracentrifugation (at an RCF 366,000 gravity) it is possible to remove all the solids from asphaltene. The major components of the solids are alumino-silicates—ultrafine clays, *i.e.* crystallites with a lateral extension of less than 100 nm and thickness of less than 10 nm. Pyrite, titanium oxide, chelated vanadium and nickel, along with 18% carbon in the form of toluene-insoluble organic matter, comprise the rest of the material.

4.0 Experimental Probes into the Molecular Structure of Asphaltene

Since the earliest days, the question of the molecular structure of asphaltene has been one of the most puzzling and challenging problems of petroleum chemistry. In terms of fundamental research more efforts have been expended on the investigation of the molecular and colloidal structure of asphaltene than on any other single issue of petroleum chemistry but in spite of this, progress has been slow. The evolution of our conception of the asphaltene molecule was not accidental, it followed from and was the direct consequence of the complexity of the problem, the randomness of the structure of the molecule, its intractability due to involatility arising from the relatively high MW of the basic units and its tendency to agglomeration. Just the determination of the MW of asphaltene in itself is a formidable problem, partly because of the ever-present association equilibria shifting with experimental conditions, partly because of the polydispersity of the basic molecular units and partly because of the different kinds of aggregates present. The high MW and its broad distribution along with the randomness of structure makes possible the involvement of a large number of structural units combining randomly in many different ways to form large numbers of different structures of variable sizes. It was not known and it could not be readily established whether there were any hidden principles underlying the apparent covalent structural randomness and it has been long and vigourously debated whether native petroleum asphaltene represents any chemically distinct class of molecules. Adding to the confusion was the definition of asphaltene as a solubility class, thus incorporating into the precipitate a plethora of small, well-defined organic molecules and other larger molecules which structurally belonged to the resin fraction (especially in the case of n-C_5 as the precipitant), while at the same time excluding some degraded lower-MW asphaltene fragments by releasing them to the lower MW fractions. Moreover, the origin of native petroleum asphaltene was not understood and opinions were divided as to whether asphaltene was a product of the chemical aggregation of the lower-MW resinous molecules of the crude oil or of the degradation of the high-MW precursor kerogen. The close similarity between native petroleum asphaltenes from different sources, crude oils, bitumens, asphalts, *etc.* was recognized early, along with the sharp chemical distinction between petroleum- and coal-derived asphaltenes, but the differences in structure between native and thermally processed asphaltenes were not given proper attention.

Most of our structural knowledge of asphaltene evolved during the last three decades from intensive studies using modern instrumental and chemical methods of analysis. The instrumental methods are collectively characterized as non-destructive as opposed to the chemical methods (oxidative, reductive, hydrolytic, thermal) in which the sample is degraded by chemical alterations resulting in products that are amenable to chemical analyses involving instrumental methods such as the various branches of mass spectrometry (MS), gas chromatography (GC) and their combination (GC–MS), Fourier Transform infrared (FTIR), ^{1}H and ^{13}C nuclear magnetic resonance (NMR), size exclusion or gel permeation chromatography (SEC, GPC), high-performance liquid chromatography (HPLC), X-ray absorpion near edge structure (XANES) spectroscopy, *etc.*, for the detection, identification and quantitation of individual product molecules. The two basic methods, instrumental and chemical, are complementary and both are necessary and barely sufficient for the unravelling of the structure of asphaltene.

Macromolecular substances do not usually contain precisely identical molecules but instead they consist of molecules which, while being quite similar in their basic structure, differ in subtle details, especially in size. There are many natural macromolecular substances, known examples of which are starch (a polysaccharide), cellulose and lignins (the structural components of wood), humin and humic acids (the basic organic constituents of soil), and kerogen (the insoluble organic constituent of sedimentary rocks constituting the most abundant organic matter on earth, which is the precursor of petroleum, petroleum asphaltene and many other natural products). These substances are best characterized by the description of their molecules in terms of basic structural units, the mode and number of their linkages, their average MW and their MW distribution. Macromolecules are generally solids, some of which are completely insoluble in any known solvent (*e.g.* kerogen), and others (*e.g.* humic acids and asphaltene) which are soluble in some solvents. Their individual covalent molecules interact with fairly strong intermolecular forces, causing them to form aggregates. The nature of these forces, their strength, location and number of the functional groups responsible for them in the molecule are important considerations to the understanding of their molecular structure. In the case of asphaltene, as mentioned above, London dispersion forces, H-bonding, charge transfer complexation and dipole interaction have been identified as the predominant modes of molecular aggregation. Coulombic interaction and, more recently, "aromagnetism"[65] have also been suggested as potential modes in intermolecular bond formation.

In the chemical approach to the structure of macromolecules, the macromolecules are subjected to chemical manipulations causing them to degrade to smaller molecules with as few chemical changes in the released degradation products as possible. In order to preserve the structural information in the product molecules, the degradation process must be mild and effected under controlled conditions. Chemical degradation of asphaltene can be brought about by thermal, hydrolytic, reductive or oxidative means and is then followed by detailed compositional–structural investigation of the resultant degradation products. The molecules identified in the products may then be regarded as structural units covalently bound in the asphaltene with one or two bonds. Care must be taken to differentiate between genuine asphaltene degradation products and resin molecules released from the asphaltene micelles in the degradation process. Some of the resin molecules may be so strongly complexed to the asphaltene that they are difficult to remove by solvent extraction and would be only liberated by the thermal destruction of the molecular aggregate structure.

During the last two decades, numerous exploratory studies have been carried out attempting to develop suitable oxidizing and reducing agents which would yield identifiable products, characteristic of specific chemical linkages or structural units in the asphaltene molecule. Historically, the reductive approaches initially appeared to be more promising until the early 1980s, when a simple modification was introduced to the ruthenium tetroxide oxidation[66] and ruthenium-ions-catalyzed oxidation (RICO) of organic compounds with an enormous improvement in the performance and utility of the method. In this section we will discuss separately the thermal, reductive, oxidative and hydrolytic degradation processes, in that order.

4.1 Thermal degradation of asphaltenes

Thermal degradation is generally a less selective process than chemical degradations but a certain degree of selectivity is conferred to the process by its tendency to preferentially cleave the weakest bonds in the molecule. In the case of asphaltene the weakest bonds are the benzylic bonds of the alkyl aromatics, the carbon–sulfur bonds mainly in the saturated cyclic sulfides and the branching or side-chain positions in the aliphatic systems:

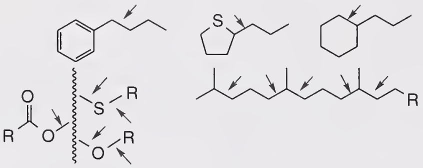

On thermolysis these bonds are expected to cleave first, especially in the lower-temperature regimes before the extensive occurrence of other, higher-energy reactions sets in.

The structural information that can be derived from thermal degradative studies is complementary in many respects to that obtainable from chemical degradative and instrumental studies and the results are also directly relevant to the reactions involved in the thermal upgrading of the bitumen and their products.

4.1.1 Thermolysis of whole asphaltenes

Asphaltenes do not have well-defined melting points. When heated under nitrogen flow, they intumesce and begin to decompose with vapor and gas evolution above 250℃. The first symptom of decomposition is the appearance of a colorless liquid (water), accompanied by swelling and flowing of the asphaltene. Around 330℃ oily products begin to distill out and around 390℃ the evolution of gases indicates the onset of rapid thermal cracking, leaving behind a brittle, vuggy char and ultimately coke.

Thermolysis studies on Athabasca and other conventional oil asphaltenes reported in the 1970s have established the presence of *n*-alkanes in the reaction products. Thus, when asphaltenes were pyrolyzed in a closed system, a smooth distribution of *n*-alkanes ranging from C_{10} to C_{50} with CPI ~1.0 and maxima at C_{14}–C_{16} was obtained.[43,67–69] Since the technique applied was not appropriate for the collection of the lower-MW gaseous and volatile members of the alkanes, the reported distribution was biased in favor of the heavier ends. Experiments carried out in a vacuum system have shown that indeed the *n*-alkane distribution extends down to methane.[70]

Since Athabasca bitumen is a severely biodegraded oil, the presence of these *n*-alkyl moieties in its asphaltene molecules shows that the supramolecular or aggregate environment exerts a protective action[43,67,68] against microbial attack, enabling the *n*-alkyl units to survive the microbial degradation of the oil. The feasibility and efficacy of this protective effect was demonstrated in the laboratory by comparing the *n*-alkane yields from a conventional oil asphaltene before and after laboratory microbial degradation. Prudhoe Bay oil was subjected to microbial degradation using a mixed bacterial culture that consumed 50% of the oil and removed all its *n*-alkane complement. Yet, the microbial processes did not affect the asphaltene fraction of the oil and no perceptible differences were apparent between the thermolysis products of the asphaltene before and after degradation.[43,67,68]

When the thermolysis is carried out in a closed system the *n*-alkanes appear without *n*-alkenes but in an inert gas-purged system,[43–45] then in addition to the *n*-alkane series, a series of 1-*n*-alkenes also appears, Figure 14.29. The emergence of this alkene series indicates that the

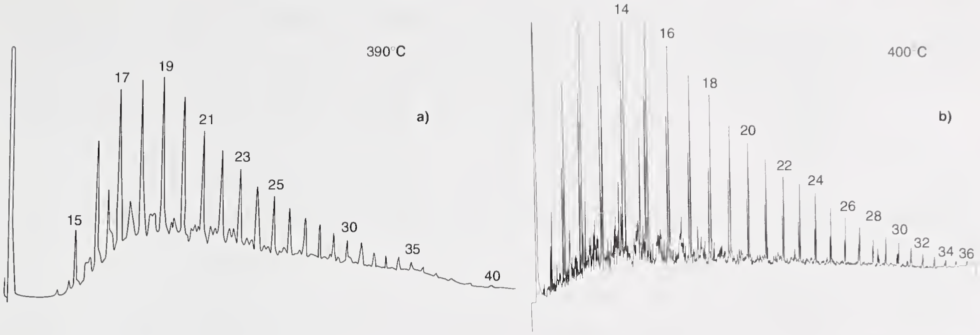

Figure 14.29 Gas chromatogram of the saturate fraction of the pyrolysis product from: a) Athabasca asphaltene at 390°C in a closed system;[44] b) Athabasca asphaltene at 400°C in a flow system.[43] The numbers above the peaks correspond to the carbon number of the alkene/alkanes.

n-alkanes were formed *via* the intermediacy of *n*-alkyl radical precursors. The non-appearance or reduced yields of the 1-*n*-alkenes in static experiments is then due to their destruction in reactions initiated by free radicals.

As can be anticipated on the basis of this premise, *n*-alkyl-free radicals will be prominent among the primary products of the thermal decomposition of asphaltene. They form mainly by the dealkylation reactions of alkylaromatics and alkylnaphthenic moieties

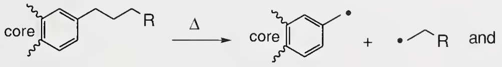

(15a)

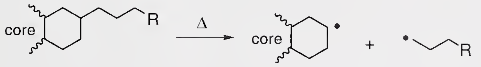

(15b)

followed by the well-known reactions of *n*-alkyl radicals [71] (E_a = activation energy)

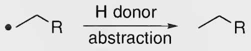

$E_{a(16)} = 10\text{–}15\ \mathrm{kcal{\cdot}mol^{-1}}$ (16)

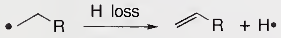

$E_{a(17)} < {\sim}40\ \mathrm{kcal{\cdot}mol^{-1}}$ (17)

(only from ethyl and propyl)

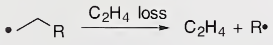

$E_{a(18)} \sim 35\ \mathrm{kcal{\cdot}mol^{-1}}$ (18)

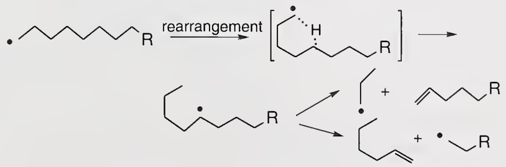

(19a)

$E_{a(19)} \sim 35\ \mathrm{kcal{\cdot}mol^{-1}}$

to give *n*-alkanes and 1-*n*-alkenes. The carbon-carbon cleavage in reaction (15) and the hydrogen abstraction in reaction (16) both preferentially (but not exclusively) take place at the weak benzylic position, α to the ring:

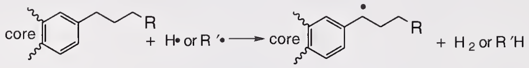

(20)

$$E_{a(20)} \sim 14\ \text{kcal·mol}^{-1}$$

The benzylic radical from the latter reaction is thermally quite reactive and readily undergoes decomposition

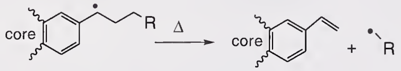

(21)

$$E_{a(21)} \sim 35\ \text{kcal·mol}^{-1}$$

to give vinylarene and an *n*-alkyl radical. This step, in conjunction with step (16), can then set up a chain reaction producing *n*-alkanes. The principal sources of 1-*n*-alkenes are reactions (19) and the ethylene- and propylene-forming reaction (17), which are more endothermic than the abstraction reaction (16) and therefore compete with the abstraction reaction more and more efficiently as the temperature is raised.

The decomposition of the *n*-alkyl radicals, reactions (18) and (19), also has a sizeable activation energy of about 35 kcal·mol^{-1} and the site of the hydrogen abstraction along the alkyl chain in reaction (20) varies with temperature. As a consequence, the size distribution of the *n*-alkane and 1-*n*-alkene products is temperature dependent and with increasing temperature, the maximum in concentration gradually shifts to lower carbon numbers. For this reason and also because of the general complexity of the thermal decomposition (in which the reactions of *n*-alkyl moieties attached to aromatic and naphthenic rings in side chains and bridges, the *n*-alkyls attached to saturated sulfides and thiophenes, and the *n*-alkyls from the *n*-alkanoic acid esters and *n*-alcohol ethers and others are lumped together), the distribution of *n*-alkanes and 1-*n*-alkenes does not give an accurate picture of their functionality or size distribution in the asphaltene. Nevertheless, thermolysis under standard conditions can be a rapid, convenient way to compare the *n*-alkyl content of asphaltenes for geochemical purposes.[44,72,73]

As the temperature is lowered just below the threshold of the main reaction to about 250°C and the reactor is purged with an inert gas, the distribution shows a marked change: as in a closed system, only *n*-alkanes (but not 1-*n*-alkenes) are produced and the concentration *versus* chain length profile becomes bimodal with maxima at C_{18} and ~C_{27}, showing a slight preference for even carbon number in the first maximum region but not in the second one, as seen in Figure 14.30. At this temperature the reaction is very slow, the product yields are low and the absence of alkenes can probably be attributed to the large activation energy difference between the

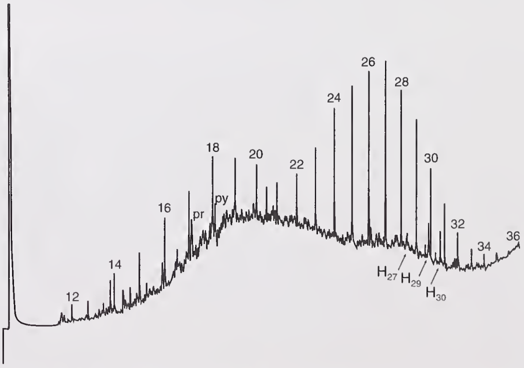

Figure 14.30 Gas chromatogram of the saturate fraction of the pyrolysis products from Peace River asphaltene at 250°C in a flow system. Pr = pristane; py = phytane; H = hopane.[44]

alkene-producing step (19a) and the hydrogen abstraction reaction (16), and possibly to the contribution of other minor reactions yielding alkanes as the primary products. An example of these could be the decomposition of *n*-alkanoic and other carboxylic acids liberated in the *in-situ* thermolysis of their esters. This reaction

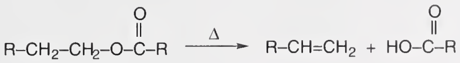

$$R-CH_2-CH_2-O-\overset{\overset{O}{\|}}{C}-R \xrightarrow{\Delta} R-CH{=}CH_2 + HO-\overset{\overset{O}{\|}}{C}-R \qquad (22)$$

is probably the energetically cheapest reaction that may occur in the pyrolysis of asphaltene (E_a for long-chain alkanoic esters is 53 kcal·mol^{-1} and would be even lower for α-branched alcohol esters[74]). Owing to the slowness of the reaction the small amounts of olefins produced could be destroyed by free radical addition reactions. Other examples of minor reactions may include the liberation of some preexisting alkanes in living and dead microorganisms present in the asphaltene (*v.i.*) and any alkanes trapped in the asphaltene.

Evidently, the bimodal distribution of alkanes is of common occurrence in the low-temperature pyrolysis of asphaltenes and is similar to that found in immature petroleums.[73]

All native, conventional oil and oil sand asphaltenes yield series of *n*-alkanes and *n*-alkenes on thermolysis in the temperature range 275 to 800°C with somewhat varying yields and concentration distributions depending on sample origin and experimental conditions—proving that all native asphaltenes contain *n*-alkyl groups as side chains or bridges.

To this point, the light hydrocarbon and other gaseous products have not been discussed. In effect, methane, followed by the C_2–C_7 hydrocarbons, represents the most abundant alkane/alkene products in the thermolysis of Alberta asphaltenes, Table 14.15. When the thermolysis is carried out in the presence of a few Torr nitric oxide the yields of hydrocarbon gases are lowered, owing to the well-known free radical scavenging ability of nitric oxide, thus providing direct evidence for the intermediacy of free radicals in the formation of hydrocarbon gases.

In addition to the *n*-alkane/1-alkene series comprising the bulk of the saturate fraction of the pyrolysis products of asphaltene a host of other hydrocarbons, mainly biomarkers, have also been identified. They embody the following:

- *n*-C_{10}–C_{50} alkanes, iso- and anteiso-alkanes, C_{27}–C_{35} hopanes, moretanes, up to about 15% of the total pentacyclics; C_{19}–C_{21}, C_{26}–C_{30} 5α and 5β steranes; and C_{16}–C_{21} acyclic isoprenoids, first detected in Athabasca and Prudhoe Bay asphaltenes;[43,67,68]
- squalene, discovered in Alberta and Utah oil sand/heavy oil and in some conventional crude oil asphaltenes;[42]
- C_{19}–C_{26} cheilanthanes, identified in Athabasca asphaltene;[75]
- methylated mono-through condensed pentacyclic aromatics in Prudhoe Bay asphaltene[67], and
- series of alkylated C_{10}–C_{30} C_nH_{2n+Z} aromatics with Z values = –6 to –16 in Athabasca asphaltene, *etc.*

In all cases studied, the important common feature that characterized the asphaltene-bound biomarkers was their significantly lower thermal maturity status, compared to their free, unbound analogs in the maltene fraction of the bitumen/crude oil. In the case of crude oils that had experienced secondary microbiological degradation, an additional difference was that the biodegradable biomarker components that had been metabolized and removed from the oil were still retained in the asphaltene, largely as structural units of the asphaltene molecules,

Table 14.15 Composition of gases[70] from the thermolysis of Athabasca (Saline Creek) and Cold Lake asphaltene as a function of temperature[a]

	Rates, 10^{-8} mol·h^{-1}·(g asph.)$^{-1}$					
	Athabasca			Cold Lake		
Temperature, °C	200	300	400	200	300	400
Wt sample, g	2.008	1.002	0.200	1.0013	0.4906	0.3091
CH_4	11.3	368.0	10,100	2.0	111	9,680
C_2H_4	5.2	37.3	1,810	14.8	12.8	1,230
C_2H_6	4.2	132	7,500	12.4	73.4	5,860
CH_3CHO	2.5	16.4	n.o.[b]			
CH_3SH	0.4	11.6	430			
CH_3COCH_3	4.2	12.3	n.d.[c]			
C_3H_6	2.8	42.5	1,660	3.0	25.4	2,830
C_3H_8	44.8	103	6,140	5.2	60.3	3,820
i-C_4H_8	1.1	31.7	1,610	n.o.[b]	19.8	3,150
i-C_4H_{10}				35.8	7.5	n.o.
n-C_4H_{10}	1.4	58.3	3,010			
1- or 2-C_4H_8	0.2	1.2	31.0	n.o.	30.5	2,670
C_5	11.1	102	3,520	1.0	688	5,910
C_6	10.1	83.0	3,390	25.4	2.1	6,560
C_7	13.7	97.4	943			
CO	60.6	307	1,770	12.4	61.6	512
CO_2	585	1,180	1,260	69.9	309	251
COS	2.6	41.7	145	n.d.[c]	29.8	199
H_2S	2.6	2,060	15,300	n.d.	1,720	10,900

[a] Each sample was heated for 5 h in a cell of volume 155 cc. [b] Not observed. [c] Not determined.

owing to the protective environment provided by the supramolecular aggregate nature of the asphaltene. Thus, because of its complete resistance to biodegradation, asphaltene can serve as a unique source of geochemical information.

The immature state of bound biomarkers also points to the catalytic nature of their isomerization since for a purely thermal reaction, the rate of isomerization should not depend on the external environment. At the same time it proves that the supramolecular aggregate environment is effective in preventing contact with the clay or mineral catalyst.[76,77]

These results were extended and amplified in studies involving the hydrous pyrolysis in closed systems of Alberta,[78] Boscan and Douk Daka (Congo)[79] asphaltenes at different temperatures by measuring tri- and pentacyclic terpanes and steranes.

The results reported at three different temperatures for Boscan asphaltene and its parent oil for comparison, are reproduced in Figure 14.31. *n*-Alkanes up to C_{39} are the major components of the saturates in both the oil and its pyrolysis products. At 250°C their distribution is bimodal, and at higher temperatures it is unimodal. The distributions of triterpanes and steranes are similar to those present in the parent oil but those in the pyrolyzates consistently manifest a younger thermal maturity age. This is best reflected in the H_{31}–H_{35} R and S epimeric ratios, the hopane/moretane ratios, and the various diastereomeric ratios of C_{27} and C_{29} steranes. It is also observed that with rising pyrolysis temperature the distributions approach those in the parent oil, *e.g.* H/M = 5.8, 6.5, 8.5 and 11.4 at 250, 290 and 330°C and in the parent oil, respectively. In other words, the young oil locked in the asphaltene undergoes increasing degrees of aging as a result of thermal stress during pyrolysis.

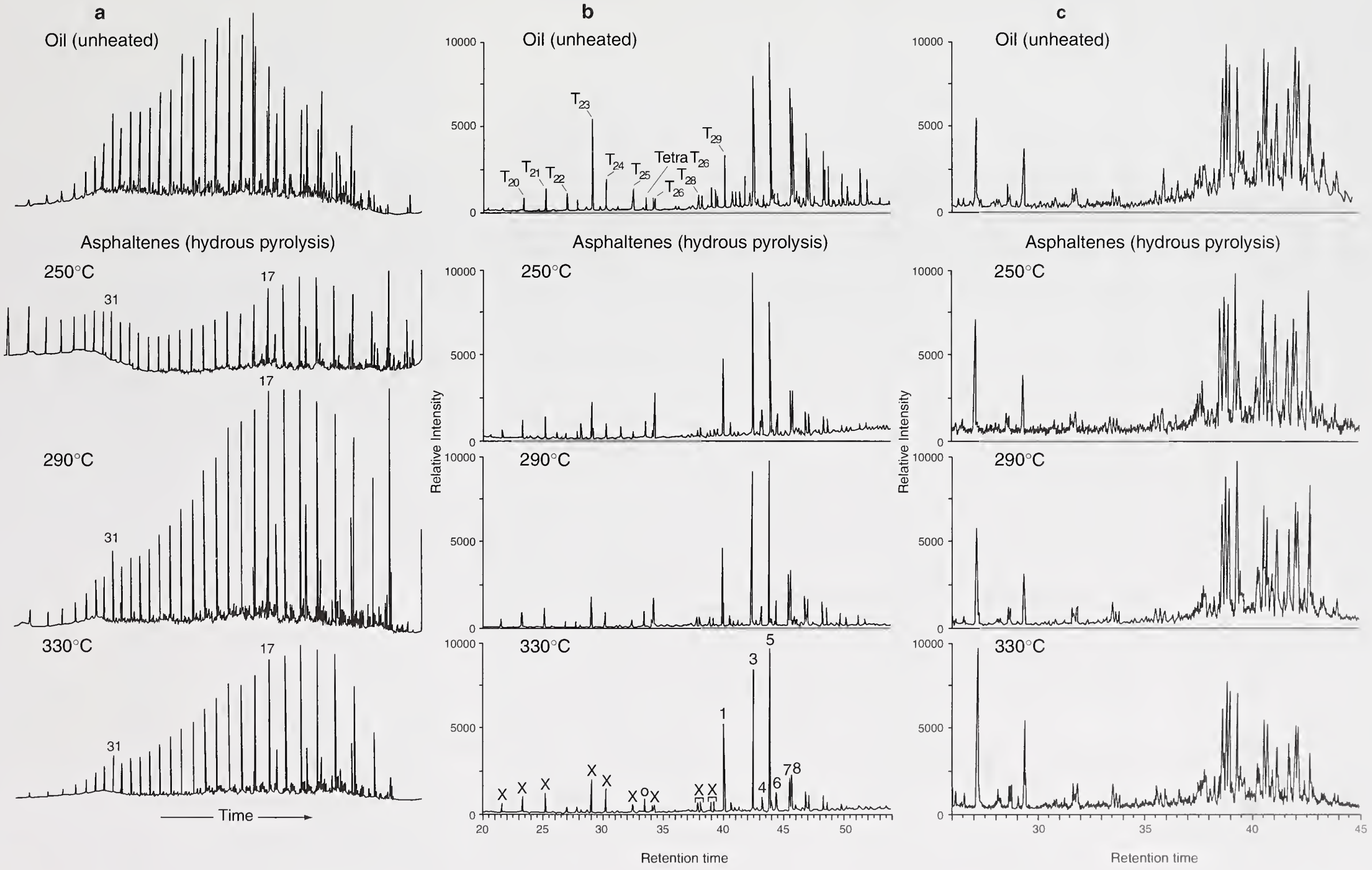

Figure 14.31 a) Gas chromatogram of alkanes; b) m/z =191 cross-scan of aliphatic hydrocarbons and c) m/z = 217 cross-scan of steranes at different temperatures from the closed system pyrolysis of Boscan asphaltene along with those of the maltene of the original oil. From D.M. Jones *et al.*, Ref. 79. © 1987, American Chemical Society.

The studies on Alberta asphaltenes included those from Wabasca, Athabasca, and Grosmont Carbonate Trend bitumens, and Lloydminster and Cold Lake heavy oils, in a total of ten samples. Preliminary investigations on the thermal stress caused by the pyrolysis indicated that under the most severe conditions employed, 330°C and 72 hours' pyrolysis time, significant thermal cracking and isomerizations in the products had taken place. This is seen from the H_{31}–H_{35} epimeric ratios and the T_{23}/H_{30} ratios in Figure 14.32. The optimum conditions for the pyrolysis are about 330°C and 24 hours' reaction time.

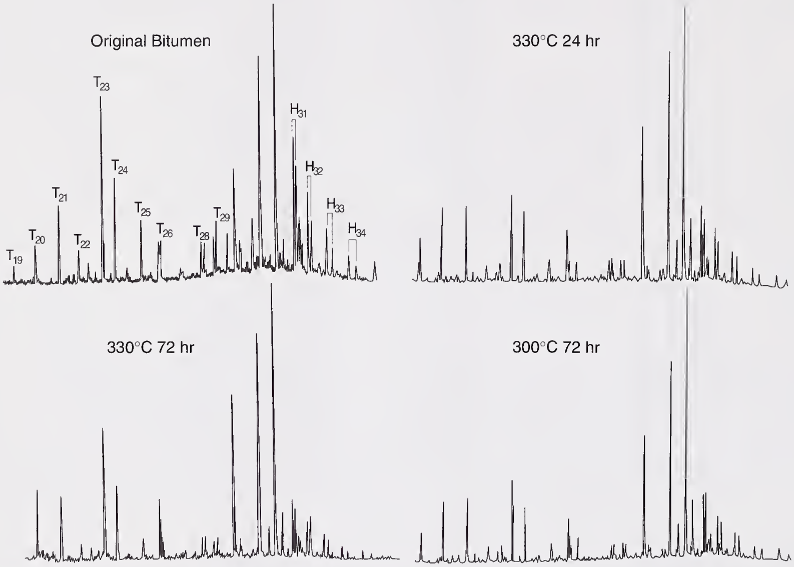

Figure 14.32 *m/z* = 191 cross-scans of aliphatic hydrocarbons from the maltene of the original oil and the closed system pyrolysis of Lloydminster asphaltene at different temperatures. T = tricyclic terpane; H = hopane. From M.G. Fowler and P.W. Brooks, Ref. 78. © 1987, American Chemical Society.

Here again, *n*-alkanes are the major pyrolysis products in spite of the fact that the parent bitumens are practically devoid of *n*-alkanes since they are severely biodegraded. Another important finding was the absence of diasteranes in the pyrolyzate, whereas in most of the parent bitumens diasteranes are the only, or the dominant, steranes present. This means that diasteranes were not components of the original biotic source material of the precursor oils of the bitumens. Also, as the *m/z* = 191 fragmentogram in Figure 14.32 shows, 18α(H)-trisnorhopane and 28,30-bisnorhopane are absent in the pyrolyzates.

Under all conditions employed in this study, all the asphaltene pyrolyzates showed less mature sterane and hopane isomerization ratios than the original bitumen but increasing thermal stress leads to more mature ratios, and they also indicated that cracking had occurred.

The close similarity of the biomarker parameters in the pyrolyzates from the ten Alberta bitumens led to the important conclusion that, with the possible exception of one of the bitumens, they all had a common origin. Moreover, it was also concluded that the pyrolysis of asphaltene is a less sensitive method for establishing correlations between degraded samples than the use of biomarkers resistant to degradation that still remain in the saturate fraction.

In bringing this section to a close, we reiterate what was obvious at the time biomarkers were first discovered in asphaltene, namely, that thermolysis is not an ideal method of liberating biomarkers from asphaltene. The reason for this is twofold. Firstly, the thermal excitation needed to cleave the C–C bond holding the biomarker molecule to the asphaltene will also cause the cleavage of other C–C bonds, as well as undesired structural changes in the biomarker molecule, thereby causing its alteration or complete destruction. Secondly, a sizeable portion of the biomarker free radicals will be lost to competing reactions, especially in closed system experiments where scavenging of the free radicals by the alkenes formed in the reaction is very efficient.

4.1.2 Thermolysis of extracted Athabasca asphaltene

As has been discussed before, asphaltenes precipitated from a methylene chloride solution of the bitumen by *n*-pentane contain, in addition to some material that may be considered to be adsorbed maltene resins (sulfides, sulfoxides, carboxylic acids, fluorenols, fluorenones, carbazoles, porphyrins, *etc.*) some hydrocarbons, along with degraded low-MW asphaltene. These materials can be removed either by GPC fractionation, repetitive precipitation or exhaustive Soxhlet extraction using a polar solvent such as acetone. The remaining asphaltene has a higher molecular weight (*e.g.* 6,300 *versus* 3,600 $g{\cdot}mol^{-1}$ for the crude asphaltene) and thermolysis of this material should afford fragment molecules that are more representative of the structure of asphaltene proper.

Some of the thermolysis[80] experiments were done on acetone-extracted Athabasca asphaltene and some on twice precipitated centrifuged n–C_5 asphaltene. The substrate asphaltene was thermolyzed in a flow system in a dilute toluene solution.[80,81] The solution, suspended above a heated surface, was allowed to fall dropwise to the surface that was kept at 430℃, in a stream of flowing nitrogen gas with a residence time for the vapor in the hot zone of about 20 seconds. The advantage of this method is that it permits the use of a larger sample size, thus producing more products, and also the large excess of toluene vapor may act as a quencher of free radicals produced in the reaction. A mobile, dark red pyrolysis oil was obtained in 34% yield. At higher thermolysis temperatures the yield increases slightly. At 460℃ the yield was 37% but GC–MS examination of the products showed that they had shorter alkyl chains, which is an indication that secondary cracking of the primary fragments had taken place. For structural studies this is undesirable. At lower temperatures, on the other hand, the yields tended to decline. Thus, 430℃ was selected as the optimum temperature under the given experimental conditions. The residue of the thermolysis, a black vuggy char, accounted for 53% of the asphaltene, leaving 13% for the gases and volatiles evolved. Of course, at the pyrolysis temperature (430℃) the toluene would be expected to undergo decomposition as well. Indeed, a blank experiment on toluene alone indicated that the toluene had undergone decomposition to an extent of a few percent but without leaving any residue in the reactor or producing any dimeric bibenzyl. Thus, it was concluded that the decomposition of the toluene carrier would not affect the asphaltene decomposition products, a conclusion which was confirmed by using perdeuterated toluene.

The pyrolysis oil was then subjected to a sequence of chemical and chromatographic steps in order to fractionate it according to compound types. As shown by the flow diagram in Appendix 14.1, first the alkenes (which would have interfered with the separation scheme) were removed by hydroboration which converts them to alcohols. This involved the treatment of the sample with a tetrahydrofuran solution of boron hydride and oxidation with 30% hydrogen peroxide in the presence of aqueous potassium hydroxide. Subsequent chromatography on silica gel produced a saturate fraction (28%, elemental analysis 2.9% S), an aromatic fraction (42%)

and a polar fraction (30%) which contained the alcohols derived from the alkenes along with other polar substances. The *n*-pentane eluent, which is labelled as saturates, contained, in addition to saturates, thiophenes and alkylbenzenes; the aromatic fraction contained sulfides along with condensed thiophenes and other aromatic class compounds.

a) Saturate fraction of the product

Considerable amounts of alkylthiophenes and minor amounts of alkylbenzenes were present in this fraction, Table 14.16. The alkylthiophenes may be separated from the rest of the fraction by silica gel chromatography following oxidation with *meta*chloroperbenzoic acid (MCPBA) to the sulfones, which are much more polar than the hydrocarbons as was discussed in Chapter 12, or by chromatography on 10% $AgNO_3$/silica gel. The residual hydrocarbon mixture was then separated chromatographically on alumina into alkanes and alkylbenzenes. Each compound class was then subjected to GC and GC–MS analysis.

Table 14.16 Gravimetric results for the separation of various fractions from Athabasca asphaltene pyrolysis oil

Fraction[a]	Wt%		Wt% estimate in orig. asphaltene
	Pyrolysis oil[b]	Asphaltene	
Saturates			
n-alkanes	18	6.1	12
alkyl benzenes	0.8	0.3	1.0
thiophenes	9	3.1	8.0
Saturates Total	28	9.5	21.0
Aromatics			
sulfides	2	0.7	2.0
condensed thiophenes	14	4.8	12
aromatics I	5.1	1.7	5.0
aromatics II	1.6	0.5	1.0
fluorenes	0.25	0.1	0.3
9-*n*-alkylfluorenes	0.3	0.1	0.3
alkylaromatics, alkylnaphthenes, others	9.0	3.0[c]	6.0
Aromatics Total	32.25	10.9	
Polars Total	30	10	
Total	**90.25**	**30.4**	**47.6**

[a] See Appendix 14.1. [b] Isolated yield. [c] Estimate

i) Alkanes

The gas chromatogram of the alkanes, Figure 14.33, shows that the series extends to at least C_{34} with a maximum around C_{14}–C_{16} which, however, is an artifact of the sample handling due to the loss of low-MW products. The true maximum would lie at shorter chains, probably at methane, as has been shown above. Small quantities of pristane, phytane and some hopanes are present. The small peaks have not been identified and would probably represent methyl branched alkanes, acyclic isoprenoids and other compounds.

ii) Alkylbenzenes

Figure 14.34 shows the gas chromatogram of the alkylbenzene fraction. At each carbon number, which extends to at least C_{28} total carbon in the molecules, a cluster of four major peaks appears.

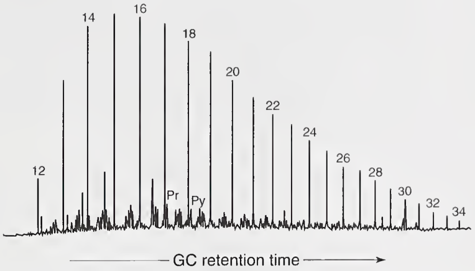

Figure 14.33 GC–FID trace of the alkanes in Athabasca asphaltene pyrolysis oil. The numbers above the peaks indicate the number of carbon atoms in the alkane. Pr = pristane and Py = phytane. From J.D. Payzant *et al.*, Ref. 80. © 1991, American Chemical Society.

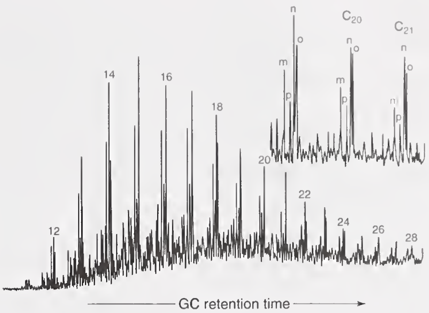

Figure 14.34 GC–FID trace of the alkylbenzenes in Athabasca asphaltene pyrolysis oil. The numbers above the clusters of peaks indicate the total number of carbon atoms in the corresponding alkylbenzenes. The insert is an expansion of the area about C_{20} recorded with a temperature program of 3°/min. Peak m: *m*-monomethyl *n*-alkyl benzene; n: *n*-alkyl benzene; o: *o*-monomethyl *n*-alkyl benzene; p: *p*-monomethyl *n*-alkyl benzene. From J.D. Payzant *et al.*, Ref. 80. © 1991, American Chemical Society.

They have been identified as being (from *m* to *o*) *meta* monomethyl-*n*-alkylbenzene, *para* monomethyl-*n*-alkylbenzene, *n*-alkylbenzene, and *ortho* monomethyl-*n*-alkylbenzene.

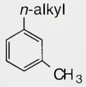

meta

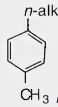

para

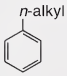

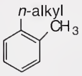

ortho

Above C_{15} the most abundant isomer of the series is the *ortho* isomer followed by the *meta* and then the *para* isomers. This distribution is taken to suggest that the least thermodynamically stable *ortho* isomer was the primary isomer which, in the maturation process of the oil, underwent isomerization to the more stable *meta* and then *para* isomer.

iii) *n*-Alkylthiophenes

The third class of compounds isolated from the *n*-pentane eluant of silica gel chromatography (9% of the pyrolysis oil) comprises *n*-alkylthiophenes, the SIR–GC–MS trace of which is shown in Figure 14.35. The major peaks are due to three distinct homologous series comprising 2-*n*-alkyl-, 2-methyl-5-*n*-alkyl and 2-ethyl-5-*n*-alkylthiophenes. These series extend to at least C_{29} with maxima between C_{10} and C_{12}.

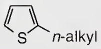

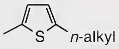

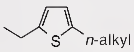

b) Aromatic fraction of the product

The 50% toluene/*n*-pentane eluent from the silica gel column contains a variety of sulfur compounds including alkylthianes, alkylthiolanes, benzo- and dibenzothiophenes, their various condensed derivatives along with aromatic hydrocarbons. The sulfides were removed first from this mixture by oxidation with tetrabutylammonium periodate to the sulfoxides as described in Chapter 12. The polar sulfoxides were chromatographically separated from the mixture, reduced back to the sulfides with $LiAlH_4$ and rechromatographed to give the sulfide fraction. The residual aromatic fraction still contains condensed thiophenes which can readily be separated by MCPBA oxidation to sulfones, reduction of the separated sulfones back to the thiophenes, followed by silica gel chromatographic separation to yield a condensed thiophene fraction. Following these steps the residual aromatics were found to contain fluorenes along with other condensed aromatic hydrocarbons. The fluorenes were isolated from the rest of the aromatics by an oxidation step to convert them to fluorenones and fluorenols as was described in Chapter 11. This base-catalyzed autooxidation with molecular oxygen in the presence of the phase transfer catalyst 18-crown-6 ether quantitatively converts nuclear alkylated fluorenes to fluorenones and 9-*n*-alkylfluorenes to 9-*n*-alkylfluorenols. The oxidized mixture was then subjected to silica gel chromatography according to the flow sheet in Appendix 14.1 yielding four fractions designated as aromatics I, aromatics II, fluorenones and fluorenols. The separated fractions were subjected to detailed GC and GC–MS analyses.

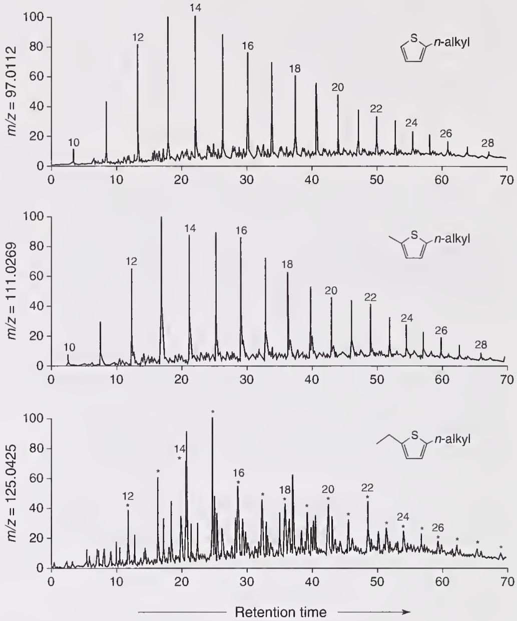

Figure 14.35 Cross-scan chromatograms for $m/z = 97$, 111 and 125 showing the thiophenes in Athabasca asphaltene pyrolysis oil. The numbers above the peaks correspond to the total number of carbon atoms in the thiophene. The peaks in the bottom panel marked by an asterisk correspond to the 2-*n*-alkyl 5-ethylthiophenes; the remaining peaks are unidentified.[81]

i) Sulfides

Several series of monocyclic sulfides were detected by GC–MS, Figure 14.36. Three five-membered ring (thiolanes) and three six-membered ring (thianes) sulfide series were identified,

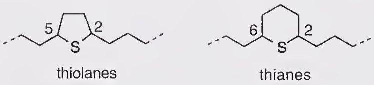

all containing an *n*-alkyl group in the 2-position and H, CH_3 or C_2H_5 in the 5 or 6 position. Thus, identified were 2-*n*-alkyl-, 2-*n*-alkyl-5-methylthiolanes and 2-*n*-alkyl-5-ethylthiolanes and 2-*n*-alkyl- and 2-*n*-alkyl-6-methylthianes up to at least C_{28}. The *cis* and *trans* isomers of 2-*n*-alkyl-6-methylthianes are well resolved but the later-eluting *trans* isomer coelutes with the unresolved isomers of the 2-*n*-alkyl-5-ethylthiolane. The maximum concentrations occur in the C_{13}–C_{17} range but, as with all the thermolysis products, the true maxima lie at even lower carbon numbers than observed because of the gradually increasing product loss with decreasing MW due to volatility. The relative concentrations of the various series follow the order:

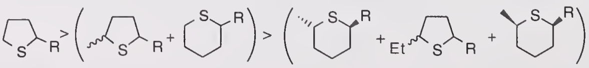

The isolation and identification of these cyclic sulfides in Athabasca asphaltene corroborate the earlier naphthalene radical anion reduction and also the ruthenium-ions-catalyzed oxidation (RICO) results (where saturated sulfones formed during the RICO of the saturated sulfide structural units of the asphaltene) were detected in the oxidized residue.

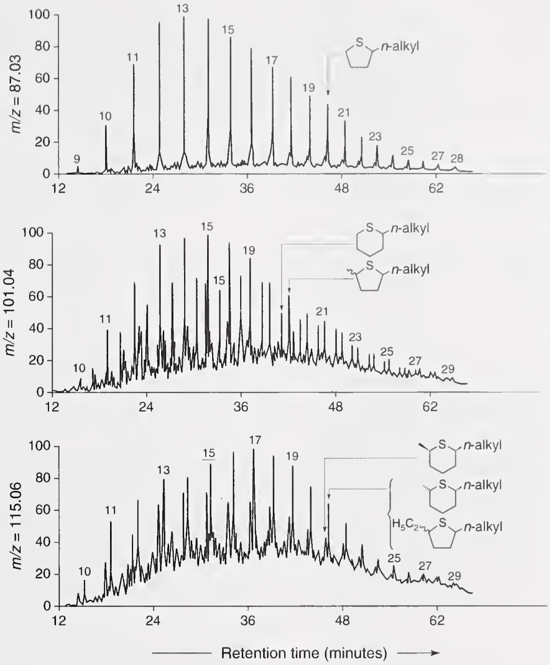

Figure 14.36 Cross-scan chromatograms for *m/z* = 87, 101 and 115 showing the *n*-alkyl sulfides in Athabasca asphaltene pyrolysis oil. The numbers above the peaks represent the number of carbon atoms in the molecule.[81]

All the cyclic sulfides identified, like the thiophenes, show a specific pattern of substitution, namely, the alkyl groups present are all *normal* and the location of substituents is always α to the sulfur. Thus, monosubstituted rings carry the *n*-alkyl groups in the 2-position and disubstituted rings in the 2,5-positions in the case of thiophene and thiolane and the 2,6-position in the case of thiane. As will become more evident in subsequent sections, this pattern of substitution is the signature of the geochemical origin of these molecules which have been preserved in the supramolecular aggregate structure of the asphaltene. Because this information is related to the nature of the biotic source material of these sulfur compounds in asphaltene, native petroleum asphaltene is a quintessential biomarker in the overall genesis of petroleum.

2-*n*-Alkylthianes and 2-*n*-alkylthiolanes with chain lengths of up to at least C_{30} have also been identified in the maltene fractions of a number of non-biodegraded petroleums. An example of the concentration distribution of these *n*-alkyl substituted monocyclic sulfides in the maltene fraction of a conventional oil has been shown in the mass chromatogram in Figure 12.40. These cyclic sulfides are not found in petroleums that have undergone secondary biodegradation in their reservoir. Their presence in non-biodegraded and their absence from biodegraded petroleum suggests that, like *n*-alkyl substituted hydrocarbons, they are biodegradable. Indeed, it has been shown in laboratory studies on model compounds and on cyclic sulfide concentrates from petroleum[82] that these compounds are biodegradable by some bacteria and fungi to thiolane-2-carboxylate, **a**, from even-carbon-number chains and thiolanylacetic acid, **b**, from odd carbon number chains:

a
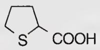

b
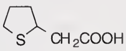

Some oxidation on the sulfur locus to sulfoxide and sulfone along with unspecified transformations of the ring have also been found to occur.

As we know from Chapter 12, thiolanes and thianes are absent from Athabasca and Alberta oil sand maltenes but they are present in the asphaltene as structural units. Here again, they were protected from biodegradation by the supramolecular aggregate structure of their molecular environment, effectively preventing the microorganisms from reaching the alkyl chains.

In contrast to the abundance of *n*-alkylthiolanes and *n*-alkylthianes, the cyclic terpenoid sulfides

e.g.

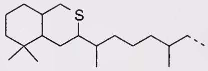

which are present in the maltene fraction of Alberta bitumens and all sulfur-containing oils are present in only very low concentrations in the asphaltene.

ii) Benzo[b]thiophenes

This group of sulfur compounds was isolated from the aromatic hydrocarbons by MCPBA oxidation followed by silica gel separation of the sulfones, reduction of the sulfones back to thiophenes with $LiAlH_4$, and again, silica gel separation of the thiophenes. Benzo[b]thiophenes are of such high abundance in Athabasca asphaltene pyrolysis oil that they are easily concentrated from the pyrolysis oil by a simple chromatographic procedure. Their mixture is dominated by series of 2,4-di-*n*-alkyl substituted derivatives. Similarly, substituted benzo[b]-thiophenes have been reported in various petroleums and other pyrolyzates.

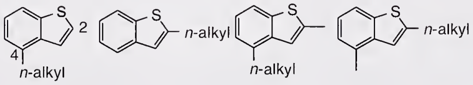

The most abundant member in the series is 2,4-dimethylbenzo[b]thiophene and the relative concentration in the series declines gradually as the length of the side chain increases up to C_{16} for both the 2-methyl-4-*n*-alkyl and 4-methyl-2-*n*-alkyl series, as can be seen from the mass chromatogram in Figure 14.37. The two analogous series, 2-*n*-alkyl- and 4-*n*-alkylbenzo[b]thiophenes are present in comparable but somewhat lower concentrations than the thiophene and cyclic sulfide series, Figures 14.35 and 14.36, with the 4-*n*-alkyl isomers being somewhat more abundant than the 2-*n*-alkyl isomers. However, it should be remarked that during the isolation procedure, when the sulfones are reduced back to thiophenes, the $LiAlH_4$ reagent partially hydrogenates the 2,3 double bond and therefore converts a fraction of the benzothiophenes to the corresponding benzothiolanes. Thus, the true yield of the benzothiophenes would be higher than the measured value. The concentration of the *n*-alkylbenzothio-

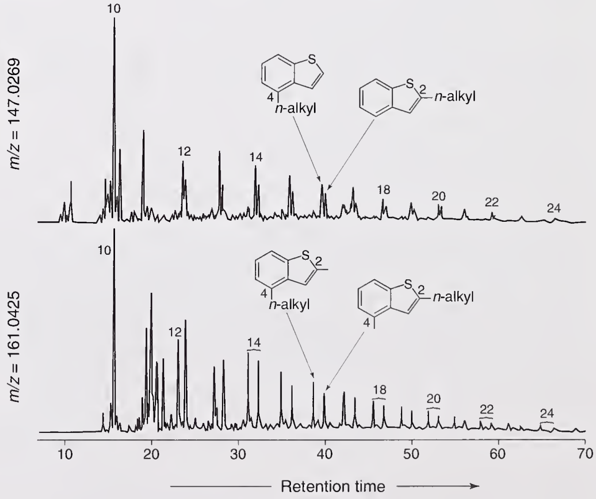

Figure 14.37 Cross-scan chromatograms for m/z = 147 and 161 showing the *n*-alkyl benzo[*b*]thiophenes in the pyrolysis oil of Athabasca asphaltene. The numbers above the peaks correspond to the total number of carbon atoms in the benzo[b]thiophenes.[81]

phenes declines monotonically with increasing length of the alkyl chain as found for the former two series. This distribution of benzo[b]thiophenes is in contrast to the distributions of thiophenes and the cyclic sulfides in the pyrolysis oil, which both go through a maximum around C_{13}–C_{16}. The difference is probably not real and is related to variations in vapor pressure and volatility loss differences in the analytical procedures.

As we have seen with the thiophenes and the cyclic sulfides, the pattern of substitution here again is highly specific and is restricted to either the 2-, the 4- or both the 2- and 4-positions in the molecule.

iii) Dibenzothiophenes

The condensed thiophene fraction contains *n*-alkyl substituted dibenzothiophenes which are concentrated in the fraction after chromatographic removal of the benzo[b]thiophenes. Unlike the maltenes of Alberta bitumens and heavy oils and the Bellshill Lake conventional oil which contain only minor amounts of benzothiophenes compared to dibenzothiophenes (*cf.* Chapter 12), in the Athabasca asphaltene pyrolysis oil the dibenzothiophenes are somewhat less abundant than the benzo[b]thiophenes. The dibenzothiophenes are complex mixtures as can be seen from the mass chromatogram displayed in Figure 14.38 where the peaks correspond to the following structures:

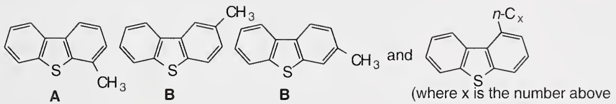

(where x is the number above the peaks in Figure14.38)

Their distribution is quite similar in all the samples studied, showing only minor variations, and the most abundant homologous series comprises the 1-*n*-alkyldibenzothiophenes. In the Athabasca sample the 1-methyl derivative is present in the highest concentration. The length of the alkyl chains extends from C_1 to C_{12} in the asphaltene but in the biodegraded Athabasca, Cold Lake and Peace River maltenes the chain is truncated at C_7 (*cf.* Chapter 12). Lloydminster heavy oil is incompletely biodegraded and the chain length goes up to C_{12} as in the asphaltene. This observation suggests that the microorganisms which were responsible for the secondary microbial degradation of the oil were capable of metabolizing only those members of the series which had a chain length of greater than C_7, but in the asphaltene even these members were protected against the microbial attack by the supramolecular aggregate environment. It has been shown that certain organisms which attack *n*-alkyl aromatic molecules will attack only when the *n*-alkyl side chain exceeds a critical length. As with the *n*-alkylbenzo[b]thiophene series, the concentration distribution of the dibenzothiophenes in the asphaltene pyrolysis oil exhibits a monotonic decline with increasing length of the alkyl chain; however, we have seen that in the maltenes the distribution is different and varies from sample to sample but overall the concentration decreases with increasing chain

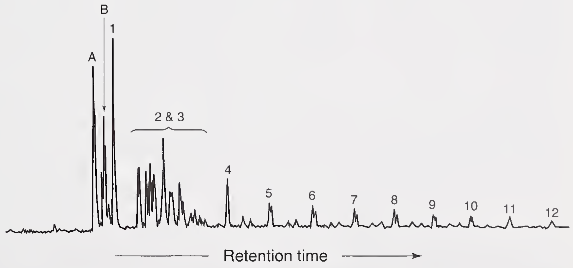

Figure 14.38 Cross-scan chromatogram for $m/z = 197$ showing the *n*-alkyl dibenzothiophenes in the pyrolysis oil of Athabasca asphaltene. Peak assignments are given in the text.[81]

length. The concentration of the 1-methyl isomer relative to the other monomethyl isomers decreases with increasing depth of burial or thermal maturity of the various petroleums, as the thermodynamically least stable 1-methyl isomer is converted into the other, more stable isomers. Accordingly, the relative distribution of the three resolvable monomethyl isomers in the Athabasca asphaltene and maltene is about the same.

On close inspection of the mass chromatogram of the *n*-alkyldibenzothiophenes, Figure 14.38, the extended-side-chain compounds appear as incompletely resolved doublets. The first of these doublet peaks corresponds to the 1-*n*-alkyldibenzothiophene. The second one must correspond to a structurally similar series of compounds which could have formed from the main 1-*n*-alkyl series by some rearrangement during the thermolysis process, since the maltene fraction of the Athabasca bitumen does not contain this second, minor series. However, the second series is discernible in small amounts in the mass chromatogram of the Lloydminster maltene, which is less extensively biodegraded than the other bitumen maltenes. Therefore, an alternative possibility regarding the origin of the minor series is that it was native to the oil but was removed from the oil in the course of biodegradation.

As encountered before, the pattern of substitution is again highly specific and involves only *n*-alkyl groups which are restricted to a single position in the main series of dibenzothiophenes.

The distribution of thiophenes in the pyrolysis oil of Athabasca asphaltene has also been investigated by field ionization mass spectrometry.[83] As seen from the plots of the relative abundances against the number of carbon atoms in the molecules in Figure 14.39, the relative abundance of benzothiophenes, $C_nH_{2n-10}S$, is slightly higher than that of dibenzothiophenes, $C_nH_{2n-16}S$, and the maximum in both cases occurs at C_3 substitution. Also plotted are the distributions of benzothiophenes with one condensed naphthenic ring or with a cyclohexyl group, $C_nH_{2n-12}S$:

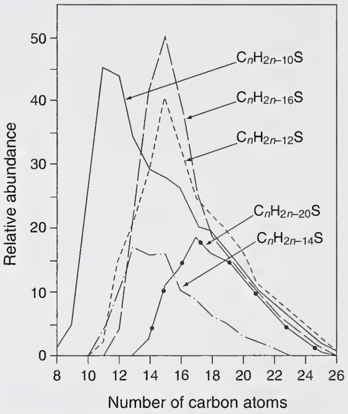

Figure 14.39 Distribution of the aromatic sulfur compounds in the pyrolysis oil of Athabasca asphaltene as determined by field ionization mass spectroscopy. From J.D. Payzant *et al.*, Ref. 83. © 1979, Elsevier.

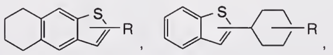

benzothiophenes having two condensed naphthenic rings, two cyclohexyl rings or a decalinyl group, $C_nH_{2n-14}S$:

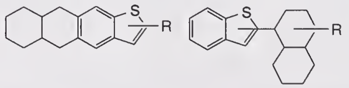

and dibenzothiophenes with two condensed naphthenic rings, two cyclohexyl rings or a decalinyl group, $C_nH_{2n-20}S$:

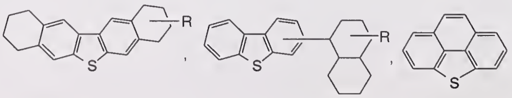

, *etc.*

or similar structures. They extend in carbon number to about 26. From a comparison with the corresponding plots for the same series in the maltene fraction of the bitumen shown in Figure11.38 it is seen that dibenzothiophene, relative to the other series, is much more abundant in the maltene than in the pyrolysis oil of the asphaltene, and the maxima of the series are somewhat shifted to higher carbon numbers, 17–18. These results from field ionization experiments are in agreement with those obtained from GC–MS studies.

iv) Fluorenes

The next structurally important class of compounds is represented by fluorene and alkylfluorenes. These compounds were isolated in oxidized form from the aromatic fraction of the pyrolysis oil after removal of the condensed thiophenes by oxidation to fluorenones and fluorenols followed by silica gel chromatography according to the separation scheme in Appendix 14.1. The method of oxidation employed quantitatively converts nuclear alkylated fluorenes to fluorenones and 9-alkylfluorenes to 9-alkylfluorenols, as was discussed in Chapter 11.

The aggregate amount of fluorenones and fluorenols

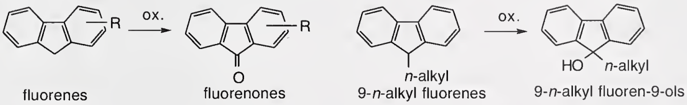

isolated from the pyrolysis oil (*ca* 0.2% of the asphaltene) was less than the amounts of any of the other structural units identified, *n*-alkanes, *n*-alkylbenzenes, *n*-alkylsulfides or *n*-alkylthiophenes. From this observation one may conclude that fluorenes are less abundant structural units in Athabasca asphaltene than the other identified units, but it would be erroneous to assume that the measured product yields should be representative of the concentration of the fluorene structural units in the asphaltene. Fluorenes, and especially 9-alkylfluorenes, contain easily abstractable hydrogens and could readily undergo hydrogen transfer reaction with alkyl radicals produced during thermolysis. This would essentially lead to their destruction and thus a drastically reduced yield in the products, resulting in an underestimation of their concentration in the asphaltene.

The GC–MS data for the fluoren-9-ols are shown in Figure 14.40. Several series of fluoren-9-ols are evident, and prominent among them is the series with a 9-*n*-alkyl substituent. The length of the *n*-alkyl side chain extends from methyl to C_{13} with maximum concentration at C_1. As the length of the chain increases, the concentration monotonically declines in much the same fashion as with the 1-*n*-alkyldibenzothiophene series. This distribution by carbon number is different from that found for fluoren-9-ols and 9-*n*-alkylfluorenes in the maltene fraction of Athabasca bitumen, Chapter 12, in that the relative abundance of 9-methylfluoren-9-ol is considerably greater and the length of the 9-*n*-alkyl groups extends to higher carbon numbers in the asphaltene pyrolysis oil. Thus, we observe here the same relationship in the side chain distribution of the materials from the asphaltene as compared to the materials from the maltene as we found in the case of the 1-*n*-alkyldibenzothiophene series, namely, that the side chains are longer in the asphaltene, extending to C_{13}, than in the maltene where they extend to C_8 only. This trend underscores the validity of the argument in favor of the microbial removal of the longer-chain members from the maltene. The cause of the heightened importance of the first members in the series, 9-methylfluorene and 1-methyldibenzothiophene, relative to the higher members of their respective series in the asphaltene pyrolysis oil compared to the maltene could be the result of the preferential production of short side-chain molecules during laboratory

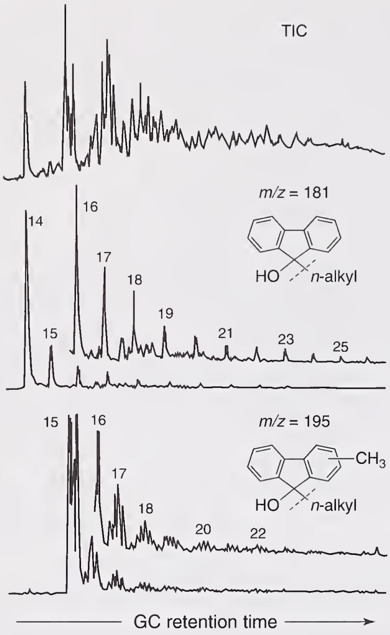

Figure 14.40 GC–MS of the fluorenols from Athabasca asphaltene pyrolysis oil. Upper trace, total ion current; middle trace, m/z = 181, the base peak of the mass spectra of 9-*n*-alkyl fluoren-9-ols; bottom trace, m/z = 195, the base peak of the mass spectra of monomethyl-9-*n*-alkyl fluoren-9-ols. The numbers above the peaks correspond to the total number of carbon atoms in the fluorenols. From J.D. Payzant, *et al.*, Ref. 80. © 1991, American Chemical Society.

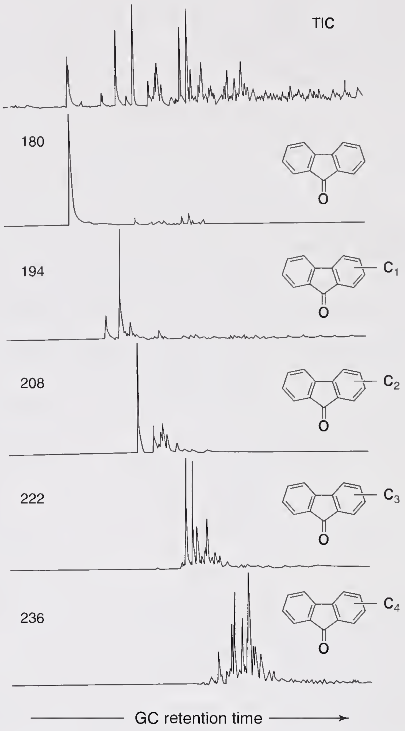

Figure 14.41 GC–MS chromatograms of the fluorenones from Athabasca asphaltene pyrolysis oil. TIC is the total ion current; descending panels are mass chromatograms of the molecular ions. From J.D. Payzant, *et al.*, Ref. 80. © 1991, American Chemical Society.

thermolysis. A certain degree of distortion in chain length and concentration distribution in the thermolysis process is unavoidable.

The concentration distribution of the nuclear monomethylated fluoren-9-ols in the bottom panel of Figure 14.40 shows incomplete resolution of the isomers. At most carbon numbers the presence of four isomers is evident, corresponding to the four isomeric positions of the nuclear methyl group in the molecule. The most abundant members of the series are the isomeric nuclear monomethylated 9-*n*-alkylfluoren-9-ols. The concentration of the higher members of the series, as with the non-nuclear methylated series, rapidly falls off with increasing chain length of the 9-*n*-alkyl group. Thus, here again we observe the repetition of the specificity of substitution, namely, the substituents are *n*-alkyl and only *n*-alkyl groups, and the site of substitution is restricted to the 9-position in the aromatic system.

The GC–MS data for fluorenones are reproduced in Figure 14.41. At least three of the possible four isomeric C_1-fluorenones are present, and one of them is in far greater concentration than the rest combined. Also, the 14 possible isomeric C_2–fluorenones are represented by only six peaks in the mass chromatogram, one of which is as large as the rest combined. The C_3- and

C_4-fluorenones also display numerous but much fewer peaks than the number of possible isomers, clearly manifesting the non-random occurrence of possible isomers.

The total amount of fluorenols and fluorenones recovered from the pyrolysis oil of the high-molecular-weight portion of Athabasca asphaltene is about 0.2% of the asphaltene. It will be recalled from Chapter 12 that the *n*-pentane-precipitated crude Athabasca asphaltene contains oxidized fluorene derivatives such as nuclear methylated fluorenones, fluorenols as well as their benzo and dibenzo derivatives complexed to the asphaltene. Also, the maltene fraction of the Athabasca bitumen contains significant amounts of fluorene, 9-*n*-alkylfluorene, fluorenone, 9-*n*-alkylfluoren-9-ols and their nuclear methylated derivatives. Thus, the total amount of fluorenes, fluorene derivatives and fluorene structural elements in the whole bitumen may be estimated to well exceed 1%.

The nuclear alkylated fluorenone and fluorene derivatives in the maltene are dominated by the dimethyl derivatives with relative isomeric abundance in the order 1,4 > 2,4 > 3,4 > 2,3. These fluorene derivatives probably originated from the degradation of the asphaltene and became partially oxidized by water-dissolved oxygen or microbes during the microbial degradation of the reservoir. Thus, fluorene was originally a significant structural unit in Athabasca asphaltene.

v) Aromatics I and II

The gas chromatograms of these two aromatic fractions are shown in Figure 14.42. The Aromatics I fraction comprises mainly alkylated naphthalenes and biphenyls. The carbon and *Z* numbers (C_nH_{2n+Z}) shown above the major cluster of peaks are derived from GC–MS analysis and correspond to the major peaks in the clusters. Evidently, many isomers are present. The peaks $C_{11,12}$; $Z = -12, -14$ represent methylnaphthalenes and biphenyl:

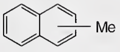

$C_{11}H_{10}$
$Z=-12$

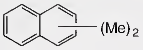

$C_{12}H_{12}$
$Z=-12$

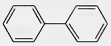

$C_{12}H_{10}$
$Z=-14$

and the peaks $C_{13,14}$; $Z= -12, -14$ correspond to:

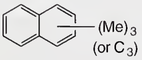

$C_{13}H_{14}$
$Z=-12$

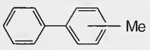

$C_{13}H_{12}$
$Z=-14$

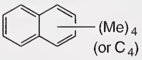

$C_{14}H_{16}$
$Z=-12$

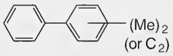

$C_{14}H_{14}$
$Z=-14$

Subsequent clusters would correspond to higher alkyl derivatives.

Of the various alkylated naphthalenes and biphenyls, the most abundant are the di- and trimethyl derivatives. This finding for Athabasca asphaltene is in agreement with the results on the thermolysis of Prudhoe Bay crude oil asphaltene where the distribution of the various alkyl naphthalenes was found to follow the order: dimethyl > trimethyl > monomethyl > desmethyl > tetramethyl > pentamethyl. The presence of naphthalenes in the pyrolysis oil of Athabasca asphaltene is also in line with the detection of the benzene-1,2-dicarboxylic acids and their methyl derivatives in the RICO products of the asphaltene (*v.i.*). The biphenyl structure, on the other hand, cannot be detected by RICO because the resultant oxalic acid would be further oxidized and destroyed by the oxidants present. Nevertheless, the presence of biphenyl linkages in higher aromatic molecules has been established by the detection of the benzene-1,2,4-tri- and 1,2,3,5-tetracarboxylic acids in the oxidation products (*v.i.*).

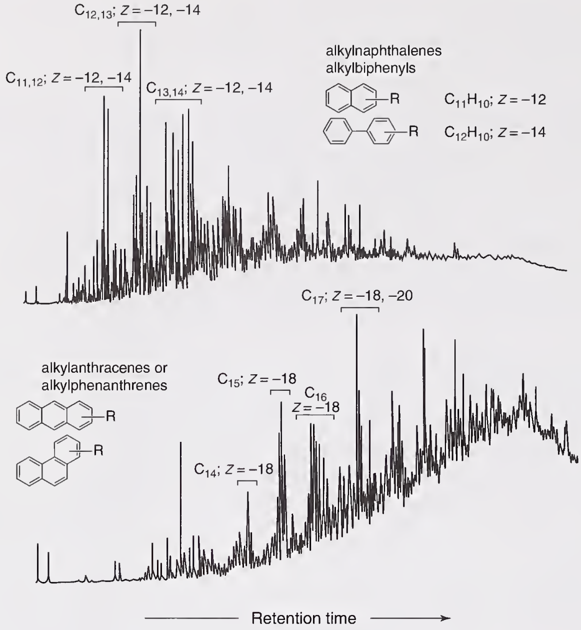

Figure 14.42 Gas chromatograms of the Aromatics I (upper panel) and Aromatics II (lower panel) fractions in Athabasca asphaltene pyrolysis oil. The carbon and *Z* numbers above selected clusters of peaks were derived from GC–MS data. From J.D. Payzant, *et al.*, Ref. 80. © 1991, American Chemical Society.

The Aromatics II fraction is also a complex mixture of alkyl aromatic compounds which comprises mainly methyl and alkylphenanthrenes and anthracenes. Thus, the peaks clustered on C_{17} correspond to

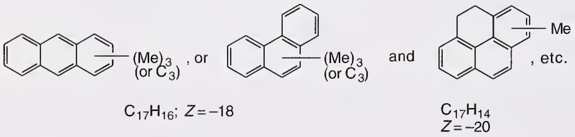

In the RICO products both of the expected isomeric benzenetetracarboxylic acids, the 1,2,3,4- from phenanthrene and the 1,2,4,5-isomer from anthracene have been detected.

In other studies on the thermolysis of Athabasca asphaltene alkylpyrenes and alkylchrysenes

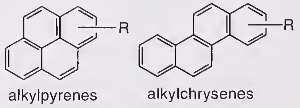

have also been identified in the pyrolysis oil, in addition to the aromatic compounds discussed above.

In the pyrolysis oil of Prudhoe Bay crude oil asphaltene,[67] alkylnaphthalenes, alkylphenanthrenes, alkylchrysenes and alkylpicenes

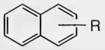

alkylnaphthalenes

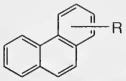

alkylphenanthrenes

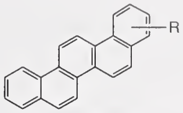

alkylpicenes

have been shown to be present. The concentration distribution of alkylchrysenes followed the order: desmethyl > monomethyl > dimethyl > trimethyl.

Field ionization studies of the aromatic fraction of the Athabasca pyrolysis oil, Figure 14.43, revealed the presence of the following homologous series of aromatic hydrocarbons:

C_nH_{2n-6} alkylbenzenes C_8–C_{28}

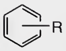

C_nH_{2n-8} alkyltetralins or alkylcycloalkylbenzenes C_{11}–C_{28}

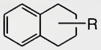

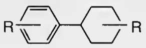

C_nH_{2n-10} alkylindenes C_{12}–C_{28}

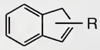

alkyloctahydroanthracene/phenanthrene

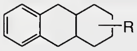

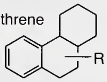

C_nH_{2n-12} alkylnaphthalenes C_{12}–C_{28}

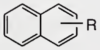

C_nH_{2n-14} alkylbiphenyls alkyltetrahydroanthracene/phenanthrene C_{12}–C_{28}

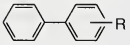

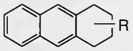

alkylcycloalkylnaphthalenes

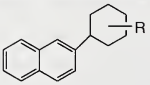

acenaphthene

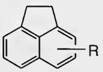

C_nH_{2n-16} alkylfluorenes alkylcyclohexenenaphthalenes C_{13}–C_{28}

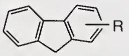

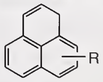

acenaphthylene

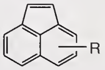

, etc.

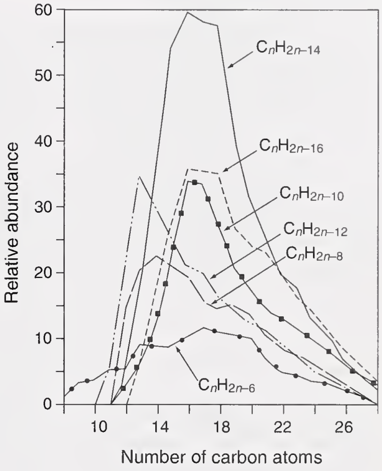

Figure 14.43 Distribution of the aromatic hydrocarbons in the pyrolysis oil of Athabasca asphaltene as determined by field ionization mass spectrometry. From J.D. Payzant, *et al.*, Ref. 83. © 1979, Elsevier.

Comparison with the plots in Figure 11.37 for the aromatic hydrocarbons in the maltene fraction of Athabasca bitumen suggests similarities in the concentration distributions of these hydrocarbons except that, as with the dibenzothiophenes, Figures 11.38 and 14.39, the maxima in the pyrolysis oil occur at slightly lower carbon numbers than in the maltene—at C_{13}–C_{17} rather than C_{17}–C_{20}. This can be due to the shortening of the alkyl chains during the thermolysis.

c) Polar fraction of the product

The polar fraction of the pyrolysis oil (Appendix 14.1) amounted to 30%, or 12.9% of the asphaltene. In the course of the main study of the saturate and aromatic fractions of this oil it was necessary to remove the alkenes produced in the thermolysis by hydroboration, converting them to alcohols prior to the chromatographic class separation step. As a result, the chromatographically-separated polar fraction contained substantial quantities of a complex mixture of alcohols and was unsuitable for further studies on the structural units of asphaltene. Therefore, using fresh oil from the pyrolysis of acetone-extracted asphaltene, the chromatographic class separation was repeated, but without the prior hydroboration step, and the resulting polar fraction was subjected to various analytical procedures. The complete separation sequence is illustrated in Appendix 14.2.

First, in order to separate any carboxylic acids that might have been present, the polar fraction was methylated with ethereal diazomethane, chromatographed, and the separated methyl esters analyzed by GC. A short series of C_{14}–C_{18} *n*-alkanoic acid methyl esters, dominated by the C_{16} and C_{18} members, and a *n*-$C_{\overline{18}}$ ester were detected.

Next, the basic nitrogen compounds were removed by complexation with $CuCl_2 \cdot 2\,H_2O$. The complex was filtered, decomposed with water and the free base was dissolved in CH_2Cl_2 and analyzed by GC–MS. Two series of nitrogen compounds, an alkylpyridine and an alkylquinoline series, were detected:

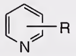
alkylpyridine

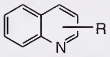
alkylquinoline

or

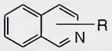
alkyl*iso*quinoline

The mass spectra of some representative members of each series in the pyrolysis oil are shown in Figure 14.44. The dominant fragmentation in the pyridines, loss of a methyl group, suggests the presence of an ethyl group in both compounds. Some C_9H_{19} pyridines were also detected. The major series of basic nitrogen compounds found was that of alkylquinolines (or alkyl*iso*quinolines) with C_2 through C_{10} substituents. In most cases the mass spectrum consists only of the molecular ions but, in cases where fragmentation occurs, it is possible to draw structural inferences. Three different mass fragmentograms for three isomeric C_5-substituted quinolines are also seen in Figure 14.44. The top panel is most likely an alkylquinoline bearing an ethyl group in the 8-position where facile hydrogen atom loss can take place:

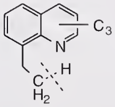

The middle and bottom panels show losses of methyl groups from two isomeric, ethyl-C_3-substituted quinolines.

The nitrogen base isolated amounted to only about 0.2% of the asphaltene and represents only a fraction of the total present.

The FTIR spectrum of the residual polar material following alkanoic acid methyl ester and nitrogen base removal showed the presence of OH (~3260 cm^{-1}) and several carbonyl functionalities (1650–1700 cm^{-1}). Quinolinols were not present. Therefore, any alcohols which could have been present were derivatized with *t*-butyldimethylsilyl chloride to their silyl ethers and analyzed by GC. Identified were a series of primary *n*-alkanols from C_{10} to C_{21}, a tetralinol and benzyl alcohol. All these alcohols were also found to be present in the acetone extract of the native asphaltene but in a somewhat different distribution, namely, the primary *n*-alkanols detected in the extract occurred in a concentration distribution $C_{12} > C_{10} > C_{14} > C_{18} > C_{17} > C_{16} > C_{19}$ with only traces of the other odd-carbon-number members being present.

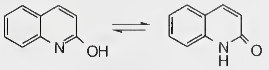

Alcohols have also been detected in the aromatic, resin and asphaltene fractions of Athabasca bitumen after saponification and in the process water from the hot-water separation. They differ in type, quantity and relative abundance depending upon whether their source was the asphaltene, aromatic or resin fraction of the bitumen. The *n*-alcohols detected were in the C_8–C_{30} range and in general were dominated by the even carbon members in all fractions. In the asphaltene *n*-C_{12} through *n*-C_{30} primary alcohols bound to the asphaltene *via* ester and ether bonds with a maximum at *n*-C_{14} (*v.i.*) were detected. In addition four sterols, comprising 24-ethylcholesterol, β-sitosterol, a C_{29} ($Z = -10$), a C_{30} ($Z = -12$) sterol and a C_{31} ($Z = -12$) enol along with some hopanols were observed. The presence of several other alcohols was noted but their structures were not elucidated.

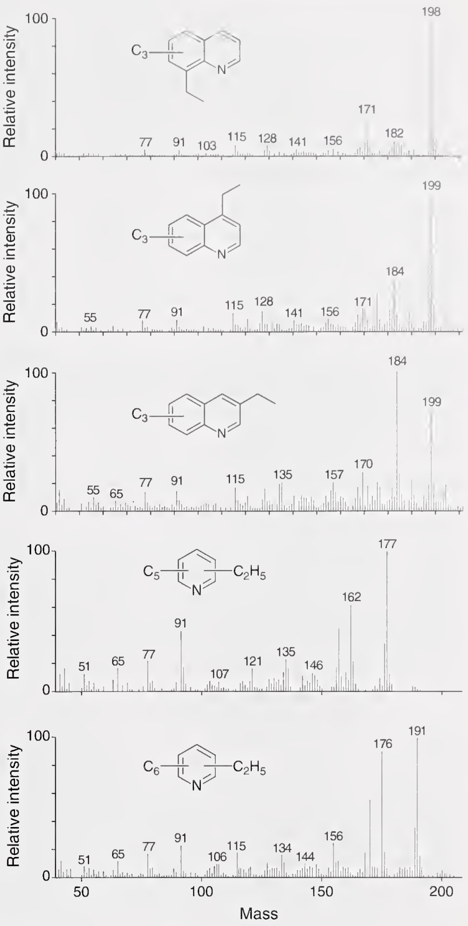

Figure 14.44 Mass spectra of C_7- and C_8-substituted pyridines and three isomeric C_5-substituted quinolines from the polar fraction of Athabasca asphaltene pyrolysis oil.

The residue of the polar fraction of the pyrolysis oil after removal of the alcohols showed strong carbonyl absorptions in the IR spectrum around 1750 cm^{-1} and a weak OH absorption around 3340 cm^{-1}, indicating that carboxylic acid esters may be present. Consequently, in order to reduce the carboxylic acid esters to their corresponding alcohols, the residual polar fraction was subjected to treatment with $LiAlH_4$,

$$RCH_2COOR' \xrightarrow{LiAlH_4} RCH_2CH_2OH \qquad (23)$$

which resulted in a drastic reduction of the carbonyl absorption intensity and a marked increase in the OH absorption intensity. After derivatization with butyldimethylsilylchloride and column chromatography, the resulting nonpolar fraction yielded the gas chromatogram shown in Figure

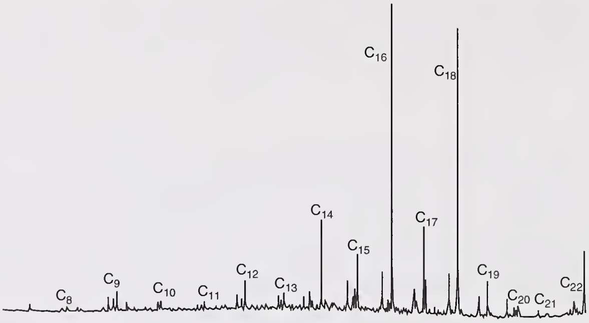

Figure 14.45 Gas chromatogram of the silylated alcohols obtained from $LiAlH_4$ reduction of the *n*-alkanoic acid esters in the residual pyrolysis oil. The peak labels refer to the chain lengths of the *normal* alcohols. From T.W. Mojelsky, E.M. Lown and O.P. Strausz, "Structural Units of Athabasca Asphaltene Pyrolysis Oil: The Polar Fraction", Progress Report to AOSTRA, Res. Proj. #810, June, 1991.

14.45. The major peaks correspond to primary *n*-alkanols and their concentration distributions, featuring strong preference for the even carbon numbers, especially C_{16} and C_{18}, are similar to those of the free *n*-alkanoic acid products found in the pyrolysis oil as mentioned above, and also those generated from the thermal cleavage and from the hydrolysis of side-chain ester groups, which will be shown later. The asphaltene acetone extract also contained a series of *n*-alkanoic acids in a distribution nearly identical to that in Figure 14.45. Thus, it can be concluded that (primarily *n*-alkanoic) carboxylic acids in the C_8–C_{22} range are present in the asphaltene, to some extent as adsorbed free acids, but mainly as esters, and perhaps to a lesser extent as anhydrides and salts. Most of the free acids can be removed from the asphaltene by acetone extraction but the esters remain in the asphaltene (*v.i.*) because they are covalently bound to the asphaltene core.

d) Product yields

Gravimetric yields for the various fractions of the Athabasca asphaltene pyrolysis oil are given in Table 14.16. The yield of the pyrolysis oil is 34% and the losses due to gas and volatile evolution correspond to 13% of the asphaltene. The measured product yields represent only a small fraction of the concentrations of the particular compound classes present in the asphaltene. This feature is a characteristic attribute of the thermolysis of highly complex mixtures as will be discussed later in this chapter where this theme will be enlarged upon in more detail.

Not surprisingly all the principal structural units identified are sulfur compounds, primarily thiophenes and condensed thiophenes dominated by benzothiophenes. In contrast, the predominant thiophenes in the maltene are the dibenzothiophenes and thiophenes are practically absent.

A portion of the benzothiophenes in the asphaltene pyrolysis oil may arise from the thermal dehydrogenation of benzothiolanes during pyrolysis. (Direct evidence for the presence of benzothiolanes in the asphaltene is lacking, but benzothiolanes have been detected in the maltene fraction of the bitumen.) The FIMS data (Figure 14.43) also reveal significant concentrations of alkyl-substituted $C_nH_{2n-10}S$, $C_nH_{2n-12}S$, $C_nH_{2n-14}S$, $C_nH_{2n-16}S$ and $C_nH_{2n-20}S$ series of compounds.

From the standpoint of structural information on the asphaltene molecule the important result of these investigations on the thermal decomposition products of asphaltene is the definite identification of a number of principal structural elements in the molecule. These are as follows:

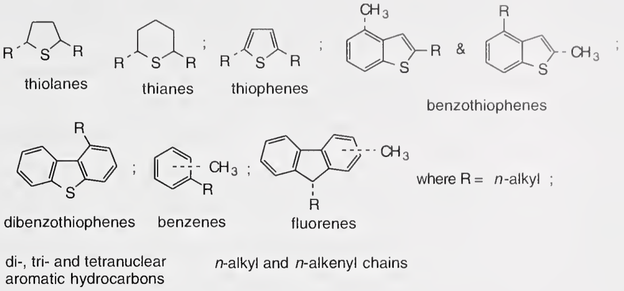

Moreover, by combining the pyrolysis results with ^{13}C NMR data it can be estimated that the above structural elements, along with the *n*-alkanoic acid esters, *n*-alkanol esters and ethers, contribute a minimum of 36% (but more likely 38–40%) to the mass of the asphaltene.

e) Flash pyrolysis with toluene-d$_8$ as the carrier

The asphaltene flash pyrolysis experiment was also done using toluene-d$_8$ as solvent. Under these conditions any free radicals formed during carbon bond scission would incorporate a deuterium atom if the solvent were the source of hydrogen atoms for the stabilization of the free radicals. However, careful GC-MS examination of the *n*-alkane products clearly showed the absence of any deuterium incorporation, indicating that the hydrogen-transfer reactions are taking place in the condensed phase rather than in the gas or vapor phase.

4.2 Reductive degradation of asphaltenes

Reductive degradation, like chemical degradation in general, is more selective than thermal degradation and can be directed to cleave specific bonds with a high degree of selectivity. Of the many known reducing agents used in organic chemistry, the degradation reactions of only two, namely the naphthalene radical anion (NRA) and nickel boride (NiB) with asphaltene have been studied in detail. These reagents are efficient in cleaving the sulfide C–S bonds but they also reduce the carbon–carbon double bonds and some of the other linkages which may be present in the asphaltene.

4.2.1 Naphthalene radical anion reduction

The NRA reagent reacts with any acyclic sulfides present in the asphaltene[84] by the electron transfer desulfurization reaction

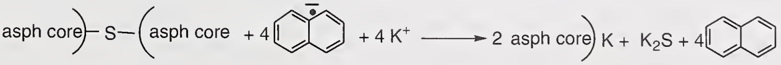

(24)

In a subsequent step the resultant organopotassium compounds are then stabilized by reaction with a suitable alkyl halide, in the reported case, *n*-octyl iodide:

$$\text{asph. core)K} + n\text{-}C_8H_{17}I \longrightarrow \text{core-}n\text{-octyl} + KI \qquad (25)$$

Other linkages possibly present in the asphaltene that will be cleaved by NRA include:

- carboxylic acid esters, 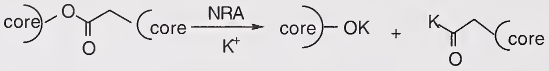 (26)

- aryl and benzyl ethers, 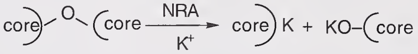 (27)

- hydrogen bondings, 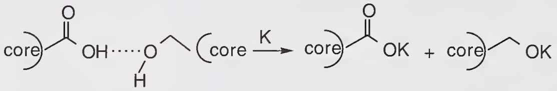 (28)

and essentially all other intermolecular bonds including aromatic stacking, Coulombic interactions, acid–base and other complexations. Reaction 24 illustrates the case of an asphaltene molecule in which two core segments are attached *via* a sulfide linkage. Upon desulfurization by NRA the asphaltene molecule falls apart into two core segments, effectively reducing the MW by a factor of slightly more than two. Experimentally, it was found[84] that the MW of the reduced Athabasca n-C_5-asphaltene—after correction for n-octyl group uptake —dropped to 580 from the initial value of 5,920 g·mol^{-1}. When the experiment was repeated with acetone-extracted asphaltene having a MW of 9,884 g·mol^{-1}, the MW dropped to 534 g·mol^{-1}. These observations indicated that the asphaltene molecules are built of core segments separated by C–S–C and some C–O–C(O)– covalent linkages and these covalent molecules are interconnected by aromatic stacking, hydrogen bonding, Coulombic and acid–base intermolecular bonds, as may be schematically represented by the equation

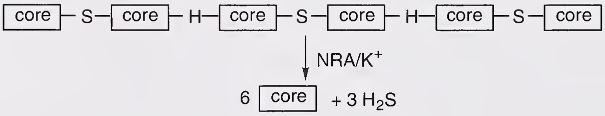 (29)

where the rectangles represent the asphaltene cores and H indicates any intermolecular bonds.

Now, the number of core segments in the sample asphaltene were

$$5{,}920/580 = 10.2$$

held together by 9.2 bonds in the whole asphaltene and

$$9{,}884/534 = 18.5$$

held together by 17.5 bonds in the acetone extracted asphaltene.

As can be seen, the NRA reaction has the unique and highly useful ability of being capable of bringing about the decomposition of the asphaltene supramolecule to its core segments by cleaving the sulfide and oxygen bridges and all intermolecular bonds. In the process, on the average about 46% of the sulfur is removed. A more accurate view of the desulfurization process and the cleavage of the sulfide bridges could be obtained from the NiB reduction of the asphaltene, as will be discussed in the following section.

Here, it is also mentioned that NRA and other mild degradative[37,67,68,75,85] treatments of Athabasca and Nigerian oil sand asphaltenes have been reported to produce a host of biological markers including n-alkanes, di-, tri- and pentacyclic terpanes, steranes and unidentified aromatic and polar molecules. These products are important sources of highly valuable molecular structural and geochemical information and point to the complexity of the mechanism for reductive degradation of asphaltene.

Among other reducing agents tried, $LiAlH_4$ has been shown to decrease the MW of Athabasca (Mildred Lake) asphaltene[86] from 6,110 to 3,547 g·mol^{-1} in a single-step process and Li in ethylenediamine effects the same reduction in three successive steps. The decrease in MW was attributed to cleavage of sulfide or ether bonds.

4.2.2 Nickel boride reduction

The reduction of asphaltene with NiB, prepared *in situ* from the reaction of $NiCl_2{\cdot}xH_2O$ with $NaBH_4$ in CH_3OH/THF solution, is thought to be a cleaner reaction which is essentially restricted to the cleavage of C–S bonds and the removal of sulfur as H_2S/NiS.[87–89] The reaction has been shown to be highly efficient, giving >98% yields from dialkylsulfide, dialkylpolysulfide, alkylthiol, alkyl- and dialkylthiolane and thiophene model compounds.

Detailed studies of the NiB reduction of acetone-extracted Athabasca n-C_5-asphaltene (high-MW asphaltene, HMA) and of the asphaltene in the acetone extract (low-MW asphaltene, LMA), Figure 14.46, included the identification of some of the desulfurization products and measurements of the molecular weight and compositional changes in the reduced asphaltenes.

The yields of products according to compound classes using the procedure shown in Appendix 14.3 are listed in Table 14.17. The total product yields for the HMA and LMA are around 4–5% and 16–20% and in the compound classes follow the order: saturates << polars ≤

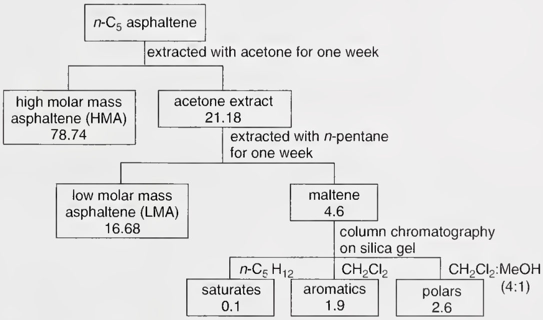
n-C5 asphaltene
extracted with acetone for one week
high molar mass asphaltene (HMA) 78.74
acetone extract 21.18
extracted with n-pentane for one week
low molar mass asphaltene (LMA) 16.68
maltene 4.6
column chromatography on silica gel
n-C5 H12
CH2Cl2
CH2Cl2:MeOH (4:1)
saturates 0.1
aromatics 1.9
polars 2.6

Figure 14.46 Procedure for isolating high-MW and low-MW asphaltene and occluded maltene fractions from crude n-C_5-asphaltene. From P. Peng *et al.*, Ref. 37. © 1997, American Chemical Society.

Table 14.17 Yields of compound classes (wt% of starting asphaltene) from the NiB desulfurization of Athabasca asphaltenes

	HMA sample A			HMA sample B		
	Sat.	Arom.	Polar	Sat.	Arom.	Polar
Protonated	0.050	1.93	1.87	0.11–0.13[a]	2.12–2.45[a]	2.08–2.74[a]
Deuterated[b]	0.047	2.61	2.04	0.11	1.97	1.87

	LMA sample A		
	Sat.	Arom.	Polar
Protonated	0.32	10.0	5.9
Deuterated	0.32, 0.36[c]	12.2, 12.5[c]	7.0–10.2[c]

[a] Range of three determinations. [b] Deuterated products are from reduction with $NaBD_4$ and CD_3OD. [c] Two determinations.

aromatics. Only the small amounts (0.05–0.35%) of the saturate fractions, comprising mostly biomarkers, were analyzed and their compositions will be discussed later.

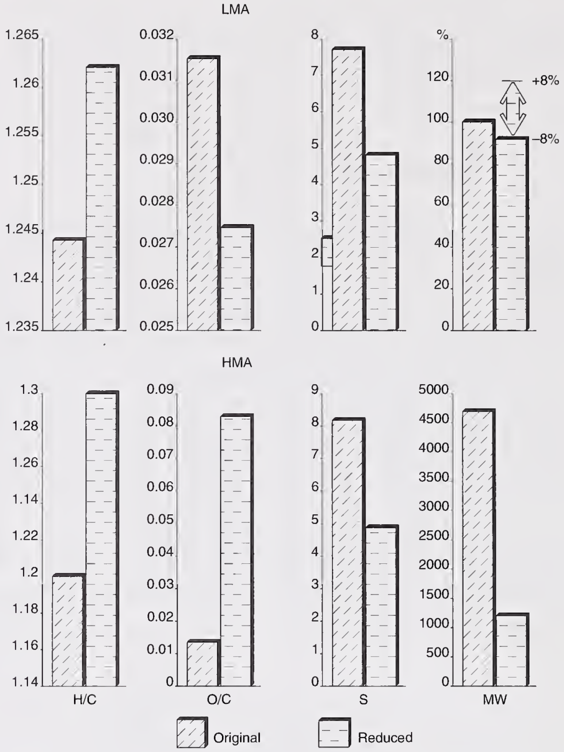

Figure 14.47 Elemental data for the original and NiB-desulfurized low-molecular-weight (LMA) and high-molecular-weight (HMA) asphaltene. From P. Peng *et al.*, Ref. 37. © 1997, American Chemical Society.

The MW of the HMA decreased from 4,630–5,170 g·mol^{-1} to about 1,220 g·mol^{-1} but that of the LMA remained essentially unchanged at 1,210–1,660 g·mol^{-1}, Figure 14.47. At the same time the $(H/C)_a$ ratio increased and the sulfur content decreased in both asphaltenes, the latter by 42% and 39% in the HMA and LMA. The O/C ratio decreased in the LMA and increased in the HMA; this latter phenomenon was also encountered in the NRA reduction of bitumen, the HBF_4 superacid-catalyzed hydrocracking of bitumen[90] and the HBF_4/H_2 liquefaction of coal;[91] thus it appears to be of general occurrence in the hydrocracking of carbonacious materials. The oxygen increase was shown to be a post-hydrocracking process taking place upon exposure of the hydrocracked material to air. Its progress can be monitored by measuring the intensity of the characteristic IR absorption bands for the $-CO_2H$ and sec-alcohol C–O stretches at 1705, 3440 and 1080 cm^{-1}. According to ^1H and ^{13}C NMR and FTIR data, the reactive entities responsible for the oxygen uptake are conjugated polyenes.

Now, returning to the NiB reaction we can write:

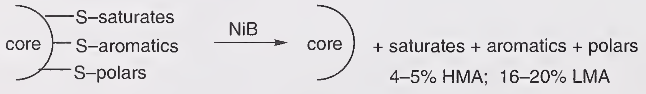
core
S–saturates
S–aromatics
S–polars
NiB
core
+ saturates + aromatics + polars
4–5% HMA; 16–20% LMA

(30)

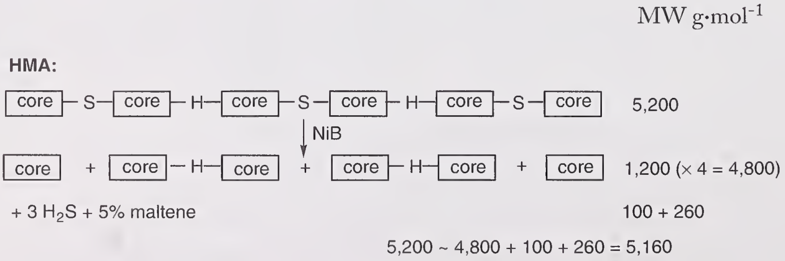
MW g·mol^{-1}
HMA:
core
S
core
H
core
S
core
H
core
S
core
5,200
NiB
core
+
core
H
core
+
core
H
core
+
core
1,200 (× 4 = 4,800)
+ 3 H$_2$S + 5% maltene
100 + 260
5,200 ~ 4,800 + 100 + 260 = 5,160

(31)

and **LMA:**

$$\text{asph} \xrightarrow{\text{NiB}} \text{asph} + 16\text{–}20\%\ \text{maltene} \qquad (32)$$

In order to estimate the number of sulfide bridges broken in the desulfurization step, it is necessary to take into account any interfering side reactions that could affect the apparent molecular mass change. One of these is the cleaving of the sulfide side chains producing low-MW saturates, aromatics and resins as well as some volatiles, which can lower the MW of the residual asphaltene up to 5–10%; another possibility is cleavage of the ester groups in the asphaltene. However, unlike the NRA reagent, NiB does not reduce alkanoic ester bonds[89] and should not substantially affect the existing hydrogen bonds. However, the extensive refluxing in methanol solution required (16 h) can cause transesterification in the existing ester groups,

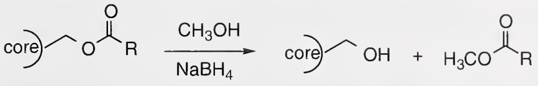

(33)

liberating new alcoholic hydroxyl groups on the asphaltene core and thereby increasing hydrogen bonding and molecular aggregation. This hypothesis was tested in an auxiliary experiment in which the HMA was subjected to the same procedure as applied in the NiB desulfurization experiments, but without the $NiCl_2$ reagent. It was indeed found that the molar mass of the HMA had increased from its initial value of 4,630 (in this particular experiment) to 5,460 g·mol^{-1}. Moreover, it was also observed that in the basic hydrolysis with NaOH the residual asphaltene partially lost its solubility, presumably because of the molar mass increase due to the creation of alcoholic and other highly polar functionalities, causing extensive aggregation of the asphaltene molecules. The small amount of residual asphaltene that could be solubilized had a molar mass of 5,630 g·mol^{-1}—a comparable but larger increase than that with $NaBH_4$ as the base.

Other complications in the overall reaction include oxygen uptake from air by the reduced material owing to its high reactivity with respect to molecular oxygen, and the strong adsorption of about 30% of the asphaltene to the black, solid NiB residue so that it could only be recovered by Soxhlet extraction with pyridine. This residue had the same elemental composition as the original asphaltene but there was an increase in the mineral content up to 6%, and in MW which, after correction for reagents-induced aggregation, amounted to 34%. This MW increase can partly be attributed to the incorporation of NiB into the asphaltene and it appears that this strongly-adsorbed asphaltene was effectively shielded against reaction with the NiB reagent.

Desulfurization, Figure 14.47, breaks up the HMA molecule aggregates by converting them to their covalent core segments, resulting, after correction for the above two side effects, in an approximately four-fold drop in the molar mass.

The four-fold reduction in MW requires at least a ~2% decrease in the sulfur content of the reduced asphaltene (if the core segments in the asphaltene form a linear array, as in Eq. (31) and assuming that upon C–S cleavage the sulfur is quantitatively removed from the molecule). The difference between the experimental value, 3.3%, and the 2% value estimated from Eq. (31), 1.3%, then corresponds to the sulfur removed in the cleavage of the low-MW appendages also connected to the core by sulfide linkages, and in cyclic sulfides and thiophenes.

Although it is probably fortuitous, it is to be noted that the MW of the reduced HMA core segment is about the same as the MW of the LMA.

The results of the NiB reduction validate the conclusion drawn from the earlier NRA reduction studies insofar as the existence of sulfide bridges connecting core segments in Athabasca asphaltene is concerned. This is an important feature of Athabasca (and of other Alberta) oil sand asphaltenes and is largely responsible for the singularly desirable property possessed by all Alberta oil sand and heavy oil asphaltenes, that of facile degradability on coking and hydrocracking, thereby precluding excessive coke formation. Sulfide bridges also connect small structural units comprising saturated, aromatic and polar molecules to the asphaltene core.

With regard to the evolution of the model of sulfide-bridged core segments,

$$\boxed{\text{core}}-\text{S}-\boxed{\text{core}}-\text{S}- \quad , \textit{etc.},$$

their existence in Athabasca asphaltene was first reported in 1964 using $LiAlH_4$, in 1967 using Li/ethylenediamine[86], in 1977 using NRA,[84] and in 1986 their presence was confirmed by the appearance of sulfones in the aliphatic residue from the ruthenium-ions-catalyzed oxidation.[92] They appeared to account for about 25% of the sulfur in asphaltene. Shortly thereafter, the homologous series of *n*-alkyl-substituted thiolanes and thianes discussed above (section 4.1.2 b) were isolated from the pyrolysis oil of Athabasca asphaltene.[81] At this point it became problematic to distinguish between acyclic and cyclic sulfur linkages as bridging elements and the possibility of cyclic sulfide bridges breaking up in the NRA electron transfer reactions, Eq. (24), had to be taken into account for the following reason. In the K/naphthalene/THF NRA electron transfer system the product anions were stabilized by octyl iodide. Among the octylated products identified were some octyl and C_{10}-naphthalenes. The C_2 unit (in the latter product required to convert the C_8-naphthalene to the C_{10}-naphthalene) had to come from THF. Thus, formally

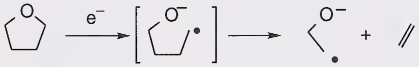

(34)

Therefore, the possibility of the analogous reaction with thiolanes being more facile and becoming the major reaction could not be discounted.

Now, it has been firmly established that in NiB reduction cyclic sulfides are desulfurized without cleavage of the carbon skeletons and therefore the molecular weight decrease of the reduced asphaltene is only possible as a result of the breakup of acyclic sulfur bridges.

Detailed discussions of the reduction and their ramifications with regard to the molecular structure of asphaltene and asphaltene aggregates will follow in Section 6 of this chapter.

a) Saturates from the NiB desulfurization

The precipitate formed from a solution of Athabasca bitumen upon *n*-pentane addition contained 4.6% occluded maltene, 16.7% LMA and 78.7% HMA (Figure 14.47). The asphaltenes were separately reduced with NiB and the saturate fractions of the compound class separated products along with that of the occluded maltene, Table 14.17, were subjected to detailed analysis. The composition of the occluded maltene saturates was similar to that of the bulk bitumen maltene saturates and therefore it is not considered further here.

i) HMA saturates

This fraction was rich in biomarkers and contained *n*-alkanes, alkylcyclohexanes, tricyclic terpanes, steranes, hopanes and gammacerane; all of them were originally bound to the asphaltene by sulfide bridges. Two different Athabasca samples, A and B, were studied.

1. Alkanes

The *n*-alkanes were separated from the cyclic compounds by urea adduction and their distribution is shown in Figure 14.48. These *n*-alkanes could have been present as alkyl side chains, in 2-*n*-alkylthiolanes and thianes, thiophenes, 2,5-di-*n*-alkylthiolanes, 2,6-di-*n*-alkylthianes, or thiophenes attached to the asphaltene by a sulfur atom at one end or both ends of the chain. Differentiation among these possibilities can be accomplished by the use of deuterium labeling. Indeed, MS analysis, Figure 14.49, shows the incorporation of d_1 to d_8 atoms into the *n*-alkane products when deuterated reagents were used in the reduction. The most abundant isotopomers were the d_2–d_5 alkanes, suggesting the prominence of the following structures:

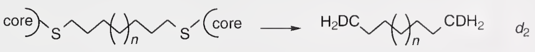

(35)

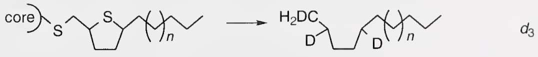

(36)

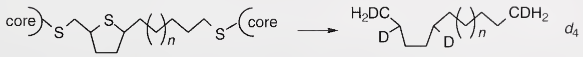

(37)

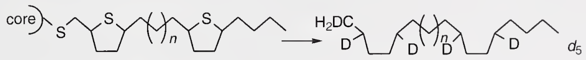

(38)

and to a lesser extent,

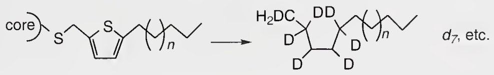

(39)

The yield of the *n*-alkane products from the NiB desulfurization is much less than the combined yield of cyclic sulfides and thiophenes produced in the thermolysis of asphaltene. This can be due partly to the incompleteness of the desulfurization (42%) but even if reasonable allowance is made for this, the alkane yield is still two orders of magnitude less than that of thianes + thiolanes + thiophenes in the thermolysis. This discrepancy shows that sulfur-attached *n*-alkyls, 2-*n*-alkyl-, 2,5-di-*n*-alkylthiolanes, thiophenes and 2,6-di-*n*-alkylthianes, are much less abundant than their C–C bond attached counterparts. Also, the sulfur-attached species, as indicated by their OEPs listed in Table 14.18, were probably incorporated into the asphaltene core at an early stage of diagenesis.

The irregular distribution of the *n*-alkanes apparent in the mass chromatogram (Figure 14.48) is an instrumental artifact and the correct concentration distribution is shown by the gas chromatogram. The small peaks appearing between the *n*-alkane peaks are due to branched alkanes, of which the mid-monomethyl branched series are designated with an asterisk. Sample B HMA showed a similar alkane distribution but with a less pronounced OEP.

The immediate sources of the alkanes are the *n*-alkyl, and alkylated cyclic sulfides and thiophenes. In the cyclic sulfides, thermally-induced sulfur migration along the chain in a single three-carbon-atom step has been shown to be facile:

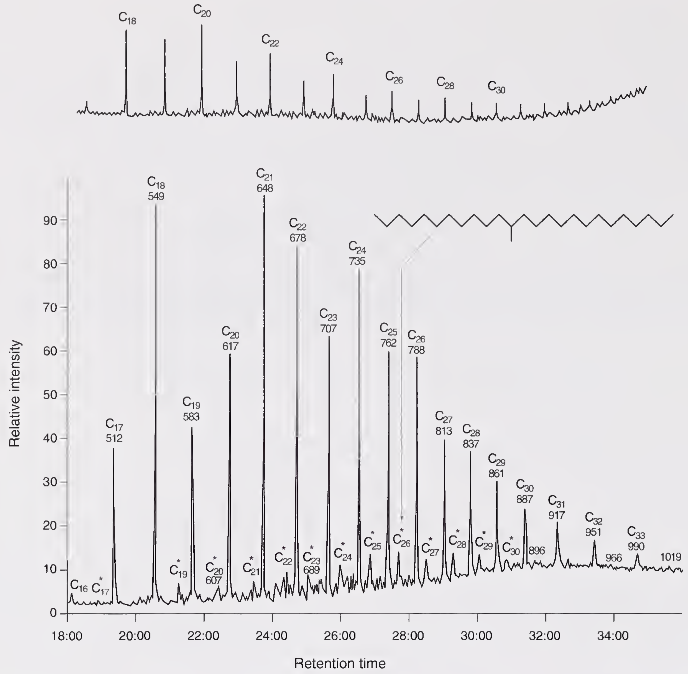

Figure 14.48 Gas chromatogram (top) and total ion current mass chromatogram (bottom) of the urea adduct from the NiB desulfurization of high-molecular-weight asphaltene showing the *n*-alkanes and mid-chain methylalkanes (*). The true concentration distribution is best represented by the gas chromatogram. From P. Peng *et al.*, Ref. 37. © 1997, American Chemical Society.

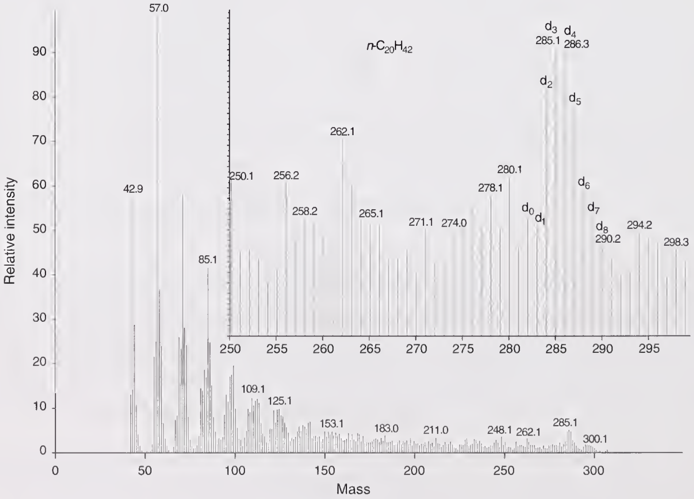

Figure 14.49 Mass spectrum of deuterated n-$C_{20}H_{42}$ from the $Ni_2B/NaBD_4/CH_3OD$ desulfurization of high-molecular-weight asphaltene. The enlarged scan portion (inset) shows the presence of d_0–d_8 isotopomers. From P. Peng *et al.*, Ref. 37. © 1997, American Chemical Society.

Table 14.18 Geochemical characterization of saturates from the NiB desulfurization of asphaltene

Sample	*n*-alkanes C(max.)	OEP[a]	Pr/Ph[b]	$C_{29}S/(R+S)^c$	$C_{27}{}^d$	$C_{28}{}^d$	$C_{29}{}^d$	$C_{31}S/(R+S)^c$	$(2+5)/(3+4)^f$	$G/C_{30}{}^g$
Maltene(A)								60.98		0.12
LMWA(A)	16,18	0.59	0.51	36.57	44.77	20.93	34.30	36.99		0.064
HMWA(A)	18	0.82		22.11	36.50	21.93	41.57	35.71	1.67	0.35
HMWA(B)	20	0.92		23.30	42.96	16.92	40.12			

[a] $(n\text{-}C_{17} + 6 \times n\text{-}C_{19} + n\text{-}C_{21})/(4 \times n\text{-}C_{18} + 4 \times n\text{-}C_{20})$; [b] Pristane/phytane; [c] C_{29}-20S, ααα sterane/(C_{29}-20S, ααα + C_{29}-20R, ααα sterane) × 100; [d] % of total steranes; [e] C_{31}-22S, αβ hopane/(C_{31}-22S, αβ + C_{31}-22R, αβ hopane) × 100; [f] [C_{32}(S + R) + C_{35}(S + R) αβ hopane]/[C_{33}(S + R) + C_{34}(S + R) αβ hopane]; [g] Gammacerane/C_{30}-αβ hopane.

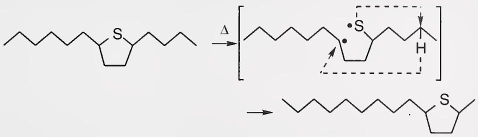

(40)

It is conceivable that methyl migration may also be operative to some extent:

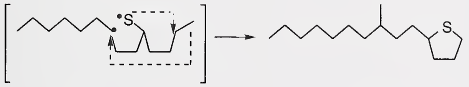

(41)

This would seem to tally with the observation that the most abundant positional isomers, the 6, 9 and 12 isomers, differ in the methyl position by three carbon units as in the case of sulfur migration in cyclic sulfides.[81]

Alternatively, the primary source of the mid-methyl carbon skeleton could have been mid-methyl bacterial fatty acids or alcohols. In this connection it is noteworthy that although there are reports of mid-methyl alkanes in modern sediments and organisms, most of the mid-methyl alkanes were actually found in early Paleozoic and Proterozoic oils and sediments. Hence, the presence of these compounds in the asphaltene may be an indication of a Paleozoic origin for the bitumen.

2. Alkylcyclohexanes

Alkylcyclochexanes have been reported in Ordovician samples where they all show a similar carbon number distribution with an odd-to-even predominance in the C_{14}–C_{24} range. In the short (C_{14}–C_{19}) series of cycloalkanes detected in the urea nonadduct fraction, Figure 14.50, however, no such preference is evident.

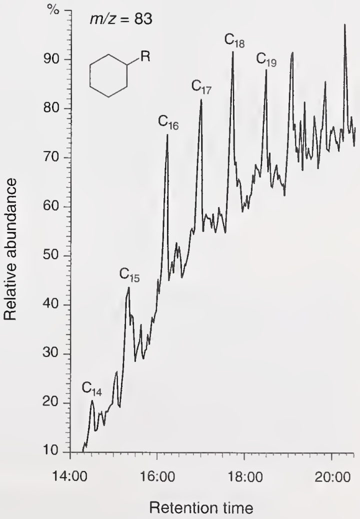

Figure 14.50 Cross scan chromatogram for *m/z* = 83 showing the presence of C_{14}–C_{19} alkylcyclohexanes from the NiB desulfurization of high-molecular-weight asphaltene. From P. Peng *et al.*, Ref. 37. © 1997, American Chemical Society.

The presence of alkylcyclohexanes would seem to support a Paleozoic origin for the bitumen, in apparent agreement with the presence of the mid-methylalkanes.

3. Tricyclic terpanes

Tricyclic terpanes are present in a distribution similar to that in the maltene, Figure 14.51, which is consistent with a carbonate source rock for the bitumen. Deuteration experiments suggest that these tricyclanes are preferentially bound to the asphaltene core *via* two sulfide linkages positioned in the isoprenoid side chain, Figure 14.52. Cleavage of these sulfide bonds can give rise, at least conceptually, to the precursor of the ubiquitous tetracyclic terpenoid sulfides occurring in nearly all sulfur-containing crude oils:

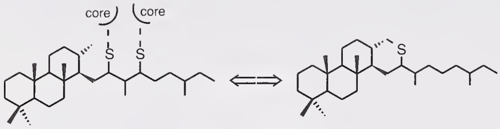

(42)

4. Steranes

Steranes are present as regular C_{27}–C_{30} steranes with C_{27} and C_{29} as the predominant members, Figure 14.53. The distribution of the geologic (S) and biologic (R) epimers (around the C–20 chiral center), Table 14.18, and the absence of diasteranes (in sharp contrast to the maltene steranes) clearly demonstrate that the asphaltene steranes are immature. The absence of diasteranes is also consistent with anoxic, clay-poor carbonate source rock. Because these asphaltene steranes have undergone minimal alterations, their carbon number distribution is a more reliable indicator of their original input distribution than is the carbon number distribution of the steranes or diasteranes in the maltene. The C_{28}/C_{29} sterane ratio for marine oils varies with age and has been found to have values in the 0.4–0.7 range for Upper Paleozoic and Lower Jurassic oils. The value for the asphaltene steranes, 0.42–0.53, would be consistent with an Upper Paleozoic age for the bitumen.

Unlike the tricyclanes, the steranes are bound to the asphaltene by a single sulfide bridge attached to the AB ring system rather than to the side chain, Figure 14.54. This particular mode of bonding may be related to the fact that pentacyclic sterane sulfides appear to be present only in low concentrations in the maltene.

5. Hopanes

The concentration of the hopanes is smaller than that of the tricyclanes or the steranes, Figure 14.55, and their concentration distribution corresponds to highly-reducing marine conditions during deposition. The epimeric ratios at C–22 in the C_{31}, C_{32} and C_{35} 17α,21β hopanes, Table 14.18, are significantly below the equilibrium value, in contrast to the situation in the occluded maltene where they are close to the equilibrium value—indicating a mature state for the occluded maltene and thermal immaturity for the asphaltene.

The main mode of bonding to the asphaltene core, Figure 14.56, involves multiple linkages in the side chain and the presence of the hexacyclic hopanoic sulfides in the maltene appears to validate the correlation between the mode of bonding in the asphaltene and the occurrence of the corresponding disulfides in the maltene,

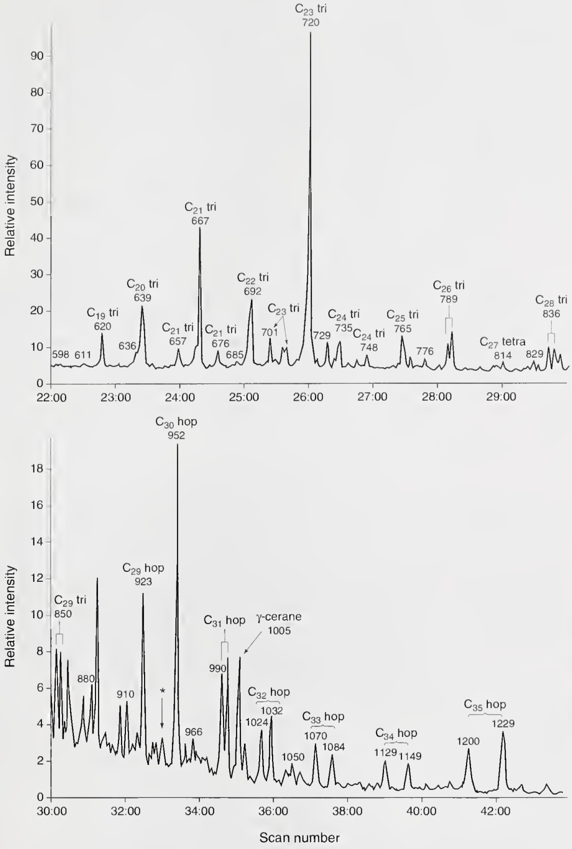

Figure 14.51 Cross scan chromatogram for $m/z = 191$ showing the distribution of C_{19}–C_{29} tricyclic, C_{27} tetracyclic, C_{29}–C_{35} pentacyclic terpenoid hydrocarbons and gammacerane from the NiB desulfurization of high-molecular-weight asphaltene. *28,30 Bisnorhopane. From P. Peng *et al.*, Ref. 37. © 1997, American Chemical Society.

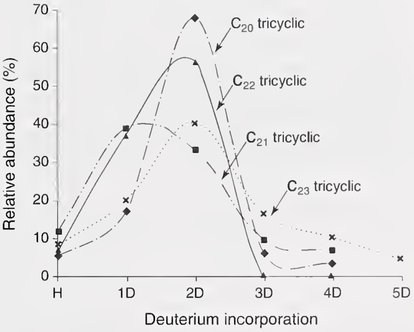

Figure 14.52 Relative abundances of d_0–d_5 tricyclic terpanes from the NiB/NaBD$_4$/CH$_3$OD desulfurization of high-molecular-weight asphaltene. From P. Peng *et al.*, Ref. 37. © 1997, American Chemical Society.

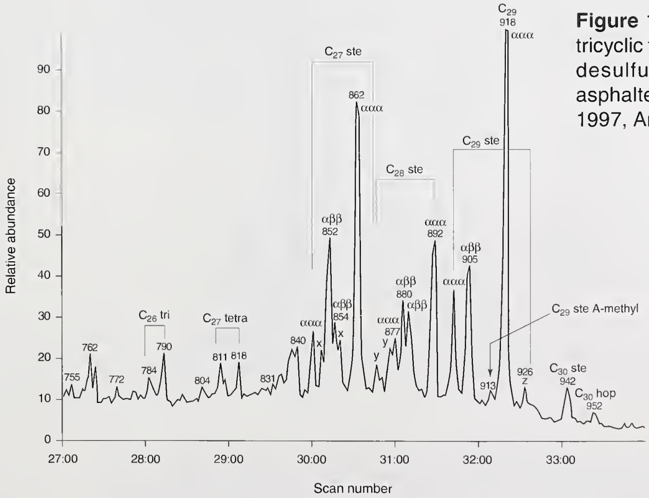

Figure 14.53 Cross scan chromatogram for $m/z = 217$, showing the distribution of the C_{27}–C_{30} steranes from the NiB desulfurization of high-molecular-weight asphaltene. From P. Peng *et al.*, Ref. 37. © 1997, American Chemical Society.

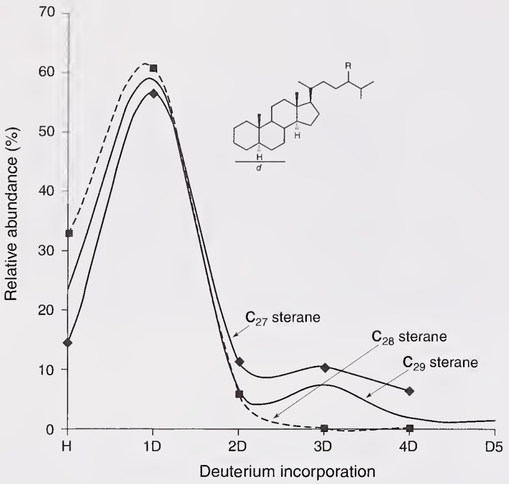

Figure 14.54 Relative abundances of d_0–d_4 C_{27}–C_{29} steranes from the NiB/NaBD$_4$/CH$_3$OD desulfurization of high-molecular-weight asphaltene. From P. Peng *et al.*, Ref. 37. © 1997, American Chemical Society.

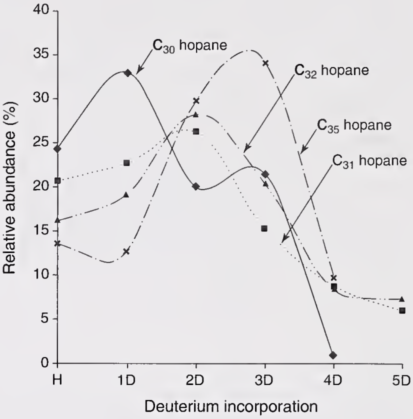

Figure 14.56 Relative abundances of d_0–d_5 hopanes from the NiB/NaBD$_4$/CH$_3$OD desulfurization of high-molecular-weight asphaltene. From P. Peng *et al.*, Ref. 37. © 1997, American Chemical Society.

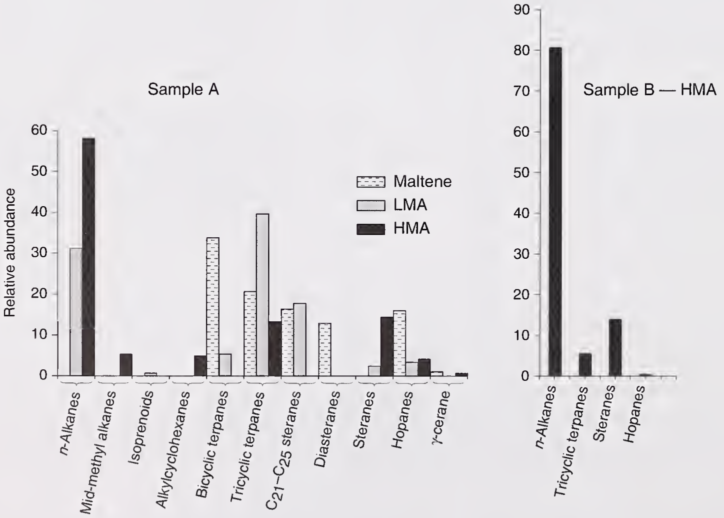

Figure 14.55 Relative concentration distributions of the hydrocarbon biomarkers from the NiB desulfurization of: (left) high- and low-molecular-weight asphaltene and maltene occluded in the crude asphaltene precipitate from one sample of Athabasca bitumen, and (right) high-molecular-weight asphaltene from a different sample of Athabasca bitumen. From P. Peng *et al.*, Ref. 37. © 1997, American Chemical Society.

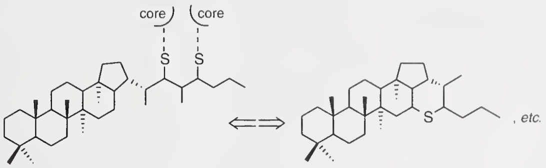

(43)

6. Gammacerane

Gammacerane is present in low concentrations in all three fractions studied, Table 14.18, indicating a hypersaline depositional environment or stratified water column. The gammacerane index ($G/\alpha\beta H_{30}$) is highest in the HMA and the gammacerane concentration is highest in the occluded maltene. Gammacerane has been found in petroleum corresponding to an age as early as the late Proterozoic.

ii) LMA saturates

The desulfurization product yields from sample A LMA, Table 14.17, were several times higher than those from the HMA of either sample. Here again only the saturates were investigated. Their composition, while in general being similar to the HMA saturates, exhibits characteristic differences.

1. *n*-Alkanes

Their distribution is similar to that of the HMA *n*-alkanes but here the odd-to-even preference is even more pronounced.

2. Bicyclic terpanes

Bicyclic terpanes represent a new class of compounds not found in HMAs, indicating a secondary origin for this series. Their distribution is similar to those in the bulk maltene. Their uptake of two deuterium atoms upon reduction in the presence of deuterated solvents reflects two sulfide linkages to the asphaltene core. Drimanes

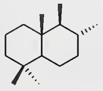

8β(H)-drimane

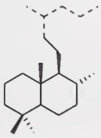

homodrimanes

are ubiquitous in sediments and crude oils and are thought to have bacterial origins. Again, as we observed with hydrocarbons linked by multiple sulfide bonds, their sulfides—which range from C_{17} to C_{31}—

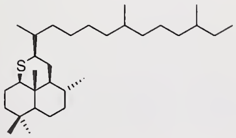

are present in the maltene fraction of the bitumen.

3. Tricyclic terpanes

In addition to the main series,

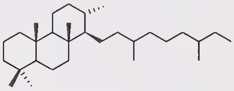

there are a number of isomers not seen in the HMA saturates.

4. Steranes

The steranes exhibit major differences from the HMA steranes with respect to maturity status, which is higher here, Table 14.18 (20S/[S + R] = 36.6% *vs* 22.1%), and in the appearance of a series of C_{21}–C_{25} steranes, Figure 14.57.

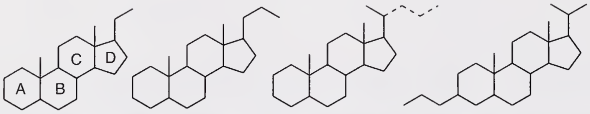

pregnane (C_{21}) bisnorcholane (C_{22}) C_{22}–C_{25} steranes 20-methyl-3-propylpregnane, *etc.*

The mode of attachment of the latter series to the asphaltene core, Figure 14.58, is also distinctly different from that of the regular C_{27}–C_{29} steranes in that it involves two sulfide linkages in the side chain in contrast to the single sulfide linkage in the AB ring system in the regular steranes.

ααα and αββ-pregnanes and -bisnorcholanes are present in Alberta bitumen maltenes where they could have originated at least in part from the thermocatalytic cleavage of higher steranes. In general they are associated with hypersaline lacustrine sediments, where they could have formed from unknown precursors that are indigenous to hypersaline environments. Since the C_{21}–C_{25} steranes are absent from the HMA, they either originated from the steranes in the LMA during diagenesis of the oil or from secondary biotic source materials. Most pregnane hormones found in nature are devoid of such complicating alkyl substitution and no organism is known to produce C_{23}–C_{25} steranes. Nonetheless, a secondary origin appears most likely at this time. Their absence from the bitumen maltene suggests that they are readily biodegradable.

Another significant variation in sterane distributions is the absence of diasteranes from the asphaltene and their presence in the maltene. Here again the diasteranes were formed from regular steranes or from secondary biotic source materials in the maltene. They are more resistant to biodegradation than are regular steranes and survived the biodegradation of the precursor oil of the bitumen.

5. Hopanes

The hopanes are similar to those from the HMA except that they are richer in minor isomers and show a slightly more mature character.

6. Pristane/phytane

The pristane/phytane ratio, 0.51, is indicative—in agreement with other biomarker characteristics—of a reducing depositional environment for the bitumen precursor oil source rock.

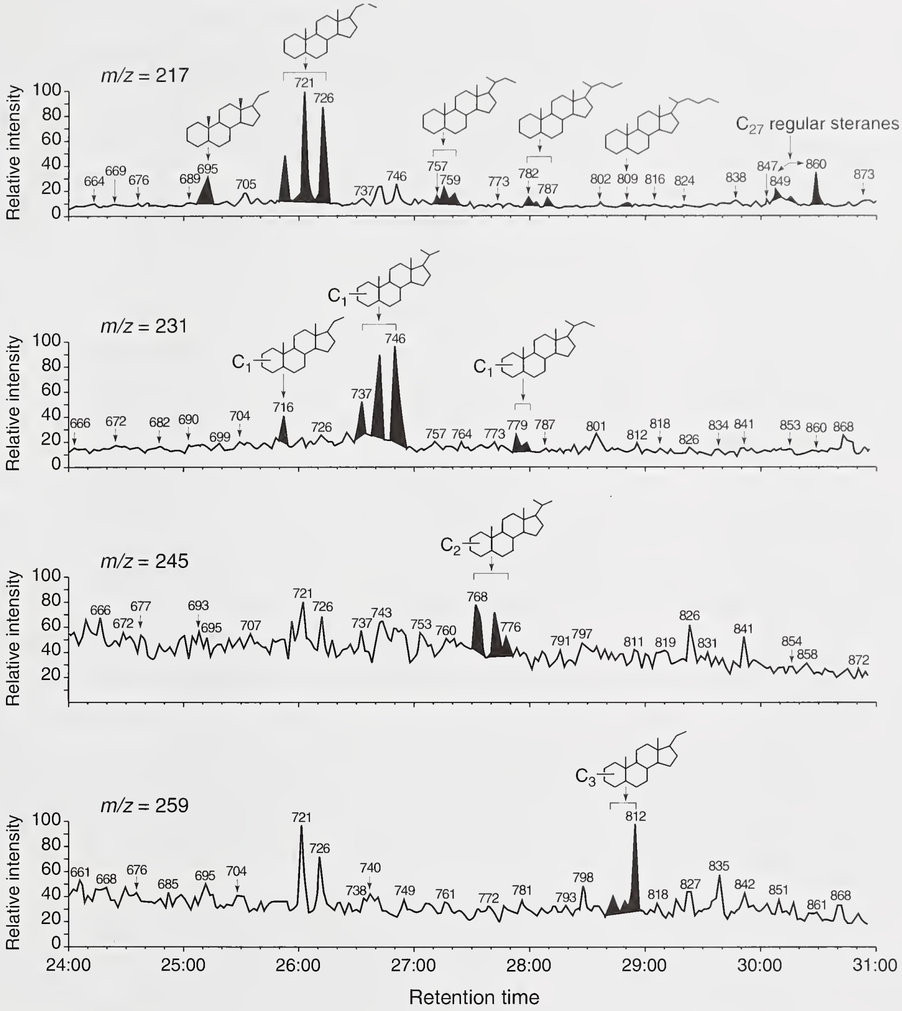

Figure 14.57 Cross-scan chromatograms for *m/z* = 217, 231, 245 and 259, showing the distribution of the C_{21}–C_{25} steranes from the NiB desulfurization of low-MW asphaltene. For the A-ring alkylated species the indicated structures are consistent with the EIMS but have not been proved. From P. Peng *et al.*, Ref. 37. © 1997, American Chemical Society.

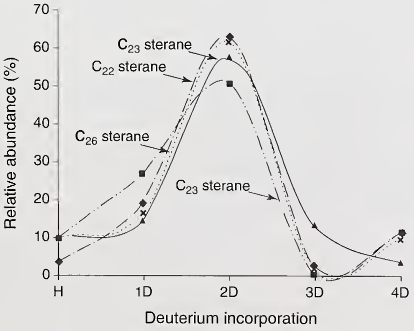

Figure 14.58 Relative abundances of d_0–d_5 C_{22}, two C_{23} and the C_{26} steranes from the NiB/$NaBD_4$/CH_3OD desulfurization of high-MW asphaltene. From P. Peng *et al.*, Ref. 37. © 1997, American Chemical Society.

iii) Summary and conclusions from the NiB reduction experiments

The three fractions—LMA, HMA and occluded maltene—isolated by solvent extraction from *n*-pentane-precipitated Athabasca asphaltene have different MWs and elemental and molecular compositions, and, upon NiB reduction, the asphaltenes release different quantities of *n*-pentane solubles: the yields from the LMA are four times higher than those from the HMA.

The MW of the residual asphaltene from the HMA is about four times less than that of the starting asphaltene, whereas that of the residual asphaltene from the LMA is essentially unchanged. The decrease in the MW of the reduced HMA is attributed to the presence of sulfide bridges holding together, on average, four molecular core segments. From an industrial point of view this is an important, desirable property of the covalent asphaltene molecule and this feature is largely resposible for the low inherent coke yield in the upgrading operation. The *n*-pentane-soluble products are considered to be originally attached to the asphaltene core by sulfide bridges as well. These products comprise saturate $<<$ polar $\leq$ aromatic fractions, of which only the saturates have been analyzed.

The saturated hydrocarbon biomarkers from all three fractions are similar yet characteristically different; the differences reflect variations in their apparent thermal maturity status and also leaves open the possibility of different biotic source materials. The least mature distribution is displayed by the HMA and the most mature by the occluded maltene where the concentration distributions are identical to those in the bulk maltene.

The gradation in apparent maturity is attributed to differences in the availability of external catalysts (clay, various light and heavy minerals). Asphaltene, by virtue of its high molar mass and tendency for aggregation, provides an environment that effectively prevents contact between its internal structure and external catalysts. Also, the biomarkers in the asphaltene are present in chemically bound form which, in itself, would—in most cases—reduce somewhat the efficiency of the catalytic reactions. Thus, the slowness of the maturation process in asphaltene is a consequence of the supramolecular, aggregate structure of asphaltene and, at the same time, points to the catalytic nature of the maturation processes.

Since the biomarkers liberated from the HMA are less mature than those from the other fractions, they have undergone fewer secondary chemical alterations and therefore they reflect more reliably the biomarker distribution as it existed in the young oil. Thus, the distribution of biomarkers unambiguously points to a carbonate source rock for the bitumen, and may also indicate a Paleozoic age. The observed biomarker characteristics, namely:

- absence of diasteranes
- low pristane/hopane ratio
- high hopane 29 index
- high hopane 32 and 35 indices
- presence of C_{30} sterane
- high gammacerane index
- high C_{23} and high ΣC_{20}–C_{25} tricyclic terpane index

when taken together with the high sulfur content and high V/Ni value provide strong evidence for a marine, carbonate source rock of the precursor oil along with a strongly reducing, hypersaline depositional environment, further validating the conclusions drawn from the biomarker distributions in the maltene. Indications for the age of the oil are much weaker. Thus, the value of the C_{28}/C_{29} sterane ratio along with the presence of gammacerane, mid-chain monomethylalkanes and the C_{14}–C_{20} alkylcyclohexanes may point to a Paleozoic age.

The lower OEP value found for the thermally more mature LMA suggests secondary incorporation of thermally young biomarkers from external sources *via* sulfide linkages. This conclusion is further supported by the observation of even-carbon-number dominated fatty acids from the thermolysis of the naphthenic residue from the RICO of Athabasca asphaltene; these were originally bound to the asphaltene in ester form. Additional evidence comes from various hydrolysis studies to be discussed below.

In the LMA the steranes show a distinctly higher state of maturity. Here, the percentage concentration of the steranes is lower, but diasteranes are still absent. Instead, C_{21}–C_{25} steranes, A-ring C_1–C_3 alkylated pregnanes and higher steranes appear. The diasteranes in the maltene could have and probably were formed mainly from the isomerization of the regular steranes in the maltene but it is unlikely that the A-ring-alkylated pregnanes and steranes also originated from the regular steranes. Instead, these biomarkers for the time being may be assumed to have been incorporated into the LMA *via* multiple sulfide linkages from secondary biotic sources.

Indeed, the marked differences between the biomarker profiles of the LMA and HMA, such as the distribution of α-branched *n*-alkyls on the aromatic moieties, the presence of the mid-methylalkanes and alkylcyclohexanes in the HMA and of the C_{21}–C_{25} steranes, and bicyclic terpanes in the LMA and their absence in the counterpart asphaltene may suggest biotic sources additional to the original source material for Athabasca asphaltene, perhaps from secondary microbial degradation or through the mixing of different oils. This latter possibility would not be inconsistent with the distribution of biomarkers attached to aromatic carbon (*v.i.*) either. As a general conclusion we may state that the results obtained from asphaltene are consistent with those obtained from the maltene (*cf.* Chapter 13) but they provide additional informations which were not obtainable from the maltene studies.

Some of the biomarkers—*e.g.* alkylthiolanes—are present in much greater concentration in C–C than in C–S forms.

In closing this section on NiB desulfurization we have to keep in mind that asphaltene is a highly complex chemical entity featuring not only many different functional groups and moieties but that any given one of these groups and moieties, depending on their location in the host molecule, can be activated, deactivated, sterically hindered, *etc.*, and thus can exhibit quite different reactivities with respect to NiB. Some examples of this diversity are the following:[89]

- heptadecanol, octadecanoic acid, octadecanoic acid methyl ester do not react, whereas
- phytol and chlorophyll *a* do react, yielding phytane and phytene;
- in cholesterol and ergosterol the ring double bonds do not react, but the double bond in the side chain does react.

The reactivity of course would also be affected by the experimental conditions of the reaction, *e.g.* ratio of reagents to substrate, duration of the experiment, *etc.* With respect to bond cleavage reactions leading to MW reduction in the residual asphaltene, it can be concluded from the available information[89] that the only interference could come from the reactions of activated carboxylic acid esters—if such bonds connecting asphaltene core segments exist.

4.3 Hydrolytic degradation of asphaltenes

Carboxylic acid esters are regular components of Alberta oil sand asphaltenes and petroleum asphaltenes in general. The ester bonds can be readily broken by saponification (basic hydrolysis) and the liberated acids or alcohols separated and analyzed, Figure 14.59. One of the ester components, the alcohol or the acid, must be anchored to the asphaltene, otherwise the ester molecule would be soluble in pentane and acetone and should not be present in HMAs, *i.e.*

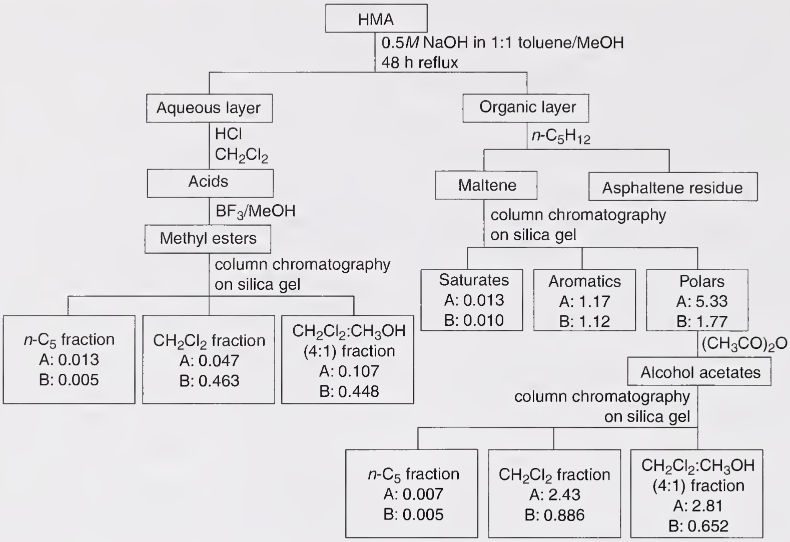
HMA
0.5*M* NaOH in 1:1 toluene/MeOH
48 h reflux
Aqueous layer
HCl
CH_2Cl_2
Acids
BF_3/MeOH
Methyl esters
column chromatography on silica gel
n-C_5 fraction A: 0.013 B: 0.005
CH_2Cl_2 fraction A: 0.047 B: 0.463
CH_2Cl_2:CH_3OH (4:1) fraction A: 0.107 B: 0.448
Organic layer
n-C_5H_{12}
Maltene
Asphaltene residue
column chromatography on silica gel
Saturates A: 0.013 B: 0.010
Aromatics A: 1.17 B: 1.12
Polars A: 5.33 B: 1.77
$(CH_3CO)_2O$
Alcohol acetates
column chromatography on silica gel
n-C_5 fraction A: 0.007 B: 0.005
CH_2Cl_2 fraction A: 2.43 B: 0.886
CH_2Cl_2:CH_3OH (4:1) fraction A: 2.81 B: 0.652

Figure 14.59 Flow chart for the basic hydrolysis of samples A and B high-MW asphaltene and chromatographic fractionation of the products. The numbers are percentage yields in terms of the starting asphaltene. From P. Peng *et al.*, Ref. 37. © 1997, American Chemical Society.

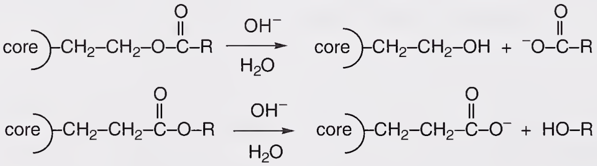

$$\text{core}\text{-}CH_2\text{-}CH_2\text{-}O\text{-}\overset{O}{\overset{\|}{C}}\text{-}R \xrightarrow[H_2O]{OH^-} \text{core}\text{-}CH_2\text{-}CH_2\text{-}OH + {}^-O\text{-}\overset{O}{\overset{\|}{C}}\text{-}R$$

$$\text{core}\text{-}CH_2\text{-}CH_2\text{-}\overset{O}{\overset{\|}{C}}\text{-}O\text{-}R \xrightarrow[H_2O]{OH^-} \text{core}\text{-}CH_2\text{-}CH_2\text{-}\overset{O}{\overset{\|}{C}}\text{-}O^- + HO\text{-}R \qquad (44)$$

Figures 14.60 and 14.61 show cross-scan mass chromatograms displaying the monocarboxylic acids isolated from HMA samples A and B after saponification.[37] In both cases the soluble acid fractions are dominated by even-carbon-number *n*-alkanoic acids from C_{14} to C_{27} with the C_{16} and C_{18} acids being the most prevalent. Trace quantities of the C_{20} and C_{21} tricyclic terpenoid acids are also in evidence in sample A. This distribution is quite similar to that found for the carboxylic acids in the thermolysis products of HMA (Figure 14.45), the *n*-alkanoic acid distribution in the Athabasca asphaltene acetone extract and the alkaline aqueous extract of the oil sand (Figure 13.55). The even-to-odd preference of all these *n*-alkanoic acids is indicative of a young thermal maturity status and they probably represent the metabolic products of the aerobic microorganisms which caused the secondary microbial degradation of the precursor oil to the present-day bitumen. Incorporation of the acids in ester form into the asphaltene structure protected them from microbial or thermocatalytic destruction.

The alcohols liberated in the hydrolysis of sample B HMA were also examined. The hydrolysis products were chromatographically separated according to compound classes (Figure 14.59) and the alcohol constituents of the polar fraction were acetylated and then chromatographically separated. The mass chromatogram in Figure 14.62 reveals a short series of even-carbon-number *n*-alcohols in the C_{12}–C_{24} range with a maximum at C_{14}. The almost complete absence of the odd members of the series here again points to a young thermal age, and these ester-bound alcohols and also the free *n*-alcohols found in various fractions of Athabasca bitumens are probably also related to the secondary biodegradation of the original oil.

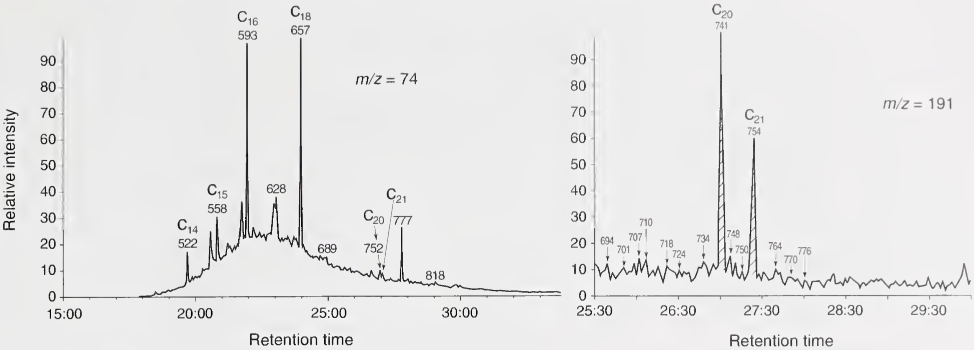

Figure 14.60 Cross-scan mass chromatograms for *m/z* = 74 and 191, showing the *n*-alkanoic and terpenoid acids produced in the basic hydrolysis of sample A high-MW asphaltene. From P. Peng *et al.*, Ref. 37. © 1997, American Chemical Society.

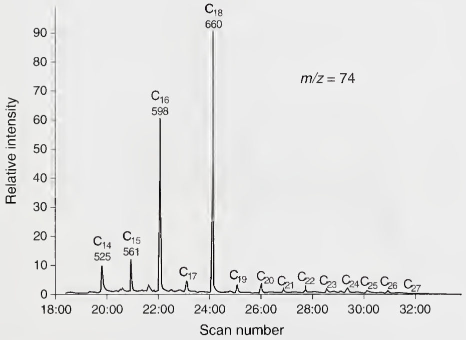

Figure 14.61 Cross-scan mass chromatogram for *m/z* = 74, showing the *n*-alkanoic acid distribution from the basic hydrolysis of sample B high-MW asphaltene. From P. Peng *et al.*, Ref. 37. © 1997, American Chemical Society.

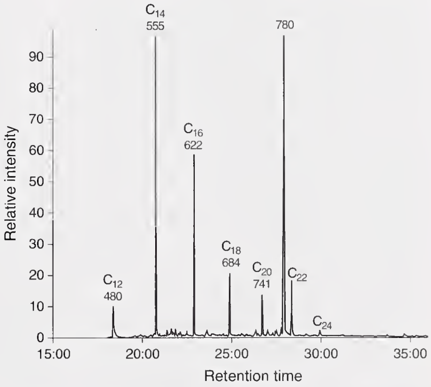

Figure 14.62 Total ion current chromatogram of the alcohols (analyzed as acetates) from the basic hydrolysis of sample B high-MW asphaltene. From P. Peng *et al.*, Ref. 37. © 1997, American Chemical Society.

The esterified products were measured gravimetrically, their yields being given in Figure 14.59. The total yield of hydrolysis products from sample A-HMA was 6.7% and from sample B-HMA, 3.8%. The yields of methyl ester concentrates were 0.05% and 0.46% and those of the alcohol acetates, 2.43 and 0.89%, respectively. Thus, considerable variation may occur in the ester contents from sample to sample. The other products contain a carboxylic or alcoholic hydroxyl group in addition to other polar functional groups; in the chromatographic separation they collect in the CH_3OH/CH_2Cl_2 eluant; their composition has not been examined.

The presence of ether linkages in sample B-HMA has been established by the BBr_3/CH_2Cl_2 cleavage of the ether bond, followed by $LiAlH_4$ reduction of the bromides to the hydrocarbons, Figure 14.63:

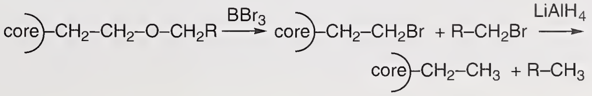

$$\text{core)}\!-CH_2-CH_2-O-CH_2R \xrightarrow{BBr_3} \text{core)}\!-CH_2-CH_2Br + R-CH_2Br \xrightarrow{LiAlH_4} \text{core)}\!-CH_2-CH_3 + R-CH_3 \qquad (45)$$

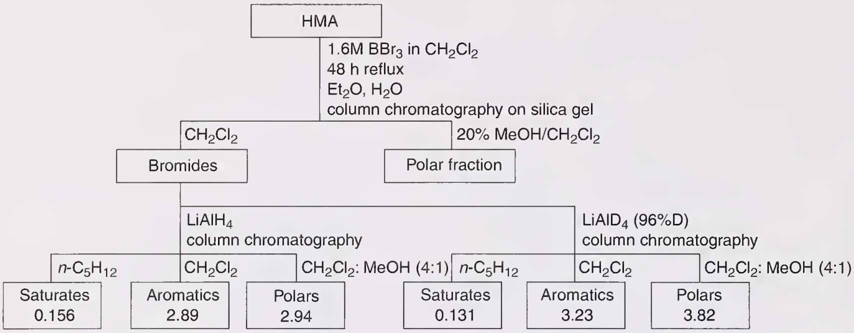
HMA
1.6M BBr_3 in CH_2Cl_2
48 h reflux
Et_2O, H_2O
column chromatography on silica gel
CH_2Cl_2
20% MeOH/CH_2Cl_2
Bromides
Polar fraction
$LiAlH_4$
column chromatography
$LiAlD_4$ (96%D)
column chromatography
n-C_5H_{12}
CH_2Cl_2
CH_2Cl_2: MeOH (4:1)
n-C_5H_{12}
CH_2Cl_2
CH_2Cl_2: MeOH (4:1)
Saturates 0.156
Aromatics 2.89
Polars 2.94
Saturates 0.131
Aromatics 3.23
Polars 3.82

Figure 14.63 Flow chart for the BBr_3 cleavage of C–O bonds in sample B high-MW asphaltene and chromatographic fractionation of the products. The numbers are percentage yields in terms of the starting asphaltene. From P. Peng *et al.,* Ref. 37. © 1997, American Chemical Society.

This procedure also liberates the alcohols from the ester bond in the form of bromides and therefore the resultant bromides will be a mixture derived from ether-bound and ester-bound alcohols. Accordingly, the total product yield from the BBr_3 cleavage experiment is higher, 6–7%, compared to the 3.8% yield and the 1.54% yield of alcohol acetates from basic hydrolysis. The mass chromatogram in Figure 14.64 shows a series of n-alkanes ranging from C_{12} to C_{30} along with trace quantities of hopanes (from their ethers). The n-alkanes feature a peculiar bimodal distribution with maxima at C_{16} and C_{26}. Portions of the even-numbered peaks from C_{12} to C_{24} come from the hydrolysis of the ester bonds and this series is devoid of odd-carbon-number members. The rest of the material comes from the cleavage of the ether bonds and this series, with a maximum at C_{26}, displays an odd-to-even ratio which is less biased in favor of the even members. Thus, it appears that the esters in the HMA are the residue of microbial metabolic products from the secondary degradation of the precursor oil whereas at least part of the ethers could be components of the original biotic source material of the bitumen.

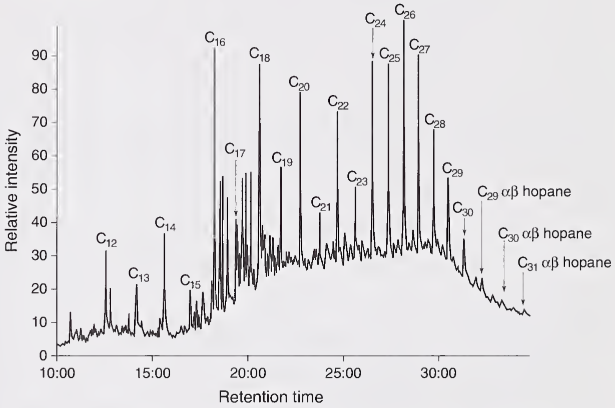

Figure 14.64 Total ion current mass chromatogram showing the n-alkanes and some hopanes formed after reduction of the bromide products from the BBr_3-induced cleavage of the ether and ester bonds in sample B high-MW asphaltene. From P. Peng *et al.,* Ref. 37. © 1997, American Chemical Society.

4.4 Oxidative degradation of asphaltenes by ruthenium ions-catalyzed oxidation (RICO)

This method permits the selective oxidation and near quantitative removal of aromatic carbon from asphaltene and other petroleum fractions, while leaving the structural integrity of aliphatic units intact.

Ruthenium ions-catalyzed oxidation (RICO) has been used in organic chemistry for the selective oxidation of organic compounds since 1953. However, the method did not become generally applicable until 1981 when the use of acetonitrile as a co-solvent was introduced.[66] The reaction is carried out in a water-carbon tetrachloride–acetonitrile mixed solvent. Acetonitrile is thought to prevent the precipitation of lower-valent ruthenium carboxylate complexes, thereby improving the selectivity and efficiency of the reaction. The effective oxidant is ruthenium tetroxide, RuO_4, a reddish-orange compound which melts near room temperature and is much more soluble in carbon tetrachloride than in water. It is formed *in situ* in the system by the oxidation of a lower-valent ruthenium salt, such as $RuCl_3 \cdot 3H_2O$, with an oxidant like sodium metaperiodate, $NaIO_4$, which in itself does not attack the substrate. Only small quantities of the ruthenium salt are required since it is effectively a catalyst:

$$\mathrm{Ru(III)} \xrightarrow{\mathrm{NaIO_4}} \mathrm{Ru(VIII)} \xrightarrow[\text{reducing agent}]{\text{org.}} \mathrm{Ru(III)/Ru(II)} \xrightarrow{\mathrm{NaIO_4}} \mathrm{Ru(VIII)} \qquad (46)$$

Under these conditions benzene is oxidized to carbon dioxide and water. Aliphatic substitution increases the reactivity and the site of attachment is excised preferentially in the form of a carboxylic acid of the substituent. Thus, an alkylbenzene yields an alkanoic acid as the principal product,

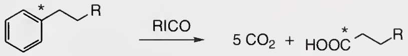

(47)

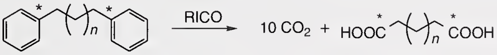

(48)

Carboxylic groups on an aromatic ring can cause deactivation of the ring against further oxidation and when two or more carboxylic groups are present the reaction stops, yielding benzene carboxylic acids from the oxidation of condensed aromatic ring structures.

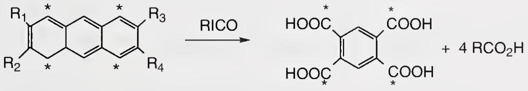

(49)

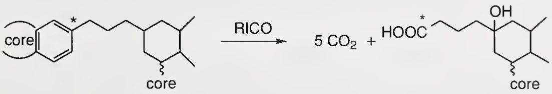

(50)

As indicated by the asterisks, the site of attachment of the alkyl group becomes the carboxylic carbon in the acid formed. Also, tertiary hydrogen may be oxidized to hydroxyl and ether to ester.

Thus, from these generalized reactions it is seen that the RICO method can play a highly useful role in the investigation of the molecular structure of asphaltene. It is potentially capable of yielding information on the following structural details:

- the kinds of alkyl groups attached to aromatic rings, *normal* or branched; their concentrations and chain length distributions;
- the kinds of alkyl bridges between aromatic rings, their concentrations and chain length distributions;
- the kinds of alkyl bridges connecting an aromatic ring to a naphthenic ring; their concentrations and chain length distributions;

- the kinds of alkyl groups connected to naphthenic rings;
- the nature of aromatic condensation;
- the types of biomarkers attached to aromatic carbons in the asphaltene core *via* aliphatic carbons; and
- indications about the nature of aliphatic core segments.

Detailed studies using RICO have been reported on Athabasca and other bitumen asphaltenes and some heavy oil and conventional asphaltenes. When Athabasca asphaltene was subjected to RICO the following products were obtained:

- a homologous series of *n*-alkanoic acids from C_2 to ~C_{33} along with several minor series of other alkanoic acids;
- a homologous series of α,ω-di-*n*-alkanoic acids from C_4 to ~C_{32} along with some other di- and tricarboxylic acids;
- a number of isomeric benzene di-, tri- and tetracarboxylic acids, benzene ketocarboxylic acids, and their nuclear methylated derivatives, along with benzene penta- and hexacarboxylic acids;
- series of carboxylic acids of saturated biomarkers;
- a non-distillable oxidized residue;
- carbon dioxide.

The alkanoic acids can be accurately analyzed as free acids, but the analysis is difficult and for this reason the acids in practice are converted to their esters or the acid salts are esterified with the appropriate alcohol in the presence of BBr_3 and analyzed as such. The low-MW members up to C_6 can be measured as *e.g.* their phenacyl or octadecyl esters,

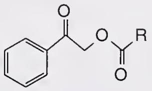

,

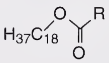

and the rest as their methyl or octyl esters. The diacids can be measured either as the dimethyl or dioctyl ester.

4.4.1 Low-MW products from Athabasca asphaltene

a) Alkyl side chains attached to aromatic carbon

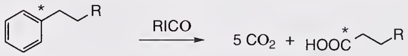

(47)

A gas chromatogram showing the low molar mass C_2–C_9 free acids[93][*] and the methyl esters of the C_{9+} acids[94] from another asphaltene sample is reproduced in Figure 14.65. The number of alkyl groups determined this way is plotted as a function of the chain length of the *n*-alkyl group in Figure 14.66. These *n*-alkyl groups were originally present as alkyl side chains attached to aromatic rings. The dominant series of monocarboxylic acids produced have a *normal* chain

---

[*] It should be pointed out that the volatile C_2–C_9 free acids were recovered in a vacuum system without any loss. In the esterification with diazomethane, however, substantial losses in the low molar mass portion of the methyl esters is unavoidable. Another complication is experienced in the determination of the acetic acid produced in the oxidation of methyl aryl structures because acetic acid is also produced in the hydrolysis/oxidation reactions of the acetonitrile cosolvent-phase transfer agent. This requires that the oxidation reaction be repeated using propionitrile as cosolvent instead of acetonitrile. Small quantities of acetic acids could be produced even in this system.

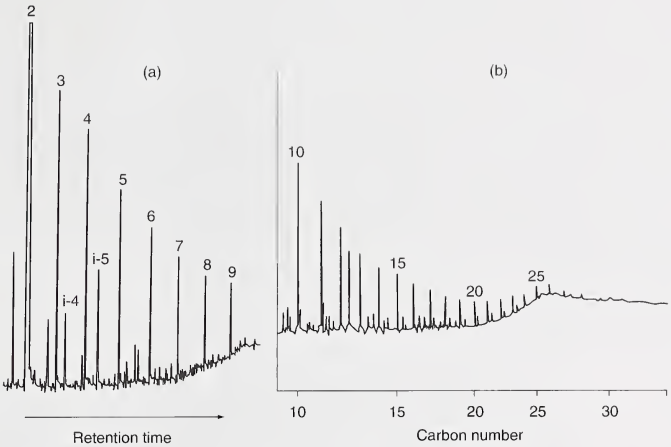

Figure 14.65 Gas chromatogram of the low-molar-mass C_2–C_9–*n*- and *iso*- acids[93] (a) along with the *n*-alkanoic methyl esters[94] (b) from the RICO of Athabasca asphaltene.

and the concentrations of the α-methyl, α-ethyl, α-*n*-propyl and α-*n*-butyl acids which elute between the peaks of the *normal* acids amounted to a fraction of the total aliphatic monocarboxylic acids. The length of the side chains extends from C_1 to ~C_{32} and beyond with a maximum concentration (~1.1 C per 100 C atoms in the asphaltene) at C_1 and the concentration decreases at first rapidly, then more gradually with increasing chain length.

The total number of carbon atoms in the *n*-alkyl side chains is 9.9 C per 100 C and the total number of *n*-alkyl groups, 2.5 per 100 C atoms. In other words, 9.9% of the carbon in Athabasca *n*-C_5-asphaltene is present in 2.5 *n*-alkyl side chains (per 100 C atoms) attached to aromatic rings in mono- through polynuclear aromatic and heteroaromatic compounds.

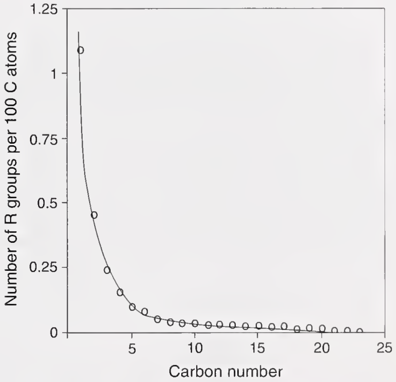

Figure 14.66 Distribution of *n*-alkyl groups attached to aromatic moieties in Athabasca asphaltene.

The alkanoic acid distributions were also determined in the high-MW and low-MW fractions of the asphaltene. The acids from the two oxidized fractions were separately methylated, fractionated by urea adduction into adduct (UA) and nonadduct (UNA) fractions and analyzed by GC and GC–MS. The gas chromatograms in Figures 14.67 and 14.68 show that both the HMA and LMA contain *n*-alkyl aromatics with *n*-alkyl chain lengths up to C_{33} and beyond, and while the HMA UA comprises a fairly clean suite of *n*-alkanoic methyl esters the LMA UA contains substantial concentrations of other homologous series of *n*-alkanoic esters, namely, homologous series of α-methyl, α-ethyl, α-*n*-propyl and α-*n*-butyl branched *n*-alkanoic acid methyl esters. On adduction chromatography, these branched esters become concentrated in the UNA fraction.

Figures 14.69–14.73 show the characteristic fragment ions m/z = 74, 88, 102, 116 and 130 for the α-H, α-methyl, α-ethyl, α-*n*-propyl and α-*n*-butyl branched acid methyl esters in the UNA fraction of the HMA, as predicted by the McLafferty rearrangement mechanism:

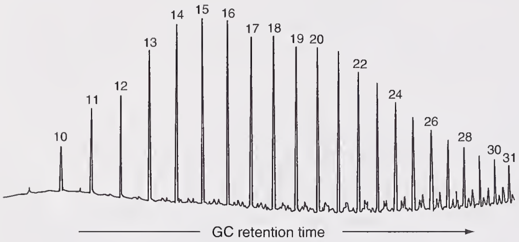

Figure 14.67 Gas chromatogram of the urea adduct fraction showing the *n*-alkanoic acid methyl esters from the RICO of high-MW asphaltene. The numbers refer to the carbon numbers of the corresponding acids. From O.P. Strausz *et al.*, Ref. 93. © 1999, American Chemical Society.

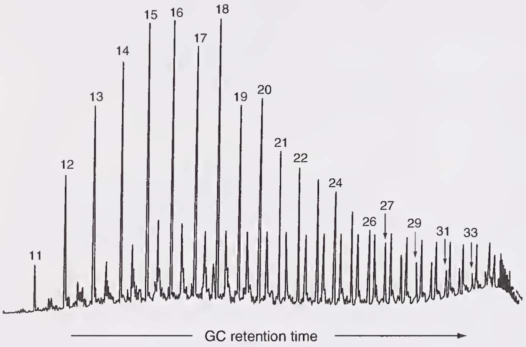

Figure 14.68 Gas chromatogram of the urea adduct fraction showing the *n*-alkanoic acid methyl esters from the RICO of low-MW asphaltene. The numbers refer to the carbon numbers of the corresponding acids. From O.P. Strausz *et al.*, Ref. 93. © 1999, American Chemical Society.

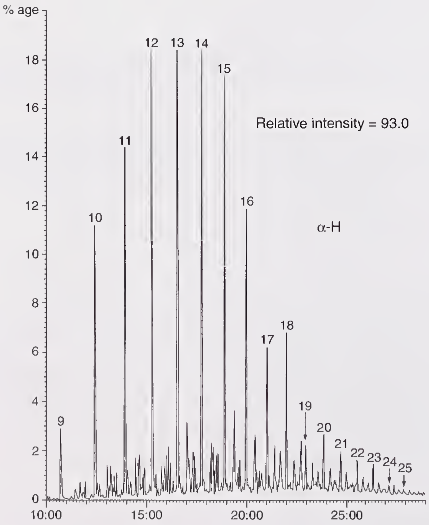

Figure 14.69 Cross scan chromatogram for *m/z* = 74 showing the distribution of the *n*- alkanoic methyl esters from the RICO of the UNA fraction of high-MW asphaltene. From O.P. Strausz *et al.*, Ref. 93. © 1999, American Chemical Society.

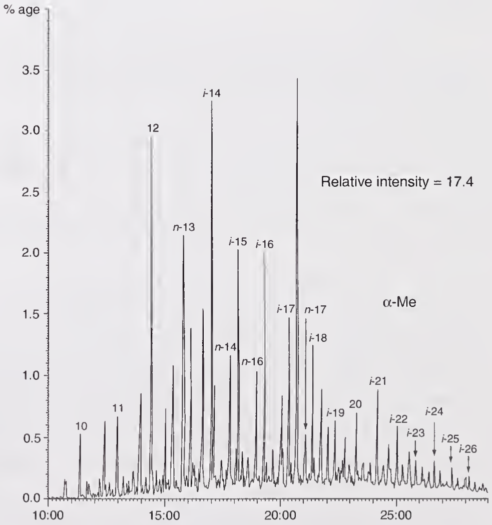

Figure 14.70 Cross scan chromatogram for *m/z* = 88 showing the distributions of the CH_3-branched alkanoic methyl esters from the RICO of the UNA fraction of high-MW asphaltene. From O.P. Strausz *et al.*, Ref. 93. © 1999, American Chemical Society.

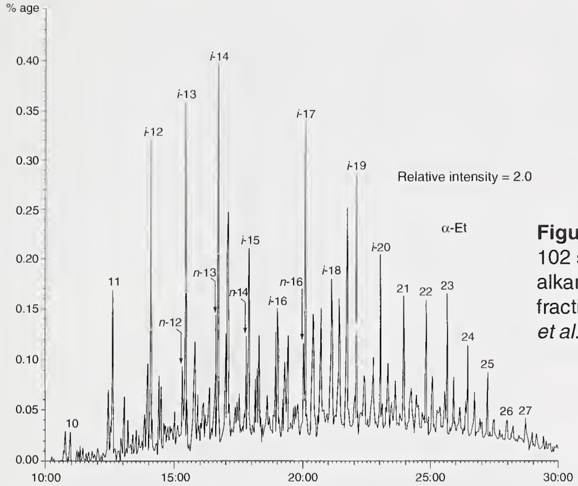

Figure 14.71 Cross scan chromatogram for *m/z* = 102 showing the distribution of the C_2H_5-branched alkanoic methyl esters from the RICO of the UNA fraction of high-MW asphaltene. From O.P. Strausz *et al.*, Ref. 93. © 1999, American Chemical Society.

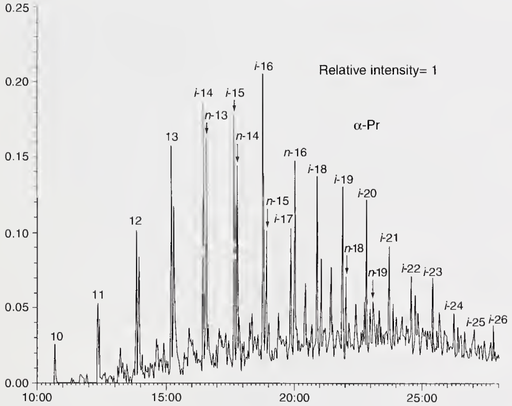

Figure 14.72 Cross scan chromatogram for *m/z* = 116 showing the distribution of the C_3H_7-branched alkanoic methyl esters from the RICO of the UNA fraction of high-MW asphaltene. From O.P. Strausz *et al.*, Ref. 93. © 1999, American Chemical Society.

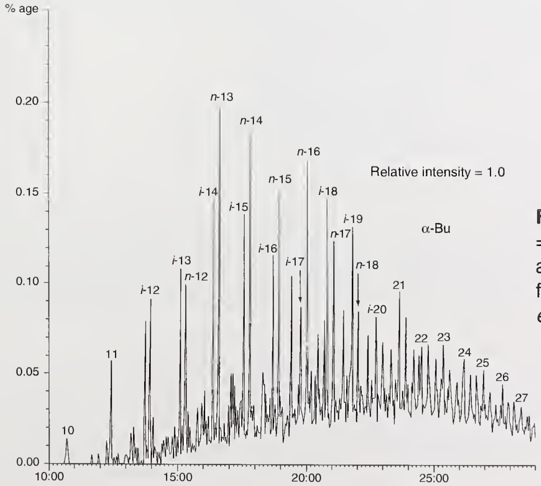

Figure 14.73 Cross scan chromatogram for *m/z* =130 showing the distribution of C_4H_9-branched alkanoic methyl esters from the RICO of the UNA fraction of high-MW asphaltene. From O.P. Strausz *et al.*, Ref. 93. © 1999, American Chemical Society.

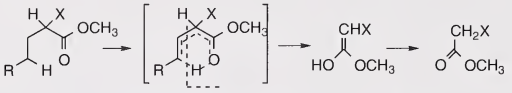
H
X
OCH3
R
H
O
CHX
HO
OCH3
CH2X
O
OCH3

(51)

where X = H, CH_3, C_2H_5, C_3H_7, C_4H_9, giving rise to
m/z = 74, 88, 102, 116, 130.

Note the gradual change in ion intensity, manifesting the rapid decline in concentration with increasing size of the branched moiety.

The appearance of these acid series in the RICO products of Athabasca asphaltene proves the presence of the following structural elements in the asphaltene:

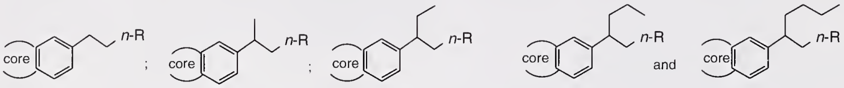
core
n-R
;
core
n-R
;
core
n-R
core
n-R
and
core
n-R

in decreasing order of importance. The carbon range for the side chains is C_1–C_4 and for R up to C_{34}. At high carbon numbers in the LMA UA series, the branched acids concentration exceeds that of the nonbranched counterparts (Figure 14.68).

In the RICO products from the HMA, series of cyclic monocarboxylic acids concentrated in the UNA fraction were also detected. Among them, series of tricyclic terpenoid (cheilanthanoic) acids in the C_{21}–C_{29} range and pentacyclic terpenoid (hopanoic) acid methyl esters in the C_{28}–C_{33} range were identified,

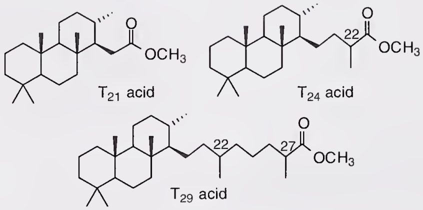
O
OCH3
T_{21} acid
22
O
OCH3
T_{24} acid
22
27
O
OCH3
T_{29} acid

(the T number specifies the carbon number in
the acid portion of the esters)

the *m/z* = 191 cross scans of which are shown in Figure 14.74. The presence of the stereomeric components of the ≥T_{24} members due to the chirals centers at C–22 and C–27 are clearly evident. The peaks labelled H_{28}–H_{33} are hopanoic acid methyl esters:

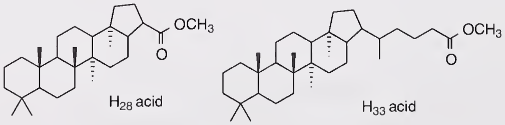
OCH3
O
H_{28} acid
OCH3
O
H_{33} acid

These terpenoid acids were also detected as free acids in the polar fraction of the maltene but here they were all originally attached as hydrocarbon appendages to aromatic rings, the carboxylic carbon corresponding to the aromatic carbon of the site of attachment to the asphaltene core, *e.g.*

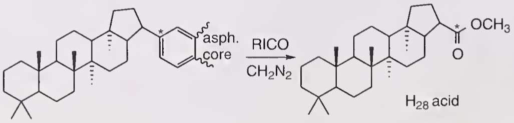
*
asph.
core
RICO
CH2N2
*
OCH3
O
H_{28} acid

(52)

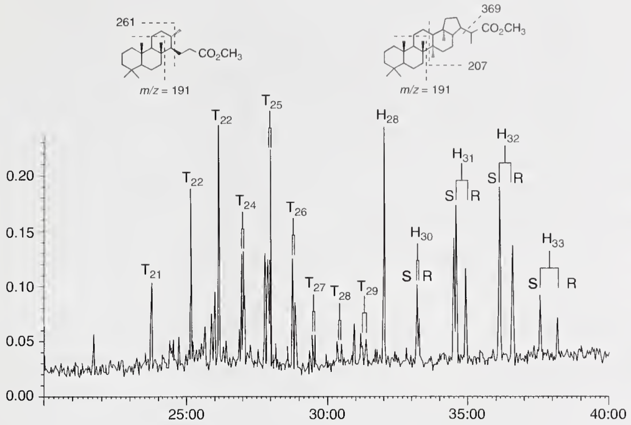

Figure 14.74 Cross scan chromatogram for *m/z* = 191 showing the distributions of the tricyclic and pentacyclic acid methyl esters in the UNA fraction of the RICO products of high-MW asphaltene. The numbers refer to the carbon numbers of the corresponding acids. From O.P. Strausz *et al.*, Ref. 93. © 1999, American Chemical Society.

The distribution of the acids from the RICO of the HMA (after making allowance for the extra carbon excised from the aromatic ring), while similar in some respects, is not identical to that of the free acids or the parent hydrocarbons in the maltene, or the hydrocarbons from the NiB reduction of the HMA. Thus, while the epimeric ratio S/(S + R) of the C_{32} and C_{33} member acids here is 0.60, about the same as in the hydrocarbons from the maltene, the carbon number distribution is different from that in the free acids; more importantly, the epimeric ratio is very different from that found in the NiB-reduced hydrocarbon products, 0.36, from the HMA. This difference in the epimeric ratios suggests that the sulfur-bound hopanes and the aromatic-carbon-bound hopanes in the HMA were incorporated into the HMA at different stages of diagenesis, the sulfur-bound hopanes probably at an early, immature stage and the aromatic-carbon-bound hopanes at a late stage of diagenetic or catagenetic alterations when they were already in a mature state. This points again to the possibility of the precursor oil of the bitumen being a mixture of two (or more) different oils.

As discussed before, cheilanthanoic and hopanoic acids occur in the maltene but steranoic acids are conspicuously absent. However, in the RICO of the HMA two sets of steranoic acids were observed, one is the C_{21}–C_{24} and the other is the C_{28}–C_{30} set, showing different sites of attachments to the aromatic rings, Figures 14.75 and 14.76

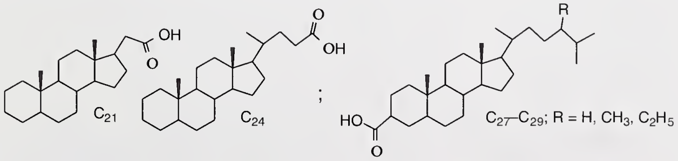

as is the case for their sulfide-bound analogs, evidently retaining the positions of the functional groups in their probable precursors. None of these naphthenic carboxylic acids was detected in the LMA.

Comparing the distribution of hydrocarbon biomarkers in the HMA, it is noted that C_{21}–C_{24} steranes were absent in the sulfide-bound biomarkers but are present in low concentrations in the aromatic-carbon-bound biomarkers. This finding lends additional support to the proposition discussed previously in this chapter, that the incorporation of terpenoid sulfides and biomarkers into the aromatic moieties of the asphaltene occurred at different stages of

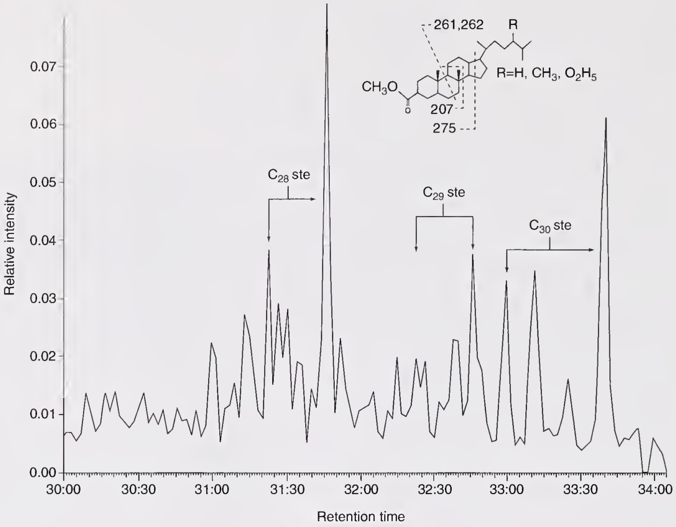

Figure 14.75 Cross scan chromatogram for *m/z* = 275 showing the C_{28}–C_{30} tetracyclic acid methyl esters from the RICO of the UNA fraction of high-MW asphaltene. The numbers refer to the carbon numbers of the corresponding acids. From O.P. Strausz *et al.*, Ref. 93. © 1999, American Chemical Society.

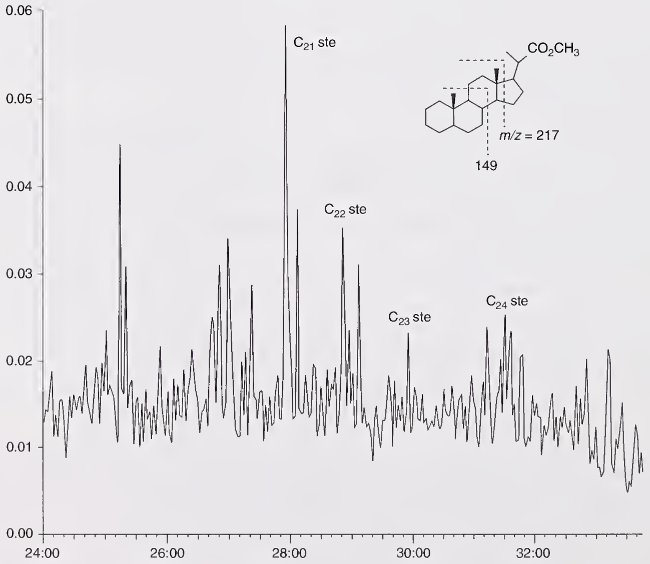

Figure 14.76 Cross scan chromatogram for *m/z* = 217 showing the C_{21}–C_{24} tetracyclic (steroid) acid methyl esters from the RICO of the UNA fraction of high-MW asphaltene. The numbers refer to the carbon numbers of the corresponding acids. From O.P. Strausz *et al.*, Ref. 93. © 1999, American Chemical Society.

maturity and that the precursor oil of Athabasca bitumen might have migrated and accumulated in their present-day reservoirs about 100 or as early as 200 million years ago.[79] The early-mature–mature status of the bitumen, however, would appear to be more consistent with a 100 million years date. If the oils forming the blend had different degrees of thermal maturity then the presence of the two sets of biomarkers in the HMA, a less mature and a more mature set, could be explained. On the other hand, since the mechanism of incorporation of both the sulfide-bound and the aromatic-carbon-bound biomarkers is unknown, the possibility that the apparent difference in thermal maturity is somehow related to the mechanism of their incorporation into the HMA cannot be definitely discounted.

Sulfur incorporation into the organic sediments occurs at an early diagenetic age and therefore at this point it is believed that the sulfur-bound biomarkers are residues of the original primary biotic source material in the HMA. This would be consistent with the general biomarker and bulk composition of Alberta bitumens; moreover, the vast quantity of sulfur distributed so uniformly in them is not likely to have come from secondary sources.

The absence of these cyclic biomarker acids from the RICO products of the LMA is an unexpected feature which again underscores the sharp division between the LMA and HMA.

Finally, it should be pointed out that the results of the hydrolysis experiments described in section 4.3 exclude the possibility that the carboxylic acids in the RICO experiments could have arisen as a consequence of ether or ester bond cleavages.

The mode of incorporation of the biomarker molecules into the asphaltene aromatics is not clearly understood, but the precursors are thought to be the various alcohol derivatives of the biomarkers. Thus, in the case of hopanes,these could be the various hopane polyols which have been discussed in the literature:[96]

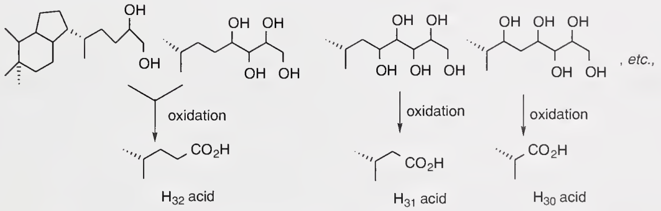

and the various hopanols, *e.g.* α,β C_{29-31} hopanols occurring in low concentrations in free and ether-bound states in the bitumen.[37] Incorporation into the aromatic framework of the asphaltene then may take place at the alcohol stage in competition with oxidation of the alcohols to acids.

The distribution of the cheilanthanoic acids is different from anything we have encountered before. The maximum concentration occurs at C_{25}, implicating the C_{24} alcohol as the probable precursor:

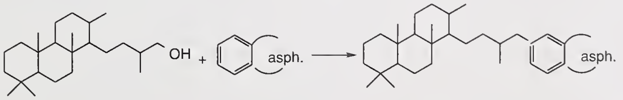

(53)

As expected, the C_{23} member is missing and epimeric splitting of the GC peak occurs at $C_{\geq 24}$.

For steranes and pregnanes the alcoholic functional group is at the same positions—the C-3 and the side-chain terminus—as the sulfur in the sulfide-attached compounds. In addition to the above series, small quantities of regular isoprenoid acid esters (including pristane and phytane) and some β-methyl alkanoic acid esters and, in the case of LMA, perhaps some 2-alkanones and other branched acid esters, were also detected.

In concluding this section we point out that the selectivity observed here for the incorporation of aliphatic biomarkers in the asphaltene *via* C_{aliph}–C_{arom} or C–S–C bonds is of general validity, as will be shown later in this chapter, and it reflects the functional group position in the incorporating biomarker molecule. Reversing this argument, it also follows that regular steranes and their shorter side-chain relatives, the pregnanes, have their functional groups in different locations within the molecule and therefore the pregnanes do not appear to be the derivatives of the regular steranes, but rather molecules originating from different biotic source material. Also, the observed substitution pattern militates against the possibility of a trans-alkylation mechanism. Led by the above considerations in retrospect it would seem likely that at least some of the α-branched alkyl side chains on the aromatic carbons also originate from a Friedel-Crafts-type substitution reaction of the appropriate alcohol with the aromatic structures of the asphaltene. However, it should also be pointed out that Friedel-Crafts alkylation with alkyl halides often leads to isomeric alkylated products, *e.g.*

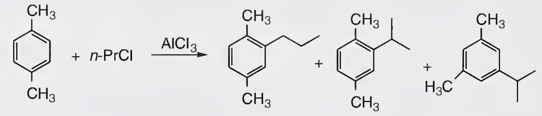

(54)

and thus, the α-branched alkyl aromatics could have arisen from alkylation with *n*-alcohols.[97]

b) Alkyl bridges connecting two aromatic units

The oxidation of aromatic units connected by an alkyl bridge yields alkanoic dicarboxylic acids.

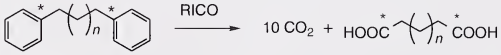

(48)

n-Alkyl (*n*-alkenyl or polymethylene) bridges should yield α,ω-di-*n*-alkanoic acids as has indeed been found experimentally. A gas chromatogram of the methyl esters of the diacids is shown in Figure 14.77. The carbon range for the diacids is from 4 to at least 26, corresponding to methylene bridges of 2 to at least 24 carbons and, as can be seen from the methylene bridge concentration *versus* methylene bridge length plot in Figure 14.78, the concentration of the bridges falls off monotonically with growing length as for the *n*-alkyl side chains except for the first member, the C_4 acid, which is present in a lower concentration than the next member, the C_5 acid. The number of carbon atoms present in bridges connecting two aromatic rings is calculated to be 3.8 and the number of bridges, 0.61 per 100 C atoms in the asphaltene.

The shortest-chain acid that could be detected under the severe experimental conditions employed was C_4, representing a dimethylene bridge in the asphaltene. Shorter-than-C_4-chain acids probably were formed in the oxidation, but C_3 and C_2 acids which would represent a methylene bridge and a biphenyl linkage in the asphaltene, respectively, could not have been detected even though biphenyl linkages are present in the asphaltene (*v.i.*) because these acids are readily oxidized to carbon dioxide in RICO under the severe experimental conditions employed. The C_1 and C_2 bridges are chemically more reactive than the longer ones owing to the increased reactivity of the benzylic bonds activated by two aromatic ring systems and therefore during thermal maturation the concentration of such compounds would be more rapidly depleted than that of compounds with longer bridges. This may explain the low concentration found for the C_2 bridge.

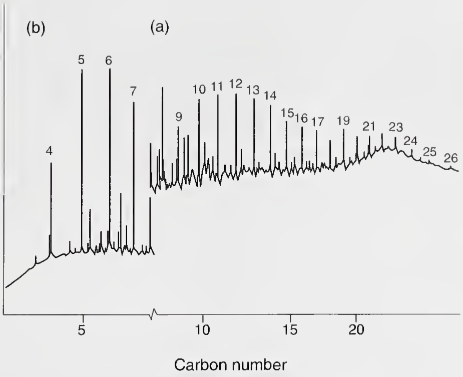

Figure 14.77 Gas chromatograms of the α,ω-di-*n*-alkanoic acid methyl esters from the RICO of Athabasca asphaltene. a) Organic phase; b) water phase. The numbers above the peaks correspond to the carbon numbers of the esters.

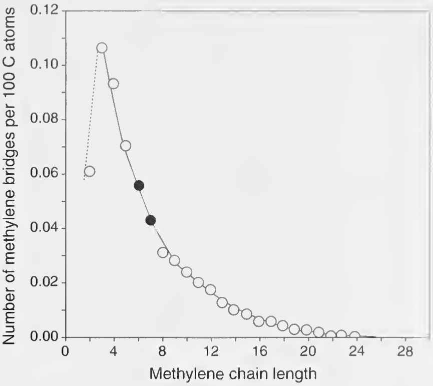

Figure 14.78 Distribution of methylene bridges attached to aromatic moieties in Athabasca asphaltene. C_6 and C_7 are interpolated values.

c) Aromatic units

The presence of two or more carboxylic or other electron-withdrawing groups on a benzene ring is known to deactivate the ring against further reaction in RICO , thereby preventing the complete oxidation of aromatic carbons to CO_2:

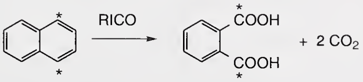
*
*
RICO
*
COOH
COOH
*
+ 2 CO₂

(55)

Consequently, a third group of acids detected and identified was a suite of benzenedi- through hexacarboxylic acids which, after methylation to convert them to their methyl esters, gave the gas chromatogram reproduced in Figure 14.79. The following esters were identified:[94]

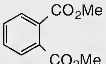
CO₂Me
CO₂Me

1

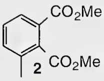
CO₂Me
CO₂Me

2

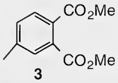
CO₂Me
CO₂Me

3

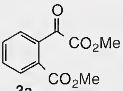
O
CO₂Me
CO₂Me

3a

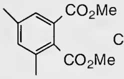
CO₂Me
CO₂Me

4

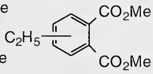
C₂H₅
CO₂Me
CO₂Me

5

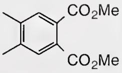
CO₂Me
CO₂Me

6

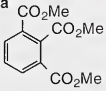
CO₂Me
CO₂Me
CO₂Me

7

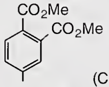
CO₂Me
CO₂Me
CO₂Me

8

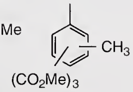

9

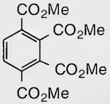
CO₂Me
CO₂Me
CO₂Me
CO₂Me

10

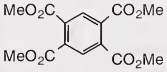
MeO₂C
CO₂Me
MeO₂C
CO₂Me

11

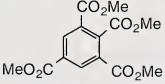
CO₂Me
CO₂Me
MeO₂C
CO₂Me

12

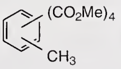

13

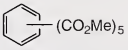

14

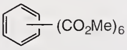

15

Therefore, the appearance of these benzenecarboxylic acids is a consequence of the presence of condensed aromatic hydrocarbons in the asphaltene. To account for the products identified, as

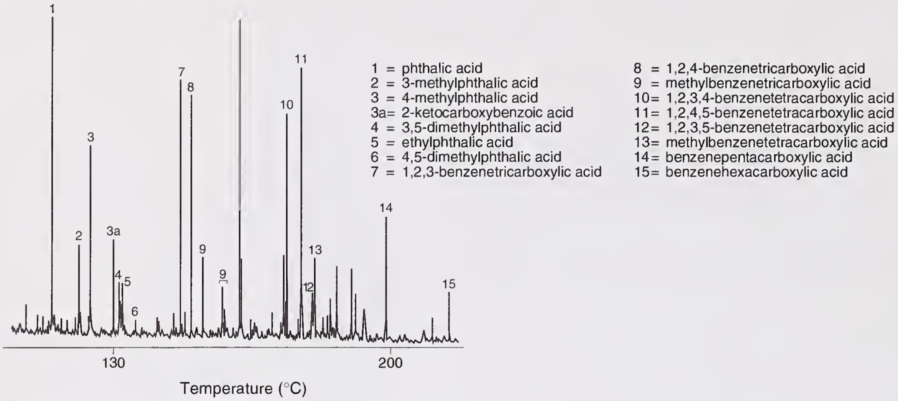

Figure 14.79 Gas chromatogram of the methyl esters of benzenepolycarboxylic acids produced from the RICO of Athabasca asphaltene.

examples, the following types of condensed aromatic nuclei may be considered:

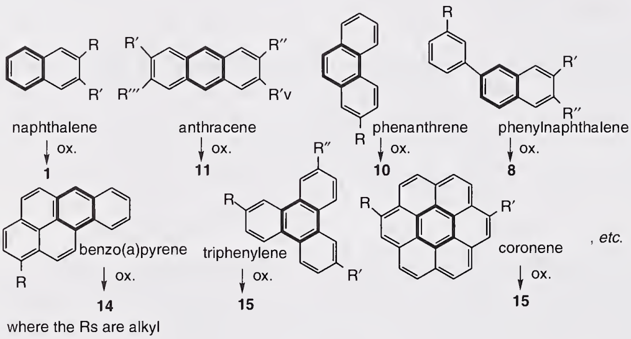
R
R′
naphthalene
ox.
1
R′
R″
R‴
R′v
anthracene
ox.
11
R
phenanthrene
ox.
10
R
R′
R″
phenylnaphthalene
ox.
8
benzo(a)pyrene
R
ox.
14
R
R″
R′
triphenylene
ox.
15
R
R′
coronene
ox.
15
, etc.
where the Rs are alkyl

The benzene ring that remains intact is indicated in the structure by boldface, and the directly adjoining aromatic carbons would be oxidized to carboxylic groups to form the corresponding benzenepolycarboxylic acids. However, in most cases, more than one oxidation route giving different benzenepolycarboxylic acids is possible. For example, triphenylene can lead to benzenedicarboxylic acid in addition to benzenehexacarboxylic acid; experimentally, both acids were found to be produced in a statistical ratio of about 3:1.[*]

The appearance of these products provides evidence for the presence of anthracene, phenanthrene, pyrene, benzpyrene, triphenylene, coronene, *etc.*, type hydrocarbons and of biaryl linkages in the asphaltene molecules. On the other hand, the absence of other than the 1,2-isomer of benzenedicarboxylic acid in the oxidation products suggests that there are no benzene rings in the condensed systems of asphaltene that would be involved in more than one biaryl bond.

Of course, heteroaromatic systems would also undergo oxidative degradation. Thus, benzothiophene is oxidized completely and dibenzothiophene is quantitatively converted to its

---

[*] Recently, unsubstituted coronene has been reported to yield 10 (30.1%), 15 (1.9%) and 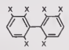 (25.1%) where X = $-CO_2H$.[98]

sulfone. Alkyl-substituted (above C_1) dibenzothiophenes, however, would be oxidized to alkanoic acids because alkyl substitution enhances the reactivity of the aromatic ring and alters the nature of the end products. Both the nature of the products and their yields may be dependent on the reaction conditions of temperature, reaction time, solvents ratio and cooxidant to substrate ratio.

A list of the RICO reactions of model compounds is given in Appendix 14.4. In many cases the product recovery is less than quantitative and even with simple alkylbenzenes such as propylbenzene and tridecylbenzene side products such as the alkylphenone and shorter chain homologous acids are formed in low yields. Nonetheless, with the particular alkylaromatics that are the principal reaction centers in petroleum asphaltenes, the reactions involved are relatively clean and proceed with high efficiency, resulting in good product yields. The side reactions producing small yields of the lower homologous acids do not seriously interfere with the quantitative aspects of the oxidation reactions because the small losses in the yields of the expected alkanoic acid due to the formation of lower homologous acids are compensated for by equivalent reaction from the next higher homolog, *etc.* Also, the high cooxidant-to-substrate ratios used in the asphaltene oxidation reactions probably had a diminishing effect on the alkylphenone yields by oxidizing the alkylphenones further to the alkanoic acids. Even though there are many complicating minor reactions occurring, as will be discussed below, the overall reaction is remarkably clean and efficient, and there can be little doubt that the results and the inferences from them with regard to the structure of the asphaltene molecules are on the whole valid and meaningful.

d) Other types of reactions occurring in RICO

Thus far, we have considered only the oxidation of aromatic carbon to carbon dioxide and carbonyl functionalities. However, other reactions may also take place parallel to the oxidation of aromatic carbon, but at a slower rate. These include transformation of primary alcohols to carboxylic acids, secondary alcohols to ketones, ethers to esters, sulfides and thiophenes to sulfones (sulfinic, sulfonic esters), and even reactive tertiary and secondary C–H bonds in bridgehead positions to alcohols:

$$R{-}(CH_2)_n{-}CH_2OH \xrightarrow{RICO} R{-}(CH_2)_n{-}CO_2H \tag{56}$$

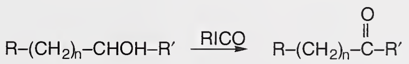

$$R{-}(CH_2)_n{-}CHOH{-}R' \xrightarrow{RICO} R{-}(CH_2)_n{-}\overset{\overset{O}{\|}}{C}{-}R' \tag{57}$$

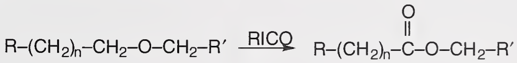

$$R{-}(CH_2)_n{-}CH_2{-}O{-}CH_2{-}R' \xrightarrow{RICO} R{-}(CH_2)_n{-}\overset{\overset{O}{\|}}{C}{-}O{-}CH_2{-}R' \tag{58a}$$

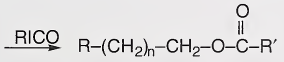

$$\xrightarrow{RICO} R{-}(CH_2)_n{-}CH_2{-}O{-}\overset{\overset{O}{\|}}{C}{-}R' \tag{58b}$$

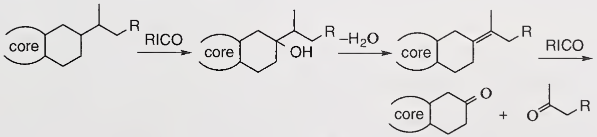

(59a)

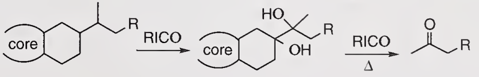

(59b)

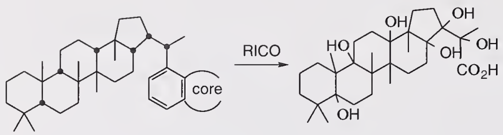

(60)

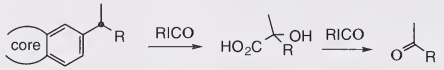

(61)

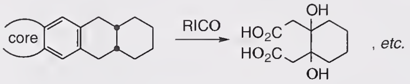

(62)

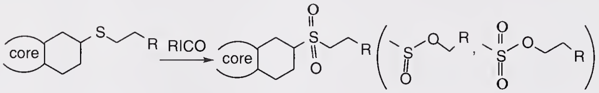

(63)

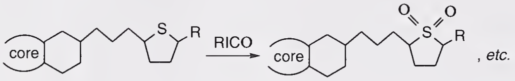

(64)

These reactions are interesting and important in their own right and in addition, they might have an impact on the directions and yields of the reactions discussed in the preceeding sections.

Thus, if the alkanol chain is attached to an aromatic ring, reaction (56) would yield an α,ω-di-*n*-carboxylic acid:

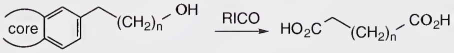

(65)

This would interfere with the determination of the yield of the diacids from the cleavage of the polymethylene bridges in reaction (48), which is of paramount importance with regard to the elucidation of the molecular structure of asphaltene (*v.i.*). That the concentrations of aromatic-anchored *n*-alkanols and *n*-alkanoic acids are not high enough to cause significant distortion of the α,ω-di-*n*-alkanoic acid yields from reaction (65) was shown by a study of the molecular weight variation upon esterification of the acids with diazomethane, followed by esterification of the alcohols with acetic anhydride. The VPO MW of the asphaltene decreased from 5,166 to 4,694 $g \cdot mol^{-1}$ upon diazomethane treatment and then to 4,090 $g \cdot mol^{-1}$ upon subsequent acetic anhydride treatment. These results suggest the presence of one hydrogen bond in ten asphaltene molecules due to carboxylic OH, and 1.7 hydrogen bonds in ten asphaltene molecules due to alcoholic OH. However, if any of these functionalities are present, they should not all be in terminal positions on the alkyl chains; they could also be present in secondary and tertiary positions and on the naphthenic and aromatic rings. This view is supported by the detection of tetralin alcohol, benzyl and a C_7-benzyl alcohol in the pyrolysis products of asphaltene.

That the *n*-alcohol or *n*-alkanoic acid side chains cannot significantly contribute to the production of α,ω-di-*n*-alkanoic acids also follows from the observation that:

- upon basic hydrolysis or BBr_3 cleavage of the C–O bonds in the asphaltene, large amounts of alcohol and acid products are produced: this indicates that the concentrations of free *n*-alkanoic acids and *n*-alkanolic side chains on aromatic carbons must be minimal, *i.e.* the acids are present mainly as esters and the alcohols, as esters and ethers; moreover,
- both the alkanoic acids and the alcohols produced in the above reactions exhibit strong even-

carbon-number preference, in contrast to the α,ω-di-*n*-alkanoic acid series which has a CPI value of about unity; and

- the value of the acid number of the HMA is low.

Reaction (59) may occur in the RICO of the LMA where, among the various α-branched *n*-alkanoic acid products, a series of 2-*n*-alkanones has been tentatively identified.

Reaction (60) indicates oxidation of all eligible (bridgehead) hydrogens. This, of course, would not necessarily occur, but even if a single one of these hydrogens is oxidized, the yield of the hopanoic (cheilanthanoic, steranoic, *etc.*) acid products would be underestimated since the oxidized acids would not have been detected in the analytical procedure employed.

Among the reaction products there are a series of tentatively identified compounds that can be indicative of the types of products represented by reactions (61) and (62). These were analyzed after methylation of their carboxylic moieties and acetylation of their alcoholic groups:

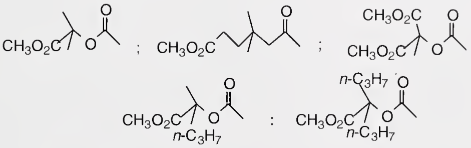

They are thought to be formed from the structural elements

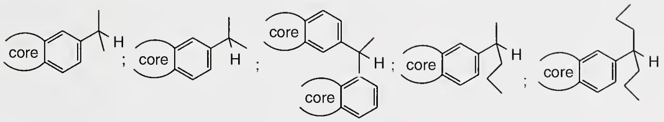

Sulfides are oxidized to sulfones in RICO and possibly to:

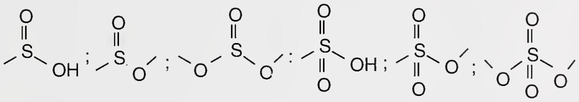

These species exhibit strong characteristic IR absorptions around 1310–1350, 1120–1160, 1125–1135, 1200, 1090, 1010–1080 and 1156–1260 cm^{-1}, Appendix 14.5, which are made even more complicated by the absorptions of alcoholic and carboxylic moieties present. According to the FTIR and ^{1}H, ^{13}C NMR spectra (*v.i.*) the aromatic carbon content of the oxidized residue is ≤5% of the aromatic carbon in the asphaltene and therefore the sulfur-containing species are mostly aliphatic.

4.4.2 High-MW products

a) Elemental composition

The RICO of asphaltene also yields a non-distillable oxidized residue that is rich in valuable structural information. With Athabasca asphaltene the yield of this residue is ~41% and its elemental composition is C: 65%; H: 7.6%; S: 4.7%; N: 0.8% and O: ~20%. The NMR spectrum shows a low aromatic carbon content, suggesting that the oxidation was fairly complete and that the residue consists mainly of oxidized aliphatic materials. The IR and ^{33}S NMR spectra of the residue show the presence of saturated sulfones and possibly other $>SO_x$ species.

When the whole asphaltene was fractionated (by acetone extraction) into LMA (890 g·mol^{-1}, 16%) and HMA asphaltene (6,800 g·mol^{-1}, 84%) and each fraction subjected to RICO, the aggregate MW of the acids produced is about the same as the MW of the asphaltene in the case of the LMA, but for the HMA it is only about 1/5 that of the asphaltene, showing that in this case extensive degradation had taken place. This behavior is somewhat reminiscent of that observed in the NiB desulfurization experiments where the MW of the LMA did not change, within experimental error, whereas that of the HMA was reduced about fourfold. The chemical changes taking place during the two reactions are, however, quite different; in the NiB reduction they involve only the cleavage of the sulfide bonds whereas here they involve the destruction of the nearly entire aromatic framework. The LMA and HMA oxidation products were methylated with diazomethane for further studies. The MWs of the resulting methylated products were about 40% lower because esters do not form association complexes as readily as do carboxylic acids.

Following methylation the products were separated by GPC into five different MW fractions. The MW distribution of the fractions, along with their yields and elemental compositions, are given in Appendix 14.6. The most striking aspect of the data is the unveiling of the presence of high-MW naphthenic-aliphatic core fragments in the oxidation products with number average molecular weights of ~5,500 (LMA–1) to ~8,700 (Aw1) g·mol^{-1}. Thus, it appears that about 15% of the native *n*-C_5-asphaltene has a non-aromatic core with molecular weight exceeding 5,000 g·mol^{-1}, although some molecular association owing to the presence of alcohols and polar SO compounds is likely. It is also seen from the data that the oxidized residue from the HMA has a higher proportion of the higher MW fractions than the oxidized residue from the LMA, as expected.

All fractions contain nitrogen, oxygen and sulfur and in concentrations that vary from fraction to fraction. The LMA products contain more sulfur than the HMA products even though the sulfur content of the LMA is lower than that of the HMA. Thus, the sulfur remaining in the oxidation products is 52% of the original amount present in the asphaltene in the case of LMA and 19% in the case of HMA, giving a value for the whole, native asphaltene of 25%. The sulfur is primarily present in the form of saturated sulfones as indicated by the intense IR absorption[93,99] bands at 1300 and 1130 cm^{-1}, characteristic of sulfones, and the ^{33}S NMR spectrum.[100] Also, since the NMR spectra of the oxidation products show a low aromatic carbon content, the sulfones could only have formed from the oxidation of saturated sulfides. These results are in agreement with the presence of cyclic terpenoid sulfoxides in the LMA, *n*-alkyl-substituted thianes and thiolanes, and acyclic sulfides as structural units in the HMA. In auxiliary studies (Appendix 14.4) it was shown that indeed alkyl and aryl sulfides can be converted in good yields to their sulfones in RICO. From the NiB experiments it was also estimated that 42% of the sulfur in the HMA was present as sulfides which, in the oxidation residue, decreased to 19%. The remainder of the sulfur, ~58%, should be present as *n*-alkyl-substituted thiophenes, benzo-, dibenzo- and higher condensed thiophenes, some of which have been detected in the thermolysis products of asphaltene.

The presence of sulfides in asphaltenes is important, not only with regard to the molecular structure and origin of asphaltenes, but also with relation to their chemical behavior during thermal processing of the bitumen. Unambiguous evidence in support of the original claim for the presence of saturated sulfides in asphaltene[84] was obtained in the RICO of Athabasca asphaltene in 1986 by IR spectroscopy,[92] later confirmed by ^{33}S NMR spectroscopy[100] in 1987, and was fully corroborated by the isolation of *n*-alkyl thiolanes and thianes[81] from the pyrolysis oil and biological markers from the NiB reduction[37] of this and other asphaltenes.[99,101,102] With the advent of X-ray Absorption Near Edge Structure (XANES) spectroscopy,[103] sulfides and other sulfur compounds have been detected in a variety of asphaltenes.[104,105]

Inspection of the compositional data on the GPC fractions in Appendix 14.6 shows a definite trend in the distribution of sulfur. Sulfur is most abundant in fraction 2 for both the LMA and HMA, followed by fractions 1>3>4>5 for the HMA. The intensities of the sulfone IR absorptions also vary, fractions 1–3 displaying the most intense absorption and fractions 4 and 5 showing very weak absorptions even though their sulfur content is still substantial.

The nitrogen content of asphaltene is also greatly reduced in the course of RICO and only about 50% of the original amount present in the asphaltene remains in the oxidation products. The distribution of the residual nitrogen among the GPC fractions of the esters exhibits the same trend for the LMA and HMA, namely, the highest-MW fractions contain significantly more nitrogen than any of the lower-MW fractions and the percent concentration goes through a minimum in fraction 3. The true trend, however, may be somewhat distorted by the incorporation of nitrogen into the esters during diazomethane treatment of the acids. The fate of the lost nitrogen is not known.

During the oxidation process, as expected, large quantities of oxygen are incorporated into the residue, mainly in the form of carboxylic, sulfone and alcoholic hydroxyl groups. The oxygen contents of the GPC fractions show little variation except that the highest-MW fractions contain more oxygen than any of the remaining fractions. Particularly large concentrations of oxygen are found in the water-soluble portions of the residues (34% for LMA and 26% for the whole asphaltene).

The H/C atomic ratios of the acids are significantly higher than in the asphaltenes owing to the excision and removal of aromatic hydrogen and carbon with a low $(H_{arom}/C_{arom})_a$ ratio of ~0.2. A further increase in the H/C atomic ratio takes place during the esterification of the acids owing to the addition of a methylene group with an H/C atomic ratio of 2.0. In the GPC fractions of the esters the H/C atomic ratios exhibit a slightly increasing trend with decreasing molecular weight of the fractions.

b) Pyrolytic fragments

The oxidized residue also contains information on the molecular structure of asphaltene. As we have seen, the positions where the aromatic attachments were excised were converted to carboxylic acids. Some of these carboxylic groups remained anchored to the residue as evidenced by the high oxygen content of the residue and the detection of carboxylic groups by NMR and IR spectroscopy. In order to further probe into the structural details of the oxidized naphthenic-aliphatic core of the asphaltene, the oxidized residue after methylation was subjected to mild thermolysis. The following principal thermolysis products were identified:[106]

- homologous series of *n*-alkanes and *n*-1-alkenes, Figure 14.80,
- homologous series of 2-methyl-*n*-alkanones, *n*-alkanoic and alkenoic acid methyl esters, Figure 14. 81, and
- a short series of unesterified, free *n*-alkanoic acids, Figure 14.82.

The *n*-alkanes and *n*-1-alkenes are formed principally by the cleavage of the *n*-alkyl side chains on the (oxidized) naphthenic core:

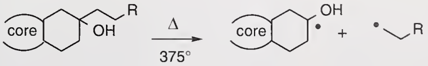

(66)

followed by the stabilization reactions of the alkyl radicals:

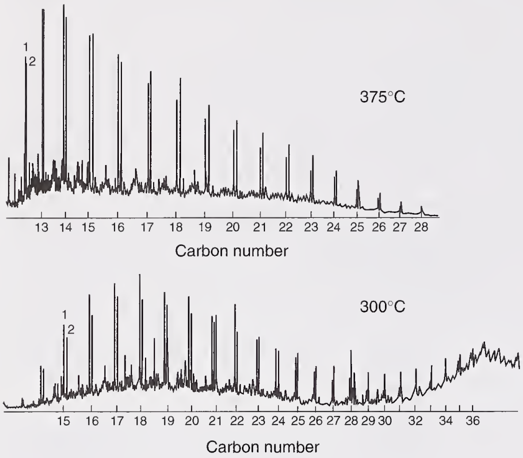

Figure 14.80 Gas chromatograms of the *n*-alkanes (2) and *n*-1-alkenes (1) liberated from the pyrolysis of the nondistillable ester residue from the RICO of Athabasca asphaltene.[106]

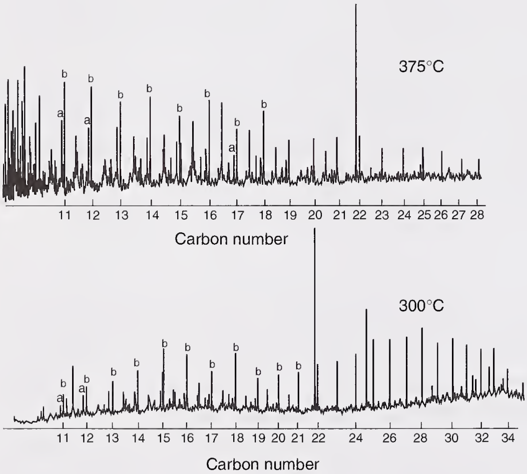

Figure 14.81 Gas chromatograms of the *n*-alkenoic (a) and *n*-alkanoic (b) methyl esters liberated from the pyrolysis of the nondistillable ester residue from the RICO of Athabasca asphaltene. The minor peaks are series of *n*-alkenoic acid methyl esters and 2-methyl *n*-alkanones.[106]

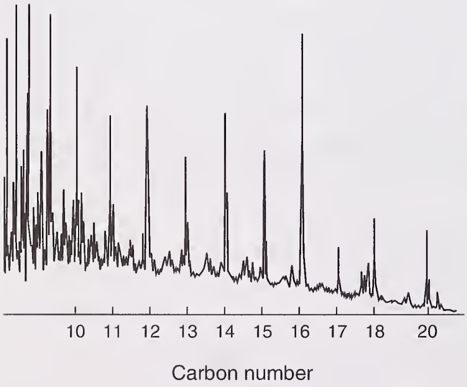

Figure 14.82 Gas chromatograms of the free *n*-alkanoic acids liberated from the pyrolysis of the nondistillable ester residue from the RICO of Athabasca asphaltene.[106]

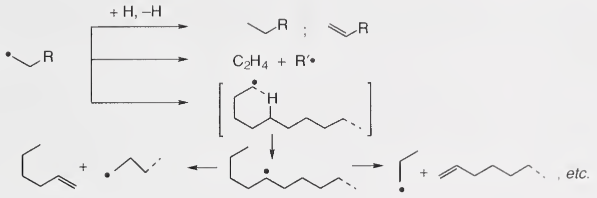

+ H, –H
R
R'•
C$_2$H$_4$
H
, etc.

(67)

where R = *n*-alkyl, as well as by the stepwise cleavage of the polymethylene bridges between two naphthenic rings:

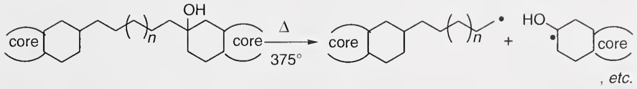

core
OH
HO
Δ
375°
n
, etc.

(68)

Similarly, the esters are produced by the cleavage of the *n*-alkanoic acid methyl esters attached to the naphthenic core at their alkyl end:

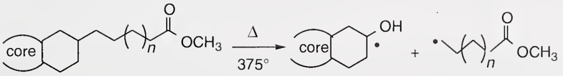

core
O
OCH$_3$
OH
Δ
375°
n

(69)

followed by the stabilization reactions:

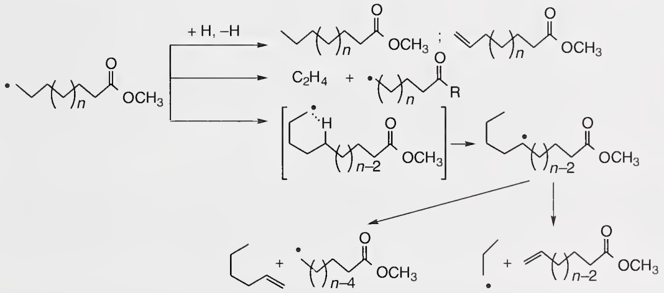

+ H, –H
O
OCH$_3$
C$_2$H$_4$
R
H
n
n–2
n–4

(70)

The chain-end carboxylic groups were formed during RICO of the aromatic portion of the asphaltene, and the carboxylic carbon was originally the site of attachment of the alkyl bridge to the aromatic ring in the asphaltene:

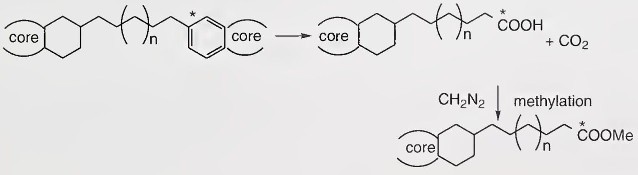

core
n
*
COOH
+ CO$_2$
CH$_2$N$_2$
methylation
COOMe

(71)

Finally, the *n*-alkanoic acids must have originated from the thermal decomposition of *n*-alkanoic acid esters originally present in the asphaltene with their alcoholic portion covalently bonded to the naphthenic core:

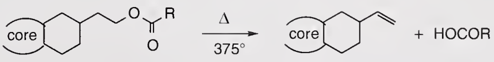

core
O
R
Δ
375°
+ HOCOR

(72)

This interpretation is supported by the detection of similar series of *n*-alkanoic acids in the thermolysis and in the saponification of the asphaltene as well, as discussed in a previous section of this chapter.

The results obtained are highly informative and provide clear evidence for the presence of naphthenic-attached *n*-alkyl side chains (and/or bridges), polymethylene bridges connecting an aromatic with a naphthenic ring, and *n*-alkanoic acid esters covalently bound to the naphthenic core in the asphaltene molecule by their original alkanol components.

The three product fractions were chromatographically separated and their quantities estimated gravimetrically. In every case the lower-MW, volatile C_{15}– portions of the fractions were lost and therefore the results underestimate the true values. The loss, however, can be estimated if it is assumed that the chain length distribution of the alkyl groups in the aliphatic systems is the same as in the aromatic systems. With this assumption it was possible to estimate that in Athabasca asphaltene 3.2% of the carbon is present as naphthenic-attached chains, 1.3% as polymethylene bridges connecting two naphthenic rings, 5.1% as polymethylene bridges connecting a naphthenic with an aromatic ring, and 3.9% as *n*-alkanoic acids in naphthenic-anchored esters.

With additional reasonable assumptions, more structural details can be elucidated. Thus, assuming an average chain length of 14 for the *n*-alkanoic acids in the form of esters (based on the measured distribution of the *n*-alkanoic acids (*v.i.*)) the number of *n*-alkanoic acids is estimated to be 0.3 acids per 100 C atoms. Also, from the fact that the number of carbon atoms present in polymethylene bridges connecting two aromatic units, 3.8 per 100 C atoms, is not very different from the number of carbon atoms in bridges connecting an aromatic to a naphthenic unit (5.1 per 100 C atoms), it may be assumed that the average length of the bridges would be the same and thus the number of bridges between naphthenic and aromatic units is estimated to be 0.82 bridges per 100 C atoms.

As noted from the general reaction scheme for the RICO oxidation of aromatic compounds, most of the aromatic carbon is oxidized in the process to carbon dioxide, the amount of which can be measured directly. The value found was 29 CO_2 per 100 C atoms in the asphaltene. Now we can make material balances separately for aromatic and alkyl carbons. The details are given in Table 14.19. As seen, the RICO products account for 90% of the aromatic carbon and about 100% of the alkyl carbon originally present in the asphaltene as determined by NMR measurements (*v.i.).* Qualitative analysis of a portion of the oxidized residue, namely the one that was adsorbed to the inorganic solids, revealed the presence of carboxylic acids and other oxidized molecules not detected before, Table 14.20. Some of these indicate the existence of branched alkyl bridges between aromatic carbons.

The data collected in Table 14.19 illustrate the strengths and pitfalls of the separate RICO and NMR approaches to the study of the molecular structure of asphaltene and the need for, and benefits of, combining the two.

The experimental execution of NMR measurements is simpler and faster than the lengthy procedures involved in RICO and gives directly and accurately the percentage distribution of aromatic, alkanoic, naphthenic, terminal and branched methyl carbons, as well as the aliphatic, aromatic, methyl, methylene, *etc.* protons. Still, from these data, while the existence of fairly long *n*-alkyl groups in asphaltene follows directly, it would be difficult to distinguish among the many possibilities regarding the chemical environment of these *n*-alkyl moieties and specify whether they are attached only to aromatic carbons or to both aromatic and naphthenic carbons.

Table 14.19 Distribution of carbon (per 100 C) in Athabasca asphaltene

C_{arom}		$C_{alk.}$	ΣR[a]	CH_3 terminal
2.5	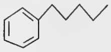	9.9	2.5	2.5
1.2	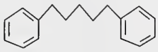	3.8	0.6	–
0	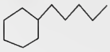	3.2	0.8	0.8
0	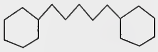	1.3	0.2	–
0.8	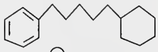	5.1	0.8	–
0.3	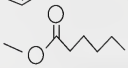	3.9	0.3	0.3
~2.0	as C_{arom} in oxidized residue			
~1–2	as benzene carboxylic acids			
29.0	as CO_2[*]			
≥38	total from RICO	27	5.2	3.6
≤42	from NMR	27	–	~3.9

[a] Total number of alkyl groups.

Neither is it possible from the NMR data alone to establish the presence or absence of *n*-alkyl bridges, alkanoic acid esters, ethers or the length distribution of the *n*-alkyl moieties. Only RICO in combination with NiB reduction, OH^{-}/BBr_3 hydrolysis and thermolysis studies can deliver these types of structural information: the determination of alkyl chains and bridges on aromatic carbons can be accomplished quantitatively while the rest of the numerical values can be obtained as semiquantitative estimates.

4.4.3 Oxidative degradation of other Alberta asphaltenes

Preliminary RICO studies have been done on other asphaltenes from the Western Canada Sedimentary Basin including a Peace River native and steam-produced oil sand asphaltene, a Carbonate Triangle asphaltene and a heavy oil asphaltene from the Lloydminster deposit.[94]

As for the case of Athabasca asphaltene, each of these asphaltenes on RICO yielded a series of *n*-alkanoic acids, Figure 14.83, α,ω-di-*n*-alkanoic acids, Figure 14.84, and benzene carboxylic acids, Figure 14.85, (analyzed as their methyl esters) with very similar distributions in approximately the same carbon range. The gravimetric results of these experiments are listed in Table 14.21.

---

[*] In a study of Gudao vacuum residue asphaltene, that will be discussed in section 4.4.4 of this Chapter, Wang *et al.* claimed that the CO_2 value of 29C/100C reported by Mojelsky *et al.* is too high because the CO_2 yield from their sample amounted to only 15.5C/100C coupled with a total carbon recovery of 98.2% which, however in reality was probably 73% or so, as shown in Appendix 14.6. Wang *et al.* also suggested that the source of error was adsorption of solvent vapor on the ascarite absorber. But, in CO_2 analysis the gas stream is always dried before entering the ascarite absorber. Also, Su *et al.* reported a similar value, 27.5C/100C from an Arabian residue asphaltene.

Table 14.20 Compounds identified in the solid adsorbate from the RICO of Athabasca asphaltene and which have not been observed in the organic or aqueous phase

Compound identified	Possible precursor	Compound identified	Possible precursor
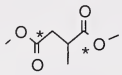	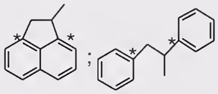	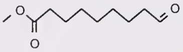	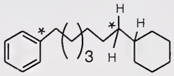
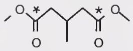	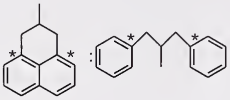	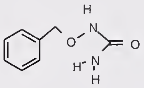	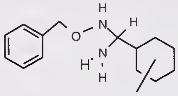 ?
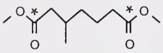	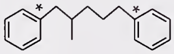	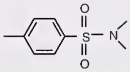	?
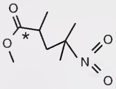	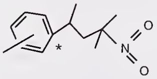	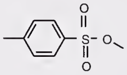	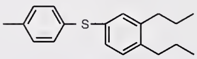 ?
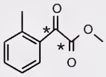	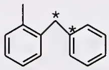	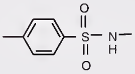	?
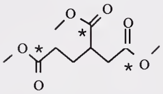	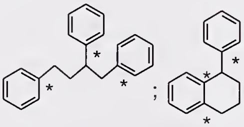	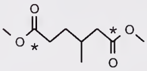	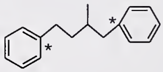
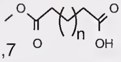 n = 3,7	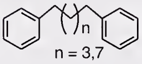 n = 3,7	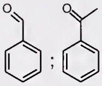	?
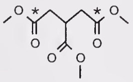	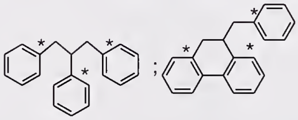		

The smooth distribution of the *n*-alkanoic acids in Figure 14.83 is perturbed by the appearance of a slight excess of the C_{16} and C_{18} members. This excess comes from small quantities of the C_{16} and C_{18} acids produced from the microbiological degradation of the precursor oil that became trapped in the asphaltene micelles and were subsequently liberated when the asphaltene molecules were destroyed during the oxidation process, or, alternatively, they might have been formed by the slight hydrolysis of *n*-alkanoic acid esters under the acidic conditions of the oxidation process. It is noteworthy that even this slight, subtle feature in the concentration distribution of the acids is so clearly recognizable in each case, with the exception of the steam-treated Peace River sample where the increased thermal stress and water washing appear to have diminished the excess amounts of the C_{16} and C_{18} members.

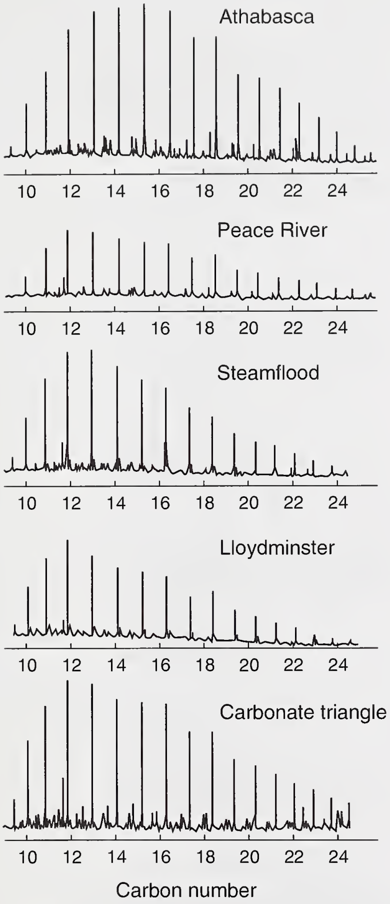

Figure 14.83 Gas chromatograms of *n*-alkanoic acid methyl esters from the RICO of various Alberta asphaltenes. From T.W. Mojelsky *et al.*, Ref. 94. © 1992, American Chemical Society.

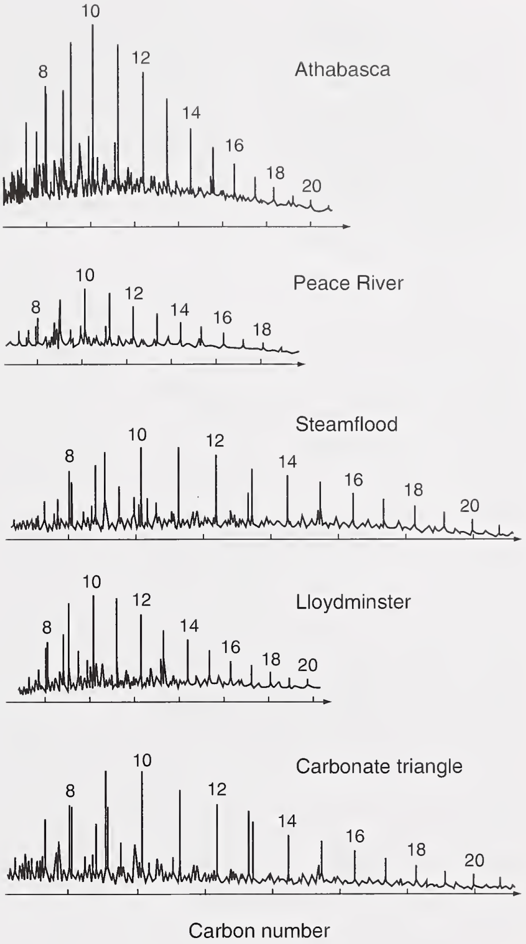

Figure 14.84 Gas chromatograms of α,ω-dicarboxylic acid methyl esters from the RICO of various Alberta asphaltenes. From T.W. Mojelsky *et al.*, Ref. 94. © 1992, American Chemical Society.

Table 14.21 Yields of products (wt% of oxidized residue) from the 375°C pyrolysis of the oxidized residues[a,b]

Asphaltene source	Alkanes + alkenes	Me esters of *n*-alkanoic acids	Free *n*-alkanoic acids
Lloydminster	1.1	7.8	3.7
Peace River	5.6	8.1	5.9
Steamflood	3.6	5.7	5.7
Carbonate Triangle	8.0	6.7	5.0

[a]From Ref. 94. [b]The yield of oxidized residue is taken as 40% of the asphaltene.

The distribution of α,ω-di-*n*-alkanoic acids and the kinds of benzenecarboxylic acids produced in the oxidation are also similar in all of the asphaltenes, again with the exception of the steam-treated Peace River sample. In the latter case, the concentrations of peaks 2 through 9 relative to peak 1, the 1,2-benzenedicarboxylic acid, which is the most abundant in all the samples, are greatly reduced.

The similarities in the nature of the products, as well as their carbon ranges and concentration distributions, from the five asphaltene samples studied further extends to the pyrolysis products of the oxidized naphthenic/alkanoic residua. These can be seen from the gas chromatograms reproduced in Figure 14.86 for the *n*-alkanes + *n*-1-alkenes, and in Figure 14.87 for the *n*-alkanoic acids. From the latter it is also evident that all five samples show a distinct preference for the even-carbon-number members of the *n*-alkanoic acids in the C_7–C_{22} range dominated by the C_{14}–C_{16}–C_{18} members, and the presence of two or three smaller peaks around C_{18} in addition to the *n*-octadecanoic acid. These small peaks are thought to be due to the monounsaturated *n*-C_{18}-9-*cis* and *n*-C_{18}-11-*cis* acids and the diunsaturated *n*-C_{18}-9-12-*cis,cis* acid, as have been found in other studies on Athabasca oil sands (*cf.* Chapter 8). The presence of these acids provides additional evidence for a not-too-distant microbiologial degradation[107] of the oils that were the precursors of the bitumens.

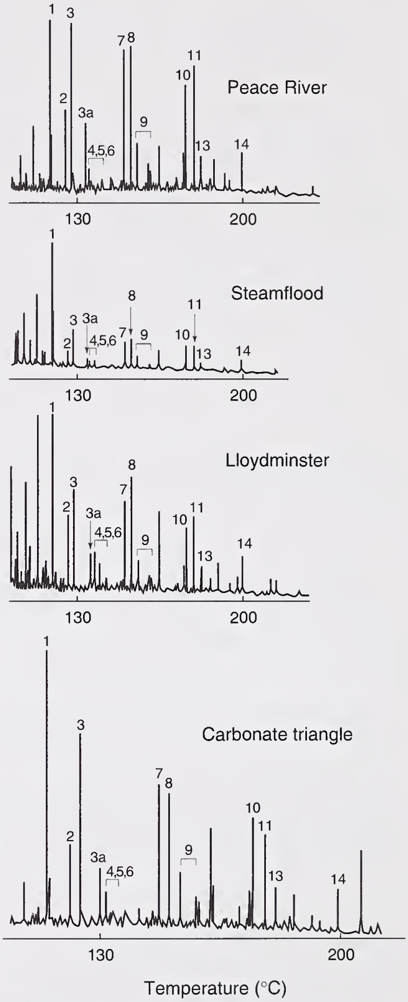

Figure 14.85 Gas chromatograms of the benzenepolycarboxylic acid methyl esters from the RICO of various Alberta aphaltenes. Peak labels as in Figure 14.83. From T.W. Mojelsky *et al.*, Ref.94. © 1992, American Chemical Society.

These comparative studies have brought to light the close similarities in the molecular structures of the five asphaltene samples investigated and suggest that all five asphaltenes originated from *n*-alkane-derived kerogens, in corroboration with independent observations made in other studies on the similarities between various Alberta oil sand maltene components and asphaltenes. The results discussed above are also comparable to those derived from the RICO study of the nondistillable (230°C, 10^{-3} Torr) portions of the saturate, aromatic and polar fractions of Athabasca bitumen. The findings, taken together, constitute clear evidence that the high-MW portions of the deasphaltened bitumen are composed of incompletely degraded asphaltene fragments in which the *n*-alkyl moieties were also at least partially protected from microbial attack and that these high-MW portions were derived from asphaltene. This is in sharp contrast with the mainly terpenoid composition of the lower molecular weight distillable portions of Athabasca bitumen.

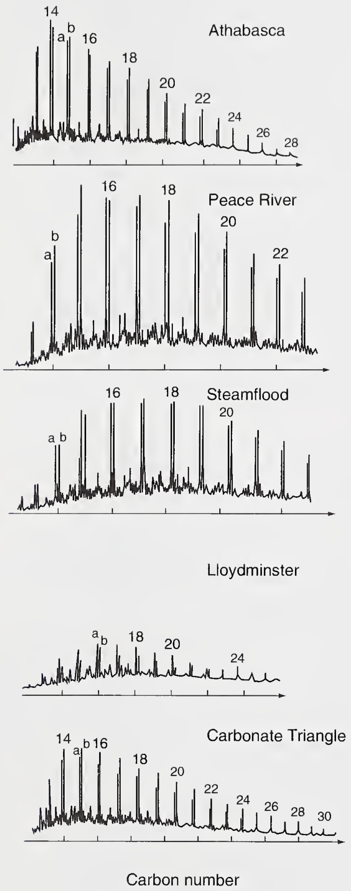

Figure 14.86 Gas chromatograms of the 1-alkenes (a) and *n*-alkanes (b) from the 375°C pyrolysis of the (methylated) oxidized residues of various Alberta asphaltenes. From T.W. Mojelsky *et al.*, Ref.94. © 1992, American Chemical Society.

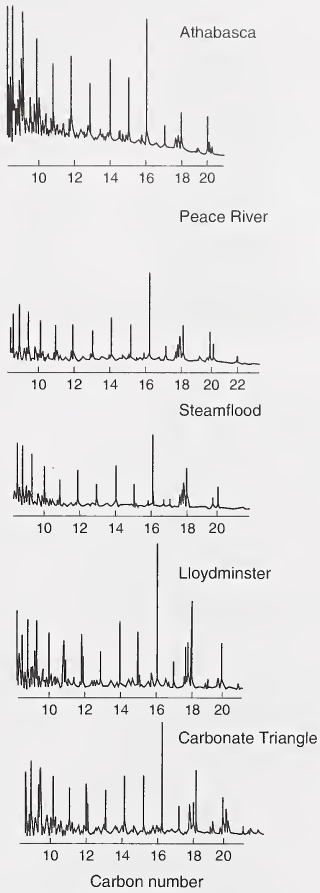

Figure 14.87 Gas chromatograms of the carboxylic acids from the 375°C pyrolysis of the (methylated) oxidized residues of various asphaltenes. From T.W. Mojelsky *et al.*, Ref.94. © 1992, American Chemical Society.

4.4.4 Foreign asphaltenes

One important question regarding the compositional–structural data on Athabasca and other Alberta asphaltenes discussed in the above sections concerns their generality and representativeness for native petroleum asphaltenes. No fractions of petroleums (including asphaltenes) from any two different sources can be expected to have identical compositional–structural properties because these properties are determined by the entire history of the oil, including the biotic source material of the oil, the nature of its source rock and its depositional environment; moreover, these properties are further modified by the age, diagenetic and thermal history (depth of burial), water washing, microbial alterations and reservoir conditions of the parent oil. Useful information in this regard was obtained from studies on asphaltenes from the following sources:

Sample	C	H	N	O	S	MW (VPO)
			%			g·mol^{-1}
Athabasca (HMA)[37]	81.2	8.1	1.1	1.3	8.2	5,000
Boscan[99]	81.1	8.0	1.1	1.4	6.1	10,000[a]
Duri[99]	87.4	8.2	1.5	2.1	0.4	8,200[a]
X[108]	86.4	7.1	1.5	1.0	2.3	6,000
Gudao[109]	85.2	9.4	1.7		3.6	3,960
Saline Lake[110]	73.3	8.9	1.7	3.0	9.3	
Arabian[111]	83.7	7.5	0.84	–	6.8	–
Jinghan[102]	73.8	8.7	1.24	3.0	14.9	3,442
Jinghan 2[102]	75.8	10.4	1.4	4.4	4.0	5,061

[a] MM_p/GPC

- a low-sulfur, light, conventional Duri crude oil from Indonesia;
- a high-sulfur Boscan heavy oil from Venezuela;
- a medium-sulfur, light, conventional crude oil (X);
- a high-sulfur, immature crude oil from a saline lake basin in China (Saline Lake);
- two different Jinghan oils and kerogens from China;
- a vacuum resid from China (Gudao); and
- a vacuum resid from an Arabian crude mixture.

Elemental compositional data for these asphaltenes are as follows:

As demonstrated by the chromatograms in Figure 14.88, all these samples contained aromatic-attached *n*-alkyl side chains and smaller quantities of branched *n*-alkyls. Table 14.22 lists the measured numbers of side chains and carbon atoms in them. The values (with the exception of the immature oils from China) lie in the range 1.5–3.9 and 6.6–11.4 per 100 C-atoms, in spite of the obvious differences among the parent oils and the *n*-alkane contents of their maltene fractions. For all asphaltenes studied, the carbon range of the *n*-alkyl chains extends from 1 to about 34, with monotonically decreasing concentrations as the chain length increases. The immature oils from China are again the exception, in that the number of alkyl side chains per 100 C atoms in the asphaltene is significantly lower than in mature oil asphaltenes, owing—at least in part—to their lower aromatic content. Also, their alkyl side chain distribution displays a slight preference for the even carbon numbers (the latter feature is also apparent in the Duri chromatograms). Figure 14.89 shows the presence of the α-methyl, -ethyl and -*n*-propyl branched alkanoic acids in the Saline Lake sample.

Similar data for the polymethylene bridges connecting aromatic carbons in these asphaltenes are seen in Figure 14.90 along with plots of the number of bridges as a function of length. The numerical data listed in Table 14.23 also show relatively narrow ranges for the number of bridges, 0.43–1.0, and carbon atoms in the bridges, 3.7–7.6 per 100 carbon atoms.

The benzenepolycarboxylic acid chromatograms are shown in Figure 14.91. A comparison of the gas chromatograms in Figures 14.65, 14.67, 14.77, 14.79, 14.88, 14.90 and 14.91 and the analytical data in Tables 14.22 and 23 reveals a remarkable similarity in the nature and distribution of the alkyl substituents on the aromatic systems in the asphaltene molecules and in the nature and distribution of the benzenepolycarboxylic acid products from the RICO of the vastly different mature asphaltenes. The three immature asphaltenes from China, while generally similar to the others, show some distinctive features probably related to their immature state and the Gudao and Arabian vacuum resid asphaltenes feature—perhaps in part as a result

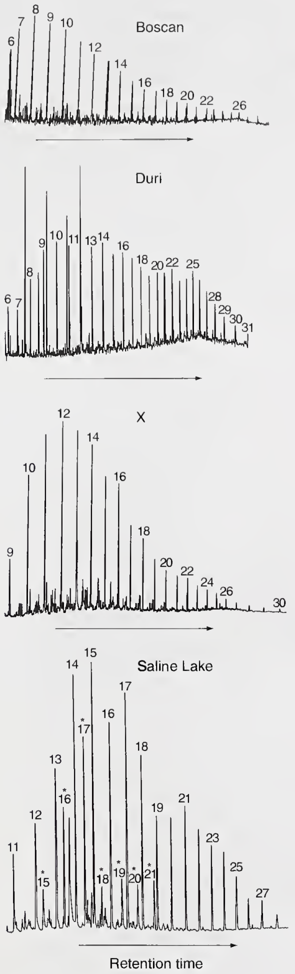

Figure 14.88 GC–MS total ion current chromatograms of the alkanoic acid methyl esters from the RICO of Boscan, Duri, X and Saline Lake asphaltenes. The numbers refer to the chain lengths of the esters and the asterisks denote isoprenoid acid esters. The Boscan and Duri plots are from O.P. Strausz *et al.*, Ref. 99. © 1999, American Chemical Society; X, from Ref. 108; Saline Lake, from P. Peng *et al.*, Ref. 110. © 1999, American Chemical Society.

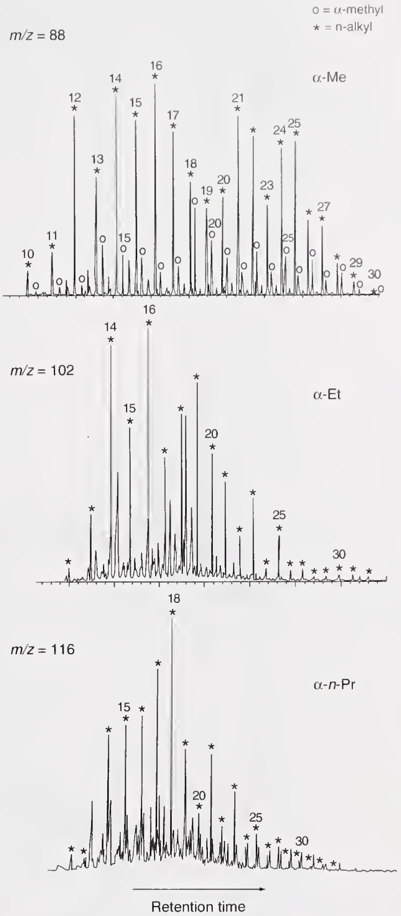

Figure 14.89 GC–MS cross-scan (*m/z* = 88, 102 and 116) chromatograms showing the presence of α-methyl, -ethyl, and -*n*-propyl branched alkanoic acids in the Saline Lake asphaltene. The numbers refer to the chain lengths of their methyl esters. From P. Peng *et al.*, Ref. 110. © 1999, American Chemical Society.

of their thermal history—a much higher percentage of benzene penta- and hexacarboxylic acids than native asphaltenes.

All the asphaltenes studied so far have *n*-alkyl side chains attached to aromatic systems in a nearly smooth distribution with monotonically declining concentrations from C_1 to about C_{30-35}. In the Saline Lake asphaltene the alkyl distribution is not completely smooth but displays a slight preference for the C_{15}, C_{17}, C_{21} members, which after correction for the C_{arom} site of attachment, would correspond to C_{14}, C_{16} and C_{20} preference, revealing the immature state of

Table 14.22 Aromatic-attached *n*-alkyls in petroleum asphaltenes

Sample	No. of alkyls	No. of C-atoms	Ave. chain length
	per 100 C in asphaltene		
Athabasca	2.5	9.9	4.0
Boscan	1.5	6.6	4.4
Duri	1.5	10.5	6.8
X	1.9	11.4	6.1
Gudao	2.1	~7.4	3.5
Arabian	3.9	5.5	
	(C_2–C_5)	(C_2–C_5)	

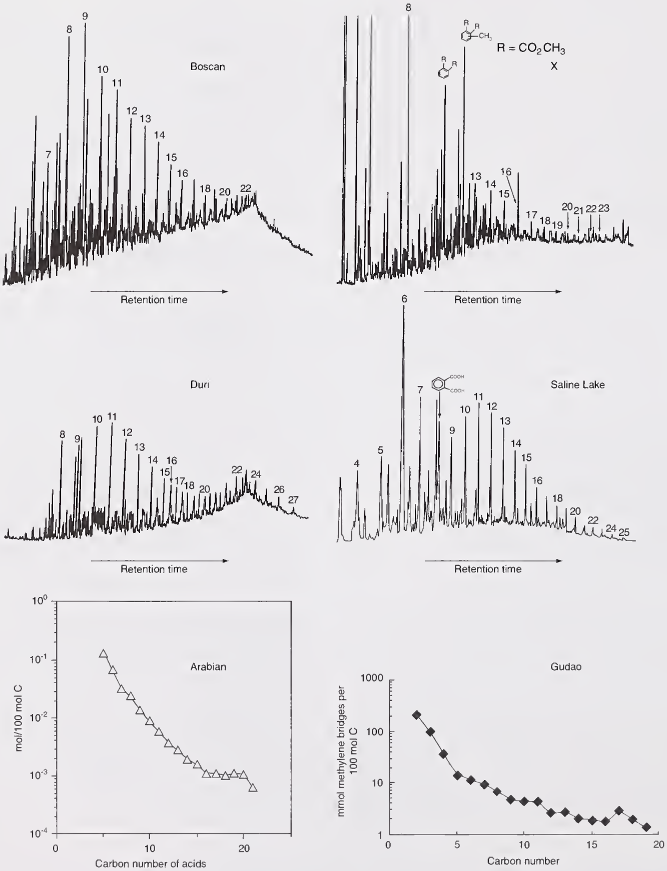

Figure 14.90 Gas chromatograms of the α,ω-di-*n*-carboxylic acid methyl esters from the organic phases of the RICO of Boscan, Duri and X asphaltenes and the combined phase of the RICO of the Saline Lake asphaltene, along with plots of the number of bridges as a function of length for the Gudao and Arabian asphaltenes. The numbers refer to the chain lengths of the esters. The Boscan and Duri plots are from O.P. Strausz *et al.*, Ref. 99. © 1999, American Chemical Society; X from Ref. 108; Saline Lake from P. Peng *et al.*, Ref. 110. © 1999, American Chemical Society; Gudao from W. Zijun *et al.*, Ref. 109. © 1997, Marcel Dekker; Arabian from Y. Su *et al.*, Ref. 111. © 1998, American Chemical Society.

Table 14.23 Polymethylene bridges connecting two aromatic carbons in petroleum asphaltenes

Sample	No. of bridges	No. of C-atoms	Ave. bridge length
	per 100 C in asphaltene		
Athabasca	0.61	3.8	6.2
Boscan	0.58	3.7	6.4
Duri	1.03	7.6	7.4
Gudao	0.43	3.8	8.8
Arabian	0.45*	–	–

*Includes some tri- and higher carboxylic acids

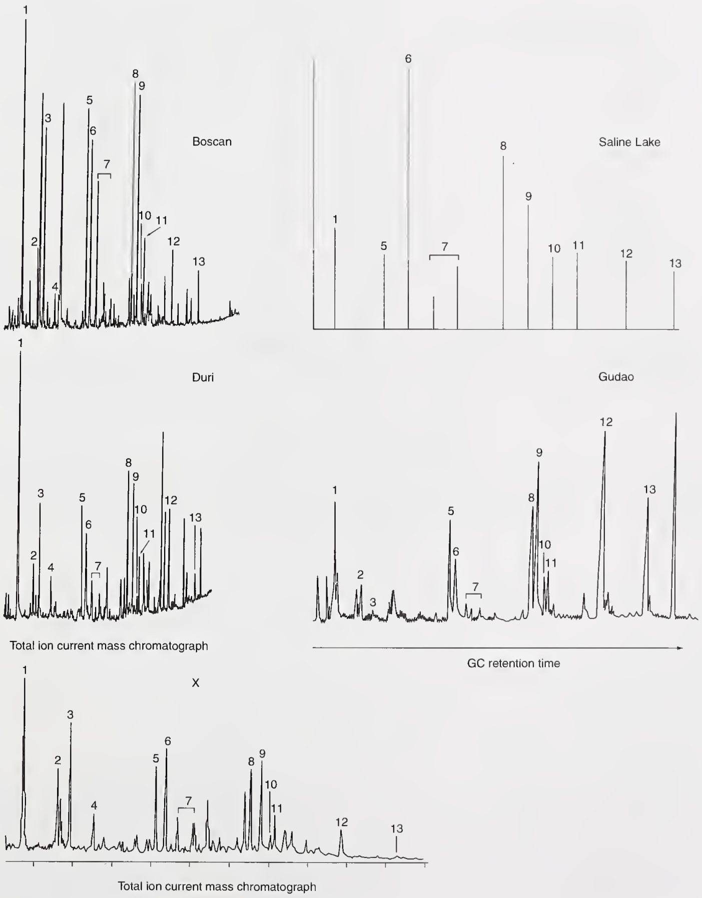

Figure 14.91 Total ion current mass chromatograms of the benzenepolycarboxylic acid methyl esters from the RICO of Boscan, Duri and X asphaltenes, and gas chromatograms of the same esters from the Saline Lake (schematic plot) and Gudao asphaltenes. The data for the last two samples are quantitative. 1 = 1,2-di-; 2 = 3-Me-1,2-di-; 3 = 4-Me-1,2-di-; 4 = keto 1,2-di-; 5 = 1,2,3-tri-; 6 = 1,2,4-tri-; 7 = Me-tri-; 8 = 1,2,3,4-tetra-; 9 = 1,2,4,5-tetra-; 10 = 1,2,3,5-tetra-; 11 = Me-tetra-; 12 = penta-; 13 = hexa-carboxylic acids. The Boscan and Duri plots are from O.P. Strausz *et al.*, Ref. 99. © 1999, American Chemical Society; X from Ref. 108; Saline Lake from P. Peng *et al.*, Ref. 110. © 1999, American Chemical Society; Gudao from W. Zijun *et al.*, Ref. 109. © 1997, Marcel Dekker.

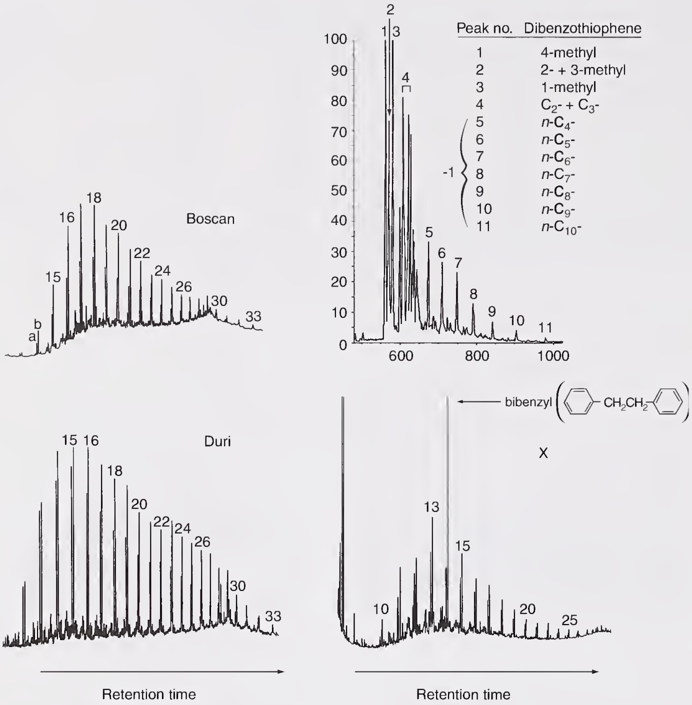

Figure 14.92 Gas chromatograms of the n-alkanes and n-alkenes from the pyrolysis of the nondistillable residues from the RICO of Boscan, Duri and X asphaltenes, along with that of the dibenzothiophenes from the Boscan asphaltene. From O.P. Strausz *et al.*, Ref. 99. © 1999, American Chemical Society.

this oil. The mature asphaltenes may show a slight preference for the C_{14}, C_{16}, C_{18}, *etc.* members of the n-alkanoic acid products from the RICO reaction. However, this phenomenon is the result of secondary processes, and may be due to the incorporation of small amounts of free n-alkanoic acids from very recent biological processes may be present in the asphaltene into the reaction products. These n-alkanoic acids show a marked even-to-odd preference, with particularly high concentrations of the C_{14}, C_{16} and C_{18} members.

In an analogous fashion the presence of α,ω-di-n-alkanoic acids among the RICO products is a manifestation of the existence of polymethylene bridges connecting aromatic carbons in the asphaltene molecule. In quantitative measurements, the distribution of these acids declines more or less monotonically from C_5 up to C_{28} and beyond. The reverse trend $C_4 < C_5$ observed in some instances is attributed to the lower concentration of C_2 bridges in the asphaltene owing to the high reactivity of 1,2-diarylethanes. In the Saline Lake sample the C_6 (adipic) acid concentration is exceptionally high, which provides unambiguous evidence for the abundance of aromatic condensed, unsubstituted cyclohexane rings

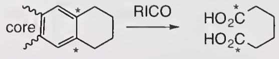

(58)

in this asphaltene. None of the other asphaltenes showed this feature.

In every case, along with the dominant *n*-alkyl appendages, smaller amounts of α-methyl, -ethyl, -*n*-propyl and -*n*-butyl branched alkyl appendages are also present but their total concentrations are much lower than that of the *n*-alkyls.

As noted above, the alkyl substitution in all the asphaltenes studied exhibits quite similar characteristics but even more striking is the almost identical nature and distribution of the benzenepolycarboxylic acid products from the RICO of the mature Alberta, Boscan and Duri asphaltenes, Table 14.24. The combined effects of heat and water washing appear to be reflected by the differences in the Peace River core and waterflood samples.

The total yield of the benzenepolycarboxylic acids is low, of the order 0.6–2% of the asphaltenes.

Table 14.24 Distribution of benzenepolycarboxylic acids from the RICO of various asphaltenes

	Gudao[109]	Arabian[111]	Saline Lake[110]
Total yield of di- through hexacarboxylic acids; mol/100C			
	0.26	0.125	0.0574
Percentage distribution			
di-	11	9	12
tri-	9	15	42
tetra-	35	32	38
penta-	29	22	5
hexa-	18	22	4
	Athabasca*	Duri[99]	Boscan[99]
Percentage distribution			
di-	31	40	38
tri-	21	19	21
tetra-	26	21	21
penta-	15	14	9
hexa-	7	7	10

* Correction factors for sensitivity differences from reference 109.

The hexaacid yields from the two vacuum resid asphaltenes (Gudao and Arabian) are 1.8–2.5 times higher than those from other mature asphaltenes (Athabasca, Duri and Boscan). This is attributable in part to differences in the analytical procedures, in part to alterations in the aromatic fractions of the whole native asphaltenes during vacuum distillation (~350°C?) due to the lower thermal stability of the more open kata condensed components of the asphaltene compared to the peri condensed structures, and in part to the fractionation caused by the higher volatility of the low-MW, kata condensed components. Of course, we cannot exclude the possibility that the difference is due to the difference in the compositions of the native asphaltenes or to all the above factors.

The near equivalence of the kinds and distributions of the benzenepolycarboxylic acid RICO products from the mature asphaltenes means that, like the alkyl substituents on the aromatic carbons, the modes of aromatic condensation must be quite similar as well. The generally low concentrations of the hexaacid suggests that pericondensed aromatic structures in native *n*-C_5-petroleum asphaltenes may be present but in relatively low concentrations. This is in agreement with the abundance of small aromatic fragments (benzenes, thiophenes, naphthalenes, quinolines, and three- and four-ring aromatic structures) in the thermolysis products[67–69] of asphaltenes and the magnetic susceptibility[112] and NMR[113] properties of asphaltenes.

The observed commonality further extends to structural features brought to light in other experiments.[111,114,115] Thus, the presence of *n*-alkyl appendages on naphthenic carbons in the Boscan, Duri and X asphaltenes is manifested, by analogy with the Alberta asphaltenes, by the presence of *n*-alkane/*n*-alkene series in the pyrolysis products of the methylated nondistillable residue from the RICO of these asphaltenes, Figure 14.92. The pyrolyzates also contained series of *n*-alkanoic/*n*-alkenoic acid methyl esters (C_{11}–C_{25}) and free *n*-alkanoic acids (C_8–C_{25}), proving the presence of the structural elements comprising polymethylene bridges connecting an aromatic to a naphthenic system and ester-bound *n*-alkanoic acid side chains on the naphthenic systems in the asphaltenes. The latter series, as in the case of Alberta asphaltenes, exhibit a marked preference for the even-carbon members up to C_{20} with the C_{16} member being the most abundant. Beyond C_{20}, this preference may vanish.

Data are also available on the sulfur compounds in the high-sulfur Boscan asphaltene. Thus, 2-*n*-alkylthiolanes and -thianes along with the 2,5- and 2,6-di-*n*-alkyl analogs are present in homologous series (C_{12}–C_{27}) along with the bicyclic terpenoid sulfide series (C_{13}–C_{24}) in the pyrolysis products, proving the existence of these molecules as side chains or bridges between ring systems in the asphaltene molecules. Also, the distribution of 1-*n*-alkyldibenzothiophenes, Figure 14.92, is similar to that found in the pyrolysis products of Athabasca asphaltene.

Results concerning the nature and distribution of biomarkers liberated in the RICO of the immature asphaltenes from China and in the RICO, NiB reduction and C–O bond cleavage of Athabasca and the two different Jinghan asphaltenes lend further support to the proposition of remarkable structural similarities in the intrinsic molecular structure of native petroleum asphaltenes. Thus, desulfurization and C–O cleavage yielded similar series of *n*-alkanes, steranes, isoprenoids, cheilanthanes, hopanes and gammacerane; and RICO yielded much the same monocarboxylic, α,ω-di-*n*-alkanoic and benzenepolycarboxylic acids along with the carboxylic acid derivatives of all the above biomarker molecules.

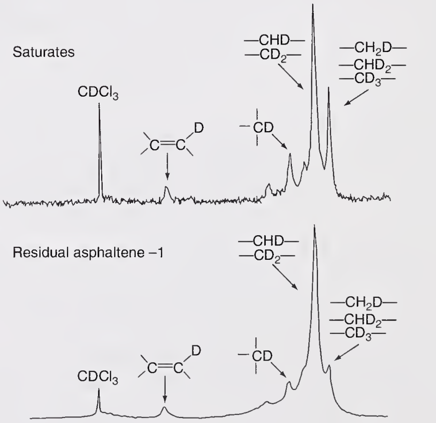

Figure 14.93 ^2H NMR spectra of the products after NiB reduction of the C–S bonds in Jinghan asphaltenes. From P. Peng *et al.*, Ref. 102. © 1999, American Chemical Society.

In the course of studies on foreign asphaltenes, some important information that came to light is related to the question of how the sulfide sulfur bridges are attached to the asphaltene molecules. HMAs of the two Jinghan samples studied were subjected to NiB reduction using deuterated reagents and the reduced asphaltenes and hydrocarbon products of the reaction were subjected to ^2H·NMR examination, Figure 14.93.[110] There, one can clearly see that in the asphaltenes the predominant deuterated moiety is the methylene moiety in both samples, indicating that the sulfur atoms bridging asphaltene core segments are attached predominantly to naphthenic carbon or mid-chain methylene carbon. In the saturates products, while deuterated methylenes are predominant, deuterated methyl groups are also prominent, suggesting that the alkyl appendages are attached to the sulfur atom in the asphaltene at their chain end, terminal positions.

Wet chemical methods, as demonstrated in this and previous chapters, are powerful approaches to the exploration of the composition and molecular structure of asphaltene. They are complementary to instrumental spectroscopic methods which will be discussed in a later section of this chapter.

5.0 Spectroscopic Probes Into the Molecular Structure of Asphaltene

Spectroscopic methods provide essential supplementary information (to the chemical methods) about molecular structure. Mass spectrometry, nuclear magnetic resonance and Fourier Transform infrared spectroscopy are indispensable tools in contemporary investigations of molecular structure. In the exploration of the molecular structure of asphaltene, UV–visible and electron paramagnetic resonance spectroscopy also play a useful role.

Mass spectrometry has been discussed in previous chapters and some of its aspects will be revisited later. NMR, FTIR, UV-vis and EPR spectroscopic studies of asphaltene will now be briefly reviewed.

5.1 Nuclear magnetic resonance spectroscopy

This method can yield detailed information about the composition, structure and conformation of pure organic molecules. In the case of very large molecules and complex mega-component mixtures, the spectrum becomes complicated and less informative. In such an environment the resonances of the many magnetically slightly different carbon atoms will be somewhat displaced relative to one another; they then may broaden into sharp bands or coalesce into broad continua. Thus, as seen by comparing the NMR spectrum of Athabasca asphaltene with that of *n*-tridecylbenzene,[113] Figure 14.94, some of the sharp resonance line in the latter are broadened and others are coalesced into broad continua in the asphaltene spectrum. Here, the aromatic resonances between 110 and 160 ppm form a continuum, but the resonance lines of the alkyl groups in the 14–37 ppm range, although broadened, retained their character. This can be explained in terms of the presence of very large numbers of magnetically similar aromatic carbon atoms and alkyl carbon atoms: the difference is that the immediate molecular environment around the central carbons in the alkyl groups effectively isolates them from the influence of the rest of the molecule, whereas around the aromatic carbons it does not. For example, all the terminal methyl carbons in a long alkyl chain, $CH_3–(CH_2)_n–$, isolated from the rest of the molecule by three or more methylene groups ($n \geq 3$), exhibit resonances near 14.174 ppm (relative to tetramethylsilane) and all mid-chain carbons, $CH_3–(CH_2)_n–(CH_2)_{mid\text{-}chain}–(CH_2)_n–$ with $n \geq 2$ exhibit resonances in the narrow range 29.441–29.759, Table 14.25 and Figure 14.95. However, in the aromatic region, 110–160 ppm, the resonances form a continuum with weak structural features owing to the overlap of tertiary and quaternary carbons and the lack of shielding from the influence of the molecular environment. Similar considerations apply for the naphthenic resonances underlying the alkyl resonances in the 10–40 ppm range.

The NMR samples used can be in the solid or solution (usually $CDCl_3$) phase but the latter are preferred because the experimental techniques for solution phase spectra are simpler,

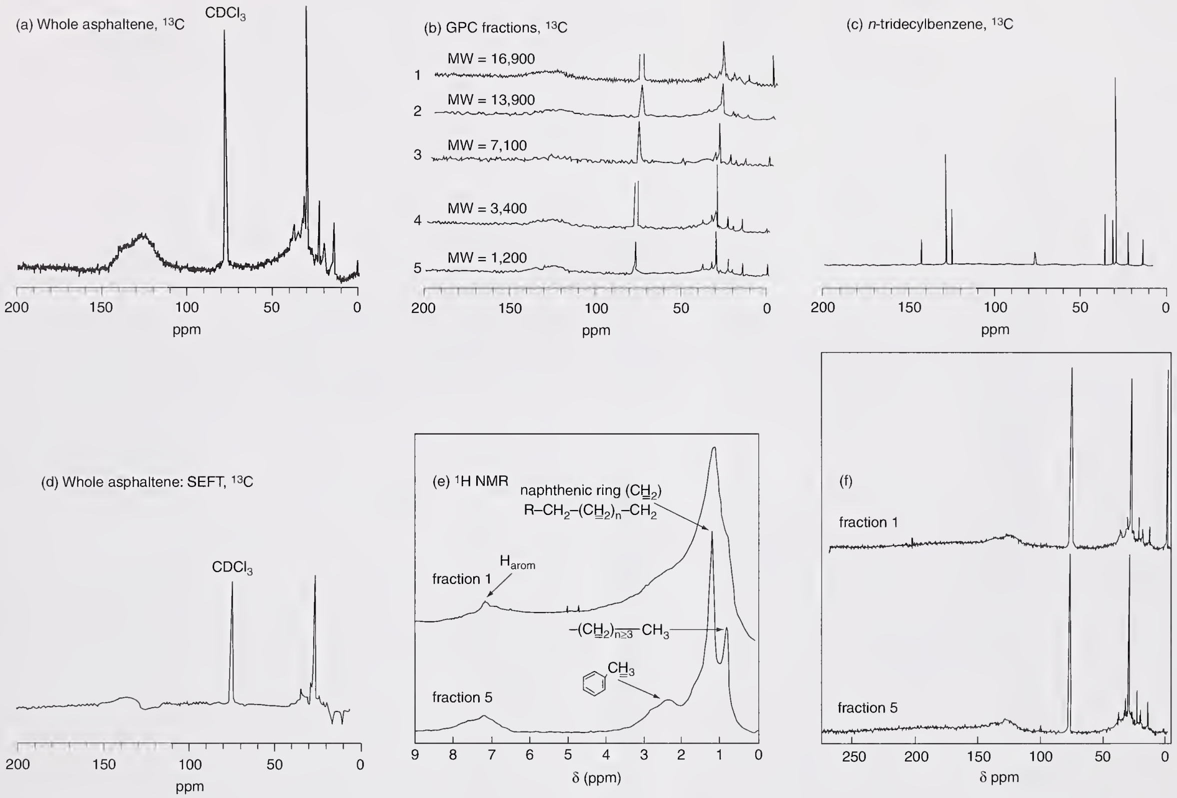

Figure 14.94 a)–c) ^{13}C NMR spectra of whole Athabasca asphaltene, the GPC fractions of Athabasca asphaltene, and of *n*-tridecylbenzene; d) Spin Echo Fourier Transformed NMR spectrum of whole Athabasca asphaltene. From N. Cyr et al., Ref. 113. © 1987, Elsevier Science. e) ^1H and f) ^{13}C NMR spectra of fractions 1 and 5. From T.M. Ignasiak *et al.*, Ref. 38. © 1983, Elsevier Science.

Table 14. 25 ^{13}C NMR spectral assignments (in ppm, relative to tetramethylsilane) in the asphaltene spectrum of Figure 14.95.

0–70	C_{al} aliphatic carbons
110–160	C_{ar} aromatic carbons
14.174	$\overset{*}{C}H_3-(CH_2)_n-$ n ≥ 3 ; 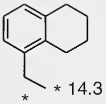
19.705 19.742 19.811 19.860	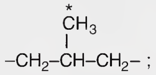 $-CH_2-\underset{}{CH}(\overset{*}{C}H_3)-CH_2-$; 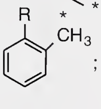; 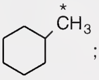; 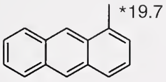
22.540 22.743	$CH_3-\overset{*}{C}H_2-(CH_2)_n-$ n ≥ 2 ; 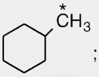; 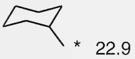
27.139 27.172 27.237	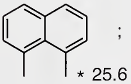; 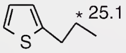; 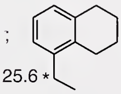; 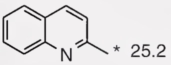; 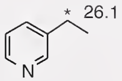 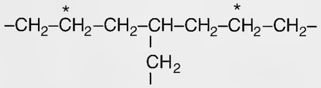 $-CH_2-\overset{*}{C}H_2-CH_2-\underset{\substack{\vert\\ CH_2\\ \vert}}{CH}-CH_2-\overset{*}{C}H_2-CH_2-$; 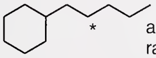 also peaks in the 25.9–27.5 range, not marked in the figure
27.969 28.055 28.099 28.132 28.303 28.343 28.660 28.734 28.758 28.880 28.937 29.157	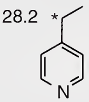; 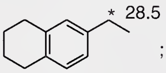; 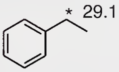; 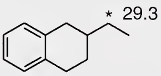
29.441 29.482 29.759	$CH_3-CH_2-CH_2-(\overset{*}{C}H_2)_n-CH_2-CH_2-$; 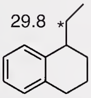
31.804 31.967 32.150	$CH_3-CH_2-\overset{*}{C}H_2-(CH_2)_n-$; 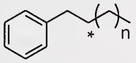; 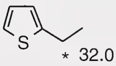
32.845	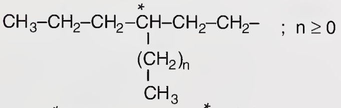 $CH_3-CH_2-CH_2-\underset{\substack{\vert\\ (CH_2)_n\\ \vert\\ CH_3}}{\overset{*}{C}H}-CH_2-CH_2-$; n ≥ 0
37.140 37.164 37.229 37.303 37.380 37.420 37.473	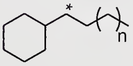 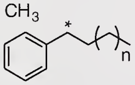 n ≥ 1 ; 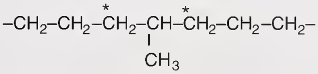 $-CH_2-CH_2-\overset{*}{C}H_2-\underset{\substack{\vert\\ CH_3}}{CH}-\overset{*}{C}H_2-CH_2-CH_2-$

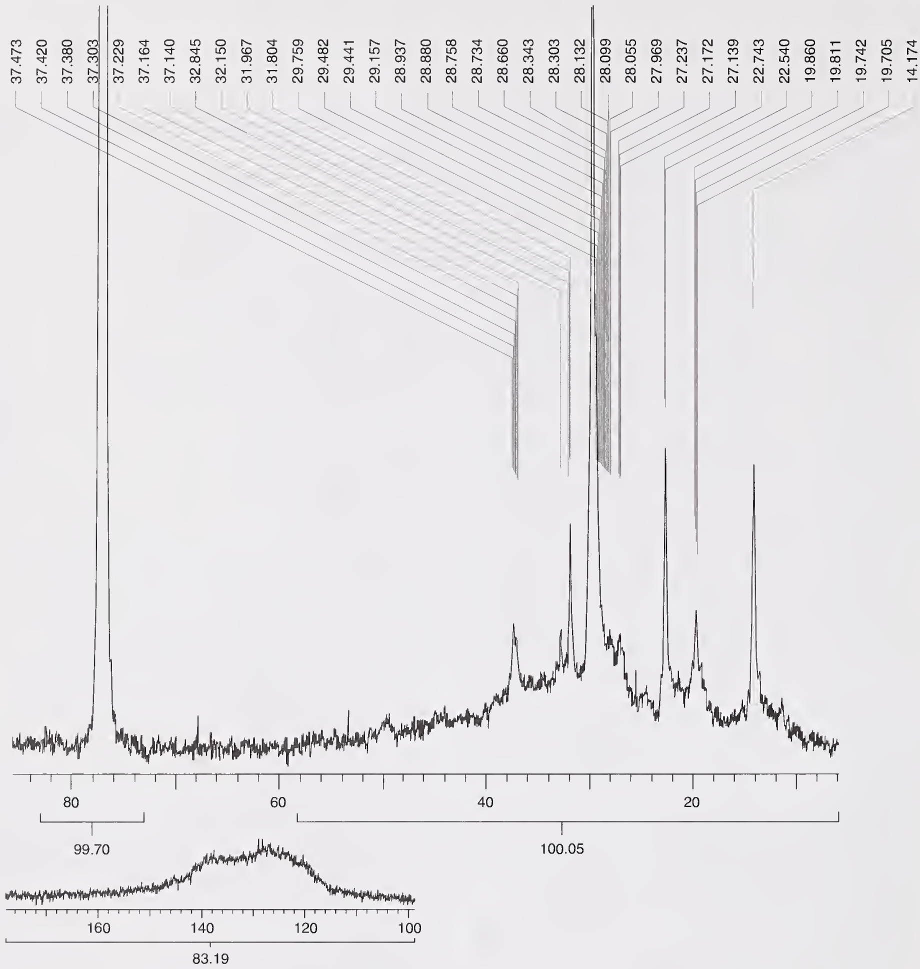

Figure 14.95 High-resolution 500-MHz ^{13}C NMR spectrum of Athabasca asphaltene.

the spectra are free of distortions and the resolution and accuracy are superior. Both solid- and liquid-phase ^{13}C and ^{1}H spectra for Athabasca and other Alberta asphaltenes have been reported.

In addition to the fully relaxed 400 MHz inverse gated decoupled ^{13}C spectrum of whole Athabasca asphaltene, Figure 14.94 also shows the Spin Echo Fourier Transform (SEFT) spectrum, which is equivalent to the currently used attached proton test (APT) spectrum. This allows differentiation between methyl and methine carbons on the one hand, and methylene and quaternary carbons on the other. The former show a negative spin in the SEFT spectrum and the latter, positive signals. Also shown in Figure 14.94 are the ^{13}C NMR spectra of the five GPC fractions of asphaltene and the ^{1}H NMR spectra of fractions 1 and 5; the analyses are given in Table 14.26.

The spectrum of the whole asphaltene is similar to those of the nondistillable fractions of the saturate, aromatic and polar fractions, featuring a broad hump in the 10–60 ppm region due to naphthenic carbons, with superimposed sharp peaks representing primary, secondary

Table 14.26 Analysis of Athabasca asphaltene and its GPC fractions.[a]

GPC fraction	1	2	3	4	5	Whole asphaltene
Yields (wt%)	22.5	30.5	13.6	11.1	20.8	
MW	16,900	13,700	7,100	3,400	1,200	3,600
Number of carbon atoms per 100 C atoms of major carbon types (solution state results)						
C aliphatic	65	66	61	59	52	57
C aromatic	35	34	39	41	48	43
Number of carbon atoms per 100 C atoms of major carbon types (solid state results)						
C aliphatic	58	60	65	69	63	58
C aromatic	42	40	35	31	37	42
Aliphatic carbon types per 100 C						
C terminal methyl	2	2	2	3	3	3
C branch methyl	2	2	1	1	1	2
C β-methylene	2	2	2	3	3	3
C mid-chain methylene	12	12	8	8	7	10
C other methylene	6	6	6	9	9	9
Average chain length	12	12	9.5	8	7.7	9
Proton types per 100 C						
H aliphatic	115	116	116	120	111	
H methyl	31	27	26	32	21	
H methylene, methine	67	66	66	65	62	
H 2.1–5.0 ppm	17	22	25	22	28	
H aromatic	7	7	8	9	12	
H_{arom}/C_{arom}	0.20	0.21	0.20	0.22	0.25	

[a] From N. Cyr et al., Ref. 113.

and tertiary carbons in mainly straight chains, and a 110–160 ppm hump due to aromatic resonances. The approximate ratios of aromatic, alkyl and naphthenic carbons determined from the spectrum are 43, 27, 30. The alkyl resonances, the most conspicuous characteristic of the spectrum, indicates the presence of fairly long unbranched or methyl-branched alkyl chains. These resonances represent the sum of alkyl resonances due to *all* the alkyl structural elements in the asphaltene, some of which have been identified and are listed in Chapters 12 and 13, and some others as follows:

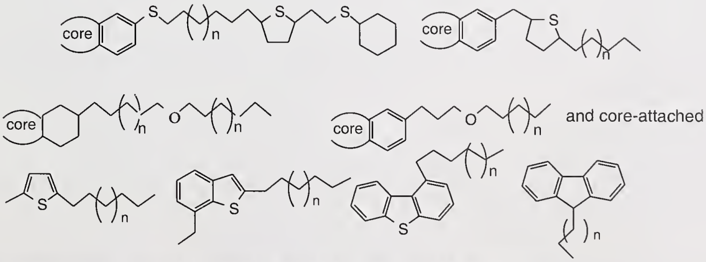

cheilanthanoic, steranoic, hopanoic, isoprenoid, etc., attachments where the length of the *n*-alkyl side chains can vary from C_1 up to C_{20}.

Consequently assignments to individual compounds is not possible.

The 500 MHz ^{13}C spectra of whole Athabasca and Cold Lake asphaltenes are reproduced in Figure 14.96. They show a close similarity which extends to all Alberta oil sand asphaltenes and even beyond, to the asphaltenes of many unrelated conventional and extra heavy oils from different parts of the world (*v.i.*). This characteristic asphaltene spectrum appears to be deceptively simple and does not give much hint of the enormous structural complexity of its carrier. The characteristic "asphaltene spectrum" displayed by the nondistillable fractions of the maltene compound classes points to the genetic relationship bonding these fractions of the maltene to the asphaltene and this, in turn, suggests that the heavy, nondistillable fraction of the oil sand maltene comprises, at least in part, degraded low-MW asphaltene. Because of their still relatively high molecular weights and attendant aggregate structures, these fractions provided a protective environment against chemical, thermocatalytic and microbial degradation of the alkyl moieties enclosed in them, while the alkyl moieties outside this protective environment were destroyed by secondary biodegradation.

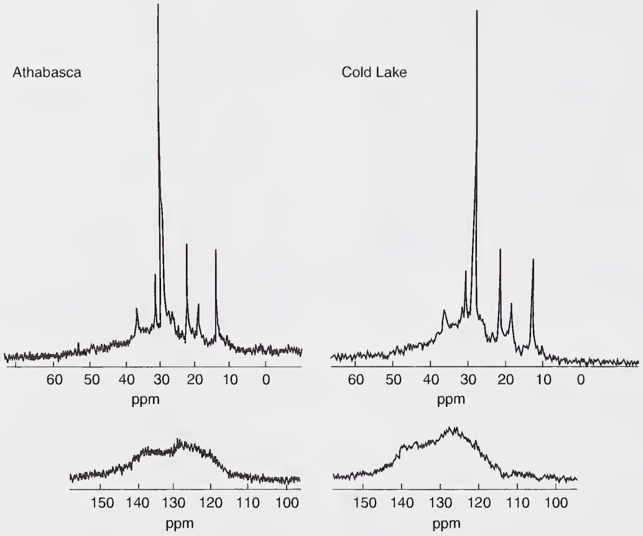

Figure 14.96 500-MHz ^{13}C NMR spectra of Athabasca and Cold Lake asphaltenes.

GPC fractionation of Athabasca asphaltene according to molecular weight does not appear to reveal significant qualitative structural differences among the fractions, with the exception of the lowest-MW (1,200 g·mol^{-1}) 20.8% fraction, which appears to be nearly identical to the 21–22% acetone-soluble asphaltene (MW 1,210 g·mol^{-1}). With increasing molecular weight the following trends can be noted in the molecular structure of the fractions:

- aromaticity: ↓
- apparent alkyl chain length: ↑
- number of terminal methyls: ↓
- number of branched methyls: ↑
- H_{arom}: ↓
- H_{arom}/C_{arom}: ↓
- H/C: ↓
- S content: ↑
- O content is highest in the lowest-MW fraction.

In order to illustrate the close similarity among the typical "asphaltene spectrum", the ^{13}C and some ^{1}H NMR spectra of a number of asphaltenes from foreign sources are displayed in Figures 14.97–14.103.[99,110,114,117] They represent petroleums from different continents,

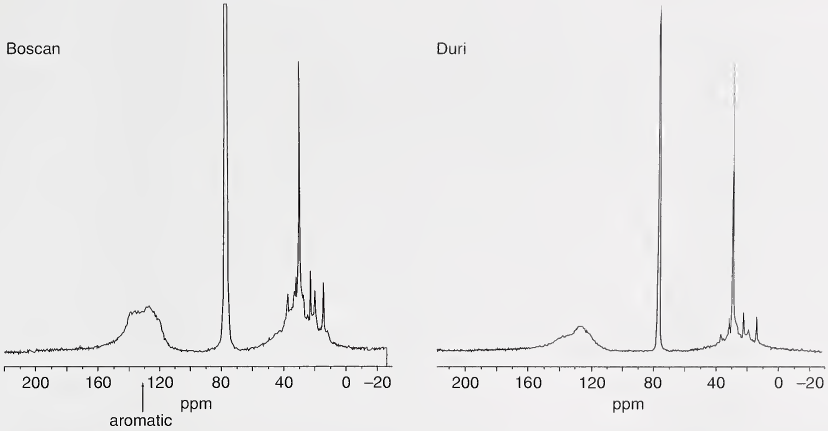

Figure 14.97 500-MHz ^{13}C NMR spectra of Boscan and Duri asphaltenes. From O.P. Strausz *et al.*, Ref. 99. © 1999, American Chemical Society.

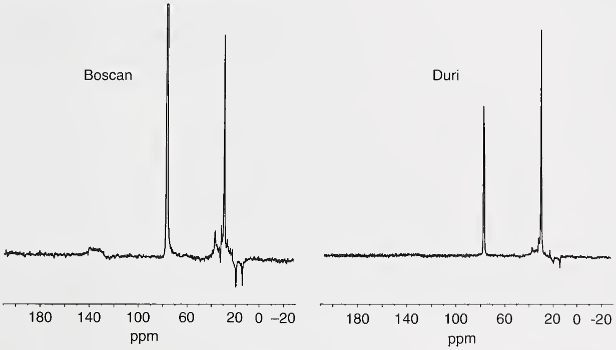

Figure 14.98 500-MHz ^{13}C NMR APT spectra of Boscan and Duri asphaltenes. From O.P. Strausz *et al.*, Ref. 99. © 1999, American Chemical Society.

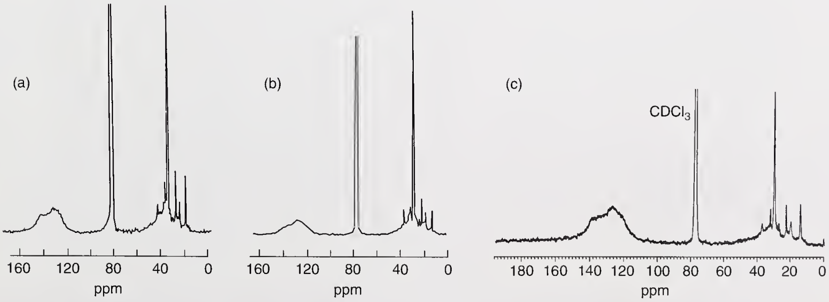

Figure 14.99 Comparison of Athabasca (a), Utah (b) and Arabian residue (c) asphaltenes. The Athabasca and Utah spectra are from L.S Kotlyar *et al.,* Ref. 117. © 1988, Elsevier Science. The Arabian residue spectrum is from L. Artok *et al.*, Ref. 114. © 1999, American Chemical Society.

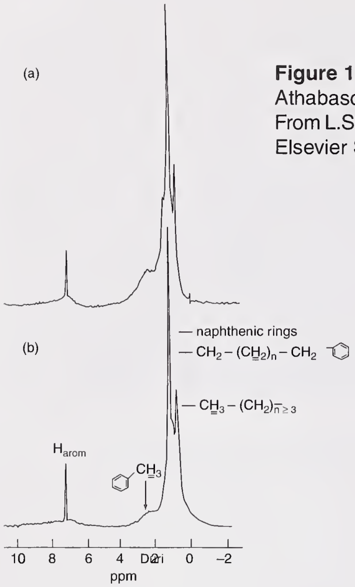

Figure 14.100 ^1H NMR spectra of (a) Athabasca and (b) Utah asphaltenes. From L.S Kotlyar *et al.*, Ref. 117. © 1988, Elsevier Science.

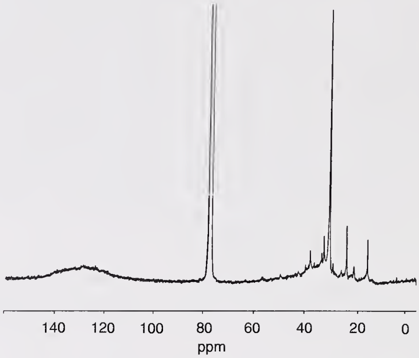

Figure 14.101 ^{13}C NMR spectrum of Saline Lake asphaltene. From P. Peng *et al.*, Ref. 110. © 1999, American Chemical Society.

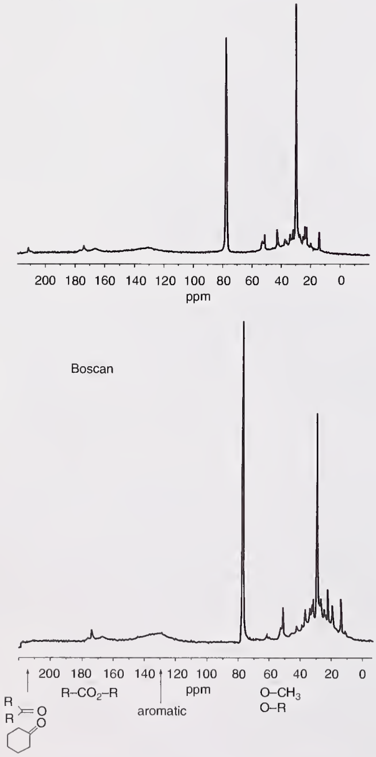

Figure 14.102 500-MHz ^{13}C NMR spectra of the oxidized residues from the RICO of Boscan and Duri asphaltenes. From O.P. Strausz *et al.*, Ref. 99. © 1999, American Chemical Society.

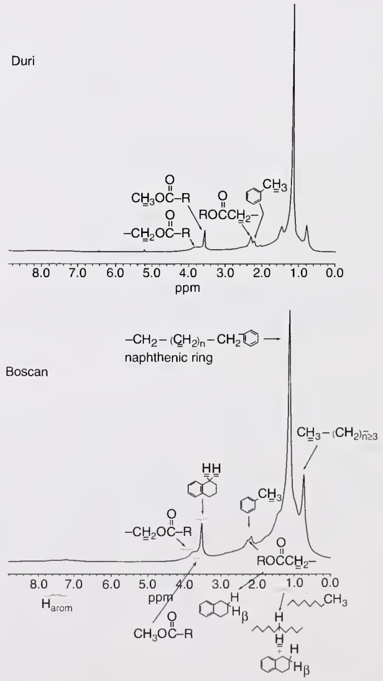

Figure 14.103 500-MHz ^1H NMR spectra of the oxidized residues from the RICO of Boscan and Duri asphaltenes. From O.P. Strausz *et al.*, Ref. 99. © 1999, American Chemical Society.

different origins with different depositional, temporal, thermal and microbial histories, yet all these spectra are characterized by unresolved aromatic absorption at 110–160 ppm and unresolved naphthenic absorption at 10–50 ppm, the latter being superimposed by sharp alkyl bands at 10–40 ppm. In the alkyl absorption, the mid-chain methylene band absorption (29–30 ppm) is much more intense than the terminal or branched methyl absorption at 14–15 and 19–20 ppm, pointing to the presence of long *n*-alkyl side chains and *n*-alkyl bridges between ring structures, in agreement with the RICO and thermolysis results. Considering the terminal and branched methyl, and midchain methylene resonances, the NMR spectra suggest that the length of the alkyl chains in the Duri asphaltene is greater and the branching is smaller than in the Boscan asphaltene, which again correlates well with the results of the RICO experiments. The spectra are, however, due to chains as well as bridges and therefore the apparent "chain length" is determined by the ratio of bridges to chains and not only the ratio of mid-chain methylenes to terminal methyls.

After chemical alterations the residual asphaltenes still preserve some of the characteristic molecular structural elements of the original asphaltene, but of course in significantly modified forms. For example, the nondistillable residues from the RICO of Boscan and Duri asphaltenes display a modified ^{13}C NMR spectrum, Figure 14.102, in which the aromatic resonances are markedly reduced, and new resonances representing the $O–CH_3$, $O–CH_2–R$ and $R–CO_2–R$ carbons of ester groups and the C=O carbon of alkyl- and cycloalkylketones appear. The C_{arom} content of the residue is considerably reduced relative to the starting asphaltene and represents only 4.6% based on the aromatic carbon content of the starting Duri asphaltene and 9.4% for the starting Boscan asphaltene. Nevertheless, the spectra still bear significant resemblance to the original asphaltene spectra, providing clear evidence for the presence of long-chain alkyl and alkenyl bridge moieties on the naphthenic core of the asphaltene molecule, in agreement with the thermolysis studies. The ^{1}H NMR spectra of these oxidized residues, Figure 14.103, are also informative and indicate the presence of methyl, methylene, CH_3–phenyl, H_{arom}, α and β (to aromatic) CH_2 and various ester protons. These NMR spectra may be useful in the elucidation of the structure of the nondistillable residue and for the quantification of C_{arom}, H_{arom}, C–carbonyl, C–ketone, *etc.*

Over the past 20–25 years several methods have been described in the literature attempting to yield more in depth information from NMR and other spectroscopic measurements on the molecular structure of asphaltene. One of these methods,[116] with the aim of delineating the size of polynuclear aromatic core structure, is based on the line shape determination in solid-state ^{13}C NMR spectra under static condition exploiting the chemical shift anisotropy of the different carbon atoms. It is possible to extract the principal values of the chemical shift anisotropy second rank tensor from such spectra. Inner aromatic carbons have an axially symmetric tensor with maximum intensity in the 160–190 ppm range while outer aromatic carbons have an orthorombic symmetry tensor with maximum intensity in the 140–100 ppm range. The proportion of the band intensities at 170 and 100 ppm was then taken as a qualitative-semiquantitative measure of the size of the polycondensed aromatic cores. For seven different asphaltenes investigated by this method the intensity ratios fell in the range of 5–7 condensed ring in the aromatic core on a scale based on the measured intensity ratios for standard polynuclear aromatic compounds ranging from anthracene to coronene and graphite.

Comparison with results from other ^{13}C NMR data led the authors to the conclusion that the average asphaltene molecule features a number (3–4) of polycondensed aromatic core built of 5–7 rings joined together by "some heteroatom and aliphatic linkages".[116]

To conclude this section we can state that the ^{13}C NMR spectra provide clear and convincing evidence for a common blueprint underlying the unique molecular architecture of all petroleum asphaltenes.

5.2 Fourier transform infrared spectroscopy

Like the NMR spectra, the FTIR spectra are informative but give no clue about the extreme complexity of asphaltenes. The spectrum of Athabasca asphaltene, Figure 14.104, shows the following absorptions:

cm^{-1}	assignment
700–900	arom CH out-of-plane bend and $(CH_2)_n$ rock
900–1000	arom CH in-plane bend
1032.3	S=O stretch
1070	arom C–H in-plane bend
1113.7	C–OH and C–O–C stretch
1263.4	C–O–C stretch
1376.6	CH_3 sym bend
1456.3	CH_2 scissor and CH_3 asym bend
1599.4	arom ring and C=O in ketones
~1710, ~1730	C=O in alkanoic acids and *n*-alkanoic acid esters stretch; weak shoulders
~1980–2040	arom CH out-of-plane-bend overtone and combination
2852.9	CH_2 and CH_3 sym stretch
2923.8	CH_2 and CH_3 asym stretch
~3050	arom CH stretch and comb.
3100–3500	OH polymeric stretch
3213.19	polymeric OH
~3470	dimeric OH
3619.8	SiO–H stretch from clay or free OH stretch
3695.95	SiO–H stretch from clay (kaolin)

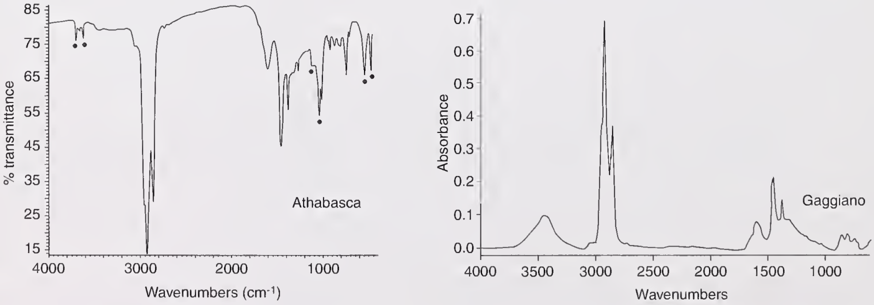

Figure 14.104 FTIR spectrum of Athabasca and Gaggiano[116] asphaltene. Peaks labelled with dots are due to clay minerals.

The last two absorption bands at 3619.8 and 3695.95 suggest that the sample contained a significant quantity of clay minerals, Appendix 14.7.

After RICO of the Boscan and Duri asphaltenes, the nondistillable oxidized residues yielded FTIR spectra[99] shown in Figure 14.105. For reference, the spectrum of 2-*n*-dodecylthiane-1,1-dioxide is also shown. The two asphaltene spectra are similar and feature broad polymeric OH absorptions at 2600–3400 cm^{-1} due to tertiary alcohols, weak absorptions in the 1900–2100 cm^{-1} range, presumably due to the overtone and combination bands of highly substituted aromatic rings; the characteristic aromatic and C=O absorption at 1600 cm^{-1}, showing that some aromatic carbons have resisted oxidation to CO_2; intense ester carbonyl absorption at 1740 cm^{-1}; and a broad, ill-resolved band structure due to C–O–C, C–OH, $=SO_2$, CH_3, CH_2, *etc.* The appearance of the OH absorption bands is indicative of the presence of tertiary alcohols originating from the oxidation of tertiary C–H bonds during the RICO reaction. The appearance of the broad band structure at 1100–1400 cm^{-1} provides evidence for the existence of aliphatic sulfides in the asphaltene; upon RICO these sulfides are oxidized to SO_2-, SO_3- and SO_4-containing species (*cf.* Appendix 14.5). Aromatic sulfides and thiophenes would be oxidized as well, but they would be destroyed rather than converted to their sulfones. The intense CH_2 and CH_3 absorptions around 2850 and 2920 cm^{-1} reveal the existence of long-chain alkyls, in agreement with the ^{13}C and ^{1}H NMR spectra.

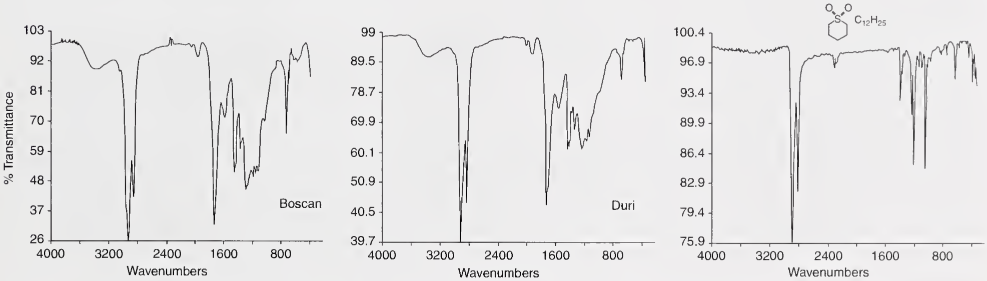

Figure 14.105 FTIR spectra of the oxidized residues from Boscan and Duri asphaltenes and 2-*n*-dodecylthiane-1,1-dioxide. From O.P. Strausz *et al.*, Ref. 99. © 1999, American Chemical Society.

5.3 Ultraviolet–visible spectroscopy

Whole, native petroleum asphaltenes have a dark brown color, but when their low-molecular-weight portions are removed by acetone extraction, gel permeation chromatography, or successive reprecipitations, the residual high-molecular-weight asphaltene is black. It is noted here that asphaltene, whether solid or in solution, does not exhibit a red color—even at extreme dilution—contrary to some earlier reports.

The absorption spectra of asphaltenes are characterized by a broad, featureless continuum covering the entire visible range and extending into the ultraviolet down to 250 nm and beyond. The only distinctive attribute of these spectra is a weak band appearing at 412 nm, which is identified with the Soret band of the vanadyl porphyrin complexes[118] which are concentrated in the low-molecular-weight asphaltene separated by acetone extraction or GPC fractionation. The complexes from Athabasca asphaltene have been isolated from the acetone extract and analyzed at the molecular level[40], *cf.* Figure 12.86.

Asphaltenes exhibit fluorescence when irradiated with UV light. The emission band system is a continuum with a maximum around 450–500 nm and extends from 340 nm to about 650 nm and beyond (when λ_{exc} is 300 nm). It may show some very weak, irregular and uninterpretable structure and, on the whole, it is not much more informative than the absorption spectrum. Moreover, interpretation of the spectrum is further complicated by the intervention of intramolecular exciplex (excimer) species, and self-absorption processes (the re-absorption of shorter-wavelength radiation of one species by longer-wavelength-absorbing other species, re-emitting longer-wavelength fluorescence).

As a consequence, the UV–visible spectroscopy of asphaltene is not of great value for the identification of specific structural units; nonetheless it can still yield useful information with regard to compositional variations.

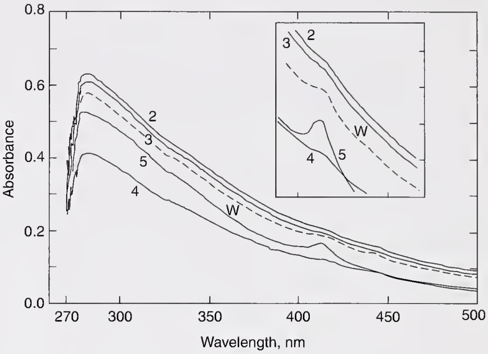

Figure 14.106 Absorption spectra of Athabasca asphaltene (W) and its GPC fractions 2–5, concentration 19.2 mg·L^{-1}. Inset: concentration 60 mg·L^{-1}. From T. Yokota *et al.,* Ref. 118. © 1986, Elsevier Science.

Absorption spectra for the GPC-separated fractions of Athabasca asphaltene and the whole asphaltene[118] (Table 14.12) are shown in Figure 14.106. The onset of light absorption lies above 600 nm and the absorbances increase smoothly into the ultraviolet, reaching a maximum corresponding to the absorption onset of the solvent, around 260 nm in chloroform. The absorbance of fraction 1 (not shown) is very similar to that of fraction 2. The Soret band at 412 nm is most intense in fraction 5; in the spectra of the other fractions it is faint, becoming less noticeable with incresing MW. At a constant weight concentration the absorbances of fractions 1–4 are different and show an increasing trend with increasing MW of the fraction. The absorbance of fraction 5 does not follow this trend and lies between those of fractions 3 and 4.

In general, the UV-visible spectra of asphaltenes is attributed to the $\pi^*\leftarrow\pi$ transitions of their aromatic constituents, although other chromophores such as carbonyls, sulfoxides and vanadyl porphyrins are known to be present. The spectra of linear acenes consist of three $\pi^*\leftarrow\pi$ transition bands (E_1, E_2, B) whose molar absorptivities are approximately 10^5, 10^4 and 10^2 ($L^3 \cdot mol^{-1} \cdot cm^{-1}$). The energy of HOMO-LUMO separation and the position of λ_{max} for each absorption band depends on the number of condensed aromatic rings and λ_{max} increases with the number of condensed rings. The onset of absorption in the linear acene series also increases with the number of rings and so does the short-wavelength tail end of their emission spectra (benzene: 265 and 280; naphthalene: 290 and 320; anthracene: 380 and 390; tetracene: 475 and 485; pentacene: 580 and 590 nm for absorption and emission, respectively). These spectral characteristics are substantially affected by the mode of condensation in non-linearly condensed aromatic structures and by substitution. Alkyl, naphthyl, ester, ether, *etc.* substituents can cause large bathochromic shifts and increases in the molar absorptivity and fluorescence yields.

The relatively high absorptivity of fraction 5 in Athabasca asphaltene is partly due to its high aromatic carbon content and partly to its high resin content. In the cases of fractions 1–4, however, the absorptivity varies in inverse proportion to the aromatic carbon content, *cf.* Table 14.12. This trend then must be due to the increasing concentration levels of larger condensed aromatic units (with high absorptivities) in the asphaltene molecules with increasing MWs of the fractions. A similar conclusion can be reached from EPR spectroscopic studies (*v.i.*).

Fluorescence spectra from the whole asphaltene and its fractions are displayed[118] in Figure 14.107. As seen, the fluorescence intensity (in terms of quantum units) at a given weight concentration is inversely proportional to the MW of the fraction*; when the concentration is increased from 3 to 60 mg·L^{-1} the intensity increases and the spectra shift toward the red. These concentrations are well below the critical micelle or aggregate concentration of asphaltene in benzene (0.5–4 g·L^{-1}) and therefore the absorbing species must be dissociated asphaltene molecules. The minima at 412 nm are due to the self-absorption of the emitted light by the vanadyl porphyrin complexes and the maxima around 395 nm can be identified with the most prominent Raman band of the benzene solvent. The emission intensities exhibit a clear trend: at a constant weight concentration the emission intensity increases as the average MW decreases, reaching a maximum value in fraction 5. The change that is evident in the spectral profile upon concentration increase is probably due to inner filtering effects and intermolecular exciplex/excimer formations.

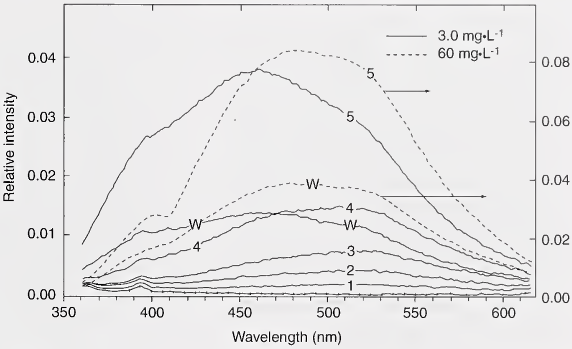

Figure 14.107 Emission spectra (λ_{ex} = 350 nm) of Athabasca asphaltene (W) and its GPC fractions 1–5. From T. Yokota *et al.*, Ref. 118. © 1986, Elsevier Science.

Excitation, emission and (height adjusted) absorption spectra for fraction 5 are shown in Figure 14.108.[118] According to the theory of excitation spectra, the profile of the normal excitation spectrum should match that of the absorption spectrum. As seen from the figure this is indeed the case, indicating that essentially all the excited singlet species are participating in the fluorescence processes and that no significant amount of scattering (Tyndall effect) is affecting the absorption spectrum.

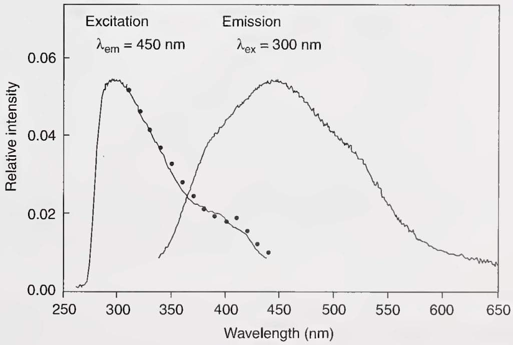

Figure 14.108 Emission and excitation spectra of fraction 5, 2.0 mg·L^{-1}.(• • • •, absorption spectrum, from Figure 14.106). From T. Yokota *et al.*, Ref. 118. © 1986, Elsevier Science.

From the above discussion it is clear that the most fluorescent fraction of the asphaltene is the lowest-MW fraction, which is known to be rich in small aromatic molecules, including the following:

---

*A similar phenomenon has recently been reported for coal pitch fractions: A.A. Herod, M.-J. Lazaro, M. Domin, C.A. Islas and R. Kandiyoti, Fuels, 79 (2000) 323.

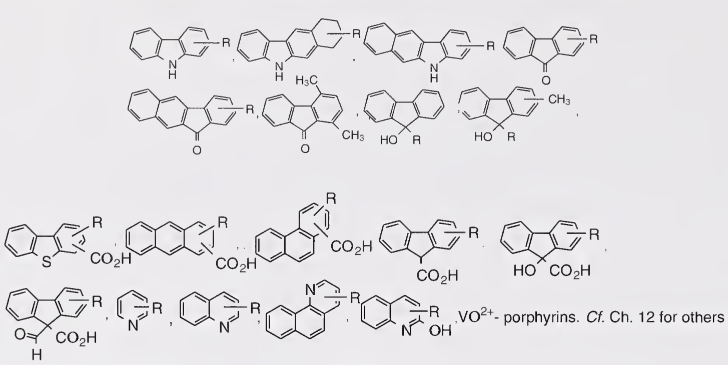

The percentage integrated fluorescence yields corrected for light absorption at λ_{exc} = 350 nm and at a concentration of 3.0 mg·L^{-1} in benzene solution were calculated to be 1.8, 4.0, 7.4, 23 and 51% of the total for fractions 1–5, respectively. Thus, more than half of the fluorescence from the whole asphaltene comes from the lowest-MW fraction and the two highest-MW fractions (14,000–17,000 g·mol^{-1}, amounting to over half of the whole asphaltene) contributes a mere 5.8% to the total fluorescence. The implication, then, is that the fluorescence originates from the free, substituted, aromatic complement and the small aromatic structural segments of the asphaltene, and that the large aromatic clusters fluoresce either very weakly or not at all. The fluorescence yield for aromatic molecules is known to be highly variable and changes with the size, condensation mode and nature and degree of substitution. Rigidity in the molecule enhances the fluorescence.

The position of the emission maximum also varies from fraction to fraction and λ_{max} is found near 450, 510 and 530 nm for fractions 5, 4 and 3–1, respectively. This trend suggests that the average size of aromatic clusters increases progressively with the MW of the fraction. If the emission from fraction 5 is from a monomeric absorber then it would be equivalent to a di- or higher substituted anthracene, phenanthrene, benz[a]anthracene, benzo[c]phenanthrene, triphenylene, pyrene, chrysene, coronene, *etc.* molecule. An alternative possibility is that the emission is from an intramolecular exciplex (excimer) species, as will be discussed below. Increasing concentrations up to 5 mg·L^{-1} have no effect on either the position of λ_{max} or the integrated fluorescence yield. Above 5 mg·L^{-1} the fluorescence yield starts to drop owing to intermolecular energy transfer, bimolecular reactions and self-absorption processes. At 10 mg·L^{-1} the fluorescence yield is about 12% lower than at 1–5 mg·L^{-1} and at 60 mg·L^{-1} it is four times lower.

It is well known from organic photochemistry[119] that flexible polymethylene-bridged bichromophoric aromatic hydrocarbons may readily undergo intramolecular energy transfer processes (from the higher to the lower energy units), *e.g.*

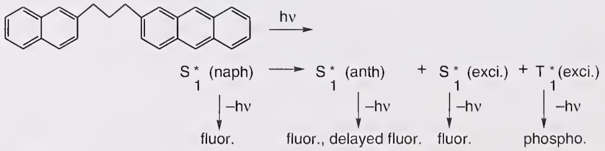

where the S_1^* (exciplex) fluorescence may be considerably shifted to the red, compared to the fluorescence of the monomers: λ_f(naph) < λ_f(anth) < λ_f(exci.); the efficiency of exciplex fluorescence for simple mono- through trinuclear aromatic chromophores depends on the chain length and may maximize at the shortest length[119c] after which it may gradually decline (to a length of up to 12 units) at some intermediate length[119a] or may be independent of length[119c] over a range.

Now, militating against the involvement of any exciplex/excimer species in the photophysics of asphaltene are the interpretations of results obtained from extensive spectroscopic and fluorescence lifetime studies carried out on a select suite of asphaltenes over the past decade.[120,121] In these studies, the fluorescence spectra of a light crude oil and some asphaltenes were compared under identical conditions and it was shown that the emission from the light oil featured two intense short wavelength bands, one around 280 nm and one around 320 nm, originating from monoaromatic and dinuclear condensed aromatic molecules, respectively which in practical terms are missing from all asphaltene spectra studied thus far[120], Figure 14.109. The lack of significant spectral emission from these small aromatics was then interpreted as being due to their small population in asphaltenes. But this is not the case. Alkylated benzene, thiophene (nonfluorescent), fluorene, naphthalene, biphenyl and benzothiophene (the most abundant compound class in the asphaltene molecule) along with various other small aromatic molecules have been detected in significant concentrations in the mild thermolysis products of asphaltene, *cf.* section 4.1.2 of this chapter. These structural units are present in bi- and multichromophoric molecules which have the capacity to undergo intramolecular transfer of energy from the higher energy chromophore to the lower energy chromophore. Thus, the intervention of intramolecular exciplexes would shift the fluorescence spectrum of the asphaltene to the red.

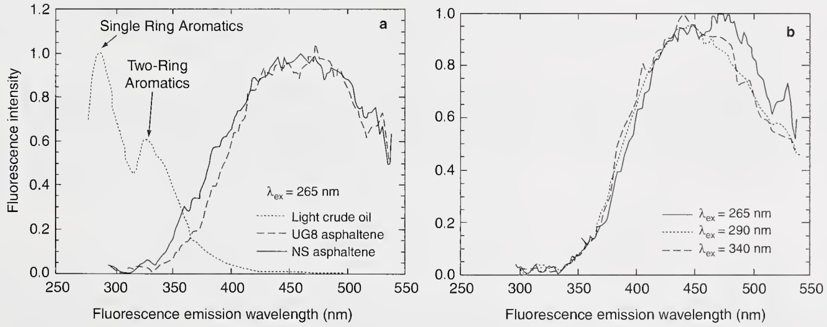

Figure 14.109 a) Fluorescence emission spectra of two asphaltenes and a light crude; b) Fluorescence emission spectra of an asphaltene with different excitation wavelengths. From C.Y. Ralston, *et al.*, Ref. 120. © 1996 American Chemical Society.

At this point in order to understand the nature of the problem involved in the interpretation of the photophysical results it is necessary to take a brief digression from asphaltene chemistry into the land of photophysics.

The experimental techniques employed in the investigation of exciplex, excimer chemistry and inter- and intramolecular energy transfer processes between two chromophores involve time resolved spectroscopy, radiative life time and quantum yield measurements for fluorescence and phosphorescence. For example, one method to detect the occurrence of intramolecular energy transfer is to selectively excite the higher energy chromophoric moiety of a bichromophoric molecule and observe the fluorescence and/or phosphorescence emerging from the lower energy chromophoric moiety of the molecule. Innumerable examples of these methods have been described in the literature.

In the study of asphaltenes and crude oils reported in references 120 and 121 narrow spectral band filters were used for selected spectral ranges with a 40 nm gap between exciting and emitting light. Fluorescent lifetimes, τ_F, were then measured on the nanosecond time scale. Decay plots for fluorescence are reproduced in Figure 14.110 and the kinetic equation (equation (1) in reference 120) used for the extraction of fluorescence lifetime from the experimental data is as follows:

$$k_F = k_F^0 + k_Q[Q] + k_{ET}[Q'] + k_{Q^*} + k_{ET^*}, \tag{74}$$

where, k_f is the measured fluorescence decay rate, k_F^0 is the intrinsic fluorescence decay rate of the chromophores, k_Q is the collisional quenching rate with the quencher of concentration [Q], k_{ET} is the intermolecular energy transfer rate with chromophores of concentrations [Q′], k_{Q^*} is the rate of singlet ⟶ triplet intersystem crossing, and k_{ET^*} is the rate of intramolecular energy transfer, process 1 ⟶ 2.

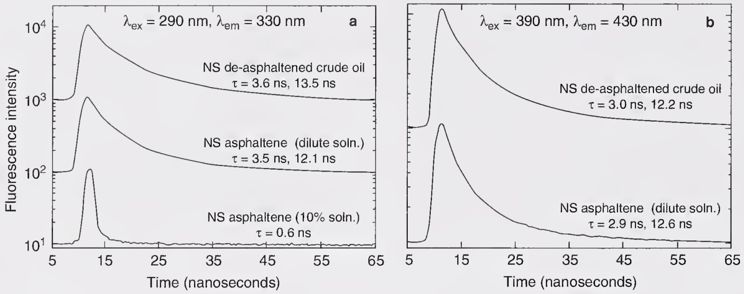

Figure 14. 110 Fluorescence decay curves for a two-ring aromatics, a) and b) roughly four-to-seven ring aromatics for an asphaltene and its deasphaltened crude oil. From C.Y. Ralston, *et al.*, Ref. 120. © 1996 American Chemical Society.

$$\boxed{\text{Ch I}}\!-\!(\text{CH}_2)_n\!-\!\boxed{\text{Ch II}} + h\nu \longrightarrow \boxed{\text{Ch I}}^*\!-\!(\text{CH}_2)_n\!-\!\boxed{\text{Ch II}} \tag{75}$$

$$\boxed{\text{Ch I}}^*\!-\!(\text{CH}_2)_n\!-\!\boxed{\text{Ch II}} \xrightarrow{\text{ET}} \boxed{\text{Ch I}}\!-\!(\text{CH}_2)_n\!-\!\boxed{\text{Ch II}}^* \tag{76}$$

At low concentrations of the bichromophoric absorber, the asphaltene bimolecular quenching rates are negligibly slow and the kinetic equation is reduced to

$$k_F = k_F^0 + k_{Q^*} + k_{ET^*}, \tag{77}$$

In so far as the experiments in Figure 14.110 are concerned* the experimentally determined fluorescence decay times for asphaltenes are all in the range (12 ± 2) x 10^{-9} sec. As a reference the decay times of the corresponding deasphaltened crude oils were also determined and shown in Figure 14.110 as well. The decay times of the deasphaltened crudes were very similar to their asphaltene counterparts and the deviations did not exceed ±2 x 10^{-9} sec.

Now, the interpretation of the results with all of its far reaching consequences depends entirely on whether the 12 x 10^{-9} second lifetimes obtained for the dilute asphaltene solutions is “considered” to be long or short. The authors of reference 120 state that “The long lifetimes obtained for dilute asphaltene solution indicate that energy transfer and quenching effects are not dominant for the two-ring aromatics.” So, let us examine the magnitude of the τ_F values in a more objective way.

---

*The emerging fluorescence is a composite of a large number of components originating from different species present in different concentrations, with different fluorescence quantum yields and radiative lifetimes, giving rise to multiexponential overall decay kinetics. The dominant spectral components will arise from the most intense, slowest decaying excited chromophores.

For asphaltene, the principal two-ring aromatic absorber in the spectral range of excitation, 290 ± 2 nm, is naphthalene, Appendix 14.8. The reported measured fluorescence lifetime of this molecule,[119d] Appendix 14.9, is 96×10^{-9} sec with an intersystem crossing quantum yield of ~0.4, giving a fluorescence quantum yield of 0.6. (Therefore, the intrinsic fluorescence lifetime, $\tau_F^0 = \tau_F/\phi_F = 96 \times 10^{-9}/0.6 = 160 \times 10^{-9}$ sec.) The measured fluorescence lifetimes for the two asphaltenes and deasphaltened oils reported in reference 120 are in the $12–14 \times 10^{-9}$ sec range, that corresponds to 85% quenching by the intramolecular energy transfer process, reaction (76). Yet the authors in reference 120 conclude that energy transfer effects are not “dominant” for the two-ring aromatics!?

The above fluorescence lifetime does not register all the intramolecular processes taking place in the system. There are two types of processes not registered:

a) where the excitation energy of Ch II lies between the energy of excitation and the energy of light selected for fluorescence monitoring: for such cases the fluorescence emitted from Ch II could be registered as emission from Ch I; and
b) where the excitation energies of Ch I and Ch II are so close that the reverse process of reaction (76) could have some significance.

The occurrence of either or both of these processes would lead to a slight underestimation of the importance of intramolecular energy transfer as expressed by the measured value of τ_F.

The “long” lifetime in reference 120 evidently refers to the deasphaltened oil as a standard, for the authors here appear to have assumed that in this case there should be no bichromophoric molecules present and thus the measured lifetime would reflect the intrinsic lifetime + intersystem crossing processes in the deasphaltened oil,

$$1/\tau = 1/\tau_F^0 + k_{Q^*}. \tag{78}$$

Whatever the case may be—”long” or “short”, deasphaltened oil standard or not, the conclusion drawn from the interpretation of the experimental results rests on a basic **assumption**. If this assumption is wrong so goes the conclusion and everything else that follows from it. And surely, the assumption that the measured lifetimes for asphaltenes are inconsistent with the occurrence of intramolecular energy transfer is a mistaken idea that led to the misinterpretation of the results and ultimately to a host of wrong conclusions.

Fluorescence spectra have also been reported[120,121a] for several other crude oil asphaltenes. Shown in Figure 14.111 are the fluorescence spectra of four different crude oil asphaltenes and a coal asphaltene. For the crude asphaltenes the maxima in the spectra lie in the same spectral range (at the same excitation wavelength in highly dilute solution) ~460–530 nm as those for the MW fractions of Athabasca asphaltene, Figure 14.107, manifesting the effect of the MW distribution. The quantum yield of fluorescence is low, lying in the range of a few hundredths and in a given asphaltene it is MW dependent.

Fluorescence spectroscopy has also been proposed as a method for the MW determination of asphaltene.[120,121] The idea is contingent upon the non-operativeness of intramolecular energy transfer that has been shown above to be completely wrong. Consequently, the method is wholly inappropriate for the MW measurement of asphaltene as will be discussed in section 6.7.4.

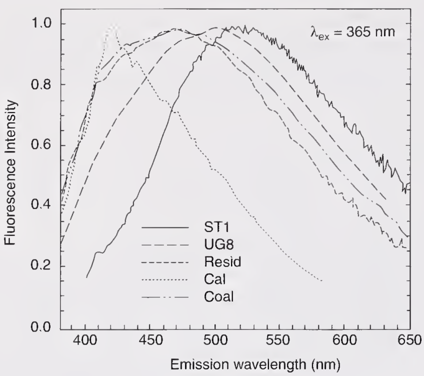

Figure 14.111 Fluorescence spectra for a series of asphaltenes. From H. Groenzin and O.C. Mullins, Ref. 121. © American Chemical Society.

Going back to the nature of the fluorescence it should be remarked that in more complex systems where exciplexes would have some stability through charge-transfer complexation in their ground electronic states, the bridging chain length dependence of the fluorescence may be modified or even disappear altogether, and exciplex absorption may compete with absorption by individual aromatic moieties, also resulting in a bathochromic shift in the absorption spectrum. Indeed the presence of intramolecular and/or intermolecular charge transfer triplet state, doublet–doublet radial ion pairs in equilibrium with their ground singlet state, doublet-doublet radical ion pairs has been established by EPR spectroscopy

$$A\colon + \colon B \rightleftharpoons [\overset{(-)}{A\colon\cdot}\cdot\cdot\overset{(+)}{B}]^1 \rightleftharpoons [\overset{(-)}{A\colon\cdot}\cdot\cdot\overset{(+)}{B}]^3$$

as will be discussed in the following section of this chapter. Their role in the fluorescence spectroscopy has not been investigated, but must not be ignored.

Lastly, the MW dependence of the fluorescence yield may be rationalized by invoking intramolecular quenching of the S_1^* state of the monomers in the exciplexes, with or without the intervention of the triplet state of the exciplex. Such processes would be more efficient with increasing sizes of the condensed polyaromatic moieties, the concentrations of which should be higher with increasing MW.

These general conclusions are in agreement with conclusions drawn from RICO, thermolysis, NiB and NRA reduction, NMR and magnetic susceptibility studies, pointing to the presence of relatively small aromatic units as free entities and structural segments in the larger asphaltene core. Also, the conclusion that the size of aromatic condensation grows with the average MW of the fraction is supported by EPR studies of these fractions.

5.4 Electron paramagnetic resonance (EPR) and electron nuclear double resonance (ENDOR) spectroscopy

In general, petroleum asphaltenes, petroleum resins, coals, kerogens and charred organic materials are paramagnetic, manifesting the presence of stable free radicals. Bitumens, whole oil sands and even the extracted mineral matrix of some oil sands (including Alberta oil sands) possess free radicals and are EPR active. Fulvic acids, humic acids and humins—constituents of soil—also contain free radicals in concentrations comparable to those in the above substances. The nature of the free radicals in these materials, their distributions and concentrations, can be investigated by EPR, ENDOR and related spectroscopic methods. A considerable volume of literature exists on this topic going back to 1954, the date of discovery of EPR in charred materials.[122] The first EPR spectra of a crude oil and crude oil products were reported in the period 1958–1961.[123–126]

The EPR spectra of Athabasca, Peace River and Cold Lake asphaltenes—like those of asphaltenes in general— are complex and quite similar to one another, all indicating the presence of at least two very different kinds of free radicals, one which was identified in early studies as the vanadium radical ion in vanadyl porphyrin (VO^{2+}–porphyrin) complexes[122–124] and the other as a mixture of EPR spectroscopically-similar carbon free radicals.[122,123,125,126] The former are bound to the asphaltene by adsorptive forces and can be largely removed from the asphaltene by solvent extraction, whereas the latter are intimately associated with, and form part of, the asphaltene bulk material. (Vanadium atoms in other than the four-valent state have not been detected with certainty in carbonaceous materials.) The concentrations of the organic free radicals in the asphaltene are relatively high, at least in terms of free spin chemistry, and lie in the range $0.8–20 \times 10^{18}$ $spins \cdot g^{-1}$ asphaltene.

The study of these paramagnetic species in fossil fuels can give information on the biotic source material of the fossil fuels, the nature of their source rocks, depositional environment and diagenetic/catagenetic history, since vanadyl porphyrins are considered to be valuable biomarkers in petroleum and have a historic role in biomarker chemistry. On the other hand, the organic free radicals are indigenous to the structure of their host molecules and thus they reflect the covalent molecular structure of asphaltene and related species in crude oils and bitumens; they may also play a pivotal role in the thermal chemistry of the bitumen[127] during upgrading operations.

5.4.1 The vanadyl porphyrin spectrum

The V^{4+} (VO^{2+}) ion has one unpaired electron in its d-orbital which interacts with the nuclear spin to produce a hyperfine spectrum (hfs). The spin value of the unpaired electron is 1/2 which vectorially combines with the nuclear spin of the V atom, 7/2, to give a $(2I + 1) = (2 \times 7/2 + 1) = 8$ hyperfine line spectrum. However, axially symmetric paramagnetic species, if randomly oriented in a powder, display two sets of characteristic lines corresponding to the orientation of the symmetry axis (the V=O bond of the vanadyl ion) parallel and perpendicular to the external magnetic field (of the EPR spectrometer), effectively doubling the number of hyperfine lines in the spectrum, Figure 14.112. The anisotropy disappears when the adsorbed vanadyl porphyrins are desorbed from the asphaltene with a polar solvent at elevated temperature. Under these conditions the spectrum is transformed reversibly into an isotropic spectrum of only eight hyperfine lines. From relative spectral intensity measurements at different temperatures, desorption energies of 41.8 and 58.5 $kJ \cdot mol^{-1}$ have been reported for two different asphaltenes. (Note: nickel porphyrins are diamagnetic and thus cannot be detected by EPR spectroscopy.) Prior to the advent of atomic absorption, inductively coupled plasma and nuclear activation spectro-

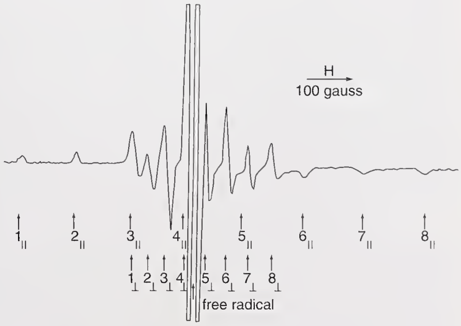

Figure 14.112 EPR spectrum of Athabasca asphaltene. The lines labeled $1_{\perp}$ to $8_{\perp}$ belong to the VO^{2+} cation. From S. Niizuma *et al.*, Ref. 128. © 1977, Elsevier Science.

scopies, EPR spectroscopy was suggested to be the definitive tool for the analysis of VO^{2+} in petroleum.

Vanadium was also found in asphaltene-associated clays[129] (P.R. Spring tar sand) and in coal inclusions in Athabasca oil sands.[130]

5.4.2 The organic free radicals spectrum

In contrast to the vanadyl porphyrin spectrum, the organic free radicals spectrum consists of a single, intense line without any hyperfine structure (hfs), Figure 14.112. The absence of hfs precludes the unambiguous assignment of the spectrum. Several causes for the absence of an hfs have been suggested, for example:

- there may be more than one structurally similar free radical present, each having different hfs and g-factors, causing extreme line broadening;
- molecular tumbling, in large micelles, a glass or in the solid asphaltene, may fail to average out electron dipolar and anisotropic nuclear hyperfine interactions and thus the width of the absorption line depends on the state of aggregation of the sample;
- the occurrence of electron dipole–dipole interaction which, from the formula $\Delta B = g\beta Nd[5.1S(S + 1)]$, based on Van Vleck's dipolar broadening theory, can by itself account for 30–40% of the experimental line width (ΔHpp = 0.591 at a microwave power of about 0.04 mW). However, this broadening effect can be somewhat reduced by the electron exchange-narrowing phenomenon which occurs when wave functions of similar molecules overlap sufficiently to allow a rapid exchange of electon spins.
- the spin–lattice relaxation time of carbon radicals is long, of the order of 10^{-6} s, and as illustrated for the case of Athabasca asphaltene in Figure 14.113,[131] saturation can occur readily even at low microwave power, down to tenths of a milliwatt. If line broadening at zero power is homogeneous, then saturation can cause line broadening. The shape of the free radical line in asphaltene has been shown to be invariant with respect to saturation, indicating that the saturation occurring is inhomogeneous;
- the occurrence of g-anisotropy broadening, *etc.*

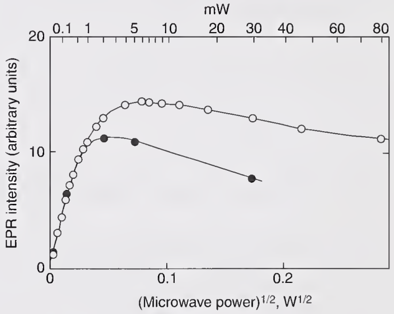

Figure 14.113 Power saturation of the EPR signal of the paramagnetic species in Athabasca asphaltene: O at 10°C; ● at –140°C. From Ref. 131.

Thus, it can be seen that the disappearance of hfs and the broadening of the absorption line is the result of numerous complex phenomena, the overall effects of which cannot be evaluated precisely. Nevertheless, it is clear that the single line at g = 2 does not necessarily signify a single doublet radical species but can be due to a set of different, but structurally similar, doublet or even triplet radicals. That the signal indeed represents a mixture of doublet and triplet radical species is indicated by the temperature variation of its intensity and the ENDOR spectrum of the free radicals, although other interpretations have also been offered.

The EPR signal intensity at g = 2 varies with temperature in most of the asphaltene samples studied, even after correction for the Curie effect,[128] Figure 14.114, and this has been attributed to the presence of close-lying singlet and triplet state diradicals in addition to the doublet monoradicals.[132-136] The population of the triplet level increases with increasing temperature from the lower-lying singlet reservoir. From the temperature study done at low (0.04 mW) microwave power, it was determined that the triplet state in Athabasca asphaltene lies about 300 cm^{-1} above the singlet state[128] and that, at room temperature, approximately 65% of the absorption comes from doublet species. (It is also possible that more than one singlet state, separated by 1,000–2,000 cm^{-1}, exists.) Other values reported for S_o–T_1 state separation include P.R. Spring,[136], Mara[134] and Bakerville[134] asphaltenes with wavenumbers 127, 419 and 710.

The spin concentration, after correction for saturation effects and assuming that all the absorption was due to doublet-state free radicals, was 3.1×10^{18} spins·g^{-1} asphaltene. This corresponds to about one unpaired spin per ~ 100–200 asphaltene molecules. Other values reported for Athabasca asphaltene were 0.6,[137] 1.2,[138] 1.3 and 5.8×10^{18} spins·g^{-1} asphaltene. For other asphaltenes the values reported are in the range $1–10 \times 10^{18}$ spins·g^{-1} asphaltene, most of them in the $(3 \pm 2) \times 10^{18}$ subdomain. (The apparent measured spin concentration is dependent on whether or not the signal is saturated. Spin saturation leads to low apparent concentration values.)

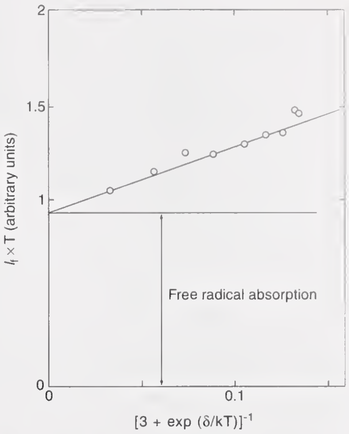

Figure 14.114 Analysis of the temperature dependence of the EPR signal intensity for Athabasca asphaltene. From Ref. 131.

In kerogens, spin densities have been found to correlate with depth of burial and geothermal gradient, and thus with the thermal stress history of the reservoir.[139] Similar correlations would be expected to apply for asphaltene and the spin density of asphaltene should also increase with increasing thermal stress experienced by the host oil.

A method auxillary to EPR spectroscopy is ENDOR spectroscopy. Here the EPR signals are saturated to a steady-state distribution and then the distribution is perturbed by a nuclear spin transition induced by a sweeping radio wave irradiation while saturation of the EPR transition is continued, and the intensity of its absorption is observed. Since the EPR spectrum of the asphaltene carbon radicals is readily saturated, Figure 14.113, it is easy to see why ENDOR spectroscopy can be easily adapted for use in the study of the carbon radicals in asphaltene over a wide temperature range. When the radio wave radiation frequency matches the frequency of the nuclear spin, a transition to a higher nuclear spin state takes place, causing a change in the population of the EPR levels that ultimately results in an increase in the EPR absorption. This increase occurs at two different radio frequencies, the separation of which depends on the strength of the hyperfine coupling.

Representative ENDOR spectra[131] of Athabasca asphaltene are shown in Figure 14.115. They are superior to EPR spectra in that they reveal more features. The interpretation of ENDOR spectra, however, is subject to considerable conjecture. Thus the appearance of the D and S bands in various samples has been attributed by several authors to different causes and these bands have been assigned at various times to:

- a contribution from a freely rotating radical and a more rigid radical in coal-derived oil;
- contributions from more than one kind of radical in solid coal;
- two different matrix ENDOR spectra arising from the interaction of the unpaired electron with two different nearest protons in a conventional crude oil; and

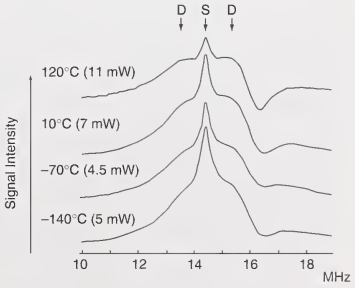

Figure 14.115 Temperature dependence of the ENDOR signal of Athabasca asphaltene. From Ref.131.

- the presence of doublet state (S) monoradicals and triplet state (D) diradicals in Athabasca asphaltene.

From these conflicting interpretations, it is evident that our understanding of the origin of these ENDOR spectra is less than satisfactory. Nonetheless, for reasons given below, we prefer the assignment of the spectra shown in Figure 14.115 to doublet state (S) monoradical and triplet state (D) diradical matrix effects.[136]

The central S band in Figure 14.115 occurs at the free proton frequency, 14.4 MHz, and the two D bands occur at 15.2 and 13.8 MHz. The concentration ratio of the two radicals, estimated from the ratio of their respective absorption band areas, changes reversibly with temperature, Table 14.29, higher temperatures favoring the triplet species. From the numerical agreement between the concentration ratios calculated from the EPR and ENDOR measurements, we conclude that the results obtained from the ENDOR studies validate the conclusions drawn earlier from the EPR studies by revealing separately the absorption bands of the doublet and triplet species. The singlet diradical species which provides the reservoir for the triplet diradical species does not have unpaired spins and therefore cannot be detected by EPR or ENDOR spectroscopic methods.

Table 14.29 Temperature dependence of the triplet/doublet free radical ratio in Athabasca asphaltene

Temperature (°C)	Triplet/doublet ratio	
	from ENDOR[a]	from EPR
120	1.00	–
~40	0.56	0.55
10	0.50	0.51
–70	0.31	0.34
–140	0.23	0.12

[a] Normalized values. From Ref. 131.

At this point we may raise the question, is the free radical distribution in asphaltene homogeneous or is there a trend relating distribution to some property of the asphaltene? A few studies addressing this question have been reported in the literature.

In a series of experiments involving six different asphaltenes, the asphaltenes were fractionated according to MW by GPC and the spin concentrations (along with other EPR parameters) were measured in each of the fractions.[140] As seen from Figure 14.116, in the MW range 1,000–~10,000 g·mol^{-1} there is a significant increase in the number of spins per g asphaltene for all the samples. Beyond a certain MW some of the samples show a levelling off while others a decline in spin concentration. This break in the spin concentration *vs* MW trend suggests that the few percent of the asphaltene having the highest MW has a molecular structure different from the rest (which may involve clay organics). Below 1,000 g·mol^{-1} the sample materials consist mainly of co-precipitated resins and therefore any trend which appears in the plots below 1,000 g·mol^{-1} should not be directly correlated with the asphaltene.

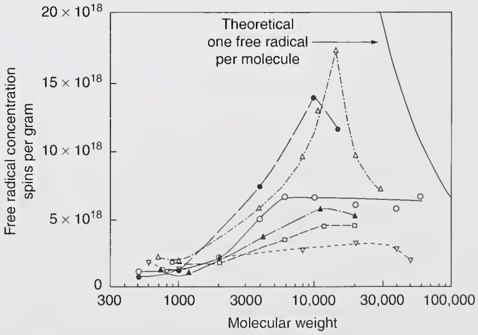

Figure 14.116 Free radical concentration as a function of MW of the GPC fractions of natural asphalt (O), and crude oil asphaltenes from Venezuela. (∇), California (Δ), Arabian I (▲), Arabian II (□) and Sumatra (●). From J. Q. Adams *et al.*, Ref. 140. © 1966, American Chemical Society.

In a similar study, Athabasca asphaltene was fractionated according to MW by GPC into five fractions, as described earlier, and the

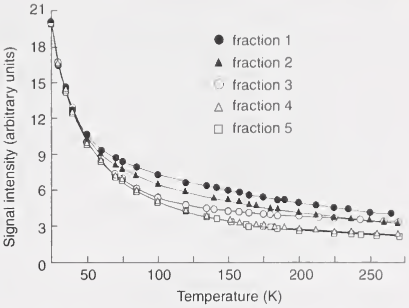

Figure 14.117 Signal intensity variation for the five asphaltene GPC fractions as a function of temperature. The solid lines through the data points represent best fits to the theoretical equation $I = \frac{A}{T} + \frac{B}{[\exp(\Delta_i / kT) + 3]} \cdot \frac{1}{T}$.

EPR signal intensity for each fraction was measured as a function of temperature[141] from 273 to 25K, Figure 14.117. The data derived are listed in Table 14.30. As was found in the above study, the spin concentrations increase with increasing MW of the fraction and, at the same time, the g-values decrease; significantly, the percent triplet content of the radicals also increases.

In an earlier study, Athabasca asphaltene was fractionated by GPC into 15 fractions, and spin densities and g-values were measured for each fraction.[137] However, neither the MWs nor the weight percents of the fractions were determined and correlation can only be established with the sequential number of the fractions, which is not sufficiently meaningful. In spite of this shortcoming, the data are still informative: the spin densities of the first seven fractions—representing a major part of the material—exhibited a monotonic decline with the sequential number of the eluted fractions (and presumably with decreasing MW); however, beyond fraction 7, the spin density of each subsequent fraction increased monotonically and in the last two fractions, 14 and 15, the spin densities (1.2×10^{18} and 1.5×10^{18}) exceeded the spin density in fraction 1, 1.0×10^{18} spins·g^{-1}. Similar measurements were made on the resin fraction of Athabasca bitumen. In this case the spin densities were one order of magnitude lower but their variation resembled that observed for the asphaltene, showing a monotonic decline from fractions 2 to 6 and a slow gradual rise from fractions 6 to 15.

Table 14.30 Free radicals in the GPC fractions of Athabasca asphaltene

MW	Wt% of asph.	g-value[a]	Radicals	Aggregates	%		No. of C_{arom} per aggregate
			g asph. × 10^{18}	spin	triplet	C_{arom}	
16,900	22.5	2.90	2.4	15	23	35	394
13,700	30.5	3.05	2.0	20	20	34	310
7,100	13.6	3.10	2.1	40	18	39	184
3,400	11.1	3.25	1.4	130	7	41	93
1,200	20.8	3.30	1.3	400	5	48	38

[a] $(g\text{–}2) \times 10^3$. Aggregates/spin in whole asphaltene ~ 60; MW by VPO.

Data on asphaltene, maltene, resins and ion exchanger fractions of Cold Lake asphaltene are tabulated in Table 14.31. The spin density varies in the order asphaltene > heavy resins > light resins > maltene. Some data on anion exchanger fractions of Athabasca asphaltene are also included in Table 14.31. It would appear that in the anion and cation exchanger fractions the highest spin densities occur in the medium acidic and medium basic subfractions.

In a more recent study,[142] Cerro Negro asphaltene was fractionated by sequential dialysis–solvent (acetone/tetrahydrofuran) extraction into eight basic and six composite fractions. For each fraction MW, spin density, aromaticity and other properties were measured, Table 14.32. As can be noted, one peculiar feature of the data is that the solvent extracts have higher MWs than the residues. And if extrapolation is meaningful, the MW of the final residue, R_7, should be much less than 3,260 g·mol^{-1} (that of R_3) since the MW of the combined extract $F_4 + F_5 +$

Table 14.31 EPR parameters for Cold Lake and Athabasca bitumen fractions[a,b]

Sample	$(g–2) \times 10^3$	$\Delta B pp^c$, mW	Spin density, $spins \cdot g^{-1} \times 10^{17}$
Cold Lake			
Asphaltene	3.3	0.54	9.2
Maltene	3.7	0.60	0.29
Resins I	3.5	0.67	0.12
Resins II	3.5	0.54	1.0
MALTENE:			
Anion exchanger:			
n-C_5	3.6	0.59	0.081
Benzene	3.3	0.57	0.98
Bz/MeOH	3.6	0.59	1.8
Bz/MeOH/CO_2	3.3	0.52	3.4
Cation exchanger:			
n-C_5	3.4	0.53	
Benzene	3.2	0.66	0.051
Bz/MeOH	3.6	0.58	2.9
Bz/MeOH/*i*-PrN	3.5	0.51	1.7
Athabasca			
ASPHALTENE:			
Anion exchanger:			
Benzene	3.5	0.57	5.0
Bz/MeOH	3.5	0.54	2.9
Bz/MeOH/CO_2	3.5	0.61	7.4
CH_2Cl_2/CO_2	3.4	0.59	2.4
AcOH/Bz	3.1	0.72	8.4
AcOH/THF	3.6	0.54	4.4
Whole asphaltene	3.4	0.59	6.0

[a] From K.F. Schultz and M.L. Selucky, Ref. 137. © 1981, Elsevier. [b] In air. [c] Peak-to-peak width.

Table 14.32 Properties of Cerro Negro asphaltene fractions (F_i) and residues (R_i) obtained by acetone–THF extraction[a,b]

Solvent fractions	F_1	F_2	F_3	F_4	F_5	F_6	F_7
%[c]	15	4.6	10.3	21.9	13.4	11.6	6.31
MW[d]	1800	4500	4600	5300	5700	5700	5500
f_a^f	0.47	0.46	e	0.53	0.57		0.57
$S_d \times 10^{18g}$							0.8

Residues	R_1	R_2	R_3	R_4	R_5	R_6	R_7
%[c]	85.0	80.0	69.8	47.9	34.8	23.2	13.0
MW[d]	2900	e	3260	e	e	e	e
f_a^f	0.51		0.50		0.56		0.57
$S_d \times 10^{18g}$	0.8		3.21		4.1		8.8

[a] From S. Acevedo *et al.*, Ref. 142. [b] Solvent sequence: % acetone 1:60, 2:50, 3:40, 4:30, 5:20, 6:10, 7:0. [c] Between 1.6 and 1.3 g asphaltene in the membrane. Average of three experiments. [d] GPC. [e] Owing to very low solubility in THF, MW could not be measured. [f] $f_a = C_{arom}/(C_{aliph} + C_{arom})$. [g] Number of spins per gram of sample. S_d(native Cerro Negro asphaltene) = 9.2×10^{18} $spins \cdot g^{-1}$.

$F_6 + F_7$ is about 5,600 g·mol^{-1}. Yet the final, insoluble residue, R_7, appears to have the highest spin density of all the fractions. (In GPC and ion exchanger separation all of the separated fractions are soluble.) This is contradictory to the results on asphaltenes discussed above (Figures 14.116 and 14.117, Table 14.30) where the spin densities were found to increase monotonically or peak around a MW of 10,000 g·mol^{-1}, but may be in agreement with the observations made on the narrower GPC cuts of Athabasca asphaltene. It was also observed that refluxing the Cerro Negro asphaltene with tetrahydrofuran significantly (~3.2-fold) reduced the spin density. This may be attributed to some reaction between tetrahydrofuran (or some impurity in it?) and the more reactive fraction of the free radicals. Another peculiarity of the results is that spins appear to be created in the course of the extraction process, since the sum of the spins in F_7 and R_7 exceeds that in R_1 by a factor of 1.76 (even though some spins are likely to be associated with fractions F_2–F_6 as well). Thus, spins should not necessarily be conserved; they could be created and destroyed in the course of solvent extraction. Indeed, it has been reported that treatment of chars with organic solvents can lead to an increase in spin concentrations.[143] The phenomenon was attributed to the introduction of diamagnetic solvent (tetralin, naphthalene) molecules between the aromatic sheets, causing separation of the strongly interacting free radicals in the char.

A complicating and generally overlooked factor in the interpretation of the distribution of spin density is the presence of mineral matter, mainly fine clay,[129,130] in the asphaltene. For example, crude n-C_5 Athabasca asphaltene from CH_2Cl_2-extracted bitumen contains 3.2% clay (*cf.* Fig. 14.104). The clay content can be reduced by high-speed ultracentrifugation but this is seldom done and the clay or ash contents of most of the asphaltenes studied have not been measured. It has also been shown that upon GPC fractionation the clay contents of the separated fractions vary and increase with increasing MW of the fraction. With Athabasca asphaltene, the highest MW (22.5%) fraction contains 8.8% clay, comprising 62% of the total clay in the whole asphaltene. The significance of the presence of clay is that, as will be discussed below, the mineral matter of Athabasca oil sand is also paramagnetic and exhibits EPR absorption closely resembling that of the asphaltene, with the same g value of 2.003. Moreover, from the EPR measured spin densities of the bitumen and the CH_2Cl_2-extracted sand[144,145] it is clear that in this case the spin density in the clean sand is twice as high as in the bitumen, Table 14.33. From these observations it would appear likely that the clay and other mineral components of the asphaltene are, to some extent, responsible for the observed EPR absorption, especially in the high-MW fractions, but resolution of this problem must await the results of more detailed experimental studies.

Some interesting data revealing variations of spin density in bitumen and extracted sand with the nature of the extracting solvent as well as with the origin of the whole oil sands are listed in Table 14.33. In bitumen, the apparent spin density varies within about a factor of two, $(1.7–3.7) \times 10^{17}$ spins·g^{-1}, depending on the nature of the extracting solvent. The only exception is the hot-water-separated bitumen in which the spin density is about 3–6 times lower, 0.6×10^{17} spins·g^{-1}. However, since the bitumen content of the oil sand used in this study was 10%, only 10% of the spin densities in the separated, neat bitumen— $\sim 2.5 \times 10^{17} \times 10/100 = 2.5 \times 10^{16}$ spins·g^{-1}—is due to spins in the bitumen component of the oil sand. This is about one-half of the spin density measured for the whole oil sand, 5×10^{16} spins·g^{-1}. The apparent contradiction regarding the difference in spin densities between solvent-extracted and hot-water-separated bitumen is then due to the fact that substances containing free spins, such as clays, fine minerals, humic matter, resins, *etc.* are partially removed in the hot water extraction process and form colloidal suspensions in water. During solvent extraction on the other hand,

Table 14.33 Number of spins·g^{-1} in solvent-extracted bitumen and sand[a,b]

Solvent	Bitumen	Sand
Carbon disulfide	3.7×10^{17}	2.2×10^{16}
Carbon tetrachloride	3.4×10^{17}	2.6×10^{16}
Toluene	1.8×10^{17}	2.5×10^{17}
Chloroform	2.1×10^{17}	5.12×10^{17}
Tetrahydrofuran	1.7×10^{17}	5.08×10^{17}
Dichloromethane	2.5×10^{17}	5.0×10^{17}
Hot water extracted	6×10^{16}	1.8×10^{16}
Whole oil sand	5×10^{16}	
Utah oil sand[c]	6.03×10^{17}	no EPR line

[a] Unless otherwise noted, data are from Athabasca oil sand. [b] From Ref. 144. [c] From Ref. 145.

the only components removed from the bitumen + sand (whole oil sand) are the dissolved and entrapped gases and volatiles, which have no free spins associated with them. Thus, as can be seen, the variance in the free spin contents of the extracted bitumens can be easily rationalized. This, however, is not the case with the variation of the spin densities in the extracted sand. Here, some of the solvents (H_2O, CS_2, CCl_4) act as would be expected, *i.e.*, yield extracted sand with spin densities such that the sum of the spin densities in the separated bitumen + sand is smaller or about equal to the spin density of the whole oil sand: for example, for CS_2 solvent $(3.7 \times 10^{17} \times 0.1) + (2.2 \times 10^{16} \times 0.9) = 5.7 \times 10^{16}$ spins·g^{-1}. The other solvents (toluene, $CHCl_3$, THF, CH_2Cl_2) yield "activated" sand with spin densities an order of magnitude greater than the spin density of the whole oil sand. In the sand component of the whole oil sand a fraction of the spin density arises from a contribution from the strongly-bound asphaltic and humic matter, and a fraction may come from paramagnetic metal ions, primarily Fe^{3+} (g = 2.003) and also Mn^{2+} (g = 1.99–2.0024), *etc.* The removal of the organic matter by some solvents then may cause changes in the crystal fields of these paramagnetic ions, resulting in their apparent higher spin densities. From this, it follows that the distribution of spin density in the sand is not uniform but should be much higher in the clays and fines than in the coarse sand. Alternatively, the same explanation may apply as in the case of char "activation" by solvent molecules (see above).

The average spin density of organic solvent-extracted bitumens is 2.5×10^{17} spins·g^{-1}. The asphaltene content in Athabasca bitumen is typically 16–17%. Consequently, if all the free spins in the bitumen belong to its asphaltene component then the spin density of the asphaltene should be about 1.5×10^{18} spins·g^{-1}, which is close to the average experimentally measured value for asphaltene. Consequently, the resin and polyaromatic fractions of the bitumen cannot contribute much to the spin density of the bitumen, as documented by the data in Table 14.31.

Returning to the EPR spectrum of Athabasca asphaltene, the sample asphaltene had been subjected to centrifugation until its initial 3.2% ash content was reduced to 0.9%; the EPR measurements were made on this sample. From the available data we can estimate the contribution of this ash to the total spins in the asphaltene. In the highest-MW fraction the ash content was 1.3%: in the case of CH_2Cl_2-extracted sand this would represent less than 10^{16} spins·g^{-1} in the asphaltene. The measured spin density was 2.4×10^{18} spins·g^{-1} and thus the contribution of the sand-bound spins to the total spin is not significant. If, however, the spins are concentrated in the intrinsically-bound residual clay organics in the asphaltene, then their contribution to the asphaltene spin density could be more significant.

Finally, in addition to the paramagnetic metal ions in the extracted sand, aromatic radical cations arising from electron transfer reactions between chemisorbed aromatic molecules and clay may also contribute to the spin density of the sand. Such a reaction was suggested to occur between styrene adsorbed on dry kaolinite and the Al^{3+} ion, resulting in the formation of a radical cation.[146] Reactions of this kind could also explain the increase in spin density observed under certain conditions in some of the solvent-extracted sand. Also, kaolinite clays associated with Tertiary brown coal formation are known[143] to exhibit organic free radical signals at g = 2.0025–2.0038.

Aside from Athabasca and P.R. Spring oil sands, the EPR spectroscopy of only one other extracted oil sand has been studied, a Utah oil sand. Here, the CH_2Cl_2-extracted sand was found to be EPR inactive.

EPR data for a number of asphaltenes and bitumens are listed in Table 14.34. From a study of P.R. Spring asphaltene it was concluded that both doublet monoradicals and, owing to exchange-coupled spins, ground singlet state and excited triplet state radical pairs are present. The origin of the isotropic exchange interaction was thought to be related to the presence of similar heteroatoms in alternate sheets of the aromatic stack. The percentage distribution of doublet–triplet state radicals was calculated to be 43 and 57 at room temperature, compared to

Table 14.34 EPR parameters of various bitumens and their fractions

Sample	T(K)	$(g–2)\times 10^3$	ΔBpp (mT)	Spins·g^{-1} $\times 10^{18}$	Reference
Bitumens:					
P.R. Spring	300	3.4	0.53		136
	81	3.4	0.60		136
Athabasca			0.06–0.37		137
Utah			0.6		145
Maltene:					
P.R. Spring	300	3.4	0.57		136
Asphaltenes:					
P.R. Spring	300	3.3	0.54	10	136
Athabasca	~296	3.4	0.59	1.2	138
	296	3.2	0.59	3.1	a
Peace River	~296	3.3	0.56	0.97	138
Cold Lake			0.92		
Wabasca	~296	3.3	0.56	1.6	138
Gilwood	~296	2.8	0.56	12	138
Boscan	~296	3.4	0.85	1.8	133,135
Cerro Negro			9.2		
Villafortuna		2.8	6.3	7.9	
Gaggiano		2.9	5.1	3.1	147
Brent		2.9	6.1	5.3	147
Arabian Light		3.1	6.4	2.9	147
Safaniya		3.2	5.9	2.7	147
Belayim		3.1	6.3	3.2	147
Gela		3.4	5.8	1.4	147
Baxterville	~296	3.0	0.57	4.39	133,135
Mara	~296	3.0	0.67	1.68	133,135
Ragusa	~296	2.7	0.54	2.12	133,135

[a] S. Niizuma, unpublished results.

the values 65 and 35 for Athabasca asphaltene. These values are averages across the entire MW spectrum of the asphaltene since the spin concentration and triplet-to-doublet radical distribution varies with the MW, Table 14.30, and they both tend to increase with increasing MW. It is important to emphasize that these properties also appear to correlate monotonically with the chemical properties of the asphaltene fractions, namely, the higher spin concentration and higher triplet concentration fractions feature higher propensity for polymerization and insoluble coke formation upon thermal treatment.[38]

5.4.3 The nature of the free radicals

The idea that all stable neutral carbon free radicals are polyaromatic π radicals has widespread currency in organic free radical chemistry. This class of free radicals can be divided into two main groups, one is represented by the triarylmethyl radicals and the other by the odd, alternant perinaphthyl-type radicals. Carbon free radicals without some stabilizing effects in their structure are highly reactive and under ordinary conditions have short lifetimes. Stabilization effects—either through kinetic, thermodynamic or both—can increase the lifetime of radicals. When the lifetime is increased above a millisecond the radical becomes **persistent** and persistent radicals sometimes are stable indefinitely. Kinetic stabilization implies a steric effect, crowding around the radical center, whereas thermodynamic stabilization implies mainly resonance effects, the delocalization of the unpaired electron over the entire π electron system of the molecules, which can be represented by mesomeric structures. Usually, both kinetic and thermodynamic effects are operative, along with some characteristic structural uniqueness.

a) *Triaryl radicals*

The prototype is the triphenylmethyl radical discovered by Gomberg in 1900, marking the beginning of free radical chemistry.

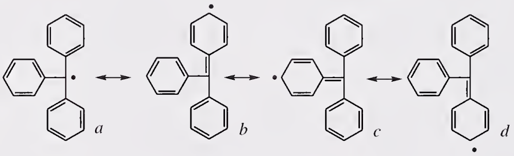

mesomeric structures of triphenylmethyl

In the stabilization of the triphenylmethyl radical, steric effects are considered to play a dominant, and delocalization, a minor, role. Delocalization is not efficient because, instead of being coplanar, the aromatic rings are disposed as in a three-bladed propeller. In solution, the radical is in equilibrium with the dimer formed from mesomers *a* plus *b*. Stable triaryl radicals are represented among others by the tri-(*p*-phenylphenyl) methyl and bisdiphenylene phenyl allyl radicals

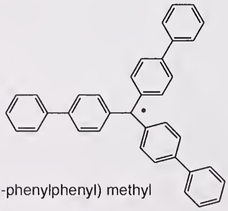

tri-(p-phenylphenyl) methyl

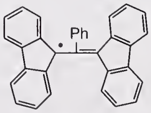

bisdiphenylene phenyl allyl

b) Perinaphthyl radicals

Hydrocarbons containing conjugated chains and cyclic conjugated molecules containing only rings with even numbers of carbon belong to a type of molecule called **alternant**. In an alternant system the atoms can be divided into two classes such that atoms of one class are bonded only to atoms of the other class:

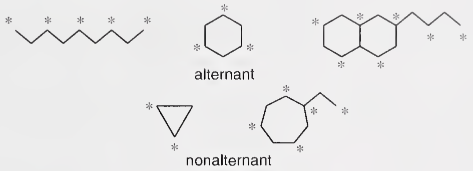
alternant
nonalternant

An alternant hydrocarbon is termed "even" if it has an even number of π orbitals and "odd" if it has an odd number of π orbitals. Odd alternant hydrocarbons have a nonbonding level about which the π orbitals, occurring in pairs, are symmetrically disposed. For odd molecules all bonding orbitals are doubly occupied and the nonbonding orbital is singly occupied. The simplest example of an odd alternant hydrocarbon π orbital manifold is that of the allyl radical, Figure 14.118.[148]

Perinaphthyl is the simplest example of an odd alternant aromatic π radical:

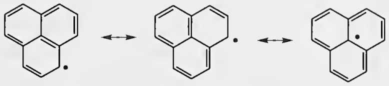

The perinaphthyl radical has remarkable stability in the absence of air and has been identified in a 150°C boiling petroleum distillate. Some alkylated and larger condensed derivatives

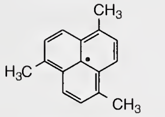

trimethyl perinaphthyl

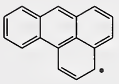

benzanthranyl

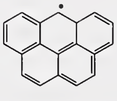

naphthanthranyl

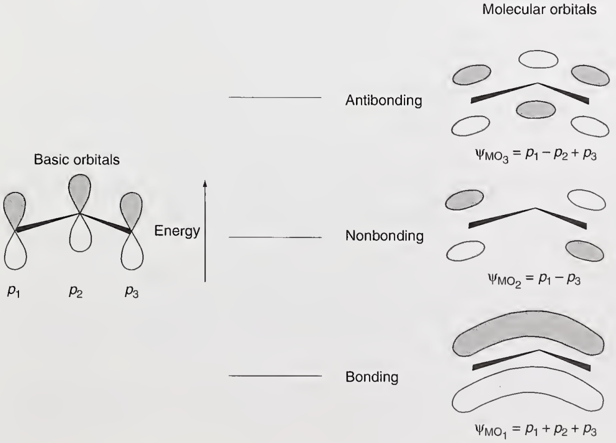
Molecular orbitals
Antibonding
$\Psi_{MO_3} = p_1 - p_2 + p_3$
Basic orbitals
Energy
Nonbonding
$\Psi_{MO_2} = p_1 - p_3$
p_1
p_2
p_3
Bonding
$\Psi_{MO_1} = p_1 + p_2 + p_3$

Figure 14.118 The π molecular orbitals of the allyl radical (right) constructed from the three basis *p* orbitals (left). From T.H. Lowry and K.S. Richardson, Ref. 148. © Harper & Row, 1987.

are even more thermally stable than perinaphthyl. The very high stability of these odd alternant hydrocarbon radicals is directly attributable to resonance stabilization through delocalization over the entire π orbital of the molecule, as indicated by their large number of mesomeric structures, and the inability of the radical site to convert to an aromatic double bond by the loss of a hydrogen atom. The odd alternant radicals have been proposed[127] to represent the most stable family of neutral hydrocarbon radicals.

It has also been suggested that the unpaired electrons in carbonaceous materials are associated with trivalent carbon atoms located either at the edges of aromatic rings or at internal ring sites. Extensive studies carried out on various chars, model compounds and coals led to the identification of perinaphthyl and related radicals in these systems and provided an experimental foundation for this proposal.[127]

c) Radical ions

In the case of petroleum asphaltene there is no direct spectroscopic evidence for the presence of perinaphthyl or any other specific class of neutral monoradicals, but on the other hand, there is no evidence dictating their exclusion either. However, strong evidence points to the presence of radical ions and radical ion pairs in petroleum asphaltenes. EPR data on solid and solution phase asphaltenes and electrical conductivity[149–152] and dielectric relaxation measurements[150,151,153,154] on asphaltene solutions concordantly led to the conclusion that radical ions formed in charge-transfer processes between aromatic sheets and their singlet and triplet state radical ion pairs represent princial groups of radicals present, in agreement with earlier EPR data. These radical ion pairs may be envisaged as being responsible for the positive departure from the Curie law of the signal intensity in the EPR spectrum of asphaltenes. The activation energy measured for the apparent increase in spins could then be assigned to the singlet→triplet transition in the radical ion pairs. (Triplet state doublet-doublet and even some higher spin state, like quintet state triplet–triplet neutral radical pairs, have been extensively studied and their EPR spectra recorded in low-temperature inert matrices.[155]) It should also be noted that the radical cations and radical anions of condensed aromatic (and other organic) molecules are quite stable entities and some of them can be kept indefinitely, under appropriate conditions.[97,156] In connection with the Athabasca sand-associated free radicals, the possible participation of radical cations formed via electron transfer from condensed aromatic donors to an aluminum ion in the clay (kaolinite) needs to be considered as well.[143,146]

In closing this section on the EPR and ENDOR studies on Alberta and other asphaltenes we may summarize the main conclusions as follows:

- vanadyl porphyrin and stable aromatic carbon free radical ions are present, but the existence of neutral free radicals of the odd, alternant, polycondensed aromatic π, perinaphthyl types cannot be dismissed either;
- in addition to doublet-state monoradicals, triplet state doublet-doublet radical ion pairs and, by inference, singlet state doublet-doublet radical ion pairs are present in probably all petroleum asphaltenes;
- the triplet state radical ion pairs are thought to represent the lowest excited state of the singlet state radical ion pairs formed in charge-transfer processes between (identical heteroatom-containing) alternate parallel sheets in the aromatic stacks of asphaltene aggregates containing isotropic exchange-coupled spins;
- the activation energy (~ 120–600 cm^{-1}, 300 cm^{-1} for Athabasca asphaltene) for triplet radical ion pair formation corresponds to the S_o–T_1 state energy separation;

- GPC separation according to MW shows that the radicals are not distributed uniformly across the bulk of the asphaltene, but both doublet and triplet radical concentrations increase with increasing MW, along with the triplet-to-doublet ratios;
- the trend in radical concentration variation often parallels the number of aromatic carbons in the molecule, indicating an expected correlation with the size of the aromatic sheets in the molecule;
- in Athabasca asphaltene the triplet radical ion pairs comprise about 35% of the paramagnetic radicals, and in the highest-MW fraction the radical concentration is about one radical per 15 aggregates;
- the radicals are indigenous to the structures of the asphaltene fractions;
- above room temperature the growth in radical concentration becomes more rapid with temperature, indicating the possible existence of a second singlet reservoir with a triplet–singlet energy separation of 1600 cm^{-1}. At 200°C the radical concentration increases to 10^{19} spins·g^{-1} asphaltene; this behaviour points to the high stability of the radical ion pairs and raises the possibility that the ion pairs are resistant against dissociation upon dilution of their solution; moreover, both ionic and neutral free radicals would be expected to act as nuclei for aggregation of the asphaltene molecules by permanent dipole-induced dipole and charge transfer interactions; these properties may impact the physical and chemical characteristics of asphaltene, for example MW dependence of fluorescence yield, propensity for aromatic condensation in thermal processes, *etc.*;
- the concentration distribution of free radicals, paralleling the reactivity variation of the GPC-fractionated Athabasca asphaltene, suggests a direct relationship with MW variation: the higher-MW fractions contain more radicals and are more reactive chemically, pointing to the potential role of stable free radical intermediates in the upgrading chemistry of bitumen;
- vanadyl porphyrin complexes and carbon radicals are also present in the resins fractions of crude oils and bitumens, including Athabasca bitumen; and
- the solvent-extracted sand from Athabasca oil sand is paramagnetic with a g-value of 2.003. The paramagnetism may be attributed to the presence of humic matters, bound resins, clay-adsorbed aromatic cations formed *via* electron transfer from condensed aromatic molecules to Al^{3+} ions in kaolinite, or paramagnetic metal ions, primarily Fe^{3+}, or any combination of the above.

5.5 Magnetic susceptibility

An important problem in the molecular structural study of asphaltene is the degree of aromatic condensation. Some insight into this problem can be obtained from measurements of the diamagnetic susceptibility. For highly-condensed aromatic molecules the diamagnetic susceptibility has large negative values. The diamagnetic susceptibility of some asphaltenes has been determined[112] by measuring the total magnetic susceptibility using the Faraday method which gives the sum of the diamagnetic and paramagnetic susceptibilities. The paramagnetic susceptibility was then measured by EPR and deducted from the total susceptibility value from the Faraday method. The measured values were then compared to the calculated values obtained by Pascal's rules and their differences, which should have had large negative values if highly-condensed aromatic structures had been present, ranged from -0.21 to $+1.47 \times 10^{-7}$ e.m.u/C.G.S. g^{-1}. These values, in agreement with the results obtained from solid state ^{13}C NMR studies, section 5.1, point to a relatively low degree of average aromatic condensation in asphaltene.

5.6 Conductivity and dielectric properties

Using ion exchanger chromatographic columns, asphaltenes can be separated into acidic (~40%), basic (~23%), amphoteric (~16%) and neutral fractions. In light of this and the reasons cited in sections 5.4.2 and 5.4.3 of this chapter, the presence of some ionic species in asphaltene can be expected. This has indeed been proved in studies on the electrical conductivity and dielectric properties of asphaltenes. Asphaltene solutions have been shown to behave as typical organic ions[149,151] in media of low-to-moderate dielectric constant. Thus, from electrical conductivity measurements on a C_5 native asphaltene, it was concluded that about 8–10% of the asphaltene contained ionizable materials and that the measurement of conductivity is a suitable method for the detection of asphaltene precipitation in crude oil.[151] The ionic components have been stated to be the least-soluble components of asphaltene and furthermore, it was also suggested that ion pairing and dipole–dipole interactions play a role in asphaltene aggregation and solubility phenomena.[149–154] This, however, cannot be the primary cause of aggregation since the concentration of ions is low and insufficient to cause extensive aggregation even if they act only as nucleation centers.

Conductivity and dielectric property measurements on a vacuum residue asphaltene gave indications that the charges within an asphaltene colloid exchange rapidly between asphaltene molecules, but there is virtually no exchange between colloids. In these studies it was also concluded that self-association of asphaltene is likely due to charge transfer between asphaltene molecules.[150,151,154]

Unfortunately, in neither of these studies were any precautions taken to remove the chemisorbed resins (which may contain carboxylic acids and strong bases) or clays from the asphaltene samples and this omission may obscure the picture somewhat. Nevertheless, the main conclusion—namely, that ionic species are present in asphaltene—is certainly correct and appears to lend credence to the existence of radical ion pairs, as postulated from EPR and ENDOR spectroscopic studies.

6.0 The covalent structure of the asphaltene molecule

The results obtained from chemical investigations on asphaltenes discussed in the preceding sections have brought to light a wealth of information regarding the structure of these molecules as well as the geochemical history of the parent oil. The homologous series and suites of compounds identified give valuable insight into their structural units and elements. These components are assumed to be bound together in the asphaltene molecule by one or two single bonds, from which they can be excised structurally intact.

All asphaltenes investigated to date, including those from severely biodegraded oils, were found to contain copious quantities of *n*-alkyl type structural elements. Thus, thermolysis of an asphaltene always yields *n*-alkanes and *n*-alkyl substituted benzo- and dibenzothiophenes, thiolanes, thianes, for example, and a host of other *n*-alkyl substituted species. The *n*-alkyl moieties may be associated with aromatic or naphthenic carbons, either as side chains or bridges. Also present are *n*-alkanoic ethers and esters as side chains, and possibly bridges. In line with the chemical results, the ^{13}C NMR spectrum of the asphaltene clearly reveals the presence of alkyl ($CH_2 > CH_3 > CH$) groups, but does not permit differentiation between alkanoic side chain, bridge, ether, ester or sulfide functionalities and it cannot be determined whether attachment of these groups is to aromatic or naphthenic carbon.These questions can only be determined to a significant extent by chemical methods of analysis—primarily by a combination of the thermal decomposition, RICO, NRA, NiB reduction, OH^- hydrolysis and BBr_3 C–O bond cleavage reactions. Further complicating the molecular architecture are the alkyl, ester, ether and cyclic hydrocarbon biomarker appendages on the aromatic and naphthenic core segments of the asphaltene molecule.

These structural features strongly influence the stacking ability of the aromatic sheets and the molecular shape-dependent kinetic and rheologic properties (Stokes' Law, frictional coefficients, diffusion, viscosity, scattering phenomena, *etc.*) as well as the solubility and chemical properties of the asphaltene. Consequently, a precise knowledge of these properties is a prerequisite to the understanding of asphaltene chemistry. In the following, each of these structural elements will be examined individually.

6.1 Structural elements from thermolysis

All the products, Tables 14.35 and 14.36, were formed in free radical reactions. In order to develop some idea about the mode of attachment of these molecules to the asphaltene and arrive at an estimate of their concentration in the asphaltene, the relevant features of the chemistry of the free radicals involved need to be reiterated. Thus, what we have to keep in mind is as follows:

Table 14.35 Homologous series of alkylaromatic compounds identified in Athabasca asphaltene[a]

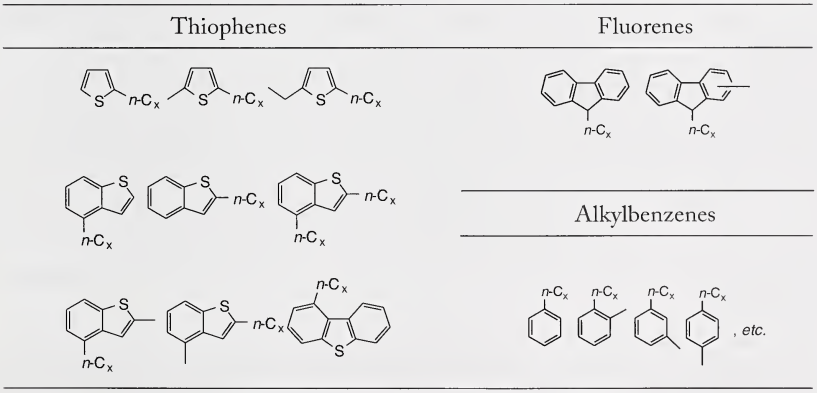

[a] C_{total} up to 29. n-C_x = n-alkyl.

Table 14.36 Homologous series of alkylnaphthenic compounds identified in Athabasca asphaltene[a]

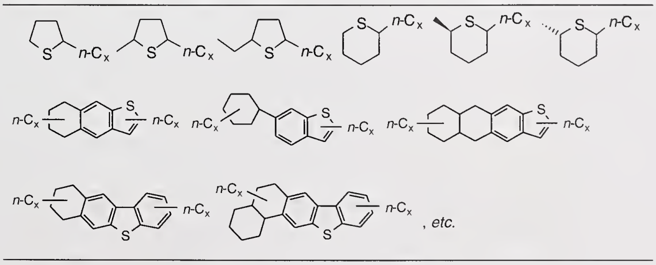

[a] C_{total} up to 29. n-C_x = n-alkyl.

- long alkyl chains, free or attached, are not created in low-severity thermolysis; the presence of these compounds in the thermolysis products is proof of their preexistence in the substrate;
- the most probable thermal reaction of long-chain alkylaromatics is the cleavage of the weak benzylic C–C bond in the side chain (reaction 15a);
- long-chain *n*-alkylcycloalkanes preferentially lose their side chain by cleavage at the attachment site (reaction 15b);
- the formation of long *n*-alkyl- chain-containing cyclic products is proof of their preexistence in the substrate;
- in all these reactions the primary products are free radicals, the reasonably well-known reactions (16–21) of which lead to the formation of the final products;
- all the product molecules must have preexisted in the asphaltene as structural units attached to the molecular core by one or, at the most, two, covalent bonds. The alkyl side chains are preeminent candidates for the sites of attachment. Indeed, experimental validation of this statement has been presented in section 4.4.4 of this chapter. Since all the principal products are produced with the intermediacy of free radicals, they are accompanied by the production of their alkene counterparts in about 65–100% or, on the average, about 85% yield, based on the yield of the measured alkane products.

6.1.1 *n*-Alkanes

In the thermolyis of each of the several dozens of different asphaltenes reported in the literature, series of C_1 up to C_{50} *n*-alkanes (and, depending on the experimental conditions, 1-alkenes) were found to be principal products, in yields of up to 30% or higher, even when the maltene fraction of the bitumen was devoid of *n*-alkanes. The appearance of the *n*-alkanoic and α,ω-di-*n*-alkanoic acid series in the RICO reaction products is proof for the presence of portions of *n*-alkanoic structural elements as side chains and bridges on aromatic rings. Thus, the RICO method is an invaluable tool for the quantitative determination of these structural elements and it also shows that *n*-alkyl and *n*-alkanoic ester side chains are significant structural elements of the naphthenic portion of the asphaltene as well, along with bridges between naphthenic and aromatic carbons.

Returning to the *n*-alkane products, their yield from Athabasca *n*-C_5-asphaltene was about 6.1% (not including the *n*-1-alkenes), Table 14.16. Correcting for the alkene product (about 85% of *n*-alkanes) the true yield would increase to 11.2% in terms of the asphaltene. The total amount of alkyl carbon, from ^{13}C NMR and RICO determinations, was about 27% of the carbon in the asphaltene and the carbon in the 11.2% *n*-alkanes represents 12% of the carbon in the asphaltene. In the GC determination of the *n*-alkane yield, Figure 14.29, most of the low-MW material below about C_{15} was lost, Table 14.15. This material represents short-chain alkanoic structural elements in the asphaltene, as is evident from RICO measurements, Figures 14.66 and 14.78, as well as short-chain alkane fragments from the typical alkyl degradation reactions 18 and 19. Therefore, the true total alkane yield must be significantly higher than 12%.

We can conclude that the bulk of the *n*-alkanes (and *n*-alkenes) arises from the cleavage of the alkyl side chains and bridges on the aromatic and naphthenic rings and there is a smaller contribution from the decompositions of alkanoic acids and (as we know from the OH^- and BBr_3 cleavage reactions) ester and ether side chains (and probably bridges).

6.1.2 Alkylbenzenes

Homologous series of C_{12}–C_{28} *n*-alkyl- and methyl-*n*-alkylbenzenes were formed in a combined yield of 0.3%, Table 14.16. These molecules must have been attached to the asphaltene through their alkyl moieties since bonds directly attached to the benzene ring would not cleave readily under the mild thermolysis conditions. Hence, the attachment of the alkylbenzenes was most likely by a single bond and the methyl alkylbenzenes could have been attached either by one or two bonds. This is a general principle which applies to all alkylated ring compounds: in the case of a single alkyl group, the attachment is by one bond while in the case of two or more alkyl goups, attachment could be by one or two bonds. In either case the appearance of C_{12}–C_{28} alkylbenzene products shows that dealkylation of the asphaltene to produce alkanes is incomplete, which explains the relatively low yield of alkanes, ≤ 50%. Losses due to the formation of alkenes, volatility of low-MW products formed from primary radicals, and radical fragmentations, would suggest that the measured yields of the alkylbenzene products represent not more than 30–40% of the alkylbenzene structural units present in the asphaltene molecule. Thus, we conclude that alkylbenzenes are authentic structural elements in the asphaltene molecule in a concentration of about 0.8–1.0%.

6.1.3 Thiophenes

C_{10}–C_{29} homologous series of alkyl- and dialkylthiophenes, along with some related unidentified molecules, were produced in a yield of about 3.1%. Here, as in the case of the rest of the principal products, the same logic that was applied in the alkylbenzene case tells us that the measured products—which, in this case, are highly reactive and vulnerable to destruction by free radical attack—could not represent more than about 30% of the alkylthiophene structural units in the asphaltene molecule. Thus, a conservative estimate of the concentration of alkylthiophenes in the asphaltene molecule would be about 8%. (It should be pointed out that a fraction of the thiophenes could have come from the corresponding alkylthiolanes (Figure 14.36) which, in thermolysis, have been shown to produce thiophenes.[81])

6.1.4 Sulfides

Alkyl- and dialkylthiolanes and thianes produced in C_{10}–C_{29} homologous series in a measured yield of about 0.7% are also highly vulnerable to free radical attacks. Their concentration in the asphaltene molecule as structural units may be estimated to be not less than 2%.

6.1.5 Condensed thiophenes

This compound class represents the most abundant product, 4.8%, in the pyrolysis of asphaltene. Benzothiophenes and dibenzothiophenes are the most stable types of organosulfur compounds and they are ubiquitous in sulfur-containing petroleums. In the maltene fractions of Alberta bitumens dibenzothiophenes are more abundant, while in the asphaltene pyrolysis oil, benzothiophenes predominate. Like the previously-mentioned products, the members of this class are also all alkylated and they comprise benzo-, dibenzo-, monocyclohexanobenzo-, and dicyclohexanodibenzothiophenes in the C_{10}–C_{26} range. Other higher condensed derivatives are undoubtedly also present. The measured product yields in this case are estimated to be about 40% of the concentration of these structural units in the asphaltene, which therefore should be around 12%.

6.1.6 Condensed aromatics

This compound class comprises alkylated di- through pentacondensed aromatics, biphenyls, indenes, their cycloalkyl derivatives, *etc.* in the range C_{10}–C_{30} in a measured yield of 2.4%. On the basis of the foregoing considerations this would represent an approximately 6% contribution by these structural units to the mass of the asphaltene.

6.1.7 Additional compounds

These include di- through pentacyclic monoaromatics, *cf.* Figures 11.2, 11.3, 11.5, and 11.6, tetracyclic triaromatics, Figure 11.14, and the series of alkylnaphthalenes, -tetralins, -octahydrophenanthrenes, fluorenes, tetrahydrophenanthrenes, *etc.* and their isomeric series shown in Figure 14.43, alkylpyridines and quinolines, *n*-alcohols, C_8–C_{22} alkanoic acids, fluorenols, like in Figure 12.64, *etc.*, along with a gamut of low-concentration level biomarkers, in a combined yield of at least 3%, corresponding to concentrations in the asphaltene of at least 6%.

6.1.8 Combined yield

Essentially all the principal structural units identified, Table 14.16, had a carbon skeleton that could have originated from straight-chain carbon percursors and/or were slightly alkylated, mainly by *n*-alkyl groups. The combined yield of structural units identified, on the basis of the above studies on Athabasca asphaltene, may be estimated to comprise about 48% of the asphaltene; of this amount, about one-half, or 24% of the asphaltene is estimated to have cyclic and the rest, acyclic structures.

6.1.9 Pattern of substitution in alkylated cyclic compounds

The positions of the alkyl substituents on the aromatic ring systems have been identified for a number of small ring homologous series, Table 14.35, and for the cyclic sulfide series shown in Table 14.36. For the entire group, an unexpected common pattern of substitution by the *n*-alkyl groups has emerged, namely, that by appropriate ring opening the entire molecule can be stretched out into a straight-chain carbon skeleton, as highlighted below:

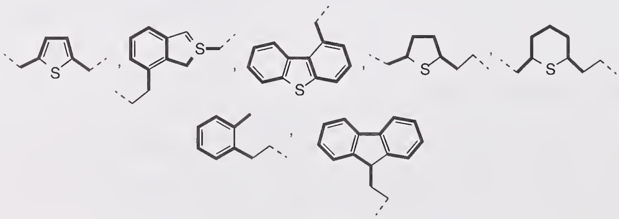

Scheme 14.1

This is a common, underlying architectural principle of these groups of molecules produced in the thermolysis of asphaltene. It clearly and unequivocally establishes that **they originated from *normal* alkanoic type biotic source materials**. In the present context however, the relevant feature of all the above aromatic structures is that upon RICO, they would all be destroyed without yielding any benzenepolycarboxylic acids.

6.2 Reductive degradation

NRA and NiB reduction both cause large decreases in MW and sulfur content. The lowering of MW is more extensive in the NRA reaction because this reagent, in addition to breaking the C–S bonds in sulfides, also cleaves all the intermolecular bonds along with the C–O bonds of esters. The NRA reaction follows an ionic path, reactions 24–28, and the asphaltene radical anion intermediates produced do not undergo aromatic stacking because of the strong Coulombic repulsion. They ultimately stabilize themselves by forming hydraromatics, *e.g.*

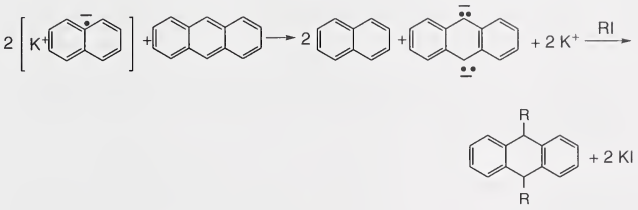

(79)

NiB cleaves the C–S bonds in sulfides only.

Details of the two reaction systems are as follows:

Experimental observations:
- NiB reduction: $-S_{5.17}\cdot mol^{-1}$; (VPO) MW 4,800 → 1,200 $g\cdot mol^{-1}$
- NRA reduction: $-S_{11.9}\cdot mol^{-1}$; (VPO) MW 9,884 → 534$g\cdot mol^{-1}$

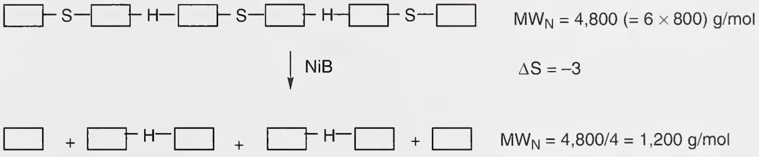

(80)

where "H" represents **all** intermolecular bonds the dominant variety of which is the aromatic stacking. The difference $S_{5.17} - S_3 = S_{2.17}$ is in cyclic sulfides, thiophenes and in low-MW sulfide appendages.

In the case of the higher MW asphaltene, NRA treatment removed about 11.9 S atoms from the molecule of which 6 or 7 were in bridging positions,

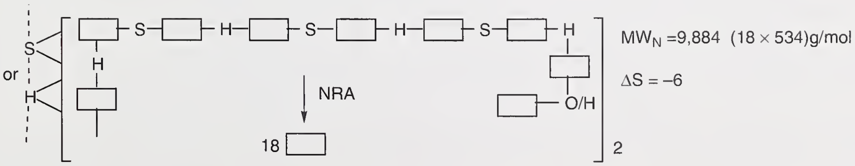

(81)

and the rest in cyclic sulfides, thiophenes and in maltene molecules bridging to the asphaltene. In the reaction, O/H represents an ester oxygen or any one of the intermolecular bonds designated by H. The NRA reaction cleaves the ester bond and therefore reaction (81) is the same with an ester O or with H. In order to create the 18 particles required to reduce the MW_N to the measured value of 534 $g\cdot mol^{-1}$, 17 bonds had to be broken. Of these bonds, a few could be ester bonds but the number of oxygen atoms, according to elemental analysis, is only 8.1, of which a considerable portion is present in the form of side chain ester and ether appendages, fluorenones, fluorenols and other oxygen functionalities; consequently, the number of ester bridges in the molecule cannot be much more than one or two. In this experiment the MW of the sample used was twice the MW of the sample used in the NiB reaction and therefore in the former sample the asphaltene supramolecules may be viewed as the dimer of the latter. Now, depending on the nature of bond joining the two monomers in the dimer, whether it is an intermolecular bond or a sulfide bond, the number of sulfur atoms bridging core segments together can be $2 \times 3 = 6$ or $2 \times 3 + 1 = 7$ leaving $11.9 - 6 = 5.9$ or $11.9 - 7 = 4.9$ S atoms associated with cyclic sulfides, thiophenes and low-MW sulfide appendages. In the monomeric asphaltene supramolecule there were 2.17 S associated with such environments for each 3 S in core bridging position. Therefore, in the dimeric supramolecule the expected number would be $2.17 \times (6/3) = 4.34$ or $2.17 \times (7/3) = 5.06$ depending on whether the two monomers are bridged together by an intermolecular bond or a sulfide linkage. The much better self consistency of the data, 4.34 versus 5.9 or 5.06 versus 4.9 for the sulfide bridged structure lends credence to the validity of the sulfide bridged structure.

So, in this way it was possible to establish the number of sulfide bridges in the asphaltene supramolecule from the NiB reduction reaction (75) and the MW_N of the covalent asphaltene core segments from the NRA reaction (81). Therefore, the NiB reaction of the monomeric supramolecule reaction (80) can be rewritten as reaction (82).

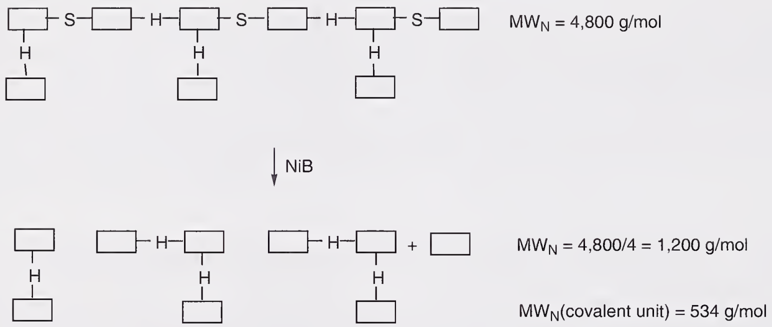

(82)

Thus, without increasing the number of intermolecular bonds the core MW_N was 800 $g{\cdot}mol^{-1}$ and with the increase it fell to 534 $g{\cdot}mol^{-1}$, without affecting the MW of the desulfurization products. What will, however, be affected is the MW_N of the fully dissociated molecule (upon infinite dilution), which will have values of 1,600 and 800, respectively:

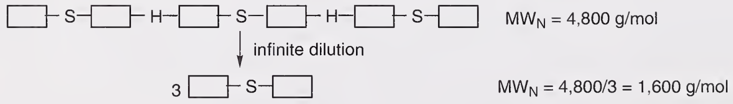

(83)

and

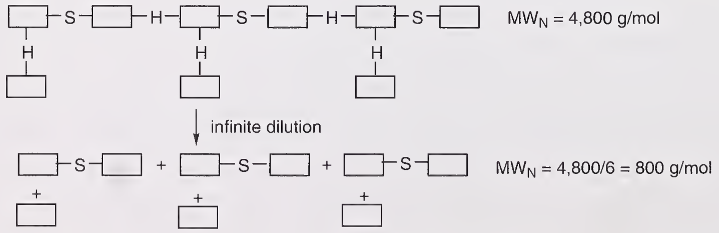

(84)

and with one ester bond,

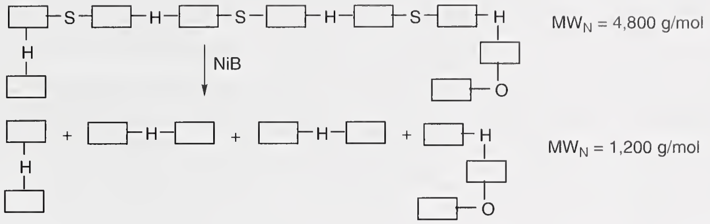

(85)

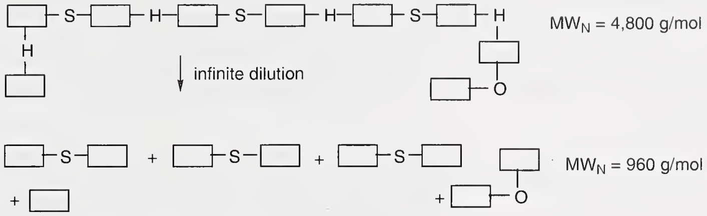

(86)

The experimental values of MW_N(covalent unit), 534 g·mol^{-1}, from the NRA reaction where all the sulfur bridges, ester bridges and intermolecular bonds were broken, and MW_N = 1,200 g·mol^{-1} from the NiB reaction where only the the sulfur bridges were broken, agree with reaction schemes 81, 82, 85, 86; however, the MW_N upon infinite dilution, as will be shown in Section 6.7, best agrees with reaction schemes 81, 85, 86. Thus, to summarize the interpretation of results, it appears that the Athabasca sample studied contained sulfide sulfur- and ester-bridged covalent molecules and intermolecular forces-bound molecules. The approximate amount of material present in sulfur-bridged molecules, as can be seen from the results, represents about two-thirds by weight (number average) of the asphaltene (not taking into consideraton the sulfide bridges between an asphaltene core and a maltene molecule) and the oxygen-bridged material in ester linkages, about 22% of the asphaltene.

Detailed NRA and NiB reduction studies have been carried out only on Athabasca asphaltene, however, there can be little doubt that sulfur containing asphaltenes, that most asphaltenes are, all feature sulfide bridged structure in proportion with their sulfur content. A crude estimate of the importance of such structures may be that low sulfur asphaltenes with sulfur content ≤3% would contain up to 22%, medium sulfur asphaltenes with sulfur content in the range 3–6% up to 44% and asphaltenes above 6% sulfur up to 67% sulfur bridged structures.

Now, the low value of MW_N for the covalent core segments, 534 g·mol^{-1}, imposes limits on the average size of the nuclear condensed aromatic sheets in the molecule. Thus, the number of aromatic carbon atoms,

$$C_{ar} = (534 \times \%C/100 \times f_a)/12 = 534 \times 0.80 \times 0.42/12 = 15$$

present in the core segments corresponds to up to four rings, *e.g.*

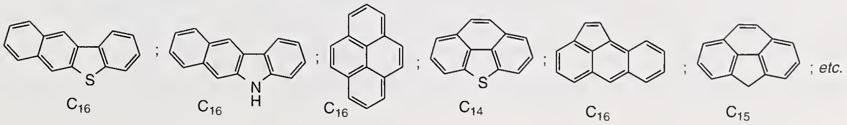

The NRA reduction of Athabasca asphaltene provided the first experimental evidence for the low degree of nuclear aromatic condensation in asphaltene which, at that time, was contrary to contemporary consensus, and it is corroborated by the identification of the host of one- through four- and some five- and six-ring condensed aromatic structures among the products.

It has to be stressed that all data are number averages and considerable dispersity could occur in the distribution, as indicated by the abundance of the 1–4-ring nuclear condensed aromatics in the thermolysis products. For example, a ten percent presence of molecules with MW 3,000 $g{\cdot}mol^{-1}$ would cause an increase in the MW_N of the NRA products from 534 to only 582 $g{\cdot}mol^{-1}$.

The differentiation in the sulfide species is reflected in the difference between the sulfide sulfur removed, 5.17 S and that used in the MW reduction, 3 S (NiB) and about 11.9 and 7.0 (NRA). The difference, 2.17 S (NiB) and 4.9 (NRA) is then due to the ~5% low-MW products, Tables 14.17 and Figure 14.55, and the rest to the desulfurization of the thiophenes and cyclic sulfides:

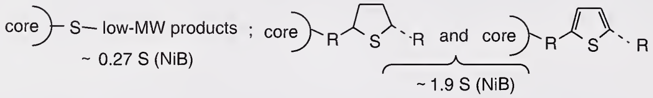

with distribution as indicated. The 1.9 S in the molecule with MW_N 240 (C_{15}) would correspond to a combined sulfide + thiophene content of about 9.5 wt% in the asphaltene, in good agreement with the 10% value estimated from thermolysis, Table 14.16.

The extent of desulfurization is 42% in HMA and 38% in LMA (NiB), well within the range 0–50% reported for various asphaltenes by XANES analysis.[103–105]

6.3 Oxidative degradation

From the previous section we know that the covalent asphaltene molecules are not built of a single aromatic sheet but a considerable fraction of them contain flexible aliphatic sulfide and ester C–O–C linkages. In addition to such bridges alkyl bridges are also present.

The RICO method provides a powerful tool for the investigation of several aspects of the structure of asphaltene, reactions 47–50, 52 and 55–65. In addition to providing a precise method for the determination of the distribution of alkyl side chains attached to aromatic moieties in the molecule, it is the only method capable of yielding reliable information on the distribution of alkyl bridges connecting aromatic carbons, and aromatic to naphthenic carbons. This latter feature is vitally important with regard to the elucidation of the architecture of the asphaltene molecule. More specifically, RICO is the method of analysis that can explore the structure of the asphaltene core segments and answer the question of whether they comprise a single aromatic–naphthenic unit with some alkyl side arms, or whether there are several aromatic moieties connected by various bridges in them. The physical and chemical properties associated with the two molecular architectures are quite different, and this impacts the behavior of the molecule in a major way. As is amply evident from the above, alkyl bridges are present in Athabasca (Table 14.19) and in every other asphaltene investigated by the RICO method. In addition to the two types of alkyl bridges and sulfide and ester bridges mentioned before, alkyl bridges may also exist between naphthenic carbons, and ester and ether bridges, between any type of carbon atoms. Indeed, the alkylated cyclic products from the thermolysis of Athabasca asphaltene listed in Table 14.35 were originally attached to the asphaltene *via* the side chain bridges:

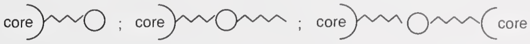

where O represents a cyclic moiety or either $-CH_2-$, $-O-$, $-O-C(O)-$ or $-S-$ linkages. The mono- to tetranuclear cyclic components of the thermolysis products are estimated to comprise 24 wt% of the asphaltene and the alkyl components, about 24 wt%. The remainder is then mainly composed of higher-condensed cyclic structural units. Some indication about the mode and extent of their condensation can be obtained from the benzene polycarboxylic acid (BPA) products from their RICO reaction. Since the yields of BPA depend on the experimental conditions and, more importantly, aliphatic substitution accelerates their oxidation and the aromatics being highly substituted, the yield of benzene polycarboxylic acids is low and depends more on the pattern of aliphatic substitution than on the mode of condensation. As a consequence, these products carry only qualitative information. Nonetheless, the limited information they provide is still useful since they permit a glimpse into the mode of aromatic condensation in the asphaltene molecule: they indicate the presence of the following structural elements:

Product (R = CO_2H)	Precursor
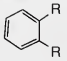	terminal benzene rings (unsubstituted and mono- and di-C_1 and C_2 substituted)
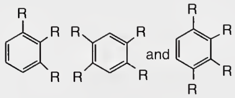	kata-condensed rings
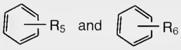	pericondensed rings
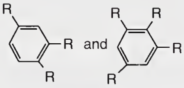	biaryl linkages with a single linkage per ring;

(the biaryl linkages permit rotation about the aryl–aryl bond and thus could be viewed as the simplest bridge connecting aromatic to aromatic units.)

How the reaction paths and yields are affected by the number and positions of the aliphatic substituents is illustrated by the following examples:

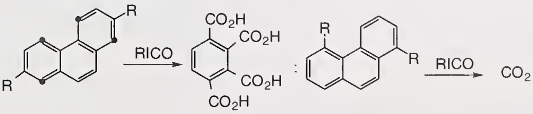

(87)

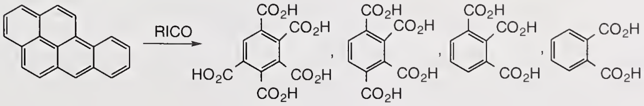

(88)

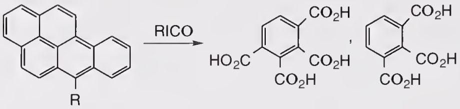

(89)

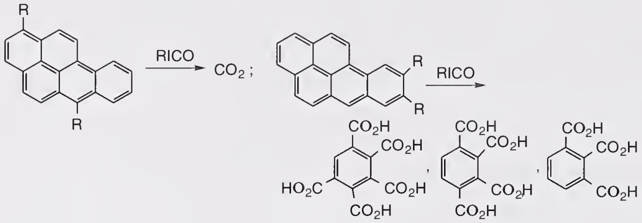

(90)

Since the average number of substituents on an aromatic ring system is more than two, the product distribution cannot be unambiguously related to the structure of the aromatic substrate.

Observed characteristics of the benzene PBA distributions from all asphaltenes studied are:

- absence of monoacids;
- presence of 1,2-diacids;
- absence of 1,3 -and 1,4-diacids :
- presence of 1,2,3-, 1,2,4-, 1,2,3,4-, 1,2,4,5- and 1,2,3,5-(tri- and tetraacids);
- absence of 1,3,5-triacids;
- presence of penta- and hexaacids.

This distribution indicates the presence of biaryl linkages, with the limitation of one biaryl linkage on a given ring and is consistent with the identified aromatic structural units in the thermolysis products; however, examples of identified structural units for the penta- and hexaacids are missing. The only indication for the possible existence of pericondensed aromatic structures in the asphaltene molecule comes from the appearance of these acids in the RICO products. Nevertheless, this does not constitute proof in itself because, as the example of the tetranuclear aromatic triphenylene and phenylphenanthrene molecules show,

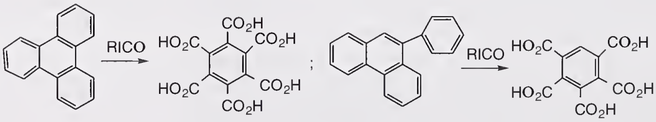

(91)

the existence of large, fully pericondensed aromatic structures is not an *a priori* requirement for penta- and hexaacid production.

6.3.1 Bridges between ring structures

The manifestation of the existence of bridges between ring structures is an important and unique piece of structural information learned from RICO. In order to validate this conclusion it is necessary to ascertain the potential role of other conceivable sources of the evidence—the α,ω-di-*n*-alkanoic acid series in the reaction products. Among the alternative sources to consider, the following come to mind:

i) 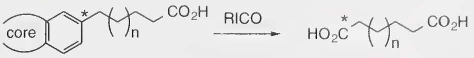 (92a)

ii) 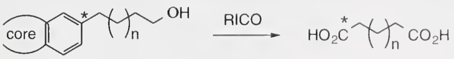 (92b)

iii) 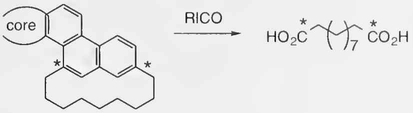 (92c)

i) and ii) can be discounted because of the unit value of the odd/even carbon preference in the diacids, as opposed to the high even preference observed in the acid and alcohol components of side-chain esters and ethers, and also because of the relatively low acid number of the asphaltene compared to the number of moles of diacids produced and the low yields of *n*-alkanoic acids and alcohols in the thermolysis of asphaltene, and their high even-to-odd preference. Moreover, bridges between aromatic and naphthenic rings on thermolysis after RICO and methylation (reactions 71 and 69) produces *n*-alkanoic acids in yields comparable to those of the diacids, again with a unit value of even-to-odd preference;

iii) large aromatic-condensed aliphatic ring structures have not been found in petroleum. They are relatively rare in nature; their stability would depend on the chain length and mode of attachment to the aromatic rings and should not exhibit a smooth concentration distribution, in contrast to experimental findings.

Thus, it can be concluded that indeed, the unbranched polymethylene moieties are regular structural elements in asphaltene. The length of the diacids extends up to at least C_{27} in Athabasca, and to 36 in immature asphaltenes and their total concentration lies in the reported range 0.45–1.0 per 100 C in the asphaltene. The concentration may exhibit a maximum around C_4–C_6, after which it declines monotonically.

6.3.2 Additional products identified in RICO experiments

The same biomarker molecules as those identified in the NiB reduction were also found here except that, instead of being in hydrocarbon forms, they were present in oxidized forms as their carboxylic acid derivatives. This indicates that, unlike the hydrocarbons from the NiB reaction which were attached to the asphaltene molecule as sulfide appendages, these biomarkers were attached to the aromatic moieties by C_{arom}–C_{aliph} linkages and became converted to the acid in the RICO process, as shown by the example of hopanoic acid:

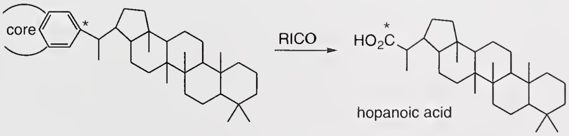 (93)

6.4 HO^- and BBr_3 cleavage of the C–O bonds

Detailed C–O bond cleavage studies have revealed additional significant details about the covalent structure of the asphaltene molecule, showing the presence of *n*-alkanoic ester and ether side chains and various other more complex C–O–C-bound unidentified appendages.

Basic hydrolysis of the esters in the asphaltene produced series of *n*-alkanoic acids and *n*-alcohols which were bound by ester linkages to their asphaltene-anchored counterparts. Both the acids and the alcohols showed strong even-to-odd preference, and RICO studies proved that at least a portion of the ester side chains were associated with the naphthenic moieties in the asphaltene.

The BBr_3 reaction showed the existence of *n*-alkanoic ether side chains, also with a strong even-to-odd preference, and extending to higher carbon numbers than the alcohols in esters. Here, some hopanol ethers were also detected.

Both the esters and ethers could form bridges between cyclic moieties but this would be difficult to detect directly. Indirect evidence from FTIR, NRA and NiB reductions appear to point to the existence of ester bridges.

6.5 The nature of the remainder of the asphaltene core

The total concentration of the structural units in Athabasca asphaltene that have been accounted for on the basis of the thermolysis products, Table 14.16, amounted to 48%. Another few percent can be attributed to missing *n*-alkyls on the basis of the deficit between the *n*-alkyl content of 27% calculated from ^{13}C NMR and RICO results and the 24% estimate from the thermolysis products. This brings the unaccounted fraction of Athabasca asphaltene to about 50 wt%. Regrettably, not much is known about the structure of this material or how the identified structural units are attached to this core material. In this latter respect, however, some insight has been obtained from a study conducted on the immature Jinghan asphaltenes.[102] Two different samples were subjected to deuterated NiB reduction and the reduced asphaltenes were examined by ^2H NMR spectroscopy in order to determine the distribution of deuterium atoms taken up in the course of the reduction. As seen in the spectra shown in Figure 14.93,[102] in both samples the dominant position for the incorporated deuterium atoms was the methylene, followed to a much smaller extent by the methyl and methine positions; in one of the samples there was a very small contribution from vinyl and toluene methyl positions. These findings prove that the sulfide sulfur attached to the asphaltene is mainly attached to midchain or naphthenic carbons:

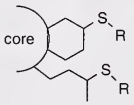

In the same experiment it was also shown that in the Jinghan I sample the sulfur-attached (10%) *n*-alkyls, *n*-alkylthiolanes, thiophenes and thianes are attached at the terminal position of the *n*-alkyl side chain, as indicated by the well-developed methyl resonances (0.8 ppm) in the *n*-alkane products, Figure 14.93.[102] The other resonances (methylene, methine, toluene methyl) are due to the deuterodesulfurization-produced various molecules from the sulfides and thiophenes,

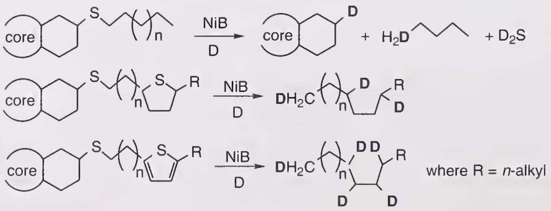

(94a)

(94b)

(94c)

Thus, we can conclude that in the case of Jinghan asphaltene the sulfide sulfur atom attached to the asphaltene core is attached predominanly *via* the agency of a naphthenic or a mid-chain methylene carbon and the alkyl groups, alkylthianes, thiolanes and thiophenes are attached to the sulfur atom at the terminal position of the alkyl chain. These results are also revealing with regard to the bonding of the sulfur bridges connecting core segments in the asphaltene molecule. Evidently, in both Jinghan asphaltenes the sulfide bridge sulfur is attached to aliphatic carbons, as mentioned above, and primarily to naphthenic and mid-chain methylene groups,

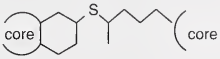

endowing the molecule with considerable flexibility and internal rotational, vibrational, *etc.*, degrees of freedom. Hence, it appears that aromatic-attached sulfur is present entirely as thiophenic sulfur and the rest, as cyclic and acyclic aliphatic sulfides.

The results obtained are probably applicable to most petroleum asphaltenes and would adequately describe the sulfur bridges in them. In combination with the RICO observation that the alkyl side chains and bridges are predominantly attached at their terminal position, it appears to be reasonable to assume that cycloalkyls would also be attached at the terminal positions of their alkyl chains.

As has been pointed out before, each of the principal series of compounds identified in the thermolysis products of Athabasca asphaltene can be subjected to bond cleavages in such a manner that the rings would stretch out into a straight-chain carbon skeleton. This common underlying architectural principle applies to a minimum of 48% of Athabasca asphaltene, Table 14.35, showing that at least this fraction must have originated from *n*-alkanoic source materials.

These discoveries, made in the late 1980s,[80,81,94] were quite unexpected inasmuch as Athabasca and Alberta oil sand bitumens in general, being biodegraded oils, are practically devoid of *n*-alkanes. Yet, as it turned out, their asphaltene and high-MW fractions are not only rich in *n*-alkyl moieties, but their ring skeletons, naphthenic and aromatic alike, are at least partly *n*-alkane derived! As has been shown by compositional and chemolysis studies, the asphaltenes of the Alberta oil sand bitumens, carbonate bitumen and heavy oils are chemically quite similar and consequently the conclusion drawn above for the origin of Athabasca oil sand asphaltene applies to all Alberta asphaltenes. Moreover, all asphaltenes studied by these methods (Boscan, Duri, Prudhoe Bay, Saline Lake, Jinghan, Gudao, Arabian) were found to be quite similar to Alberta asphaltenes. During the 1980s numerous studies[67–73] reported the appearance of *n*-alkanes and 1-*n*-alkenes in the thermolysis products of various asphaltenes from worldwide deposits of various origins, ages and histories, involving conventional oils, heavy oils and bitumens. Conversely, there has been no published report on the existence of a native petroleum asphaltene which, on thermolysis, would **not** have yielded a series of *n*-alkanes. Consequently, it would be sensible to assume that all—or at least most—native petroleum asphaltenes contain—*n*-alkyl side chains and bridges attached to aromatic and naphthenic rings, even when the maltene fraction of the oil is devoid of *n*-alkanes (as is the case for Alberta bitumens) and therefore a substantial portion of all asphaltenes must have originated from *n*-alkanoic source materials. These observations and their interpretations point to the all-important biomarker properties of asphaltenes, which go beyond the significance of conventional biomarkers usually occurring in quite low concentrations, and carry unique information related to the bulk origin of asphaltenes and crude oils. They identify one specific compound class in the biotic source material as the key player in petroleum genesis. The long-chain *n*-alkanoic precursors were probably derived from the long-chain fatty acids and *n*-alkanols of lipids and lipid-like substances in the debris of dead organisms. Lipids have been known to play a dominant role in the formation of petroleum along with less important contributions from proteins, carbohydrates, lignins and pigments.

The recognition of the structural principles of the asphaltene molecule also requires modification of the earlier view of asphaltenes as random organic geomacromolecules, in which the emphasis was on randomness and largeness of molecular size, by taking into consideration the high degree of structural order hidden under the apparent arbitrary ensemble.

What is also important from this discourse in molecular structure is the proposition that, in addition to *n*-alkanoic-derived thermolysis products identified, additional quantities of *n*-alkanoic-derived material remained locked up in the residue. These represent, in addition to the smaller nuclear condensed aromatics, penta- and higher condensed nuclear aromatic compounds which may have undergone additional condensations during thermolysis.

Another source material that quantitatively is of much less importance, yet is so clearly recognizable, is the family of terpenoid biomarkers, mostly isoprenoids, the hopanes, steranes, cheilantanes, drimanes, acyclic isoprenoids, *etc.* These molecules were incorporated into the aromatic portion of the asphaltene molecule probably *via* their alcoholic hydroxyl functionality in a Friedel–Crafts type reaction.[157] This points to the possibility of the incorporation of *n*-alkanol source materials into the aromatic portions of asphaltene, thereby increasing the carbon number of the asphaltene molecule beyond that of the naturally-occurring *n*-alkanoic acids and *n*-alkanols and introducing branching, incompatible with the cyclization of single-strain *n*-alkanoic chains. Therefore, even molecules which would apparently not conform to *n*-alkanoic branching in the asphaltene could have been formed from purely alkanoic materials.

In addition to a Friedel–Crafts type pathway, these biomarkers are also incorporated into the asphaltene *via* sulfide, ether and ester linkages, as we have seen earlier, but evidence for any role that would have been played by transalkylation reaction is lacking.

6.6 The size of the polyaromatic sheets

Early workers, using primarily X-ray diffractions measurements, tended to overestimate the size of the polynuclear condensed aromatic sheets. In the late 1950s, primarily from IR, NMR and X-ray diffraction studies, it was concluded that aromatic and alkyl structures are prominent in asphaltene, but there was no indication of the presence of naphthenic structure. From X-ray diffraction measurements on a series of solid asphaltenes in the 1960s it was inferred that the covalently bound asphaltene molecule is composed of alternating sequences of *normal* alkyl moieties and islands of condensed aromatic disks.[158] Around that time there were a number of circumstances prevailing which, in combination, led to the general belief that the aromatic portions of petroleum asphaltenes must be highly condensed. These circumstances arose from the overestimation of the structural significance of the X-ray diffraction signal attributed to large aromatic disks, the failure of instrumental methods to detect the presence of naphthenic structural elements, the lack of chemical approaches to the structural investigation of asphaltene and the consequent nonexistence of chemical knowledge, and last but not least, the well-recognized propensity of asphaltenes for coke formation.

One of the two main bands observed in the X-ray diffraction pattern of solid asphaltene, the (002) band at 350 pm, is an intermolecular peak arising from interference between aromatic molecules;[159] the other, the γ band near 450 pm, reflects intermolecular order of saturated hydrocarbon chains. In early work it was thought that, from measurements of the intensities of these bands, with the assumption that all the aromatic carbons in the asphaltene are present in polyaromatic sheets, average values for some parameters of the molecular aggregates could be derived. Average derived diameters of the polyaromatic sheets in nine different asphaltenes were between 9 and 17 Å, and somewhat lower, between 8.5 and 11 Å, in the resins. For Athabasca asphaltene, values of 14–15 Å were reported, depending on MW, and 6.0–9.1 Å for the polar, lower-MW asphaltene fractions. Recently, however, it has been questioned[159] whether an intermolecular peak like the (002) peak which arises from interference *between* aromatic molecules can be related to the size of the aromatic molecules. Instead, the (100) and (110) peaks arising from *intramolecular* interferences *within* a benzenoid molecule have been suggested to be more suitable for this purpose, but even here many nonaromatic-type structures (naphthenes, heterocyclics, fullerenes, *etc.*) can lead to misinterpretation of the results.

In light of these developments and the new chemical results revealing that a large portion of the aromatic carbon is present in relatively small molecules from thiophene and benzene to tri- and tetrabenzothiophenes, *etc.*, lying outside the large polyaromatic centers and therefore not contributing to the diffraction intensity, the significance of the X-ray data is obscure. What appears likely is that the average diameter of the polyaromatic centers depends on MW and that it tends to increase with increasing MW of the asphaltene. This conclusion is also supported by EPR measurements which revealed a trend of increasing concentrations of stable organic free radicals in the GPC-separated fractions of Athabasca asphaltene with increasing MW of the fractions.[141] Since the aromaticity of the fractions varies in the opposite direction, that is, it decreases slightly with increasing MW of the fractions, the higher concentrations of free radicals in the heavier fractions cannot be due to a higher degree of aromaticity, but rather, it must be due to the larger average size of the polyaromatic centers which affords greater stabilization[127,160] by delocalization of the unpaired electron.

6.7 The covalent MW of asphaltene

The determination of MW* for the vast majority of organic compounds is a simple, routine laboratory operation. Not so for asphaltene. In effect, scores of researchers have expended a great deal of effort over the past 75 years trying to develop a reliable, precise method for the measurement and interpretation of the MW of asphaltene. Whereas for a single compound the MW can be unambiguously and precisely defined in terms of a single number, that is not possible for asphaltene. Determination of the MW and MW distribution of the covalent molecules forming the fundamental units in asphaltene is a formidable task which has not been brought to full completion yet. Many of the difficulties arise from the following circumstances:

- structural and size diversity of the random asphaltene molecules with unknown precise structures;

---

*There are numerous methods involving various physical principles available for MW measurement. They can be divided into various categories depending on whether they measure absolute or relative values, and whether they represent equilibrium or nonequilibrium processes. Scattering-based methods (light, SAXS, SANS) are absolute nonequilibrium methods and those based on colligative properties (cryoscopy, osmometry, ebulliometry) represent absolute equilibrium methods. MS and fluorescence-based methods are neither equilibrium nor nonequilibrium methods. Viscosity, surface tension, VPO and GPC are relative methods.

- the propensity of the asphaltene molecules for aggregation by a variety of different types and strengths of intermolecular forces, leading to the formation of sizeable polydispersed supramolecules;
- the characteristic dominant structural feature of dense atomic centers interconnected with varying lengths of polymethylene (up to at least C_{24}) and C–S–C and C–O–C ester bridges, methylene and biphenyl C–C linkages;
- inexact operational definition coupled with insufficient instruction for the isolation of "pure" asphaltene.

The MW of asphaltene and its measurement are huge and contentious topics and any attempt to review them in this monograph would be out of context. Instead, we will restrict our purview to a limited outline of selected current developments.

Petroleum asphaltenes in solution have been traditionally thought of as micellar aggregates of several high-MW covalent asphaltene molecules that were "peptized" in crude oil by lower-MW resin molecules. Then in 1979 it was shown[161] that GPC of very dilute solutions of Athabasca n-C_5-asphaltene features a trimodal distribution, indicating three different MW distribution domains. Moreover, it was also found that the distribution depends on the "age" of the asphaltene solution and with increasing time, over several weeks, redistribution slowly takes place, primarily towards later-elution (lower size and MW). This phenomenon provides unambiguous evidence for a dynamic equilibrium in asphaltene solutions between low-MW single molecules and their aggregates. At that time it was felt that given sufficient time (or shifting the equilibrium by other means) the dissociation would go to completion. However, that was not always experimentally observed. Subsequent studies on asphaltenes prepared by conventional solvent precipitation with n-C_5 revealed the presence of substantial concentrations of non-asphaltenic substances (low-MW hydrocarbons and resins) in the precipitated asphaltene.[39–41] This, along with the observation that the fluorescence yield from dilute solutions of asphaltene depends on the MW of the GPC-separated fractions of the asphaltene,[118] and the experimental observation of equipartitioning[36] of the non-asphaltenic substances between the n-C_5 precipitant and the precipitating asphaltene, necessitated the revision of this assumption.

6.7.1 MW from chromatographic and chemical studies

When Athabasca asphaltene was subjected to GPC separation on a Styragel 1000Å column at concentrations well above 0.05% solutions in CH_2Cl_2, the chromatogram was a regular unimodal symmetrical peak, Figure 14.119.[161] Repeating the experiment under the same conditions at or below 0.05% concentrations, the chromatogram featured a trimodal distribution, the latest-eluting peak of which was completely detached from the other two overlapping earlier-eluting peaks, Figure 14.120.[161] The same figure also shows the chromatograms of the separated fractions.[161,162] The results of repetitive analyses on each fraction are seen in Figure 14.121.[162] The approximate relative peak areas are plotted in the form of bar diagrams positioned at the elution time of the peak maxima. The measured area of peak III was corrected for the presence of the 22% acetone solubles, assuming that all these materials would elute with the lowest-MW peak III and the total residue was then normalized to 100%. This then led to an approximate distribution for peaks I, II and III of 27.7, 31.2 and 41.1%. The highest-MW fraction, as seen from the figure, underwent extensive redistribution to longer retention time (lower MW) upon standing five days in the dark at room temperature under a nitrogen atmosphere. After five days the residue amounted to about 18%. Microscopic examination of the stored solution prior to chromatographic analysis showed no signs of any precipitate. Consequently, the occurrence of

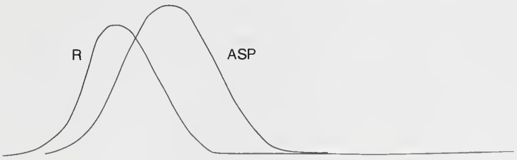

Figure 14.119 GPC separation of Athabasca asphaltene and resins (>> 0.05% solution). From M.L. Selucky *et al.*, Ref. 161. © 1981, American Chemical Society.

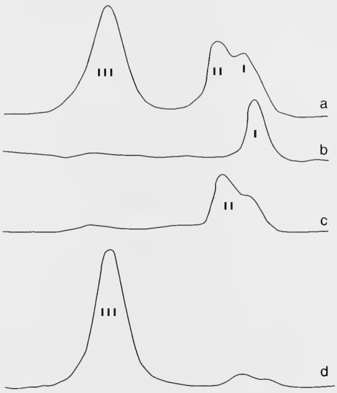

Figure 14.120 GPC of Athabasca asphaltene (a) in a 0.05% solution and (b–d) rechromatographed peaks I, II and III. From O.P. Strausz *et al.*, Ref. 162. © 2002, American Chemical Society.

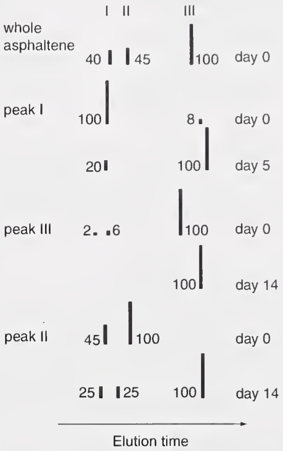

Figure 14.121 Time study of changes in the GPC profiles of fractions I–III in Figure 14.120. From O.P. Strausz *et al.*, Ref. 162. © 2002, American Chemical Society.

redistribution is proof that at least 82% of this material consists of molecular aggregates which, upon standing in CH_2Cl_2, slowly dissociate into their low-MW components. It will also be noted that after five days the retention time of the redistributed fraction I is significantly longer (and MW lower) than was that of the lowest-MW fraction III. This observation suggests that even the lowest-MW fraction III shows some degree of aggregation. Indeed, after 14 days peak III is seen to have drifted to somewhat longer retention time, indicating some degree of association in the zero day solution. Peak II is incompletely separated from peak I in the fresh solution, and also after 14 days' standing. Therefore, they are best treated as a single peak. This gives a 33% residue after 14 days.

Similar observations of redistribution processes were also made on two chromatographic subfractions, namely the benzene/MeOH (5.3%, MW 1,450 g·mol^{-1}) subfraction which was the lowest-MW subfraction (on an IRA-904 anion exchanger column), and the benzene (10.9%, MW 5,300 g·mol^{-1}) highest-MW subfraction (on an A-27 anion exchanger column), Figures 14.122 and 14.123.[161,162] In the former experiment, the redistribution was followed up to 45 days, at which time 13% residue was still apparent, and in the latter case the experiment was conducted for 14 days, after which conversion to only 13 % was observed.

The major conclusions from this study can be summarized as follows:

- at sufficiently low concentrations, ≤ 0.05%, the GPC chromatograms of solutions of Athabasca asphaltene and their ion exchanger chromatographic subfractions display considerable polydispersity which, in some cases, may be manifested by the appearance of a number of discrete peaks in the chromatogram;

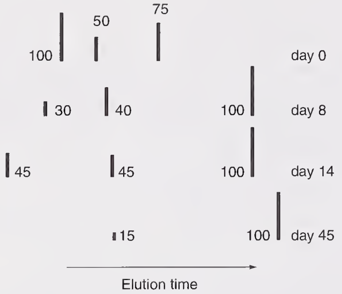

Figure 14.122 Time study of changes in the GPC profiles of the acidic Bz/MeOH fraction of Athabasca asphaltene. From O.P. Strausz *et al.*, Ref. 162. © 2002, American Chemical Society.

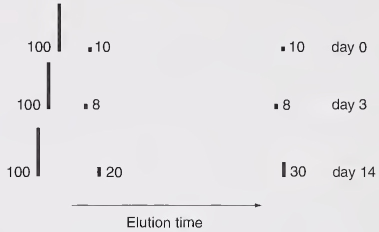

Figure 14.123 Time study of changes in the GPC profiles of the acidic Bz fraction of Athabasca asphaltene. From O.P. Strausz *et al.*, Ref. 162.© 2002, American Chemical Society.

- the GP chromatograms of the various asphaltene subfractions exhibit characteristic differences;
- in dilute solutions, ≤ 0.05%, upon standing in the dark at room temperature in an inert atmosphere, a slow but extensive redistribution of the asphaltene molecular units takes place, manifested by a drift of the GPC peaks to longer retention times, *i.e*, smaller aggregate sizes;
- the various high-MW fractions converted to low-MW entities after 14 days, from 13% to 87%, with the exception of the lowest-MW fraction III of the whole asphaltene, where 100% was converted to still lower-MW moieties. Even after 45 days, one fraction left a significant amount of high-MW residue behind. In the whole Athabasca asphaltene the unconverted residue is estimated to be ~16%.
- the occurrence of redistribution provides unambiguous proof for the presence of molecular aggregates comprising a sizeable portion of the asphaltene;
- the GPC method gives an insight into the details of molecular and aggregate size distribution without distorting or affecting it; moreover, it makes possible the separation of the distinct molecular aggregates.

The splitting of GPC peaks into discrete bands, which has recently been also observed in the GPC of coal tar pitches,[163] is an interesting molecular phenomenon. To gain information about the nature and role of the chemistry involved here, one of the acidic subfractions eluting (after cyclo-C_6, benzene, benzene/MeOH) with MeOH/CO_2 was further separated into its four components yielding ~ 0.05% solutions. The FTIR spectra of these fractions, along with their chromatograms, are shown in Figure 14.124.[161] As seen, the hydroxylic H-bonding region (3600–2500 cm^{-1}) features a large, sharp peak in the first, shortest retention time spectrum then gradually decreases and becomes broader in the subsequent ones. Other progressive changes include an increase in the carboxylic carbonyl absorption (1700–1725 cm^{-1}) relative to that of the aromatic one (1600 cm^{-1}) and a decrease in absorption and articulation over the range 1250–1000 cm^{-1} due to carboxylic acids, alcohols, *etc.* The IR spectra reveal different chemical compositions in the four different MW fractions and this points to the continuous nature of the changes in the chemical compositions of these four different size aggregate fractions. Clearly, the highest-MW aggregates are formed from those molecules which have the highest aromatic, carboxylic acid and perhaps alcohol contents. These findings are consistent with asphaltene being a typical representative of a random self-assembling supramolecular system. In these aggregates the intermolecular interactions, according to molecular mechanics calculations[164] on model asphaltenes that have a large aromatic moiety, are dominated at the equilibrium distances by van der Waals forces, and Coulombic forces contribute only about 10%. It then follows that for

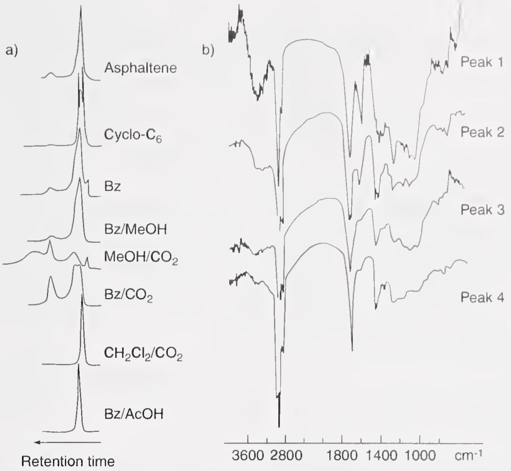

Figure 14.124 a) GPC of acidic subfractions of Athabasca asphaltene. b) FTIR spectra of the four components of the MeOH/CO_2 subfractions. From O.P. Strausz *et al.*, Ref. 162. © 2002, American Chemical Society.

this type of asphaltene the primary interaction is between the electron-rich aromatic systems followed by H-bonding, and probably radical ion pairs formed in intermolecular charge transfer processes, along with weak complexations owing to the acid, base and amphoteric components present. H-bonding, involving carboxylic acids and, less efficiently, alcohols, has also been computed to possess sizeable adsorption enthalpies and thus contributes to the aggregation. If the aromatic regions are small or not readily available for bond formation, H bonding may become the dominant intermolecular force. Consequently, it follows that molecules rich in these types of adsorption sites will tend to form larger and more stable aggregates than the other ones. Molecular recognition processes will favor the interaction between molecules of complementary shapes that have the least steric interference, and have the strongest H-bonding sites. Molecules that fulfill these requirements will form the most stable aggregates.

Returning to Figure 14.121, we note that the ultimate redistribution retention times estimated to correspond to approximately 1,000 g·mol^{-1} MW for the individual covalent asphaltene molecule are nearly the same for all these fractions, showing that the size of the covalent molecules forming the aggregates is about the same in the three different size aggregates, except of course for the nondissociated residues, about which no statement in this regard can be made.

Now, we summarize the available information discussed in this section concerning the aggregation number and MW of the individual covalent asphaltene molecules.

- from GPC studies it was established that the whole asphaltene with (VPO) MW 4,000 g·mol^{-1} dissociates, upon extreme dilution, into four approximately 1,000 g·mol^{-1} covalent molecules giving an average aggregation number of four;
- from NiB reduction it was found that the MW was reduced from about (VPO) 4,800 to about 1,200 g·mol^{-1}, about fourfold;
- from NRA reduction the (VPO) MW of the reduced asphaltene was 534 g·mol^{-1} (Section 4.2.1). This reagent reduces and cleaves all the C–S$_{\text{sulfide}}$ bonds, the C–O ester bonds, and cleaves all the intermolecular bonds. The latter effect is a corollary of the ionic nature of the NRA reduction mechanism,

$$\boxed{}\!-\!\mathrm{S}\!-\!\boxed{} \xrightarrow{\mathrm{NRA}} \boxed{}^{-}(\mathrm{K}^{+}) + \mathrm{S}^{2-}(2\mathrm{K}^{+}) + \boxed{}^{-}(\mathrm{K}^{+}) \tag{95}$$

which, in parallel with C–S bond cleavage, converts the liberated aromatic core of the asphaltene to an asphaltene radical anion. The strong Coulombic repulsion among identically-charged asphaltene fragments would then prevent their aggregation.
- the structure that appears best to agree with all the experimental observations for the asphaltene used in the NiB reduction is

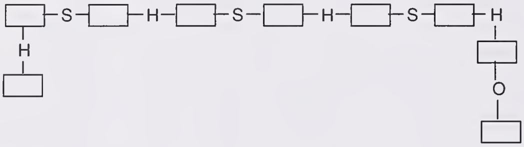

MW_N = 4,800 g/mol

MW_N from NiB reduction =1,200 g/mol

MW on ∞ dilution = 960 g/mol (96)

- the identical size of the asphaltene core segments, 534 $g{\cdot}mol^{-1}$, deduced from the NRA and NiB reactions, lends support to the validity of the above argument and establishes the average size of the aromatic core segments in the asphaltene around 534 $g{\cdot}mol^{-1}$.
- the value of the MW_N sets the total number of C atoms in the asphaltene core molecule as $(534 \times 0.8)/12 = 35.6$, and

  C_{arom} as $35.6 \times 0.42 = 15$

  C_{aliph} as 20.6

  Since the total number of alkyl bridges in the asphaltene core–S–core and core–O–core molecules are (Table 14.19):

  0.61 between C_{arom}–C_{arom}

  0.8 between C_{arom}–C_{naph}

  0.2 between C_{naph}–C_{naph}

  1.61 total/100 C

  then the total number of bridges in the core–S–core and core–O–core molecule is $1.61 \times 0.712 = 1.15$ per molecule, and now assuming 20 C_{arom} per bridge, the number of C_{arom} in bridges in the molecule is $1.15 \times 20 = 23$.
- there are four core–X–core (X = S or O) molecules in the aggregate and thus the number of C_{arom} in these molecules is $23 \times 4 = 92$ out of the 120 C_{arom} total. Therefore, 92/120 = 76.7% of C_{arom} in the core–X–core bridged molecules are in alkyl bridges as well.
- similarly, for the one orphan core segment in the aggregate, 11.5 of the 15 C_{arom} is in alkyl-bridged structures; thus, the total number of C_{arom} in alkyl-bridged structures in the aggregate is 103.5 out of the 135 C_{arom} in the aggregate.
- some hypothetical structural models exemplifying the compositional requirements for aromatic carbons outlined above are shown below (where C^*_{arom} = that portion of aromatic carbons which are attached to alkyl bridges). The alkyl and naphthenic components of these structures are to be appended by the appropriate kind and number of units to bring their total carbon number in the molecule to 20 and 22, respectively:

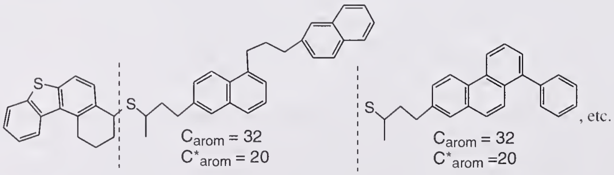

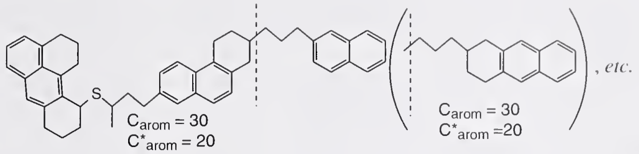
$C_{arom} = 30$
$C^{*}_{arom} = 20$
$C_{arom} = 30$
$C^{*}_{arom} = 20$
, *etc.*

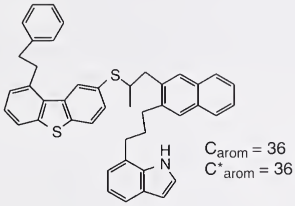
$C_{arom} = 36$
$C^{*}_{arom} = 36$

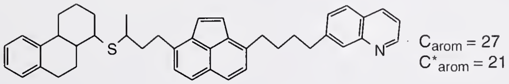
$C_{arom} = 27$
$C^{*}_{arom} = 21$

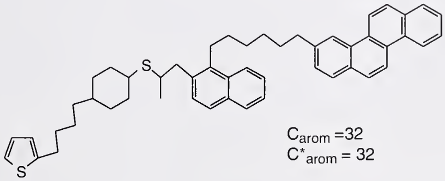
$C_{arom} = 32$
$C^{*}_{arom} = 32$

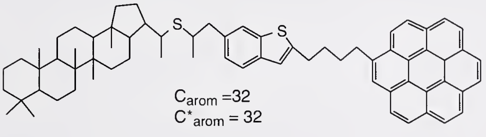
$C_{arom} = 32$
$C^{*}_{arom} = 32$
,

where any one out of three 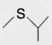 sulfide moieties can be replaced by the ester moiety.

- in the definition of bridged structure used above the bridge that was taken into account was the purely alkenyl bridge. But, as it is clear from the structures each molecule contains one bridge in which a sulfur (or oxygen) atom is also involved and if that is taken also into consideration, as it should be, all cyclic structural units are in bridged structure.
- the sulfur-bridged structure is easily broken up in thermal or hydrocracking operations with the release of lower-MW materials, and therefore it is much preferable to condensed thiophenic sulfur which is difficult to remove and has a tendency to undergo aromatic condensation reactions with the formation of polymers and ultimately coke.
- the bridged moieties endow the asphaltene molecule (comprising collections of small aromatic and naphthenic segments) with a rather loose and flexible molecular skeleton with great numbers of intramolecular rotational degrees of freedom.
- the structure and architecture of the asphaltene, deduced from the above detailed chemical studies, contrasts the one postulated earlier in the literature featuring a single rigid disk with some alkyl side arms.[120,121] On the other hand, it is in line with those deduced from diamagnetic/paramagnetic and NMR spectroscopic measurements reporting an average aromatic condensation of six[116] or less.[112]

- indications are that the structure established for Athabasca asphaltene is of general validity and should be applicable (with appropriate modifications) to most crude oil asphaltenes with S(O) content dependent weight.
- it is important to keep in mind that the acetone-soluble LMA behaves differently: it undergoes a similar degree of desulfurization in NiB reduction without any significant change in MW. Thus, a sulfide-bridged molecular structure is a characteristic of only the HMA. On the other hand, on NiB reduction the LMA releases more (16–20%) maltene material. In the whole asphaltene the two processes occur in parallel.
- interestingly, this property of the asphaltene manifests itself in the reversal of the magnitude of the measured MW for the whole and extracted asphaltene in the NRA reduction: before reduction of the asphaltene,

  $$\text{MW (extracted)} > \text{MW (whole)}$$

  but after reduction

  $$\text{MW (extracted)} < \text{MW (whole)}.$$

  This is because the 22% LMA in the whole asphaltene retains its original MW of 1,200 g·mol^{-1} but the MW of the 78% HMA is lowered on reduction to 534 g·mol^{-1}. The calculated MW of about 577 g·mol^{-1} is in agreement with the experimental value.
- The combination of results from the three different experiments, the direct observation of the slow dissociation of Athabasca asphaltene in dilute solution, the cleaving of the sulfide bonds by NiB reduction and the cleaving of the sulfide and all intermolecular bonds in the NRA reduction can be summarized as follows:

	MW_N/g·mol^{-1}	
asphaltene sample (corrected)	4,800	9,884
from NRA reduction	–	534
from NiB reduction	1,200	–
on ∞ dilution (exptl)	~ 1,000	–
on ∞ dilution predicted from structure	960	–

The value for ∞ dilution obtained in these studies is about half that reported recently (1,800 g·mol^{-1}) from VPO and interfacial tension measurements.[165] Thus, it would appear that in the VPO measurements the asphaltene was not fully dissociated. The strongest of the intermolecular bonds (in the radical ion pairs?) would be the most difficult to cause to dissociate and therefore the dimeric form would be quite persistent.

If the picture outlined above is correct then the results can be interpreted as meaning that the LMA does not contain any intermolecular bonds except the low concentration of triplet state radical ion pairs detected by EPR (Table 14.30) due to intramolecular charge transfer bonds.

Moreover, it also follows from the above data that about 80% of the LMA contains only cyclic sulfides whereas the remaining 20% contains about two acyclic sulfide bonds per molecule which on NiB reduction produce ~ 20% maltenes,

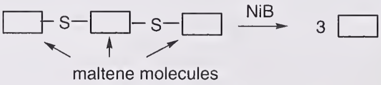

while leaving the MW of the residual LMA unaffected. This observation strongly suggests that the aromatic and resins fractions of the maltene contain acyclic sulfides with one sulfide bond per molecule. Thus, the following picture emerges

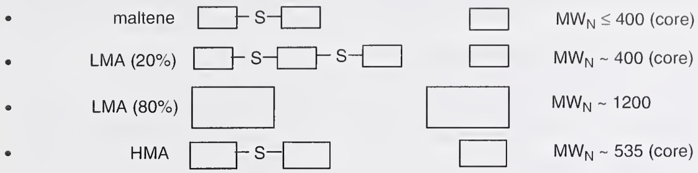

6.7.2 MW distribution

The mode of MW distribution in a colloidal system can significantly impact the properties of the system. The distribution in an associative system like an asphaltene solution may occur on two levels, the covalent molecular and the supramolecular level. In asphaltene solutions the distribution envelope is quite broad (*cf.* Figures 14.17, 14.18 and 14.116) and may extend from a few hundreds to many tens of thousands g·mol^{-1}.

The average MW of a polydisperse system can be defined in different ways, the two most common ones of which are the number average, MW$_N$, (obtained from VPO, *etc.*) and the weight average, MW$_W$, (obtained from light scattering, *etc.*),

$$MW_N = \frac{\Sigma_i n_i M_i}{\Sigma_i n_i} \; ; \; MW_W = \frac{\Sigma_i w_i M_i}{\Sigma_i w_i} .$$

From the above definition it follows that MW$_W$/MW$_N$ ≥ 1 and only when the system is monodisperse does the equality apply. The deviation of this ratio from unity is a measure of polydispersity which is an important characteristic of colloidal solutions.

As we have seen before, the properties, such as EPR, UV-fluorescence, NMR spectra, solubility, chemical composition of GPC separated Athabasca asphaltene fractions vary considerably. Therefore, it would be difficult to establish the cause–effect relationship, meaning whether the size separation is caused by chemical variations or the chemical variation by size fractionations.

MW distribution calculated from data obtained by different methods may have very different forms. The plots in Figure 14.125 illustrate the point. Plotted here are the theoretical results for a condensation polymer. The upper panel shows the number fraction distribution as would be obtained from MS (MALDI TOF) mea-

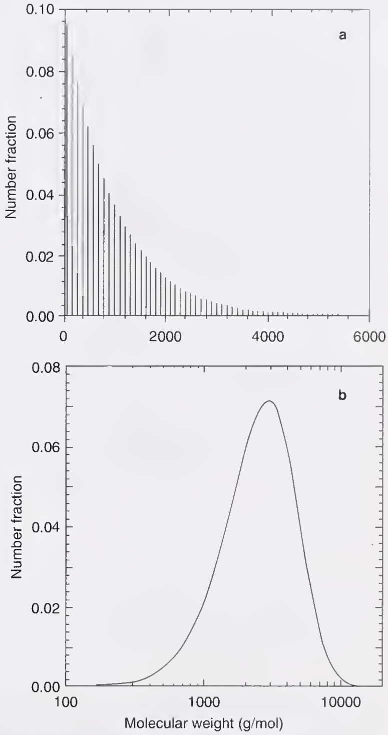

Figure 14.125 Simulated distribution for a wide polymer distribution from , *e.g.*, a polycondensation reaction (a) plotted on a linear and (b) plotted on a logarithmic scale. From M.W.F. Nielen, "MALDI Time-of-Flight Mass Spectrometry of Synthetic Polymers", Mass Spectr. Rev., 18 (1999) 309, after C. Jackson, B. Larsen, C. McEwen, "Comparison of Most Probable Peak Values as Measured for Polymer Distributions by MALDI Mass Spectrometry and Size Exclusion Chromatography", Anal. Chem., 68 (1996) 1303.

surements and the lower panel the weight fraction distribution from size exclusion chromatographic measurement. The shape of the curves and the peak MW (MW_P) values are vastly different from the two measurements. In the former case MW_P is the monomer mass, in sharp contrast to the latter case where MW_P is the weight average molecular weight, MW_W.

6.7.3 MW from mass spectrometric studies

The advent of the ionization desorption technique in mass spectrometry, with its various modifications, has made possible the MS investigation of many man-made and natural high-MW organic solids. The technique has matured to the point that it has made sizeable impacts on polymer chemistry and, in some instances, has even led to the creation of new fields in science, for example proteomics, the MW and structural study of proteins. However, advancement was not uniformly progressive in every area, and in the application of the technique for asphaltene some inconsistency remains. This is evident from the data of the comparative study[166] of an Athabasca 525+°C residue's GPC fractions employing VPO, ^{252}Cf-plasma desorption ionization mass spectrometry (PDMS), GPC and matrix-assisted laser desorption ionization mass spectrometry (MALDI-MS), Table 14.37. It is seen from the data that the various methods yield significantly different values, but similar trends throughout the fractions. The numerical values among VPO, GPC and MALDI are closer to one another than to PDMS, Figure 14.126, which consistently reports lower values. Fraction 1, with VPO MW_N 3,228 g·mol^{-1} by and large should correspond to the asphaltene content of the residue. The VPO, GPC and MALDI values correlate quite well for this fraction with an average value of 3,076 g·mol^{-1} as compared to the MW_N (PDMS) value of 790 g·mol^{-1}. The PDMS spectrum, Figure 14.126b, is unimodal with a maximum at an extremely low value of around 100 g·mol^{-1} , following which there is a

Table 14.37 Molecular weights of Athabasca 525+ °C residue GPC fractions[166]

Fraction	MN(VPO) g·mol^{-1}	MN(PDMS) g·mol^{-1}	MW(PDMS) g·mol^{-1}	M(GPC) g·mol^{-1}	MALDI[a] *m/z*
1	3,228	790	1,360	3,200	2,800
2	1,319	590	1,005	1,400	1,400
3	1,047	540	840	480	<1,000
4	911	540	830	390	<1,000
5	1,682	630	1,020	430	<1,000
feed	1,682	630	1,020	430	<1,000

[a] At maximum peak intensity

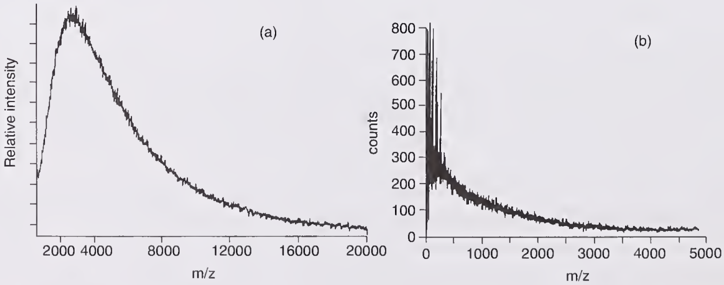

Figure 14.126 MW distributions of fraction 1 from Athabasca 525+ °C residue by a) MALDI and b) PDMS. From M. Domin *et al.*, Ref. 166. © 1999, American Chemical Society.

monotonic decline up to at least 4,800 g·mol^{-1}. The MALDI spectrum is quite different, featuring a broader maximum at 2,800 g·mol^{-1} with a gradual decline to at least 20,000 g·mol^{-1}—which is far too high for the basic monomeric unit of asphaltene. Also, the correlation of the MALDI maximum with the VPO value does not lend credence to the MALDI spectrum as representative of the monomeric distribution of asphaltene.

Another laser desorption study involving Athabasca and Cold Lake asphaltenes reported the LD high-resolution MS pyrolysis of these materials.[167] Here, whole n-C_5-asphaltenes were used and these contained substantial quantities of resinous materials (*cf.* Figure 14.46); at that time the authors were unaware that "high-MW materials may be greatly underestimated when the determinations take place in the presence of a greater abundance of low-MW material".[168] Also, the MS was run in the reflector mode for it was also not known at that time that "removal of the MALDI-TOF instrument's reflector from the flight pass improves the sensitivity to high-MW material".[166] Conseqently the reported spectrum[167] is inundated by well-resolved, low *m/z* peaks of resin and pyrolysis fragment molecules.

Among the numerous LDI, MALDI, field ionization desorption MS investigations of asphaltenes we mention only one more, namely, the LDI-MS study on solvent precipitation-separated fractions of a residue asphaltene.[169] The spectra of three fractions obtained are shown in Figure 14.127. Spectrum AS6 was obtained on the highest-MW fraction, AS2 on the most soluble fraction and AS4 is an intermediate fraction. The overall shapes of all three spectra are similar; following the 0–100 *m/z* range, a U-shaped valley is apparent, going into maximum intensities at *m/z* 300, 350 and 500 for samples AS2, AS4 and AS6. The AS6 spectrum extrapolates well beyond *m/z* 2,000, where its intensity is about 15% of the maximum value. Evidently, LDI causes significant fragmentations, or multiple ionizations, of the covalent molecules and aggregates of the asphaltene. In view of the presence of sulfide bridges and other weak, reactive linkages in asphaltenes, this is not surprising.

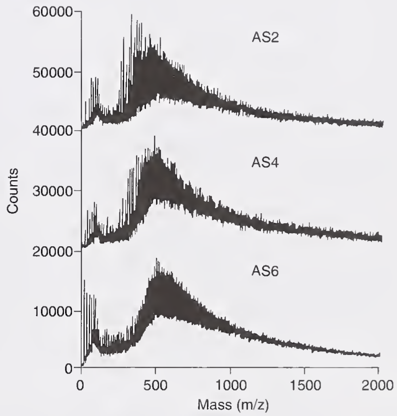

Figure 14.127 LDI MS spectra of three asphaltene subfractions. From M.-G. Yang and S. Eser, Ref. 169.

In conclusion, it appears that LDI–MS in asphaltene chemistry may not be as useful as in, for example, the chemistry of proteins or polyethylene polymers which lack the low dissociation energy, weak linkages so abundantly present in asphaltene (sulfide bridges, benzylic C–C, alkylfluorenes, tertiary C–C bonds in biomarkers, in alkyl cycloalkanes, in α-alkyl branched alkyl aromatics, *etc.*). Also, the extreme polydispersity of the asphaltene mass distribution, featuring molecular mass peaks at every *m/z* values above 200 atomic mass unit into the thousands, is a serious, experimentally complicating factor, making it impossible to differentiate between molecular and fragment ions. This is an especially critical problem since the mechanism of LDI follows a step-wise route, requiring the absorption of at least three of the λ = 337 nm photons of the N_2 laser used in most LDI work, whereas two-photon absorption is sufficient to cause the rupture of the strongest single bond in the asphaltene molecule. Therefore, extensive fragmentation at the weak linkages must occur and this can then be followed by subsequent ionization of the fragments.

6.7.4 MW from molecular rotational correlation time–fluorescence depolarization (RCT–FDP)

This spectroscopic method has been used mainly to determine the size of **rigid** molecules of a pure compound or simple mixtures of pure compounds in solution. It has now been applied to the molecular size determination of asphaltene molecules. However, the asphaltene molecule, as it is amply evident from the foregoing dicussions, is an ensemble of small-ring aromatic chromophores linked together by flexible alkyl, aliphatic sulfide, ester and biaryl bridges which, if there is a representative structure for the antipode of a rigid molecular structure that must be the asphaltene molecule. The claim that the asphaltene molecule has a rigid disk-like structure and thus providing validation for the application of the RCT-FDP method for asphaltene MW measurement was based on the erroneous, invalid conclusions from fluorescence lifetime measurements as was discussed in section 5.3.

Aside from the structural problems which in themselves would be sufficient reason to disqualify RCT–FDP as a valid method for the measurement of the MW of asphaltene, there is the additional problem concerning the nature of the fluorescence: its quantum yield is strongly dependent on the MW[118] (Section 14.5.3) and the possibility exists that the high-MW fractions do not fluoresce at all; in the case of whole Athabasca n-C_5-asphaltene, we have seen that 51% of the emission originates from the 22% lowest-MW fraction and only 1.8% from the 22% highest-MW fraction. Moreover, the fluorescence and even the absorption spectra can be affected by the intervention of intramolecular exciplexes and strongly-bound dimeric species such as the triplet-state charge-transfer doublet-doublet radical ion pairs seen in the EPR spectra and their ground-state counterparts in the fluorescence mechanism.

In addition to the methods discussed above, there are a variety of others to measure MW, each with its own advantages and associated problems. The VPO method stands out with its simplicity and reliability in providing accurate upper limits for number average MWs and, in combination with time-resolved GPC of highly dilute solutions, should be a potential route to the exact measurement of MW_Ns and MW distributions.

6.8 The fifth compound class of petroleum

In the compositional characterization of petroleum, as has been discussed in previous chapters, it is general practice to fractionate the oil into the four compound classes designated by the 'SARA' acronym. Simple, single-step separation never leads to pure fractions because there is always some material carried over from or left behind in the other fractions; this can be minimized by further analytical refinements. Thus, the saturate fraction from the initial silica gel column chromatographic separation in most cases contains some oxygen and sulfur compounds, some aromatics and even some asphaltene-like material; the aromatics contain large quantities of heteroatoms, resins and also asphaltene-like materials; and the resin or polar fraction contains some polynuclear condensed aromatic hydrocarbons and asphaltenes. Therefore, it would be unreasonable to expect that asphaltene would be an exception and be isolated in "pure" state by a single-step precipitation or any other single-step operation, regardless of how we view asphaltene—as a mere solubility class or as molecules whose structures are characterized by ensembles of polynuclear and naphthenic condensed aromatic and heteroaromatic hydrocarbons.

A fraction of the crude asphaltene comprises materials which are wholly or nearly so soluble in the precipitant but these materials can precipitate with the asphaltene due to adsorption or absorption to the asphaltene aggregate (although a portion remains in the liquid phase). Therefore, this portion of the crude asphaltene can be viewed as precipitant soluble in the absence of asphaltene, but in the presence of asphaltene this portion becomes equipartitioned between the liquid bulk phase and the desolved asphaltene phase. The latter includes not only the "precipitating" asphaltene but the "precipitated" asphaltene as well. (section 2.1.2). If the solid asphaltene is collected by filtration, washed and dissolved, a new equipartitioning equilibrium state will be reached by the release of some of the precipitant solubles into the liquid phase. Upon reprecipitation, another portion of the precipitant solubles will remain in the liquid solution. In the case of *n*-C_5-Athabasca asphaltene, after the sixth reprecipitation,[36] the combined precipitant solubles amounted to 21.9 wt% of the crude asphaltene, or 28.0 wt% of the residual, precipitant-insoluble asphaltene (section 2.1.2 and Figure 14.14). The chemical composition, chemical and physical properties of this material are quite different from those of the residual asphaltene: its color is deep reddish-brown compared to the black color of the residual asphaltene, its MW is about one-half that of the initial crude asphaltene , and the residual asphaltene MW is about twice that of the crude asphaltene. It contains[39–41] cyclic terpenoid sulfoxides, aliphatic and aromatic alcohols and carboxylic acids, ketones, alkylcarbazoles and various condensed carbazoles, porphyrins, and other resinous substances admixed with some lower-MW asphaltene fragments. Mixing this material wholly or partly into the asphaltene, as is done when following standard procedures, obscures the true chemical and physical character of the asphaltene and confuses the interpretation of research results. This 28% fraction of the precipitant-insoluble asphaltene is also an important element in the compositional characterization of crude oils, the quantity and quality of which would vary from crude oil to crude oil. This pre-asphaltene could also play an important role in the solubilization of asphaltene and its quantity in the oil, and its composition should be monitored. Back extrapolation from a few reprecipitations would also permit the estimation of the amount of pre-asphaltene that was associated with the asphaltene in its natural state in the oil, and this then could probably be correlated with the stability of the colloidally-dispersed state of the asphaltene solution. Therefore, it would appear highly desirable to introduce this precipitant-soluble fraction into the compositional characterization of crude oils as the fifth compound class fraction.

An interesting demonstration of the effect of this pre-asphaltene on the properties of the residual asphaltene has been described recently[170] in connection with the effect of low-concentration water on the micellization of asphaltene. Water induces the micellization of *n*-C_7-asphaltene. However, when the pre-asphaltene material, representing the difference material between *n*-C_7-asphaltene and *n*-C_5-asphaltene, was added to the *n*-C_7-asphaltene, then water ceased to be effective in inducing micellization. Evidently, this pre-asphaltene material adsorbs more strongly than water to the active sites in the asphaltene, preventing adsorption of water and thereby hindering micellization.

Repeated re-precipitations admittedly are time- and work-intensive processes. However, essentially the same pre-asphaltene fraction can also be isolated by acetone extraction of the crude asphaltene. When Athabasca crude asphaltene was Soxhletted for one week, the yield and MW of the pre-asphaltene fraction in the solution was practically identical to those obtained after six re-precipitations. There was only one noticeable difference in properties, namely, 76.4% of the combined pre-asphaltenes after the sixth re-precipitation was soluble in *n*-pentane whereas the pre-asphaltene from the acetone extraction released only 21.7% material after one week's Soxhletting in *n*-pentane.

Lastly, as mentioned in section 2.1.2, the pre-asphaltene fraction can also be separated from the crude asphaltene by GPC. The lowest-MW (1,200 $g{\cdot}mol^{-1}$) 20.8% fraction isolated from Athabasca asphaltene by GPC was practically the same material as the pre-asphaltene from the previously-mentioned separations.

In summary, the pre-asphaltene could be defined as that portion of *n*-C_5-asphaltenes that can be removed by one week's Soxhlet extraction of the asphaltene in acetone. Acetone is the choice solvent for this separation because it separates according to characteristic natural differences in composition and properties, Table 14.38. Other low-solvent-power solvents would also dissolve fractions of the asphaltene on prolongued Soxhletting (Figure 14.15, Table 14.5) but the separation would not be as satisfactory.

Table 14.38 Differences in properties between pre-asphaltene and asphaltene

	pre-asphaltene (LMA)	asphaltene (HMA)
MW	low	high
color	reddish-brown	black
Changes upon NiB reduction		
MW	no change	reduced
O-content	reduced	increased
Products from NiB reduction		
isoprenoids	x	—
bicyclic terpanes	xx	—
pregnanes	xx	—
C_{21}–C_{25} steranes	x	—
mid-Me-alkanes	—	x
steranes maturity	higher	lower
Products from RICO		
tricyclic carboxylic acids	—	x
pentacyclic carboxylic acids	—	x
steranoic carboxylic acids	—	x
pregnanoic carboxylic acids	—	x

7.0 The origin of asphaltene

From previous sections of this chapter we found that beneath the apparent surface randomness of the chemical composition of asphaltene, which has been amply emphasized in the past, there lies a wealth of high chemical order with a unifying generic principle, namely, that the bulk of the chemical constitutents of petroleum asphaltene consists of *normal* alkanoic-derived hydrocarbons and heterocycles with minor amounts of pigments some cyclic terpenoids and other biotic source materials. Therefore, the historical view of asphaltene as merely a solubility class material of petroleum comprising randomly fused organic matter must be abandoned. It is true that solvent precipitation produces a crude asphaltene with substantial amounts of complexed resinous substances and occluded hydrocarbons, but with appropriate solvent precipitation and extraction procedures most of these extraneous substances can be removed, permitting the isolation of a structurally defined asphaltene fraction as molecular ensembles of *n*-alkylaromatic and naphthenoaromatic hydrocarbons and heterocycles linked together with flexible alkyl, biaryl, ester and aliphatic sulfide linkages with characteristics specific for *n*-alkyl progenitors. Thus, the procedural difficulties in separation should not obscure our recognition of the distinct molecular structural characteristics of asphaltene and our conceptual understanding of its basic chemistry. It then directly follows that, contrary to the historical view in which asphaltene is considered as merely a solubility class, with the often explicit corollary that it is not a compound class and that it does not even have a "definite composition", asphaltene in reality comprises a broad variety of polydispersed molecular ensembles with highly specific characteristics and substitutional patterns, which were generated by the cyclization, aromatization and condensation of *normal* fatty acids and alcohols from the lipid components of the sedimentary organic matter in which the *n*-alkanoic skeleton remained preserved and is recognizable today. This structural feature endows asphaltene with a unique biogenetic information content and in this sense asphaltene should be considered as a unique biomarker which identifies the principal source material of not only itself but of the associated parent oil, and it manifests the types of chemical transformations taking place during the chemical evolution of petroleum. Thus, the knowledge of the asphaltene structure achieved represents a major contribution to the theory of petroleum formation by revealing that *normal* fatty acids were the major biotic source materials.

The proposition that the principal source materials of petroleum were *normal* alkanoic acids[171–174] is not new. It has been suggested repeatedly in the past but until the identification of the *n*-alkylaromatic and *n*-alkyl cyclic sulfide thermolysis products and the recognition of their structural commonality, no substantive evidence for their role in petroleum generation has been found.

Schematic 14.1, illustrating the carbon skeleton of the identified principal thermolysis products of asphaltene, reveals that these compounds originated from the cyclization of single *n*-alkyl chains

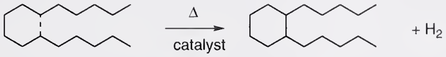

(97)

rather than from the fusion of two chains.

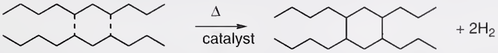

(98)

Such dehydrogenation-cyclization steps would be only slightly endothermic, but would possess a high activation energy and a low preexponential factor and consequently could only occur at prohibitively high temperatures. In the presence of a suitable catalyst, however, these reactions could and indeed have been shown to occur[175] quite readily in the 550–600°C range on the tenths-of-a-second time scale to give, in good yields, alkylbenzenes and higher condensed alkylaromatics from n-C_9 to n-C_{14} alkanes.

n-Alkanoic acids also decompose readily in the presence of appropriate catalysts.[171–174,176] Thus, montmorillonite promotes decarboxylation with the production of one-carbon-atom-shorter-chain *n*-alkanes, calcium carbonate promotes β cleavage with the loss of two carbon atoms and the production of two-carbon-atoms-shorter-chain *n*-alkanes and kaolin catalyzes decarboxylation and the extensive isomerization and cracking of the resultant hydrocarbons. These decarboxylation reactions have been studied using, as working materials, palmitic (n-C_{16}), stearic (n-C_{18}) and behenic (n-C_{22}) acids. Many of the experiments were carried out in sealed glass ampoules at temperatures between 200 and 300°C. Under these conditions behenic acid over kaolinite as catalyst gave C_2–C_{28} hydrocarbons in yields amounting to several percent in 300–1300 hours' experiments. Preponderant among the cracked C_2–C_7 products were isoalkanes, especially at the lower temperatures. With rising temperature the total amounts of products, the *normal* to *iso* alkane ratio and the relative combined amounts of cyclic products detected, cyclopentane, methylcyclopentane, cyclohexane and 1,3-dimethylcyclopentane, all increased. Small quantities of branched alkylbenzenes were also detected but not measured.

Smectic clay catalysts have been postulated to feature two types of catalytic sites. Lewis acid sites, characterized by octahedrally coordinated Al^{3+}/Fe^{3+} ions exposed at the edges of smectite crystallites, may act as electron acceptors, promoting free radical formation. A second source of catalytic activity has been attributed to the strong Brønsted acid character of cation exchange smectites arising from dissociation of the interlayer water molecules, which is favoured by tetrahedral substitution. Such strong Brønsted acids show superacidic properties capable of converting hydrocarbons to carbonium ions. Accordingly, the decomposition of carboxylic acids over these catalysts has been thought to proceed *via* two parallel mechanisms, one involving free radicals and leading to *normal* hydrocarbon products, and the other involving carbonium ions and leading to extensive cracking and isomerization of the *normal* alkyl chains and the production of branched hydrocarbons.

Smectic clays also catalyze the thermal decomposition of alkanes. Thus, *n*-octacosane, $C_{28}H_{58}$, has been shown to decompose over bentonite to yield high concentrations of branched and cyclic alkanes.

Apparent activation energies for the decarboxylation and hydrocarbon cracking reactions over Ca-montmorillonite have also been determined. Behenic acid was found to decompose with an activation energy of 31 kcal mol^{-1}, heneicosane with 6.1 kcal mol^{-1} and heneicosane in a heneicosane-stearic acid mixture with 6.4 kcal mol^{-1}.

From results obtained in flow experiments and IR examination of the solid products of the reaction, it became evident in the mid 1980s that the decomposition of carboxylic acids is a complex reaction, the primary step of which involves (in addition to a minor decarboxylation process to produce *n*-alkyl radicals or carbonium ions) the intervention of the acid anhydride which, in turn, may undergo decarboxylation to give a ketone:[176]

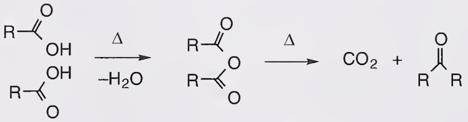

(99)

The nature of the action of smectic clay catalysts and the mechanism of fatty acid and alkane decomposition reactions over these clays are not well understood; nevertheless, it is now well established that these catalysts are effective in promoting the decomposition of fatty acids and aliphatic hydrocarbons by lowering their activation energy requirements and that these catalytic effects have played an important role in the natural diagenesis of sedimentary organic matter.

Returning to the cyclization and aromatization reactions of *n*-alkanoic acids and *n*-alkanes, as we have seen above, these processes can be facile under thermocatalytic conditions and can conceivably take place at deeper burial depths during the diagenetic/catagenetic maturation of the sedimentary matter. Cyclization–aromatization should take place sequentially:

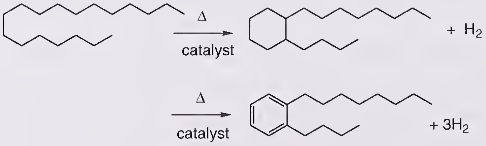

(100)

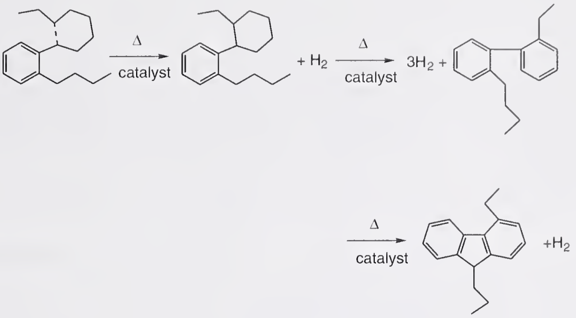

(101)

A measure of the progress of the cyclization-aromatization processes may be defined as the ratio of the concentrations of the polymethylene bridges connecting two aromatic ring systems to those of the *n*-alkyl side chains attached to aromatics. Thus, taking a benzene ring for the aromatic structure, the concentration of 1,3-diphenylpropane may be compared to that of *n*-nonyl benzene, through the ratio of their respective carboxylic acid product yields from the RICO reaction

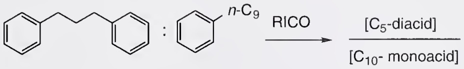

(102)

or

$$\sum_{C=3}^{C=16}(\text{number of bridges}) \,/\, \sum_{C=9}^{C=22}(\text{number of chains})$$

in the C_3–C_{16} range for bridges and C_9–C_{22} for chains. This ratio should be an expression of an intrinsic property of the asphaltene, reflecting its maturation history (thermal stress, availability and nature of catalysts, *etc.*). The upper limit for carbon numbers in the summation is dictated by the upper limit of C_{28} for the bulk of the naturally occurring *n*-alkanoic acids and *n*-alkanols. Higher carbon number molecules may arise from:

- a combination of two strains of alkanoic precursors;
- Friedel–Crafts type aromatic substitution with *n*-alkanols and *n*-alkanol-*n*-carboxylate;[157]
- transalkylation reactions;
- condensation of $\leq C_{28}$ compounds.

8.0 Micelles: to be or not to be?

Colloidal systems consist of a homogeneous medium and particles dispersed therein which have at least one dimension within the range of about 1 nm to 1 μm. Colloid chemistry has been termed the science of large molecules, small particles and surfaces. Most colloidal systems including petroleums are microheterogeneous and on multistage ultrafiltration the colloid particles are held back on filters with different pore sizes. On ultrafiltration of petroleum the asphaltene particles can be separated from the maltene with filters of pore diameter ≤ 35 nm. Employing a set of filters with successively smaller pore diameters down to 5 nm, a filtration residue remains on each filter. The asphaltene particles lie in the 10–35 nm range and the resin particles, in the 5–10 nm range. It has been reported that the removal of colloids (5–35 nm) from petroleum in general results in a light yellow dispersion medium which fluoresces with a light blue color. Thus, the brown-black color of petroleum arises from the colloidal asphaltene and resin contents.

Ultracentrifugation studies[177] in the late 1950s and ultrafiltration experiments[178] in the 1960s have shown petroleums to be polydispersed colloidal systems, as had been deduced earlier from flow behaviour and MW measurements. The MW of petroleum asphaltenes in solution shows a broad distribution continuum ranging from about 1,000 to several tens of thousands and even up to several hundred thousands depending on the method of determination and the experimental conditions. Using vapor pressure osmometry, the MW_Ns of most petroleum asphaltenes lie in the 2,500–6,000 domain and are dependent on concentration, temperature and the nature of the solvent. This dependence is a consequence and manifestation of the association equilibrium of the covalent asphaltene (and complexed resin) molecules to form aggregates or micelles in solution. GPC of highly dilute asphaltene solution permits direct observation of the slow MW decrease of colloidal asphaltene aggregates.

Micelle formation induces abrupt changes in various transport and equilibrium properties of solutions of highly surface-active materials with changing concentration. This is illustrated schematically in Figure 14.128 for the variation of osmotic pressure, turbidity, surface tension and molar conductivity with concentration for the case of aqueous solutions of sodium dodecyl sulfate. It is seen from these plots that at a fairly well-defined concentration, the rate with which these properties change with concentration abruptly increases or decreases. The rate of change for osmotic pressure decreases and that for turbidity increases, suggesting that at the critical concentration where all these changes take place, molecular association—micelle formation—becomes significant. The concentration where all the sudden changes take place is the critical micelle concentration (CMC). Fatty acid soap and simple detergent (like sodium dodecyl sulfate) micelles, which are the best investigated and understood micelles, are spherical in shape and have fairly well-defined aggregation numbers (which are dependent on the carbon chain length) with a value of ~50 for sodium dodecyl sulfate at the CMC at room temperature. Such surfactants are therefore nearly monodisperse.

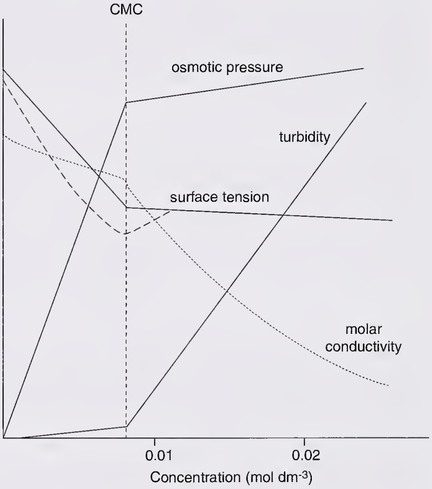

Figure 14.128 Physical properties of sodium dodecylsulfate solutions at 25°C. Reproduced, with permission, from D.J. Shaw, "Introduction to Colloid and Surface Chemistry", 3rd Ed., Butterworths, London (1980).

In the micelle, the lipophilic (preferentially organic solvent soluble) hydrocarbon chains of the dodecyl sulfate anions are oriented towards the interior of the micelle and the polar hydrophilic (preferentially water soluble) sulfate groups are on the outside in contact with the aqueous medium, giving rise to a spherical micelle, Figure 14.129. Above the CMC the spherical shape of the micelles becomes gradually distorted, changing into cylindrical rods or flattened disks and ultimately, at high concentrations of the surfactant, they form liquid crystals and other "mesomeric phases". The micelles are in dynamic equilibrium with the monomer in the solution and the monomers are associated with the micelle for only a very short time, of the order of 10^{-5}–10^{-6} s.

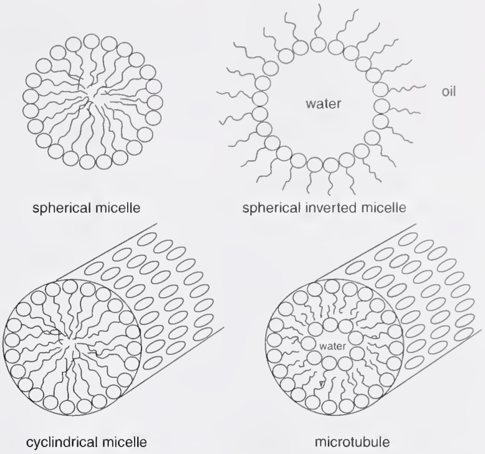

Figure 14.129 Simplified representations of different types of micelles. After R.J. Hunter, Foundations of Colloid Science, Vol. 1, Clarendon Press, Oxford, 1987.

The process of micellization is entropy-driven,[179] and the negative value of the free energy of micellization originates from the large positive value of the entropy of micellization since the enthalpy change of the process usually has a small positive or negative value:

$$\Delta G_{mic} = \Delta H_{mic} - T\Delta S_{mic} \qquad (103)$$

At first glance this would appear to be counter-intuitive for micellization—the aggregation of monomolecularly-dispersed surfactant molecules into micelles—because ΔS_{mic} would be expected to be negative. Therefore, the origin of the entropy increase must be the entropy increase of the water. In liquid water the molecules are associated by forming hydrogen bonds. When the hydrocarbon tail of a surfactant molecule is imbedded in the water one might assume that the hydrogen bonds will be ruptured and that the entropy of water will increase. This, however, is not the case; on the contrary, water molecules at the surface of the cavity form a more ordered network of hydrogen-bonded water molecules, as if the hydrocarbon chains were nucleation sites, with an attendant decrease in entropy. Now, removing the surfactant from the water and placing it in the micelle allows the cavity to revert to the structure of pure water. Thus, the highly-organized cavity walls return to a normal hydrogen-bonded liquid with an increase in entropy. The enthalphy difference between ordered water in the cavity and the hydrogen-bonded water in pure water is small, which explains the small value of ΔH_{mic}.

The explanation given above for the entropy-dominated association of surfactant molecules is called the hydrophobic effect. In terms of this hydrophobic effect micelle formation is accounted for, without reference to any special affinity between the associating species, as the expulsion of the surfactant molecules from the water.

The essential feature of aqueous micellar systems is that, as the monomer is introduced into the solution, its concentration reaches a critical value at which the concentration remains nearly stationary and any additional monomer introduced enters the micellar structure. Thus, aqueous micelles are a special type of supramolecules whose kinetics of formation are reminiscent of the phenomenon of phase equilibrium (constant vapor pressure of a liquid, constant concentration of a saturated solution) rather than the kinetics of chemical equilibrium. This behavior can be attributed to the requirement that energetically, some minimum value for n (the number of monomeric units) is necessary before the exclusion of hydrophobic tails from the aqueous medium becomes effective. Once the concentration of the monomer in the solution reaches the critical n value for aggregates to be formed, i.e. $(\text{monomer})_n \rightleftharpoons$ micelle, any additional amounts of an amphipathic molecule (a molecule consisting of two parts, each of which having an affinity for a different phase) added to the solution goes into the micelle. For this reason, aqueous micelles are sometimes called pseudophases.

Micelle formation is hindered by thermal motion and the repulsion between electric charges on head groups, if present, and consequently a low value for CMC would be expected to be favored by:

i) increasing length of the alkyl chain, as is found to be the case experimentally, *e.g.* for a C_8 chain the CMC is 140×10^{-3} mol·L^{-1} and for C_{18}, 0.23×10^{-3} mol·L^{-1} in the case of sodium *n*-alkyl sulfate in water at 40 °C;
ii) lowering the temperature, and
iii) addition of simple salts for the case of ionic surfactants.

Micellization may occur in nonaqueous solvents as well but nonaqueous micellar systems differ in their basic properties from aqueous systems as will be discussed below.

Asphaltene dissolved in an organic solvent represents quite a different system than simple soap or analogous detergent solutions with respect to molecular composition, size, shape and distribution of polar and nonpolar groupings and, even more importantly, with respect to heterogeneity of composition and size distribution. Consequently, in asphaltene solutions the micelles that can form will have no resemblance to the well-defined micelle structures and shapes of surfactants. Nevertheless, numerous studies published in the literature[180] since the early 1980s of the interfacial tensions and other properties of asphaltene solutions along with the heat of dilution of concentrated solutions of asphaltene in organic solvents show the existence of a CMC, Figure 14.130, and the presence of micelle-like aggregates. When a concentrated toluene solution of asphaltene, 50 g·L^{-1}, was diluted with 2,4-dimethylpyridine, which is a considerably better solvent than toluene, the micelles became more extensively solvated and partly broke up to smaller aggregates or to monomeric covalent molecules. The process of dilution is accompanied by the evolution of heat, that is, ΔH_{dil} is negative. The heat that evolved per gram solute was lower above the CMC, which had a value of 3.9 g·L^{-1}, than below the CMC, implying that the break-up of the micelles is an endothermic process. An approximate value for the micellization enthalpy could then be estimated from the difference of the extrapolated line representing the monomeric portion of the plot and the experimental line above the CMC. This procedure gave $\Delta H_{mic} \approx -7$ J/(g·L^{-1} asphaltene) above a concentration of 4 g·L^{-1} asphaltene, which may be compared to the range reported for ionic and nonionic surfactants: $\Delta H_{mic} = -6$ to $+16$ kJ·mol^{-1}.

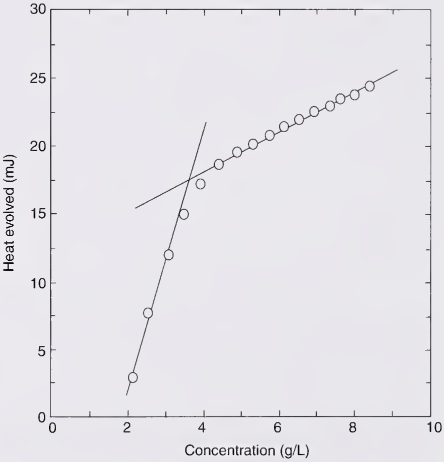

Figure 14.130 CMC determination of asphaltenes in 2,4-dimethylpyridine from calorimetric titration curve. From S.I. Anderson and K.S. Birdi, Ref. 180. © 1991, Academic Press.

The value of the CMC determined in this way, 3.9 g·L^{-1}, is quite low, in fact lower than the concentrations where most of the physical measurements reported in the literature on asphaltene solutions have been performed. Therefore, practically all the data in the literature on the properties of asphaltene solutions appear to apply to the micellar state rather than to the monomeric state of asphaltene. CMC values reported in the literature in the 1980s and 1990s ranged from 0.25 g to 4.9 g asphaltene/L of solvent.

Ternary mixtures of asphaltene, a solvent and a precipitant have CMC's which are dependent on composition. With increasing precipitant content in the mixture the composition approaches the precipitation point of asphaltene—that is, the compatibility of asphaltene with the solvent mixture decreases—and the asphaltene is expected to aggregate more readily.

Asphaltene has been treated in the literature as an inverted micelle in its natural state, in which the polar groups are oriented toward the center, Figure 14.129. The driving force for the orientation of the polar groups towards the center was thought to originate from hydrogen bonding, charge transfer or salt formation. Indeed, micelles are known to exist in nonaqueous solvents and the aggregation of surfactants has been investigated in various organic solvents although much less extensively than in water.

As was mentioned above, micellization in nonpolar media differs in several important aspects from aqueous aggregation. The most prominent of these differences is the absence of the hydrophobic effect. In aqueous micellization the amphipathic species are relatively passive, they are squeezed out of solution by the water. In contrast to this, the amphipathic molecules in nonpolar solvents play an active role in the formation of inverted micelles which are held together by specific interactions between the "head" groups in the core of the micelle. The solubility parameter difference between the alkyl or hydrocarbon tail of the amphipathic molecule and the solvent can be a stabilizing influence and a contributing factor to inverted micelle formation. In this respect, for example, the enthalpy and entropy values measured for the micellization of potassium benzenesulfonate in heptane, $\Delta H_{\text{mic}} = -79.5$ kJ·mol^{-1} and $\Delta S_{\text{mic}} = -62.8$ J·K^{-1}·mol^{-1} are revealing and show that, in contrast to aqueous systems, the large negative value of the free energy of micellization comes from the large negative enthalpy change and that the entropy change opposes micellization. Another difference between aqueous and nonaqueous systems is the size of the initial aggregate formed. For aqueous micelles *n* has values of the order of 30–50 or higher, while for the inverted micelles *n* has values of ten or less. The corollary of the small aggregation numbers is the breakdown of the phase model for micellization and the more appropriate applicability of the chemical equilibrium model. When the micelle is very small the whole picture of a polar core shielded from a nonaqueous medium by a mantle of lyophilic (solvent soluble) tail groups is no longer valid.

An unexpected turn in our understanding of the micellization of asphaltene solutions took place very recently. In 2000 it was reported[165] that the interfacial tension of Athabasca and Cold Lake asphaltene solutions in 1,2-dichlorobenzene or in toluene *vs* water varied linearly with concentration on a logarithmic scale, Figure 14.131, without the expected break, characteristic of micellar systems, indicating the absence of micelle formation. This follows from the known relation of a linear decrease in surface tension with the logarithm of increasing surfactant concentration when the interface is saturated with surfactant at equilibrium with the bulk phase. However, reaching the CMC, the surface tension becomes constant because all additional surfactant molecules entering the system become part of the surface-inactive micelle and thus the concentration of free surfactant molecules remains unchanged.

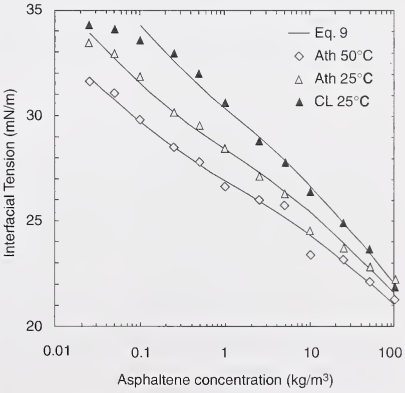

Figure 14.131 Interfacial tension of Athabasca (Ath) and Cold Lake (CL) *n*-C_5 asphaltenes in toluene *vs* water. The departure from linearity is the consequence of using mass concentration instead of molar concentration. From H.W. Yarranton *et al.*, Ref. 165. © 2000, American Chemical Society.

In the following year it was reported[170] that moisture in the solution profoundly influences the aggregation behavior of asphaltene. In meticulously dried solvents, the break in the plot of heat of dilution evolved during isothermal calorimetric titration *vs* asphaltene concentration disappeared, indicating a stepwise association rather than a classical micellar association, Figure 14.132. Repeating the same experiment in the presence of 0.013% water in the solvent caused the plot to show the familiar curvature characteristic of micellar systems. Moreover, it was also found that the value of the CMC is function of the quantity of water present, Figure 14.133 exhibiting a bell-shaped relation. The presence of water also affects the solubility of asphaltene in the solvent toluene: the asphaltene solubility of 80 g·L^{-1} in dry toluene dropped to 30 g·L^{-1} in water-saturated toluene (0.047% w/w). Conversely, the solubility of water in toluene exhibited a nearly linear increase with asphaltene concentration and at 20 g·L^{-1} asphaltene concentration it rose from 0.047% (in the absence of asphaltene) to 0.1%. In the intermediate range between 0. 2 and 8–20 g·L^{-1} asphaltene, there appeared to be some departure from linearity, which was interpreted as being caused by the restructuring of the water–asphaltene aggregates, leading to a better uptake of water.

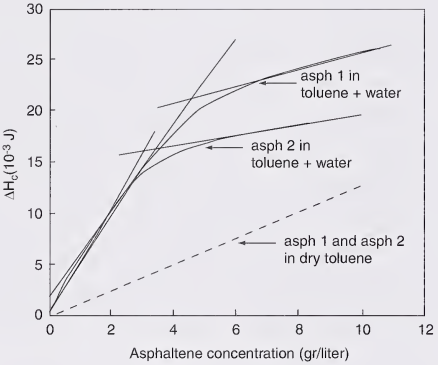

Figure 14.132 Cumulated heat of titration *vs* asphaltene concentration in toluene in the absence and presence of water (0.013%) for two different asphaltenes. From S.I. Andersen *et al.*, Ref. 170. © 2001, American Chemical Society.

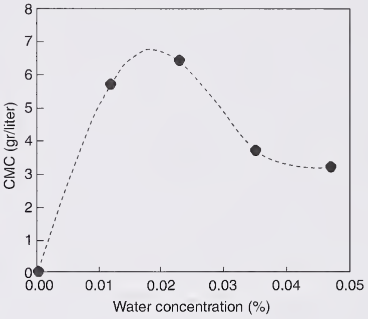

Figure 14.133 Apparent CMC of an asphaltene *vs* water content in toluene at 35 °C. From S.I. Andersen *et al.*, Ref. 170. © 2001, American Chemical Society.

The effect of resin content on the behavior of asphaltene was also reported for one particular asphaltene. Interestingly, the titration plot for 0.01% water content featured a significantly different behavior for *n*-C_7 asphaltene and *n*-C_5 asphaltene: the former was characterized by a relatively high heat of dilution and a CMC of about 3 g·L^{-1} whereas the latter, by a much lower heat of dilution and no CMC.

An average value for the Gibbs free energy of the transference of water into the solution was also determined to be around –13.4 kJ·mol^{-1} at 293 K, which lies in the lower range of hydrogen bonding.

The observations and data described above point to the role of the formation of water bridges *via* hydrogen bonds connecting asphaltene species. It was estimated that 1.2 molecules of water associate with one molecule of asphaltene (of MW 1,000 g·mol^{-1}) and therefore there is the possibility of multiple bridge formation in any given asphaltene species:

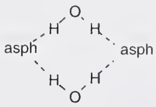

In the case of monomeric asphaltene molecules, 2.4 bridges are possible and in the case of asphaltene aggregates, *e.g.*

$$\text{asph}_n\text{---}\ (\text{HOH})\text{---}\ \text{asph}_n$$

2.4n bridges are possible on the average. Alternatively, these water molecules may be present as microdroplets in the polar inner core of the asphaltene reverse "micelle". The relatively low value of the hydrogen bond strength then explains the observation that the presence of the difference resin (n-C_5 asphaltene – n-C_7 asphaltene) can affect the behavior of the asphaltene. Resins are the best solvents for asphaltene and, for example, possess an order of magnitude larger heat of solution for asphaltene compared to toluene or xylene. Therefore, they can be expected to bind much more strongly to the active binding sites in the asphaltene than the water molecule.

Bridge formation would lead to increases in the MW of the asphaltene. This effect, in conjunction with the occupancy of the surface-active sites by the water molecule, blocking them from the solvent molecules, would lead to the lowering of the solubility of the asphaltene—as has been experimentally observed.

Lastly, enthalpies of dissociation were estimated from calculations[181] on hypothetical model asphaltene molecules. The experimental data, –1 to –2.1 kcal·mol^{-1}, agree with the computed data for a water bridge between two nitrogen atoms in two different asphaltene molecules, –2.1 kcal·mol^{-1}. The heat of aromatic stacking of the same two asphaltene molecules has also been calculated and found to be –6.3 kcal·mol^{-1}, significantly higher than for the water bridges.

Properties of micelles have been investigated by various methods, *e.g.* surface tension, viscosity, SANS, SAXS measurements. The kinetics of micellization, for example, have been probed through measurements of surface tension.[182,183] Here, asphaltene solutions below and above the CMC were demicellized by heating the solution to elevated temperatures, 250 °C, for a period of time and then the temperature was rapidly quenched, during which the surface tension was monitored as a function of time, Figure 14.134. In both cases a drop in surface tension was observed that was attributed to increased concentrations of adsorbed asphaltenes at 250°C due to less solvation of the asphaltene molecules. The plot in Figure14.134a is for an asphaltene solution below the CMC and Figure 14.134b is for an asphaltene

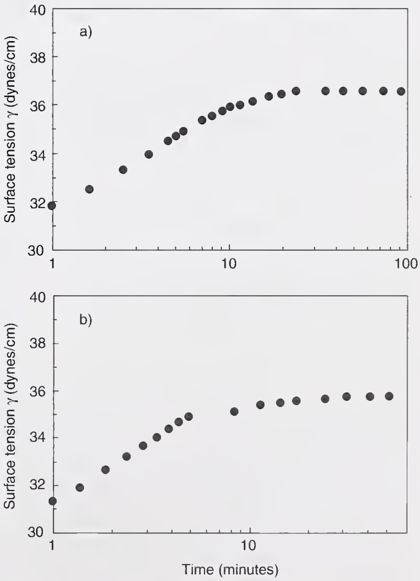

Figure 14.134 Dynamic surface tension of a) 0.01 wt% and b) 0.5 wt% asphaltene in pyridine as a function of time after quenching to 25 °C. From E.Y. Sheu, Ref. 183. ©1996, IOP Publishing Ltd.

concentration above the CMC. In the latter case at least two distinct processes may be anticipated, desorption of asphaltene molecules from the surface layer (plus their solvation), and their micellization. If this assumption is correct then it may be possible to observe both processes sequentially in the solution with concentration above the CMC and to observe only one process, desorption, in the solution with concentration below the CMC. Employing the simple kinetic equation

$$\gamma(t) = \gamma_\infty[1 - e^{-kt}] \tag{104}$$

where γ is the surface tension and k is the rate constant which can be determined from the plot of ln $(1 - \gamma(t)/\gamma_\infty)$ *vs* t, Figure 14.135. When the concentration is greater than the CMC, k(desorption) = 0.36 min^{-1} and, as seen from Figure 14.135b, the desorption step is followed by the slower self-association step with a rate constant of 0.13 min^{-1}, that is the micellization tends to slow down the desorption. The kinetic equation (104) decribes the reaction rate of a process which is first order in the concentration of the reactant. Whereas it is easy to see that the desorption step would obey first-order kinetics, it is not so easy to rationalize how the aggregation step could be a first-order process. The slow rate of both processes is an indication that they have some activation energies associated with them. Obviously, the restoration of room-temperature equilibrium involving water is a more complex reaction system than that indicated by the simple rate equation.

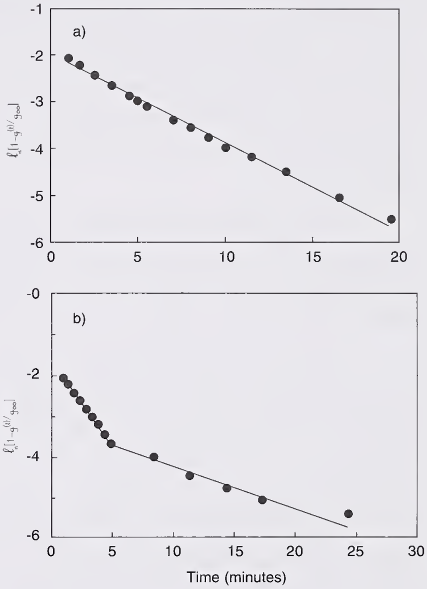

Figure 14.135 Plots of Eq. (104) for a) 0.01 wt% and b) 0.5 wt% asphaltene in pyridine. From E.Y. Sheu, Ref. 183. © 1996, IOP Publishing Ltd.

Viscosity, SANS and SAXS measurements have been used to study the aggregation of asphaltene in toluene /*n*-heptane solutions.

Intrinsic viscosities of asphaltene solutions in toluene /*n*-heptane were measured as a function of solvent compositions, Figure 14.136.[184] The intrinsic viscosity is defined as

$$[\eta]_{\text{intr}} = \lim_{\theta \to 0} \frac{\eta_{\text{rel.}} - 1}{\theta} \tag{105}$$

where θ is the volume fraction of asphaltene and η_{rel} is the ratio of solution viscosity to solvent viscosity. The value of $[\eta]_{\text{intr}}$ is obtained from the slope of the relative viscosity *vs* asphaltene volume fraction plot at low volume fractions. The intrinsic viscosity varies with the heptane content in the solvent, as seen in Figure 14.137. Now the intrinsic viscosity has been suggested to be a measure of the ratio of the hydrodynamic volume of the aggregate (containing asphaltene and solvating solvent trapped inside the particle) to the volume occupied by the asphaltene only:[186]

$$V_{\text{hydro}}/V = [\eta]/2.5 \tag{106}$$

The changes in intrinsic viscosities with heptane content in the solvent then reflect variations in the hydrodynamic volume of the aggregates. The variations are the results of two opposing

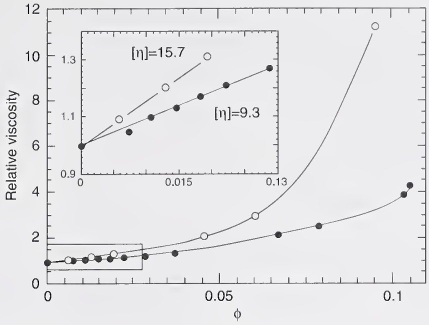

Figure 14.136 Relative viscosities *vs* volume fractions, ϕ, for an asphaltene in pure toluene (●) and in 55/45 wt% toluene/heptane (O). The intrinsic viscosities [η] correspond to the slopes of the linear portion of the viscosity curves at low volume fractions (inset). From D. Fenistein *et al.*, Ref. 184. © 1998, American Chemical Society.

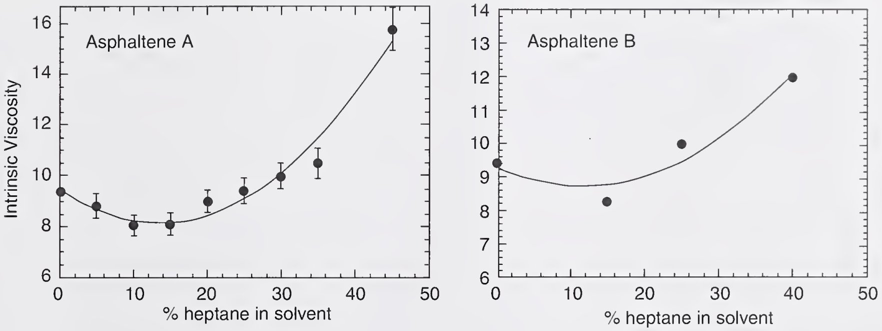

Figure 14.137 Intrinsic viscosities of asphaltenes A and B as a function of heptane concentration in toluene. From D. Fenistein *et al.*, Ref. 184. © 1998, American Chemical Society.

effects, a desolvation (densification) of the aggregates (induced by the decrease in solvent power) and an aggregation between asphaltene entities (induced by an enhanced attraction). As seen from Figure 14.137, at low heptane concentrations desolvation, which lowers $[\eta]_{intr}$, is more important than aggregation, which increases $[\eta]_{intr}$. But above 15% heptane, aggregation accelerates, causing rapid increases in $[\eta]_{intr}$.

SANS studies, which are capable of providing more quantitative information on the aggregation process, were also carried on this same system.[184] Weight average MW_Ws and weight average molecular volumes, V_W, of aggregates were measured at various percentage concentrations of fully deuterated *n*-heptane in fully-deuterated toluene solutions. The results, tabulated below,

n-C_7, %	MW_W/g·mol^{-1}	V_W/Å^3
0	112,800	157,300
15	132,500	184,900
35	328,600	458,400
45	1,178,600	1,644,00

show a modest increase in MW_W and a corresponding increase in V_W upon addition of 15% *n*-C_7 to toluene, but upon further dilution the MW_W and V_W increase rapidly. From the scattering measurements another volume, the effective volume—representing asphaltene plus solvent trapped inside—the analog of the hydrodynamic volume, can be defined as:

$$V_{\text{scatt.}} = 4/3\pi(5/3)^{3/2}R_{gz} \qquad (107)$$

where R_{gz} is the z-average radius of gyration. The ratio

$$V_{\text{hydro}}/V_{\text{scatt}} = \Psi = \frac{2\eta}{5}\;\frac{3\,V_w}{4\pi R^3_{gz}(5/3)^{3/2}}$$

has values between 0.3 (at 15% n-C_7) and 0.15 (at 45% n-C_7) meaning that V_{scatt} is about 3.4 to 6.6 times larger than V_{hydro}. The ratios of the asphaltene to the total volume of the aggregate, V_W/V_{scatt} and V/V_{hydro}, are different and both are small, with values of 2–3% and 15–20% for 45% n-C_7.

The above results have been interpreted[184] to show that asphaltenes, instead of being dense objects, form open aggregates in solution, and the largest of these aggregates have a self-similar internal structure characterized by an apparent (fractal) exponent (d, such that $MW_W \sim R^d_{gz}$) with a value of about 2 (for distances intermediate between the size of the whole aggregate and the size of the structural unit). It also describes how the MW of the whole asphaltene aggregate increases with its size (radius of gyration) when the heptane fraction in the solution is increased. Because this exponent is well below 3, it has been stated that these aggregates cannot be described by the conventional model of solvated spherical molecules, "although there is a possibility that their structural units are the result of some micellar type of association between molecules". From these considerations, the asphaltene aggregates studied have been classified as belonging to the nonequilibrium, reaction-limited colloidal aggregation (RLCA) model colloidal system. The nonequilibrium aggregation processes lead to aggregates that progressively fill up the whole space and gradually penetrate into each other, resulting in equilibrium-quiescent gels after long enough times.

In RLCA, the structural units come into contact by diffusion, but the interparticle interaction potential displays a potential barrier ΔV that needs to be overcome for the entities to join, Figure 14.138.[184]

Support for the existence of a potential barrier comes from the observation of a slow variation in the SANS scattering spectra[186] in dilute solutions of asphaltene, and increases in the viscosity[187] over periods of many days.

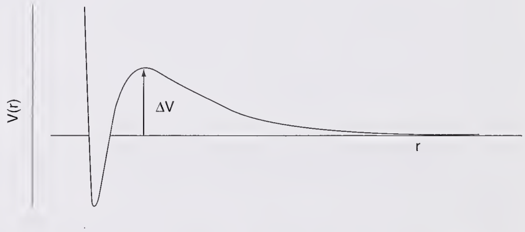

Figure 14.138 Schematic form of interparticle potentials V(r) as a function of the interparticle distance r for RLCA. From D. Fenistein *et al.*, Ref. 184. © 1998, American Chemical Society.

The results of these physical measurements and their interpretation, specifically the openness of the aggregate structure, the smallness of the ratio of asphaltene to the total volume of the aggregate, and the existence of a potential energy barrier for aggregation, are consistent with the looseness of the molecular structure derived from chemical studies.

As was noted from the data in the table above, the MW_Ws are all large numbers. The number average MW_N was not reported in reference 184 but SANS and SAXS MW_W and MW_N values have been given in other publications. The one quoted here[188] reports MW_W and MW_N values for a 2% asphaltene solution in toluene as 113,000 and 64,800 from SANS measurement and 105,170 and 13,226 g·mol^{-1} from SAXS measurement (same sample). SANS measurements were done in deuterated toluene because scattering is on the nuclei of hydrogen and deuterium and the contrast term between them is large. SAXS measurements were done in toluene and here, scattering is on the electrons and the contrast term between polynuclear condensed aromatics and toluene is large. As seen from the data, the MW values are all large even for MW_N and especially in the SANS data. The reason for the high values, and the differences beween the SAXS and SANS results have not been adequately explained. The scattering methods probe not only the solute, as do the VPO and colligative methods, but the solvation and internally-trapped solvents associated with the molecule/aggregate as well. The binding energies for the solvents evidently are too low for the VPO method to perceive them as being part of the aggregate.

In these scattering measurements the asphaltene concentrations were kept low in order to avoid interference from interparticle interactions. For concentrated solutions, other approaches are needed. One of these, with attention to concentrated regimes,[189] is said to characterize the data in terms of a correlation length which is indicative of proximity to phase separation, rather than the radius of gyration, which is more indicative of individual colloids. In a binary mixture of particles A and B, the correlation length characterizes the length over which a region is "A" rich as opposed to "B" rich. The correlation length varies with the position to phase separation and as the critical temperature and concentration associated with phase separation is approached, the correlation length increases and ultimately diverges at the critical point. In a single-phase mixture of any number of components the concentration will fluctuate and thus a correlation length can be measured. The lack of phase separation does not imply lack of structure aside the length scale of the constituent molecules. Figure 14.139 depicts the variation of correlation length (obtained from X-ray scattering measurements) for n-C_7-separated Cold Lake asphaltene in n-dodecane/1-methylnaphthalene solutions. With decreasing aromaticity the correlation length increases until precipitation begins at the maximum.

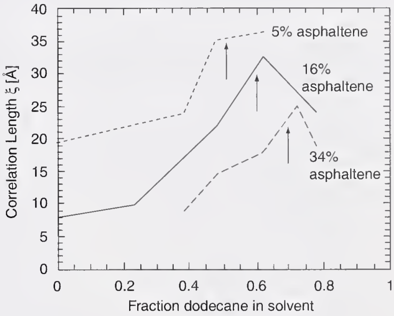

Figure 14.139 Measured correlation length *vs* weight fraction of dodecane in the solvent 1-methylnaphthalene for three concentrations of asphaltenes. The arrows indicate approximately where phase separation occurs. After E.B. Sirota, Ref. 189.

When dry asphaltenes are studied, a peak in the scattering appears at a wave vector, $q = 2\pi/d$, corresponding to a distance $d = 38$Å. The shape of the curve indicates short-range local order and the existence of a characteristic "inter-object distance". According to the author,[189] it does not reveal the size of an object, but rather the average distance between the centers of neighboring objects. One way of elucidating local structures is to "swell" the system with a solvent and observe the behavior of the scattering curve, indicating that the maximum shifts to smaller wave vectors, q, with increasing dilution. From the shape of the variation of the interparticle distance with dilution, it is possible to determine that swelling is two-dimensional (*vs* $MW_W \sim R_{gz}^2$) indicating **locally** rod-like entities where the solvent increases their separation. The conclusion from this study is illustrated by the phase diagram shown in Figure 14.140 where the concentrated single-phase solutions of asphaltene are viewed as "swollen asphaltenes".

The one disturbing element in the results is the relationship between dilution of asphaltene in a good solvent and correlation length, predicting increasing correlation lengths with increasing dilution, which is contrary to intuitive expectation and experiment.

There are numerous studies in the literature reporting on the size and shape of asphaltene particles in various solvents. These are collected in Table 14.39.

The size and shape variation with temperature is an interesting phenomenon which has potential implications with respect to the thermal processing of crude oils.[190]

Pressure also has an effect on asphaltene aggregation,[191] as concluded from SAXS measurements: decreasing pressure causes increasing aggregation, and this can have important consequences in oil recovery and high-pressure refining operations. This conclusion is in agreement with experimental measurements (*cf.* Section 2.2.4).[57]

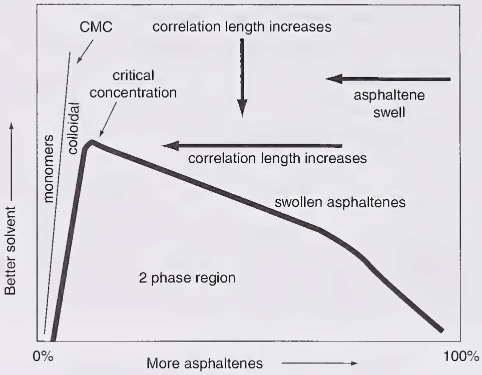

Figure 14.140 Schematic phase diagram of asphaltenes and solvent quality. After E.B. Sirota, Ref. 189.

Table 14.39 Shapes and sizes of colloidal asphaltenes from different studies

Solvent	Shape	Ave. particle radius, Å	Ref.
cis-decahydro-naphthalene	polydisperse sphere	43–44	1
mineral oil		44–56	1
benzene	monodisperse sphere	43–44	2
decalin		43–52	2
benzene, THF, pyridine	polydisperse disk-like	45–90	3
toluene	polydisperse sphere	30–60; 30–32; 33	4–6
toluene	polydispersed sphere[a]	33	7
toluene	polydispersed fractal aggregate[b]	61	8
toluene	polydispersed fractal aggregate[b]	69	8
resid oil	polydispersed sphere	30–60	9
d_{10}-1-methylnaphthalene, 20 °C	rod, polydispersed in length	$20 \times 2–5 \times 10^2$	10
d_{10}-1-methylnaphthalene, 200 °C	rod, polydispersed in length	12×65	10
d_{10}-1-methylnaphthalene, >340 °C	uniform spheres	12	10
toluene XAXS[c]	disk-shape, height 10	8–160	11
toluene, SANS[c]	disk-shape, height 8	8–20	11

[a] Athabasca asphaltene. [b] Fractal exponent $MW_w \sim R_{gz}^2$. [c] Same sample.

References: 1. C.W. Dwiggins, J. Phys. Chem., 69 (1965) 3500. 2. S.S. Pollack and T.F. Yen, Anal. Chem., 42 (1970) 623. 3. J.C. Ravey, G. Ducouret and D. Espinat, Fuel, 67 (1988) 1560. 4. E.Y. Sheu, K.S. Liang, S.K. Sinha and R.E. Overfield, J. Colloid Interface Sci., 153 (1992) 399. 5. D.A. Storm, E.Y. Sheu and M.M. De Tar, Fuel, 72 (1993) 977. 6. E.Y. Sheu, D.A. Storm and M.M. De Tar, J. Non-Cryst. Solids, 131–133 (1991) 341. 7. Y. Xu, Y. Koga and O.P. Strausz, Fuel, 74 (1995) 960. 8. D. Fenistein, L. Barré, D. Broseta, D. Espinat, A. Livet, J.-N. Roux and M. Scarsella, , Langmuir, 14 (1998) 1013. 9. R.E. Overfield, E.Y. Sheu, S.K. Sinha and K.S. Liang, Fuel Sci. Technol. Int., 7 (1989) 611; E.Y. Sheu, K.S. Liang, S.K. Sinha and R.E. Overfield, Prep.–Pap. Am. Chem. Sic. Div. Petrol. Chem., 35 (1990) 813; E.Y. Sheu, M.M. De Tar, D.A. Storm and S.J. DeCanio, Fuel, 71 (1992) 299. 10. R.E. Winans and J.E. Hunt, “An Overview of Resid Characterization by Mass Spectrometry and Small Angle Scattering Techniques”, Prepr. Pap.—Am. Chem. Soc., Fuel Chem., 42 (1999) 725. 11. Ch. Bardon, L. Barré, D. Espinat, V. Guille, M.H. Li, J. Lambard, J.C. Ravey, E. Rosenberg and T. Zemb, Fuel Sci. Technol. Int., 14 (1996) 203.

Progress of aggregation in the solution phase ultimately leads to phase separation and the precipitation of solid asphaltene. In the solution phase, increasing aggregation is accompanied with an increasing degree of solvation and amount of solvent incorporation into the aggregate. However, at some point in the course of precipitation the asphaltene must undergo desolvation but the mechanism of this process is not known. The appearance of the solid asphaltene particle then requires a different detection method from the SAXS, SANS methods employed for the study of the aggregates in the solution phase. In one of the studies to be described a commercial Laser Particle Analyzer (LPA), based on the time resolved attenuation of the incident laser beam intensity was employed and in a second study photon correlation spectroscopy, based on the broadening of light scattering spectrum which then can be related to the mean particle size in the scattering medium was employed.

For self evident reasons in technological problems caused by asphaltene aggregation, the size, shape and composition of the asphaltene aggregates may be critical process parameters. In order to gain insight into the governing factors that determine these properties of the aggregates, studies have been carried out on the effect of asphaltene content of the parent oil, precipitant-to-oil ratio, temperature and pressure on the particle size distribution. Some aspects of the kinetics of the flocculation process have also been explored.

Employing the LPA it was determined[192] that in the precipitant-to-oil ratio domain of 5:1 to 10:1 the asphaltene aggregate average particle size is described by a unimodal, log-normal distribution, Figure 14.141, although in some cases bimodal distribution composed of two log-normal distribution fitted the data. As the figure shows, the mean particle size is a function of the precipitant-to-oil ratio and tends to shift from 196 ± 59 µm at 5:1 *n*-C_7:Cold Lake bitumen volume ratio to 286 ± 82 µm at 40:1 *n*-C_7:bitumen volume ratio. It was also found that in the *n*-C_7:bitumen volume ratio change of ca 8–40 the total amount of asphaltene flocculated and the mean particle size of the asphaltene particles increased in nearly the same proportion indicating that the weight increase was mainly due to the increase in size of the already flocculated particles. The particle size distribution also had a strong dependence on the asphaltene content of the crude; light crudes with asphaltene content of 0.5–0.8 wt% produced precipitates with mean particle sizes of 4.5 ± 1.2 µm and heavy oils with asphaltene content 9.2, 12.2 and 18.1 wt% generated precipitates with mean particle sizes of 210 ± 65, 221 ± 68 and 291 ± 78 µm, respectively at the 40:1 *n*-C_7-to-crude volume ratio.[192]

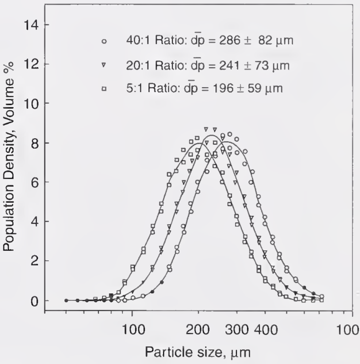

Figure 14.141 Particle size distributions: Cold Lake bitumen with *n*-heptane at three volume ratios. From K.A. Ferworn *et al.*, Ref. 192. © 1993, American Chemical Society.

Overall, the results obtained[193] on four crude oils using *n*-C_5 as precipitant suggest, with the exception of one oil, a slight increase of the mean asphaltene particle size with an increase in pressure and with a decrease in temperature, Figure 14.142; however, no effect of crude oil molar mass is apparent.

In experiments with the two highest molar mass crude oils (Cold Lake bitumen and an oil with molar mass of 483 kg·kmol^{-1}) "superagglomerates" were observed[193] at T ≥ 75°C which is attributed to the softening and adhesion of asphaltene particles.

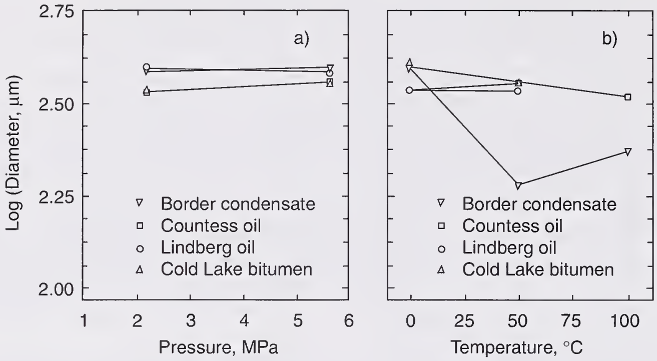

Figure 14.142 Effects of pressure and temperature on mean asphaltene particle size: a) at 0°C, b) at 2.2 MPa. From B.B. Nielsen *et al.*, Ref. 193. © 1994, Americal Chemical Society.

Precipitation of asphaltene in the above-mentioned studies was brought about by the addition of a fairly large excess, ≥ 5 volume ratio, of precipitant to the neat crude or bitumen. In the studies described below[194] a lower proportion of the precipitant, ≤ 3 was added to a toluene solution of the oil. This, then permitted to explore the kinetics of the early phases of the flocculation process.

The kinetics of flocculation slightly above the threshold seen in Figure 14.143 show the growth of the asphaltene particles in time. This growth process extends to a period of 1.5–2 hours.

In the asphaltene flocculation two processes can be distinguished which can be separated by a slight shaking of the suspension, Figure 14.144. Without shaking, the process of flocculation goes on continuously by forming fractal-like flocs with a very loose structure. Above a size of 1.5–2 µm the growth of flocs is accompanied by sedimentation. The fractal aggregates are very unstable: a slight shaking destroys them, leading to the formation of particles of a very stable size—the basic aggregates. However, the formation of the fractal flocs restores immediately after the shaking stops, Figure 14.145. The characteristic time of formation of the basic aggregates, when the particle size is being saturated is about one hour, but for a given oil changes with the toluene-to-*n*-C_7 ratio, Figure 14.146.

Based on the above observations the flocculation of asphaltene can be divided into three stages:

- the first is a nucleation stage corresponding to the formation of asphaltene clusters of critical size (observable by SAXS and SANS methods) and leading to the appearance of very small (0.05 µm) basic aggregates (requiring several minutes);
- during the second stage the clusters grow into the basic aggregates by absorbing smaller particles from the solution; and
- the third stage is the formation and growth of the fractal structures.

As is evident from the foregoing, the flocculation of asphaltene is a complex process, the understanding of which may provide means to the control of aggregate size, distribution and structure.

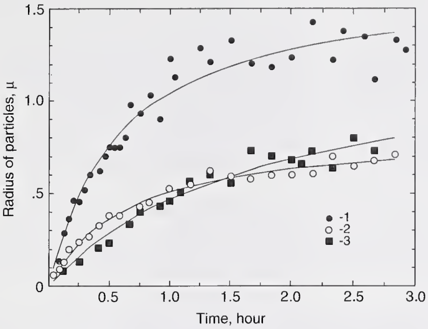

Figure 14.143 Initial stage of flocculation: 1. Arabian Light, 35/65 toluene/*n*-C_7; 2. Boscan, 25/75; and 3. Arabian Heavy, 35/65. From M.A. Anisimov, *et al.*, Ref. 194. © 1995, American Chemical Society.

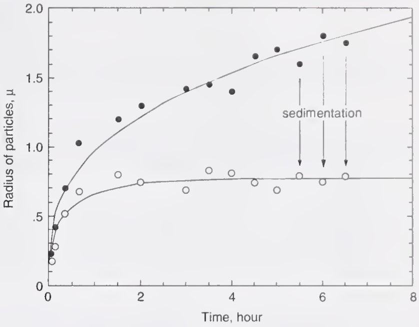

Figure 14.144 Two mechanisms of asphaltene flocculation in toluene/*n*-C_7 solution. From M.A. Anisimov, *et al.*, Ref. 194. © 1995, American Chemical Society.

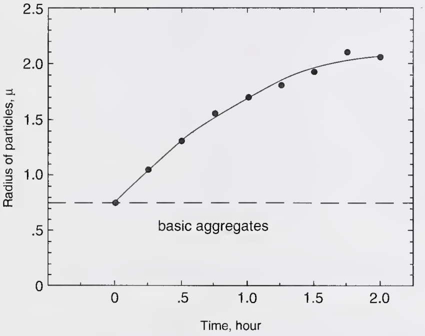

Figure 14.145 Fractal aggregate formation. Zero time is the moment when shaking stops. From M.A. Anisimov, *et al.*, Ref. 194. © 1995, American Chemical Society.

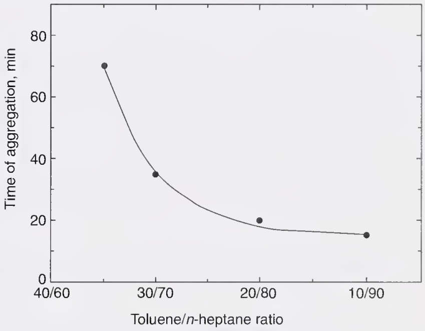

Figure 14.146 Characteristic time of basic aggregate formation as a function of toluene/*n*-C_7 volume ratio. From M.A. Anisimov, *et al.*, Ref. 194. © 1995, American Chemical Society.

Bibliography

1. B.C. Bockrath and F.K. Schweighardt, "Coal Derived Asphaltenes" in *Chemistry of Asphaltenes*, Advan. Chem. Series 195, J.W. Bunger and N.C. Li, Eds., American Chemical Society, Washington, D.C., 1981.
2. J. Marcusson, "The Chemical Structure of Natural Asphalts", Z. Angew. Chem., 29 (1916) 346.
3. O.G. Strieter, "Determining the Components of Asphalts and Crude Oils", Nat. Bureau of Standards J. Res., 26 (1941) 415.
4. D.S. Pasternak and K.A. Clark, "The Components of the Bitumen in Athabasca Bituminous Sand and Their Significance in the Hot Water Flotation Process", Research Council of Alberta Report No. 58, 1951, Edmonton, Canada.
5. a) J. Marcusson, "The Optically Active Constituents of Petroleum", Chem.-Z., 31 (1907) 419. b) H.P. Walden, "Optical Activity and Origin of Petroleum", Chem.-Z., 30 (1906) 1155. c) R. Zsigmondy, *Zur Erkenntnis der Kolloide*, Jena, 1905.
6. F.J. Nellensteyn, "Manufacture and Constitution of Asphaltic Bitumen", Dissertation, Technische Hoogeschool, Delft, 1923; "Theoretical Aspect of the Relation of Bitumen to Solid Matter", World Petr. Congr. Proc., 2 (1933) 616; J. Inst. Petr. Technol., 10 (1924) 311.
7. J.Ph. Pfeiffer, *The Properties of Asphaltic Bitumen*, Elsevier, Amsterdam, 1950.
8. J.Ph. Pfeiffer and R.N. J. Saal, "Asphaltic Bitumen as Colloid System", J. Phys. Chem., 44 (1940) 139.
9. J. Murgich, D. Merino-Garcia, S.I. Andersen, J.M. del Rio and C. Lira-Galeana, "Molecular Mechanics and Microcalorimetric Investigations of the Effect of Molecular Water on the Aggregation of Asphaltene in Solutions" Langmuir, 18, (2002) 9080.
10. G. Gonzales, S.M. Saraiva and L.C. doc. Marques, "Electrokinetic Study of Asphaltene Particles", 1st Int. Symp. Colloid Chem. in Oil Prod., Rio de Janeiro, 1995, Abstracts p. 224.
11. D.L. Mitchell and J. G. Speight, "The Solubility of Asphaltenes in Hydrocarbon Solvents", Fuel, 52 (1973) 149.
12. L.W. Corbett and U. Petrossi, "Differences in Distillation and Solvent Separated Asphalt Residua", Ind. Eng. Chem. Prod. Res. Dev., 17 (1978) 342.
13. J.H. Hildebrand, "Solubility", J. Am. Chem. Soc., 38, (1916) 1452; "Solubility and Internal Pressure", *ibid.*, 39, (1917) 2297; J. Hildebrand and R. Scott, *Solubility of Non-electrolytes*, 3rd Ed., Reinhold, New York, 1949.
14. J.H. Hildebrand, J.M. Prausnitz and R.L. Scott, *Regular and Related Solutions*, Van Nostrand Reinhold, Princeton, N.J., 1970.
15. a) Ch. Hansen and A. Beerbower, "Solubility Parameters" in *Kirk–Othmer Encycl. Chem. Technol.*, 2nd ed., Suppl. vol., A. Standen, Ed., Wiley, New York, 1971; b) A.F.M. Barton, *CRC Handbook of Solubility Parameters and Other Cohesion Parameters*, 2nd ed., CRC Press, Boca Raton, 1991; c) R.C. Weast, *CRC Handbook of Chemistry and Physics*, 68th ed., CRC Press, Boca Raton, 1987.
16. F.J. Nellensteyn, "The Relation of the Micelle to the Medium in Asphalt", J. Inst. Petr. Technol., 14 (1928) 134.
17. J.W.A Labout, "Constitution of Asphaltic Bitumen" in *The Properties of Asphaltic Bitumen*, J. Ph. Pfeiffer, Ed., Elsevier, Amsterdam, 1950, p. 28.
18. F. Sutherland, "A Proposed Model of Asphaltene Solution Behaviour", MSc Thesis, Imperial College, London, 1982.
19. N.E. Burke, R.E. Hobbs and S.F. Kashou, "Measurement and Modeling of Asphaltene Precipitation", J. Petr. Technol., Nov. (1990) 1440.
20. J.N. Caldos, M. Thomas, E. Behar and K. Rajagopal, "Influence of Solvents and the Asphaltene Content on the Flocculation Threshold of Crude Oils and Asphaltene Solutions", Abstracts, 1st Int. Symp. Colloid Chem. in Oil Production, Rio de Janeiro, 1995, p. 17.

21. F.X. Wang and J.S. Buckley, "A Two-Component Solubility Model of the Onset of Asphaltene Flocculation in Crude Oils", Energy & Fuels, 15 (2001) 1004.

22. K.D. Mannistu, H.W. Yarranton and J.H. Masliyah, "Solubility Modeling of Asphaltenes on Organic Solvents", Energy & Fuels, 11 (1997) 615.

23. A. Hirschberg, L. N. J. de Jong, B.A. Schipper and J.G. Meyer, "Influence of Temperature and Pressure on Asphaltene Flocculation", Soc. Petr. Eng. J., 24(3) (1984) 283.

24. S.I. Andersen, "Hysteresis in Precipitation and Dissolution of Petroleum Asphaltenes", Fuel Sci. Technol. Int., 10 (1992) 1743.

25. H.W. Yarranton and J.H. Masliyah, "Molar Mass Distribution and Solubility Modeling of Asphaltenes", AIChE J., 12 (1996) 3533.

26. S.I. Andersen, "Dissolution of Solid Boscan Asphaltenes in Mixed Solvents", Fuel Sci. Technol. Int., 12 (1994) 1551.

27. I.A. Wiehe and S.K. Liang, "Asphaltenes, Resins and Other Petroleum Macromolecules", Fluid Phase Equilibria, 117 (1996) 201.

28. R.B. Long, "The Concept of Asphaltene" in *Chemistry of Asphaltenes*, J.W. Bunger and N.C. Li, Eds., Advan. Chem. Series 195, American Chemical Society, Washington, D.C., 1981.

29. Z. Zhang and L.G. Hepler, "Heats of Solution of Athabasca Bitumen, Asphaltenes, and Maltenes in Toluene and Xylene and of Bitumen in Methylene Chloride", AOSTRA J. Res., 2 (1986) 267.

30. a) J.A. Bichard, *Oil Sands Composition and Behavior Research, Research Papers of J.A. Bichard 1957–1965*, Alberta Oil Sand Technology and Research Authority, Edmonton, 1987; b) S.I. Andersen, "Flocculation Onset Titration of Petroleum Asphaltenes", Energy & Fuels, 13 (1999) 315; c) E.W. Mertens, ASTM Bull. (1960) 40 (TP 218).

31. J.S. Buckley, G.J. Hirasaki, Y. Liu, S. von Drasek, J.X. Wang and B.S. Gill, "Asphaltene Precipitation and Solvent Properties of Crude Oils", Petr. Sci. Technol., 16 (1998) 251.

32. G. Hotier and M. Robin, "Action de Divers Diluants sur les Produits Pétroliers Lourds: Mesure, Interprétation et Prévision de la Floculation des Asphaltènes", Rev. Inst. Franç. Pétrol., 38 (1983) 101.

33. T. Ignasiak, Z. Frakman and O.P. Strausz, "Solvent Extraction as a Method of Fractionating Asphaltene on the Preparative Scale", Progress Report to AOSTRA, Research Project 142A, *Chemical Studies on Resins and Asphaltenes*, Jan.–June, 1983.

34. W. Liang, G. Que and Y. Chen, University of Petroleum, China, private communication.

35. Juan Murgich, Centro di Quimica, Instituto Venezolano Investigationes Cientificas, private communication.

36. M. Torres, E.M. Lown and O.P. Strausz, unpublished results, 1989.

37. P. Peng, A. Morales-Izquierdo, A. Hogg and O.P. Strausz, "Molecular Structure of Athabasca Asphaltene: Sulfide, Ether and Ester Linkages", Energy & Fuels, 11 (1997) 1171.

38. a) T.M. Ignasiak, L. Kotlyar, N. Samman, D.S. Montgomery and O.P. Strausz, "Preparative Gel Permeation Chromatography of Athabasca Asphaltene and the Relative Polymer-Forming Propensity of the Fractions", Fuel, 62 (1983) 363. b) K.M. Semple, N. Cyr, P.M. Fedorak and D.W. Westlake, "Characterization of Cold Lake Heavy Oil: Variations in Chemical Structure and Composition with Molecular Size", Can. J. Chem., 68 (1990) 1092.

39. Z. Frakman, T. Ignasiak, D.S. Montgomery and O.P. Strausz, "Nitrogen Compounds in Athabasca Asphaltene: The Carbazoles", AOSTRA J. Res., 3 (1987) 131.

40. Z. Frakman, T. Ignasiak, D.S. Montgomery and O.P. Strausz, "Nitrogen Compounds in Athabasca Asphaltene: The Vanadyl Porphyrins", AOSTRA J. Res., 4 (1988) 171.

41. Z. Frakman, T. Ignasiak, E.M. Lown and O.P. Strausz, "Oxygen Compounds in Athabasca Asphaltene", Energy & Fuels, 4 (1990) 263.

42. N. Samman, T. Ignasiak, C.-J Chen , O.P. Strausz and D.S. Montgomery, "Squalene in Petroleum Asphaltenes", Science, 213 (1981) 1381.

43. O.P. Strausz, "The Molecular Structure and Chemistry of Oil Sands Asphaltene", Final Report to AOSTRA, Agreement #30, 1977–1979.

44. D.D. McIntyre, D.S. Montgomery and O.P. Strausz, "Asphaltene Pyrolysis Distillates from Athabasca Bitumen and Cretaceous Heavy Oils Related to Depth of Burial and Degree of Weathering", AOSTRA J. Res., 2 (1986) 251.

45. T.D. Cyr, "Bicyclic, Tricyclic and Pentacyclic Terpanes", AOSTRA Fellowship Report, University of Alberta, October, 1983.

46. O.P. Strausz, E.M. Lown and T. W. Mojelsky, "Oil-Soluble Catalysts for the Hydrocracking of Athabasca Bitumen", Prepr., Am. Chem. Soc. Div. Petrol. Chem., 40 (1995) 741.

47. M.A.G. Teixeira, "Average Molecular Structure of Asphaltenes and Fractions and Their Tendency to Deposition", 1st Int. Symp. Colloid Chem. in Oil Prod., Rio de Janeiro, 1995, Abstracts p. 216.

48. A. Hammami, D. Chang-Yen and F.A. Nighswander, "An Experimental Study of the Effect of Paraffinic Solvents on the Onset and Bulk Precipitation of Asphaltene", Fuel Sci. Technol. Int., 13 (1995) 1167.

49. J.C. Monin and R. Pelet, "Asphaltene Fractionation and Characterization by Liquid Chromatography", in *Advan. Org. Geochem. 1981,* M. Bjorøy *et al.*, Eds., Wiley-Heyden Ltd., Chichester, 1983, p. 839.

50. S. Kawanaka, S.J. Park and G.A. Mansoori, "Organic Deposition from Reservoir Fluids: A Thermodynamic Predictive Technique", SPE Reservoir Eng., 6 (1991) 185.

51. J.G. Speight, R.B. Long and T.D. Trowbridge, "Factors Influencing the Separation of Asphaltenes from Heavy Petroleum Feedstocks", Fuel, 63 (1984) 616.

52. A. Hirschberg and L. Hermans, "Asphaltene Phase Behaviour: A Molecular Thermodynamic Model", Collect. Colloq. Semin., Inst. Franç. Pétr., 40 (1984) 492.

53. H. Rassamdana, B. Dabir, M. Nematy, M. Farhani and M. Sahimi, "Asphalt Flocculation and Deposition: I. The Onset of Precipitation", Am. Inst. Chem. Eng. J., 42 (1996) 10.

54. S.I. Andersen, "Effect of Precipitation Temperature on the Composition of *n*-Heptane Asphaltenes", Fuel Sci. Technol. Int., 12 (1994) 51; *ibid.*, 13 (1995) 579.

55. L.H. Ali and K.A. Al-Ghannarn, "Investigations into Asphaltenes in Heavy Crude Oils. I. Effect of Temperature on Precipitation by Alkane Solvents", Fuel, 60 (1981) 1043.

56. B. Fuhr, C. Cathrea, L. Coates, H. Kabra and A.I. Majeed, "Properties of Asphaltenes from a Waxy Crude", Fuel, 70 (1991) 1293.

57. a) C. Lhioreau, J. Briant and R. Tindy, "Influence de la Pression sur la Floculation des Asphaltènes", Rev. Inst. Franc. Petrol., 22 (1967) 797. b) R. Angulo, A. Borges, M. Fonseca and C. Gil, "Experimental Asphaltene Precipitation Study. Phenomenological Behavior of Venezuelan Live Crude Oils", in "Proceedings, 1st Int. Symp. Colloid Chem. in Oil Prod.: Asphaltenes and Wax Deposition", Rio de Janeiro, Brazil, November 26–29, 1995, Abstracts p. 109.

58. K. Takamura and E.E. Isaacs, "Interfacial Properties", in *AOSTRA Technical Handbook on Oil Sands, Bitumens and Heavy Oils*, L.G. Hepler and C. Hsi, Eds., Alberta Oil Sands Technology and Research Authority, Edmonton, AB, 1989, p. 99.

59. J.G. Speight and S.E. Moschopedis, "On the Molecular Nature of Petroleum Asphaltenes" in *The Chemistry of Asphaltene*, ACS Symp. Series 195, J.W. Bunger and C. Li, Eds., American Chemical Society, Washington, D.C., 1981, p. 3.

60. J.A. Curiale, "Distribution and Occurrence of Metals in Heavy Crude Oils and Solid Bitumens: Implications for Petroleum Exploration"; Exploration for Heavy Crude Oil and Bitumen, AAPG Res. Conf., Santa Maria, CA Oct. 29–Nov. 2, 1984.

61. L. Lopez, S. Lo Monaco, F. Galarranga, A. Lira and C. Crur, "V/Ni Ratio in Maltene and Asphaltene Fractions of Crude Oils from West Venezuelan Basin: Correlation Studies", Chem. Geol., 119 (1995) 255.

62. F.S. Jacobs and R.H. Filby, "Solvent Extraction of Oil-Sand Components for Determination of Trace Metals by Neutron Activation Analysis", Anal. Chem., 55 (1983) 74.

63. F.S. Jacobs, F.W. Bachelor and R.H. Filby, "Determination of Trace Elements in GPC Fractions of Oil-Sand Asphaltenes by INAA", Proc., 5th Int. Conf. Nuclear Methods in Env. Energy Res., April, 1984, Univ. Missouri, Columbia, MI.

64. L.S. Kotlyar, B.D. Sparks, J.R. Woods and K.H. Chung, "Solids Associated with the Asphaltene Fraction of Oil Sands Bitumen," Energy & Fuels, 13 (1999) 346.

65. R.Z. Syunyaev, "The Role of Aromagnetism in the Hierarchy of Intermolecular Forces in Asphaltene Aggregates", Int. Symp. on Science and Technology of Hydrocarbon Dispersed Systems, Nat. Academy I.M. Gubkin of Oil and Gas, Moscow, October 1997.

66. P.H.J Carlsen, T. Katsuki, V.S. Martin and K.B.Sharpless, "A Greatly Improved Procedure for Ruthenium Tetroxide Catalyzed Oxidation of Organic Compounds", J. Org. Chem., 46 (1981) 3936.

67. I. Rubinstein, C. Spyckerelle and O.P. Strausz, "Pyrolysis of Asphaltenes: A Source of Geochemical Information", Geochim. Cosmochim. Acta, 43 (1979) 1.

68. I. Rubinstein and O.P. Strausz, "Thermal Treatment of Athabasca Oil Sand Bitumen and its Component Parts", Geochim. Cosmochim. Acta, 43 (1979) 1887.

69. R.G.S. Ritchie, R.S. Roche and W. Steedman, "Pyrolysis of Athabasca Tar Sands: Analysis of the Condensible Products from Asphaltene", Fuel, 58 (1979) 523.

70. O.P. Strausz, K.N. Jha and D.S. Montgomery, "Chemical Composition of Gases in Athabasca Bitumen and in Low-Temperature Thermolysis of Oil Sand, Maltene and Asphaltene", Fuel, 56 (1977) 114; K.N. Jha, D.S. Montgomery and O.P. Strausz, "Chemical Composition of Gases in Alberta Bitumens and in Low-Temperature Thermolysis of Oil Sand Asphaltenes and Maltenes", in *Oil Sand and Oil Shale Chemistry*, Verlag Chemie Int., New York, N.Y., 1978, p. 33.

71. I. Safarik and O.P. Strausz, "The Thermal Decomposition of Hydrocarbons. Part I. *n*-Alkanes ($C \geq 5$)", Res. Chem. Intermed., 22 (1996) 275.

72. F. Behar and R. Pelet, "Characterization of Asphaltenes by Pyrolysis and Chromatography", J. Anal. Appl. Pyrolysis, 7 (1984) 121; F. Behar, R. Pelet and J. Roucaché, "Geochemistry of Asphaltenes", Org. Geochem., 6 (1984) 587; A.-Y. Huc, F. Behar and J.-C Roussel, Proc., 1st Int. Symp. Heavy Crude Oils Petrol. Residue, Lyon, 1984, p. 438; F. Behar and R. Pelet, "Pyrolysis–Gas Chromatography Applied to Organic Geochemistry. Structural Similarities Between Kerogens and Asphaltenes from Related Rock Extracts and Oils", J. Anal. Appl. Pyrolysis, 8 (1985) 173; M.M. Ekwenchi, E.M. Lown, D.S. Montgomery and O.P. Strausz, "High Temperature Pyrolysis of Petroleum Asphaltenes", AOSTRA J. Res., 1 (1984) 127; M.M. Ekwenchi, A.O. Oladapo and O.P. Strausz, "Estimation of Thermal Maturity Status of Petroleum Asphaltenes and Maltenes", Fuel, 68 (1989) 1532.

73. G.W. Mushrush and R.N. Hazlett, "Pyrolysis of Alkyl Compounds Containing Long Unbranched Alkyl Groups", Ind. Eng. Chem. Fundam., 23 (1984) 288.

74. R. Alexander, P.G. Kralert and R.I. Kagi, "Kinetics and Mechanism of the Thermal Decomposition of Esters in Sediments", Advan. Org. Geochem. 1991, Org. Geochem., 19 (1992) 133.

75. C.M. Ekweozor and O. P. Strausz, "Tricyclic Terpanes in Athabasca Oil Sands: Their Geochemistry", in *Advances in Organic Geochemistry 1981*, M. Bjøroy *et al.*, Eds., Wiley Heyden, London, U.K., 1983, p. 746; C.M. Ekweozor and O.P. Strausz, "18,19-Bisnor-13bH, 14aH-Cheilantane: A Novel Degraded Tricyclic Sesterterpenoid-Type Hydrocarbon from the Athabasca Oil Sands", Tetrahedron Lett., 23 (1982) 2711.

76. T.D. Cyr, "Carboxylic Acids in the Bitumens and Bound to the Mineral Matter of Alberta Oil Sands", AOSTRA Fellowship Report, June, 1982; T.D. Cyr and O.P. Strausz, "The Structures of Tricyclic

Terpenoid Carboxylic Acids and Their Parent Alkanes in the Alberta Oil Sands", J. Chem. Soc. Chem. Commun., (1983) 1028; T.D. Cyr amd O.P. Strausz, "Bound Carboxylic Acids in the Alberta Oil Sands", Org. Geochem., 7 (1984) 127.

77. C.F. Hoffmann and O.P. Strausz, "Bitumen Accumulation in Grosmont Platform Complex, Upper Devonian, Alberta, Canada", Am. Assoc. Petrol. Geol. Bull., 70 (1986) 1113.

78. M.G. Fowler and P.W. Brooks, "Organic Geochemistry of Western Canadian Tar Sands and Heavy Oils. 2. Correlation of Tar Sands Using Hydrous Pyrolysis of Asphaltenes", Energy & Fuels, 1 (1987) 459.

79. D.M. Jones, A.G. Douglas and J. Connan, "Hydrocarbon Distributions in Crude Oil Asphaltene Pyrolyzates. 1. Aliphatic Compounds", Energy & Fuels, 1 (1987) 468.

80. J.D. Payzant, E.M. Lown and O.P. Strausz,"Structural Units of Athabasca Asphaltene: The Aromatics with a Linear Carbon Framework", Energy & Fuels, 5 (1991) 445.

81. J.D. Payzant, D.S. Montgomery and O.P. Strausz, "The Identification of Homologous Benzo[b]thiophenes, Thiophenes, Thiolanes and Thianes Possessing a Linear Carbon Framework in the Pyrolysis Oil of Athabasca Asphaltene", AOSTRA J. Res., 4 (1988) 117; J.D. Payzant, D.D. McIntyre, T.W. Mojelsky, M. Torres, D.S. Montgomery and O.P. Strausz, "The Identification of Homologous Series of Thiolanes and Thianes Possessing a Linear Carbon Framework from Petroleums and Their Interconversion Under Geological Conditions", Org. Geochem., 14, (1989) 461.

82. P.M. Fedorak, J.D. Payzant, D.S. Montgomery and D.W. Westlake, "Microbial Degradation of *n*-Alkyltetrahydrothiophenes Found in Petroleum", Appl. Environ. Microbiol., 54 (1988) 1243.

83. J.D. Payzant, I. Rubinstein, A.M. Hogg and O.P. Strausz, "Field-Ionization Mass Spectrometry: Application to Geochemical Analysis", Geochim. Cosmochim. Acta, 43 (1979) 1187.

84. T. Ignasiak, A. Kemp-Jones and O.P. Strausz, "The Molecular Structure of Athabasca Asphaltene. Cleavage of the Carbon–Sulfur Bonds by Radical Ion Electron Transfer Reactions", J. Org. Chem., 42 (1977) 312.

85. C.M. Ekweozor, "Characterization of the Non-Asphaltene Products of Mild Chemical Degradation of Asphaltenes", Org. Geochem., 10 (1986) 1053; "Tricyclic Terpenoid Derivatives from Chemical Degradation Reactions of Asphaltenes", Org. Geochem., 6 (1984) 51.

86. H. Szawatsky and D.S. Montgomery, "The Reduction of Asphaltenes", Fuel, 43 (1964) 453; H. Szawatsky, M.L. Boyd and D.S. Montgomery, "The Application of Hydrocarbon Structural Group Analyses to Mildred Lake and Abasand (Alberta) Asphaltenes and Their Reduction Products", J. Inst. Petrol., London, 53 (1967) 162.

87. T.G. Back, K. Yang and H.R. Krouse, "Desulfurization of Benzo- and Dibenzothiophenes with Nickel Boride", J. Org. Chem., 57 (1992) 1986.

88. S. Schouten, D. Pavlovic, J.S. Sinninghe Damsté and J.W. de Leeuw, "Nickel Boride: an Improved Desulfurization Agent for Sulfur-Rich Geomacromolecules in Polar and Asphaltene Fractions", Org. Geochem., 20 (1993) 901.

89. W.A. Hartgers, J.F. Lopez, F.X.C. de las Heras and J.O. Grimalt, "Sulfur Binding in Recent Environments. I. Lipid By-Products from Ni_2B Desulfurization", Org. Geochem., 25 (1996) 353.

90. O.P. Strausz, T.W. Mojelsky, J.D. Payzant, G.A. Olah and G.K. Surya Prakash, "Upgrading of Alberta's Heavy Oils by Superacid-Catalyzed Hydrocracking", Energy & Fuels, 13 (1999) 558.

91. G.A. Olah, M.R. Bruce, E.H. Edelson and A. Husain, "Superacid Coal Chemistry. 1. $HF:BF_3$ Catalyzed Depolymerization—Ionic Hydroliquefaction of Coals Under Mild Conditions", Fuel, 63 (1984) 1130; G.A. Olah and A. Husain, "Superacid Coal Chemistry. 2. Model Compound Studies Under Conditions of $HF:BF_3:H_2$ Catalyzed Mild Coal Liquefaction", Fuel, 63 (1984) 1427; G.A. Olah, M.R. Bruce, E.H. Edelson and A. Husain, "Superacid Coal Chemistry. 3. Electrophilic Substitution of Coals under 'Stable Ion' Conditions and the Conversion of Functionalized Coals with the $HF:BF_3:H_2$ Liquefaction System", Fuel, 63 (1984) 1432. G.A. Olah, "Liquefaction of Coals Using Recyclable Superacid Catalysts", U.S. Patent 4,394,247 (1983).

92. T.W. Mojelsky, D.S. Montgomery and O.P. Strausz, "The Side Chains Associated with the Undistillable Aromatic and Resin Components of Athabasca Bitumen", AOSTRA J. Res., 2 (1986) 177.

93. O.P. Strausz, T.W. Mojelsky, F. Faraji, E.M. Lown and P. Peng, "Additional Structural Details on Athabasca Asphaltene and Their Ramifications", Energy & Fuels, 13 (1999) 207.

94. T.W. Mojelsky, T.M. Ignasiak, Z. Frakman, D.D. McIntyre, E.M. Lown, D.S. Montgomery and O.P. Strausz, "Structural Features of Alberta Oil Sand Bitumen and Heavy Oil Asphaltenes", Energy & Fuels, 6 (1992) 83.

95. Wm.C. Gussow, "Migration of Reservoir Fluids", Soc. Petrol. Eng., Am. Inst. Mining Eng., 42nd Ann. Meeting, Houston, TX, SPE Reprint 1870; —, Soc. Petrol. Eng., Am. Inst. Mining Eng., J. Petrol. Technol., 20 (1968) 353; —, *Petroleum Exploration,* McGraw-Hill Yearbook Science and Technology, (1970) 297; —, "The East Texas Field—a New Interpretation", 24th Int. Geol. Congr., Montreal, 1972, Rept. Sec. 5, Mineral Fluids, 82; —, *9th World Petroleum Congress, Proceedings*, Panel Discussion 3, p. 203; Discussion SP 1, 372.

96. G. Ourisson and M. Rohmer, "Hopanoids. 2. Biohopanoids: A Novel Class of Bacterial Lipids", Account Chem. Res., 25 (1992) 403.

97. G.A. Olah and A. Molnar, *Hydrocarbon Chemistry,* John Wiley & Sons, New York, 1995, p. 161.

98. S. Murata, Y. Tani, M. Hiro, K. Kidena, L. Artok, M. Nomura and M. Miyake, "Structural Analysis of Coal Through RICO Reaction: Detailed Analysis of Heavy Fractions", Fuel, 80 (2001) 2099.

99. O.P. Strausz, T.W. Mojelsky, E.M. Lown, I. Kowalewski and F. Behar, "Structural Features of Boscan and Duri Asphaltenes", Energy & Fuels, 13 (1999) 228.

100. D.D. McIntyre and O.P. Strausz, "Sulfur-33 Nuclear Magnetic Resonance of Oxidized Petroleum Asphaltene", Magn. Res. Chem., 25 (1987) 36.

101. J.S. Sinninghe Damsté, A.C. Kock-van Dalen, J.W. de Leeuw and P.A. Schenck, "Identification of Homologous Series of Alkylated Thiophenes, Thiolanes, Thianes and Benzothiophenes Present in Pyrolyzates of Sulfur-Rich Kerogens", J. Chromatogr., (1988) 435.

102. P. Peng and O.P. Strausz, "Chemical Structure and Biomarker Content of Jinghan Asphaltenes and Kerogens", Energy & Fuels, 13 (1999) 248.

103. J. Goulon, C. Esselin, P. Friant, C. Berthé, J.F. Muller, J.-L. Poncet, R. Guilard, J.-C. Escalier and B. Neff, "Structural Characteristics by X-ray Absorption Spectroscopy (EXARS/XANES) of the Vanadium Chemical Environment in Various Asphaltenes", Collect. Colloq. Semin., Inst. Franç. Pétrol., 40 (1984) 158.

104. G.N. George and M.L. Gorbaty, "Sulfur K-Edge X-Ray Absorption Spectroscopy of Petroleum Asphaltenes and Model Compounds", J. Am. Chem. Soc., 111 (1989) 3182.

105. G.S. Waldo, O.C. Mullins, J.E. Penner-Hahn and S.P. Cramer, "Determination of the Chemical Environment of Sulfur in Petroleum Asphaltenes by X-Ray Absorption Spectroscopy", Fuel, 71 (1992) 53.

106. T.W. Mojelsky, D.S. Montgomery and O.P. Strausz, "Pyrolytic Probes into the Aliphatic Core of Oxidized Athabasca Asphaltene Nondistillable Ester Residue", AOSTRA J. Res., 3 (1986) 43.

107. A.S. Mackenzie, G.A. Wolff and J.R. Maxwell, "Fatty Acids in some Biodegraded Petroleums. Possible Origins and Significance", Proc., 10th Int. Meet. Org. Geochem., Univ. Bergen, Norway, Sept. 14–18, 1981; Adv. Org. Geochem., (1981) 637.

108. I. Kowalewski, F. Behar and O.P. Strausz, to be published.

109. Z. Wang, W. Liang, G. Que and J. Qian, "Structural Characterization of Gudao Asphaltene by Ruthenium Ion Catalyzed Reaction", Petr. Sci. Technol., 15 (1997) 559.

110. P. Peng, J. Fu, G. Sheng, A. Morales-Izquierdo, E.M. Lown and O.P. Strausz, "Ruthenium Ions-Catalyzed Oxidation of an Immature Asphaltene: Structural Features and Biomarker Distribution", Energy & Fuels, 13 (1999) 228.

111. Y. Su, L. Artok, S. Murata and M. Nomura, "Structural Analysis of Asphaltene Fraction of Arabian Mixture by Ruthenium Ions-Catalyzed Oxidation Reaction", Energy & Fuels, 12 (1998) 1265.

112. S. El-Mohamed, M.-F. Achard, F. Hardouin and H. Gasparoux, "Correlations Between Diamagnetic Properties and Structural Characters of Asphaltenes and Other Heavy Petroleum Products", Fuel, 65 (1986) 1501.

113. N. Cyr, D.D. McIntyre, G. Toth and O.P. Strausz, "Hydrocarbon Structural Group Analysis of Athabasca Asphaltene and its GPC Fractions by ^{13}C NMR", Fuel, 66 (1987) 1709.

114. L. Artok, Y.Su, Y. Hirose, M. Hosokawa, S. Murata and M. Nomura, "Structure and Reactivity of Petroleum-Derived Asphaltenes", Energy & Fuels, 13 (1999) 287.

115. L. Artok, S. Murata, M. Nomura and S. Satoh, "Reexamination of the RICO Method", Energy & Fuels, 12 (1998) 391.

116. V. Calemma, P. Iwanski, M. Nali, R. Scotti and L. Montanari, "Structural Characterization of Asphaltenes of Different Origins", Energy & Fuels, 9 (1995) 225.

117. L.S. Kotlyar, J.A. Ripmeester, B.D. Sparks and J. Woods, "Study of Organic Matter Derived from Utah and Athabasca Oil Sands", Fuel, 67 (1988) 1529.

118. T. Yokota, F. Scriven, D.S. Montgomery and O.P. Strausz, "Absorption and Emission Spectra of Athabasca Asphaltene in the Visible and Near Ultraviolet Regions", Fuel, 65 (1986) 1142.

119. a) N.J. Turro, *Modern Molecular Photochemistry*, Benjamin/Cummings Publ. Co., Menlo Park, CA 1978; b) F.C. de Schryver and N. Boens, "Excited State Behaviour of some Bichromophoric Systems", in Advan. Photochem., 10 (1977) 359; c) D.O. Cowan and R.L. Drisko, "Elements of Organic Photochemistry", Plenum Press, New York, N.Y. 1976; d) R.S. Becker, "Theory and Interpretation of Fluorescence and Phosphorescence, Wiley Interscience, New York, N.Y. 1969.

120. C.Y. Ralston, S. Mitra-Kirtley and O.C. Mullins, "Small Population of One to Three Fused-Aromatic Ring Moieties in Asphaltenes", Energy & Fuels, 10 (1996) 623.

121. H. Groenzin and O.C. Mullins, a) "Molecular Size and Structure of Asphaltenes from Various Sources", Energy & Fuels, 14 (2000) 677; b) "Asphaltene Molecular Size and Structure", J. Phys. Chem., A, 103 (1999) 11237; and references therein.

122. J. Uebersfeld, A. Etienne and J. Combrisson, Paramagnetic Resonance, a new Property of Coal-Like Materials", Nature, 174 (1954) 614; F.H. Winslow, W.O. Baker and W.A. Yager, "Odd Electrons in Polymer Molecules", J. Am. Chem. Soc., 77 (1955) 4751.

123. D.E. O'Reilly, "Paramagnetic Resonance of Vanadyl Etioporphyrin I."J. Chem. Phys., 29 (1958) 1188.

124. A.J. Saraceno, D.T. Fanale and N.D. Coggeshall, "An Electron Paramagnetic Resonance Investigation of Vanadium in Petroleum Oils", Anal. Chem., 33 (1961) 500.

125. H.S. Gutowsky, R.B. Ray, R.L. Rutlege and R.R. Unterberger, "Carbonaceous Free Radicals in Crude Petroleum", J. Chem. Phys., 28 (1958) 744.

126. A.J. Saraceno and N.D. Coggeshall, "Effect of Dissolved Oxygen on the Spin–Lattice Relaxation Time of Free Radicals in Petroleum Oils", J. Chem. Phys., 34 (1961) 260.

127. I.C. Lewis and L.S. Singer, "Electron Spin Resonance and the Mechanism of Carbonization" in *Chemistry and Physics of Carbon*, P.L. Walker Jr. and P.A. Thrower, Eds., Marcel Dekker, New York, 1981.

128. S. Niizuma, C.T. Steele, H.E. Gunning and O.P. Strausz, "Electron Spin Resonance Study of Free Radicals in Athabasca Asphaltene", Fuel, 56 (1977) 249.

129. V.M. Malhotra and H.A. Buckmaster, "34 GHz E.P.R. Study of Vanadyl Complexes in Various Asphaltenes", Fuel, 64 (1985) 335.

130. M.B. Hocking and P.I. Premovic, "Coal Inclusions in the Athabasca Tar Sands", Geochim. Cosmochim. Acta, 42 (359) 1978.

131. S. Niizuma, M. Iwaizumi and O.P. Strausz, "ENDOR Study of Free Radicals in Athabasca Asphaltene", AOSTRA J. Res., 7 (1991) 217.

132. C.S. Wen, G.V. Chilingarian and T.F. Yen, "Properties and Structure of Bitumen", in *Bitumens, Asphalts and Tar Sands*, G.V. Chilingarian and T.F. Yen, Eds., Development in Petrol. Sci. Ser. 7, Elsevier, Amsterdam, 1978.

133. T.F. Yen and S.R. Sprang, "Contribution of EPR Analysis Toward Diagenetic Mechanisms in Bituminous Deposits", Geochim. Cosmochim. Acta, 41 (1977) 1007.

134. T.F. Yen and D.K. Young, "Spin Excitations of Bitumens", Carbon, 11 (1973) 33.

135. T.F. Yen, J.G. Erdman and A.J. Saraceno, "Investigation of the Nature of Free Radicals in Petroleum Asphaltenes and Related Substances by Electron Spin Resonance", Anal. Chem., 34 (1962) 694.

136. V.M. Malhotra and W.R.M. Graham, "Characterization of P.R. Spring (Utah) Tar Sand Bitumen by the EPR Technique: Free Radicals", Fuel, 62 (1983) 1255.

137. K.F. Schultz and M.L. Selucky, "EPR Measurements on Asphaltene and Resin Fractions from Various Separation Methods", Fuel, 60 (1981) 951.

138. R.M. Elofson, K.F. Schultz and B. Hitchon, "Geochemical Significance of Chemical Composition and EPR Properties of Asphaltenes in Crude Oils from Alberta, Canada", Geochim. Cosmochim. Acta, 41 (1977) 567.

139. N. Qin and J. Wang, "The Use of Free Radicals of Organic Matter to Determine Paleogeothermal Gradient", Org. Geochem., 28 (1998) 77.

140. J. Q. Adams, K.H. Altgelt, R.L. LeTourneau and L.P. Lindeman, "Free Radical Concentrations in Gel Permeation Fractions of Asphaltenes From Different Crude Oils", Am. Chem. Soc. Div. Petrol Chem. Preprints, 11 (1966) B-140.

141. P. Raghunathan, S. Niizuma, E.M. Lown and O.P. Strausz, unpublished results.

142. S. Acevedo, G. Escobar, M.A. Ranaudo, J. Piñate and A. Amorin, "Observations About the Structure and Dispersion of Petroleum Asphaltenes Aggregates Obtained from Dialysis Fractionation and Characterization", Energy & Fuels, 11 (1997) 774.

143. A. Jezierski, F. Czechowski, J. Drozd, M. Yerzykiewicz and B. Witek, Mol. Phys. Rep., 18/19 (1997) 115.

144. K.C. Khulbe, R.S. Mann, G. Lamarche and A.-M. Lamarche, "Electron Spin Resonance Study of the Thermal Decomposition of Solvent Extracted Athabasca Tar Sand Bitumen", Fuel Proc. Technol., 31 (1992) 91.

145. L.R. Rudnick and C.A. Audeh, "Thermal Chemistry of a Utah Tar Sand: An EPR Characterization", Ind. Eng. Chem. Res., 27 (1988) 1366.

146. B.K.G. Theng, *The Chemistry of Clay-Organic Reactions*, Halsted Press, U.K., 1974, p. 271.

147. L. Montanari, M. Clericuzio, G. Del Piero and R. Scotti, "Asphaltene Radicals and Their Interaction with Molecular Oxygen: an EPR Probe of Their Molecular Characteristics and Tendency to Aggregate", Appl. Magn. Res., 14 (1998) 81.

148. T.H. Lowry and K.S. Richardson, *Mechanism and Theory in Organic Chemistry*, 3rd Ed., Harper & Row, New York, 1987.

149. S. Penzes and J.G. Speight, "Electrical Conductivities of Bitumen Fractions in Non-Aqueous Solvents", Fuel, 53 (1974) 192.

150. E.Y. Sheu, D.A. Storm and M.M. De Tar, "Asphaltenes in Polar Solvents", J. Non-Crystalline Solids", 131–133 (1991) 341.

151. E.Y. Sheu, M.M. De Tar and D.A. Storm, "Dielectric Properties of Asphaltene Solutions", Fuel, 73 (1994) 45.

152. P. Fotland and H. Anfindsen, "Electrical Conductivity of Asphaltenes in Organic Solvents", Fuel Sci. Technol. Int'l, 14 (1996)101.

153. E.Y. Sheu, "Physics of Asphaltene Micelles and Microemulsions—Theory and Experiment", J. Phys.: Condens. Matter, 8 (1996) A125.

154. E.Y. Sheu, D.A. Storm and M.B. Shields, "Dielectric Response of Asphaltenes in Solvent", Energy & Fuels, 8 (1994) 552.

155. See, for example, H. Murai, I. Safarik, M. Torres and O.P. Strausz, "Triplet Ground-State Benzoylphenylmethylene and its Quintet Ground-State Triplet–Triplet Radical Pair", J. Am. Chem. Soc., 110 (1988) 1025 and references therein.

156. G.A. Olah, G.K.S. Prakash and J. Sommer, *Superacids*, J. Wiley & Sons, New York, 1985.

157. D. Rigby, T.D. Gilbert and J.W. Smith, "The Synthesis of Alkylaromatic Hydrocarbons and its Geochemical Implications", Org. Geochem., 9 (1986) 255.

158. T.F. Yen, J.G. Erdman and S.S. Pollack, "Investigation of the Structure of Petroleum Asphaltenes by X-Ray Diffraction", Anal. Chem., 33 (1961) 1587; J.P. Dickie and T.F. Yen, "Macrostructures of the Asphaltic Fractions by Various Instrumental Methods", Anal. Chem., 39 (1967) 9, 1847.

159. L.B. Ebert, "Comment on the Study of Asphaltenes by X-Ray Diffraction", Fuel Sci. Technol. Int., 8 (1990) 563); L.B. Ebert, "X-Ray Diffraction of Stacked Aromatic Molecules Revisited: Can One Determine Aliphatic Carbon Abundance from a Diffraction Peak Related to Intermolecular Aromatic Interactions?", Fuel Sci. Technol. Int., 13 (1995) 941.

160. H.L. Retcofsky, "Magnetic Resonance Studies of Coal", in *Coal Science*, Vol. 1, Eds. M.L. Gobarty, J.W. Larsen and I. Wender, Academic Press, New York, 1982, p. 51.

161. M. Selucky, S.S, Kim, F. Skinner and O.P. Strausz, "Structure-Related Properties of Athabasca Asphaltene and Resins", presented in the Petrol. Chem. Div., Fall Meeting of the American Chemical Society, Washington, D.C., 1979; M. Selucky, S.S, Kim, F. Skinner and O.P. Strausz, "Structure-Related Properties of Athabasca Asphaltene and Resins as Indicated by Chromatographic Separation" in *Chemistry of Asphaltenes*, J.W. Bunger and N.C. Li, Eds., Advances in Chemistry Series 195, American Chemical Society, Washington, D.C., 1981, p. 83.

162. O.P. Strausz, P. Peng and J. Murgich, "About the Colloidal Nature of Asphaltenes and the MW of Covalent Units", Energy & Fuels, 16 (2002) 809.

163. M.J. Lazaro, C.A. Islas, A.A. Herod and R. Kandiyoti, "Calibration of Size Exclusion Chromatography in 1-Methyl-2-Pyrrolidinone for Coal-Derived Materials Using Standards and Mass Spectrometry", Energy & Fuels, 13 (1999) 1212.

164 J. Murgich, J. Abanero and O.P. Strausz, "Molecular Recognition in Aggregates Formed by Asphaltene and Resin Molecules from the Athabasca Oil Sand", Energy & Fuels, 13 (1999) 278; J. Murgich and O.P. Strausz, "Molecular Mechanics of Aggregates of Asphaltenes and Resins of Different Types of Crude Oils", Petrol. Sci. Technol., 19 (2001) 231.

165. H.W. Yarranton, H. Aboudwarej and R. Jakher, "Investigation of Asphaltene Association with Vapor Pressure Osmometry and Interfacial Tension Measurements", Ind. Eng. Chem. Res. 39 (2000) 2916.

166. a) M. Domin, A. Herod. R. Kandiyoti, J.W Larsen, M.-J. Lazaro, S. Li and P. Rahimi, "A Comparative Study of Molecular Weight Distribution", Energy & Fuels, 13 (1999) 552. b) For a detailed recent review on MALDI-TDF-MS see M.W.F. Nielen , "MALDI Time of Flight Mass Spectrometry of Synthetic Polymers", Mass Spectr. Rev., 18 (1999) 309.

167. J.P. Matthews, S. EPRe and P. Rahimi, "Preliminary Results on the Molecular Structures of the Athabasca and Cold Lake Asphaltenes", Prepr. Pap.—Am. Chem. Soc., Div. Fuel Chem., 42 (1999) 783.

168. A.A. Herod, M.-J. Lazaro, M. Domin, C.A. Islas and R. Kandiyoti, "Molecular Mass Distributions and Structural Characterization of Coal Derived Liquids", Fuel, 79 (2000) 323.

169. M.-G. Yang, and S. Eser, "Fractionation and Molecular Analysis of Vacuum Residue Asphaltenes", Prepr. Pap.—Am. Chem. Soc., Div. Fuel Chem., 42 (1999) 768.

170. S.I. Andersen, J.M. del Rio, D. Khvostitchenko, S. Shakir and C. Lira-Galeana, "Interaction and Solubilization of Water by Petroleum Asphaltenes in Organic Solution", Langmuir, 17 (2001)307.

171. J.W. Jurge and E. Eisma, "Petroleum Hydrocarbons: Generation from Fatty Acids", Science, 144 (1964) 1451.

172. E. Eisma and J.W. Jurge, "Fundamental Aspects of the Diagenesis of Organic Matter and the Formation of Hydrocarbons", Proc. 7th World Petrol. Congress, Vol. 2, 1967, p. 61.

173. A. Shimoyama and D.W. Johns, "Catalytic Conversion of Fatty Acids to Petroleum-Like Paraffins and Their Maturation", Nature phys. Sci., 232 (1971) 140; "Formation of Alkanes from Fatty Acids in the Presence of $CaCO_3$", Geochim. Cosmochim Acta, 36 (1972) 87; W.D. Johns and A. Shimoyama, "Clay Minerals and Petroleum-Forming Reactions During Burial and Diagenesis". Am. Assoc. Petrol. Geol.Bull., 56 (1972) 2160.

174. W.D. Johns, "Clay Mineral Catalysis and Petroleum Generation", Ann. Rev. Earth Planet. Sci., 7 (1979) 183; Dev. Sedimentol. 35, (1982) 655.

175. W. Henderson, G. Eglinton, P. Simmonds and J.E. Lovelock, "Thermal Alteration as a Contributory Process to the Genesis of Petroleum", Nature, 219 (1968) 1012; Z. Ismailov, A.A. Kacimov, V.C. Aliev, N.K. Rzaev and R.B. Orudzev, "The Effect of Temperature on the Product Yield in the Dehydrogenation Process of the Higher (C11–C14) Paraffins on Oxide Catalysts", Azerbaijan Chem. J., No. 1 (1988) 34; A.A. Kasimov, V.S. Alief, B.G. Ter-Sarkisov, Z.I. Ismailov and N.K. Rzaev, "Identification of the Variation of the Monoolefin Yield in the Formation of Aromatic Hydrocarbons in the Dehydrogenation Process of (C11–C14) *n*-Paraffins", Azerbaijan Chem. J., No. 2 (1983) 33.

176. Z. Aizenshtat, I. Miloslavsky and L. Heller-Kallai, "The Effect of Montmorillonite on the Thermal Decomposition of Fatty Acids under 'Bulk Flow' Conditions", Org. Geochem., 7 (1984) 85.

177. B.R. Ray, P.A. Witherspoon and R.E. Grim, "A Study of the Colloidal Characteristics of Petroleum Using the Ultracentrifuge", J. Phys. Chem., 61 (1957) 1296; P.A. Witherspoon and R.E. Grim, "Size and Shape of Asphaltic Particles in Petroleum", Producers Monthly, 24 No. 10 (1960) 20.

178. H.J. Neumann, "Kolloid Chemische Untersuchungen an Asphaltenen", Brennstoff Chem., 46 (1965); H.J. Neumannn, B. Paczynska–Lahme and D. Severin, "Composition and Properties of Petroleum", Geology of Petroleum, Vol. 5, H. Beckman, Ed., Halsted Press, New York, 1981.

179. D. Myers, *Surfaces, Interfaces and Colloids*, 2nd ed., Wiley–VCH, New York, 1999; D.J. Shaw, *Introduction to Colloid and Surface Chemistry*, Butterworth-Heinemann, Oxford, 1992; C. Tanford, *The Hydrophobic Effect*, Wiley–Interscience, New York, N.Y. 1980.

180. S.I. Andersen and K.S. Birdi, "Aggregation of Asphaltenes as Determined by Calorimetry", J. Colloid Interface Sci., 142 (1991) 497; S.I. Andersen and S.D. Christensen, "The Critical Micelle Concentration of Asphaltenes as Measured by Calorimetry", Energy & Fuels, 14 (2000) 38.

181. J. Murgich, C. Lira-Galeana, D. Merino-Garcia and S.I. Andersen, "Molecular Mechanics and Microcalorimetric Investigations of the Effects of Molecular Water on the Aggregation of Asphaltenes in Solutions", Langmuir, 18 (2002) 9080.

182. E.Y. Sheu, M.M. de Tar, D.A. Storm and S.J. De Canio, "Aggregation and Kinetics of Asphaltenes in Organic Solvents", Fuel, 71 (1992) 299.

183. E.Y. Sheu, "Physics of Asphaltene Micelles and Microemulsions—Theory and Experiment", J. Phys.: Condens. Matter, 8 (1996) A125.

184. D. Fenistein, L. Barré, D. Broseta, D. Espinat, A. Livet, J.-N. Roux and M. Scarsella, "Viscosimetric and Neutron Scattering Study of Asphaltene Aggregates in Mixed Toluene/Heptane Solvents", Langmuir, 14 (1998) 1013.

185. E.Y. Sheu, M.M. de Tar and D.A. Storm, “Rheological Properties of Vacuum Residue Fractions in Organic Solvents”, Fuel, 70 (1991) 1151; “Structure, Interaction and Phase Transition of Vacuum Residue in Apolar Solvents”, Fuel Sci. Technol. Int.’l, 10 (1992) 607.

186. E.Y. Sheu, K.S. Liang, S.K. Sinha and R.E. Overfield, “Polydispersity Analysis of Asphaltene Solutions in Benzene”, J. Colloid Interface Sci., 153 (1992) 399.

187. S.El Mohamed, F. Hardouin and H. Gasparoux, “Floculation des Produits Lourds du Pétrole”, J. Chim. Phys., 85 (1988) 135.

188. Ch. Bardon, L. Barré, D. Espinat, V. Guille, M.H. Li, J. Lambard, J.C. Ravey, E. Rosenberg and T. Zemb, “The Colloidal Structure of Crude Oils and Suspensions of Asphaltenes and Resins”, Fuel Sci. Technol. Int., 14 (1996) 203.

189. E.B. Sirota, “Swelling Asphaltenes”, Petrol. Sci. Technol., 16 (1998) 415.

190. R.E. Winans and J.E. Hunt, “An Overview of Resid Characterization by Mass Spectrometry and Small Angle Scattering Techniques”, Prepr. Pap.—Am. Chem. Soc., Div. Fuel Chem., 42 (1999) 725.

191. N.F. Carnahan, L. Quintero, D.M. Pfund, J.L. Fulton, R.D. Smith, M. Capel and K. Leontaritis, “A Small Angle X-Ray Scattering Study of the Effect of Pressure on the Aggregation of Asphatene Fractions in Petroleum Fluids under Near-Critical Solvent Conditions”, Langmuir, 9 (1993) 2035.

192. K.A. Ferworn, W.Y. Svreck and A.K. Mehrotra, “Measurement of Asphaltene Particle Size Distribution in Crude Oils diluted with *n*-Heptane”, Ind. Eng. Chem. Res., 32 (1993) 955.

193. B.B. Nielsen, W.Y. Svreck and A.K. Mehrtotra, “Effects of Temperature and Pressure on Asphaltene Partricle Size Distribution in Crude Oils with *n*-Pentane”, Ind. Eng. Chem. Res., 33 (1994) 1324.

194. M.A. Anisimov, I.K. Yudir, V. Nikitin, G. Nikolaenko, A. Chernoutsan, H. Toulhoat, D. Frot and Y. Briolant, “Asphaltene Aggregation in Hydrocarbon Solutions Studied by Photon Correlation Spectroscopy”, J. Phys. Chem., 99 (1995) 9576.

Appendix 14.1

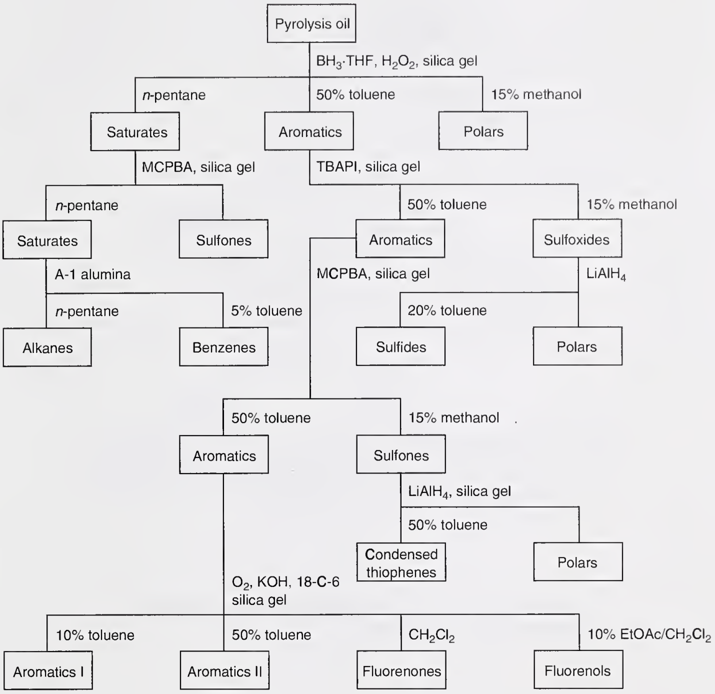
Pyrolysis oil
BH3·THF, H2O2, silica gel
n-pentane
50% toluene
15% methanol
Saturates
Aromatics
Polars
MCPBA, silica gel
TBAPI, silica gel
n-pentane
Saturates
Sulfones
50% toluene
15% methanol
Aromatics
Sulfoxides
A-1 alumina
MCPBA, silica gel
LiAlH4
n-pentane
5% toluene
20% toluene
Alkanes
Benzenes
Sulfides
Polars
50% toluene
15% methanol
Aromatics
Sulfones
LiAlH4, silica gel
50% toluene
Condensed thiophenes
Polars
O2, KOH, 18-C-6 silica gel
10% toluene
50% toluene
CH2Cl2
10% EtOAc/CH2Cl2
Aromatics I
Aromatics II
Fluorenones
Fluorenols

Flow diagram for the analysis of pyrolysis products of Athabasca asphaltene. From J.D. Payzant *et al.*, Ref. 80. © 1991, American Chemical Society.

Appendix 14.2

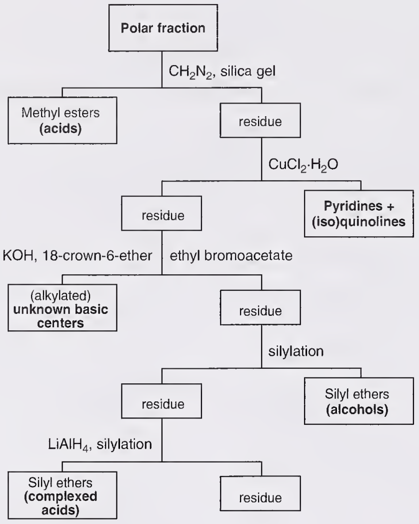
Polar fraction
CH_2N_2, silica gel
Methyl esters (acids)
residue
$CuCl_2 \cdot H_2O$
residue
Pyridines + (iso)quinolines
KOH, 18-crown-6-ether
ethyl bromoacetate
(alkylated) unknown basic centers
residue
silylation
residue
Silyl ethers (alcohols)
$LiAlH_4$, silylation
Silyl ethers (complexed acids)
residue

Flow diagram for the analysis of pyrolysis products of Athabasca asphaltene.

Appendix 14.3

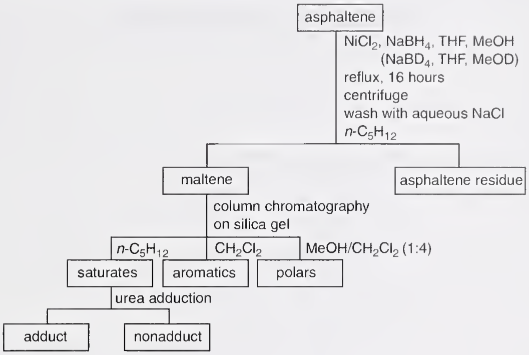
asphaltene
NiCl2, NaBH4, THF, MeOH
(NaBD4, THF, MeOD)
reflux, 16 hours
centrifuge
wash with aqueous NaCl
n-C5H12
maltene
asphaltene residue
column chromatography
on silica gel
n-C5H12
CH2Cl2
MeOH/CH2Cl2 (1:4)
saturates
aromatics
polars
urea adduction
adduct
nonadduct

Flow diagram for the analysis of products from the NiB reduction of Athabasca asphaltene. From P. Peng *et al.*, Ref. 37. © 1997, American Chemical Society.

Appendix 14.4
Products and their yields from the RICO of various organic compounds

Substrate	Products[a]	% Product recovery	Ref.
benzene	"vigorous explosion"		1
phenanthrene	phanthraquinone	28	1
diphenyl sulfide	diphenyl sulfone	31	1
methyl benzyl sulfide	methyl benzyl sulfone	58	1
pyridylphenylmethane	4′-pyridylphenone	67	2
cyclohexylbenzyl ether	cyclohexylbenzoate	90	2
propylbenzene	butyric acid (95); propiophenone (5)	76	3
tridecylbenzene	tetradecanoic acid(91); tridecanophenone (9)	70	3
tetralin	adipic acid (75); 1-tetralone (8); glutaric acid (17)	100	3
bibenzyl	succinic acid (35); hydrocinnamic acid (63)		3
4-pentylbiphenyl	hexanoic acid (51); benzoic acid (54); 4-pentylbenzoic acid (38)	74	3
phenanthrene	phthalic acid (5); diphenic acid (91); phenanthrenequinone (4)	100	3
triphenylene	phthalic acid (75); benzene hexacarboxylic acid (25)	55	9
9,10-dihydrophenanthrene	succinic acid (2); phthalic acid (7); diphenic acid (55); 3-(2-carboxyphenyl)-propionic acid (32)	81	8
1-decene	nonanoic acid	89	4
phenylcyclohexane	cyclohexanecarboxylic acid	94	4
1-methylnaphthalene	phthalic acid; 3-methylphthalic acid	"good yield"	5
isochroman	isochromone	95	6
4-benzyloxobenzoic acid	4-hydroxybenzoic acid; benzoic acid		6
4-nitroethoxybenzene	ring attacked products		6
9,10-dihydroanthracene[b]	anthrone; anthraquinone; anthracene; phthalic acid		6
pentadecylbenzene[b]	hexadecanoic acid (69); shorter homologous acids; pentadecylphenone	65	6
2,2-diphenylpropane	dimethylmalonic acid		7
6-hydroxytetralin	glutaric acid; succinic acid		7
6-methoxytetralin	glutaric acid; succinic acid		7
2-tetralone	succinic acid		7
lignite coals	"phthalic and other polybenzene- carboxylic acids"		8
diheptyl sulfide	diheptyl sulfone	99	9
dibenzyl sulfide	dibenzyl sulfone	88	9
diphenyl sulfide	diphenyl sulfone	85	9
dibenzothiophene	dibenzothiophene sulfone	~100	9
n-alkyl thiolanes and thianes	thiolane and thiane sulfones	~100	9
benzothiophene	completely oxidized		9
1-hexadecene	pentadecanoic acid	93	9
1,12-diphenyl dodecane	1,12-tetradecanedicarboxylic acid	100	9

---

[a] From T.W. Mojelsky *et al.*, Ref. 94. © 1992, American Chemical Society. [b] Numbers in brackets indicate % distribution.
[c] Depends upon co-oxidant to substrate ratio.

References

Appendix 14.4

1. C.J. Djerassi and R.R. Engle, J. Am. Chem. Soc., 75 (1953) 3838. Note: acetonitrile as co-solvent was not used.
2. P.F. Schuda, M.B. Cichowicz and M.R. Heinmann, Tetrahedron Lett., (1983) 3829.
3. L.M. Stock and K. Tse, Fuel, 62 (1983) 974.
4. P.H.J. Carlson, T. Kalsuhi, V.S. Martin and K.B. Sharpless, J. Org. Chem., 46 (1981) 3936.
5. E.S. Olson and B.W. Farnum, Preprints, Am. Chem. Soc., Div. Fuel Chem., 26 (1981) 60.
6. W.H. Isley, R.A. Zingaro and J.H. Zoeller, Fuel, 65 (1986) 1216.
7. E.S. Olson, J.W. Diehl, M.L. Froehlich and D.J. Miller, Fuel, 66 (1987) 968.
8. E.S. Olson, J.W. Diehl, M.L. Froehlich and D.J. Miller, Preprints, Am. Chem. Soc., Div. Fuel Chem., 31 (1986) 97.

(9) T.W. Mojelsky, T.M. Ignasiak, Z. Frakman, D.D. McIntyre, E.M. Lown, D.S. Montgomery and O.P. Strausz, Energy & Fuels, 6 (1992) 83.

Appendix 14.5

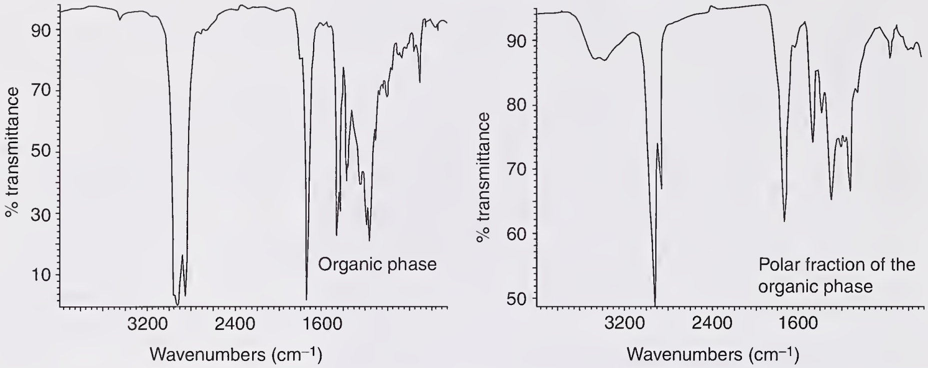

FTIR spectra of oxidized Athabasca asphaltene. From O.P. Strausz *et al.*, Ref. 93. © 1999, American Chemical Society. For characteristic absorptions of -SO$_x$-species, *cf. Infrared Absorption Spectroscopy*, Koji Nakamishi, Holden-Day San Francisco and Nancodo Co. Ltd., Tokyo, 1964.

Appendix 14.6*

Elemental analysis of low-molecular-weight (LMA) and high-molecular-weight (HMA) Athabasca asphaltenes and their RICO products

Sample	Source	Yield, wt %		wt% (DAF)					Ash, %	H/C	MW[b]
		1	2[a]	C	H	N	O	S			
substrate	LMA	100	16	78.32	8.37	0.96	4.39	7.96	0.00	1.28	890
	HMA	100	84	79.29	7.84	1.09	3.83	9.95	2.03	1.19	6800
acids	LMA	48.5	7.8	61.36	7.56	0.55	23.73	6.81	23.00	1.48	880
	HMA	35.2	29.6	64.37	7.83	0.77	21.79	5.24	11.42	1.46	1400
Me-esters	LMA	61.5	9.9	66.73	8.73	0.92	18.10	5.52	–	1.57	530
	HMA	46.5	39.1[c]	70.49	7.68	0.69	17.41	3.72	4.25	1.57[c]	780
	LMAw[d]	19.0	3.0	54.35	6.14	1.05	34.22	4.24	9.90	1.36	390
	HMAw[d]	10.0	8.4								
GPC fractions of esters											
	LMA–1	11.8	1.9	65.45	7.87	1.34	19.40	5.93	0.96	1.44	5470
	LMA–2	11.6	1.9	66.74	8.61	0.71	17.61	6.32	8.98	1.55	1200
	LMA–3	14.5	2.3	67.37	8.87	0.58	17.71	5.48	8.34	1.58	660
	LMA–4	13.4	2.1	67.54	8.89	0.67	18.22	4.68	4.75	1.58	430
	LMA–5	10.1	1.6	69.14	9.31	0.83	17.99	2.73	0.77	1.62	300
	HMA–1	16.1	13.5	61.70	7.50	2.10	23.94	4.76	6.90	1.46	8230
	HMA–2	10.4	8.7	68.72	8.81	0.93	16.53	4.98	9.21	1.54	1200
	HMA–3	7.4	6.2	69.67	9.45	0.47	16.94	3.47	5.92	1.63	660
	HMA–4	7.3	6.2	70.16	9.93	0.62	16.94	2.36	0.88	1.70	450
	HMA–5	5.4	4.5	70.12	9.68	0.88	18.01	1.31	0.83	1.66	300
	Aw[d] 1	3.3	3.3	60.42	6.32	1.34	26.47	5.45	3.39	1.26	8690

[a] 1 = wt% of substrate; 2 = wt% of the native asphaltene. [b] In benzene. [c] The excessive weight increase is due to the $-(CH_2)_n-$ polymer formed from diazomethane; [d] Water layer. [e] Calculated from GPC fractions. From T.W. Mojelsky *et al.*, Ref. 94. © 1992, American Chemical Society.

* As mentioned in sections 4.4.2 and 4.4.4 Wang *et al.*,[109] determined the carbon yield from CO_2 plus the carbon yield from the diazomethane methylated oxidation products and claimed to have obtained 98.2% recovery. This claim was erroneous for the following reasons:

- evaporation losses were neglected;
- the carbon content increase due to methylation was neglected; and
- most importantly Wang *et al.*,[109] were not aware of the polymerization reactions of the methylene and diazomethane molecules occurring parallel to the methylation of the carboxyl functionality leading to olefinic products with a broad MW distribution. Had they scrutinized the data in the table above published in reference 94, they would have noted the dramatic weight increase that accompanies the methylation of the acids. The weight increase amounts to 25–35% corresponding to an average of 44% increase in carbon content. If our data are applicable to their reaction conditions, as probably is the case, then it is possible to estimate that their true carbon yield from the reaction must have been around 73%. Therefore (quite aside from the logical error of assuming that all asphaltenes should yield identical product distribution) their argument that since they obtained 98.2% carbon recovery with 15.5 %C yield from CO_2 it follows that any higher than 15.5 %C yield from CO_2 must be erroneous.

Appendix 14.7

Oil sand bitumen extracted with benzene or methylene chloride contains 0.5–1.0% clay minerals concentrated in the asphaltene fraction of the bitumen. The content of the clay minerals in the asphaltene can be reduced, in the present instant from 3.2% to 0.5% by successive centrifugation without affecting the chemical composition.

IR studies of the asphaltene and isolated clays and X-ray diffraction studies of the clays, Figures 14.7.1 and 14.7.2, reveal the following features*:

- the FTIR spectrum of asphaltene with 3.2% clay content, Figure 14.7.1a, displays the characteristic absorption bands of kaolin, Figure 14.7.2a, namely bands in the 400–600, 950–1100 and 3600–3700 cm^{-1} ranges. The last of the bands at 3695.95 cm^{-1} attributed to outer OH vibrations is characteristic of kaolin;
- according to the X-ray diffraction data, the clay is a mixture of kaolin minerals with illite interstratified with less than 10% smectite and some quartz in trace amounts. No evidence presented itself for the existence of discrete swelling clay minerals in the asphaltene;
- in the step-wise removal of the clay from the bitumen and asphaltene by centrifugation it was observed that the clay from the bitumen, Figure 14.7.2b, strongly resembles that of standard kaolin, the first 0.9% clay removed from the asphaltene, Figure 14.7.2c, indicates the presence of adsorbed water (broad bands at ≈ 3400 cm^{-1} and 1630 $cm^{-1)}$ that may be associated with illite. The absorption at ≈ 1450 cm^{-1} suggests the presence of some carbonates in the clays. The last 0.4% clay removed from the residual 0.9% clay to reduce its final amount to 0.5%, Figure 14.7.2d, while still clearly bears the characteristics of the kaolin family minerals indicating changes in band intensities and articulation in the 950–1100 cm^{-1} region as well as the growth of the 2800–3000 and 1600–1750 bands showing the presence of strongly adsorbed organic matter;
- the FTIR spectrum of the asphaltene with a residual clay content of 0.5%, Figure 14.7.1d, lacks the clay absorption bands; the residual absorption at 1032 is due to the S=0 stretch vibration in sulfoxides;
- the progressively smaller size fractions of the clay material from successive centrifugation of the asphaltene corresponds closely to a change from well-crystalized, ordered kaolinite to highly disordered kaolinite as determined by X-ray diffraction measurements; with decreasing crystallinity and particle size, the clay has an increasing affinity towards organic matter;
- reasonable rectilinear relations have been established between clay and ash levels and the intensity of the 1040 cm^{-1} IR absorption of asphaltene.

---

* T.M. Ignasiak, L. Kotlyar, F.J. Longstaffe, O.P. Strausz and D.S. Montgomery, “Separation and Characterization of Clay from Athabasca Asphaltene”, Fuel, 62 (1983) 353.

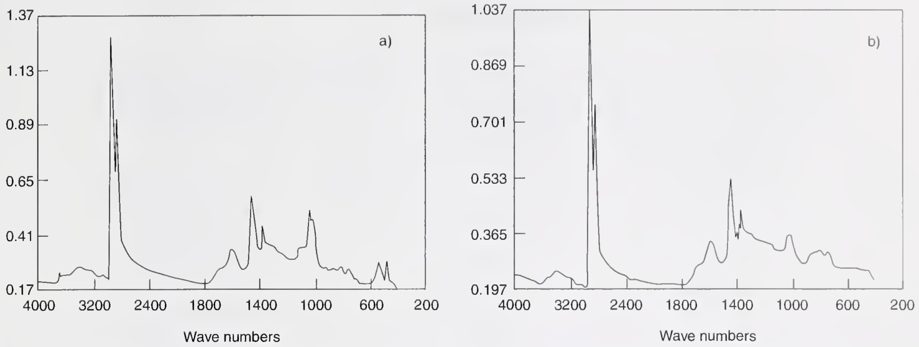

Figure 14.7.1 FTIR spectra of asphaltene containing a) 3.2%, and b) 0.5% clay (2 mg sample per 300 mg KBr).

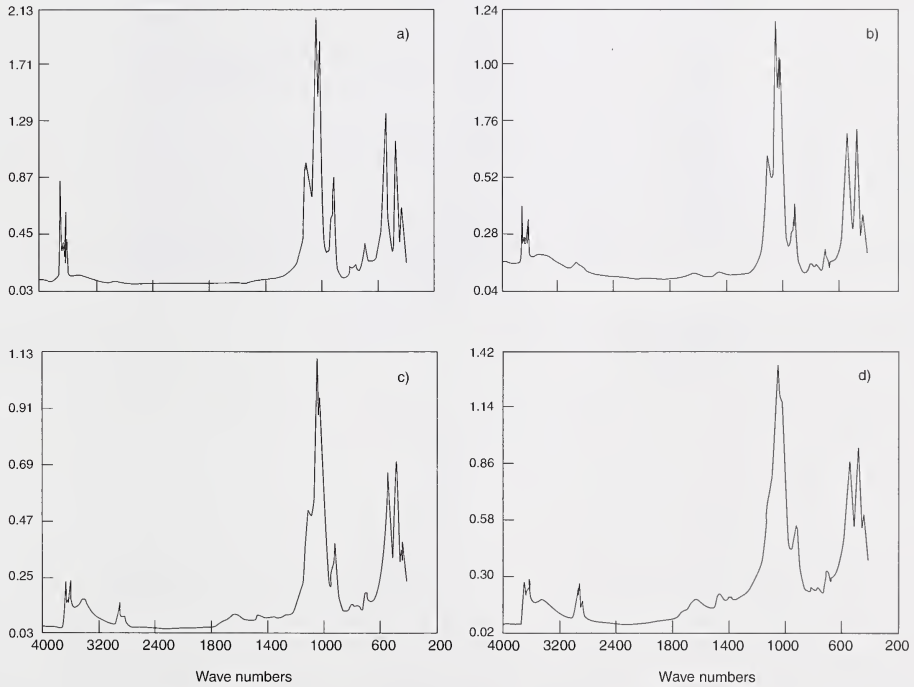

Figure 14.7.2 FTIR spectra of the clay minerals removed from the bitumen and asphaltene, a) Kaolin standard, b) clay removed from bitumen, c) the first 0.9% clay from the asphaltene and d) is the 0.4% clay removed from asphaltene with 0.9% clay content (1 mg sample per 300 mg KBr). From T.M. Ignasiak *et al.*, Fuel 62 (1983) 353. © 1983, Butterworth-Heinemann.

Appendix 14.8

Some of the Lower Homologous Series of Alkyl Aromatic Compounds Identified in Athabasca Asphaltene

Z number in C_nH_{2n-Z}	Formula
-6	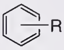
-8	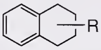
-10	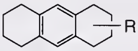
-12	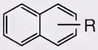
-14	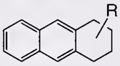 ; 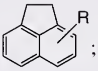 ; 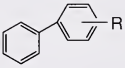
-16	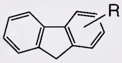 ; 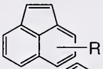
-18	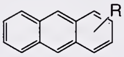 ; 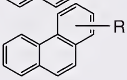

Z number in $C_nH_{2n-Z}S$	Formula
-4	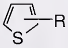
-10	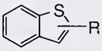
-12	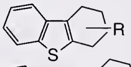
-14	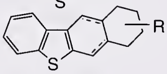
-16	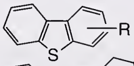
-20	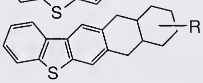

Cf., also references 39–41, 67, 68, 80, 81, 83 and Table 14.16 along with Figures 14.34, 14.35, 14.37–14.44.

Appendix 14.9

Fluorescence Lifetimes and Quantum Yields of Small Aromatic Compounds[119d]

	Lifetime, nsec	Quantum yield
Benzene*	29	0.07
Toluene*	34	0.17
Naphthalene*	96	0.23
1-Methylnaphthalene*	67	0.25
2-Methylnaphthalene*	59	0.32
Biphenyl*	16	0.18
Anthracene*	4.9	0.36
Phenanthrene*	71	0.15
Naphthacene	6.4	0.21
Benz(a)anthracene	60	0.20
Chrysene*	44.7	0.23
Triphenylene†	36.6	0.08
Pyrene*	400	0.32
Perylene*	6.4	0.94
Fluorene*	10	0.80
Biphenyl*	16	0.18
Acenaphthene*	46	0.60

* Have been detected in Athabasca asphaltene.

† Probably present in Athabasca asphaltene.

Epilogue

Bitumen, being a class of crude oil, has its chemistry closely tied to petroleum chemistry which in the past three and a half decades underwent—like science and technology in general—deep-rooted metamorphosis and this period has witnessed the birth and spectacular advancement of modern petroleum chemistry. During this time chemical foundations for new, technologically more advanced, cleaner, neater, environmentally more benign technologies have been developed. The organic chemistry of petroleum has made impressive progress and organic geochemistry, biomarker chemistry have become mature sciences. This era also coincided with the emergence and rapid growth of the modern oil sand industry in Alberta.

The major achievement, at least from an epistemological point of view of modern petroleum chemistry, is the scientifically sound elucidation of the origin of petroleum and the laying down of foundations for the theory of petroleum sciences. In oil sand chemistry this is parallelled by the elucidation in some detail of the origin of Alberta oil sand bitumen.

Over the course of history there have been several suggestions put forth as to the origin of Alberta oil sand bitumen which include:

- abiogenic gas hydrates, methane, ethane, *etc.*, polymerization;
- deep earth explosion hurling abiogenic high-quality crude oil from deep within the earth crust or mantle to the surface;
- the extraterrestrial "intergalactic oil freighter" hypothesis;
- biogenic origin from organic sediments deposited in the present day reservoir rocks;
- biogenic origin from organic sediments deposited in sedimentary source rocks from where after diagenetic and some catagenetic maturation the oil generated migrated to its present day reservoir rocks.

For the reader of this book it must already be clear at this point that the only correct reconstruction of the history of the origin of bitumen is the last-mentioned one.

From the chemical composition of the oil it is now possible to tell what kind of living organisms provided the biotic source material in what kind of environment, in what kind of source rocks and under what kind of conditions were the biotic source materials deposited. The knowledge gained provides invaluable aid in oil exploration and in the elucidation of the chemical composition of the bitumen. All this became possible because of the success and rapid advancement made in the discovery of the vast number of biological molecules present in crude oils which can be used as biological markers. A good number of these biological molecules have been discovered in Alberta bitumens. They include the important homologous and quasihomologous series of bi-through hexacyclic terpenoid sulfides, *n*-alkyl substituted monocyclic-five- and six-membered ring sulfides, their mildly oxidized derivatives the cyclic terpenoid sulfoxides, homologous series of *n*-alkylsubstituted thiophenes, benzothiophenes, dibenzothiophenes, fluorenes, fluorenols, fluorenones, asphaltene-attached *n*-alkyl ethers, esters, cyclopropyl, steranoic, hopanoic carboxylic acids, some alcohols, *etc.*

The cyclic terpenoid sulfides are regular constituents of all sulfur containing petroleums and the *n*-alkyl substituted mono cyclic sulfides are regular constituents of all non-biodegraded oils. They occur not only in free form, but also in chemically bound forms. Acyclic sulfides are also present and they play an important role in the structural construction of the asphaltene molecules. Sulfides comprise a sizeable weight fraction of the bitumen.

Also, as was discovered in Alberta bitumen, the hydrocarbon frameworks of the terpenoid sulfide molecules constitute the most important hydrocarbon type biological markers in the bitumen. They occur as free hydrocarbons in the saturates and aromatic fractions and in derivatized state as carbocyclic acids, alcohols and of course as sulfides and sulfoxides in the resins. They are also present as sulfide, ester, ether and C_{arom}–C bound appendages in the asphaltene.

The role played by microbiological processes in the alteration of petroleum discovered in the mid 1950s by Russian scientists had found application in explaining certain features of Alberta crude oils in the early 1970s. It then quickly became a widely accepted tenet that Alberta bitumens are the residues of the microbiological degradation of some medium grade conventional crude oils which later have been described on the basis of their biological marker content and some other compositional characteristics as early mature–mature marine carbonate oils, deposited under strongly reducing conditions in a saline aquatic environment. This feature of the history of the bitumen explains the absence of the *n*-alkane and other biodegradable complements of conventional crude oils. The story then neatly explains one of the essential compositional attributes of the bitumen, namely, that its hydrocarbon fraction is largely comprises mixtures of cyclic terpenoid (steroid) biological markers and their isomerization, ring opening, degradation and aromatization products.

The hydrocarbon biomarkers are usually present in homologous or quasihomologous series extending over a carbon range with each member occurring in several and sometimes many isomeric forms.

Among the other important characteristics of the bitumen are its high polar and asphaltene content and high heteroatom content. These properties partly originate from the precursor oil (*e.g.* high sulfur, vanadium, V/Ni) and partly are the consequences of their microbiological and associated water washing and oxidative history. Biodegradation causing the removal of the *n*-alkanes and other hydrocarbons does not appear to consume components of the resin fraction and thereby increases their relative amount in the biodegraded residue. The heaviest fraction of the bitumen, the asphaltene, is also impervious to biodegradation and consequently its proportion in the residue is also significantly enhanced.

The resin fraction contains series of *n*-alkanoic and bi-through pentacyclic terpenoid carboxylic acids and series of aromatic carboxylic acids from the interruption of the biodegradation of longer than C_8 *n*-alkyl aromatics along with *n*-alkanols, terpenols, steroid alcohols, homologous series of *n*-alkyl benzothiophenes, dibenzothiophenes, fluorenes, fluorenols, fluorenones along with sulfoxides, pyridines, quinolines, quinolinoles and a host of other compounds.

Asphaltene, the heaviest fraction of the bitumen is, in contrast to the maltene, mainly composed of *n*-alkylaromatics and *n*-alkyl sulfur aromatics along with their naphtheno aromatic counterparts. The alkyl groups are present as side chains on, and bridges between, cyclic molecules and they, along with the small amounts of terpenoid and steroid biomarkers were protected against biodegradation, catalytic degradation and other alterations over geologic times. This is because an intrinsic property of asphaltene is its capacity to form high-MW aggregates either by the Guldberg-Waage mass action or a micellar mechanism. The latter mechanism is tied to the presence of moisture as has been recently discovered. Another characteristic property of asphaltene is its propensity to adsorb resins. The adsorbed resins may stabilize the dissolved asphaltene in the bitumen and also may influence its aggregation mechanism. The protective effect of the asphaltene in preserving the chemical integrity of its structure is then due to the high MW aggregate/micellar nature of its solution.

The structure of the covalent asphaltene molecules, the nature of their aggregates and adsorption complexes are difficult problems to elucidate and have historically been one of the central problems in petroleum chemistry. Complicating the problem is the polydisperse distribution of the aggregates built on polydispersely distributed covalent asphaltene molecules.

The salient features of the covalent Athabasca asphaltene molecules have recently been shown to be the following:

- existence of a common central core unit with a MW_N of about 540 $g{\cdot}mol^{-1}$;
- existence of molecules built from two core units which are bridged together by a sulfide sulfur;
- existence of molecules built from two core units which are joined together by an ester oxygen atom;
- the number of core units present in the three kinds of environments are in the approximate proportion of 1:6:2, respectively;
- about 42% of the carbon is aromatic, 27% *n*-alkanoic and 31% is naphthenic;
- the structure of core units features aromatic, naphthenoaromatic core segments along with their sulfur aromatic and naphthenoaromatic counterparts which are interconnected via alkyl, sulfide, ester, biaryl and aryl-naphthenic linkages;
- the above structures endow the asphaltene molecules with a loose and flexible molecular skeleton with great number of internal rotational and vibrational degres of freedom impacting its kinetic and rheological properties;
- in sharp contrast to the maltene fraction of the bitumen, the asphaltene fraction possesses long *n*-alkyl and some α–branched *n*-alkyl side chains from C_1 up to over C_{30} which were protected from biodegradation. They furnish clear evidence that the precursor oil had a sizable complement of *n*-alkanes;
- the position of the *n*-alkyl groups in the aromatics and cyclic sulfide products from the pyrolysis of asphaltene is highly specific, permitting the stretching out of the molecule in a straight chain by the cleavage of a few, appropriate bonds;
- this feature of the architecture of the asphaltene molecule is a clear manifestation that the cyclic components, including the aromatic and naphthenic structures were formed by the cyclization and aromatization reactions of *n*-alkanoic compounds; *n*-alkanoic acids, *n*-alkanols: thus, the molecular structure of asphaltene contains important geochemical information pointing to its biomarker character;
- the acetone extract of the native *n*-C_5 Athabasca asphaltene with a MW_N of about 1200 $g{\cdot}mol^{-1}$ contains low-MW resins and apparently two kinds of asphaltenes, one featuring minor amounts of two or more sulfide bridged units and the one without sulfide bridges. The MW_N of the latter is close to that of the dimeric core unit, 2 × 540 = 1100, or an ester oxygen bridged dimeric core unit.

From the preceedings it follows that the two principal biotic source materials of Athabasca bitumen and petroleum in general were the cyclic terpenoid plus steroid compounds on the one hand and *n*-alkanoic acids plus alcohols on the other. Knowledge of the origin, biotic source material and history of the bitumen furnishes this important information pertaining to the composition of the bitumen. Bitumen is one of the most complex chemical systems known and without taking advantage of the wealth of chemical knowledge that has accumulated in organic geochemistry and biomarker chemistry interrelated to the origin, biotic source material and history of petroleum it would have hardly been possible to get as far as we did in the understanding of the chemistry of oil sand bitumen. This is the reason why anyone interested in the chemistry of bitumen should have some familiarity with its history. One simple example of the many that one could quote is the general feel we get for the overall composition of the lower hydrocarbon fractions of the bitumen just from comparing their ring number and carbon number distribution with those of the cyclic hydrocarbon biomarkers. The excellent correlation that one finds for the saturate fraction and the cyclic biomarkers and also between the lower aromatics and the cyclic biomarkers constitutes clear cut evidence that these fractions of the bitumen originated from the isomerization, ring opening, degradation and aromatization of the cyclic biomarkers in the oil and thus they have a close structural relationship with the cyclic terpenoid and steroid biomarkers.

Also, the above outline of the molecular structure and architectural principles of the asphaltene renders understandable the low yields of asphaltene and coke in the upgrading step of the bitumen. The sulfide and ester bonds being the weakest in the asphaltene molecule cleave readily at low temperatures causing marked reduction in MW, increased solubility and thereby reduced phase separation what is the immediate cause of coke formation. In this regard the role of the high concentrations of resins needs mentioning. Resins are the best solvents for asphaltenes and are responsible for the stability of the asphaltene solution in the maltene.

To sum it all up in one sentence we can say that the bitumens and heavy oils are exceedingly complex chemical systems and an in-depth, detailed knowledge of their composition and other related properties are prerequisite for the developing of optimal strategies and process technologies for their upgrading and conversion to synthetic crude oils.

Subject Index

List of Abbreviations:
Ath. = Athabasca; PR = Peace River; Lloyd. = Lloydminster; CL = Cold Lake
HMA = high-molecular-weight asphaltene; LMA = low-molecular-weight asphaltene; MW = molecular weight;
NRA = naphthalene radical anion; RICO = ruthenium ions-catalyzed oxidation

abiogenic oxidation 11,19
acid–base reactions 44
acid number 430
acyclic terpenoid biomarkers 398
adduction chromatography
  of the saturate fraction 195 *illus.*,216
alkaline earth carbonates 37
alkyl
  bridges in Ath. asph. 552,553 *illus.*
  n- groups in Ath. asph. 545
alterations of crude oils 19 *illus.*
amphipathic molecule 639,641
amphiphilic components 35
analcime 135
Andrade equation 104–106
anoxic 12
API gravity 90,95,99–102,109,113,403,404,421 *illus.*
  correlations 103 *illus.*
  of biodegraded oil 419,422
API gravity scale 89
Arabian asphaltene
  RICO 568–573
aromatic fraction
  contents 219 *table*
  Ath. distillables, composition 220–240, 254 *illus.*
  Ath. nondistillables
    NMR 241/242 *illus.*
    RICO 248,252
    thermolysis products 241
  CL composition 220 *table*,254 *illus.*
  Lloyd. composition 254 *illus.*
aromatization 238
ash content 93,95 *table*,112
asphaltene
  aggregation 640,642,644 ,651 *illus.*
    shapes, radius 648 *illus.*
    size 649 *illus.*,650 *illus.*
    – volume 645 *table*,646
  conductivity and dielectric properties 606
  content 113,125 *table*
    in biodegraded oil 422
    variation with depth 126,127 *table*
  correlation length 647 *illus.*
  covalent structure 606
  definition, general properties 459,460
  elemental composition 493,494/495 *tables*
  EPR parameters 601 *table*
flocculation threshold 479,480,650,651 *illus.*
fluorescence
  decay curves 590
  lifetime 590,591
  spectra 589
interparticle potentials 646 *illus.*
micellar properties 462
micelles 637
critical micelle concenration (CMC) 638,640, 642 *illus.*,644,648 *illus.*
  enthalpy of dissociation 643
  formation 638–640
  inverted 641
  properties 643
  reverse 643
  shape 638
  structure 638,639 *illus.*
micellization 633
MW
  determination
    from chemical studies 625,626,628 *table*
from chromatographic studies 622–624, 628 *table*
    from fluorescence spectra 591,592
from small angle neutron scattering 645 *table*,646
    from small angle X-ray scattering 647
  distribution curves 488 *illus.*,629 *illus.*
  of GPC fractions 487 *illus.*
nature of core 618
nitrogen content 495
origin 634
oxygen content 495
polyaromatic sheets, size 620,621
precursors of:
  n-alkanoic types 620
  cyclic terpenoid types 620
precipitation 464
  –point calculation 469,471
  potential 486; – scale 480 *illus.*
  procedures 487
    ASTM 487
    Syncrude 487
    UOP 487
  yield
    effect of oxygen and light 493
from various precipitants 468 *table*,485 *illus.*

      vs contact time 489,490 *illus.*
    vs no. of re-dissolutions/reprecipitations 483 *illus.*
      vs MW of precipitant 490 *illus.*
      vs pressure 492 *illus.*
      vs solvent solubility parameters 467 *illus.*
      vs solvent carbon number 465 *illus.*
      vs solvent surface tension 466
      vs temperature 490,491 *illus., tables*
      vs volume precipitant 488/489 *illus.*
  radius of gyration 647
  separation 120,461
  size of polyaromatic sheets 620
  solubility
    calculations 471,472 *illus.*
    characteristics 46
    critical solubility point 479
    parameters 465,466,469,470 *table*,473,474 *illus.*,477/478 *illus.*,481
      vs refractive index 481 *illus.*
    phase diagram 475 *illus.*
  solvency 480
  Soxhlet extractions 484 *table*
  sulfide bridges 527
  sulfur content 495
  surface tension and viscosity of solutions 644/645 *illus.*
  swelling 647
  trace metals in – 495
  ultracentrifugation 638
  ultrafiltration 638
  X-ray studies 620
asphaltic aggregates 96
asphaltites 89
asphalts 89
Ath. asphaltene
  absorption spectra 586 *illus.*
  acetone extract
    preparation 305,525 *illus.*
    fractionation 306 *illus.*,525 *illus.*
  alkyl bridges in – 626
  ash level 497
  biotic source materials 610
  C_{arom} in – 626
  C_{naph} in – 626
  clay minerals in 670,671 *illus.*
  covalent MW 621
  dissociation 625
  distribution of carbon 563 *table*
  ester bridges 611
  fluorescence spectra 587 *illus.*
    yields 588
  EPR
    parameters 598
    spectrum 593/594 *illus.*
    temperature dependence 595 *illus.*
  fluorescence, excitation spectra 587 *illus.*
  geochemical classification of trace elements 497 *table*
  GPC (Bio-Beads) fractions 496 *table,* 580
    free radicals in - 597 *table*
    NMR spectra 576 *illus.*,578 *illus.*
      assignments 577 *table*,579 *table*
  GPC (Styragel) fractionation 622
    FTIR spectra of fractions 625 *illus.*
    time profiles of fractions 623/624 *illus.*
  heat of solution 475 *table*
  high-MW (HMA) properties 526,634 *table*, 669 *table*
    analysis of RICO fractions 669 *table*
    NiB reduction 525
      analysis of products 665 *illus.*
      saturate products 528–535
  hydrolytic degradation 539
  intermolecular intractions 624
  low-MW (LMA) properties 526,634 *table*,669 *table*
    analysis of RICO fractions 669 *table*
    NiB reduction 525
      saturate products 535–537
  MW
    determination from
      chromatographic studies 622–624, 628 *table*
      chemical studies 611,625,626,628 *table*
      mass spectrometric studies 630 *table*
      molecular rotational correlation time–fluorescence depolarization 632
    distribution from MS 630 *illus.*
    of covalent core segments 613
  NMR studies 575,584 *illus.,tables*
  NRA reduction 523
  RICO 542
    distillable products 544–557
    nondistillable residue 557
      composition 557
      thermolysis products 559,560 *illus.*
  spin concentration 595,599
  structural elements from
    C–O bond cleavage 617
    thermolysis 607–610
    reductive degradation 611
    RICO 614–616
  sulfide bridges 612
  structural models 626,627 *illus.*
  thermolysis of whole asphaltene 500–507
  thermolysis of HMA 507–523, 607
    analysis of pyrolysis oil 663/664 *illus.*

    - *n*-alkane products, yields 608
    - alkylaromatic products 607 *table.*
    - alkylbenzene products 609
    - alkylnaphtenic products 607 *table*
    - composition of the pyrolysis oil 508 *table*
    - condensed aromatics 610
    - thiophenes, condensed thiophenes, sulfides 609
  - trace element concentrations 487 *table*,497
  - triplet/doublet free radical ratio 596 *table.*
- Athabasca oil sands
  - distillates properties 108 *table*
  - gases evolved
    - vs temperature 181 *table*
    - vs depth 183 *table*
    - vs time at 130°C 185 *table*
    - vs time at 170°C 186 *table*
    - vs time and temperature 184 *table, illus.*
    - in the presence of oxygen 186 *table*, 187 *illus.*
- Attapulgus clay 123
- axial 74
- algae (phytoclasts) 13
  - blue-green, 10

- bacteria 10
- Banff reserves 25
- Baumé scale 89
- Bingham model 106
- biodegradation 16,17,90,204,386,389,390,400, 403,417
  - effect on
    - oil quality 422
    - pristane/phytane ratio 422
  - extent of – 419 *illus.*
  - of Athabasca 423 *illus.*,425 *illus.*
  - of Bellshill Lake 405,420 *illus.*,421 *illus.*,425 *illus.*
  - of hydrocarbon biomarkers 418,420 *illus.*,422–424
  - of oil sand bitumens 421 *illus.*,423 *illus.*
  - of Prudhoe Bay 405 *table*,418 *illus.*,421 *illus.*, 423 *illus.*,425 *illus.*
  - of thiolanes 406
- biomarker
  - products from NiB reduction of Ath. asph. 534
  - ratios (steranes) 393 *table*
- bitumen
  - reserves 25 table
  - API gravity 100 *table*,103 *illus.*,125 *table*
  - asphaltene content 125 *table*,127 *table*
  - class composition 120,124 *table*
  - class separation procedures 122/123 *illus.*
  - compositional variations 126
  - definition, characterization, separation 89,121
  - density–viscosity correlation 106 *illus.*
  - elemental composition 93,94 *table*,121 *table*
  - EPR parameters 601 *table*
  - displacement 57/58 *illus.*
  - distillation data 95 *table*,112 *table*
  - oil/water/solids analyses 93 *table*
  - pressure effect 106
  - saturation 30
  - spin density 600 *table*
  - sulfur content 125 *table*
  - Suncor coker feed characterization 95
  - thermal properties 107
    - carbon residue 110
    - heat of combustion 116
    - latent heats of vaporization/fusion 115
    - liquid–solid transition 107
    - specific/latent heat 114
  - trace element
    - concentrations 97 *table*,98 *table*,497 *table*
    - geochemical classification 497 *table*
  - viscosity 100 *table*,104 *illus.*,105 *table*
  - viscosity–molecular weight correlation 106 *illus.*
- Bluesky/Gething
  - geology 31
  - reserves 25
- Blueridge reserves 25
- boiling point 90
  - equation 110
  - correlations with carbon number, MW 111 *illus.*
- Boscan asphaltene
  - thermolysis 504,505 *illus.*
  - NMR 581 *illus*
  - RICO 568–573
    - FTIR of residue 585 *illus.*
    - NMR of residue 582 *illus.*
- bottom water 145
- bound carboxylic acids 45
- bridges
  - between ring structures 616
  - biaryl linkages between ring structures 616
  - polymethylene between aromatic carbons 571 *table*, 617
  - sulfur bridges 619
- buffer capacity 37

- calcite 135
- Calmar reserves 25
- capillary
  - effect 40
  - forces 58 *illus.*, 61
  - number 61 *illus.*
  - pressure 15,40,42 *illus.*,61
- carbon cycle 11
- Carbon Preference Index (CPI) 87,404,430
- carbon reservoirs 11 *table*

carbon residue 112
  correlation between MCR, RCR and CCR 112 *illus.*
  Conradson (CCR) 112,113 *table*,112 *table*
  microcarbon (MCR) 112,113*table*, 114 *table*
  Ramsbottom (RCR) 112,113 *table*, 114 *table*
carbonate
  minerals 38
  Triangle asphaltene
    RICO of – 565/566 *illus.*,557 *illus.*
catagenesis 11,12
centrifugation method of extraction 91
Cerro Negro asphaltene 598 *table*
chair conformation 74
chalcopyrite 37
chemisorbed organic matter 183 (see also humic, fulvic acids)
chert 135
chirality 80
chlorite 135
chromatographic effects 101
chromatography
  silica-alumina 122 *illus.*
  anion exchanger 123 *illus.*
CL asphaltene
  compositions of GPC fractions 496 *table*
  EPR parameters 598
  gases from thermolysis 504
  NMR spectrum 580
CL oil sands
  gases evolved 182 *table*
clay 29,159
  – humate complex 171 *illus.*
  minerals 35,671 *illus.*
    surface areas and cation exchange capacities 168 *table*
  organics 29
  suspensions 55 *illus.*
Clearwater
  geology 31
  reserves 25
cloud point 107
coke formation 96,110
cold water process 61
colloidal dipersions 91
conductivity and dielectric properties 606
conformational energies 75 *table*
connate water 35,38,39,47,50,55,56,60,145
  and the hot water process 57,58
  and chemisorbed acids 157
  composition 145,146 *tables*
  dissolved solids 145,147
  water-soluble salts 147
contact angle 40
coordination complexing 170
Cretaceous deposits 24
crystal sufaces 50
cyanobacteria 10

dealkylation 238
deasphalting 17
Debolt/Shunda
  geology 31
  reserves 25
Debolt formation geology 24,31
demetalation of porphyrins 436
density of
  biodegraded oil 422
  bitumen 95,99,101 *illus.*
  bitumen distillates 108 *table*
  hydrotreated products 108 *table*
depth of burial
  effect on gravity, sulfur and asphaltene content 101 *illus.*
  effect on sulfides 408,411
  effect on sulfoxides 416
  effect on thiophenes 297 *table*,349,417
Devonian
  Beaverhill Lake Formation 23
  De Formation 189
diagenesis 11,12,388
diaromatic subfraction composition 223–229, 238 *table*
diastereomers 81
disjoining pressure 56 *illus.*,59 *illus.*
dissolved solids in connate water 145,147
distillation
  curves 111 *illus.*
  properties 108 *table*
dolomite 135
double layer
  interaction energies 59
  repulsive force 58
Duri asphaltene
  RICO 568–573
    FTIR of residue 585 *illus.*
    NMR of residue 582 *illus.*

eclipsed forms 73
electric charges
  in oil sands 39
electric double layer 43
  of the bitumen/water interface 50, 51 *illus.*
  of the mineral/water interface 53 *illus.*,54 *illus.*
electrical properties (interface) 44,50
electrostatic bonding 169
enantiomers 80,81

ENDOR (electron nuclear double resonance) spectroscopy 592
  temperature dependence 595 *illus.*
epimerization reactions 388
epimers 81,199,549
EPR (electron paramagnetic resonance) spectroscopy 592
  EPR spectrum of Athabasca asphaltene 593/594 *illus.*
    temperature dependence 595/597 *illus.*
  parameters for Cold Lake and Athabasca bitumen 598 *table* ,601 *table.*
  spin concentration 595; of Cero Negro asphaltene 598 *table*, 599, 600 *table*
    MW dependence 596 *illus.*
equatorial 74
ester bond cleavage 539,540
ether bond cleavage 541,542 *illus.*
eunoxic 12
euphotic zones 10
extraction efficiencies 92,152 *table*

Faraday effect 120
feedstocks for chemicals 2
feldspar 135,159
field ionization mass spectrometry (FIMS) 190,212
fines 29,33,34,59,98,135
  content 30
  effect on bitumen recovery 37 *illus.*
  organic carbon content 158,159,165
  trace element concentrations 97,170 *tables*
flocculation threshold 479
Flory-Huggins term 471
fluorescence spectrum 587/589 *illus.*, 592 *illus.*
  fluorescence decay curves 590 *illus.*
  fluorescence lifetime 590/591,673 *table*
  intramolecular energy transfer 588/589, 591
  MW determination method 591
formation water
  composition 144 *table*
  types 143,144 *illus.*
free radicals
  allyl radicals: molecular orbitals 603
  perinaphthyl radicals 603
  triaryl radicals 602
  free radical concentration MW dependence 597 *table*
froth composition 170
FTIR (Fourier Transform Infrared) 91,140, 584,
  spectra of Athabasca and Gaggiano asphaltene 584 *illus.*
    RICO residues from Boscan and Duri asphaltenes 585 *illus.*

Fuller's earth 121

gas hydrates 215
gases from asph. thermolysis 504 *table*
GC–MS (gas chromatography–mass spectroscopy) 91
genesis of petroleum 12
geological timetable 22 *illus.*
geology of Alberta deposits 21
  Ath. 23,24
  PR 25
  Carb. Tri. 24
  CL 26
  Lloyd. 26
Graminis reserves 25
grain size distribution 136,139/140 *tables*
Grand Rapids
  geology 31
  reserves 25
graphite 16
gravity 99
Grosmont geology 24 *illus.*,31
Grosmont-Nisku reserves 25
group adsorption energies 269
Gudao asphaltene
  RICO 568–573

$(H/C)_{atomic}$ ratios 13,69,94–96,113
  in asphaltenes 494 *table* ,495
  in asphaltene acetone extract fractions 306
  in biodegraded oil 422
  in aromatic fraction 220 *table*
  in insoluble material 160 *table*
  in polar fraction 261
    in polar subfractions 262
    in nondistillable polars 346
    in NiB reduced asph. 526 *illus.*
  in saturate fraction 190
heat
  of combustion 116/117 *tables*
  of vaporization and fusion 115,116 *table*
heteroatoms in bitumen 96
Hildebrand solubility parameter 465,466
Hildebrand-Scatchard equation 471
HPLC–MS (high-pressure liquid chromatography–mass spectrometry) 91
HO^- and BBr_3 cleavage of the C-O bond 617
Hondo reserves 25
hot water separation 30,38,39,43,48,50,92,100, 135,165,172,179
  physical chemistry of 57,61
hydrocarbon generation 451
hydrogen bond 169,170 *illus.*,171
hydrophobic effect 639,641

hydrostatic pressure 61
hysteresis 485

illite 135,140,159,169
inertinites 13
insoluble organic matter 151
  bitumen-related 151
    extraction methods 152 *table*
    composition 152 *table*
  non-bitumen related 158
    characterization 158, 174 *illus.*
    composition 160
    distribution 168 *illus.*
    fractionation 159 *illus.*
    in sludge 174 *illus.*
    polar fractions 163 *illus.*
interfaces 39
interfacial
  effects in *in-situ* recovery 61
  energy 50
  film 46 *illus.*; – creation 47
  forces in the hot water process 58 *illus.*
  phenomena 46
  properties of oil sands 39
  relationships 39
  tension 39,40,42 *table*,43 *illus.*,44 *illus.*,45 *illus.*,46–48,479,628,641 *illus.*
    in the hot water process 57 *illus.*
intramolecular energy transfer 588,589,591
ion
  concentration in connate water 146 *table*
  dissociation 50
  adsorption 50
  dissolution 50
Ireton reserves 25
isomerism 77

Jinghan asphaltene 568,574,618

kaolinite 59,135,159,168,169
Karl Fischer titration 92
kerogen 87,407
  evolution 160 *illus.*

Langmuir model 45
latent heat of fusion 115,116 *table*
latent heat of vaporization 109,114,115,116 *table*
Leduc reserves 25
liptinites 13
liquid–vapor transition 109
Lloydminster
  asphaltene
    RICO of – 565/566 *illus.*,557 *illus.*
  upgrader production 6
London–van der Waals forces 55
Lower Cretaceous sands 21
lyophilic group 641

macerals 13
maltene
  EPR parameters 598 *table*,601 *table*
  class separations
    SARA 121,122 *illus.*,123,124 *table*,125,190
    USBM-API-60 121,122 *illus.*,123,124 *table*,190
    SAPA 121 *illus.*,124,125
  elemental analysis 121 *table*
  chromatographic fractionation 191 *illus.*,192 *table*, 193 *table*
  trace element concentrations 497 *table*
magnetic susceptibility 605
  diamagnetic – 605
  paramagnetic – 605
  Faraday method 605
maltene EPR parameters 598 *table*
marcasite 37,135
marine
  deposits 35
  sediments 13
mass spectrometry
  cross scans 196
  fast atom bombardment (FAB) 445
  field ionization (FI) 212
  matrix-assisted laser desorption ionization (MALDI) 630 *illus.*,*table*
  single ion recording (SIR) 196
  total ion current (TIC) 195
metagenesis 11,12
metamorphism 12
McMurray Formation 23
McMurray-Wabiska
  geology 31
  reserves 25
meso molecules 81
metal sulfates 37
mica 135
micelles 637
  critical micelle concenration (CMC) 638,640,642 *illus.*,644
  formation 638–640
  inverted 641
  shape 638
  structure 638,639 *illus.*
micellization 633
microbial degradation 14,16
microbiological processes 101
microorganisms 12
  aerobic 12

  anaerobic 12
migration 451 *illus.*
  primary 14,15,437 *illus.*
  secondary 15,436,437 *illus.*
minerals 135,136 *table*,137/138 *tables*
  chemical formulas 138 *table*
  in oil sand ore 159 *table*
Mississipian limestones 21
Mississipian Shunda formation geology 24
molar refraction of bitumen 118
molecular orbitals of allyl radical 603
molecular sieve adduction 216
monoaromatic subfraction composition 220–223, 236 *table*
montmorillonite 168,169
MW 90
  measurement 621,630
  of asphaltenes 494 *table*
  of desulfurization products 612
  of reduced Ath. asphaltene 524,526

naphthalene radical anion reduction of Ath. asph. 523
  mechanism 524
natural gas 1
neutral nitrogen compounds 123
  in polar fraction 266
neutral resins 123
neutron activation analysis 97
Newton's law 102
NiB reduction of Ath. asph. 525
  compound class yields 525 *table*
  elemental analysis of products 526 *illus.*
Nisku formation geology 24
NMR (nuclear magnetic resonance) 91,575,
  spectra 576 *illus.*
  assignments 577 *table*
  analysis of Athabasca asphaltene 579 *table*
  spectra of Athabasca and Cold Lake asphaltene 580 *illus.*
  ^{1}H spectra of Athabasca and Utah asphaltenes 582 *illus.*
    of RICO residues of Boscan and Duri asphaltenes 582 *illus.*
  ^{2}H NMR of products from NiB reduction of Jinghan asph. 574 *illus.*
  high resolution spectrum of Athabasca asphaltene 578 *illus.*
  spectra of Boscan, Duri, Utah, Arabian asphaltenes 581 *illus.*, Saline Lake 582 *illus*
  of RICO residues of Boscan and Duri asphaltenes 582 *illus.*
nondistillable aromatics
  composition 240
  NMR studies 240,241 *illus.*
  thermolysis 242
    n-pentane eluent 242
    pyrolysis oil fractionation procedure 243 *illus.*
nondistillable polars
  composition 346
  pyrolysis 349
    fractionation 350 *illus.*
  NMR studies 347,348 *illus.*

Odd Even Preference (OEP) 87
oil
  consumption 1
  demand 2,4 *illus.*
  flotation 49 *illus.*
  generation curve 402 *illus.*
  production 1,2,4 *illus.*
  products 3,4 *illus.*
  reserves 2,6,21 *illus.*
  resources 2,6
  –/water/solids analyses 93 *table*
oil sand
  composition 29, 30 *illus.*, 37,170 *table*, 172 *illus.*
  composition and particle size 173 *illus.*
  deposits 22 *illus.*
  geological attributes 31 *table*
  microstructure 34,35,55
  resources 5 *illus.*
  saturation 36 *illus.*
  spin density 600 *table*
optical activity 9,119
optical properties of bitumen 118
optical rotation 119
origin of petroleum 9
oxidation reactions
  fluorenes to fluorenones and fluorenols 255
  catalytic 179
  in oil sands 37
  microbiological 179
  ruthenium ions-catalyzed 248,252,542
    mechanism 543
  sulfides to sulfoxides 245
  thiophenes to thiophene sulfones 246
oxygen content of biumen, 96

Paleozoic
  formations 24
  rocks 25
particle associations 55 *illus.*
Pascal's rules 605
petrochemical family tree 3 *illus.*
Pekisko reserves 25
peptide linkages 83

pH
  effect on interfacial tension 43,46,49 *illus.*
  effect on quartz solubility 148
  effect on surface crystal charges 169,172
  effect on surface tension 50
  effect on zeta potential 51,53,54
  in the hot water process 39,43,58,59
  of minerals in oil sands 37,38
  of the connate water 145,148,149
photosensitizers 10
photosynthesis 9,10,11
phototrophs 10
phytoplanktons 10, 13
pigments 85
point of zero charge (pzc) 53,54
polar fraction
  H/C ratio 261
  molecular weight 261
  subfractions
    elemental composition 262,263 *illus.*, 264 *table*
    fractionation 262,263 *illus.*
    infrared spectra 265 *illus.*,267 *illus.*
  thermolysis 369,370
porosity of reservoir rock 30
potash 135
potential energy curves 59 *illus.*
pour point 107
PR asphaltene
    RICO of – 565/566 *illus.*,557 *illus.*
PR sands
  gases evolved 182 *table*
process streams solids (NMR) 173 *illus.*
process water 438
pyrites 37, 38,134
pyrobitumens 89
pyrolysis oil
  of Ath. asph. 500–507
  of nondistillable aromatics 241–251
  of nondistillable polars 346–369

quartz 135,139,159
  solubility 148

racemate 80
radical ions, radical ion pairs 604
Ramsbottom carbon residue 75 *table*
Rankin scale 91
reduction reactions
  molecular weight of covalent core segments 613
  molecular weight of products 613
  reductive degradation by NRA and NiB 611
  sulfide bridge cleavage 525
    number of sulfide bridges 612
  sulfide, oxygen bridge cleavages 523
  sulfides to hydrocarbons 278
  sulfoxides to sulfides 245,278
refractive index
  vs asph precipitation 381
  of bitumen 90,118 *table*, 119
  of crude oils 482
refractivity intercept method 119
repulsive interactions 74
reservoir
  gases 179
    composition 181/182 *tables*,184–186 *tables*
  sources 143
  types 143,144 *illus.*
  water 143
resin fraction definition 121,261
resonance energy 77
ring opening 238
ring strain 74
ruthenium ions-catalyzed oxidation (RICO) 614, 666 *table*
  of Ath. asph. 542–557
  of Carb. Tri., Lloyd. and PR asphaltenes 565 *illus.*
  of nondistillable aromatics 248
  of nondistillable polars 361
  precursors of benzene polycarboxylic acids 615

Saline Lake asphaltene 568
  NMR 582
  RICO 569 *illus.*
saponification of
  Ath. asph. 539,540
  ore sands 152
SARA procedure 121,122 *illus.*,123,124 *table*, 125,190
SAPA procedure 123 *illus.*,124
saturate fraction 189
  composition
    Ath. 190,205 *illus.*,206 *illus.*
    Carb. Tri. 204 *illus.*
    CL 202–205 *illus.*
    Lloyd. 205 *illus.*
    PR 206 *illus.*
    Venezuela 204 *illus.*
  content 190
  fractionation 191 *illus.*,192/193 *tables*
  NMR 209 *illus.*
  nondistillable Ath. fraction 208
    NMR, 209
    thermolysis 210
saturates from NiB reduction of HMA 528–535
  geochemical classification 531
Saybolt viscosity 90

sea water composition 144 *table*
sedimentary organic matter 9,11,12
    evolution 14 *illus.*
sedimentary rocks 14
shale bed waters 143
shale stringers 143
siderite 135
silica 135,169
silicates 135
silt 29
small angle neutron scattering 645
smectic clays 636
smectite 135,140,159
solubilities of hydrocarbons 427 *illus.,table*, 428 *illus.*
solvation energy 467
solvent extraction 91
solvent power 482
Soret band of porphyrins 335,336,337 *table*
source
    materials correlation with petroleum properties 404 *table*
    rock, 14
        bitumen class compositional data 15 *illus.*
        correlation with petroleum properties 404 *table*
Soxhlet extraction of asphaltene 483
specific dispersion method 119
specific gravity
    and asphaltene content 17 *illus.*
    of bitumen 90,99
specific heat 114–116 *tables*
specific rotation 119
spreading rate parameter 48
stereoisomers 81
sulfate ion 37
sulfide bridges in asph. 527
sulfonic acids 39
sulfur
    content of bitumen 94,96,97,101,125 *table*,404
    elemental 37
    incorporation 407,551
sulfuric acid 37,38
Suncor production 6
surface
    energy 50
    tension 40, 41 *table*, 42 *illus.*,43,48,49,50
        and particle size 173 *illus.*
        and asphaltene yield 466
surfactants 35,39,43
    carboxylate anions 39,43149,157
    sulfonate anions 39
Syncrude Batch Extraction Test (SBET) 164
Syncrude production 6

tailings organic matter
    composition 165 *table*
    fractionation 164 *illus.*
thermal cracking properties 91
thermal maturation 17
thermal maturity ratios 402 *illus.*
    from bridges and chains 637
    from hopanes 381,382,384,395,401
    from porphyrins 436
    from steranes 388,391,401,402
    diasterane/sterane 389,390
    dibenzothiophene (DBTI) 297 *table*,349, 417 *illus.*
    tricyclics/(tricyclics+hopanes) 395
thermal processes 16, 17 *illus.*,101
thermocatalytic processes 101,179
thiourea adduction 216
total ion current mass chromatogram 195
trace metal analyses
    in bitumens 97 *table*,98 *table*,132/133 *tables*
    in mineral solids 138 *table*
Treibs scheme 435 *illus.*
triaromatic subfraction composition 229–229
Turner Valley Formation 189

Universal Oil Product (UOP) 91
Upper Devonian
    Grosmont formation geology 25
    limestones 21
Upper Ireton reserves 25
urea adduction 216
USBM-API-60 procedure 121,122 *illus.*,123,124 *table*,125,190,262
Ultraviolet-visible spectra 585
    absorption spectra of Ath. asphaltene 586 *illus.*

van der Waals
    equation of state 479
    forces 169,171,215
van Krevelen diagram 13
vanadium/nickel content of bitumen 101
vermiculite 168,169
viscosity 90,99,102
    data 95 *table*,98,104 *illus.*,109 *table*
    – density correlation 106 *illus.*
    dynamic 101
    – gravity constant (vgc) 90
    kinematic 101,104,107
    – molecular weight correlation 106 *illus.*
    of biodegraded oil 422
    of distillates 108 *table*,109 *table*
    of hydrotreated products 108 *table*,109 *table*
    pressure dependence 106

- Saybolt – 90,99,103
- shear dependence 105 *table*
- SUS 99
- temperature dependence 104 *illus.*,105 *table*

viscosity-gravity constant (vgc) 90
vitrinite reflectance 12,402
vitrinites 13,14

Wabamum reserves 25
water–flood oil recovery 61
water displacement 91
water pockets 145
water washing 16,17,96,101,157,402,408,409, 426,429 *illus.*
- effect on sulfides 411 *illus.*,412 *illus.*,414 *illus.*
- effect on sulfoxides 410 *illus.*
- geological setting 427 *illus.*

Watson characterization factor 91
Wentworth scale 135,139/140 *tables*
Western Canada Sedimentary Basin 21,421 *illus.*

X-ray diffraction 140, 620
X-ray fluorescence spectroscopy 98

zeta potential
- 50,51 *illus.*, 52 *illus.*
- of Na–kaolinite particles 55 *illus.*
- of the mineral/water interface 53 *illus.*,54 *illus.*

zooplanktons 13

Chemical Index

List of Abbreviations:

Ath. = Athabasca; PR = Peace River; Lloyd. = Lloydminster; CL = Cold Lake
HMA = high-molecular-weight asphaltene; LMA = low-molecular-weight asphaltene; MW = molecular weight;
NRA = naphthalene radical anion; RICO = ruthenium ions-catalyzed oxidation

- abietic acid 394
- acetaldehyde 180,183
- acetic acid 93
- acyclic
  - alkanes 69
  - isoprenoids 189
    - in Cold Lake saturates 201
    - in Leduc saturates 214 *table*
- adamantane 207,208
- adduction chromatography 216
- alcohols 87
  - biomarkers 432
  - in pyrolysis oil of nondistillable aromatics 250,251 *illus.*
  - in pyrolysis oil of nondistillable polars 366, 367 *table*
  - produced by RICO of the nondistillable polars 362,363 *illus.*
  - n-
    - from saponification of Ath. asph. 540, 541 *illus.*
    - from thermolysis of Boscan asph. 505 *illus.*
    - from thermolysis of whole Ath. asph. 501/502 *illus.*
    - in pyrolysis oil of Ath. HMA 521,522 *illus.*
    - in the polars 316 *illus.*,376
    - in the process water 445
- aldehyde 87
- alginic acid 84
- alkanes
  - *n*- 189
    - concentration in Ath. asph. 608
    - from BBr_3 cleavage of ester bonds in Ath. asph. 542 *illus.*
    - from NiB reduction of HMA 529,530 *illus.*, 531 *table*
    - from NiB reduction of LMA 535
    - in Ath. saturates 204
    - in CL saturates 201 *illus.*,204
    - in Lloyd. saturates 204
    - in pyrolysis oil of Ath. HMA 509 *illus.*
    - in pyrolysis oil of nondistillable aromatics 242,243 *illus.*
    - in pyrolysis oil of nondistillable polars 349
    - in pyrolysis oil of nondistillable residue from RICO of Ath. asph. 560 *illus.*
    - in pyrolysis oil of nondistillable residue from RICO of Boscan, Duri and X asph. 572 *illus.*
    - in the process water 439
    - mode of attachment in asph. 608
  - diphenyl- 357
  - *iso*- 711,72
- alkanoic acids
  - bound to the sand 153,154/155 *illus.*
  - *n*-
    - from saponification of Ath. asph. 540, 541 *illus.*
    - in biodegraded oils 430
    - in the polars 274,304,376
    - in pyrolysis oil of Ath. HMA 520
    - in pyrolysis oil of nondistillable polars 364
    - source materials of asph. 635
- alkanoic acids from RICO
  - α,ω-di-*n*- 572
    - from Ath. asph. 552,553 *illus.*
    - Boscan, Duri, X, Saline Lake, Gudao, Arabien 570 *illus.*
    - from Carb. Tri., Lloyd.and PR asphaltenes 565 *illus.*
    - from nondistillable aromatics 248,252, 253 *illus.*
    - from nondistillable polars 361,362 *illus.*
    - precursor polymethylene bridges 617
  - benzenepolycarboxylic
    - from Ath. asph. 553,554 *illus.*
    - from Carb. Tri., Lloyd. and PR asphaltenes 565 *illus.*
    - from nondistillable aromatics 253 *illus.*
    - in pyrolysis oil of nondistillable aromatics 242,253 *illus.*
    - in pyrolysis oil of nondistillable polars 362,363 *illus.*
    - precursors 615 *table*
  - branched 569
  - *iso*-
    - from Ath. asph. 544,545-547 *illus.*
  - hopanoic 548,549 *illus.*
  - *n*-
    - from Ath. asph. 544,545/546 *illus.*
    - from Carb. Tri., Lloyd. and PR 565 illus.
    - from Boscan, Duri, X, Saline Lake 569 *illus.*
    - from nondistillable aromatics 248,249 *illus.*,252

    - from nondistillable polars 361,362 *illus.*
    - in pyrolysis oil of nondistillable residue 560 *illus.*
  - steranoic 549,550 *illus.*
  - tricyclic terpenoid
    - from Ath. asph. 548,549 *illus.*,551
- alkenes 189
- *n*-alkyls
  - aromatic attached in asphaltenes 570 *table*
- aluminum silicate-organic complexes 35
- amino acids 83
- anhydrides in the polars 311,312 *illus.*
- *anteiso*alkanes 71,72
- anthracene 77,78,87,554
  - benzofluoro- 87
  - dibenzo- 87
  - fluoro- 87
  - in pyrolysis oil of Ath. HMA 518,519 *illus.*
  - methylcarboxylate 307
- anthrene
  - azafluoro- 330
- aromatic hydrocarbons
  - biodegradation of – 424
  - concentration in Ath. asph. 609
  - distribution in Ath., CL and Lloyd. 254 *illus.*
  - in Ath. asph. 672 *table*
  - mono- 222 *illus.*,223 *table,*238 *table*
    - distribution 236 *table*
  - di- 224 *illus.*,226 *illus.*,238 *table*
  - tri- 228 *illus.*,229,231,239 *table*
  - tetra- 235 *illus.*, 239 *illus.*
- azaarenes in the maltene 326
  - elemental analysis 327 *table*
  - identified Ath., 329,332 *tables*, Cold Lake, 331 *table*

- basic nitrogen compounds (see azaarenes)
- BBr$_3$ cleavage of ester bonds in Ath. asph. 541, 542 *illus.*
- benzenes (alkyl) 77
  - concentration in asph. 609
  - in the monoaromatic subfraction 221,222 *illus.*
  - in pyrolysis oil of Ath. HMA 509 *illus.*,519
  - in pyrolysis oil of nondistillable aromatics 241,245
  - in pyrolysis oil of nondistillable polars 349,350 *table*,357
  - mode of attachment in asph. 609
  - distribution from various asphaltenes 573 *table*
  - from Boscan, Duri, X, Saline Lake, Gudao asphaltenes 571 *illus.*
- benzothiophenes
  - alkyl-, cycloalkyl-
    - in the monoaromatic fraction 222 *illus.*
    - in the diaromatic fraction 224–227 *illus.*
- bicyclic terpenoid acids
  - chemisorbed to the ore 153
- bicyclic terpenoid sulfides 199
  - in pyrolysis oil of nondistillable aromatics 245,247 *illus.*
- bicycloalkanes 75
- bicyclodecane 75
- bicyclic terpenoid
  - hydrocarbons 191 *illus.*
  - sulfides
    - in the triaromatic fraction 230 *illus.*
- biological markers (biomarkers) 9,189
- biphenyl 78
  - in pyrolysis oil of Ath. HMA 517,518/519 *illus.*
- biphytane 73,201
- butane 70,73
  - 2-iodo- 80
  - 2-chloro-3-iodo- 81
- butyl radicals 72
- butyric acid 93

- Ca^{2+} ions 35,38,39,56
- carbazoles 79,87
  - alkyl-
    - in the asphaltene acetone extract 322
    - in the triaromatic subfraction 234 *illus.*
    - in the polar fraction 266,268 *illus.*
  - alkylbenzo-
    - in the asphaltene acetone extract 322,323
    - in the polar fraction 266
  - alkylcyclohexane-
    - in the polar fraction 266, 268 *illus.*
  - alkylcyclohexanebenzo-
    - in the asphaltene acetone extract 322,323
    - in the polar fraction 266
  - alkylbenzo-
    - biomarkers for migration distances 436–438 *illus.*
    - in the asphaltene acetone extract 325 *illus.*
    - in the polar fraction 266,268 *illus.*
  - alkyldibenzo-
    - in the asphaltene acetone extract 322, 325 *illus.*
    - in the polar fraction 266,268 *illus.*
  - concentrations
    - in the polar fraction 269 *illus.*
    - in the asphaltene acetone extract 324 *table*,326
- carbohydrates, 12,83,167
- carbonate, bicarbonate ions 10
  - in the connate water 145,148
- carboxylates in the connate water 148

carboxylic acids 87,93,149
  biomarkers 429–431
  bound to the sand 152 *illus./table*,153 *table*,171
    identification 153,156 *tables*
    distribution 154,155 *illus.*
  in the asphaltene acetone extract 307,431
  in the polars 449 *illus.*
    hexacyclic terpenoid 273 *illus.*
    naphthenic 272 *illus.*
    pentacyclic (hopanoic) 272 *illus.*,303
    reduced to hydrocarbons 301 *illus.*
    tetracyclic terpenoid 273 *illus.*
    tricyclic terpenoid 272 *illus.*,273 *illus.*, 299 *illus.*,300,375
  in the process water 445,448 *illus.*
  in pyrolysis oil of the nondistillable polars 364
carotene 408
carotenoids 10
cellulose 13,84
cheilanthane 87,197,204 (see also tricyclic terpanes)
  bisnor- 377,389
  carboxylic acid 87
chitin 84
m-chloroperbenzoic acid 246
chlorophyll 9,10,11,85,337,375,398,399
  a,b 85
  bacterio 85,399
  in Treibs scheme 435
cholestane 199,377,378,390
  dia- 377,378,390
  methyl-, ethyl- 378
cholesterol 83,387,388,457
chrysene 78,87,357
Cl$^-$ ions 51
coronene 78,554
cyclic saturated hydrocarbons
  in Athabasca saturates 194 *illus.*,198 *table*,199, 205
  in Carb. Tri. saturates 206 *illus.*
  in CL saturates 200, 202–205 *illus.*,205
  in Lloyd. saturates 204,205
  in PR saturates 206 *illus.*
  in Venezuela saturates 206 *illus.*
cycloalkanes 73
cyclohexane 73,74
  alkyl 199
  cis-1,4-dimethyl 74,79
  cis-1,3-dimethyl 81
  trans-1,4-dimethyl 75,79
  conformational energies 75
  dodecyl 214
cyclopentane 73,74

decalin 199
decane 70
diasterane 87,199
diastereomers 199,302
dibenzothiophene maturity index (DBTI) 297 *table*, 349
drimane 87,196,197,288,377,397
  from NiB reduction of LMA 535
  sulfide/sulfoxide 87

eicosane 70,214
ester bond cleavage 539,540
ethane 70
ether 87
  bond cleavage 541,542 *illus.*

farnesane 73,398,399
fatty acids chemisorbed to the ore 156,157
Fe^{2+} ions 39
FeCl$_3$ complexes 163
fluorene 78,87
  9-alkyl- 78
  alkylaza- 328
  aza- 364
  biomarker 432
  9-carbomethoxy-
    -9-methoxy- 310
    -9-formyl- 310
    -9-acetyl- 310
    9-acetaldehyde- 310
    9-1-hydroxyethyl- 310
  -carboxylic acid 87
  in Ath. aromatic fraction 255,256,257 *illus.*
  in pyrolysis oil of Ath. HMA 515,516 *illus.*, 519 *illus.*
  in pyrolysis oil of nondistillable polars 357
  methylcarboxylate 308
fluorene-9-ols 87,317
  9-carbomethoxy- 309
  9-*n*-alkyl 78
    in the asphaltene acetone extract 318
    in the polars 271 *illus.*,317 *illus.*,319 *illus.*
    from fluorenes in the aromatics 256, 257 *illus.*
fluorene-9-ones 78,87
  biomarkers 432
  in the maltene 314,315 *illus.*
  in the asphaltene acetone extract 314,315 *illus.*,316
  in the polars
    alkyl- 270 270 *illus.*
    alkylbenzo- 270
  from fluorenes in the aromatics 256,257 *illus.*
formic acid 93
fructose 83

- fulvic acids 29,33,60
  - bound to clays 171
  - evolution 160 *illus.*
  - in oil sands ore 152
    - FTIR spectrum 162 *illus.*
    - NMR spectrum 162 *illus.*
- gammacerane 87,379,384,385,535
- gases evolved (composition) 181,182,184, 185 *tables*
- glucose 10,83
- glyceryl
  - diether 83
  - tetraether 83

- H^+ ions 38,39
- hemes 375
- heptane 70
- hexane 70
  - alkylcyclo- from NiB reduction of Ath. HMA 531 *illus.*
- hopane 87,190,198,380,383,384,388
  - carboxylic acid 87
  - disulfide in the triaromatic subfraction 234
  - sulfide/sulfoxide 87
- hopanes
  - bacteriohopanetetrol 387,388,397,457
  - benzo- 379
    - in the process water 448 *illus.*
  - bishomo- 378,383,384
  - bisnor- 378,382,383,384
  - distribution 382, *illus.*,383 *illus.*385/386 *illus.*, 396 *illus.*
  - from BBr_3 cleavage of ester bonds in Ath. asph. 542 *illus.*
  - from NiB reduction of Ath. HMA 532,533 *illus.*
  - from NiB reduction of Ath. LMA 536
  - from thermolysis of Ath. asph. 503
  - from thermolysis of Lloyd. asph. 506 *illus.*
  - homo- 378,381,382,383,384
  - in the process water 439,441,448 *illus.*
  - in the saturates 191,198 *table*
  - nor- 382,383,384,
    - and biodegradation 385,423
  - norhomo- 384
  - norbishomo- 384
  - pentakishomo- 378,383
  - seco- 231,377,379,393,402
    - in the process water 442 *illus.*,446 *illus.*, 447 *illus.*
  - thermal maturity indices 401
  - tetrakishomo- 378,383,
  - trishomo- 378,383,
  - trisnor- 379,382,383,384,385
  - trisnorneo- 379,383
  - Z plots 239 *illus.*
- hopanetetrol 83
- hopanoic acids 273,431
  - from RICO of asphaltene 617
- hopene 387
- humic acids 29,33,60
  - bound to clays 171
  - evolution 160 *illus.*
  - in oil sand ore 152; in tailings 164,165,166; in oil sands and in overburdens 166
  - FTIR spectrum 161 *illus.*
  - NMR spectra 166 *illus.*,167 *illus.*,174 *illus.*
  - evolution 160 *illus.*
- humic
  - materials 33,35,140,157,171
  - matter/inorganic complexes 35
- humic–inorganic complexes 60
- humin 29,33,60
- hydrocarbon sources 14 *illus.*
- hydrocarbons
  - in the reservoir gases 180
  - cyclic- in the saturates 194 *illus./table*,198 *table*

- indene 78
  - in pyrolysis oil of Ath. HMA 519 *illus.*
- iron 10
- iron
  - oxide 171
  - sulfates 3
  - sulfides 147
- isoprene 196,376

- K^+ ions 35
- kerogen 12,13,14,89,433
  - evolution 160 *illus.*
- ketones 87
  - biomarkers 431,432
  - in pyrolysis oil of nondistillable polars 366, 368 *illus.*
- Lewis acid 163,207
- lignin 12,84,85
- lycopane 73,379,398

- methane 69
- methylene chloride 92
- mica 135
- Mg^{2+} ions 35,38,39
- monoaromatic hydrocarbons distribution 221, 222 *illus.*
- monocyclic sulfides (see thianes, thiolanes)
- moretane 378,381
  - bisnor- 378
  - from thermolysis of asph. 503
  - nor- 378

  trisnor- 379

Na^+ ions 51
$NaCl$ 61
$NaOH$ 61,62
naphthalene 77,78,87,554
  alkyl-
    in the diaromatic fraction 225,227
    in pyrolysis oil of Ath. HMA 517,518/519 *illus.*
    in pyrolysis oil of nondistillable polars 357
  alkyldecahydro-
    in pyrolysis oil of nondistillable aromatics 245
  alkyltetrahydro-
    in pyrolysis oil of nondistillable aromatics 241,245
    in pyrolysis oil of nondistillable polars 349,352 *table*,357
  radical anion (NRA) reduction of asph. 523
neopentane 180,185
naphthenes 96
neutral nitrogen compounds (see also azaarenes) 123
neutral resins 123
Ni^+ 339
NiB reduction of Ath. asph. 525
Ni contents 338 *illus.,table*
nonane 70,71
nondistillable aromatics 240
  thermolysis 241
nondistillable polars pyrolysis oil fractionation 350/351 *illus.*
norpristane 73

octane 70
  6-ethyl-2-methyl 71
organic carbon 9,11,14
organic matter 12
oxygen functionalities 79

pectin 84
pentacosane 70
pentacyclic hydrocarbons (see hopanes)
pentadecane 70
pentane 70
  2,2-dimethyl 71
  2,2,4-trimethyl 71
  6-ethyl-2-methyl 71
pentyl radicals 72
perinaphthyl radicals 603
perylene 87
phenanthrene 77,78,87,96,554
  alkyl-
    in pyrolysis oil of nondistillable aromatics 241,245
    in pyrolysis oil of nondistillable polars 357
  alkyltetrahydro-
    in pyrolysis oil of nondistillable aromatics 241
  aza- 364
  phenanthridine
  methylbenzo- 326
phytane 73,189,200,214,379,398,399
phytol 398,399
picene 87
pollens 13
polyaromatic fraction (see nondistillable aromatics)
polysaccharides 10,83,84
polysilicic acids 148
porphyrins 9,10,79,87,335,375
  alkyl substituents 339
  benzo- 343,344 *illus.*
  complexed to Ath. asphaltene 342,343 *illus.*
  concentrations 338 *table*,345 *table*
  demetalated 342,343 *illus.*,344 *illus.*
  di-DPEP 337
  DPEP 335,336,337435 *illus.*,436
    benzo- 337
    tetrahydrobenzo- 337
  etio 86,335,336,337,436
  etio/benzo-DPEP ratio 341 *table*
  etio/benzo-etio ratio 341 *table*
  etio/DPEP ratio 339–341 *table*,342
  etio/THBD ratio 341 *table*
    benzo- 337
    tetrahydrobenzo- 337
  in Ath bitumen 339
  molecular weights 338 *table*
  phyllo 353,36
  rhodo 335,336,343
  separation from bitumen fractions 340 *illus.*
  THBD/benzo-DPEP ratio 341 *table*
  UV spectra 336 *illus.*
  vanadyl - 339,345,434,436

  V/Ni ratio 337,338
pregnane 377,389
pristane 73,189,200,214,379,398,399
pristane/phytane ratio 400,404,422,536
propane 70
propionic acid 93
proteins, 12,13,83
pyrene 78,87,357
  alkylaza- 328,330
  benzo- 554
pyridines (alkyl) 78,87
  in pyrolysis oil of Ath. HMA 520,521 *illus.*

  in pyrolysis oil of nondistillable aromatics 250
  in pyrolysis oil of nondistillable polars 364,365 *table*
  in the maltene 327,329 *table*,330
pyrrole 85

quinolines (alkyl) 87
  benzo-, in the aromatic fraction 233
  in pyrolysis oil of Ath. HMA 520,521 *illus.*
  in pyrolysis oil of nondistillable aromatics 250
  in pyrolysis oil of nondistillable polars 364, 365 *table*
  in the maltene
    alkyl 329 *table*,330
    alkylbenzo- 327,238 *table*
    alkyldibenzo- 330
    alkyldimethylbenzo- 326
    alkylhydroxy- 332
    alkyltetrahydrodibenzo- 330
quinolone 87
  in Ath. maltene 333
  in pyrolysis oil of nondistillable polars 366, 367 *illus.*
  thio- 87,334

Raney nickel reduction of sulfides 283
22R/22S epimers 199,304
ruthenium ions-catalyzed oxidation 248,252,542

silicate ion 148
silicic acid 148
S/N ratio classification 433
sodium chloride in connate water 145
spores 13
squalane 379
squalene 83,387,388,405
    from thermolysis of asph. 503
steranes 87,190,199 *illus.*,204,380,389
  biodegradation of 423,424
  biomarker ratios 393 *table*,404
  dia- 389,423,532
  distribution 387 *illus.*,389 *illus.*,390 *illus.*,391
  from NiB reduction of Ath. HMA 532,533 *illus.*
  from NiB reduction of Ath. LMA 536,537 *illus.*
  from thermolysis of Ath. asph. 503
  from thermolysis of Boscan asph. 505 *illus.*
  in the process water 439,443 *illus.*
  monoaromatic 379,391,392 *illus.*,402
    in the process water 443 *illus.*,444 *illus.*
  tetracyclic - 375,
  triaromatic 87,229,231,391,392 *illus.*,402
    in the process water 444 *illus.*
sterol-sterene-sterane conversions 388 *illus.*
sucrose 83
sulfate in the connate water 145,407
sulfide bridges in asph. 527
sulfides 87
  complexed to asphaltene 293
  concentartion in Ath. asph. 609
  contents in oils 295 *table*,409 *table*
  from sulfoxides 279,280 *illus.*,281 *illus.*
  in the triaromatic subfraction 229,230 *illus.*
  in pyrolysis oil of nondistillable aromatics 245, 247 *illus.*
  in pyrolysis oil of nondistillable polars 354, 356 *illus.*
  in the maltene
    monocyclic 291 *illus.*,292 *illus.*
    bicyclic terpenoid 283 *illus.*,284,285 *illus.*
      as biomarkers 408,410–412 *illus.*
    hexacyclic terpenoid 289,415,416 *illus.*
    pentacyclic terpenoid 290 *illus.*,415
    tetracyclic terpenoid 286 287 *illus.*,413, 414 *illus.*
    tricyclic terpenoid 288 *illus.*,411,412 *illus.*
  in the polars 277
  oxidation to sulfoxides 282
  reduction to saturates 283
sulfonic acids 449
sulfoxides
  as biomarkers 409
  complexed to asphaltene 293
  contents in oils 295
  conversion to sulfides and saturates 278 *illus.*
  in the polars 274,277
    bicyclic 274,275 *illus.*,410 *illus.*
    tricyclic 274,275 *illus.*,397
    tetracyclic 274,275 *illus.*,411
    pentacyclic 274,275 *illus.*
    hexacyclic 274,275 *illus.*
    relative concentrations 275 *table*, 276 *illus.*
  in the triaromatic subfraction 229
  in the maltene
    analysis as sulfides, 279,280 *illus.*,281 *illus.*
    bicyclic terpenoid 282,283 *ilus.*,287 *illus.*
    contents 280 *table*
    hexacyclic terpenoid 289
    IR, FIM spectra 279 *illus.*
    pentacyclic terpenoid 293
    separation/isolation 278 *illus.*
    tetracyclic terpenoid 286,287 *iilus.*
    tricyclic terpenoid 288 *illus.*,289 *illus.*

tannins 13
terpanes
  bicyclic 191, *illus.*,375,380,386,397
    from NiB reduction of LMA 535
    in the process water 441 *illus.*

  - mono - 376,398
  - sesqui- 376
  - sesquiter- 376
  - tricyclic 199, *illus.*,274,375–377,383,393, 394 *table*
    - concentration 395
    - distribution 382 *illus.*,383 *illus.*,384 *table*,385 *illus.*,386 *illus.*,396 *illus.*
    - from NiB reduction of Ath. HMA 532, 533 *illus.*
    - from NiB reduction of Ath. LMA 536
    - from saponification of Ath. asph. 540, 541 *illus.*
    - from thermolysis of Ath. asph. 503
    - from thermolysis of Lloyd. asph. 506 *illus.*
    - genetic relationships 16 *illus.*
    - in the process water 441 *illus.*
  - tetra- 376
  - tetracyclic 375 (see steranes)
  - pentacyclic (see hopanes)
- terpenoid acids
  - biomarkers 430
  - chemisorbed to the ore 153
- terpenoid hydrocarbons in the saturates 191 *illus.*, 193 *illus.*
- tetracontane 70
- tetracyclic hydrocarbons Z plots 239 *illus.*
- tetralin 77
  - alkyl 90
  - in the monoaromatic subfraction 221 *illus.*
  - in pyrolysis oil of Ath. HMA 519 *illus.*
- thianes (alkyl) 78,87
  - concentration in Ath. asph. 609
  - sulfoxide 87
  - in Bellshill Lake oil 292 *illus.*
  - in pyrolysis oil of Ath. HMA 510,511 *illus.*
  - in pyrolysis oil of nondistillable aromatics 247 *illus.*
- thiolanes (alkyl) 78,87
  - carboxylic acids 406
  - concentration in Ath. asph. 609
  - in Bellshill Lake oil 292 *illus.*
  - in pyrolysis oil of Ath. HMA 510,511 *illus.*
  - in pyrolysis oil of nondistillable aromatics 247 *illus.*
  - in pyrolysis oil of nondistillable polars 348, 352 *table*,354,356 *illus.*
  - sulfoxide 87
- thiophenes 87
  - alkyl - 78
    - in pyrolysis oil of Ath. HMA 509,510 *illus.*
    - in pyrolysis oil of nondistillable polars 349, 352 *table*,352 *illus.*
  - alkylbenzo- 78
    - in the aromatic fraction 222 *illus.*
  - alkyldibenzo- 78
    - in biodegraded oil 422
    - in pyrolysis oil of nondistillable polars 352 *illus.*
    - in pyrolysis oil of RICO residue from Boscan asphaltene 572 *illus.*
  - benzo- 87
    - in the aromatic fraction 224 *illus.*,225, 226 *illus.*,227
    - in pyrolysis oil of Ath. HMA 512 *illus.*, 514 *illus.*
    - in the pyrolysis oil of nondistillable polars 356 *illus.*
  - concentration in Ath. asph. 609
  - content 404
  - cycloalkanobenzo 78
  - cycloalkylbenzo- in the aromatic fraction 222 *illus.*
  - dibenzo - 87
  - in the aromatic fraction 227 *illus.*,228
    - in pyrolysis oil of Ath. HMA 513/514 *illus.*
    - in the pyrolysis oil of Ath. nondistillable aromatics 246
    - in the pyrolysis oil of nondistillable aromatics 246,356 *illus.*
    - methylcarboxylate 307
  - maturity index (DBTI) 297 *table*, 349
  - in CL, Ath. and Lloyd. aromatics 255 *illus.*
  - in the maltene 296,297,298 *illus.*, *table*
    - separation scheme 296 *illus.*
  - tribenzo- in the aromatic fraction 228
- triacontane 70
- tridecane, 2,6,10-trimethyl 73
- triphenylene 554
- triphenylmethyl radical 602

- undecane 70

- V/Ni ratios 98,101,338,339
- V contents, 338 *illus.*, *table*
- VO^{2+}, 339,346 *illus.*
  - EPR spectrum 593

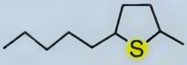

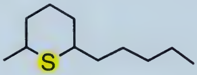

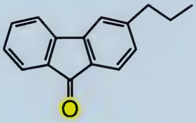

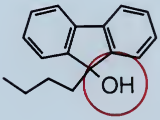

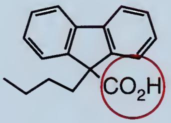

1.5 million trees have been planted as part of site reclamation.

NATIONAL LIBRARY OF CANADA
Bibliothèque nationale du Canada
3 3286 52865751 9

Bitumens upgraders at
Syncrude Canada Ltd.
near Fort McMurray